PROCEEDINGS OF WAVES 2007

THE 8TH INTERNATIONAL CONFERENCE ON MATHEMATICAL AND NUMERICAL ASPECTS OF WAVES

Editors: Nick Biggs, Anne-Sophie Bonnet-Bendhia, Peter Chamberlain, Simon Chandler-Wilde, Gary Cohen, Houssem Haddar, Patrick Joly, Stephen Langdon, Eric Lunéville, Beatrice Pelloni, Dominique Potherat, Roland Potthast

University of Reading
23rd – 27th July 2007

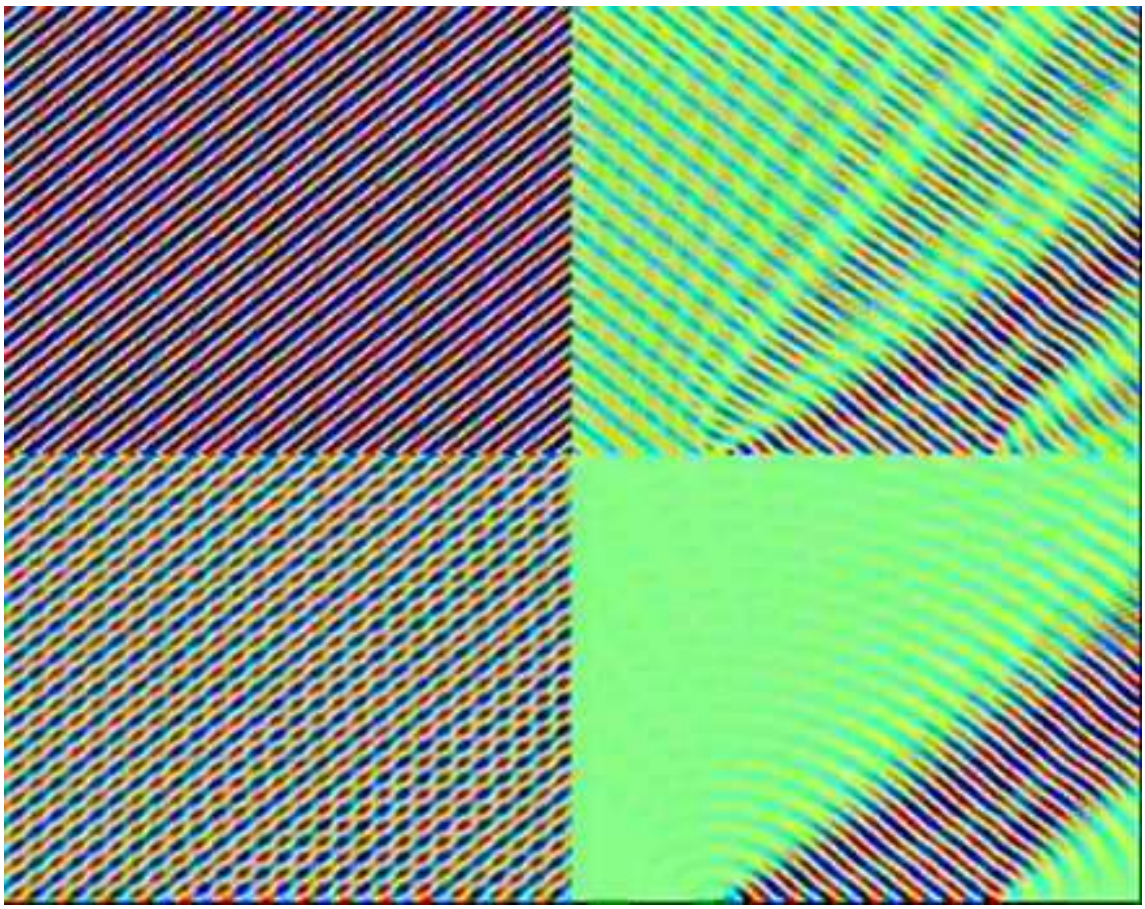

University of Reading

INRIA

PREFACE

As we are writing we are looking forward to the 8th International Conference on Mathematical and Numerical Aspects of Waves (Waves 2007) which will be held in a month's time, from 23 to 27 July 2007, at the University of Reading, organised jointly with INRIA. This meeting is the 8th in a sequence which started in Strasbourg in 1991. Commencing with that first meeting, this series has been one of the main venues where significant advances in the analysis and computational modelling of wave phenomena are discussed and where exciting new applications are presented.

We expect this 8th conference to maintain the strong traditions of its predecessors. In addition to plenary talks by Mark Ablowitz, Annalisa Buffa, Weng Cho Chew, Tom Hagstrom, Andreas Kirsch, John Toland, and Ross McPhedran, we are expecting approximately 180 varied and interesting contributed talks. This proceedings contains accounts, in the form of 2-3 page short papers or extended abstracts, of all the papers to be presented at the Waves 2007 meeting.

As the reader of this proceedings will see, major themes of the conference include periodic media and photonic crystals, metamaterials and propagation in complex and random media, nonlinear wave phenomena in optics and fluid dynamics, inverse problems and optimization, numerical methods for time domain problems, resonances and trapped modes, finite element methods for the Helmholtz equation and Maxwell system, absorbing boundary conditions, elastic waves, gravity waves, and brain waves and cognitive neurodynamics. The conference includes an embedded Workshop on High Frequency Propagation and Scattering, as a follow-up satellite meeting of the 2007 Isaac Newton Institute Programme on Highly Oscillatory Problems: Computation, Theory and Application, and many of the papers describe very recent developments by participants in that five-month programme which finishes next month.

It is pleasure to thank our co-organisers, from INRIA, ENSTA, and Reading, for their efforts in putting this proceedings together. While all have contributed, thanks are especially due to Houssem Haddar and Jing-Rebecca Li of INRIA, who supervised the submission and reviewing process, and Nick Biggs of Reading who supervised the production of the proceedings. It is a pleasure also to thank the following for their direct or indirect financial support for the Waves 2007 meeting and its embedded workshop: the Isaac Newton Institute, Cambridge, the Institute of Mathematics and its Applications, SIAM UK, INRIA, and the University of Reading Computational Science Theme.

Simon Chandler-Wilde and Patrick Joly,

on behalf of the Waves 2007 Organising Committee:

Nick Biggs, Anne-Sophie Bonnet-Bendhia, Peter Chamberlain, Simon Chandler-Wilde, Gary Cohen, Hossem Haddar, Patrick Joly, Steve Langdon, Jing-Rebecca Li, Eric Lunéville, Beatrice Pelloni, Roland Potthast.

June 2007

Table of Contents

Plenary Speakers

Nonlinear waves in optics and fluid dynamics

Mark J. Ablowitz
University of Colorado, Department of Applied Mathematics, Boulder, Colorado, U.S.A.
Email: mark.ablowitz@colorado.edu

Abstract

Nonlinear waves arise naturally in optics and fluid dynamics. An extremely important class of special solutions are localized waves, often termed solitons or solitary waves, arise naturally in nonlinear optics and fluid dynamics. In optical communications, asymptotic analysis leads to the "classical" and "dispersion-managed" (DM) nonlocal nonlinear Schrödinger (NLS) equations which have localized pulses as special solutions. Recent research has shown that similar dispersion-managed equations explain observed phenomena in mode-locked lasers. Both in nonlinear optics with quadratic nonlinearity and water waves, a nonlocal NLS type equation arises which reduce to the standard NLS equation in appropriate limits. Here localized modes are fundamentally important in the study of wave collapse. In water waves the classical equations can reformulated as a system of two equations for the wave height and for the velocity potential evaluated on the free surface. One of the equations is a nonlocal equation and one is a local nonlinear PDE. This system reduces to known asymptotic limits in shallow and deep water. Included in these asymptotic reductions are the Boussinesq, Benney-Luke and nonlinear Schrödinger equations.

Discussion

Obtaining localized waves to the governing equations of nonlinear optics and fluid dynamics are of keen scientific interest. One of the best known examples dates back to J. Scott Russell [1] who observed the propagation of solitary waves in shallow canals in Edinburgh, Scotland. This provided motivation for the seminal works of Boussinesq [2] and of Korteweg-deVries (KdV) [3] who derived the approximate equations governing water waves in shallow water, which they showed possess solitary wave solutions. Subsequent numerical and analytical studies of the KdV equation led to the concept of solitons cf. [4]. Solitons in the KdV equation are solitary waves which interact elastically in the sense that the velocity and amplitude are the same in the limit of large distances before and after a collision.

In nonlinear optics solitary waves are usually called solitons, despite the fact that they generally do not interact elastically. We will refer to solitons in this broader context. In optical fibers solitons were predicted to exist in 1973 [5, 6]. They were subsequently demonstrated experimentally by Molleneauer [7]; [see also 8, 9, for additional references and historical background]. In order to improve and enhance optical communications various technological difficulties had to be overcome; some of the more important developments include: i) all-optical amplifiers which are used to counteract damping; and ii) dispersion-management (DM) [10, 11] in which strong variations in the underlying dispersion of the fibers are employed to significantly reduces penalties (e.g. reducing the effects of four wave mixing [12] and reducing the size of frequency and timing shifts [13]) that arise in multi-channel communications systems. DM systems are of keen technological interest and have been recently installed in commercial communications environments. Dispersion-managed systems also give rise to localized pulse solutions [11]. In [14] a nonlocal equation which governs strongly dispersion-managed communications systems was derived by the asymptotic method of multiple scales. This asymptotic equation, termed the DMNLS (dispersion managed nonlinear Schrödinger equation) equation is nonlocal. It admits solitary wave solutions which were found numerically in [14], [see also 15, 16], and were rigorously proven to exist in [17]. DM systems also give rise to other special solutions of the DMNLS equation, in particular quasi-linear pulse solutions [18, 19].

Another nonlocal system of equations which arises in both optics and water waves is also of interest. The system is called the NLSM equation or the nonlinear Schrödinger equation coupled to a mean term. In nonlinear optics it arises in quadratic nonlinear media under the quasi-monochromatic assumption. In [20, 21] it is shown that with quadratic nonlinearity introduced, the classical nonlinear Schrödinger equation (NLS) is modified to have coupling to a mean term. In water waves similar systems were found earlier, first by Benney and Roskes [22], [see also 23, who introduced surface tension] and later by Davey and Stewartson [24] who put the equations into a simpler form. The stationary localized waves of this equation are fundamentally important in the study of wave collapse which can occur in these systems.

An numerical method to to find localized waves was re-

cently introduced [25]; see also [14, 26] for related methods. The main ideas are to go to Fourier space, then renormalize variables to obtain an algebraic system coupled to a nonlinear integral equation. The localized mode is determined from a convergent fixed point iteration scheme. The method is termed spectral renormalization, or SPRZ. We have found the method of coupling to be remarkably effective and straight forward to implement.

In Bose-Einstein condensates a multi-dimensional NLS equation with a parametrically forced external potential is the governing equation. This system supports dispersive shock waves and they have been experimentally observed. The theory and experiments are described in recent papers [27–29].

In the study of water waves one needs to determine the free surface, which appears as an unknown in the basic formulation. For two dimensional water waves, where the free surface evolves as a function of one space dimension and time, there are various techniques which can be used to eliminate the vertical coordinate and to reduce the problem to the evaluation of the motion of the wave height and velocity potential on a fixed domain. Effective methods used in the two dimensional water wave problem include conformal mapping and singular integral equations, both of which make use of complex analytic techniques [see e.g. 30–33]. In the three dimensional problem, where the free surface evolves as a function of two space dimensions and time, the situation is more difficult and one loses the possibility of employing standard complex analysis.

Zakharov [34] showed that the wave height η and velocity potential ϕ evaluated on the free surface, are canonically conjugate variables and the water wave equations are formulated as a Hamiltonian system. Craig and Sulem [35] employed these variables and introduced an elegant Dirichlet-Neumann operator $G(\eta)$ associated with the velocity potential which eliminated the vertical coordinate from the formulation. The operator $G(\eta)$ is obtained as a series, which is valid for small η. This formulation was used in [36] to find small amplitude/long wave approximations including the Boussinesq, Korteweg-deVries (KdV) and Kadomtsev-Petviashvili (KP) equations. The Dirichlet-Neumann operator methodology, which employs high order series approximations to a modified version of G, has been employed to perform interesting computational investigations cf. [37].

In [38] an explicit nonlocal formulation of water waves in 2+1 dimensions was constructed. The original equations with unknown boundary conditions are replaced by an integro-differential equation and a nonlinear partial differential equation, both of which are formulated in a known domain. The vertical coordinate is removed from the determining equations. These two equations can be used to determine the wave height and the velocity potential on the free surface. From this system well known asymptotic equations, in both shallow and deep water with surface tension included are obtained. In particular, this nonlocal system leads to the Benney-Luke (BL) and [39] and Kadomtsev-Petviashvili (KP; cf. [4]) equations in shallow water and the NLS equations in deep water. The SPRZ method can be used to find lump type solutions to these equations.

Acknowledgments

This work was partially supported by U.S. Air Force Office of Scientific Research under FA4955-06-1-0237, NSF grants DMS–0505352, DMS–0602151.

References

[1] J. S. Russell. Report on waves. In *Report of the 14th meeting of the British Association*, pages 311–390. John Murray, London, 1845.

[2] J. Boussinesq. Essai sur la théorie des eaux courantes. *Mémoires présentés par divers savants à l'Académie des Sciences*, 23:1–680, 1877.

[3] D.J. Korteweg and G. de Vries. On the change of form of long waves advancing in a rectangular canal, and on a new type of long stationary waves. *Phil. Mag.*, 39:422–443, 1895.

[4] M. J. Ablowitz and H. Segur. *Solitons and the Inverse Scattering Transform*. SIAM Publications, Philadelphia, Philadelpia, 1981.

[5] A. Hasegawa and F. D. Tappert. Transmission of stationary nonlinear optical pulses in dispersive dielectric fibres. I. Anomalous dispersion. *Applied Physics Letters*, 23(3):142–144, 1973.

[6] A. Hasegawa and F. D. Tappert. Transmission of stationary nonlinear optical pulses in dispersive dielectric fibres. II. Normal dispersion. *Applied Physics Letters*, 23(4):171–172, 1973.

[7] L. F. Mollenauer, R. H. Stolen, and J. P. Gordon. Experimental observation of picosecond pulse narrowing and solitons in optical fibers. *Phys. Rev. Lett.*, 45:1095–1098, 1980.

[8] A. Hasegawa and Y. Kodama. *Solitons in Optical Communciations*. Oxford University Press, Oxford, 1995.

[9] L. F. Molleneauer and J. P. Gordon. *Solitons in Optical Fibers : Fundamental and Applications to Telecommunications*. Academic Press, London, 2006.

[10] C. Lin, H. Kogelnik, and L. G. Cohen. Optical-pulse equalization of low-dispersion transmission in single-mode fibers in the 1.3 – 1.7-μm spectral region. *Optics Letters*, 5(11):476–478, 1980.

[11] J. H. B. Nijhof, N. J. Doran, W. Forysiak, and F. M. Knox. Stable soliton-like propagation in dispersion managed systems with net anomalous, zero and normal dispersion. *Electronics Letters*, 33(20):1726–7, 1997.

[12] M. J. Ablowitz, G. Biondini, S. Chakravarty, and R. L. Horne. Four-wave mixing in dispersion-managed return-to-zero systems. *Journal of the Optical Society of America B*, 20(5):831–845, 2003.

[13] M. J. Ablowitz, A. Docherty, and T. Hirooka. Incomplete collisions in strongly dispersion-managed return-to-zero communication systems. *Optics Letters*, 28(14):1191–1193, Jul 2003.

[14] M. J. Ablowitz and G. Biondini. Multiscale pulse dynamics in communication systems with strong dispersion management. *Optics Letters*, 23(21):1668–70, 1998.

[15] M. J. Ablowitz, G. Biondini, and E. Olson. On the evolution and interaction of dispersion-managed solitons. In *Massive WDM and TDM Soliton Transmission Systems*, edited by Akira Hasegawa, pages 362–7, Kyoto, Japan, 2000. Kluwer Academic Publishers.

[16] I. R. Gabitov and S. K. Turitsyn. Averaged pulse dynamics in a cascaded transmission system with passive dispersion compensation. *Optics Letters*, 21(5):327–329, 1996.

[17] V. Zharnitsky, E. Grenier, S. K. Turitsyn, Ckrt Jones, and J. S. Hesthaven. Ground states of dispersion-managed nonlinear schrödinger equation. *Physical Review E*, 62(5):7358–64, 2000.

[18] M. J. Ablowitz, T. Hirooka, and G. Biondini. Quasi-linear optical pulses in strongly dispersion-managed transmission systems. *Optics Letters*, 26(7):459–461, 2001.

[19] M. J. Ablowitz and T. Hirooka. Managing nonlinearity in strongly dispersion-managed optical pulse transmission. *Journal of the Optical Society of America B*, 19(3):425–439, 2002.

[20] M. J. Ablowitz, G. Biondini, and S. Blair. Multi-dimensional pulse propagation in non-resonant chi((2)) materials. *Physics Letters A*, 236(5-6):520–524, 1997.

[21] M. J. Ablowitz, G. Biondini, and S. Blair. Nonlinear schrodinger equations with mean terms in nonresonant multidimensional quadratic materials. *Physical Review E*, 63(4):046605, Apr 2001.

[22] D. J. Benney and G. J. Roskes. Wave instabilities. *Studies in Applied Mathematics*, 48:377–385, 1969.

[23] V. D. Djordjevic and L. G. Redekopp. 2-dimensional packets of capillary-gravity waves. *Journal of Fluid Dynamics*, 79(23):703–714, 1977.

[24] A. Davey and Stewarts.K. 3-dimensional packets of surface-waves. *Proceedings Of The Royal Society Of London Series A-Mathematical Physical And Engineering Sciences*, 338(1613):101–110, 1974.

[25] M. J. Ablowitz and Z. H. Musslimani. Spectral renormalization method for computing self-localized solutions to nonlinear systems. *Optics Letters*, 30(16):2140–2142, Aug 2005.

[26] V. I. Petviashvili. Equation of an extraordinary soliton. *Sov. J. Plasma Phys.*, 2:254–263, 1976.

[27] M. A. Hoefer, M. J. Ablowitz, E. A. Coddington, I. Cornell, P. Engels, and V. Schweikhard. On dispersive and classical shock waves in bose-einstein condensates and gas dynamics. *Physical Review A*, 74:023623, 2006.

[28] M. A. Hoefer and M. J. Ablowitz. Interactions of dispersive shock waves. *Physica D, submitted*, preprint, 2007.

[29] Shu Jia Wenjie Wan and Jason W. Fleischer. Dispersive superfluid-like shock waves in nonlinear optics. *Nature Physics*, 3:46–51, 2007.

[30] M. S. Longuet-Higgens and E. D. Cokelet. The deformation of steep surface waves on water i. a numerical method of computation. *Proc. Roy. Soc. London A*, 1:350, 1976.

[31] B. Fornberg. A numerical method for conformal-mappings. *SIAM Journal on Scientific and Statistical Computing*, 1(3):386–400, 1980.

[32] J. W. Dold. An efficient surface-integral algorithm applied to unsteady gravity-waves. *Journal Of Computational Physics*, 103(1):90–115, Nov 1992.

[33] V. E. Zakharov, A. I. Dyachenko, and O. A. Vasilyev. New method for numerical simulation of a nonstationary potential flow of incompressible fluid with a free surface. *European Journal Of Mechanics B — Fluids*, 21(3):283–291, 2002.

[34] V. E. Zakharov. Stability of periodic waves of finite amplitude on the surface of a deep fluid. *J. Appl. Mech. Tech. Phys.*, 2:190–194, 1968.

[35] W. Craig and C. Sulem. Numerical simulation of gravity-waves. *Journal Of Computational Physics*, 108(1):73–83, 1993.

[36] W. Craig and M. D. Groves. Hamiltonian long-wave approximations to the water-wave problem. *Wave Motion*, 19(4):367–389, 1994.

[37] W. J. D. Bateman, C. Swan, and P. H. Taylor. On the efficient numerical simulation of directionally spread surface water waves. *Journal of Computational Physics*, 174(1):277–305, Nov 2001.

[38] M. J. Ablowitz, A. S. Fokas, and Z. Musslimani. On a new nonlocal formulation of water waves. *Accepted by Journal of Fluid Mechanics*, 2006.

[39] D. J. Benney and J. C. Luke. Interactions of permanent waves of finite amplitude. *Journal of Mathematics and Physics*, 43:455, 1964.

Advances in Mimetic Finite Differerences

F. Brezzi[†,‡*], **A. Buffa**[†,*]
[†] Istituto di Matematica Applicata e Tecnologie Informatiche, CNR Pavia. Italy
[‡]IUSS Istituto Universitario di Studi Superiori, Pavia, Italy.
[*]Email: brezzi@imati.cnr.it, annalisa@imati.cnr.it

Abstract

In this work, new mimetic finite difference discretizations of second order differential equations are introduced. Our analysis will include the relevant cases of diffusion problems, electromagnetics. The methods we propose are intimately linked with the theory of cochains and their use as discrete differential forms.

Introduction

We are interested in solving numerically differential problems whose unknowns can be thought as differential forms, pretty much in the spirit of [1], but going beyond the finite element techniques. When treating this family of differential problems there are two main setting available: the language of differential forms and the one of functional analysis of partial differential equations. Here we basically choose the second one, just using the classification coming from differential geometry.

Our differential problems will be set in a bounded domain Ω which is supposed to be a bounded polyhedron in $\mathbb{R}^3$ and we will always consider homogeneous essential boundary conditions. This choice is made just for simplicity and does not affect generality.

All problems we treat can be considered in the context of electromagnetic phenomena, and we present them in this framework.

Electrostatics: Given a charge density ρ, the electric scalar potential verifies

$$-\mathrm{div}\,\boldsymbol{\varepsilon}\mathbf{grad}\,p = \rho \tag{0.1}$$

where $\boldsymbol{\varepsilon}$ is the electric permittivity tensor. Potentials are evaluated on points, and can be interpreted as differential $0-$forms. Let us recall that this problem comes from:

$$\mathrm{div}\,\mathbf{D} = \rho \qquad \mathbf{D} = \boldsymbol{\varepsilon}\mathbf{grad}\,p \tag{0.2}$$

after elimination of the electric induction $\mathbf{D}$. In this case, ρ must be interpreted as a 3-form, $\mathbf{D}$ is the electric induction and it is known through fluxed: thus is a $2-$form.

Magnetostatics: Given a current density $\mathbf{J}$, the vector potential $\mathbf{u}$ verifies:

$$\mathbf{curl}\,\boldsymbol{\mu}^{-1}\mathbf{curl}\,\mathbf{u} = \mathbf{J}. \tag{0.3}$$

$\mathbf{u}$ can be interpreted as a $1-$form and can be evaluated through integrals along lines. Most often the problem (0.3) is made wellposed by adding the gauge: $\mathrm{div}\,\mathbf{u} = 0$. Problem (0.3) comes from the standard magnetostatics:

$$\mathrm{div}\,\mathbf{B} = 0 \qquad \mathbf{curl}\,\mathbf{H} = \mathbf{J} \qquad \mathbf{B} = \boldsymbol{\mu}\mathbf{H} \quad \text{on } \Omega \tag{0.4}$$

where $\boldsymbol{\mu}$ is the magnetic permeability, $\mathbf{H}$ the magnetic field and $\mathbf{B} = \mathbf{curl}\,\mathbf{u}$ the magnetic induction. It is well known that the magnetic field $\mathbf{H}$ can be interpreted as a differential 1-form, while the magnetic induction $\mathbf{B}$ can be sought as a differential 2-form, i.e., it is known through fluxes.

Cochains

Given the domain Ω, we are given with a polyhedral partition $\mathcal{T}_h$ of Ω, N vertices $V_1, V_2, ...V_{\mathsf{N}}$, E edges $e_1, e_2, ..., e_{\mathsf{E}}$, F faces $f_1, f_2, ..., f_{\mathsf{F}}$ and P elements $P_1, \ldots, P_{\mathsf{P}}$.

We can naturally define four types of unknowns attached to the partition $\mathcal{T}_h$:

• node unknowns whose values are attached to vertices and are to be interpreted as the *value of a scalar function* at each node;

• edge unknowns whose values are attached to edges and are to be interpreted as the *circulation of a vector field* on the edge;

• face unknowns whose values are attached to faces and are to be interpreted as the *flux of a vector field* across the face;

• element unknowns whose values are attached to element and are to be interpreted as the *integral of a scalar function* over the element.

We denote the corresponding space of all node unknowns by $\mathcal{N}$, that of all edge unknowns by $\mathcal{E}$, that of all face unknowns by $\mathcal{F}$, and that of all element unknowns by $\mathcal{P}$.

Signs of elements in these spaces will depend on the orientation of edges and faces. We consider then the orientation fixed once and for all.

In the Mimetic Finite Differences (MFD) framework these spaces are used as discretization spaces for the problems mentioned above. $\mathcal{N}$ is the natural discretization space for the scalar potential p in (0.1), i.e., for $0-$forms; $\mathcal{E}$ is the natural discretization space for $1-$forms, i.e. $\mathbf{u}$ and $\mathbf{H}$ in (0.3)-(0.4); $\mathcal{F}$ can be interpreted as discrete $2-$forms and as discretiztion of $\mathbf{D}$ or $\mathbf{B}$ in (0.2) and (0.4). Finally, the right candidate to discretize ρ, and $3-$forms in general, is indeed $\mathcal{P}$.

For algebraic topology, $\mathcal{N}$, $\mathcal{E}$, $\mathcal{F}$ and $\mathcal{P}$ are co-chain spaces and form a complex, a co-chain complex, together with the co-boundary operator. We defer the reader to [3] for an application of these concepts to the formalization of MFD.

The co-boundary operator is a collection of operators linking our spaces one upon the other. When co-chains are interpreted as discrete differential forms, then co-boundary operator is seen as discretization of standard differential operator d, that is, in our simplified setting, as $\mathbf{grad}$, $\mathbf{curl}$, div depending on the space on which it acts. Here we adopt a self evident notation (as it is standard in MFD):

• The $\mathcal{GRAD}$ operator, from $\mathcal{N}$ to $\mathcal{E}$, defined as follows: for each edge e with vertices (V_1, V_2) and oriented from V_1 to V_2

$$\Big(\mathcal{GRAD}\, u\Big)\Big|_{e} = u|_{V_2} - u|_{V_1}. \tag{0.5}$$

• The $\mathcal{CURL}$ operator, from $\mathcal{E}$ to $\mathcal{F}$, defined as follows: for each element $\varphi \in \mathcal{E}$ and for each face f we denote by $e_1, e_2, ..., e_{\mathsf{E}_f}$ the edges sharing the face f and we suppose they are endowed with the orientation induced by the orientation of f. We consider the corresponding values $\varphi_1, \varphi_2, ..., \varphi_{\mathsf{E}_f}$ of φ with the sign corresponding to the orientation just chosen. Then $\mathcal{CURL}\,\varphi$ *on the face* f *is defined as*

$$\Big(\mathcal{CURL}\,\varphi\Big)\Big|_{f} = \sum_{i=1}^{\mathsf{E}_f} \varphi_i. \tag{0.6}$$

• The $\mathcal{DIV}$ operator, from $\mathcal{F}$ to $\mathcal{P}$, defined as follows: let $f_1, ..., f_{\mathsf{F}_P}$ be all the faces of an element P, and for each $\sigma \in \mathcal{F}$ let $\sigma_1, ..., \sigma_{\mathsf{F}_P}$ be its values on each face assumed to be oriented outward with respect to P. Then $\mathcal{DIV}\,\sigma$ *is defined as*

$$\mathcal{DIV}\,\sigma = \sum_{k=1}^{\mathsf{F}_P} \sigma_k. \tag{0.7}$$

It is interesting to note that, taking in the spaces $\mathcal{N}$, $\mathcal{E}$, $\mathcal{F}$, $\mathcal{P}$ the obvious canonical basis (after choosing an orientation of the edges, faces and elements in an arbitrary way, but once and for all), then the matrices associated with the operators $\mathcal{GRAD}$, $\mathcal{CURL}$, and $\mathcal{DIV}$ are the incidence matrices.

Scalar products

It is rather obvious to see that each of the spaces $\mathcal{N}$, $\mathcal{E}$, $\mathcal{F}$ and $\mathcal{P}$ can be considered as a *linear vector space over* $\mathbb{R}$, introducing in an obvious way the sum of two elements of the same space or the multiplication by a real number. What we recalled above can be found in a number of papers dealing with theoretical approximations of differential forms: it is elegant, it is simple.

However, if one wants to use co-chains as discrete differential forms in order to approximate boundary value problems for partial differential equations, then, apparently, little can be done unless we introduce suitable *scalar products*. In particular, scalar products are an implicit discretization of the discretize Hodge-* operators that, in turn, are substantial in describing the properties of the material we are dealing with (even when the problem is set in the vacuum).

If we want to obtain robust and reliable numerical methods, we need to define scalar products able to mimic the L^2-inner product, possibly weighted with material parameters. "To mimic" means here that the scalar product needs to have some exactness property which garantees "the bit of" consistency which is needed to get convergence.

As it is natural, scalar products are constructed element by element, and the global L^2-like inner product is then obtained by summing over the elements.

Here we provide scalar products following a general strategy based on *reconstruction operators*. Let us see it, as an example, on the case of the space $\mathcal{N}|_P$, i.e., the node unknowns attached to nodes $V \subset \partial P$, $P \in \mathcal{T}_h$. To every $u \in \mathcal{N}|_P$ we associate a (smooth enough) function $R_{\mathcal{N}}(u)$ such that $R_{\mathcal{N}}(u)|_V = u|_V$ for all vertex V, and define the scalar product element by element as:

$$[u,\, v]_{\mathcal{N},P} := \int_P R_{\mathcal{N}}\, u\, R_{\mathcal{N}}\, v \,\mathrm{d}P \tag{0.8}$$

This can be rather easily done in a tetrahedron, giving raise to the usual Lagrangian finite elements. If P is a tetrahedron the same idea applies to $\mathcal{E}$, $\mathcal{F}$ producing *edge* and *face* elements. It is clear, however, that this procedure applied on a general polyhedron can rely only upon suitable submeshing as proposed in [6].

A different approach was used however in other cases: a pioneering paper is [2], and recently the approach has

been formalized in [5] for $\mathcal{F}$ type spaces. The idea is to use minimal consistency and prove that: *any scalar product would do the work*, provided it has the right scaling and is "exact on constants". The meaning of being "exact on constants" is the following, e.g., on $\mathcal{N}|_P$: the result of the integral

$$\int_P (R_{\mathcal{N}} u) c \, \mathrm{d}P \tag{0.9}$$

for a constant c, can be expressed in terms of c and u is a closed form for any "good" reconstruction operator[1]. We can then set for $c \in \mathbb{R}$:

$$[u, \Pi_{\mathcal{N}} c]_{\mathcal{N},P} := \int_P (R_{\mathcal{N}} u) c \, \mathrm{d}P, \tag{0.10}$$

where $\Pi_{\mathcal{N}} c$ is just the evaluation of the constant on each vertex in ∂P. As a consequence, we known how to compute the scalar product of a constant field against any $u \in \mathcal{N}|_P$ and we say it is "exact" on constants. Formula (0.10) defines "a part of" the scalar product, and the rest can be chosen arbitrarily just preserving the right scaling.

In the paper [4], we construct scalar products on $\mathcal{N}$, $\mathcal{E}$, $\mathcal{F}$ and $\mathcal{P}$ having this property which is also proved to be sufficient to obtain robust numerical methods. They are all defined as sum of contributions local to the single element. We denote these scalar products as $[\cdot,\cdot]_{\mathcal{N}}$, $[\cdot,\cdot]_{\mathcal{E}}$, $[\cdot,\cdot]_{\mathcal{F}}$ and $[\cdot,\cdot]_{\mathcal{P}}$ and we present their use in the definition of new numerical schemes.

Cochains discretizations

We propose here to use cochains as a discretization strategy for the differential problems mentioned in the Introduction. We denote by $\mathcal{N}_0$, $\mathcal{E}_0$, $\mathcal{F}_0$ the spaces where the natural boundary conditions are imposed; e.g., $\mathcal{N}_0$ will be the space of nodes unknowns which are zero on each node on the boundary of the computational domain Ω. For simplicity, we suppose all material tensors to be reduced to constants. During the talk, we will treat the general case.

The discretization of (0.1) will then be: Find $p_h \in \mathcal{N}_0$ such that for all $q_h \in \mathcal{N}_0$

$$\varepsilon [\mathcal{GRAD}\, p_h, \mathcal{GRAD}\, q_h]_{\mathcal{E}} = [\Pi_{\mathcal{N}} \rho, q_h]_{\mathcal{N}}. \tag{0.11}$$

where $\Pi_{\mathcal{N}}$ denotes the evaluation of ρ on nodes. The one of (0.2) will in turn be: Find $\mathbf{D}_h \in \mathcal{F}$, $p_h \in \mathcal{P}$ such that for all $\mathbf{F}_h \in \mathcal{F}$, $q_h \in \mathcal{P}$

$$\begin{aligned} \varepsilon^{-1} [\mathbf{D}_h, \mathbf{F}_h]_{\mathcal{F}} - [p_h, \mathcal{DIV}\, \mathbf{F}_h]_{\mathcal{P}} &= 0 \\ [\mathcal{DIV}\, \mathbf{D}_h, q_h]_{\mathcal{P}} &= [\Pi_{\mathcal{P}} \rho, q_h]_{\mathcal{P}} \end{aligned} \tag{0.12}$$

[1] Among others, reconstruction operators must preserve constants: if v are the nodal values of a constant c, then $R_{\mathcal{N}}(v) = c$. The same rationale is applied to the other spaces.

where $\Pi_{\mathcal{P}}$ denotes the integral of ρ on each element $P \in \mathcal{T}_h$. This problem has been studied in [5]. We turn now to magnetostatics. The discretization of (0.3) together with the gauge $\operatorname{div} \mathbf{u} = 0$, is: Find $\mathbf{u}_h \in \mathcal{E}_0$ and $p_h \in \mathcal{N}_0$ such that for all $\mathbf{E}_h \in \mathcal{E}_0$, $q_h \in \mathcal{N}_0$

$$\begin{aligned} \mu^{-1} [\mathcal{CURL}\, \mathbf{u}_h, \mathcal{CURL}\, \mathbf{E}_h]_{\mathcal{F}} - [\mathcal{GRAD}\, p_h, \mathbf{E}_h]_{\mathcal{E}} &= \\ = [\Pi_{\mathcal{E}} \mathbf{J}, \mathbf{E}_h]_{\mathcal{E}} & \\ [\mathbf{u}_h, \mathcal{GRAD}\, q_h]_{\mathcal{E}} &= 0 \end{aligned} \tag{0.13}$$

where $\Pi_{\mathcal{E}}$ does the following: for each edge of the mesh, it computes the circulation of $\mathbf{J}$ on the edge. Thus, $\Pi_{\mathcal{E}} \mathbf{J}$ is an element of $\mathcal{E}$. We do not propose here a discretization of (0.4), since it is either equivalent to (0.12) or to (0.13). A discretization which computes both a magnetic field in $\mathcal{E}$ and a magnetic induction in $\mathcal{F}$ is not available.

Now, the open questions are the following:
(i) Are these discrete problems wellposed ?
(ii) Do they verify error estimates ?
(iii) What can we say on the spectral properties ?

All these questions will be addressed during the talk and are the object of the paper [4].

References

[1] D. N. Arnold, R. S. Falk, and R. Winther. Finite element exterior calculus, homological techniques, and applications. *Acta Numer.*, 15:1–155, 2006.

[2] J. Baranger, J.-F. Maitre, and F. Oudin. Connection between finite volume and mixed finite element methods. *RAIRO Modél. Math. Anal. Numér.*, 30(4):445–465, 1996.

[3] P. B. Bochev and J. M. Hyman. Principles of mimetic discretizations of differential operators. In *Compatible spatial discretizations*, volume 142 of *IMA Vol. Math. Appl.*, pages 89–119. Springer, New York, 2006.

[4] F. Brezzi and A. Buffa. Scalar products of discrete differential forms. Technical report, IMATI-CNR, 2007. in preparation.

[5] F. Brezzi, K. Lipnikov, and M. Shashkov. Convergence of the mimetic finite difference method for diffusion problems on polyhedral meshes. *SIAM J. Numer. Anal.*, 43(5):1872–1896 (electronic), 2005.

[6] Yu. Kuznetsov and S. Repin. New mixed finite element method on polygonal and polyhedral meshes. *Russian J. Numer. Anal. Math. Modeling*, 18(3):261–278, 2003.

Computational Electromagnetics: The Quest for Faster Algorithms

W. C. Chew[1], **M. K. Li, A. J. Hesford, and C. P. Davis**
U. Illinois, Urbana, IL 61801-2991, USA
Email: w-chew@uiuc.edu
[1] On LOA to be with The U. of Hong Kong

Abstract

In this talk, the recent development of fast algorithms will be discussed for simulating complex structures where the objects can be a tiny fraction of the wavelength, and yet wave physics is important. The equivalence principle algorithm will be presented to separate circuit physics from wave physics, so that complex problems can be solved. Then the solution of complex radiation problem using parallel computers and special preconditioning techniques will be discussed. Furthermore, the diagonalization of the vector addition theorem will be presented. We will discuss on how to solve the high frequency problem in a frequency independent manner. The talk will end by presenting some future challenge problems.

Introduction

Integral equation solvers (IESs) are, in general, more complex to implement compared to differential equation solvers (DESs). This is due to the need for the Green's function method, which generally involves the evaluation of singular integrals. Moreover, due to the dense matrix system, acceleration solution methods have to be invoked before IESs are competitive with differential equation solvers [1]. Also, linearity of the media has to be assumed before frequency-domain and Green's-function techniques can be used. In contrast to DESs, the advantage of IESs, lies in the smaller number of unknowns and favorable scaling properties for memory and CPU requirements. DESs are simple to implement, but usually exhibit worse scaling properties when applied to surface scattering problems. The presence of grid-dispersion error worsens their scaling properties for large scale computing. On the other hand, DESs in the time domain can easily account for nonlinear phenomena. Hence, for an area replete with nonlinear physics, such as computational mechanics or computational fluid dynamics, DESs outrank integral equation solvers in popularity [2]. IESs also have the advantage of satisfying the radiation condition automatically, whereas in DESs, absorbing boundary conditions have to be used, or the mesh has to be truncated with a boundary integral equation.

Many electrical engineering and electromagnetics phenomena can be modelled with linear equations. Hence, Green's function and IESs are rather popular in this arena. The advantages of IESs in electromagnetics make them popular for solving a number of scattering problems. This is especially so when they have been accelerated with fast algorithms [3].

However, when IESs are modelled with complex structures, convergence issue is a main concern. Still the scaling of computational load with problem is another concern.

Integral Equation Solvers for Complex Structures

In the following, several advances in integral equation solvers made recently are discussed. First, techniques on how to improve convergence when highly complex structures are encountered are presented. Then, we follow that with a presentation on a way to diagonalize the vector addition theorem, which is very important for the design of fast algorithms for electromagnetics and elastic wave problems. Then the issue of arriving at frequency independent solution for some scattering problem is addressed.

Equivalence Principle Aglorithm

The equivalence principle algorithm (EPA) is a good way to domain decompose a larger problem into smaller problems. It also allows regions of low frequency physics (circuit physics) to be separated from the regions of mid frequency physics (wave physics). The use of EPA allows a larger problem to be broken down into a sum of smaller problems, so that only smaller problems need to be solved at one time. Then the solution to the larger problem is accomplished by rigorously concatenating the smaller problems together.

Recently, we have developed an equivalence principle algorithm that allows the equivalence surface to cut through metal, and break an object involving metal into smaller objects [4], [5].

EPA also allows one to use one technique to solve the smaller problems, while a different technique is used to solve the larger problem. This is important since the physics at the micro-scale is quite different from the physics at the macro-scale.

Parallelization for Radiation Problems

Scattering problems are generally more benign compared to the radiation problem. The reason being that in the scattering problem, the object is usually excited by a source placed far away. Hence, the current on the scatterer is usually quite smooth. However, for the radiation problem, the excitation source is usually placed right on the scatterer, and hence, the induced current on the scatterer is quite singular. In terms of eigenfunction expansions, the current covers a broader spectrum in the radiation problems compared to the scattering problem. Hence, the convergence rate in radiation problem is usually slower compared to that of the scattering problems, due to the larger range of eigenfunctions being excited.

Recently, we have successfully connected a code for antenna radiation, named FastAnt, with a parallel solver, ScaleME [6]. This is necessary due to the slower convergence rate of the radiation problem, as well as the additional cost of designing preconditioners for the radiation problem. To ameliorate the convergence issue, we have designed the self-box inclusion (SBI) preconditioner [7] to help reduce the number of iterations needed in solving the problem.

Recently, in combining FastAnt with ScaleME, we have reworked the preconditioning strategy so that reasonably large radiation problems can be solved. We will demonstrate the solution of radiation due to a complex antenna on top of an automobile.

Diagonalization of Vector Addition Theorem

Electromagnetic and elastic wave problems are inherently vector in nature. Electromagnetic and elastic wave fields can be expressed in terms of vector wave functions, and the vector addition theorem can be used to change the coordinates of the vector wave functions. Recently, we have successfully derived some important mathematical identities [8]. They are useful to diagonalize the vector addition theorem. The use of such vector addition theorem will save memory, as well as making the solving of electromagnetic problems more natural using fast algorithms.

Furthermore, the successful diagonalization of the vector addition theorem for translation means that a mixed-form fast multipole algorithm (MF-FMA) can be easily designed. Such MF-FMA is important in modeling multiscale structures that may be encountered in circuits and antenna structures.

High-Frequency Method

There is a need to arrive at frequency independent method for high frequency scattering. A naive computational electromagnetics method will have resource increase as the frequency increases. However, as the frequency becomes very high, the wave physics becomes ray-like or particle-like. The phase variation can be separated from the envelope variation. At even higher frequencies, the phase becomes random, making a ray behave like a particle. There is a need to develop numerical methods that can gradually transition from the wave-like nature to particle-like nature of waves [9], [11], [10]. We will show our recent advances made in this arena regarding the scattering solution by a strip which is frequency independent [12].

Some Examples

Shown in this section are some examples of numerical simulation results. More will be discussed at the conference.

References

[1] W. C. Chew, J. M. Jin, E. Michielssen, and J. M. Song, (editors), *Fast and Efficient Algorithms in Computational Electromagnetics*, Artech House, Boston, MA, 2001.

[2] W. C. Chew, "What a CFD person should know about CEM and vice versa?" *CCEM Research Report*, 2004.

[3] W. C. Chew, "Computational Electromagnetics—the Physics of Smooth versus Oscillatory Fields," *Philo. Trans. Royal Soc. London Series A, Math., Phys. Eng. Sci.* vol. 362, no. 1816, pp. 579-602, March 15, 2004.

[4] M. K. Li and W. C. Chew, "A Domain Decomposition Scheme Based on Equivalence Theorem," *Micro. Opt. Tech. Lett.*, v. 48, no. 9, pp. 1853-1857, Sept. 2006.

[5] M. K. Li and W. C. Chew, *IEEE Trans. Antenn. Propag.*, vol. 55, no. 1, pp. 130-138, 2007.

[6] A. J. Hesford and W. C. Chew, "A Distributed-Memory, Parallel MLFMA for the Solution of Radiation and Scattering Problems in Complex Environments," *Antennas Progation Symposium,* Honolulu, June 2007.

[7] H. Y Chao, *Ph.D. Thesis*, Dept. ECE, U. Illinois, Urbana-Champaign, January 2003.

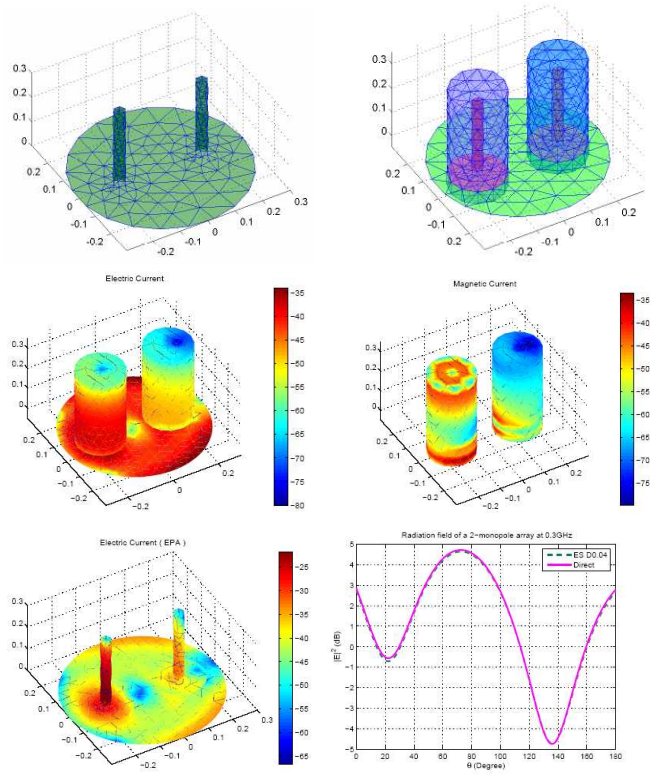

Figure 1: Demonstration of the equivalence principle algorithm where two monopoles on a ground plane (top left) is broken into subproblems using equivalence surfaces (top right). The interaction are via electric (middle left) and magnetic (middle right) equivalence currents on equivalence surfaces. The bottom figures show the resultant calculated electric current on the antennas and the radiation pattern compared to the direct approach.

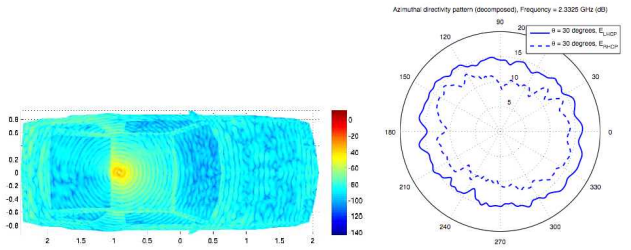

Figure 2: Radiation of an antenna on a car. Simulation parameters: 1,101,219 total unknown current elements 7-level MLFMA SBI preconditioner used in the vicinity of the antenna Excitation frequency: 2.3325 GHz (bottom of XM band) Total runtime (12 processors): 48 minutes, 150 iterations.

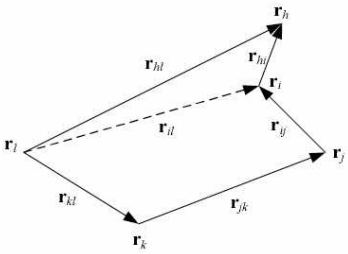

Figure 3: The vector addition theorem can be used to factorize the dyadic Green's function.

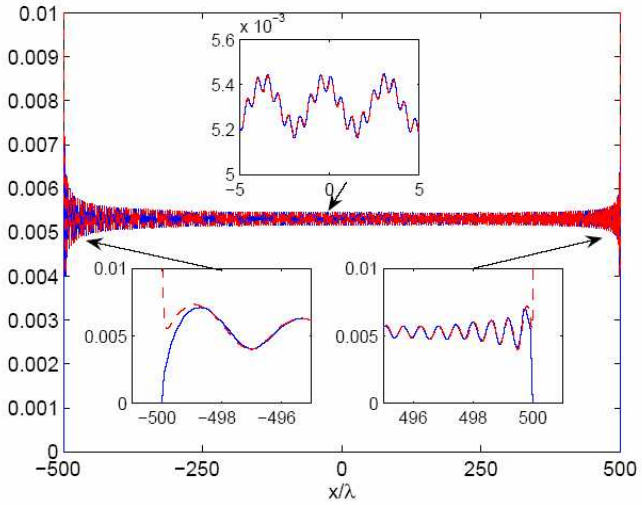

Figure 4: Total current for a 1000λ strip using $N = 30$ nodes and either the MoM or the minimally-varying MoM, which cannot be distinguished at this resolution. The numerical solutions agree with the GTD away from the strip edges, where the GTD breaks down.

[8] W. C. Chew, "Diagonalization of the vector addition theorem," *Communications in Computational Physics,* accepted for poublication.

[9] D.-H. Kwon, R. Burkholder, and P. Pathak, *IEEE Trans. Ant. Prop.*, vol. 49, pp. 583 591, April 2001.

[10] S. Langdon and S. Chandler-Wilde, *SIAM J. Numerical Analysis*, vol. 43, no. 6, pp. 24502477, 2006.

[11] O. Bruno, C. Geuzaine, J. Monro, and F. Reitich, *Phil. Trans. R. Soc. of London Series A*, vol. 362, pp. 629645, March 2004.

[12] C. P. Davis and W. C. Chew, "Order-1 Quadrature Rules for Flat Facets," *Antennas Progation Symposium,* Honolulu, June 2007.

ON COMPLETE RADIATION BOUNDARY CONDITIONS AND OPTIMAL ABSORBING LAYERS

T. Hagstrom[†,*], **T. Warburton**[‡]

[†]Department of Mathematics and Statistics, The University of New Mexico, Albuquerque, NM 87131 USA.
[‡]Computational and Applied Mathematics, Rice University, Houston, TX 77005 USA.
[*]Email: hagstrom@math.unm.edu

Abstract

We introduce an exact representation of waves propagating in a half space, which we call the complete plane wave representation. It expresses the time-domain wave field as a superposition of outgoing propagating modes and decaying evanescent modes. A finite approximation to this representation is derived via appropriate quadrature rules. Local radiation boundary condition sequences are then constructed which are exact when applied to the finite representation, and the conditions are extended to polygonal domains by identifying them with a non-standard PML admitting a closure akin to the PML corner layers. Numerical experiments suggest that the new conditions lead to dramatic improvements in the long time accuracy of simulations with a complexity estimate comparable to optimal nonlocal approximations. The new complete radiation boundary conditions thus combine easy implementation, geometric flexibility, and spectral convergence with essentially uniform long time accuracy.

Introduction

As radiation to the far field is a typical feature of wave propagation problems, the efficient and accurate simulation of waves requires methods to accurately impose such conditions at artificial boundaries located as closely as possible to scatterers and other inhomogeneities. In recent years, a number of new methods have been introduced which are capable of delivering arbitrary accuracy for models which are isotropic and homogeneous in the far field. These include:

i. Fast, low-memory approximations to exact, nonlocal formulations [1], [2], [3], [4];

ii. Local boundary condition sequences [5], [6], [7], [8];

iii. Reflectionless absorbing layers (PML) [9], [10], [11];

iv. Fast evaluations of the retarded potential [12];

v. Construction and fast evaluation of equivalent sources [13], [14].

(See the recent review articles [15], [16] for more details and a more extensive reference list.)

Although all the algorithms mentioned above can be efficient in some settings, at least those with which the authors are most familiar, (i-iii), are all suboptimal in others. (The algorithm in [12] does satisfy what we would define as an optimal complexity estimate, though we have no experience with its practical performance, while a complete analysis of the algorithms in [13], [14] is unknown to us.)

The algorithms in class (i.) are based on a factorization of the nonlocal operators into spatial and temporal pieces. The spatial part is handled by a fast transform algorithm and the temporal part is compressed either by global exponential approximations [1], [2] or piecewise exponential approximations [3], [4]. To guarantee an accuracy, ϵ, up to a time, T, for a wavelength, λ, the algorithm of [1], [2] requires a boundary operator described by:

$$P_{\text{nonlocal}} \leq C \ln \frac{1}{\epsilon} \cdot \ln \frac{cT}{\lambda} \tag{1}$$

functions per harmonic where C will denote some constant. We believe this estimate is optimal. However, although the associated computational cost is small compared with the cost of the interior solve, the factorization only exists for special boundaries: spheres, cylinders and planes. Thus, for example, if one wishes to solve the scattering problem for a high aspect ratio object, the need to solve in a spherical domain leads to significant additional costs. In addition, although fast spherical harmonic transforms exist [17], [18], they are expensive.

Algorithms in class (ii.), though conceptually quite simple, were generally only used at lowest order, and thus provided only limited accuracy with no real possibility of effecting convergence. To enable their use at arbitrary order in polygonal domains, a special auxiliary variable reformulation was introduced in [19], [20]. However, although the methods were found to be spectrally convergent at fixed times, their accuracy rapidly degraded at large times. (See, e.g., the analyses in [21], [22].) The resulting estimate of the number of auxiliary functions needed is:

$$P_{\text{local}} =\leq C \ln \frac{1}{\epsilon} \cdot \frac{cT}{\lambda}, \tag{2}$$

which is obviously quite bad for $\frac{cT}{\lambda} \gg 1$.

Algorithms in class (iii.), the perfectly matched layers, have been the most successful of all those mentioned. From the start, they combined the features of easy implementation, error control, and geometric flexibility. In particular, they can be implemented by simply solving an augmented system of equations in the layer region (including corner layers), and convergence can be achieved simply by thickening the layer. However, PMLs, too, suffer from long time nonuniformities [22], [23]. It is less straightforward to write down complexity estimates for PML as they depend on the discretization of the layer. In particular, one can certainly use a somewhat coarser mesh towards the end. However, under the assumption of a uniform resolution one finds that the number of points across the layer should satisfy:

$$P_{\text{PML}} =\leq C \ln \frac{1}{\epsilon} \cdot \sqrt{\frac{cT}{\lambda}}, \tag{3}$$

confirming their superiority to the standard local conditions.

In this work we examine the root cause of the long-time nonuniformities for the two local methods, and develop methods to dramatically improve their accuracy. In particular we will write down a complete plane wave representation of the wave field which includes both propagating and evanescent modes. It will be seen that with an explicit treatment of modes of both types optimal complexity estimates can evidently be achieved for local boundary condition sequences. We also note that our auxiliary variable formulation can be interpreted as a non-standard PML, thus showing that PMLs with optimal complexity estimates exist. We will consider the construction of optimal standard PMLs in the future.

Complete Plane Wave Expansions

Consider a planar artificial boundary, $x = 0$, and a field or field component u which satisfies the scalar wave equation. Using a Fourier-Laplace transformation with Dirichlet data given on the plane $x = -\delta$ we derive for $x > -\delta$:

$$\hat{u}(x, k_y, k_z, s) = e^{-(s^2+c^2k_x^2+c^2k_y^2)^{1/2}\frac{x+\delta}{c}}\hat{u}_0, \tag{4}$$

Computing the inverse transforms to form u and in particular choosing $\Re(s) = 0$ as an inversion contour we can break the integrals into two pieces according to the exponent, $-\gamma x/c$. We express imaginary exponents as:

$$-\cos\theta\frac{sx}{c}, \;\; \theta \in [0, \frac{\pi}{2}], \tag{5}$$

and real exponents as:

$$-\sigma x, \;\; \sigma \geq 0. \tag{6}$$

We obtain (see [25] for more details and [24] for an alternative derivation):

$$\begin{aligned} u(x, y, z, t) &= \int_0^{\frac{\pi}{2}} \Phi\left(ct - x\cos\phi, y, z, \phi\right) d\phi \\ &\quad + \int_0^{\infty} e^{-\sigma(x+\delta)} \Upsilon(y, z, t, \sigma) d\sigma, \end{aligned} \tag{7}$$

The standard radiation boundary condition sequences only explicitly treat the propagating modes, that is the first integral in (7). Their accuracy can be estimated via their complex reflection coefficients. Assuming a boundary located at $x = 0$ and the Padé approximants of order p [6] this coefficient takes the form:

$$\hat{R}_{\text{local}} \propto \left(\frac{s-\gamma}{s+\gamma}\right)^{2p} e^{-\gamma\delta/c}. \tag{8}$$

If we consider s imaginary and γ real corresponding to the evanescent modes we see that the reflection coefficient is independent of p. To prove convergence at all we must consider $\Re(s) = O(T^{-1}) > 0$ in which case the factor is bounded by $1 - O(T^{-1})$. Applying Parseval's relation the estimate (2) follows.

Similarly one can derive a reflection coefficient for standard PML. The details depend on the termination condition at the edge of the layer, but the essential factor is:

$$\hat{R}_{\text{PML}} \propto e^{-2L\gamma\left(\frac{s+\alpha+\bar{\sigma}}{c(s+\alpha)}\right)}. \tag{9}$$

Here L is the layer width, $\bar{\sigma}$ is the average absorption, and α is the complex frequency shift parameter. Note that if s is imaginary and γ is real the real part of the exponent is:

$$-2L\gamma\frac{|s|^2 + \alpha^2 + \alpha\bar{\sigma}}{c(|s|^2 + \alpha^2)} \tag{10}$$

which is again much better than the expression for the boundary conditions but which still vanishes when $\gamma = 0$. Taking $\Re(s) = O(T^{-1})$ and $\alpha = 0$ (which is not optimal) estimate (3) follows.

Boundary condition formulation

Following the treatment of analogous expressions in deriving the translation formulas for the fast multipole method, approximate (7) by some quadrature rule:

$$\begin{aligned} u(x, y, z, t) &\approx \sum_{j=0}^{n_p-1} w_j \Phi_j(ct - x\cos\theta_j, y, z) \\ &\quad + \sum_{j=1}^{n_e} d_j e^{-\sigma_j x} \Upsilon_j(t, y, z). \end{aligned} \tag{11}$$

Local boundary conditions with $n_p + n_e$ auxiliary functions can now be constructed which are exact on this approximate representation independent of the unknown functions Φ_j and Υ_j. Following [19], [20] we recursively define for $j = 0, \ldots, n_p - 1$:

$$\left(\cos\theta_j \frac{\partial}{\partial t} + c\frac{\partial}{\partial x}\right)\psi_j = \left(\cos\theta_j \frac{\partial}{\partial t} - c\frac{\partial}{\partial x}\right)\psi_{j+1} \tag{12}$$

with $\psi_0 = u$ and for $j = 1, \ldots, n_e$:

$$\left(\sigma_j + \frac{\partial}{\partial x}\right)\psi_{n_p+j-1} = \left(\sigma_j - \frac{\partial}{\partial x}\right)\psi_{n_p+j} \tag{13}$$

Assuming (11) is exact we note that each subsequent term in the recursion involves one fewer term in the sum. That is, the operators on the left-hand sides of (12) and (13) are chosen to annihilate terms in the approximate representation. We may then conclude:

$$\psi_{n_p+n_e} = 0. \tag{14}$$

We now impose (12)-(14). Upon proving by induction that each of these auxiliary fields satisfies the governing equations, one derives evolution equations along the boundary $x = 0$ by eliminating the normal derivatives. This leads to the local boundary condition sequences. Alternatively, one can interpret the recursions as a finite volume discretization of a PML (with nonstandard parameters). (See [26], [27] for related ideas). In particular, if we perform a Laplace transform in time the equations formally resemble a discrete PML with frequency-dependent grid spacings:

$$\frac{\hat{\psi}_{j+1} - \hat{\psi}_j}{\left(\frac{2c}{s\cos\theta_j}\right)} = \frac{1}{2}\left(\frac{\partial\hat{\psi}_{j+1}}{\partial x} + \frac{\partial\hat{\psi}_j}{\partial x}\right), \tag{15}$$

$$\frac{\hat{\psi}_{j+1} - \hat{\psi}_j}{\left(\frac{2}{\sigma_j}\right)} = \frac{1}{2}\left(\frac{\partial\hat{\psi}_{j+1}}{\partial x} + \frac{\partial\hat{\psi}_j}{\partial x}\right). \tag{16}$$

For first order systems

$$u_t + Au_x + Bu_y + Cu_z = 0, \tag{17}$$

the approximate boundary conditions now take the following form. For $0 \le j \le n_p$:

$$\begin{aligned}(\cos\theta_j A - I)\frac{\partial\psi_j}{\partial t} - B\frac{\partial\psi_j}{\partial y} - C\frac{\partial\psi_j}{\partial z} \quad &= \\ (\cos\theta_j A + I)\frac{\partial\psi_{j+1}}{\partial t} + B\frac{\partial\psi_{j+1}}{\partial y} + C\frac{\partial\psi_{j+1}}{\partial z}, &\end{aligned} \tag{18}$$

and for $1 \le j \le n_e$:

$$\begin{aligned}-\frac{\partial\psi_{n_p+j}}{\partial t} - B\frac{\partial\psi_{n_p+j}}{\partial y} - C\frac{\partial\psi_{n_p+j}}{\partial z} + \sigma_j A\psi_{n_p+j} \quad &= \\ \frac{\partial\psi_{n_p+j+1}}{\partial t} + B\frac{\partial\psi_{j+1}}{\partial y} + C\frac{\partial\psi_{n_p+j+1}}{\partial z} + \sigma_j A\psi_{n_p+j+1}, &\end{aligned} \tag{19}$$

truncated by:

$$\psi^{\text{in}}_{n_p+n_e+1} = 0, \tag{20}$$

with $\frac{\partial\psi^{\text{out}}_0}{\partial t}$ computed from the interior. (Here "in" and "out" refer to normal characteristic variables.) Note that the discretization of these conditions is straightforward as they are of the same type as the interior equations.

To use these conditions on polygonal domains, corner and edge compatibility conditions must be derived to provide boundary conditions for the auxiliary hyperbolic systems. Here, as first noted by Guddati and Lim [27], the PML interpretation is useful, allowing the construction of corner compatibility conditions in analogy with standard corner layers. Precisely,

$$\begin{aligned}&\frac{\partial\psi_{k+1,j+1}}{\partial t} + \frac{\partial\psi_{k,j}}{\partial t} + \frac{\partial\psi_{k+1,j}}{\partial t} + \frac{\partial\psi_{k,j+1}}{\partial t} \\ &+S_j A\left(\psi_{k+1,j+1} - \psi_{k+1,j} + \psi_{k,j+1} - \psi_{k,j}\right) \\ &+S_k B\left(\psi_{k+1,j+1} - \psi_{k,j+1} + \psi_{k+1,j} - \psi_{k,j}\right) \quad = 0,\end{aligned} \tag{21}$$

where

$$S_j w \equiv \begin{cases} \cos\theta_j \frac{\partial w}{\partial t}, & j \le n_p, \\ \sigma_{j-n_p} w, & j > n_p. \end{cases} \tag{22}$$

Truncate by:

$$\psi^{\text{in}}_{k,n_p+n_e+1} = \psi^{\text{in}}_{n_p+n_e+1,j} = 0, \tag{23}$$

with $\frac{\partial\psi^{\text{out}}_{k,0}}{\partial t}$, $\frac{\partial\psi^{\text{out}}_{0,j}}{\partial t}$ computed from the edges. (Here the meanings of in and out are based on the local characteristics in the normal directions. The truncations are combined for $k = j = n_p + n_e + 1$.) We refer to [28] for more details and to [29] for implementations for second order equations.

We have not yet proven error estimates for the new conditions. However, we have obtained excellent results in our numerical experiments so far and we have also carried out numerical evaluations of the complex reflection coefficients. In our experiments we have used a combination of Gauss-Radau and Yarvin-Rokhlin nodes to define the boundary condition parameters:

$$\theta_j = \frac{\pi(c_j + 1)}{4}, \quad j = 0, \ldots, n_p - 1, \tag{24}$$

where c_j are the left endpoint Gauss-Radau nodes on $[-1, 1]$ and

$$\sigma_j = \delta d_j, \;\; j = 0, \ldots, n_e, \tag{25}$$

where d_j are the Yarvin-Rokhlin nodes [30] and δ is a length scale parameter. In practice we choose this to be the minimum separation between inhomogeneities and the artificial boundary. For our error estimates we have made the slightly unrealistic choice of $\delta = 5\lambda$ and set $n_p = n_e$. Numerical evaluation of the reflection coefficient then yields the optimal estimate:

$$n_p + n_e \leq C \ln \frac{1}{\epsilon} \cdot \ln \frac{cT}{\lambda}. \tag{26}$$

As a simple numerical experiment we have compared all three local methods for Maxwell's equations with $c = 1$ and a field produced by transversely 1-periodic point sources located a distance 2 from the artificial boundary. These have Gaussian time signature which is effectively zero at the initial time. We resolve the fields very accurately using 8th order spatial differencing combined with the standard 4th order Runge-Kutta method in time. (The 8th order one-sided spatial differences are stabilized by adding one subcell grid point as discussed in [31].)

The results, displayed in Figure 1, confirm the theoretical predictions. The 30-term Padé conditions are accurate up to $t = 20$ but the error eventually grows to 3×10^{-2}. The 19-point PML, with parameters optimized to equidistribute the error in time, is significantly more accurate with errors oscillating near 10^{-4} with eventual growth to about 8×10^{-4}. However with 30 terms of the new conditions the maximum error remains below 7×10^{-7} and is probably dominated by the discretization error. Further experiments in [25], [28] confirm this excellent performance.

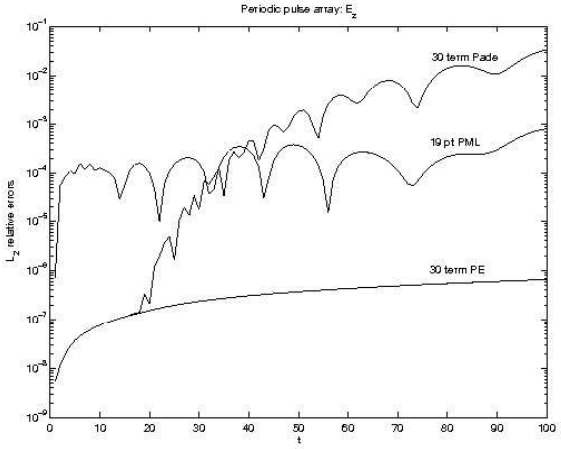

Figure 1: Errors for various 30-term approximate boundary conditions. Maxwell's equations with transversely periodic point sources.

Extensions and Conclusions

Given the positive results obtained so far, we are hopeful that the new local boundary condition sequences based on complete plane wave representations will provide a fully satisfactory solution to the radiation boundary condition problem for homogeneous, isotropic wave systems. In particular, they are easy to implement, geometrically flexible, and appear to be as accurate as the less flexible nonlocal approaximations derived in [1], [2].

We have so far only just started to consider extensions of the complete plane wave expansion to other problems. One case where we have had some preliminary success is that of lattice waves. Here we approximate the boundary conditions derived in [32] used for multiscale computations of crack problems at low temperature. It is still unclear if methods such as these can be constructed for general anisotropic systems. However, we do believe that the linearized Euler equations will admit an analagous representation, following the transformation used in [11] to derive a stable PML. Of course we would also like to apply the complete plane wave representation to optimize the parameters in a standard PML. A direct approach would be to tune the grid spacings and absorption profiles to minimize the errors for the functions in the approximate representation. We hope to carry out such a construction in the near future.

Acknowledgements

The first author was supported in part by ARO Grant DAAD19-03-1-0146 and NSF Grant DMS-0610067. Both authors were also supported in part by AFOSR contract FA9550-05-1-0473. Any conclusions or recommendations expressed in this paper are those of the authors and do not necessarily reflect the views of AFOSR, ARO, or NSF.

References

[1] B. Alpert, L. Greengard and T. Hagstrom, "Rapid evaluation of nonreflecting boundary kernels for

time-domain wave propagation", SIAM J. Numer. Anal., vol. 37, pp. 1138-1164, 2000.

[2] B. Alpert, L. Greengard and T. Hagstrom, "Nonreflecting boundary conditions for the time-dependent wave equation", J. Comput. Phys., vol. 180, pp. 270-296, 2002.

[3] C. Lubich and A. Schädle, "Fast convolution for non-reflecting boundary conditions", SIAM J. Sci. Comput., vol. 24, pp. 161-182, 2002.

[4] R. Hiptmair and A. Schädle, "Non-reflecting boundary conditions for Maxwell's equations", Computing, vol. 71, pp. 265-292, 2003.

[5] E. Lindman, "Free space boundary conditions for the time dependent wave equation", J. Comput. Phys., vol. 18, pp. 66-78, 1975.

[6] B. Engquist and A. Majda, "Absorbing boundary conditions for the numerical simulation of waves", Math. Comp., vol. 31, pp. 629-651, 1977.

[7] A. Bayliss and E. Turkel, "Radiation boundary conditions for wave-like equations", Comm. Pure and Appl. Math., vol. 33, pp. 707-725, 1980.

[8] R. Higdon, "Numerical absorbing boundary conditions for the wave equation", Math. Comp., vol. 49, pp. 65-90, 1987.

[9] J.-P. Bérenger, "A perfectly matched layer for the absorption of electromagnetic waves", J. Comput. Phys., vol. 114, pp. 185-200, 1994.

[10] P. Petropoulos, "Reflectionless sponge layers as absorbing boundary conditions for the numerical solution of Maxwell's equations in rectangular, cylindrical and spherical coordinates", SIAM J. Appl. Math., vol. 60, pp. 1037-1058, 2000.

[11] D. Appelö, T. Hagstrom and G. Kreiss, "Perfectly matched layers for hyperbolic systems: General formulation, well-posedness and stability", SIAM J. Appl. Math., vol. 67, pp. 1-23, 2006.

[12] A. Ergin, B. Shanker, and E. Michielssen, "Fast evaluation of three-dimensional transient wave fields using diagonal translation operators", J. Comput. Phys., vol. 146, pp. 157-180, 1998.

[13] V. Ryaben'kii, S. Tsynkov and V. Turchaninov, "Global discrete artificial boundary conditions for time-dependent wave propagation", J. Comput. Phys., vol. 174, pp. 712-758, 2001.

[14] O. Bruno and D. Hoch, "Exact nonreflecting boundary conditions based on equivalent sources for time dependent scattering problems", in preparation, 2007.

[15] T. Hagstrom, "New results on absorbing layers and radiation boundary conditions, appearing in Topics in Computational Wave Propagation, M. Ainsworth, P. Davies, D. Duncan, P. Martin and B. Rynne, eds., pp. 1-42, Springer-Verlag, 2003.

[16] T. Hagstrom and S. Lau, "Radiation boundary conditions for Maxwell's equations: A review of accurate time-domain formulations", J. Comput. Math., in press, 2007.

[17] M. Mohlenkamp, "A fast transform for spherical harmonics", J. of Fourier Anal. and Applic., vol. 5, pp. 159-184, 1999.

[18] D. Healy, D. Rockmore, P. Kostelec and S. Moore, "FFTs for the 2-sphere - Improvements and variations", J. Fourier Anal. Applic., vol. 9, pp. 341-385, 2003.

[19] T. Hagstrom and T. Warburton, "High-order local radiation boundary conditions: Corner compatibility conditions and extensions to first order systems", Wave Motion, vol. 39, pp. 327-338, 2004.

[20] D. Givoli, T. Hagstrom and I. Patlashenko, "Finite element formulation with high order absorbing boundary conditions for time-dependent waves, Comput. Meth. Appl. Mech., vol. 195, pp. 3666-3690, 2006.

[21] J. Diaz and P. Joly, "An analysis of higher-order boundary conditions for the wave equation", SIAM J. Appl. Math., vol. 65, pp. 1547-1575, 2005.

[22] A. de Hoop, P. van den Berg and R. Remis, "Absorbing boundary conditions and perfectly matched layers - an analytic time-domain performance analysis", IEEE Trans. on Magnetics, vol. 38, pp. 657-660, 2002.

[23] J. Diaz and P. Joly, "A time-domain analysis of PML models in acoustics", Computer Meth. Appl. Mech. Engrg., vol. 195, pp. 3820-3853, 2006.

[24] E. Heyman, "Time-dependent plane-wave spectrum representations for radiation from volume source distributions", J. Math. Phys., vol. 37, pp. 658-681, 1996.

[25] T. Hagstrom and T. Warburton, "Complete local radiation boundary conditions and optimal absorbing layers for isotropic waves", in preparation, 2007.

[26] S. Asvadurov, V. Druskin, M. Guddati and L. Knizherman, "On optimal finite difference approximation of PML", SIAM J. Numer. Anal., vol. 41, pp. 287-305, 2003.

[27] M. Guddati and K.-W. Lim, "Continued fraction absorbing boundary conditions for convex polygonal domains", Int. J. Num. Meth. Engng., vol. 66, pp. 949-977, 2006.

[28] T. Warburton and T. Hagstrom, "Complete local radiation boundary conditions for electromagnetic scattering", in preparation, 2007.

[29] A. Mar-Or, D. Givoli, and T. Hagstrom, "High-order local absorbing boundary conditions for the wave equation: Extensions and improvements", in preparation, 2007.

[30] N. Yarvin and V. Rokhlin, "Generalized Gaussian quadratures and singular value decompositions of integral operators, SIAM J. Sci. Comp., vol. 20, pp. 699-718, 1998.

[31] T. Hagstrom and G. Hagstrom, "Grid stabilization of high-order one-sided differencing I: First order hyperbolic systems", J. Comput. Phys., vol. 223, pp. 316-340, 2007.

[32] G. Wagner, E. Karpov, and W. Liu, "Molecular dynamics boundary conditions for regular crystal lattice", J. Comput. Phys., vol. 193, pp. 1579-1601, 2003.

INVERSE SCATTERING PROBLEMS FOR THE TIME-HARMONIC MAXWELL SYSTEM

Andreas Kirsch[†,*]
[†]University of Karlsruhe, 76128 Karlsruhe, Germany
[*]Email: kirsch@math.uni-karlsruhe.de

Abstract

In this talk we study the following electromagnetic scattering problem. Let $k = \omega\sqrt{\varepsilon_0\mu_0} > 0$ be the wave number with frequency ω, electric permittivity ε_0, and magnetic permeability μ_0 in vacuum. An incident plane electromagnetic field of the form

$$\begin{aligned} H^i(x;\theta,p) &= p\, e^{ik\theta\cdot x} \text{ and} \\ E^i(x;\theta,p) &= -\frac{1}{i\omega\varepsilon_0}\operatorname{curl} H^i(x;\theta,p) \\ &= -\sqrt{\frac{\mu_0}{\varepsilon_0}}\,(\theta\times p)\, e^{ik\theta\cdot x}\,. \end{aligned}$$

is scattered by a non-magnetic inhomogeneous medium with space dependent electric permittivity $\varepsilon = \varepsilon(x)$ and conductivity $\sigma = \sigma(x)$. Here, $\theta \in S^2 = \{x \in \mathbb{R}^3 : |x| = 1\}$ denotes the direction of the incident plane wave and $p \in \mathbb{C}^3$ with $p\cdot\theta = \sum_{j=1}^3 p_j\theta_j = 0$ the polarization vector.

We assume that $\varepsilon \equiv \varepsilon_0$ and $\sigma \equiv 0$ outside of some bounded domain. The pair (E^i, H^i) satisfies the time harmonic Maxwell system in vacuum, i.e.

$$\operatorname{curl} E^i - i\omega\mu_0 H^i = 0 \quad \text{in } \mathbb{R}^3,$$

$$\operatorname{curl} H^i + i\omega\varepsilon_0 E^i = 0 \quad \text{in } \mathbb{R}^3\,.$$

The total fields are superpositions of the incident and scattered fields, i.e. $E = E^i + E^s$ and $H = H^i + H^s$ and satisfy the Maxwell system

$$\operatorname{curl} E - i\omega\mu_0 H = 0 \quad \text{in } \mathbb{R}^3, \tag{1}$$

$$\operatorname{curl} H + i\omega\varepsilon E = \sigma E \quad \text{in } \mathbb{R}^3\,. \tag{2}$$

Furthermore, the tangential components of E and H are continuous on interfaces where σ or ε are discontinuous. Finally, the scattered fields have to satisfy the Silver-Müller radiation condition

$$\sqrt{\frac{\mu_0}{\varepsilon_0}}\, H^s(x)\times x - |x|E^s(x) = \mathcal{O}\left(\frac{1}{|x|}\right) \tag{3}$$

uniformly w.r.t. $\hat{x} = x/|x|$ as $|x|$ tends to infinity.

In this talk we will always work with the magnetic field H only. This is motivated by the fact that in our case of a non-magnetic medium the magnetic field is divergence free.

Eliminating the electric field E from the system (1), (2) leads to

$$\operatorname{curl}\left[\frac{1}{\sigma - i\omega\varepsilon}\operatorname{curl} H\right] - i\omega\mu_0 H = 0$$

i.e.

$$\operatorname{curl}\left[\frac{1}{\varepsilon_r}\operatorname{curl} H\right] - k^2 H = 0 \quad \text{in } \mathbb{R}^3$$

where ε_r denotes the (complex valued) relative permittivity given by

$$\varepsilon_r(x) = \frac{\varepsilon(x)}{\varepsilon_0} + i\,\frac{\sigma(x)}{\omega\,\varepsilon_0}\,.$$

We note that $\varepsilon_r \equiv 1$ outside of some bounded domain. The incident field H^i satisfies

$$\operatorname{curl}^2 H^i - k^2 H^i = 0 \quad \text{in } \mathbb{R}^3\,.$$

The Silver-Müller radiation condition (3) turns into

$$\operatorname{curl} H^s(x)\times\hat{x} - ikH^s(x) = \mathcal{O}\left(\frac{1}{|x|^2}\right) \tag{4}$$

as $|x|$ tends to infinity. The continuity of the tangential components of E and H translates into analogous requirements for H^s and $\operatorname{curl} H^s$.

From the Silver-Müller radiation condition (4) one concludes that H^s has the asymptotic form

$$H^s(x) = \frac{\exp(ik|x|)}{4\pi|x|}\, H^\infty(\hat{x}) + \mathcal{O}\left(\frac{1}{|x|^2}\right)$$

uniformly w.r.t. $\hat{x} = x/|x|$. The vector field H^∞ is called the far field pattern of H^s. It depends on the wave number k, the direction of observation $\hat{x}$, and the direction θ and polarization p of the incident field. We write $H^\infty = H^\infty(\hat{x};\theta,p)$ und suppress the dependence on k since we keep k fixed. H^∞ is tangential, i.e. satisfies $H^\infty(\hat{x};\theta,p)\cdot\hat{x} = 0$ for all $\hat{x},\theta \in S^2$ and $p \in \mathbb{C}^3$ with $p\cdot\theta = 0$.

In our talk we concentrate on the **inverse scattering problem** which is to determine (properties of) ε_r from

the knowledge of the far field patterns $H^\infty(\hat{x};\theta,p)$ for all $\hat{x},\theta \in S^2$ and polarization vectors p.

In the first part we recall some properties of the far field patterns $H^\infty(\hat{x};\theta,p)$ and the corresponding far field operator $F : L_t^2(S^2) \to L_t^2(S^2)$ defined by

$$(Fp)(\hat{x}) \;:=\; \int_{S^2} H^\infty\big(\hat{x};\theta,p(\theta)\big)\, ds(\theta)\,, \quad \hat{x} \in S^2.$$

Here, $L_t(S^2)$ denotes the L^2-space of tangential vector fields on S^2.

In the second part we present the Factorization Method which is a relatively new approach for determing the support D of $\varepsilon_r - 1$. This method avoids the computation of (a sequence of) forward problems, is therefore extremely fast (at least for constant background media) and does not need a priori information on the type of boundary conditions or the number of connectivity components of the scatterer. The Factorization Method is based on a decomposition of F in the form

$$F \;=\; H^* T\, H$$

with some explicitely given integral operator $H : L_t^2(S^2) \to L^2(D)$ and some isomorphism T from $L^2(D)$ onto itself. It can be shown that the support D of $\varepsilon_r - 1$ consists of exactly those points $z \in \mathbb{R}^3$ for which the function

$$\phi_z(\hat{x}) \;=\; \frac{ik}{4\pi}\,(\hat{x}\times p)\times \hat{x}\, e^{-ik\hat{x}\cdot z}\,, \quad \hat{x}\in S^2\,,$$

is in the range of H^*. Under certain assumptions on ε_r and the support D the range of H^* can be expressed by the range of an operator $F_\#$ which can be easily computed from the data operator F. Combining these results yields a very explicit representation of the characteristic function of D.

One of the important assumptions mentioned above is that k^2 is not an eigenvalue of the following unconventional system of linear homogeneous differential equations:

$$\begin{aligned}
\operatorname{curl}\left[\frac{1}{\varepsilon_r}\operatorname{curl} v\right] - k^2 v = 0 \text{ in } D\,,\\
\operatorname{curl}^2 w - k^2 w = 0 \text{ in } D\,,\\
\nu\times v \;=\; \nu\times w \text{ on } \partial D\,,\\
\frac{1}{\varepsilon_r}\,\nu\times\operatorname{curl} v \;=\; \nu\times\operatorname{curl} w \text{ on } \partial D\,.
\end{aligned}$$

We will report on some properties of this "interior transmission eigenvalue problem".

KNOWLEDGE OF OUR GAPS IN PHOTONIC CRYSTALS

R. C. McPhedran[†,*], **K. B. Dossou**[‡], **L. C. Botten**,[‡], **A. A. Asatryan**,[‡],**C. M. de Sterke**[†]
[†] CUDOS, School of Physics, University of Sydney, Sydney, NSW 2006, Australia
[‡] CUDOS, Department of Mathematical Sciences, University of Technology, Sydney, NSW 2007, Australia
[*]Email: ross@physics.usyd.edu.au

Abstract

We consider defect modes created in total gaps of 2D photonic crystals by changing a property such as the dielectric constant or radius of a single cylinder. Using an asymptotic method based on the dominant contribution to the Green's function from the band edge, we derive a simple exponential law which links the frequency difference between the defect mode and the band edge to the change in dielectric constant. We present numerical results which show the accuracy of the exponential law, for TE and TM polarizations, hexagonal and square arrays and for the first and second gaps.

Introduction

The original motivation for the study of photonic crystals was to create bandgaps for light by analogy with those for electrons in semiconductors, and to employ structural modification to induce localized states in the gaps, the analogue of localized states for electrons induced by doping. In recent years, attention has turned to the unusual in-band properties of photonic crystals, and in particular to possibilities for photon manipulation *at the band-edge* [1], [2].

Here, we focus on properties of defect states *at the gap-edge*. We employ a Bloch function representation of the Green's function, and show that near the gap-edge this is dominated by a single term, contributed by the Bloch edge wave function. The frequency dependence of this term in two dimensions for parabolic band-edge dispersion is logarithmic in $|\omega - \omega_{be}|$, the difference in the frequency in the gap and that at the band edge. We show that this asymptotic procedure gives rise to an exponential dependence of $|\omega - \omega_{be}|$ on the inverse of the parameter giving rise to the defect state. This type of result is derived in the tight-binding case for electrons in the solid state literature, but the derivation described here does not rely on tight-binding and is framed quite generally, requiring in essence only that the density of states at the band-edge be non-zero.

We describe the asymptotic technique for two-dimensional photonic crystals in which the distribution of dielectric constant is altered, as in [4]. We also consider the case of Dirichlet boundary conditions, in which the radius of one cylinder in a square array of cylinders is altered to generate a defect. This is a particularly interesting special case, in that there is a low-frequency band edge whose cut-off frequency is known analytically, as is the curvature at the band edge. This means that the important parameters of the formula for the frequency of the defect mode can be estimated analytically.

Numerical Examples

The analytic estimates for the behaviour of modes near gap edges are verified using a numerical method called the Fictitious Source Superposition Method (FSS) [5]. This method is particularly well suited to modelling the behaviour of such modes, which are spatially very extended, and thus difficult to model using supercell or PML techniques.

Fig. 1 shows the comparison between the normalized inverse wavelength d/λ as determined numerically and the asymptotic formula appropriate to the Dirichlet case:

$$\delta\omega = Ae^{\frac{S}{\delta a}}, \tag{1}$$

where $\delta\omega = |\omega - \omega_{be}|$, $\omega = 2\pi c/\lambda$, A is determined numerically, and S is the sensitivity, which can be determined analytically. In the case shown, S is positive, so defects are formed by decreasing the radius: $\delta a = 0.1 - \rho_d$. Note that the exponential form of equation (1) is particular to two dimensions, which is an intermediate case between the power law asymptotics of one dimension and the three dimensional case, where the density of states at the band edge is zero.

Figs. 2 and 3 give respectively a line plot and a surface plot of the defect wave function. Note the mixture of the oscillating Bloch function and the exponential decay in the former, and the four positive peaks near the centre of the defect in the latter. The wave function goes to zero within each cylinder, as is evident from Fig. 2, where the small radius of the central cylinder makes this feature less obvious than in other cylinders.

References

[1] M. Ibanescu , S.G. Johnson, D. Roundy, C. Luo, Y. Fink, and J.D.Joannopoulos," Anomalous disper-

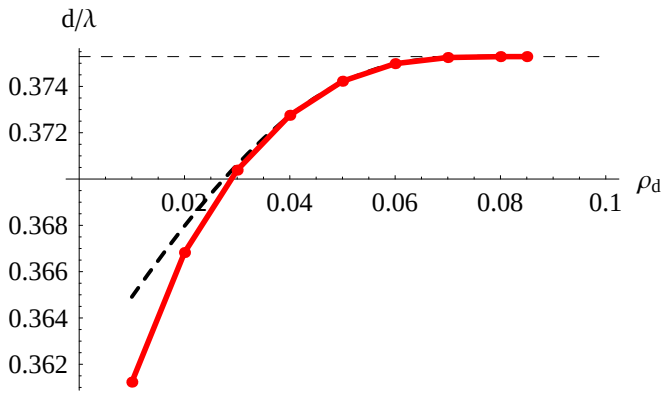

Figure 1: Normalized reciprocal wavelength d/λ for defects formed by changing the radius of a single cylinder to ρ_d, in a square array (period d) of cylinders with radius $0.1d$. Dashed line: exponential fit; solid line-FSS results. Dirichlet boundary conditions.

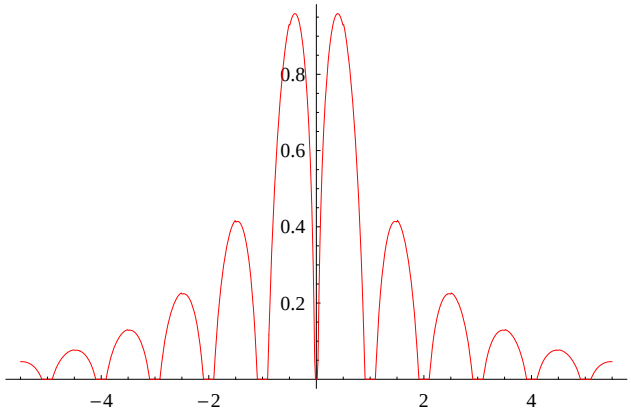

Figure 2: Line plot (along an axis through the centre of the defect) of the wave function of the defect formed by reducing the radius of a single cylinder to $0.03d$ for a square array of cylinders with radius $0.1d$ and Dirichlet boundary conditions.

sion relations by symmetry breaking in axially uniform waveguides", Phys. Rev. Lett., vol.92,063903 (2004).

[2] A. Figotin and I. Vitebskiy I, "Slow light in photonic crystals", Waves in Random and Complex Media, vol. 16, 293-382 (2006).

[3] E.N. Economou, "Green's Functions in Quantum Physics", Springer-Verlag (Berlin, 1983).

[4] K.B.Dossou, R.C.McPhedran, L.C. Botten, A.A. Asatryan and C. M. de Sterke, "Gap-edge Asymptotics of Defect Modes in 2D Photonic Crystals", Optics Express, vol. 15, 4753-4762 (2007)

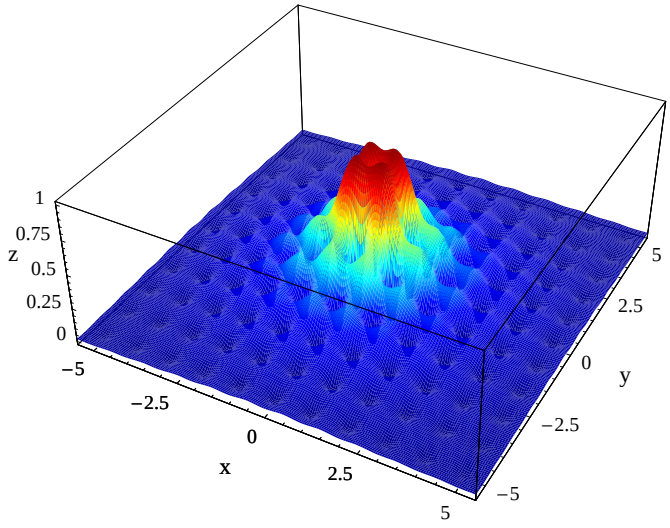

Figure 3: Surface plot of the wave function of the defect formed by reducing the radius of a single cylinder to $0.03d$ for a square array of cylinders with radius $0.1d$ and Dirichlet boundary conditions.

[5] K.B. Dossou, L.C. Botten, S. Wilcox, R.C. McPhedran, R.C., C.M. de Sterke, N.A. Nicorovici, N.A. and A.A. Asatryan, "Exact Modelling of Generalized Defect Modes in Photonic Crystal Structures", Physica B, vol. 394, 330-334 (2007).

Hydroelastic Waves

J. F. TOLAND

Introduction

By a hydroelastic wave is meant the steady irrotational periodic motion under gravity of an inviscid incompressible liquid when the top streamline is in contact with a frictionless elastic sheet. Such problems have been of interest since GREENHILL's paper [7] in the nineteenth century up to the present day, for example in the theory of very large floating structures (VLFS), or platforms (VLFP) (see [1] and the references therein) and flow under ice [8], [9], [11]. Recently there have been mathematical studies of small amplitude solutions [8], [10], [11], and numerical studies [5], [6], [9] of large amplitude solutions, to nonlinear models.

The question of existence for large-amplitude two-dimensional waves on flows of infinite depth when the sheet's elastic response to stretching and bending may be strongly nonlinear, when its mass is neglected, was formulated in [13] as a variational problem. For a class of problems where the stored energy is a sum of the effects of bending and stretcing the existence of waves propagating with arbitrarily large speeds was established by maximizing a Lagrangian. This lecture is on [3], [14] in which we develop the variational approach to deal with a heavy sheet and a more general elastic responses. That case is more complicated for the following reason.

A hydrodynamic wave is steady when the fluid's Eulerian velocity field is stationary in a reference frame moving with the wave. On the other hand, as the wave passes, the material points in the surface sheet move relative to each other according to the dynamical equations of solid mechanics in Lagrangian coordinates with the forces of gravity and the pressure exerted by the fluid acting on them. We will show the existence of travelling waves for which the Eulerian velocity of the fluid and Lagrangian velocity of the elastic sheet are stationary, but not constant, in a reference frame moving with the wave. Such waves are given by non-trivial solutions of a free-boundary value problem for the stream function.

The Physical Problem

We consider hydroelastic travelling waves that are periodic and travel with speed c_0 without changing form on the surface of an inviscid fluid which is at rest at infinite depth and occupies the region beneath a thin elastic sheet. Throughout the wavelength is normalized to be 2π and we assume that the fluid's velocity field is irrotational in the (x, y)-plane, 2π-periodic in the x direction, and stationary with respect to a frame moving with velocity c_0.

The material points of the sheet on the surface are supposed to move periodically in time with respect to a frame that is translating horizontally with speed d. This drift velocity d might be zero, in which case the material points move periodically with respect to the fluid at rest at infinite depth. If $c_0 d < 0$, the surface sheet drifts in the opposite direction to that of wave propagation.

The intersection of the sheet with the plane $z = 0$ is supposed to behave dynamically like a uniform, thin, hyperelastic rod, as described by ANTMAN [2, Ch. 4], with a stored-energy function that depends on both stretch and curvature. By the reference section is meant the line $y = z = 0$ and steady travelling waves are sought which satisfy the constraint that at any moment of time

($\star$) *the material in an interval of length* 2π *of the reference section is deformed to become one period of the hydroelastic wave surface.*

Mathematical Formulation

We suppose that the position, at time t, of the point with Lagrangian coordinates $(X, 0)$ is given by

$\boldsymbol{R}(X,t) := \big(X + dt + u(X - ct), v(X - ct)\big)$

where u and v are 2π-periodic and c, $d \in \mathbb{R}$. Let $c_0 = c + d$. Then the wave profile $\mathcal{S}_t$ at time t is

$$\begin{aligned}\{(X + dt + u(X - ct), v(X - ct)) : X \in \mathbb{R}\}\\ = \mathcal{S}_0 + (c_0 t, 0).\end{aligned}$$

The second line shows that $\mathcal{S}_t$ describes a fixed profile $\mathcal{S}_0$ propagating from left to right with-

out changing shape at a constant speed c_0; the first line shows that points on the surface have time period $2\pi/c$ relative to a frame moving with speed d. So c_0 is the wave speed and d is the drift velocity of the material in the surface sheet, both calculated relative to the fluid at rest at infinite depth. We suppose throughout that $c_0 \geq 0$ and $d \in \mathbb{R}$.

The elasticity of the surface membrane is defined as follows. Let $s \in [0, 2\pi]$ denotes a point of the reference sheet (the X-axis) and let $\boldsymbol{r}(s) \in \mathcal{S} = \{\boldsymbol{r}(s) : s \in \mathbb{R}\}$ denote its position after deformation, so that $|\boldsymbol{r}'(s)|$ is the stretch at $\boldsymbol{r}(s)$. Let $\hat{\sigma}(\boldsymbol{r}(s))$ denote the curvature of $\mathcal{S}$ at $\boldsymbol{r}(s)$. Then the elastic energy stored in in one period is

$$\int_0^{2\pi} |\boldsymbol{r}'(s)| \boldsymbol{e}\big(|\boldsymbol{r}'(s)|, \hat{\sigma}(\boldsymbol{r}(s))\big) ds.$$

With c and ρ given, let ϖ be defined by

$$\varpi(\gamma, \sigma) = \nu \Leftrightarrow \nu^2(\boldsymbol{e}_1(\nu, \sigma) - c^2\rho/2) = \gamma.$$

and let $\gamma = \gamma(\sigma, \eta)$ depends on the height and curvature, η and σ, and the density and velocity, ρ and c, via the formula

$$\int_{\mathcal{S}} \frac{d\varsigma}{\varpi(\gamma + g\rho\eta(\varsigma), \sigma(\varsigma))} = 2\pi,$$

where ς denotes arc length along one period the surface. This is to ensure that $(\star)$ in the Introduction is satisfied. Let $\underline{\boldsymbol{e}}(\nu, \sigma) := \boldsymbol{e}(\nu, \sigma) - (c^2\rho/2)\nu$ and, for any real numbers γ_1 and σ_1, let

$$\underline{v}(\gamma_1, \sigma_1) = \underline{\boldsymbol{e}}(\varpi(\gamma_1, \sigma_1), \sigma_1) + \frac{\gamma_1}{\varpi(\gamma_1, \sigma_1)},$$

$$\underline{v}_2(\gamma_1, \sigma_1) = \frac{\partial \underline{v}}{\partial \sigma_1}(\gamma_1, \sigma_1) = \underline{\boldsymbol{e}}_2\big(\varpi(\gamma_1, \sigma_1), \sigma_1\big),$$

and

$$\underline{N}(s) = \underline{v}\big(\gamma(\sigma, \eta) + g\rho\eta(s), \sigma(s)\big) - \sigma(s)\underline{v}_2\big(\gamma(\sigma, \eta) + g\rho\eta(s), \sigma(s)\big).$$

Then we can deduce from the mechanics [2] that the pressure exerted on the sheet by the fluid beneath is determined by its position and curvature (alone) through the formula

$$P(\varsigma) = \frac{d^2}{d\varsigma^2}\big(\underline{v}_2(\gamma + g\rho\eta(\varsigma), \sigma(\varsigma))\big) - \sigma(\varsigma)\underline{N}(\varsigma) + \frac{g\rho\cos\theta(\varsigma)}{\varpi(\gamma + g\rho\eta(\varsigma), \sigma(\varsigma))},$$

in which $\gamma = \gamma(\sigma, \eta)$, $\underline{N}$ is given above and ϑ is the angle between the surface and the horizontal.

Note that this formula for P depends only on the *geometric shape* of the sheet section and does not require knowledge of the displacement of the material points in the undeformed sheet section.

The unknown region occupied by the liquid is characterized by the kinematic requirement that the surface is a streamline and the dynamic condition that the pressure in the fluid and the effect of gravity yield the force needed to deform the sheet. Therefore the existence of a steady hydroelastic wave with speed c_0, when the drift velocity is d and $(\star)$ holds, corresponds to the existence of a non-self-intersecting smooth curve $\mathcal{S}$ in the plane which is 2π-periodic in the horizontal direction for which there exists a solution of the following system:

$$\begin{aligned} \Delta\psi &= 0 \text{ below } \mathcal{S}, \\ \psi &\equiv 0 \text{ on } \mathcal{S} \text{ (kinematic condition)}, \\ \nabla\psi(x, y) &\to (0, c_0) \text{ as } y \to -\infty, \end{aligned}$$

with the dynamic (pressure) boundary condition

$$\frac{1}{2}|\nabla\psi|^2 + g\eta = \frac{c_0^2}{2} - P(\varsigma) \text{ on } \mathcal{S}\,.$$

Are there any nontrivial solutions of this problem? In [13] we use a variational argument based on Zakharov's Hamiltonian system [15] as formulated in [4] to prove the existence of travelling waves when the surface density is zero.

Hypotheses and Main Result

Roughly speaking the main hypotheses on the stored-energy function is:

> $\boldsymbol{e}_{11} > \kappa$, where $\kappa \geq 0$ is a constant, and the mapping
>
> $$(t, \sigma) \mapsto \boldsymbol{e}(1/t, \sigma) \qquad \text{(H)}$$
>
> is strictly convex and tends to ∞ sufficiently rapidly as $t \to \infty$ or 0, and as $|\sigma| \to \infty$.

Suppose that $g > 0$, $\rho \geq 0$, $c_0 \geq 0$ and $d \in \mathbb{R}$ are given. Let $c = c_0 - d$ and suppose that $c^2\rho \leq \kappa$. Suppose also that

$$c_0^2 + c^2\rho + \frac{g^2\rho^2}{\boldsymbol{e}_{11}(1, 0) - c^2\rho} > g + \boldsymbol{e}_{22}(1, 0).$$

Then there exists a non-zero solution of the hydroelastic wave problem. In particular, if $c_0^2 + \rho^2$ is sufficiently large there exist waves for all values of c with $c^2\rho \leq \kappa$. A special case occurs when ρ is sufficiently large (depending only on $\boldsymbol{e}$ and g) and c is sufficiently small (depending on ρ and $\boldsymbol{e}$). For example, when ρ is sufficiently large, there exist waves for all c_0 and d with $c_0^2 + d^2$ sufficiently small; c_0 and d may have opposite sign and either of c_0 or d may be zero.

The case $c = c_0 = d = 0$ and ρ is sufficiently large is included. This limiting case corresponds to *static hydroelastic waves* in which there is no motion in the surface sheet or in the fluid and elastic stresses are balanced by hydrostatic pressure.

Thus, depending on the density of the surface sheet, very slow, or very fast hydroelastic waves are proved to exist, and the drift can have either sign depending on circumstances.

References

[1] A. Andrianov, Hydroelastic Analysis of Floating Structures. PhD Thesis, Technische Universiteit Delft September 2005. www.library.tudelft.nl/dissertations

[2] S. S. Antman, Nonlinear Problems of Elasticity. First Edition. Springer-Verlag, New York, 1995.

[3] P. Baldi and J. F. Toland, Steady periodic water waves under nonlinear elastic membranes. In preparation.

[4] A. I. Dyachenko, E. A. Kuznetsov, M. D. Spector, and V. E. Zakharov, Analytic description of the free surface dynamics of an ideal fluid (canonical formalism and conformal mapping), Physics Letters A **221** (1996), 73–79.

[5] L. K. Forbes, Surface waves beneath an elastic sheet. Part 1. High-order series solution, J. Fluid Mech., **169** (1986) 409 - 428.

[6] L. K. Forbes, Surface waves beneath an elastic sheet. Part 2. Galerkin solutions, J. Fluid Mech., **188** (1988) 491 - 508.

[7] A. G. Greenhill, Wave motion in hydrodynamics, Amer. J. Math. **9** (1) (1886) 62-96. http://jstor.org

[8] M. Haragus-Courcelle and A. Il'ichev A, Three-dimensional solitary waves in the presence of additional surface effects, Euro. J. Mech. B Fluids, **17** (5) (1998), 739-768.

[9] G. M. Hegarty and V. A. Squire, Large amplitude periodic waves beneath an ice sheet, In "Ice in the Environment: Proc 16th IAHR International Symp. on Ice, Vol. 2, 310-317. Dunedin, New Zealand, 2002.

[10] G. Iooss and F. Dias, Water-waves as a spatial dynamical system. In Handbook of Mathematical Fluid Dynamics, edited by S. Friedlander and D. Serre, Elsevier 2003.

[11] E. Parau and F. Dias, Nonlinear effects in the response of a floating ice plate to a moving load, J. Fluid Mech. **460** (2002), 281-305.

[12] E. Shargorosky and J. F. Toland, Bernoulli free-boundary problems, to appear in Memoirs of Amer. Math. Soc. www.maths.bath.ac.uk/∼jft/

[13] J. F. Toland, Steady periodic hydroelastic waves, pre-print, 2006.

[14] J. F. Toland, Periodic hydroelastic travelling waves, pre-print, 2007.

[15] V. E. Zakharov, Stability of periodic waves of finite amplitude on the surface of deep fluid, Jour. Appl. Mech. Tech. Phys. **2** (1968), 190-194.

Department of Mathematical Sciences
University of Bath
Bath
BA2 7AY
UK
jft@maths.bath.ac.uk

Isaac Newton Institute Satellite Workshop on High Frequency Wave Propagation and Scattering

Organisers: Simon Chandler-Wilde (University of Reading), Ivan Graham (University of Bath), Stephen Langdon (University of Reading) and Valery Smyshlyaev (University of Bath)

WELL-CONDITIONED INTEGRAL EQUATIONS FOR HIGH-FREQUENCY SCATTERING PROBLEMS

François Alouges[‡], **David P. Levadoux**[†,*]
[†]ONERA, Chemin de la hunière, 91761 Palaiseau, France
[‡] Université Paris XI, 91405 Orsay, France
[*]Email: david.levadoux@onera.fr

Abstract

We present a new class of integral equations dedicated to the iterative solution of harmonic scattering problems. We conjecture a localization of the so-called admittance operator with increasing frequency, which allows us to construct an approximate model able to be efficiently discritized. The general framework of the formalism consists of factorizing the Calderón projector with a regularizing boundary operator $\widetilde{A}$ built with this approximation of the admittance. An important feature of the approach is to directly inform about the optimal operator A for which the resulting equation becomes trivial (whose underlying operator is identity). Therefore, in such a framework, building well-conditioned integral equations becomes to exhibit as pertinent as possible approximations $\widetilde{A}$ of A.

Introduction

The relevance of integral methods for solving scattering problems in harmonic regime requires no further proof. Using them in combination with fast multi-pole algorithms and iterative solvers enables one to accurately solve problems involving hundreds of thousands of unknowns. However, the efficiency of iterative methods depending on the condition number of the linear systems, it becomes absolutely crucial to have either high-performance pre-conditioners or intrinsically well-conditioned integral formulations. It is in this strategic field, that the french aerospace lab ONERA has been conducting fundamental research for the past few years.

The main research theme, begun in 1998 [9], is based on a generalized combined source integral equation (GCSIE) [10] [11] [8], also called later generalized Brakhage-Werner integral equation by different authors [3] [7]. Very close in spirit, but in the area of direct integral equation methods is the generalized combined field integral equation (GCFIE) of Contopanagos *et al.* [6] and Adams [1]. The goal of both methods is to find a way to incorporate in the integral equation formalism, some information on the scattering phenomenon. Eventually, it turns out that both GCSIE and GCFIE depend on the choice of an operator $\widetilde{Y}$, which should be an approximation of the admittance of the diffracting body. Indeed, the construction of the equation is done in such a way that in the limiting case where this approximation is exact, the integral operator to be inverted becomes the identity (this is also true for GCFIE although it has not been noticed by the authors). Thus, we need to construct computable approximations of the admittance such that the operator underlying the equation appears as a mathematically controllable perturbation of the identity (small or compact). When the GCSIE or GCFIE are discretized, we then arrive at a linear system which is close to the identity and hopefully, by its very nature, well-conditioned.

After recalling the principle of the method, we apply it to the problem of scattering by a perfect electric conductor, making explicit the approximation of the admittance operator that was used. We then discuss suitable modifications for handling different boundary conditions (impedance or Leontovitch). Numerical results show the efficiency of the method, both in terms of reliability (for complex geometries) and in terms of iterations and speed.

A general formalism

Most boundary value problems in wave scattering read as

$$\text{Find } w \in W \text{ such that } Bw = u_0 \,, \tag{1}$$

where $u_0 \in \mathcal{D}'(\Gamma)$ is a distribution on the boundary Γ of a compact set D, W a functional space of admissible wave solutions usually defined on $\mathbb{R}^3 \setminus D$, and B a boundary trace operator. Moreover, W can be parameterized with the help of a potential $\mathcal{C}$

$$w = \mathcal{C}(\gamma_0 w, \gamma_1 w) \,,$$

where $(\gamma_0 w, \gamma_1 w)$ stand for the Cauchy data of $w \in W$. Since (1) is well-posed there exists an operator A defined by

$$A : \, Bw \mapsto (\gamma_0 w, \gamma_1 w) \,,$$

and therefore

$$B\mathcal{C}A = \mathrm{Id} \,. \tag{2}$$

The integral equations we present are built on the model:

$$\text{Find } u \in \mathcal{D}'(\Gamma) \text{ such that } B\mathcal{C}\widetilde{A}u = u_0 \,, \tag{3}$$

where $\widetilde{A}$ is meant to be an approximation as close as possible to A. In view of (2), the linear system produced after the discretization of (3) is expected to be well-conditioned. Although the general framework of this formalism is not confined to Maxwell problems, we restrict now our presentation to this field of applications. Therefore, $\mathcal{C}$ is given by the Stratton-Chu formula

$$\mathcal{C}(\mathbf{u},\mathbf{v}) = \mathcal{L}\mathbf{v} - \mathcal{K}\mathbf{u} \tag{4}$$

where $\mathcal{L} = -\frac{1}{ik}\nabla\times\nabla\times\mathcal{G}$, $\mathcal{K} = \nabla\times\mathcal{G}$, and $\mathcal{G}$ is the vector potential.

The perfect electrical conductor problem

Although already relevant, one of the simplest applications of this framework is to consider the electromagnetic problem of the perfect electrical conductor (PEC). There, $(\gamma_0,\gamma_1) = (\mathbf{n}\times, \frac{1}{ik}\mathbf{n}\times\text{curl})$ ($\mathbf{n}$ being the unit outward normal to Γ and k the wave number) and $B = \gamma_0$. Here, it is easily seen that $A = (\mathrm{Id}, Y)$ where Y is the classical admittance operator, and hence approximating A becomes approximating Y. In (3) we will have $\widetilde{A} = (\mathrm{Id}, \widetilde{Y})$

A quite natural way to build approximations of the admittance is to pull back onto the boundary Γ of the scatterer, the well known admittance of the tangent plane. Viewing the admittance of the plane as the trace of a potential, say $-2\mathbf{n}\times\mathcal{L}$, we are obviously conveyed to import this formula onto the boundary and to consider the first approximation $\widetilde{Y} = -2\mathbf{n}\times\mathcal{L}$. The resulting equation turns out to be a compact perturbation of the identity, but suffers from irregular frequencies. A solution to remove these spurious modes is to localize this first approximation. While Contopanagos *et al.* [6] and Adams [1] propose to introduce a damping coefficient in the wave number, we suggest to use a quadratic partition of unity (U_p,χ_p)[1] on the boundary, leading to the following pseudo-local approximation

$$\widetilde{Y} = -2\sum_p \chi_p\,\mathbf{n}\times\mathcal{L}\,\chi_p \quad . \tag{5}$$

This technique has been thoroughly studied in [5], [4], [2]. One of its foremost features is that it leads to an equation without internal resonance frequency, and shows a condition number independent of both the mesh refinement and the frequency. Concerning experimental results, we point out that, for instance, the Channel cavity, which models an aircraft air intake was processed at 7 GHz ($300\,000$ unknowns) in half the computational time usually needed with a classical equation (FIG. 1). Another technique to approximate Y has been proposed in [7].

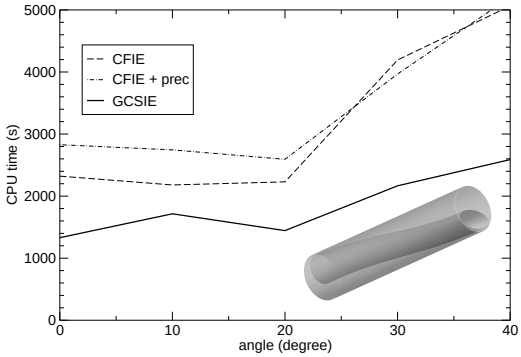

Figure 1: *Resolution time in function of the incidence for the Channel cavity at* 7 *GHz (around* $300\,000$ *DoF).*

Let us note that for PEC problem, a well-conditioned direct formulation can as well be designed when the excitation is given by an incident electromagnetic wave $(\mathbf{E}^{\mathrm{inc}},\mathbf{H}^{\mathrm{inc}})$. Indeed, starting from the well-known combined field integral equation

$$\mathbf{n}\times\mathcal{K}\mathbf{J} + \mathbf{J} + \alpha\mathcal{L}_{|\tan}\mathbf{J} = \mathbf{n}\times\mathbf{H}^{\mathrm{inc}} - \alpha\mathbf{E}^{\mathrm{inc}}_{|\tan}\,, \tag{6}$$

and replacing coupling coefficient α with $-Y\mathbf{n}\times$ leads to

$$\mathbf{n}\times\mathcal{K}\mathbf{J} + \mathbf{J} - Y\mathbf{n}\times\mathcal{L}\mathbf{J} = \mathbf{J}\,. \tag{7}$$

As before, approximating Y by $\widetilde{Y}$ and solving

$$\mathbf{n}\times\mathcal{K}\mathbf{J} + \mathbf{J} - \widetilde{Y}\mathbf{n}\times\mathcal{L}\mathbf{J} = \mathbf{n}\times\mathbf{H}^{\mathrm{inc}} + \widetilde{Y}\mathbf{n}\times\mathbf{E}^{\mathrm{inc}} \tag{8}$$

should give a well-conditioned equation.

Problems with impedance boundary conditions

In this kind of problem, the boundary operator B is given by

$$B\mathbf{E} = \mathbf{E}_{\tan} + \mathbf{n}\times\mathbf{H}\,. \tag{9}$$

Writing A in coordinates (A_E, A_H), we have $A_H = YA_E$ and setting $\mathbf{u} = B\mathbf{E}$, (9) becomes $\mathbf{u} = -\mathbf{n}\times A_E\mathbf{u} + YA_E\mathbf{u}$, so that

$$A_E = (Y - \mathbf{n}\times)^{-1}\,. \tag{10}$$

Looking at the principal symbol of A_E, we propose the following approximation

$$\widetilde{A}_E = \mathbf{n}\times(\Pi_{\mathrm{star}} + 2ikG_0)\,, \tag{11}$$

[1] $(U_p)_p$ is a set of patches recovering Γ, and $(\chi_p)_p$ a family of truncation functions with support in U_p and such that $\sum_p \chi_p^2 = 1$.

where $\Pi_{\rm star}$ is the Helmholtz projector onto the curl free vector-fields and G_0 is the tangential trace of the convolution with the Green function of the Laplacian. Taking $\widetilde{A} = (\widetilde{A}_E, \widetilde{Y}\widetilde{A}_E)$, one can show that (3) is well-posed, and the underlying operator is a compact perturbation of identity.

References

[1] R. J. Adams. Combined field integral equation formulations for electromagnetic scattering from convex objects. *IEEE Trans. Antennas Propag.*, 52(5):1294–1303, May 2004.

[2] F. Alouges, S. Borel, and D. P. Levadoux. A stable well-conditioned integral equation for electromagnetism scattering. *J. Comp. Appl. Math*, 2006, accepted.

[3] X. Antoine and M. Darbas. Alternative integral equations for the iterative solution of acoustic scattering problems. *Quart. J. Mech. Appl. Math.*, 58(1):107–128, 2005.

[4] S. Borel. *Étude d'une équation intégrale stabilisée pour la résolution itérative de problèmes de diffractions d'ondes harmoniques en électromagnétisme*. PhD thesis, Université Paris XI, 2006.

[5] S. Borel, D. P. Levadoux, and F. Alouges. A new well-conditioned integral formulation for Maxwell equations in three-dimensions. *IEEE Trans. Antennas Propag.*, 53(9):2995–3004, September 2005.

[6] H. Contopanagos, D. Dembart, M. Epton, J. J. Ottusch, V. Rokhlin, J. Visher, and S. Vandzura. Well-conditioned boundary integral equations for three-dimensional electromagnetic scattering. Technical Report YALEU/DCS/RR-1198, Yale University, June 2000.

[7] M. Darbas. Generalized combined field integral equations for the iterative solution of the three-dimensional maxwell equations. *Applied Mathematics Letters*, 19(8):834–839, August 2006.

[8] D. P. Levadoux. Stable integral equations for the iterative solution of electromagnetic scattering problems. *C. R. Physique*, 7(5):518–532, 2006.

[9] D. P. Levadoux and B. L. Michielsen. Analysis of a boundary integral equation for high frequency Helmholtz problems. In *Waves Conference*, pages 765–767, Golden, Co, 1-5 June 1998.

[10] D. P. Levadoux and B. L. Michielsen. An efficient high-frequency boundary integral equation. In *Antennas and Propagation Society International Symposium*, volume 2, pages 765–767, Orlando, FL, 11-16 July 1999.

[11] D. P. Levadoux and B. L. Michielsen. Nouvelles formuations intégrales pour les problèmes de diffraction d'ondes. *M2AN*, 38(1):157–175, January/February 2004.

A NEW DISCRETIZATION PROCEDURE USING OSCILLATING FINITE ELEMENT POLYNOMIALS FOR HELMHOLTZ PROBLEMS

A. Amara[†,*], **A. Bernardini**[†,*], **R. Djellouli**[‡,*]
[†]INRIA Futurs, Magique 3D team,
Laboratoire de Mathématiques Appliquées, CNRS-UMR5142,
Université de Pau et des Pays de l'Adour, BP 1155, 64013 Pau cedex, FRANCE.
[‡]Department of Mathematics, California State University Northridge,
18111 Nordhoff Street, Northridge, CA91330-8313, USA.
[*]Email: mohamed.amara@univ-pau.fr, angela.bernardini@univ-pau.fr, rabia.djellouli@csun.edu

Abstract

We propose a new class of hybrid-mixed-type solution methodology for solving high-frequency Helmholtz problems. The proposed approach distinguishes itself from similar discontinuous Galerkin methods by a local approximation of the solution with oscillated finite elements polynomials that satisfy the wave equation. We enforce a weak continuity of the solution across the element interfaces by Lagrange multipliers. Preliminary numerical results are presented to illustrate the potential of the proposed method.

Introduction

The numerical solution of waves phenomenas has adquired great attention during the last century. Despite the tremendous progress that has been made in the recent years, the challenge of efficient computation at high wavenumbers is still considered as an unsolved problem by current numerical techniques. Indeed, standard computational methods such as Galerkin finite element methods (FEM) are unable to cope with rapid oscillation because they become prohibitely expensive to resolve the waves and control numerical dispersion errors. For example, solving an acustic scattering with Q2 finite elements when $ka = 10$, where k is the wave number and a is the dimension of the considered submarine-like scatterer, requires to solve a system of almost 10 million complex unknowns [1], when scatterer applications require to solve exterior Helmholtz problem when $ka > 200$.

Research efforts on reducing the computational cost for mid- and high-frequency problems have been and are currently directed in many different venues, e.g. (a) mesh-dependent augmented Galerkin techniques such as stabilized methods [2], and (b) multi-scale methods such as partition of unity methods [3], residual free bubbles [4], and discontinuous Galerkin methods (DGM) [5]. We propose a new hybrid-mixed-type formulation for solving mid- and high-frequency wave problems in which the solution is approximated locally by oscillated finite elements polynomials that satisfy the wave equation. In addition, a weak continuity of the solution is enforced by the introduction of Lagrange multipliers along the element interfaces. Due to the discontinuous nature of the approximation element-level static condensation is enabled. The computational cost of the proposed method is then simplified, and mainly given by the total number of Lagrange multipliers degrees of freedom and by the sparsity pattern of the resulting matrix.

The approach we propose here combines the features of standard Galerkin finite elements techniques in terms of implementation complexities and the oscillating aspect of the shape functions needed for approximating high frequency waves.

The mixed-hybrid variational formulation

Let $\Omega \subset \mathbb{R}^d$ be a d-dimensional, open, bounded region with smooth boundary $\partial\Omega$.

Find $u : \Omega \to \mathbb{R}$ such that

$$\begin{cases} \Delta u + k^2 u = f\,, & \text{in} \quad \Omega \\ \frac{\partial u}{\partial \nu} = iku + g\,, & \text{on} \quad \partial\Omega \end{cases} \tag{1}$$

where $k > 0$ is the wave number, $\partial/\partial\nu$ denotes the normal derivative and $f : \Omega \to \mathbb{R}$ and $g : \partial\Omega \to \mathbb{R}$ are given functions. The second equation in (1) is a representation of a class of inhomogeneous Robin boundary conditions.

Let $\mathcal{T}_h$ be a regular triangulation of Ω into subdomain K with boundary ∂K. The subdomain K is either a triangular-shapad or a quadrilateral-shaped element. We focus in this abstract on the case where the subdomains K are rectangular-shaped elements. Let h denote the stepsize of the trangulation. We consider the following hybrid variational formulation:

Find $(u, \lambda) \in \mathcal{V} \times \mathcal{M}$ such that

$$\begin{cases} a(u, v) + b(v, \lambda) = F(v)\,, & \forall v \in \mathcal{V} \\ b(u, \mu) = 0\,, & \forall \mu \in \mathcal{M} \end{cases} \tag{2}$$

where the bilinear form $a(\cdot,\cdot)$ and $b(\cdot,\cdot)$, and the right-hand side F are given by:

$$\begin{aligned} a(u,v) &= \sum_{K\in\mathcal{T}_h}\left(\int_K(\nabla u\cdot\nabla v - k^2uv)dx \right. \\ &\quad \left. -ik\int_{\partial K\cap\partial\Omega} uvds\right), \quad \forall u,v\in\mathcal{V} \quad (3) \\ b(v,\mu) &= \sum_{K\in\mathcal{T}_h}\int_{\partial K}\mu^K v ds\,,\ \forall(v,\mu)\in\mathcal{V}\times\mathcal{M} (4) \\ F(u) &= \sum_{K\in\mathcal{T}_h}\left(\int_{\partial K\cap\partial\Omega} gvds \right. \\ &\quad \left. -\int_K fvdx\right), \quad \forall v\in\mathcal{V} \quad (5) \end{aligned}$$

where $\mathcal{V}$ and $\mathcal{M}$ denote the following spaces

$$\begin{aligned} \mathcal{V} &= \{v\in L^2(\Omega): v|_K\in H^1(K)\}, \\ \mathcal{M} &= \{\mu\in\prod_{K\in\mathcal{T}_h} L^2(\partial K): \mu=0 \quad \text{on} \quad \partial\Omega \quad \text{and} \\ &\quad \forall K,K'\in\mathcal{T}_h, \mu^K+\mu^{K'}=0 \quad \text{on} \quad \partial K\cap\partial K'\}. \end{aligned}$$

Now, let $\mathcal{V}_h$ and $\mathcal{W}_h$ denote two finite-dimensional space satisfying

$$\mathcal{V}_h\subset\mathcal{V}\,,\quad \mathcal{W}_h\subset\mathcal{W}. \quad (6)$$

The basic idea in our method is to seek an approximate solution $(v_h,\lambda_h)\in\mathcal{V}_h\times\mathcal{W}_h$ to the variational problem (2). We chose to approximate the primal variable u using a linear combination of finite element polynomials that oscillate with the frequency. The oscillated aspect of these shape functions with respect to the wavenumber ka is illustrated in Fig. 1. More specifically, we construct the space $\mathcal{V}_h$ as follows:

$$\begin{aligned} \mathcal{V}_h &= \{v_h\in\mathcal{V}: v|_K=\sum_{l=1}^{2}\left(\sum_{j=1}^{2}u_j^l\Lambda_j(x)e^{(-1)^l iky}\right. \\ &\quad \left.+\sum_{j=3}^{4}u_j^l\Lambda_j(y)e^{(-1)^l ikx}\right), u_j^l\in\mathbb{C}\} \quad (7) \end{aligned}$$

where Λ_j is an one-dimensional Lagrange polynomial.

The dicrete space $\mathcal{M}_h$ is given by

$$\begin{aligned} \mathcal{M}_h &= \{\mu_h\in\mathcal{M}: \forall K\in\mathcal{T}_h \quad \text{and} \quad \forall e_j^K\in\partial K: \\ &\quad \mu_j^K=\mu|_{e_j^K}\in\mathbb{C}, 1\le j\le 4\} \quad (8) \end{aligned}$$

where e_j^K represents the element edges. In particular we approximate the Lagrange multipliers field by

$$\mu_h=\mu_0+\mu_1 s, \quad (9)$$

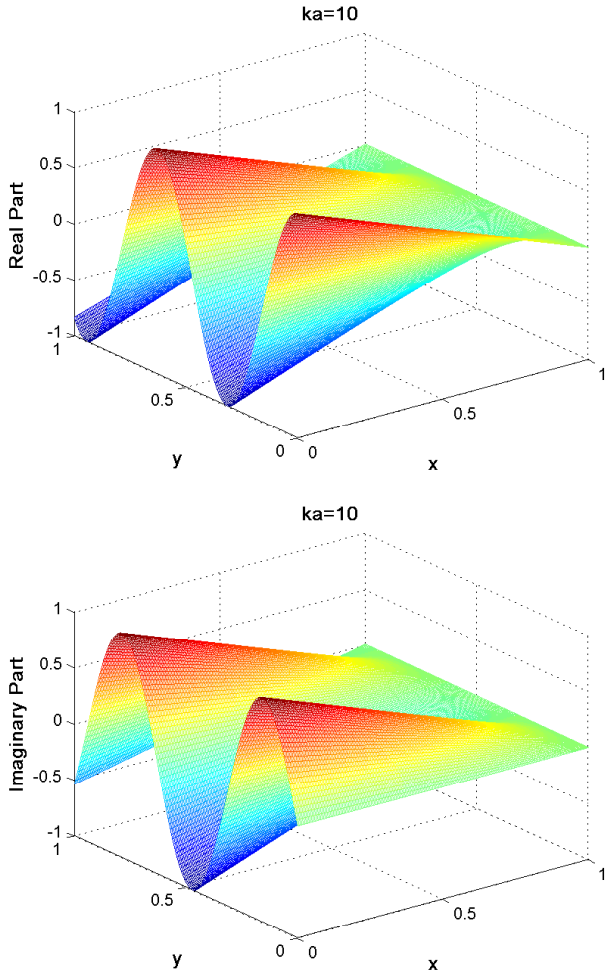

Figure 1: Dependence of the shape function $\Lambda_1(x)e^{iky}$ with respect to the wave number $ka=10$.

where s is varying along one element edge. μ_h has similarly expression along all three other edges of the element. From now on we refer to our element as the OP-8-2 element, (OP for oscillated polynomials, 8 for eight shape functions for element, 2 for two Lagrange multipliers dofs per edge).

Numerical results

In this section we present preliminary results obtained for a two-dimensional model problem discretized by a uniform rectangular-shaped mesh. We consider the Helmholtz problem (1) where Ω is an $a\times a$ square domain, and the functions f and g are chosen so that the exact solution is a plane wave propagating in a given direction $\mathbf{d}=(cos\,\theta, sin\,\theta)$

$$u^{ex}(x,y)=e^{ik\mathbf{d}\cdot\mathbf{x}}.$$

We vary the angle θ of propagation in the interval $[0, 2\pi)$ and for each angle we measure the relative error by the following H^1 modified norm which takes into account the jump of the solution along the element edges

$$||u-u^{ex}||_{\widehat{H^1}} = \left(\sum_{K\in\mathcal{T}_h} ||u-u^{ex}||^2_{H^1(K)} + \sum_{\partial K\in\mathcal{T}_h} |||[u]|||^2_{L^2(\partial K\cap\partial K')} \right)^{1/2} \quad (10)$$

The proposed method is compared with both the standard finite element method equipped with the Q2 elements and the DGM equipped with the R-8-2b elements. We must point out that the main difference between the porposed method and the DGM formulation is the approximation at the element level. The latter approach approximates the solution by planar waves. Because of space limitation, we present comparison results obtained for $ka = 30$ only. Fig.2 shows the dependence of the relative errors with respect to the angle of propagation when $ka = 30$.

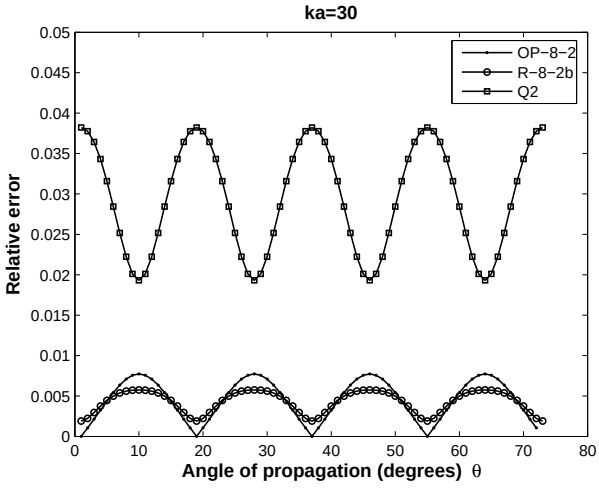

Figure 2: Performance comparison when $ka = 30$.

The preliminary results obtained from the numerical investigation performed in the case of waveguide problems reveal:

- The OP-8-2 elements exhibit superiority with respect to the standard Q2 element. We must point out that since we use static condensation procedure, the size of the resulting linear system is smaller that the size of the system obtained when using Q2 finite elements discretization.
- The performance of proposed solution methodology is overall comparable to the DGM method. The elements OP-8-2 and R-8-2b deliver results with the same level of accuracy. However, the proposed method is more versatile than DGM because it can be applied to unstructured meshes with either triangular-shaped elements or quadrilateral-shaped elements, and its extension to three-dimensional problems is conceptually straightforward.

ACKNOWLEDGMENTS

The authors acknowlegde the support by INRIA/CSUN Associate Team Program.

References

[1] R. Tezaur, A. Macedo, C. Farhat and R. Djellouli, "Three-dimensional finite element calculations in acoustic scattering using arbitrarily shaped convex artificial boudaries", Internat. J. Numer. Meths. Engrg., vol. 53, pp. 1461-1476, 2002.

[2] I. Babuška, F. Ilhlenburg, E. T. Paik and S. A. Sauter, "A generalized finite element method for solving Helmholtz equation in two dimension with minimal pollution", Comput. Meths. Appl. Mech. Engrg., vol. 128, pp. 325-359, 1995.

[3] I. Babuška and J. M. Melenk, "The partition of the unity method", Intenat. J. Numer. Meths. Engrg., vol. 40, pp. 727-758, 1997.

[4] L. P. Franca, C. Farhat, A. P. Macedo and M. Lasoinne, "Residual-free bubbles for the Helmholtz equation", Intenat. J. Numer. Meths. Engrg., vol. 40, pp. 4003-4009, 1997.

[5] C. Farhat, I. Harari and U. Hetmaniuk, "A discontinuous Galerkin method with Lagrange multipliers for the solution of the Helnholtz problems in the mid-frequency regime", Comput. Meths. Appl. Mech. Engrg., vol. 192, pp. 1389-1419, 2003.

Accuracy improvement of the finite element solution of time-harmonic scattering problems using asymptotic microlocal techniques

X. Antoine[†,*], **C. Geuzaine**[‡]
[†]Institut Elie Cartan Nancy (IECN), University Henri Poincaré, INRIA Corida Team,
Office 307, B.P. 239, F-54506 Vandoeuvre-lès-Nancy Cedex, France
[‡]University of Liège, Department of Electrical Engineering and Computer Science,
Montefiore Institute, Sart-Tilman, Bldg. B28, Parking P32, B-4000, Liège, Belgium
[*]Email: Xavier.Antoine@iecn.u-nancy.fr

Abstract

The aim of this paper is to propose an approach for improving the accuracy of the finite element solution of time-harmonic scattering problems, and in particular acoustic scattering by sound-hard, convex obstacles. The method uses approximate microlocal analysis techniques developed for the fast solution of high-frequency problems. After a detailed presentation of the methodology, we provide a numerical example for a two-dimensional problem to validate our approach.

Introduction

Many developments have been proposed over the last decade to improve the accuracy of the classical finite element solution of time-harmonic scattering problems at high frequencies. Indeed, the finite element solution is known to suffer from *pollution effects* when the wavenumber increases, leading to ever costlier computations as the mesh spacing must decrease faster than the wavelength [1]. In this paper we propose a method which strongly reduces this problem. The very basic ideas are 1) the *a priori* determination of an approximate phase in the bounded computational domain using microlocal analysis techniques and 2) the computation of a slowly varying wave field over the domain through a classical finite element formulation. All these points are developed below and a numerical example is given to validate the proposed approach.

The classical formulation

We investigate the numerical solution of the time-harmonic acoustic scattering problem of a plane wave $u^{\rm inc}(\mathbf{x}) = e^{ik\nu\cdot\mathbf{x}}$ by a sound-hard obstacle $\Omega^- \subset \mathbb{R}^d$, $d \geq 1$, with $\mathcal{C}^1$ closed boundary Γ. The real-valued positive wavenumber k is related to the wavelength λ by the relation $k = 2\pi/\lambda$ while the normalized incidence vector direction is ν. We set $\Omega^+ := \mathbb{R}^d \backslash \overline{\Omega^-}$ as the exterior domain of propagation associated with Ω^-. The spatial variable is denoted by $\mathbf{x} = (x_1, ..., x_d)$. The boundary value problem writes

$$\begin{array}{ll} \Delta u + k^2 u = 0, & \text{in } \Omega^+, \\ \partial_{\mathbf{n}_\Gamma} u = g := -\partial_{\mathbf{n}_\Gamma} u^{\rm inc}, & \text{on } \Gamma, \\ \lim\limits_{|\mathbf{x}|\to+\infty} |\mathbf{x}|^{(d-1)} (\nabla u \cdot \dfrac{\mathbf{x}}{|\mathbf{x}|} - iku) = 0. & \end{array} \tag{1}$$

The operator Δ is the Laplacian operator and $\mathbf{a}\cdot\mathbf{b}$ designates the hermitian inner product of two d-dimensional complex-valued vector fields $\mathbf{a}$ and $\mathbf{b}$. The outwardly directed unit normal vector to Ω^- is $\mathbf{n}_\Gamma$. In a suitable functional setting, this problem is known to be well-posed.

To approximate the solution to problem (1), we consider a smooth convex fictitious boundary Σ enclosing the scatterer Ω^-. We set Ω_b as the bounded computational domain delimited by Γ and Σ. We only consider the second-order Bayliss-Gunzburger-Turkel-like (BGT2-like) Artificial Boundary Condition (ABC) derived in [2]. We restrict our attention to this approach to show that the proposed solution is flexible in terms of code implementation even if other truncation techniques like PML could also be used and adapted to the proposed strategy. The BGT2-like ABC on Σ is given by

$$\partial_{\mathbf{n}_\Sigma} u = {\rm div}_\Sigma(A\nabla_\Sigma u) - \beta u, \ \text{ on } \Sigma, \tag{2}$$

where $\mathbf{n}_\Sigma$ designates the outwardly directed unit normal vector to Σ, the operator ${\rm div}_\Sigma$ is the surface divergence of a tangential complex-valued vector field and ∇_Σ is the surface gradient operator of a complex-valued scalar surface field, all these quantities being defined over Σ. Furthermore, the operator A is a complex-valued tensor field and β is a complex-valued scalar function. The variational formulation consists in computing $u \in H^1(\Omega_b)$ such that

$$a(u, v) = \ell(v), \tag{3}$$

for any test-function $v \in H^1(\Omega_b)$. The sesquilinear form $a(\cdot,\cdot)$ is defined by

$$\begin{array}{r} a(u,v) = (\nabla u, \nabla v)_{0,\Omega_b} - k^2 (u,v)_{0,\Omega_b} \\ +(A\nabla_\Sigma u, \nabla_\Sigma v)_{0,\Sigma} + (\beta u, v)_{0,\Sigma}, \end{array} \tag{4}$$

and the linear form ℓ appearing in the right-hand side is: $\ell(v) = -(g, v)_{0,\Gamma}$. We define $(\cdot,\cdot)_{0,D}$ as the hermitian inner product of two complex-valued scalar or vector square-integrable fields u and v of $L^2(D)$, D specifying the integration domain.

The finite element solution consists in introducing a covering Ω_h of Ω_b using some tetrahedrons K: $\Omega_h = \cup_{K\in\mathcal{K}_h} K$, where $\mathcal{K}_h$ designates a triangulation of the domain. The corresponding interpolated boundaries associated with Γ and Σ are respectively denoted by Γ_h and Σ_h. The p-finite element version of (3) yields the discrete formulation: find $u_h \in V_h$ such that

$$a_h(u_h, v_h) = \ell_h(v_h), \tag{5}$$

for any test-function v_h of V_h, setting

$$\begin{aligned} a_h(u_h, v_h) = (\nabla u_h, \nabla v_h)_{0,\Omega_h} - k^2(u_h, v_h)_{0,\Omega_h} + \\ +(A_h \nabla_{\Sigma_h} u_h, \nabla_{\Sigma_h} v_h)_{0,\Sigma_h} + (\beta_h u_h, v_h)_{0,\Sigma_h} \end{aligned} \tag{6}$$

and: $\ell_h(v_h) = -(g_h, v_h)_{0,\Gamma_h}$. The classical finite element space of order p is given by

$$V_h := \{v_h \in \mathcal{C}^0(\overline{\Omega_h}) / v_{h\,|K} \in \mathbb{P}_p(K), \forall K \in \mathcal{K}_h\},$$

where $\mathbb{P}_p$ is the space of polynomials of degree less than or equal to p.

The improved formulation

Our proposed approach can be roughly decomposed into two successive steps

1) an *a priori* determination over the computational domain Ω_b of an approximate phase $\tilde{\phi}$ through the solution $\tilde{u}$ to a one-way wave propagation evolution equation, with initial condition $\tilde{u}_0$ approximating the trace of the field u on Γ; and

2) the calculation of the true solution u through the computation of a slowly varying envelope $\mathbb{A} = e^{-ik\tilde{\phi}}u$, solution to a weak formulation solved by a classical finite element procedure.

The two following subsections explain in detail how to treat efficiently these two points.

Step 1: computing the approximate phase $\tilde{\phi}$

If the obstacle Ω^- was sound-soft instead of sound-hard (i.e., if the Neumann boundary condition on Γ in (1) was replaced with the Dirichlet condition $u = u^{\text{inc}}$), then the construction of the initial condition $\tilde{u}_0$ for the one-way wave propagation evolution equation would be trivial: the exact trace of the field u on Γ being known, we would set $\tilde{u}_0 = u^{\text{inc}}$ on Γ [3].

For the sound-hard obstacle we are interested in here, however, the exact trace of u on Γ is unknown and the construction of $\tilde{u}_0$ relies on the knowledge of the Dirichlet-to-Neumann operator on Γ. In order to efficiently compute an approximation of the trace in the high-frequency regime, our approach is to use the On-Surface Radiation Condition (OSRC) proposed in [4], which, for a given normal derivative trace on Γ, expresses an approximation φ of the exact trace of u through the relation

$$\Lambda\varphi = g, \quad \text{on } \Gamma, \tag{7}$$

where Λ is the pseudo-local OSRC operator given by

$$\Lambda = ik\sqrt{1+X}. \tag{8}$$

Then, we simply set $\tilde{u}_0 = \varphi$. The symmetrical partial differential operator X is: $X = \text{div}_\Gamma(k_\varepsilon^{-2}\nabla_\Gamma\cdot)$, defining the complex wavenumber k_ε by $k_\varepsilon = k + i\varepsilon$, with $\varepsilon = 0.4k^{1/3}\mathcal{H}_\Gamma^{2/3}$, where $\mathcal{H}_\Gamma$ is the mean curvature on Γ. The numerical solution of (7)-(8) can be obtained efficiently through the introduction of complex Padé approximants of the square-root in conjunction with a surface finite element method [4], [5].

Once the surface field $\tilde{u}_0 := \tilde{A}e^{ik\tilde{\phi}}$ is known on Γ, the corresponding surface phase function $\tilde{\phi}$ can be computed. To solve this *phase unwrapping* problem, we consider the known field $\tilde{u}_0$ and differentiate the relation $e^{ik\tilde{\phi}} = \tilde{u}_0/\tilde{A}$, assuming that the surface field is not equal to zero. Taking the real part of the equation, one gets

$$\nabla_\Gamma\tilde{\phi} = \mathbf{F} := \Re\left(\frac{1}{ik}\frac{\tilde{A}}{\tilde{u}_0}\nabla_\Gamma\left(\frac{\tilde{u}_0}{\tilde{A}}\right)\right), \tag{9}$$

where the surface vector field $\mathbf{F}$ is known. If one fixes the value of $\tilde{\phi}$ at an arbitrary surface point $\mathbf{x}^*$ where $\tilde{u}_0$ is non-zero and one takes the surface divergence of equation (9), then a continuous determination of the phase $\tilde{\phi}$ can be computed as the unique solution to the well-posed surface partial differential equation

$$\begin{cases} -\Delta_\Gamma\tilde{\phi} = -\text{div}_\Gamma\mathbf{F}, & \text{on } \Gamma, \\ \tilde{\phi}(\mathbf{x}^*) = \arg\left(\dfrac{\tilde{u}_0(\mathbf{x}^*)}{\tilde{A}(\mathbf{x}^*)}\right). \end{cases} \tag{10}$$

The numerical solution can be easily obtained by a surface finite element method, similarly to the OSRC technique [5].

To extend the phase in the whole computational domain, our approach consists in developing an approximate forward propagating equation according to a privileged direction. This can be done by the application of

microlocal analysis methods. Here, we will only consider the lowest-order approximation

$$\tilde{u}(\mathbf{x}) = \tilde{u}(\mathbf{x}_0)e^{ik||\mathbf{x}-\mathbf{x}_0||}, \tag{11}$$

where $\mathbf{x}$ is an exterior point in the computational domain and $\mathbf{x}_0$ its projection onto Γ (see [3] for the use of a more complex forward propagating technique based on the solution of the Eikonal equation). Since the phase $\tilde{\phi}(\mathbf{x}_0)$ is known at $\mathbf{x}_0$ by the previous step, the phase at point $\mathbf{x}$ of Ω^+ is finally given by

$$\tilde{\phi}(\mathbf{x}) = \tilde{\phi}(\mathbf{x}_0) + ||\mathbf{x} - \mathbf{x}_0||. \tag{12}$$

Step 2: computing the exact solution u through $\mathbb{A}$

In a way similar to what was done in [6] for boundary integral equations, let us use the ansatz $u = \mathbb{A}e^{ik\tilde{\phi}}$, and let us recall that $\tilde{\phi}$ is known from step 1. Then, replacing u by this expression in the weak formulation (4) and taking some test-functions $v = \mathbb{B}e^{ik\tilde{\phi}}$, we obtain the following weak formulation: find $\mathbb{A} \in H^1(\Omega_b)$ such that

$$\mathcal{A}(\mathbb{A}, \mathbb{B}) = \mathcal{L}(\mathbb{B}), \tag{13}$$

for all $\mathbb{B} \in H^1(\Omega_b)$. The sesquilinear form $\mathcal{A}$ is given by

$$\begin{aligned}
&\mathcal{A}(\mathbb{A}, \mathbb{B}) = (\nabla\mathbb{A}, \nabla\mathbb{B})_{0,\Omega_b} \\
&+ik\left((\mathbb{A}\nabla\tilde{\phi}, \nabla\mathbb{B})_{0,\Omega_b} - (\nabla\mathbb{A}, \mathbb{B}\nabla\tilde{\phi})_{0,\Omega_b}\right) \\
&-k^2((1 - ||\nabla\tilde{\phi}||^2)\mathbb{A}, \mathbb{B}))_{0,\Omega_b}(A\nabla_\Sigma\mathbb{A}, \nabla_\Sigma\mathbb{B})_{0,\Sigma} \\
&+ik\left(((A\nabla_\Sigma\tilde{\phi})\mathbb{A}, \nabla_\Sigma\mathbb{B})_{0,\Sigma} - (A\nabla_\Sigma\mathbb{A}, \mathbb{B}\nabla_\Sigma\tilde{\phi})_{0,\Sigma}\right) \\
&+k^2((A\nabla_\Sigma\tilde{\phi}, \nabla_\Sigma\tilde{\phi})\mathbb{A}, \mathbb{B}))_{0,\Sigma} + (\beta\mathbb{A}, \mathbb{B})_{0,\Sigma}
\end{aligned} \tag{14}$$

and the linear form $\mathcal{L}$ by: $\mathcal{L}(\mathbb{B}) = -(f, \mathbb{B})_{0,\Gamma}$, with $f = ge^{-ik\tilde{\phi}}$ and $\tilde{\phi}$ given. Even if the formulation seems complicated at first sight, all the quantities can be however easily obtained through simple assembling procedures available in most finite element codes.

A numerical result

To show the improvement related to our approach, we consider a simple two-dimensional test-case. The computational domain is composed of a circular scatterer with radius $R_0 = 1$ and a fictitious circular boundary Σ with radius $R_1 = 2$. The incident wave is plane. Figure 1 shows the relative $L^2(\Omega_b)$-error over the concentric computational domain according to k for two densities of discretization points per wavelength $n_\lambda = \lambda/h$, using the linear finite element method. We can see that, compared to the classical approach, the new formulation leads to a significant accuracy improvement. More two- and three-dimensional test-cases will be presented during the talk and further numerical results will be discussed.

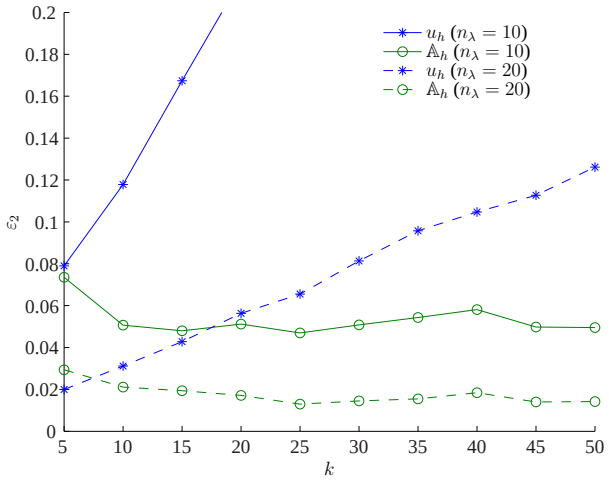

Figure 1: Relative L^2 error ε_2 vs. wavenumber k for the classical (u_h) and improved ($\mathbb{A}_h$) formulations.

References

[1] L. L. Thompson, A review of finite element methods for time-harmonic acoustics, *J. Acoust. Soc. Am.* **119** (3), (2006), pp. 1315-1330.

[2] X. Antoine, H. Barucq and A. Bendali, Bayliss-Turkel-like radiation conditions on surfaces of arbitrary shape, *J. Math. Anal. Appl.* **229** (1999), pp. 184-211.

[3] C. Geuzaine, J. Bedrossian and X. Antoine, An amplitude finite element formulation for scattering problems, *Proceedings of the 16th International Conference on the Computation of Electromagnetic Fields*, Aachen, Germany, June 24-28, 2007.

[4] X. Antoine, M. Darbas and Y.Y. Lu, An improved surface radiation condition for high-frequency acoustic scattering problems, *Comput. Meth. Appl. Mech. Engrg.* **195** (33-36) (2006), pp. 4060-4074.

[5] X. Antoine, Advances in the On-Surface Radiation Condition Method: Theory, Numerics and Applications, Book Chapter for Computational Methods in Acoustics, to appear (2007).

[6] O. Bruno, C. Geuzaine, J. Monro and F. Reitich, Prescribed error tolerances within fixed computational times for scattering problems of arbitrarily high frequency: the convex case, *Phil. Trans. Roy. Soc., A*, **362** (2004), pp. 629–645.

Quantized asymptotics of high frequency oscillations in high contrast media

N. Babych[†,*], **Yu. Golovaty**[‡,*]

[†]University of Bath, Bath, United Kingdom
[‡]Lviv National University, Lviv, Ukraine
[*]Email: n.babych@bath.ac.uk

Abstract

We study stable forms of eigenvibrations for inhomogeneous media consisting of two parts with strongly contrasting stiffness and mass density. In this work we treat a critical case for the *high frequency vibrations*, namely the case when the order of mass density inhomogeneity is the same as the order of stiffness inhomogeneity, with heavier part being softer. Two non-classical effects are discussed, firstly the appearance of limit problem with nonlinear dependance on the spectral parameter and secondary the quantized multi-dimensional WKB or geometrical optics asymptotic expansions of the high frequency resonances.

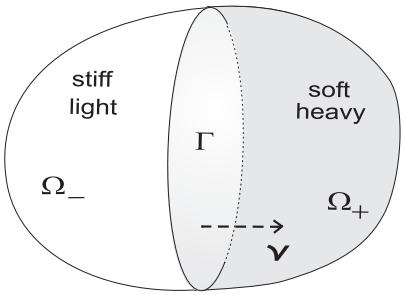

Figure 1: Configuration of the body

Problem statement

Let a soft and heavy body part Ω_+ be complemented by a stiff and relatively light body part Ω_- forming a bounded domain $\Omega = \Omega_- \cup \Gamma \cup \Omega_+$ of $\mathbb{R}^d$, $d \geq 2$, with smooth interface Γ. We assume that domains Ω, Ω_- and Ω_+ have Lipschitz boundaries. For the sake of simplicity the surfaces $\partial\Omega$ and Γ are supposed to intersect at the right angle. We consider stiffness K_ε and mass density R_ε of the form

$$K_\varepsilon = \begin{cases} k(x), & x \in \Omega_- \\ \varepsilon\kappa(x), & x \in \Omega_+ \end{cases} \qquad R_\varepsilon = \begin{cases} \varepsilon r(x), & x \in \Omega_- \\ \rho(x), & x \in \Omega_+ \end{cases}$$

with all functions being positive and smooth in the closures $\overline{\Omega}_-$ and $\overline{\Omega}_+$ respectively. We consider body configuration such that $\partial\Omega \cap \partial\Omega_\pm \neq \emptyset$ (see Figure 1). Let ν be the unit normal to Γ. We assume that eigenvibrations of the body are described by the self-adjoint eigenvalue problem

$$-\mathrm{div}\,(K_\varepsilon(x)\nabla u^\varepsilon) = \lambda^\varepsilon R_\varepsilon(x) u^\varepsilon, \quad x \in \Omega, \qquad (1)$$

$$u^\varepsilon\big|_{\partial\Omega} = 0, \qquad (2)$$

understood in the weak sense, i.e. implying the following interface conditions on Γ

$$u^\varepsilon_-\big|_\Gamma = u^\varepsilon_+\big|_\Gamma, \quad k\frac{\partial u^\varepsilon_-}{\partial\nu}\Big|_\Gamma = \varepsilon\kappa\frac{\partial u^\varepsilon_+}{\partial\nu}\Big|_\Gamma. \qquad (3)$$

The inferior indices $-$ and $+$ denote the restrictions of a function defined in Ω to the subdomains Ω_- and Ω_+.

We investigate the question how the eigenvibrations of the media, namely eigenvalues λ^ε and eigenfunctions u^ε, change if the parameter ε tends to 0. More precisely, we are looking for the stable forms of eigenvibrations, namely for the sequences of pairs λ^ε and appropriately normalized u^ε with non-trivial limits as $\varepsilon \to 0$.

Low frequencies

Elastic problems with simultaneous perturbations of stiffness and mass density, either with other geometries or at different perturbation rates, were studied in [1–3].

It is well-known that for each fixed $\varepsilon > 0$ the spectrum of problem (1)-(3) is real and discrete, consisting of eigenvalues with finite multiplicity that form a sequence $0 < \lambda^\varepsilon_1 < \lambda^\varepsilon_2 \leq \cdots \leq \lambda^\varepsilon_n < \cdots \to \infty$ as $n \to \infty$. The corresponding eigenfunctions $\{u^\varepsilon_n\}_{n=1}^\infty$ form an orthogonal basis in the weighted real L_2-space with the scalar product

$$(\phi,\psi)_\varepsilon = \varepsilon\int_{\Omega_-} r(x)\phi\,\psi\,dx + \int_{\Omega_+}\rho(x)\phi\,\psi\,dx.$$

Moreover, for each number n the eigenvalue branch λ^ε_n is a continuous function of $\varepsilon \in (0,1)$ such that $\lambda^\varepsilon_n \leq c_n\varepsilon$ with positive constant c_n independent of ε.

Studying asymptotic behaviour as $\varepsilon \to 0$ of each eigenvalue branch λ^ε_n with fixed number n and corresponding eigenfunctions u^ε_n (appropriately normalized), we imme-

diately have the convergence

$$\varepsilon^{-1}\lambda_n^\varepsilon \to \lambda_n, \quad u_n^\varepsilon \to \begin{cases} 0 & \text{in} \quad \Omega_- \\ v_n & \text{in} \quad \Omega_+ \end{cases} \qquad \text{as} \quad \varepsilon \to 0,$$

where λ_n is an eigenvalue and v_n is the corresponding eigenfunction of the limit problem

$$-\text{div}\,(\kappa(x)\nabla v) = \lambda\rho(x)v \quad \text{in} \quad \Omega_+, \quad u^\varepsilon\big|_{\partial\Omega_+} = 0.$$

The asymptotic expansions in power series of ε for the eigenelements λ_n^ε and u_n^ε could be constructed and justified by a standard procedure. Since each eigenvalue tends to zero as $\varepsilon \to 0$, the corresponding eigenvibrations are referred to as low frequency vibrations. Nevertheless, the convergence to the limits is not uniform with respect to number n. Moreover, all low frequency vibrations vanish in Ω_- as $\varepsilon \to 0$. This naturally poses the question on the possibility of constructing other non-trivial limits of eigenvibrations addressed next.

High frequencies. Discussion and results

Since the asymptotics of eigenelements with fixed number n leads immediately to the low frequencies, the only other non-trivial stable forms of vibrations could be found among eigenfunctions $u^\varepsilon_{n(\varepsilon)}$ with numbers $n(\varepsilon) \to \infty$. Also, similarly to [4], these *high frequency vibrations* have a discrete dependence on ε (see Figure 2).

We hence construct certain sequences of small parameter $\varepsilon_r \to 0$ such that at certain energy levels

$$\lambda_\varepsilon := \lambda^{\varepsilon_r}_{n(\varepsilon_r)} \sim \varepsilon^{-1}\mu + \mu_1 \tag{4}$$

the corresponding eigenfunctions $u_\varepsilon := u^{\varepsilon_r}_{n(\varepsilon_r)}$ with unit norm in $L_2(\Omega)$ converge weakly in $L_2(\Omega)$ to functions of the form

$$U = \begin{cases} w & \text{in} \quad \Omega_-, \\ 0 & \text{in} \quad \Omega_+. \end{cases}$$

We have to mention that the asymptotic expansions for high frequency eigenelements are constructed under certain strong additional restrictions. Using the WKB-expansions we require Ω_+ to be the tube of rays with the base Γ for the corresponding eikonal equation (see Figure 3 and the next section for the specification). The tube of rays is supposed to be free from the focal points.

The high frequency levels μ and corresponding limit forms of vibrations w are described by a family of the following problems, parametrized by $\delta \in [0, \pi)$ in the boundary condition,

$$-\text{div}\,(k(x)\nabla w) = \mu r(x) w, \quad x \in \Omega_-, \tag{5}$$

$$w\big|_{\partial\Omega_-\cap\partial\Omega} = 0, \tag{6}$$

$$\sqrt{\mu\kappa\rho}w\big|_\Gamma \cos\delta + k\tfrac{\partial w}{\partial\nu}\big|_\Gamma \sin\delta = 0, \ \delta \in [0,\pi). \tag{7}$$

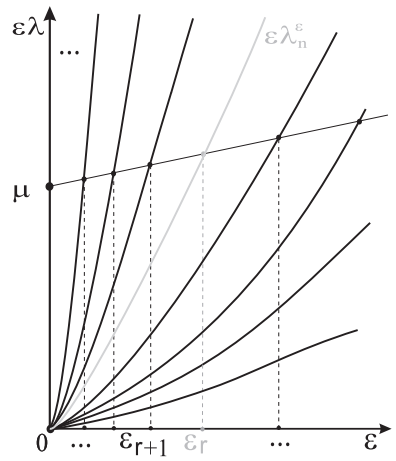

Figure 2: High frequencies: eigenvalues

Notice that (5) – (7) have a non-linear dependence on the spectral parameter μ. In the space

$$H_*(\Omega_-) = \{\phi \in H^2(\Omega_-): \quad \phi|_{\partial\Omega_-\cap\partial\Omega} = 0\}$$

the family of problems (5) – (7) admits variational formulation

$$\int_{\Omega_-} k\nabla w\nabla\phi\,dx + \sqrt{\mu}\,\text{cotan}\,\delta \int_\Gamma \sqrt{\kappa\rho}\,w\phi\,d\gamma = \mu\int_{\Omega_-} r\,w\phi\,dx, \quad \forall\phi \in H_*(\Omega_-). \tag{8}$$

It can be shown that the union of spectra for problems (5) – (7) contains all the positive real semi-axis. Namely, for any positive μ_0 there exists $\delta_0 \in [0,\pi)$ with a non-zero eigenfunction $w \in H_*(\Omega_-)$ satisfying (8) for all $\phi \in H_*(\Omega_-)$ with $\delta = \delta_0$ and $\mu = \mu_0$. The distinguishing feature of this result is that the high frequency levels μ which we can approach by the eigenelements λ_ε with non-trivial limits of u_ε fill in the continuum set $\mathbb{R}_+$ (contrary to e.g. the discrete spectrum for the high frequency limits in the purely stiff problem [4]).

Asymptotic expansions

Under the above assumptions we construct asymptotic expansions of high frequency eigenelements using combination of the power series technique and WKB-approximations, namely

$$\begin{aligned} \lambda_\varepsilon &\sim \mu\varepsilon^{-1} + \mu_1 + \dots + \mu_j\varepsilon^{j-1} + \dots \\ u_\varepsilon &\sim \begin{cases} \sum\limits_{j=0}^{\infty} w_j(x)\varepsilon^j, & \Omega_- \\ \sum\limits_{j=0}^{\infty} \langle a_j(x), N\Big(\frac{S(x)}{\varepsilon}\Big)\rangle\varepsilon^j, & \Omega_+ \end{cases} \end{aligned} \tag{9}$$

where $\langle\cdot,\cdot\rangle$ denotes a scalar product in $\mathbb{R}^2$,

$$N(\tau) = (\cos\tau, \sin\tau)$$

and the phase function $S = \sqrt{\mu}S_0$ with S_0 being a solution of eikonal equation $c(x)|\nabla S_0(x)|^2 = 1$ in Ω_+ with $c(x) = \kappa(x)\rho(x)^{-1}$. Our geometrical assumptions, which were mentioned above, could be explained now more specifically. We suppose Γ to be a wave front that is to say the vector field ∇S_0 changes in the orthogonal to Γ direction. Further the wave front moves along rays that are projections of bicharacteristics to the coordinate space. Finally, the front comes to $\partial\Omega$ simultaneously along the rays as follows. Namely, first we solve the Hamilton system for $H(x,p) = c(x)|p|^2 - 1$,

$$\frac{dx_\xi}{dt} = 2c(x)p_\xi, \quad \frac{dp_\xi}{dt} = -|p_\xi|^2\nabla c(x)$$

with the initial conditions

$$x_\xi(0) = \xi \in \Gamma, \quad p_\xi(0) = c(x)^{-1/2}\nu.$$

Let for $t \in (0,h)$ the rays $x_\xi(t)$ do not intersect (for all $\xi \in \Gamma$). Then we formalize all our geometrical assumptions to the requirement

$$\Omega_+ = \{x \in \mathbb{R}^d | \quad x = x_\xi(t), \quad t \in (0,h), \quad \xi \in \Gamma\}.$$

In particular, if smooth Γ coincides with $\partial\Omega_-$ then Ω_+ is a "shell" surrounding Ω_- and $\partial\Omega$ is an equidistant surface relative to Γ in the metric $c(x)^{-1/2}|dx|$.

Finally, we fix the phase function $S_0(x_\xi(t)) = 2(t-h)$. Hence, we consider short-wave asymptotic expansions (9) along the rays x_ξ. The specifics of such approach lies in peculiar boundary conditions that have to be satisfied after the transport equations for the coefficients $a_j(x_\xi)$ are solved. In particular, according to the transport equations the leading terms transform to the form

$$\langle a_0, N(\varepsilon^{-1}S)\rangle = \alpha\langle\beta_0, N(\gamma_\varepsilon S_0)\rangle,$$

where $\alpha = J^{-1/2}(\rho\kappa)^{-1/4}$ depends on the geometrical spreading $J(t,\xi) = \det\frac{\partial x_\xi(t)}{\partial(t,\xi)} > 0$, $\gamma_\varepsilon = \frac{\sqrt{\mu}}{\varepsilon} + \frac{\mu_1}{2\sqrt{\mu}}$, $\beta_0 \in \mathbb{R}^2$ is an arbitrary constant vector.

Then transmission conditions (3) imply

$$\begin{array}{rcl} \alpha\langle\beta_0, N(\gamma_\varepsilon S_0)\rangle|_\Gamma & = & w_0|_\Gamma, \\ \sqrt{\mu\rho\kappa}\alpha\langle\beta_0, N'(\gamma_\varepsilon S_0)\rangle|_\Gamma & = & k\frac{\partial w_0}{\partial\nu}|_\Gamma. \end{array} \qquad (10)$$

Since according to our assumptions $S_0(\xi) = -2h$ does not depend on $\xi \in \Gamma$, relations (10) are satisfied after the quantization $2h\gamma_\varepsilon = \delta + 2\pi r$, $r \in \mathbb{N}$. The latter fixes the sequence of small parameter

$$\varepsilon_r = \frac{2h\sqrt{\mu}}{\delta + 2\pi r - h\mu_1/\sqrt{\mu}}, \quad r \in \mathbb{N},$$

for each selected direction $\varepsilon^{-1}\mu + \mu_1$ of asymptotics (4) for λ_ε. Moreover, (2) gives $\beta_{0,1} = 0$ and then (10) implies (7), which depends on μ nonlinearly. For the chosen asymptotic direction characterized by μ and μ_1 with simple eigenvalue μ of (5) – (7) we construct on this way complete asymptotic expansions for the above selected series of λ_ε and u_ε.

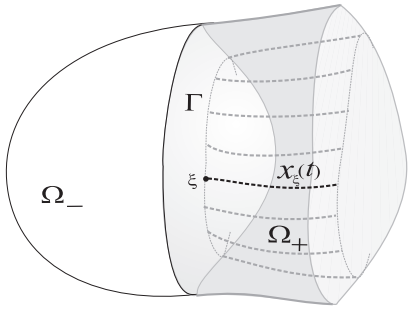

Figure 3: Tube of rays

Acknowledgements

The authors are grateful to V.P. Smyshlyaev and I.V. Kamotski for the helpful discussions.

References

[1] J. Sanchez Hubert , E. Sanchez Palencia, Vibration and coupling of continuous systems. Asymptotic methods, Berlin etc.: Springer-Verlag. xv, 1989.

[2] N. Babych, Yu. Golovaty, "Asymptotic analysis of vibrating system containing stiff-heavy and flexible-light parts", Submitted to Nonlinear boundary problem.

[3] D. Gomez, M. Lobo, S. Nazarov, E. Perez, "Spectral stiff problems in domains surrounded by thin bands: Asymptotic and uniform estimates for eigenvalues", J. Math. Pures Appl. 85 (2006), pp. 598-632.

[4] Yu. Golovaty , N. Babych, "On WKB asymptotic expansions of high frequency vibrations in stiff problems", in Proceedings of the Conference Equadiff '99, Berlin 1999. Singapore: World Scientific. Vol. 1: 103-105, 2000.

RAPID SOLUTION OF THE WAVE EQUATION IN UNBOUNDED DOMAINS: ABRIDGED VERSION

L. Banjai[†,*], **S. Sauter**[‡,*]
[*]Mathematical Institute, University of Zürich, Switzerland
Email: [†]lehelb@math.unizh.ch, [‡] stas@math.unizh.ch

Abstract

We propose and analyze a new fast method for the numerical solution of time-domain boundary integral formulations of the wave equation. Discretization in time is achieved by Lubich's convolution quadrature method and in space by a Galerkin boundary element method. We show that the arising block Toeplitz system is after a small perturbation equivalent to a a decoupled system of discretized Helmholtz equations. Each of these systems can efficiently be solved by a fast data-sparse method (e.g. FMM, panel clustering). Further savings can be achieved by noticing that in some cases the solutions of many of the Helmholtz problems can be replaced by zero. Finally the proposed method is inherently parallel.

We prove that the excellent stability and optimal convergence of the convolution quadrature are inherited by the new method. These results thereby pave the way to the efficient solution using fast data-sparse techniques.

1 Introduction

Boundary value problems governed by the wave equation arise in many physical applications such as electromagnetic wave propagation or the computation of transient acoustic waves. Since such problems are typically formulated in unbounded domains, the method of integral equations is an elegant tool to transform this partial differential equation to an integral equation on the bounded surface of the scatterer.

In this paper we represent the solution of the wave equation as a single layer potential thereby arriving at a boundary integral formulation of the problem. For disretisation we employ the convolution quadrature method in time [5], [6] and a Galerkin boundary element method in space.

The coefficient matrix in the arising system of linear equations is a block-triangular Toeplitz matrix consisting of N blocks of dimension $M \times M$, where N denotes the number of time steps and M is the number of spatial degrees of freedom. Due to the non-localness of the arising boundary integral operators, the $M \times M$ matrix blocks are densely populated.

In the literature, there exist (at least) two alternatives to solve this system efficiently. In [3], an FFT-technique is employed which makes use of the Toeplitz structure of the system matrix and the computational complexity is reduced to $\mathcal{O}\left(M^2 N \log^2 N\right)$, while the storage complexity stays at $\mathcal{O}\left(M^2 N\right)$. In [2], [4] the $M \times M$ block matrices are approximated by data sparse representations based on a cutoff and panel-clustering strategy. This leads to a significant reduction of the storage complexity while the computational complexity is reduced compared to the naive approach (cost: $\mathcal{O}\left(N^2 M^2\right)$) but increased compared to the FFT approach.

In this paper, we will propose a third approach which combines the advantages of the FFT-technique with the data sparse approximation: The block Toeplitz system is transformed to a decoupled system of discretized Helmholtz problems which can then be efficiently solved by fast data sparse approximations. Thereby we reduce *both* the storage and complexity estimates to $\mathcal{O}(MN \log^a N)$, for a small $a \geq 1$. A full version of the paper [1], where all the results stated here are proved, is in preparation.

2 Integral formulation of the wave equation

Let $\Omega \subset \mathbb{R}^3$ be a Lipschitz domain with boundary Γ. We consider the homogeneous wave equation

$$\partial_t^2 u = \Delta u \qquad \text{in } \Omega \times (0,T) \tag{1 a}$$

$$u(\cdot,0) = \partial_t u(\cdot,0) = 0 \qquad \text{in } \Omega \tag{1 b}$$

$$u = g \quad \text{on } \Gamma \times (0,T) \tag{1 c}$$

on a time interval $(0,T)$ for some $T > 0$. For its solution, we employ an ansatz as a *single layer potential*

$$u(x,t) = \int_0^t \int_\Gamma k(x-y, t-\tau)\phi(y,\tau) d\Gamma_y d\tau \tag{2}$$

for $(x,t) \in \Omega \times (0,T)$ and where $k(z,t)$ is the fundamental solution of the wave equation,

$$k(z,t) = \frac{\delta(t - \|z\|)}{4\pi\|z\|}, \tag{3}$$

$\delta(t)$ being the Dirac delta distribution. The ansatz (2) satisfies the homogeneous equation (1 a) and the initial conditions (1 b). The extension $x \to \Gamma$ is continuous and hence, the unknown density ϕ in (2) is determined via the

boundary condition (1 c), $u(x,t) = g(x,t)$. This results in the boundary integral equation for ϕ,

$$\int_0^t \int_\Gamma k(x-y, t-\tau)\phi(y,\tau) d\Gamma_y d\tau = g(x,t) \qquad (4)$$

for all $(x,t) \in \Gamma \times (0,T)$.

3 Time and space discretisation

For the time discretisation, we employ the convolution quadrature approach which has been developed by Lubich in [5], [6]

We split the time interval $[0,T]$ into $N+1$ time steps of equal length $\Delta t = T/N$ and compute an approximate solution at the discrete time levels $t_n = n\Delta t$. The continuous convolution operator is replaced by a discrete convolution operator, and the resulting semi-discrete problem is given by

$$\sum_{j=0}^{n} \int_\Gamma \omega_{n-j}^{\Delta t}(\|x-y\|)\phi_{\Delta t,j}(y) d\Gamma_y = g(x,t_n), \qquad (5)$$

for all $n = 1, \ldots, N, \quad x \in \Gamma$.

If the time discretisation is related to a multistep method defined by its generating polynomial $\gamma(\zeta)$ (see [5]) the kernel functions $\omega_n^{\Delta t}(d)$ are implicitly defined by

$$\hat{k}\left(d, \frac{\gamma(\zeta)}{\Delta t}\right) = \sum_{n=0}^{\infty} \omega_n^{\Delta t}(d)\zeta^n.$$

Here, $\hat{k}$ denotes the Laplace transform of the original kernel $\hat{k}(d,s) = \frac{e^{-sd}}{4\pi d}$. For the rest of this paper we consider the BDF2 multistep method defined by $\gamma(\zeta) = \frac{1}{2}(\zeta-1)(\zeta-3)$.

For the space discretisation, we employ a standard Galerkin boundary element method. The space of piecewise constant, discontinuous functions is denoted by $S_{-1,0}$ and the space of continuous, piecewise linear functions by $S_{0,1}$ The general notation is S for the boundary element space and $(b_m)_{m=1}^M$ for the basis. The mesh width is denoted by h. For the space-time discrete solution at time t_n we employ the ansatz

$$\phi_{\Delta t,h,n}(y) = \sum_{m=1}^{M} \phi_{n,m} b_m(y)\,, \qquad (6)$$

where $(\phi_{n,m})_{m=1}^M \in \mathbb{R}^M$ are the nodal values of the discrete solution at time step t_n.

We impose the integral equation not pointwise but in a weak form: Find $\phi_{\Delta t,h,n} \in S$ of the form (6) such that

$$\sum_{j=0}^{n}\sum_{m=1}^{M} \phi_{j,m} \int_\Gamma \int_\Gamma \omega_{n-j}^{\Delta t}(x-y) b_m(y) b_k(x) d\Gamma_y d\Gamma_x = \int_\Gamma g(x,t_n) b_k(x) d\Gamma_x \quad (7)$$

for all $1 \le k \le M$ and $n = 1, \ldots, N$. This can be written as a linear system

$$\sum_{j=0}^{n} \mathbf{A}_{n-j}\phi_{j,\star} = \mathbf{g}_{n,\star}\,, \qquad n = 0, \ldots, N\,, \qquad (8)$$

with

$$(\mathbf{A}_n)_{k,m} := \int_\Gamma \int_\Gamma \omega_n^{\Delta t}(x-y) b_m(y) b_k(x) d\Gamma_y d\Gamma_x\,,$$

and

$$\mathbf{g}_{n,\star} = \left(\int_\Gamma g(x,t_n) b_k(x) d\Gamma_x\right)_{k=1}^{M}.$$

4 Transformation to a decoupled system of Helmholtz problems

Let us define $\omega_n^{\Delta t} := 0$ for $n = -N, -N+1, \ldots, -1$. With this definition we can extend the sum in (7) to $j = 0, 1, \ldots, N$ to obtain

$$\sum_{j=0}^{N}\sum_{m=1}^{M} \phi_{j,m} \int_\Gamma \int_\Gamma \omega_{n-j}^{\Delta t}(x-y) b_m(y) b_k(x) d\Gamma_y d\Gamma_x = \int_\Gamma g_{\Delta t,n}(x) b_k(x) d\Gamma_x. \quad (9)$$

The next step in our method is to replace each $\omega_n^{\Delta t}$ by the trapezoid rule approximation of the Cauchy integral representation. The details and an error estimate are given in the following proposition. For clearer exposition we introduce some extra notation. Let $\zeta_{N+1} := \exp(-2\pi i/(N+1))$ and $\kappa_l := i\gamma(\lambda\zeta_{N+1}^l)/\Delta t$. Then we notice that

$$\hat{k}(\|x-y\|, \gamma(\lambda\zeta_{N+1}^l)/\Delta t) = G_{\kappa_l}(\|x-y\|),$$

where $G_\kappa(\cdot)$ is the fundamental solution of the Helmholtz operator $\Delta + \kappa^2 \cdot$:

$$G_\kappa(d) = \frac{e^{i\kappa d}}{4\pi d}.$$

Proposition 4.1 *Let $N \in \mathbb{N}$, $d > 0$, $\Delta t = T/N$, and $\lambda < e^{-\Delta t}$ be given. There exists a constant $C > 0$ independent of the parameters such that, for $-N \le j \le N$,*

$$|\omega_j^{\Delta t}(d) - \frac{\lambda^{-j}}{N+1} \sum_{l=0}^{N} G_{\kappa_l}(d)\zeta_{N+1}^{-lj}| \le Ce^{2T}\frac{\lambda^{N+1}}{d}.$$

Substituting the above approximation in to (9) we obtain a new system

$$\frac{\lambda^n}{N+1} \sum_{l=0}^{N} \left(\hat{A}_l\, \hat{\phi}_{l,\star}\right)_k \zeta_{N+1}^{-nl} = \int_\Gamma g(x,t_n) b_k(x) d\Gamma_x,$$

where

$$\hat{\phi}_{l,\star} := \sum_{j=0}^{N} \lambda^j \tilde{\phi}_{j,\star} \zeta_{N+1}^{lj}$$

and

$$(\hat{A}_l)_{k,m} = \int_\Gamma \int_\Gamma G_{\kappa_l}(\|x-y\|) b_m(y) b_k(x) d\Gamma_y d\Gamma_x.$$

Note that the unknowns (in the time domain) of the above systems are denoted by $\tilde{\phi}_{j,m}$. The approximation $\tilde{\phi}_{\Delta,h,n} \in S$ at time t_n is then given analogously to (6) Now, notice that if we take the Fourier transform of both sides we obtain $N+1$ decoupled problems:

$$\hat{A}_l \hat{\phi}_{l,\star} = \int_\Gamma \hat{g}_{\Delta t,l}(x) b_\star(x) d\Gamma_x, \tag{10}$$

where

$$\hat{g}_{\Delta t,l}(x) = \sum_{n=0}^{N} \lambda^n g_(x,t_n) \zeta_{N+1}^{ln}.$$

Therefore we have indeed reduced the problem of solving numerically the wave equation to a system of Helmholtz problems with wavenumbers κ_l, $l = 0, 1, \ldots N$.

The stability and convergence of the new method can be derived using the techniques developed in [6] and [2].

Theorem 4.2 *Let g be sufficiently compatible and smooth (see [6]) and let $S = S_{m-1,m}$ for $m \in \{0,1\}$. Then if $\lambda^{N+1} \le Ch\Delta t^8$, the solution $\tilde{\phi}_{\Delta t,h,n}$ exists and satisfies the error estimate*

$$\|\tilde{\phi}_{\Delta t,h,n} - \phi(\cdot,t_n)\|_{H^{-1/2}(\Gamma)} \le C_g(\Delta t^2 + h^{m+3/2}),$$

where C depends on T and C_g depends on the right-hand side g.

5 Fast solution of the decoupled systems

To solve the N dense systems from the previous section, fast methods (e.g. FMM, panel clustering) designed for high-frequency Helmholtz problems (see e.g. [7]), can be applied. In these methods dense sub-blocks of the matrix are replaced by data-sparse (e.g. low rank) matrix approximations. It is then possible to solve each dense $M \times M$ system (10) in $\mathcal{O}(M \log^a M)$, for some small $a \ge 0$, time and storage complexity. The conditions on the error introduced so that the stability and optimal convergence is preserved are developed in [1].

To reduce the costs even further we notice that if $\partial_t^r g(x,0) = \partial_t^r g(x,T) = 0$, for $r = 0, 1, \ldots R$ (corresponding to a smooth, time limited incoming signal) only $\mathcal{O}(N^{3/R})$ systems need to be solved (see [1]). In fact if $\partial_t^r g(x,0) = \partial_t^r g(x,T) = 0$, for all $r \ge 0$ then we expect to only have to solve $O(\log N)$ systems. For supporting numerical evidence see [1].

References

[1] L. Banjai and S. Sauter. "Rapid solution of the wave equation in unbounded domains", *In preparation*, 2007.

[2] W. Hackbusch, W. Kress, and S. Sauter. "Sparse convolution quadrature for time domain boundary integral formulations of the wave equation", Technical Report 116, MPI for Mathematics in the Sciences, Leipzig, 2005.

[3] E. Hairer, C. Lubich, and M. Schlichte. "Fast numerical solution of nonlinear Volterra convolution equations", SIAM J. Sci. Stat. Comput., 6(3):532–541, 1985.

[4] W. Kress and S. Sauter. "Numerical treatment of retarded boundary integral equations by sparse panel clustering", Technical Report 17-2006, Universität Zürich, 2006.

[5] C. Lubich. "Convolution quadrature and discretized operational calculus I", Numer. Math., 52:129–145, 1988.

[6] C. Lubich. "On the multistep time discretization of linear initial-boundary value problems and their boundary integral equations", Numer. Math., 67:365–389, 1994.

[7] V. Rokhlin. "Diagonal forms of translation operators for the Helmholtz equation in three dimensions", Appl. Comput. Harmon. Anal.,1:82–93, 1993.

KRYLOV SUBSPACE BASED ACCELERATION STRATEGIES FOR THE SOLUTION OF HIGH-FREQUENCY MULTIPLE SCATTERING PROBLEMS

Y. Boubendir[†], **F. Ecevit**[‡,*], **F. Reitich**[†]
[†]School of Mathematics, University of Minnesota, Minnepolis, MN 55455, USA
[‡]Max Planck Institute for Mathematics in the Sciences, 04103 Leipzig, Germany
[*]Email: ecevit@mis.mpg.de

Abstract

A recently developed integral equation method can deliver scattering returns with prescribed error tolerances in fixed computational times for single-scattering problems of arbitrarily high frequency. To encompass multiple-scattering effects while preserving a frequency independent operation count, recent extensions of the approach are based on a spectrally convergent Neumann series to decompose the overall scattering return into a superposition of single-scattering contributions. For cases wherein the series is slowly convergent, these implementations have relied on analytic continuation mechanisms (Padé approximation) to reduce the number of iterations necessary to reach a prescribed error tolerance. Here, we present a new Krylov-subspace method that provides a further significant reduction in the number of iterations while still retaining the frequency-independent computational cost.

Introduction

Oscillatory problems, such as those that arise in connection with acoustic, elastic or electromagnetic simulations, have provided significant impetus to the design of advanced numerical algorithms for decades and particularly over the last twenty years. As a result, an array of sophisticated simulation schemes (based on e.g. finite elements, finite differences, multi-resolution analyses or boundary integral equations) have been devised to efficiently tackle these applications. Today, such algorithms enable the virtual analysis of large practical configurations that may span up to a few hundred wavelengths. The very nature of these approaches, however, limits their applicability at higher frequencies since the numerical resolution of field oscillations translates to a commensurately higher number of degrees of freedom and this, in turn, can easily lead to impractical computational times.

A recently developed scattering simulator (based on the *rigorous* solution of integral equation formulations which incorporate asymptotic phase information), on the other hand, has demonstrated the capability of delivering solutions in prescribed error tolerances within fixed computational times for single-scattering problems of arbitrarily high frequency [1]. To encompass multiple-scattering effects, recent extensions of the approach are based on the iterated evaluation of a suitable Neumann series that reduces the overall problem to a sequence of single-scattering events. This series converges spectrally, with a rate that can be asymptotically determined; see [2–4]. As such it is amenable to acceleration via Padé approximation, and use of this latter technique can be shown to provide a substantial reduction in the number of iterations to reach a prescribed tolerance. Here, we present a new Krylov-subspace method that provides a further significant reduction in the number of iterations while still retaining the frequency-independent operation count.

High-frequency Multiple Scattering Formulation

For simplicity of presentation, we consider here the (exterior) sound soft acoustic scattering problem from a bounded obstacle $K \subset R^n$ $(n = 2, 3)$

$$\begin{cases} \Delta u(x) + k^2 u(x) = 0, & x \in R^n \backslash \overline{K}, \\ u(x) = -u^{\mathrm{inc}}(x) = -e^{ik\alpha\cdot x}, & x \in \partial K, \\ \lim\limits_{|x|\to\infty} |x|^{(n-1)/2} \left[\left(\frac{x}{|x|}, \nabla u(x) \right) - iku(x) \right] = 0 \end{cases}$$

and recall that its solution can be recast, through the use of Green's identities, in the form of an integral equation

$$\eta(x) - \int_{\partial K} \frac{\partial G(x,y)}{\partial \nu(x)} \, \eta(y) \, ds(y) = 2 \, \frac{\partial u^{inc}(x)}{\partial \nu(x)} \qquad (1)$$

for the (unknown) *physical* quantity η (normal velocity of the total field in acoustics) confined to the scattering surface ∂K where $G = -2\Phi$ and Φ is the outgoing fundamental solution to the Helmholtz equation. When the scatterer is composed of several (disjoint) substructures $K = \cup\{K_\sigma : \sigma \in \mathcal{I}\}$, equation (1) can be written as

$$(I - R)\eta = f \qquad (2)$$

where $f = [f_{\sigma_1}, \ldots, f_{\sigma_{|\mathcal{I}|}}]^t$, $f_\sigma = 2\partial u^{inc}/\partial\nu|_{\partial K_\sigma}$, $\eta = [\eta_{\sigma_1}, \ldots, \eta_{\sigma_{|\mathcal{I}|}}]^t$, $\eta_\sigma = \eta|_{\partial K_\sigma}$ and the operator R is defined for $x \in \partial K_\sigma$ as

$$(R_{\sigma\tau}\eta_\tau)(x) = \int_{\partial K_\tau} \frac{\partial G(x,y)}{\partial \nu(x)} \, \eta_\tau(y) \, ds(y) \, .$$

Inverting the diagonal part of the equation in (2) yields

$$(I - T)\eta = g \tag{3}$$

where $g_\sigma = (I - R_{\sigma\sigma})^{-1} f_\sigma$, $T_{\sigma\tau} = (I - R_{\sigma\sigma})^{-1} R_{\sigma\tau}\delta_{\sigma\tau}$ and δ is the Kronecker symbol. Considering the series solution to (3)

$$\eta = \sum_{m=0}^{\infty} \eta^m = \sum_{m=0}^{\infty} T^m g\,,$$

we note that

$$\eta^m\big|_{K_{\sigma_m}} = \sum_{\substack{\sigma_0,\ldots,\sigma_{m-1}\in\mathcal{I} \\ \sigma_j\neq\sigma_{j-1}}} T_{\sigma_m\sigma_{m-1}} T_{\sigma_{m-1}\sigma_{m-2}} \cdots T_{\sigma_1\sigma_0} g_{\sigma_0}\,, \tag{4}$$

for each $\sigma_m \in \mathcal{I}$, and each summand in (4) corresponds, in the limit of infinite frequency, to a group of rays that reflect through $\partial K_{\sigma_0}, \ldots, \partial K_{\sigma_{m-1}}$ and arrive at ∂K_{σ_m}. Thus the phase $\varphi_m(x)$, for $x \in \partial K_{\sigma_m}$, of the corresponding summand can be evaluated a priori as

$$\varphi_m(x) = \alpha \cdot x^{m,0}(x) + \sum_{j=0}^{m-1} |x^{m,j+1}(x) - x^{m,j}(x)|$$

where the points

$$(x^{m,0}(x), \ldots, x^{m,m-1}(x)) \in \partial K_{\sigma_0} \times \cdots \times \partial K_{\sigma_{m-1}}$$

satisfy the law of reflection throughout to finally arrive at $x^{m,m}(x) := x \in \partial K_{\sigma_m}$. Knowledge of the phases φ_m, in turn, allows for their extraction in the recursive application of the operators $T_{\sigma\tau}$ and thus for the fast, frequency independent, evaluation of the latter. In more detail, for a given sequence $\{\sigma_m\}_{m\geq 0} \subset \mathcal{I}$ with $\sigma_m \neq \sigma_{m+1}$, letting

$$\eta_0 = g_{\sigma_0} \quad \text{and} \quad \eta_m = T_{\sigma_m\sigma_{m-1}}\eta_{m-1}\,,\ (m \geq 1)$$

we have $\eta_m = \eta_m^{\text{slow}} e^{ik\varphi_m}$, and thus

$$\eta_m^{\text{slow}} - e^{-ik\varphi_m} R_{\sigma_m\sigma_m}(e^{ik\varphi_m}\eta_m^{\text{slow}}) = F^{\text{slow}} \tag{5}$$

where

$$F^{\text{slow}} e^{ik\varphi_m} = R_{\sigma_m\sigma_{m-1}}(e^{ik\varphi_{m-1}}\eta_{m-1}^{\text{slow}})$$

is twice the normal velocity of the field scattered off $\partial K_{\tau_{m-1}}$ evaluated on ∂K_σ. In the form (5) the advantages of the formulation become rather clear, as it entails only discretizations of slow modulations and integrations that can be localized to the neighborhood of critical points; see [2, 5].

Enhanced Convergence by Analytic Continuation

As has recently been shown (see [2–4]), within the context of several interacting convex structures, the (spectral) convergence of the Neumann series is governed by the underlying geometrical configuration. More precisely, considering for simplicity the case of two cylindrical convex structures K_1 and K_2, the (high-frequency) rate of convergence of the Neumann series is given, asymptotically as $k \to \infty$, by

$$\mathcal{R}_k = e^{2ikd}\left(\sqrt{r} + \sqrt{r-1}\right)^{-1} \tag{6}$$

where $d = \operatorname{dist}(K_1, K_2)$, $r = (1 + d\kappa_1)(1 + d\kappa_2)$ and κ_j are the curvatures at the distance minimizing points. The spectral rate in (6) suggests that, as long as $r > 1$, the series can be interpreted as a power series in an artificial parameter z evaluated at $z = 1$. At high-frequencies, the radius of convergence of this series will thus be limited (it will approach R_k^{-1}) but its convergence can be enhanced via classical Padé approximation; see [5].

A New Krylov-subspace Based Acceleration Strategy

Although, as shown in [5] (see also Figure 1), the use of Padé approximation significantly accelerates the convergence of multiple scattering iterations, it is not optimal from this perspective. In the present context, a most relevant property of the Padé approximants relates to the possibility of evaluating these from the sole knowledge of the iterates $T^m g$, whose calculation can be done in frequency independent times. Indeed, the new high-frequency integral equation approach allows for the efficient evaluation of the Krylov subspace associated with the operator T or, equivalently, that of $I - T$. And this, in turn, suggests that a best approximation to the solution of equation (3) can alternatively be garnered through the application of optimized Krylov subspace methods (e.g. GMRES).

In more detail, and letting $A = I - T$, a basis $p_0, p_1, \ldots, p_{m-1}$ for the Krylov subspace

$$\mathcal{K}_m(A, g) = \operatorname{span}\{g, Ag, \ldots, A^{m-1}g\}$$

can be effectively computed through the classical recursion

$$p_{j+1} = A\,p_j + \sum_{i=0}^{j} \beta_{ij}\,p_i \tag{7}$$

provided efficient evaluations of $A^m g$ can be attained. Clearly, a most natural approach would rely on the *binomial theorem*

$$A^m = \sum_{j=0}^{m} \binom{m}{j} (-1)^j\, T^j \tag{8}$$

as this reduces the problem to the fast evaluation of the iterates $T^j g$ entering the Neumann series. We note, however, that the convergence of this Krylov-subspace technique is strongly affected by the *direct* use of (8) as it impairs the approximation of each projection A^m (see Figure 1). On the other hand, owing to (8), we have

$$\mathcal{K}_m(A, g) = \text{span}\{g, Tg, \ldots, T^{m-1}g\}\,,$$

and thus, the representation

$$p_j = \sum_{i=0}^{j} \gamma_{ij} T^i g \tag{9}$$

delivers the *stable* recursion (see [6])

$$\begin{aligned} p_{j+1} &= (I - T)p_j + \sum_{i=0}^{j} \beta_{ij} p_i \qquad (10)\\ &= \sum_{i=0}^{j} \gamma_{ij} T^i g + \sum_{i=0}^{j} \gamma_{ij} T^{i+1} g + \sum_{i=0}^{j} \beta_{ij} p_i \end{aligned}$$

replacing the combined use of (7) and (8).

Numerical Example

In Figure 1, we present a comparison of (a) the Neumann series; (b) the Padé approximation; (c) a Krylov subspace method (GMRES) based on the binomial formula (8); and (d) the alternative implementation of the latter based on the decomposition (9) leading to equation (10). Here we have considered the configuration in Figure 1 (top) consisting of two elliptical cylinders with centers at $(0, 0)$ and $(0, -4.5)$, and major/minor axes $10/1$ and $7/2$. The illumination is provided by a plane wave with direction along the major axes and wavenumber $k = 40$. The bottom figure displays the number of reflections versus the relative L^∞ error between the exact solution and the approximations obtained by the four aforementioned schemes.

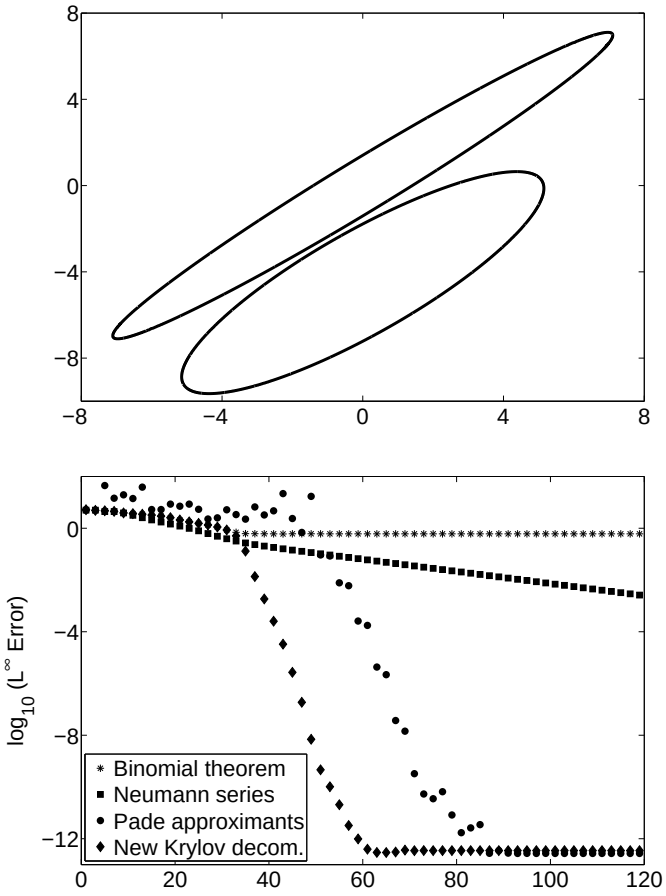

Figure 1: Top: A configuration with two ellipses. Bottom: Number of reflections vs. logarithmic plot of L^∞ error.

References

[1] O. Bruno, C. Geuzaine, J. Monro and F. Reitich, "Prescribed error tolerances within fixed computational times for scattering problems of arbitrarily high frequency: the convex case," Phil. Trans. Roy. Soc. London **362** (2004), 629–645.

[2] F. Ecevit and F. Reitich, "Analysis of multiple scattering iterations for high-frequency scattering problems. I: The two-dimensional case," Max Planck Institute for Mathematics in the Sciences, Preprint **137** (2006), 1–37.

[3] A. Anand, Y. Boubendir, F. Ecevit and F. Reitich, "Analysis of multiple scattering iterations for high-frequency scattering problems. II: The three-dimensional scalar case," Max Planck Institute for Mathematics in the Sciences, Preprint **147** (2006), 1–27.

[4] F. Ecevit, W. Hackbusch and R. Kriemann, "Analysis of vector electromagnetic equations for trapping obstacles," in preparation.

[5] O. Bruno, C. Geuzaine and F. Reitich, "On the $\mathcal{O}(1)$ solution of multiple-scattering problems," IEEE Trans. Magn. **41** (2005), 1488–1491.

[6] Y. Boubendir, F. Ecevit and F. Reitich, "Acceleration of an iterative method for the evaluation of high-frequency multiples scattering effects," in preparation.

AN ERROR ESTIMATE FOR THE UWVF

Annalisa Buffa[‡] **and Peter Monk**[†,*]
[†]Department of Mathematical Sciences, University of Delaware, Newark, DE 19716, USA
[‡]Instituto di Matematica Applicata e Tecnologie Informatiche, Via Ferrata 1, 27100 Paria, Italy.
[*]Email: monk@math.udel.edu

Abstract

The Ultra Weak Variational Formulation of the Helmholtz equation is a variational method, discretized using a plane wave basis, for approximating the Helmholtz equation. The method has proved used at frequencies where standard finite element methods become very expensive. To date, convergence is proved only on the boundary of the computational domain, but is always observed throughout the domain. In this paper we provide the first convergence proof in a global norm. The proof is based on intepreting the scheme as a discontinuous Galerkin method.

Introduction

Complete families of solutions have been investigated as a means of approximating partial differential equations for many years (see for example the early paper of Trefftz [15] and the book of Herrera [7]). In order to control approximation error and the conditioning of the resulting linear system, it is desirable to use multiple complete families associated with different subregions of the domain of the differential equation. The solution on each subregion must then be constrained by approximately enforcing transmission conditions between elements and also approximately enforcing boundary conditions in order to generate a global approximate solution (an alternative approach, the Partition of Unity Finite Element Method (PUFEM) [12], [13], constructs a continuous approximation but is more difficult to use when the sound speed is discontinuous).

One method for weakly enforcing the transmission conditions is the Ultra Weak Variational Formulation (UWVF). We shall be concerned with an error analysis of the discrete UWVF for the Helmholtz equation proposed by Cessenat and Després [2], [3], [4]. This method has been extended to other equations and tested computationally in several studies [2], [3], [11], [9], [10] and has proved to be a useful computational tool at mid-range frequencies. In numerical comparisons with other methods using complete families (in particular the PUFEM [8] and least squares method [6]) it has been found to provide similar accuracy although it is more generally applicable than PUFEM and usually better conditioned than least squares. In all these studies global convergence of the method under mesh refinement is observed (until the mesh is so fine that ill-conditioning prevents further improvement in the error [11]). In the work of Cessenat and Després, convergence is proved on the boundary of the computation domain. In this paper we shall use techniques from the analysis of the discontinuous Galerkin method to provide a global L^2 error estimate. This is a preliminary reports on results presented in more detail in [1].

Description of the UWVF

In this section we shall describe the UWVF for a simple model problem for the Helmholtz equation. Suppose $\Omega \subset \mathbb{R}^3$ is a bounded polyhedral domain in $\mathbb{R}^3$ with boundary $\Gamma = \partial\Omega$ and unit outward normal $\boldsymbol{n}$. We wish to approximate the function $u = u(\boldsymbol{x})$ that satisfies

$$\Delta u + k^2 u = 0 \text{ in } \Omega, \tag{1}$$

where $k > 0$ is the wave-number. The field u is assumed to be subject to the impedance boundary condition

$$\frac{\partial u}{\partial n} - ik\eta u = g \text{ on } \Gamma. \tag{2}$$

Here $g \in L^2(\Gamma)$ is a given function, and η is a given real, uniformly bounded and uniformly positive continuous function of position on Γ. Note that $\eta = 1$ corresponds to a low order absorbing boundary condition which allows the UWVF to approximate scattering problems.

Now suppose Ω is covered by a regular and quasi-uniform mesh of tetrahedra of maximum diameter h. We shall enumerate the tetrahedra $K_1, K_2, \ldots, K_{N_h}$. The continuous UWVF governs the upwind fluxes on the boundary of each tetrahedron in the mesh. Defining $u_j = u|_{K_j}$ we set

$$\chi_j = \left(\eta u_j + \frac{1}{ik}\frac{\partial u_j}{\partial n_j}\right)\Big|_{\partial K_j}, \ 1 \le j \le N_h.$$

The appropriate solution space is then $X = \prod_{j=1}^{N_n} L^2(\partial K_j)$. We define $\vec{\mathcal{X}} = (\mathcal{X}_1, \ldots, \mathcal{X}_{N_n})$ and consider $\vec{\mathcal{X}} \in X$. In order to state the UWVF

we need two special operators. The first is denoted $F : X \to X$ and is defined as follows. If $\mathcal{Y}_j \in L^2(\partial K_j)$, then let $w_j \in H^1(K_j)$ satisfy

$$\Delta w_j + k^2 w_j = 0 \quad \text{in} \quad K_j,$$
$$\eta w_j + \frac{1}{ik}\frac{\partial w_j}{\partial n_j} = \mathcal{Y}_j \quad \text{on} \quad \partial K_j,$$

and set $F_j(\mathcal{Y}_j) = -\nu w_j + \frac{1}{ik}\partial w_j/\partial n_j$. Here η is given from the boundary condition on $\partial K_j \cap \Gamma \neq \emptyset$ and otherwise is usually chosen to be $\eta = 1$.

In addition let $\Pi : X \to X$ be defined by

$$\Pi\chi_j|_{\partial K_j \cap \partial K_\ell} = \chi_\ell \text{ if } \partial K_j \cap \partial K_\ell \neq \emptyset,$$
$$\Pi\chi_j|_{\partial K_j \cap \Gamma} = 0 \text{ if } \partial K_j \cap \Gamma \neq \emptyset.$$

In deriving the UWVF, Cessenat and Després [2], [3] show that $\vec{\mathcal{X}} \in X$ satisfies

$$\langle \vec{\mathcal{X}}, \vec{\mathcal{Y}} \rangle - \langle \Pi\vec{\mathcal{X}}, F(\vec{\mathcal{Y}}) \rangle = \langle \tilde{g}, F(\vec{\mathcal{Y}}) \rangle \tag{3}$$

for all $\vec{\mathcal{Y}} \in X$ where $\langle \cdot, \cdot \rangle$ is the inner produce on X defined by

$$\langle \vec{\mathcal{X}}, \vec{\mathcal{Y}} \rangle = \sum_{j=1}^{N_h} \int_{\partial K_j} \frac{1}{2\eta} \mathcal{X}_j \bar{\mathcal{Y}}_j \, dA.$$

This inner product defines a norm $\|\cdot\|_X$ on X. In addition $\tilde{g} = g$ on Γ and $\tilde{g} = 0$ on faces interior to Ω. Cessenat and Després show that (3) has exactly one solution corresponding to the upwind fluxes of (1) - (2). Equation (3) can be derived simply by intergration by parts as in [2], [3] or via discontinuous Galerkin techniques [5], [10], [1]. It is the latter view that we take in order to prove convergence.

To discretize the UWVF, let $\mathbf{d}_\ell^{K_j},\ 1 \le \ell \le p$, denote p_j linearly independent unit vectors (typically chosen, for example, to be quadrature points on the unit sphere). Then set

$$M_{K_j}^h = \text{ span } \left\{ \exp(ik\mathbf{d}_\ell^{K_j} \cdot \boldsymbol{x}),\ 1 \le \ell \le p_j \right\}.$$

For each j, the discrete space X_j^h is the impedance trace of $M_{K_j}^h$. Thus

$$X_j^h = \left\{ \eta w_j + \frac{1}{ik}\frac{\partial w_j}{\partial n_j} \;\middle|\; w_j \in M_{K_j}^h \right\}.$$

Then the global discrete space is $X^h = \prod_{j=1}^{N_h} X_j^h$. The discrete UWVF is to seek $\vec{\mathcal{X}}^h \in X^h$ such that

$$\langle \vec{\mathcal{X}}^h, \vec{\mathcal{Y}}^h \rangle - \langle \Pi\vec{\mathcal{X}}^h, F(\vec{\mathcal{Y}}^h) \rangle = \langle \tilde{g}, F(\vec{\mathcal{Y}}^h) \rangle$$

for all $\vec{\mathcal{Y}}^h \in X^h$. This problem is also proved to have a unique solution by Cessenat and Després. Note that the action of F on any element of X^h is easy to compute.

Error Estimates

The convergence of the UWVF was studied in [2], [3] where it is shown that

$$\left\| \frac{1}{\sqrt{2\eta}} (\mathcal{X}_j - \mathcal{X}^h) \right\|_{L^2(\Gamma)}^2 \le 4 \|(I - P_h)\vec{\mathcal{X}}\|_X^2, \tag{4}$$

where P_h is the X-orthogonal projection of X onto X^h. In fact, this estimate is a very slight extension of the results in [2], [3] since in [1] we have derived the method and results when $\nu \neq 1$.

In [1] we provide details of the proof of the following theorm that proves convergence throughout Ω, at least if the solution u is sufficiently smooth.

Theorem 1 *Let $u_j^h \in M_{K_j}^h$ be such that*

$$\nu u_j^h - (1/ik)\, \partial u_j^h/\partial n_j = \mathcal{X}_j^h \text{ on } \partial K_j.$$

Then if $\nu = 1$ and u^h is defined by $u^h|_{K_j} = u_j^h$ we have the error estimate

$$\|u - u^h\|_{L^2(\Omega)} \le C h^{-1/2} \|(I - P_h)\vec{\mathcal{X}}\|_X. \tag{5}$$

Remark 1 *We might hope for a power of $h^{1/2}$ in this result. When $\vec{\mathcal{X}}$ is smooth enough and $p_j = 2\mu + 1$ for all j, Cessenat and Després show that in 2D*

$$\|(I - P_h)\vec{\mathcal{X}}\|_X \le C h^{\mu - \frac{1}{2}}$$

where C depends on u and μ. Our estimate (5) also holds in 2D so in that case

$$\|u - u^h\|_{L^2(\Omega)} \le C h^{\mu - 1}.$$

This proves convergence, at least for smooth data in 2D provided $\mu > 1$.

This theorem is proved via a more basic result. Let $a(\vec{\mathcal{X}}, \vec{\mathcal{Y}}) = \langle \vec{\mathcal{X}}, \vec{\mathcal{Y}} \rangle - \langle \Pi\vec{\mathcal{X}}, F(\vec{\mathcal{Y}}) \rangle$ and define, for a face f with between K_1 and K_2,

$$[u]_f = u_1 \boldsymbol{n}_1 + u_2 \boldsymbol{n}_2,\ [\mathbf{v}]_f = \mathbf{v}|_{K_1} \cdot \boldsymbol{n}_1 + \mathbf{v}|_{K_2} \cdot \boldsymbol{n}_2.$$

We prove, using techniques from the theory of discontinuous Galerkin methods, that

$$\sum_{f:\text{interior face}} \int_f \frac{\eta}{2} |[u]_f|^2 + \frac{1}{2\eta} \left| [\frac{1}{ik}\nabla u]_f \right|^2 dA$$
$$+ \sum_j \int_{\Gamma \cap \partial K_j} \frac{1}{2\eta} |F_j(\mathcal{X}_j)|^2 \, dA = \text{Re}\left(a(\vec{\mathcal{X}}, \vec{\mathcal{X}}) \right).$$

Using estimates for $a(\vec{\mathcal{X}} - \vec{\mathcal{X}}^H, \vec{\mathcal{X}} - \vec{\mathcal{X}}^h)$ from [3] and defining $e^h = u - u^h$ we then verify that

$$\begin{aligned} & \sum_{f:\text{interior face}} \int_f \frac{\eta}{2} |[e^h]_f|^2 + \frac{1}{2\eta} \left| [\frac{1}{ik} \nabla e^h]_f \right|^2 dA \\ + & \sum_j \int_{\Gamma \cap \partial K_j} \frac{1}{2\eta} |F_j(\mathcal{X}_j - \mathcal{X}_j^h)|^2 dA \\ \leq & \; 2\|(I - P_h)\vec{\mathcal{X}}\|_X^2 \end{aligned} \tag{6}$$

This is our basic estimate and it holds for general η. The left hand side defines a mesh dependent norm on the solution space, and estimate (6) ensures convergence. However the norm in which (6) proves convergence is non-standard.

We can make the estimate more explicit using the following result from [14] that when $\eta = 1$,

$$\begin{aligned} & \|e^h\|^2_{L^2(\Omega)} \leq \\ & \frac{C}{h} \left[\sum_{f:\text{interior faces}} \|[\nabla e^h]_f\|^2_{L^2(f)} + k^2 \|[e^h]_f\|^2_{L^2(f)} \right. \\ & \left. + \sum_{f:\text{boundary faces}} \|\partial e^h / \partial n - ike^h\|^2_{L^2(f)} \cdot \right] \end{aligned}$$

This estimate and (6), together with (4) then proves (5).

Conclusion

We have summarized the proof of two basic error estimates for the UWVF. These show that the method converges, at least when the exact solution is smooth. Efforts are now underway to improve the power of h and the regularity needed for these results.

References

[1] A. BUFFA AND P. MONK, *Error estimates for the ultra weak variational formulation of the Helmholtz equation*. In preparation.

[2] O. CESSENAT, *Application d'une nouvelle formulation variationnelle aux équations d'ondes harmoniques. Problèmes de Helmholtz 2D et de Maxwell 3D.*, PhD thesis, Université Paris IX Dauphine, 1996.

[3] O. CESSENAT AND B. DESPRÉS, *Application of the ultra-weak variational formulation of elliptic PDEs to the 2-dimensional Helmholtz problem*, SIAM J. Numer. Anal., 35 (1998), pp. 255–99.

[4] ——, *Using plane waves as base functions for solving time harmonic equations with the Ultra Weak Variational Formulation*, Journal of Computational Acoustics, 11 (2003), pp. 227–38.

[5] G. GABARD, *Discontinuous Galerkin methods with plane waves for time-harmonic problems*. to appear.

[6] P. GAMALLO AND R. ASTLEY, *A comparison of two Trefftz-type methods: The ultraweak variational formulation and the least-squares method, for solving shortwave 2-D Helmholtz problems*. In Press.

[7] I. HERRERA, *Boundary Methods: an Algebraic Theory*, Pitman, 1984.

[8] T. HUTTUNEN, P. GAMALLO, AND R. ASTLEY, *Comparison of two wave element methods for the Helmholtz problem*. Submitted.

[9] T. HUTTUNEN, J. KAIPIO, AND P. MONK, *The perfectly matched layer for the ultra weak variational formulation of the 3D Helmholtz equation*, Int. J. Numer. Meth. Eng., 61 (2004), pp. 1072–92.

[10] T. HUTTUNEN, M. MALINEN, AND P. MONK, *Solving Maxwell's equations using the Ultra Weak Variational Formulation*. to appear in *J. Comp. Phys.*, 2006.

[11] T. HUTTUNEN, P. MONK, AND J. KAIPIO, *Computational aspects of the Ultra Weak Variational Formulation*, J. Comput. Phys., 182 (2002), pp. 27–46.

[12] J. MELENK, *On generalized finite element methods*, PhD thesis, University of Maryland, College Park, MD, 1995.

[13] J. MELENK AND I. BABUŠKA, *The partition of unity finite element method: Basic theory and applications*, Comput. Meth. Appl. Mech. Eng., 139 (1996), pp. 289–314.

[14] P. MONK AND D. WANG, *A least squares method for the Helmholtz equation*, Comput. Meth. Appl. Mech. Eng., 175 (1999), pp. 121–36.

[15] E. TREFFTZ, *Ein gegenstück zum Ritz'schen verfahren*, in Proc. 2nd Int. Congr. Appl. Mech., Zurich, 1926, pp. 131–137.

Condition Number Estimates for Combined Potential Integral Operators in Acoustic Scattering

S. N. Chandler-Wilde[†,*], **I. G. Graham**[‡], **S. Langdon**[†], **M. Lindner**[†],
[†]Department of Mathematics, University of Reading, Reading RG6 6AX, UK.
[‡]Department of Mathematical Sciences, University of Bath, Bath BA2 7AY, UK.
[*]Email: S.N.Chandler-Wilde@reading.ac.uk

Abstract

We study the classical combined field integral equation formulations for time-harmonic acoustic scattering by a sound soft bounded obstacle, namely the indirect formulation due to Brakhage-Werner/Leis/Panich, and the direct formulation associated with the names of Burton and Miller. We obtain lower and upper bounds on the condition number, emphasising dependence on the frequency, the geometry of the scatterer, and the coupling parameter.

Introduction

We consider the classical problem of scattering of a time-harmonic acoustic wave by a bounded, sound soft obstacle occupying a compact set $\Omega \subset \mathbb{R}^d$ ($d = 2$ or 3) with Lipschitz boundary Γ. The wave propagates in the exterior domain $\Omega_e = \mathbb{R}^d \setminus \Omega$ and we suppose that the medium of propagation in Ω_e is homogeneous, isotropic and at rest, and that a time harmonic ($\mathrm{e}^{-\mathrm{i}\omega t}$ time dependence) pressure field u^i is incident on Ω. Denoting by $c > 0$ the speed of sound, we assume that u^i is an entire solution of the Helmholtz equation with *wave number* $k = \omega/c > 0$. We wish to find the resulting time-harmonic acoustic pressure field u which satisfies the Helmholtz equation $\Delta u + k^2 u = 0$ in Ω_e and the sound soft boundary condition $u = 0$ on $\Gamma := \partial\Omega_e$, and is such that the scattered part of the field, $u^s := u - u^i$, satisfies the Sommerfeld radiation condition.

Let $\Phi(x, y)$ denote the standard free-space fundamental solution of the Helmholtz equation, given, in the 2D and 3D cases respectively, by $\Phi(x, y) := \frac{\mathrm{i}}{4} H_0^{(1)}(k|x-y|)$ and $\Phi(x, y) := \exp(\mathrm{i}k|x-y|)/(4\pi|x-y|)$, for $x, y \in \mathbb{R}^d$, $x \neq y$, where $H_0^{(1)}$ is the Hankel function of the first kind of order zero.

It was proposed independently by Brakhage & Werner, Leis, and Panich (see [5]), as a means to obtain an integral equation uniquely solvable at all wave numbers, to look for a solution to the scattering problem in the form of the *combined single- and double-layer potential*

$$u^s(x) := \int_\Gamma \frac{\partial\Phi(x,y)}{\partial\nu(y)}\varphi(y)\,ds(y) - \mathrm{i}\eta \int_\Gamma \Phi(x,y)\varphi(y)\,ds(y), \quad x \in \Omega_e, \tag{1}$$

for some non-zero value of the *coupling parameter* $\eta \in \mathbb{R}$. (In this equation $\partial/\partial\nu(y)$ is the derivative in the normal direction, the unit normal $\nu(y)$ directed into Ω_e.) The function u^s, given by (1), satisfies the scattering problem if and only if φ satisfies a second kind boundary integral equation on Γ, see [5] or [4, §4]. This integral equation, in operator form, is

$$(I + D - \mathrm{i}\eta S)\varphi = g, \tag{2}$$

where I is the identity operator, S and D are *single-* and *double-layer potential operators*, defined by

$$S\varphi(x) := 2\int_\Gamma \Phi(x,y)\,\varphi(y)\,ds(y), \quad x \in \Gamma, \tag{3}$$

and

$$D\varphi(x) := 2\int_\Gamma \frac{\partial\Phi(x,y)}{\partial\nu(y)}\,\varphi(y)\,ds(y), \quad x \in \Gamma, \tag{4}$$

and $g := -2u^i|_\Gamma$.

We treat (2) as an operator equation on the space $L^2(\Gamma)$. The right hand sides of (3) and (4) are well-defined, for general Lipschitz Γ, almost everywhere on Γ, as Cauchy principal values, and the operators D and S so-defined are bounded operators on $L^2(\Gamma)$. Further, choosing $\eta \neq 0$ ensures that (2) is uniquely solvable in $L^2(\Gamma)$, that is

$$A := I + D - \mathrm{i}\eta S \tag{5}$$

is invertible as an operator on $L^2(\Gamma)$. See [1] for further details, where, in fact, it is shown that A is invertible as an operator on the Sobolev space $H^s(\Gamma)$, for $0 \leq s \leq 1$.

Let

$$D'\varphi(x) := 2\int_\Gamma \frac{\partial\Phi(x,y)}{\partial\nu(x)}\,\varphi(y)\,ds(y), \quad x \in \Gamma,$$

and $A' := I + D' - \mathrm{i}\eta S$ denote the formal adjoint operators of D and A, respectively. While the operator A appears in the standard indirect combined field boundary integral formulation of the exterior sound soft scattering problem, its adjoint A' appears in the standard direct boundary integral formulation (see e.g. [5], [1], [2]).

In this paper we are interested in upper and lower estimates for the *condition number*

$$\text{cond } A \;:=\; \|A\|\,\|A^{-1}\|,$$

and so in estimates for the norms $\|A\|$ and $\|A^{-1}\|$. Our emphasis is on the limit $k \to \infty$, on understanding the dependence on the coupling parameter η, and on exploring the influence of the shape of Γ. (Note that, since A' is the adjoint of A, $\|A'\| = \|A\|$ and $\|A'^{-1}\| = \|A^{-1}\|$, so that $\text{cond } A' = \text{cond } A$). These questions have received attention before, see [6], [2], [3], [4], and the references therein. But we note that, with the exception of recent bounds in [2], [3], [4], rigorous estimates valid in the limit as $k \to \infty$ have not been obtained. Moreover, research to date has focussed almost entirely on the circle/sphere case where Fourier analysis methods are possible. The estimates we list below address these gaps in the literature and show that the behaviour of $\text{cond } A$ as a function of k depends strongly, and in a subtle way, on the geometry of Γ.

In the remainder of the paper we will summarise the main results we have obtained; proofs will appear elsewhere. Throughout, by $a \lesssim b$ we will mean that for every $K > 0$ there exists $C > 0$, such that $a \le Cb$ for $k \ge K$. By $a \approx b$ we will mean that $a \lesssim b$ and $b \lesssim a$.

A Summary of Previous Results

Most previous work has focussed on the case where Γ is a circle or sphere, when A has spherical harmonics as its eigenfunctions and the singular values of A are known explicitly. The following is the state of the art. The bound on $\|A^{-1}\|$ is from [2] for $\eta = k$ and from [4] otherwise. The other bounds are from [2], [3].

Theorem 1 *If Γ is a circle or a sphere, then $\|S\| \lesssim k^{-2/3}$, $\|D\| \lesssim 1$, and $\|A^{-1}\| \lesssim 1 + k/|\eta|$, so that, if $2/3 \le \epsilon \le 1$ and $|\eta| \approx k^{\epsilon}$, then $\text{cond } A \lesssim k^{1/3}$.*

We note that $|\eta| \approx k$ is the usual recommendation as the best value for the coupling parameter for large k (e.g. [6]), but that $|\eta| \approx k^{2/3}$ is suggested recently in [3].

The above bound on $\|A^{-1}\|$ is a special case of the following more general result from [4], proved via a Rellich type identity. Recall that we assume throughout that Γ is Lipschitz, so that this result holds for a piecewise smooth, starlike, Lipschitz boundary.

Theorem 2 *If Γ is piecewise C^2 and strictly starlike (precisely, for some point x_c in the interior of Γ and some $c > 0$ it holds that $(x - x_c) \cdot n(x) \ge c$, for almost all $x \in \Gamma$), then $\|A^{-1}\| \lesssim 1 + k/|\eta|$.*

New Bounds on $\|S\|$, $\|D\|$, $\|A\|$, $\|A^{-1}\|$ and $\text{cond } A$

Our first observation follows from the fact that S and K are smoothing operators on smooth parts of Γ.

Lemma 3 *In both 2D and 3D, if a part of Γ is C^2, then $\|A\| \ge 1$, $\|A^{-1}\| \ge 1$.*

For the general Lipschitz case we give in the next theorem upper bounds on the norms of S and D on $L^2(\Gamma)$ obtained via interpolation. E.g. (where $\|\cdot\|_p$ denotes the norm of an operator considered as acting on $L^p(\Gamma)$), we have that

$$\begin{aligned}\|S\| &= \|S\|_2 \le \max\{\|S\|_1, \|S\|_\infty\} \\ &= \sup_{x\in\Gamma} \int_\Gamma |\Phi(x,y)|\; ds(y).\end{aligned}$$

This technique applies in modified form to D, and gives bounds in both the 2D ($d = 2$) and 3D ($d = 3$) cases. (For a proof for the 2D case when Γ is smooth, see [2].)

Theorem 4 *$\|S\| \lesssim k^{(d-3)/2}$ and $\|D\| \lesssim k^{(d-1)/2}$.*

We note the gap for large k between the bounds in Theorems 1 and 4, especially in 3D. However, in the 2D case the above results are almost sharp for some Lipschitz boundaries as the following lower bounds show.

Theorem 5 *In the 2D case: (i) if Γ contains a straight line section, then $\|S\| \gtrsim k^{-1/2}$ and $\|A\| \gtrsim 1 + |\eta|k^{-1/2}$; (ii) there exists a Lipschitz Γ such that $\|D\| \gtrsim k^{1/2-\varepsilon}$ for every $\varepsilon > 0$.*

The following is a sketch of the proof of the first statement. Choose disjoint sections, Γ_1 and Γ_2, of the straight line part of Γ, and choose $\phi \in L^2(\Gamma_1)$ with $\phi(y) = \exp(\mathrm{i}ky \cdot t)$ on Γ_1 and ϕ zero elsewhere, where t is a unit vector parallel to Γ_1 and Γ_2, pointing from Γ_1 to Γ_2. Then, uniformly for $x \in \Gamma_2$,

$$S\phi(x) \approx \int_{\Gamma_1} |\Phi(x,y)| ds(y) \approx k^{-1/2}.$$

Since also $D\phi = 0$ on Γ_2, this gives that $\|S\phi\| \gtrsim k^{-1/2}$ and $\|D - \mathrm{i}\eta S\| \gtrsim |\eta|k^{-1/2}$ while $\|\phi\| \lesssim 1$, so that $\|S\| \gtrsim k^{-1/2}$ and $\|D - \mathrm{i}\eta S\| \gtrsim |\eta|k^{-1/2}$.

This idea can be refined to give the following lower bound on $\|S\|$.

Theorem 6 *Suppose (in the 2D case) that Γ is locally C^2 in a neighbourhood of some point x^* on the boundary. Then $\|S\| \gtrsim k^{-2/3}$. More generally, adopt a local coordinate system OX_1X_2 with origin at x^* and the X_1 axis in the tangential direction at x^*, so that, near x^*, Γ coincides with the curve $\{x^* + t^*X_1 + n^*f(X_1) : X_1 \in \mathbb{R}\}$,*

for some $f \in C^2(\mathbb{R})$ with $f(0) = f'(0) = 0$; here t^* and n^* are the unit tangent and normal vectors at x^*. Then if, for some $N \in \mathbb{N}$, Γ is locally C^{N+1} near x^*, i.e. $f \in C^{N+1}(\mathbb{R})$, and if also $f'(0) = f^{(2)}(0) = \cdots = f^{(N)}(0) = 0$, then $\|S\| \gtrsim k^{-(N+1)/(2N+1)}$.

Note that it follows from Theorem 1 that the above bound is sharp for $N = 1$ in the case of a circle and, by Theorem 4, it is sharp in the limit $N \to \infty$ when $k^{-(N+1)/(2N+1)} \to k^{-1/2}$. Similar lower bounds can be given for D as follows.

Theorem 7 *In the 2D case, suppose x^1 and x^2 are distinct points on Γ, that Γ is C^2 in (at least one-sided) neighbourhoods Γ^1 and Γ^2 of x^1 and x^2, and that $x^1 - x^2$ is not parallel to both t^1 and t^2, where t^j is the tangent vector to Γ^j at x^j. Then $\|D\| \gtrsim 1$. If $x^1 - x^2$ is parallel to exactly one of t^1 and t^2, then $\|D\| \gtrsim k^{1/8}$.*

The only upper bounds on $\|A^{-1}\|$ we know are Theorems 1 and 2. The following 2D bound for a class of 'trapping' geometries shows that $\|A^{-1}\|$ grows more quickly with k when Γ is not starlike. This result is suggestive that the choice $\eta \approx k^{2/3}$ has merit.

Theorem 8 *If Ω_e contains a rectangle, two opposite sides of which, distance d apart, are part of Γ, then, for values of k for which $kd = n\pi$, with $n \in \mathbb{N}$, it holds for $\eta \lesssim k$ that $\|A^{-1}\| \gtrsim k^{1/2}$. Thus, by theorem 5, if Γ is also piecewise smooth then, for $|\eta| \approx k^{2/3}$, $\operatorname{cond} A \gtrsim k^{2/3}$, while, for $|\eta| \approx k$, $\operatorname{cond} A \gtrsim k$.*

Combining Theorem 2, Lemma 3, Theorem 4, and Theorem 5(i), we have the following bounds on $\operatorname{cond} A$ for the usual choice $|\eta| \approx k$.

Corollary 9 *For $|\eta| \approx k$: (i) for a starlike, piecewise smooth obstacle in d dimensions, $\operatorname{cond} A \lesssim k^{(d-1)/2}$; (ii) for a convex polygon in 2D the bound in (i) is sharp, i.e. $\operatorname{cond} A \approx k^{1/2}$.*

Numerical Results

In this section we present approximations to operator norms obtained by computing the norms of the corresponding matrices when the operators are discretised with a piecewise constant Galerkin boundary element method with an orthonormal basis and five elements per wavelength. In table 1 we present approximations to $\|S\|$ and $\|D\|$ when Ω is the unit circle. We also show estimated values of p and q, on the assumption that $\|S\| \sim k^p$ and $\|D\| \sim k^q$. The results clearly match the upper and lower bounds in theorems 1, 6 and 7. In table 2 we present approximations to $\|A\|$ and $\|A^{-1}\|$, with $\eta = k$, for a domain satisfying the conditions of theorem 8 with $d = \pi/5$. We also show estimated values of p and q, assuming that $\|A\| \sim k^p$ and $\|A^{-1}\| \sim k^q$. The results are consistent with the bound on $\operatorname{cond} A$ in theorem 8.

k	$\|S\|$	p	$\|D\|$	q
10	2.9156×10^{-1}	-0.66	1.0611	-0.05
20	1.8431×10^{-1}	-0.69	1.0215	-0.02
40	1.1394×10^{-1}	-0.68	1.0078	-0.00
80	7.1116×10^{-2}	-0.68	1.0061	-0.00
160	4.4380×10^{-2}	-0.67	1.0029	-0.00
320	2.7914×10^{-2}		1.0013	

Table 1. Values of $\|S\|$ and $\|D\|$, unit circle.

k	$\|A\|$	p	$\|A^{-1}\|$	q
10	4.9211	0.15	3.3989	0.65
20	5.4603	0.18	5.3373	0.68
40	6.1688	0.26	8.5387	0.73
80	7.4100	0.28	14.1509	0.73
160	8.9683	0.34	23.4338	0.67
320	11.3684		37.2691	

Table 2. Values of $\|A\|$, $\|A^{-1}\|$, trapping domain.

References

[1] S. N. Chandler-Wilde and S. Langdon, "A Galerkin boundary element method for high frequency scattering by convex polygons", SIAM J. Numer. Anal., 45:610–640 (2007).

[2] V. Domínguez, I. G. Graham and V. P. Smyshlyaev, "A hybrid numerical-asymptotic boundary integral method for high-frequency acoustic scattering", Numer. Math., 106:471–510 (2007).

[3] L. Banjai and S. Sauter, "A refined Galerkin error and stability analysis for highly indefinite variational problems", SIAM J. Numer. Anal. 45:37–53 (2007).

[4] S. N. Chandler-Wilde and P. Monk, "Wave-number-explicit bounds in time-harmonic scattering", to appear in SIAM J. Math. Anal.

[5] D. L. Colton and R. Kress, Integral equation methods in scattering theory, John Wiley, New York, 1983.

[6] R. Kress and W. T. Spassov, "On the condition number of boundary integral operators for the exterior Dirichlet problem for the Helmholtz equation", Numer. Math., 42:77–95 (1983).

ULTRA-WEAK VARIATIONAL FORMULATION AND INTEGRAL REPRESENTATION USING A MULTILEVEL FAST MULTIPOLE METHOD

E. Darrigrand[†,*], **P. Monk**[‡,*]

[†]IRMAR - Université de Rennes 1, Campus de Beaulieu, 35042 Rennes cedex, France
[‡]Department of Mathematical Sciences, University of Delaware, Newark, DE 19716, USA
[*]Emails: eric.darrigrand-lacarrieu@univ-rennes1.fr , monk@math.udel.edu

Abstract

To solve the time-harmonic Maxwell equations in exterior domains at high frequency, volume based methods have the drawback of needing an artificial boundary far from the obstacle. Integral formulations enable one to avoid this difficulty by solving a problem on the surface of the obstacle, but imply dense systems with bad condition numbers. In this paper we describe a coupling of the Ultra-Weak Variational Formulation (UWVF), a volume based method using plane wave basis functions, and an integral representation of the unknown field to obtain an exact artificial boundary condition. The use of different fast evaluation techniques is suggested.

Introduction

The Ultra-Weak Variational Formulation (UWVF) is a volume based numerical method for solving the time-harmonic Maxwell system on a bounded domain developed by B. Després and O. Cessenat ([2]). It uses local plane wave solutions on a finite element mesh to approximate the field. By varying the number of plane wave basis functions from element to element the UWVF can discretize the electromagnetic field with a coarser volume mesh in comparison to more classical methods like low order finite elements or finite differences. However, to approximate scattering on an unbounded domain, the UWVF requires an artificial boundary Γ_{ext} sufficiently far from the obstacle. A simple absorbing boundary condition on Γ_{ext} (as used in the original UWVF) implies a large domain around the obstacle and so a large number of degrees of freedom.

In this paper we consider the use of an integral representation of the unknown field on Γ_{ext} due to C. Hazard and M. Lenoir ([6]) as we suggested in [4]. In particular, the unknown on the artificial boundary Γ_{ext} is defined thanks to the unknown field values on a third boundary Σ taken closer to the boundary of the obstacle Γ_{int}. The artificial boundary Γ_{ext} can then be taken very close to the third boundary Σ. However, this method requires the evaluation of integral operators which are expensive by direct means. A thorough study of the numerical complexity show that the use of the integral representation does not greatly increase the cost of the UWVF if the integral calculation is performed using a Fast Multipole Method (FMM) (see for example [5]). The first section of this paper gives a brief presentation of the UWVF. In the second section, we explain the application of the integral representation and give a rigorous result on the numerical complexity when using fast evaluation methods or not. The last section presents encouraging numerical results obtained using the FMM.

Ultra-Weak Variational Formulation

To solve a scattering problem for the time-harmonic Maxwell equations in an exterior domain Ω we need to find the electric field E and magnetic field H such that the following equations hold:

$$\left.\begin{array}{l} \nabla \wedge E - \imath\omega\mu H = -m\,, \\ \nabla \wedge H + \imath\omega\varepsilon E = j\,, \\ \nabla \cdot (\varepsilon E) = 0\,, \\ \nabla \cdot (\mu H) = 0\,, \end{array}\right\} \quad \text{in } \Omega, \tag{1}$$

where m and j are given data functions specifying the current sources, ε and μ are positive functions of position and $\omega > 0$ is the angular frequency of the field. For use with the UWVF, the boundary condition on $\partial\Omega = \Gamma_{\text{int}} \cup \Gamma_{\text{ext}}$ is written in the following non standard form ([2])

$$\begin{array}{rl} & -\mid \sqrt{\varepsilon} \mid E \wedge \nu + (\mid \sqrt{\mu} \mid H \wedge \nu) \wedge \nu \\ = & Q(\mid \sqrt{\varepsilon} \mid E \wedge \nu + (\mid \sqrt{\mu} \mid H \wedge \nu) \wedge \nu) + g\,, \end{array} \tag{2}$$

where $Q = 0$ on Γ_{ext} and g is computed from the incident wave to give a low order Absorbing Boundary Condition (ABC).

The UWVF is based on the decomposition of the domain Ω into tetrahedra $\{\Omega_k\}_{k=1,\ldots,K}$ and the unknowns are defined on the boundaries of these tetrahedra. This variational formulation is defined on the Hilbert space $V = \prod_{k=1}^{K} L_t^2(\partial\Omega_k)$ where $L_t^2(\partial\Omega_k)$ is the space of square integrable tangential fields on $\partial\Omega_k$ the boundary of Ω_k, and the scalar product is given by $(\mathcal{X}, \mathcal{Y})_V = \sum_k \int_{\partial\Omega_k} \mathcal{X}_{/\partial\Omega_k} \overline{\mathcal{Y}_{/\partial\Omega_k}}$. Under the assumption that ε and μ are positive constants on each Ω_k, (E, H) is found

through the restriction of the field (E_k, H_k) to $\partial\Omega_k$, where $(E_k, H_k) = (E, H)_{/\Omega_k}$. The method then solves for an unknown impedance trace $\mathcal{X} \in V$, defined by $\mathcal{X}_{/\partial\Omega_k} \in L^2_t(\partial\Omega_k)$ and

$$\mathcal{X}_{/\partial\Omega_k} = \sqrt{\varepsilon_{/\partial\Omega_k}}(E_k \wedge \nu_k) + \sqrt{\mu_{/\partial\Omega_k}}((H_k \wedge \nu_k) \wedge \nu_k)\,,$$

where $\varepsilon_{/\partial\Omega_k}$ and $\mu_{/\partial\Omega_k}$ are quantities defined by the values of ε and μ on each side of $\partial\Omega_k$ (see [4] for details), and ν_k is the exterior normal to $\partial\Omega_k$.

The UWVF of Maxwell's equations ([2]) is then given by finding $\mathcal{X} \in V$ such that

$$(\mathcal{X}, \mathcal{Y})_V - (\Pi\mathcal{X}, F\mathcal{Y})_V = (\widetilde{b}, \mathcal{Y})_V \quad \text{for all } \mathcal{Y} \in V, \quad (3)$$

for all $\mathcal{Y} \in V$ given by $\mathcal{Y}_{/\partial\Omega_k} = \sqrt{\varepsilon_{/\partial\Omega_k}}(E'_k \wedge \nu_k) + \sqrt{\mu_{/\partial\Omega_k}}((H'_k \wedge \nu_k) \wedge \nu_k)$ where the fields (E'_k, H'_k) satisfy the adjoint Maxwell problem

$$\left\{ \begin{array}{l} \nabla \wedge E'_k - \imath\omega\overline{\mu_{\Omega_k}} H'_k = 0 \text{ in } \Omega_k\,, \\ \nabla \wedge H'_k + \imath\omega\overline{\varepsilon_{\Omega_k}} E'_k = 0 \text{ in } \Omega_k\,. \end{array} \right.$$

In (3), $\widetilde{b} \in V$ is derived from the right hand side of (1) and g given in (2). Π and F are local operators defined in [4] following [2], such that Π is the operator which involves the boundary condition (2) through the function Q.

By taking a finite dimensional subspace $V_h \subset V$ and using basis functions $Z_i, i \in J$, a Galerkin discretization of (3) leads to problem of finding $\mathcal{X}_h = \sum_{i\in J} X_i Z_i \in V_h$ such that $(\mathcal{X}_h, \mathcal{Y}_h)_V - (\Pi\mathcal{X}_h, F\mathcal{Y}_h)_V = (\widetilde{b}, F\mathcal{Y}_h)_V$ for all $\mathcal{Y}_h \in V_h$. Equivalently, in matrix/vector form we seek to compute $X = [X_1, \cdots, X_{\mathrm{card}(J)}]^T$ such that

$$(D - C)X = b\,, \quad (4)$$

where D is the matrix with (i,j)th entry $(Z_j, Z_i)_V$ and C has (i,j)th entry given by $(\Pi Z_j, F Z_i)_V$. The data vector b is derived from the right hand side above.

As usual for the UWVF, on each Ω_k we use a basis generated by taking the impedance trace of p_k plane waves satisfying the adjoint Maxwell system on Ω_k ($p_k/2$ directions with two polarizations for each direction). At least six plane waves (and usually more) are used per element.

The UWVF then leads to a system of size $(\sum_{k=1}^K p_k)$. The number of plane waves p_k must be chosen depending on the local wavelength and diameter of the element. Suppose the electromagnetic parameters of the domain are constant and define the wave number $\kappa = \omega\sqrt{\varepsilon\mu}$. The UWVF enables one to reduce the number of elements in the mesh, in comparison with a more classical volume method. Of course, the complexity of the method is then linked to the number of elements in the mesh and the number of basis functions per element. Let us introduce another parameter: K_0 denotes the average number of tetrahedra taken in one dimension so that $K \sim K_0^3$. As a volume method, the UWVF method leads to a sparse system. The number of degrees of freedom is of order $K_0^3\, p$ and the complexity of the algorithm is $\mathcal{O}(K_0^3\, p^2)$ where p denotes the average number of basis functions per tetrahedra which typically satisfies $K_0\, p \sim \kappa$.

Use of an Integral Representation within the UWVF

For simplicity, we now suppose $\varepsilon = \mu = 1$ so that Σ can be taken equal to Γ_{int} (i.e. the scatterer is not penetrable and the exterior medium is homogeneous). The idea presented by C. Hazard and M. Lenoir in [6] consists of replacing the low order absorbing boundary condition $-E \wedge \nu + (H \wedge \nu) \wedge \nu = -E_0 \wedge \nu + (H_0 \wedge \nu) \wedge \nu$ on Γ_{ext} by the boundary condition

$$\begin{array}{rl} & -E \wedge \nu + (H \wedge \nu) \wedge \nu \\ = & -E^s \wedge \nu + (H^s \wedge \nu) \wedge \nu - E_0 \wedge \nu + (H_0 \wedge \nu) \wedge \nu\,, \end{array}$$

where (E^s, H^s) are given by the Stratton-Chu formula ([3]) in terms of field values on $\Sigma = \Gamma_{\text{int}}$ involving the tangential components of the fields E and H on $\Sigma = \Gamma_{\text{int}}$. As shown in [4], these components can be computed from the degrees of freedom of the UWVF.

The system (4) becomes $(D - C - \widetilde{C})X = b$ where $\widetilde{C}$ couples the degrees of freedom on Γ_{int} and Γ_{ext}. The matrix $\widetilde{C}$ can be split into different discrete integral operators $\widetilde{C}_i\,,\ i = 1, ..., 4$ of the form

$$(\widetilde{C}_i\, \mathcal{X}_h)_{kl} = \int_{\Sigma^{\text{ext}}_{kk}} c_k\, S_i(\mathcal{X}_h) \cdot \overline{F\mathcal{Y}_{kl}}\, d\gamma_{\text{ext}}\,,$$

where Σ^{ext}_{kk} is the face on Γ_{ext} of a tetrahedron which interacts with the exterior boundary, c_k depends only on ε and μ on Σ^{ext}_{kk}, F is the local operator introduced in (3), and S_i is a global operator which comes from the Stratton-Chu formula, for instance $(S_1(\mathcal{X}))(x)$ equals to

$$\left(-\int_{\Gamma_{\text{int}}} f_Q(y)\, \nabla_y G(x,y) \wedge \mathcal{X}(y)\, d\gamma(y) \right) \wedge \nu(x)\,,$$

where f_Q is a function involving Q and ε, ν is the exterior normal to the surface $\Sigma = \Gamma_{\text{int}}$ and $G(x,y) = \exp(\imath\kappa|x-y|)/(4\pi|x-y|)$ is the fundamental solution for the Helmholtz equation. These integral operators can be evaluated by the FMM.

The integral representation aims to reduce the distance of the absorbing boundary from the scatterer to a number

of elements independent of κ. We then have a number of elements in the mesh of order K_0^2. This reduces the complexity related to the volume calculation. However the cost of the integral calculation would be very large unless treated carefully since the integral operators give rise to a matrix with large dense blocks. This cost is controlled thanks to the FMM.

A thorough study of the complexity of the new algorithm leads to the results in Table 1 with or without the integral representation (IR), using or not a 1-level (1L) or multilevel (ML) FMM. We also studied the consideration of a use of the FMM with no close interactions. This would lead to an algorithm adapted to the case of meshes with local refinements. Finally, the double mesh concept introduced by Zhou *et al* ([1]) is considered as a way to keep using relatively coarse meshes for the UWVF and ensuring a good accuracy of the geometry for the integral representation.

Table 1: Complexity estimates

Method	Cost
UWVF	$K_0\kappa^2$
UWVF + IR	$\kappa^2 + \kappa^4$
UWVF + IR + 1L-FMM	$\kappa^2 + \kappa^3$
UWVF + IR + ML-FMM	$\kappa^2 + \kappa^2 \ln^2 \kappa$
UWVF + IR + ML-FMM with double mesh	$\kappa^2 + \kappa^2 \ln^2(\kappa)p$
UWVF + IR + 1L-FMM without close interaction	$\kappa^2 + \kappa^3$
UWVF + IR + ML-FMM without close interaction	$\kappa^2 + \kappa^2 \ln^2 \kappa$

Numerical Results and concluding remarks

The first numerical results obtained with a 1-level FMM (see [4]) illustrate the theoretical statements about the complexity of the algorithm. The results were obtained for approximating the problem of scattering by a perfectly conducting sphere, in particular the unit sphere (Γ_{int}) with the wavenumber $\kappa = 4\text{m}^{-1}$. The exterior boundary Γ_{ext} is a concentric sphere. We tried different meshes. They are named "Sxxx" where "xxx" denotes the distance between Γ_{int} and Γ_{ext} in centimeters. In Figure 1, we show the radar cross section predicted by the code UWVF+IR+1L-FMM compared to the exact Mie series. It gives very accurate results even for S025 when the code UWVF applied to S200 is already lightly in disagreement with the Mie series.

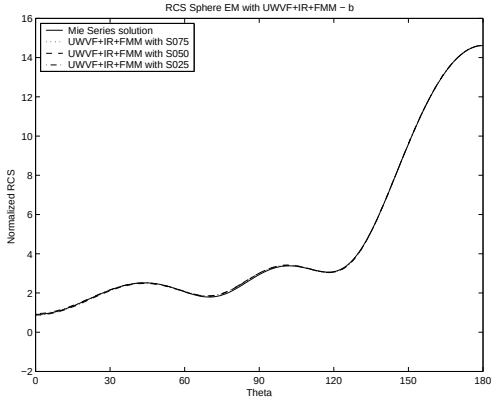

Figure 1: UWVF+IR+1L-FMM (S025, S050, S075).

These first results show the strong benefit of the use of the integral representation regarding the accuracy. We plan to present results using a ML-FMM. In this case the theoretical study predicts the same accuracy for a lower cost.

References

[1] T. Abboud, J.-C. Nédélec and B. Zhou, "Improvement of the Integral Equation Method for High Frequency Problems", Third international conference on mathematical aspects of wave propagation phenomena, SIAM, pp. 178-187, 1995.

[2] O. Cessenat and B. Després, "Using Plane Waves as Base Functions for Solving Time Harmonic Equations with the Ultra Weak Variational Formulation", J. Comput. Acoust., vol. 11, pp. 227-238, 2003.

[3] D. Colton and R. Kress, Inverse Acoustic and Electromagnetic Scattering Theory, 2nd ed., Springer Verlag, New York, 1998.

[4] E. Darrigrand and P. Monk, "Coupling of the Ultra-Weak Variational Formulation and an Integral Representation using a Fast Multipole Method in Electromagnetism", J. Comput. and Applied Math., to appear, available online.

[5] E. Darve, "The Fast Multipole Method: Numerical Implementation", J. Comput. Phys., vol. 160 (1), pp. 195–240, 2000.

[6] C. Hazard and M. Lenoir, "On the Solution of Time-Harmonic Scattering Problems for Maxwell's Equations", SIAM J. Math. Anal., vol. 6, pp. 1597-1630, November 1996.

A HIGH FREQUENCY PARAMETRIX: A ADAPTED TOOL FOR WAVE PROPAGATION?

Philippe J. Delorme[†,*]

[†]Numerical Simulations & Aero-acoustics Department, ONERA, Chatillon, 92300, France
[*]email: Philippe.Delorme@onera.fr

Abstract

The Parametrix is an usual and efficient theoretical tool for hyperbolic systems and usually requires the hypothesis of strictly hyperbolicity. But most hyperbolic systems coming from Physics are described by the general "Friedrich systems" but are not strictly hyperbolic. If this tool is applied to those systems, that hypothesis is not at all necessary, and so, the parametrix covers a great part of the waves propagation. Moreover it can describe complex phenomena like waves coupling or medium-wave interactions leading to instabilities.

Introduction

In the field of waves propagation, mathematical results like existence, uniqueness, boundary conditions and continuity are fairly well-settled at the present time. But the qualitative behavior of the solutions remains a difficult task maybe why the phenomena are complex: One can quote: interactions medium-wave like polarization or injection of energy and instabilities, creation of one wave by another like backscattering or creation of sound by flow in aeroacoustic, or lateral or Rayleigh waves. In addition the tools to predict the behavior of waves are completely of different nature. For stratified media, the Fourier transform leads to an ordinary differential equation and by the inverse Fourier transform and the steepest descent method, a far-field approximation of the solution is obtained. An another approach is the traditional perturbation method: if the medium is assumed quasi homogeneous, a fixed-point method can be exhibited by using the Green (Matrix-valued) function: this is the task of the Lippmann-Schwinger method (or the Born method when the first iteration is enough). Roughly speaking, the multi-pole method is similar to a Taylor development of the Schwarz Kernel in function of the derivatives of the Green function. For high frequencies (or rapidly oscillating initial conditions) the Wigner method is adequate but doesn't take into account the interaction between waves. The goal of this presentation is to promote a method to compute the Schwarz Kernel, the generalization to the inhomogenous media of the Green function. One doesn't obtain this kernel stricto-sensus but a "paramatrix" i.e. a theoretical tool, which is well-known by the mathematicians. This method is an important tool for the scattering theory. At the first sight, this method is not well-suited to describe the physics of the wave propagation: the general theory is rather difficult (at least for the author!): for example in [1] the entire demonstration covers pp. 262-281. But if one applies it only to the Friedrich's systems, which cover the most important cases of waves, this method seems understandable (c.f. [2]) and has deep connections with physics like energetic balance. After a short presentation of the "Friedrich's systems" of the linear hyperbolic systems, we give a sketch of this method and how to get from Green Kernel in homogeneous case to Schwarz Kernel in in-homogeneous one. In the previous works the parametrix method requires the hypothesis of strict hyperbolicity, which is a too strong hypothesis for covering the domain of usual waves: In fact the good hypothesis is the strong hyperbolicity and we show ,even in this case, that we are able to built a parametrix (at least for Friedrich's systems). Then we give some connections with complex phenomena arising for waves propagation in in-homogeneous medium like medium-waves or interactions between elementary waves. To conclude we give the present limits: they stay still important but they don't seem insurmountable.

Short presentation of the "Friedrich system"

Acoustics, Aero-acoustics, Elasticity, Electromagnetism, Quantic Mechanics can be described by first order linear partial differential equations.

Definition:

The most general *Friedrich system* are described by:

$$\partial_0 \phi + A^i(x)\, \partial_i \phi + B(x)\phi = h(t,x) \qquad (1)$$

with A^i symmetric, h is the source, B the multiplication matrix The dispersion matrix $J(x,\xi) = A^i.\xi_i$ (we use the "Einstein rule") has real eigenvalues and is diagonalizable. If all the eigenvalues are simple the system is *strictly-hyperbolic*, if not, the system is only *strongly hyperbolic* (the case of *weakly-hyperbolic* systems concerns un-diagonalizable matrices, they are not Friedrich systems). Most systems cited supra are not strictly hyperbolic but strongly hyperbolic.

Energy balance:

The energy balance of eq. (1) is:

$$\partial_0 \frac{1}{2}\Sigma\phi^2 + \partial_{\rm i}[\frac{1}{2}\phi^t A^i(x)\phi] + \phi^t.\Sigma.\phi = \phi^t h$$

$$\text{with} \quad \Sigma = B + B^t - \partial_{\rm i} A^i \tag{2}$$

The matrix Σ has not a defined sign and so the system can lose or gain energy. This balance allows essentially the existence of instabilities. The systems described in [3] can easily be putted in the form of eq. (1) . In this case the matrix Σ is equal to 0 (no energetic action of the medium on the waves).

Sketch of the parametrix method for Friedrich's systems

Generalities

The general context is the pseudo-differential operators context. S^k is the space of the (matrix-valued) symbol homogeneous of order k in ξ. One tries to extend the x in-dependent mathematical structure to the x dependent case. We only deal with problem without boundary conditions.

Homogeneous case

By use of the Fourier transform and the diagonalizibility of the symbol matrix $A^i\xi_i$ the Green kernel is (see [2] for more details):

$$K(t, x-y) = \int d\xi \sum_k exp(2i\pi[(x-y).\xi) - \lambda_k(\xi)t]).P_k(\xi)$$

where $\lambda_k(\xi)$ is the k-th eigenvalue of the symbol $A^i\xi_i$ (homogeneous of degree 1 in ξ)and $P_k(\xi)$ its projector (homogeneous of degree 0 in ξ) The Green kernel (a convolution kernel) is the sum of elementary kernel associated with each eigenvalue. One can say that the solution is the sum of different *elementary waves*. For $t \to 0$ one has $K \to \delta(x-y)$.

Non-homogeneous case

For propagation in a non-homogeneous medium, the parametrix generalizes the previous kernel:

$$K(t, x, y) \simeq \int_{\sim} d\xi dy \Sigma_k exp(2i\pi[\psi_k(t, x, \xi) - y.\xi]).Q_k(t, x, \xi) \tag{3}$$

where :

- $\simeq$ is a parametrix, equal to left side up to a regular function of $S^{-\infty}$
- $\int_{\sim} d\xi$ is a oscillatory integral of a Fourier Integral Operator (FIO)
- $\psi_k(t, x, \xi)$ is the k-th phase function homogeneous of order 1 in ξ
- $Q_k(t, x, \xi)$ are the amplitude (matrix-valued) functions
- $Q_k(t, x, \xi)$ are symbols and have an ansatz $Q_k(t, x, \xi) \sim \Sigma_{j=0}^{\infty} Q_k^{-j}(t, x, \xi)$ where each $Q_k^{-j}(t, x, \xi)$ is homogeneous of order -j in ξ.

The clue is the homogeneity with respect to ξ, a kind of ansatz with respect the small parameter is $1/|\xi|$ which measures the level of inhomogeneities. Now we have to apply the operator $\partial_0 \phi + A^i(x)\,\partial_{\rm i}\,\phi + B(x)\phi$ to each kth wave and identify the terms of same order of homogeneity in ξ with the special case for the zero-order:

$$2i\pi[\partial_0 \psi_k I + \partial_{\rm i} \psi_k A^i]Q_k^{-j-1} + [\partial_0 I + A^i\,\partial_{\rm i} + B]Q_k^{-j} = 0 \tag{4}$$

The *first step* is to determine the phase functions thanks the zero-order: There is a solution only if $det[\partial_0 \psi_k I + \partial_{\rm i} \psi_k A^i] = 0$ and in that case, ψ_k is solution of the non-linear partial differential system of order 1: $\partial_0 \psi_k + \lambda_k(x, \partial_{\rm i} \psi_k) = 0$ where $\lambda_k(x, p_i)$ is the kth eigenvalue of $A^i p_i$. The resolution of that equation requires the resolution of the bicharacteristic (Hamiltonian) system with an initial value which is chosen, by analogy with the uniform case, to be equal to $x\xi$. In addition the phase function is homogeneous of degree 1 in ξ :

$$\frac{dt}{1} = \frac{dx^i}{D^i\lambda} = -\frac{dp_i}{\partial_{\rm i}\,\lambda} = \frac{d\psi}{0} \tag{5}$$

where $D^i = \frac{\partial}{\partial p_i}$ The solution is local in time, i.e. it does not exist for any time. The *second step* consists in determining the amplitude Matrices and it is rather complicate. By using the "mobil reference frame", by setting $Q = X^t\tilde{Q}$, $J = X^t.\Lambda.X$, where X is the matrix of the eigenvectors and Λ is diagonal, the recurrence relation (4) can be written mutatis mutandis:

$$2i\pi[\Lambda(x, \partial_{\rm i} \psi_k) - \lambda_k I]\tilde{Q}_k^{-j-1} + [\partial_0 I + \tilde{A}^i\,\partial_{\rm i} + \tilde{M}]\tilde{Q}_k^{-j} = 0 \tag{6}$$

To keep it simple assume the symbol matrix J has only 2 eigenvalues λ_1 and λ_2. We begin determining the amplitude matrix of the kernel associated with the first wave (first eigenvalue) and we omit the index and the $\tilde{}$, i.e:

$$\tilde{Q}_k = \sum_{j=0}^{-\infty} \begin{pmatrix} A^{(j)} & B^{(j)} \\ C^{(j)} & D^{(j)} \end{pmatrix} \tag{7}$$

(the remaining index concerns the degree of homogeneity). Eq.(6) becomes:

$$\left[\begin{array}{cc} 0 & 0 \\ 0 & \lambda_2(x,\partial_i\psi)-\lambda_1(x,\partial_i\psi) \end{array}\right]\cdot\left[\begin{array}{cc} A^{(j)} & B^{(j)} \\ C^{(j)} & D^{(j)} \end{array}\right] - i/(2\pi)\left[\begin{array}{cc} L_1^1 & L_1^2 \\ L_2^1 & L_2^2 \end{array}\right].\cdot\left[\begin{array}{cc} A^{(j-1)} & B^{(j-1)} \\ C^{(j-1)} & D^{(j_1)} \end{array}\right]=0 \quad (8)$$

The operator L_1^1 can be written by utilizing the relation$A^i = D^i(A^i p_i)$ in the "mobil reference frame":

$$L_1^1 = I_1(\partial_0 + D^i\lambda_1\,\partial_i) + \tilde{M}_1^1$$

In the recurrence relation eq.(8) or more generally eq.(6) there is not coupling from one column to another. Let begin with the first column (A, C). For $j = 0$ one has $C^{(0)} = 0$. For $j = -1$, (8) gives $L_1^1(A^{(0)}(t, x, \xi) = 0$ or more explicitly:

$$\partial_0\,A^{(0)} + D^i\lambda_1\,\partial_i\,A^{(0)} + \tilde{M}_1^1 A^{(0)} = 0$$

If one expresses $A^{(0)}(x, \xi)$ in function of the constants of the motion of (5), we have only the ordinary differential equation to solve $\frac{d}{dt}A^{(0)} + \tilde{M}_1^1 A^{(0)} = 0$. When $t = 0$ A is equal to I_1, so $A(0)$ is determined. One has to check $A^{(0)}$ (written in the initial frame) is homogeneous of degree 0 in ξ. Then for j=-1 thanks to (8) it is possible to compute $C^{(1)}$ by:

$$(\lambda_2 - \lambda_1)(x, \partial_i\,\psi).C^{(1)} - i/(2\pi)L_1^2(A^{(0)}) = 0$$

and $C^{(1)}$is homogeneous of degree -1 in ξ. Then one can compute $A^{(1)}$ thanks the initial condition $A^{(1)}(0) = 0$. By recurrence the first column is determined at each order. The computing of the second column seems be the same at the first sight but actually the initial condition $(t = 0)$ is missing. This condition is given thanks the computation of the second column of the second kernel (corresponding to λ_2). Obviously this calculus doesn't depend on the simplicity of the eigenvalues.

Interpretation in terms of waves propagation

Of course the previous analysis promotes the high frequency point of view.

quasi homogeneous media

When one studies the propagation through a medium the first point is the existence of different elementary waves. Those waves can be "simple" if the dimension of the eigenprojector is one or "polarizable" if the dimension is greater than 1. For constant or quasi constant medium the highest terms (degree zero) shows that those waves don't interact between themselves: The elementary waves propagate "along their own rays" following their own law of propagation (hamiltonian). The medium can absorb or furnish energy to the wave and the level can be evaluated thanks the projection of the matrix Σ of (2) on the relative eigenspace. So instabilities can be explained.

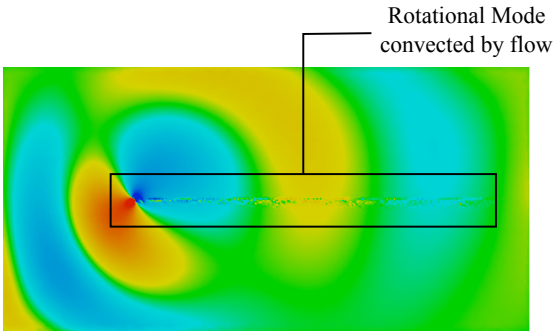

Figure 1: Hydrodynamic wave created by acoustic wave in a shear layer

next terms

The non-block-diagonal terms (like C or B of the previous section)) are equal to zero at the order zero but not at order greater than 1: they explain the interaction between different elementary waves. Wave of the first kind can create wave of second kind (or be created c.f. figure 1)

Conclusions

This method allows one to understand , at high frequency, phenomena like the energetic exchanges between the mediums and the waves. Of course, some problems remain: for instance

- boundary conditions,
- the structure of the temporal group,
- the parametrix is not valid for any time, so what are exactly the limitations in time?
- what about numerical calculations?

References

[1] Jean Dieudonne "Elements d'analyse, tome 8, chapitre 23 " *Gauthiers-Villars*

[2] Ph. J. Delorme "Study of the aero-acoustical phenomena by use of a high frequency parametrix" *Proc. of Wave'05 pp.44-46*(2005)

[3] G. Papanicolaou & L. Ryzhic " Waves and transport" *IAS/Park City Mathematics Series Vol.5 pp. 307-381* (1999)

SPECTRAL METHODS FOR THE INTEGRAL EQUATIONS OF TIME-HARMONIC MAXWELL PROBLEMS

E. Demaldent[†,*], **D. Levadoux**[†], **G. Cohen**[‡]
[†]Electromagnetism and Radar Department, ONERA, chemin de la Hunière, 91761 Palaiseau, FRANCE
[‡]INRIA Rocquencourt, Domaine de Voluceau, 78153 Le Chesnay, FRANCE.
[*]Email: edouard.demaldent@onera.fr

Abstract

Spectral methods were successfully used within finite element methods for solving Maxwell equations [1]. These formulations are based on the two families of Nédélec edge elements, with Gauss and Gauss-Lobatto quadrature points. The purpose of our talk is to show how these techniques can be applied to integral equations of Maxwell problems, in time-harmonic domain. For these formulations, the main advantage of the spectral elements is to provide a cheap way to compute the double integral of the Green's function, with more accurate solutions.

High-Order Integral Methods

It is well known that high-order schemes provide a significant reduction of the number of unknowns and yield more accurate solutions. As the Method of Moment (MoM) with Galerkin testing results in optimal convergence for scattering problems, one should try to expand MoM low-order basis functions into their higher-order form [2]. Unfortunately, this increases dramatically matrix fill time, thus rendering classical high-order MoM useless. By contrast, high-order point-based discretizations such as the Nyström method, excel with their low pre-computation time [3][4][5]. However, these schemes do not enforce current continuity, and an increase of the total number of unknowns is required to reach Galerkin's optimal far field error. Various authors have developed high-order MoM schemes with efficient pre-computation time. S.D. Gedney's studies [6] are particularly interesting : a transformation is performed on the outer integral to speed up the matrix fill time.

Here we present a new, high-order, MoM formulation which leads to optimal error with minimal pre-computation time. Our scheme can be interpreted as a point-based formulation too. It differs from the previous ones in the sense that the acceleration's technique ensues in a natural way (no particular transformation is needed). In fact, the main principle of our studies is close to the one used in [5], but is performed onto an Hdiv-conformal formulation, so that we enforce current continuity.

Discretization

Our research focuses on the field integral equations (EFIE-MFIE-CFIE). Although no special treatment is required on their variational formulations, one should have knowledge of the process performed to weaken the singular behaviour of the EFIE. Applying Stokes'theorem, the use of Hdiv functions allows us to handle the double gradient operator within the Dyadic Green's function (1). Therefore, we deal with divergence terms of basis functions.

$$\left(k^2\mathbf{Id} + \nabla\nabla\right) G(\mathbf{r}, \mathbf{r}') \qquad (1)$$

Our variational spaces slightly differ from the ones described in [2] : the choice of the Lagrange polynomials is made in order to fulfill a spectral elements method. In other words, their roots have to be the Gauss-Lobatto and/or Gauss quadrature rule points. Furthermore, the two families of Nédélec edge elements have been implemented on quadrilateral patches (which are under bilinear/quadratic/cubic parametrization).

Let Γ be the approximation of the surface scatterer. We read $\Gamma_h = \{K_i\}_{i=1}^{Ne}$, where K_i are the basic quadrilateral elements. Let $\widehat{K}$ be the unit square and $\mathbf{F}$ the conform mapping of $\mathbb{R}^3$, such that $\mathbf{F}(\widehat{K}) = K, K \in \Gamma_h$. $\mathbf{DF}$ is the Jacobian matrix of $\mathbf{F}$ and J=det($\mathbf{DF}$). (u, v) denotes the $2D$-coordinates on $\widehat{K}$, and $\{\mathbf{e}_1, \mathbf{e}_2\}$ the canonical basis of $\mathbb{R}^2$.

The set of Lagrange polynomials in $1D$, whose roots are the Gauss-Lobatto (Gauss) points of order k, is read GL^k (G^k). We introduce two spaces on $\widehat{K}$:

$$\widehat{U}^{k,k+1} = (GL^{k+1} \otimes G^k)\, \mathbf{e}_1 \oplus (G^k \otimes GL^{k+1})\, \mathbf{e}_2$$
$$\widehat{V}^{k,k} = \textstyle\sum_{i=1}^{2} (GL^k \otimes GL^k)\ \mathbf{e}_i$$

The approximate space for first class of elements is :

$$U^{k,k+1} = \{\mathbf{\Phi} \in H_{\text{div}}(\Gamma)\ ; \quad \forall K \in \Gamma_h, \mathbf{\Phi}_{|K} \in |J|^{-1}\, \mathbf{DF}\, \widehat{U}^{k,k+1}\}$$

The approximate space for second class of elements is :

$$V^{k,k} = \{\mathbf{\Phi} \in H_{\text{div}}(\Gamma)\ ; \quad \forall K \in \Gamma_h, \mathbf{\Phi}_{|K} \in |J|^{-1}\, \mathbf{DF}\, \widehat{V}^{k,k}\}$$

The divergence of $\mathbf{\Phi}_{|K}(\mathbf{r})$, $\mathbf{r} = \mathbf{F}(u, v)$, is read :

$$\text{div}(\mathbf{\Phi}_{|K}(\mathbf{r})) = |J|^{-1}\, \partial g l^{k+1}(u) \times g^k(v)$$
$$\text{div}(\mathbf{\Phi}_{|K}(\mathbf{r})) = |J|^{-1}\, \partial g l^{k}(u) \times g l^k(v)$$

with : $gl^k \in GL^k$, $g^k \in G^k$,
$\mathbf{\Phi} \in U^{k,k+1}$ and $V^{k,k}$, respectively.

Operators' particularities

In order to complete the discretization's intoduction, one should emphasize the operators' behavior which is specific to the approximate space selected. The EFIE is commonly considered as the most accurate one, but it seems that this is only true for RWG basis functions (first family on triangular mesh). Actually, using Rooftop basis functions (first family on quadrilateral mesh) makes the CFIE more efficient, whereas the MFIE's best results are performed on the second family. These phenomenons are showed in Figure 1. Here we employ usual quadrature rules (Gauss) and low-order basis functions. The sphere's mapping is realized with straight-edge elements.

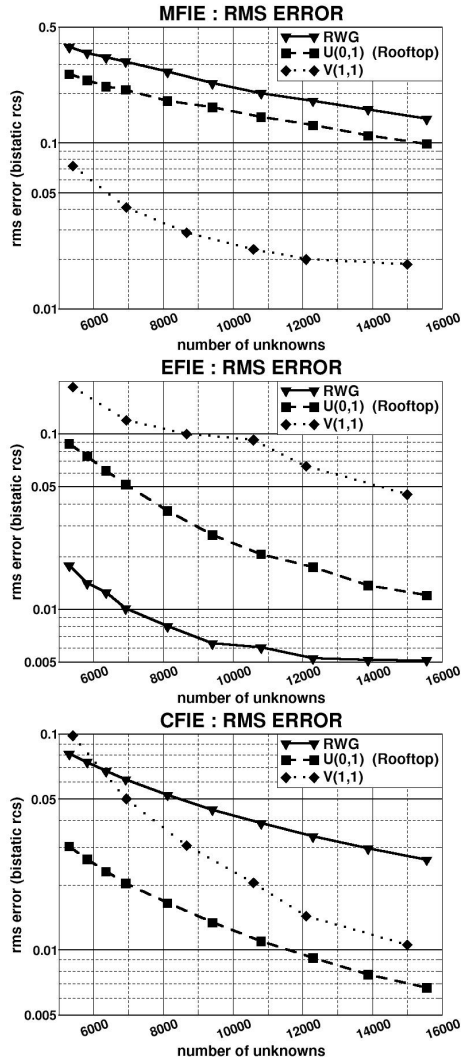

Figure 1: *PEC sphere R=1m. Frequency = 1 GHz. RMS error for MFIE-EFIE-CFIE with low-order basis functions.*

High-Order Spectral Elements

Hdiv Spectral Elements

The approximate spaces we have introduced, used within Gauss and Gauss-Lobatto quadrature rules, describe spectral elements methods.

Let $\{(\xi,\omega)_q^{gl}, q=1,k+1\}$ be the $1D$ Gauss-Lobatto rule's points and weights of order k ($(\xi,\omega)_q^g$ the Gauss' ones). Then we have :

$$gl_i^k(\xi_q^{gl}) = \delta_i^q \;\;,\;\; g_i^k(\xi_q^g) = \delta_i^q \;\;;\;\; 1 \leq i,q \leq k+1 \quad (2)$$

The Gauss-Lobatto rule gives us points on edges, so that the Hdiv property is easily observed. The first family is more complicated in the sense that we have to modify the quadrature rule with the function's direction. We work on a GL/G quadrature rule on the first direction in $2D$, G/GL rule on the second one.

Integral estimations of basis functions and their divergence over K are achieved as follow : $\forall \mathbf{\Phi}_{i,j} \in V^{k,k}$,

$$\int_K \mathbf{\Phi}_{i,j}(\mathbf{r})\, \partial K \;\simeq\; \omega_i^{gl}\, \omega_j^{gl}\, \mathbf{DF}(\xi_i^{gl},\xi_j^{gl})\, \mathbf{e} \quad (3)$$

$$\int_K \mathrm{div}(\mathbf{\Phi}_{i,j}(\mathbf{r}))\, \partial K \;\simeq\; \omega_j^{gl} \sum_{q=1}^{k+1} \omega_q^{gl}\, \partial gl_i^k(\xi_q^{gl}) \quad (4)$$

where $1 \leq i,j \leq k+1$ are the polynomial indexes.
The sum over q in (4) slow down the calculation. Recovering the Dyadic Green's function (1) for far interactions makes us evaluate each double integral on one pair of quadrature points. To overcome the singular behavior of self-term matrix elements, one has to develop quadrature rules under polar coordinates and adaptative orders in the inner integral.

Notice that the approximation's properties of spectral elements converge exponentially with respect to the order. As a consequence, our technique isn't effective with low-order basis functions (order 0,1), for reasonable unknowns' density. Moreover, Gauss rule converges faster than Gauss-Lobatto. That's the reason why accurate results come earlier using the first family, in comparison to the second one.

Numerical Results

As we said in the first part, various authors have dealt with point-based schemes. We propose to use our method on simulations presented in [5][6].

- *PEC sphere R=1m, freq.=1.2GHz*

This case is computed in [5], using second-order basis functions on triangular patches, and a 4-level MLFMA.

We display our results for the first class of quadrilateral elements. The MGCR solver is used with a relative error norm of 10^{-4}.

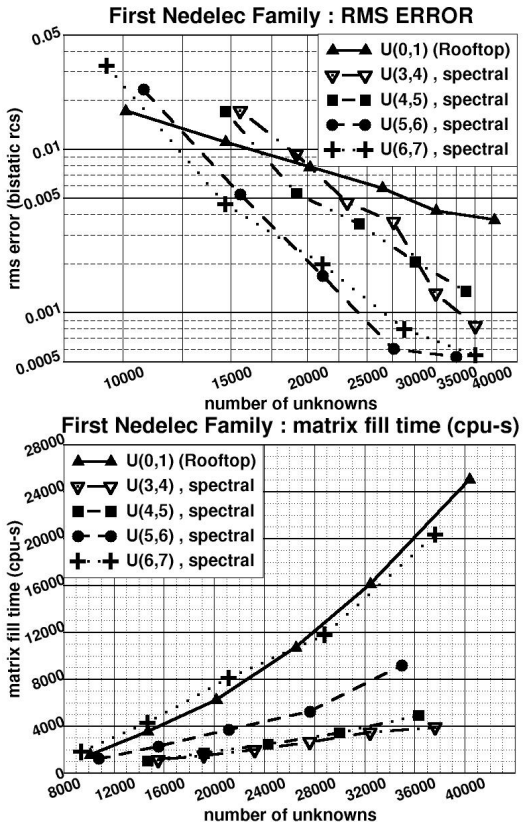

Figure 2: *PEC sphere R=1m. Frequency=1.2GHz. CFIE = 0.5 EFIE + 0.5 MFIE*

The use of the Dyadic Green's function makes the pre-computation time even lower than for low-order schemes. As the number of far interactions increases quadratically with the total number of unknowns, this behavior is amplified in large size problems. As an example, a 2.1GHz test using $60{,}000$ unknowns was made with Rooftop functions against five-order second-kind functions : 14h38 of calculation and a 6.7^{-3} rms error for Rooftop, versus 3h and 4.7^{-3} for the higher-order one.

- *Sphere PEC R=1m, freq.=95MHz ($k_o a = 2$)*

Results are given for both EFIE and MFIE in [6]. If we are more accurate with the EFIE, this trend is reversed with the MFIE. However, the polar quadratures introduced to evaluate singular integrals aren't strong enough to reach extra-precision : we choose to ensure a 10^{-3}-10^{-4} precision only, in order to limit the increase of pre-computation time. Here the order of the mapping function $\mathbf{F}_i$ is adaptative within the subspace's choice : $V^{6,6} \rightarrow 6^{th}$order.

Operator	Subspace	nUnk	Matrix fill time (cpu-s)	RMS error
EFIE	$U^{3,4}$	1728	38	3.49^{-4}
MFIE	$V^{4,4}$	2160	19	1.00^{-4}
CFIE	$U^{3,4}$	1728	53	2.59^{-4}
CFIE	$V^{6,6}$	2016	180	4.43^{-5}

Conclusion

The spectral elements method is efficient in higher-order MoM. The two families we've introduced provide more accurate solutions and a significant reduction of the matrix fill time.

Implementing a fast multipole method is the next step to accomplish. Then, we will adapt the hybrid finite element-boundary integral method used within high-order spectral elements, to handle inhomogeneous media.

References

[1] G. Cohen, M. Duruflé, "Non Spurious Spectral-Like Element Methods for Maxwell Equations", to appear in J. of Comp. Math.,2007.

[2] R.D. Graglia, D.R. Wilton, A.F. Peterson, "High Order Interpolatory Vector Bases for Computational Electromagnetics", IEEE Transactions on Antennas and Propagation,vol.45(3),pp 329-342,March 1997

[3] L.F. Canino, J.J. Ottusch, M.A. Stalzer, J.L. Visher, S.M. Wandzura, "Numerical Solution of the Helmholtz Equation in 2D and 3D Using a High-Order Nyström Discretization", J. of Computational Physics,vol.146,pp 627-663,1998

[4] O.P. Bruno, L.A. Kunyansky, "A Fast, High-Order Algorithm for the Solution of Surface Scattering Problems: Basic Implementation, Tests, and Applications", J. of Computational Physics,vol.169(1),pp 80-110,2001

[5] K.C. Donepudi, J.M. Jin, W.C. Chew, "A Grid-Robust Higher-Order Multilevel Fast Multipole Algorithm for Analysis of 3-D Scatterers", Electromagnetics,vol.23,pp 315-330,2003

[6] S.D. Gedney,"High-Order Method-of-Moments Solution of the Scattering by Three-Dimensional PEC Bodies Using Quadrature-Based Point Matching", Microwave and Optical Technology Letters,vol.29(5),June 2001

Numerical implementation of a Galerkin scheme for solving a BIE in high-frequency problems

V. Domínguez[†,*], **I.G. Graham**[‡,**]

[†]Universidad Pública de Navarra, Campus de Arrosadía s/n, 31006 Pamplona, Spain
[‡]University of Bath, Bath BA2 7AY, United Kingdom
[*]Email: victor.dominguez@unavarra.es
[**]Email: igg@maths.bath.ac.uk

Abstract

In this work we propose a numerical implementation of a Galerkin method for a boundary integral equation appearing in high frequency problems. The numerical scheme, proposed in [3], requires in practice a low number of unknowns to approximate the slow part of the solution with high accuracy. However, the assembly of the matrix requires the computation of double integrals of highly oscillating functions. We show how these integrals can be computed efficiently. Finally, we present some numerical experiments to illustrate the theoretical results.

The continuous problem

Let Γ be a convex, closed and simply connected smooth curve in $\mathbb{R}^2$. For $\widehat{\mathbf{a}}$ a unit vector we construct the plane wave $u_i(\mathbf{x}) = \exp(ik\mathbf{x}.\hat{\mathbf{a}})$ with $k >> 1$. The problem we want to solve is

$$\left| \begin{array}{rcl} \Delta u_s + k^2 u_s &=& 0, \qquad \text{on ext}\,\Gamma \\ u_s|_\Gamma &=& -u_i|_\Gamma \\ \partial_r u_s(z) - iku_s(z) &=& o(|z|^{-1/2}), \end{array} \right.$$

∂_r denoting the radial derivative. The scattered wave can be written in terms of the single layer potential

$$u_s = -\mathcal{S}_k\lambda := -\int_\Gamma \phi_k(\cdot - \mathbf{x})\lambda(x)\,\mathrm{d}\sigma(x)$$

with $\lambda = \partial_n(u_i + u_s)$ and ϕ_k the fundamental solution of the Helmholtz equation.

The density λ, which has a clear physical meaning, is the unique solution of the combined field integral equation (also known as Burton-Miller formulation)

$$\mathcal{R}_k\lambda := \tfrac{1}{2}\lambda + \mathcal{D}_k\lambda - ik\mathcal{V}_k\lambda = g_k, \qquad (1)$$

where $g_k = \partial_n u_i - iku_i$. In the expression above, $\mathcal{V}_k$ and $\mathcal{D}_k$ are the single layer and the adjoint of the double layer operator.

Numerical method

As a numerical solution of (1) we propose that given by

$$\left| \begin{array}{l} \lambda_h \in X_h \\ \displaystyle\int_\Gamma \overline{\xi}_h \mathcal{R}_k\lambda_h = \int_\Gamma \overline{\xi}_h g_k, \quad \forall \xi_h \in X_h \end{array} \right.$$

The discrete space X_h will be specified later. We assume that a Cea's lemma-type result holds

$$\|\lambda - \lambda_h\|_{L_2(\Gamma)} \leq B_k \min_{\xi_h \in X_h} \|\lambda - \xi_h\|_{L_2(\Gamma)},$$

where $B_k > 0$ depends on k but it is independent of X_h and λ. We point out that this result holds for the circle and the sphere (see [3]), where $B_k \approx k^{1/3}$. The case of an arbitrary curve remains as an open problem (see [2] for some new results in this direction).

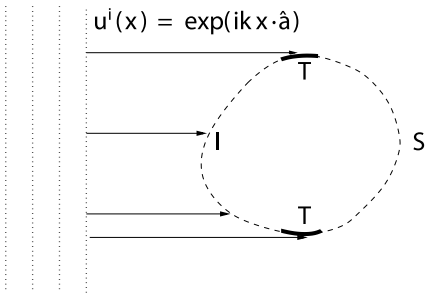

Figure 1: Partition of the curve

Consider $\gamma : [0, L] \to \Gamma$ an arc-length parameterization, with L the length of the curve. Let $0 < t_1 < t_2 < L$ be such that the plane wave impinges tangentially on Γ at $\gamma(t_1)$ and $\gamma(t_2)$. We divide Γ into four well-defined zones (see Figure 1): the illuminated part (**I**), the shadow (**S**) and the transition zones (**T**), usually referred to as Fock domains. Take $\varepsilon, \delta > 0$ and define for appropriate constants α_i, β_i, the intervals

$$\begin{array}{rcl} \Lambda_1 &:=& [t_1 - \beta_1 k^{-1/3+\delta}, t_1 + \alpha_1 k^{-1/3+\varepsilon}] \\ \Lambda_2 &:=& [t_2 - \alpha_2 k^{-1/3+\varepsilon}, t_2 + \beta_2 k^{-1/3+\delta}] \end{array}$$

for the Fock domains and

$$\begin{array}{rcl} \Lambda_3 &:=& [t_1 + \alpha_1 k^{-1/3+\varepsilon}, t_2 - \alpha_2 k^{-1/3+\varepsilon}] \\ \Lambda_4 &:=& [0, L] \setminus \bigcup_{j=1}^3 \Lambda_j. \end{array}$$

corresponding to the illuminated and the shadow part respectively.

The discrete spaces are constructed as follows

$$X_h \;:=\; \bigoplus_{j=1}^{3} \left\{ \chi_j \, p_m \, \exp(\mathrm{i}\, k\, \gamma(\cdot)\cdot \widehat{\mathbf{a}}) \;\middle|\; p_m \in \mathbb{P}_{d_j} \right\}$$

where $\chi_j \in L^\infty(\mathbb{R})$ is the characteristic function of the interval Λ_j and $\mathbb{P}_{d_j}$ the set of polynomials of degree d_j. Notice that in the shadow part, a zero approximation of the function is used.

Theorem ([3]) Let $\varepsilon = 1/9 > \delta > 0$. Then for all n and d_i ($i = 1, 2, 3$) with $6 \le n \le d_i + 1$, there exists $C_n > 0$ independent of k such that

$$\|\lambda - \lambda_h\|_{L_2(\Gamma)} \le C_n \, k^{5/9} B_k \left[\sum_{i=1}^{3} \left[\frac{k^{1/9}}{d_i} \right]^n + \exp(-c_0 k^\delta) \right].$$

Restricting ourselves to the circle, where the precise estimate $B_k \approx k^{1/3}$ is available, we check that taking $d_i \approx k^{1/9}$ is enough to keep the accuracy of the solution (notice that $\|\lambda\|_{L_2(\Gamma)}$ grows proportional to k as k goes to infinity).

Numerical implementation

Each entry of the matrix of the Galerkin method requires the approximation of double integrals of high oscillating functions. The applicability of the method relies heavily on designing efficient quadrature rules for these integrals. This problem can be reduced to the computation of

$$\iint_{\Lambda_i \times \Lambda_j} \exp(ik\Psi(s,t)) M(s,t)\, \mathrm{d}s\, \mathrm{d}t \qquad (2)$$

for large values of k. Here M is a non-oscillating, smooth function, except on the diagonal where a logarithmic singularity occurs, and Ψ is the so-called phase function:

$$\Psi(s,t) = |\gamma(s) - \gamma(t)| - (\gamma(s) - \gamma(t)) \cdot \widehat{\mathbf{a}}.$$

The first term of Ψ comes from the asymptotics of the fundamental solution ϕ_k for large values of k, whereas the second term arises from the complex exponential included in the discrete space.

For the sake of simplicity, we describe the quadrature for $\Lambda_3 \times \Lambda_3$, and we leave as a final comment how to proceed in remaining cases. We first split D into $D^+ \cup D^-$ where $D^+ = \{(s,t) \mid (s,t) \in \Lambda_3 \times \Lambda_3,\ t \ge s\}$ (D^- is defined accordingly). Then, for the integral on D^+, we introduce the change of variables

$$s = s, \quad \tau = \Psi(s,t).$$

Letting $\Psi_s = \Psi(s,\cdot)$, the jacobian is given by

$$j(s,\tau) = \frac{1}{|\partial_t \Psi(s, \Psi_s^{-1}(\tau))|} = \frac{1}{|\Psi_s'(\Psi_s^{-1}(\tau))|}$$

Lemma For all $s, t \in \Lambda_3$, $\partial_t \Psi(s,t) \neq 0$.

Hence, the change of variable is valid. Let $d \in \mathbb{R}$, and $r_1(\tau)$, $r_2(\tau)$ functions describing the transformed domain in such a way

$$\iint_{D^+} \exp(ik\Psi(s,t)) M(s,t) \mathrm{d}s \mathrm{d}t = \int_0^d f(\tau) \exp(ik\tau) \mathrm{d}\tau,$$

with

$$f(\tau) = \int_{r_1(\tau)}^{r_2(\tau)} M(s, \Psi_s^{-1}(\tau)) j(s, \Psi_s^{-1}(\tau))\, \mathrm{d}s.$$

The oscillating term appears now written in a simpler form. Next we apply modified Clenshaw-Curtis formulas, which roughly speaking, consist of replacing f by a piecewise polynomial f_m, which interpolates f at the Chebyshev nodes in each subinterval, and take

$$\int_0^d f(\tau) \exp(ik\tau)\, \mathrm{d}\tau \approx \int_0^d f_m(\tau) \exp(ik\tau)\, \mathrm{d}\tau.$$

Notice that the latter integral can be now evaluated exactly. Clearly, the error behaves as $\|f - f_m\|_{L_p(0,d)}$. The function f is actually smooth, except at $0, d$ and at the points where r_1 or r_2 fails to be smooth (usually, only one). The use of refined meshes for f_m is enough to obtain good approximations for this integral.

On the other hand, the evaluation of f can be carried out effectively using Gaussian rules. However, the jacobian of the change of variables blows up as $(\tau, s) \to (0, t_1)$. This phenomenon becomes relevant as $k \to \infty$ (see the definition of Λ_3), so that the evaluation of f has to be done carefully in the vicinity of $\tau = 0$ for large values of k.

Approximation of the integral in the rest of the domains

The strategy developed above can be adapted to approximate the remaining integrals, provided that $\partial_t \Psi(s,t) \neq 0$ in the domain of integration. This is satisfied, for k high enough, on $\Lambda_1 \times \Lambda_2$. On the other hand, for $\Lambda_1 \times \Lambda_3$ a geometric restriction on the domains, which turns out to be very natural, must be satisfied.

Finally, the integration on the Fock domain has some peculiarities. To gain insight on it, let $D := \Lambda_1 \times \Lambda_1$ and consider D^+, for $t \ge s$, and D^-, $t \le s$ as before. For D^-

the same techniques used before work again. The change of variable, however, is not valid in D^+ because

$$\partial_\alpha^{|\alpha|}\Psi(t_1, t_1^+) = 0, \quad \alpha \in \{s, t, ss, st, tt\}.$$

Hence $k|\Psi(s,t)| \leq Ck^{1/3}$ for $(s,t) \in D^+$. Therefore the oscillations of the integrand (see (2)) on D^+ are not so strong to rule out the use of standard rules, at least for moderate values of k. For higher values of k, a new splitting of D^+ can be considered, so that in one of the new subdomains the change of variables is again applicable, whereas in the other one the integrand is almost non-oscillating.

Numerical experiment

Let Γ be the unit circle and take $\widehat{\mathbf{a}} = (1, 0)$. As a test problem we have taken

$$\int_a^b \int_s^b M(s,t) \exp(ik\Psi(s,t))\, \mathrm{d}s\, \mathrm{d}t$$

(which corresponds to the integration in the illuminated part) where $a = \pi/2 + \pi/100$ and $b = 3\pi/2 - \pi/100$.

We first take $M_1(s,t) = 1$ and $M_2(s,t) = \log(t-s)$ for $k = 0$ (to have an exact solution to compare with). Next table shows the number of points used in the evaluation, the error E_i of our formula for M_i, and the CPU spent in the evaluation

# Points	E_1	E_2	Time of CPU
5922	$6.0\mathtt{E}-08$	$2.0\mathtt{E}-07$	$5.2''$
20341	$4.9\mathtt{E}-10$	$1.4\mathtt{E}-9$	$15''$
67536	$8.1\mathtt{E}-15$	$4.3\mathtt{E}-14$	$49''$

The experiments have been done in Matlab running on a computer with a Core 2 Duo processor and 2GB of RAM memory. Figure 2 shows the transformed domain and the points used for the evaluation for the first rule. Let us emphasise that the performance of the formula is better as it seems at first sight. This is because the bulk of the time is spent in the computation of Ψ_s^{-1}. However, these values should be computed only once, and can be reused to compute more integrals on the same domain. This is what we do in the next experiment with

$$M_3(s,t) = H_0^{(1)}(2k|\sin(\tfrac{s-t}{2})|) \exp(-2ik|\sin(\tfrac{s-t}{2})|).$$

which is a complex non oscillating function. The quadrature rules T_1 with 5922 points and T_2 with 67536 points have been applied with the following result

k	Time of CPU for T_1	Time of CPU for T_2
5	$0.16''$	$0.58''$
50	$0.17''$	$0.45''$
500	$0.19''$	$0.47''$
5000	$0.17''$	$0.45''$

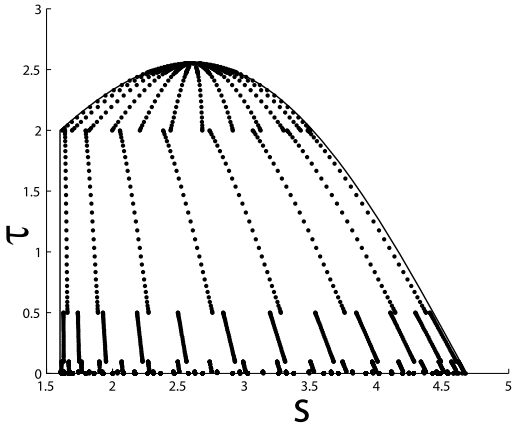

Figure 2: Points use for the quadrature rule T_1

Finally, the relative errors for T_1, when T_2 is taken as the exact value, are presented here

k	50	500	5000	50000
Error	$3.68\mathtt{E}-5$	$1.54\mathtt{E}-5$	$6.48\mathtt{E}-6$	$4.70\mathtt{E}-6$

References

[1] O.P. Bruno, C.A. Geuzaine, J.A. Monro, F. Reitich "Prescribed error tolerances within fixed computational times for scattering problems of arbitrarily high frequency: the convex case", in Philos. Trans. R. Soc. Lond. Ser. A Math. Phys. Eng. Sci. vol 362, pp. 629645, 2004.

[2] S. Chandler-Wilde, P. Monk "Wave-number-explicit bounds in time-harmonic scattering", University of Reading preprint, 2006. Submitted for publication.

[3] V. Domínguez, I.G. Graham, V.P. Smyshlyaev. "A hybrid numerical-asymptotic boundary integral method for high-frequency acoustic scattering". Published online in Numer. Math.

[4] J.M. Melenk, S. Langdon "An hp-BEM for high frequency scattering by convex polygons", Book of Abstracts of IABEM 2006.

Robust boundary integral methods in high frequency acoustic scattering

V. Domínguez[†,*], **I.G. Graham**[‡,**], **V.P. Smyshlyaev**[‡,***]
[†]Universidad Pública de Navarra, Campus de Arrosadía s/n, 31006 Pamplona, Spain
[‡]University of Bath, Bath BA2 7AY, United Kingdom
[*]Email: victor.dominguez@unavarra.es
[**]Email: igg@maths.bath.ac.uk
[**]Email: vps@maths.bath.ac.uk

Abstract

In this talk we discuss the numerical solution of the problem of acoustic plane wave scattering by a 2D convex smooth sound-soft object using hybrid numerical-asymptotic methods.

In recent joint work with Víctor Domínguez (Pamplona) and Valery Smyshlyaev (Bath) we developed Galerkin methods with oscillatory basis functions for this problem and proved that the resulting discretisations are almost uniformly accurate as the wave number k increases.

The key components of the analysis are:

(i) Estimates for the continuity and coercivity of the boundary integral operators explicitly in terms of k.

(ii) A proper description of the asymptotic behaviour of the solution in a format suitable for numerical analysis, by further development of the classical asymptotics results for this problem.

(iii) Design of suitable ansatz spaces for use in the Galerkin method and the analysis of their consistency error.

(iv) Construction of quadrature methods for the highly oscillatory Galerkin integrals.

In the talk we will describe recent results on this programme of work concentrating on items (i) - (iii). The talk by Victor Dominguez in the same minisymposium is linked to this talk and will concentrate on item (iv).

Some of the results presented in these two talks are in the recent paper [1].

A recent review of high frequency boundary integral methods is contained in [2].

References

[1] V. Domínguez, I.G. Graham, V.P. Smyshlyaev. "A hybrid numerical-asymptotic boundary integral method for high-frequency acoustic scattering", Numer. Math. DOI:10.1007/s00211-007-0071-4 (2007).

[2] I.G. Graham, Robust boundary integral methods in high frequency scattering, in **Computational Electromagnetism and Acoustics**, Oberwolfach Report 5/2007 (Eds. R. Hiptmair, R.H.W. Hoppe, P.Joly and U. Langer) (2007). Available electronically at http://www.maths.bath.ac.uk/∼igg/publications

FAST DIRECTIONAL MULTILEVEL SOLVER FOR INTEGRAL FORMULATIONS OF WAVE SCATTERING

Björn Engquist and Lexing Ying
Department of Mathematics, University of Texas at Austin, Austin, TX 78712, USA
Email: (engquist,lexing)@math.utexas.edu

Abstract

This paper describes a new directional multilevel algorithm for solving N-body or N-point problems resulted from integral formulations of wave scattering applications. These problems are difficult since the kernel involved is oscillatory. The starting point of our approach is the observation that the interaction between two point sets has a low rank separable representation as long as they follow an angular separation condition. In order to construct the separable representations numerically, we introduce an efficient procedure based on random sampling. Finally, the resulting low rank representations are embedded in a hierarchical multiscale and multidirectional framework to accelerate the far field computation in an optimal way. This new algorithm is proved to have $O(N \log N)$ complexity, and the numerical results demonstrate the effectiveness of the algorithm in engineering examples.

Introduction

Boundary integral methods for high frequency scattering problems result in very large and dense linear systems of equations. For a scattering surface in three dimensions the number of unknowns typically scales as the square of frequency in order to achieve a prescribed accuracy. When iterative methods are used to solve these systems a bottleneck is matrix vector multiplications with very large matrices. If the kernel in the boundary integral operator is smooth away from the diagonal the fast multipole method (FMM) provides an efficient technique for the matrix vector multiplication, [2]. When the size of the matrix is $N \times N$ the computational complexity can be reduced from the standard $O(N^2)$ to $O(N \log N)$ or $O(N)$. The original FMM does, however, not apply directly to problems with the oscillatory kernels corresponding to high frequency scattering. A new version is needed.

Our application is a potential formulation of the Helmholtz equation in R^3 and the challenge is to develop a fast evaluation method for Gf, where the matrix $G = G(x_j, x_k)$ corresponds to a discretization of,

$$\int G(x,y)f(y)dy, \quad G(x,y) = \frac{e^{2\pi i|x-y|}}{|x-y|}.$$

Even if the focus is on the Helmholtz kernel the technique discussed here generalizes to other oscillatory kernels. In [3] Rokhlin develops a fast solver for special oscillatory kernels. It couples the original FMM to high frequency asymptotics. Our new method is somewhat closer in form to his original FMM.

The low computational complexity in the new method is based on approximate low rank interaction between sets of points. This is also the case in the original FMM when applied to non-oscillatory kernels. The interaction between quadrature point sets that are well separated can be efficiently approximated by a low rank interaction. This is not true for highly oscillatory kernels. It is not enough that the point sets are well separated but we show that they should also satisfy directional constraints.

Algorithm

The new directional multilevel algorithm for solving problems with highly oscillatory kernels can be proved to have $O(N \log N)$ computational complexity for any given accuracy. The key is to exploit low rank far field interaction in different directions. The interaction between a set of points contained in a ball of radius r and a well-separated region has an approximate low rank representation, as long as the well-separated region belongs to a cone with a spanning angle of O($1/r$) and is at a distance which is at least O(r^2) away from the ball. See figure 1.

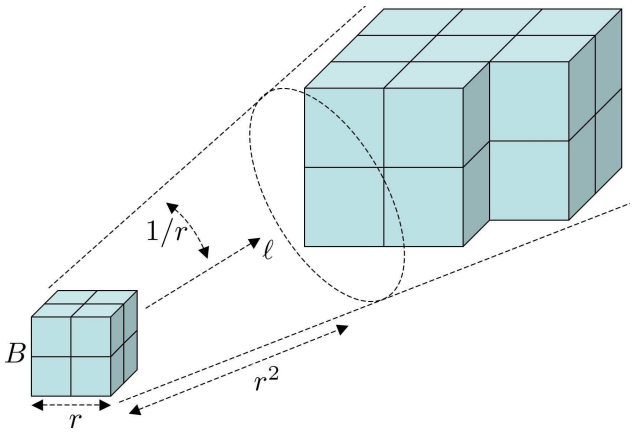

Figure 1: Boxes in an octree belonging to two directionally separated regions.

The directional low rank property follows from a directional separated representation of the Helmholtz kernel,

$$\left| G(x,y) - \sum_{j=1}^{J(\varepsilon)} a_j(x) b_j(y) \right| \leq C\varepsilon.$$

A theorem states that there exist functions a_j and b_j such that the number of terms $J(\varepsilon)$ is independent of the frequency, x and y as long as x and y belong to directionally separated sets. For details see [1].

The proof is constructive but in practice a more efficient algorithm is based on random sampling in order to generate the separated, low rank representation. A subset of the interaction matrix corresponding to directionally separated sets is compressed. The compressed form is achieved by QR decompositions applied to randomly selected subsets of rows and columns. In the compressed form a large number of points is replaced by a finite set of equivalent densities, compare [4]. This random process is imbedded in a hierarchical multiscale and multidirectional strategy. A brief description of the algorithm is as follows.

The first step is to construct an octree of boxes that contain all quadrature points. See figure 1 for a sample of such boxes. Then ascending in the octree visit the boxes in the low frequency regime. These boxes have width less than one wavelength and their outgoing non-directional equivalent densities are computed, see [4]. The next step is again to ascend in the octree and visit the boxes in the high frequency regime. Here the new algorithm is used to determine the outgoing directional equivalent densities.

We then descend in the octree and visit the boxes in the high frequency regime. For every such box and for each direction, transform the outgoing directional equivalent densities to the incoming potentials. Finally go down the octree and focus on the low frequency regime. Transform the outgoing non-directional equivalent densities and add to the incoming potentials.

Numerical Results

The new directional multilevel algorithm is highly efficiency already at a modest number of unknowns and scales as predicted with larger number of points. See table 1. In this numerical example the focus is on the fast matrix vector multiplications. The quadrature points are randomly distributed on the surface. Other geometries give similar substantial improvement over the standard $O(N^2)$ algorithm.

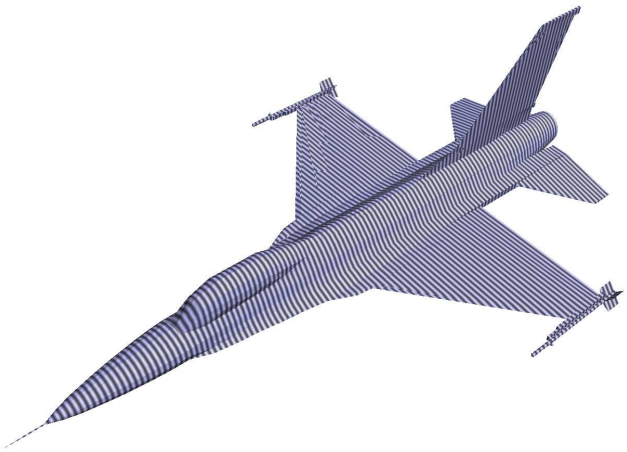

(K, ε)	N	T_a(sec)	Speedup	ε_a
(32, 1e-4)	1.87e+5	5.00e+1	8.34e+1	6.13e-4
(64, 1e-4)	7.46e+5	2.27e+2	2.90e+2	6.69e-4
(128,1e-4)	2.98e+6	1.04e+3	9.87e+2	6.89e-4
(256,1e-4)	1.19e+7	5.04e+3	3.25e+3	7.63e-4
(32, 1e-6)	1.87e+5	1.18e+2	3.44e+1	2.72e-6
(64, 1e-6)	7.46e+5	6.12e+2	1.07e+2	3.30e-6
(128,1e-6)	2.98e+6	3.07e+3	3.45e+2	4.16e-6
(32, 1e-8)	1.87e+5	2.38e+2	1.71e+1	6.34e-8
(64, 1e-8)	7.46e+5	1.29e+3	5.14e+1	8.10e-8
(128,1e-8)	2.98e+6	6.42e+3	1.64e+2	6.55e-8

Table 1: Results on an airplane model. K: number of wavelengths across computational domain, ε: error tolerance, N: total number of unknowns, T_a: computation time for new algorithm, Speedup: the speedup factor over the $O(N^2)$ algorithm, ε_a: error in computed matrix vector product.

References

[1] B. Engquist and L. Ying. "Fast directional multilevel algorithms for oscillatory kernels", SIAM J. Sci. Comp., to appear.

[2] L. Greengard and V. Rokhlin. "A fast algorithm for particle simulations", J. Comput. Phys., 73(2), 325-348, 1987.

[3] V. Rokhlin. "Rapid solution of integral equations of scattering theory in two dimensions", J. Comput. Phys., 86(2):414-439, 1990.

[4] L. Ying, G. Biros, and D. Zorin. "A kernel-independent adaptive fast multipole algorithm in two and three dimensions", J. Comput. Phys., 196(2):591-626, 2004.

High-frequency integral evaluation algorithms for three dimensional obstacle scattering

M. Ganesh[†,*], **I. H. Sloan**[‡,+]
[†]Department of Mathematical and Computer Sciences, Colorado School of Mines, Golden, USA.
[‡]School of Mathematics and Statistics, University of New South Wales, Sydney, Australia.
[*]Email: mganesh@mines.edu [+]Email: i.sloan@unsw.edu.au

Abstract

A key component of surface integral equation based simulation of acoustic/electromagnetic waves scattered by three dimensional obstacles is the efficient evaluation of several integrals defined on the surface of the obstacles. The computational complexity of evaluating such integrals depends on the incident wave frequency, scatterer size and shape, and singularities at observation directions. In this work we describe algorithms for efficient evaluation of such integrals for a class of smooth three dimensional scatterers with diameter that is a large multiple of the wavelength of the incident wave.

Introduction

In this short presentation, we describe some oscillatory surface integrals arising in a three dimensional homogeneous medium for time–harmonic acoustic waves (corresponding details for electromagnetic waves are in [4], [8], [9]) and briefly discuss some problems and efficient approaches for evaluation of such integrals. We are interested in computing an approximation to the *radiating solution* u of the exterior Helmholtz equation

$$\triangle u(\boldsymbol{x}) + k^2 u(\boldsymbol{x}) = 0, \qquad \boldsymbol{x} \in \mathbb{R}^3 \setminus \overline{D}, \tag{1}$$

where $D \subset \mathbb{R}^3$ is assumed to be a bounded connected domain with boundary ∂D and a connected complement $\mathbb{R}^3 \setminus \overline{D}$. The fundamental requirement for our singularity-free surface integral equation reformulation of (1) is that there must exist a point inside D that is a suitable origin for a spherical coordinate system, in which each component of coordinates $\boldsymbol{x} = (x_1, x_2, x_3)$ on the two dimensional surface ∂D has a spherical-Fourier series representation through spherical angles (θ, ϕ). In (1), $k > 0$ is called the wavenumber and we use the standard notion of *radiating solution* [4], i.e. u satisfies the Sommerfeld radiation condition

$$\lim_{r\to\infty} r\,(\partial u/\partial r - iku) = 0, \tag{2}$$

where $r = |\boldsymbol{x}|$ and the limit is assumed to hold uniformly in all directions $\boldsymbol{x}/|\boldsymbol{x}|$.

Problem Formulation

One of the advantages of using a surface integral ansatz (combined with a surface integral equation) to represent the exterior acoustic field u is that the radiation condition (2) is automatically satisfied by the ansatz. For example, assuming that (1) has a unique radiating solution, under appropriate regularity assumptions, by Green's theorem, the radiating solution $u(\boldsymbol{x})$, for $\boldsymbol{x} \in \mathbb{R}^3 \setminus \overline{D}$, can be represented as [4, Theorem 2.4]:

$$u(\boldsymbol{x}) = \int_{\partial D} \left[\frac{\partial \Phi(\boldsymbol{x}, \boldsymbol{y})}{\partial n(\boldsymbol{y})} u(\boldsymbol{y}) - \Phi(\boldsymbol{x}, \boldsymbol{y}) \frac{\partial u}{\partial n}(\boldsymbol{y}) \right] ds(\boldsymbol{y}), \tag{3}$$

where

$$\Phi(\boldsymbol{x}, \boldsymbol{y}) := \frac{1}{4\pi} \frac{\exp(ik|\boldsymbol{x} - \boldsymbol{y}|)}{|\boldsymbol{x} - \boldsymbol{y}|} \tag{4}$$

is the fundamental solution of the Helmholtz equation and $\boldsymbol{n}(\boldsymbol{y})$ denotes the unit outward normal to ∂D at the point $\boldsymbol{y} \in \partial D$. Further, the radiating solution u has the asymptotic behavior of an outgoing spherical wave [4, Theorem 2.5]:

$$u(\boldsymbol{x}) = \frac{e^{ik|\boldsymbol{x}|}}{|\boldsymbol{x}|} \left\{ u_\infty(\hat{\boldsymbol{x}}) + O\left(\frac{1}{|\boldsymbol{x}|}\right) \right\},$$

as $|\boldsymbol{x}| \to \infty$ uniformly in all directions $\hat{\boldsymbol{x}} = \boldsymbol{x}/|\boldsymbol{x}|$. Here, the function u_∞ is known as the acoustic *far field pattern* of u, and it is defined on the unit sphere (denoted throughout by ∂B). Computation of the far field pattern plays an important role in inverse scattering theory, to identify the shape of the scatterer [4]. In electromagnetic scattering, representation of the corresponding electric far field pattern is required to compute the bistatic and monostatic radar cross sections of the obstacle [8], [9].

For the exterior field ansatz (3), if we know the radiating solution u and its normal derivative only on the surface ∂D, then a computable surface integral representation of the far field pattern u_∞ can be obtained, based on the asymptotics of the fundamental solution:

$$\Phi(\boldsymbol{x}, \boldsymbol{y}) = \frac{e^{ik|\boldsymbol{x}|}}{4\pi|\boldsymbol{x}|} \left\{ e^{-ik\hat{\boldsymbol{x}}\cdot\boldsymbol{y}} + O(\frac{1}{|\boldsymbol{x}|}) \right\}. \tag{5}$$

In general, acoustic (and electric) far field representation essentially involves replacing $\Phi(\boldsymbol{x}, \boldsymbol{y})$ in

the exterior acoustic (and electric) field ansatz by $e^{-ik\hat{\boldsymbol{x}}.\boldsymbol{y}}/(4\pi)$ [4], [7], [8], [9].

Using the direct representation formula (3) (or other types of indirect representations [4], [7], [8], [9]), and depending on the boundary condition associated with the three dimensional Helmholtz equation (or the Maxwell equations in electromagnetic case), the exterior radiating solution and its far field pattern can thus be computed, essentially by solving a surface integral equation (for the unknown density in the exterior field ansatz) and evaluation of various singularity-free surface integrals in the exterior field ansatz (due to evaluation points away from the surface ∂D) and the far field formula. The boundary condition is determined by the physical properties of the obstacle (such as sound–soft, sound–hard, absorbing in acoustic case; perfectly conducting, dielectric in electromagnetic case) and the type of incident wave, which has wavelength $\lambda = 2\pi/k$, impinging on the obstacle (such as a plane wave).

For example, in the case of a scalar acoustic plane-wave $u^{\mathrm{i}}(\boldsymbol{x}) := e^{ik\boldsymbol{x}.\hat{\mathbf{d}}}$ impinging on a sound-soft obstacle D with a fixed direction $\hat{\mathbf{d}} \in \partial B$, the total field $u^T = u^{\mathrm{i}} + u$ must vanish on the surface ∂D, and so the boundary condition associated with the Helmholtz equation (1) for the exterior scattered field is $u(\boldsymbol{x}) = -u^{\mathrm{i}}(\boldsymbol{x})$ for $\boldsymbol{x} \in \partial D$. Using the fact that plane-wave is an entire solution of the Helmholtz equation, (3), and the Green's formula for $u^{\mathrm{i}}(\boldsymbol{x})$, the scattered and far fields can be computed by evaluating the singularity-free surface integrals [4]

$$u(\boldsymbol{x}) = -\int_{\partial D} \Phi(\boldsymbol{x},\boldsymbol{y}) v(\boldsymbol{y}) ds(\boldsymbol{y}),\ \boldsymbol{x} \in \mathbb{R}^3 \setminus \partial D, \quad (6)$$

$$u_\infty(\hat{\boldsymbol{x}}) = -\int_{\partial D} \frac{e^{-ik\hat{\boldsymbol{x}}.\boldsymbol{y}}}{4\pi} v(\boldsymbol{y}) ds(\boldsymbol{y}), \quad \hat{\boldsymbol{x}} \in \partial B, \quad (7)$$

where the unknown density function $v := \frac{\partial u^T}{\partial n}$ satisfies the weakly–singular surface integral equation

$$v + \mathcal{K}'v - i\mathcal{S}v = 2\frac{\partial u^{\mathrm{i}}}{\partial n} - 2iu^{\mathrm{i}}, \qquad \text{on} \quad \partial D \quad (8)$$

with $\mathcal{K}'$ being the normal derivative of the single-layer acoustic operator $\mathcal{S}$, which is defined by

$$\mathcal{S}\psi(\boldsymbol{x}) := 2\int_{\partial D} \Phi(\boldsymbol{x},\boldsymbol{y})\psi(\boldsymbol{y}) ds(\boldsymbol{y}), \quad \boldsymbol{x} \in \partial D. \quad (9)$$

High-frequency Problems

The example surface integrals described above exhibit typical oscillatory behavior of integrals that arise in general computational acoustic and electromagnetic scattering problems.

In three dimensional computational acoustics and electromagnetics, for high-frequency scattering (i.e. the diameter of the obstacle is $c\lambda$ with, say, $c \geq 100$), the computational cost of evaluating all of the highly oscillatory surface integrals required to discretize the weakly-singular surface integral equation using standard fully-discrete algorithms (using quadrature) is prohibitive. The situation is similar for standard quadrature based evaluation of singularity-free high-frequency surface integrals for exterior field and radar cross section visualization using thousands of points and directions. The present work is concerned with design and analysis of efficient algorithms for approximating such high-frequency surface integrals.

For high-frequency problems, by considering the boundary of a convex obstacle locally (in a leading order approximation) as a plane at each point, one may use appropriate asymptotics (physical optics or Kirchhoff approximation [13]) for the illuminated region and special approximations for the shadow and transition zones to reduce the number of unknowns and the number of integrals required for the discretization, with accuracy increasing as the wavenumber k increases (specifically accuracy $\mathcal{O}(k^{-\alpha})$ for $\alpha > 0$). Such an approach has recently been implemented successfully and analyzed in various ways for computational high-frequency acoustic scattering by single and multiple two dimensional convex obstacles in [2], [5], [6], [11], [12] and related references therein. However, for high-frequency acoustic scattering by three dimensional convex obstacles one encounters substantial difficulties in such approximations and computations, for example in finding stationary points of various types, and efficient approximations in shadow and transition regions. For recent, but limited progress, in this area for acoustic scattering by three dimensional convex obstacles, we refer to [1], [10] and references therein.

Three dimensional high-frequency scattering simulations through surface integral equations have two main difficulties: $1/r$ type singularities and high-oscillations. For designing high-order algorithms, even for low frequency problems, it is important to treat singularities exactly. Such an analytic approach, for example, requires specific parametric and coordinate details to take advantage of the Jacobian in coordinate transformation to cancel out the singularity. This approach combined with a specific parameterization of the obstacle (as specified in the Introduction) was used to design the efficient spectrally-accurate low to medium frequency three dimensional acoustic scattering algorithm in [7] and elec-

tromagnetic scattering algorithm in [8], [9]. A similar approach (with local polar coordinate system) was used to design a high-order algorithm for acoustic scattering in [3]. The 'exact treatment of singularities' approach is crucial when tackling the difficulties associated with the highly-oscillatory nature of various surface integrals arising in high-frequency scattering simulations. Although algorithms and analysis in [7], [8], [9] are applicable for any frequency problem, for practical realization these algorithms are not efficient for very high-frequency case.

In this work we explore variants of the recent three dimensional scattering algorithms [1], [7], [8], [9], [10] for high-frequency integrals defined on the surface of smooth convex three dimensional obstacles that facilitate exact treatment of singularities for acoustic and electromagnetic scattering.

High-frequency scattering by a connected non-convex three dimensional obstacle (and hence multiple scattering by non-convex obstacles) is an even more challenging open problem. Any algorithm that facilitates efficient simulations to measure the bistatic and monostatic radar cross section of three dimensional connected non-convex obstacles with large diameter $c\lambda$ would be a major breakthrough in scattering, even for the case $50 \leq c \leq 500$. The asymptotics approximation approach may not be efficient or suitable for the three dimensional non-convex case. We plan for a non-asymptotic based approach for non-convex obstacle scattering using certain compression techniques (such as those used in wavelets based algorithms to compute approximate solutions of boundary integral equations).

Acknowledgments

Support of the Australian Research Council is gratefully acknowledged.

References

[1] O. P. Bruno and C. A. Geuzaine. An $\mathcal{O}(1)$ integration scheme for three-dimensional surface scattering problems. *J. Comp. Appl. Math.*, to appear, 2007.

[2] O. P. Bruno, C. A Geuzaine, J. A. Monro, and F. Reitich. Prescribed error tolerances within fixed computational times for scattering problems of arbitrarily high frequency: the convex case. *Philos. Trans. R. Soc. Lond. Ser. A Math. Phys. Eng. Sci.*, 362:629–645, 2004.

[3] O. P. Bruno and L. A. Kunyansky. A fast, high-order algorithm for the solution of surface scattering problems: Basic implementation, tests, and applications. *J. Comput. Phys.*, 169:80–110, 2001.

[4] D. Colton and R. Kress. *Inverse Acoustic and Electromagnetic Scattering Theory*. Springer, 1998.

[5] V. Domínguez, I. G. Graham, and V. P. Smyshlyaev. A hybrid numerical-asymptotic boundary integral method for high-frequency acoustic scattering. *Numer. Math.*, to appear, 2007.

[6] F. Ecevit and F. Reitich. Analysis of multiple scattering iterations for high-frequency scattering problems. I: The two-dimensional case. *Preprint*, 2006.

[7] M. Ganesh and I. G. Graham. A high-order algorithm for obstacle scattering in three dimensions. *J. Comput. Phys.*, 198:211–242, 2004.

[8] M. Ganesh and S. C. Hawkins. A spectrally accurate algorithm for electromagnetic scattering in three dimensions. *Numer. Algorithms*, 43:25–60, 2006.

[9] M. Ganesh and S. C. Hawkins. A hybrid high-order algorithm for radar cross section computations. *SIAM J. Sci. Comput., to appear*, 2007.

[10] M. Ganesh, S. Langdon, and I.H. Sloan. Efficient evaluation of highly oscillatory acoustic scattering surface integrals. *J. Comp. Appl. Math.*, to appear, 2007 (doi:10.1016/j.cam.2006.03.029).

[11] C. Geuzaine, O. Bruno, and F. Reitich. On the $\mathcal{O}(1)$ solution of multiple-scattering problems. *IEEE Trans. Magnetics*, 41:1488–1491, 2005.

[12] S. Langdon and S. N. Chandler-Wilde. A wavenumber independent boundary element method for an acoustic scattering problem. *SIAM J. Numer. Anal.*, 43:2450–2477, 2006.

[13] R. B. Melrose and M. E. Taylor. Near peak scattering and the corrected Kirchhoff approximation for a convex obstacle. *Adv. in Math.*, 55:242–315, 1985.

NON-CONFORMING FINITE ELEMENTS FOR WAVE SIMULATIONS ON LARGE GEOMETRIES

B. Heubeck[†,*], **C. Pflaum**[†], **G. Steinle**[‡]
[†]Department of System Simulation (LSS), University of Erlangen-Nuremberg, 91058 Erlangen, Germany
[‡]Infineon Technologies AG, Development Center Munich, 85579 Neubiberg, Germany
[*]Email: britta.heubeck@informatik.uni-erlangen.de

Abstract

We present a new approach to simulate waves on large geometries. This method is based on newly developed Finite Elements, so-called Trigonometric Finite Wave Elements (TFWE), which are constructed by linear elements as well as by trigonometric functions such that the one-dimensional Helmholtz equation is exactly solved under certain conditions. In comparison with the Transfer Matrix Method the TFWE method offers as good results, but it can be extended to higher dimensions and it can be applied to time-dynamic problems. In two dimensions the TFWE are non-conforming elements. The analysis of TFWE shows that these elements approximate functions with certain oscillation properties more accurate than standard Finite Elements. Thus, a Finite Element discretization with TFWE leads to a smaller system of equations, which eases the solving process. Numerical results obtained by applying the TFWE method to the simulation of the wave equation for Distributed Feedback lasers are presented.

Derivation and Convergence of the Trigonometric Finite Wave Elements

Our aim is to solve the two-dimensional wave equation

$$-2\mathrm{i}\frac{k^2}{\omega}\frac{\partial E}{\partial t} = -\triangle E - k^2 E, \tag{1}$$

which is coupled with a pair of partial differential equations for the carrier density called drift diffusion equation (see [1]):

$$\begin{aligned}\frac{\partial n_A}{\partial t} &= \nabla(D_A \nabla n_A) + \frac{n_B}{\tau_{cap}} - \frac{n_A}{\tau_{esc}} - r_{rec,A},\\ \frac{\partial n_B}{\partial t} &= \nabla(D_B \nabla n_B) + \eta_{i,leck}\frac{j_{inj}}{q d_B} - \frac{n_B}{\tau_{cap}}\frac{d_A}{d_B}\\ &\quad + \frac{n_A}{\tau_{esc}}\frac{d_A}{d_B} - r_{rec,B}.\end{aligned}$$

In standard simulations the above wave equation is reduced to the following stationary one-dimensional Helmholtz equation:

$$-\frac{\partial^2 E}{\partial x^2} - k^2 E = 0 \quad \text{on} \quad \Omega =]0, L[, \tag{2}$$

where $k : \Omega \to \mathbb{R}$ is a piecewise constant function such that k is constant on the intervals $s_j =]p_{j-1}, p_j[$, $j = 1, ..., N$, $p_j = \frac{L}{N} j$ and $N \in \mathbb{N}$. Let us abbreviate $k_j = k\left(\frac{p_{j-1}+p_j}{2}\right)$.

A common and well-established method to solve the time-periodic Helmholtz equation (2) is the Transfer Matrix Method (TMM). The idea of this method is that the solutions of (2) are contained in $\mathcal{C}^1(\Omega)$ and that E has the form

$$E(z) = \alpha_j \exp(-\mathrm{i}k_j z) + \beta_j \exp(\mathrm{i}k_j z) \text{ for } z \in s_j, \tag{3}$$

where the coefficients α_j and β_j, $j \in \{1, ..., N\}$, have to satisfy two continuity equations resulting from the continuity of E and $\frac{dE}{dz}$ at the grid points p_j.

But general simulations require time-dependent, two-dimensional discretizations of (1), which cannot be obtained by the TMM. Standard Finite Element methods cannot be applied, as for resolving the wave appropriately, a huge amount of grid points is needed. Furthermore, the Beam Propagation Method is not suitable, as by this method it is very difficult to simulate internal reflections.

We propose a new Finite Element method, which provides for the one-dimensional Helmholtz equation as good results as the TMM, but which can be extended to two and three dimensions and can also be applied to time-dynamic calculations. The new method is similar to the method described in [2], however, the two-wave ansatz cannot be applied to simulate internal reflections, which appear in Distributed Feedback (DFB) lasers. Let us explain the new method in one dimension. The idea is to construct new basis functions by multiplying $v^h_{p_j}(z)$ with trigonometric cosine and sine functions, which approximate the behavior of an oscillating wave. In case of linear Finite Elements, $v^h_{p_j}(z)$ denotes the nodal basis function, which is 1 at p_j and 0 at all other grid points p_i, $i \neq j$, where $h = \frac{L}{N}$ is the mesh size of the discretization grid. Now we can define the following basis functions at grid point p_j:

$$B_j^{\cos}(z) := \cos\big(k(z)(z - p_j)\big) v^h_{p_j}(z),$$

$$B_j^{\sin}(z) := \sin\big(k(z)(z - p_j)\big) v^h_{p_j}(z),$$

and

$$B_j^{mix}(z) := mix\big(k(z)(z-p_j)\big)v_{p_j}^h(z)$$
$$:= \begin{cases} -\sin\big(k_j(z-p_j)\big)v_{p_j}^h(z) & \text{if } z \le p_j \\ \sin\big(k_{j+1}(z-p_j)\big)v_{p_j}^h(z) & \text{if } z > p_j. \end{cases}$$

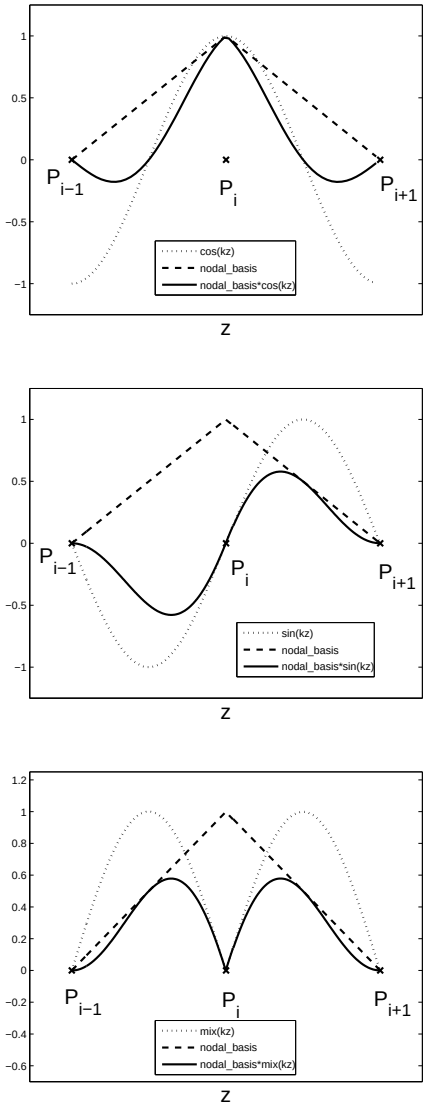

Figure 1: Cosine, Sine, and Mixed Basis Function

These basis functions are called Trigonometric Finite Wave Elements and span the space

$$V_h := \Big\{ u \in H^1(\Omega) \quad | \quad u(z) = \sum_{j=0}^{N} a_j B_j^{\cos}(z) + b_j B_j^{\sin}(z) + c_j B_j^{mix}(z), \; a_j, b_j, c_j \in \mathbb{C}, \; c_0 = c_N = 0 \Big\}.$$

Introducing suitable boundary conditions, which can be handled by TMM as well as by TFWE, we can show that the solutions (3) of the one-dimensional Helmholtz equation derived by the TMM are contained in the space spanned by the TFWE (see [3]).

An important advantage of the TFWE method in comparison with the TMM is that it can be applied to general wave number coefficients k and in two and more dimensions:

Let $\Omega =]0, L[\times]0, W[$ and let $k \in L^\infty(\Omega)$ such that k is a continuous function on each subdomain $]H(j-1), Hj[\times[0, W]$, $j = 1, ..., m$, where $H = \frac{L}{m}$ and $m \in \mathbb{N}$. Now, we introduce two meshsizes $h_x = \frac{L}{N_x}$ and $h_y = \frac{W}{N_y}$ and the meshsize tuple $\boldsymbol{h} := (h_x, h_y)$, where $N_x = nm$, $n \in \mathbb{N}$, and $N_y \in \mathbb{N}$. This leads to the grid points $p_{ij} := (x_i, y_j) := (ih_x, jh_y)$ and grid cells $r_{ij} = [x_{i-1}, x_i]\times]y_{j-1}, y_j[$, $i \in \{1, ..., N_x\}$, $j \in \{1, ..., N_y\}$, such that $\bigcup_{j=1}^{N_y}\bigcup_{i=1}^{N_x} \bar{r}_{ij} = \Omega$.

Now, let $k_{\boldsymbol{h}}$ be the interpolant of k at the midpoints of each cell r_{ij} such that $k_{\boldsymbol{h}}$ is piecewise constant on $\mathring{r}_{ij}$. This means that $k_{\boldsymbol{h}}(x, y) := k_{ij} := k(\frac{x_{i-1}+x_i}{2}, \frac{y_{j-1}+y_j}{2})$ for every $(x, y) \in \mathring{r}_{ij}$. We construct the TFWE in two dimensions by taking the tensor product of the one-dimensional TFWE and the linear nodal basis functions in y-direction. Thus, we get the following basis functions at grid point p_{ij}:

$$B_{ij}^{\cos}(x, y) := \cos\big(k_{\boldsymbol{h}}(x, y)(x - x_i)\big)v_{x_i}^{h_x}(x)v_{y_j}^{h_y}(y),$$

$$B_{ij}^{\sin}(x, y) := \sin\big(k_{\boldsymbol{h}}(x, y)(x - x_i)\big)v_{x_i}^{h_x}(x)v_{y_j}^{h_y}(y),$$

and

$$B_{ij}^{mix}(x, y) := mix\big(k_{\boldsymbol{h}}(x, y)(x - x_i)\big)v_{x_i}^{h_x}(x)v_{y_j}^{h_y}(y),$$

where

$$mix\big(k_{\boldsymbol{h}}(x, y)(x - x_i)\big) = \begin{cases} -\sin\big(k_{\boldsymbol{h}}(x, y)(x - x_i)\big) & \text{if } x \le x_i \\ \sin\big(k_{\boldsymbol{h}}(x, y)(x - x_i)\big) & \text{if } x > x_i. \end{cases}$$

As these basis functions are discontinuous in y-direction, let us define the space $\Omega_{\boldsymbol{h}} := \bigcup_{i=1}^{N_x}\bigcup_{j=1}^{N_y} r_{ij}$ and the corresponding seminorm

$$|u|_{H^1(\Omega_{\boldsymbol{h}})} := \left(\sum_{i=1}^{N_x}\sum_{j=1}^{N_y} \int_{r_{ij}} \Big|\frac{\partial u}{\partial x}(x, y)\Big|^2 + \Big|\frac{\partial u}{\partial y}(x, y)\Big|^2 d(x, y) \right)^{\frac{1}{2}}.$$

Then these TFWE span the space

$$V_{\boldsymbol{h}}^{2D} := \Big\{ u \in H^1(\Omega_{\boldsymbol{h}}) \big|\ u(x,y) = \\ = \sum_{j=0}^{N_y} \sum_{i=0}^{N_x} a_{ij} B_{ij}^{\cos}(x,y) + b_{ij} B_{ij}^{\sin}(x,y) \\ + c_{ij} B_{ij}^{mix}(x,y) \quad \forall (x,y) \in \Omega, \\ a_{ij}, b_{ij}, c_{ij} \in \mathbb{C},\ c_{0j} = c_{N_x j} = 0 \Big\}.$$

Remark. As $H^1(\Omega_{\boldsymbol{h}}) \not\subseteq H^1(\Omega)$, the Finite Element space $V_{\boldsymbol{h}}^{2D} \not\subseteq H^1(\Omega)$ is non-conforming.

Let us consider the following weak problem derived from a time discretization of (1):

Find $u \in H^1(\Omega)$ such that $a(u,v) = \boldsymbol{f}(v),\ \forall v \in H^1(\Omega)$, where

$$a(u,v) := \int_\Omega \big(\nabla u(x,y) \nabla \bar{v}(x,y) - k^2 u(x,y) \bar{v}(x,y) \\ + \mathrm{i}\beta u(x,y) \bar{v}(x,y) \big) d(x,y)$$

and $\beta > 0$.

Let us assume that the solution u satisfies the Oscillation Assumption:

Assumption 1 (Oscillation Assumption) *Let $u \in H^2(\Omega_{\boldsymbol{h}})$ be a function oscillating with an angular frequency ω similar to ck, where c is the velocity of light. In mathematical notation this means that u can be written as*

$$u = u^+ \exp(\mathrm{i}kx) + u^- \exp(-\mathrm{i}kx),$$

where $u^+ \exp(\mathrm{i}kx) \in C(\Omega)$, $u^- \exp(-\mathrm{i}kx) \in C(\Omega)$, $|\frac{d^2 u^+}{dx^2}|_{L^2(\hat{\Omega}_{\boldsymbol{h}})} \ll |\frac{d^2 u}{dx^2}|_{L^2(\Omega)}$, and $|\frac{d^2 u^-}{dx^2}|_{L^2(\hat{\Omega}_{\boldsymbol{h}})} \ll |\frac{d^2 u}{dx^2}|_{L^2(\Omega)}$.

Herein, $|u|_{X(\hat{\Omega}_{\boldsymbol{h}})}$ defines the X-norm of the space $\hat{\Omega}_{\boldsymbol{h}} := \bigcup_{i=1}^{N_x} \bigcup_{j=1}^{N_y} \overset{\circ}{r}_{ij}$.

Theorem 1 *Let $u \in H^2(\Omega)$ satisfy Assumption 1. Then, there exists a constant c independent of $h := \max\{h_x, h_y\}$ such that*

$$|u - u_{\boldsymbol{h}}|_{H^1(\Omega_{\boldsymbol{h}})} \leq ch \Big(|u^+|_{H^2(\hat{\Omega}_{\boldsymbol{h}})} + |u^-|_{H^2(\hat{\Omega}_{\boldsymbol{h}})} \Big)$$

holds.

The proof of this theorem can be found in [3].

Application and Numerical Results

Finally, we present numerical simulation results for the optical wave in DFB lasers achieved by the TFWE method. We solved the weak form of (1) numerically, where laser resonators of different size emitting at wavelength $1300nm$ were considered. In Figure 2 a laser resonator of size $30\mu m \times 130\mu m$ with a small stripe width of size $2\mu m$ was chosen, whereas in Figure 3 a laser resonator of size $120\mu m \times 130\mu m$ with a large stripe width of size $40\mu m$ is shown. Herein, the photon density n is defined by $n = \frac{\epsilon}{2\hbar\omega}(|E|^2)$.

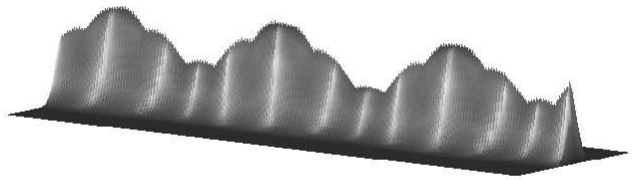

Figure 2: Photon density n: mode of first order is achieved by a small stripe width s

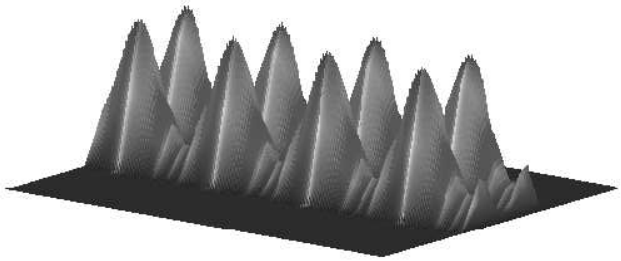

Figure 3: Photon density n: mode of higher order due to a "large" stripe width s

References

[1] G. Steinle, "Neuartige monolithische InAlGaAsN Vertikallaserdioden: langwellige Emission bei $1.3\mu m$, Monitordiodenintegration, Modellierung", Ph.D. thesis, Institute of Optoelectronics, Ulm University, Germany, 2002.

[2] K. Altmann, C. Pflaum, and D. Seider, "Three-Dimensional Finite Element Computation of Laser Cavity Eigenmodes", Applied Optics-LPE, vol. 43, n° 9, pp. 1892-1901, 2004.

[3] B. Heubeck, C. Pflaum, and G. Steinle, "New Finite Elements for Large-Scale Simulation of Optical Waves", in preparation.

WHY IS A SHOCK NOT A CAUSTIC?

C. J. Howls[†,*]
[†]School of Mathematics, University of Southampton, Highfield, Southampton, SO17 1BJ
[*]Email: c.j.howls@maths.soton.ac.uk

Abstract

We discover, identify and examine an apparently critical asymptotic paradox that underlies nonlinear smoothed-shock formation. Fortunately for anyone modelling shocks, the issue can be resolved by the newly discovered "higher order Stokes phenomenon". A pedagogical example is used to explain the problem, but we also indicate the generality of the idea.

Introduction

A vast toolbox of asymptotic techniques exists for attacking and interpreting smoothed nonlinear shock formation, one of the most obvious being matched expansions. Here we take an exponential asymptotic approach and apply to the pedagogical problem of a Burgers equation that develops a smoothed shock.

$$u_t + uu_x = \epsilon^2 u_{xx},$$
$$u(x,0) = \frac{1}{1+x^2},\ \epsilon \to 0^+,$$

for $-\infty < x < +\infty, t > 0$. Within large classes, the particular boundary data chosen does not change the main conclusions of the work.

We use asymptotic expansions in ϵ that take into account exponentially small terms that grow spatially in x to generate the shock wave transition. A smoothed shock can be said to occur when two such exponential terms exchange dominance over a narrow range of x.

Thus far will be familiar territory to many, as there is an intimate link between the matched asymptotic approach and exponential asymptotics: the former is here the leading order behaviour of the latter.

Coalescence of exponents and caustics

From 1-D WKB analysis, it is well-known that "turning points" (or "caustics") can arise in asymptotic approximations when two exponents coalesce. The simplest example of this is the expansion of the Airy function $\mathrm{Ai}(z)$ which has expansions

$$2\sqrt{\pi}\mathrm{Ai}(z) \sim \begin{cases} z^{-1/4}\exp(-\frac{2}{3}z^{3/2}), & z \to +\infty, \\ 2|z|^{-1/4}\sin(\frac{2}{3}|z|^{3/2}+\frac{\pi}{4}), & z \to -\infty. \end{cases}$$

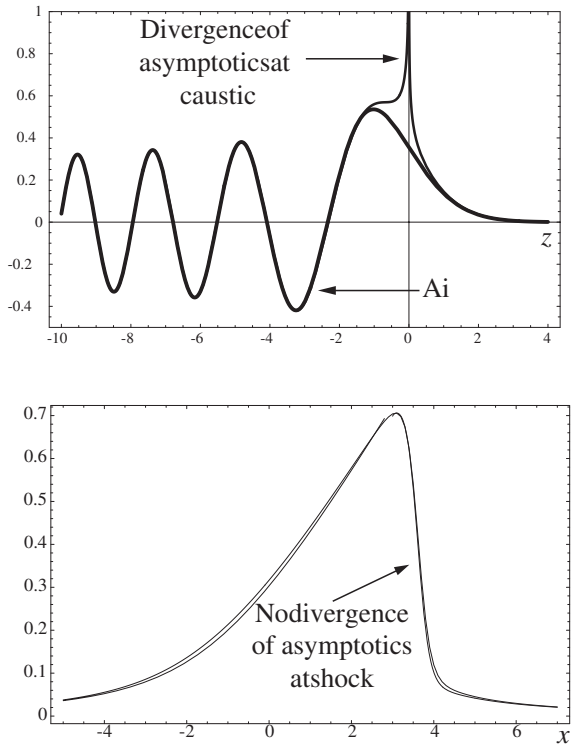

Figure 1: Comparison of asymptotic behaviours for the Airy function (top) and Burgers (bottom, with $\epsilon = 0.05$) at points where the exponents involved are equal. For the Airy function every term in the asymptotics is singular at the caustic at $z = 0$. For Burgers, there is no such divergence at the shock, where the exponents are also equal as they exchange dominance.

As $z \to 0^-$ the two exponents generating the sine function coalesce. Simultaneously the prefactor $|z|^{-1/4}$ diverges and the expansion breaks down. A turning point or caustic exists at $z = 0$. An exponential asymptotic study shows that actually every term in the expansions are singular. This is because they take the asymptotic form of a factorial divided by a power of the difference in the exponents. For example for $z > 0$,

$$2\sqrt{\pi}\mathrm{Ai}(z) \sim z^{-1/4}\exp(-\tfrac{2}{3}z^{3/2})\sum_{r=0}^{\infty} a_r(z)$$
$$a_r(z) \sim \frac{(r-1)!}{2\pi(\frac{4}{3}z^{3/2})^r},\ r \to \infty.$$

Exponential asymptotics shows that this behaviour of the coefficients is generic at a turning point/caustic.

Nonlinear asymptotic paradox

Returning to the nonlinear smoothed shock, we now encounter a paradox. If the shock transition is caused by an exchange of dominance, and therefore the coalescence of exponents, then why does the exponential asymptotic (or matched asymptotic) expansion remain non-singular at the shock position?

Higher order Stokes phenomenon

The resolution of this problem comes by considering sub-sub-dominant terms. For then, once discovers the influence of the "Higher Order Stokes Phenomenon".

At an ordinary "Stokes Phenomenon" an asymptotic expansion can acquire an exponentially subdominant term a set of parameters is crossed, the Stokes set. In a single complex dimension, the Stokes sets are just lines that run between turning points and/or infinity. In other regions of parameter space, this may grow to dominate. In the case of the Airy function $\mathrm{Ai}(z)$ a Stokes phenomenon occurs across the Stokes line $\arg(z) = 2\pi/3$ and a second exponentially-prefactored contribution is born that grows to help form the sinusoidal approximation when $\arg(z) = \pi$.

At a "Higher Order Stokes Phenomenon", (HOSP) the activity of a Stokes line changes. This may cause a Stokes line to "switch off" at a perfectly regular point in space. This effect was first observed by Berk et al [1], and then discussed at length in different contexts by Kawai et al [2], Howls *et al* [3] and Chapman and Mortimer [4].

The mechanism for the switching-off of the activity of the Stokes line is a change in the Riemann-sheet structure of the Borel plane, a natural dual space to work in when attacking problems with exponential asymptotics. This change in structure requires at least three singularities in the Borel plane, each singularity corresponding to a different asymptotic contribution in the original coordinates. At a HOSP, at least three Borel plane singularities are colinear, so that, as viewed from one of the singularities, a second eclipses a third. At this eclipse the third singularity passes through a cut from the second and onto a different Riemann sheet from the first. The first and third singularities can then no-longer interact directly, and so a Stokes phenomenon between the associated asymptotic contributions can no-longer take place. It is important to stress that no change in the leading order or first subdominant behaviour occurs at a HOSP. This partially explains why their effects had not been noticed before, even in the asymptotics of integrals involving three or more saddles.

Role of the HOSP in smoothed shocks

In the context of the Burgers example, we can show that a higher order Stokes curve surrounds the shock region. The associated HOSP switches off the activity of a Stokes line along the real axis in the shock region By itself, the lack of a Stokes line on the real axis is of lesser importance. That the associated Borel plane singularities have consequently changed the structure of the Borel plane however is of vital importance. For then the singularities that apparently coalesce (along with the asymptotic exponents) at the actual shock position as the exponents change dominance, do not in fact do so, because they are now on different Riemann sheets. This means that, since the dominant behaviour of the coefficients cannot involve the exponent arising from the singularity on the different Riemann sheet, the individual terms in the expansion cannot become singular at the shock. Hence the exponential asymptotic (and so matched asymptotic) expansion cannot become singular at the shock.

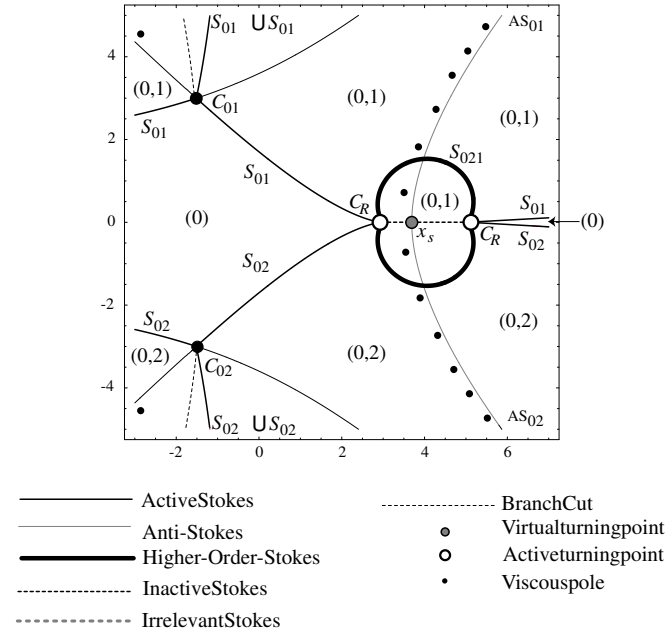

Figure 2: Location of the Stokes, anti-Stokes, higher-order Stokes lines, together with the poles, caustics and shock location x_s (a virtual caustic, due to the HOSP) in the complex x-plane surrounding the shock region for times after smoothed shock formation, both for $\epsilon = 0.075$. The numbers in brackets within a Stokes region, denote the family of Borel singularities that are contributing to the asymptotics.

Full details and diagrams are included [4]. This approach is not dependent on the existence of a Cole-Hopf-type solution to Burgers' equation and can be generalised to other Riemann-type nonlinear shock equations.

References

[1] H.L. Berk, W.M. Nevins, K.V. Roberts, K. V. "New Stokes lines in WKB theory", J. Math. Phys. 23, 9881002 (1982).

[2] T.Aoki, T.Kawai, Y.Takei, "On the exact steepest descent method: a new method for the description of Stokes curves", J. Math. Phys. 42 , 3691-3713, (2001).

[3] C.J.Howls, P.J. Langman A.B. Olde Daalhuis, "On the higher order Stokes phenomenon", Proc. R. Soc. Lond. Ser. A Math. Phys. Eng. Sci. 460, 2285-2303, (2004).

[4] S.J.Chapman, C.J.Howls, J.R.King, A.B. Olde Daalhuis, "Why is a shock not a caustic? The higher order Stokes phenomenon and smoothed shock formation.", submitted to "Nonlinearity", (2007).

AN INTEGRATION SCHEME FOR THE 2D PARTITION OF UNITY BOUNDARY ELEMENT METHOD IN WAVE PROPAGATION

M. E. Honnor and J. Trevelyan
School of Engineering, Durham University, UK
Email: m.e.honnor@durham.ac.uk

Abstract

In this paper we concentrate on the highly oscillatory integrals that arise in the 2D partition of unity boundary element method in wave propagation. The integrations are performed using the numerical steepest descent method. The method is based on Cauchy's integral theorem and replaces the integral over the real interval by an equivalent integral along a path in the complex plane such that the integrand is no longer oscillatory along the path and exhibits exponential decay.

Introduction

We address frequency domain problems of linear wave scattering governed by the Helmholtz equation

$$\nabla^2\phi + k^2\phi = 0 \tag{1}$$

where k is the wavenumber, given by $k = 2\pi/\lambda$ where λ is the wavelength, and ϕ is the acoustic pressure or wave elevation. ϕ is complex since it contains both magnitude and phase information. We consider the solution of (1) in the unbounded 2D region Ω resulting from the scattering by an object of boundary Γ of an incident plane wave, $\phi^i = Ae^{ika\cdot x}$, where A is the incident wave amplitude and a is the unit vector describing its direction. The scattering boundary, Γ, is considered in the present work to provide a sound-hard Neumann condition

$$\frac{\partial\phi}{\partial n} = 0 \tag{2}$$

where n is the unit normal pointing outward from Ω. Conventional treatment of (1) to (2) yields a boundary integral equation, assuming a smooth boundary, as

$$\frac{\phi}{2} + \int_\Gamma \frac{\partial G^*}{\partial n}\phi d\Gamma = \int_\Gamma G^*\frac{\partial\phi}{\partial n}d\Gamma + \phi^i \tag{3}$$

where we collocate on the boundary, Γ, and G^* is the fundamental solution, or Green's function. BEM discretisation of equation (3) gives [1]

$$Hu - Gq = 0 \tag{4}$$

where the terms in the influence matrices are found by evaluation of the boundary integrals in (4) over a discretisation of Γ. Considering an arbitrary collocation point and element of boundary Γ_e, the integrations for the matrix terms relating to node j on the element are

$$H_j = \int_{\Gamma_e} \frac{\partial G^*}{\partial n}N_j d\Gamma = \int_{-1}^{1} \frac{\partial G^*}{\partial n}N_j J d\xi \tag{5}$$

$$G_j = \int_{\Gamma_e} G^* N_j d\Gamma = \int_{-1}^{1} G^* N_j J d\xi \tag{6}$$

where N_j is the shape function for the node j, and G^* is the fundamental solution, or Green's function, given by

$$G^* = \frac{i}{4}H_0(kr) = \frac{1}{4}\left[iJ_0(kr) - Y_0(kr)\right] \tag{7}$$

where r is the distance from the collocation point and $H_0(z)$ is a Hankel function of the first kind and of order 0. We show the decomposition of $H_0(z)$ into Bessel functions of the first and second kind, $J_0(z)$ and $Y_0(z)$ respectively. Substituting equation (7) into equations (5) and (6) gives

$$H_j = \int_{-1}^{1} \frac{k}{4}\frac{\partial r}{\partial n}\left[Y_1(kr) - iJ_1(kr)\right]N_j J d\xi \tag{8}$$

$$G_j = \int_{-1}^{1} \frac{1}{4}\left[iJ_0(kr) - Y_0(kr)\right]N_j J d\xi \tag{9}$$

Partition of Unity

Melenk and Babuka [2] presented the Partition of Unity Method where the approximation space is enriched by functions known to populate the solution. In the PUBEM, we enrich N_j in a plane wave expansion, leading to a set of shape functions $N_j e^{ik(xCos\theta_q + ySin\theta_q)}$, $q = 1, 2, ..., m$, giving

$$H_{j_q} = \int_{-1}^{1} \frac{k}{4}\frac{\partial r}{\partial n}\left[Y_1(kr) - iJ_1(kr)\right] N_j e^{ik(xCos\theta_q + ySin\theta_q)} J d\xi \tag{10}$$

$$G_{j_q} = \int_{-1}^{1} \frac{1}{4} \left[iJ_0(kr) - Y_0(kr) \right] N_j e^{ik(xCos\theta_q + ySin\theta_q)} J d\xi \qquad (11)$$

The plane wave directions in the basis, θ_q, are usually uniformly distributed around the unit circle. The values of θ_q and m may be chosen *a priori* according to the required value of τ, or may be selected adaptively according to an error indicator.

Integration scheme

The numerical evaluation of the integrals (10) and (11) requires the evaluation of the Bessel functions of the first and second kind of orders 0 and 1. Press et al. [3] give routines for evaluation of the Bessel functions and use different formulae for $|kr| < 8$ and $|kr| \geq 8$. Because of the overwhelming number of non-singular integrations performed with $|kr| \geq 8$ in PUBEM we concentrate on this case.

Substituting the equations from [3], for $|kr| \geq 8$ into the integrals (10) and (11) gives

$$G_{j_q} = \int_{-1}^{1} \frac{1}{4} \sqrt{\frac{a_0}{kr}} \left[p_0 e^{i\left(kr - b_0 + \frac{\pi}{2}\right)} - \frac{8}{kr} q_0 e^{i(kr - b_0)} \right] N_j e^{ik(xCos\theta_q + ySin\theta_q)} J d\xi \qquad (12)$$

$$H_{j_q} = \int_{-1}^{1} \frac{k}{4} \frac{\partial r}{\partial n} \sqrt{\frac{a_1}{kr}} \left[\frac{8}{kr} q_1 e^{i(kr - b_1)} - p_1 e^{i\left(kr - b_1 + \frac{\pi}{2}\right)} \right] N_j e^{ik(xCos\theta_q + ySin\theta_q)} J d\xi \qquad (13)$$

where a_0, b_0, p_0, q_0, a_1, p_1, q_1 come from the series approximations to Bessel functions [3]. Equations (12) and (13) give four integrals of the type

$$I_n = \int_{-1}^{1} f_n(\xi)\, e^{ikg(\xi)} d\xi \qquad (14)$$

In order to evaluate the oscillatory integrals of equation (14) we use the numerical steepest descent method [4]. The method is based on Cauchy's integral theorem and replaces the integral over the real interval $\xi \in (-1, 1)$ by an equivalent integral along a path in the complex plane such that the integrand is no longer oscillatory along the path, but instead exhibits exponential decay. We denote with h the complex plane. The required paths start at $h = (-1 + 0i)$ and are found to go to ∞ before returning to $h = (+1 + 0i)$. The situation can be complicated by the presence of stationary points in $\xi \in (-1, 1)$. In order to simplify the method we start with the ideal case, with no stationary points, as shown in Figure1, where the arrowheads at c and d represent the curves going to and coming back from ∞ respectively. Rather than integrating the oscillatory integrals along the element from a(-1,0) to b(1,0) we deform the integral path into the complex plane to a-c, c-d, d-b shown in Figure 1. We choose the integration paths a-c and d-b in the complex plane such that

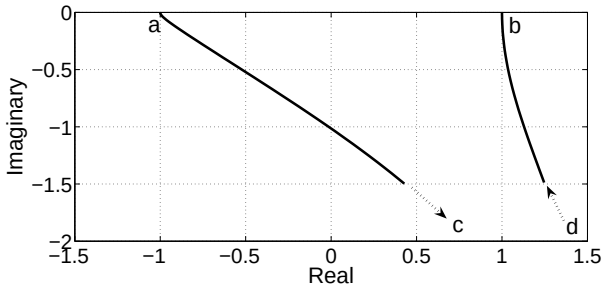

Figure 1: Integration paths in the complex plane *h*

$$g(h) = g(\xi) + ip \qquad (15)$$

The integrals in equation (14) are then transformed to

$$I_n = \left| e^{ikg(\xi)} \int_0^{\infty} f_n(h)\, e^{-kp} \frac{\partial h}{\partial p} dp \right|_{\xi=-1}^{\Gamma a-c} - \left| e^{ikg(\xi)} \int_0^{\infty} f_n(h)\, e^{-kp} \frac{\partial h}{\partial p} dp \right|_{\xi=1}^{\Gamma b-d} \qquad (16)$$

The first term on the right hand side of equation (16) is the integral along the path a-c in Figure 1, and the second term considers path d-b; we have changed the direction and sign of the second term. The integral along the path c-d vanishes since e^{-kp} is zero at $p = \infty$. In equation (16) $\partial h / \partial p$ is complex and is obtained from taking the derivative of equation (15) giving

$$\frac{\partial h}{\partial p} = \frac{i}{g'(h)} \qquad (17)$$

We integrate each term of equation (16) using Gauss-Laguerre numerical integration. The integrals along paths a-c and b-d in Figure 1 are non-oscillatory and can be integrated very accurately using very few Gauss points. The integration paths given by equation (15) need only be

found at the Gauss points for the Gauss-Laguerre integration. We do this by using Newton-Raphson iteration to solve equation (15) using a linear truncated Taylor series for $g(h)$ from the previous Gauss point to find the starting value for the Newton-Raphson iteration.

The case of stationary points is a little more involved. A stationary point is located where $g'(\xi_{SP}) = 0$, $\xi_{SP} \in (-1, 1)$. Figure 2 shows the integration paths a-c, c-d, d-

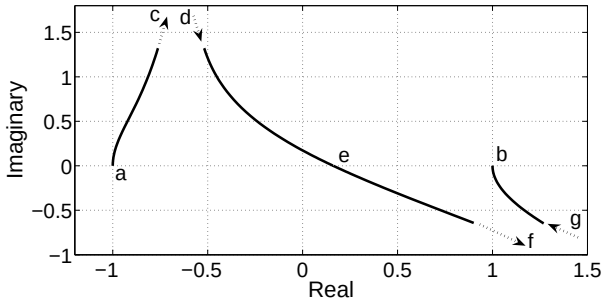

Figure 2: Integration paths in the complex plane *h* with a stationary point at $\xi_{SP} = 0.1613$

e-f, f-g, g-b for the integration with a stationary point at e, $\xi_{SP} = 0.1613$. The integration path d-e-f crosses the real axis at the stationary point, e at ξ_{SP}. The integral along the paths c-d and f-g vanishes since e^{-kp} is zero at $p = \infty$. The integrals in equation (14) are then transformed to

$$I_n = \left| e^{ikg(\xi)} \int_0^\infty f_n(h)\, e^{-kp} \frac{\partial h}{\partial p} dp \right|_{\xi=-1}^{\Gamma a-c} - \left| e^{ikg(\xi)} \int_0^\infty f_n(h)\, e^{-kp} \frac{\partial h}{\partial p} dp \right|_{\xi=\xi_{SP}}^{\Gamma e-d} + \left| e^{ikg(\xi)} \int_0^\infty f_n(h)\, e^{-kp} \frac{\partial h}{\partial p} dp \right|_{\xi=\xi_{SP}}^{\Gamma e-f} - \left| e^{ikg(\xi)} \int_0^\infty f_n(h)\, e^{-kp} \frac{\partial h}{\partial p} dp \right|_{\xi=1}^{\Gamma b-g} \quad (18)$$

Notice there are two paths for increasing p at the stationary point, e, and care needs to be taken to distinguish between paths e-d and e-f in Figure 2 since they have opposite signs in equation (18). The contribution along path e-d has a negative sign since the path is coming back to the real axis, and the contribution along path e-f has a positive sign since the path is going away from the real axis. At the stationary point we need both paths satisfying equation (15); to do this, we take the quadratic truncated Taylor series for $g(h)$ giving two values for the starting value for the Newton-Raphson iteration, at the first Gauss point, one of which starts the curve e-d and the other of which starts path e-f in Figure 2. Once we have found the first Gauss point on the two curves we revert back to the linear truncated Taylor series for subsequent points along each curve.

At the stationary point $g'(h) = 0$, which means that the $\partial h/\partial p$ term in equation (18), given by equation (17), is infinite. To overcome this we use a Telles type transformation [5] where the Jacobian of the transformation is zero at the singularity.

Results

Numerical tests on scattering by a cylinder of radius a, with wavenumber k such that $ka = 240\pi$, show that the scheme presented herein uses 365×10^6 integration points, comparing favourably with the 8.8×10^9 points used for comparable accuracy in previous works with conventional Gauss-Legendre on the real interval.

References

[1] R.D. Ciskowski and C.A. Brebbia, Boundary Element Methods in Acoustics, Computational Mechanics Publications, Southampton, 1991.

[2] J.M. Melenk and I. Babuka, "The Partition of Unity Finite Element Method. Basic Theory and Applications", Computer Methods in Applied Mechanics and Engineering, 139, pp 289-314, 1996.

[3] W.H. Press, S.A. Teukolsky, W.T. Vetterling and B.P. Flannery, Numerical Recipes in Fortran 77, The Art of Scientific Computing, Second Edition, Cambridge University Press, Cambridge, 2003.

[4] D. Huybrechs and S. Vandewalle, "On the evaluation of highly oscillatory integrals by analytic continuation", SIAM Journal on Numerical Analysis, 44, pp 1026-1048, 2006.

[5] J.C.F. Telles, "A self-adaptive co-ordinate transformation for efficient numerical evaluation of general boundary element integrals", International Journal for Numerical Methods in Engineering, 24, pp 959-973, 1987.

EFFICIENT COMPUTATIONS IN HIGH FREQUENCY SCATTERING PROBLEMS

D. Huybrechs[†,*]

[†]Dept. Computer Science, K.U.Leuven, Leuven, Belgium
[*]Email: daan.huybrechs@cs.kuleuven.be

Abstract

Methods for the numerical simulation of high frequency scattering problems invariably involve one or more highly oscillatory integrals, either implicitly or explicitly. The presence of oscillatory integrals is explicit in a natural way in integral equation methods, where the kernel function of the integral operator under consideration itself may be highly oscillatory. As such, methods for the numerical evaluation of oscillatory integrals are highly relevant for the construction of new methods for solving such integral equations. In this paper, we explore the relation between these two problems and we describe an application to the case of high frequency scattering by convex obstacles.

Introduction

The discretization of integral equations using boundary element methods naturally leads to large and dense matrices. For non-oscillatory problems, the dense matrix is highly redundant. It can be compressed in many ways, e.g., using wavelets, the fast multipole method or hierarchical matrices. We will see that in some cases, perhaps unexpectedly, much redundancy in the matrix representation also appears in the highly oscillatory case. The redundancy is in fact much higher than in the non-oscillatory case. Also, it is more easily exploited numerically. Here, we will show how one can obtain a sparse, but highly accurate, representation of a particular oscillatory integral operator. The operator appears in the problem of scattering by a smooth two-dimensional obstacle.

The method we describe has the characteristics of an asymptotic method. There are two major issues that require special attention in such methods. The first is that asymptotic expansions are generally divergent. The second is the existence of the Stokes phenomenon: an asympotic expansion may change form discontinuously as one parameter of the problem passes a crucial value. We will see how both issues can be resolved by incorporating the asymptotic behaviour of the solution into a more traditional boundary element method.

This work has been inspired by earlier results using a similar approach. An efficient implementation that also takes advantage of the localisation principle was described in [1]. A compression of the matrix representation was described in [2]. We believe the biggest differences here, compared to the given references, is a more effective treatment of the oscillatory integrals involved and the much improved sparsity that results. A detailed account of the method can be found in [4].

Oscillatory integrals

Highly oscillatory integrals represent a challenge for traditional quadrature approaches, such as composite interpolatory Gaussian or Newton-Cotes quadrature. The underlying polynomial interpolation requires resolving the wavelengths of the integrand, which naturally leads to a high computational cost for increasing frequency.

Now consider the following model integral,

$$I = \int_a^b f(x) e^{ikg(x)} \,\mathrm{d}x \tag{1}$$

with smooth functions f and g and a large frequency parameter k. This integral can be evaluated very effectively by deforming the integration path onto the so-called paths of steepest descent. This leads to a sum

$$I = F(a) - F(b) + O(e^{-kP}), \quad k \to \infty,$$

with $P > 0$ and with the line integrals $F(x)$ given by

$$F(x) = e^{ikg(x)} \int_0^P \tilde{f}(p) e^{-kp} \mathrm{d}p, \tag{2}$$

where $\tilde{f}$ is a smooth function that depends on f. This procedure turns the integrand into a non-oscillatory function that exhibits exponential decay. The numerical evaluation of $F(x)$ leads to a numerical method that requires only few evaluations of the original integrand. Moreover, the accuracy increases rapidly with increasing frequency [5].

A different method was proposed in [3]. These authors constructed a *Filon-type* quadrature rule using derivatives,

$$I \approx Q[f] := \sum_{l=0}^{L} \sum_{j=0}^{d} w_{l,j} f^{(j)}(x_l). \tag{3}$$

The error of this rule behaves as $O(k^{-s-1})$, where s depends on the number of derivatives that are used. The

number of quadrature points L is small and, more importantly, independent of k. This method has the advantage that it has the form of a classical quadrature rule and that it can be applied to functions f that are not analytic. The weights $w_{l,j}$ in this quadrature rule are given by oscillatory integrals themselves – they can be evaluated very efficiently using the method of [5] described above.

The succes of both of these methods hinges on the existence of an asymptotic expansion of I in terms of k^{-1},

$$I \sim \sum_{j=0}^{\infty} a_j k^{-\delta(j+1)}, \quad k \to \infty, \tag{4}$$

where $0 < \delta \leq 1$ depends on the behaviour of g. The coefficients in this expansion depend solely on the behaviour of f and g near the critical points of the integrand. They are the endpoints a and b of the integration interval and the so-called *stationary points*: all points $\xi_l \in [a, b]$ such that $g'(\xi_l) = 0$. The quadrature points in (3) include all the critical points. The coefficients a_j themselves are not computed or estimated.

An oscillatory integral equation

Consider the oscillatory integral operator

$$(Kf)(t) = \int_0^1 \frac{i}{4} H_0^{(1)}(k|\kappa(t) - \kappa(\tau)|) f(\tau)\, \mathrm{d}\tau, \tag{5}$$

that arises in the problem of two-dimensional time-harmonic scattering by a bounded obstacle Γ, given by $\kappa : [0, 1] \to \Gamma$, with $|\nabla\kappa(\tau)| = 1$ for simplicity. Since

$$H_0^{(1)}(z) \sim \sqrt{\frac{2}{\pi z}} e^{i(z-\frac{1}{4}\pi)}, \quad z \to \infty,$$

the integral Kf closely resembles the model integral (1). One can evaluate Kf efficiently and very accurately using a Filon-type method,

$$(Kf)(t) \approx \sum_{l=0}^{L} \sum_{j=0}^{d} w_{l,j}(t) f^{(j)}(x_l(t)).$$

The weights and the quadrature points now depend on t.

In general, the solution q of the integral equation $Kq = u^i$ may itself be oscillatory. In some cases, one can predict the oscillatory behaviour of q. For example, if Γ is convex and $u^i(t) = e^{ikg^i(t)}$, geometrical optics predicts

$$q(t) = q_s(t) e^{ikg^i(t)} \tag{6}$$

where $q_s(t)$ is almost non-oscillatory. This holds in the part of the obstacle that is visible to the incoming wave

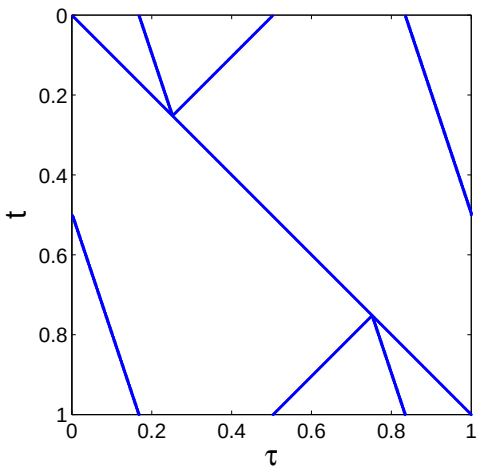

Figure 1: Location of the critical points $\tau \in [0, 1]$ as a function of the collocation point $t \in [0, 1]$.

$u^i(t)$. The function $q_s(t)$ is mildly oscillatory but rapidly decaying in the shadow region. The transition occurs at the so-called shadow boundaries – the points where the incoming wave is tangential to the boundary Γ.

A sparse discretization

Our approach will be to substitute the ansatz (6) into the integral equation and to solve for the function q_s,

$$q_s(t) \approx q_c(t) := \sum_{m=1}^{N} c_m \phi_m(t). \tag{7}$$

Collocating in the points t_n, $n = 1, \ldots, N$, yields the system $Ac = b$ with entries

$$A_{n,m} = (K\phi_m e^{ikg^i})(t_n) \text{ and } b_n = u(t_n). \tag{8}$$

Even if the basis functions ϕ_m are only locally supported, the matrix A is dense. Row n corresponds to a discretisation of the oscillatory integral $(Kq_s e^{ikg^i})(t_n)$. An alternative is to use a Filon-type method,

$$(Kq_s e^{ikg^i})(t_n) \approx \sum_{l=0}^{L} \sum_{j=0}^{d} w_{l,j}(t_n) q_s^{(j)}(x_l(t_n)). \tag{9}$$

From (7) we obtain the necessary derivatives

$$q_s^{(j)}(t) \approx q_c^{(j)}(t) = \sum_{m=1}^{N} c_m \phi_m^{(j)}(t).$$

Hence, everything can again be expressed as a linear combination of the coefficients c_m. The typical locations of

the critical points $x_l(t_n)$ are shown in Figure 1. The diagonal corresponds to the singularity of the kernel function. The other lines represent stationary points.

If the basis functions ϕ_m are locally supported, only few basis functions are non-zero at the critical points. The matrix representation based on (9) then becomes highly sparse, with non-zero elements distributed approximately as in Figure 1. However, the ansatz (6) is not valid near the shadow boundaries. As a result, the Filon-type quadrature rule does not apply. Following [1], the wavelengths are resolved in a small region of size $O(k^{-1/3})$ around the shadow boundaries. We approximate q_s by 0 in the shadow region away from the shadow boundaries. The Filon-type rule is now used only where it applies. For other parts of the matrix, we revert to a small dense part with elements elements $A_{n,m}$ as given by (8). This leads to a matrix $\tilde{A}$ with a sparse structure as shown in Figure 2.

Accuracy and computation time

The construction of the sparse matrix requires the computation of the weights

$$w_{l,j}(t_n), \quad n = 1, \ldots, N.$$

They are given by oscillatory integrals that can be computed efficiently following [5]. These integrals become easier to evaluate as the frequency increases. As an immediate result, the computation time of the method actually decreases with increasing frequency. Numerical results on timing and accuracy can be found in [4].

There are two sources of errors in this scheme. First, one has the error of the overall collocation scheme, depending on the size of the boundary region and the number of unknowns. Second, an additional quadrature error is introduced by using (9). The two sources of the error can be analysed separately, since the sparse representation asymptotically approximates the dense matrix. This is the subject of ongoing research. A similar approach was already analysed in [6].

Concluding remarks

The dense matrix representation in this particular scattering problem can be approximated asymptotically by a small and highly sparse matrix, resulting in large savings. This approximation improves with increasing frequency. The two major disadvantages of asymptotic methods that were mentioned in the introduction are resolved by considering the problem in a boundary element setting. At lower frequencies, one can increase the size of the dense parts to gradually fill up the matrix, reducing to a classical dence boundary element method discretization for q_s. The features of the transitional shadow boundary regions are not captured in the ansatz that was used. This problem, too, is resolved by locally reducing to a regular dense discretization.

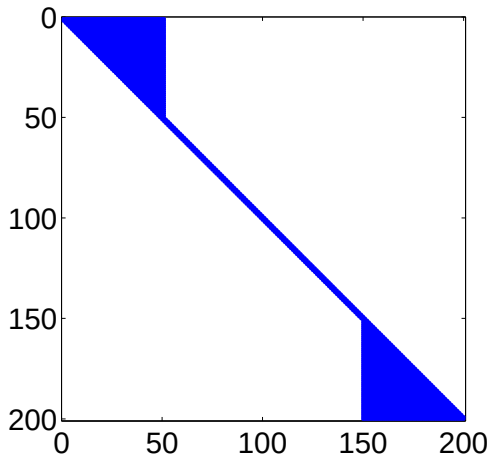

Figure 2: The sparse discretization matrix $\tilde{A}$.

References

[1] O. Bruno et al, “Prescribed error tolerances within fixed computational times for scattering problems of arbitrarily high frequency: the convex case”, Phil. Trans. R. Soc. Lond. A, vol. 362, pp. 629-645, 2004.

[2] E. Giladi, “Asymptotically derived boundary elements for the Helmholtz equation in high frequencies”, J. Comput. Appl. Math., vol. 198, pp. 52-74, 2007.

[3] A. Iserles and S. P. Nørsett, “Efficient quadrature of highly oscillatory integrals using derivatives”, Proc. R. Soc. Lond. Ser. A, vol. 461, pp. 1383-1399, 2004.

[4] D. Huybrechs and S. Vandewalle, “A sparse discretisation for integral equation formulations of high frequency scattering problems”, SIAM J. Sci. Comput., to appear.

[5] D. Huybrechs and S. Vandewalle, “On the evaluation of highly oscillatory integrals by analytic continuation”, SIAM J. Numer. Anal., vol. 44, pp. 1026-1048, 2006.

[6] V. Dominguez et al, “A hybrid numerical-asymptotic boundary integral method for high-frequency acoustic scattering”, Numer. Math., vol. 106, pp. 471-510, 2007.

Eulerian computational methods for high frequency waves through interfaces

Shi Jin[†,*]
[†]Department of Mathematics, University of Wisconsin, madison, WI 53706, USA
[*]Email: jin@math.wisc.edu

Abstract

High frequency waves through interfaces can be approximated, in the limit of infinite frequency, a Liouville equation that corresponds to a Hamiltonian system with a *discontinuous* Hamiltonian. We introduce an interface condition– that corresponds to wave transmission and reflection–for the Liouville equation, and then develop numerical schemes using this interface condition. The numerical schemes can capture the high frequency waves through the interface without resolving the high frequency. Extensions to thin quantum barriers and to the computation of diffraction by using the Geometric Theory of Diffraction will also be discussed.

Introduction

By using the Wigner transform, the high frequency limit of a linear symmetric hyperbolic system or the linear Schrödinger equation in quantum mechanics has the limiting equation for the energy or density distribution $f(t,x,p)$ governed by the linear Liouville equation:

$$\partial_t f + \nabla_p H \cdot \nabla_x f - \nabla_x H \cdot \nabla_p f = 0\,, \qquad (1)$$
$$f(x,p,0) = |A_0(x)|\delta(p - \nabla S_0(x))\,. \qquad (2)$$

where $A_0(x)$ and $S_0(x)$ are the inital density (energy) and phase respectively.

In the case of wave equation, $H(x,p) = c(x)|p|$, where $c(x)$ is the local sound speed, while for the Schrödinger equation, $H(x,p) = 1/2|p|^2 + V(x)$ with $V(x)$ the potential.

Compared to the classical WKB analysis, the Wigner approach is valid beyond the caustics, thus is valid globally in time. The above limit has been justified when H is smooth.

When the medium is inhomogeneous, the potential $V(x)$ or the local wave speed c is discontinuous, creating a sharp potential barrier or interface where waves can be partially reflected and partially transmitted as in Snell-Descartes' Law of Refraction. This gives rise to new mathematical and numerical challenges not faced in the smooth Hamiltonian case.

Methods

For problem (1)-(2), we introduce an interface condition at the point of interface, say $x = 0$, for $p > 0$, [2]:

$$f(0^+,p^+) = \alpha_T f(0^-,p^-) + \alpha_R f(0^+,-p^+) \quad (3)$$
$$H(0^-,p^-) = H(0^+,p^+) \quad (4)$$

For a sharp interface, $0^+ = 0^-$. Here α_T and α_R are the transmission and reflection coefficients respectively,

$$0 \le \alpha_T, \alpha_R \le 1\,, \qquad \alpha_T + \alpha_R = 1\,.$$

(3) is the conservation of density. The first term on the right hand side corresponds to the transmission, while the second term corresponds to the reflection. For wave reflection, the velocity or momentum simply changes sign. For transmission, however, the momentum or velocity changes according to the Hamiltonian or energy conservation (4). In geometrical optics, (4) is equivalent to the *Snell Law of Refraction.*

We now define the solution to (1)-(2) by solving the Liouville equation (1) on both sides of the interface, and then connect the solution through the interface condition (3)-(4). This provides a mathematically well-posed initial value problem to the linear Liouville equation (1) which is a linear transport equation with singular (discontinuous and measure-valued) coefficients. This also motivates our numerical methods.

The basic idea of our numerical method [1] is to incorporate (or immerse) the interface condition (3)-(4) into the numerical flux in the x-direction. This gives a class of finite difference schemes that are L^1 and L^∞ stable, under a hyperbolic CFL condition $\Delta t = O(\Delta x, \Delta p)$. We have also developed finite volume methods and particle methods.

Applications

This method is very generic. We will discuss its applications in semiclassical limit of the linear Schrödinger equation [1], geometric optics [2], elastic wave [3], and even diffuse interfaces [5].

We will also extend it to a semiclassical computation of thin quantum barriers [4]. The basic idea is the following:

- Solve a time-independent Schrodinger equation for the local barrier/well to determine the scattering data (in 1d these are α_T and α_R)
- Solve the classical liouville equation elsewhere, using the scattering data at the interface

Since we solve the (stationary) quantum mechanics only in a preprocessing step, this "multiscale" method allows us to compute the quantum tunneling with a computational cost of classical mechanics.

We have also generalized the interface condition (3)-(4) to include the diffraction effect by utilizing the Geomatric Theory of Diffraction [6].

References

[1] S. Jin and Xin Wen, "Hamiltonian-preserving schemes for the Liouville equation with discontinuous potentials", Comm. Math. Sci. vol. 3, pp. 285-315, 2005.

[2] S. Jin and Xin Wen, " Hamiltonian-preserving schemes for the Liouville equation of geometrical optics with partial transmissions and reflections", SIAM J. Num. Anal. vol 44, pp. 1801-1828, 2006.

[3] S. Jin and Xiaomei Liao, " A Hamiltonian-preserving scheme for high frequency elastic waves in heterogeneous media", J. Hyperbolic Diff Eqn. vol. 3, No. 4, pp. 741-777, 2006.

[4] S. Jin and K. Novak, "A Semiclassical Transport Model for Thin Quantum Barriers" Multiscale Modeling and Simulation, vol . 5(4), pp. 1063-1086, 2006.

[5] S. Jin, Xiaomei Liao and Xu Yang, "Computation of interface reflection and regular or diffuse transmission of the radiative transfer equation and its diffusion limit", SIAM J. Sci. Comp., submitted.

[6] S. Jin and Dongsheng Yin, "Computational high frequency waves through curved interfaces via the Loiuville equation and Geometric Theory of Diffraction", J. Comp. Phys., submitted.

A COMPARISON OF NON REFLECTING BOUNDARY CONDITIONS FOR PUFEM IN 2D EXTERIOR HELMHOLTZ PROBLEMS AT HIGH WAVE NUMBERS

O. Laghrouche[†,*], **J. Trevelyan**[‡]

[†]School of the Built Environment, Heriot-Watt University, Edinburgh EH14 4AS, UK
[‡]School of Engineering, Durham University, Durham DH1 3LE, UK
[*]Email: o.laghrouche@hw.ac.uk

Abstract

To solve wave scattering problems in unbounded media using the finite element method, it is necessary to truncate the domain at some artificial boundary and to apply a suitable non reflecting boundary condition (NRBC) allowing the outgoing waves to radiate away towards infinity. Usually, an approximation of the Sommerfeld radiation condition is applied at a sufficiently large distance from the scatterer, which leads to solutions in large computational domains. Such techniques are practical at low wave numbers where the artificial boundary is only a few wavelengths from the scatterer. As the wave number increases, the distance between the scattering object and the artificial boundary increases as well in terms of the wavelength, and hence the use of NRBC based on asymptotic expansions become computationally expensive. In this work, exact and approximate NRBC are implemented with the Partition of Unity Finite Element Method (PUFEM) to solve short wave scattering problems governed by the Helmholtz equation in two dimensions. A comparison of the performance of the NRBC is carried out based on the accuracy of the results, ease of implementation and computational cost.

Introduction

Many authors have developed finite elements which incorporate knowledge about the problem to be solved. The approach is based on the enrichment of the solution space by analytical solutions to the Helmholtz equation usually in the form of plane waves. These elements are capable of containing many wavelengths per nodal spacing and therefore allow us to relax the traditional requirement which consists to take around ten nodal points per wavelength. The reader is directed to reference [1] for a survey of the activity which took place up to 2004. More recent work could be found, for example, in [2], [3] and [4]. Regarding the NRBC for exterior wave problems, again so much activity has been taking place in this area. The used references are [5] and [6], among others. In this work, two type of exact NRBC are implemented, namely the Robin boundary condition and the DtN map. In the case of approximate boundary conditions, three different boundary conditions are used. Those are of Bayliss, Gunzburger and Turkel (BGT), Engquist and Majda (EM), and Feng (F). Different orders of the approximate boundary conditions are also considered. The problem of interest is a simple model of an acoustic plane wave scattering from a rigid circular cylinder, for which the exact solution is known.

Formulation

The problem of a plane wave scattered by a rigid object D in unbounded media is considered in two dimensions. The incident plane wave of potential Φ_i is scattered by the rigid body of boundary Γ_S. The diffracted potential Φ satisfies the following problem

$$(\nabla^2 + k^2)\Phi = 0 \quad \text{outside } D \tag{1}$$

$$\boldsymbol{\nabla}\Phi \cdot \boldsymbol{n} = -\boldsymbol{\nabla}\Phi_i \cdot \boldsymbol{n} \quad \text{on } \Gamma_S \tag{2}$$

$$\lim_{r\to\infty} r^{\frac{1}{2}}\left(\frac{\partial\Phi}{\partial r} - \mathrm{i}k\Phi\right) = 0 \tag{3}$$

where ∇^2 denotes the Laplacian operator, $\boldsymbol{\nabla}$ is the gradient vector operator, k is the wave number, $\boldsymbol{n}$ is the outward normal vector to the line boundary Γ_S and i is the complex imaginary such that $\mathrm{i}^2 = -1$. The time variable is removed by considering a harmonic steady state. The region of interest Ω around the scatterer is bounded by an artificial circular boundary Γ_R of radius R at which special conditions must be imposed to appear transparent to the propagating waves.

The differential equation (1) is multiplied by an arbitrary weight function Ψ and then integrated by parts in Ω to give the weak form

$$\int_\Omega \left(\boldsymbol{\nabla}\Psi \cdot \boldsymbol{\nabla}\Phi - k^2\Psi\Phi\right)\, d\Omega - \int_{\Gamma_R} \Psi\boldsymbol{\nabla}\Phi \cdot \boldsymbol{n}\, d\Gamma = \int_{\Gamma_S} \Psi\boldsymbol{\nabla}\Phi_i \cdot \boldsymbol{n}\, d\Gamma \tag{4}$$

where the integral along the outer boundary Γ_R is treated by considering different NRBC.

The computational domain Ω is meshed into n-noded finite elements and the diffracted potential Φ is expressed

as a combination of plane waves.

$$\Phi = \sum_{j=1}^{n} \sum_{l=1}^{m} N_j(\boldsymbol{\eta})\, e^{\mathrm{i}k\boldsymbol{\xi}_j^l \cdot \boldsymbol{r}}\, A_j^l \qquad (5)$$

where the coefficients A_j^l are the amplitudes of the set of m plane waves associated with each vertex j. The plane waves are chosen to be evenly distributed such that $\boldsymbol{\xi}_l^T = (\cos\alpha_l, \sin\alpha_l)$ with $\alpha_l = 2\pi l/m$. The geometry of each finite element is described by the coordinate transformation $\boldsymbol{r} = \mathcal{T}(\boldsymbol{\eta})$ between the global coordinates $\boldsymbol{r} = (x, y)$ and the local coordinates $\boldsymbol{\eta} = (\eta, \zeta) \in [-1, 1]^2$. A Galerkin weighting is adopted and therefore the weighting functions Ψ are products of polynomial shape functions and chosen plane waves. A high order Gauss-Legendre integration scheme is used to evaluate the element matrices, which are of dimension $nm \times nm$.

Numerical results - example

We consider the problem of a horizontal plane wave of unit amplitude impinging a rigid circular cylinder of unit radius, a. The computational domain extension is given by $1 \leq R/a \leq 1.25$. The measure of the accuracy of the model is based on the L_2 norm error, $\epsilon_2 = ||\Phi - \tilde{\Phi}||_{L_2(\Omega)}/||\tilde{\Phi}||_{L_2(\Omega)} \times 100\%$, where $\tilde{\Phi}$ is the exact solution of the diffracted potential. We also define the parameter τ as the number of degrees of freedom (DOF) per wavelength used to solve the problem. A mesh containing one layer of 9-noded finite elements around the cylinder and 23 elements in total is used (Figure 1). At each nodal point we use 30 plane waves. Figure 2 shows an example of contour plots of the real part of the diffracted potential around the cylinder for ka=100 when the DtN boundary condition is imposed on the outer boundary Γ_R. In this case, 60 integration points are employed per element in each spatial direction for the evaluation of the element matrices and 3 DOF are used to model each wavelength. The L_2 error is very satisfactory, $\epsilon_2 = 0.1\%$.
Further results compare the accuracy of different local and non-local NRBC at relatively high wave numbers.

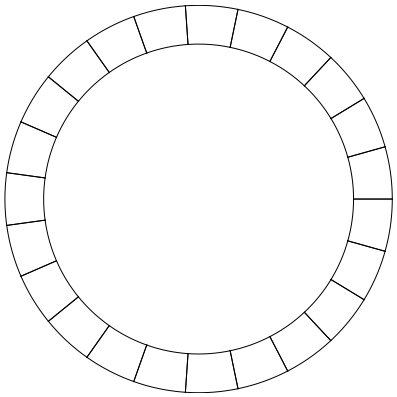

Figure 1: Mesh of the computational domain.

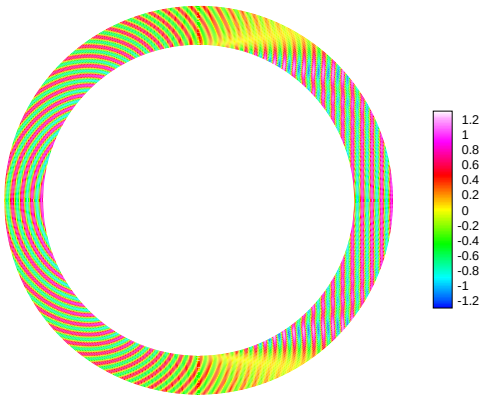

Figure 2: Real part of the diffracted potential, $ka = 100$, $\lambda/a = 0.06$, $\tau = 3$, $\epsilon_2 = 0.1\%$.

References

[1] P. Bettess, O. Laghrouche and E. Perrey-Debain (Eds.), Theme Issue on Short Wave Scattering, Phil. Trans. R. Soc. Lond. A, 362, 2004.

[2] O. Laghrouche, P. Bettess, E. Perrey-Debain and J. Trevelyan, "Wave interpolation finite elements for Helmholtz problems with jumps in the wave speed", Comput. Methods Appl. Mech. Engrg., 194, pp.367-381, 2005.

[3] T. Strouboulis, I. Babuška and R. Hidajat, "The generalized finite element method for Helmholtz equation: Theory, computation, and open problems", Comput. Methods Appl. Mech. Engrg., 195, pp.4711-4731, 2006.

[4] L. Zhang, R. Tezaur and C. Farhat, "The discontinuous enrichment method for elastic wave propagation in the medium-frequency regime", Int. J. Numer. Methods Engrg., 66, pp.2086-2114, 2006.

[5] D. Givoli, Numerical methods for problems in infinite domains, Amsterdam, Elsevier Science Publishers, 1992.

[6] J.J. Shirron and I. Babuška, "A comparison of approximate boundary conditions and infinite element for exterior Helmholtz problems", Comput. Methods Appl. Mech. Engrg., 164, pp.121-139, 1998

A FULLY DISCRETE COLLOCATION METHOD FOR HIGH FREQUENCY SCATTERING BY CONVEX POLYGONS

S. Langdon[†,*], **D. Huybrechs**[‡], **S. N. Chandler-Wilde**[†]

[†]Department of Mathematics, University of Reading, Reading RG6 6AX, UK.
[‡]Katholieke Universiteit Leuven, Department of Computer Science, Celestijnenlaan 200A, B-3001 Leuven, Belgium.
[*]Email: s.langdon@reading.ac.uk

Abstract

We consider the numerical solution of the problem of time-harmonic acoustic scattering in two dimensions by a sound soft convex polygon. Standard boundary or finite element methods with piecewise polynomial approximation spaces have a computational cost that grows at least linearly with respect to the frequency of the incident wave. By including in the approximation space the products of plane wave basis functions with piecewise polynomials supported on a graded mesh, with the grading optimally adapted to the decay of the diffracted waves away from corners of the polygon, it has previously been shown that an error of best approximation that depends only logarithmically on the frequency of the incident wave can be achieved. To achieve this result via a Galerkin scheme requires the numerical evaluation of many highly oscillatory double integrals; to avoid this difficulty, a related collocation scheme has also previously been proposed. Some potential improvements to this scheme are discussed here.

Introduction

We consider the numerical solution of the exterior Helmholtz problem

$$\Delta u^s + k^2 u^s = 0, \quad \text{in } D := \mathbb{R}^2 \backslash \Upsilon, \tag{1}$$

where Υ is a convex polygon and $k > 0$ (the wavenumber) is some arbitrary positive constant, with boundary condition

$$u^s(\mathbf{x}) = -u^i(\mathbf{x}) := -\mathrm{e}^{\mathrm{i}k\mathbf{x}.\mathbf{d}}, \quad \mathbf{x} \in \Gamma, \tag{2}$$

where Γ is the boundary of Υ and $\mathbf{d}$ is the direction of the incident wave, together with the Sommerfeld radiation condition

$$\lim_{r\to\infty} r^{1/2}\left(\frac{\partial u^s}{\partial r}(\mathbf{x}) - \mathrm{i}k u^s(\mathbf{x})\right) = 0, \tag{3}$$

where $r = |\mathbf{x}|$ and the limit holds uniformly in all directions $\mathbf{x}/|\mathbf{x}|$. This boundary-value problem can arise when modelling the scattering of an acoustic incident plane wave by an infinite sound soft cylinder with polygonal cross section. Here we are concerned with solving (1)–(3) numerically in the case that k may be large.

Integral equation formulation

Using Green's theorem we can write the total acoustic field $u(\mathbf{x}) := u^s(\mathbf{x}) + u^i(\mathbf{x})$ as

$$u(\mathbf{x}) = u^i(\mathbf{x}) - \int_\Gamma \Phi(\mathbf{x},\mathbf{y})\frac{\partial u}{\partial \mathbf{n}}(\mathbf{y})\,\mathrm{d}s(\mathbf{y}),$$

where $\Phi(\mathbf{x},\mathbf{y}) := (\mathrm{i}/4)H_0^{(1)}(k|\mathbf{x}-\mathbf{y}|)$ is the standard fundamental solution for the Helmholtz equation and $\mathbf{n}$ is the normal vector directed out of Υ. Thus our problem reduces to finding the complementary boundary data $\partial u/\partial \mathbf{n} \in L^2(\Gamma)$, and to do this we solve the well known second kind integral equation

$$(I + K)\frac{\partial u}{\partial \mathbf{n}} = f, \quad \text{on } \Gamma\backslash\{S\}, \tag{4}$$

where S is the set of corners of Ω, $f := 2\partial u^i/\partial \mathbf{n} + 2\mathrm{i}\eta u^i$, and for $v \in L^2(\Gamma)$

$$Kv(\mathbf{x}) := 2\int_\Gamma \left(\frac{\partial \Phi(\mathbf{x},\mathbf{y})}{\partial \mathbf{n}(\mathbf{x})} + \mathrm{i}\eta\Phi(\mathbf{x},\mathbf{y})\right) v(\mathbf{y})\,\mathrm{d}s(\mathbf{y}),$$

where η is a coupling parameter, with $\eta \in \mathbb{R}\backslash\{0\}$ ensuring that (4) has a unique solution (we refer to [3] for details).

To achieve a good approximation to the solution of (4) when k is large, we begin by separating off the leading order asymptotic behaviour in the limit $k \to \infty$. To that end, we define $\phi := \frac{1}{k}\frac{\partial u}{\partial \mathbf{n}} - \Psi$, where

$$\Psi(\mathbf{x}) := \begin{cases} \frac{2}{k}\frac{\partial u^i}{\partial \mathbf{n}}(\mathbf{x}) & \text{on illuminated sides} \\ 0, & \text{on shadow sides,} \end{cases}$$

and then we solve numerically

$$(I + K)\phi = F := f - \Psi - K\Psi. \tag{5}$$

Approximation space and boundary integral methods

It is shown in [3] that the solution ϕ of (5) can be written as

$$\phi(s) = \mathrm{e}^{\mathrm{i}ks} v_+(s) + \mathrm{e}^{-\mathrm{i}ks} v_-(s), \quad \text{for } s \in [0, L],$$

where $\mathbf{x}(s), s \in [0, L]$ parametrises Γ, and where the functions v_+ and v_- and all their derivatives are highly peaked near the corners of the polygon and rapidly decaying away from the corners. The oscillatory nature of $\phi(s)$ is thus represented exactly by the terms $\mathrm{e}^{\pm \mathrm{i}ks}$, and so to approximate ϕ all that is required is to approximate the smooth functions $v_\pm$. These functions decay sufficiently quickly away from the corners of the polygon that they can be approximated by piecewise polynomials on a graded mesh, with the number of degrees of freedom required to maintain the accuracy of their best L^2 approximation growing only logarithmically with respect to k as $k \to \infty$.

More specifically, the approximation space used in [1] and [3] is defined as follows: for $A > \lambda = 2\pi/k > 0$, $q > 0$, $N = 2, 3, \ldots$, the mesh $\Lambda_{N,A,\lambda,q} := \{y_0, \ldots, y_{N+\hat{N}_{A,\lambda,q}}\}$ consists of the points $y_i = \lambda \left(\frac{i}{N}\right)^q$, $i = 0, \ldots, N$, together with the points $y_{N+j} := \lambda \left(\frac{A}{\lambda}\right)^{j/\hat{N}_{A,\lambda,q}}$, $j = 1, \ldots, \hat{N}_{A,\lambda,q}$, where $\hat{N}_{A,\lambda,q} = \lceil N^* \rceil$, the smallest integer greater than or equal to N^*, with $N^* = \frac{-\log(A/\lambda)}{q \log(1-1/N)}$. Assuming $L_j > \lambda$, $j = 1, \ldots, n$, where L_j denotes the length of the jth side of the polygon, we define $q_j := (2\nu+3)/(2\pi/\Omega_j - 1)$, $j = 1, \ldots, n$, (where Ω_j is the external angle at the jth corner, and ν denotes the degree of the approximating piecewise polynomial) and the two meshes

$$\Gamma_j^+ := \tilde{L}_{j-1} + \Lambda_{N,L_j,\lambda,q_j}, \quad \Gamma_j^- := \tilde{L}_j - \Lambda_{N,L_j,\lambda,q_{j+1}},$$

where $\tilde{L}_j := \sum_{m=1}^{j} L_m$.

Letting $\mathrm{e}_\pm(s) := \mathrm{e}^{\pm \mathrm{i}ks}$, $s \in [0, L]$, we then define

$$V_{\Gamma_j^+,\nu} := \{\sigma \mathrm{e}_+ : \sigma \in \Pi_{\Gamma_j^+,\nu}\},$$
$$V_{\Gamma_j^-,\nu} := \{\sigma \mathrm{e}_- : \sigma \in \Pi_{\Gamma_j^-,\nu}\},$$

for $j = 1, \ldots, n$, where

$$\Pi_{\Gamma_j^+,\nu} := \{\sigma \in L^2(0, L) : \sigma|_{(\tilde{L}_{j-1}+y_{m-1}, \tilde{L}_{j-1}+y_m)} \text{ is a polynomial of degree} \le \nu, \text{ for } m = 1, \ldots, N + \hat{N}_{L_j,\lambda,q_j}, \text{ and } \sigma|_{(0,\tilde{L}_{j-1})\cup(\tilde{L}_j,L)} = 0\},$$

$$\Pi_{\Gamma_j^-,\nu} := \{\sigma \in L^2(0, L) : \sigma|_{(\tilde{L}_j-\tilde{y}_m, \tilde{L}_j+\tilde{y}_{m-1})} \text{ is a polynomial of degree} \le \nu, \text{ for } m = 1, \ldots, N + \hat{N}_{L_j,\lambda,q_{j+1}}, \text{ and } \sigma|_{(0,\tilde{L}_{j-1})\cup(\tilde{L}_j,L)} = 0\},$$

with the points of the mesh $\Lambda_{N,L_j,\lambda,q_j}$ given by $y_0, \ldots, y_{N+\hat{N}_{L_j,\lambda,q_j}}$, and the points of the mesh $\Lambda_{N,L_j,\lambda,q_{j+1}}$ given by $\tilde{y}_0, \ldots, \tilde{y}_{N+\hat{N}_{L_j,\lambda,q_{j+1}}}$.

Our approximation space is then the linear span of $\bigcup_{j=1,\ldots,n}\{V_{\Gamma_j^+,\nu} \cup V_{\Gamma_j^-,\nu}\}$. Note that on each side of the polygon this gives us two overlapping meshes, one graded to each corner.

The question then arises of how to select the best L^2 approximation from the approximation space. In [3] a Galerkin scheme is proposed, for which both stability and convergence are proved. However, the implementation of this scheme requires the evaluation of many highly oscillatory double integrals, typically of a form similar to

$$\int_{-b}^{-a} \int_c^d \left[H_0^{(1)}(k\sqrt{s^2+t^2}) + \frac{\mathrm{i}tH_1^{(1)}(k\sqrt{s^2+t^2})}{\sqrt{s^2+t^2}} \right] . \mathrm{e}^{\mathrm{i}k(\sigma_j t - \sigma_m s)} \, \mathrm{d}t \, \mathrm{d}s,$$

where $0 \le a < b$, $0 \le c < d$, $\sigma_j, \sigma_m = \pm 1$. Numerical evaluation of these integrals by standard (e.g. Gaussian quadrature) schemes can be prohibitively expensive, with the number of degrees of freedom needing to grow like k^2 to maintain accuracy as $k \to \infty$. To avoid this difficulty, an alternative collocation scheme is proposed in [1]. Implementation of this scheme only requires evaluation of highly oscillatory single integrals, typically of a form similar to

$$\int_a^b \left[H_0^{(1)}(k\sqrt{s_m^2+t^2}) + \frac{\mathrm{i}tH_1^{(1)}(k\sqrt{s_m^2+t^2})}{\sqrt{s_m^2+t^2}} \right] \mathrm{e}^{\mathrm{i}k\sigma_j t} \, \mathrm{d}t, \tag{6}$$

where $a < b$, $\sigma_j = \pm 1$, and the collocation points s_m are defined as the midpoints of the intervals of the graded meshes. Numerical results in [1] suggest that this collocation scheme achieves a similar level of accuracy to that attained by the Galerkin scheme of [3], but with a reduced computational cost (the cost of evaluating the integrals (6) by standard Gaussian quadrature need only grow with order k to maintain accuracy as $k \to \infty$). However, the nature of the approximation space means that this naive choice of collocation points may lead to ill-conditioned systems. Moreover, the mesh grading proposed in both [3] and [1] near the corners of the polygon does not appear to be optimal in some ways. We now consider possible improvements to the scheme of [1].

Proposed improvements to the collocation scheme

Mesh grading near each corner

For the scheme of [1], we define $\alpha_j = 1-\pi/\Omega_j$, where Ω_j is the external angle at the jth corner: if $\Omega_j = \pi$ then there is no corner at all, in which case $\alpha_j = 0$; if $\Omega_j = 2\pi$ so that the corner becomes a sharp point, then $\alpha_j = 1/2$. For all other values of Ω_j, $\alpha_j \in (0, 1/2)$. In [1], [3], the grading of the mesh near the corner is $q_j = (2\nu+3)/(1-2\alpha_j)$. However, in the case that $\Omega_j = \pi$, i.e. if there is no corner, then this gives $q_j = 2\nu + 3$, which seems to be too severe. Ideally, as $\Omega_j \to \pi$ the grading would satisfy $q_j \to 1$, for all ν. At the other extreme we would expect that as $\Omega_j \to 2\pi$, i.e. as the corner becomes a sharp point, then we should have $q_j \to \infty$, which is exactly what we see. In L^2, when $\Omega_j = 2\pi$ the decay is $r^{-1/2}$, and thus in L^2 everything blows up as $\Omega_j \to 2\pi$. However these results can be improved: in L^2, a reduced mesh grading can be applied. Alternatively, we could work in L^1.

Specifically, the main approximation result in [3] is Theorem 4.2, which states that for a function $f \in C^\infty$ that satisfies

$$|f^{(m)}(s)| \leq C_m k^m (ks)^{-\alpha-m},$$

for $ks \leq 1$, where $\alpha \in (0, 1/2)$, then if $q = (2\nu+3)/(1-2\alpha)$ it follows that

$$\|f - P_N^* f\|_2 \leq C_\nu \frac{(1+\log\frac{kL}{C})^{1/2}}{k^{1/2} N^{\nu+1}},$$

where C and C_ν are absolute constants, L is the length of the boundary, and P_N^* is the orthogonal projection onto the approximation space. Although this grading is optimal in the sense that it allows us to derive identical error bounds on each mesh interval (equidistributing the error), in fact, we can show that the same approximation result holds in L^2 for any q satisfying

$$\frac{2\nu+2}{1-2\alpha} < q \leq \frac{2\nu+3}{1-2\alpha}.$$

To achieve a mesh grading that makes more sense as $\Omega_j \to \pi$, i.e. to achieve a grading that becomes uniform as the corner disappears, it is necessary to work in L^1 near the corner and L^2 away from the corner.

Improved definition of collocation points

The collocation points of [1] were defined as the midpoints of each interval of Γ_j^+ and Γ_j^-. However, as the meshes overlap this leaves open the possibility that two mesh points may be very close to each other, leading to ill-conditioned systems. Instead, we now use an alternative algorithm for determining the collocation points that should result in a well-conditioned system. The idea is to split each side of the polygon in half, so that the grid points corresponding to the $\mathrm{e}^{\mathrm{i}ks}$ are bunched in one half and well spaced in the other, and the grid points corresponding to the $\mathrm{e}^{-\mathrm{i}ks}$ are bunched in the other half, and well spaced where the others are bunched. Collocation points are then defined first on the bunched halves, as the midpoints of each interval. It remains to place collocation points on the widely spaced halves. In [1] these were placed at the midpoints, but here we propose computing the two "dense" collocation points to either side of the midpoints, and then moving the points to the midpoints of the "dense" points, so as to maximise the distance between collocation points. Numerical experiments on a range of examples indicate that this approach leads to an improvement in the conditioning of the linear system.

Integral evaluation

Numerical evaluation of integrals of the form (6) which arise in the collocation scheme can be expensive. To maintain accuracy as $k \to \infty$, the number of degrees of freedom required by standard Gaussian quadrature must grow at least with order k, due to the oscillatory nature of the integrand. Instead, we propose to use the numerical method of steepest descents approach developed by Huybrechs and Vandewalle in [4], which is well adapted to evaluating integrals of this type. Indeed the cost of this scheme does not increase as $k \to \infty$.

Further details will appear in [2].

References

[1] S. Arden, S. N. Chandler-Wilde and S. Langdon, "A collocation method for high frequency scattering by convex polygons", J. Comp. Appl. Math., 204:334–343, 2007.

[2] S. N. Chandler-Wilde, D. Huybrechs and S. Langdon, "A fully discrete wavenumber independent boundary integral method for scattering by convex polygons", in preparation.

[3] S. N. Chandler-Wilde and S. Langdon, "A Galerkin boundary element method for high frequency scattering by convex polygons", SIAM J. Numer. Anal., 45:610–640, 2007.

[4] D. Huybrechs and S. Vandewalle, "On the evaluation of highly oscillatory integrals by analytic continuation", SIAM J. Numer. Anal., 44:1026–1048, 2006

Eulerian Gaussian Beams for High Frequency Wave Propagation

Shingyu Leung[†,*], **Jianliang Qian**[‡,**], **Robert Burridge**[§,***]

[†] Department of Mathematics, University of California, Irvine, CA 92697-3875, USA
[‡] Department of Mathematics and Statistics, Wichita State University, Wichita, KS 67260-0033, USA.
[§] 13200 Mountain Shadow Road NE, Albuquerque, NM 87111, USA.
*Email: syleung@math.uci.edu, **Email: qian@math.wichita.edu, ***Email: burridge@erl.mit.edu

Abstract

The traditional Gaussian beam summation method is based on Lagrangian ray tracing and local ray centered coordinates. We propose a new Eulerian formulation of Gaussian beam theory which adopts global Cartesian coordinates, level sets and Liouville equations, yielding uniformly distributed Eulerian traveltimes and amplitudes in phase space simultaneously for multiple sources. The time harmonic wavefield can be constructed by summing up Gaussian beams with ingredients provided by the new Eulerian formulation. Numerical experiments indicate that the Gaussian beam summation method yields accurate asymptotic wave fields even at caustics. The new method may be used for seismic modeling and migration.

Introduction

The method of Gaussian beam summation is powerful for seismic wave modeling and migration in the high frequency regime; see [1] and references therein. In contrast to the geometrical ray theory in which the ray amplitude is unbounded at caustics, a Gaussian beam constructed around a central ray always has guaranteed regular behavior at caustics and interference of multiple arrivals is achieved by summing up a bundle of Gaussian beams. We propose a purely Eulerian Gaussian beam summation method that combines the Gaussian beam ansatz introduced in [5] with the paraxial Liouville formulation developed recently in [3]; the resulting Eulerian method is easy to implement and computationally efficient.

Gaussian beams are approximate asymptotically valid solutions to hyperbolic partial differential equations which are concentrated near a single curve through the domain. The existence of such solutions has been known to the applied mathematician since sometime in the 1960s, and these solutions have been used to obtain results on propagation of singularities in hyperbolic PDEs ([2], [5]).

Traditional Gaussian beams are constructed by using local ray coordinates. As a result, one has to compute the normal distance from every observation point to the central ray of every Gaussian beam, which is computationally cumbersome and expensive. To overcome this difficulty, one may use local geographical coordinates in the vicinity of an observation point, which only partially solves the problem. To implement Gaussian beam summation in a global Cartesian coordinate, we adopt the ansatz proposed in [5] and [6] to construct Gaussian beams along central rays without resorting to local ray-centered coordinates. Mathematically, this ansatz constructs an approximate traveltime function with an imaginary part as a Taylor expansion around a central ray by using traveltime derivatives on the central ray; to some extent, the approximate traveltime function in the traditional Gaussian beam summation can be obtained from the new approximate traveltime function by using a local ray-centered coordinate transformation. To have an Eulerian formulation capturing multiple arrivals and caustics, we adopt Liouville equations in a paraxial setting ([3]) to parametrize multiple sources and receivers; see these papers and the references therein for recent progress in Eulerian geometrical optics.

Methods

Eikonal Equations

Consider the reduced wave equation for $U(x,z,\omega)$,

$$\nabla^2 U(x,z,\omega) + \frac{\omega^2}{v^2(z,x)} U(x,z,\omega) = -\delta(x-x_s)\delta(z-z_s), \quad (1)$$

in the physical domain,

$$\Omega = \{(x,z) : x_{\min} \le x \le x_{\max}, 0 \le z \le z_{\max}\},$$

where ω is frequency, $v(z,x)$ the velocity at point (z,x), and (z_s,x_s) the coordinates of a source point.

Applying the standard geometrical optics ansatz to the above equation, we have the eikonal and transport equations for traveltime τ and amplitude A:

$$\left(\frac{\partial \tau}{\partial x}\right)^2 + \left(\frac{\partial \tau}{\partial z}\right)^2 = \frac{1}{v^2(x,z)}, \quad (2)$$

$$\nabla\tau \cdot \nabla A + \frac{1}{2} A \nabla^2 \tau = 0, \quad (3)$$

with corresponding initial conditions.

In some seismic applications, the traveltime field is needed only in regions where

$$\frac{\partial \tau}{\partial z} \geq \frac{\cos\theta_{\max}}{v} > 0,$$

i.e., along downgoing rays making an angle $\pm\theta_{\max}$, $\theta_{\max} < \frac{\pi}{2}$ with the vertical; this is the so-called sub-horizontal rays, where sub-horizontal means oriented in the positive z-direction. To enforce this condition, we modify the eikonal equation as an evolution equation in depth, resulting in the following form of the eikonal equation,

$$\frac{\partial \tau}{\partial z} - \sqrt{\frac{1}{v^2} - \left(\frac{\partial \tau}{\partial x}\right)^2} = 0, \ z \geq 0, \quad (4)$$

$$\tau(0,x) = \tau_0(x), \quad \text{Im}\ \tau_0 \geq 0, \quad (5)$$

$$\nabla\tau|_{z=0} = \xi(x), \quad (6)$$

where $\tau_0(x)$ and $\xi(x)$ are given complex smooth functions satisfying the compatibility conditions:

$$\frac{\partial \tau_0}{\partial x} = \xi_1(x), \quad (7)$$

$$\xi_2(x) - \sqrt{\frac{1}{v^2(0,x)} - \xi_1^2(x)} = 0. \quad (8)$$

At the point source, $(z_s, x_s) = (0, x_s)$, we specify initial conditions,

$$\tau_0(x_s) = 0, \quad (9)$$

$$\xi_1(x_s;\theta_s) = \frac{\sin\theta_s}{v(0,x_s)}, \quad |\theta_s| \leq \theta_{\max} < \frac{\pi}{2}, \quad (10)$$

where $(x_s, \theta_s) \in \Omega_p$,

$$\Omega_p = \{(x,\theta) : x_{\min} \leq x \leq x_{\max}, -\theta_{\max} \leq \theta \leq \theta_{\max}\}.$$

Accordingly, we construct an approximation of τ in the neighborhood of the source by,

$$\tau_0(x;x_s) = \tau_0(x_s) + \xi_1(x_s;\theta_s)\cdot(x - x_s) \quad (11)$$

$$+ i\frac{\epsilon}{2}(x - x_s)^2\cos^2\theta_s, \quad (12)$$

where ϵ is a positive number. The constructed τ_0 satisfies the required initial condition at the source.

To apply Gaussian beam theory ([5], [6]) we let the axis, or central ray, of a beam be given by $x = X(z)$, travel time by $\tau = T(z)$ and, we introduce the Hamiltonian

$$H(z,\ X,\ p) = -\sqrt{\frac{1}{v^2(z,X)} - p^2}, \quad (13)$$

where $p(z) = \tau_x(z, X(z))$. Then we need from the ray tracing system,

$$\dot{X}(z) = H_p = \frac{p}{\sqrt{\frac{1}{v^2} - p^2}}, X|_{z=0} = x_s; \quad (14)$$

$$\dot{p}(z) = -H_X = \frac{-v_X}{v^3\sqrt{\frac{1}{v^2} - p^2}}, p|_{z=0} = \xi_1(x_s;\theta_s); \quad (15)$$

$$\dot{T}(z) = \frac{1}{v^2\sqrt{\frac{1}{v^2} - p^2}}, T|_{z=0} = \tau_0(x_s); \quad (16)$$

here $\dot{}$ denotes the total derivative with respect to z. To emphasize the dependence on the initial conditions, we will write $X = X(z) = X(z;x_s,\theta_s)$, $p = p(z) = p(z;x_s,\theta_s)$, and $T = T(z) = T(z;x_s,\theta_s)$; for the sake of clarity of notation we may also suppress the dependence on (x_s,θ_s) when it is clear from the context.

Next we consider the variations of $X(z;x_s,\theta_s)$ and $p(z;x_s,\theta_s)$ along the ray with respect to the initial point $x_s = \alpha$, and we define $B(z;x_s,\theta_s) = \frac{\partial p(z;x_s,\theta_s)}{\partial\alpha}$ and $C(z;x_s,\theta_s) = \frac{\partial X(z;x_s,\theta_s)}{\partial\alpha}$. Then we have the following dynamic ray tracing (DRT) system,

$$\dot{B}(z) = -H_{X,p}B - H_{X,X}C, B(0) = i\epsilon\cos^2\theta_s, \quad (17)$$

$$\dot{C}(z) = H_{p,p}B + H_{p,X}C, C(0) = 1, \quad (18)$$

where $\epsilon > 0$,

$$H_{p,p} = \frac{1}{(1 - v^2\ p^2)\sqrt{\frac{1}{v^2} - p^2}},$$

$$H_{X,X} = \frac{(v\ v_{X,X} - 3v_X^2)(1 - v^2\ p^2) + v_X^2}{v^4(1 - v^2\ p^2)\sqrt{\frac{1}{v^2} - p^2}},$$

$$H_{p,X} = H_{X,p} = \frac{p\ v_X}{v\ (1 - v^2\ p^2)\sqrt{\frac{1}{v^2} - p^2}}.$$

The width of the beam is $\sqrt{2/(\epsilon\omega\cos^2\theta_s)}$ in the x-direction and is $\sqrt{2/(\epsilon\omega)}$, independent of θ_s, orthogonally to the beam axis. Then Gaussian beam theory implies that $\text{Im}(BC^{-1})$ remains positive if it is positive initially, i.e. if ϵ is positive.

Because $\tau_x = p$ and $\tau_{xx} = \delta p/\delta x = (\partial p/\partial\alpha)/(\partial x/\partial\alpha) = B/C$, near a central ray emanating from x_s with the initial takeoff angle θ_s we have the following approximate solution in the neighborhood of X,

$$\tau(z,x;x_s,\theta_s) = T(z;x_s,\theta_s) + p(z)\cdot(x - X(z)) + \frac{1}{2}(x - X(z))^2 B(z)C^{-1}(z), \quad (19)$$

where p, X, B and C depend on (x_s,θ_s) as well. Let the angle the central ray of a beam makes with the z-direction at z be the arrival angle $\Theta(z;x_s,\theta_s)$, and let

$p(z) = \frac{\sin\Theta(z)}{v(z,X(z))}$. Then, by the ray tracing system (14), (15) and (16), we have

$$\frac{dX}{dz}(z) = \tan\Theta, \quad X(0) = x_s, \tag{20}$$

$$\frac{d\Theta}{dz}(z) = \frac{1}{v}(v_z \tan\Theta - v_x), \quad \Theta(0) = \theta_s, \tag{21}$$

$$\frac{dT}{dz}(z) = \frac{1}{v(z,X(z))\cos\Theta(z)}, \quad T|_{z=0} = 0, \tag{22}$$

where θ_s varies from $-\theta_{\max} \le \theta_s \le \theta_{\max} < \pi/2$. As a result, the DRT system, (17) and (18), becomes

$$\dot{B}(z) = -H_{X,p}B - H_{X,X}C, B(0) = i\epsilon\cos^2\theta_s, \tag{23}$$

$$\dot{C}(z) = H_{p,p}B + H_{p,X}C,\ C(0) = 1, \tag{24}$$

where $\epsilon > 0$, $H_{X,X}$, $H_{X,p}$, and $H_{p,p}$ are defined accordingly.

Finally, the amplitude along a paraxial ray is

$$A(z; x_s, \theta_s) = \frac{\sqrt{C(0)v(z, X(z))\cos\theta_s}}{\sqrt{v(z_s, x_s)C(z; x_s, \theta_s)\cos\Theta(z)}}, \tag{25}$$

which is nonzero everywhere.

We note that when the paraxial assumption is not available, we may construct the Gaussian beam summation directly by using the approach presented in [5] and [6].

Lagrangian Gaussian beam superposition

The wavefield due to one Gaussian beam parameterized with initial take-off angle θ_s is

$$\Psi(z, x; x_s, \theta_s) = \psi_0 A(z; x_s, \theta_s)\exp[i\omega\tau(z, x; x_s, \theta_s)], \tag{26}$$

where $\tau(x, z; x_s, \theta_s)$ is given by (19) with $p(z) = \frac{\sin\Theta(z;x_s,\theta_s)}{v(z,X(z;x_s,\theta_s))}$. Here the radiation factor

$$\psi_0 = \frac{1}{4\pi}\exp\left[\frac{i\pi}{2}\right], \tag{27}$$

and can be determined by the stationary phase method.

To compute the wavefield generated by a point source at x_s, we integrate over all the possible rays emanating from the source,

$$U(z, x; x_s) = \int_{-\pi/2}^{\pi/2} \Psi(z, x; x_s, \theta_s)d\theta_s. \tag{28}$$

What does equation (28) mean? According to equations (20) and (21), given x_s, $\theta_s \in [-\theta_{\max}, \theta_{\max}]$, there is one ray emanating from the source x_s and take-off angle θ_s to reach $(X(z; x_s, \theta_s), \Theta(z; x_s, \theta_s)) \in \Omega_p$ at depth z; varying θ_s from $-\theta_{\max}$ to $\theta_{\max}$ traces out a curve,

$$\gamma(z; x_s) \subset \Omega_p,$$

where $\gamma(0; x_s) = \{(x_s, \theta_s) : -\theta_{\max} \le \theta_s \le \theta_{\max}\}$ is a vertical line in Ω_p. We note that $\gamma(z; x_s)$ can be considered as a curve parametrized by θ_s, while the z-variable indicates the evolution of the curve under the ray tracing equations (20) and (21). Consequently, the summation formula (28) simply states that at depth z the integration is carried out with respect to the curve parameter θ_s along the curve $\gamma(z; x_s)$.

To carry out the above summation process, we need to choose a numerical quadrature formula, solve the ray tracing equations and the dynamical ray tracing system with takeoff angles at the quadrature sampling points, construct a Gaussian beam along each ray, and sum up Gaussian beams to obtain wavefield at each observation point. Because the above process is based on the Lagrangian ray tracing, we look for an Eulerian approach using Gaussian beams.

Eulerian Gaussian beams

We apply the level set based Eulerian method for computing multivalued traveltimes in paraxial formulation as developed in [3] and references therein to construct Eulerian Gaussian summation methods; see [4] for more details.

References

[1] V. Cerveny, M. Popov, and I. Psencik. Computation of wave fields in inhomogeneous media-Gaussian beam approach. *Geophys. J. R. Astr. Soc.*, 70:109–128, 1982.

[2] L. Hormander. On the existence and the regularity of solutions of linear pseudo-differential equations. *L'Enseignement Mathematique*, 17:99–163, 1971.

[3] S. Leung, J. Qian, and S. Osher. A level set method for three dimensional paraxial geometrical optics with multiple sources. *Comm. Math. Sci.*, 2:657–686, 2004.

[4] S. Y. Leung, J. Qian, and R. Burridge. Eulerian Gaussian beams for high frequency wave propagation. Preprint, 2006.

[5] J. Ralston. Gaussian beams and the propagation of singularities. Studies in partial differential equations. MAA Studies in Mathematics, 23. Edited by W. Littman. pp.206-248., 1983.

[6] N. Tanushev, J. Qian, and J. Ralston. Mountain waves and Gaussian beams. SIAM J. Multiscale Modeling and Simulation (to appear), 2007.

A NEW INTEGRAL FORMALISM FOR TRANSMISSION PROBLEMS OF ELECTROMAGNETISM

David P. Levadoux
ONERA, Chemin de la hunière, 91761 Palaiseau, France
Email: david.levadoux@onera.fr

Abstract

Taking inspiration from a previous work on the construction of some "inherently pre-conditioned" integral equations [4] for scattering problems, we present a new class of boundary integral equations for transmission problems of electromagnetism. As the previous one, the new formalism is dependent of the choice of a boundary operator playing the role of a preconditioner. We propose few models of such preconditioning operators whose vocation is to approach as well as possible an optimal operator identified as a the exterior Calderón projector of the transmission problem. Indeed, if the preconditioning operator is taken as the Calderón projector, the resulting equation becomes trivial (the underlying operator is the identity). For this reason, the linear systems resulting from the discretization of such a formalism are suspected to be well-conditioned.

Introduction

A motivation of this work is to give a continuation to the integral equation method elaborated at ONERA since 1998 [5] to speed up the resolution time of the perfect electrical conductor (PEC) problem in the time-harmonic domain. The method is based on a generalized combined source integral equation [6] [7] [4] depending on the choice of a boundary operator whose vocation is to approximate as close as possible the exterior admittance of the conductor. Indeed, the construction of the equation is done in such a way that in the limiting case where this approximation is exact, the integral operator to be inverted becomes the identity. An efficient approximation allows in practice to reduce by half the computational time of problems involving more than $300\,000$ unknowns, and containing big cavities [3] [2] [1]. Such encouraging results call for an extension of the method. See for instance in these proceedings, the extension we propose in an other abstract to the impedance boundary-value problems.

Here, we are interested in application of the methodology to transmission problems formally read as

$$\text{Find } \mathbf{E} \in W \text{ such that } B\mathbf{E} = (\mathbf{u}, \mathbf{v}) \qquad (1)$$

where $\mathbf{u}$, $\mathbf{v}$ are current distributions ${\mathcal{D}'}_T(\Gamma)$ on a bounded closed surface Γ of $\mathbb{R}^3$, B a two-components boundary trace operator, and W being the space of all radiating electric fields defined on $\mathbb{R}^3\backslash\Gamma$ and having a tangential trace on Γ.

We set Ω^- (resp. Ω^+) the volume enclosed in (resp. exterior to) Γ to which is associated a wave number k_- (resp.k_+). The application from Ω^- (resp. Ω^+) of the tangential trace operator $\gamma_{EH} = (\mathbf{n}\times, \frac{1}{ik}\mathbf{n}\times\nabla)$ is noted γ^-_{EH} (resp. γ^+_{EH}), $\mathbf{n}$ being the outward unit normal to Γ.

Now and for all the sequel, we restrict the study to the classic transmission problem governed by the jump trace operator

$$B = \gamma^+_{EH} - \gamma^-_{EH} \ . \qquad (2)$$

Framework of the new formalism

We call *Calderón potential* the underlying potential $\mathcal{C}$ induced by the resolution of the well-posed problem (1) equipped with $B = \gamma^+_{EH} + \gamma^-_{EH}$, *i.e.* $\mathcal{C}(\mathbf{u}, \mathbf{v}) = \mathbf{E}$. In the particular case $k_- = k_+$ the Calderón potential, we decide to note $\mathcal{V}$, is known explicitly as

$$\mathcal{V}(\mathbf{u}, \mathbf{v}) = \mathcal{L}\mathbf{v} - \mathcal{K}\mathbf{u}$$

where $\mathcal{L} = \frac{1}{ik}\nabla\times\nabla\times\mathcal{G}$, $\mathcal{K} = \nabla\times\mathcal{G}$ and $\mathcal{G}$ being the well-known vector potential.

For any potential $\mathcal{U} : {\mathcal{D}'}_T(\Gamma) \rightarrow W$, we adopt the following notations

$$\mathcal{U}^+ = \mathcal{U}_{|\Omega^+} \qquad\qquad U^+ = \gamma^+_{EH}\mathcal{U}^+ \ .$$

The general framework of our new formalism consists to seek the solution $\mathbf{E}$ of (1)-(2) in the form

$$\mathbf{E}^+ = \mathcal{V}^+\widetilde{C}^+(\mathbf{u}', \mathbf{v}') \quad \mathbf{E}^- = -\mathcal{V}^-(\mathrm{Id} - \widetilde{C}^+)(\mathbf{u}', \mathbf{v}')$$

where $(\mathbf{u}', \mathbf{v}')$ is a solution of the boundary equation

$$\left(V^+\widetilde{C}^+ + V^-(\mathrm{Id} - \widetilde{C}^+)\right)(\mathbf{u}', \mathbf{v}') = (\mathbf{u}, \mathbf{v}) \qquad (3)$$

and $\widetilde{C}^+$ a boundary operator being an approximation of the Calderón projector C^+. The main feature of this formalism is that if $\widetilde{C}^+ = C^+$, then the underlying operator of (3) is the identity. Therefore, it is expected that a good approximation of C^+ should results in a well-conditioned equation (3).

Approximation of the Calderón projector

We recall that the exterior admittance operator Y^+ links the components of the Cauchy data of any field $\mathbf{E} \in W^+$ as

$$Y^+ : \mathbf{n} \times \mathbf{E} \mapsto \mathbf{n} \times \mathbf{H} \ .$$

We analogously define the interior admittance operator Y_-. Reading C^+ with the admittance operators gives

$$C^+ = \begin{pmatrix} A & -Y^+A \\ Y^+A & A \end{pmatrix} \tag{4}$$

where $A = Y^+(Y^+ - Y_-)^{-1}$. One can show that modulo a -1 order operator, A is equal to

$$\widetilde{A} = \frac{k_+k_-}{k_+ + k_-}\left(\frac{1}{k_+}\Pi_{\text{loop}} + \frac{1}{k_-}\Pi_{\text{star}}\right) \tag{5}$$

where Π_{loop} and Π_{star} are the projectors onto the solenoidal and irrotational currents of the Helmoltz decomposition. Coming back to (4) and noticing that $(Y^+)^2 = -\text{Id}$, we suggest to adopt as an approximation of C^+

$$\widetilde{C}^+ = \begin{pmatrix} \widetilde{A} & -\widetilde{Y}^+\widetilde{A} \\ \widetilde{Y}^+\widetilde{A} & -(\widetilde{Y}^+)^2A \end{pmatrix} \tag{6}$$

where $\widetilde{Y}^+$ is an approximation of Y^+ we have to build.

Approximation of the exterior admittance

The problem to deal with a good approximation of the exterior admittance of a surface pervade number of numerical problems in wave propagation simulation. Many solutions have been proposed going from the basic Sommerfeld condition to the more advanced techniques of perfect matched layers. Therefore, we don't pretend in this early work to present an optimal solution resulting from comparisons between different competitive solutions. Nevertheless, the experience we get in the numerical implementation of this kind of formalism for the PEC problem, suggests some solutions which are perhaps relevant.

Let us recall that we aim a model $\widetilde{Y}^+$ of admittance leading to an equation (3)-(6)-(5) always well-posed at any frequency and being a compact perturbation of identity, in order to deal after discretization with a well-conditioned linear system easy to solve iteratively. The model designed for the PEC problem and having given proof of its efficiency uses a quadratic partition of unity (POU) (U_p, χ_p)[1] as follows

$$\widetilde{Y}^+ = -\frac{2}{ik_+}\mathbf{n} \times \sum_p \chi_p \left(\nabla G \nabla \cdot + k_+^2 G\right) \chi_p \ , \tag{7}$$

G being the convolution with the elementary solution of the Helmholtz equation. But the problem we have to face when reusing this model is that the resulting equation (3) can only be shown injective without the Fredholm property (compact perturbation of identity). On the other hand, modifications claimed to restore the Fredholm property seems to ask harshly the question of injectivity. For instance, the Fredholm property can be preserved if instead of a quadratic POU we have a regular POU whose each χ_p function is associated to a cut-off function $\overline{\chi_p}$ such that $\overline{\chi_p} = 1$ on the support of χ_p. Then, equation (3)-(6)-(5) equipped with

$$\widetilde{Y}^+ = -\frac{2}{ik_+}\mathbf{n} \times \sum_p \overline{\chi_p} \left(\nabla G \nabla \cdot + k_+^2 G\right) \chi_p \tag{8}$$

is a compact perturbation of identity. Although the proof of the injectivity is probably unreachable without further constraints on the cut-off functions $\overline{\chi_p}$, such a model is attractive and should be experimented in the future.

A mid-term solution able to preserve in (3) both the injectivity and the Fredholm property is given by this new model

$$\widetilde{Y}^+ = -\frac{2}{ik_+}\mathbf{n} \times (\nabla \sum_p \chi_p G_0 \chi_p \nabla \cdot \ + k_+^2 \sum_p \chi_p G \chi_p)$$

where $\{\chi_p\}_p$ is once again a quadratic POU, and G_0 the convolution with the elementary solution of the Laplace equation.

References

[1] F. Alouges, S. Borel, and D. P. Levadoux. A stable well-conditioned integral equation for electromagnetism scattering. *J. Comp. Appl. Math*, 2006, accepted.

[2] S. Borel. *Étude d'une équation intégrale stabilisée pour la résolution itérative de problèmes de diffractions d'ondes harmoniques en électromagnétisme*. PhD thesis, Université Paris XI, 2006.

[3] S. Borel, D. P. Levadoux, and F. Alouges. A new well-conditioned integral formulation for Maxwell equations in three-dimensions. *IEEE Trans. Antennas Propag.*, 53(9):2995–3004, September 2005.

[1] $(U_p)_p$ is a set of patches recovering Γ, and $(\chi_p)_p$ a family of truncation functions with support in U_p and such that $\sum_p \chi_p^2 = 1$.

[4] D. P. Levadoux. Stable integral equations for the iterative solution of electromagnetic scattering problems. *C. R. Physique*, 7(5):518–532, 2006.

[5] D. P. Levadoux and B. L. Michielsen. Analysis of a boundary integral equation for high frequency Helmholtz problems. In *Waves Conference*, pages 765–767, Golden, Co, 1-5 June 1998.

[6] D. P. Levadoux and B. L. Michielsen. An efficient high-frequency boundary integral equation. In *Antennas and Propagation Society International Symposium*, volume 2, pages 765–767, Orlando, FL, 11-16 July 1999.

[7] D. P. Levadoux and B. L. Michielsen. Nouvelles formuations intégrales pour les problèmes de diffraction d'ondes. *M2AN*, 38(1):157–175, January/February 2004.

AN hp-BEM FOR HIGH FREQUENCY SCATTERING BY CONVEX POLYGONS

J. M. Melenk[†,*], **S. Langdon**[‡]
[†]Institut für Analysis und Scientific Computing, TU Wien, A-1040 Wien, Austria.
[‡]Department of Mathematics, University of Reading, Reading RG6 6AX, UK.
[*]Email: melenk@tuwien.ac.at

Abstract

Time harmonic acoustic scattering by convex polygons is considered. Standard schemes with piecewise polynomial approximation spaces have a computational cost that grows at least linearly with respect to the wavenumber. Here we extend a h-version Galerkin boundary element method scheme for this problem developed by Chandler-Wilde and Langdon to an hp-version of the BEM, for which we demonstrate an exponential convergence rate with respect to the order of the polynomials whilst maintaining only logarithmic dependence on the wavenumber. The question of how to set up the stiffness matrix with work independent of the wavenumber is also addressed.

1 Introduction

Consider time harmonic acoustic scattering by convex polygons. An integral equation based method effective for high frequencies was recently proposed in [1]. Using a detailed regularity analysis of the solution, an h-version trial space was proposed that has approximation properties depending only logarithmically on the wavenumber. The key features are the ability to identify the leading order (in the wavenumber) behaviour of the solution and a precise characterization of the solution behaviour near the vertices of the polygon. Since the approximation order is fixed, the achievable convergence rate is algebraic. Here, we begin in §2 by reformulating as an integral equation. In §3 we extend the scheme of [1] to the hp-version of the BEM, for which the solution can be approximated at an exponential rate from the trial space; the problem size required to achieve a given accuracy grows only logarithmically with the wavenumber. Numerical results are presented in §4. In §5 we address the question of how to set up the stiffness matrix with work independent of the wavenumber. Finally in §6 we present some conclusions.

2 Integral equation formulation

Consider acoustic scattering of a time harmonic incident plane wave $u^i(\mathbf{x}) := \mathrm{e}^{\mathrm{i}k\mathbf{d}.\mathbf{x}}$ by a sound soft convex polygon Ω. Here $\mathbf{d}$ denotes the direction of the incident wave, with $|\mathbf{d}| = 1$. The total acoustic field u satisfies

$$-\Delta u - k^2 u = 0, \text{ in } \mathbb{R}^2\backslash\bar{\Omega}, \quad u = 0, \text{ on } \partial\Omega,$$

with $u^s := u - u^i$ satisfying the Sommerfeld radiation condition, where $\partial\Omega$ denotes the boundary of Ω. To solve, we begin by reformulating as a boundary integral equation for the unknown Neumann data $\partial_n u$:

$$\left(\frac{1}{2}I + K' + \mathrm{i}\eta V\right)\partial_n u = f := \partial_n u^i + \mathrm{i}\eta u^i, \qquad (1)$$

where $V\psi(\mathbf{x}) := \int_{\partial\Omega}\Phi(\mathbf{x},\mathbf{y})\psi(\mathbf{y})\,\mathrm{d}\mathbf{y}$ and $K'\psi(\mathbf{x}) := \int_{\partial\Omega}\frac{\partial\Phi(\mathbf{x},\mathbf{y})}{\partial\mathbf{n}(\mathbf{x})}\psi(\mathbf{y})\,\mathrm{d}\mathbf{y}$ are the usual single and double layer potentials, with $\Phi(\mathbf{x},\mathbf{y}) := \frac{i}{4}H_0^1(k|\mathbf{x}-\mathbf{y}|)$ denoting the fundamental solution of the two-dimensional Helmholtz problem and $\mathbf{n}$ the unit outward normal. The classical Galerkin method for solving (1) is then:
given $V_N \subset L^2(\partial\Omega)$ find $\psi_N \in V_N$ such that

$$\left\langle\left(\frac{1}{2}I + K' + \mathrm{i}\eta V\right)\psi_N, v\right\rangle_{L^2} = \langle f, v\rangle_{L^2}, \text{ for all } v \in V_N. \qquad (2)$$

It remains to choose a good approximation space V_N.

3 Design of an hp-BEM space

As shown in [1], the total acoustic field can be decomposed into the incident field u^i, the "reflected" field u^r, and the "diffracted" field u^d. For high frequencies, the leading order behaviour of $\partial_n u$ (away from the corners) consists of the incident and reflected fields, giving

$$\partial_n u \sim \Psi := \begin{cases} 2\partial_n u^i & \text{on lit sides,} \\ 0 & \text{on shadow sides.} \end{cases}$$

The idea is then to write $\partial_n u = \Psi + k\phi$, and solve for the diffracted part ϕ. Thus we want to design an approximation space V_N in such a way that ϕ can be approximated well. To achieve this, it is shown in [1] that for each edge $\Gamma_j = \{A_j + \frac{s}{L_j}(A_{j+1} - A_j) : s \in (0, L_j)\}$ (with A_j and A_{j+1} the corners of the edge, L_j the length of the edge and ω_j the external angle at the corner A_j as shown in figure 1), the diffracted part ϕ can be written in the form

$$\phi(s) = \mathrm{e}^{\mathrm{i}ks}v_j^+(s) + \mathrm{e}^{-\mathrm{i}ks}v_j^-(L_j - s).$$

Further, with $\alpha_j = 1 - \frac{\pi}{\omega_j} \in (0, 1/2)$, v_j^+ satisfies

$$\left|(v_j^+)^{(m)}(s)\right| \le Cm!k^m \begin{cases} \sqrt{m+1}(ks)^{-\alpha_j - m} & \text{for } ks \le 1 \\ (ks)^{-1/2-m} & \text{for } ks \ge 1 \end{cases},$$

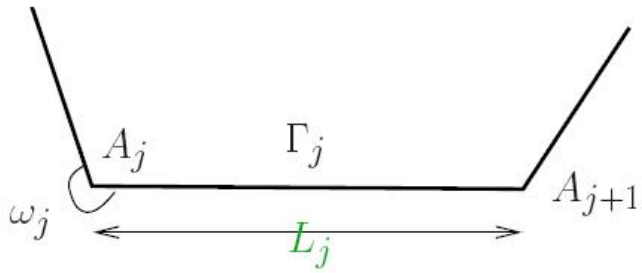

Figure 1: Notation for a polygon edge

for $m = 0, 1, \ldots$, with an analogous result holding for v_j^-. This is used in [1] to design an h-version Galerkin scheme with an approximation space consisting of the products of plane waves with piecewise polynomials supported on a graded mesh, with the mesh grading adapted in an optimal way to the rates of decay of ϕ away from the corners, such that the number of degrees of freedom required to achieve a prescribed level of accuracy need only grow logarithmically with respect to k in order to maintain accuracy as $k \to \infty$. Here we achieve a similar result, but by using an hp ansatz space we improve the convergence rate such that the approximation error decreases exponentially with respect to the order of the polynomials. Our hp ansatz space consists of a geometric mesh with L layers refined towards the vertex A_j of the edge Γ_j, as shown in figure 2. We then have the following approximation result.

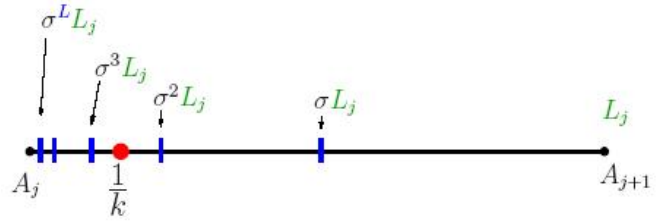

Figure 2: hp ansatz space

Theorem 1 *Let $\mathcal{T}_L^+$ ($\mathcal{T}_L^-$) be a geometric mesh with $O(L)$ layers refined towards A_j (A_{j+1}), and define*

$V_N^+ := \mathrm{e}^{\mathrm{i}ks} \times$ *piecewise polynomials of degree p on $\mathcal{T}_L^+$,*

$V_N^- := \mathrm{e}^{-\mathrm{i}ks} \times$ *piecewise polynomials of degree p on $\mathcal{T}_L^-$,*

and $\alpha = \min\{\alpha_j, \alpha_{j+1}\} \in (0, 1/2)$. Then there exists a constant b such that for $V_N := V_N^+ + V_N^-$ (so that $\dim V_N \sim pL$),

$$\inf_{v \in V_N} \|\phi - v\|_{L^2(\Gamma_j)} \lesssim k^{-1/2} \left[k^{1/2-\alpha} \mathrm{e}^{-bL} + \sqrt{\log k}\, \mathrm{e}^{-bp} \right].$$

Thus if we choose $L \sim \log k + p$ we then have

$$\begin{aligned} \inf_{v \in V_N} \|\phi - v\|_{L^2(\Gamma_j)} &\lesssim k^{-1/2}(1 + \sqrt{\log k})\mathrm{e}^{-bp}, \\ &\lesssim k^{-1/2}\mathrm{e}^{-bp+\log(\log k)}, \end{aligned}$$

and thus exponential convergence with respect to p, provided $p \gtrsim \log(\log(k))$, with $\dim V_N \sim p^2 + p \log k$.

4 Numerical results

As a numerical experiment we consider scattering by a square of side length 2π, whose sides lie on the x_1 and x_2 axes, with incident angle $\pi/4$ measured from the downward vertical. The L^2 errors (scaled by $\sqrt{k}$) and relative L^2 errors are shown in table 1. The "exact" solution ϕ was computed using the h-version scheme of [1], with many degrees of freedom. The number of degrees of freedom used here for each problem is denoted by DOF.

Table 1: Errors for hp scheme, scattering by a square

k	p	L	DOF	$\sqrt{k}\|\phi - \phi_N\|_2$	$\frac{\|\phi-\phi_N\|_2}{\|\phi\|_2}$
5	0	1	16	2.3×10^0	1.0×10^0
	1	3	64	5.4×10^{-1}	2.5×10^{-1}
	2	5	144	1.1×10^{-1}	5.1×10^{-2}
	3	7	256	4.5×10^{-2}	2.1×10^{-2}
10	0	1	16	2.3×10^0	1.1×10^0
	1	3	64	4.9×10^{-1}	2.3×10^{-1}
	2	5	144	1.1×10^{-1}	5.4×10^{-2}
	3	7	256	6.5×10^{-2}	3.1×10^{-2}
20	0	1	16	1.9×10^0	9.5×10^{-1}
	1	3	64	4.9×10^{-1}	2.4×10^{-1}
	2	5	144	1.0×10^{-1}	5.2×10^{-2}
	3	7	256	4.1×10^{-2}	2.1×10^{-2}
40	0	1	16	1.9×10^0	9.8×10^{-1}
	1	3	64	5.1×10^{-1}	2.7×10^{-1}
	2	5	144	9.3×10^{-2}	4.9×10^{-2}
	3	7	256	3.7×10^{-2}	2.0×10^{-2}

5 Quadrature for oscillatory integrals

In order to set up the linear system (2) it is necessary to evaluate many highly oscillatory double integrals, some of which have singularities (due to the singularities in V and K at $\mathbf{x} = \mathbf{y}$). As a model integration problem we consider the numerical evaluation of

$$\int_{s=0}^{1} \int_{t=0}^{1} \mathrm{e}^{\mathrm{i}k\{\pm s \pm t + d(s,t)\}} \kappa(s,t) g(s,t)\, \mathrm{d}s\, \mathrm{d}t, \quad (3)$$

where κ has a singularity at $s = t = 0$, g is smooth, and $d(s,t)$ represents the distance between the points $\mathbf{x}(s)$

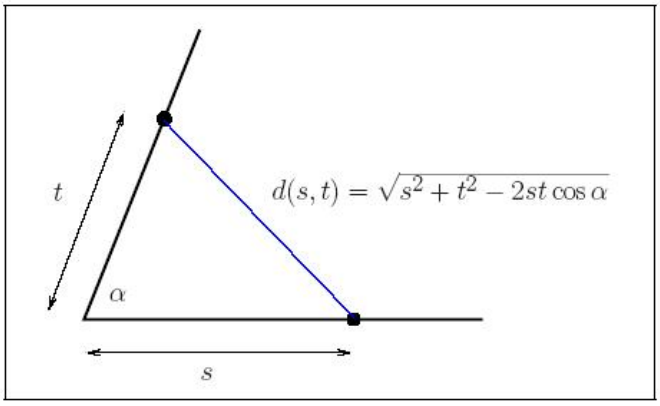

Figure 3: Geometry for model integration problem

and $\mathbf{y}(t)$, as shown in figure 3. To evaluate (3), we split the inner integral into $t < s$ and $t > s$, and consider a quadrature routine for the integration over the triangle $\{(s,t) : 0 < s < 1, 0 < t < s\}$ (the method for the case $t > s$ follows analogously). Making the substitution $\tau := \pm s \pm t + d(s,t)$, we get the integral

$$\int_\tau \mathrm{e}^{\mathrm{i}k\tau} \underbrace{\int_s \kappa(s,t(s,\tau))g(s,t(s,\tau))\frac{\partial t}{\partial \tau}\,\mathrm{d}s}_{=:f(\tau)}\,\mathrm{d}\tau.$$

Then the function $f(\tau)$ has a singularity only at $\tau = 0$. The evaluation of oscillatory integrals of the form $\int_a^b \mathrm{e}^{\mathrm{i}kx} f(x)\,\mathrm{d}x$ in the case that f is smooth has received much recent attention in the literature (see e.g. [2]). For polynomials π, integrals of the form $\int_0^1 \mathrm{e}^{\mathrm{i}kx}\pi(x)\,\mathrm{d}x$ can be evaluated analytically. The classical Filon quadrature approach is then to approximate the function f by a polynomial $I_p f$, so

$$\int_0^1 \mathrm{e}^{\mathrm{i}kx} f(x)\,\mathrm{d}x \approx \int_0^1 \mathrm{e}^{\mathrm{i}kx}(I_p f)(x)\,\mathrm{d}x =: F_p(k,f).$$

This approach yields the error estimate

$$\left|\int_0^1 \mathrm{e}^{\mathrm{i}kx} f(x) - F_p(k,f)\right| \le \|f - I_p f\|_{L^1(0,1)}.$$

In the case that f is singular one can use an hp-Filon quadrature approach. Assuming that f has a "typical" singularity at $x = 0$, we define $\mathcal{T}_L$ to be the geometric mesh on $(0,1)$ with L layers refined towards 0, similar to the mesh shown in figure 2. We define $I_{p,L}f$ to be the piecewise polynomial approximation to f on $\mathcal{T}_L$, and then make the approximation

$$\int_0^1 \mathrm{e}^{\mathrm{i}kx} f(x)\,\mathrm{d}x \approx \int_0^1 \mathrm{e}^{\mathrm{i}kx}(I_{p,L}f)(x)\,\mathrm{d}x =: F_{p,L}(k,f).$$

This yields the error estimate

$$\left|\int_0^1 \mathrm{e}^{\mathrm{i}kx} f(x) - F_{p,L}(k,f)\right| \le \|f - I_{p,L}f\|_{L^1(0,1)}.$$

Choosing $L \sim p$ leads to exponential convergence, with work $O(Lp+p^2)$ independent of k. Numerical results for a simple model example are shown in figure 4.

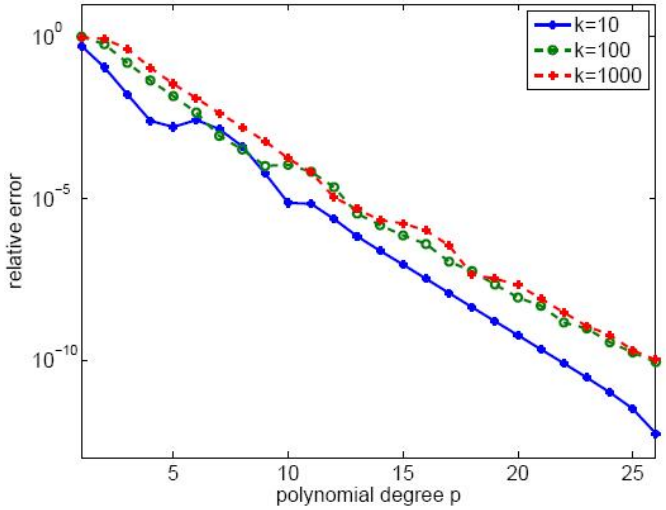

Figure 4: Numerical evaluation of $\int_0^1 \int_0^s \frac{\mathrm{e}^{\mathrm{i}k(s+t+\sqrt{s^2+t^2})s}}{(s^2+t^2)^{5/4}}\,\mathrm{d}t\,\mathrm{d}s$

6 Conclusions

In this paper we have designed an hp-BEM space that can approximate, in L^2, the solution $\partial_n u$ at an exponential rate (with respect to the polynomial degree p), subject to the weak side constraints $p \gtrsim \log(\log k)$, and $L \sim \log k + p$, where L is the number of layers of geometric refinement. The total problem size is then $N \sim Lp \sim p(p + \log k)$. To deal with integrands that are highly oscillatory and that have singularities, we propose an hp-Filon quadrature technique, giving k-independent exponential convergence (in the number of quadrature points) for the absolute errors.

References

[1] S. N. Chandler-Wilde and S. Langdon, "A Galerkin boundary element method for high frequency scattering by convex polygons", SIAM J. Numer. Anal., 45:610–640, 2007.

[2] A. Iserles, "On the numerical quadrature of highly-oscillating integrals I: Fourier transforms", IMA J. Numer. Anal., 24:365–391, 2004.

High Frequency Scattering By Convex Curvilinear Polygons

M. Mokgolele[‡,*], **S. Langdon**[‡], **S. N. Chandler-Wilde**[‡]

[‡]Department of Mathematics,University of Reading, Whitenights, P. O. Box 220, Berkshire RG6 6AX, UK
[*]Email: m.mokgolele@reading.ac.uk

Abstract

Acoustic and electromagnetic wave scattering problems can be formulated as the Helmholtz equation with appropriate boundary conditions. The computational cost of standard schemes for these problems grows in direct proportion to the frequency of the incident wave. Recently *Chandler-Wilde and Langdon* have proposed a novel Galerkin boundary element method to solve the problem of acoustic scattering by a sound soft convex polygon, with computational cost that depends only logarithmically on the frequency. They achieved this by incorporating into the approximation space the products of plane wave basis functions with piecewise polynomials supported on a graded mesh, with smaller elemets adjacent to the corner of the polygon. In this paper we extend their scheme to problems of scattering by curvilinear polygons.

1 Introduction

Consider the two-dimensional problem of scattering of a time-harmonic acoustic incident plane wave

$$u^i(\mathbf{x}) = e^{ik\mathbf{x}.\mathbf{d}}, \quad \text{in} \quad D := R^2\backslash\overline{\Omega},$$

where $\mathbf{d} \in R^2$ is a unit vector representing the direction of the incident field. The scattered field $u^s := u - u^i$ (where u denotes the total field) satisfies

$$\Delta u^s + k^2 u^s = 0 \quad \text{in} \quad D, \quad u^s = -u^i \quad \text{on} \quad \Gamma,$$

and also the Sommerfeld radiation condition (see e.g. [3]), where Γ denotes the boundary of the obstacle Ω. Using Green's theorem and following the usual coupling procedure we obtain a second kind boundary integral equation for $\frac{\partial u}{\partial \mathbf{n}}$

$$\frac{1}{2}\frac{\partial u}{\partial \mathbf{n}}(\mathbf{x}) + \int_\Gamma \left(\frac{\partial \Phi(\mathbf{x},\mathbf{y})}{\partial \mathbf{n}(\mathbf{x})} + \mathrm{i}\eta\Phi(\mathbf{x},\mathbf{y}) \right) \frac{\partial u}{\partial \mathbf{n}}(\mathbf{y})\, \mathrm{d}s(\mathbf{y})$$

$$= f(\mathbf{x}), \quad \mathbf{x} \in \Gamma, \qquad (1)$$

where $\frac{\partial u}{\partial \mathbf{n}} \in L^2(\Gamma)$ is the unknown boundary data, $\Phi(\mathbf{x},\mathbf{y}) := \frac{i}{4}H_0^{(1)}(k|\mathbf{x}-\mathbf{y}|)$ is the fundamental solution of the Helmholtz equation in $2D$, $H_0^{(1)}$ is the Hankel function of first kind of order zero, $\mathbf{n}$ is the normal direction directed out of Ω, $f(\mathbf{x}) := \frac{\partial u^i(\mathbf{x})}{\partial \mathbf{n}} + i\eta u^i(\mathbf{x})$, and $\eta \in R\backslash\{0\}$ is the coupling parameter. The total field throughout D is determined by

$$u(\mathbf{x}) = u^i(\mathbf{x}) - \int_\Gamma \Phi(\mathbf{x},\mathbf{y}) \frac{\partial u}{\partial \mathbf{n}}(\mathbf{y}) ds(\mathbf{y}), \quad \mathbf{x} \in D.$$

In this paper we consider the numerical solution of (1) in the case that Γ is a curvilinear polygon. In §2 we introduce our numerical method, in §3 we present some numerical results and in §4 we present our conclusion.

2 Galerkin Boundary Element Method

We begin by parametrising (1) on the boundary of a curvilinear polygon such as that shown in Fig.1.

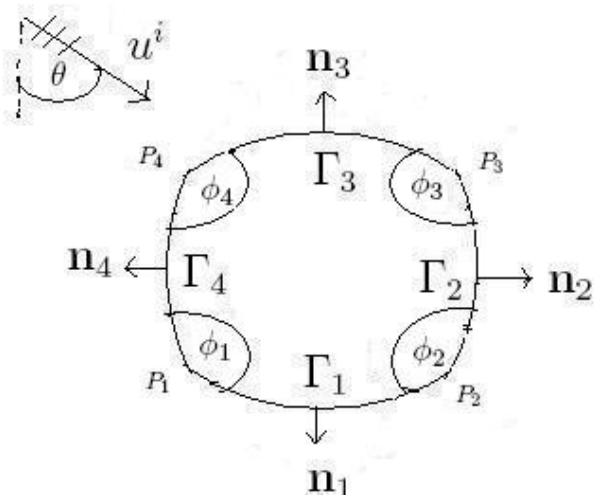

Figure 1: Scattering by a curvilinear polygon

We write the boundary as $\Gamma = \bigcup_{j=1}^{n_{sd}} \Gamma_j$, where Γ_j, $j = 1, ..., n_{sd}$ are the n_{sd} sides of the polygon, ordered so that Γ_j, $j = 1, ..., n_{sh}$, are in shadow, (so that $\mathbf{n}_j.\mathbf{d} > 0$ for $j = 1, ..., n_{sh}$), and Γ_j, $j = n_{sh}+1, ..., n_{sd}$ are illuminated, (so that $\mathbf{n}_j.\mathbf{d} < 0$ for $j = n_{sh}+1, ..., n_{sd}$), with j increasing anticlockwise as shown in Fig 1. Here $\mathbf{n}_j = (n_{j1}, n_{j2})$ is the normal derivative to the line Γ_j. For simplicity we assume here that $\mathbf{n}_j.\mathbf{d} \neq 0$ $\forall\ j = 1, ..., n_{sd}$. If this were not the case, special care would be needed in the "transition zone" around

the shadow boundary $\mathbf{n}_j.\mathbf{d} = 0$, (see e.g. [4]). We denote the vertices of the polygon by $P_j = (p_j, q_j)$, for $j = 1, ..., n_{sd}$. We set $P_{n+1} = P_1$, so that for $j = 1, ..., n_{sd}$, Γ_j is the line joining P_j with P_{j+1}.

If we denote $\gamma_j(s)$, for $j = 1, ..., n_{sd}$ as the arc length parameterisation of the curve Γ_j then $\mathbf{x} \in \Gamma$ can be represented by

$$\mathbf{x}(s) = P_j + \gamma_j\left(s - \sum_{m=1}^{j-1} L_m\right),$$

$$\text{for} \quad s \in (P_j, P_{j+1}) \quad j = 1, ..., n_{sd}, \tag{2}$$

where L_j is the length of Γ_j, $j = 1, ..., n_{sd}$. The interior angle given by $\phi_j \in (0, \pi)$, $j = 1, ..., n_{sd}$ is the angle between the tangents to Γ_{j-1} and Γ_j at P_j. The angle of the incident plane wave is given by θ, which is measured anticlockwise from the downward vertical as shown in Fig 1.

We rewrite (1) in parametrised form as

$$\phi(s) + \int_0^L K(s,t)\phi(t)dt = \tilde{F}(s), \tag{3}$$

$$\text{where} \quad \phi(s) := \frac{1}{k}\frac{\partial u}{\partial \mathbf{n}}(\mathbf{x}(s)), \quad L = \sum_{j=1}^{n_{sd}} L_j,$$

$$K(s,t) := 2\left(\frac{\partial \Phi(\mathbf{x}(s), \mathbf{x}(t))}{\partial \mathbf{n}(\mathbf{x}(s))} + \mathrm{i}\eta\Phi(\mathbf{x}(s), \mathbf{x}(t))\right)|\mathbf{x}'(t)|$$

and $\tilde{F}(s) := \frac{2}{k}f(\mathbf{x}(s))$. We begin by separating the leading order behavior, in the limit as $k \to \infty$. We define

$$\Psi(s) := \begin{cases} \frac{2}{k}\frac{\partial u^i}{\partial \mathbf{n}}(\mathbf{x}(s)), & \text{on illuminated sides,} \\ 0, & \text{on shadow sides,} \end{cases}$$

then $\varphi(s) := \phi(s) - \Psi(s)$ represents the difference between the exact solution of (3) and the solution in the high frequency limit. Substituting into (3) we get

$$\varphi(s) + \mathcal{K}\varphi(s) = F(s), \quad s \in [0, L]. \tag{4}$$

$$\text{where} \quad \mathcal{K}\psi(s) := 2\int_0^L K(s,t)\psi(t)dt,$$

$$F(s) := \frac{2}{k}f(s) - \Psi(s) - 2\int_0^L K(s,t)\Psi(t)dt.$$

We are going to solve (4) by a Galerkin boundary element method. We use the same mesh grading and approximation space as that used by *Chandler-Wilde and Langdon* in [1,2] for the case where Γ_j is a straight line. For $A > \lambda := 2\pi/k$ we define a composite graded mesh on $[0, A]$, with a polynomial grading on $[0, \lambda]$ and a geometric grading on $[\lambda, A]$. For $N = 2, 3, ...$, the mesh $\Lambda_{N,A,q_j} := \{y_0, ..., y_{N+N_A}\}$ consists of the points $y_i := \lambda(i/N)^{q_j}$, $i = 0, ..., N$, where $q_j := (2\nu + 3)/(1 - 2\alpha_j)$ (where $\alpha_j := 1 - \pi/(2\pi - \phi_j)$), together with the points $y_{N+j} := \lambda(A/\lambda)^{j/N_A}$, $j = 1, ..., N_A$,, where $N_A = \lceil N^* \rceil$, is the smallest integer greater than or equal to N^*, with $N^* = -\log|A/\lambda|/(q_j \log(1-1/N))$ chosen to ensure a smooth transition between the two parts of the mesh. We choose our approximate space $V_{\Gamma,\nu}$ to be the union over all sides of polygon of piecewise polynomials of order ν supported on the mesh Γ_j^+ multiplied by e^{iks}, with piecewise polynomials of order ν supported on the mesh Γ_j^- multiplied by e^{-iks}, where $\Gamma_j^+ := P_j + \Lambda_{N,A,q_j}$ and $\Gamma_j^- := P_{j+1} - \Lambda_{N,A,q_{j+1}}$. Then our Galerkin method approximation $\varphi_N \in V_{\Gamma,\nu}$ is defined by

$$(\varphi_N, \rho) + (\mathcal{K}\varphi_N, \rho) = (F, \rho), \quad \text{for all} \quad \rho \in V_{\Gamma,\nu}. \tag{5}$$

3 Numerical Results

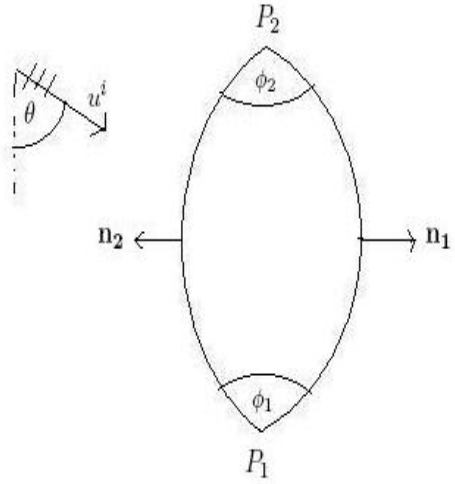

Figure 2: Scattering by a two sided curvilinear polygon

We solve (1) on a two sided curvilinear polygon, which is parametrised by

$$\begin{aligned} \mathbf{x}(s) &= a_j + r\cos(s/r - b_j) \\ \mathbf{y}(s) &= r\sin(s/r - b_j) \end{aligned} \tag{6}$$

for $(\mathbf{x}(s), \mathbf{y}(s)) \in \Gamma_j$, where

$$\begin{aligned} a_1 = -a, \quad b_1 = \cos^{-1}(a/r) \\ a_2 = a, \quad b_2 = 3\cos^{-1}(a/r) - \pi \end{aligned}$$

with $r = 3$ and $a = 1.5$, as shown in Figure 2. We take here the incident angle $\theta = \pi/2$, and $\nu = 0$ in (5). We fix $N = 4$ and increase k. The actual and relative L_2 errors are shown in Table 1. Here ϕ is computed using the same method with a larger number of degree of freedom. Here M_N denotes the total number of degrees of freedom. It is clear from the results that the relative errors remain roughly constant as k increases.

Table 1: Relative errors, Scattering by curvilinear polygon

k	M_N	$\|\phi - \phi_N\|$	$\|\phi - \phi_N\|_2 / \|\phi\|_2$
5	20	2.1058x10^{-1}	3.8363x10^{-1}
10	24	1.2401x10^{-1}	3.3347x10^{-1}
20	24	7.9625x10^{-2}	3.0512x10^{-1}
40	28	5.3473x10^{-2}	3.0133x10^{-1}

4 Conclusions

In this paper we have described a Galerkin scheme for solving a second kind boundary integral equation on the boundary of a curvilinear polygon. We have demonstrated the robustness of the numerical scheme as the wavenumber increases by numerical experiments. Ideas regarding the rigorous error analysis of this problem will appear in [5].

References

[1] S. Arden, S. N. Chandler-Wilde, and S. Langdon, "A Collocation method for high frequency scattering by convex polygons", J. Comp. Appl. Math., 204(2007) 334-343.

[2] S. N. Chandler-Wilde and S. Langdon, "A Galerkin boundary element method for high frequency scattering by convex polygons", SIAM J. Numer. Anal., 45(2007) 610-640.

[3] D. Colton and R. Kress, "Integral Equation Methods in Scattering Theory", Wiley, 1983.

[4] V. Dominguez, I. G. Graham, and V. P. Smyshlyaev, "A hybrid numerical-asymptotic boundary integral method for high-frequency acoustic scattering", Numer. Math., DOI:10.1007/s00211-007-0071-4(2007).

[5] M. Mokgolele, S. Langdon and S. N. Chandler-Wilde, "High Frequency Scattering By Convex Curvilinear Polygons", in preparation.

Numerical comparison of different fast multipole methods for solving the radiosity equation

J. Morice[†,*], **K. Mer-Nkonga** [‡,*] **and A. Bachelot** [†,*]
[†] Université Bordeaux I, MAB, Avenue des facultés 33405 Talence, France.
[‡] CEA-CESTA, BP 2, 33114 Le Barp, France.
[*]Email: jacques.morice@math.u-bordeaux1.fr, katherine.nkonga@cea.fr, Alain.Bachelot@math.u-bordeaux1.fr.

A fast method for solving the radiosity equation is considered by using the Fast Multipole Method (FMM), in the context of heat transfer calculations. This equation models radiative exchanges between gray diffuse surfaces without participating media [10]. The radiosity equation plays also an important role in obtaining realistic image in computer graphics [17]. This equation writes, for a polyhedral surface S of $\mathbb{R}^3$:

$$\begin{aligned} \forall x \in S, \;\; B(x) &= \epsilon(x)\sigma T^4(x) \\ &+ \rho(x) \int_S V(x,y)\, G(x,y) B(y) d\sigma_y, \end{aligned}$$

with B the radiosity, ϵ the emissivity, ρ the reflectivity, T the temperature and σ the Stefan-Boltzmann constant. The visibility $V(x,y)$ equals 1 if the two points x and y see each other ($[x,y] \cap S = \{x,y\}$) and cancels otherwise. The radiosity kernel G is given by:

$$G(x,y) = \frac{(x-y).n_x (y-x).n_y}{|x-y|^4}, \qquad (1)$$

where n_x is the inner unit normal to the surface S at point x.After discretization of the whole surface by finite elements, the size of the system generated can be quite large, and consequently the cost of solving this system is important in time (with an iterative method: $O(N^2)$ where N is the number of elements) and memory.

Three classes of fast methods to solve this problem have been developed. Firstly, classical hierarchical methods (HM) for sets of plane surfaces and their generalization to initial curved surfaces with clustering [17] in computer graphics, and secondly a $\mathcal{H}$-matrix approximation, constructing with ACA, of the system matrix in heat transfer [2] and thirdly methods based on an expansion of the integral kernel: panel clustering [1] and FMM [8] in computer graphics. In the first class, a hierarchical representation of interactions between initial plane surfaces (or shape factor matrix) is constructed by adaptively subdividing planar surfaces into sub-surfaces according to a local error of interaction between two surfaces. The cost of this method is linear with respect to the refined surfaces, but quadratic in the initial plane elements of discretization. An improvement of HM, clustering has a quasi-linear cost in the initial plane surfaces by grouping elements into volume clusters. In practice, HM and clustering encounter problems of iterative robustness and prediction of accuracy which are unacceptable in radiative heat transfer. In ACA, the low rank block of the original matrix is approximated by a combination of a few rows and a few columns of this block which is constructed algebraically. Moreover, there is no guarantee for a good approximation in some configurations. Panel clustering reduces the cost in grouping elements of discretization. This method applied to the radiosity equation [1] is based on the clustering of elements with the same unit normal. Hence, this panel clustering does not allow to accelerate radiosity equation for an initial curve surface.

To accelerate iterative solution of the radiosity equation, we propose then to use FMM as in [8] [11]. This method was introduced for N-body problems [13] and used in many other physical applications: electromagnetics problems [4], [14], [18], molecular dynamics [20] ... Based on an expansion of the kernel of the integral equation, this method reduces the interaction generated by the kernel between elements of the mesh to interactions between multipole boxes and so accelerates matrix-vector products of iterative methods. By using the multi-level FMM (MLFMM), we can evaluate solution system with a cost of $O(N \ln(N))$ for the unoccluded case ($V \equiv 1$).

A FMM expansion for a kernel K approximates interactions between two points x and y inside boxes B_{x_0} and B_{y_0} respectively of centers x_0 and y_0, by a separation of variables x and y: mainly

$$K(x,y) \simeq \sum_i L_i(x,x_0) \sum_{i'} T_{i,i'}(x_0,y_0) M_{i'}(y,y_0),$$

where $T_{i,i'}$ is the transfer or M2L operator,L_i and M_i are respectively the local and multipole functions. The radiosity kernel (1) depends on the surface, due to the normal. Thus, to construct a FMM independent of the surface for this equation, we need to investigate a FMM expansion for an auxiliary kernel that doesn't depend on the surface. We are interested in this work on a FMM expansion for $1/r^4$ as in [8] [11].

A FMM method based on a Taylor expansion for smooth kernels has been proposed in [19]. A limitation of

this method is the computing with accuracy of the derivatives of kernel (operators of transfer steps is defined with these derivatives).

A multipole expansion based on the expansion of $1/r^\gamma$ ($\gamma \in \mathbb{N}^*$) with the Gegenbauer polynomials was used to solve the Fokker-Planck-Landau's equation ($\gamma = 3$) [9]. In [7], this multipole expansion is expressed with Spherical Harmonics (SH) to solve the radiosity equation ($\gamma = 4$). With the multipole expansion in [7] and a formula in [16], Karapurkar *et al.* introduced a FMM expansion for the radiosity kernel with SH [8] (SH method). The Rotational Translation Coaxial Decomposition (RTCD) of [6], primary used for Laplace's equation ($\gamma = 1$), uses properties of SH to accelerate transfers between boxes. In [11], the RTCD was extended for $\gamma \in \mathbb{N}^*$ and it was used to improve the FMM proposed in [8] to solve the radiosity equation.

In [11], we have discussed a new fast method for general kernels inspired by the method of Gimbutas and Rokhlin [5]: Reduced SVD method (R-SVD). The resulting scheme is based on an approximation of the kernel by the truncation of a *reduced* Singular Value Decomposition of an expansion of tensor products of Legendre polynomials. The approximation of the kernel defined by an expansion of tensor products is equivalent to an interpolation of the kernel. This approximation is calculated with evaluations of kernel on interpolation points and hence is applicable to a wide variety of kernels. A proof of convergence of the approximation given by tensor products for an asymptotic smooth kernel is given in [3].

Previously in [11], we have introduced a comparison process for surface interaction problems or for particles interaction problems with particles on a surface, that takes into account the empty boxes in the octree, for different MLFMMs in the non adaptive case. This process was used to compare theoretically MLFMMs for the kernel $1/r^4$ [11] and for the radiosity kernel [12].

For the radiosity equation, a comparative study of these multilevel fast multipole methods (Taylor method, SH method, RTCD method and R-SVD method) will be presented, based on numerical experiments; the conclusions obtained will be compared to the one of the theoretical comparisons of [11] [12].

References

[1] K. Atkinson and D. Chien, "A fast matrix-vector multiplication method for solving the radiosity equation",*Adv. Comput. Math.*, vol. 12, pp. 51–74, 2000.

[2] M. Bebendorf and S. Rjasanow,"Matrix Compression for the Radiation Heat Transfer in Exhaust Pipes", *In Multifields Problems: stat of the art, A.-M. Sndig, W. Schielen, W. L. Wendland (eds.) Springer Verlag*, pp. 183–192, 2000.

[3] S. Borm and L. Grasedyck, "Low-Rank Approximation of Integral Operators by Interpolation", *Computing*, vol. 72, pp. 325–332, 2004.

[4] E. Darve, "The fast multipole method I: error analysis and asymptotic complexity", *SIAM Journal on Numerical Analysis*, vol. 38, pp. 98–128, 2000.

[5] Z. Gimbutas and V. Rokhlin,"A generalized fast multipole method for non-oscillatory kernels", *SIAM J. Sci. Comput.*, vol. 24, pp. 796–817, 2002.

[6] N. A. Gumerov and R. Duraiswami,"Comparison of the efficiency of translation operators used in the fast multipole method for the 3D Laplace equation", *UMIACS Techincal Report* 09, 2005.

[7] A. Hausner, "Multipole expansion of light", *IEEE Transactions on vizualisation and computer graphics*, vol. 3, pp. 12–22, 1997.

[8] A. Karapurkar, N. Goel and S. Chandran, "The Fast Multipole Method for Global Illumination", *In ICVGIP 2004*,pp. 119–125, 2004.

[9] M. Lemou, "Multipole expansion of the Fokker-Planck-Landau operator", *Numer. Math.*, vol. 78, pp. 597–618, 1997.

[10] M. F. Modest, Radiative heat transfer, second edition, Academic Press second edition, 2003.

[11] J. Morice, k. Mer-Nkonga and A. Bachelot, "Fast Multipole Method for solving the radiosity equation", *In ENUMATH 2005*, Santiago de compostella, Spain, pp. 609–617, 2005.

[12] J. Morice, k. Mer-Nkonga and A. Bachelot, "Comparison of different fast multipole methods for solving the radiosity equation", *In BETEQ 2006*, Paris, France (in press).

[13] V. Rokhlin, "Rapid solution of integral equations of classical potential theory", *J. Comput. Phys.*, vol. 60, pp. 187–207, 1985.

[14] V. Rokhlin, "Rapid solution of integral equations of scattering theory in two dimension", *J. Comput. Phys.*, vol. 86, pp. 414–439, 1990.

[15] Y. Saad, Iterative methods for sparse linear systems, PWS Publishing co, 1996.

[16] R.A. Sack, ”Three dimensional addition theorem for arbitrary functions involving expansions in spherical harmonics”, *J. Math. Phys.*, vol. 5, 252–259, 1964.

[17] F. Sillion, ”Clustering and volume scattering for hierarchical radiosity calculations”, *In Fifth Eurographics Workshop on rendering*, Darmstadt,Germany, pp 105–117, 2004.

[18] J. M. Song and C.-C. Lu and W. C. Chew”, ”Multilevel Fast Multipole Algorithm for Electromagnetic Scattering by Large Complex Objects”, *IEEE Trans. on Antennas and Propag.*, vol. 45, pp. 1488–1493, 1997.

[19] J. Tausch, ”The Variable Order Fast Multipole Method for Boundary Integral Equations of the Second Kind”, *Computing*, vol. 72, pp 267–291, 2004.

[20] C. A. White and M. Heat-Gordon, ”Rotation around the quartic momentum barrier in fast multipole method calculations”, *J. Chem. Phys.*, vol. 105, pp. 5061–5067, 1996.

SOLUTION OF HIGH FREQUENCY WAVE PROPAGATION PROBLEMS BY A FAST MULTIPLE-PATCH PHASE SPACE METHOD

M. Motamed[†,*], **O. Runborg**[†]
[†]School of Computer Science and Communication, Royal Institute of Technology (KTH), Stockholm, Sweden
[*]Email: mohamad@nada.kth.se

Abstract

We present a multiple-patch phase space method for computing trajectories on two-dimensional manifolds possibly embedded in a higher-dimensional space. The dynamics of trajectories are given by systems of ordinary differential equations (ODEs). We split the manifold into multiple patches where each patch has a well-defined regular parameterization. The ODEs are formulated as *escape* equations, which are hyperbolic partial differential equations (PDEs) in a three-dimensional phase space. The escape equations are solved in each patch, individually. The solutions of individual patches are then connected using suitable inter-patch boundary conditions. Properties for particular families of trajectories are obtained through a fast post-processing.

We apply the method to two different wave propagation problems: the creeping ray contribution to monostatic radar cross section computations and the multivalued travel-time of seismic waves in multi-layered media.

Introduction

We present a fast, multiple-patch phase space method for computing trajectories on two-dimensional compact manifolds possibly embedded in a higher-dimensional space. The dynamics of the trajectories we consider are given by systems of ODEs in a phase space. In many problems we need to compute a large number of trajectories, i.e., the dynamical systems of ODEs need to be integrated for many different initial conditions. Examples include seismic migration, tomography and geodesics computation in computational geometry and robotics.

Our motivation for this comes from high frequency wave propagation problems, where the problem of scattering of a time-harmonic incident field by a bounded scatterer is considered. The total field is split into an incident and a scattered field. The scattered field in the region outside the scatterer is given by the Helmholtz equation. The computational cost of direct numerical simulations grows algebraically with the frequency. Therefore, at high frequencies, numerical methods based on approximations of the Helmholtz equation are needed. A survey of this research effort is given in [1].

Recently, the authors extended the fast phase space method [2] to efficiently computing all possible creeping rays on a hypersurface, [3]. This method is based on escape equations which are time-independent PDEs in a three-dimensional phase space. The escape solutions, computed by a fast marching method, contains information for all incident angles. The phase and amplitude of the field are then extracted by a fast post-processing. It is computationally attractive when the solution is sought for many different sources but with the same index of refraction. However, it is only applicable for the scatterer surfaces with simple geometries. It assumes that the surface is represented by a single parameterization, and therefore surfaces with coordinate singularities cannot be treated, and the singularity has to be excised. This problem can be resolved by splitting the scatterer surface into several simpler surfaces (patches) with explicit parameterizations such that multiple patches collectively cover the scatterer surface in a non-singular manner.

In this paper, we consider a two-dimensional compact manifold M embedded in $\mathbb{R}^d$ and compute trajectories on the manifold. We first consider the case when the manifold is represented by a single regular parameterization and modify the fast phase space method [2], [3] to a more general class of problems. Second, we consider the case when the manifold is represented by an atlas of charts and modify the single-patch phase space method to this case. We present applications in computing creeping rays and seismic waves, together with sample numerical results from a prototype implementation of the scheme.

Multiple-Patch Phase Space Scheme

We consider a two-dimensional compact manifold M embedded in $\mathbb{R}^d$ and want to compute trajectories on M. Since we are interested in applications to wave propagation problems, it is natural to consider the trajectories as rays, and we will use this terminology henceforth. We consider two cases: when the manifold is represented by a single regular parameterization, and when the manifold is represented by an atlas of charts. In both cases, dynamics of rays are given by systems of three first-order ODEs, set in a phase space. These equations describe the rate of change of the rays' location and direction together with any other information transported along the ray trajecto-

ries.

We let M be represented by a single regular parameterization. First, the system of ODEs are formulated as time-independent Eulerian PDEs in phase space, known as escape equations. These equations are linear hyperbolic equations and are solved by a version of Fast Marching algorithm [2]. PDE solutions give the escape point, length and other information for rays with all possible starting points in the phase space. These solutions are then post-processed to extract properties for particular ray families.

For the more complicated and realistic case when the manifold M cannot be represented by one regular parameterization, we let M be described by an atlas of charts or multiple patches. The system of ODEs in each chart (patch) are formulated as escape PDEs and solved numerically on a fixed computational grid in phase space. The solutions to the PDEs in each chart are then connected using suitable inter-patch boundary conditions. Information for a particular family of rays are extracted through a fast post-processing.

Discretizing the phase space domain into N^3 grid points, the total complexity of the algorithm, including solving the escape PDEs and post-processing, is $\mathcal{O}(N^3 \log N)$. This is expensive for computing the field for only one source point. For example by using wave front tracking or solvers based on the surface eikonal equation, the complexity is $\mathcal{O}(N^2)$. However, if the solutions are sought for many source points, the phase space method can be more efficient. See next section for such an example.

Application to Wave Propagation Problems

We consider the application of the multiple-patch phase space method to compute two different types of wave propagation problems; creeping ray computations, where the computational domain is a two-dimensional scatterer surface embedded in $\mathbb{R}^3$, and seismic wave computations, where the domain is a two-dimensional multi-layered medium with different wave speeds in each layer.

First, we consider a balloon, as a scatterer surface. We split the surface into multiple patches (Figure 1a) and compute the contribution of *backscattered* creeping rays to mono-static RCS, i.e., the rays that propagate on the surface of the scatterer and return in the opposite direction of incident waves. We assume that the incoming amplitudes are one at attachment points on the shadow line and compute the backscattered amplitude at detachment points on the shadow line. The escape PDEs describing creeping rays are solved in each patch, individually. The creeping rays on the scatterer are then computed by connecting all individual solutions. The inter-patch boundaries are treated by the continuity of characteristics. Figure 1b shows the amplitude of backscattered rays in a polar coordinate system for all incident directions $\Psi \in [0, 360]$.

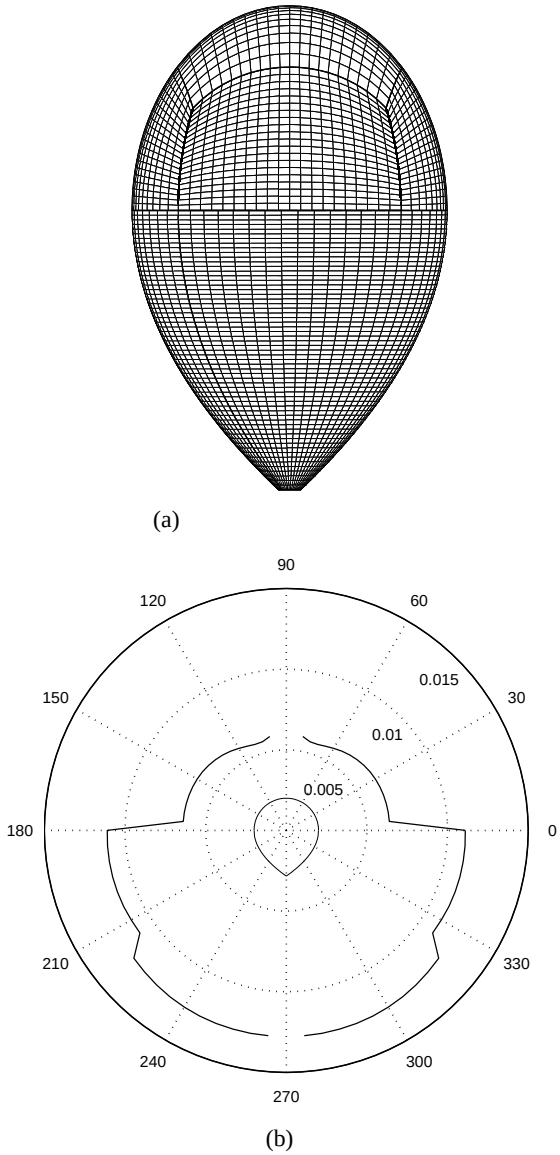

(a)

(b)

Figure 1: Figure (a) shows the balloon divided into 6 patches. Figure (b) shows total amplitude of the backscattered creeping rays (with frequency $\omega = 1$) for all illumination directions.

Next, we consider a multi-layered medium $M = [0, 6]^2$ consisting of three layers with different wave speeds (Figure 2b). The equiarrival curves, i.e., the locus of all points in physical domain which have the same travel-time, from

a source point at $\mathbf{x}_0 = (3, 6)$ are shown in Figure 2a. The inter-patch boundaries are treated by Snell's law and the law of reflection.

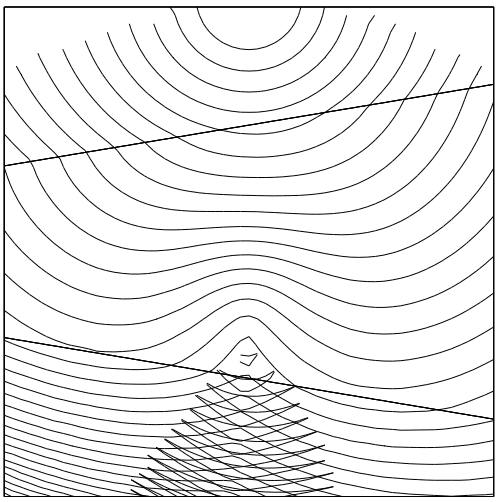

(a)

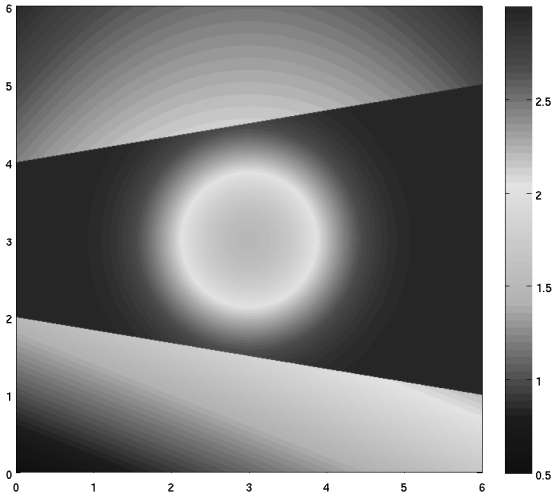

(b)

Figure 2: Figure (a) shows the equiarrival curves of seismic rays for a source point on the top of the domain. Figure (b) shows the medium consisting of three layers and the wave speed field.

We can track both reflected and transmitted ray families. Figure 3 shows the equiarrival curves of reflected rays from the bottom interfaces, being trapped in the middle layer.

Conclusion

We have modified the single-patch phase space method for computing creeping rays to a multiple-patch method for computing trajectories on two-dimensional manifolds possibly embedded in a higher-dimensional space. The dynamics of trajectories are given by systems of first-order ODEs in a phase space. We split the manifold into multiple patches where each patch has a well-defined regular parameterization. The escape equations, which are hyperbolic PDEs in a three-dimensional phase space, are derived and solved in each patch, individually, using a second-order version of the fast marching method. The solutions of individual patches are then connected using suitable inter-patch boundary conditions. Properties for particular families of trajectories are obtained through a fast post-processing. For some applications, the complexity of the method is attractive. Such applications include mono-static and bi-static RCS computations, antenna coupling problems, and travel-time computations of seismic waves when the solution is sought for many different sources.

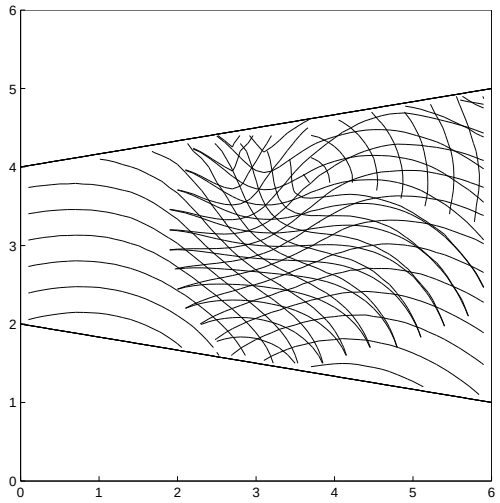

Figure 3: The equiarrival curves of reflected seismic rays from the bottom interfaces.

References

[1] B. Engquist and O. Runborg, "Computational High Frequency Wave Propagation", Acta Numerica, vol. 12, pp. 181-266, 2003.

[2] Fomel, S. and Sethian, J. A., "Fast phase space computation of multiple arrivals", Proceedings of the National Academy of Sciences of the United States of America, vol. 99, pp. 7329-7334, 2002.

[3] M. Motamed and O. Runborg, "A Fast Phase Space Method for Computing Creeping Rays", Journal of Computational Physics, vol. 219, pp. 276-295, 2006.

A WAVEFRONT GAUSSIAN BEAM METHOD FOR HIGH-FREQUENCY WAVE PROPAGATION

M. Motamed[†], **O. Runborg**[†,*]

[†]School of Computer Science and Communication, Royal Institute of Technology (KTH), Stockholm, Sweden
[*]Email: olofr@nada.kth.se

Abstract

We present a wavefront method based on Gaussian beams for computing high-frequency wave propagation problems. Unlike standard geometrical optics, Gaussian beams compute the correct solution of the field also at caustics. The method tracks a front of Gaussian beams with two particular initial values for width and curvature which allows the direct recreation of any other beam propagating from the initial front into the medium. This is used to approximate the field with different, optimally chosen, beams in different points on the front.

Introduction

The Gaussian beam method is an asymptotic method for computing high-frequency wave fields in smoothly varying inhomogeneous media. It was proposed by Popov [1], based on an earlier work of Babic and Pankratova [2]. The method was first applied by Katchalov and Popov [3] and Cerveny et al. [4] to describe high-frequency seismic wave fields by the summation of paraxial Gaussian beams. It was later applied to seismic migration by Hill [5], [6]. For a rigorous mathematical analysis of Gaussian beams we refer to [7]. The main advantage of this method is that Gaussian beams give the correct solution also at caustics where standard geometrical optics breaks down.

In the Gaussian beam method, the initial/boundary condition for the wave field is decomposed into initial conditions for Gaussian beams. Individual Gaussian beams are computed by ray tracing, where quantities such as the curvature and width of beams are calculated from ordinary differential equations (ODEs) along the central ray of the beams. The contributions of the beams concentrated close to their central rays are determined by Taylor expansion. The wave field at a receiver is then obtained as a weighted superposition of the Gaussian beams situated close to the receiver.

In this paper, we present a wavefront method for computing Gaussian beams. Wavefront methods have been been very successful for standard geometrical optics as they provide a simple mechanism for controlling the resolution and accuracy of the numerical approximation [8]. Using them with Gaussian beams is not as straightforward since the beam method strongly depends on the distribution and width of the beams at the initial front. We show how one can use two canonical beams in the wavefront method and from these afterwards recreate any other beam. This is used to approximate the field with different, optimally chosen, beams in different points on the front. We present a numerical example to verify the efficiency of the algorithm.

Gaussian Beam Equations

We consider a ray Ω in a two-dimensional Cartesian coordinate system x, y

$$\begin{aligned} \frac{dx}{d\tau} &= V\,\cos\theta \\ \frac{dy}{d\tau} &= V\,\sin\theta \\ \frac{d\theta}{d\tau} &= \frac{\partial V}{\partial x}\,\sin\theta - \frac{\partial V}{\partial y}\,\cos\theta \end{aligned} \tag{1}$$

where τ is the real-valued travel-time along the ray, variable $V = V(x, y)$ is the wave propagation velocity and θ is the angle between the tangent of the ray and the positive x-axis. We introduce the orthogonal ray-centered coordinates τ, q, where q is the axis perpendicular to the ray at point τ with the origin on the ray. In these coordinates, the paraxial Gaussian beam solution closely concentrated about the central ray Ω is given by

$$u(\tau, q, \omega) = A(\tau, q)\,\exp\{i\omega T(\tau, q)\}, \tag{2}$$

where ω is the angular frequency, and the complex-valued amplitude A and the phase T are given by Taylor expansions

$$A \approx A(\tau, 0) = \sqrt{V(x(\tau), y(\tau))/Q(\tau)}, \tag{3}$$

$$T \approx T(\tau, 0) + qT_q(\tau, 0) + \frac{q^2}{2}T_{qq}(\tau, 0) = \tau + \frac{q^2}{2}\,\frac{P(\tau)}{Q(\tau)}. \tag{4}$$

The complex-valued scalar functions P and Q satisfy the dynamic ray tracing system

$$\begin{aligned} \frac{dQ}{d\tau} &= V^2\,P \\ \frac{dP}{d\tau} &= -\frac{1}{V}\,(V_{xx}\,\sin^2\theta - \\ &\quad - 2V_{xy}\,\sin\theta\,\cos\theta + V_{yy}\,\cos^2\theta)\,Q \end{aligned} \tag{5}$$

Note that the Gaussian beam wavefield is evaluated only at a region along its central ray at which the ray-centered coordinate system is regular, that is, a region at which the normals to the ray do not intersect.

As initial data for (5), we choose

$$Q(0) = Q_0 > 0, \qquad P(0) = i. \tag{6}$$

One can show that this choice will guarantee that two important conditions are satisfied along the ray:

1. $Q(\tau) \neq 0$,
2. $Im(P(\tau)/Q(\tau)) > 0$.

The first condition guarantees the regularity of the Gaussian beam (with finite amplitudes at caustics). The second condition guarantees the concentration of the solution close to the ray.

Now assume that we want to compute the wave field in a two-dimensional domain generated by an incoming wave at $x = 0$. We first decompose the incoming wave into Gaussian beams and compute them. The wave field at a fixed receiver point R is then calculated by a weighted summation of paraxial Gaussian beams connected with rays Ω_m passing in the vicinity of R,

$$U(R) = \sum_m \Psi_m \, u_m(\tau_R, q_R, \omega), \tag{7}$$

where $u_m(\tau_R, q_R, \omega)$ is the wave field of the Gaussian beam (2) concentrated close to the ray Ω_m. The weight Ψ_m, the initial position, direction and Q_0 for each beam are chosen such that U at $\tau = 0$ approximates the incoming wave at $x = 0$.

Choice of Shape of Gaussian Beams

In order to have a good accuracy in the Taylor expansions (3)-(4), we should have beams which are as narrow as possible. We show here how to choose the initial data Q_0 to achieve this.

We specify two real-valued solutions of (5), (Q_1, P_1) and (Q_2, P_2), by the initial conditions

$$(Q_1, P_1)(0) = (1, 0), \quad (Q_2, P_2)(0) = (0, 1). \tag{8}$$

It is easy to show that the complex solutions of (5) with the initial data (6) can then be expressed as

$$Q = Q_0 \, Q_1 + i \, Q_2, \qquad P = Q_0 \, P_1 + i \, P_2. \tag{9}$$

The half-width of the Gaussian beam will then be

$$L(\tau) := \left(\frac{1}{2} \omega \, Im(P/Q) \right)^{-1/2} = \left(\frac{2(Q_0^2 \, Q_1^2 + Q_2^2)}{\omega \, Q_0} \right)^{1/2}. \tag{10}$$

We then choose the Q_0 which gives at a receiver a minimum value of the quantity $L(\tau)$,

$$Q_0^{opt}(\tau) = \left| \frac{Q_2(\tau)}{Q_1(\tau)} \right|. \tag{11}$$

Note that Q_0 is a function of τ, meaning that we have different optimal initial conditions at different points along the beam central ray.

Wavefront Method

In this section we will show how to construct the wavefront Gaussian beam method. We assume the exact phase space wave front is described by $(\mathbf{x}(\tau, r), \theta(\tau, r))$ at travel-time τ, where $\mathbf{x} = (x, y)$ and θ is the angle between the front's normal and the x-axis. The variable r represents the parameterization along the front induced by the parameterization of the source. Let $\mathbf{x}_j^n \approx \mathbf{x}(n\Delta\tau, j\Delta r)$ and $\theta_j^n \approx \theta(n\Delta\tau, j\Delta r)$, where (j, n) represents a marker (grid point) on a front at $\tau = n\Delta\tau$. We initialize the markers on the initial front at $\tau = 0$ as $(\mathbf{x}_j^0, \theta_j^0) = (\mathbf{x}(0, j\Delta r), \theta(0, j\Delta r))$. Each marker is then updated by a standard ODE-solver, applied to the ray tracing system (1). When the resolution of the wave front deteriorates, new markers are inserted and computed by interpolation from the old markers. We add a new marker between markers (j, n) and $(j + 1, n)$ if

$$|\mathbf{x}_{j+1}^n - \mathbf{x}_j^n| \geq \text{TOL} \qquad \text{or} \qquad |\theta_{j+1}^n - \theta_j^n| \geq \text{TOL},$$

for some tolerance TOL. In parallel with computing $(\mathbf{x}_j^n, \theta_j^n)$, we also compute the real-valued functions (Q_1, P_1) and (Q_2, P_2) by solving the dynamic ray tracing system (5) with the initial conditions (8). We note that via (9) we can recreate beams with *any* initial Q_0 value from these.

Now assume we want to compute the wave field at a marker (j, n) on the front at $\tau = n\Delta\tau$. We choose a region $\mathcal{R}$ on the front in both sides of the marker in which the Taylor expansion of travel-times of Gaussian beams are accurate enough. We discretize $\mathcal{R}$ into $2M + 1$ grid points. For each grid point we find the Gaussian beam passing through it. By interpolating $\mathbf{x}_j^n$ and θ_j^n we obtain the points and directions on the initial front of those beams. Similarly we can approximate the (Q_1, P_1) and (Q_2, P_2) values of the beams by interpolation. From these we pick the optimal initial Q_0 value of each beam according to (11). Next, we compute Ψ_m with $m = 1, \ldots, 2M + 1$ such that U in (7) at $\tau = 0$ locally approximates the wave field at the initial front. The complex-valued functions P, Q at each grid point in $\mathcal{R}$ are

then obtained by (9). The total wave field at the marker (j, n) is calculated by (7) with u_m given by (2)-(4). Finally, the wave field carried by all markers on wave fronts are interpolated down on a regular cartesian grid.

Remark 1. *Note that in wave front construction it is computationally more efficient to rewrite the Gaussian beam solution (2) and the summation (7) in the Cartesian coordinates and avoid computing q. See [9].*

Numerical Example

We consider a rectangular domain $\mathcal{D} = [0, 200] \times [0, 40]$ with a variable V. A point source at the origin generates a wave that is refracted as it propagates through the domain. Figure 1a shows the central rays of the Gaussian beams, and Figure 1b shows the corresponding wave fronts. The total wave field is shown in Figure 2 along the line $y = 0$ with $x \in [100, 135]$. The amplitude is bounded at the caustic ($x = 120$) but increases with higher frequency, as expected.

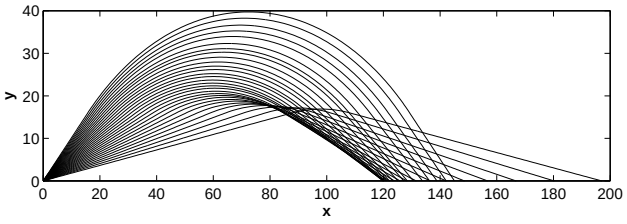

(a)

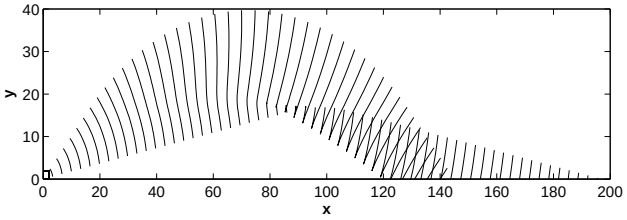

(b)

Figure 1: Figure (a) shows the central rays of Gaussian beams from a point source at the origin. Figure (b) shows the corresponding wave fronts.

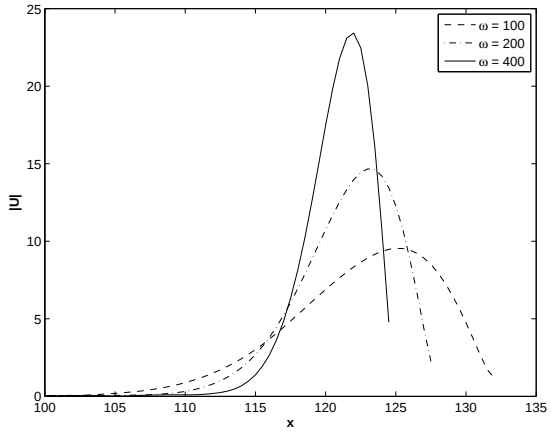

Figure 2: The absolute value of the wave field $|U|$ along a line at $y = 0$ with $x \in [100, 135]$ for different frequencies.

References

[1] M. M. Popov, "A New Method of Computation of Wave Fields Using Gaussian Beams", Wave Motion, vol. 4, pp. 85-97, 1982.

[2] V. M. Babic and T. F. Pankratova, "On Discontinuities of Green's Function of the Wave Equation with Variable Coefficient", Problemy Matem. Fiziki, vol. 6, Leningrad University, Saint-Petersburg, 1973.

[3] A. P. Katchalov and M. M. Popov, "Application of the Method of Summation of Gaussian Beams for Calculation of High-frequency Wave Fields", Sov. Phys. Dokl. , vol. 26, pp. 604-606, 1981.

[4] V. Cerveny, M. M. Popov and I. Psencik, "Computation of Wave Fields in Inhomogeneous Media - Gaussian Beam Approach", Geophys. J. R. Astr. Soc., vol. 70, pp. 109-128, 1982.

[5] N. R. Hill, "Gaussian Beam Migration", Geophysics, vol. 55, No. 11, pp. 1416-1428, 1990.

[6] N. R. Hill, "Prestack Gaussian-Beam Depth Migration", Geophysics, vol. 66, No. 4, pp. 1240-1250, 2001.

[7] J. Ralston, "Gaussian Beams and the Propagation of Singularities", In Studies in partial differential equations, vol. 23 of MAA Stud. Math., pp. 206-248, Math. Assoc. America, Washington, DC, 1982.

[8] B. Engquist and O. Runborg. Computational high frequency wave propagation. *Acta Numerica*, 12:181–266, 2003.

[9] L. Klimes, "Expansion of a High-frequency Time-harmonic Wavefield Given on an Initial Surface into Gaussian Beams", Geophys. J. R. astr. Soc., vol. 79, pp. 105-118, 1984.

High-frequency Multiple-Characteristic Wave Propagation

C. Nolan[†,*], **G. Uhlmann**[‡,*]
[†]Dept. of Maths & Statistics, University of Limerick, Castletroy, Ireland
[‡]Dept. of Math, University of Washington, Seattle, USA
[*]Email: Clifford.Nolan@ul.ie

Abstract

We present recent progress on representing high-frequency waves traveling anisotropic electromagnetic and elastic materials. The main issue addressed by this work is how to handle multiple characteristics, for which standard geometrical optics techniques fail. This failure manifests itself in a blowup of the polarisation vector. Naively, the resolution to this problem lies in the use of polar coordinates in phase space. There is also an interesting connection with the harmonic oscillator, through the use of a Hermite transformation that is used in our construction.

Introduction

The study of wave propagation in anisotropic media where the wave speeds depend on direction of propagation is very challenging. A better understanding of a geometrical optics representation of such waves would be of significant practical benefit, both to academics and practitioners alike.

The propagation of singularities and geometrical optics solutions for scalar partial differential operators of real principal type like the acoustic wave equation is well understood. By Egorov's theorem, one may conjugate the operator via an invertible Fourier integral operator to the operator D_{x_n}. The construction of the solution basically follows directly from this result ([4]).

However, most differential equations in mathematical physics have characteristics with variable multiplicity and do not fit the principal type model. In such instances, striking phenomena occur when the characteristic (wave) speeds co-incide. An example of such a phenomenon is that of conical refraction in a biaxial crystal [1], such as topaz. Melrose and Uhlmann [8] constructed a microlocal parametrix for the Cauchy problem for Maxwell's equations in a biaxial crystal with double involutive characteristics. Singularities along the double characteristics (optical axis) propagate along a cone; the cone of conical refraction (see [10]). The propagation of singularities for a class of symmetric systems with double characteristics satisfying a generic condition has been extensively studied in [5] and [6]. The propagation of singularities depends on the behavior of the bicharacteristic flow near the double characteristic variety.

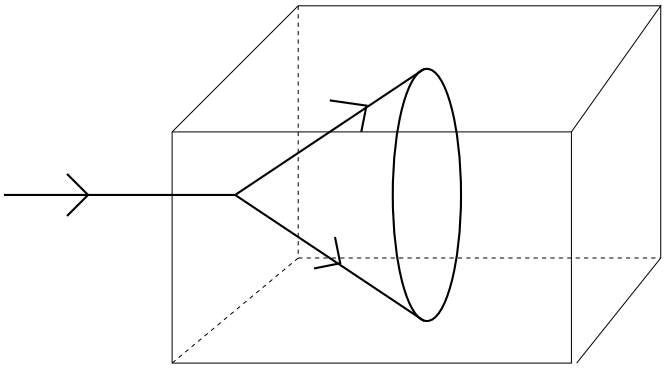

Figure 1: Splitting of a single ray impinging on a biaxial crystal into an internal ray conoid. This is the classic example of (internal) conical refraction, associated to multiple characteristic speeds crossing.

A step toward the construction of parametrices for generic symmetric systems was realized in [3]. Braam and Duistermaat consider a system of symmetric pde's, and microlocally conjugate it to normal form, when the system satisfies a generic condition

Our main goal here is to develop a high-frequency solution operator of the Cauchy problem associated to the Braam-Duistermaat normal form, and apply this to solve the Cauchy problem for a generic class of Maxwell's equations as well as a generic class of equations of elastodynamics.

1 Reduction to Normal Form

To start, we recall the main result of ([3], theorem 5), which states that under generic conditions, one may conjugate a symmetric system of partial differential equations to a first order block system:

$$\begin{bmatrix} D_t + D_{x_1} & x_1 D_{x_2} & 0 \\ x_1 D_{x_2} & \pm(D_t - D_{x_1}) & 0 \\ 0 & 0 & E_1^{\pm} \end{bmatrix} \tag{1}$$

where both signs can ocurr and $E_1^{\pm}$ is an elliptic operator. In this sense, it suffices to understand the solution for the upper 2×2-block sub-system. The conjugation is achieved by pre- and post- multiplication of the original

partial differential operator by Fourier integral operators of the appropriate order (this is why a first order system appears above).

Multiplying across the negative cofactor matrix of the upper 2×2 block of (1), yields the system

$$\left(\pm\partial_t^2 \mp \partial_{x_1}^2 - x_1^2 \partial_{x_2}^2 + R_2^{\pm} + P_1^{\pm} + R_0^{\pm} \right) \tag{2}$$

where

$$\begin{aligned} P_1^{\pm} &= A^{\pm}\partial_{x_2} + R_1^{\pm} \\ A^{\pm} &= \begin{bmatrix} 0 & \pm 1 \\ -1 & 0 \end{bmatrix} \end{aligned} \tag{3}$$

and $R_2^{\pm}, R_1^{\pm}$ are second order scalar and first order non-scalar operators respectively, whose symbols are flat and vanish respectively at the double characteristic set Σ_2, defined by

$$\Sigma_2 := \{(t, x, \tau, \xi) : \ \tau = \xi_1 = x_1 = 0\} \tag{4}$$

2 Conjugation to Principal-Type

From now on, we concentrate on the plus sign in the normal form. A key step in our construction is to now conjugate the latter operator by an Singular integral operator associated to the Hermite transformation

$$\begin{aligned} x_1 &= \sqrt{2k/\eta_2}\ \cos\theta \\ \xi_1 &= -\sqrt{2k\eta_2}\ \sin\theta \\ x_2 &= y_2 + (k/2\eta_2)\ \sin 2\theta \\ \xi' &= \eta' \\ x_i'' &= y_i'' \end{aligned} \tag{5}$$

Notice that this transformation pulls back the principal symbol of the normal form (2) to the operator on the circle times a reduced number of space-time variables:

$$P := \partial_t^2 - 2\partial_\theta \partial_{y_2} \tag{6}$$

This new operator is therefore of principal-type.

3 Solution Operator

Since we have now obtained an operator of principal-type, one might be tempted to think that the solution from here on in is simple, based on our opening remarks, but this is not true since we are dealing with a system. In fact the solution operator for the Cauchy problem

$$\begin{aligned} Pu &= 0 \\ u|_{t=0} = u_0, \ \ u_t|_{t=0} &= u_1 \end{aligned} \tag{7}$$

turns out to be a formed by a Fourier-series-integral pair. The solution operator for the case of $u_1 = 0$ for example is of the form

$$u = \sum_{\pm, k \geq 0} \int \begin{bmatrix} e^{i\phi_{\pm}^{(1)}(t,k,\eta')} & 0 \\ 0 & e^{i\phi_{\pm}^{(2)}(t,k,\eta')} \end{bmatrix} e^{i\left(\ (4k+1)(\theta - \tilde{\theta}) + (y' - \tilde{y}')\cdot\eta' \ \right)} e_{\pm}(t, y', k, \eta')\ u_0(\tilde{\theta}, \tilde{y}')\ d\tilde{\theta} d\tilde{y}' d\eta' \tag{8}$$

where $\phi_{\pm}^{(j)}$ are phase functions to be determined and $e_{\pm}$ is a 2×2 matrix of symbols also to be determined. Appropriate initial conditions on the matrices $e_{\pm}$ can be given to recover the initial conditions on u.

Remarks:

1. The $k = 0$ Fourier coefficient term does not propagate singularities within the double characteristic variety. The underlying reason for this is due to the fact that time-derivative coefficient in the transport operator $M_{\pm}$ contains a factor $\sqrt{k\eta_2}$ (for large k), whereas in [8], the coefficient contained a factor analogous to k which necessitated a conical refraction correction term that led to propagation of singularities within the double characteristic variety. The $k > 0$ terms propagate singularities along characteristics of the principal type operator (6).

2. Due to the brevity of this article we have hidden many details, and in particular the appearance of the operator P_1^+ in the standard form (2) creates a quite a complication in the construction of the solution.

3. Notice that we have only taken positive frequencies as the data is in the image of Hermite transformation and we have only taken every other odd frequency due to the fact that after rescaling θ, the data are odd under a shift by a quarter cycle.

4. We also need to examine the specific pde systems governing electromagnetism and linear elasticity. In solving the Cauchy problem associated to (1), we are implicitly assuming that the canonical transformation in [3] applied to bring the original partial differential operator to the normal form can be chosen so that it preserves the space-likeness of $\{(t, x) : \ t = 0\}$ and so we still have to check that this can be arranged in the case of electromagnetism and linear elasticity.

4 Propagation of singularities

To understand how singularities of solutions to $(2)_+$ propagate (c.f. [3]), we have seen that it is sufficient to understand propagation of singularities of the differential operator P. It is easy to compute the characteristics of this simple characteristic operator. If we then transform these characteristics back via the singular Hermite transformation, we find that singularities are propagated along curves of the form

$$\begin{aligned} t(s) &= -\tau^0 s \\ \tau(s) &= \tau^0 \\ x_1(s) &= \sqrt{\alpha/\beta}\sin(2\beta s) \\ x_2(s) &= 2\alpha s - (\alpha/2\beta)\sin(2\beta s) \\ x_i(s) &= x_i^0,\ 3 \le i \le n \\ \xi_1(s) &= \xi_1^0 \cos(2\beta s) \\ \xi_i(s) &= \xi_i^0,\ 2 \le i \le n \end{aligned} \tag{9}$$

where α is zero exactly at a double characteristic point, $\alpha \ll \beta$ and x_i^0, ξ_i^0 are constants. Also, τ^0 must be such that the above curve lies in Char(P).

We can obtain a qualitative picture of the propagation of singularities near the double characteristic points by examining (9) for $\alpha \ll \beta$. In the case of $(2)_+$, we observe a narrowly winding helix (with x_2 almost proportional to the parametrization of (9), and x_1, ξ_1 oscillating with small amplitude). The qualitative propagation of singularities described here agrees with the description in [3] and ([2], fig. 4).

5 Concluding Remarks

We have presented a compressed summary of how one can develop high-frequency solutions for wave equations in generic anisotropic materials. For more details we refer the reader to [9].

Acknowledgement: The first author acknowledges support from Science Foundation Ireland and the second author acknowleges support from a J. S. Gugenheim fellowship.

References

[1] M. Born and E. Wolf, "Principles of Optics", Pergamon Press, (1959).

[2] R. Burridge, "The singularity on the plane lids of the wave surface of elastic media with cubic symmetry", Quart. Journ. Mech. and Applied Math., 20(1), 41-56, (1967).

[3] P.J. Braam and J.J. Duistermaat, "Normal forms of real symmetric systems with multiplicity", Indag. Math. (N.S.) 4(4), 407–421 (1993).

[4] J. Duistermaat and L. Hörmander, "Fourier Integral Operators II", Acta Mathematica 128, 183–269 (1972).

[5] V. Ivrii, "On wave fronts of solutions of the system of crystal optics", Soviet Math. Dokl. 20, 139–141 (1977).

[6] V. Ivrii "Wave fronts of solutions of symmetric pseudodifferential systems", Siberian Math. J. 20, 557–578 (1979).

[7] R. Melrose, "The wave equation for a hypoelliptic operator with symplectic characteristics of codimension two", J. Analyse Math. 44, 134–182 (1985).

[8] R. Melrose and G. Uhlmann, "Microlocal structure of involutive conical refraction", Duke Math. J. 46, 571–582 (1979).

[9] C.J. Nolan and G. Uhlmann "Parametrices for symmetric systems with multiplicity", Wave Motion, 44(4), pp. 231–247 (2007).

[10] M. Taylor, "Pseudodifferential Operators", Princeton University Press, Princeton, New Jersey, (1981).

[11] G. Uhlmann, "Light intensity distribution in conical refraction", Comm. Pure and App. Math. 35, 69–80, (1982).

A diffusion-like equation for mode mixing in large diameter multimode optical fibres

E. Perrey-Debain[†,*], **I.D. Abrahams**[††]

[†]Laboratoire Roberval, Université de Technologie de Compiègne
60205 Compiègne BP 20529 France
[††]School of Mathematics, University of Manchester,
Oxford Road, Manchester, M13 9PL, UK
[*]Email: emmanuel.perrey-debain@utc.fr

Abstract

This paper investigates the evolution of the distribution of propagating modes in a graded-index multimode optical fibre with random imperfections. For large diameter fibres, the high number of propagating modes can be handled by moving to a continuum limit, which leads to differential equations of diffusion type.

Introduction

Large diameter multimode fibres are finding increasing application in short- and medium-distance networks for communications in buildings, aircraft, trains, cars, etc. Their attractiveness stems from their low cost, and from the ease by which they may be spliced together (because of their large core size) and excited using inexpensive sources, couplers, splitters and connectors. In practice, the small random variations of the optical and geometrical properties of fibres from the ideal model are impossible to avoid. These perturbations may be microscopic random bends, ellipticity of the cross-section, or index of refraction fluctuations, introduced during manufacture. Perturbations having a sufficiently high spatial frequency influence the signal propagation as a result of mode coupling; their cumulative effects may become important after a long propagation length so that they need to be taken into account when calculating the power attenuation, the signal distortion and the bandwidth of the fibre. This is particularly relevant to plastic optical fibres for which experimental and theoretical results indicate that the modes are highly coupled [1], [2]. Mode coupling mechanisms, radiation loss and intermodal dispersion are conveniently described by the coupled power theory [3] describing the evolution of the average optical power carried by the propagating modes. When the number of guided modes becomes too large, a direct algebraic treatment of the coupled system is ruled out because of the computational overhead. In this paper, we show that the coupling process can be ideally described in terms of a diffusion equation in which the mode number is treated as a continuous variable.

Evolution equations

We aim to study the propagation of electromagnetic waves with frequency ω, $[\mathbf{E},\mathbf{H}](\mathbf{r})\mathrm{e}^{-\mathrm{i}\omega t}$ in perturbed round optical fibres of internal core radius a with a refractive index of the form $n^2(\mathbf{r}) = n_0^2(1-2\Delta[(X/a)^2+(Y/a)^2])-\delta n^2(\mathbf{r})$ in the waveguide region $X^2+Y^2\leq a^2$ and $n^2(\mathbf{r})=n_c^2$ in the infinite cladding, $X^2+Y^2>a^2$. Here $\mathbf{r}=(X,Y,Z)$ is the position vector, Z is the guide axis and X,Y are the transverse coordinates. We call κ the vacuum wavenumber and we introduce the usual waveguide parameter $V=\kappa n_0 a\sqrt{2\Delta}$, which is large for multimode fibres. The profile height parameter Δ is assumed to be small and backscattering is ignored so that, under the appropriate scaling

$$\boldsymbol{x}=(x,y)=(X,Y)\frac{\sqrt{V}}{a} \quad \text{and} \quad z=Z\frac{\sqrt{2\Delta}}{a}, \tag{1}$$

the problem can be formulated as the following Schrodinger-type equation for the envelope of the transverse electric field Ψ as

$$\mathrm{i}\frac{\partial\Psi}{\partial z}=(\mathrm{H}+\delta\mathrm{H})\Psi, \tag{2}$$

where H is the z-independent Hamiltonian

$$\mathrm{H}\Psi=-\frac{1}{2}\left(\frac{\partial^2}{\partial x^2}+\frac{\partial^2}{\partial y^2}-v\right)\Psi. \tag{3}$$

The potential v stands for the quadratic well of finite depth $v(\boldsymbol{x})=|\boldsymbol{x}|^2$ where $|\boldsymbol{x}|\leq\sqrt{V}$ and $v(\boldsymbol{x})=V$ otherwise. We introduce the small parameter ϵ which characterizes the relative amplitude of the perturbation δn^2 and we define the normalized perturbation shape function $\bar{h}$ as $\delta n^2=\epsilon(n_0^2-n_c^2)\bar{h}$ so that $|\bar{h}|\sim 1$. The z-dependent perturbed Hamiltonian can then be shown to be $\delta\mathrm{H}(\boldsymbol{x},z)=\frac{1}{2}\epsilon V\bar{h}(\boldsymbol{x},z)$. Following the standard perturbation theory [3], [4], [5], Ψ is expanded in the eigenmode basis of the unperturbed operator H as

$$\Psi(\boldsymbol{x},z) = \sum_{\mathbf{n}} a_{\mathbf{n}}(z)\Psi_{\mathbf{n}}(\boldsymbol{x})\mathrm{e}^{-\mathrm{i}\beta_{\mathbf{n}}z} \tag{4}$$

$$+ \sum_{l}\int a_l(\beta,z)\Psi_l(\beta,\boldsymbol{x})\mathrm{e}^{-\mathrm{i}\beta z}\mathrm{d}\beta. \tag{5}$$

The first summation extends over all the discrete spectrum of the guided modes satisfying the eigenvalue problem

$$\mathrm{H}\Psi_{\mathbf{n}} = \beta_{\mathbf{n}}\Psi_{\mathbf{n}}. \tag{6}$$

Guided modes propagate without attenuation and their propagation constants lie in the range $0 < \beta_{\mathbf{n}} < \beta_c$ where $\beta_c = V/2$ is the cut-off wavenumber. The integral in (5) extends over the continuum spectrum of H corresponding to the radiation modes and the discrete summation extends over their azimuthal dependence (index l). Now, if the guided modes are weakly coupled over a distance which is large compared to the correlation length of the random process δH then the ensemble average power $A_{\mathbf{n}}(z) = \langle |a_{\mathbf{n}}(z)|^2 \rangle$ can be shown to satisfy the master equation system [3], [6]:

$$\frac{1}{\epsilon^2}\frac{\mathrm{d}A_{\mathbf{n}}}{\mathrm{d}z} = \sum_{\mathbf{m}} \mathrm{W}_{\mathbf{n}\to\mathbf{m}}(A_{\mathbf{m}} - A_{\mathbf{n}}) - \alpha_{\mathbf{n}}A_{\mathbf{n}}, \tag{7}$$

where the transition probability matrix coefficients $\mathrm{W}_{\mathbf{n}\to\mathbf{m}}$ are given from the spectral density of the coupling coefficients

$$C_{\mathbf{n},\mathbf{m}}(z) = \int_{\mathbb{R}^2} \Psi_{\mathbf{n}}(\boldsymbol{x})\bar{h}(\boldsymbol{x},z)\Psi_{\mathbf{m}}(\boldsymbol{x})\mathrm{d}\boldsymbol{x} \tag{8}$$

evaluated at the wavenumber spacing $(\beta_{\mathbf{m}} - \beta_{\mathbf{n}})$, i.e.,

$$\mathrm{W}_{\mathbf{n}\to\mathbf{m}} = \beta_c^2\langle |\mathcal{F}[C_{\mathbf{n},\mathbf{m}}](\beta_{\mathbf{m}} - \beta_{\mathbf{n}})|^2\rangle \tag{9}$$

where the operator $\mathcal{F}$ stands for the usual Fourier transform. Therefore, the condition for appreciable coupling between the two modes is that the perturbation $\bar{h}$ must both induce a substantial overlap integral in $C_{\mathbf{n},\mathbf{m}}$ and have spatial frequency support at $\beta_{\mathbf{m}} - \beta_{\mathbf{n}}$. The positive quantities $\alpha_{\mathbf{n}}$ take into account the averaged coupling between mode $\mathbf{n}$ and the modes of the continuum of the radiation modes.

The continuous model

In the limit of large V, the set of orthonormal functions $\Psi_{\mathbf{n}}(\boldsymbol{x}) = \psi_\nu(x)\psi_\mu(y)$ (we identify the mode index $\mathbf{n}$ (in bold) with the multi-index (ν,μ)) where

$$\psi_\nu(x) = \frac{1}{\sqrt{\pi^{1/2}2^\nu\nu!}}H_\nu(x)e^{-x^2/2} \tag{10}$$

and H_ν denote the usual Hermite polynomials, are good approximations to the exact solutions of (6) except for modes near cut-off, $\beta_{\mathbf{n}} \approx V/2$ (the eigenvalues are given by $\beta_{\mathbf{n}} = \nu + \mu + 1$). These latter high order modes carry non-negligible power in the vicinity of the core-cladding interface and therefore suffer from very high radiation loss, so we can ignore them by imposing the cut-off condition $A_{\mathbf{n}} = 0$ for $\nu + \mu \geq \beta_c$. Now, we assume that the normalized perturbation $\bar{h}$ is sufficiently regular so that it can be fairly approximated by its truncated Taylor expansion as

$$\bar{h}(\boldsymbol{x},z) = \left(\bar{h} + x\frac{\partial\bar{h}}{\partial x} + y\frac{\partial\bar{h}}{\partial y} + \dots\right)(0,0,z). \tag{11}$$

Here, derivatives of $\bar{h}$ are random functions of the waveguide axis z and participate in the mode mixing dynamics. Using both the polynomial expansion (11) and the analytical form of the guided modes (10), it can be shown [7] that there exists a polynomial series $w_{\mathbf{s}}(\tilde{\nu},\tilde{\mu})$ where $\mathbf{s} \in \mathbb{Z}^2$ and $(\tilde{\nu},\tilde{\mu}) \in \mathbb{R}^2$ (the *continuous* counterpart of $\mathbf{n} = (\nu,\mu)$) such that the transition probability matrix from mode $\mathbf{n}$ to mode $\mathbf{n}+\mathbf{s}$ has the analytical form

$$\mathrm{W}_{\mathbf{n}\to\mathbf{n}+\mathbf{s}} = \beta_c^2\, 2w_{\mathbf{s}}(\mathbf{n} + \mathbf{s}/2). \tag{12}$$

This form is perfectly suited for a continuous approach (see [8] for the 1D case). Let us introduce a continuous function $\tilde{A}(\tilde{\nu},\tilde{\mu},z)$ such that $\tilde{A}(\mathbf{n},z) = A_{\mathbf{n}}(z)$ for all guided modes. By direct application of Taylor's theorem, the transition probability operator may be written formally as

$$\begin{aligned}\sum_{\mathbf{m}} \mathrm{W}_{\mathbf{n}\to\mathbf{m}}(A_{\mathbf{m}} - A_{\mathbf{n}}) &= \beta_c^2 \sum_{\mathbf{s}\in\mathbb{Z}^2} \frac{\partial}{\partial\mathbf{s}}\left(w_{\mathbf{s}}\frac{\partial\tilde{A}}{\partial\mathbf{s}}\right)(\mathbf{n}) \\ &+ \beta_c^2\mathcal{T}(\tilde{A})(\mathbf{n}),\end{aligned} \tag{13}$$

where $\frac{\partial}{\partial\mathbf{s}} \equiv \mathbf{s}\cdot\left(\frac{\partial}{\partial\tilde{\nu}},\frac{\partial}{\partial\tilde{\mu}}\right)$ stands for the directional derivative and the term $\mathcal{T}(\tilde{A})$ contains the Taylor series remainder. Let us now employ the small parameter $\varepsilon = 1/V$. As the number of guided modes goes tends to infinity, i.e. $\varepsilon \to 0$, it can be shown that the function $w_{\mathbf{s}}$ admits the asymptotic limit: $w_{\mathbf{s}}(\tilde{\mathbf{n}}) = W^0_{\mathbf{s}}(u,v) + \mathcal{O}(\varepsilon)$, where (u,v) are the normalized continuous variables $(u,v) = 2\varepsilon(\tilde{\nu},\tilde{\mu}) = \beta_c^{-1}\tilde{\mathbf{n}}$. Similarly, we may assume that there exits a regular function γ such that $\gamma(\mathbf{n}) = \alpha_{\mathbf{n}}$ for all modes below cut-off and admitting the regular expansion: $\gamma(\tilde{\mathbf{n}}) = \gamma_0(u,v) + \mathcal{O}(\varepsilon)$. Thus, at leading order, the discrete evolutionary coupled system (7) can be modelled as the following diffusion-like equation

$$\frac{1}{\epsilon^2}\frac{\partial\tilde{A}}{\partial z} = \mathcal{D}\tilde{A} = (\nabla\cdot\mathsf{D}\nabla - \gamma)\tilde{A}, \tag{14}$$

where $\nabla \equiv (\partial/\partial u, \partial/\partial v)^T$ and D is the symmetric matrix

$$\mathsf{D} = \sum_{\mathbf{s}=(\zeta,\eta)\in\mathbb{Z}^2} \begin{pmatrix} \zeta^2 & \zeta\eta \\ \zeta\eta & \eta^2 \end{pmatrix} W^0_{\mathbf{s}}(u,v), \tag{15}$$

V	ε	λ_1 (dis.)	λ_2 (dis.)
20	0.05	-3.34	-9.34
40	0.025	-3.49	-9.71
80	0.0125	-3.58	-9.93
120	0.0083	-3.61	-10.0
∞	0	-3.67 (cont.)	-10.1 (cont.)

Table 1: Evolution of the first two eigenvalues of the discrete system (7) as V increases. The last line corresponds to the continuous diffusion operator (17).

which can be interpreted as a diffusion tensor controlling the average transfer of modal power at the 'mode number' $\tilde{\mathbf{n}} = \beta_c(u, v)$.

Applications

Let us consider typical deformations observed in optical fibres as illustrated in Figure 1 (bar symbol denotes the normalized coordinates $\bar{x} = X/a$ and $\bar{y} = Y/a$). We suppose that the microbending and ellipticity perturbations $\delta x, \delta y, \delta a$ and δb are independent random processes with respect to the normalized waveguide axis z. The associated diffusion tensor then has the diagonal form

$$\mathsf{D} = \begin{pmatrix} C_{\delta x}u + C_{\delta a}u^2 & 0 \\ 0 & C_{\delta y}v + C_{\delta b}v^2 \end{pmatrix}, \qquad (16)$$

where constants $C_{\delta x}, C_{\delta y}, C_{\delta a}$ and $C_{\delta b}$ respectively contain the spectral density of the processes $\delta x, \delta y, \delta a$ and δb. The solution of (14) can be conveniently obtained via projection on the eigenmode basis U_i verifying

$$\mathcal{D}U_i = \tilde{\lambda}_i U_i. \qquad (17)$$

There is no analytical solution to this eigenvalue problem in the general case. To simplify the analysis, we consider the microbending problem where the horizontal and vertical deviations are statistically identical, i.e. we take $C_{\delta x} = C_{\delta y}$ in (16) and we ignore the ellipticity: $C_{\delta a} = C_{\delta b} = 0$. In the lossless scenario ($\gamma = 0$), it can be shown that (17) is separable and admits analytical solutions. In Table 1, we compare the first two eigenvalues of the discrete system (7) with its continuous counterpart (17) (we take $C_{\delta x} = 1$ and eigenmodes are conveniently normalized to yield comparable results) demonstrating that the theoretically predicted behaviour is achieved.

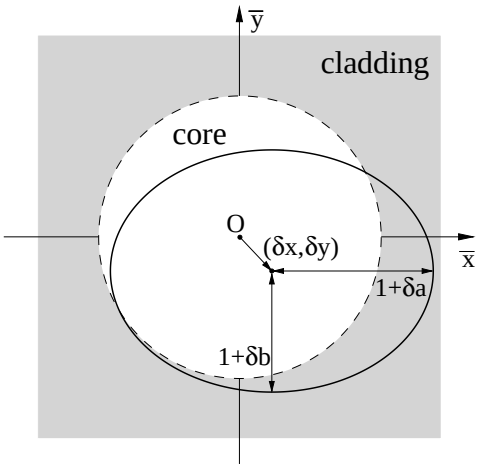

Figure 1: Typical deformations observed in optical fibres: Eccentricity (micro-bending) and ellipticity. Dashed line: unperturbed fibre. Solid line: fibre under deformation.

References

[1] A.F. Garito, J. Wang, R. Gao, "Effects of random perturbations in plastic optical fibers", Science, vol. 281, pp. 962-967, 1998.

[2] S.E. Golowich, W. White, W.A. Reed, E. Knudsen, "Quantitative estimates of mode coupling and differential modal attenuation in perfluorinated graded-index plastic optical fiber", J. Ligh. Tech., vol. 21, pp. 111-121, 2003.

[3] D. Marcuse, Theory of Dielectric Optical Waveguides, Academic Press, New York, 1991.

[4] A.W. Snyder, J.D. Love, Optical Waveguide Theory, London: Chapman and Hall, 1983.

[5] L.D. Landau, E.M. Lifshitz, Quantum Mechanics (Non-relativistic Theory), third ed., Oxford: Pergamon Press Ltd, 1977.

[6] J. Garnier, "Energy distribution of the quantum harmonic oscillator under random time-dependent perturbation", Phys. Rev. E, vol. 60, pp. 3676-3687, 1999.

[7] E. Perrey-Debain, I.D. Abrahams, "A band factorization technique for transition matrix element asymptotics", Comp. Phys. Comm., vol. 175, pp. 315-322, 2006.

[8] E. Perrey-Debain, I.D. Abrahams, "A diffusion analysis approach for multimode random optical waveguides", Proc. 7th Inter. Conf. Mathematical and Numerical Aspects of Wave Propagation, Brown University, U.S., pp. 267-269, 2005.

ON THE MATRIX CONDITION NUMBER OF FINITE ELEMENT APPROXIMATIONS TO THE FREQUENCY DOMAIN MAXWELL'S EQUATIONS

Christoph Schwarzbach[†,*], **Klaus Spitzer**[†]
[†]Institute of Geophysics, TU Bergakademie Freiberg, Freiberg, Germany
[*]Email: schwarzb@geophysik.tu-freiberg.de

Abstract

Finite element (FE) approximations to the solution of Maxwell's equations can be based upon different formulations as boundary value problems. We investigate two different approaches in frequency domain: the classical curl-curl formulation and a mixed formulation which explicitly takes into account the equation of continuity for conducting media. The frequency dependent condition number of the FE system matrix is computed for a homogeneous medium model problem. It reveals that the mixed approach introduces stability for low frequencies. Additionally, largely unequal weights given to the two partial differential equations of the mixed formulation significantly affect the matrix condition number.

The study is extended to an anisotropic Perfectly Matched Layer (PML). The resulting coefficients of the partial differential equation (PDE) as a function of frequency can be bounded by introducing a complex frequency shift. However, anisotropy grows with decreasing frequency in the relevant frequency range and, thus, deteriorates the matrix condition number.

Introduction

Electromagnetic methods in geophysics cover a broad frequency spectrum. Even at the highest frequencies used, the damping of electromagnetic waves cannot be neglected because of the inherent electrical conductivity present within the earth. Therefore, it is interesting to study the damped wave equation over a frequency range of several orders of magnitude.

Numerical simulations are a key tool to understanding the physics of geophysical measurements, interpreting their data and improving acquisition techniques. Restricting ourselves to time harmonic fields and Fourier synthesizing if required we end up with a system of linear equations which is obtained by the Finite Element Method (FEM) from frequency domain Maxwell's equations [1]. This paper presents a numerical experiment with different formulations of boundary value problems that lead to stable or unstable behaviour of the frequency dependent FE system matrix condition number.

A model problem

Consider the unit cube $\Omega = [0,1]^3\,\mathrm{m}^3$ with homogeneous constitutive parameters magnetic permeability $\mu = \mu_0$, electric permittivity $\varepsilon = 8\varepsilon_0$ and electric conductivity $\sigma = 0.01\,\mathrm{S/m}$. μ_0 and ε_0 denote the free space quantities which are related to the vacuum speed of light $c = 1/\sqrt{\mu_0\varepsilon_0} \approx 3 \cdot 10^8\,\mathrm{m/s}$. We will examine the solution of the frequency domain Maxwell's equations for frequencies $f = 10^5 \ldots 10^8\,\mathrm{Hz}$.

The domain Ω is discretized by a regular mesh consisting of 5^3 hexahedrons of size $h = 0.2\,\mathrm{m}$. Maxwell's equations are numerically solved using FEMSTER [2] with a family of quadratic FE base functions ($p = 2$). Therefore, a sufficient sampling of wavelengths of at least ten samples is provided. The algorithm of Higham and Tisseur [3] is combined with a direct solver from PARDISO [4], [5] to estimate the 1-norm FE system matrix condition number κ_1.

Boundary value problems

Standard curl-curl equation approach

A standard approach of solving Maxwell's equations in frequency domain is combining them to form a second order PDE that reads in terms of the electric field vector $\boldsymbol{E}$ as

$$\operatorname{curl}(\mu^{-1} \operatorname{curl} \boldsymbol{E}) - i\omega(\sigma - i\omega\varepsilon)\boldsymbol{E} = i\omega\boldsymbol{j_s}. \qquad (1)$$

Here, i denotes the imaginary unit, $\omega = 2\pi f$ the angular frequency and $\boldsymbol{j_s}$ an applied source current density. If $\boldsymbol{E}$ is a sufficiently smooth solution of eq. (1) and $\omega \neq 0$, the divergence of eq. (1) can be taken, revealing that $\boldsymbol{E}$ also fulfils the equation of continuity

$$-\operatorname{div}(\sigma - i\omega\varepsilon)\boldsymbol{E} = \operatorname{div}\boldsymbol{j_s}. \qquad (2)$$

To complete the PDE (1) posed on Ω, homogeneous Dirichlet or Neumann boundary conditions are applied on the boundary $\Gamma = \partial\Omega$,

$$\boldsymbol{n} \times \boldsymbol{E} = 0 \qquad (3)$$

$$\text{or} \quad \boldsymbol{n} \times (\mu^{-1} \operatorname{curl} \boldsymbol{E}) = 0, \qquad (4)$$

where $\boldsymbol{n}$ is the outward normal vector on Γ.

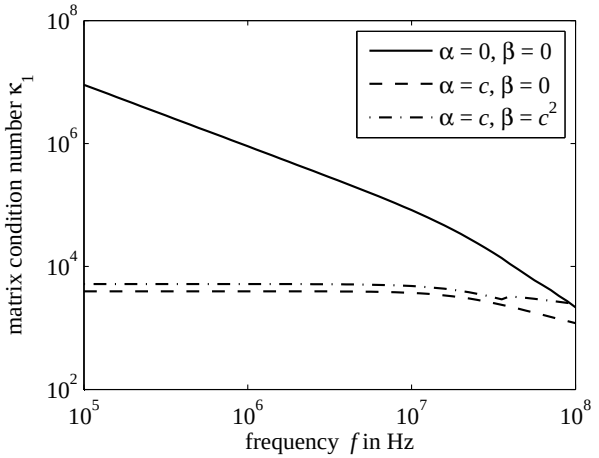

Figure 1: Frequency dependence of the 1-norm FE system matrix condition number for the Dirichlet boundary condition problems.

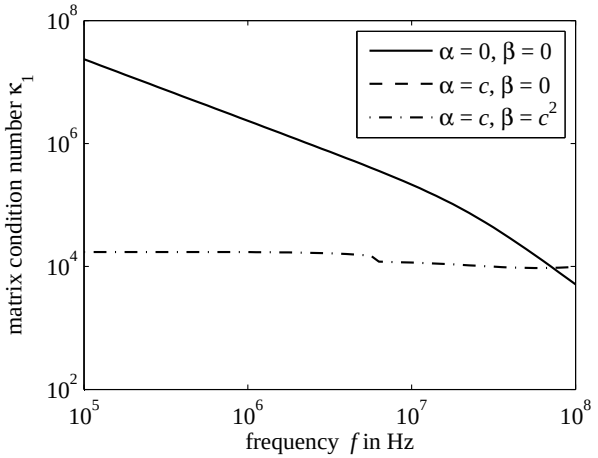

Figure 2: Frequency dependence of the 1-norm FE system matrix condition number for the Neumann boundary condition problems. Note that the matrix is singular for $\alpha = c$, $\beta = 0$.

The condition number κ_1 of the resulting FE system matrix is depicted by the continuous line '$\alpha = 0$, $\beta = 0$' (cp. eqs (5) and (6)) in Figs 1 and 2. The kernel of the curl operator causes κ_1 to increase exponentially with decreasing frequency. For small ω, the curl-curl term dominates the zeroth order term and the solution can be spoiled by gradients of a scalar function. This behaviour can be avoided using a mixed formulation.

Mixed approach

The equation of continuity (2) is explicitly taken into account by extending the system of equations (1) and (2) by a scalar variable V,

$$\begin{aligned} \operatorname{curl}(\mu^{-1} \operatorname{curl} \boldsymbol{E}) - i\omega(\sigma - i\omega\varepsilon)\boldsymbol{E} \\ + \alpha(\sigma - i\omega\varepsilon) \operatorname{grad} V = i\omega \boldsymbol{j_s} \qquad (5) \\ -\alpha \operatorname{div}(\sigma - i\omega\varepsilon)\boldsymbol{E} + \beta V = \alpha \operatorname{div} \boldsymbol{j_s}, \qquad (6) \end{aligned}$$

where α is a scalar constant and β a scalar function. These assumptions ensure that the resulting discrete system has a symmetric coefficient matrix. The appropriate boundary conditions read

$$\begin{aligned} \boldsymbol{n} \times \boldsymbol{E} = 0, \qquad V = 0 \qquad (7) \\ \text{or} \quad \boldsymbol{n} \times (\mu^{-1} \operatorname{curl} \boldsymbol{E}) = 0, \qquad \boldsymbol{n} \cdot \operatorname{grad} V = 0. \qquad (8) \end{aligned}$$

Taking the divergence of eq. (5) we learn that V implicitly fulfils

$$-\alpha^2 \operatorname{div}(\sigma - i\omega\varepsilon) \operatorname{grad} V + i\omega\beta V = 0. \qquad (9)$$

The choice $\beta \neq 0$ leads to a denser FE system matrix than $\beta \equiv 0$. In the case of the Neumann boundary condition (8), however, the zeroth order term $i\omega\beta V$ is crucial: If $\beta \equiv 0$, the solution of eq. (9) in terms of V is non-unique and $\kappa_1 = \infty$. For all other cases, a constant κ_1 is achieved for low frequencies using the mixed formulation (Figs 1 and 2).

The particular value of α is important. It can be interpreted as giving appropriate weights to both differential equations and the two unknowns $\boldsymbol{E}$ and V. Fig. 3 illustrates that the matrix condition number, as a function of α, has a pronounced minimum and is exponentially increasing away from the minimum. Note that, for the choice of PDEs (5) and (6), α is in the order of the vacuum speed of light c.

Extension to Perfectly Matched Layers

Most geophysical simulation problems are naturally posed on unbounded domains. Numerical methods like the FEM usually require the restriction to a bounded domain. The unavailability of appropriate boundary conditions for the auxiliary boundary introduced to obtain a finite simulation volume makes attractive the technique of Perfectly Matched Layers (PML) [6]. Therefore, we extend our model study by a Complex Frequency Shifted (CFS), anisotropic PML [7] which replaces all scalar constitutive parameters $\eta = \mu, \varepsilon, \sigma$ by tensors $\eta \operatorname{diag}(1/d, d, d)$, where

$$d = 1 + i \frac{bx^n}{\omega + i\omega_0} \qquad (10)$$

can be considered as a complex valued stretching of the first spatial coordinate x. y and z remain unaffected. In particular we choose $n = 1$, $b = 3.45 \cdot 10^8\,\mathrm{Hz/m}$,

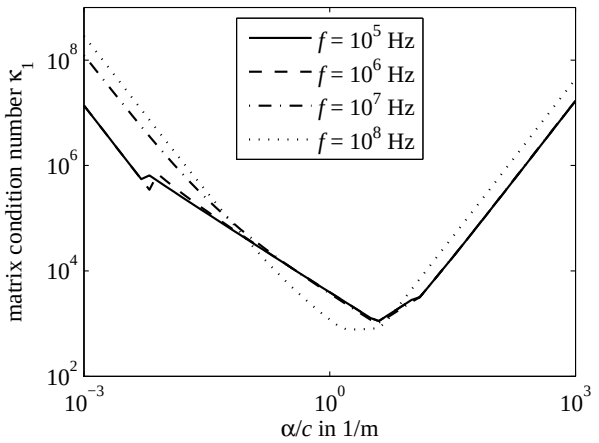

Figure 3: Dependence of the 1-norm FE system matrix condition number κ_1 on the weight constant α for the Dirichlet boundary condition and $\beta = 0$.

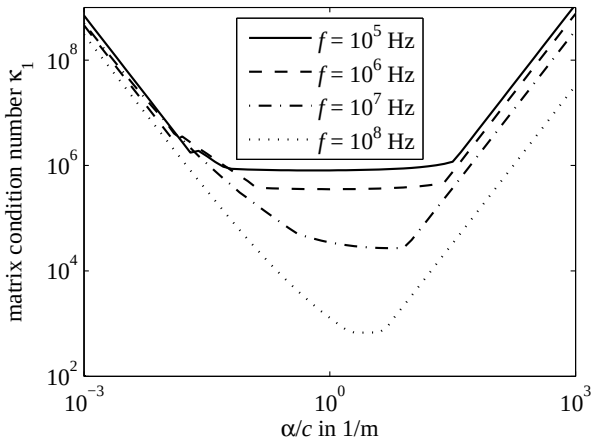

Figure 4: Dependence of the 1-norm matrix condition number κ_1 on the weight constant α for the CFS PML with Dirichlet boundary condition and $\beta = 0$.

$\omega_0 = 8.485 \cdot 10^5$ Hz. The complex frequency shift $i\omega_0$ guarantees that the constitutive parameters are bounded for low (real) frequencies ω. However, for $\omega \gtrapprox \omega_0$, the anisotropy factor, i. e., the ratio of the largest and smallest tensor eigenvalues increases with decreasing frequency. A constant level is only reached at lower frequencies. The effect of growing anisotropy can be seen in Fig. 4. The important role of the weight constant α observed before is confirmed.

Conclusions

Taking explicitly into account the divergence condition, i. e., the equation of continuity, may render stable the resulting boundary value problem and its discrete FE equivalent when solving the frequency domain Maxwell's equations for low frequencies. Giving matching weights to the curl-curl equation and the equation of continuity has been illustrated to be important. An approximately well-balanced formulation can be obtained if eq. (5) is divided by the vacuum speed of light c and rewritten in terms of wavenumber $k = \omega/c$ instead of the angular frequency ω.

The mixed approach works well for the classical Maxwell's equations. Their anisotropic PML extension introduces additional frequency dependencies and a low frequency instability. Introduction of a complex frequency shift to the PML establishes bounds to all coefficients of the boundary value problem and its discrete FE equivalent. However, the anisotropy, introduced to improve the performance of boundary conditions, significantly deteriorates the FE system matrix condition number for low frequencies.

References

[1] P. Monk, Finite Element Methods for Maxwell's Equations. Oxford University Press, Oxford, 2003.

[2] P. Castillo, R. N. Rieben and D. A. White, "FEMSTER: An Object Oriented Class Library of Discrete Differential Forms", in Proceedings of the 2003 IEEE International Antennas and Propagation Symposium, vol. 2, pp. 972–976, Columbus, OH, 2003.

[3] N. J. Higham and F. Tisseur, "A Block Algorithm for Matrix 1-norm Estimation, with an Application to 1-norm Pseudospectra", SIAM Journal on Matrix Analysis and Applications, vol. 21, no. 4, pp. 1185–1201, 2001.

[4] O. Schenk and K. Gärtner, "Solving Unsymmetric Sparse Systems of Linear Equations with PARDISO", Journal of Future Generation Computer Systems, vol. 20, no. 3, pp. 475–487, 2004.

[5] O. Schenk and K. Gärtner, "On Fast Factorization Pivoting Methods for Sparse Symmetric Indefinite Systems", Electronic Transactions on Numerical Analysis, vol. 23, pp. 158–179, 2006.

[6] J. P. Berenger, "A Perfectly Matched Layer for the Absorption of Electromagnetic Waves", Journal of Computational Physics, vol. 114, pp. 185–200, 1994.

[7] M. Kuzuoglu and R. Mittra, "Frequency Dependence of the Constitutive Parameters of Causal Perfectly Matched Anisotropic Absorbers", IEEE Microwave and Guided Wave Letters, vol. 6, no. 12, pp. 447–449, 1996.

Pseudo-differential operators for embedding formulae

A. V. Shanin[†,*], **R. V. Craster** [‡]
[†]Moscow State University, Russia, [‡]Imperial College, London, UK,
[*]Email: shanin@ok.ru

Abstract

A new technique to derive an embedding formula is considered. Instead of a differential operator, a pseudo-differential one is proposed. The advantage is that for wedge problems one can obtain an embedding formula smoothly depending on the opening angle.

An overview of the embedding procedure

One possible method to derive an embedding formula is as described in [1]. It consists of three steps:

1. Apply a differential operator K to the field u. The differential operator should both eliminate the incident wave and maintain the boundary conditions.

2. Using reciprocity express the local asymptotics of the solution in terms of the so-called "edge Green's functions" $\hat{u}_j$, i.e. specially constructed multipole fields with sources located at the edges.

3. Compensate the singularities at the edges by adding an appropriate combination of edge Green's functions. By applying the uniqueness theorem, establish an identity of the form $K[u] = \sum_j C_j \hat{u}_j$, where C_j are constants depending on the angle of incidence. If necessary, it is possible to convert this formula into a relation for directivities.

Currently (see [1]) an embedding formula is available for wedge-like geometries, having rational angles, like $\pi q_j/p_j$. The derivation of embedding formulae requires the application of a differential operator of order P, which is the least common multiple of all p_j in the configuration. The most disturbing issue relating to embedding is the absence of continuity of the formula vs. the angles of the structure.

Pseudo-differential operator

Here we propose to replace the differential operator with a pseudo-differential one. The pseudo-differential operator has a continuous parameter μ, which in the simplest case should be equal to π/Φ, where Φ is the opening angle; thus the new operator can handle problems with irrational angles.

Unfortunately, currently the embedding formula is constructed only for wedges, so its practical value is questionable, however it gives a better understanding of embedding procedure.

The main problem under consideration is as follows: In the sectorial area $0 < \varphi < \Phi$, $0 < r < \infty$ the field obeys the Helmholtz equation

$$\Delta u + k_0^2 u = 0 \tag{1}$$

with time dependence of all variables having the form $e^{-\mathrm{i}\omega t}$.

The Dirichlet boundary conditions are considered so:

$$u = -e^{-\mathrm{i}k_0 x\cos\psi} \qquad \text{at } \varphi = 0, \tag{2}$$

$$u = 0, \qquad \text{at } \varphi = \Phi \tag{3}$$

We introduce a family of integral operators

$$K_\mu[u](x,y) = \int_\Gamma [w_\mu \partial_n u - u\,\partial_n w_\mu]\,dl, \tag{4}$$

where

$$w_\mu(\rho,\alpha) = H_\mu^{(1)}(k_0 r)\cos[\mu(\pi-\alpha)], \tag{5}$$

and the contour of integration is shown in Fig. 1. Note that for each point (x,y) we define its own contour.

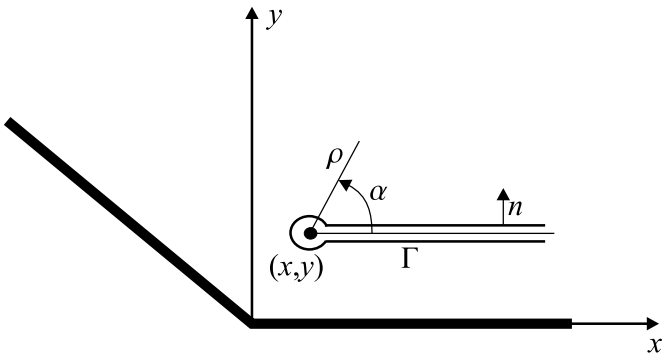

Figure 1: Contour of integration

The trigonometric function in (5) is chosen to eliminate the integral of $\partial_n u$ along the straight parts of the contour.

Properties of the operator

Several propositions concerning the operator K_μ can be proved.

1. The operator K_μ maps solutions of the Helmholtz equation into solutions of Helmholtz equation.

2. If $\mu = n$, n is an integer, then

$$K_n[u] = 4e^{i(n-1)\pi/2} T_n\left(\frac{i}{k_0}\frac{\partial}{\partial x}\right), \qquad (6)$$

where T_n is the Tchebyshev's polynomial. The operator on the right-hand side has been introduced in [1] for rational angles.

3. Let

$$v(r,\varphi) = \exp\{-\mathrm{i}k_0 r\cos(\psi-\varphi)\} \qquad (7)$$

be a plane wave coming from direction ψ. Then

$$K_\mu[v](x,y) = G(\psi)\, v(x,y), \qquad (8)$$

where

$$G(\psi) = 4e^{-i(\mu+1)\pi/2}\cos[\mu(\pi-\psi)]. \qquad (9)$$

4. Let the field obey boundary condition (2). Then

$$[K_\mu - G(\psi)]\, u = 0. \qquad (10)$$

5. Let u satisfy boundary condition (3) and radiation condition. Let us also define

$$\mu = \pi m/\Phi, \qquad (11)$$

where m is an integer, then

$$K_\mu[u] = 0 \qquad \text{at } \varphi = \Phi.$$

6. Let u satisfy the radiation condition, then $K_\mu[u]$ also satisfies radiation condition.

7. We set

$$v(r,\varphi) = J_\nu(k_0 r)e^{\pm \mathrm{i}nu\varphi}, \qquad \nu > 0. \qquad (12)$$

with $0 < \mu < \nu$, then $K_\mu[v]$ near the origin obeys Meixner's conditions.

If $\nu \geq \mu$ then near the origin the field is as follows:

$$K_\mu[v] = -4e^{\pi\mathrm{i}(\nu-\mu)}\sin(\pi\nu)H^{(1)}_{\nu-\mu}(k_0 r)e^{\pm\mathrm{i}\nu\varphi} + \text{Meixner terms} \qquad (13)$$

All these properties enable one to use the operators K_μ in the embedding procedure instead of $T_n(\mathrm{i}/k_0\partial_x)$.

The work is supported by EPSRC, RFBR-07-02-00803 and NSh-1575.003.2 grants.

References

[1] R.V.Craster, A.V.Shanin, Embedding formula for diffraction by wedge and angular geometries, Proc. Roy. Soc. Lond. A, (2005) V.461, P.2227–2242.

Minisymposium on Brain Waves and Cognitive Neurodynamics

Organisers: Peter beim Graben, Roland Potthast and Doug Saddy (University of Reading)

FOCK SPACE REPRESENTATIONS IN NEURAL FIELD THEORIES

Peter beim Graben[†,*], **Sabrina Gerth**[‡], **Douglas Saddy**[†] **and Roland Potthast**[§]
[†]**Dept. of Clinical Language Sciences, University of Reading, UK**
[‡]**Inst. for Linguistics, University of Potsdam, Germany**
[§]**Dept. of Mathematics, University of Reading, UK**
[*]**Email: p.r.beimgraben@reading.ac.uk**

Abstract

We outline a computational model of syntactic language processing based on Smolensky's Fock space representations of symbolic expressions using spherical wave functions. Symbolic computation, regarded as nonlinear operators acting upon these waves, provides a discrete sequence of training patterns that could be used to solve the inverse problem of neural field theories in order to determine the synaptic connectivity/weight kernels. The solutions of a neural field equation should then provide a model of event-related brain potentials that are elicited by syntactic processing problems.

Introduction

The difference between linguistic competence and performance becomes most obvious in the processing of *garden path sentences* such as "the lawyer charged the defendant was lying" [1], where an initially preferred interpretation of "the defendant" as an direct object of "charged" has to revised. *Psycholinguistics* investigates such effects that are due to *processing strategies* in performance rather than to syntactic competence e.g. by means of event-related brain potentials (ERP). Figure 1 illustrates the spatio-temporal ERP dynamics elicited by the processing of dispreferred object-verb-subject (ovs) sentences (solid curves) compared to default subject-verb-object sentences (svo) (dotted curves) in German [2], [3]. Evidently, the brain waves related to the disambiguating words diverge around 600 ms after stimulus presentation where the ovs condition exhibits a *syntactic positivity shift (P600)*.

Complementarily, *computational psycholinguistics* [4] is concerned with computational models of such experimental data that can provide insights into the nature of the cortical processes. Here, we shall outline a model of language-related brain waves in a neural field theory [5].

Fock Space Representations

The construction of our computational model comprises four steps: (1) a context-free toy grammar (CFG) and a processing automaton (the *parser*) [6] are (2) represented by activation vectors and a dynamics in a neural network using Smolensky's [7] *tensor product representations*. However, (3) these representations exhibit several disadvantages (cf. [8]) which could be remedied in an infinite setup, leading to (4) a representation by spherical wave functions.

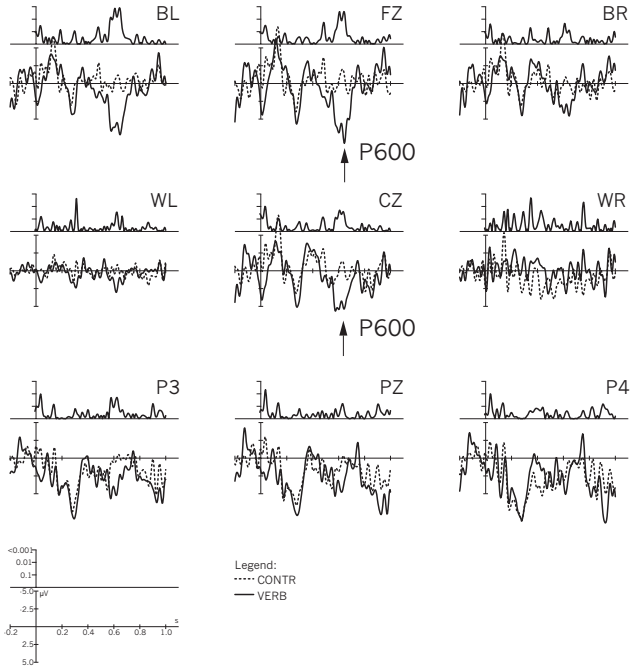

Figure 1: ERPs from a language processing experiment. "CONTR" refers to svo, "VERB" to ovs.

Grammars

The sentence material of the ERP experiment [2], [3], $L = \{\mathtt{svo}, \mathtt{ovs}\}$, can be generated by the CFG [6] $G = G_1 \cup G_2$, where $G_1 = (\{\mathtt{s}, \mathtt{v}, \mathtt{o}\}, \{S, VP\}, \{S \rightarrow \mathtt{s}VP, VP \rightarrow \mathtt{vo}\}, S)$ and $G_2 = (\{\mathtt{s}, \mathtt{v}, \mathtt{o}\}, \{S, VP\}, \{S \rightarrow VP\mathtt{s}, VP \rightarrow \mathtt{ov}\}, S)$ where G_1, G_2 are locally unambiguous CFGs [9] reflecting the different processing strategies: G_1 generates the string svo while G_2 supplies ovs.

Following [7], structured symbolic expressions such as lists or trees can be represented as activation vectors in a neural network by tensor products

$$\mathbf{v} = \bigoplus_n \mathbf{f}_n \otimes \mathbf{r}_n \qquad (1)$$

of "filler", $\mathbf{f}_n$, and "role" vectors, $\mathbf{r}_n$, respectively. For the given case, elementary "fillers" are the variables $\mathtt{s}, \mathtt{v}, \mathtt{o}, S, VP \in \mathbb{R}^5$ of G, regarded as "spins", and "roles" are the positions ROOT $= |0\rangle$, LEFT DAUGHTER $= |1\rangle$, and RIGHT DAUGHTER $= |2\rangle \in \mathbb{R}^3$ of a labeled binary tree.

Equation (1) allows for recursion. In our example, the phrase structure tree for the sentence svo, $[_S \mathtt{s}[_{VP}\mathtt{vo}]]$, assumes the representation $S|0\rangle \oplus \mathtt{s}|1\rangle \oplus VP|02\rangle \oplus \mathtt{v}|12\rangle \oplus \mathtt{o}|22\rangle$, where $|k_1 k_2\rangle$ is the "two-particle state" $|k_1\rangle \otimes |k_2\rangle$. In general, these vectors are elements of the "many particle" Fock space

$$\mathcal{F} = \bigoplus_{n=1}^{\infty} \mathcal{V}_F \otimes \bigotimes_{k=1}^{n} \mathcal{V}_R \tag{2}$$

where $\mathcal{V}_\mathcal{F}$ is a finite vector space spanned by the elementary fillers (analogous to particle spins) and $\mathcal{V}_R$ is a vector space of elementary roles.

Parsers

Since the grammars G_1, G_2 are locally unambiguous, the strings svo and ovs can be deterministically processed, e.g. by *top-down parsers* which successively construct the phrase structure trees by predicting the input [6]. Let us here consider the grammar G_1. The stack of a top-down parser is initialized with the start symbol of a grammar, $S|0\rangle$. As S is a nonterminal symbol, the content of the stack is replaced by the tensor product representation of the unique rule expanding S, i.e., by $S|0\rangle \oplus \mathtt{s}|1\rangle \oplus VP|2\rangle$. Next, the parser finds the nonterminal filler VP which is replaced by the representation $VP|0\rangle \oplus \mathtt{v}|1\rangle \oplus \mathtt{o}|2\rangle$, yielding the complete tree given above. Therefore, the automata are described by maps $\alpha : \mathcal{F} \to \mathcal{F}$ acting in the following way: each nonterminal filler $\mathbf{f}_n$ occurring in Eq. (1) is recursively replaced by a complex filler corresponding to the rule with left-hand-side $\mathbf{f}_n$.

A similar approach using minimalist grammars [10] gave the state space trajectories in a two-dimensional PCA projection of a 275,562-dimensional Fock space, shown in Fig. 2 [8].

Problems

The trajectories plotted in Fig. 2 were obtained by using linearly dependent role vectors because the dimension of the activation space became 1,879,048,192 using linearly independent ones [8]. Unfortunately, the treatment of these representations was numerically not feasible.

However, the very high space dimensions required even for finite language models is only one problem of Smolensky's proposal. Others are

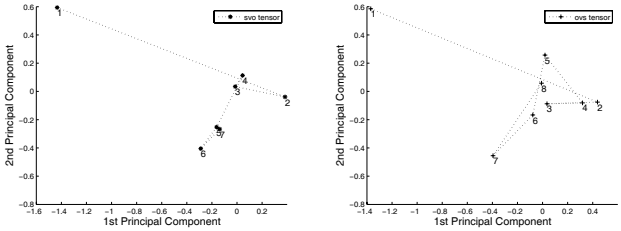

(a) (b)

Figure 2: PCA projections of a "minimalistic" Fock space representation for language processing. (a) Trajectory of the svo parse, (b) that of the ovs parse.

- the processing of lists of unbounded length or of trees with arbitrary recursion depth, respectively, requires *infinite* dimensional spaces,
- but, only vertices have symbolic representations (brain state in-the-box model [7]); therefore
- most states occupy a meaningless vacuum; meaningful states are rather improbable.

Smolensky's solution of the dimensionality problem to use always finite-dimensional representations with linearly dependent role and/or filler vectors does not seem to be appropriate as it leads to cross-talk [7], thereby preventing a faithful mapping between the symbolic and the connectionist dynamics. Thus, Smolensky stresses that there is no *implementation* of symbolic processes in neural dynamics [11]. Since we are looking for such implementations, yet, we shall allow for infinite-dimensional Fock spaces to encounter the dimensionality problem in the following.

Wave functions

Our starting point are the linearly independent elementary role vectors of our CFG model. These can be identified with a triplet of angular momentum states: $|0\rangle \cong |1,0\rangle, |1\rangle \cong |1,-1\rangle, |2\rangle \cong |1,1\rangle$, which, in turn, have an $L_2(S)$ representation by spherical harmonics $|\ell m\rangle \cong Y_{\ell m}(\vartheta, \varphi)$ at the unit sphere S. This appears as a suitable choice as these functions are often used as basis functions of EEG waves and neural fields.

In the next step, tensor products of the role vectors are to be computed. In our notation, $|12\rangle$, e.g., denotes the left daughter of the right daughter of the tree's root, and is given as $|12\rangle = |1\rangle \otimes |2\rangle = |1,-1\rangle \otimes |1,1\rangle \cong Y_{1,-1}(\vartheta_1, \varphi_1) Y_{1,1}(\vartheta_2, \varphi_2)$.

In quantum theory, the product states $|\ell_1 m_1\rangle \otimes |\ell_2 m_2\rangle$ belong to different multipletts with total angular momentum ℓ given by the Clebsch-Gordan sums $|\ell, m, \ell_1, \ell_2\rangle = \sum_{m_1, m_2 = m - m_1} \langle \ell_1 m_1 \ell_2 m_2 | \ell m \ell_1 \ell_2 \rangle |\ell_1 m_1 \ell_2 m_2\rangle$ [12]. Thus, we can map the roles described by the tensor products $|\ell_1 m_1\rangle \otimes |\ell_2 m_2\rangle$ onto a family of spherical wave functions $Y_{\ell m}(\vartheta, \varphi)$ obeying the triangle relation $|\ell_1 - \ell_2| \leq \ell \leq \ell_1 + \ell_2$. Finally, a phrase structure tree will be represented by "spinors"

$$\Psi(\vartheta, \varphi) = \sum_{\ell, m} \mathbf{f}_{\ell m} Y_{\ell m}(\vartheta, \varphi) \tag{3}$$

with the elementary fillers $\mathbf{f}_{\ell m}$ denoting the tree labels.

Neural Field Theory

In the preceding sections we outlined a way how to represent symbolic content by tensor products in an infinite-dimensional Fock space of spherical wave functions $Y_{\ell m}(\vartheta, \varphi)$. Correspondingly, symbolic computation, such as language processing α, will be represented by (presumably nonlinear) operators $\mathbf{A}_\alpha : \Psi(\vartheta, \varphi) \rightarrow \Phi(\vartheta, \varphi)$. A time-discrete trajectory of these wave functions $\{\Psi_t | t \in \mathbb{N}_0\}$ describes a cognitive process with initial condition Ψ_0.

These functions can be regarded as stationary solutions of a neural field equation [5]

$$\begin{aligned} & \tau(x) \frac{\partial \Psi(x,t)}{\partial t} + \Psi(x,t) = \\ = & \int_{-\infty}^{t} \mathrm{d}t' \int_S \mathrm{d}x' \, w(x,x') \times \\ \times & \; G(t-t') \, f \left[\Psi \left(x', t' - \frac{||x - x'||}{c} \right) \right] \end{aligned} \tag{4}$$

at the unit sphere, $x = (\vartheta, \varphi)$. Here, $\tau(x)$ describes the neural time constants, the kernel $w(x, x')$ the synaptic connectivity and weights, $G(t - t')$ the postsynaptic impulse response, f the activation function and c the propagation velocity of neural activity.

Regarding Ψ_t as *training patterns* for the field equation, the *inverse problem* of determining the kernel $w(x, x')$ from the solutions Ψ_t, entails a cognitive implementation by a neural field theory. Such a model would be able to predict the dynamics of ERPs evoked by processing problems such as garden path sentences [1], [2], [3].

References

[1] L. Osterhout, P. J. Holcomb, and D. A. Swinney. Brain potentials elicited by garden-path sentences: Evidence of the application of verb information during parsing. *J. Exp. Psych. LMC*, 20(4):786 – 803, 1994.

[2] P. beim Graben, D. Saddy, M. Schlesewsky, and J. Kurths. Symbolic dynamics of event-related brain potentials. *Phys. Rev. E*, 62(4):5518 – 5541, 2000.

[3] D. Saddy and P. beim Graben. Measuring the neural dynamics of language comprehension processes. In T. Witruk, A. D. Friederici, and T. Lachmann, editors, *Basic Fuctions of Language, Reading and Reading Disorder*, pages 41 – 60. Kluwer Academic Publishers, Boston, 2002.

[4] R. L. Lewis. Computational psycholinguistics. In *Encyclopedia of Cognitive Science*. Macmillan Reference Ltd., 2000.

[5] C. J. Rennie, P. A. Robinson, and J. J. Wright. Unified neurophysical model of EEG spectra and evoked potentials. *Biol. Cybern.*, 86:457 – 471, 2002.

[6] J. E. Hopcroft and J. D. Ullman. *Introduction to Automata Theory, Languages, and Computation*. Addison–Wesley, Menlo Park, California, 1979.

[7] P. Smolensky and G. Legendre. *The Harmonic Mind. From Neural Computation to Optimality-Theoretic Grammar*, volume 1: Cognitive Architecture. MIT Press, Cambridge (MA), 2006.

[8] S. Gerth. Parsing mit minimalistischen, gewichteten Grammatiken und deren Zustandsraumdarstellung. Master's thesis, Universität Potsdam, 2006.

[9] P. beim Graben, B. Jurish, D. Saddy, and S. Frisch. Language processing by dynamical systems. *Int. J. Bif. Chaos*, 14(2):599 – 621, 2004.

[10] E. P. Stabler. Derivational minimalism. *SLNCS 1328*, pages 68 – 95. Springer, New York, 1997.

[11] P. beim Graben. Incompatible implementations of physical symbol systems. *Mind and Matter*, 2(2):29 – 51, 2004.

[12] A. R. Edmonds. *Angular Momentum in Quantum Mechanics*. Princeton University Press, 1957.

Exotic dynamics in a firing rate model of neural tissue with threshold accommodation

S. Coombes[†], **M. R. Owen**
School of Mathematical Sciences
University of Nottingham
Nottingham
NG7 2RD, UK.
[*]Email: stephen.coombes@nottingham.ac.uk

Abstract

Many of the equations describing the dynamics of neural systems are written in terms of firing rate functions, which themselves are often taken to be threshold functions of synaptic activity. Dating back to work by Hill in 1936 it has been recognized that more realistic models of neural tissue can be obtained with the introduction of state-dependent dynamic thresholds. In this paper we treat a specific phenomenological model of threshold accommodation that mimics many of the properties originally described by Hill. Importantly we explore the consequences of this dynamic threshold at the tissue level, by modifying a standard neural field model of Wilson-Cowan type. As in the case without threshold accommodation classical Mexican-Hat connectivity is shown to allow for the existence of spatially localized states (bumps) in both one and two dimensions. Importantly an analysis of bump stability in one dimension, using recent Evans function techniques, shows that bumps may undergo instabilities leading to the emergence of both breathers and traveling waves. Moreover, a similar analysis for traveling pulses leads to the conditions necessary to observe a stable traveling breather. In the regime where a bump solution does not exist direct numerical simulations show the possibility of self-replicating bumps via a form of bump splitting. Simulations in two space dimensions show analogous localized and traveling solutions to those seen in one dimension. Indeed dynamical behavior in this neural model appears reminiscent of that seen in other dissipative systems that support localized structures, and in particular those of coupled cubic complex Ginzburg-Landau equations. Further numerical explorations illustrate that the traveling pulses in this model exhibit particle like properties, similar to those of dispersive solitons observed in some three component reaction-diffusion systems.

A full account of this work can be found in S Coombes and M R Owen 2007 *Exotic dynamics in a firing rate model of neural tissue with threshold accommodation*, AMS Contemporary Mathematics "Fluids and Waves - Recent Trends in Applied Analysis", to appear[1].

Introduction

The mathematical modeling of neural tissue can trace its roots back to work by Beurle [3] in the 1950s and later by Griffith [11], [12] in the 1960s. To overcome the difficulties of modeling the large numbers of neurons and synapses in even a small piece of cortex these authors advocated continuum descriptions in which space is continuous and macroscopic state variables are mean firing rates. These early models were later improved and refined in the work of Wilson and Cowan [22], Nunez [20] and Amari [1], and are still in use today as models of large scale brain activity. We shall refer to such models and their variants as neural field theories. To date neural field theories have found applications in understanding brain slice preparations [14], EEG rhythms [16], [19], visual hallucinations [9], [4], short term memory [17], motion perception [10], representations in the head-direction system [23] and feature selectivity in the visual cortex [2]. For recent reviews of the dynamics of neural fields we refer the reader to [5], [6]. Typically they take the form of integral or integro-differential equations. Although they do not capture the details of the fast ionic currents underlying spiking neural behavior, neural field theories can incorporate realistic non-local axo-dendritic synaptic interactions provided that spike-trains can be replaced by firing rates. In practice this assumption seems to be useful when dealing with slow synaptic interactions. The firing rate in such models is often taken to be a threshold function of the synaptic activity. Typically, as a constant current is increased, most cortical neurons switch from a resting constant potential to an active mode. In the active mode, either trains of spikes are generated or bursts of spikes. Since the majority of cells in cortical networks fire repetitively [21], we shall focus our attention on this case. A common choice to fit the firing rate function is a sigmoid function of pre-synaptic activity u in the form

[1] http://eprints.nottingham.ac.uk/archive/00000457/

$f = f(u-h)$, where

$$f(u) = \frac{1}{1+\exp(-\beta u)}. \tag{1}$$

Here the parameter h is identified as a threshold whilst β measures the steepness of the sigmoid. Interestingly the notion of a threshold goes back a long way in the history of neuroscience. Even in the absence of any detailed model of neural tissue Hill [13] in 1936 described the fruitfulness of thinking of neural tissue as possessing a threshold for excitability. Indeed, at the single neuron level the notion of a threshold model can be traced back as far as 1907 to Lapicque [18].

In more detail we will discuss a generic neural field model with synaptic activity $u = u(x,t)$, $x \in \mathbb{R}$, $t \in \mathbb{R}^+$, governed by the integral equation

$$u = \eta * w \otimes f(u-h). \tag{2}$$

Here, the symbol $*$ represents a temporal convolution in the sense that

$$(\eta * f)(x,t) = \int_0^t \eta(s) f(x,t-s)\mathrm{d}s, \tag{3}$$

and $\otimes$ represents a spatial convolution such that

$$(w \otimes f)(x,t) = \int_{-\infty}^{\infty} w(y) f(x-y,t)\mathrm{d}y. \tag{4}$$

The function $\eta(t)$ (with $\eta(t) = 0$ for $t < 0$) represents a synaptic filter, whilst $w(x)$ is a synaptic footprint describing the anatomy of network connections. Typically, however, neural field theories such as the one above do not incorporate any of the slow intrinsic processes known to modulate tissue response. In particular we are drawn to the observation of Hill that thresholds are dependent upon the state of the tissue. We quote directly from his 1936 paper[2] [13]:

.... *The critical value of V required for excitation, i.e., the threshold U, might have been constant and independent of the previous history of the nerve. If the current lasts only for a very short time this is true. If, however, the current lasts longer, the threshold rises, as is shown by the well-known fact that a slowly increasing current has a higher threshold than a quickly increasing one. The change of threshold is gradual, it takes place as a consequence of, and at a speed determined by, the change of "local potential" produced in the nerve by the passage of current. There is, therefore, a second time-factor in electric excitation, viz., that defining the rate of change of threshold U.*
We shall use the term "accommodation" to describe the fact that the threshold U rises when the "local potential" V is maintained. It is known that "accommodation" disappears of itself, i.e., U reverts gradually to its original value U_0 when the nerve is allowed to return to its original resting state ...

[2]We are indebted to John Rinzel for bringing the work of A V Hill to our attention.

If we identify the "local potential" described by Hill with synaptic activity u then a simple phenomenological model of threshold accommodation can be written as

$$h_t = -(h-h_0) + \kappa g(u-\theta). \tag{5}$$

Here h and h_0 are identified with the U and U_0 described by Hill, whilst the nonlinear function $g(u)$ describes the effects of the accommodation process on the threshold evolution. We also assume that accommodation is itself a threshold process and interpret θ as a threshold for accommodation, whilst the parameter $\kappa > 0$ measures the strength of accommodation. For later convenience we write the dynamics for h in the integrated form

$$h = h_0 + \kappa \eta_h * g(u-\theta), \tag{6}$$

where $\eta_h(t) = \mathrm{e}^{-t}$ for $t > 0$ and is zero otherwise. In the absence of threshold accommodation (i.e. with $\kappa = 0$) it is known that models with short-range excitation and long range inhibition, or so-called Mexican-hat connectivity, can support spatially localized solutions. Indeed such solutions are known to exist for sufficiently steep sigmoids [15] and has motivated much analysis in the limit that the firing rate function f approaches a Heaviside step function, i.e. as $\beta \to \infty$ in (1). To illustrate how the form of nonlinear threshold accommodation (5) can lead to exotic dynamics at the network level, we will focus on the case of Mexican-hat connectivity with Heaviside firing rate function. Moreover, so that we may study instabilities of spatially localized states in a tractable mathematical fashion we will also restrict our attention to the case that $g(u)$ is also a Heaviside. Hence, throughout the rest of this paper we work with the choice $g(u) = f(u) = H(u)$, where H is a Heaviside function such that $H(x) = 1$ for $x \geq 0$ and is zero otherwise. Moreover, we shall take $\eta(t) = \alpha \mathrm{e}^{-\alpha t} H(t)$ and $w(x) = (1-|x|)\mathrm{e}^{-|x|}$, representing an exponential synaptic response in a network with short-range excitation and long-range inhibition. The extension to other synaptic filters and footprints is straightforward [7]. A preliminary account of the work in this paper first appeared in [8].

References

[1] S Amari, *Homogeneous nets of neuron-like elements*, Biological Cybernetics **17** (1975), 211–220.

[2] R Ben-Yishai, L Bar-Or, and H Sompolinsky, *Theory of orientation tuning in visual cortex*, Proceedings of the National Academy of Sciences USA **92** (1995), 3844–3848.

[3] R L Beurle, *Properties of a mass of cells capable of regenerating pulses*, Philosophical Transactions of the Royal Society London B **240** (1956), 55–94.

[4] P C Bressloff, J D Cowan, M Golubitsky, P J Thomas, and M Wiener, *Geometric visual hallucinations, Euclidean symmetry and the functional architecture of striate cortex*, Philosophical Transactions of the Royal Society London B **40** (2001), 299–330.

[5] S Coombes, *Waves, bumps, and patterns in neural field theories*, Biological Cybernetics **93** (2005), 91–108.

[6] ———, *Neural fields*, Scholarpedia (2006), 2125.

[7] S Coombes, G J Lord, and M R Owen, *Waves and bumps in neuronal networks with axo-dendritic synaptic interactions*, Physica D **178** (2003), 219–241.

[8] S Coombes and M R Owen, *Bumps, breathers, and waves in a neural network with spike frequency adaptation*, Physical Review Letters **94** (2005), 148102(1–4).

[9] G B Ermentrout and J D Cowan, *A mathematical theory of visual hallucination patterns*, Biological cybernetics **34** (1979), 137–150.

[10] M A Geise, *Neural field theory for motion perception*, Kluwer Academic Publishers, 1999.

[11] J S Griffith, *A field theory of neural nets: I: Derivation of field equations*, Bulletin of Mathematical Biophysics **25** (1963), 111–120.

[12] ———, *A field theory of neural nets: II: Properties of field equations*, Bulletin of Mathematical Biophysics **27** (1965), 187–195.

[13] A V Hill, *Excitation and accommodation in nerve*, Proceedings of the Royal Society of London. Series B, Biological Sciences **119** (1936), 305–355.

[14] X Huang, W C Troy, Q Yang, H Ma, C R Laing, S J Schiff, and J Wu, *Spiral waves in disinhibited mammalian neocortex*, The Journal of Neuroscience **24** (2004), 9897–9902.

[15] K Kishimoto and S Amari, *Existence and stability of local excitations in homogeneous neural fields*, Journal of Mathematical Biology **7** (1979), 303–318.

[16] P l Nunez, *Neocortical dynamics and human EEG rhythms*, Oxford University Press, 1995.

[17] C R Laing, W C Troy, B Gutkin, and G B Ermentrout, *Multiple bumps in a neuronal model of working memory*, SIAM Journal on Applied Mathematics **63** (2002), 62–97.

[18] L Lapicque, *Recherches quantitatives sur l'excitation électrique des nerfs traitée comme une polarisation*, J. Physiol. Pathol. Gen. **9** (1907), 620–635.

[19] D T J Liley, P J Cadusch, and M P Dafilis, *A spatially continuous mean field theory of electrocortical activity*, Network **13** (2002), 67–113.

[20] P L Nunez, *The brain wave equation: a model for the EEG*, Mathematical Biosciences **21** (1974), 279–297.

[21] E L White, *Cortical circuits: Synaptic organization of the cerebral cortex. Structure, function, and theory*, Birkhauser, 1989.

[22] H R Wilson and J D Cowan, *Excitatory and inhibitory interactions in localized populations of model neurons*, Biophysical Journal **12** (1972), 1–24.

[23] K Zhang, *Representation of spatial orientation by the intrinsic dynamics of the head-direction cell ensemble: a theory*, Journal of Neuroscience **16** (1996), 2112–2126.

A SOLUTION TO THE DYNAMICAL INVERSE PROBLEM OF EEG GENERATION USING SPATIOTEMPORAL KALMAN FILTERING

Andreas Galka[†,‡,*], **Tohru Ozaki**[‡]
[†]Department of Neurology, University of Kiel, Schittenhelmstrasse 10, 24105 Kiel, Germany
[‡]Institute of Statistical Mathematics (ISM), Minami-Azabu 4-6-7, Tokyo 106-8569, Japan
[*]Email: andreas@ism.ac.jp

Abstract

We discuss a state-space approach to dynamical modeling of multivariate time series obtained from spatially extended dynamical systems; as an example we consider the human electroencephalogram (EEG). Since the assumed true states are unobserved and high-dimensional, their estimation represents an "ill-posed" inverse problem. By discretizing both time and space and assuming a stochastic autoregressive dynamics, derived from a wave equation, it is possible to recast the problem as a filtering problem and apply the Kalman filter to it. Additional approximations are introduced into the Kalman filter in order to obtain an efficient implementation by exploiting the spatial structure of the problem, yielding the "spatiotemporal Kalman filter". The model is fitted to time series data using likelihood maximization.

Introduction

In many fields of science (such as oceanography, geophysics, engineering, physiology or medicine) spatially extended systems are studied which evolve in time according to some possibly complicated dynamics. It is a typical situation that the relevant state variables of such systems cannot be observed directly, but only through an observation function; in many cases this function performs a projection of the high-dimensional true state space of the system onto an observation space of much lower dimension. The task of retrieving estimates of the true states from such observations represents a typical inverse problem. Due to the absence of a simple invertible relationship between state and observation such problems are ill-posed, i.e. the solutions ("inverse solutions") are unstable and ambiguous.

As an example, we mention the neural activity of human brain, which can be observed noninvasively by recording the electroencephalogram (EEG). The resulting multivariate time series represent only an indirect reflection of the actual brain dynamics taking place in space and time. For purposes of clinical diagnosis and brain research, it would be desirable to obtain estimates of the unobserved internal states of brain, i.e. estimates of the *sources* of the EEG; these estimates would then also be functions of space and time. This task represents the *inverse problem of EEG generation*.

Most previous attempts to solve this inverse problem, e.g. *Low Resolution Electromagnetic Brain Tomography* (LORETA) [1], were ignoring the temporal dimension of the problem, i.e. they processed the data sampled at each instant of time independently. Here we present a framework for a dynamical approach to this problem, taking into account all data sampled until a given instant of time and connecting them by a dynamical model. This is accomplished by casting the problem into the shape of a state space filtering problem.

Model

Let the unobserved true states of the system be given by a vector field $\boldsymbol{j}(\boldsymbol{r},t)$, where $\boldsymbol{r}$ and t denote space and time, respectively; in the case of the human brain, $\boldsymbol{j}(\boldsymbol{r},t)$ denotes the *primary current density*, i.e. the field of current dipoles resulting from synaptic transmission processes in neural dendrites. In the linear approximation, the dynamics in a spatially extended passive medium can be described by *stochastic* partial differential equations, such as the linear wave equation

$$\frac{\partial^2 \boldsymbol{j}(\boldsymbol{r},t)}{\partial t^2}+2\zeta\omega\frac{\partial \boldsymbol{j}(\boldsymbol{r},t)}{\partial t}+\omega^2\boldsymbol{j}(\boldsymbol{r},t)=b\frac{\partial^2 \boldsymbol{j}(\boldsymbol{r},t)}{\partial \boldsymbol{r}^2}+\boldsymbol{\eta}(\boldsymbol{r},t)$$

where $\boldsymbol{\eta}(\boldsymbol{r},t)$ denotes a stochastic driving noise term.

In practical work, the volume of brain is discretized into a rectangular grid of *voxels*, and also the wave equation is transformed into a discrete-time dynamical model; the resulting model for the evolution of the primary current density $\boldsymbol{j}(v,t)$ (where v labels voxels) represents a linear *state space model*. By stacking the $\boldsymbol{j}(v,t)$, a *global* state vector $\mathbf{X}(t)$ is defined; let N_v and N_x denote the number of voxels and the dimension of $\mathbf{X}(t)$, respectively; since the dimension of $\boldsymbol{j}(v,t)$ is 3, we have $N_x = 3N_v$.

The state space model is then given by two equations: First by the second-order multivariate autoregressive model (derived from the wave equation)

$$\mathbf{X}(t) = \mathsf{A}_1\mathbf{X}(t-1) + \mathsf{A}_2\mathbf{X}(t-2) + \boldsymbol{\mathcal{H}}(t) \qquad (1)$$

where $\mathsf{A}_1, \mathsf{A}_2$ denote transition parameter matrices (of size $3N_v \times 3N_v$), and $\boldsymbol{\mathcal{H}}$ denotes the global gaussian white noise vector, for which we define the covariance matrix[1] $\mathsf{C}_{\mathcal{H}} = \mathscr{E}(\boldsymbol{\mathcal{H}}\boldsymbol{\mathcal{H}}^\dagger)$; and second by the linear observation equation

$$\mathbf{Y}(t) = \mathsf{K}\mathbf{X}(t) + \boldsymbol{\mathcal{E}}(t) \quad , \tag{2}$$

where $\mathbf{Y}(t)$ denotes the vector of observations (such as EEG voltages), with dimension N_y, K denotes an observation matrix of dimension $N_y \times N_x$, and $\boldsymbol{\mathcal{E}}(t)$ denotes a vector of observational gaussian white noise, with dimension N_y, for which we define the covariance matrix $\mathsf{C}_{\mathcal{E}} = \mathscr{E}(\boldsymbol{\mathcal{E}}\boldsymbol{\mathcal{E}}^\dagger)$.

Method of analysis

The observation matrix K (in the case of the EEG also known as *lead field matrix*) can approximately be derived by electromagnetic theory; since usually $N_y \ll N_x$, solving equation (2) for $\mathbf{Y}(t)$ by least-squares methods requires techniques like pseudo-inversion and regularization (as employed in the LORETA method). This needs to be done for each time point t, ignoring the temporal order of the data (and, thus, the dynamical model equation (1)), such that a considerable amount of information is discarded.

Spatiotemporal Kalman filter

As an alternative, we propose to apply Kalman filtering to the state space model consisting of equations (1) and (2). It is well known that, for given estimates of the model parameters $\mathsf{A}_1, \mathsf{A}_2, \mathsf{C}_{\mathcal{H}}, \mathsf{C}_{\mathcal{E}}$, the Kalman filter provides optimal linear estimates of the states $\mathbf{X}(t)$ in an efficient way. Since the Kalman filter operates by predicting states and observations, it can fully utilize the information contained in the temporal ordering of the data, including the direction of time. We also mention that a further improvement of the state estimates can be obtained by applying an additional smoothing filter which runs backwards through time (while the Kalman filter runs forward). For a detailed presentation of Kalman filtering and smoothing we refer to Grewal & Andrews [2].

However, due to the large state space dimension N_x (which can easily exceed 10000), it is advisable to simplify the application of the Kalman filter, in order to avoid explicit numerical operations with huge matrices. For this purpose, we have designed a *spatiotemporal Kalman filter*. Its core idea is to replace a single $(3N_v)$-dimensional filtering problem by a set of N_v coupled 3-dimensional filtering problems, each of which is localized at a single voxel. Details can be found in Galka *et al.* [3].

This simplification becomes possible only by assuming that $\mathsf{C}_{\mathcal{H}}$ is diagonal; this, however, is a strong assumption which in general will not be true for the set of local state vectors $\boldsymbol{j}(v,t)$. But if we take a second-order spatial derivative of $\boldsymbol{j}(v,t)$, it is reasonable to expect that the non-zero off-diagonal elements of $\mathsf{C}_{\mathcal{H}}$ will become much smaller. We denote this transformation by $\tilde{\mathbf{X}}(t) = \mathsf{L}\mathbf{X}(t)$; L denotes a *Laplacian* matrix. Consequently we formulate the filtering problem entirely in $\tilde{\mathbf{X}}(t)$ instead of $\mathbf{X}(t)$; the lead field matrix K then has to be replaced by $\mathsf{K}\mathsf{L}^{-1}$.

Note that equation (1) represents an autoregressive model of second order, while state space models always need to be first-order models; by augmenting the state vector $\tilde{\mathbf{X}}(t)$ by a time-delayed copy $\tilde{\mathbf{X}}(t-1)$, equation (1) can easily be rewritten as a first-order autoregressive model, but at the price of doubling the effective state dimension. The transition parameter matrix of the new model is given by the $(6N_v \times 6N_v)$ matrix $\left(\begin{smallmatrix} \mathsf{A}_1 & \mathsf{A}_2 \\ \mathsf{I} & 0 \end{smallmatrix}\right)$.

Instead of using a time-delayed copy, as done in [3], also a time-advanced copy may be used, which has the advantage of avoiding the "temporal blurring" of the components of the state vector: The advanced components of the augmented state vector have then the interpretation of "predicted future states at time t" [4]. In this case the new transition parameter matrix is given by $\left(\begin{smallmatrix} \mathsf{A}_1 & \mathsf{I} \\ \mathsf{A}_2 & 0 \end{smallmatrix}\right)$.

Parameter estimation

The model, as presented above, depends on a set of 4 parameter matrices, $\mathsf{A}_1, \mathsf{A}_2, \mathsf{C}_{\mathcal{H}}, \mathsf{C}_{\mathcal{E}}$, which are unknown and need to be estimated from the data as well; this step requires computation-intensive numerical optimization. As the quantity to be maximized we choose the logarithmic likelihood:

$$\mathcal{L} = \sum_{t=1}^{N_t} \left(\log |\mathsf{R}(t)| + \Delta\mathbf{Y}^\dagger(t)\, \mathsf{R}^{-1}(t)\, \Delta\mathbf{Y}(t) + N_y \log(2\pi) \right)$$

where $\Delta\mathbf{Y}(t)$ denotes the observation prediction error (i.e. the *innovation*) of the Kalman filter at time t, $|\mathsf{R}(t)|$ the determinant of the observation prediction error covariance matrix at time t and N_t the length of the analyzed time series. The Kalman filter readily provides $\Delta\mathbf{Y}(t)$ and $|\mathsf{R}(t)|$ during its forward pass through the data.

In order to decrease the dimension of the parameter space, a number of constraints need to be applied: Most elements of $\mathsf{A}_1, \mathsf{A}_2$ are set to zero, only the diagonal values may be non-zero, but they assume only two common values for all voxels, say a_1 and a_2; for A_1 also those matrix elements corresponding to directly neighboring pairs

[1] $\mathscr{E}(.)$ denotes expectation.

of voxels are allowed to be non-zero, but again they all assume a common value, say b_1. Also $\mathsf{C}_{\mathcal{H}}$ and $\mathsf{C}_{\mathcal{E}}$ are constrained to be diagonal with one common value each, say σ_η and σ_ϵ. Through these constraints the number of parameters is reduced to 5.

We note that choosing a non-zero value of the parameter b_1 has the important benefit of ensuring *observability* of the state space model [3]; it is precisely this property which renders it possible – at least in theory –, to obtain estimates of the unobserved state vector from an observation vector of much smaller dimension, provided a time series of sufficient length is analyzed.

The numerical optimization is carried out by a sequence of Broyden-Fletcher-Goldfarb-Shanno (BFGS) secant method steps and Nelder-Mead simplex method steps; convergence can be accelerated by limiting some steps to subsets of parameters. Still the optimization procedure easily consumes hours, if not days, of time, depending on the time series length N_t, the number of EEG channels N_y and the number of voxels N_v. Typical values of our analyses are $N_t = 512$, $N_y = 18$, $N_v = 3433$.

Results

We have applied the state space modeling, as described above, to various simulated and real time series, both for human EEG; for the detailed results see [3]. For the case of simulations we can compare directly the inverse solution with the true sources; we find that if the *true* dynamical model is employed (i.e. the model which has created the data), the inverse solution becomes very close to the true states. This is not a trivial result, since at each time point we are still estimating 3*3433 unknown states from just 18 observed values.

On the other hand, employing simple dynamical models leads to inverse solutions which are similar to LORETA solutions. This motivates the search for improved dynamical models.

We have also derived an estimator of the log-likelihood of LORETA, which can be compared with the log-likelihood of the state space model. This comparison reveals the state space model to provide a considerably better modeling of given data than LORETA. Furthermore we have derived estimators of the error of the inverse solutions for LORETA and for state space modeling (in fact, such error estimates are provided naturally by the state estimation covariance matrix of Kalman filtering), and we find that state space modeling achieves much smaller errors than LORETA (where the error renders the solutions statistically insignificant most of the time). These results were obtained both for simulations and for real EEG data.

References

[1] R.D. Pascual-Marqui, C.M. Michel, D. Lehmann; "Low resolution electromagnetic tomography: a new method for localizing electrical activity in the brain", Int. J. Psychophysiol., vol. 18, pp. 49-65, 1994.

[2] M.S. Grewal, A.P. Andrews; Kalman filtering: theory and practice using MATLAB, Wiley-Interscience, New York, 2001.

[3] A. Galka, O. Yamashita, T. Ozaki, R. Biscay, P.A. Valdés-Sosa; "A solution to the dynamical inverse problem of EEG generation using spatiotemporal Kalman filtering", NeuroImage, vol. 23, pp. 435-435, 2004.

[4] H. Akaike, T. Nakagawa; Statistical analysis and control of dynamic systems, Kluwer, Dordrecht, 1988.

CORTICAL NETWORK DYNAMICS WITH TIME DELAYS REVEAL FUNCTIONAL CONNECTIVITY IN RESTING BRAIN

Anandamohan Ghosh*, **Young-Ah Rho, Viktor Jirsa**
Laboratoire Mouvement et Perception, Universite de la Mediterranee, 13288 Marseille, France
Rolf Kötter
Department of Cognitive Neuroscience, Radboud University Medical Center, 6500HB Nijmegen, The Netherlands
Anthony Randal McIntosh
Rotman Research Insitute of Baycrest Centre, University of Toronto, Toronto, Ontario M6A 2E1, Canada
*Email: Anandamohan.Ghosh@univmed.fr

Abstract

Cortical dynamics of resting brain exhibits spontaneous neuronal activity. We study neuronal dynamics of a human anatomical network, represented as a connection matrix, by modelling neuronal masses at each location by FitzHugh-Nagumo oscillators and also incorporating time-delayed coupling. We identify the stability region in the connectivity strength and time delay plane and show its robustness by subjecting the model to perturbations. The complex spatiotemporal data is analysed by principal component analysis to reveal the underlying functional connectivity. We find strong evidence that prefrontal, parietal and cingulate cortex forms an active network in a resting brain.

Introduction

Neuronal oscillations have intrigued neuroscientists over the last few decades. Following the pioneering work of Hodgkin-Huxley single neuron oscillations have been well studied [1] while the collective behaviour of assembly of neurons, neuronal masses, has evoked new interests in understanding behavioural patterns. Cortical neurons exhibit behaviour dependent oscillating networks that have manifold implications. Neuronal oscillations in cortical networks have been detected in a resting brain, say, during sleep and are conjectured to play crucial role in information processing, memory, perception and consciousness [2].

Functional imaging studies have been widely used in detecting task related neural activity. In such studies a task or stimulus is responsible for inducing change in brain activity pattern and imaging techniques such as positron emission tomography (PET) or functional MRI (fMRI) are used to detect associated responses in different regions. However, it is expected to see changes in brain activity patterns due to external stimuli. But understanding fluctuations in a resting or idling brain are more intriguing and interesting as it leads to cognitive processing. One is interested in questions like which areas of brain are activated and what are the functional relationships. Recent studies of functional connectivity in resting brain has revealed that a specific set of prefrontal and parietal cortical regions show significant increase in activity during cognitive tasks [3], [4].

Emergence of sophisticated imaging experimental tools has now made it possible to represent the cortical connections by pathways identified by anatomical tracing techniques. These facilitate theoretical investigation by emulating neuronal dynamics on cortical regions. Recent work of Honey et al [5] identifies functional network from connection matrix of macaque neo-cortex by using information theoretical measures. They have identified existence of clusters linking prefrontal and parietal regions.

In this paper, we investigate neural activity using an anatomical connection matrix of human cortex comprising of 38 sensory areas. We study dynamics on the anatomical network by modelling neuronal masses at each location by FitzHugh-Nagumo[6] oscillators and incorporating time-delayed coupling. We identify the stability region in the connectivity strength and time delay plane and show its robustness by subjecting the model to perturbations. The complex spatiotemporal data is analysed by principal component analysis to reveal the underlying functional connectivity. We find strong evidence that prefrontal, parietal and cingulate cortex are actively involved in a resting brain in agreement with existing imaging studies [3], [4], [5].

Methods

We simulated the neuronal dynamics on a connection matrix of human neo-cortex. The connectivity matrix is a weighted matrix comprising of 38 sensory nodes. This is a sparse matrix with weights ranging from 1, 2, and 3 and has some unknown connections, where experimental evidences are not strong enough to establish the connection. We assume the unknown weights to be zero and have also studied by substituting them with random weights with no change in results. The connection graph has 599

edges, with connection density = 0.42603, characteristic path length = 1.633 and clustering index = 0.568.

We simulate neuronal dynamics by assuming each neuronal mass is governed by an oscillator of the kind of FitzHugh-Nagumo model given by

$$\dot{u}(t) = g(u,v) = \tau\left[v + \gamma u - \frac{u^3}{3}\right] \quad (1)$$

$$\dot{v}(t) = h(u,v) = -\frac{1}{\tau}\left[u - \alpha + bv - I\right] \quad (2)$$

where u and v represent the fast and slow variables respectively. The network model with the coupling term having coupling strength c is given by:

$$\dot{u}_i(t) = g(u_i,v_i) - c\sum_{j=1}^{N} f_{ij}u_j(t-\Delta t_{ij}) \quad (3)$$

$$\dot{v}_i(t) = h(u_i,v_i) \quad (4)$$

where f represents the connection matrix and the time delays are computed from the distance matrix d and v is the propagation velocity,

$$\Delta t_{ij} = \frac{d_{ij}}{\mathrm{v}} \quad (5)$$

The simulations are carried out for rest state dynamics i.e. there is no external stimulus, $I = 0$, and parameter values are set as follows $\alpha = 1.05$, $b = 0.2$, $\gamma = 1.0$, $\tau = 1.25$. We vary the connection strength, c, and propagation velocity, v, to obtain the stability region from the spatiotemporal data. The stability diagram is shown in Figure 1.

It is interesting to see that by varying propagation velocity it is possible to stabilize/destabilize the system. To check for robustness we have varied the system parameters and recalculated the stability criteria. We observe that for moderate perturbations in the parameters the stability feature is robust and qualitative features are retained. While the above results confirm the resilience of the network we expect the stability feature to breakdown for random connectivity matrices. Starting from the connectivity matrix we rewire the edges by a probability, p, and by varying p obtain a completely random graph for $p = 1.0$ [7]. Now, performing the simulation and obtaining the stability index we observe that the stability feature is destroyed by systematically increasing p. This shows that the stability diagram is intrinsic feature of the underlying cortical network.

The aim of this work is to establish the functional relationship between different cortical regions. The instability that sets in the system is oscillatory in nature and tuning c or v it is possible to stabilize/destabilize the system. The nodes that set into oscillations will exhibit strong correlations depending on their functional connectivity. We have used principal component analysis on the spatiotemporal data to identify the dominant connectivity. The PCA is carried out on the spatiotemporal data in the following way: let the parameters be set to point A in Figure 1, which is a stable region and let the system run and settle to its fixed point and then tune the propagation velocity, v, such that the system is destabilized. The time at which v is decreased is indicated by the arrow and the corresponding time series is shown in Figure 2. Now performing PCA in moving windows it will be possible to see how many nodes are dominant as the system scans through stable to unstable region.

A typical result of PCA is shown in Figure 3. It is clearly evident that as destabilizing oscillations do set in the system, the spatiotemporal dynamics can have low dimensional representation in terms of two modes. Plotting the spatial modes for subsequent windows show that they have identical structure and we set a threshold -0.3, and identify those nodes having values below the threshold are most relevant. Thus we can identify the underlying functional network. (For the results shown in Figure 2 and 3 the network thus identified is shown in Figure 4.) The nodes are obtained from the first dominant PCA mode. It is observed that these areas are primarily involved in rest state brain irrespective of the region in parameter space we have analysed.

Illustrations and References

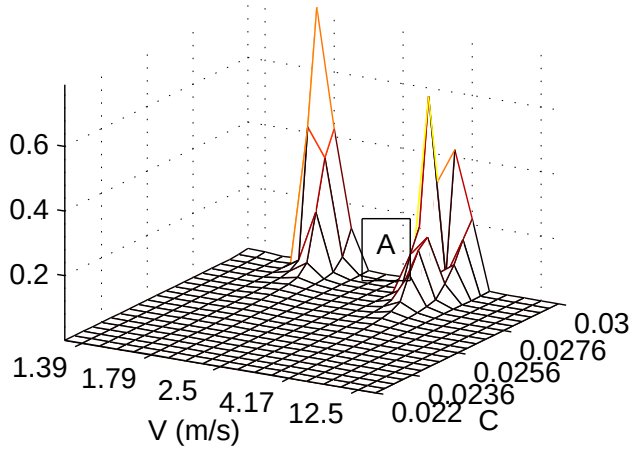

Figure 1: Stability diagram: A indicates the stable region lying between two unstable regions for $c = 0.03$.

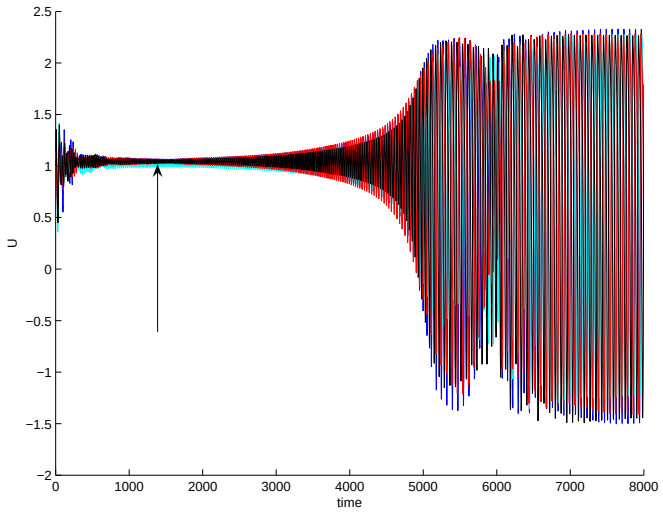

Figure 2: Time series plotted for all nodes shown for the fast variable u, details in text.

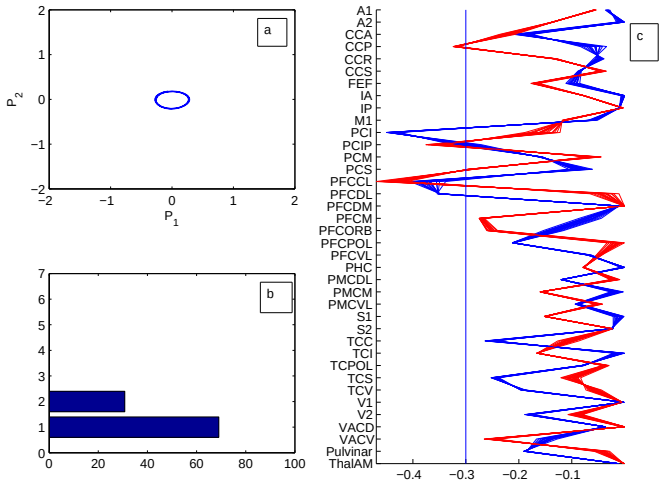

Figure 3: Results of PCA as instability sets in. (a) The phase portrait of 1st two principal components. (b) The percentile contribution of the 1st two principal components. (c) The spatial modes are shown for PCA applied on successive time windows for 1st mode (blue) and 2nd mode (red). The areas are considered active if the magnitude falls below threshold -0.3.

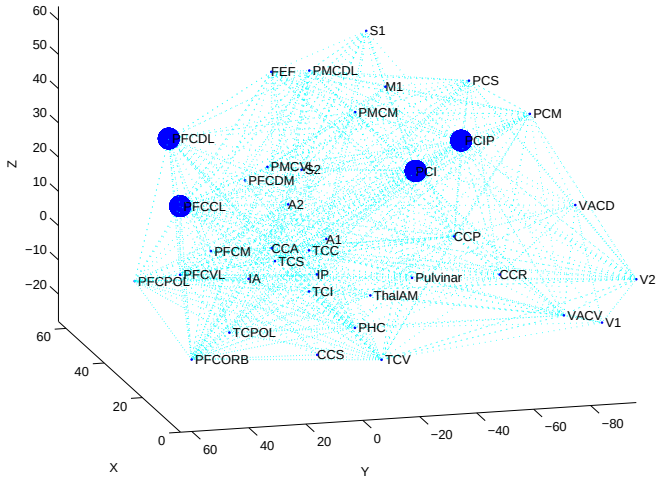

Figure 4: The functional network identified in the resting state of brain is shown as obtained from the 1st mode of the PCA.

References

[1] A. L. Hodgkin and A. F. Huxley “A quantitative description of membrane current and application to conduction and excitation in nerve”, J. Physiol., vol 117, pp. 500-544, 1954.

[2] G. Buszàki, Rhythms of the brain, Oxford University Press, 2006.

[3] M.D. Greicus, B. Krasnow, A.L. Reiss and V. Menon “Functional connectivity in the resting brain: A network analysis of the default mode hypothesis”, Proc. Natl. Acad. Sci. USA, vol 100 pp. 253-258, 2003.

[4] M.D. Fox, A.Z. Snyder, J.L. Vincent, M. Corbetta, D.C. Van Essen and M.E. Raichle “The human brain is intrinsically organized into dynamic, anticorrelated functional networks”, Proc. Natl. Acad. Sci. USA, vol 102 pp. 9673-9678, 2005.

[5] C. Honey, R. Kötter, M. Breakspear and O. Sporns “Network structure of cerebral cortex shapes functional connectivity on multiple time scales”, Proc. Natl. Acad. Sci. USA, in press 2007.

[6] R. FitzHugh, “Impulses and physiological states in models of nerve membrane”, Biophys. J., vol 1 pp. 445-466, 1961.

[7] D.J. Watts and S. H. Strogatz “Collective dynamics of ‘small-world’ networks”, Nature vol. 393 pp. 440-442, 1998.

DYNAMIC CAUSAL MODELS FOR MAGNETO- AND ELECTROENCEPHALOGRAPHY (M/EEG)

Stefan J. Kiebel[†,*] **and Karl J. Friston**[†]
[†] **Wellcome Trust Centre for Neuroimaging, 12 Queen Square, WC1N 3BG, London, UK**
[*]**Email: skiebel@fil.ion.ucl.ac.uk**

Introduction

Magneto- and Electroencephalograms have been used for decades to measure electrophysiological brain data. In particular, the responses to short stimuli, so called event-related fields (ERFs) and potentials (ERPs) have been used as putative magneto- and electrophysiological correlates of perceptual and cognitive operations. However, the exact neurobiological mechanisms underlying their generation are largely unknown. This is unfortunate, because MEG and EEG measure temporally well-resolved activity related directly to neuronal dynamics. Being able to infer about the system underlying these dynamics would make it possible to test cognitive hypotheses that see the brain as a dynamic hierarchical network.

Previous studies have shown that ERP-like responses can be reproduced by brief perturbations of model cortical networks [1], [7], [5], [6], [10]. The parameterization of these models is neurobiologically plausible and makes them valuable tools to look at the system 'brain'.

In particular, the Jansen & Rit neural mass model [5] explains ERPs by the output of a few coupled damped oscillators. When one combines dynamic networks of these cortical oscillators with the M/EEG observation function (i.e., the leadfield), one obtains a full spatiotemporal forward model for evoked responses [7]. Inversion of this forward model can be done using a Bayesian expectation-maximization (EM) algorithm [1].

Dynamic Causal Modelling

In Fig. 1, the ordinary differential equations of the temporal model aspect are shown. This coupled system, consisting of three neural masses (pyramidal cells, excitatory and inhibitory interneurons), describes the dynamics of one cortical area. For a bifurcation analysis of this model, see [4]. Output is generated as the depolarisation of the pyramidal cells, which causes extra-cellular current due to a voltage difference between their apical and basal dendrites. Interesting inferences can be made by postulating the differences between ERPs (e.g., different conditions of an experimental paradigm) due to a modulation of connection strength, either within- or between areas [8].

The full spatiotemporal model is inverted using a Bayesian Expectation-Maximization algorithm [2], [1], under the assumption of a normal observation error. We use informative priors on most of the parameters, which are known to lie in some physiological range.

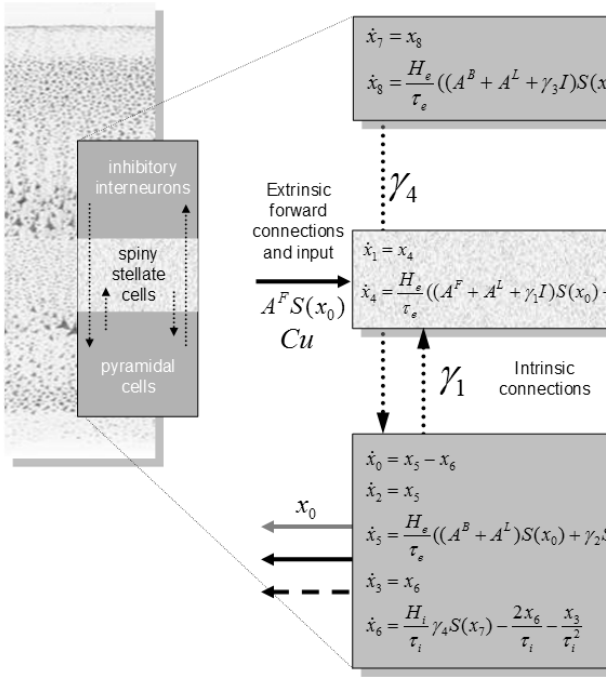

Figure 1: System of coupled 1st order differential equations describing the dynamics of a single cortical area. H_e, H_i, τ_e, τ_i are the maximum amplitudes and the decay times of a transmembrane-potential function, the function S is a sigmoid, u is the input, the matrix C the input efficacy, and $\gamma_1, \gamma_2, \gamma_3, \gamma_4$ control the connections strengths between subpopulations. Matrices A^F, A^B, A^L encode (long-range) connections strengths between cortical areas.

Importantly, the model evidence can be used for model comparison to select the best model among several candidate models. These candidate models can be predictions derived from competing cognitive or neurophysiological hypotheses. Results are typically reported over subjects, and the posterior means of the best model are inspected using confidence intervals. In a first application,

we have shown that the mismatch-negativity (MMN), a well-known M/EEG phenomenon, can be explained by a modulation of forward and backward connections, and can thus be construed as learning about the auditory environment [3].

Currently, our group uses this model, and variants of it, for analysis of evoked responses, time-frequency power data (Chen et al., in preparation), and local field potentials [9]. Ongoing work aims at making the model stochastic, i.e., allowing noise on the states x to take into account uncertainty about the neuronal states. The inversion of the stochastic model will be done using a Variational Bayes algorithm (Daunizeau et al., in preparation).

Conclusions

Dynamic Causal Modelling (DCM) is a new tool to analyse electrophysiological data based on neural mass models and their Bayesian inversion. The difference to conventional M/EEG analysis approaches is that DCM operates with physiologically grounded parameters, i.e., inferences can be related to the underlying system, the brain.

References

[1] David,O., Kiebel,S.J., Harrison,L.M., Mattout,J., Kilner,J.M., and Friston,K.J. Dynamic causal modeling of evoked responses in EEG and MEG. *Neuroimage*, 30: 1255 – 1272, 2006.

[2] Friston,K.J., Harrison,L., and Penny,W. Dynamic causal modelling. *Neuroimage*, 19: 1273 – 1302, 2003.

[3] Garrido,M., Kilner,J.M., Kiebel,S.J., Stephan,K.E., and Friston,K.J. Dynamic Causal Modeling of evoked potentials: A reproducibility study. *Neuroimage*, in press.

[4] Grimbert, F. and Faugeras, O. Bifurcation Analysis of Jansen's Neural Mass Model. *Neural Computation*, 18: 3052 – 3068 (2006).

[5] Jansen,B.H. and Rit,V.G. Electroencephalogram and visual evoked potential generation in a mathematical model of coupled cortical columns. *Biol.Cybern.*, 73: 357 – 366, 1995.

[6] Jirsa, V. Information processing in brain and behavior displayed in large-scale scalp topographies such as EEG and MEG. *Int. J. Bifurc.Chaos*, 14: 679 – 692, 2004.

[7] Kiebel,S.J., David,O., and Friston,K.J. Dynamic causal modelling of evoked responses in EEG/MEG with lead field parameterization. *Neuroimage*, 30: 1273 – 1284, 2006.

[8] Kiebel,S.J., Garrido, M., and Friston,K.J. Dynamic causal modelling of evoked responses: The role of intrinsic connections. *Neuroimage*, in press.

[9] Moran, R.J., Kiebel S.J., Stephan K.E., Reilly R.B., Daunizeau J., Friston K.J. A neural mass model of spectral responses in electrophysiology. *Neuroimage*, in press.

[10] Rennie, C.J., Robinson, P.A., Wright, J.J. Unified neurophysical model of EEG spectra and evoked potentials. *Biol. Cybern.*, 86: 457 – 471, 2002.

Magnetic Tomography for the Brain - Uniqueness and Nonuniqueness of Source Reconstructions

R. Potthast[†,*]
[†] Department of Mathematics, University of Reading, United Kingdom
[*]Email: r.w.e.potthast@reading.ac.uk

Abstract

We discuss the uniqueness and non-uniqueness of current reconstruction problems from measurements of the magnetic field outside of the region where the currents flow. Current reconstructions are of importance for magnetic brain imaging, where event related magnetic fields can be used to find regions of enhanced activity within the brain. Here, we study the mathematical theory behind such reconstructions. In particular, we will analyse the null-space $N(W)$ of the Biot-Savart integral operator W and provide characterizations of $N(W)$ and $N(W)^{\perp}$. We will construct particular elements in the null-space. Further, for the reconstruction of currents in single wire-lines or with a discrete set of sources, we will prove uniqueness for source reconstruction.

Introduction

We assume that we know the current distribution j in the domain $\Omega \subset \mathbb{R}^3$. We need to model the magnetic field from which we target to reconstruct the current density j. Magnetic fields H of currents j are calculated via the *Biot-Savart integral operator*, defined by

$$(Wj)(x) := \frac{1}{4\pi} \int_{\Omega} \frac{j(y) \times (x-y)}{|x-y|^3}\, dy, \quad x \in \mathbb{R}^3 \quad (1)$$

for $j \in L^2(\Omega)$. For details about this representation and its relation to Maxwell's equations we refer to [5]. The problem of magnetic tomography consists of solving the equation

$$Wj = H_{meas} \quad \text{on } \partial G, \quad (2)$$

where G is some domain with sufficiently smooth boundary such that $\overline{\Omega} \subset G$ and H_{meas} denotes some measured magnetic field on ∂G. Here, we need to supply appropriate conditions on the current densities j under consideration via the spaces on Ω and ∂G.

The simulation of currents has been studied in [5]. The uniquenss and non-uniqueness of current reconstructions is our topic here. Different approaches to current and obstacle reconstruction from measured magnetic fields are under development, compare [1], [2], [8], [7]. In particular, a general *Tikhonov regularization approach* is employed in [5], the *point source method* for field reconstructions and the no-response test in [4]. We also would like to refer to related work on real data reconstructions for the industrial *fuel-cell application* of magnetic tomography in [2]. Here we relate these results to the medical application, where currents and sources in the brain are under investigation.

Non-uniqueness for source reconstructions

An important problem for magnetic tomography is given by the uniqueness question. Does a magnetic field measured on ∂G determine the current distribution in Ω? This question naturally leads to basic subproblems. *First*, do the measurements on ∂G determine the analytic magnetic field in the exterior of Ω? *Second*, if the field is determined on Ω_e, does it uniquely determine the current distribution j in Ω. We will first give a simple example which demonstrates the strong non-uniqueness of the general magnetic tomography problem.

Consider a vectorial function $m \in C_0^2(\Omega)$ and define $j := \triangle m$. We calculate

$$\begin{aligned} (Wj)(x) &= \text{curl} \int_{\Omega} \frac{1}{4\pi} \frac{1}{|x-y|} \triangle m(y) dy \\ &= \text{curl} \int_{\Omega} \triangle_y \frac{1}{4\pi} \frac{1}{|x-y|} m(y) dy \\ &= 0, \quad x \notin \overline{\Omega} \end{aligned} \quad (3)$$

where we used Green's second theorem and $\triangle_y \frac{1}{|x-y|} = 0$ for $y \neq x$. The full nullspace is characterized via the following result [1].

THEOREM 1.1 *The nullspace of the Biot-Savart integral operator (1) is given by the set*

$$N(W) = \left\{ \text{curl } v : \ v \in H_0^1(\Omega), \text{div } v = 0 \right\}. \quad (4)$$

Thus there is a large nullspace. Special elements of the nullspace have been constructed in [1], compare Figure 1.

Connected to the uniqueness question is the characterization of the orthogonal space $N(W)^{\perp}$ of the nullspace $N(W)$ with respect to the $L^2(\Omega)$ scalar product

$$(\varphi, \psi)_{L^2(\Omega)} = \int_{\Omega} \overline{\varphi(y)} \psi(y)\, dy. \quad (5)$$

The space $N(W)^{\perp}$ is particularly interesting since the standard Tikhonov regularization projects the solution density j onto the space $N(W)^{\perp}$.

The following theorem is due to Kühn [4], extending results of [1].

THEOREM 1.2 *The* orthogonal space *of* $N(W)$ *is characterized by*

$$N(W)^{\perp} = \{j \in H_{\text{div }=0}(\Omega) : \exists q \in L^2(\Omega) \; s.th. \; \text{curl } j = \text{grad } q\}, \tag{6}$$

where $H_{\text{div }=0}(\Omega)$ *denotes the set of densities* j *in* H^1 *with* $\text{div } j = 0$.

An important *conclusion* of this result now follows from $\text{div } j = 0$ via $\text{curl curl } = -\triangle + \text{grad div}$. We derive

$$\triangle j = -\text{curl curl } j = -\text{curl grad } q = 0 \tag{7}$$

for each element of $N(W)^{\perp}$. Equation (7) is to be understood in $H^{-1}(\Omega)$. Thus the cartesian components of the current density j are weak solutions to Laplace's equation and via standard regularity results they are also a strong solution to Laplaces equation. As it is well known solutions of the Laplace equation satisfy a maximum-minimum principle, i.e. these functions take their maximum or minimum on the boundary of a domain. This is a strong limitation to the reconstruction algorithm via Tikhonov regularization which needs to be investigated further.

Uniqueness of ohmic currents with known background and of source locations

Here we show some further uniqueness results in magnetic tomography. We call currents *ohmic* when they do not have sources in the set Ω. A result about ohmic currents has been shown in [4], [1].

THEOREM 1.3 *Let* j *be an ohmic current in* Ω*, i.e. the current does not have any cources in the interior. Then we have*

$$j \perp_{\sigma} N(W) \tag{8}$$

with orthogonality with respect to the scalar product

$$(\varphi, \psi)_{\sigma} := \int_{\Omega} \varphi(y) \cdot \sigma(y)^{-1} \overline{\psi(y)} dy. \tag{9}$$

The theorem shows that if σ is known, then the currents are in exactly the right space for unique reconstruction. However, if σ would be known we could calculate the currents by solving the forward problem and would not need the magnetic field measurements. Usually σ is unknown, that is the crucial point. In this sense the result of Theorem 1.3 does not help to answer the uniqueness question nor does it provide an algorithm for the reconstruction. However, if σ is close to a homogeneous function, then the scalar product is close to the standard L^2 scalar product and we can employ an approximation argument. In this case we conclude that Tikhonov regularization will calculate a reasonable reconstruction by projecting onto the space $N(W)^{\perp}$ instead of the close space $N(W)^{\perp_{\sigma}}$.

We now finish with some uniqueness results for particular settings.

THEOREM 1.4 *The current in a discrete wire grid* $\mathcal{G}$ *is uniquely determined by its magnetic field measured on the boundary* ∂G *outside of the domain* Ω *containing* $\mathcal{G}$.

The result [1] is due to the fact that the magnetic field $H(x)$ generated by a wire line γ with non-vanishing current has a singularity for $x \to \gamma$.

Next, assume that the current is coming from a finite set of discrete sources

$$H_j(x) = \beta_j \times \nabla \Phi(x, z_j), \quad x \in \mathbb{R}^3 \tag{10}$$

where

$$\Phi(x, z) = \frac{1}{4\pi} \frac{1}{|x - z|}, \quad x \neq z, \tag{11}$$

with source points $z_1, ..., z_N$, $z_j \neq z_k$ for $j, k \in N \in \mathbb{N}$ and source strength $\beta_j \in \mathbb{R}^3$, which also describes the direction of the local current β_j. This model for biomedical imaging is described in [3], Chapter 7.3. In this case, the measured magnetic field H is given by

$$H(x) = \sum_{j=1}^{N} \beta_j \times \nabla \Phi(x, z_j), \quad x \in \mathbb{R}^3 \tag{12}$$

With the same argument as for Theorem 1.4 we derive the following basic result on source reconstruction.

THEOREM 1.5 *The location* z_j *as well as the direction and strength* β_j *of any set of discrete sources is uniquely determined by its magnetic field measured on the boundary* ∂G *outside of the domain* Ω *containing the source points* $z_1, z_2, ..., z_N$.

Proof. First, we note that as shown in [5] the measurements of H on ∂G uniquely determine H in the exterior of G. By analyticity of the fields in $M := \mathbb{R}^3 \setminus \{z_1, ..., z_N\}$ it determines the field in M. Clearly, in z_j, $j = 1, ..., N$, the fields are singular. Thus the source points z_j are uniquely determined by the field itself.

The strength of the singularity can now be used to both calculate the length and direction of the vector β_j, i.e. the direction and strength of the sources, as follows. We note that the gradient $\nabla\Phi(x,z)$ has the direction

$$d = -\frac{x-z}{|x-z|}. \tag{13}$$

The vector product $\beta \times d$ is zero only if $d \parallel \beta$, which determines the direction of β from the knowledge of H up to a sign. The size and sign of β can now be calculated for example by evaluation of $H(x)$ at a point x such that $x - z \perp \beta$ and division by $|x-z|$. □

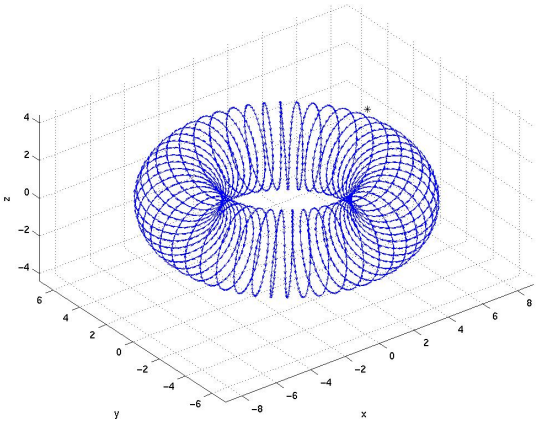

Figure 1: Element of the nullspace of the Biot-Savart integral operator.

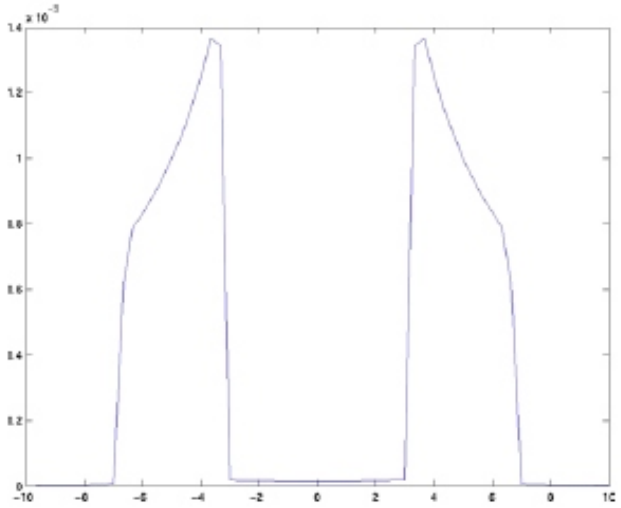

Figure 2: We show the magnetic field on a line crossing the above ring. Here, the field inside is large, outside close to zero.

References

[1] Hauer, K.-H., Kühn, L. and Potthast, R.: "On uniqueness and non-uniqueness for current reconstruction from magnetic fields." Inverse Problems 21 (2005) 1-13.

[2] Hauer, K.-H., Potthast, R., Stolton, D. and Wüster, T.: "Magnetotomography - A New Method for Analysing Fuel Cell Performance and Quality." Journal of Power Sources 143 (2005), 67-74.

[3] Kaipio, J. and Sommersalo, E.: *Computational and Statistical Methods for Inverse Problems* Springer 2004.

[4] Kühn, L.: Magnetic Tomography - On the Nullspace of the Biot-Savart Operator and Point Sources for Field and Domain Reconstruction. Dissertation Göttingen 2005.

[5] Kühn, L., Kreß, R. and Potthast, R.: "The reconstruction of a current distribution from its magnetic fields." Inverse Problems 18, 1127-1146 (2002).

[6] Kühn, L. and Potthast, R.: "On the convergence of the finite integration technique for the anisotropic boundary value problem of magnetic tomography." Math. Meth. Appl. Sciences 26 (2003), 739-757.

[7] Potthast, R.: A survey about sampling and probe methods for inverse problems. Topical Review. Inverse Problems 22 (2006), R1-47.

[8] Potthast, R., Stratis, I.G. and Yannacopoulos, A.N.: "On the stochastic magnetic tomography problem", submitted for publication.

BIFURCATIONS TO SEIZURE WAVEFORMS IN MACROSCALE MODELS OF HUMAN EEG

Serafim Rodrigues[†], Anton V. Chizhov[†], Jorge Goncalves[†], Michael Breakspear[†], and John R. Terry[†,*]

[†]Department of Engineering Mathematics, University of Bristol, BS8 1TR, UK
[*]Email: J.R.Terry@bristol.ac.uk

The brain is a multi-scale system with a complex hierarchical organization, which has been studied using several experimental techniques. This hierarchical organization varies from the level of the single neuron to that of whole brain regions. As these scales change, so the techniques for modelling the recorded activity alter from probabilistic (in some sense) to structured. Equally, the temporal dynamics vary from discrete events (i.e. spikes) to continuous rhythmic activity as may be observed via scalp EEG. Systematic experimental results on the multi-scale characteristics of the brain have motivated a number of theoretical approaches. In particular, under the *dynamical hypothesis* [1], mathematical models have been proposed to successfully describe these levels of experimentally recorded phenomena. For example, at the microscale, the Hodgkin-Huxley model [2] and related conductance-based models successfully explain the temporal dynamics of an individual neuron. Whilst at the macroscopic scale, *Neural field* models [3], [4], [5], *Neural mass* models [6], [7], [8] and models based on *Population density* [9] are employed to describe dynamical activity of LFP and EEG. To analyse complex systems, techniques such as *separation of scales* can be employed to enable mathematical analysis. However, it is not apparent that a physiological equivalent of separation of scales exists in the brain and is still a source of debate among neuroscientists. One explanation for the uncertainty of this approach in neuroscience is the fact that many processes in the brain operate on several spatial and/or temporal scales, hence providing strong interactions between them. For instance, neurons produce spikes whose timing is in some cases up to a millisecond precise [10]. On the other hand, there are examples showing that a lot of information is transmitted between neurons via variations in the average firing rate, which occur in the time scales of hundreds of milliseconds [11]. Thus, it is unclear when and how to 'coarse-grain' in order to move from one scale to another, as well as if this procedure is valid at all. Despite this, mathematical techniques have been developed, two approaches in particular are widely used to study neural field models. One approach by Ermentrout [12] utilizes thermodynamic theory which describes the activity of all neurons within a population by a single macroscopic variable. A similar derivation, which holds for averaging over Poisson inputs for a large network, used in conductance based models was introduced by Shriki [13].

One area of importance is the modelling of human EEG using macroscopic models, as it has been suggested that tracking dynamical changes in this models could be applicable in diagnosis of neurological disorders [14], [15]. The purpose of this talk is to give an overview of our recent work in this area, focussing on the use of macroscale models in studying human EEG. In particular we observe that the transition to generalized seizure states is linked to bifurcations arising out of a variation of a parameter representing the strength of connectivity between cortex and the specific relay nuclei in the thalamus. Since the parameters of these macroscale models considered are lumped together, they do not have a direct physical interpretation. However, by developing a mapping between scales, some understanding of the relationship between parameters at the macroscale and physiological parameters of reduced conductance-based models can be obtained. We will discuss techniques for achieving such mappings, as well as outline how these approaches may be used in epilepsy seizure prediction.

References

[1] T. V. Gelder. The dynamical hypothesis in cognitive science. *Behavioral and Brain Sciences*, 21:615–665, 1988.

[2] A. L. Hodgkin and A. F. Huxley. A quantitative description of membrane current and its application to conduction and excitation in nerve. *Journal of Physiology*, 117:500–44, 1952.

[3] H. R. Wilson and J. D. Cowan. Excitatory and inhibitory interactions in localized populations of model neurons. *Biophysical Journal*, 12:1–24, 1972.

[4] P. L. Nunez. *Neocortical Dynamics and Human EEG Rhythms.* Oxford University Press, 1995.

[5] V. K. Jirsa and H. Haken. Field theory of electromagnetic brain activity. *Phys. Rev. Lett.*, 77:960, 1996.

[6] W. J. Freeman. *Mass Action In The Nervous System. Examination of the Neurophysiological Basis of Adaptive Behavior through the EEG.* Academic Press New York San Francisco London, 1975.

[7] F. H. Lopes da Silva, A. Hoeks, H. Smits, and L. H. Zetterberg. Model of brain rhythmic activity. the alpha rhythm of the thalamus. *Kybernetik*, 15:27–37, 1974.

[8] B. H. Jansen and V. G. Rit. Electroencephalogram and visual evoked potential generation in a mathematical model of coupled cortical columns. *Biol. Cybern*, 73(357-366), 1995.

[9] A. Omurtag, B. W. Knight, and L. Sirovich. On the simulation of large populations of neurons. *Journal of computational neuroscience*, 8:51–63, 2000.

[10] M. J. Berry, D. K. Warland, and M. Meister. The structure and precision of retinal spike trains. *Proc. Natl. Acad. Sci. USA*, 94(10):5411–5416, 1997.

[11] A. Borst and F. E. Theunissen. Information theory and neural coding. *Nat. Neurosci.*, 2(11):947–957, 1999.

[12] B. Ermentrout. Reduction of conductance based models with slow synapses to neural nets. *Neural Comp.*, 6:679–695, 1994.

[13] O. Shriki, D. Hansel, and H. Sompolinsky. Rate models for conductance-based cortical neuronal networks. *Neural Comp.*, 15:1809–1841, 2003.

[14] M. Breakspear, J. A. Roberts, J. R. Terry, S. Rodrigues, N. Mahant, and P. A. Robinson. A unifying explanation of primary generalized seizures through nonlinear brain modeling and bifurcation analysis. *Cerebral Cortex*, 16:1296–1313, 2006.

[15] S. Rodrigues, J. R. Terry, and M. Breakspear. On the gensis of spike-wave activity in a mean-field model of human thalamic and cortico-thalamic dynamics. *Physics Letters A*, 355:352–357, 2005.

CORTICAL WAVES AND THE DEVELOPMENT OF CORTICAL ANATOMY

J. J. Wright[†,‡,*] **and P.D. Bourke**[§]

[†]**Liggins Institute and Department of Psychological Medicine, University of Auckland, Auckland, New Zealand.**
[‡]**Brain Dynamics Centre, University of Sydney, Sydney, Australia.**
[§]**WASP, University of Western Australia, Perth, Western Australia, Australia.**
[*]**Email: jj.w@xtra.co.nz**

Abstract

The transmission of waves through the neurons of the cortical mantel, and the development of synapses related to learning, can give rise to the complex structure of neural connections which emerges during growth of the visual cortex.

Synaptic connections in V1

In the visual cortex (V1) and cortex generally, the density of synaptic couplings generated by each neuron declines with distance from the soma of the cell of origin, at two scales — that of the local intra-cortical connections (at the V1 macrocolumnar scale), versus the longer intracortical connections [10], [4], [7]. Thus, visual information can reach each macrocolumn-sized area, from the whole, or a substantial part, of V1. It has been proposed [17] that via the mediation of waves of brain activity, *local maps* of synaptic connections emerge at the macrocolumnar scale, which form a tiling of V1, each local map being a representation of the visual field — the *global map* — projected to V1 by the visual pathway.

Cortical waves and synchronous fields

At all scales, the cortex of the brain supports traveling waves of depolarization of the cortical cells, mediated by axonal and dendritic transmission. Theoretically, these waves selectively eliminate of out-of-phase activity during wave interference [15], [9], [16], [5] explaining the observed occurrence of *synchronous oscillation* (e.g., [11]). Because of the decline of synaptic density with distance, the spatial covariance (the magnitude of synchronous oscillation) between any pair of pyramidal neurons in V1 declines with distance Thus, covariance of activity (the average magnitude of synchronous oscillation) in V1 declines with distance at both the global, V1, scale, and the local, macro-columnar, scale. This effect can provide a metric for organization of the local maps from the global map, as follows.

Learning rules and constraints on stable solutions

At each synapse the co-incidence of pre and post synaptic activity, $r_{Q\varphi}$, over a short epoch, t, is given by

$$r_{Q\varphi} \propto \sum_t Q_e(t) \times \varphi_e(t)\,, \tag{1}$$

where $Q_e(t) \in [0,1]$ is the postsynaptic firing rate, and $\varphi_e(t) \in [0,1]$ is the presynaptic firing rate. A Hebbian multiplication factor, H_s, operating on the gain of synapses at steady rates of pre- and post-synaptic firing, in simplest form, is

$$H_s = H_{\max} \exp(-\lambda / r_{Q\varphi})\,, \tag{2}$$

where λ is a suitable constant.

With changes in $r_{Q\varphi}$, H_s can increase or decline over time. Fields of synchronous oscillation organize the values of $r_{Q\varphi}$ through the cortical field.

Synapses can approach a stable state only by approaching either one of two extremes – with $r_{Q\varphi}$ approaching a maximum (*saturated state*) or a minimum (*sensitive state*) respectively. (These states can correspond to different physiological forms on different time scales.)

Competition occurring for metabolic resources within axons adds a further constraint to stable end-points for synaptic development [6] — viz: the proportion of saturated and sensitive synapses must be uniform along axons.

Overall synaptic stability

All positions in V1, $\{P_{j,k}\}$, can be given an ordered numbering in the complex plane, $1 \ldots, j, \ldots, k, \ldots, 2n$, and all positions within a representative macrocolumn located at P_0, $\{p_{j,k}\}$, can be similarly numbered. The total perturbation of synaptic gains in all the synapses from V1 entering the macrocolumn, $\Psi(pP)$, and the total perturbation of synaptic gains within the macrocolumn, $\Psi(pp)$,

can be written

$$\Psi(pP) = \sum_{j=1}^{j=n}\sum_{k=1}^{k=n}\sigma_{SAT}(p_jP_k)S_{SAT}(p_jP_k) + \quad (3)$$
$$\sum_{j=1}^{j=n}\sum_{k=1}^{k=n}\sigma_{SENS}(p_jP_k)S_{SENS}(p_jP_k)$$

$$\Psi(pp) = \sum_{j=1}^{j=n}\sum_{k=1}^{k=n}\sigma_{SAT}(p_jp_k)S_{SAT}(p_jp_k) + \quad (4)$$
$$\sum_{j=1}^{j=n}\sum_{k=1}^{k=n}\sigma_{SENS}(p_jp_k)S_{SENS}(p_jp_k)\,,$$

where $\sigma_{SAT}(p_jP_k, p_jp_k)$ and $\sigma_{SENS}(p_jP_k, p_jp_k)$ are densities of synapses approximately saturated, or approximately sensitive, and $S_{SAT}(p_jP_k, p_jp_k)$ and $S_{SENS}(p_jP_k, p_jp_k)$ are the corresponding variations of synaptic gains over a convenient short epoch. Since densities of synapses decline with distances of cell separation, then as a simple arithmetic property of sums of products, approximation to minimization of $\Psi(pp)$ requires synapses connecting neurons separated by short distances to most closely approach either maximum saturation, or maximum sensitivity. An analogous requirement is imposed on minimization of $\Psi(pP)$, and metabolic uniformity requires that both sensitive and saturated synapses from each axon must remain locally in equal ratio.

A stable solution meeting these requirements can be found in a unique topology, mapping the global to the local map This can be described by renumbering $\{P_{j,k}\}$ as $\{P_{j1,j2,k1,k2}\}$, and $\{p_{j,k}\}$ as $\{p_{j1,j2,k1,k2}\}$, the subscript numbers $1,\ldots,j1,\ldots,j2,\ldots,n,(n+1),\ldots,j2,\ldots,k2,\ldots,2n$ can be ascribed in the global map so that $j1$ and $j2$ are located diametrically opposite and equidistant from P_0, while in the local map $j1$ and $j2$ have positions analogous to superimposed points located on opposite surfaces of a Möbius strip. This generates a *Möbius projection* (the *input map*) from global to local, and a *Möbius ordering* within the local map. That is,

$$\frac{P_{jm}^2}{|P_{jm}|} \rightarrow p_{km}, \qquad m \in \{1,2\} \quad (5)$$

and

$$p_{jm} \rightarrow p_{km} \qquad m \in \{1,2\}\,. \quad (6)$$

Evolution of these patterns of synaptic connections is shown in Figs. 1 and 2. In Eq. (5) the mapping of widely separated points in the global map converge to coincident points on opposite surfaces of the local map's Möbius representation. In Eq. (6) the density of saturated synaptic connections now decreases as $|j1-k1|$ and $|j2-k2|$, while the density of sensitive couplings decreases as $|j2-k1|$ and $|j1-k2|$.

Anatomically, this requires $j1$ and $j2$ in the local map to represent two distinct groups of neurons. To attain maximum synaptic stability within the local map an intertwined mesh of saturated couplings forms, closed after passing twice around the local map's centre, with sensitive synapses locally linking the two turns of the mesh together. In this fashion both saturated and sensitive synapses decline in density with distance, as required. The input map is of corresponding form, conveying an image of the activity in V1 analogous to projection onto a Möbius strip.

Since the projection of the global map upon the local map conserves relative correlations in the global map as a function of distance, convergence toward the stable configuration will be facilitated by a modification of the Hebbian rule with a recently demonstrated physiological basis — the *spatio-temporal learning rule* [13], [14] in which covariance among afferent synapses, as well as pre-postsynaptic neurons, facilitates the strength of synaptic connection.

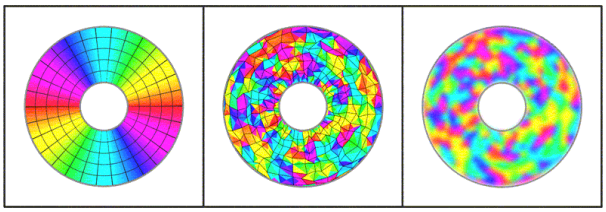

Figure 1: Initial conditions for local evolution of synaptic strength. *Left*. The global field (V1) in polar co-ordinates. Central defect indicates the position of a local area of macro-columnar size. Polar angle is shown by the color spectrum, twice repeated. *Middle*. Zones of random termination (shown by color) of lateral axonal projections from global V1 in the local area. Central defect is an arbitrary zero reference. *Right*. Transient patterns of synchronous oscillation generated in the local area, mediated by local axonal connections.

Monosynaptic interactions between adjacent local maps

Adjacent local maps form in approximately mirror image relation, as shown in Fig. 3, because in that configuration homologous points within the local maps have densest saturated and sensitive synaptic connections, thus meeting minimization requirements analogous to those of

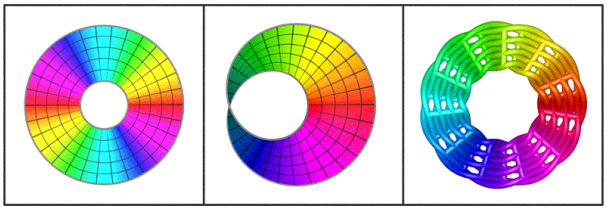

Figure 2: Evolution of synaptic strengths to their maximally stable configuration. *Left*. The global field (V1), as represented in Fig. 1. *Middle*. Saturated synaptic connections input from the global field now form a Möbius projection of the global field, afferent to the local neuronal field, and forming a local map. *Right*. Saturated local synapses, within the local map, form a mesh of connections closed over $0 - 4\pi$ radians. The central defect now corresponds to the position within the local map, of the local map within the global map. Sensitive synapses (not shown) link adjacent neurons as bridges between the $0 - 2\pi$ and $2\pi - 4\pi$ limbs of the mesh of saturated connections (Wright 2006).

Eq. (3) and Eq. (4).

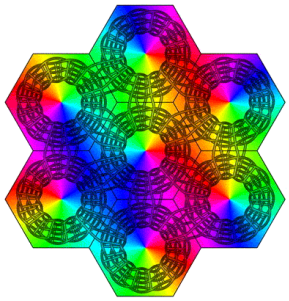

Figure 3: Organization of saturated coupling within and between local maps, and the approximate mirror symmetry of orientation preference in adjacent local maps (Wright 2006).

Conformity to experimental data

These principles can accounts for response preferences of V1 neurons to visual stimuli, orientation preference singularities, linear zones and saddle points, connections between cells of similar orientation preference in adjacent macrocolumns [3], ocular dominance columns [8], occurrence of direction preference fractures always in odd numbers around singularities [12] and the dynamic variation of orientation preference with stimulus velocity, stimulus orientation relative to direction of motion, and stimulus extension, discovered by Basole et al. [2].

References

[1] D. M. Alexander, P. D. Bourke, P. Sheridan, O. Konstandos, and J. J. Wright. Emergent symmetry of local and global maps in the primary visual cortex: self-organization of orientation preference. *Proceedings Complex Systems*, 98: 25 – 31, 1998.

[2] A. Basole, L. E. White and D. Fitzpatrick. Mapping multiple features of the population response of visual cortex. *Nature*, 423: 986 – 990, 2003.

[3] W. H. Bosking, Y. Zhang, B. Schofield and D. Fitzpatrick. Orientation selectivity and the arrangement of horizontal connections in tree shrew striate cortex. *J. Neuroscience*, 17(6): 2112 – 2127, 1997.

[4] V. Braitenberg and A. Schüz. *Anatomy of the Cortex: Statistics and Geometry*. Springer-Verlag, New York. 1991.

[5] C. L. Chapman, P. D. Bourke and J. J. Wright. Spatial eigenmodes and synchronous oscillation: coincidence detection in simulated cerebral cortex. *J. Math. Biol.*, 45: 57 – 78, 2002.

[6] S. Grossberg and J. R. Williamson. A neural model of how horizontal and interlaminar connections of visual cortex develop into adult circuits that carry out perceptual grouping and learning. *Cerebral Cortex*, 11: 37 – 58, 2001.

[7] D. T. J. Liley and J. J. Wright. Intracortical connectivity of pyramidal and stellate cells: estimates of synaptic densities and coupling symmetry. *Network*, 5; 175 – 189, 1994.

[8] K. Obermayer and G. G. Blasdel. Geometry of orientation and ocular dominance columns in monkey striate cortex. *J. Neuroscience*, 13(10): 4114 – 4129, 1993.

[9] P. A. Robinson, C. J. Rennie and J. J. Wright. Synchronous oscillations in the cerebral cortex. *Physical Review*, E 57: 4578 – 4588, 1998.

[10] D. A. Scholl. *The Organization of the Cerebral Cortex*. Wiley, New York. 1956.

[11] W. Singer Putative functions of temporal correlations in neocortical processing. In: C. Koch and J. L. Davis (Eds.) *Large Scale Neuronal Theories of the Brain*. MIT Press, Cambridge Mass., London, 1994.

[12] N. V. Swindale, D. Shoham, A. Grinvald, T. Bonhoeffer, and M. Hubener. Visual cortical maps are optimised for uniform coverage. *Nature Neuroscience*, 3(8): 822 – 826, 2000.

[13] M. Tsukada, T. Aihara, and H. Saito. Hippocampal LTP depends on spatial and temporal correlation of inputs. *Neural Networks*. 9: 1357 – 1365, 1996.

[14] M. Tsukada and X. Pan. The spatio-temporal learning rule and its efficiency in separating spatiotemporal patterns. *Biological Cybernetics*, 92: 139 – 146, 2005.

[15] J. J. Wright. EEG simulation: variation of spectral envelope, pulse synchrony and 40 Hz oscillation. *Biological Cybernetics*, 76:181 – 184, 1997.

[16] J. J. Wright, P. D. Bourke and C. L. Chapman. Synchronous oscillation in the cerebral cortex and object coherence: simulation of basic electrophysiological findings. *Biological Cybernetics*, 83:341 – 353, 2000.

[17] J. J. Wright, D. M. Alexander and P. D. Bourke. Contribution of lateral interactions in V1 to organization of response properties. *Vision Research*, 46: 2703 – 2720, 2006.

Minisymposium on Inverse Problems

Organisers: Houssem Haddar (INRIA) and Roland Potthast (University of Reading)

RESOLUTION IMPROVEMENT OF ANALYTICAL CONTINUATION METHOD BY MULTIVIEW DATA

I. Akduman[†], M. Çayören[†], A. Yapar[†] and L. Crocco[‡]
[†] Istanbul Technical University, Electrical and Electronics Engineering Faculty, 34469, Maslak, Istanbul, Turkey
[‡] CNR-IREA, Institute for Electromagnetic Sensing of Environment, I-80124, Naples, Italy
*Email: akduman@itu.edu.tr

Abstract

An analytical continuation method for the reconstruction of perfectly conducting bodies was introduced by Çayören et al [1]. The method based on a special representation of the scattered field in terms of single layer potential and Taylor series expansion, and yields very accurate results in the illuminated part of the object for a single illumination at a fixed frequency. In this study, a procedure is proposed to improve the resolution of the reconstructions by using multi-view configuration. The numerical studies shows that this approach yields quite accurate reconstructions and is robust against noise on the data.

Introduction

In [1], a simple method to determine the shape of a 2D PEC target located in an infinite homogeneous space was introduced. In that work the body, whose size is assumed to be comparable to the wavelength, is reconstructed using a single plane wave at a fixed frequency by measuring the corresponding the scattered field over a circular domain. The basic idea of the method is that the region external to the body can be fictitiously separated into two parts by a circle which covers the object. Such a circle is chosen close to the minimum one enclosing the scatterer, whose radius is either a priori known or extracted through a simple processing of measured data [2]. The scattered field in the region external to the circle is then expressed in terms of a single-layer potential [3], whose density function is achieved solving a properly regularized inverse problem. Conversely, the field inside the circle is represented through a Taylor series expansion [4], whose (few) coefficients are computed using the field arising from the single-layer potential representation. By applying the condition that the total electric field must vanish on the unknown boundary the problem is recast as the solution of a non-linear equation which is solved through the application of the Newton's method. Despite its simplicity, the method is quite general as it can reconstruct both convex and concave surfaces in the low frequency region. For high frequencies the method gives only satisfactory reconstructions in the illuminated part and is not robust against the noise on data.

In this work, the method is extended to the multi-incidence case. To this aim the body is illuminated by a certain number of plane waves and for each illumination the reconstruction is obtained through the method given in [1]. Then by taking the reconstructed portions in the illuminated parts and combining them with an averaging procedure at the connection points, a new reconstruction is obtained. This new approach provides quite accurate reconstructions in the high frequency regime.

An Analytical Continuation Method for Shape Reconstruction

The two-dimensional scattering problem which is considered here is illustrated in Figure 1. In this configuration D is a perfectly conducting cylindrical body whose boundary ∂D is defined by the parametric equation $\rho = f(\phi)$, $\phi \in (0, 2\pi)$ where (ρ, ϕ) are the cylindrical polar coordinates. The body D is located in a homogeneous infinite space whose electromagnetic constitutive parameters are ε, μ_0 and σ.
The inverse scattering problem considered here consists in recovering the shape of the body D, i.e., the function $f(\phi)$, from a set of measurements of the scattered wave on a circular domain. To this aim, the body D is illuminated by N time-harmonic plane waves $\vec{E}_n^i = (0, 0, u_n^i(\rho, \phi))$ with incidence angles θ_n, $n = 1, ..N$.

For each incident field the region outside the object is separated into two parts by a circle which is assumed to be the minimum one with radius a covering the object. The scattered field in the region $\rho > a$ is represented in terms of a single layer potential

$$u_n^s(\rho, \phi) = \frac{i}{4} \int_0^{2\pi} H_0^{(1)}(k\sqrt{\rho^2 + a^2 - 2\rho a \cos(\phi - \tau)}\,)\Psi_n(\tau) a d\tau, \quad (1)$$

with an unknown density function Ψ_n on the circle $\rho = a$ [3], where $H_0^{(1)}$ denotes the zero order Hankel function of the first kind while k is the wavenumber.

Then the use of the measured data on the circle $\rho = R$, say $u_n^s(R, \phi)$, leads the following equation for the unknown density function Ψ_n

$$A\Psi_n = u_n^s(R, \phi) \quad (2)$$

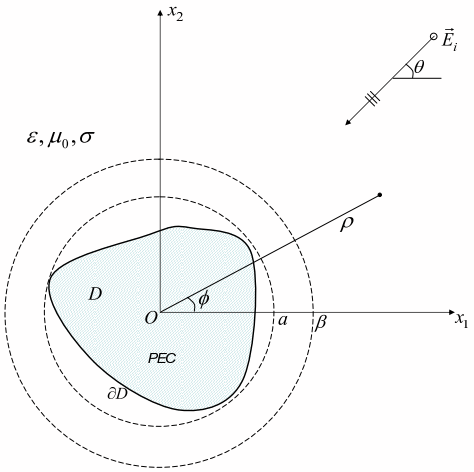

Figure 1: Geometry of the problem.

where the integral operator A is given by

$$A\Psi = \frac{i}{4}\int_0^{2\pi} H_0^{(1)}(k\sqrt{R^2+a^2-2Ra\cos(\phi-\tau)}\,)\Psi(\tau)ad\tau. \tag{3}$$

The operator A has an analytic kernel and therefore the equation (2) is ill-posed. For this reason, some kind of regularization has to be applied and only an approximation of the sought function Ψ_n can be achieved. Here we applied the truncated SVD algorithm as a regularization procedure [5].

Let us now turn to the interior region $f(\phi) < \rho < a$. Within the approximation introduced by the TSVD inversion the total field $u_n = u_n^s + u_n^i$ in this region can be obtained by using the field $u_n^s(\rho,\phi)$ given by (1). In particular, $u_n(\rho,\phi)$ is expanded into a Taylor series in terms of ρ around the circle $\rho = \beta$, where $a \leq \beta$, see Figure 1, as follows [4]:

$$u_n(\rho,\phi) = \sum_{m=0}^{M} c_m^n \left(\frac{\rho-\beta}{\lambda}\right)^m + R_M^n(\rho,\phi),\ \ \rho \in (f(\phi),\beta]. \tag{4}$$

with coefficients

$$c_m^n = \frac{\lambda^m}{m!}\frac{\partial^m u_n(\beta,\phi)}{\partial\rho^m} \tag{5}$$

and remainder term $R_M^n(\rho,\phi)$, where λ is the wavelength.

The m'th order derivatives of $u_n(\rho,\phi)$ at $\rho = \beta$ appearing in the right hand side of (5) can be obtained from (1).

Since the total field $u_n(\rho,\phi)$ in the whole region $\rho > f(\phi)$ can be estimated through (1) and (4), the reconstruction of the boundary ∂D can now be achieved by searching those points where this latter field vanishes which leads the non-linear equation

$$F_n(f) = 0 \tag{6}$$

where F_n is the operator given by

$$F_n(f) = \sum_{m=0}^{M} c_m^n \left(\frac{\rho-\beta}{\lambda}\right)^m = 0. \tag{7}$$

after neglecting the remainder term. Note that, for given data, the coefficients c_m^n in (7) are all known. Thus the reconstruction problem is reduced to the solution of non-linear equation (6) for the unknown function f. This non-linear equation is solved through a linearization procedure in the Newton sense which results in the iteration procedure

$$F_n'(f_i)\Delta f_{i+1} = -F_n(f_i),\ \ i = 0,1,2,3,.... \tag{8}$$

for Δf_{i+1} to obtain a sequence of approximations through $f_{i+1} = f_i + \Delta f_{i+1}$.

Note that the solution of (6) is a function of incident direction thus for each illumination the above method will give a solution f_n, $n = 1,..N$. As mentioned earlier the above method yields satisfactory reconstructions of the illuminated part of the object for the high frequency regime. Thus each solution f_n has an accurate part in the illuminated region of the object. By considering this fact one can get a high resolution image by combining the accurate parts of each reconstructed surface function f_n. In this procedure, the reconstructions at the connection points are obtained by simply averaging two adjacent solutions.

Numerical Results

In this section we provide some numerical results which demonstrate the validity and effectiveness of the method. In all cases, the body is illuminated by plane waves of incidence directions $\theta_1 = 0$, $\theta_2 = \pi/2$, $\theta_3 = \pi$ and $\theta_4 = 3\pi/2$ and the body is assumed to be located in free-space. The scattered field data are synthetically generated by solving the associated forward problem through the mixed double and single-layer potential approach [3]. The number of measurement points is 200 and a random noise is added to the simulated data. In particular, a random term $n_l|u_m^s|e^{2ir_d\pi}$ is added to each scattered field

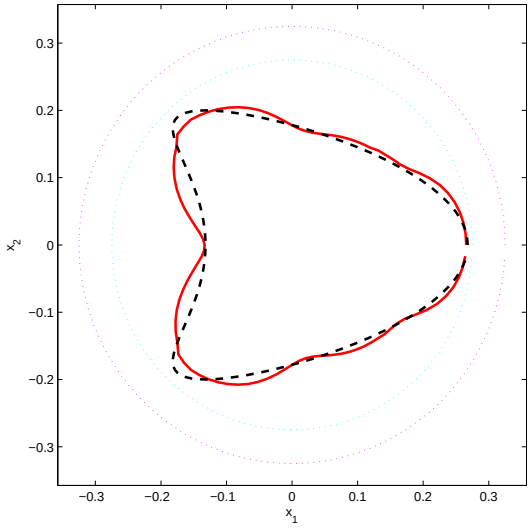

Figure 2: Exact geometry (dashed line) ; reconstructed shape with noisy data (solid line); .

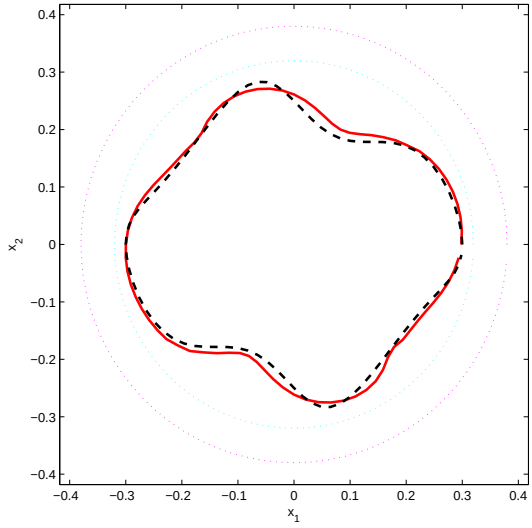

Figure 3: Exact geometry (dashed line) ; reconstructed shape with noisy data (solid line); .

value u_n^s, n_l being the noise level and r_d a random variable between 0 and 1. As a first example we consider a kite shaped object. In this case the operating frequency is chosen as $f = 700MHz$. The number of terms which is taken in the Taylor expansion is $M = 4$. The radius of the minimum circle covering the object is chosen as $a = 0.275$ and the scattered field is expanded in to Taylor series around the circle $\beta = 0.325$. Figure 2 illustrates the exact and reconstructed shapes for a given data containing 5% noise. As it can be observed, the reconstruction is quite accurate and is quite robust against noise on data.

The second example is related to a "potato"-shaped body. The exact and reconstructed shapes are presented in Figure 3 where the reconstruction is obtained for $a = 0.32$, $\beta = 0.38$, $M = 4$, and $f = 600MHz$. From the illustrative examples given above, one can conclude that the proposed method is capable of providing quite satisfactory reconstructions in the multi-view configuration. With the proposed approach the method given in [1] is extended to the high frequency regime. Note that, as only few seconds are required on a standard PC to achieve these results, the method is indeed very fast, simple and effective.

References

[1] M. Çayören, I. Akduman, A. Yapar and L. Crocco,"A new algorithm for the shape reconstruction of perfectly conducting objects", Inverse Problems, vol. 23, pp. 1087-1100, 2007.

[2] L. Crocco, M. D'Urso, T. Isernia, "Testing the contrast source extended Born inversion method against real data: the TM case", Inverse Problems, vol. 21, pp. S33-S50, 2005.

[3] D. Colton and R. Kress, Inverse Acoustic and Electromagnetic Scattering Theory, 2nd. ed. Springer-Verlag, Berlin Heidelberg New York 1999.

[4] I. Akduman, R. Kress and A. Yapar, "Iterative Reconstruction of Dielectric Rough Surface Profiles at Fixed Frequency", Inverse Problems, vol. 22, pp. 939-954, 2006.

[5] O. M. Bucci, L. Crocco, and T. Isernia, "Improving the reconstruction capabilties in inverse scattering problems by exploitation of close-proximity setups", J. Opt. Soc. Am. A, vol. 16, n. 7, pp. 1788-1798, 1999.

Field Reconstructions for 3d Rough Surface Scattering

C. Burkard[†,*], **R. Potthast**[†,*]
[†]University of Reading
[*]Email: c.b.burkard@reading.ac.uk, r.w.e.potthast@reading.ac.uk

Abstract

We study the reconstruction of *three-dimensional* rough surfaces via a potential approach. Using single-layer potentials for the solution of shape reconstruction problems has first been suggested by Kirsch-Kress in the case of bounded obstacles. We describe the original realization and discuss its advantages and problems. Then, we survey recent modifications by Schulz-Potthast using the *range-test* of Sylvester, Kusiak and Potthast and a hybrid method as realized by Serranho and Kress. Numerical results in three dimensions for field reconstructions via the potential ansatz are shown.

Introduction

We consider the scattering of time-harmonic acoustic waves by an unbounded rough surface in three dimensions. The corresponding direct problem is formulated by the Helmholtz equation, the Dirichlet boundary condition and some radiation property, [1]. Our aim is to reconstruct the shape of the surface by recovering the total field from the knowledge of some measured values on a plane Γ_h as well as the incident plane wave u^i and the boundary condition.
The unknown rough surface Γ is a surface which can be described by an strictly positive, bounded continuous function i.e.

$$\Gamma = \{x \in \mathbb{R}^3 : x_3 = f(x_1, x_2)\}$$

and, for $(x_1, x_2) \in \mathbb{R}^2$,

$$f_- < f(x_1, x_2) < f_+.$$

Notations. In the following x, y, z denote points in $\mathbb{R}^3$ with coordinates (x_1, x_2, x_3) resp. $(y_1, y_2, y_3), (z_1, z_2, z_3)$. The points mirrored at the $x - y$ plane will be denoted by x', y', z' as abbreviation for $(x_1, x_2, -x_3)$ resp. $(y_1, y_2, -y_3), (z_1, z_2, -z_3)$.

The Direct and the Inverse Problem

We consider the scattering by the surface Γ in the upper half-space bounded, where the incident field is due to a point source in $z \in \mathbb{R}^3$ be defined by $u^i(x) = \Phi(x, z)$, where Φ is the standard fundamental solution of the Helmholtz equation

$$\Phi(x, y) := \frac{1}{4\pi} \frac{e^{ik|x-y|}}{|x-y|}\,,\ x, y \in \mathbb{R}^3, x \neq y\,.$$

The formulation of a well-posed boundary integral equation can be found in [1],[2]. The numerical treatment is investigated in [4].

For the inverse problem we assume the knowledge of the incident field and measurements of the scattered field on a finite plane with height h to the origin. The goal is to reconstruct the total field and the unknown scattering surface. Here, we discuss the reconstruction of the field via a single-layer approach as suggested by Kirsch-Kress 1986, see [3]. We will discuss recent work on this method and related algorithms as given by the range test and a hybrid scheme.

The mathematical and computational modelling of the two- and three-dimensional direct and inverse problem for *bounded obstacles* is well studied, [3], [12]. Furthermore, the Kirsch-Kress Method and its relations to other similar methods as well as its convergence for bounded obstacles is discussed in [9] and in [10]. The inverse problem for *unbounded rough surfaces* in two dimensions can be found in [8], where the rigorous analysis of the point source method is discusssed.

The Kirsch-Kress Method

We define the single layer potential via

$$S\varphi(x) := \int_{\Gamma_t} G(x, y)\varphi(y) ds(y) \tag{1}$$

for all $x \in \mathbb{R}^3 \backslash \Gamma_t$. Here, G is the half-space Green's function for the Helmholtz equation

$$G(x, y) = \Phi(x, y) - \Phi(x, y'),\ x, y \in \mathbb{R}^3, x \neq y$$

and Γ_t is a test surface given by

$$\Gamma_t = \{x \in \mathbb{R}^3 : x_3 = t, t > 0\} \tag{2}$$

where we assume that $0 < t < f_+$. We define the horizontal finite measurement plane by

$$\Gamma_h = \{x \in \mathbb{R}^3 : x_3 = h, |x_1| \leq A, |x_2| \leq A\}$$

for a given constant $A > 0$ and $h > f_+$. We consider the knowledge of the scattered field on Γ_h. For the solution of the inverse problem, we make the ansatz

$$u^s(x) = -v(x) - \Phi(x, z') \, , x \in \Gamma_h,$$

i.e. the near field data is given by the sum of the mirrored point source $\Phi(\cdot, z')$ and a remainder v. Then we seek the part $v(x), x \in \Omega$ of the scattered field in form of a single layer potential, i.e. solve approximately the integral equation

$$S\varphi(x) = v(x) \quad , x \in \Gamma_h \, . \tag{3}$$

The single layer potential is well defined and it is a bounded operator from $L^2(\Gamma_h)$ to $L^2(\mathbb{R}^3 \backslash \Gamma_t)$. Specially, we will work with the restriction

$$S_h\varphi(x) := \int_{\Gamma_t} G(x, y)\varphi(y)ds(y) \tag{4}$$

for $x \in \Gamma_h$, whose adjoint operator is given by

$$S_h^*\varphi(y) = \int_{\Gamma_h} \overline{G(x, y)}\varphi(x)ds(x) \tag{5}$$

for $y \in \Gamma_t$. The restriction of the single layer potential is injective and has a dense range. For approximately solving the integral equation we apply the Tikhonov regularisation, that is to solve the equation

$$\alpha\varphi_\alpha + S_h^* S_h\varphi_\alpha = S_h^* v \tag{6}$$

with a regularisation parameter $\alpha > 0$ instead of solving $S\varphi(x) = v(x) \, , x \in \Gamma_h$. The approximate total field is then evaluated via the densitiy φ_α i.e.

$$S\varphi_\alpha(x) = v_\alpha(x) \quad , x \in \mathbb{R}^3 \backslash \Gamma_t \, , \tag{7}$$

and

$$u_\alpha = u^i - v_\alpha - \Phi(\cdot, z') = -v_\alpha + G(\cdot, z'). \tag{8}$$

The zeros of the exact total field represent the location of the scattering surface in case of Dirichlet boundary condition. Therefore, we seek the scattering surface as the location of the minimum of u_α in a norm sense.

Kirsch and Kress originally used the potential approach with some fixed auxilliary surface Γ. However, if the scattered field u^s is not analytically extensible up the the whole domain above Γ, then the equation (3) is not solvable and in general the single-layer potential does not converge towards the scattered field in neighborhood of the unknown surface. Kirsch and Kress overcame this problem by a combination of the solution of (3) with the search for the unknown shape. This leads to an optimization problem in which both the field and the surface is reconstructed simultaneously.

The simultaneous optimization within the Kirsch-Kress scheme is much more costly than solving just the linear equation (3) and subsequently evaluating the minimum curve to find the unknown shape. Different alternatives have been suggested and tested recently, one of which is the search of a proper surface Γ via a *range-test* by Kusiak, Potthast and Sylvester. Secondly, one could try to set up an iterative method for the search of Γ in which the potential approach for field reconstruction is just one tool. This has been carried out via a *hybrid method* by Kress and Serranho.

The Range Test

For finding a surface Γ on which the single-layer potential yields reasonable reconstructions to the scattered field we use the range-test suggested by Sylvester, Kusiak and Potthast [5]. A detailed discussion for the case of bounded obstacles is contained in [9] and [10]. The basic idea of the range-test is to check the solvability of the equation (3). This can be carried out either by observation of the norm $\|\varphi_\alpha\|$ of its solution in the limit $\alpha \to 0$ as suggested in the original paper [5] or by use of the approximation quality of the right-hand side suggested by Jakubik and Potthast [7]. Note that the range-test is a *generalized sampling scheme* as investigated in [12].

The Hybrid Method

As an alternative solution to overcome the solvability issue for the Kirsch-Kress method Kress and Serranho [6] recently suggested to combine the potential approach with an iterative method, such that the single-layer is used for field reconstructions on some iteration surface which is modified following a local Newton method. Some convergence analysis for this approach can be found in [11].

Numerical Examples

We choose a discretization of the finite planes Γ_h and Γ_t with points $x^{j,h} = (x_1^j, x_2^j, h)$ resp. $x^{j,t} = (x_1^j, x_2^j, t), j = 1, ..., N$. Then, the discretisation of the Tikhonov euqation leads to the matrix equation

$$\boldsymbol{\alpha I} + \mathbf{S_h^* S_h \varphi_\alpha} = \mathbf{S_h^* v} \, , \tag{9}$$

where we take notice of the numerical treatment of the singularity in the kernels of these operators introduced in [4]. In the following examples we choose $\alpha = 10^{-6}$

and reconstruct the total field via the single layer potential ansatz for given incident field. Let the source point be in $(-3, 0, 15)$ and the test surface Γ_t with $t = 0.5$ for solving the inverse problem.

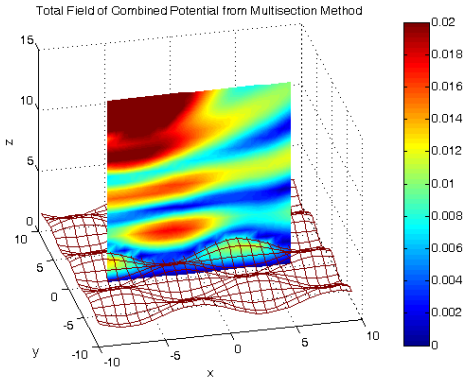

Figure 1: Simulated field via multi-section method, point source in $(-3, 0, 15)$

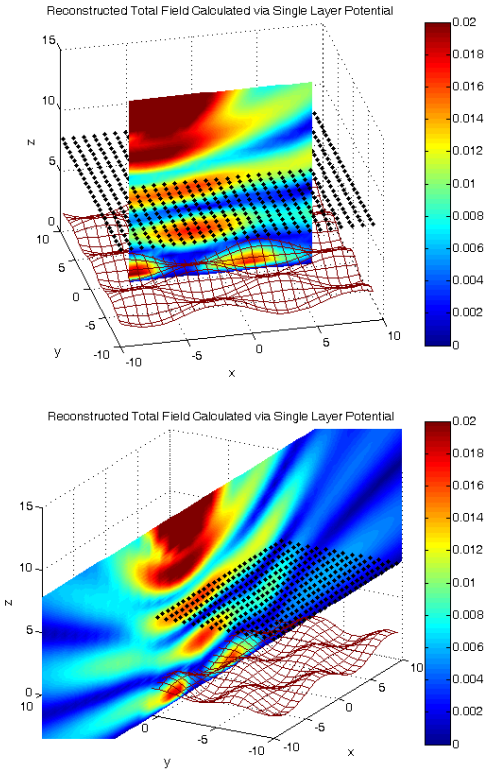

Figure 2: Reconstructed field via the single layer potential ansatz, where the measurement points are shown by black dots.

References

[1] S. Chandler-Wilde, E. Heinemeyer, R. Potthast, Acoustic scattering by middly rough unbounded surfaces in three dimensions, Proc. R. Soc. A, 2006.

[2] S. Chandler-Wilde, E. Heinemeyer, R. Potthast, A well posed Integral Equation Formulation for the Three-Dimensional Rough Surface Scattering, Proc. R. Soc. A, 2006.

[3] D. Colton, R. Kress, Inverse acoustic and electromagnetic scattering theory , 2. ed., Springer, Berlin, Heidelberg, 1998.

[4] E. Heinemeyer, R. Potthast, S.N. Chandler-Wilde, Fast evaluation of potentials and potential-operators arising from 3D acoustic rough surface scattering problems, Proceedings of Waves 2007.

[5] S. Kusaik, R. Potthast and J. Sylvester: A range test for determining scatterers with unknown physical properties." Inverse Problems 19, 533-547, 2003.

[6] R. Kress and P. Serranho, A hybrid method for two-dimensional crack reconstruction. Inverse Probl. 21, No.2, 773-784, 2005.

[7] P. Jakubik and R. Potthast: Testing the integrity of some cavity - the Cauchy problem and the range test. Applied Numerical Mathematics, at press.

[8] C. Lines, Inverse Scattering by Rough Surfaces, PhD thesis, Departement of Mathematics, Brunel University, 2003.

[9] R. Potthast, J. Schulz, From the Kirsch-Kress Potential Method via the Range Test to the Singular Sources Method, Journal of Physics: Conference Series 12, 116 - 127, 2005.

[10] R. Potthast, J. Schulz, A multiwave range test for obstacle reconstructions with unknown physical properties,Journal of Computational and Applied Mathematics, 2006.

[11] R. Potthast, *Point-sources and Multipoles in Inverse Scattering*, Chapman & Hall, London 2001.

[12] R. Potthast, A survey on sampling and probe methods for inverse problems, Topical Review for Inverse Problems 22, R1-R47, 2006.

INVERSE SCATTERING FOR ANISOTROPIC MEDIA

F. Cakoni[†,*], **D. Colton**,[†,*] **H. Haddar**[‡,*]
[†]Department of Mathematical Sciences, University of Delaware, Newark, Delaware 19716-2553, USA
[‡]INRIA, Domaine de Voluceau, Rocquencourt, B.P. 105, 78153 Le Chesnay Cedex, France.
[*]Email: cakoni@math.udel.edu

Abstract

We consider the scattering of time harmonic electromagnetic plane waves by a bounded, inhomogeneous, anisotropic dielectric medium. We use the linear sampling method to determining the support of the anisotropic inhomogeneity. Furthermore, we show that under certain assumptions a lower bound on the norm of the (matrix) index of refraction can be obtained from a knowledge of the smallest transmission eigenvalue corresponding to the medium. Numerical examples are given showing the efficaciousness of our estimates.

Introduction

Anisotropic material play a special role in electromagnetic inverse scattering theory. This is due to the fact that from far field data only the support D of the scatterer is uniquely determined [2], [11] and little can be said about the material properties of the scatterer [9]. This remains true even if multifrequency data is used. Although specific information about the material properties may be unavailable, there remains the possibility of obtaining upper or lower bounds on certain norms of the (matrix) index of refraction and it is to this task that this paper is directed. In particular, are there certain inequalities that the index of refraction must satisfy for a given measured far field pattern? For the case of a dielectric isotropic scatterer, this question was considered in [4] and [8] where it was shown that if the (scalar) index of refraction is greater than one then it is bounded below by $\lambda(D)/k^2$ where $\lambda(D)$ is the first Dirichlet eigenvalue for the Laplacian in D of the scattering obstacle and k is the first transmission eigenvalue [3]. Since D and k can be determined from the far field data [4], this then provides a lower bound for the index of refraction. In [6] it was shown that a similar inequality is valid in the case of a dielectric anisotropic media where the supremum of the (scalar) index of refraction is replaced by the Euclidean norm of the (matrix) index of refraction. We end this section by mentioning that, in all the above cases, the support of the inhomogeneity D van be reconstructed by using the linear sampling method [1] [3], without essentially requiring any a priori information on the physical properties of the scattering object.

Inverse scattering problem

We consider the scattering of electromagnetic waves by an anisotropic dielectric at fixed frequency. For a particular polarization and geometry the corresponding forward problem in the $\mathbb{R}^2$-case is given by the following set of equations, where D is the support of the scattering object such that $\mathbb{R}^2 \setminus \overline{D}$ is connected

$$\begin{aligned}
&\nabla \cdot A\nabla w + k^2 w = 0 && \text{in} \quad D\\
&\Delta u + k^2 u = 0 && \text{in} \quad D_e\\
&w - u = 0 && \text{on} \quad \partial D\\
&\frac{\partial w}{\partial \nu_A} - \frac{\partial u}{\partial \nu} = 0 && \text{on} \quad \partial D\\
&u = u^s + u^i\\
&\lim_{r\to\infty} \sqrt{r}\left(\frac{\partial u^s}{\partial r} - iku^s\right) = 0,
\end{aligned}$$

where u^s is the scattered field, u^i is the given incident field and ν is the outward normal vector to the (piecewise smooth) boundary ∂D of D. In the case of plane waves the incident field is given by $u^i := e^{ikx\cdot d}$, $d \in \Omega := \{x : |x| = 1\}$. We assume that A is a real valued 2×2 matrix-valued function whose entries are piecewise continuously differentiable functions in $\overline{D}$ with (possible) jumps along piecewise smooth curves such that A is symmetric and $\bar{\xi}\cdot A\,\xi \geq \gamma|\xi|^2$ for all $\xi \in \mathbb{C}^2$ and $x \in \overline{D}$ where γ is a positive constant. It can be shown [7] that the scattered field u^s has the asymptotic behavior

$$u^s(x) = \frac{e^{ikr}}{\sqrt{r}} u_\infty(\hat{x}, d) + O\left(r^{-3/2}\right) \qquad (1)$$

as $r \to \infty$ uniformly in $\hat{x}$ where u_∞ is the *far field pattern*.

The *inverse scattering problem* we are concerned with is to determine D and A from a knowledge of $u_\infty(\hat{x}, d)$ for all $\hat{x}, d \in \Omega$ and a range of frequencies k. In [3] it is proven that D is uniquely determined from the above data. However, it is also know [9] that the matrix A is not uniquely determined from the far field pattern for all d even if they are known for a range of frequencies k.

Solution of the inverse problem

We now define the *far field operator* $F : L^2(\Omega) \to L^2(\Omega)$ by

$$Fg(\hat{x}) := \int_\Omega u_\infty(\hat{x}, d) g(d)\, ds(d) \tag{2}$$

and introduce the far field equation

$$(Fg)(\hat{x}) = \gamma e^{-ik\hat{x}\cdot z} \qquad g \in L^2(\Omega), \quad z \in D \tag{3}$$

where $\gamma = \frac{e^{i\pi/4}}{\sqrt{8\pi k}}$ and $\gamma e^{-ik\hat{x}\cdot z}$ is the far field pattern of the fundamental solution $\Phi(x,z) := \frac{i}{4} H_0^{(1)}(k|x-z|)$ to the Helmholtz equation in $\mathbb{R}^2$ with $H_0^{(1)}$ being a Hankel function of the first kind of order zero. A reconstruction of D can be obtained by using the linear sampling method which characterizes the support D from a solution of the far field equation (3) (see e.g [3]).
In particular, from [3] we have that the *far field operator* $F : L^2(\Omega) \to L^2(\Omega)$ defined by

$$(Fg)(\hat{x}) := \int_\Omega u_\infty(\hat{x}, d) g(d) ds(d) \tag{4}$$

is injective with dense range provided k is not a *transmission eigenvalue*, i.e. a value of k for which the (homogeneous) *interior transmission problem*

$$\begin{aligned} \nabla \cdot A \nabla w + k^2 w &= 0 && \text{in} \quad D \\ \Delta v + k^2 v &= 0 && \text{in} \quad D \\ w - v &= 0 && \text{on} \quad \partial D \\ \frac{\partial w}{\partial \nu_A} - \frac{\partial v}{\partial \nu} &= 0 && \text{on} \quad \partial D \end{aligned}$$

has a nontrivial solution $w, v \in H^1(D)$. It is not known, except for the case of spherically stratified media [8], whether transmission eigenvalues exists. Now, assuming that k is not a transmission eigenvalue, ∂D can be characterized from the behavior of $\|g\|_{L^2(\Omega)}$, where g is an approximate solution of (3). Having determined D, we now want to recover information about A. We will make use of transmission eigenvalues (which we avoided when determining D) to obtain a lower bound for the Euclidian norm of A. Due to the lack of injectivity and the denseness of the range of the far field operator F, when k is a transmission eigenvalue the L^2-norm of the (regularized) solution to

$$(Fg)(\hat{x}) = \Phi_\infty(\hat{x}, z_0), \text{ for a fixed } z_0 \in D \tag{5}$$

can be expected to be large for such values of k (this is numerically verified in [6]). A validating example is shown in Figure 1. In particular, if D is the circle with radius 0.5 and $A = 1/4I$, Figure 1 shows that the transmission eigenvalues (known to exists) computed by separation of variables and by the above remark using symthetic data perfectly coincide

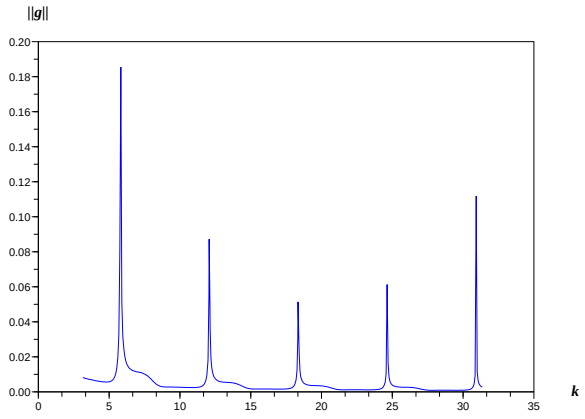

Figure 1: $\|g\|$ in terms of the wave number k for the circle. The peaks coincide with the computed transmission eigenvalues using separation of variables.

Following the idea of [5] and [10], by making an appropriate change of variable and rewriting the interior transmission problem in an equivalent variational form for a fourth order boundary value problem, in [6] it is shown that: Assume that $\bar{\xi} \cdot (A^{-1} - I)^{-1} \xi \geq \alpha |\xi|^2$ in D and for all $\xi \in \mathbb{C}^2$ where $\alpha > 0$ is a constant. Then

1. The set of transmission eigenvalues is discrete and does not accumulate at 0.

2. All transmission eigenvalues (if they exist) are such that $k^2 \geq \frac{\alpha}{1+\alpha} \lambda(D)$ where $\lambda(D)$ is the first Dirichlet eigenvalue of $-\Delta$ on D.

Recalling that $\|A^{-1}\|_2 = \sup_{\|\xi\|=1} (\bar{\xi} \cdot A^{-1} \xi)$ (e.g. the largest eigenvalue), the above result implies the following main result: Assume that $\|A^{-1}(x)\|_2 \geq \delta > 1$ for all $x \in D$, then

$$\sup_D \|A^{-1}\|_2 \geq \frac{\lambda(D)}{k^2} \tag{6}$$

where k is a transmission eigenvalue and $\lambda(D)$ is the first eigenvalue of $-\Delta$ on D. Unfortunately, if $0 < \beta \leq \|A^{-1}(x)\|_2 \leq \delta < 1$ for all $x \in D$, all we can say is that a transmission eigenvalue satisfies $k^2 \geq \lambda(D)$.

Hence, (6) provides a lower bound for the suprimum of the Euclidean norm of al matrices A that give rise to the measured far field pattern. Note that $\lambda(D)$ can be

computed since D is reconstructed by the linear sampling method, whereas the first transmission eigenvalue using the remark following (5).

We end by showing a numerical example for estimating the constant index of refraction in the case of the L-shape $D := \{[-0.5,\, 0.5]\times[-0.5,\, 0.5]\}\backslash\{]0,\, 0.5]\times]0,\, 0.5]\}$. In the following $A = 1/nI$. For more numerical examples see [6].

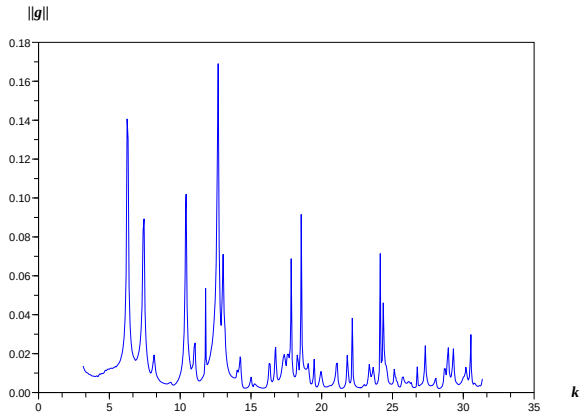

Figure 2: $\|g\|$ in terms of the wave number k for the L-shape with $A = 1/4I$

n	2.	3.	4.	6.	9.	12.	16.
k_0	15.5	8.1	6.3	4.5	3.3	2.8	2.3
$n_{\min}$	0.2	0.6	1.	1.9	3.5	4.9	7.2

Table 1: First transmission eigenvalues (k_0) and lower bounds of the index of refraction $(n_{\min})$ for the **L-shape**.

References

[1] F. Cakoni, D Colton and H Haddar, The linear sampling method for anisotropic media, J. Comp. Appl. Math., 146, pp. 285-299, 2002.

[2] F. Cakoni and D. Colton, "A uniqueness theorem for an inverse electromagnetic scattering problem in inhomogeneous anisotropic media", Proc. Edinburgh Math. Soc., 46, pp. 293-314, 2003.

[3] F. Cakoni and D. Colton, Qualitative Methods in Inverse Scattering Theory, Springer, Berlin, 2006.

[4] F. Cakoni, D. Colton and P. Monk, On the use of transmission eigenvalues to estimate the index of refraction from far field data, Inverse Problems , 23, pp. 507-522, 2007.

[5] F. Cakoni and H. Haddar, A variational approach for the solution of the electromagnetic interior transmission problem for anisotropic media, *Inverse Problems and Imaging*, (to appear).

[6] F. Cakoni, D. Colton and H. Haddar, "The computation of lower bounds for the norm of the index of refraction in an anisotropic media from far field data, *Inverse Problems and Imaging"*, (to appear).

[7] D. Colton and R Kress, Inverse Acoustic and Electromagnetic Scattering Theory, Vol. 93 in Applied Mathematical Sciences, 2nd edition, Springer, New York, 1998.

[8] D. Colton, L. Päivärinta and J. Sylvester, "The interior transmission problem", Inverse Problems and Imaging, 1, 13-28, 2007.

[9] F. Gylys-Colwell, "An inverse problem for the Helmholtz equation", Inverse Problems, 12, pp. 139-156, 1996.

[10] H. Haddar, "The interior transmission problem for anisotropic Maxwell's equations and its applications to the inverse problem", Math. Methods Appl. Sci., 27, pp. 2111-2129, 2004.

[11] P. Hähner, "On the uniqueness of the shape of a penetrable, anisotropic obstacle", J. Comp. Appl. Math.. 116, pp. 167-180, 2000.

A COUPLED BOUNDARY INTEGRAL EQUATION METHOD FOR INVERSE SOUND-SOFT SCATTERING

O. Ivanyshyn[†,*], **B. T. Johansson**[‡]

[†]Institute for Numerical and Applied Mathematics, Georg-August University of Göttingen, Lotzestr. 16–18, Göttingen, Germany

[‡]School of Mathematics, University of Birmingham, Edgbaston, Birmingham B15 2TT, UK

[*]Email: ivanyshy@math.uni-goettingen.de

Abstract

We investigate an iterative boundary integral based method for the reconstruction of the shape of a plane acoustically sound-soft obstacle from the knowledge of the far field pattern for only one incoming wave. The method is based on the representation of the scattered field as a combined acoustic double and single-layer potential together with the corresponding boundary integral for the far field. Compared with methods based on only the acoustical single-layer operator this new procedure produces accurate approximations for a wider range of wave-numbers.

Introduction

In the exterior problem for (linearised) acoustical scattering of a planar obstacle by time-harmonic waves one wishes to find a solution to the Helmholtz equation

$$\Delta u + k^2 u = 0 \quad \text{in } \mathbf{R}^2 \setminus \overline{D}, \tag{1}$$

where D is a bounded plane domain with smooth boundary Γ and $k > 0$ the wave number, subject to certain boundary conditions. For simplicity, we assume that the obstacle is sound-soft, i.e., the pressure on the boundary Γ is zero so

$$u = 0 \quad \text{on } \Gamma. \tag{2}$$

This direct scattering problem is to find $u = u^i + u^s$, where $u^i(x) = e^{ikx\cdot d}$ and d is the unit direction of the incoming wave, such that u solves (1)–(2) and the scattered wave u^s satisfies the Sommerfeld radiation condition

$$\lim_{r\to\infty} r^{1/2}\left(\frac{\partial u^s}{\partial r} - iku^s\right) = 0, \quad \text{where} \quad r = |x|,$$

uniformly in all directions. This direct scattering problem has a unique smooth solution. The far field pattern u_∞ describes the asymptotic behavior of the scattered field at large distances from the obstacle. We consider the inverse problem;

Reconstruct the boundary Γ from the knowledge of the far field pattern for only one direction of the incoming field.

This type of problem is common in applications such as medical imaging, non-destructive testing, radar and sonar obstacle detection where information is to be extracted from knowledge of the influence that the obstacle has on propagating waves. According to Colton and Sleeman [2] we have uniqueness for the inverse problem, e.g. identifiability if the obstacle is contained in a disc with radius R and $kR < C$ (the constant C is computable ≈ 3.83, see Gintides [3]).

Many different methods and procedures have been developed for the stable approximation of the solution to this inverse scattering problem, for an overview see, for example, the monograph by Colton and Kress [1].

One method, denoted as Method A, which was first considered by Sleeman [10], for the detection of a sound-soft obstacle was analysed and implemented by Johansson and Sleeman [7]. Independently, Ivanyshyn and Kress [6] proposed a related approach denoted as Method B and which is an extension of the inverse algorithm introduced by Kress and Rundell [8] for the Laplace equation. Both these methods are based on boundary integral equations for the incident field and the far field pattern, respectively, see further Ivanyshyn and Johansson [4], [5]. In [5] it was noted that the integral equations are solvable if the wave number is not an interior Dirichlet or Neumann eigenvalue. One has proposed, see [1], to find the solution of (1)–(2) in the form of a combined double and single-layer potential. This coupled integral equation is uniquely solvable for all wave numbers $k > 0$.

In this paper we modify Method A for analytical boundaries and base it on the representation of the scattered field as a combined double and single-layer potential. Given an approximation of the boundary, we solve this coupled integral equation for a density and then update the boundary approximation using this density and the integral representation of the far field pattern, see Section 2. Numerical investigations are presented in Section 3.

1 Boundary integral formulation

Assume for simplicity that the boundary Γ is given by

$$z(t) = (z_1(t), z_2(t)), \quad t \in [0, 2\pi], \tag{3}$$

where z is analytic and 2π-periodic with positive orientation and $|z'(t)| > 0$. We define the parameterised single-layer operator

$$S(z,\varphi)(t) = \int_0^{2\pi} \Phi(t,\tau)\,\varphi(\tau)\,|z'(\tau)|\,d\tau, \qquad (4)$$

and the double-layer operator

$$K(z,\varphi)(t) = \int_0^{2\pi} \frac{\partial \Phi(t,\tau)}{\partial [z'(\tau)]^\perp}\,\varphi(\tau)\,d\tau, \qquad (5)$$

where $[z'(t)]^\perp = (z_2'(t), -z_1'(t))$ is the outward normal to Γ, $\Phi(t,\tau)$ is the fundamental solution to the Helmholtz equation and $t \in [0, 2\pi]$. We search for the scattered field as a combined double and single layer potential and therefore have to find a density φ satisfying

$$\frac{\varphi(t)}{2} + K(z,\varphi)(t) - i\eta S(z,\varphi)(t) = -u^i(z(t)), \quad (6)$$

where the coupling parameter $\eta \neq 0$ is real valued. We also introduce the corresponding far field integral operators

$$S_\infty(z,\varphi)(\theta) = \gamma \int_0^{2\pi} e^{-ikx_\infty(\theta)\cdot z(\tau)}\,\varphi(\tau)\,|z'(\tau)|\,d\tau,$$

and

$$K_\infty(z,\varphi)(\theta) = -\gamma \int_0^{2\pi} ik\,g(\theta,\tau) e^{-ikx_\infty(\theta)\cdot z(\tau)}\,\varphi(\tau)\,d\tau,$$

where $g(\theta,\tau) = [z'(\tau)]^\perp \cdot x_\infty(\theta)$ and $\gamma = e^{i\pi/4}/\sqrt{8\pi k}$. Then the equation for the far field can be written as

$$K_\infty(z,\varphi)(\theta) - i\eta S_\infty(z,\varphi)(\theta) = u_\infty(\theta), \qquad (7)$$

for $\theta \in [0, 2\pi]$. Note that (7) is a non-linear and ill-posed equation for z. We assume that z' and thereby also $[z'(t)]^\perp$ are known and therefore linearise (7) with respect to z viewing z' as independent of z, by searching for an update h in the form

$$h(t) = q(t)[z'(t)]^\perp, \quad t \in [0, 2\pi]. \qquad (8)$$

From Theorem 3 in [9] we get.

Lemma 1.1. *The mappings from $C^2[0,2\pi] \to B(C[0,2\pi], C[0,2\pi])$ given by $z \mapsto S_\infty(z,\cdot)$ and $z \mapsto K_\infty(z,\cdot)$ are Fréchet differentiable (viewing z' and $[z'(t)]^\perp$ as independent of z) with derivatives*

$$(S'_\infty[z,\varphi]q)(\theta) = -i \int_0^{2\pi} E(\theta,\tau)\,\varphi(\tau)\,q(\tau)\,|z'(\tau)|\,d\tau,$$

and

$$(K'_\infty[z,\varphi]q)(\theta) = -k \int_0^{2\pi} E(\theta,\tau)\,g(\theta,\tau)\,\varphi(\tau)\,q(\tau)\,d\tau.$$

where $E(\theta,\tau) = k\gamma e^{-ikx_\infty(\theta)\cdot z(\tau)}\,g(\theta,\tau)$.

The linearised version of (7) is then

$$(K'_\infty - i\eta S'_\infty)q = u_\infty - K_\infty + S_\infty. \qquad (9)$$

Remark. The equation (7) can be linearised in several ways. Assuming that z' is unknown, one should also linearize the terms $|z'|$ and $[z']^\perp$.

2 The iterative procedure for reconstruction of the boundary

The method presented here is a variant of the method considered in [7].

1. Given z and z' solve (6) for φ.
2. Update z as $z = z + h$ with h found from (8)–(9).

The procedure is then continued by repeating the two steps until a suitable stopping criteria is satisfied.

To numerically solve (6) for the density φ, given a parametrisation z, it is effective to apply the Nyström method, see Chapter 3.5 in Colton and Kress [1] for the details.

Given a density φ and an approximation z we find the correction from (9) using Tikhonov regularization. To justify the use of the Tikhonov regularization we have

Theorem 2.1. *The operator $A := K'_\infty - i\eta S'_\infty$, where $\eta > 0$, is injective and has dense range in $L^2([0,2\pi])$.*

3 Numerical results

In order to illustrate the mathematical theory, we reconstruct a boundary curve with the parameterisation

$$z(t) = (\cos t + 0.65\cos 2t - 0.65, 1.5\sin t), \quad t \in [0, 2\pi].$$

We choose the wave number $k = 1.4$ and the direction of the incoming wave to $d = (1, 0)$. To avoid the "inverse crime", the corresponding far field pattern is numerically generated at 64 points equally distributed around the unit circle by solving the classical equations (uncoupled). Each of the components of z is approximated by

$$p(t) = a_0 + \sum_{m=1}^{7} (a_m \cos mt + b_m \sin mt), \quad t \in [0, 2\pi].$$

The initial guess is a circle with radius $R = 0.4$ located outside the obstacle. Tikhonov regularization is employed to (9) with the regularizing parameter decreasing with the number of iterations, and an H^2-penalty term is used to get smoother reconstructions. The coupling parameter is $\eta = 5$. In Figure 1a), the reconstruction after 5 ($\diamond\diamond\diamond$), 15 ($---$) and 30 ($-.-$) iterations, respectively, are shown. The analytical boundary curve is displayed as a solid line and the dotted line is the initial guess. Both the position and shape of the initial guess can be changed and the method produce similar results as long as the guess is not too far from the obstacle. However, the guess must be on the same "side" as the wave is coming from. Also the wave number can be changed. As compared with method A in [4], the procedure presented here can be applied for a wider range of wave numbers. Increasing the degree of the trigonometrical approximation does not improve the reconstruction substantially. Larger values of the coupling parameter give the same type of accuracy in about the same number of iterations. However, if η was chosen smaller than 3, then less accurate approximations are obtained.

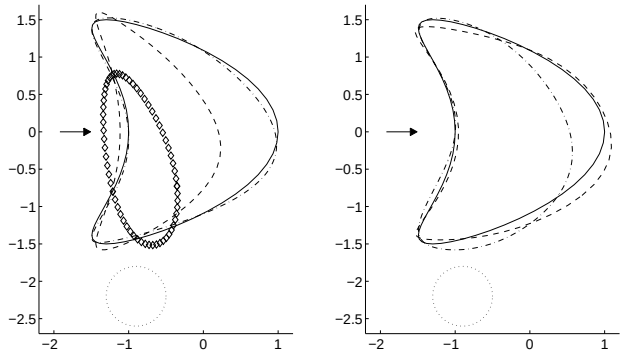

a) Exact data b) Noisy data

Figure 1: Reconstruction of a kite contour, exact data

Then 10 sets of noisy data were generated as

$$u_\infty^\delta = u_\infty + \delta \frac{\|u_\infty\|_{L^2}}{\|\eta\|_{L^2}} \eta, \tag{10}$$

with the noise level $\delta = 0.03$ and $\eta = \eta_1 + i\eta_2$ with η_1 and η_2 being normally distributed random variables. In Figure 1b), the best ($---$) and the least accurate ($-.-$) approximation are shown together with the analytical boundary curve (—) and the initial guess ($\cdots$). Noise affects most on the shadow side as expected.

Acknowledgement

Both authors wish to thank Rainer Kress and Brian Sleeman for their interest and for valuable discussions during this research. Olha Ivanyshyn acknowledges the support of her work by the Graduiertenkolleg 1023 and the support from the Computational Fluid Dynamics Centre at the University of Leeds via EST, Marie Curie funding. Tomas Johansson acknowledges grants and support from the Wenner-Gren Foundations.

References

[1] D. Colton and R. Kress, "Inverse Acoustic and Electromagnetic Scattering", Springer-Verlag, Berlin, 1998.

[2] D. Colton and B. D. Sleeman, "Uniqueness Theorems for the Inverse Problem of Acoustic Scattering", IMA J. Appl. Math., 31, pp. 253–259, 1983.

[3] D. Gintides, Local uniqueness for the inverse scattering problem in acoustics via the Faber-Krahn inequality, Inverse Problems, 21, pp. 1195–1205

[4] O. Ivanyshyn and T. Johansson, "Non-Linear Integral Equation Methods in Inverse Obstacle Scattering". Accepted for publication in J. Integral Equations Appl.

[5] O. Ivanyshyn and T. Johansson, "Boundary Integral Equations for Acoustical Inverse Sound-Soft Scattering", Submitted 2006-10-02 to Journal of Inverse and Ill-posed Problems.

[6] O. Ivanyshyn and R. Kress, "Nonlinear Integral Equations in Inverse Obstacle Scattering", In: Mathematical Methods in Scattering Theory and Biomedical Engineering (Fotiatis, Massalas, eds). World Scientific, Singapore, 39–50.

[7] T. Johansson and B. D. Sleeman, "Reconstruction of an Acoustically Sound-Soft Obstacle from one Incident Field and the Far Field Pattern", IMA J. Appl. Math., 72, pp. 96–112, 2007.

[8] R. Kress and W. Rundell, "Inverse Scattering for Shape and Impedance", Inv. Probl., 17, pp. 1075-1085, 2001.

[9] R. Potthast, "Fréchet Differentiability of Boundary Integral Operators in Inverse Acoustic Scattering", Inv. Probl., 10, pp. 431–447, 1994.

[10] B. D. Sleeman, "The Inverse Problem of Acoustic Scattering", Applied Mathematics Institute Technical Report, No. 114 A, University of Delaware, Newark, 1983.

Wave splitting in inverse scattering

R. Potthast[†,*], **J.J. Liu**[‡], **F. Ben Hassen**[◦]
[†] Department of Mathematics, University of Reading, United Kingdom
[‡] Southeast University, Nanjing, China
[◦] ENIT- University of Tunis-El Manar, BP 37, 1002 Tunis Tunisia
[*]Email: r.w.e.potthast@reading.ac.uk

Abstract

We study wave splitting procedures for acoustic scattering problems. The idea of these procedures is to split some scattered field into a sum of fields coming from different spatial regions such that this information can be used either for inversion algorithms or for active noise control.

We will show uniqueness for the general splitting problem and describe a solution algorithm via single-layer potentials.

Introduction

Inverse problems for acoustic and electromagnetic waves play an important role in many scientific and engineering applications. Medical imaging for example uses several techniques from the area of inverse problems as basic ingredients for medical examinations. Nondestructive testing employs inverse problems techniques for quality control. For a given incident wave, the impenetrable obstacle D will generate a scattered wave outside D, which is in general governed by the Helmholtz equation for acoustic waves or Maxwell equations for electromagnetic waves. The scattered wave and its far-field pattern contain information about the scatterer D such as the boundary shape and boundary type. The reconstruction of an obstacle D from the far-field pattern of its scattered wave is one of the central research topics in inverse scattering theory, see for example [4] and the topical review [6].

We present an efficient way to reconstruct the scattered wave from the far-field pattern caused by multiple obstacles. The basic idea is to *split the far-field pattern* into several parts which are essentially related to each obstacle. Correspondingly, the scattered wave is also decomposed. Please observe that our splitting *avoids any approximation* as for example employed for the Born approximation or physical optics approximation. Using this idea based on general potential theory or Green representation formula and combining it with the *point source method*, we propose a scheme which provides a reconstruction of the scattered wave at all points outside of some scatterer D with several components. This *splitting method* enables the recovery of the scattered wave outside of multiple obstacles. The method proposed in this paper, except for its intrinsic importance in *wave recovery*, is also applicable to *shape reconstruction* for multiple obstacles.

We remark that the splitting procedure in its simplest realization uses potential operators which have been constituents of the field reconstruction method of *Kirsch-Kress* [1], however used in a different way. Also, the *range-test* of Sylvester-Kusiak-Potthast [5] employs these operators. In fact, we can use the range-test to find appropriate domains G_1 and G_2 for which the splitting is valid.

Uniqueness for wave splitting

Here, we will restrict our attention to the simplest case where a field is defined in the exterior of a domain G which consists of two parts.

Assume that two domains G_1 and G_2 with $G_1 \cap G_2 = \emptyset$ and C^2-smooth boundary are given such that

$$\overline{D_1} \subset G_1 \text{ and } \overline{D_2} \subset G_2. \tag{1}$$

Set $G := G_1 \cup G_2$.

We first address the uniqueness problem for wave splitting. Consider domains G_j as given in Definition (1). Assume that we are given a decomposition $u^s = u_1^s + u_2^s$ of the scattered field u^s such that

1. u_j^s satisfies the radiation condition for $j = 1, 2$;
2. for $j = 1, 2$ the field u_j^s soles the Helmholtz equation in the exterior of G_j.
3. Both $(u_j^s)^+$ and $\frac{\partial (u_j^s)^+}{\partial \nu}$ exist in ∂G_j, where

$$(u_j^s)^+|_{\partial G_j} := \lim_{x \in \mathbb{R}^m \setminus \overline{G}_j,\, x \to \partial G_j} u_j^s(x).$$

Then the splitting of u^s is unique, i.e. for every further splitting $u^s = \tilde{u}_1^s + \tilde{u}_2^s$ with $\tilde{u}_j^s$ meeting conditions 1 – 3, we obtain $u_j^s(x) = \tilde{u}_j^s(x)$ for $x \in \mathbb{R}^m \setminus \overline{G}_j$ with $j = 1, 2$. For a proof of this uniqueness result we refer to [3].

Construction of the wave splitting

Denote by $\Phi(\cdot,\cdot)$ the free-space fundamental solution to the Helmholtz equation $\Delta u + \kappa^2 u = 0$ in $\mathbb{R}^3$. For G given in Definition 1, the single-layer potential

$$(S\varphi)(x) := \int_{\partial G} \Phi(x,y)\varphi(y)ds(y), x \in \mathbb{R}^3, \quad (2)$$

is a well-known tool in scattering theory. We express the scattered wave by single-layer approach

$$u^s(x) := (S\varphi)(x), \quad x \in \mathbb{R}^m \setminus \overline{G}. \quad (3)$$

The far field pattern of $S\varphi$ is given by the operator

$$(S^\infty\varphi)(\hat{x}) := \gamma \int_{\partial G} e^{-i\kappa\hat{x}\cdot y}\varphi(y)ds(y), \quad \hat{x} \in \mathbb{S} \quad (4)$$

with $\gamma = 1/(4\pi)$ in $\mathbb{R}^3$ and $\gamma = e^{i\pi/4}/\sqrt{8\pi\kappa}$ in $\mathbb{R}^2$, $\mathbb{S}$ is the unit sphere in $\mathbb{R}^m$. Here, the density φ lives on $\partial G = \partial G_1 \cup \partial G_2$. We denote

$$\varphi_j(y) := \varphi(y) \text{ for } y \in \partial G_j \quad (5)$$

and denote the corresponding single-layer potential operators by S_j, i.e.

$$(S_j\varphi_j)(x) := \int_{\partial G_j} \Phi(x,y)\varphi_j(y)ds(y), \quad x \in \mathbb{R}^m \quad (6)$$

and we have

$$S\varphi = S_1\varphi_1 + S_2\varphi_2. \quad (7)$$

The splitting of the far field of a scatterer $D = D_1 \bigcup D_2$ is obtained from the following three steps.

1. Solve the far-field equation

$$S^\infty\varphi = u^\infty \quad (8)$$

to generate density function φ defined in ∂G, where S^∞ is given via (4).

2. Define two functions

$$u_j^s(x) := (S_j\varphi_j)(x), \quad x \in \mathbb{R}^m \setminus \overline{G_j}, \ j = 1,2, \quad (9)$$

which can be considered as a scattered wave outside G_j, in the sense that it solves the Helmholtz equation in $\mathbb{R}^m \setminus \overline{G}_j$ and meets the radiation condition.

3. Compute the far field patterns of u_j^s defined by

$$u_j^\infty := S_j^\infty\varphi_j, \quad j = 1,2. \quad (10)$$

In this way, the far field pattern u^∞ is decomposed as

$$u^\infty = u_1^\infty + u_2^\infty. \quad (11)$$

Correspondingly, the scattered wave u^s related to u^∞ has the splitting

$$u^s(x) = u_1^s(x) + u_2^s(x), \quad x \in \mathbb{R}^m \setminus \overline{G} \quad (12)$$

from the linear superposition principle and Rellich lemma, where u_j^s is computed via (9). Moreover, u_j^s outside G_j is the scattered wave related to u_j^∞ with $j = 1,2$ again from Rellich lemma, noticing $u_j^s(x)$ defined by (9) is a radiating field.

Numerical Results

Here we demonstrate the splitting and also the reconstruction of the field via the point source method when carried out for the different parts of the field separately.

First, we show a simulation of the total field for twodimensional acoustic scattering by a sound-soft obstacle in Figure 1.

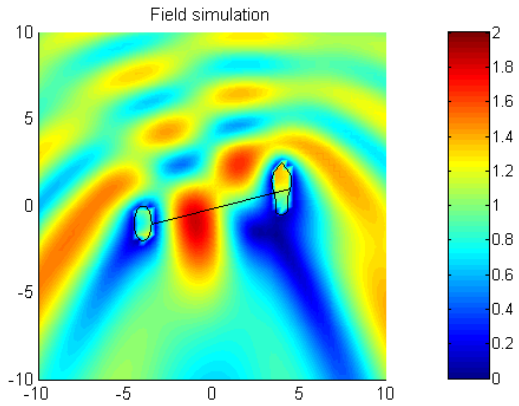

Figure 1: Simulated total acoustic field for an incident plane wave coming from above.

Second, we plot the field $u^i + u_1^s$ in Figure 2. This field is defined outside of G_1 and is a radiating solution to the Helmholtz equation. An analogous image with G_1 replaced by G_2 could be shown for $u^i + u_2^s$. Then we show a plot of the field $u^i + u_1^s + u_2^s$ in the exterior of G in Figure 3.

Clearly, the representation of the field u via splitting holds only in the exterior of the domain $G = G_1 \cup G_2$. However, to reconstruct the field in the exterior of $D_1 \cup D_2$ we can now apply reconstruction methods separately

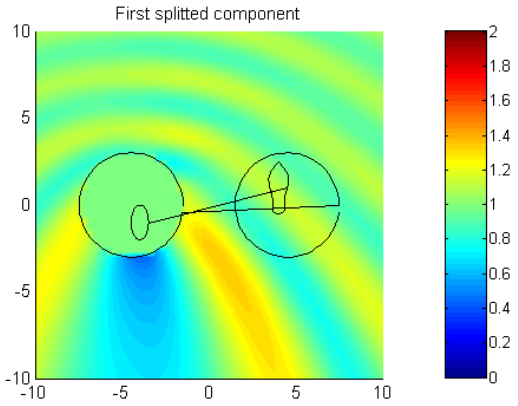

Figure 2: Sum of the incident field and the part u_1^s of the field.

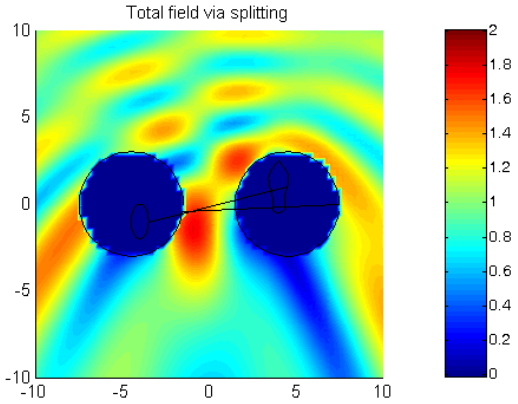

Figure 3: Total acoustic field via splitting for an incident plane wave coming from above

to u_1^∞ and u_2^∞. For example, Figure 4 shows the result of the point-source method for field reconstructions [4], [7], [2] [8] applied to reconstruct u_1^s in the exterior of D_1 and u_2^s in the exterior of D_2 and then adding the two fields plus the incident field to obtain a reconstruction of the full total field.

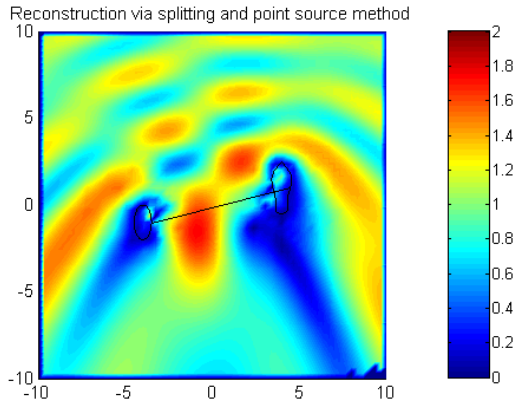

Figure 4: Reconstructed total acoustic field for an incident plane wave coming from above

References

[1] D.L.Colton, R.Kress, Inverse Acoustic and Electromagnetic Scattering Theory, 2nd edition, Springer-Verlag, Berlin, 1998.

[2] J.J.Liu, G.Nakamura, R.Potthast, A new approach and improved error analysis for reconstructing the scattered wave by the point source method, to appear in J. Comput. Maths.

[3] F.Ben Hassen, J.J.Liu, R.Potthast, On Source Analysis by Wave Splitting with Applications in Inverse Scattering of Multiple Obstacles to appear in J. Comput. Maths.

[4] R.Potthast, Point sources and multipoles in inverse scattering theory, Chapman & Hall/CRC Research Notes in Mathematics, Chapman & Hall/CRC, Boca Raton, FL, Vol.427, 2001.

[5] R.Potthast, J.Sylvester, S.Kusiak, Steven, A 'range test' for determining scatterers with unknown physical properties, Inverse Problems, Vol.19, No.3, 533-547, 2003.

[6] R.Potthast, Topical Review: A survey on sampling and probe methods for inverse problems, Inverse Problems, Vol.22, R1-R47, 2006.

[7] R.Potthast, A point-source method for inverse acoustic and electromagnetic obstacle scattering problems, IMA J. Appl. Maths., Vol.61, 119-140, 1998.

[8] R.Potthast, Sampling and Probe Methods - An Algorithmical View, Computing, Vol.75, 215-236, 2005.

A BRIEF REVIEW OF SOME MATHEMATICAL PROBLEMS OF THE LINEAR THEORY OF ELASTICITY FOR HEMITROPIC MATERIALS

I. G. Stratis[†,*]
[†]Department of Mathematics, University of Athens, Panepistimiopolis, GR 15784 Zographou, Athens, Greece
[*]Email: istratis@math.uoa.gr

Abstract

The theory of elasticity of hemitropic materials has recently been the object of rigorous mathematical analysis. The main features and results are briefly reviewed here.

Introduction

Recent technological and industrial developments, and the progress in biological and medical sciences, require the use of generalized and refined models for elastic materials. In a generalized solid continuum the usual displacement field has to be supplemented by a microrotation field. Such materials are called micropolar, or Cosserat, solids. An isotropic micropolar solid may be HEMITROPIC (equivalent terms are *noncentrosymmetric, acentric, chiral*), i.e., isotropic with respect to all proper orthogonal transformations, but not with respect to mirror reflections.

Materials may exhibit chirality on the atomic scale, as in quartz and in biological molecules (DNA), as well as on a large scale, as in composites with helical or screw–shaped inclusions, certain types of nanotubes, bone, fabricated structures such as foams, chiral sculptured thin films, and twisted fibers (for details see, e.g., [1], [4], [5], [6], [7], [8], [9], [10], [11], [17], [18], and the references therein).

Mathematical models describing the properties of elastic hemitropic materials have been proposed in the mid 1960s by Aero and Kuvshinski [1], [2] (for historical notes see also [4], [5], [16], and the references therein).

In the mathematical theory of hemitropic elasticity, the asymmetric force stress tenor and the moment stress tensor are introduced; they are kinematically related to the asymmetric strain tensor and the torsion (curvature) tensor via the constitutive equations. All these quantities are expressed in terms of the components of the displacement and the microrotation vectors; the latter satisfy a system of two coupled second order partial differential equations of dynamics. When the mechanical characteristics (displacements, microrotations, body force and body couple vectors) have harmonic time dependence (i.e. each of them is represented as a product of $exp(-i\sigma t)$ (σ being a real frequency parameter) and a function of the spatial variable x only), we have the corresponding *steady state oscillation equations* (in particular if $\sigma = 0$ we have the *equations of statics*, while if σ is complex we have the so called *pseudo–oscillation equations*, which are related to the dynamical equations via the Laplace transform).

A rigorous mathematical analysis of different aspects of the theory of hemitropic elasticity, for the steady state and the pseudo–oscillation equations, is the object of recent investigation, see [3], [12], [13], [14], [15].

Length limitations to papers in these Proceedings do not allow the inclusion of any details for the referred to results in the following sections.

Governing Equations – Fundamental Solution

The time–harmonic equations oh hemitropic elasticity

We consider the equations of hemitropic elasticity in the form

$$\begin{aligned}&(\mu+\alpha)\Delta u(x)+(\lambda+\mu-\alpha)\,\mathrm{grad}\,\mathrm{div}\,u(x)\\&+(\kappa+\nu)\Delta\omega(x)+(\delta+\kappa-\nu)\,\mathrm{grad}\,\mathrm{div}\,\omega(x)\\&+2\alpha\ \mathrm{curl}\,\omega(x)+\varrho\sigma^2u(x)=-\varrho F(x),\end{aligned}$$

$$\begin{aligned}&(\kappa+\nu)\Delta u(x)+(\delta+\kappa-\nu)\,\mathrm{grad}\,\mathrm{div}\,u(x)\\&+2\alpha\ \mathrm{curl}\,u(x)+(\gamma+\zeta)\Delta\omega(x)\\&+(\beta+\gamma-\zeta)\,\mathrm{grad}\,\mathrm{div}\,\omega(x)+4\nu\,\mathrm{curl}\,\omega(x)\\&+(\mathcal{I}\sigma^2-4\alpha)\omega(x)=-\varrho G(x),\end{aligned}$$

where u is the displacement vector, ω is the microrotation vector, Δ is the Laplacian, $\alpha,\beta,\gamma,\delta,\zeta,\kappa,\lambda,\mu,\nu$ are the material parameters, [1], ϱ is the mass density of the material, $\mathcal{I}$ is a constant characterizing the so called spin torque corresponding to the interior microrotations (i.e. moment of inertia per unit volume) and σ is the angular frequency of the considered time–harmonic fields. F and G are, respectively, the spatial parts of the body force and body couple vectors per unit mass. We remark that instead of ζ the symbol ϵ is normally used for the corresponding material parameter; nevertheless, we employ the standard use of ϵ as the period of the coefficient functions for the homogenization procedure. Note that the microrotation vector ω in the theory of hemitropic elasticity is kinematically distinct from the macrorotation vector $\frac{1}{2}\,\mathrm{curl}\,u$. Further, note that when the parameters

$\alpha, \beta, \gamma, \delta, \zeta, \kappa, \nu, \mathcal{I}$ are all equal to 0, the above system becomes the well known reduced Navier equation of classical linear elasticity.

The fundamental matrix

Let us introduce the matrix differential operator corresponding to the above system:

$$L(\partial, \sigma) := \left[\begin{array}{cc} L^{(1)}(\partial, \sigma) & L^{(2)}(\partial, \sigma) \\ L^{(3)}(\partial, \sigma) & L^{(4)}(\partial, \sigma) \end{array} \right]_{6\times 6},$$

where

$$L^{(1)}(\partial, \sigma) := [(\mu + \alpha)\Delta + \varrho\sigma^2]I_3 + (\lambda + \mu - \alpha)Q(\partial),$$

$$L^{(2)}(\partial, \sigma) = L^{(3)}(\partial, \sigma) := (\kappa + \nu)\Delta I_3 + (\delta + \kappa - \nu)Q(\partial) + 2\alpha R(\partial),$$

$$L^{(4)}(\partial, \sigma) := [(\gamma + \zeta)\Delta + (\mathcal{I}\sigma^2 - 4\,\alpha)]I_3 + (\beta + \gamma - \zeta)Q(\partial) + 4\nu R(\partial).$$

Here I_k stands for the $k \times k$ unit matrix and

$$R(\partial) := \left[\begin{array}{ccc} 0 & -\partial_3 & \partial_2 \\ \partial_3 & 0 & -\partial_1 \\ -\partial_2 & \partial_1 & 0 \end{array} \right]_{3\times 3}, Q(\partial) := [\,\partial_k \partial_j\,]_{3\times 3}.$$

Due to the above notation, our system can be rewritten in matrix form as

$$L(\partial, \sigma)U(x) = \Phi(x),$$
$$U(x) = (u(x), \omega(x))^\top, \quad \Phi(x) = (-\varrho\, F(x), -\varrho\, G(x))^\top.$$

A long technical procedure, [12], leads to the following form for the fundamental matrix

$$\Gamma(x, \sigma) = \sum_{j=1}^{6} \Gamma^{(j)}(x, \sigma),$$

where

$$\Gamma^{(j)} = \left[\begin{array}{cc} L^{(4)}(\partial, \sigma)M(\partial) & -L^{(2)}(\partial, \sigma)M(\partial) \\ -L^{(2)}(\partial, \sigma)M(\partial) & L^{(1)}(\partial, \sigma)M(\partial) \end{array} \right] \ell_j(x),$$

$$M(\partial) = a(\partial)[a(\partial) - b(\partial)\Delta]I_3 + \left[a(\partial)b(\partial) + [c(\partial)]^2\right] Q(\partial) + c(\partial)[a(\partial) - b(\partial)\Delta]R(\partial),$$

with

$$a(\partial) = [(\mu + \alpha)(\gamma + \zeta) - (\kappa + \nu)^2]\Delta\Delta + [(\mu + \alpha)(\mathcal{I}\sigma^2 - 4\alpha) + (\gamma + \zeta)\varrho\sigma^2 + 4\alpha^2]\Delta + \varrho\sigma^2(\mathcal{I}\sigma^2 - 4\alpha),$$

$$b(\partial) = -[(\mu + \alpha)(\beta + \gamma - \zeta) + (\lambda + \mu - \alpha)(\beta + 2\gamma) - (\delta + \kappa - \nu)^2 - 2(\kappa + \nu)(\delta + \kappa - \nu)]\Delta - [(\beta + \gamma - \zeta)\varrho\sigma^2 + (\lambda + \mu - \alpha)(\mathcal{I}\sigma^2 - 4\alpha) - 4\alpha^2],$$

$$c(\partial) = 4\,[\alpha(\kappa + \nu) - \nu(\mu + \alpha)]\Delta - 4\nu\varrho\sigma^2,$$

and

$$\ell_j(x) = q_j \frac{e^{ik_j|x|}}{|x|},$$

where $k_1, ..., k_6, q_1, ..., q_6$ are given, [12], in terms of the parameters $\alpha, \beta, \gamma, \delta, \zeta, \kappa, \lambda, \mu, \nu, \varrho, \sigma, \mathcal{I}$. This representation shows that the entries of the matrix $\Gamma^{(j)}(x, \sigma)$, and its derivatives, satisfy the Sommerfeld radiation conditions at infinity.

Solvability of BVPs

Based on the construction of the fundamental solution, and on the corresponding Green's formulae, [12], general integral representations can be derived for the solutions of the equations of hemitropic elasticity in bounded and unbounded domains; this is done by means of potential type integrals. The properties of the arising single– and double–layer potentials, as well as of certain boundary integral operators (generated by these potentials) have been studied, [12]. Uniqueness and existence theorems for solutions to the Dirichlet, Neumann, and mixed boundary value problems have been proved (by the BIEs method and the theory of pseudodifferential operators) for the case of the pseudo–oscillation equations in smooth domains ([12]) and in Lipschitz domains ([15]), and for the case of the steady state oscillation equations ([14]).

Representation Formulae

In the case of the steady state oscillation equations general representation formulae for the displacement and microrotation vectors by means of metaharmonic functions, solutions of the Helmholtz equations, with different wave numbers have been derived in [13]. There it is proved that the six components of the field vectors (three displacement and three microrotation components) can be expressed by six scalar metaharmonic functions. Moreover, it is shown that this correspondence is one–to–one. In particular, these representation formulae are applied to the construction of explicit solutions of two canonical boundary value and transmission problems for composed solids with spherical interface. In the first case both components are hemitropic with different material constants, and on the interface there are transmission conditions relating limiting values of the displacement, microrotation, force stress, and couple stress vectors (twelve conditions). In the second problem the interior ball is a usual isotropic elastic material described by the classical Lamé model, while in the exterior part there is a hemitropic material: in this case, the interface conditions relate the corresponding displacement and force stress vectors, and, in addition, on the interface there are given, either components

of the microrotation vector, or the couple stress vector (in total nine conditions). The solutions of these problems are represented in the form of Fourier–Laplace series, which, along with their first derivatives, are absolutely and uniformly convergent in closed domains, if the boundary data satisfy appropriate smoothness conditions.

Homogenization

The periodic homogenization problem for the elasticity theory of linear hemitropic materials is studied in [3]. The weak convergence of the solutions w_ϵ corresponding to the material of period $\epsilon > 0$ to a limit w_0, which is identified as the solution corresponding to an analogous "limit" homogeneous problem, is established. The coefficients of hemitropic elasticity of the limit problem are explicitly described in terms of an auxiliary cell problem.

Acknowledgement

The author acknowledges financial support from the project EPEAEK II ["Pythagoras II" Research Fellowships, title "Mathematical Analysis of Wave Propagation in Chiral Electromagnetic and Elastic Media", University of Athens)], co–funded by the European Social Fund and National Hellenic Resources.

References

[1] E.L. Aero, E.V. Kuvshinski, "Continuum theory of asymmetric elasticity. Microrotation effect", Soviet Physics–Solid State, vol. 5, pp. 1892-1899, 1964.

[2] E.L. Aero, E.V. Kuvshinski, "Continuum theory of asymmetric elasticity. Equilibrium of an isotropic body", Soviet Physics–Solid State, vol. 6, pp. 2141-2148, 1965.

[3] G. Barbatis, I.G. Stratis, "Homogenization in chiral elasticity", in Mathematical Methods in Scattering Theory and Biomedical Engineering (eds. D.I. Fotiadis, C.V. Massalas), World Scientific, 2006, pp. 94-103.

[4] J. Dyslewicz, Micropolar Thory of Elasticity, Lecture Notes in Applied and Computational Mechanics, no. 15, Springer-Velag, Berlin, 2004.

[5] A.C. Eringen, Microcontinuum Field Theories I: Foundations and Solids, Springer-Verlag, New York, 1999.

[6] Z. Haijun, O. Zhong-can, "Bending and twisting elasticity: a revised Marko–Sigga model on DNA chirality", Phys. Rev. E, vol. 58, pp. 4816-4821, 1998.

[7] R.S. Lakes, "Elastic and viscoelastic behavior of chiral materials", Intern. J. Mechanical Sci., vol. 43, pp. 1579-1589, 2001.

[8] A. Lakthakia, "Microscopic model for elastostatic and elastodynamic excitation of chiral sculptured thin films", J. Compos. Mater., vol. 36, pp. 1277-1298, 2002.

[9] A. Lakhtakia, V.K. Varadan, V.V. Varadan, "Elastic wave propagation in noncentrosymmetric isotropic media: dispersion and field equations", J. Appl. Phys., vol. 64, pp. 5246-5250, 1988.

[10] T. Mura, Micromechanics of Defects in Solids, Martinus Nijhoff, The Hague, 1987.

[11] T. Mura, "Some new problems in micromechanics", Materials Science and Engineering A, vol. 285, pp. 224-228, 2000.

[12] D. Natroshvili, L. Giorgashvili, I.G. Stratis, "Mathematical problems of the theory of elasticity of chiral materials", Applied Mathematics, Informatics, and Mechanics, vol. 8, pp. 47-103, 2003.

[13] D. Natroshvili, L. Giorgashvili, I.G. Stratis, "Representation formulas of general solutions in the theory of hemitropic elasticity", Quart. J. Mech. Appl. Math., vol. 59, pp. 451-474, 2006.

[14] D. Natroshvili, L. Giorgashvili, S. Zazashvili, "Steady state oscillation problems in the theory of elasticity for chiral materials", Journal of Integral Equations and Applications, vol. 17, pp. 19-69, 2005.

[15] D. Natroshvili, I.G. Stratis, "Mathematical problems of the theory of elasticity of chiral materials for Lipschitz domains", Math. Methods Appl. Sci., vol. 29, pp. 445-478, 2006.

[16] W. Nowacki, Theory of Asymmetric Elasticity, Pergamon Press, Oxford; PWN–Polish Scientific Publishers, Warsaw, 1986.

[17] R. Ro, "Elastic activity of the chiral medium", J. Appl. Phys., vol. 85, pp. 2508-2513, 1999.

[18] P. Sharma, "Size-dependent elastic fields of embedded inclusions in isotropic chiral solids", International Journal of Solids and Structures, vol. 41, pp. 6317-6333, 2004.

Minisymposium on Nonlinear Waves

Organisers: Mark Groves (Loughborough University) and Beatrice Pelloni (University of Reading)

RECENT RESULTS IN THE THEORY OF OCEAN WAVES

Jerry L. Bona
Department of Mathematics, Statistics, and Computer Science, University of Illinois at Chicago,
851 South Morgan St., Chicago, IL 60607, USA
Email: bona@math.uic.edu

Abstract

This lecture focuses upon one of the possible generative mechanisms for what are often termed Rogue Waves or sometimes Freak Waves. These are very big waves that appear occasionally in the deep ocean. Such waves have been reported by mariners for centuries, but have only been taken seriously fairly recently. They are unlike tsunamis in a number of ways. First, they persist in relatively small portions of space-time, unlike tsunamis which can propagate coherently for thousands of miles. Secondly, they are of truly large amplitude even in the deep ocean, whereas tsunamis are of small amplitude in deep water, often unnoticeable there in fact. Their existence only becomes clear when they enter shallower water. And while we have a pretty clear idea of the ways tsunamis can be generated, it is otherwise with Rogue waves.

Concurrence

One of the suggested mechanisms for the generation of Rogue waves is what we will call concurrence. Roughly speaking, this simply amounts to the possibility that small waves spread out in the ocean might, on occasion, get together en masse and add up to something really significant. It is our purpose to investigate the plausibility of this mechanism within the mathematical framework of classical water wave models. What is reported is joint work with Jean-Claude Saut (see [1], [2], [3]).

We begin with the Korteweg-de Vries model

$$u_t + u_x + uu_x + u_{xxx} = 0.$$

It is elementary to see that for the linearized version of this equation, a kind of dispersive focusing can occur by placing shorter and shorter wavelength compo- nents out near $x = +\infty$. It is an interesting bit of analysis to see that the initial value problem for the *nonlinear* KdV equation has the same property, which we term *dispersive blow-up*.

An immediate ob jection to this analysis as far as its application to Rogue waves is concerned is that the model is uni-directional and we are making use of waves traveling in the wrong direction. This can be remedied by consideration of a Boussinesq system of equations, which does allow for two-way propagation of waves. It turns out this system also exhibits the dispersive blow-up phenomenon. Moreover, this latter result can be generalized to a fully three dimensional Boussinesq system. Thus, an initial wave and velocity configuration that is too small to even bed seen with the naked eye can, in this approximation, concentrate wave components and, in finite time, lead to a wave with a infinite amplitude. A further ob jection can be raised, which is that the foregoing theory makes use of the unbounded group and phase velocities that obtain within certain of the Boussinesq (and the KdV) approximations. As the full Euler equations do not possess this property, it is still not clear whether or not the theory might pertain to the development of real Rogue waves by concurrence. A final result was mentioned, that grows out of the preceding. Another way of looking at what was established for the KdV equation and for Boussinesq systems is that these equations are not well posed in L^∞-type spaces. That is, no matter how small the initial data is restricted as far as its maximum values are concerned, the resulting solution can take on values as large as we like in finite time. Looked at this way, the issue is clarified. The authors have been able to show that at least the linearized, two-dimensional Euler equations are not well posed in L^∞, thereby coming closer to being able to say that concurrence is a possible mechanism for the formation of Rogue waves.

References

[1] J. L. Bona and J.-C. Saut, "Singularités dispersives de solutions d'équations de type Korteweg-de Vries", C. R. Acad. Sci. Paris, vol. 303, pp. 101–103 (1986).

[2] J. L. Bona and J.-C. Saut, "Dispersive blow-up of solutions of generalized Korteweg-de Vries equations", J. Diff. Eqns., vol. 103, pp. 3–57 (1993).

[3] J. L. Bona and J.-C. Saut, "Dispersive blow-up phenomena for nonlinear wave equations and concurrence on the ocean", in preparation (2007).

The Dirichlet to Neumann map for a moving initial/boundary value problem for the heat equation

S. De Lillo[†,*] **and A. S. Fokas**[‡]
[†]Dipartimento di Matematica e Informatica, Università degli Studi di Perugia, Via Vanvitelli 1, 06123 Perugia, Italy
Istituto Nazionale di Fisica Nucleare, Sezione di Perugia
[‡]Department of Applied Mathematics and Theoretical Physics, University of Cambridge, Cambridge, CB3 OWA, U.K.
[*]Email: delillo@pg.infn.it

Extended Abstract

We construct the Dirichlet to Neumann map for the linear heat equation posed on a domain whose boundary varies with time.

Let $q(x,t)$ satisfy the heat equation in a simply connected domain D,

$$q_t(x,t) = q_{xx}(x,t),\ (x,t) \in D \subset \mathbf{R}^2. \tag{1}$$

Suppose that there exists a solution $q(x,t)$ with sufficient smoothness all the way to the boundary of D, denoted by ∂D. Then, the following *global relation* is valid for all values of the complex constant k,

$$\int_{\partial D} e^{-ikx+k^2t}[q(x,t)dx + (q_x(x,t) + kq(x,t))dt] = 0,\ k \in \mathbf{C}. \tag{2}$$

Indeed the heat equation is equivalent to the equation

$$\left[e^{-ikx+k^2t}(q_x(x,t) + kq(x,t))\right]_x - \left[e^{-ikx+k^2t}q(x,t)\right]_t = 0,$$

and then (2) follows from Green's theorem.

Equation (2) relates the Dirichlet and Neumann boundary values of the solution $q(x,t)$, thus it characterizes the *Dirichlet to Neumann correspondence*.

Let us consider the following moving boundary value problem for the heat equation (1), see Figure 1,

$$D:\ 0 < t < T,\ l(t) < x < \infty;\ \ddot{l}(t) > 0, l(0) = 0, \tag{3}$$

$$q(x,0) = q_0(x),\ 0 < x < \infty;$$
$$q(l(t),t) = g_0(t), 0 < t < T, \tag{4}$$

where T is a positive constant, the functions $l(t)$, $g_0(t)$, $q_0(x)$ have sufficient smoothness and $q_0(x)$ has sufficient decay for large x. In this particular case, the global relation (2) becomes the following equation, which is valid for *Im* $k \leq 0$:

$$\int_0^T e^{k^2t-ikl(t)}\left[q_x(l(t),t) + (\dot{l}(t) + ik)g_0(t)\right]dt = \hat{q}_0(k) - e^{k^2T}\int_{l(t)}^{\infty} e^{-ikx}q(x,T)dx \tag{5}$$

where $\hat{q}_0(k)$ denotes the Fourier transform of the initial condition $q_0(x)$. In summary:

Let $q(x,t)$ satisfy the heat equation (1) *in the domain D defined in equations* (3)*, with the initial and boundary conditions* (4)*. Suppose that there exists a solution $q(x,t)$ with sufficient smoothness and decay; the problem of characterizing the associated Dirichlet to Neumann map, reduces to the problem of solving the global relation* (5) *for the unknown function $q_x(l(t),t)$ in terms of the known functions $\hat{q}_0(k)$ and $g_0(t)$. This solution must be independent of $q(x,T)$.*

Regarding the unknown functions $q(x,T)$, we note that the evolutionary nature of the heat equation implies that this function does *not* contribute to the solution ($q(x,t)$ *cannot* depend on the future time T).

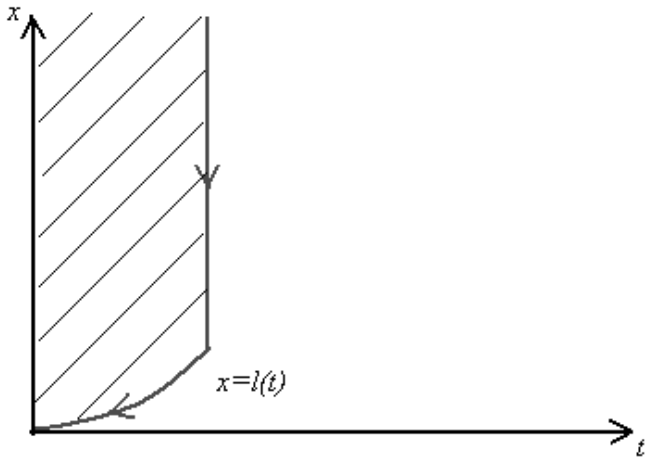

Figure 1: The domain D in the (x,t)–plane

We prove that the function $q_x(l(t),t) = g_1(t)$ satisfies the following Volterra integral equation

$$\frac{3}{4}\, g_1(t) = \frac{1}{2\sqrt{\pi}}[\frac{1}{\sqrt{t}}\int_0^\infty e^{-\frac{(l(t)-x)^2}{4t}}\dot{q}_0(x)dx$$
$$-\int_0^t \frac{e^{-\frac{(l(t)-l(s))^2}{4(t-s)}}}{\sqrt{t-s}}\dot{g}_0(s)ds] + \int_0^t g_1(s)K(s,t)ds, \quad (6)$$

where the function $K(s,t)$ is defined by the equations

$$K(s,t) = -\frac{1}{2\pi}\int_0^\infty [1 - \frac{i}{2}(\frac{\nu}{\sqrt{\nu^2 - \dot{l}(s)\nu}} +$$
$$+\frac{\sqrt{\nu^2 - \dot{l}(s)\nu}}{\nu})B(\nu,s,t)]d\nu, \quad (7)$$

$$B(\nu,s,t) = (\sqrt{\nu^2 - \dot{l}(s)\nu} + i\nu)\exp[-\nu(\dot{l}(s) - \vartheta(t,s))$$
$$(s-t) + i\sqrt{\nu^2 - \dot{l}(s)\nu}\,(2\nu - \vartheta(t,s))(s-t)], \quad (8)$$

$$\vartheta(t,s) = \frac{l(t) - l(s)}{t-s}.$$

Using the mean value theorem it follows that $\vartheta(t,s) = \dot{l}(\tau)$, $s < \tau < t$. This implies that the real part of the exponential in the right hand side of (8) is negative; hence, the kernel $K(s,t)$ decays exponentially as $\nu \to \infty$.

References

[1] S. De Lillo and A. S. Fokas, "The Dirichlet to Neumann map for the heat equation on a moving boundary", Submitted to Inverse Problems, 2007, and references therein.

Universality results for singular limits of nonlinear evolutionary PDEs

B. Dubrovin[†], **T. Grava**[†,*], **C. Klein**[‡]
[†]SISSA, via Beirut 2-4, 34014 Trieste, Italy
[‡] Max Planck Institute, Leipzig
[*]Email: grava@sissa.it

Abstract

We argue that critical behaviour near the point of gradient catastrophe of the solution of the Cauchy problem for the focusing nonlinear Schrödinger equation $i\epsilon\,\psi_t + \frac{\epsilon^2}{2}\psi_{xx} + |\psi|^2\psi = 0$ with analytic initial data of the form $\psi(x,0;\epsilon) = A(x)\,e^{\frac{i}{\epsilon}S(x)}$ is approximately described by a particular solution to the Painlevé-I equation. The critical behaviour near the point of gradient catastrophe of the solution of the Cauchy problem for any Hamiltonian perturbation of the Hopf equation $u_t + uu_x = 0$, is approximately described by a particular solution of the second member of the Painlevé-I hierarchy.

Introduction

It is well known that the solution of the Cauchy problem for the Hopf equation

$$u_t + uu_x = 0, \quad u(x,t=0) = u_0(x), \tag{1}$$

($x \in \mathbb{R}$), reaches a point of gradient catastrophe (x_c, t_c, u_c) in a finite time. The solution of the viscosity or conservative regularization of the above hyperbolic equation display a considerably different behavior. Indeed the solution of the conservative regularization has an oscillatory behaviour near the point of gradient catastrophe for the Hopf equation (see e.g. [1]). All the Hamiltonian perturbations up to the order ϵ^4, $\epsilon \ll 1$, of the hyperbolic equation (1) have been classified in [2]. They are parametrized by two arbitrary functions $c(u)$, $p(u)$, namely

$$\begin{aligned} &u_t + u\,u_x + \frac{\epsilon^2}{24}\left[2c\,u_{xxx} + 4c'u_xu_{xx} + c''u_x^3\right] + \\ &\epsilon^4\left[2p\,u_{xxxxx} + 2p'(5u_{xx}u_{xxx} + 3u_xu_{xxxx}) + \right. \\ &\left. p''(7u_xu_{xx}^2 + 6u_x^2u_{xxx}) + 2p'''u_x^3u_{xx}\right] = 0, \end{aligned} \tag{2}$$

where the prime denotes the derivative with respect to u.

For $c(u) = 24$, $p(u) = 0$ one obtains the Korteweg - de Vries (KdV) equation $u_t + uu_x + \epsilon^2 u_{xxx} = 0$, and for $c(u) = 48u$ and $p(u) = 2u$ the Camassa-Holm equation [3] up to order ϵ^4; for generic choices of the functions $c(u)$, $p(u)$ equation (2) is apparently not an integrable PDE. However it admits an infinite family of commuting Hamiltonians up to order $O(\epsilon^6)$.

It is argued in [2] and numerically proven in [4] that the generic behaviour of the solution of the Cauchy problem of (2) near the point of gradient catastrophe for the Hopf equation is described by a particular solution of the second member of the Painlevé-I hierarchy.

Next we consider the semi-classical limit of the focusing nonlinear Schrödinger (NLS) equation for the complex valued function $\psi = \psi(x,t)$

$$i\,\epsilon\,\psi_t + \frac{\epsilon^2}{2}\psi_{xx} + |\psi|^2\psi = 0, \tag{3}$$

with initial data

$$\psi(x,0;\epsilon) = A(x)\,e^{\frac{i}{\epsilon}S(x)}. \tag{4}$$

Here $\epsilon > 0$ is a small parameter. Properties of various classes of solutions to this equation have been extensively studied both analytically and numerically [5], [6], [7], [8], [9],[10], [11]. One of the striking features that distinguishes this equation from the defocusing case, is the phenomenon of *modulation instability* [12]. Namely, slow modulations of the plane wave solutions develop fast oscillations in finite time. Introducing the slow variables

$$u = |\psi|^2, \quad v = \frac{\epsilon}{2i}\left(\frac{\psi_x}{\psi} - \frac{\bar\psi_x}{\bar\psi}\right) \tag{5}$$

the equation can be recast into the following system:

$$\begin{aligned} &u_t + (u\,v)_x = 0 \\ &v_t + v\,v_x - u_x + \frac{\epsilon^2}{4}\left(\frac{1}{2}\frac{u_x^2}{u^2} - \frac{u_{xx}}{u}\right)_x = 0. \end{aligned} \tag{6}$$

The initial data for the system (6) coming from (4) do not depend on ϵ:

$$u(x,0) = A^2(x), \quad v(x,0) = S'(x). \tag{7}$$

The simplest explanation of the modulation instability then comes from considering the so-called *dispersionless limit* $\epsilon \to 0$. In this limit one obtains the following first order quasilinear system

$$\left.\begin{aligned} u_t \quad &+v\,u_x + u\,v_x = 0 \\ v_t \quad &-\ u_x + v\,v_x = 0 \end{aligned}\right\}. \tag{8}$$

This is a system of *elliptic type* because of the condition $u > 0$. Indeed, the eigenvalues of the coefficient matrix

$$\begin{pmatrix} v & u \\ -1 & v \end{pmatrix}$$

are complex conjugate, $\lambda = v \pm i\sqrt{u}$. So, the Cauchy problem for the system (8) is ill-posed in the Hadamard sense. Even for analytic initial data the life span of a typical solution is finite, $t < t_c$. The x- and t-derivatives explode at some point $x = x_c$ when the time approaches t_c. This phenomenon is similar to the gradient catastrophe of solutions to nonlinear hyperbolic PDEs.

For the full system (6) the Cauchy problem is well-posed for a suitable class of ϵ-independent initial data (see details in [13], [14]). However, the well-posedness is not uniform in ϵ. The solutions to (8) and (6) are essentially indistinguishable for $t < t_c$; the situation changes dramatically near x_c when approaching the critical point. Namely, the solution develops a zone of rapid oscillations for $t > t_c$. They have been studied both analytically and numerically in [7], [9], [11]. However, no results are available so far about the behaviour of the solutions to focusing NLS *at the critical point* (x_c, t_c). We argue that the solution of NLS near a critical point is approximately described by a solution of the Painlevé-I equation.

Painlevé equations and Universality conjecture

In [2] it is argued that the behaviour of the solution to the Hamiltonian perturbation (2) of the hyperbolic equation (1) near the point (x_c, t_c, u_c) of gradient catastrophe for the solution of (1), up to shifts, Galilean transformations and rescalings, essentially depends neither on the choice of solution nor on the choice of the equation.

Main Conjecture 1. [2] This behaviour is described near the point (x_c, t_c, u_c) by

$$\begin{aligned} &u(x,t,\epsilon) \simeq u_c + \\ &a\,\epsilon^{2/7} U\left(b\,\epsilon^{-6/7}\bar{x}; c\,\epsilon^{-4/7}(t-t_c)\right) + O\left(\epsilon^{4/7}\right), \\ &\bar{x} = x - x_c - 6u_c(t-t_c), \quad \bar{t} = t - t_c, \end{aligned} \tag{9}$$

where a, b, c are some constants that depend on the choice of the equation and the initial data evaluated at the critical point (x_c, t_c, u_c) and $U = U(X;T)$ is the unique real smooth solution to the fourth order ODE

$$\begin{aligned} X = 6T\,U - \Big[&\frac{U^3}{6} + \frac{1}{24}U_X^2 + \frac{1}{12}U\,U_{XX} \\ &+ \frac{1}{240}U_{XXXX}\Big], \end{aligned} \tag{10}$$

which is the second member of the Painlevé-I hierarchy. The relevant solution is characterized by the asymptotic behavior

$$U(X,T) = \mp(X)^{\frac{1}{3}} \mp \frac{2T}{X^{\frac{1}{3}}} + O(X^{-1}), \quad X \to \pm\infty, \tag{11}$$

for each fixed $T \in \mathbb{R}$. The existence of a smooth solution of (10) for all $X, T \in \mathbb{R}$ satisfying (11) is proved in [16]. The Main Conjecture 1 is supported numerically in [4].

Regarding the generic solution of the NLS equations near the critical point (x_c, t_c, u_c, v_c) for the system (8), it is described in terms of a particular solution of the Painlevé-I equation

$$\Omega_{\zeta\zeta} = 6\Omega^2 - \zeta. \tag{12}$$

Recall that the general solution to this equation is a meromorphic function on the complex ζ-plane. Among the many solutions, the relevant solution for our problem is the so called tritronquée solution, namely a solution Ω_0 with the asymptotic behaviour of the form

$$\Omega_0 = -\left(\frac{\zeta}{6}\right)^{1/2}\left[1 + O\left(\zeta^{-\frac{3}{4}(1-\varepsilon)}\right)\right]. \tag{13}$$

Such solution is analytic for large ζ in the sector [17]

$$|\arg\zeta| < \frac{4\pi}{5}. \tag{14}$$

Main Conjecture 2. Part 1. [15] The tritronquée solution $\Omega_0(\zeta)$ has no poles in the sector

$$|\arg\lambda| < \frac{4\pi}{5}. \tag{15}$$

We are now ready to describe the conjectural universal structure behind the critical behaviour of generic solutions to the focusing NLS.

Main Conjecture 2. Part 2. [15] Any generic solution to the NLS equations near the critical point (x_c, t_c, u_c, v_c) behaves as follows

$$\begin{aligned} &u(x,t;\epsilon) + i\sqrt{u_c}v(x,t;\epsilon) \simeq u_c + i\sqrt{u_c}v_c - \bar{t}\,re^{i\psi} + \\ &2\,\epsilon^{2/5}(3r\sqrt{u_c})^{2/5}e^{\frac{2i\psi}{5}}\Omega_0(\zeta) + O\left(\epsilon^{4/5}\right) \\ &\zeta = \left(\frac{3r}{u_c^2}\right)^{1/5} e^{\frac{i\psi}{5}}\left[\frac{-u_c\bar{t} + i\sqrt{u_c}(\bar{x} - v_c\bar{t}) + \frac{1}{2}re^{i\psi}\bar{t}^2}{\epsilon^{4/5}}\right] \end{aligned} \tag{16}$$

where $\Omega_0(\zeta)$ is the tritronquée solution to the Painlevé-I equation (12),

$$\bar{x} = x - x_c, \quad \bar{t} = t - t_c,$$

$$\bar{u} = u - u_c, \quad \bar{v} = v - v_c,$$

and r and ϕ depend on the initial data evaluated at the critical point. Numerical evidence for Main Conjecture 2 is given in [15] using spectral methods [18].

References

[1] P. D. Lax and C. D. Levermore, *The small dispersion limit of the Korteweg de Vries equation, I,II,III*, Comm. Pure Appl. Math. **36** (1983), 253-290, 571-593, 809-830.

[2] B.Dubrovin, On Hamiltonian perturbations of hyperbolic systems of conservation laws, II: universality of critical behaviour, *Comm. Math. Phys.* **267** (2006) 117 - 139.

[3] R. Camassa and D. D. Holm, An integrable shallow water equation with peaked solitons, Phys. Rev. Lett. **71** (1993), 1661-1664.

[4] T.Grava, C.Klein, Numerical study of a multiscale expansion of KdV and Camassa-Holm equation. ArXiv:math-ph/0702038.

[5] J.C.Bronski, J.N.Kutz, Numerical simulation of the semiclassical limit of the focusing nonlinear Schrdinger equation. *Phys. Lett.* **A 254** (2002) 325 - 336.

[6] R.Carles, WKB analysis for the nonlinear Schrödinger equation and instability results. ArXiv:math.AP/0702318.

[7] H.D.Ceniceros, F.-R.Tian, A numerical study of the semi-classical limit of the focusing nonlinear Schrödinger equation. *Phys. Lett.* **A 306** (2002) 25–34.

[8] C. Klein, Fourth order time-stepping for low dispersion Korteweg - de Vries and nonlinear Schrödinger equation (2006), http://www.mis.mpg.de/preprints/2006/prepr2006_133.html

[9] S. Kamvissis, K.D.T.-R.McLaughlin, P.D.Miller, *Semiclassical soliton ensembles for the focusing nonlinear Schrödinger equation.* Annals of Mathematics Studies, 154. Princeton University Press, Princeton, NJ, 2003.

[10] E.Grenier, Semiclassical limit of the nonlinear Schrödinger equation in small time. *Proc. Amer. Math. Soc.* **126** (1998) 523–530.

[11] A.Tovbis, S.Venakides, X.Zhou, On semiclassical (zero dispersion limit) solutions of the focusing nonlinear Schrödinger equation. *Comm. Pure Appl. Math.* **57** (2004) 877–985.

[12] G.P.Agrawal, *Nonlinear Fiber Optics*. Academic Press, San Diego, 2006, 4th edition.

[13] A.B.Shabat, One-dimensional perturbations of a differential operator, and the inverse scattering problem. In: *Problems in Mechanics and Mathematical Physics*, 27996. Nauka, Moscow, 1976.

[14] V.E.Zakharov, A.B.Shabat, A. B. Exact theory of two-dimensional self-focusing and one-dimensional self-modulation of waves in nonlinear media. *Soviet Physics JETP* **34** (1972), no. 1, 62-69.; translated from *Ž. Eksper. Teoret. Fiz.* (1971), no. 1, 118-134.

[15] B.Dubrovin, T.Grava, C.Klein On universality of critical behaviour in the focusing nonlinear Schrödinger equation, elliptic umbilic catastrophe and the *tritronquée* solution to the Painlevé-I equation. Preprint,http://arXiv:0704.0501.

[16] T.Claeys, M.Vanlessen, The existence of a real pole-free solution of the fourth order analogue of the Painlevé I equation. ArXiv:math-ph/0604046.

[17] P.Boutroux, Recherches sur les transcendants de M. Painlevé et l'étude asymptotique des équations différentielles du second ordre. *Ann. École Norm* **30** (1913) 265 - 375.

[18] L. N. Trefethen, *Spectral Methods in MATLAB*, SIAM, Philadelphia, PA, 2000.

INTERNAL SOLITARY WAVES IN A VARIABLE MEDIUM

R. Grimshaw[†,*]
[†]Department of Mathematical Sciences, Loughborough University, LE11 3TU, UK
[*]Email: R.H.J.Grimshaw@lboro.ac.uk

Abstract

In the coastal ocean, the interaction of a density stratified flow with topography generates large-amplitude, horizontally propagating internal solitary waves. Often these waves are observed in regions where the waveguide properties vary in the direction of propagation. We consider an extended Korteweg-de Vries equation, with variable coefficients, and use this model to describe the shoaling of internal solitary waves over the continental shelf and slope, based on the asymptotic theory of slowly-varying solitary waves together with some numerical simulations. We shall emphasize the critical role played by those special locations where the coefficient of either the quadratic, or the cubic, nonlinear term vanishes.

Introduction

An appropriate model equation is the variable-coefficient extended Korteweg-de Vries (veKdV) equation [1]

$$A_t + \alpha A A_x + \beta A^2 A_x + \delta A_{xxx} = 0\,. \tag{1}$$

Here (x,t) are transformed variables related to the usual space and time variables (χ,τ) by

$$t = \int^{\chi} \frac{d\chi}{c}\,, \quad x = t - \tau\,, \tag{2}$$

while $c(\chi)$ is the linear long wave speed for the relevant internal wave mode, whose amplitude $\eta(\chi,\tau)$ is related to the transformed amplitude by $A(x,t) = \sqrt{Q}\,\eta$. Q is the linear magnification factor, defined so that $Q\eta^2$ is the wave action flux. The coefficients $\alpha(t), \beta(t)$ and $\delta(t)$ of the nonlinear and dispersive terms respectively vary spatially, and are determined by the stratification and topography of the oceanic waveguide (see [2] for full formulas). Note that although t is a variable along the spatial path of the wave, we shall subsequently refer to it as the "time". Similarly, although x is a temporal variable, in a reference frame moving with speed c, we shall subsequently refer to it as a "space" variable.

The evKdV equation (1) possesses two relevant conservation laws,

$$\int_{-\infty}^{\infty} A\,dx \;=\; \text{constant}\,, \tag{3}$$

$$\int_{-\infty}^{\infty} A^2\,dx \;=\; \text{constant}\,, \tag{4}$$

representing conservation of mass and momentum respectively.

Slowly-varying solitary waves

We now suppose that the coefficients α, β, δ in the evKdV equation (1) are slowly varying, and write

$$\alpha = \alpha(T)\,, \quad \delta = \delta(T)\,, \quad T = \sigma\tau\,, \quad \sigma << 1\,. \tag{5}$$

These definitions enable us to define the slowly-varying condition that the width of the solitary wave should be much less than $1/\sigma$. We then invoke a multi-scale asymptotic expansion of the form

$$A = A_0(X,T) + \sigma A_1(X,T) + \cdots\,, \tag{6}$$

$$X = x - \frac{1}{\sigma}\int^{T} V(T)\,dT\,. \tag{7}$$

A is defined over the domain $-\infty < X < \infty$, and we require that A remain bounded in the limits $X \to \pm\infty$. Since we can assume that $\delta > 0$ small-amplitude waves will propagate in the negative X-direction, and so we can suppose that $A \to 0$ as $X \to \infty$. However, it will transpire that we cannot impose this boundary condition as $X \to -\infty$.

The leading term is the solitary wave,

$$A_0 = \frac{H}{1 + B\cosh K\phi}\,, \tag{8}$$

$$\text{where } V = \frac{\alpha H}{6} = \delta K^2\,,\; B^2 = 1 + \frac{6\delta\beta K^2}{\alpha^2}\,. \tag{9}$$

The amplitude is $a = H/1 + B$, and all parameters vary with T, that is $B = B(T)$ etc. The family of solutions (8) depend on a single parameter, which can conveniently be taken as B. For $\beta < 0$ there is just one branch of solutions, with $0 < B < 1$; they range from small-amplitude solitary waves of KdV-type with the familiar

"sech^2"-profile when $B \to 1$, to a limiting wave of amplitude $-\alpha/\beta$ as $B \to 0$; this limiting wave is characterized by a flat top, and is sometimes called a "table-top" wave. For $\beta > 0$ there are two branches; one has $1 < B < \infty$ and ranges from small-amplitude KdV-type waves when $B \to 1$, to arbitrarily large waves with a "sech"-profile as $B \to \infty$. The other branch has has the opposite polarity, exists for $-\infty < B < -1$, and ranges from arbitrarily large waves with a "sech"-profile to a limiting algebraic solitary wave of amplitude $-2\alpha/\beta$. Solitary waves with smaller amplitudes cannot exist, and are replaced by breathers.

The determination of how B in (8) varies with T is found either by considering the next-order term in the expansion, or equivalently by using the conservation law for momentum (4). At leading order the solitary wave (8) is substituted into (4) to give

$$G(B) = \text{constant}|\frac{\beta^3}{\delta\alpha^2}|^{1/2}, \qquad (10)$$

$$\text{where } G(B) = |B^2-1|^{3/2}\int_{-\infty}^{\infty}\frac{du}{(1+B\cosh u)^2}.$$

The integral term in $G(B)$ can be explicitly evaluated, see [1], and so these expressions provide explicit formulae for the variation of $B(T)$ as the environmental parameters vary.

But since the conservation of momentum completely defines the slowly-varying solitary wave, we see that this cannot simultaneously conserve total mass (3). This is also apparent when one examines the solution for A_1, from which it is readily shown that although $A_1 \to 0$ as $X \to \infty$, $A_1 \to D_1$ as $X \to -\infty$ where

$$VD_1 = -M_{0T}, \quad \text{and} \quad M_0 = \int_{\infty}^{\infty} A_0 dX. \qquad (11)$$

This non-uniformity in the slowly-varying solitary wave is well-known. The remedy is the construction of a trailing shelf A_s of small amplitude $O(\sigma)$ but long length-scale $O(1/\sigma)$, which thus has $O(1)$ mass, but $O(\sigma)$ momentum.

Results

The analysis of the adiabatic transformation of a solitary wave in section 2 shows that the critical points where $\alpha = 0$ (or where $\beta = 0$) are sites where we may expect a dramatic change in the wave structure [1]. Suppose first that α passes through zero, but that $\beta < 0, O < B < 1$ at the critical point $T = 0$ where $\alpha = 0$. Then as $\alpha \to 0$, it follows from (10) that $B \to 0$ and the wave profile approaches the limiting "table-top" wave. But in this limit, $K \sim |\alpha|$, and so the amplitude approaches the limiting value $a \sim -\alpha/\beta$. Thus the wave amplitude decreases to zero, but the mass M_0 of the solitary wave grows as $|\alpha|^{-1}$ and so the amplitude D_1 of the trailing shelf grows as $1/|\alpha|^4$ (11). Essentially the trailing shelf passes through the critical point as a disturbance of the opposite polarity to that of the original solitary wave, which then being in an environment with the opposite sign of α, can generate a train of solitary waves of the opposite polarity, riding on a pedestal (see [3]).

Next, let us suppose that at the critical point where $\alpha = 0$, $\beta > 0$. In this case, $1 < |B| < \infty$ and there are the two sub-cases to consider, $B > 0$ or $B < 0$, when the the solitary wave has the same or opposite polarity to α. Then, as $\alpha \to 0, |B| \to \infty$ as $|B| \sim 1/|\alpha|$. It follows from (9) that then $K \sim 1$, $D \sim 1/|\alpha|, a \sim 1, M_0 \sim 1$. It follows that the wave adopts the "sech"-profile, but has *finite* amplitude, and so can pass through the critical point $\alpha = 0$ without destruction. But the wave changes branches from $B > 0$ to $B < 0$ as $|B| \to \infty$, or *vice versa*. An interesting situation then arises when the wave belongs to the branch with $-\infty < B < -1$ and the amplitude is reducing. If the limiting amplitude of $-2\alpha/\beta$ is reached, then there can be no further reduction in amplitude for a solitary wave, and instead a breather will form.

References

[1] R. Grimshaw, E. Pelinovsky, T. Talipova, and A. Kurkin. "Simulation of the transformation of internal solitary waves on oceanic shelves" . J. Phys. Ocean., 2004, vol. 34, 2774-2779.

[2] R. Grimshaw, E. Pelinovsky and O. Poloukhina. "Higher-order Korteweg-de Vries models for internal solitary waves in a stratified shear flow with a free surface" . Nonlinear Processes in Geophysics, 2002, vol 9, 221-235.

[3] Grimshaw, R., Pelinovsky, E. and Talipova T. Solitary wave transformation in a medium with sign-variable quadratic nonlinearity and cubic nonlinearity. *Physica D*, 1999, **132**, 40-62.

MODULATING PULSE SOLUTIONS TO QUADRATIC QUASILINEAR WAVE EQUATIONS OVER EXPONENTIALLY LONG TIME SCALES

M. D. Groves
Department of Mathematical Sciences, Loughborough University, Loughborough, LE11 3TU, UK
Email: M.D.Groves@lboro.ac.uk

Abstract

This paper presents an existence proof for modulating pulse solutions to a wide class of quadratic quasilinear Klein-Gordon equations. Modulating pulse solutions consist of a pulse-like envelope advancing in the laboratory frame and modulating an underlying wavetrain; they are also referred to as 'moving breathers' since they are time-periodic in a moving frame of reference. The problem is formulated as an infinite-dimensional dynamical system with three stable, three unstable and infinitely many neutral directions. By transforming part of the equation into a normal form with an exponentially small remainder term and using a generalisation of local invariant-manifold theory to the quasilinear setting, we prove the existence of small-amplitude modulating pulses on domains in space whose length is exponentially large compared to the magnitude of the pulse.

Introduction

Consider the equation

$$\partial_t^2 u = \partial_x^2 u - u + f_1(u, \partial_x u, \partial_t u)\partial_x^2 u + f_2(u, \partial_x u, \partial_t u), \quad (1)$$

in which

(i) f_1, f_2 are analytic;

(ii) $f_i(a, -b, -c) = f_i(a, b, c),\ i = 1, 2.$ (2)

We seek modulating pulse solutions of the form

$$u(x,t) = v_1(\xi, \eta), \quad \xi = x - c_{\rm g} t,\ \eta = k_0(x - c_{\rm p} t),$$

where

(i) $v_1(\xi, \eta)$ is 2π-periodic in η and has a pulse-like profile in ξ;

(ii) $c_{\rm p} = c_{\rm p}' - \varepsilon^2$ and $c_{\rm g} = 1/c_{\rm p}$, where $c_{\rm p}'$ is the linear phase velocity $(1 + k_0^2)^{1/2}/k_0$ for a periodic wave train with wavenumber k_0.

Heuristic arguments show that one cannot in general expect a 'genuine' pulse solution for which $v_1(\xi, \eta)$ decays to zero as $\xi \to \pm\infty$ (see below), and several rigorous 'non-existence' results in this direction have indeed been published ([1], [2]). A robust result can however be obtained by generalising the definition of 'pulse' to include solutions which (i) do not necessary tend to zero as $\xi \to \pm\infty$ but certainly become very small for large values of ξ; (ii) do not necessarily exist for all $\xi \in \mathbb{R}$ but certainly exist for ξ in a very large interval of $\mathbb{R}$ [3].

Theorem

Fix a positive real number k_0. There exist positive constants ε_0 and c^* with the property that for each $\varepsilon \in (0, \varepsilon_0]$ equation (1) admits an infinite-dimensional, continuous family of modulating pulse solutions. These solutions satisfy

$$v_1(\xi, \eta) = v_1(-\xi, -\eta),$$

$$|v_1(\xi, \eta) - h^\varepsilon(\xi, \eta)| \leq {\rm e}^{-c^\star/2\sqrt{\varepsilon}}$$

for all $\eta \in \mathbb{R}$ and $\xi \in [-{\rm e}^{c^\star/2\sqrt{\varepsilon}}, {\rm e}^{c^\star/2\sqrt{\varepsilon}}]$, in which

$$h^\varepsilon(\xi, \eta) = \pm\varepsilon \left(\frac{2\check{C}_1}{\pi \check{C}_2}\right)^{1/2} {\rm sech}(\check{C}_1^{1/2}\varepsilon\xi)\cos\eta + \mathcal{O}(\varepsilon^{3/2}{\rm e}^{-\varepsilon\theta|\xi|}), \qquad 0 < \theta < \check{C}_1^{1/2}$$

(so that $\lim_{\xi \to \pm\infty} h^\varepsilon(\xi, \eta) = 0$ uniformly in $\eta \in \mathbb{R}$) and $\check{C}_1$, $\check{C}_2$ are positive constants (see Figure 1).

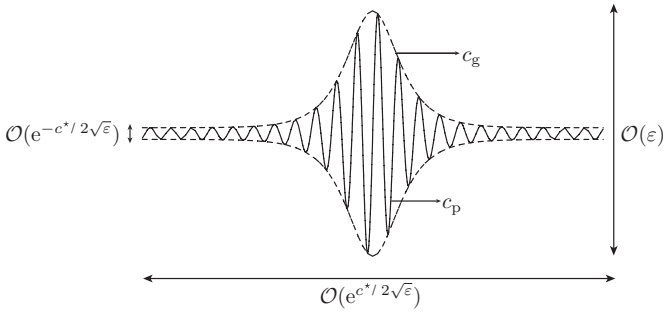

Figure 1: A modulating pulse solution

In this paper we sketch the proof of the above theorem.

Spatial dynamics

We formulate the equation for $v_1(\xi,\eta)$ as a system for (v_1,v_2), where $v_2=\partial_\xi v_1$, so that

$$\begin{aligned}\partial_\xi v_1 &= v_2, &(3)\\ \partial_\xi v_2 &= -c_3^\varepsilon k_0^2\partial_\eta^2 v_1 - c_4^\varepsilon v_1 \\ &\quad + g_0^\varepsilon(v)\partial_\eta^2 v_1 + g_1^\varepsilon(v) + g_2^\varepsilon(v)\partial_\eta v_2, &(4)\end{aligned}$$

where c_3^ε, c_4^ε and g_0^ε, g_1^ε, g_2^ε are respectively constants and analytic functions with

$$g_j^\varepsilon(v)=g_j^\varepsilon(v_1,\partial_\eta v_1,v_2),\qquad j=0,1,2;$$

the superscript ε denotes a quantity which depends analytically upon ε. We study the above system in the space

$$\mathcal{X}^s=H^{s+1}_{\rm per}(0,2\pi)\times H^s_{\rm per}(0,2\pi),\qquad s>0,$$

so that its phase space (the domain of the vector field on its right-hand side) is $\mathcal{X}^{s+1}$. Notice that g_j^ε is actually a bounded operator on $\mathcal{X}^s$.

An important consequence of the discrete symmetry (2) is that the system (3), (4) is *reversible*, that is invariant under the transformation

$$\xi\mapsto-\xi,\qquad (v_1,v_2)\mapsto S(v_1,v_2),$$

where the *reverser* $S:\mathcal{X}^s\to\mathcal{X}^s$ is defined by

$$S(v_1(\eta),v_2(\eta))=(v_1(-\eta),-v_2(-\eta)).$$

A solution to (3), (4) is said to be *symmetric* if it is invariant under the above transformation.

Spectral analysis

We may express an element of $H^s_{\rm per}(0,2\pi)$ as a Fourier series

$$\begin{aligned}v_1(\eta)&=\sqrt{\frac{1}{2\pi}}v_{1,0}\\ &\quad+\sqrt{\frac{1}{\pi}}\sum_{m=1}^{\infty}\{v_{1,m,\rm o}\sin(m\eta)+v_{1,m,\rm e}\cos(m\eta)\}\end{aligned}$$

Using this Fourier-series representation we find that $\mathcal{X}^s$ decomposes into a direct sum $\oplus_{m\in\mathbb{N}_0}E_m$ of subspaces, where

$$E_0=\{(v_{1,0},v_{2,0})\}$$

and

$$E_m=E_{m,\rm o}\oplus E_{m,\rm e},$$

$$E_{m,\rm o}=\{(v_{1,m,\rm o},v_{2,m,\rm o})\},\quad E_{m,\rm e}=\{(v_{1,m,\rm e},v_{2,m,\rm e})\}.$$

for $m\in\mathbb{N}$. We can compute the spectrum of the linearisation of (3), (4) by separately examining its restriction to each of these subspaces.

$\boldsymbol{m=0}$: We have two simple, real eigenvalues $\pm\lambda_{0,\varepsilon}=\pm(1+k_0^2)^{1/2}+\mathcal{O}(\varepsilon^2)$ in E_0.

$\boldsymbol{m=1}$: In $E_{1,\rm o}$ we have a geometrically simple and algebraically double zero eigenvalue for $\varepsilon=0$, while for $\varepsilon>0$ we have two simple real eigenvalues $\pm\lambda_{1,\varepsilon}$ which satisfy the equation $(\lambda_{1,\varepsilon})^2=2k_0\varepsilon^2(1+k_0^2)^{3/2}+\mathcal{O}(\varepsilon^4)$. The same result holds in $E_{1,\rm e}$.

$\boldsymbol{m>1}$: We have two simple purely imaginary eigenvalues in $E_{m,\rm o}$ given by $\pm{\rm i}\omega_{m,\varepsilon}$. The same result holds in $E_{m,\rm e}$.

The eigenvalue picture is summarised in Figure 2. For $\varepsilon>0$ we have a two-dimensional strongly hyperbolic part $\mathcal{X}^s_{\rm sh}=E_0$, a four-dimensional weakly hyperbolic part $\mathcal{X}^s_{\rm wh}=E_1$ and an infinite-dimensional central part $\mathcal{X}^s_{\rm c}=\oplus_{m=2}^{\infty}E_m$ of phase space; we denote the corresponding spectral projections by respectively $P_{\rm sh}$, $P_{\rm wh}$ and $P_{\rm c}$.

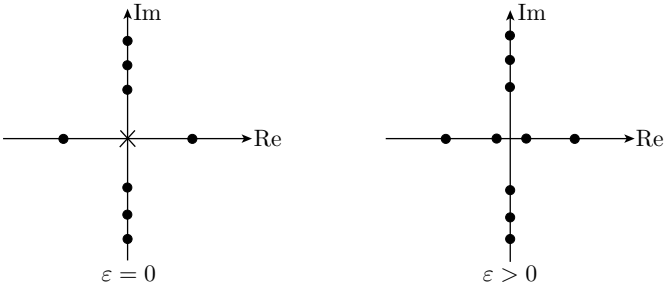

Figure 2: The spectrum of the linearised problem

A simplified problem

An examination of Figure 2 shows a qualitative difference in the spectral nature of the weakly hyperbolic subspace for $\varepsilon=0$ and $\varepsilon>0$. This observation suggests that any bifurcation phenomena take place at leading order in this subspace. We therefore write

$$z=P_{\rm wh}(v),\qquad q=P_{\rm sh,c}(v),$$

where $P_{\rm sh,c}=P_{\rm sh}+P_{\rm c}$, and formulate (3), (4) as the coupled system

$$\partial_\xi z=Kz+F^\varepsilon(z,q),\qquad K=\begin{pmatrix}0&0&1&0\\0&0&0&1\\0&0&0&0\\0&0&0&0\end{pmatrix}\quad(5)$$

and

$$\partial_\xi q_1 = q_2, \qquad (6)$$
$$= g_3^\varepsilon(z,q) + h^\varepsilon(z)$$
$$\partial_\xi q_2 = -c_3^\varepsilon k_0^2 \partial_\eta^2 q_1 - c_4^\varepsilon q_1 + \overbrace{P_{\rm sh,c}(g_1^\varepsilon(z,q))} + P_{\rm sh,c}(g_0^\varepsilon(z,q)\partial_\eta^2 q_1) + P_{\rm sh,c}(g_2^\varepsilon(z,q)\partial_\eta q_2), \qquad (7)$$

where $g_3^\varepsilon(z,0) = 0$.

Observe that

(i) $h^\varepsilon(z) = 0 \;\Rightarrow\; \{q=0\}$ is invariant;

(ii) For $h^\varepsilon = 0$ the flow in $\{q=0\}$ is controlled by the fourth-order dynamical system

$$\partial_\xi z = Kz + F^\varepsilon(z,0). \qquad (8)$$

Using the scaled variables $\check\xi = \varepsilon\xi$, $z_1(\xi) = \varepsilon\check z_1(\check\xi)$, $z_2(\xi) = \varepsilon^2\check z_2(\check\xi)$, one can write (8) as

$$\begin{aligned}
\partial_{\check\xi}\check z_{1,1} &= \check z_{2,1},\\
\partial_{\check\xi}\check z_{2,1} &= \check C_1\check z_{1,1} - \check C_2\check z_{1,1}(\check z_{1,1}^2 + \check z_{1,2}^2) + O(\varepsilon),\\
\partial_{\check\xi}\check z_{1,2} &= \check z_{2,2},\\
\partial_{\check\xi}\check z_{2,2} &= \check C_1\check z_{1,2} - \check C_2\check z_{1,2}(\check z_{1,1}^2 + \check z_{1,2}^2) + O(\varepsilon).
\end{aligned}$$

For $\varepsilon = 0$ this system has a two-dimensional invariant subspace $\{(\check z_{1,\rm e}, \check z_{2,\rm e})\}$ containing two symmetric homoclinic solutions (Figure 3).

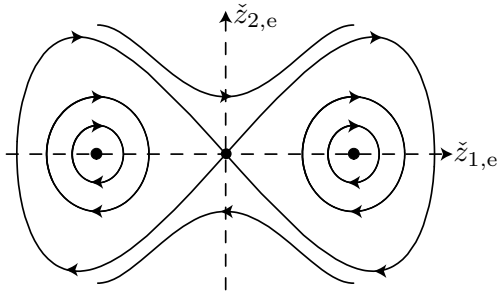

Figure 3: The $(\check z_{1,\rm e}, \check z_{2,\rm e})$ coordinate plane for $\varepsilon = 0$

Lemma

Two symmetric homoclinic solutions p^ε to (8) persist for $\varepsilon > 0$ and are estimated in unscaled coordinates by

$$|p^\varepsilon(\xi)| \le c\varepsilon \mathrm{e}^{-\varepsilon|\xi|}.$$

In the special case $h^\varepsilon = 0$ we have therefore found two symmetric homoclinic solutions $(z(\xi), q(\xi)) = (p^\varepsilon(\xi), 0)$ of (5)–(7), that is two symmetric modulating pulses which decay to zero as $\xi \to \pm\infty$.

A nonexistence result

The above 'persistence' lemma shows that the homoclinic solutions in Figure 3 survive a small perturbation (the re-introduction of the $\mathcal{O}(\varepsilon)$ terms) to become homoclinic solutions of (8). It would therefore appear reasonable to try another 'persistence' argument to show that the pulses $(p^\varepsilon, 0)$ also survive a small perturbation (the re-introduction of h^ε) to become homoclinic solutions of (5)–(7). The following heuristic argument however shows that he homoclinic solutions found in $\{q=0\}$ generically do not persist for $h^\varepsilon \neq 0$.

(i) Let us proceed formally by comparing (5)–(7) to a high-dimensional dynamical system. A homoclinic solution corresponds to a curve in phase space along which the stable and unstable manifolds intersect. Each of these manifolds is three dimensional (see Figure 2), and in general one cannot expect two three-dimensional manifolds in a high-dimensional phase space to intersect.

(ii) The situation is of actually worse than the above 'thought experiment' indicates. Equations (5)–(7) constitute a quadratic, quasilinear wave equation, and any discussion of its stable and unstable manifolds requires a global well-posedness result for this equation which is not available in a sufficiently general form.

Nevertheless, since $h^\varepsilon = 0$ is the 'good case' logic would dictate that a problem in which h^ε is very small should, in an appropriate sense, be 'close' to this good case. The following lemma shows that h^ε can be made exponentially small with respect to the bifurcation parameter ε; its proof, which relies upon the analyticity of our equations, uses ideas from a recent normal-form theory for analytic dynamical systems [4].

Lemma

There exists a change of variable which preserves the structure and yields the estimate

$$\|h^\varepsilon\| \le c\varepsilon \mathrm{e}^{-c^\star/\sqrt{\varepsilon}}$$

in the new variables.

Existence theory

We look for solutions of the form $(z,q) = (p^\varepsilon + Z, q)$, $(Z,q) \in C[0, \mathrm{e}^{c^\star/2\sqrt{\varepsilon}}]$ with

$$\|(Z(\xi), q(\xi))\| \le \mathrm{e}^{-c^\star/2\sqrt{\varepsilon}}, \qquad \xi \in [0, \mathrm{e}^{c^\star/2\sqrt{\varepsilon}}]$$

(see Figure 4). These solutions remain exponentially close to an approximate pulse p^ε for ξ in an exponentially long interval $[0, \mathrm{e}^{c^\star/2\sqrt{\varepsilon}}]$, they constitute 'half-pulses'.

Lemma

There exists a continuum of such solutions $(Z(\xi), q(\xi))$, the initial data $(Z(0), q(0))$ of which form a manifold W^{cs} in the infinite-dimensional phase space $\mathcal{X}^{s+1}$.

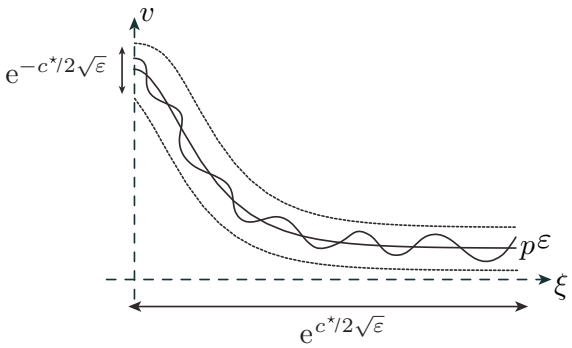

Figure 4: Solutions with initial data on W^{cs}

The above solutions are found by combining dynamical systems methods, in particular the construction of the 'centre-stable manifold' [5], and Kato's iteration scheme for quasilinear evolutionary equations [6].

Geometric arguments

The final step is to extend the 'half-pulses' constructed above to 'full pulses' which remain exponentially close to an approximate pulse p^ε for ξ in an exponentially long interval $[-\mathrm{e}^{c^\star/2\sqrt{\varepsilon}}, \mathrm{e}^{c^\star/2\sqrt{\varepsilon}}]$. We proceed by examining the geometry of the infinite-dimensional phase space $\mathcal{X}^{s+1}$.

Define the "symmetric section" $\Sigma = \mathrm{Fix}\, S$ and observe that a solution $v(\xi)$ of (3), (4) on $[0, \mathrm{e}^{c^\star/2\sqrt{\varepsilon}}]$ with $v(0) \in \Sigma$ can be extended to a symmetric solution

$$\tilde{v}(\xi) = \begin{cases} v(\xi), & \xi \geq 0 \\ Sv(-\xi), & \xi < 0 \end{cases}$$

on $[-\mathrm{e}^{c^\star/2\sqrt{\varepsilon}}, \mathrm{e}^{c^\star/2\sqrt{\varepsilon}}]$. Observe that

(i) $p^\varepsilon(0)$ lies in Σ;

(ii) W^{cs} is constructed in terms of solutions which are perturbations of p^ε.

Our approach is therefore to solve

$$(I - S)v(0) = 0, \qquad v(0) \in W^{\mathrm{cs}}$$

perturbatively around $p^\varepsilon(0)$ (see Figure 5).

Lemma

W^{cs} intersects Σ in an infinite family of points (parameterised by $P_{\mathrm{c}}(I - S)v(0)$).

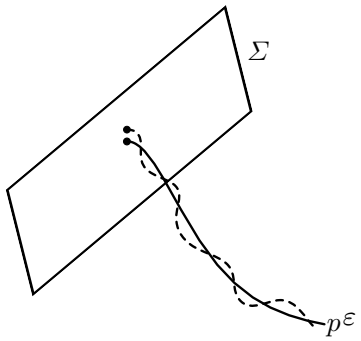

Figure 5: Symmetric pulses as perturbations of p^ε

References

[1] B. Birnir, H. McKean & A. Weinstein, "The rigidity of sine-Gordon breathers", Commun. Pure Appl. Math., vol. 47, pp. 1043–1051, 1994.

[2] J. Denzler, "Nonpersistence of breather families for the perturbed sine Gordon equation", Commun. Math. Phys., vol. 158, pp. 397–430, 1993.

[3] M. D. Groves & G. Schneider, "Modulating pulse solutions to quadratic quasilinear wave equations", preprint, 2006.

[4] G. Iooss & E. Lombardi, "Polynomial normal forms with exponentially small remainder for analytic vector fields", J. Diff. Eqns., vol. 212, pp. 1–61, 2005.

[5] E. A. Coddington & N. Levinson, Theory of Ordinary Differential Equations, McGraw-Hill, New York, 1955.

[6] T. Kato, "Quasi-linear equations of evolution, with applications to partial differential equations", in Lecture Notes in Mathematics 448, Springer, Berlin, 1974.

Inverse scattering transform for the integrable discrete nonlinear Schrödinger equation with non-vanishing boundary conditions

B. Prinari[*], **M.J. Ablowitz**[†], **G. Biondini**[‡]
[*]Dipartimento di Fisica and Sezione INFN, Università del Salento - Lecce, Italy
[†]Department of Applied Mathematics, University of Colorado - Boulder, CO
[‡]Department of Mathematics, State University of New York at Buffalo - Buffalo, NY
[*]Email: barbara.prinari@le.infn.it

The inverse scattering transform for an integrable discretization of the de- focusing nonlinear Schrodinger (IDNLS) equation with non-vanishing bound- ary values at innity is constructed. This problem was previously studied and many important results were established. In this talk, a suitable trans- formation of the scattering problem is introduced in order to address the open issue of analyticity of eigenfunctions and scattering data. Moreover, the inverse problem is formulated as a Riemann-Hilbert problem on the unit circle, and a modication of the standard procedure is required in order to deal with the dependence of asymptotics of the eigenfunctions on the potentials. Finally, soliton solutions and small amplitude limit solutions are obtained.

Introduction

We discuss the inverse scattering transform (IST) for a semi-discrete (discrete in space, continuous in time) version of the nonlinear Schrödinger (NLS) equation.

The NLS equation

$$iq_t = q_{xx} - 2\sigma\,|q|^2 q \tag{1}$$

is a universal model for weakly nonlinear dispersive waves, and $\sigma = -1$ corresponds to anomalous dispersion (focusing NLS), $\sigma = 1$ normal dispersion (defocusing NLS). In the case of normal dispersion NLS admits soliton solutions with nontrivial boundary conditions (so called dark/gray solitons)

$$q(x,t) = q_0 e^{2iq_0^2 t}\left\{\cos\alpha + \right.$$
$$\left. + i\sin\alpha\,\tanh\left[\sin\alpha\, q_0(x - 2q_0\cos\alpha\, t - x_0)\right]\right\}\,,$$

where q_0, α and x_0 arbitrary real parameters. Such solutions satisfy the boundary conditions

$$q(x,t) \to q_\pm(t) = q_0 e^{2iq_0^2 t \pm i\alpha} \qquad \text{as} \quad x \to \pm\infty\,.$$

The initial-value problem for the NLS equation on the infinite line ($-\infty < x < \infty$) can be solved via IST. In particular, the IST for NLS under nonvanishing boundary conditions was first studied in [1].

The differential-difference equation

$$i\frac{d}{dt}q_n = \frac{1}{h^2}\,(q_{n+1} - 2q_n + q_{n-1}) - \sigma|q_n|^2(q_{n+1}+q_{n-1})\,, \tag{2}$$

which is referred to here as the integrable discrete NLS (IDNLS) equation, is a $O(h^2)$ finite-difference approximation of NLS. The equation admits a Lax pair and the corresponding scattering problem is usually referred to as the Ablowitz-Ladik scattering problem (cf. [2], [3] and the monograph [4]). Besides being used as a basis for numerical schemes for its continuous counterpart, the IDNLS equation has also numerous physical applications, related to the dynamics of anharmonic lattices, self-trapping on a dimer, Heisenberg spin chains etc.

The purpose of this work is to develop the IST under nonvanishing boundary conditions for the following system of differential-difference equations on the doubly infinite lattice

$$i\frac{d}{d\tau}Q_n = Q_{n+1} - 2Q_n + Q_{n-1} - Q_n R_n\,(Q_{n+1} + Q_{n-1})\,, \tag{3a}$$

$$-i\frac{d}{d\tau}R_n = R_{n+1} - 2R_n + R_{n-1} - Q_n R_n\,(R_{n+1} + R_{n-1})\,, \tag{3b}$$

with $n \in \mathbb{Z}$. Equations (3) include the IDNLS equations (2) via the reductions $R_n = \sigma Q_n^*$, with $Q_n = hq_n$ and $\tau = t/h^2$. The IST for Eqs. (3) with vanishing boundary conditions was studied in [3]. The case of interest here, namely Eqs. (3) with $R_n = Q_n^*$ and nonvanishing boundaries, was also studied in [5], and we often refer to some key results already established there. In some important respects, however, we part from the approach in [5], and we solve the problem differently, most notably by relaxing the implicit requirement in [5] that the eigenfunctions be entire functions of the scattering parameter (which otherwise precludes the possibility of studying non-soliton solutions). We establish the analyticity properties of eigenfunctions and scattering data from the direct scattering problem for potentials in a suitable function class, we formulate the inverse problem as

a Riemann-Hilbert problem which also takes into account the asymptotic dependence (at large and small values of the scattering parameter) of the eigenfunctions on the potentials, and we discuss the small-amplitude and continuum limits of the problem.

The first step will be the discussion of the direct scattering problem. As in the continuous case, the spectral parameter of the associated scattering problem for the IDNLS equation is an element of a two-sheeted Riemann surface. Unlike the continuous system, however, for the discrete problem the Riemann surface has four branch points, located on the unit circle. The Riemann surface in the discrete case is genus 1, that is, topologically equivalent to a torus. In spite of this, due to the symmetries in the location of the branch points, the elliptic Riemann surface admits an involutive automorphism. Following [5], we therefore introduce an algebraic parametrization for the uniformization coordinate. The study of the analyticity of the scattering eigenfunctions is performed in terms of the uniformization variable. In [5] the eigenfunctions are assumed to be entire, and the equations of the inverse problem derived accordingly, which imposes strong restrictions on the class of admissible potentials. We show that in general the eigenfunctions are analytic inside or outside the unit circle of the uniform variable when $\sum_{j=\mp\infty}^{n} |Q_j - Q_\mp| < \infty$ for any finite n, where $Q_\pm = \lim_{n\pm\infty} Q_n$.

Then we discuss the asymptotic behavior of the eigenfunctions for relevant values of the scattering parameter and show this behavior explicitly depends on the potentials. We also discuss the properties of the scattering coefficients and their symmetries, as well as the discrete spectrum.

The inverse problem is formulated as a Riemann-Hilbert (RH) problem associated with analytic eigenfunctions. The formulation must be modified with respect to the standard case in order to take into account that the asymptotic behavior of the eigenfunctions for relevant values of the scattering parameter explicitly depends on the potentials, which are unknown in the inverse problem. The RH problem is then transformed into a closed linear system of algebraic-integral equations.

We obtain the time evolution of the scattering data. We discuss soliton solutions and we show how to obtain the small amplitude from the RH problem and to compare it to the Fourier transform solution obtained from the linearized equation. Finally, we briefly discuss the continuum limit of the discrete IDNLS.

References

[1] Zakharov V. E., Shabat A. B., “Interaction between solitons in a stable medium”, *Sov. Phys. JETP* **37**, 823-828 (1973)

[2] Ablowitz M.J., Ladik J.F., “Nonlinear differential-difference equations,” *Jour. Math. Phys.*, **16** (1975) 598-603

[3] Ablowitz M.J., Ladik J.F., “Nonlinear differential-difference equations and Fourier Analysis,” *Jour. Math. Phys.* **17** (1976) 1011-1018

[4] Ablowitz M. J., Prinari B., Trubatch, A. D., *Discrete and continuous nonlinear Schrödinger systems*, Cambridge University Press (2004)

[5] Vekslerchik V.E., Konotop V.V., “Discrete nonlinear Schrödinger equation under non-vanishing boundary conditions”, *Inv. Probl.* **8**, 889-909 (1992)

[6] Konotop V. V., Vekslerchik V. E., “On soliton creation in the nonlinear Schrdinger model. Discrete and continuous versions”, *J. Phys. A: Math. Gen.* **25**, pp. 4037-4042 (1992)

[7] Maruno K-i, Ohta Y., “Casorati determinant form of dark soliton solutions of the discrete nonlinear Schrödinger equation”, *J. Phys. Soc. Jpn.*, **75**, p.054002 (2006)

NUMERICAL INVESTIGATIONS OF NONLINEAR GRAVITY-CAPILLARY WATER WAVES

J.-M. Vanden-Broeck[†,*], **E. Parau**[†], **M. Cooker**[†]
[†] School of Mathematics, University of East Anglia, Norwich, NR4 7TJ, UK
[*]Email: h010@uea.ac.uk

Abstract

Three dimensional nonlinear free surface flows are considered. The fluid is assumed to be inviscid and incompressible and the flow to be irrotational. Both the effects of gravity and surface tension are included in the dynamic boundary condition. The fully nonlinear problem is solved numerically by boundary integral equation techniques. Free surface flows generated by moving disturbances are presented. Both steady and unsteady solutions are discussed. Extensions to interfacial flows are also presented. In addition three dimensional solitary waves are considered.

1 Discussion of the results

Three-dimensional capillary-gravity waves generated by a moving disturbance moving at a constant velocity c on or below a free-surface are considered. The fluid is assumed to be of infinite depth and steady solutions in a frame of reference moving with the disturbance are sought. A classical application is the calculation of the wave pattern generated by a moving ship. The problem is often modelled by potential flow and by neglecting surface tension. It is then necessary to impose the radiation condition which requires that there is no energy coming from infinity. This condition requires that the waves are behind the disturbance. It can easily be imposed numerically by forcing the free-surface to be flat at some distance in front of the disturbance (see for example [1] and [2]).

For small disturbances (insects or probes), the effect of surface tension can be significant. The situation is then more complicated. There is a minimum value c_{min} of c such that there are no waves on the free-surface when $c < c_{min}$. The value of c_{min} is given by

$$c_{min} = (\frac{4gT}{\rho})^{1/4} \qquad (1)$$

where T is the coefficient of surface tension (assumed to be constant), ρ is the fluid density and g is the acceleration of gravity. For an interface between water and air, $c_{min} \approx 0.23ms^{-1}$.

Parau, Vanden-Broeck and Cooker ([3] and [4]) calculated numerically nonlinear solutions for $c < c_{min}$. They showed that the free surface profiles are characterised by decaying oscillations in the direction of the motion of the disturbance and monotonic decay in the direction perpendicular to the direction of motion of the disturbance. As the size of the disturbance approaches zero, the solutions reduce to either a uniform stream or a three-dimensional solitary wave. There are both elevation and depresssion solitary waves. Typical profiles are shown in Figures 1 and 2. We note that our numerical results are consistent with the asymptotic results of Kim and Akylas [5] and Milewski [6] and with the rigourous findings of Groves and Sun [7].

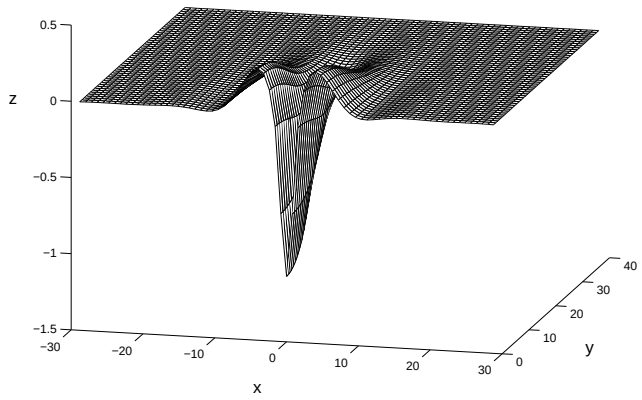

Figure 1: Depression solitary gravity-capillary wave for $\frac{c}{c_{min}} = 0.92$. Only the portion of the wave for $y > 0$ is shown. The vertical scale is exaggerated by a factor of 20.

When $c > c_{min}$, two different wave systems can occur on the free-surface. Analytic solutions have been derived by assuming a small disturbance and seeking a solution as a small perturbation around a uniform stream. These linear results show that the radiation condition forces the waves of longer wavelength to accur behind the disturbance and those of shorter wavelength to occur at the front of the disturbance.

We supplement the linear theories for $c > c_{min}$ with nonlinear computations. Since waves occur both at the front and at the back of the disturbance, the radiation condition cannot easily be imposed (as it was the case when

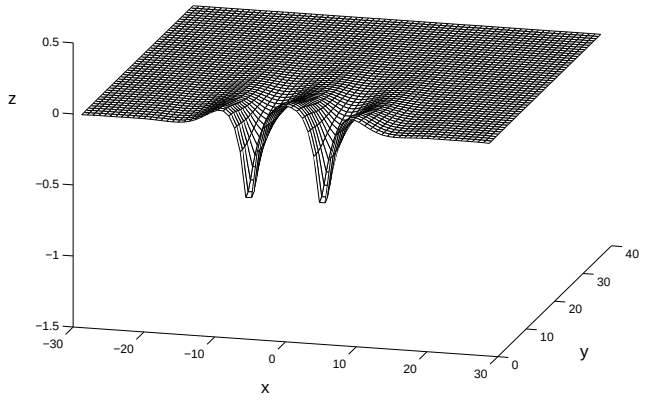

Figure 2: Elevation solitary gravity-capillary wave for $\frac{c}{c_{min}} = 0.92$. Only the portion of the wave for $y > 0$ is shown. The vertical scale is exaggerated by a factor of 20.

$T = 0$). Here we adapt to the nonlinear regime a technique introduced by Rayleigh to calculate analytically linear solutions. The idea is to include a dissipative term in the dynamic boundary condition. This term is characterised by an artificial viscosity $\mu > 0$ known as the Rayleigh viscosity. Rayleigh showed that the linear problem with $\mu \neq 0$ has a unique solution and that the correct solution satisfying the radiation condition is selected by taking the limit $\mu \to 0$.

We show that nonlinear solutions satisfying the radiation condition can be calculated numerically by using a boundary integral equation formulation in which a small Rayleigh viscosity $\mu > 0$ is introduced. The boundary integral equation formulation is based on ideas developed by [1], [2], [3] and [4]. For simplicity we assumed that the disturbance is a distribution of pressure with bounded support (qualitatively similar results can be obtained for different disturbances, for example moving submerged objects). We note that related approaches were used before for two-dimensional free-surface flows. A typical three dimensional solution for $\mu = 0.1$ is shown in Figure 3.

Our solutions are not truly non-dissipative because $\mu \neq 0$. The effect of $\mu \neq 0$ on the solutions can be estimated by comparing solutions with $\mu \neq 0$ to known solutions with $\mu = 0$. These known solutions include the solutions with $T = 0$ of Parau and Vanden-Broeck [2] and the solutions of Parau, Vanden-Broeck and Cooker ([3] and [4]) for $c < c_{min}$. In both cases we show that the effect of

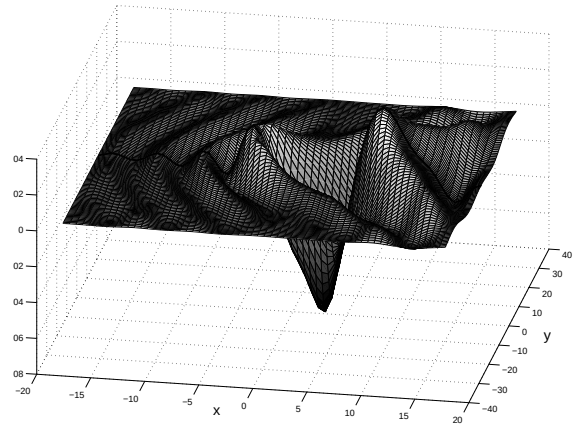

Figure 3: A typical solution for $\mu = 0.1$.

$\mu \neq 0$ is relatively small, provided μ is small.

We also present nonlinear time dependent results obtained by a boundary integral equation formulation. In particular we show how the steady gravity-capillary solutions described in the first part of the talk can be computed as the long time behaviour of a time dependent calculation.

We conclude by presenting extensions of the results for interfacial flows.

References

[1] L.K. Forbes, “An algorithm for 3-dimensional free-surface problems in hydrodynamics”, J. Comp. Physics, vol. 82, pp 330-347, 1980.

[2] E.I. Parau, J.-M. Vanden-Broeck, Eur. J. Mechanics B/Fluids, “Nonlinear two- and three-dimensional free surface flows due to moving disturbances”, vol. 21, 643-656 (2002).

[3] E.I. Parau, J.-M. Vanden-Broeck, M. Cooker, J. Fluid Mech., “Nonlinear three dimensional gravity-capillary solitary waves and related free-surface flows”, J. Fluid Mech., vol 536, pp. 99-105, 2005.

[4] E.I. Parau, J.-M. Vanden-Broeck, M. Cooker, “Three-dimensional gravity-capillary solitary waves in water of finite depth and related problems”, Phys. Fluids, vol. 17, 122101, 2005.

[5] B. Kim, T.R. Akylas, ”On gravity-capillary lumps”, J. Fluid Mech., vol 540, pp 337-351, 2005.

[6] P.A. Milewski, ”Three dimensional localized soli-

tary gravity-capillary waves", Comm. Math. Sc., vol 3, pp 89-99, 2005.

[7] M.D. Groves, M.D. Sun, "Fully localised solitary wave solutions for the three-dimensional gravity-capillary water wave problem", Arch. Rat. Mech. Anal., (in press).

Minisymposium on Periodic and Random Media

Organiser: William Parnell (University of Manchester)

A Monte-Carlo method for multiple scattering, comparison to Foldy's model

Eric Lunéville[†], **Jean-François Mercier**[†,*]

[†]Laboratoire POEMS, UMR 2706, CNRS-ENSTA-INRIA
32 Bld Victor, 75015 Paris, France
[*]Email: Jean-Francois.Mercier@ensta.fr

Abstract

The Foldy relation, classical in multiple scattering, gives the effective wavenumber of the average coherent field propagating in a layer filled with scatterers randomly arranged. The determination of this relation, based on averagings does not lead to its validity range. To quantify numerically this range (scatterers size, distance between scatterers, shape of the scatterers...) in Foldy's relation, we determine, thanks to a Monte-Carlo method, the averaged acoustic wave scattered in time harmonic regime and in 2D by rigid obstacles. To reduce the calculation times, we have developed a method based on finite elements coupled to an integral representation, similar to the boundary element method, which allows to reduce the number of freedom degrees.

We have studied the influence of the cylinders density on the quality of Foldy's approximation. We find a good agreement only for low densities. For scatterers with a more complex shape, we have made some concluding tries with square shapes.

Introduction

The Foldy's relation [1] gives in time harmonic regime, thanks to a statistical averaging, the characteristics of a homogeneous effective medium equivalent to a layer randomly filled with scatterers. This relation indicates that if k denotes the wave number of the Helmholtz equation describing the medium without scatterers ($k = \omega/c$ where ω is the frequency and c the sound speed), then the presence of scatterers leads to an effective wave number K (complex, the effective medium is dissipative). It reads $K = k + (2n/ik)f$ where f only depends on the nature and on the geometry of one scatterer and n is the scatterers density.

The average process to derive this result does not give clearly the validity ranges of Foldy's relation except that $ka \ll 1$ and $na^2 \ll 1$ where a is the "radius" of a scatterer. Our goal is to develop a finite element method in order to calculate the effective wave number and to determine the validity range of Foldy's relation: scatterer size, mean distance between scatterers, scatterer shape, boundary conditions on the scatterers, choice of randomness in the scatterers distribution... Recently experimental measures of K showed that Foldy's formula becomes inaccurate even for small surface densities (beyond 6%) [2].

The equations

The function p_{tot} denotes the total pressure in the fluid, p_{inc} is the incident wave (plane in practice) sent on the scatterers. Then the scattered pressure $p = p_{tot} - p_{inc}$ satisfies :

$$\begin{aligned} \left(\Delta + k^2\right) p &= 0 \quad (\Omega), \\ \frac{\partial p}{\partial n} &= -\frac{\partial p_{inc}}{\partial n} \quad (\Gamma), \\ &+ \quad p \text{ is outgoing at infinity.} \end{aligned}$$

Ω denotes the exterior of the scatterers and Γ is the scatterers boundary, chosen rigid. In the case of cylindrical obstacles, a semi-analytical resolution of the problem can be performed thanks to summations of Bessel's and of Hankel's functions [3]. For obstacles of complex geometry, it is necessary to use a finite element method. To reduce to a bounded calculation domain, the scatterers are surrounded by a curve Σ (see Fig. 1) on which it is required to write a condition to select the "outgoing solution". This is achieved using the integral representation

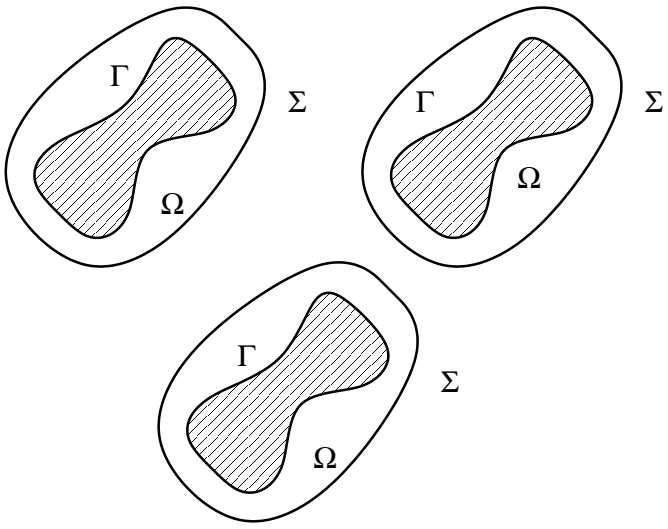

Figure 1: Problem in a bounded domain

of the outgoing solution. This method is similar to the boundary element method. For a given configuration of scatterers, the problem to solve reads:

$$\begin{aligned}
\left(\Delta + k^2\right) p &= 0 \quad (\Omega), \\
\frac{\partial p}{\partial n} &= -\frac{\partial p_{inc}}{\partial n} \quad (\Gamma), \\
\left(\frac{\partial}{\partial n_x} + \lambda\right) p(x) &= \int_\Gamma \left[p(y) \left(\frac{\partial}{\partial n_x} + \lambda\right) \frac{\partial G(x-y)}{\partial n_y} \right. \\
+ \frac{\partial p_{inc}(y)}{\partial n_y} \left(\frac{\partial}{\partial n_x} \right. &+ \left. \left. \lambda\right) G(x-y) \right] d\Gamma_y \quad (\Sigma).
\end{aligned}$$

$G(x) = H_0^{(1)}(k|x|)/4i$ is the Green function in $2D$ and $\mathbf{n}$ is the outgoing normal from Ω. To ensure that this bounded problem is equivalent to the problem in the open space, a parameter λ is introduced such that $\Im m(\lambda) \neq 0$. In the sequel, as an example we have considered cylindrical scatterers for which Ω becomes a union of crowns. The numerical method is performed thanks to the finite element code MELINA [4].

Monte-Carlo procedure

Mesh generation

The mesh of N crowns around N randomly placed scatterers is built in a rectangle of height H and of width L. In this aim first a reference crown's mesh is built. Then N random locations are chosen in the rectangle and the reference mesh is duplicated in each of these points (see Fig. 2). To adjust the size of the scatterers, a scale is also applied, whose ratio is deduced from the scatterers surface density ρ that is desired. This density is defined by $\rho = N\pi R_\Gamma^2 / S_{tot}$ where $S_{tot} = H \times L$ is the rectangle surface, which imposes the radius R_Γ of the scatterers.

As the scatterers are not punctual and since we impose no crown to overlap, the scatterers configurations do not follow a uniform statistic law. Moreover the minimal distance between two centers of scatterers is fixed to $d_{min} = 5\, R_\Gamma$ which reinforces the correlation, especially for larger densities.

Calculation of the coherent field

The frequency k and the incident wave $p_{inc} = e^{ikx}$ being fixed, for each of the N_{conf} scatterers configuration is calculated the scattered field in each crown and then on a grid (see Fig. 2), independent of the configuration, thanks to the integral representation formula. A typical scattered field obtained on the grid is drawn on Fig. 3.

The procedure to determine the mean field is the following:

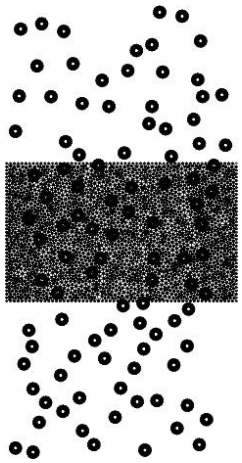

Figure 2: Mesh with the grid

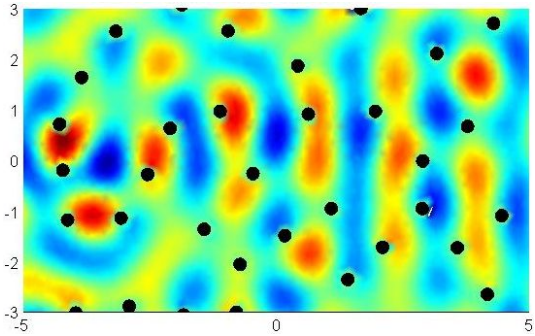

Figure 3: Scattered pressure on the grid for a particular scatterers (in black) configuration

- for $i = 1, N_{conf}$, the ith mesh is generated and the scattered field p_i is calculated on the grid,
- for $j = 1, N_{grid}$ (number of points on the grid) the mean field is determined according to the formula $p_{mean}(M_j) = \sum_{i=1}^{N_{conf}} p_i(M_j)/N_{conf}$.

Results

Influence of the number of configurations

For a density $\rho = 0.1$ the total pressure $p_{tot} = p_{inc} + p_{mean}$ has been calculated for $N = 100$ cylinders, $N_{conf} = 5$ (Fig. 4) and $N_{conf} = 44$ (Fig. 5). In the last case a plane wave is guessed but is still polluted. To get a "clean" plane wave 180 configurations are required. Then to extract the effective wave number K, first a vertical average is performed $\tilde{p}_{tot}(x) = \int_0^h p_{tot}(x,y)dy$. This improves the quality of the coherent wave (more regular). Then by seeking a representation of the pressure in the form of a plane wave $\tilde{p}_{tot}(x) = Ae^{iKx}$, A and K are identified by a less squares method. In practice to choose N_{conf}, $K(N_{conf})$ is calculated up to become constant. In

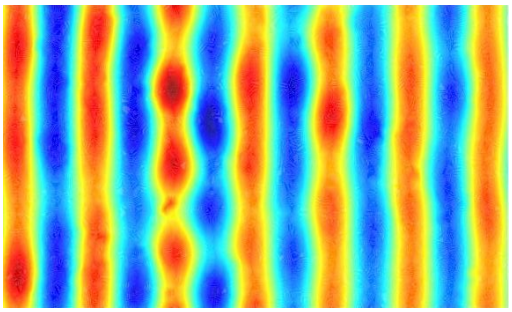

Figure 4: $N_{conf} = 5$

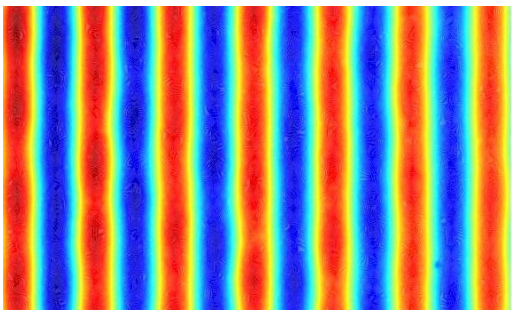

Figure 5: $N_{conf} = 44$

the worst case we obtained $N_{conf} = 200$ (obtained for $\rho = 0.1$).

Influence of the scatterer density

The Foldy relation is valid if the density ρ is small. Numerically we wanted to establish if there is a density above which the Foldy model becomes inaccurate. Drawing the imaginary parts of K_{num} and K_{foldy} (for a cylinder, $f = -\sum_{n=-\infty}^{\infty} J_n'(kR_\Gamma)/H_n'(kR_\Gamma)$ [5]) versus the density (see Fig. 6) we get that these two values remain close for $\rho \leq 0.1$. Concerning the real parts (see Fig. 7),

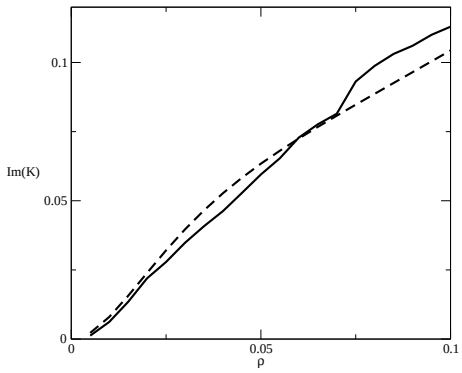

Figure 6: $- : \Im m(K_{num}), -- : \Im m(K_{foldy})$

$\Re e(K_{num})$ remains close to $\Re e(K_{Foldy})$ for $\rho \leq 0.05$ and then becomes more distant. Finally the amplitude $|A|$

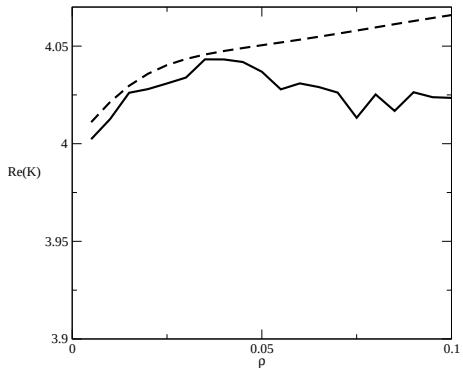

Figure 7: $- : \Re e(K_{num}), -- : \Re e(K_{foldy})$

is found to decrease continuously versus the density, starting from 0.9 for $\rho = 0.005$. $|A| = 1$ found by Foldy is not recovered: this is due to the fact that we do not study a layer of infinite height and consequently some acoustic energy is lost vertically. Our finite element method can easily be extended to non-cylindrical scatterers. Square scatterers have been considered, randomly placed and oriented. The obtained average pressure is still a plane wave, more attenuated than in the case of cylinders of same size (extra scattering by the corners).

References

[1] L.L. Foldy, "The multiple scattering of waves. I. General theory of isotropic scattering by randomly distributed scatterers", Phys. Rev., vol. 67, pp. 107-119, 1945.

[2] A. Derode, V. Mamou, A. Tourin, "Influence of correlations between scatterers on the attenuation of the coherent wave in a random medium", Phys. Rev. E, vol. 74, 036606, 2006.

[3] Y.-Y. Chen, Z. Ye, "Acoustic Attenuation by Two-Dimensional Arrays of Rigid cylinders", Phys. Rev. Letters, vol. 87 (18), 184301, 2001.

[4] D. Martin, "Code éléments finis MELINA", `http://www.maths.univ-rennes1.fr/~dmartin/melina/www/homepage.html`

[5] C.M. Linton, P.A. Martin, "Multiple scattering by random configurations of circular cylinders: second-order corrections for the effective wavenumber", J. Acoust. Soc. Am., vol. 117 (6), pp. 3413-3423, 2005.

On the effective parameters of multiple scattering media in 1D and 2D

A. Maurel
LOA, ESPCI, 10 rue Vauquelin, Paris – France
Email: agnes.maurel@espci.fr

Abstract

This work focuses on the determination of the two effective parameters that characterize a multiple scattering medium sought as an effective (homogenized) medium, namely the effective sound speed c_e and the effective density ρ_e. By considering only the single scattering processes, it is possible to derive the effective parameters, an approach that is valid for small scattering strength. Calculations are performed in 1D and exemplified by numerical results. Calculations in 2D concerns scatterers that behave as a combination of a monopole and a dipole. The results for cylinders in the low frequency limit are shown to be in agreement with results derived by a CPA type method.

1 Introduction

The problem of how a wave propagates through many scatterers is old and the literature is vast on the subject. A well established result is that the wave propagates as in a homogeneous medium with complex index or complex sound speed c_e. Solving the Green function of the multiple scattering medium is an example of how deriving the effective sound speed c_e. By using this approach, it is implicitly said that the scatterers fill the whole space. A problem that has received much less attention concerns the boundary conditions that have to be applied at an "interface" between a medium free of scatterer and a medium filled with scatterers. In other words, the characterization of the homogenized (effective) medium needs an effective density ρ_e to be determined, in addition to the effective sound speed.

The present study focuses on this problem by considering the very simple configuration of a unique scatterer able to move in an half space, say $x \geq 0$. The "mean" field averaged over all possible positions of the scatterer allows to define the reflexion and transmission coefficients of the interface $x = 0$. Generalizing this result to a N-scatterer problem is possible for small scattering strength, in which case the presented results corresponds to the first order expansion in the weak scattering strength. In 1D, we get $\rho_e/\rho = 1+n[f(\pi)-f(0)]/(2k^2)$ (with n the density of scatterers), a result that shows that the effective parameter ρ_e is linked to the anisotropy of the scatterer. In 2D, a scatterer with a monopole and a dipole contributions is considered $f(\theta) = f_1 + f_2\cos\theta$. It is shown that $\rho_e/\rho = 1 - nf_2/k^2$ with the same conclusion. The effective celerity c_e is also deduced and is shown to agree with the usual leading order result $K^2 = k^2 - nf(0)/k$ in 1D and $K^2 = k^2 - nf(0)$ 2D.

The 1D case is exemplified with numerical results in the case of a scattering due to a change in density. The 2D case is exemplified for scattering by cylinders in the low frequency limit. The results are shown to be in agreement with the results (at leading order) of Ref. [1], [2] using a CPA type approach. The main conclusion is that this childlike approach allows to derive meaningful results.

2 The one scatterer problem

We consider a unique scatterer at position $\mathbf{r}_1$ with $x_1 > 0$. The scatterer is characterized by its scattering function $f(\mathbf{r}-\mathbf{r}_1)$ so that the field solution of $(\Delta + k^2)u = 0$ in the presence of the scatterer and an incident wave u^{inc} is

$$u(\mathbf{r}) = u^{inc}(\mathbf{r}) + f(\mathbf{r}-\mathbf{r}_1)G^0(\mathbf{r}-\mathbf{r}_1)u^{inc}(\mathbf{r}_1), \quad (1)$$

with G^0 the Green function of the free space. If the scatterer moves in the half space $x > 0$ (with a probability distribution $p(\mathbf{r}_1)$), the mean field $\langle u\rangle$ is

$$\langle u\rangle(\mathbf{r}) = u^{inc}(\mathbf{r}) + \int d\mathbf{r}_1 p(\mathbf{r}_1) f(\mathbf{r}-\mathbf{r}_1)G^0(\mathbf{r}-\mathbf{r}_1)u^{inc}(\mathbf{r}_1). \quad (2)$$

For an incident wave e^{ikx}, the solution is sought in terms of an effective medium as

$$\begin{aligned} \langle u\rangle(x<0) &= e^{ikx} + r_e e^{-ikx}, \\ \langle u\rangle(x>0) &= t_e e^{iKx}, \end{aligned} \quad (3)$$

where K is the effective wavenumber and (t_e, r_e) the effective transmission and reflexion coefficients of the "fictive" interface at $x = 0$. The effective parameters (ρ_e, c_e) are simply deduced with

$$c_e = \frac{k}{K}c, \quad \rho_e = \frac{Kt_e}{k(1-r_e)}\rho. \quad (4)$$

Of course, this "one scatterer problem" (with density $n = 1/L$ in 1D, $n = 1/S$ in 2D, $L, S \to \infty$) is not very pertinent to describe an homogenized medium and the problem is then to generalized the result to a N scatterer problem. This is possible if multiple scattering processes can be neglected which means that the results hold

when the scattering strength f is small. In that case, the results correspond to first order expansion in f.

3 Derivation in 1D

3.1 Derivation of the effective parameters

In 1D, f takes two values $f(0)$, $x > x_1$ and $f(\pi)$, $x < x_1$ and we easily get, with $n \equiv 1/L$ (for N scatterers, it is sufficient to define $n = N/L$)

$$\begin{aligned}\langle u\rangle(x<0) = &\ e^{ikx} + nf(\pi)/(2ik)\int_0^L dx_1 e^{2ikx_1}e^{-ikx},\\ \langle u\rangle(x>0) = &\ e^{ikx} + nf(0)/(2ik)\int_0^x dx_1 e^{2ikx_1}e^{-ikx}\\ &+nf(\pi)/(2ik)\int_x^L dx_1 e^{ikx},\end{aligned} \tag{5}$$

from which we deduce ($L \to \infty$)

$$\begin{aligned}&r_e = nf(\pi)/(4k^2),\ \ t_e = 1 + r_e,\\ &K = k - nf(0)/(2k),\end{aligned} \tag{6}$$

where the derivation has been done expanding the solution sought in Eqn. (3) at first order in f and identifying with the expressions of Eqn. (5). The field $\langle u\rangle$ is found to be continuous across the interface while its first derivative $\langle u\rangle'$ verifies $[\langle u\rangle'] = n[f(0) - f(\pi)]/(2ik)$. We finally get

$$\begin{aligned}&c_e/c = 1 + nf(0)/(2k^2),\\ &\rho_e/\rho = 1 + n[f(\pi) - f(0)]/(4k^2).\end{aligned} \tag{7}$$

As previously said, this result is expected to be valid for a N scatterer problem for weak scattering f. It can be noticed that the effective sound speed depends only on the forward scattering (a classical result) while the effective density is found to differ from the background density ρ only when the scatterers are anisotropic.

3.2 Example of scattering due to density change

We consider the case where the scattering is due to a change in density from the background density ρ to the density ρ_0 in scatterers of size a. We introduce the filling fraction $\varphi \equiv na$, the fraction of length occupied by the scatterers ($\varphi < 1$). The corresponding scattering functions can be easily derived and we find two limits for weak scattering

- For small relative change in density $\delta\rho/\rho \equiv (\rho_0 - \rho)/\rho \ll 1$, we get $f(0) \simeq O[(\delta\rho/\rho)^2]$ and $f(\pi) \simeq 2(\delta\rho/\rho)k\sin ka + [(\delta\rho/\rho)^2]$. We thus have

$$\rho_e/\rho = 1 + \varphi(\delta\rho/\rho)\sin ka/(2ka) + O[(\delta\rho/\rho)^2]. \tag{8}$$

The result is exemplified on fig. 1(a), where the average field is numerically calculated. The first derivative $\langle u\rangle'$ exhibits a discontinuity that, for finite size scatterer ka, appears to be not well located at $x = 0$. This discontinuity is responsible for the effective density $\rho_e \neq \rho$.

- For small scatterer size or low frequency limit $ka \ll 1$, we get $f(0) \simeq -k^2a\delta\rho^2/(\rho\rho_0) + kO[(ka)^2]$, $f(\pi) \simeq k^2a(\rho_0^2 - \rho^2)/(\rho\rho_0) + kO[(ka)^2]$. We thus have

$$\rho_e/\rho = 1 + \varphi(\delta\rho/\rho)/2 + O[(ka)^2]. \tag{9}$$

The result is exemplified on fig. 1(b). This low frequency limit is probably a better limit to clearly define a discontinuity (occurring on the small length a).

Note that, in this example, the scattering function $f(0)$ is real, so their is no attenuation occurring at first order. Attenuation would appear at second order in the small parameter.

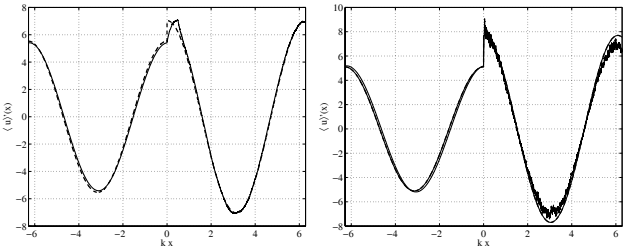

Figure 1: Illustration of the discontinuity of the the first derivative $\langle u\rangle'(x)$, responsible for an effective density $\rho_e \neq \rho$. (a) the calculation is performed by averaging 1000 realizations of 100 randomly placed scatterers with $ka = 0.5$, $\delta\rho/\rho = 0.5$, $\varphi = 0.5$ (b) same representation for 100 averages of 200 randomly placed scatterers with $ka = 0.05$, $\delta\rho/\rho = 1$, $\varphi = 0.5$. The plain line shows the numerical result and dotted line the analytical derivative of Eqn. (3).

4 Derivation in 2D

In general, the 2D scattering function is expressed as a function of the angle θ that forms the direction of $\mathbf{r} - \mathbf{r}_1$ with the incident wavenumber direction. I have not found a way to treat the general case $f(\theta)$. Instead, I consider the case of a scattering function that contains a monopole and dipole contributions $f(\theta) = f_1 + f_2\cos\theta$ [with $\cos\theta = (x - x_1)/|\mathbf{r} - \mathbf{r}_1|$].

$$\langle u\rangle(\mathbf{r}) = e^{ikx} + \int d\mathbf{r}_1 p(\mathbf{r}_1) f(\theta)\frac{H_0^{(1)}(k|\mathbf{r} - \mathbf{r}_1|)}{4i}e^{ikx_1}. \tag{10}$$

The calculation are straightforward and we get, with $n = N/S$ (S is the surface occupied by the cylinders)

$$\begin{array}{l} r_e = n(f_1 - f_2)/(4k^2), \quad t_e = 1 + r_e, \\ K = k - n(f_1 + f_2)/(2k), \end{array} \tag{11}$$

from which we deduce $[\langle u \rangle] = 0$, $[\langle u \rangle'] = -inf_2/k$ and

$$\rho_e/\rho = 1 - nf_2/k^2, \quad c_e/c = 1 + n(f_1 + f_2)/(2k^2). \tag{12}$$

Again, it can be seen that only the dipole contribution (non isotropic) gives an effective density different from the background density. Also, it can be noticed that the expression for the effective sound speed agrees with the usual law $K^2 \simeq k^2 - nf(0)/2$.

4.1 The case of cylinders

A cylinder of radius a, with density ρ_0 and sound speed c_0 in a background of density ρ and sound speed c has typically a monopole and dipole scattering contributions in the limit of low frequencies:

$$\begin{array}{l} f_1 = \pi(ka)^2 \, [1 - \rho c^2/(\rho_0 c_0^2)] + O[(ka)^2], \\ f_2 = 2\pi(ka)^2(\rho - \rho_0)/(\rho + \rho_0) + O[(ka)^2]. \end{array} \tag{13}$$

Introducing the filling fraction $\varphi \equiv n\pi a^2$, we get for the density (the effective velocity has a more complicated form)

$$\rho_e/\rho = 1 - 2\varphi(\rho - \rho_0)/(\rho + \rho_0). \tag{14}$$

Notably, for impenetrable cylinder $\rho_0 \to \infty$, we have

$$\rho_e/\rho \simeq 1 + 2\varphi, \quad c_e/c \simeq 1 - \varphi/2. \tag{15}$$

These results are the linearized version (leading order) of the results obtained in Ref. [1] using a CPA-type approach. The same expression $\rho_e/\rho \simeq (1 + \varphi)/(1 - \varphi)$ would be obtained if t_e was recasted in the form

$$t_e \simeq \frac{1}{1 - n(f_1 - f_2)/(4k^2)}, \tag{16}$$

instead of the linearized version of Eqn. (11). This resemble to the observation that K^2, rather than K is a good candidate for expansion. However, in the absence of physical argument, it appears hazardous to chose $1/t$ rather than t (this lack is the price to pay for using a crude modelization).

In Ref. [1], it is considered the case of different cylinders, namely cylinders with different densities and filling fractions. This refinement is straightforward in the presented approach since the average over f with respect to the scattering characteristics can be performed independently of the average over the scatterer positions. It is thus sufficient to replace f by $\langle f \rangle_c$ in the calculation, where $\langle . \rangle_c$ means average over the characteristics of the scatterer.

In Ref. [2], the problem of water waves propagating in periodic cylinder arrays is considered (again in a CPA type approach). In that case, the density has to be replaced by the height $h = 1/\rho$ and the effective sound speed $c = \sqrt{gh}$. It is straightforward that

$$h_e/h \simeq 1 - 2\varphi, \quad g_e/g \simeq 1 - \varphi/2, \tag{17}$$

results that appear again as a linearization of the results obtained in Ref. [2]. Again, if $1/t$ was linearized instead of t, the same expression would be obtained.

As a conclusion, the elementary approach based on single scattering process is shown to be sufficient to derive the effective parameters of a homogenized medium. Notably in 1D, it offers a nice image, because of its simplicity, of what happens in a random medium: the Eqn. (5) contains many physical informations on the reflexion and transmission processes but as well on the origin of the attenuation. Works are in progress to iterate at second order and, notably, to get informations on the hole correction.

References

[1] D. Torrent & J. Sánchez-Dehesa, "Effective parameters of clusters of cylinders embedded in a nonviscous fluid or gas", Phys. Rev. B **74**, 224305 (2006).

[2] X. Hu & C.T. Chan, "Refraction of Water Waves by periodic cylinder Arrays" Phys. Rev. Lett. **95** 154501 (2005).

Waves and faults propagating in an inhomogeneous lattice structure

G. Mishuris, A. Movchan, L. Slepyan
Department of Mathematical Sciences, University of Liverpool, Liverpool, UK

1 Abstract

We analyse a square lattice containing point masses connected by linearly elastic massless bonds. The lattice is inhomogeneous and it represents a stratified structured medium. The layers differ by particle masses, so that the cell of periodicity includes three particles, as shown in Fig. 1.

A moving fault, which is crack-like, is introduced as a line of broken bonds, and the growth of such a fault is considered as a sequence of breaks of the bonds. We note that there is no crack edge singularity, which normally appears for stress components in the continuum model.

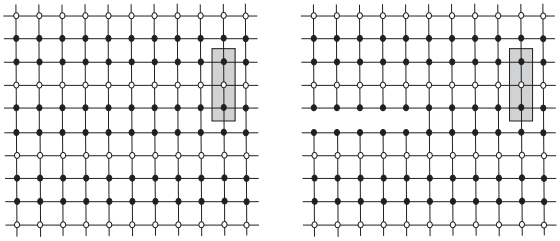

Figure 1: Inhomogeneous lattice structures: (a) Undamaged lattice, (b) Lattice with a crack.

2 Introduction

Waves in periodic structures is a classical topic (see, for example, [1], [2]). The relatively recent advance in the design of band-gap materials has resulted in a series of publications related to control of wave propagation within periodic structures ([3], [4], [5], [6], [7]).

There is also a steadily increasing number of papers on fracture in lattices. Numerical simulations of atomic lattices were initiated by the work [8], [9]. The first analytical solution for a string-like 2-D lattice model was obtained in [11]. Such lattice models were then studied in [12], [13], [14], [15], [16], [17], [18], [19], [20], [21], [22], [23], [24], [25], [26], [27].

The main results on dynamic fracture in structured media are summarized in [28].

In this paper, we discuss an analytical model, which gives the displacement field around a crack-like fault propagating in an inhomogeneous lattice. It is also shown that the propagation of the fault can be controlled via an appropriate choice of physical parameters of the lattice.

3 The lattice

In Fig. 1, the particles are shown as black or white discs, and they are assumed to have the mass m_1 or m_2, respectively.

The normalization is introduced in such a way that $(2m_1+m_2)/3 = 1$ (the average density), and $c = 1$ (the low-frequency wave speed).

The equations of motion are written for three particles within the elementary cell of the periodic structure. The displacement is denoted by $u_{j,m,n}$, where (m, n) is the multi-index giving the position of the cell $m\boldsymbol{e}^{(1)} + 3n\boldsymbol{e}^{(2)}$, whereas $j = 0, 1, 2$ is the index, which sets the particle position within the cell. The equations of motion of the intact lattice have the form:

$$\begin{aligned}
\frac{3}{2+\mu}\ddot{u}_{0,m,n} &= u_{0,m-1,n} + u_{0,m+1,n} + u_{1,m,n} \\
&\quad + u_{2,m,n-1} - 4u_{0,m,n}\,, \\
\frac{3\mu}{2+\mu}\ddot{u}_{1,m,n} &= u_{1,m-1,n} + u_{1,m+1,n} + u_{2,m,n} \\
&\quad + u_{0,m,n} - 4u_{1,m,n}\,, \\
\frac{3}{2+\mu}\ddot{u}_{2,m,n} &= u_{2,m-1,n} + u_{2,m+1,n} \\
&\quad + u_{0,m,n+1} + u_{1,m,n} - 4u_{2,m,n}\,,
\end{aligned} \tag{1}$$

where $\mu = m_2/m_1$.

4 Lattice with a propagating fault. The Wiener-Hopf problem

Consider a crack-like fault, $m < vt, t > -\infty$, propagating between the layers $(0, m, 0)$ and $(2, m, -1)$, as shown in Fig. 1b, with a constant speed, $v > 0$. We follow the "steady state" formulation and hence assume that the displacement $u_{j,m,n}(t)$ depends only on the variables j, $\eta = m - vt$ and n. The displacement functions will be denoted by $u_{j,n}(\eta)$. The following symmetry relations hold

$$\begin{aligned}
u_{0,n}(\eta) &= -u_{2,-n-1}(\eta)\,, \\
u_{1,n}(\eta) &= -u_{1,-n-1}(\eta)\,, \\
u_{2,n}(\eta) &= -u_{0,-n-1}(\eta)\,.
\end{aligned} \tag{2}$$

In terms of the Fourier transform $u^F_{j,n}(k)$ of $u_{j,n}(\eta)$ with respect to η, the equations for the undamaged lat-

tice (see (1)) become

$$\begin{aligned} \mathcal{S}_2 u^F_{0,n} - u^F_{1,n} - u^F_{2,n-1} &= 0\,, \\ \mathcal{S}_1 u^F_{1,n} - u^F_{0,n} - u^F_{2,n} &= 0\,, \\ \mathcal{S}_2 u^F_{2,n} - u^F_{0,n+1} - u^F_{1,n} &= 0\,, \end{aligned} \tag{3}$$

with

$$\begin{aligned} \mathcal{S}_1(k) &= 4 - 2\cos k + \frac{3\mu}{2+\mu}(0+ikv)^2\,, \\ \mathcal{S}_2(k) &= 4 - 2\cos k + \frac{3}{2+\mu}(0+ikv)^2\,. \end{aligned} \tag{4}$$

For the lattice with the crack Eqs. (3) are valid for $n > 0$ and for $n < -1$. For the upper half-plane we use the representation

$$\begin{aligned} u^F_{j,n}(k) &= u^F_j(k)\lambda^n(k)\,, \\ u^F_j &= u^F_{j,0}\,, \\ |\lambda| &\le 1\,. \end{aligned} \tag{5}$$

For any $n > 0$ equations (3) become

$$\begin{aligned} \mathcal{S}_2 u^F_0 - u^F_1 - u^F_2/\lambda &= 0\,, \\ \mathcal{S}_1 u^F_1 - u^F_0 - u^F_2 &= 0\,, \\ \mathcal{S}_2 u^F_2 - \lambda u^F_0 - u^F_1 &= 0\,. \end{aligned} \tag{6}$$

It follows that

$$\begin{aligned} \lambda &= P - \sqrt{P^2-1}\,, \\ P &= \frac{1}{2}\left(\mathcal{S}_1\mathcal{S}_2^2 - 2\mathcal{S}_2 - \mathcal{S}_1\right)\,. \end{aligned} \tag{7}$$

For particle displacements $u_{0,0}(\eta)$ on the crack face, we shall use the representation

$$\begin{aligned} u^F_{0,0}(k) &= u_+(k) + u_-(k)\,, \\ u_\pm(k) &= \left[u_{0,0}(\eta)H(\pm\eta)\right]^F\,, \end{aligned} \tag{8}$$

where H is the Heaviside unit step function. Let σ denote the traction on the boundary of the upper half-plane. It is assumed that the crack faces are traction free, i.e. for $\eta < 0$ we have

$$\sigma(\eta) = 0\,, \quad \sigma_- = 0\,, \tag{9}$$

whereas for $\eta > 0$

$$\sigma(\eta) = 2u_{0,0}(\eta)\,, \quad \sigma_+ = 2u_+\,. \tag{10}$$

Accordingly, we modify the first equation in the system (6), and using the relation

$$(\mathcal{S}_1\mathcal{S}_2 - 1)u^F_1 = (\mathcal{S}_2 + \eta)u^F_0 \tag{11}$$

we arrive at the functional equation of the Wiener-Hopf type for the functions $u_\pm(k)$

$$\begin{aligned} \mathcal{Q}_1(k)u_+(k) + \mathcal{Q}_2(k)u_-(k) &= 0\,, \\ \mathcal{Q}_1(k) &= \mathcal{S}_2 + 1 - \frac{\mathcal{S}_2+\lambda}{\mathcal{S}_1\mathcal{S}_2 - 1}\,, \\ \mathcal{Q}_2(k) &= \mathcal{S}_2 - 1 - \frac{\mathcal{S}_2+\lambda}{\mathcal{S}_1\mathcal{S}_2 - 1}\,, \end{aligned} \tag{12}$$

where $\mathcal{S}_{1,2}$ and λ are defined in (4) and (7), respectively.

5 Applications

The analytical solution for the dynamic fracture problem in an inhomogeneous lattice has been used to establish the connection between the crack The particular attention is given to waves corresponding to those crack-speed-dependent regions of the wavenumber axis where $\lambda = \pm 1$ and where λ is complex, that is, where $P^2 \le 1$ [see (7)].

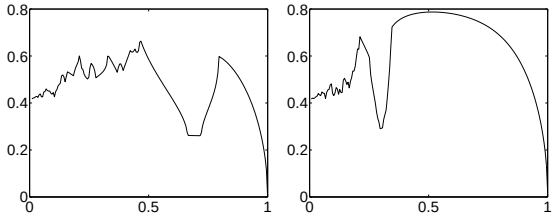

Figure 2: The energy ratio G_0/G as a function of the crack speed v for different values of the lattice contrast parameter μ. For the diagram on the left $\mu = 20$, whereas for the diagram on the right $\mu = 2$.

We evaluate the local energy release rate G_0, which is equal to the bond critical strain energy, as well as the global energy release rate G. The ratio G_0/G characterizes dissipation associated with the propagating fault within the lattice, and the results of sample computations are shown in Fig. 2. We note a considerable *energy ratio drop-down* for high-contrast lattices.

The *energy ratio drop-down* region corresponds to a highly increased dissipation, and hence to a strong increase of the crack resistance. Thus the above-mentioned increase in the lattice contrast μ creates an energy barrier against further increase of the crack speed. For the case of a crack in the inhomogeneous lattice with $2 < \mu < 10$, there exists a stability interval for sufficiently low crack speeds. We note that such an interval does not exist for a crack in a uniform lattice, as first noted in [16].

Acknowledgements. These results were obtained during the academic visit of Prof. Slepyan to Liverpool University supported by the research grant EP/D079489/1 from the

UK Engineering and Physical Sciences Research Council. Prof Mishuris was supported by the Marie Curie Transfer of Knowledge Fellowship of the European Community's Sixth Framework Programme, grant reference MTKD-CT-2004-509809.

References

[1] Brillouin, L., 1953. *Wave Propagation in Periodic Structures*. Dover, NY.

[2] Maradudin, A.A., Montroll, E.W. and Weiss, G.H., 1963. *Theory of Lattice Dynamics in the Harmonic Approximation*. Academic Press.

[3] Yablonovitch, E., 1987. Inhibited spontaneous emission in solid-state physics and electronics. Phys. Rev. Lett. 58, 2059-2062.

[4] Yablonovitch, E., 1993. Photonic band-gap crystals. J. Phys.: Condens. Matter 5, 2443-2460.

[5] John, S., 1987. Strong localization of photons in certain disordered dielectric superlattices. Phys. Rev. Lett. 58, 2486-2489.

[6] Joannopoulos, J.D., Meade, R.D., and Winn, J.N., 1995. Photonic Crystals: Molding the Flow of Light. Princeton University Press, Princeton, NJ.

[7] Johnson, S.G., and Joannopoulos, J.D., 2002. Photonic Crystals. The Road from Theory to Practice. Kluwer Acad. Publ., Boston.

[8] Thomson, R., Hsieh, C., and Rana, V., 1971. Lattice trapping of fracture cracks. J. Appl. Phys. 42, 3154-3160. (DOI:10.1063/1.1660699)

[9] Ashurst, W.T., and Hoover, W.G., 1976. Microscopic fracture studies in the two-dimensional triangular lattice. Phys. Rev. B 14, 1465-1473.

[10] Astrom, J., and Timonen, J., 1996. Crack bifurcation in a strained lattice. Phys. Rev. B 54, 9585-9588.

[11] Slepyan, L.I., 1981. Dynamics of a crack in a lattice. Sov. Phys. Dokl., 26, 538-540.

[12] Kulakhmetova, S.A., Saraikin, V.A., and Slepyan, L., 1984. Plane problem of a crack in a lattice. Mech. of Solids 19, 101-108.

[13] Fineberg, J, Gross, S.P., Marder, M., and Swinney, H.L., 1991. Instability in dynamic fracture. Phys. Rev. Lett. 67, 457-460.

[14] Fineberg, J, Gross, S.P., Marder, M., and Swinney, H.L., 1992. Instability in the propagation of fast cracks. Phys Rev B 45, 5146-5154.

[15] Marder, M., and Liu, X, 1994. Instability in lattice fracture. Phys. Rev. E 50, 188-197.

[16] Marder, M., and Gross, S., 1995. Origin of crack tip instabilities. J. Mech. Phys. Solids 43, 1-48.

[17] Marder, M., and Fineberg, J., 1996. How things break. Physics Today 49, 1-12.

[18] Kessler, D.A., 1999. Arrested cracks in nonlinear lattice models of brittle fracture. Phys. Rev. E 60, 7569-7571.

[19] Kessler, D.A., 2000. Steady-state cracks in viscoelastic lattice models. II. Phys. Rev. E 61, 2348 - 2360.

[20] Kessler, D.A., and Levine, H., 2001. Nonlinear lattice model of viscoelastic mode III fracture. Phys. Rev. E 63, 016118.

[21] Kessler, D.A. and Levine, H., 2003. Does the continuum theory of dynamic fracture work? Phys. Rev. E 68, 036118.

[22] Slepyan, L.I., 2001a. Feeding and dissipative waves in fracture and phase transition. I. Some 1D structures and a square-cell lattice. J. Mech. Phys. Solids, 49(3), 25-67.

[23] Slepyan, L.I., 2001b. Feeding and dissipative waves in fracture and phase transition. III. Triangular-cell lattice. J. Mech. Phys. Solids 49(12), 2839-2875.

[24] Heizler, S.I., Kessler, D.A., and Levine, H., 2002. Mode-I fracture in a nonlinear lattice with viscoelastic forces. Phys. Rev. E 66, 016126.

[25] Slepyan, L.I., and Ayzenberg-Stepanenko, M.V., 2002. Some surprising phenomena in weak-bond fracture of a triangular lattice. J. Mech. Phys. Solids 50(8), 1591-1625.

[26] Slepyan, L.I., and Ayzenberg-Stepanenko, M.V., 2004. Localized transition waves in bistable-bond lattices. J. Mech. Phys. Solids 52, 1447-1479.

[27] Slepyan, L.I., and Ayzenberg-Stepanenko, M.V., 2006. Crack dynamics in nonlinear lattices. Int. J. Fracture 140 (1-4), 235-242.

[28] Slepyan, L.I., 2002. Models and Phenomena in Fracture Mechanics. Springer, Berlin.

ELASTIC WAVES IN MONOCLINIC MATERIALS

William J. Parnell* **and I. David Abrahams**
School of Mathematics, University of Manchester, Manchester, UK
*Email: william.parnell@manchester.ac.uk

Abstract

We consider the problem of low frequency wave propagation through periodic fibre reinforced media where the periodic cell contains numerous fibres and hence the material possesses complex microstructure. We show how a recent homogenization scheme developed by Parnell and Abrahams [1], [2], based on classical asymptotic theory, can efficiently and reliably model such media.

Introduction

Inhomogeneous materials possessing complex microstructure are ubiquitous in science and industry. Equations governing low frequency wave propagation through such media possess rapidly varying coefficients and this poses substantial difficulties for direct numerical simulations. Homogenization theory eliminates these variations by replacing such coefficients with appropriately defined averaged quantities. This gives rise to the notion of *effective material properties*. Note the importance of *low frequency* propagation - i.e. the wavelength of propagating waves is much larger than the characteristic lengthscale of the microstructure. This is the so-called notion of *separation of scales* and the process of homogenization can only be carried out in this regime.

Many models have been developed for periodic composites. Multipole schemes based on the pioneering work of Rayleigh were developed by Zalipaev et. al. [3] and eigenstrain methods have also been used [4]. Perhaps the most well known scheme however is the method of asymptotic homogenization [5]. This is popular as it gives an algorithmic approach for determining effective properties. The main difficulty in its formulation is finding the solution to the resulting *cell problem*. For fibre reinforced media, techniques using complex variable theory and Weierstrassian elliptic functions have been developed in the statics context by Sabina et. al. [6]. It was considered in the low frequency elastodynamic context by Parnell and Abrahams [1], [2].

Traditionally, fairly simple microstructures have been modelled, such as one fibre per periodic cell. However in reality, materials possess complex microstructure and therefore there is great motivation for introducing numerous fibres into the periodic cell. The approach of Parnell and Abrahams is ideally suited to such developments and we shall describe this scheme here. Expressions are given for all *thirteen* effective elastic properties for monoclinic materials in terms of the solution to the cell problem.

Asymptotic homogenization and the cell problem

We work in Cartesian coordinates where the x_3 axis runs parallel to the fibres. The cross section of the material in the x_1x_2 plane is then defined by a *periodic cell* D of area $|D|$ which tesselates the entire plane. For ease of exposition here let us assume that each phase is isotropic. A typical periodic cell is made up from the host phase D_0 (of area $|D_0|$), of mass density ρ_0 and Lamé moduli λ_0 and μ_0 and embedded in this host phase at arbitrary locations are N fibres D_r (of area $|D_r|$) of mass densities ρ_r and Lamé moduli λ_r and μ_r, for $1 \leq r \leq N$. Again for clarity, we assume that the fibres are of circular cross section. This structure restricts the symmetry to be at most *monoclinic* (13 elastic constants).

The location of the (s,t)th periodic cell in the x_1x_2 plane is defined by the lattice vector $\mathbf{R}(s,t) = q(s\mathbf{l_1} + t\mathbf{l_2})$ for $s,t \in \mathbb{Z}$, so that q is the characteristic lengthscale of the periodic cell (and thus the microstructure) and $\mathbf{l_1}, \mathbf{l_2} \in \mathbb{R} \times \mathbb{R}$ are vectors whose components are $O(1)$.

Neglecting body forces, defining $\mathbf{x} = (x_1, x_2, x_3)$, scaling elastic properties on the host shear modulus μ_0 and nondimensionalizing lengthscales on q, Navier's equations for time harmonic waves of frequency ω in such a material are given by

$$(p(\mathbf{x}) + m(\mathbf{x}))\frac{\partial^2 u_j}{\partial x_i \partial x_j} + m(\mathbf{x})\frac{\partial^2 u_i}{\partial x_j \partial x_j} + \epsilon^2 d(\mathbf{x}) u_i = 0. \quad (1)$$

where we adopt Einstein's convention of summation over repeated subscripts. We have defined

$$m(\mathbf{x}) = \begin{cases} m_r = \mu_r/\mu_0, & \mathbf{x} \in D_r, \\ m_0 = 1, & \mathbf{x} \in D_0, \end{cases} \quad (2)$$

$$p(\mathbf{x}) = \begin{cases} p_r = \lambda_r/\mu_0, & \mathbf{x} \in D_r, \\ p_0 = \lambda_0/\mu_0, & \mathbf{x} \in D_0, \end{cases} \quad (3)$$

$$d(\mathbf{x}) = \begin{cases} d_r = \rho_r/\rho_0, & \mathbf{x} \in D_r, \\ d_0 = 1, & \mathbf{x} \in D_0. \end{cases} \quad (4)$$

and the nondimensional parameter $\epsilon = qk_0 \ll 1$ where $k_0 = \omega^2\rho_0/\mu_0$ is the shear wavenumber in the host material. Therefore a separation of scales exists and we can perform an analysis based on asymptotic homogenization. Boundary conditions on the fibre boundaries $\partial D_r, r = 1, 2, .., N$ are continuity of displacement and traction, i.e.

$$[u_j]^+_- = 0 \qquad [\sigma_{ij}n_j]^+_- = 0 \tag{5}$$

where σ_{ij} is the Cauchy stress tensor and where we have used the notation $[f(x)]^+_-$ to denote the jump in the function $f(x)$ across ∂D_r.

Asymptotic homogenization proceeds by defining the multiple scale variables

$$x_\alpha, = \xi_\alpha, \qquad x_j = \frac{1}{(\epsilon + L_2\epsilon^2 + ...)}z_j, \tag{6}$$

where $L_2 \in \mathbb{R}$ and Greek and Roman indices range from 1-2 and 1-3 respectively. On introducing $\boldsymbol{\xi} = (\xi_1, \xi_2)$ and $\mathbf{z} = (z_1, z_2, z_3)$ we note from (6) that these are short and long lengthscales respectively and there is no microscale in the x_3 direction.

An expansion in ϵ is performed for the displacements

$$u_k(\boldsymbol{\xi}, \mathbf{z}) = u_{k0}(\boldsymbol{\xi}, \mathbf{z}) + \epsilon u_{k1}(\boldsymbol{\xi}, \mathbf{z}) + O(\epsilon^2) \tag{7}$$

and since the material is doubly periodic with respect to $\boldsymbol{\xi}$, we insist that each u_{kj} possesses this symmetry.

Using (6) and (7) in the governing equation (1) and boundary conditions (5) and equating orders in ϵ we obtain a hierarchy of problems, one associated with each order in ϵ. As usual the $O(1)$ problem shows that u_{k0} is (explicitly) independent of $\boldsymbol{\xi}$ so that

$$u_{k0}(\boldsymbol{\xi}, \mathbf{z}) = U_k(\mathbf{z}). \tag{8}$$

At $O(\epsilon)$ it is advantageous to write the u_{k1} in separable form:

$$u_{k1}(\boldsymbol{\xi}, \mathbf{z}) = N_{kpm}(\boldsymbol{\xi})\frac{\partial U_p(\mathbf{z})}{\partial z_m}. \tag{9}$$

This gives rise to the resulting *cell problem* for $N_{kpm}(\boldsymbol{\xi})$. The subscripts p and m merely alter the *forcing* in the boundary conditions of the cell problem as we will see in (13)-(18), so it is useful to employ the bold font notation $\mathbf{N}_k = N_{kpm}$. On denoting the derivative of $\mathbf{N}_k$ with respect to ξ_α by $\mathbf{N}_{k,\alpha}$ the governing equations for the cell problems (in the rth phase) are of the form

$$(p_r + m_r)\mathbf{N}^r_{\alpha,1\alpha} + m_r\mathbf{N}^r_{1,\alpha\alpha} = 0, \tag{10}$$

$$(p_r + m_r)\mathbf{N}^r_{\alpha,2\alpha} + m_r\mathbf{N}^r_{2,\alpha\alpha} = 0, \tag{11}$$

$$m_r\mathbf{N}^r_{3,\alpha\alpha} = 0, \tag{12}$$

where we note again that the Greek alphabet denotes summation over the indices 1 and 2 only. Boundary conditions are continuity of $\mathbf{N}^0_k$ and $\mathbf{N}^r_k, r = 1, .., N$ across each ∂D_r and

$$\Big[(p_r + 2m_r)\mathbf{N}^r_{1,1} + p_r\mathbf{N}^r_{2,2}\Big]^+_- n_1 + \Big[m_r(\mathbf{N}^r_{1,2} + \mathbf{N}^r_{2,1})\Big]^+_- n_2 = \mathbf{A}^{r1}n_1 + \mathbf{B}^r n_2, \tag{13}$$

$$\Big[(p_r + 2m_r)\mathbf{N}^r_{2,2} + p_r\mathbf{N}^r_{1,1}\Big]^+_- n_2 + \Big[m_r(\mathbf{N}^r_{1,2} + \mathbf{N}^r_{2,1})\Big]^+_- n_1 = \mathbf{B}^r n_1 + \mathbf{A}^{r2}n_2, \tag{14}$$

$$[m_r\mathbf{N}^r_{3,\alpha}]^+_- n_\alpha = \mathbf{C}^r_\alpha n_\alpha. \tag{15}$$

Here we have defined

$$\mathbf{A}^{rj} = A^{rj}_{pm} = (p_r - p_0)\delta_{pm} + 2(m_r - m_0)\delta_{jp}\delta_{jm}, \tag{16}$$

$$\mathbf{B}^r = B^r_{pm} = (m_r - m_0)(\delta_{1p}\delta_{2m} + \delta_{2p}\delta_{1m}), \tag{17}$$

$$\mathbf{C}^r_\alpha = C^r_{\alpha pm} = (m_r - m_0)(\delta_{\alpha m}\delta_{3p} + \delta_{\alpha p}\delta_{3m}). \tag{18}$$

Note that the cell problem for $\mathbf{N}_3$ is decoupled from that for $\mathbf{N}_1$ and $\mathbf{N}_2$. The former is associated with *anti-plane* motion and the latter is associated with *in-plane* motion.

The homogenized wave equation

We obtain the effective wave equation governing the leading order displacement $U_k(\mathbf{z})$ by integrating the governing equation at $O(\epsilon^2)$ over the periodic cell, employing Green's theorem and imposing the necessary boundary conditions and double periodicity in $\boldsymbol{\xi}$. This gives

$$\begin{aligned} c^*_{11}U_{1,11} + c^*_{66}U_{1,22} + c^*_{55}U_{1,33} + c^*_{16}U_{2,11} + c^*_{26}U_{2,11} \\ + c^*_{45}U_{2,33} + 2c^*_{16}U_{1,12} + (c^*_{12} + c^*_{66})U_{2,12} \\ + (c^*_{13} + c^*_{55})U_{3,13} + (c^*_{36} + c^*_{45})U_{3,23} \\ + d^*U_1, = 0 \end{aligned} \tag{19}$$

$$\begin{aligned} c^*_{16}U_{1,11} + c^*_{26}U_{1,22} + c^*_{45}U_{1,33} + c^*_{66}U_{2,11} + c^*_{22}U_{2,22} \\ + c^*_{44}U_{2,33} + (c^*_{12} + c^*_{66})U_{1,12} + 2c^*_{26}U_{2,12} \\ + (c^*_{36} + c^*_{45})U_{3,13} + (c^*_{23} + c^*_{44})U_{3,23} \\ + d^*U_2 = 0, \end{aligned} \tag{20}$$

$$\begin{aligned} c^*_{55}U_{3,11} + c^*_{44}U_{3,22} + c^*_{33}U_{3,33} + 2c^*_{45}U_{3,12} + \\ (c^*_{13} + c^*_{55})U_{1,13} + (c^*_{23} + c^*_{44})U_{2,23} \\ + (c^*_{36} + c^*_{45})(U_{1,23} + U_{2,13}) + d^*U_3 = 0, \end{aligned} \tag{21}$$

where $U_{k,j}$ denotes the derivative of U_k with respect to z_j. The form of these effective wave equations is identical to that which governs wave propagation in a monoclinic *homogeneous* elastic medium with (engineering) elastic moduli c^*_{ij}. The coefficients therefore define the corresponding *thirteen* effective elastic moduli.

The effective elastic moduli can be written as

$$c^*_{11} = p_V + 2m_V + S_{11} + 2T_{1111}, \tag{22}$$
$$c^*_{22} = p_V + 2m_V + S_{22} + 2T_{2222}, \tag{23}$$
$$c^*_{33} = p_V + 2m_V, \tag{24}$$
$$c^*_{44} = m_V + T_{3232}, \tag{25}$$
$$c^*_{55} = m_V + T_{3131}, \tag{26}$$
$$c^*_{66} = m_V + T_{1212} + T_{2112}, \tag{27}$$
$$c^*_{12} = p_V + S_{11} + 2T_{2211} = p_V + S_{22} + 2T_{1122}, \tag{28}$$
$$c^*_{13} = p_V + S_{11}, \tag{29}$$
$$c^*_{23} = p_V + S_{22}, \tag{30}$$
$$c^*_{45} = T_{3123} = T_{3213}, \tag{31}$$
$$c^*_{16} = 2T_{1112} = T_{1211} + T_{2111}, \tag{32}$$
$$c^*_{26} = 2T_{2212} = T_{1222} + T_{2122}, \tag{33}$$
$$c^*_{36} = T_{1233} + T_{2133} = 0, \tag{34}$$

where

$$p_V = \sum_{r=0}^{N} \phi_r p_r, \qquad m_V = \sum_{r=0}^{N} \phi_r m_r, \tag{35}$$

$$S_{pm} = \sum_{r=1}^{N} (p_r - p_0) H^r_{\beta\beta pm}, \tag{36}$$

$$T_{i\beta pm} = \sum_{r=1}^{N} (m_r - 1) H^r_{i\beta pm}. \tag{37}$$

Here we have defined the so-called *H-tensor*,

$$H^r_{k\beta pm} = \frac{1}{|D|} \int_0^{2\pi} N^r_{kpm}(\boldsymbol{\xi}) n^r_\beta \; d\theta_r, \tag{38}$$

and the normal to the rth fibre is $\mathbf{n}^r = (\cos\theta_r, \sin\theta_r)$, where we have introduced the local polar coordinate system centred on the rth fibre with associated angle θ_r. The *volume fraction* of each phase is defined by $\phi_r = |D_r|/|D|$. The effective mass density is given by

$$d_* = \sum_{r=0}^{N} \phi_r d_r. \tag{39}$$

The solution to the cell problem

A detailed description of the solution to the cell problems can be found in [1], [2] and we refer the reader to these articles for more details. The methods used to solve these cell problems are based on complex variable theory, the Cauchy-Goursat solution for in-plane problems and multipole expansions of doubly periodic functions, specially constructed to enable complex microstructure to be modelled.

In summary, local solution expansions for $\mathbf{N}^r_k = N^r_{kpm}$ are posed inside the fibres and the host. In order to satisfy the double periodicity condition, these solutions must be matched to expansions of appropriately defined doubly periodic basis functions. In particular a doubly periodic basis set is assigned to each fibre within the periodic cell so that for complex microstructures, the solution comprises the superposition of N doubly periodic functions.

By implementing this scheme in Mathematica, the solutions $\mathbf{N}^r_k$ and thus the effective moduli c^*_{ij} can be computed accurately and reliably.

References

[1] Parnell, W.J. and Abrahams, I.D., "Dynamic homogenization in periodic fibre reinforced media. Quasi-static limit for SH Waves", Wave Mot., vol. 43, pp. 474-498, 2006.

[2] Parnell, W.J. and Abrahams, I.D., "Homogenization for wave propagation in periodic fibre reinforced media, I and II", Submitted to J. Mech. Phys. Sol., 2007.

[3] Zalipaev, V.V., Movchan, A.B., Poulton, C.G. and McPhedran, R.C.,"Elastic waves and homogenization in oblique periodic structures", Proc. R. Soc. Lond. A, vol. 458, pp. 1887-1912, 2002.

[4] Nemat-Nasser, S. and Hori, M., Micromechanics: Overall properties of heterogeneous materials, North-Holland, 1999.

[5] Parton, V.Z and Kudryavtsev, B.A., Engineering mechanics of composite structures, CRC Press, 1993.

[6] Sabina, F.J., Bravo-Castillero, J., Guinovart-Díaz, R., Rodríguez-Ramos, R. and Valdiviezo-Mijangos, O.C., "Overall behaviour of two-dimensional periodic composites", Int. J. Sol. Struct., vol. 39, pp. 483-497, 2002.

NUMERICAL MODELLING OF MICRO-STRUCTURE USING THE CONCEPT OF ENHANCED CONTINUUM

A. V. Pichugin* **and J. D. Kaplunov**
Department of Mathematical Sciences, Brunel University, Uxbridge UB8 3PH, UK.
*E-mail: aleksey.pichugin@brunel.ac.uk

Abstract

This paper considers the peculiarities arising in numerical implementations of theories for enhanced continua. Firstly, governing equations of such theories are often not strongly elliptic. We propose a technique for reformulating the governing equations that does not affect their truncation error. Secondly, we discuss non-physical boundary layers that correspond to extraneous integrals and are characteristic to higher-order governing equations. It is established that the effect of these boundary layers may be minimised by formulating appropriate boundary conditions. To this end, a new asymptotic procedure for deriving such boundary conditions is proposed and illustrated by a simple one-dimensional example.

Introduction

Nowadays, effective continuum theories for micro-structure are well understood and routinely used for numerical modelling. These theories are, essentially, leading order terms long-wave approximations of the associated multi-scale formulations (either discrete or continuum). The use of effective continua remains justified as long as the separation between macro- and micro-scales is well-pronounced. The numerical accuracy of these models may be further improved by taking into account higher-order refinements; this results in a variety of enhanced continuum ("strain gradient") theories. Unfortunately, the presence of higher-order terms in governing equations also results in certain unwanted features that complicate the associated computational schemes.

Consider linear harmonic vibrations of a crystalline solid, governed by the equations

$$\sigma_{mi,m} = \rho\omega^2 u_i \,, \tag{1}$$

$$\sigma_{mi} = c_{milk}\varepsilon_{lk} = c_{milk}u_{l,k} \,, \tag{2}$$

where $\boldsymbol{\sigma}$ is the stress, $\boldsymbol{\varepsilon}$ the strain, $\boldsymbol{u}$ the displacement, and c_{milk} the tensor of effective elastic constants. Commas denotes differentiation with respect to the implied spatial variable and summation over repeated indices is assumed. Equations (1)–(2) may be obtained as long-wave limits for lattice structures describing arrangements of atoms within crystals. As frequency increases, the assumptions implied in (1)–(2) become less accurate and higher-order corrections may be taken into the account. For a centro-symmetric solid they may be given by

$$\sigma_{mi} = c_{milk}\varepsilon_{lk} + \ell^2 d_{milker}\varepsilon_{lk,er} \,, \tag{3}$$

with tensor d_{milker} describing weak dispersion produced by micro-structure with a characteristic length scale ℓ^2. When constitutive equations (3) are suitably non-dimensionalised, parameter ℓ^2 may be interpreted as the ratio between a typical grain size and the wavelength.

Local stability of enhanced continua

Constitutive equations (3) are derived within the context of a perturbation procedure and only meaningful when $\ell^2 \ll 1$. It is, therefore, not surprising that (1)–(3) with $\ell^2 \gg 1$ may violate positive-definiteness of the energy functional and result in a non-uniqueness, see [1]. In elastodynamics this is usually referred to as the loss of strong ellipticity. A traditional phenomenological solution to this problem involves replacing the plus sign in (3) with a minus. However, the resulting models feature unrealistic dispersion and cannot be easily linked to explicit descriptions of micro-structure.

In scalar problems it is always possible to use equations of motion (1) to replace strain gradients in (3) with inertia corrections. In application to formally identical higher-order asymptotics for plates and shells, the authors of [2] term such models as *the theories with modified inertia.* Theories with constitutive equations similar to (3) imply non-local response and require formulating additional boundary conditions. In contrast, theories with modified inertia can be used for modelling harmonic vibrations on bounded domains using the original boundary conditions for underlying effective continuum.

The described procedure works only for scalar problems or vector problems that may be reformulated in terms of scalar potentials, see [3]. However, this approach may be generalised by noticing that since (3) implies $\sigma_{mi,m} \sim \rho\omega^2 u_i$, an arbitrary superposition of

$$c_{milk}u_{k,lm} + \ell^2 d_{milker}u_{l,kerm} = \rho\omega^2 u_i + O(\ell^4) \,, \tag{4}$$

$$\ell^2 c_{milk}u_{k,lm} = \ell^2\rho\omega^2 u_i + O(\ell^4) \,, \tag{5}$$

results in a theory with the same truncation error $O(\ell^4)$. While it is not known at present whether this procedure would enable one to ensure strong ellipticity for a three-dimensional solid with general anisotropy, paper [4] demonstrates that strong ellipticity is achievable at least in two-dimensional materials with cubic symmetry.

Boundary conditions: a model example

Since the equation obtained by superimposing (4)–(5) are singularly perturbed, they feature extraneous integrals corresponding to short-wave boundary layers. The situation is best described by considering a simple model problem for an enhanced continuum governed by

$$\frac{\partial^2 u}{\partial x^2} + \omega^2 u - \alpha^2 \ell^2 \frac{\partial^4 u}{\partial x^4} = 0\,, \tag{6}$$

in the semi-infinite domain $\Gamma = \{x | x \geqslant 0\}$. Equation (6) has two particular integrals. The first of them, $\bar{u}$, is given to the leading order by

$$\frac{\partial^2 \bar{u}}{\partial x^2} + \omega^2 \bar{u} \sim 0\,, \tag{7}$$

and is, essentially, a thought for homogenised solution that is physically relevant. The second integral u_* is described to the leading order by

$$\frac{\partial^2 u_*}{\partial x^2} - \alpha^2 \ell^2 \frac{\partial^4 u_*}{\partial x^4} \sim 0\,, \tag{8}$$

and describes a spurious non-long-wave boundary layer

$$u_* = Ce^{-x/\alpha\ell}\,. \tag{9}$$

Suppose that we want to solve a Dirichlet problem on Γ and pose a boundary condition of the form

$$u|_{x=0} = f\,. \tag{10}$$

Every solution of (6) $u = \bar{u} + u_*$ and, therefore, solutions of boundary value problem (6), (10) would implicitly assume the distorted boundary condition given by $\bar{u}|_{x=0} = f - u_*|_{x=0}$. Thus, in order to solve Dirichlet problem for the governing equation (6) we need to find a way of ensuring that $\bar{u}|_{x=0} = f$.

Fourth-order differential equation (6), certainly, requires a second boundary condition that cannot be extrapolated by considering the effective continuum. We can use this opportunity to fix the boundary layer and ensure the physicality of the solution. Let us, for example, consider the second boundary condition

$$\left.\frac{\partial u}{\partial x}\right|_{x=0} = \left.\frac{\partial \bar{u}}{\partial x}\right|_{x=0} + \left.\frac{\partial u_*}{\partial x}\right|_{x=0} = F_1\,, \tag{11}$$

with the function F_1 to be chosen later. By referring to (9) it is possible to conclude that $u_*|_{x=0} = 0$ when

$$F_1 = \left.\frac{\partial \bar{u}}{\partial x}\right|_{x=0}\,. \tag{12}$$

This implies that the numerical scheme for solving the boundary value problem (6), (10) may be implemented in two steps. Firstly, the leading order problem (7) must be solved subject to (10) to find the leading order of $\bar{u}$. Secondly, the resulting leading order solution must be differentiated to define F_1 in the additional boundary condition (11). This technique may be iterated to obtain higher-order corrections and generalised to work for the vector problems and with more complex boundary layers.

For some problems it may also be possible to find purely analytic solutions. For example, if we introduce another second boundary condition

$$\left.\frac{\partial^2 u}{\partial x^2}\right|_{x=0} = \left.\frac{\partial^2 \bar{u}}{\partial x^2}\right|_{x=0} + \left.\frac{\partial^2 u_*}{\partial x^2}\right|_{x=0} = F_2\,, \tag{13}$$

straightforward application of (7) and (9) yields

$$\frac{1}{\alpha^2\ell^2} u_*|_{x=0} = -\omega^2 \bar{u}|_{x=0} - F_2\,. \tag{14}$$

Thus, in order to satisfy the required boundary condition $\bar{u}|_{x=0} = f$ we have to select

$$F_2 = -\omega^2 f\,. \tag{15}$$

References

[1] H. Askes & E. C. Aifantis, "Gradient elasticity theories in statics and dynamics — A unification of approaches", International Journal of Fracture, vol. 139, pp. 297–304, 2006.

[2] J. D. Kaplunov, L. Yu. Kossovich, & E. V. Nolde "Dynamics of thin walled elastic bodies", New York: Academic Press, 1998.

[3] R. Burridge, P. Chadwick, & A. N. Norris, "Fundamental elastodynamic solutions for anisotropic media with ellipsoidal slowness surfaces", Proceedings of the Royal Society of London, Series A, vol. 440(1910), pp. 655–681, 1993.

[4] A. V. Pichugin, H. Askes, & A. Tyas, "Asymptotic equivalence of homogenisation procedures and fine-tuning of continuum theories", submitted for publication.

WAVE PROPAGATION ACROSS RIPPLE BEDS

R. Porter
University of Bristol, University Walk, Bristol, BS8 1TW, UK.
Email: richard.porter@bris.ac.uk

Introduction

When a train of surface gravity waves propagate across a region of non-uniform depth, reflection of waves occur. For small bed gradients and small changes in the depth of the fluid, the reflection is often very weak. An exception can occur if the bed is rippled – i.e. the bed contains a section with a number of periodically repeating undulations. In this case very significant wave reflection can occur within certain bands of wave frequency – see figs. 1a,b. Such ripple beds do occur naturally in coastal locations, their formation being a result of interaction with the coastline and self-inforcement through the morphology of the bed [1]. The high reflective property of periodic 'sand bars' can be a useful feature in coastal protection.

There have been many contributions in the literature towards the study of wave reflection by ripple beds. This is partly because the ripple bed configuration turns out to provide a stern test of the performance of approximation models developed for use in more general topographical wave scattering problems. There have also been specific efforts to exploit particular features of ripple beds (smallness in the gradient and amplitude) to predict reflection by a number of ripples. However, it has only been until fairly recently that approximate models (originally in the form of the 'modified mild-slope equations' [2]) have been able to accurately predict reflection by ripple beds when compared against experimental data [3]. The fact that, until even more recently [4], no accurate numerical results based upon the exact linear water wave theory have been available to compare against is a measure of the level of difficulty of this problem, and is the main subject of the present paper.

Of course, the phenomenon of high reflection by a large number of periods of a rippled bed is readily identifiable as 'Bragg reflection', a term originating from X-ray crystallography. That is, there are intervals of frequency where there exist coherent multiple reflections. The larger the number of periods, the greater the reflection (as a very rough first approximation, one finds that the reflected wave amplitude is proportional to the number of periods). For a wave train progressing from constant depth to an infinite number of ripple periods one expects total reflection over certain frequency bands. In this context, Bragg reflection is also readily identifiable as being associated with passing and stopping bands occurring in infinite periodic structures.

The preceding paragraph hints at the other main purpose of this work, namely to identify close connections between the scattering by finite, infinite and semi-infinite periodic ripple beds. In this sense, the present physical setting of ripple beds is somewhat unimportant and it is only the periodicity and the presence of a source of scattering into multiple wave modes within that period which is important.

Scattering by N ripples

We set out to accurately compute the wave reflection by a ripple bed with N periods. In order to make this a computationally feasible exercise, the periodicity must be exploited so that the value of N is relatively unimportant for computational purposes. Thus the scattering by a *single* period is considered and is encapsulated in either a scattering matrix $\mathcal{S}$, or a transfer matrix $\mathcal{P}$. The former relates incoming to outgoing wave amplitudes, and the latter relates wave amplitudes from left to right of the single ripple. The problem of resolving the reflection for an N-period ripple bed is then simply found by coupling each single period to its neighbour. This is done most easily by noting that the transfer matrix $\mathcal{P}_N$ for N periods is just the product of $\mathcal{P}$ with itself N times – i.e. $\mathcal{P}^N$. In order to retain the full accuracy required, not only do the wave amplitudes associated with right- and left-*propagating* waves have to be incorporated into the definition of $\mathcal{S}$ and $\mathcal{P}$, but so do the amplitudes of the infinite set of *evanescent* waves which come from separating variables in the depth variable. In practice, we work with a truncated set of M evanescent wave modes from the outset implying an approximation has been made, but assume that M will eventually be treated as a numerical parameter to determine whatever accuracy is desired. The method by which the $2(M+1)\times 2(M+1)$ matrices $\mathcal{S}$ and $\mathcal{P}$ (which, incidentally, are related to one another) are determined is based upon an integral equation formulation whose details we shall not need to go into. Suffice to say that in the formulation of integral equations, no approximation is made to the boundary of the bed nor the governing equations, whilst the formulation itself and subse-

quent numerical approximation to the solution of the integral equations and $\mathcal{S}$ and $\mathcal{P}$ ensures that certain important structural identites associated with $\mathcal{S}$ and $\mathcal{P}$ are retained. In particular, it can be shown that $\mathcal{P}$ has certain properties associated with its eigenvalues, λ_i, $i = 0, \ldots, 2M+1$, namely that $\lambda_i\lambda_j = 1$, $\lambda_i = \overline{\lambda}_k$ for some j, k not equal to i. Hence, eigenvalues occur either in real reciprocal pairs or complex conjugate pairs with unit modulus. It is useful to employ the spectral representation,

$$\mathcal{P} = \mathcal{X}\Lambda\mathcal{X}^{-1},$$

where

$$\mathcal{X}^{-1} = \begin{pmatrix} \boldsymbol{X}_{11} & \boldsymbol{X}_{12} \\ \boldsymbol{X}_{21} & \boldsymbol{X}_{22} \end{pmatrix}, \qquad \Lambda = \begin{pmatrix} \boldsymbol{\Delta} & 0 \\ 0 & \boldsymbol{\Delta}^{-1} \end{pmatrix},$$

where $\Delta = \mathrm{diag}\{\lambda_0, \ldots, \lambda_M\}$ in which the eigenvalues are ordered to contain those complex eigenvalues with argument in $(0, \pi)$ followed by the real eigenvalues with decreasing magnitude less than unity. Now $\mathcal{P}_N = \mathcal{P}^N = \mathcal{X}\Lambda^N\mathcal{X}^{-1}$ and it follows, by some careful matrix algebra designed to remove occurrences of $\boldsymbol{\Delta}^{-N}$, that the scattering matrix $\mathcal{S}_N$ for N periods can be written as

$$\mathcal{S}_N = -\begin{pmatrix} \boldsymbol{X}_{22} & \boldsymbol{\Delta}^N\boldsymbol{X}_{21} \\ \boldsymbol{\Delta}^N\boldsymbol{X}_{12} & \boldsymbol{X}_{11} \end{pmatrix}^{-1}\begin{pmatrix} \boldsymbol{X}_{21} & \boldsymbol{\Delta}^N\boldsymbol{X}_{22} \\ \boldsymbol{\Delta}^N\boldsymbol{X}_{11} & \boldsymbol{X}_{12} \end{pmatrix}$$

and is numerically robust. The reflection and transmission coefficients for N periods are identifiable as four elements in the top left positions of the 2×2 block partition of $\mathcal{S}_N$. Thus, the solution of the scattering problem is essentially determined, and it remains to establish, numerically, what values of M are required for a certain desired accuracy – see fig. 2. It is noted that if $M = 0$, the scattering process is approximated by the coupling of propagating waves only, a situation often referred to as the wide-spacing approach.

An infinitely-periodic ripple bed

For an infinitely-periodic ripple bed, Bloch-Floquet theory can be invoked to reduce the problem, again, to a single period (of length ℓ), with 'periodic' boundary conditions of the form $\phi(0, y) = \mu\phi(\ell, y)$, $\phi_x(0, y) = \mu\phi_x(\ell, y)$ where $\phi(x, y)$ is the potential satisfying Laplace's equation in the fluid, x and y are horizontal and vertical coordinates. The parameter $\mu \in \mathbb{C}$ is often written as $\mathrm{e}^{i\beta\ell}$ to make the periodicity condition explicit, where $\beta \in \mathbb{R}$ implies a passing band and there is no decay or growth at infinity; if $\beta \notin \mathbb{R}$ then there is a stopping band as waves decay in one direction along the array. The parameter $\mu(k)$ may be regarded as an eigenvalue depending upon a wavenumber $k = 2\pi/\lambda$ (λ is the wavelength) characterising the frequency. A passing band is thus associated with $\mu(k)$ taking values on the unit circle in the complex plane and since ϕ satisfies a homogeneous problem, so does $\bar{\phi}$, and so $\bar{\mu}(k)$ must also be an eigenvalue.

Numerical approximations to values of $\mu(k)$ can be found by formulating a new (homogeneous) integral equation for a single period of the bed satisfying the periodic boundary conditions on $x = 0$ and $x = \ell$. Furthermore, the structure of the integral equation itself shows that values of μ occur either as complex conjugates on the unit circle or as real reciprocal pairs. Indeed, there are not just two eigenvalues for any given value of k: there are an infinite number of eigenvalues, $\mu = \mu_i$, $i = 0, \ldots$. If $\mu_i \in \mathbb{R}$ for all i, then k lies in a stopping band. If any pair exist on the unit circle as conjugates, then k lies in a passing band.

Connections between the problems

By revisiting the scattering problem in which the fundamental quantity $\mathcal{P}$ connects amplitudes across a single period, but now imposing the periodicity conditions on ϕ, we are able to argue that the eigenvalues, λ_i, of $\mathcal{P}$, coincide with μ_i for the infinitely-periodic (Bloch) problem, in the limit as $M \to \infty$. Numerically (tab. 1) it is observed that for finite, but increasing, values of $M \geq 0$, values of λ_i approximate with ever greater accuracy the numerically obtained values of μ_i although no *a priori* estimates can be made on the proximity of λ_i to μ_i for any given value of M. We are able to go further and establish connections between the eigenvectors of $\mathcal{P}$ and the eigenfunctions of the Bloch problem.

These relationships allow us – in principle at least – to use the solution of the Bloch problem to deduce reflection and transmission scattered wave amplitudes for an N-period ripple bed, for any $N \geq 1$. Conversely, by solving the scattering problem by a single period, we can deduce eigenvalues and eigenfunctions for the Bloch problem.

A final result is that the onset of Bragg resonance is now precisely defined as being those critical values of k at which eigenvalues of infinitely-periodic problem switch from real pairs to complex conjugate pairs. That is, when $\mu = \pm 1$ or $\beta\ell = 0, \pi$. Here, it is easy to infer that these values refer simply to standing waves over the infinite periodic bed. If the bed has left-right symmetry then the critical values of k which bound intervals of Bragg resonance are just the sloshing frequencies for a single period of the bed contained between vertical walls aligned with

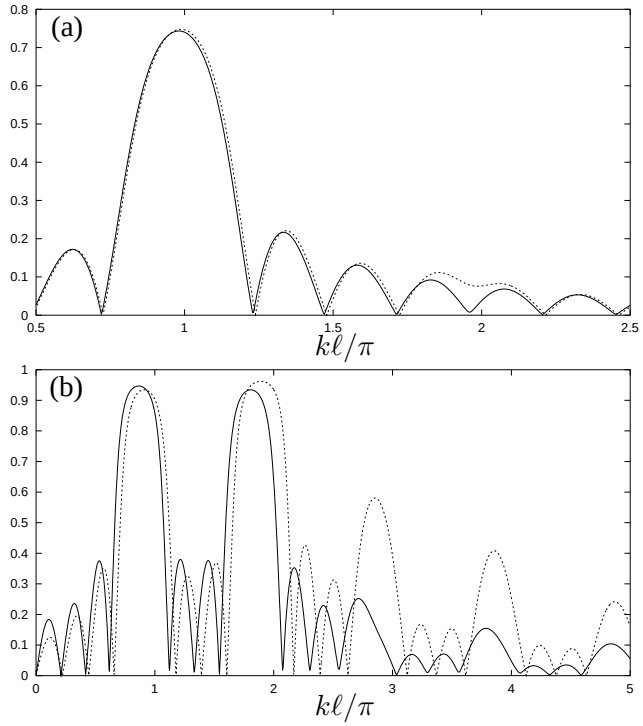

Figure 1: Reflection coefficient, $|R|$, against wavenumber for: (a) sinusoidally-varying bed, $N = 4$, $h(x) = 1 - 0.32\sin(\pi x/3.2)$; (b) doubly-sinusoidal bed, $N = 4$, $h(x) = 1 - 0.4(\sin(\pi x/2.4) + \sin(\pi x/1.2))$. Dashed curves modified mild slope equation, ref. [2].

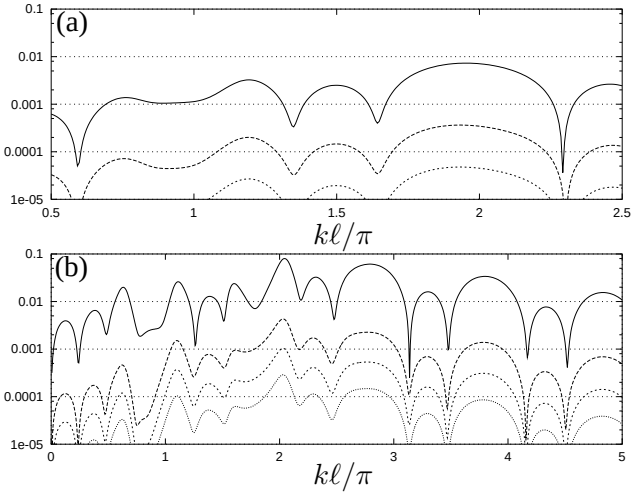

Figure 2: Convergence of reflected coefficient, $|R|$, with $M = 0, 2, 4, 6$: vertical scale measures $|R - R_e|$ where R_e uses $M = 10$. Curves correspond to configurations in fig. 1

Table 1: Comparison of eigenvalues of $\mathcal{P}$, with increasing M, from the scattering problem with those from the Bloch problem

Scattering:	$\arg(\lambda_0)$	$\lambda_1 \times 10^2$	$\lambda_2 \times 10^4$	$\lambda_3 \times 10^6$
$M = 0$	1.73112	-	-	-
$M = 1$	1.72830	0.77453	-	-
$M = 2$	1.72781	0.95100	0.21621	-
$M = 3$	1.72781	0.95224	0.42772	0.3989
$M = 4$	1.72781	0.95225	0.44779	0.1900
$M = 5$	1.72781	0.95227	0.44801	0.2395
$M = 6$	1.72781	0.95227	0.44802	0.2478
$M = 7$	1.72781	0.95227	0.44802	0.2485
$M = 8$	1.72781	0.95227	0.44802	0.2468
Bloch:	$\arg(\mu_0)$	$\mu_1 \times 10^2$	$\mu_2 \times 10^4$	$\mu_3 \times 10^6$
	1.72781	0.95227	0.44802	0.2494

the two different planes of symmetry. This interpretation can be regarded as a more sophisticated version of earlier work on ripple beds, which often quotes the Bragg resonance criteria as $k\ell = \pi$; this corresponds to the sloshing frequency for a vertically-walled vessel of width ℓ with a *horizontal* base.

A selection of numerical results demonstrating the features described above will be presented in the talk and, if time permits, a brief summary of the procedure used for considering scattering by a semi-infinite periodic ripple bed will be given.

References

[1] C.C. Mei, "Resonant reflection of surface water waves by periodic sandbars", J. Fluid Mech., vol. 152, pp. 315-335, 1985.

[2] P.G. Chamberlain, D. Porter "The modified mild-slope equation", J. Fluid Mech., vol. 291, pp. 393-407, 1995.

[3] A.G. Davies, A.D. Heathershaw, "Surface-wave propagation over sinusoidally varying topography.", J. Fluid Mech., vol. 144, pp. 419-443, 1984.

[4] R. Porter, D. Porter, "Scattered and free waves over periodic beds", J. Fluid Mech., vol. 483, pp. 129-163, 2003.

ACOUSTIC PROPAGATION IN DISPERSIONS

Brian. D. Sleeman
School of mathematics, University of Leeds, Leeds, LS2 9JT,UK
Email: bds@maths.leeds.ac.uk

Abstract

The problem of scattering of ultrasound by particles in the long wavelength limit is well known to be solvable in terms of Rayleigh expansions of the scattered fields. Such solutions are numerically ill conditioned and recent work with O. G. Harlen, M. J. Holmes, V. J. Pinfield, M. J. W. Povey and Y. Qui has sought to identify alternative methods. The scattered fields are expressed in terms of a power series expansion in the parameter Ka, (the wavenumber multiplied by the particle radius), which is small in the long wavelength region. The formulation is valid for all values of the thermal wavelength. The solution overlaps the limiting solutions for small thermal wave length, based on the geometrical theory of diffraction, [1], and very large thermal wavelength, based on low frequency theory, [2], previously developed.

Introduction

Ultrasound spectroscopy is an important technique for characterizing the physical properties of dispersions, emulsions, gels and solutions of biomolecules. It depends on a strong theoretical basis which relates ultrasound properties to particle size and the physical properties of materials. The key problems were solved for spherical particles by Rayleigh [3] and Epstein and Carhart [4]. The aim of this paper, based on the work of Pinfield.*et. al*, [5] is to formulate a numerically stable solution to the single scattering problem in such a way as to allow its extension to multiple scatterers and to nonspherical scattering particles. For $Ka \ll 1$, Kleinman's approach [6] can be used wherein the scattered field is reformulated to satisfy the radiation condition and is expressed in a certain power series in Ka. For thermal waves in which $La \ll 1$, where L is the thermal wavenumber, the Kleinman approach [2] can be used. When $La \gg 1$ the thermal wave can be studied [1] on the basis of the geometrical theory of diffraction. The idea here uses the Kleinman approach to separate the radiative terms of the waves and to define a series expansion convergent in the long acoustic wavelength limit. The significant departure from previous work is that all wave modes are expanded as a series in Ka, leaving dependence on L implicit in the coefficients. This avoids assumptions on the size of La.

Methods

Assuming an harmonic time dependence $e^{-i\omega t}$ propagational and thermal modes satisfy

$$(\Delta + K^2)\phi = 0, \quad (\Delta + L^2)\psi = 0,$$

where K and L are the complex acoustic and thermal wavenumbers respectively. To calculate the ultrasound field produced by a dispersion of particles we first consider the effect of a sound wave on a single spherical particle of radius a immersed in an infinite uniform fluid. Together with radiation conditions we have the following boundary conditions across the surface of the particle.

$$\frac{\partial}{\partial r}(\phi_0 + \phi + \psi) = \frac{\partial}{\partial r}(\phi' + \psi'),$$

$$(\phi_0 + \phi + \psi) = \hat{\rho}(\phi' + \psi'),$$

$$\Gamma_c\phi_0 + \Gamma_c\phi + \Gamma_t\psi = \Gamma_c'\phi' + \Gamma_t'\psi',$$

$$\Gamma_c\frac{\partial}{\partial r}(\phi_0 + \phi) + \Gamma_t\frac{\partial\psi}{\partial r} = \hat{\tau}\left(\Gamma_c'\frac{\partial\phi'}{\partial r} + \Gamma_t'\frac{\partial\psi'}{\partial r}\right),$$

where primed quantities refer to inside the particle,

$$\hat{\rho} = \frac{\rho'}{\rho}, \quad \hat{\tau} = \frac{\tau'}{\tau},$$

where ρ is density, τ is thermal conductivity and ϕ_0 is the incident field. The method of solution assumes the following expansion forms for the various field quantities:

$$\phi_0 = \sum_{n=0}^{\infty}\sum_{s=0}^{\infty}(iKa)^{n+2s}\left(\frac{r}{a}\right)^{n+2s}F_n(s)P_n(\cos\theta),$$

$$\phi = e^{iK(r-a)}\tilde{\phi}, \quad \psi = e^{iL(r-a)}\tilde{\psi},$$

$$(\tilde{\phi}, \tilde{\psi}) = \sum_m (iKa)^m(\tilde{\phi}_m, \tilde{\psi}_m),$$

$$\tilde{\phi}_m = \sum_{n=0}^{\infty}\sum_{j=0} A_{nmj}\frac{r^j}{a^j}\frac{a^{n+1}}{r^{n+1}}P_n(\cos\theta),$$

$$\tilde{\psi}_m = \sum_{n=0}^{\infty}\sum_{j=0}^{n+1} B_{nm}\frac{h_{nj}}{(Lr)^j}P_n(\cos\theta).$$

For the interior fields we assume the expansions

$$\phi' = \sum_m (iKa)^m\phi_m',$$

where

$$\phi_m^{'} = \sum_{n=0}^{\infty}\sum_{j=0} A_{nmj}^{'} \frac{r^j}{a^j}\frac{r^n}{a^n} P_n(\cos\theta).$$

The interior thermal field is written as

$$\psi^{'} = e^{iL^{'}(r-a)}\tilde{\psi}_{+}^{'} - e^{iL^{'}(r-a)}\tilde{\psi}_{-}^{'},$$

where

$$\{\tilde{\psi}_{+}^{'}, \tilde{\psi}_{-}^{'}\} = \sum_m (iKa)^m \{\tilde{\psi}_{+m}^{'}, \tilde{\psi}_{-m}^{'}\}$$

with

$$\tilde{\psi}_{+m}^{'} = \sum_{n=0}^{\infty}\sum_{j=1}^{n+1} B_{nm}^{'} e^{2iL^{'}a}\frac{j_{nj+}}{(L^{'}r)^j} P_n(\cos\theta),$$

and

$$\tilde{\psi}_{-m}^{'} = \sum_{n=0}^{\infty}\sum_{j=1}^{n+1} B_{nm}^{'} \frac{j_{nj-}}{(L^{'}r)^j} P_n(\cos\theta).$$

These forms are substituted into the boundary conditions and equating powers of Ka to zero. Complicated recurrence relations result which are nevertheless solvable. Full details are given in [5].

Results

Here we relate our scattering results for a single particle to the wavenumber for a dispersion of particles. The approach used is the multiple scattering theory due to Lloyd and Berry [7]. We write, for large r, the scattered field ϕ in the form

$$\phi = \frac{e^{iKr}}{r} f(\theta)$$

where

$$f(\theta) = \frac{1}{iK}\sum_{n=0}^{\infty}(2n+1)T_n P_n(\cos\theta).$$

The far field coefficients T_n are found to be given by

$$T_n = \frac{e^{-iKa}}{(2n+1)}\sum_{m=0}^{\infty}(iKa)^{m+1} A_{nmn}.$$

The multiple scattering result for the wave number of the dispersion B is

$$\left(\frac{B}{K}\right)^2 = 1 + \frac{3\phi}{K^2a^3}f(0) + \frac{9\phi^2}{4K^4a^6}\left(f^2(\pi) - f^2(0)\right) - \frac{9\phi^2}{4K^4a^6}\left(\int_0^{\pi} d\theta \frac{1}{\sin(\theta/2)}\left(\frac{d}{d\theta}f^2(\theta)\right)\right)$$

which to second order gives

$$\left(\frac{B}{K}\right)^2 = 1 - \frac{3i\phi}{K^3a^3}(T_0 + 3T_1 + 5T_2) - \frac{27\phi^2}{K^6a^6}\left(T_0T_1 + \frac{10}{3}T_0T_2 + 2T_1^2 + 11T_1T_2 + \frac{230}{21}T_2^2\right).$$

Note that here the symbol ϕ refers to the volume fraction of the dispersed particles.

Numerical experiments of the method have been carried out for sunflower oil in water with a particle diameter of $1\mu m$ [5] which show that it is numerically stable and covers all thermal wavelengths. Furthermore it is superior and more straightforward to implement than other methods. It can also be generalized to non spherical particles.

References

[1] O.G. Harlen, M.J. Holmes, M.J.W. Povey, and B.D. Sleeman, "Acoustic Propagation in Dispersions and the Geometric Theory of Diffraction", SIAM J. Appl. Math, vol. 63, pp. 834-849, 2003.

[2] O.G. Harlen, M.J. Holmes, M.J.W. Povey, Y. Qiu and B.D. Sleeman, "A Low Frequency Potential Scattering Description of Acoustic Propagation in Dispersions", SIAM J. Appl. Math, vol. 61, pp. 1906-1931, 2001.

[3] J.W. Strutt (Baron Rayleigh), "The Theory of Sound,2nd ed",Macmillan, London, 1896.

[4] P.S. Epstein and R.R. Carhart,"The Absorption of Sound in Suspensions and Emulsions. 1. Water Fog in Air, " J. Acoust. Soc. Amer.,vol. 25, pp 553-565, 1953.

[5] V.J. Pinfield, O.G. Harlen, M.J.W. Povey, and B.D. Sleeman, "Acoustic Propagation in Dispersions in the Longwavelength Limit", SIAM J. Appl. Math, vol. 66, pp. 489-509, 2005.

[6] R.E. Kleinman,"The Dirichlet Problem for the Helmholtz equation", Arch. Ration. Mech. Anal, vol 18, pp205-229, 1965.

[7] P. Lloyd and M.V. Berry,"Wave propagation through an assembly of Spheres. IV. Relations between different scattering theories", Proc. Phys. Soc, vol. 91, pp 678-688, 1967.

SLOWING DOWN AND TRANSMISSION OF WAVES IN HIGH CONTRAST PERIODIC MEDIA VIA "NON-CLASSICAL" HOMOGENIZATION

V. P. Smyshlyaev[†,*] **P. Kuchment**[‡]

[†]Department of Mathematical Sciences, University of Bath, Claverton Down, Bath BA2 7AY, UK
[‡]Department of Mathematics, Texas A& M University, College Station, TX 77843-3368, USA
[*]Email: v.p.smyshlyaev@maths.bath.ac.uk

Abstract

We study the slowing down and transmission of wave packets incident at a high-contrast rapidly oscillating periodic medium. Employing tools of "non-classical" (high-contrast) homogenization we formally derive asymptotically explicit two-scale equations displaying the desired effects of simultaneous slowing down and transparency. Those are interpreted in terms of the "coupled-resonances" effects from the standpoint of two-scale homogenization.

Introduction

The aim of this work is to study mathematically the effects of slowing down of wave packets in multi-dimensional high contrast periodic media by means of "non-classical" high contrast homogenization. The topic of slowing down of waves has been of active recent interest in physics and engineering in relation with the so-called "slow-light" effect: although ordinary optical materials do reduce speed of light in accordance with their refractive index, the reduction is very limited. Diamond for example, having one of the highest refractive indices, slows down light only by factor of 2.4. To slow down a light pulse significantly requires hence special conditions. As well as being of great intrinsic interest, slow and frozen light effects open up new possibilities for areas as diverse as optical communications, data storage, synchronizing devices for fast optical elements and much smaller electronics, etc.

Slow light has presently been generated using a variety of techniques, from introducing large material dispersion to using structurally dispersive "coupled resonances", e.g. [1]. Mathematical aspects of slowing down wave packets in truncated one-dimensional periodic structures were studied in [2],[3]. The goal has been to device media for which the group velocity in the periodic medium is small and the transmission coefficient for the truncated periodicity is not too small, i.e. to find media where a slowing down of wave packets co-exists with a transparency.

The present work studies the problem of existence and initiation of slow wave packets in a prototype *multi-dimensional* scalar ("acoustic") periodic media. This is achieved by employing methods of recently emerged "non-classical" homogenization theory for *high-contrast* periodic media, e.g. [4], [5]. Namely, upon introducing the small parameters δ of contrast in the properties of the medium and ε of the periodicity size, the asymptotic behaviour of the packets depends on the relation between δ and ε. One can then see that, in the appropriate setting, there is only one critical scaling $\delta(\varepsilon) \sim \varepsilon^2$, the so-called "double-porosity" scaling, when the phenomena at the micro and macro scales are coupled in a non-trivial way.

We show that the implementation of the above methodology of high-contrast homogenization for the problem of incidence of a wave packet at a periodic medium leads to asymptotically explicit predictions demonstrating both the effects of slowing down and transparency. On the other hand, the resulting multi-scale asymptotics for the slow wave packets appears to be qualitatively consistent with the coupled-resonators effect: the key two-scale ansatz displays microscopic oscillations only in the small inclusions (the resonators), coupled via a slower varying field in the surrounding matrix. The present work contains only a formal asymptotics analysis. The problem of rigorous justification and error bounds requires in particular a detailed analysis of the boundary layer, cf. [5] where such a rigorous analysis has been executed for a somewhat similar problem.

Problem statement

We consider a wave process described by the equation

$$v_{tt} - \operatorname{div}(a^{\varepsilon}(x)\nabla v) = 0,$$

with $x = (x_1, x') \in \mathbb{R}^n$, $n \geq 2$, and variable "stiffness" $a^{\varepsilon}(x)$, depending on small parameter ε describing both the rapid oscillations and the high contrast of the medium as follows (Figure 1). For $x_1 < 0$ the medium is uniform, i.e. $a^{\varepsilon}(x) = a_0$ is constant; for $x_1 > 0$ the medium is periodic with periodicity cell of size ε: $a^{\varepsilon}(x) = \tilde{a}^{\varepsilon}(x/\varepsilon)$, where $\tilde{a}^{\varepsilon}(y)$ is 1-periodic in y with respect to all of its arguments, i.e. with reference periodicity cell $Q = [0,1)^n$.

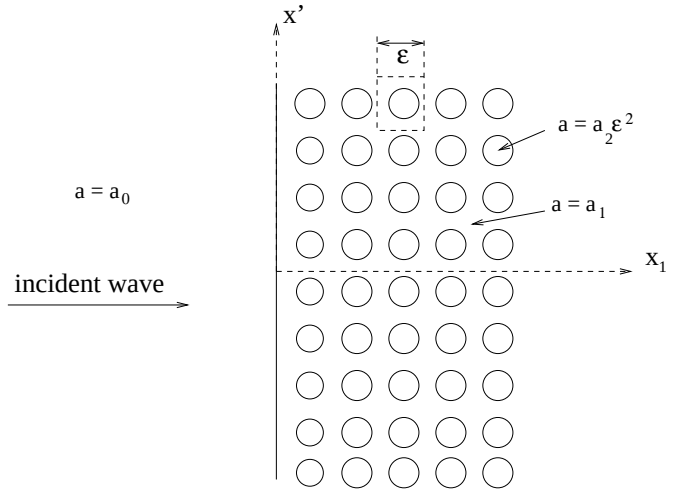

Figure 1: Geometric configuration: incidence at a rapidly oscillating high contrast medium

The periodically extended inclusions Q_2 are disconnected and the matrix $Q_1 = Q \backslash Q_2$ is connected, $\tilde{a}^\varepsilon(y) = a_1$ in Q_1 and $\tilde{a}^\varepsilon(y) = a_2\varepsilon^2$ in Q_2.

Consider a wave packet incident from the left half-space, i.e.

$$v^\varepsilon(x,t) = \int_{|\omega-\omega_0|<d} u^\varepsilon(x,\omega)\alpha(\omega-\omega_0)e^{-i\omega t}d\omega,$$

with angular frequencies from an interval of small size $2d$ around ω_0 and with

$$u^\varepsilon(x,\omega) \;=\; \begin{cases} u_{inc}(x_1,\omega) + u_r^\varepsilon(x,\omega), & x_1 < 0 \\ u_t^\varepsilon(x,\omega), & x_1 > 0, \end{cases}$$

where $u_{inc}(x_1,\omega) \;=\; \exp(ik_0(\omega)x_1)$ are the incident plane waves, $k_0(\omega) = \omega a_0^{-1/2}$, and u_r^ε and u_t^ε form the "scattered" (respectively, reflected and transmitted) component, ε-periodic in x'. It can then be shown that, for ω within the bands of the Bloch spectrum of the periodic medium and small enough ε,

$$u_r \sim R^\varepsilon(\omega)\exp(-ik_0(\omega)x_1)$$

for $x_1 \to -\infty$ where R^ε is the reflection coefficient, and for $x_1 \to +\infty$ u_t behaves as a single Bloch wave propagating in the direction x_1. This all determines the solution of the scattering problem uniquely up to possible exponentially decaying surface waves along the "interface" $x_1 = 0$ which do not matter for describing the transmitted field for $x_1 > 0$ when $\varepsilon \to 0$.

Anticipating that, for ω close to ω_0 and small ε, the transmitted field is macroscopically described by a "homogenized" field

$$u^{hom}(x_1,\omega) \;=\; T(\omega)\left(\frac{k_0(\omega)a_0}{k(\omega)a^h}\right)^{1/2}\exp(ik(\omega)x_1) \tag{1}$$

with dispersion relation $k(\omega)$, the group velocity for the homogenized transmitted wave packet is given by

$$V_g(\omega_0) \;=\; (dk/d\omega)^{-1}(\omega_0)$$

and the (normalised) transmission coefficient by $T(\omega_0)$.

High-contrast homogenization

It appears that, away from the "interface" $x_1 = 0$ containing a localized boundary layer, the limit problem for the transmitted field $u_t^\varepsilon(x,\omega)$ is *two-scale,* i.e.

$$u_t^\varepsilon(x,\omega) \;\sim\; u^{(0)}(x,x/\varepsilon)+\varepsilon u^{(1)}(x,x/\varepsilon)+\varepsilon^2 u^{(2)}(x,x/\varepsilon)+...$$

In contrast to the classical homogenization, due to the high contrast the main-order term $u^{(0)}(x,y)$ retains the dependence on the "fast" periodic variable $y = x/\varepsilon$, although only in the "soft" phase Q_2: for $x_1 > 0$,

$$u^{(0)}(x,y) \;=\; \begin{cases} u^{hom}(x_1) & \text{if } y \in Q_1 \\ u^{hom}(x_1) \;+\; v(x_1,y) & \text{if } y \in Q_2. \end{cases}$$

Application of an appropriately modified method of two-scale asymptotic expansions then results in a *coupled* system of equations for u^{hom} and v (cf. [5] Appendix A). In particular, the macroscopic part u^{hom} solves following homogenized equation with highly nonlinear dependence on the spectral parameter $\lambda = \omega^2$:

$$-\nabla\cdot\left(A^{hom}\nabla u^{hom}\right) \;=\; \beta(\omega^2)u^{hom}. \tag{2}$$

Here A^{hom} is the standard "porous" homogenized matrix with void inclusions (i.e. infinite contrast), and $\beta(\lambda)$ is an explicit function introduced by Zhikov [4]:

$$\beta(\lambda) = \lambda + \lambda^2\sum_{j=1}^{\infty}\frac{\langle\varphi_j\rangle^2}{\lambda_j-\lambda}. \tag{3}$$

Here λ_j and φ_j are the eigenvalues and the orthonormal eigenfunctions of the Laplace operator on Q_2 with Dirichlet boundary conditions, $\langle\varphi_j\rangle := \int_{Q_2}\varphi_j(y)dy$. The values of $\beta(\lambda)$ are negative in the gaps of the limit operator and positive on its bands. For $n = 3$ and Q_2 being balls $\beta(\lambda)$ is computable in elementary functions [6].

Assuming for simplicity that A^{hom} is isotropic i.e. $A^{hom} = a^h I$ (I is the unit matrix), the homogenized dispersion relation and group velocity are found from (2) to be

$$k(\omega) \;=\; \Big(\beta(\omega^2)/a^h\Big)^{1/2}, \qquad (4)$$

$$V_g(\omega_0) \;=\; \frac{\big(a^h\beta(\omega_0^2)\big)^{1/2}}{\omega_0\beta'(\omega_0)}. \qquad (5)$$

In particular, near the right ends of the "limit" bands i.e. for $\omega_0 \to (\lambda_j)^{1/2} - 0$ with $\langle\varphi_j\rangle \neq 0$, we have

$$V_g(\omega_0) \;\sim\; (a^h)^{1/2}\lambda_j^{-3/2}\langle\varphi_j\rangle^{-1}(\lambda_j - \omega_0^2)^{3/2} \;\to\; 0.$$

On the other hand, the limit reflection and transmission coefficients are found from the standard one-dimensional calculation for the original uniform medium for $x_1 < 0$ and the homogenized medium for $x_1 > 0$. Namely, we consider

$$u(x_1,\omega_0) = u_{inc}(x_1,\omega_0) + R(\omega_0)\exp(-ik_0(\omega_0)x_1)$$

for $x_1 < 0$, and $u(x_1,\omega_0) = u^{hom}(x_1,\omega_0)$ for $x_1 > 0$ described by (1), (4), with the standard continuity conditions at $x_1 = 0$ for u and for the "fluxes":

$$u(x{-}0) = u^{hom}(x{+}0),\;\; a_0u'(x{-}0) = a^h(u^{hom})'(x{+}0).$$

(The latter continuity conditions for the "homogenized fluxes" is consistent with the anticipated boundary layer analysis, cf. [5].) The result is:

$$R(\omega_0) \;=\; \frac{(a_0)^{1/2}\omega_0 \;-\; \big(a^h\beta(\omega_0^2)\big)^{1/2}}{(a_0)^{1/2}\omega_0 \;+\; \big(a^h\beta(\omega_0^2)\big)^{1/2}}, \qquad (6)$$

with $T(\omega_0) = (1 + R(\omega_0))(k(\omega_0)a^h/(k_0(\omega_0)a_0)^{1/2}$ for the transmission coefficient. In particular, $R = 0$ (zero reflection) corresponds to $\beta(\omega_0^2) = (a_0/a_h)\omega_0^2$.

The main result

We show that, for appropriately chosen ω_0 and sufficiently small ε, one can achieve simultaneously as small group velocity V_g and as small reflection coefficient as desired. More precisely:

For any $\Delta_1 > 0$ and $\Delta_2 > 0$ there exists ω_0 such that $|V_g(\omega_0)| < \Delta_1$ and $|R(\omega_0)| < \Delta_2$.

The result follows from an explicit analysis of (5) and (6), and properties of the function $\beta(\lambda)$.

Discussion

The reported results suggest the possibility of initiating in high contrast periodic media wave packets moving with slow speeds. Analysis shows that for achieving simultaneously a slow group velocity and a significant transmission one should in fact go to "higher frequency" bands of the Bloch spectrum. Microscopically, this seems to display coupled resonances and "metastability"-type effects: the described multi-scale asymptotic structure indicates that the oscillations are restricted to the soft inclusions, persisting there for sufficiently large times but eventually passing over to the neighbouring oscillators, etc, which represents macroscopically a slowly moving wave packet.

The reported work contains only a formal asymptotics analysis. The problem of rigorous justification and error bounds in somewhat similar problems of homogenization for high contrast media was addressed e.g. in [4], [5].

References

[1] J. Scheuer and A. Yariv, "Sagnac effect in coupled-resonator slow-light structures", Phys. Rev. Lett., vol. 96, No. 053901, 2006.

[2] S. Molchanov and B. Vainberg, "Slowing Down and Reflection of Waves in Truncated Periodic Media", J. Funct. Anal., vol. 231, pp. 287-311, 2006.

[3] A. Figotin and I. Vitebskiy, "Slow light in photonic crystals". Waves Random Complex Media 16, 293-382, 2006.

[4] V.V. Zhikov, *On an extension of the method of two-scale convergence and its applications*, (Russian) Mat. Sbornik **191** (2000), 31–72; English translation in Sbornik Math. **191** (2000), 973–1014; V.V. Zhikov, *Gaps in the spectrum of some elliptic operators in divergent form with periodic coefficients*. (Russian) Algebra i Analiz **16** (2004), 34–58; English translation in St. Petersburg Math. J. **16** (2005), 773–790.

[5] I.V. Kamotski and V.P. Smyshlyaev, *Localised eigenstates due to defects in high contrast periodic media via homogenisation*. BICS preprint 3/06, http://www.bath.ac.uk/math-sci/bics/preprints/BICS06_3.pdf (2006)

[6] I.V. Kamotski, personal communication (2007).

AN EMBEDDING METHOD FOR SCATTERING BY DEFECTIVE ARRAYS

Ian Thompson[†,*], **Chris M. Linton**[†]

[†]Dept. of Mathematical Sciences, Loughborough University, Loughborough, Leics. LE11 3TU, UK
[*]Email: i.thompson@lboro.ac.uk

1 Introduction

Wave scattering by arrays of bodies is an important problem in several physical contexts, including the theory of antennae and the design of offshore structures. If both the array and the incident field are periodic, the problem is relatively straightforward [1], [2]. Here we are concerned with scattering by a periodic array which has one or more elements removed; we refer to such an array as being *defective*. We will demonstrate a method whereby for a given wavenumber, scatterer size and separation, the field generated when a plane wave impinges on a defective array can be constructed from the solution to certain canonical problems. The angle of incidence and the configuration of the defect (i.e. which scatterers are removed from the array) are *embedded*; the canonical problems need not be solved again if these parameters are changed.

2 General theory

Consider the scattering of a plane wave by a defective linear array of identical circular cylinders. All lengths are nondimensionalised with reference to the distance between the axes of adjacent cylinders. Thus, we position the array so that its elements are centred at the points $(j,0)$ in the (x,y) plane, $j \in \mathbb{Z} \setminus \mathcal{D}$. Here, $\mathcal{D}$ denotes the *defect set*, the members of which correspond to the scatterers that are removed from the array. For simplicity, we consider sound soft scatterers in the long wave limit $ka \ll 1$, where k is the wavenumber, and a is the cylinder radius, although the method is not restricted to this case. The total field is given by

$$\phi^{\mathrm{t}} = \phi^{\mathrm{i}} + \phi^{\mathrm{s}} \tag{1}$$

in which ϕ^{s} does not include any contributions that are incoming toward the array, and

$$\phi^{\mathrm{i}} = \mathrm{e}^{\mathrm{i}k(x\cos\psi_0 + y\sin\psi_0)}, \tag{2}$$

where ψ_0 is the angle of incidence; see figure 1. All of the terms in equation (1) satisfy the Helmholtz equation $(\nabla^2 + k^2)\phi = 0$, and the Dirichlet boundary condition $\phi^{\mathrm{t}} = 0$ must be satisfied on the surface of the scatterers. Now the total field is composed of the incident wave, plus a contribution radiating from each of the scatterers. This latter component can be written in the form

$$\phi^{\mathrm{s}} = \sum_{j\in\mathbb{Z}\setminus\mathcal{D}} A_j \,\mathrm{H}_0^{(1)}(kr_j) + O(ka), \tag{3}$$

where $\mathrm{H}_0^{(1)}(\cdot)$ represents the Hankel function of the first kind with order 0, and r_j is the distance is the distance from the centre of scatterer j, i.e. $r_j = \sqrt{(x-j)^2 + y^2}$. The coefficient A_j is an as yet unknown amplitude. Close to the surface of scatterer p, any incoming field can be expressed in the form

$$\phi_p^{\mathrm{i}} = D_p \,\mathrm{J}_0(kr_p) + O(kr_p), \tag{4}$$

for some constant D_p, where $\mathrm{J}_0(\cdot)$ is the Bessel function of order zero. Therefore, in order to satisfy the Dirichlet boundary condition to leading order, we must have

$$A_p = -Z_0 D_p, \tag{5}$$

where

$$Z_0 = \frac{\mathrm{J}_0(ka)}{\mathrm{H}_0^{(1)}(ka)} = \left[1 + \frac{2\mathrm{i}}{\pi}\ln(ka)\right]^{-1} + O(ka). \tag{6}$$

The field incoming toward scatterer p consists of the incident wave, plus the radiation from all of the other scatterers. Evaluating this t the point $r_p = 0$ yields an expression for D_p, in view of (4). Equation (5) then becomes

$$A_p + Z_0 \sum_{\substack{j\in\mathbb{Z}\setminus\mathcal{D}\\ j\neq p}} A_j \,\mathrm{H}_0^{(1)}(k|j-p|) = -Z_0 \mathrm{e}^{\mathrm{i}kp\cos\psi_0}, \qquad p \in \mathbb{Z}\setminus\mathcal{D}. \tag{7}$$

The convergence of this infinite linear system is extremely slow, because $A_j \not\to 0$ as $|p| \to \infty$, and therefore it relies on the increasing magnitude of the argument of the Hankel function. Rather than attempting to solve it directly, we employ the infinite array subtraction method [3]. The essential idea is that, as $|p| \to \infty$ (i.e. far from the defect), $A_j \to B_j$, where B_j is the amplitude coefficient that appears in place of A_j if $\mathcal{D} = \emptyset$, i.e.

$$B_p + Z_0 \sum_{\substack{j\in\mathbb{Z}\\ j\neq p}} B_j \,\mathrm{H}_0^{(1)}(k|j-p|) = -Z_0 \mathrm{e}^{\mathrm{i}kp\cos\psi_0}, \qquad p \in \mathbb{Z}. \tag{8}$$

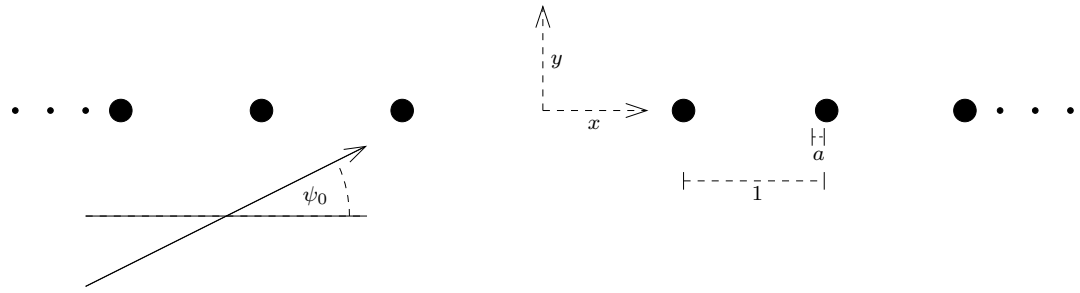

Figure 1: Schematic diagram of a defective array with $\mathcal{D} = \{0\}$.

To obtain B_j, note that in this case the entire problem is quasi-periodic, and so $B_j = \mathrm{e}^{\mathrm{i}kj\cos\psi_0}B_0$. If this is inserted into equation (8) a simple calculation shows that

$$B_0 = -Z_0/[1 + Z_0\sigma_0(k\cos\psi_0)], \tag{9}$$

where

$$\sigma_0(t) = 2\sum_{j\in\mathbb{N}} \cos(jt)\,\mathrm{H}_0^{(1)}(kj). \tag{10}$$

This is the Schlömilch series of order zero; it can be evaluated using the Twersky formula [1]

$$\sigma_0(t) = -1 - \frac{2\mathrm{i}}{\pi}\left(C + \ln\frac{k}{4\pi}\right) - \frac{2\mathrm{i}}{\gamma(t)} - \sum_{j\in\mathbb{Z}\setminus\{0\}} \frac{2\mathrm{i}}{\gamma(t+2j\pi)} - \frac{\mathrm{i}}{|j|\pi}. \tag{11}$$

Here, C is Euler's constant, and $\gamma(t) = (t^2 - k^2)^{1/2}$, with branches chosen so that $\gamma(0) = -\mathrm{i}k$, and $\gamma(t) = \sqrt{t^2 - k^2}$ for real t with $|t| > k$.

To apply the infinite array subtraction, write

$$A_j = \mathrm{e}^{\mathrm{i}kjs\cos\psi_0}B_0 + C_j, \tag{12}$$

substitute this into (7) and take known terms to the right hand side. The result is a linear system for C_j, which is expressed in a compact form by defining coefficients C_j for the absent scatterers; thus

$$C_j = -\mathrm{e}^{\mathrm{i}jk\cos\psi_0}B_0, \quad j \in \mathcal{D}, \tag{13}$$

and then

$$C_p + Z_0\sum_{\substack{j\in\mathbb{Z}\\ j\neq p}} C_j\,\mathrm{H}_0^{(1)}(k|j-p|) = 0, \quad p \in \mathbb{Z}\setminus\mathcal{D}. \tag{14}$$

The meaning of equations (13) and (14) is clarified by writing the total field in the form

$$\phi^{\mathrm{t}} = \phi^{\mathrm{i}} + \sum_{j\in\mathbb{Z}} \left[\mathrm{e}^{\mathrm{i}kj\cos\psi_0}B_0 + C_j\right]\mathrm{H}_0^{(1)}(kr_j) + O(ka). \tag{15}$$

Thus, equation (13) ensures that there is no radiation emanating from the absent scatterers. Equation (14) ensures that the field

$$\phi^{\mathrm{c}} = \sum_{j\in\mathbb{Z}} C_j\,\mathrm{H}_0^{(1)}(kr_j) \tag{16}$$

satisfies the boundary condition on all of the scatterers centred at $(j, 0)$, $j \notin \mathcal{D}$. This is necessary because the field $\phi^{\mathrm{t}} - \phi^{\mathrm{c}}$ clearly satisfies these independently. In fact, the effect of infinite array subtraction is to replace the incident wave with a distribution of line sources positioned at $(j, 0)$, $j \in \mathcal{D}$, with amplitudes given by (13). The quantity ϕ^{c} is the total field that occurs when the defective array is excited by the source distribution.

3 Single absent scatterer

If the defect set has only one member, then we shall assume without loss that $\mathcal{D} = \{0\}$. The dependence of C_j upon ψ_0 is entirely due to the amplitude of the source located at the origin which is given by (13). Therefore, we introduce a new set of coefficients which we shall denote C_j^1, and require that these satisfy the linear system (14), subject to $\mathcal{D} = \{0\}$, and

$$C_0^1 = 1. \tag{17}$$

It then follows immediately that

$$C_j = -\mathrm{e}^{\mathrm{i}jk\cos\psi_0}B_0C_j^1 \tag{18}$$

for all j. Thus, ψ_0 has now been embedded; solving (14) once is sufficient to yield the solution at all angles of incidence. Note that $C_{-j}^1 = C_j^1$ by symmetry. Also, if the source is translated from the origin to $(qs, 0)$, $q \in \mathbb{Z}$, we simply replace C_j^1 with C_{j-q}^1. This is crucial when considering defect sets with multiple members.

4 Multiple defects

If more than one scatterer is absent from the array we can still construct C_j using the coefficients C_j^1. To

achieve this, translate the source to each point $(qs, 0)$ $q \in \mathcal{D}$, and allocate it an arbitrary amplitude coefficient a_q. We then take the total field represented by (16), with C_j replaced by $a_q C^1_{j-q}$ for each q and superimpose these upon eachother. The resulting field is still given by (16), but now with

$$C_j = \sum_{q\in\mathcal{D}} a_q C^1_{j-q}, \quad j \in \mathbb{Z}. \tag{19}$$

This satisfies the boundary condition at $r_p = a$, for all $p \notin \mathcal{D}$. Indeed, it is evident that (19) is a solution to (14). To see this, recall that the set of coefficients C^1_{p-q} is a solution to (14) subject to $\mathcal{D} = \{q\}$. If (19) is substituted into (14), then, since $p \in \mathbb{Z} \setminus \mathcal{D}$, $p = q$ cannot occur.

It remains to enforce the correct source amplitudes at the points $(q, 0)$, $q \in \mathcal{D}$ by selecting appropriate values for the coefficients a_q. Thus, from equations (13) and (19), it follows that

$$-\mathrm{e}^{\mathrm{i}jk\cos\psi_0} B_0 = \sum_{q\in\mathcal{D}} a_q C^1_{j-q}, \quad j \in \mathcal{D}. \tag{20}$$

Since this is a finite linear system, as opposed to the infinite system (14) the configuration of the defect has now been embedded, along with ψ_0.

5 The canonical source problem

It remains to solve the canonical problem of an array with a single scatterer replaced by a source with unit amplitude. To achieve this, we represent the coefficients C^1_p as as integrals using a method closely related to that in [4]. The key idea is to choose the dependence of the integrand upon the parameter p in such a way that the sum in (14) can be evaluated analytically. A natural choice of ansatz is therefore

$$C^1_p = \frac{1}{2\pi\mathrm{i}} \int_{-\pi}^{\pi} f(t)\mathrm{e}^{\mathrm{i}pt}\, \mathrm{d}t, \tag{21}$$

where $f(t)$ does not depend upon p. When this is substituted into (14) (with $\mathcal{D} = \{0\}$), we find that

$$\int_{-\pi}^{\pi} f(t)[1 + Z_0\sigma_0(t)]\mathrm{e}^{\mathrm{i}pt}\, \mathrm{d}t = 0, \quad p \in \mathbb{Z} \setminus \{0\}. \tag{22}$$

This is clearly satisfied if

$$f(t) = F_0[1 + Z_0\sigma_0(t)]^{-1}, \tag{23}$$

where F_0 is a constant chosen to satisfy (17).

Now, for any k, there exists $v \in \mathbb{Z}$ such that $\pm(k + 2v\pi) \in [-\pi, \pi]$. These are branch points of the function $f(t)$. The path of integration in (21) must pass above $t = -(k + 2v\pi)$, and below $t = k + 2v\pi$ in order to yield outgoing waves at infinity. If we take $p > 0$ (for $p < 0$ we can use the symmetry relation $C^1_{-p} = C^1_p$) and close the contour in the upper half plane, the 2π periodicity of $f(t)$ means that the only contribution comes from the branch point. This can be asymptotically for large p. Indeed, a straightforward calculation shows that, as $p \to \infty$,

$$C^1_p \sim \mathrm{e}^{3\mathrm{i}\pi/4} \frac{F_0}{2Z_0} \sqrt{k/(2\pi)}\mathrm{e}^{\mathrm{i}pk} p^{-3/2}. \tag{24}$$

6 Concluding remarks

A method for solving the problem of scattering by a periodic array with one or more missing elements has been demonstrated in the limit $ka \ll 1$. For any angle of incidence, and any finite set of defects, the scattered field is constructed from the solution to a single canonical problem. An exact integral solution to this canonical problem is then derived. Evaluating this integral by quadrature can yield much more accurate results than inverting (14) by truncation. Furthermore, analysis of the integral can yield important results such as the leading order behaviour of the coefficients C_p for large p.

For larger scatterers an extra degree of complexity is introduced because the number of canonical problems to be solved turns out to be equal to the number of modes used in modelling the field radiating from each array element. Nevertheless, the same method can be applied, and in this case there are significant savings in computation time, as well as increased accuracy. Again, important results such as the amplitude of any surface waves that may be excited can be accurately obtained, and these will be shown at the meeting. The method also works for the case of an array with a finite number of scatterers replaced by objects of a different shape, under certain geometrical restrictions.

References

[1] V. Twersky. On scattering of waves by the infinite grating of circular cylinders. *IRE Trans. on Antennas and Propagation*, 10:737–765, 1962.

[2] C. M. Linton and I. Thompson. Resonant effects in scattering by periodic arrays. *Wave Motion*, 44:165–175, 2007.

[3] C. M. Linton, R. Porter, and I. Thompson. Scattering by a semi-infinite periodic array and the excitation of surface waves. *SIAM J. Appl. Math.*, accepted February 2007.

[4] I. Thompson and C. M. Linton. On the excitation of a closely spaced array by a line source. *IMA J. Appl. Math.*, accepted March 2007.

Minisymposium on Photonic Crystals and Metamaterials

Organisers: Sebastian Guenneau (University of Liverpool) and Robert Scheichl (University of Bath)

TIME-HARMONIC WAVE TRANSMISSION PROBLEMS WITH SIGN-SHIFTING MATERIAL COEFFICIENTS

A. S. Bonnet-Ben Dhia[†,*], **P. Ciarlet Jr.** [†] **and C. M. Zwolf**[†]
[†]POEMS, UMR 2706 CNRS-INRIA-ENSTA, Paris, France
[*]Email: anne-sophie.bonnet-bendhia@ensta.fr

Abstract

Some electromagnetic materials present at a particular frequency an effective dielectric permittivity and/or magnetic permeability which are negative. We consider here a scalar model problem for the simulation of wave transmission between a classical material and a "negative" one. Introducing additional unknowns, we proposed in [4] some new variational formulations of this problem, which are of Fredholm type if the contrast of permittivity is large enough, and therefore suitable for a finite elements discretization. We prove here that, surprisingly, the natural variational formulation of the problem, although not "coercive plus compact", is also suitable for a finite elements discretization. Moreover, this numerical approach is less costly than the previous ones.

1 Introduction

In electromagnetics, a number of materials can be modelled at a given frequency by taking negative values for their dielectric permittivity and/or magnetic permeability. A superconductor can be represented as a material with a negative dielectric permittivity (the London model) while homogenization theory applied to left-handed meta-materials leads to negative effective dielectic permittivity and magnetic permeability. From mathematical and numerical points of view, this leads to unsual questions. In particular, the simulation of wave transmission between a classical material and a "negative" one requires extra care. The difficulty is obvious when considering the natural variational formulation of the scalar model problem:

$$\text{div}\left(\frac{1}{\varepsilon}\nabla u\right) + \omega^2 \mu u = 0 \qquad (1)$$

when ε presents a sign shift through some interface Σ. Using integral representations on Σ, it has been proved that this transmission problem is ill-posed if the coefficient ε takes opposite constant values on each side of Σ (that is a *constrast* equal to -1) and well-posed otherwise, under the assumption that Σ is smooth [1]. More generally (non smooth interface and/or coefficients), the problem is well-posed for a large or a small absolute value of the contrast, but not for a contrast close to -1 [2].

Following an idea of [3], we proposed in [4] some new variational formulations of this transmission problem, which are proved to be of Fredholm type (for suitable contrasts) and well adapted for a finite elements discretization. The extension to the vector case (Maxwell's equations) is presented in [5].

The drawback of these formulations, especially for 3D vector problems, is their cost, since an additional vector unknown is introduced. This led us to consider more carefully the *natural* variational formulation of the problem, which gave surprisingly good numerical results.

The object of this paper is to explain this phenomenon in the scalar case : we prove "directly" that problem (1) is well-posed and that a standard finite element discretization converges in a classical manner.

2 The continuous problem

2.1 Setting of the problem

Let Ω be an open, bounded domain of $\mathbb{R}^3$ with Lipschitz boundary, which is split in two sub-domains Ω_- and Ω_+ with Lipschitz boundaries. Let $\Sigma = \partial\Omega_- \cap \partial\Omega_+$ denote the interface and $\Gamma_\pm = \partial\Omega_\pm \setminus \Sigma$. We consider two functions ε and μ defined in Ω such that ε, μ and $1/\varepsilon$ belong to $L^\infty(\Omega)$. We suppose moreover that ε is strictly positive on Ω_+ and strictly negative on Ω_-.

Let $f \in L^2(\Omega)$. We consider the following problem :
Find $u \in H^1_0(\Omega)$ such that:

$$\int_\Omega \frac{1}{\varepsilon}\nabla u.\nabla v - \omega^2 \mu u\, v = f\, v, \quad \forall v \in H^1_0(\Omega). \qquad (2)$$

2.2 The abstract theorem

Suppose V is a Hilbert space, a and c are continuous bilinear forms on V and l is a continuous linear form on V, and consider the following variational problem :

$$\begin{array}{l}\text{Find } u \in V \text{ such that} \\ a(u,v) + c(u,v) = l(v) \quad \forall v \in V.\end{array} \qquad (3)$$

Then we have the
Theorem: *Suppose :*

1. *There exists an isomorphism T of $\mathcal{L}(V)$ and a positive constant α such that*

$$|a(u,Tu)| \geq \alpha \|u\|_V^2 \quad \forall u \in V.$$

2. The operator K associated to the bilinear form c by Riesz representation is compact on V.

Then problem (3) is well-posed if and only if uniqueness holds (i.e. $l = 0 \Rightarrow u = 0$).

Proof: Problem (3) is clearly equivalent to the following:

$$\begin{array}{l}\text{Find } u \in V \text{ such that}\\ a(u, Tv) + c(u, Tv) = l(Tv) \quad \forall v \in V.\end{array} \tag{4}$$

since T is bijective, and this new problem is of Fredholm type.

2.3 Well-posedness

To apply the previous theorem to problem (2), we define the operator T as follows:

$$\forall u \in H_0^1(\Omega)\ \ Tu = \left\{ \begin{array}{lll} u & in & \Omega_+ \\ -u + 2Ru & in & \Omega_- \end{array} \right. \tag{5}$$

where Ru is defined as the unique solution $\psi \in H^1(\Omega_-)$ of:

$$\left\{ \begin{array}{lll} \text{div}\left(\frac{1}{\varepsilon}\nabla\psi\right) = 0 & in & \Omega_- \\ \psi = u & on & \Sigma \\ \psi = 0 & on & \Gamma_- \end{array} \right. \tag{6}$$

Notice that Tu belongs to $H_0^1(\Omega)$ since it is continuous across Σ and that there exists a constant C depending only on the geometry such that:

$$\int_{\Omega_-} \frac{1}{|\varepsilon|}|\nabla(Ru)|^2 \leq C\kappa(\varepsilon) \int_{\Omega_+} \frac{1}{\varepsilon}|\nabla u|^2 \tag{7}$$

where the generalized contrast is defined (in absolute value) by:

$$\kappa(\varepsilon) = \frac{\sup_{x\in\Omega_+} \varepsilon}{\inf_{x\in\Omega_-} |\varepsilon|}.$$

Moreover, T is clearly continuous and bijective, with $T = T^{-1}$. Finally, setting

$$a(u, v) = \int_\Omega \frac{1}{\varepsilon}\nabla u.\nabla v$$

elementary calculations give, $\forall u \in H_0^1(\Omega)$:

$$a(u, Tu) = \int_\Omega \frac{1}{|\varepsilon|}|\nabla u|^2 - 2\int_{\Omega_-} \frac{1}{|\varepsilon|}|\nabla(Ru)|^2 \tag{8}$$

so that, by (7), $a(u, Tu)$ is coercive *under the condition* $\kappa(\varepsilon) < 1/C$. The abstract theorem then applies in a straightforward manner, using the compactness of the embedding of $H_0^1(\Omega)$ into $L^2(\Omega)$.

3 The discrete problem

3.1 The abstract theorem

Consider again the same hypotheses as in subsection 2.2. Now V_h denotes a family of finite-dimensional subspaces of V such that :

$$\lim_{h\to 0} \inf_{v_h\in V_h} \|v - v_h\|_V = 0\ \forall v \in V, \tag{9}$$

and we consider the following discrete problem:

$$\begin{array}{l}\text{Find } u_h \in V_h \text{ such that}\\ a(u_h, v_h) + c(u_h, v_h) = l(v_h) \quad \forall v_h \in V_h.\end{array} \tag{10}$$

Moreover we suppose that there exists an operator T_h of $\mathcal{L}(V_h)$ and two positive constants β and γ independent of h such that $\forall h$:

1. $\|T_h\| \leq \gamma$.
2. $|a(u_h, T_h u_h)| \geq \beta\|u_h\|_V^2 \quad \forall u_h \in V_h$.

Then we have the

Theorem: *Problem (10) is well-posed for h small enough. Moreover, the following error estimate holds:*

$$\|u - u_h\|_V \leq \inf_{v_h\in V_h} \|u - v_h\|_V. \tag{11}$$

3.2 The finite element error

We suppose now that ε is regular on Ω_- and that V_h are classical finite element spaces associated to a quasi-uniform family of triangulations of Ω (preserving the interface Σ). We set $V_h(\Omega_\pm) = \{u|_{\Omega_\pm} | u \in V_h\}$ and $V_h^0(\Omega_\pm) = V_h(\Omega_\pm) \cap H_0^1(\Omega_\pm)$.

We define the operator T_h as follows:

$$\forall u_h \in V_h\ \ T_h u_h = \left\{ \begin{array}{lll} u_h & in & \Omega_+ \\ -u_h + 2R_h u_h & in & \Omega_- \end{array} \right. \tag{12}$$

where $R_h u_h$ is defined as the unique solution $\psi_h \in V_h(\Omega_-)$ of:

$$\left\{ \begin{array}{l} \psi_h = u_h \text{ on } \Sigma, \\ \displaystyle\int_{\Omega_-} \frac{1}{\varepsilon}\nabla\psi_h.\nabla\phi_h = 0 \quad \forall \phi_h \in V_h^0(\Omega_-). \end{array} \right. \tag{13}$$

To prove that T_h is bounded uniformly with respect to h, we just have to consider operator R_h. Let $u_h \in V_h$. Then:

$$\|R_h u_h\|_{H_0^1(\Omega_-)} \leq \|(R - R_h)u_h\|_{H_0^1(\Omega_-)} + \|Ru_h\|_{H_0^1(\Omega_-)}.$$

Moreover, since $u_h \in H_0^1(\Sigma)$, $Ru_h \in H^{3/2}(\Omega_-)$ and the classical error estimate reads:

$$\|(R - R_h)u_h\|_{H_0^1(\Omega_-)} \leq K' h^{1/2}\|u_h\|_{H_0^1(\Sigma)}.$$

Then, since the family of triangulations is quasi-uniform, the usual inverse inequality holds:

$$\|u_h\|_{H_0^1(\Sigma)} \leq K'' h^{-1/2} \|u_h\|_{H_{00}^{1/2}(\Sigma)}.$$

Putting all together and using the continuity of the trace application, we get finally for some positive constant K independent of h:

$$\|T_h u_h\|_{H_0^1(\Omega)} \leq K \|u_h\|_{H_0^1(\Omega)}.$$

This is the key result. Then one can easily establish inequalities similar to (7) and (8) in V_h, and prove well-posedness and convergence for the discrete problem.

4 Some numerical results

For the numerical validation, we consider a rectangular domain Ω splitted by Σ in two squares Ω_+ and Ω_-. The coefficient ε takes constant values $\varepsilon_\pm \in \mathbb{R}^\pm$ in $\Omega_\pm$. In order to verify *a posteriori* the error estimates (11), we use regular triangulations of Ω and we solve (2) with an *ad hoc* source term f so that the solution u is known exactly. The evolution of the relative error

$$e = \frac{\|u - u_h\|_{H^1(\Omega)}}{\|u\|_{H^1(\Omega)}}$$

as a function of the mesh diameter h is plotted on figure 1, in the particular case of a contrast $\kappa = \varepsilon_+/|\varepsilon_-| = 2.75$: the black line corresponds to a linear interpolation and the blue line to a quadratic one. The light-blue line (resp. the green line), which slope is equal to one (resp. two), is introduced just as a reference. We observe a convergence in agreement with the theoretical estimates.

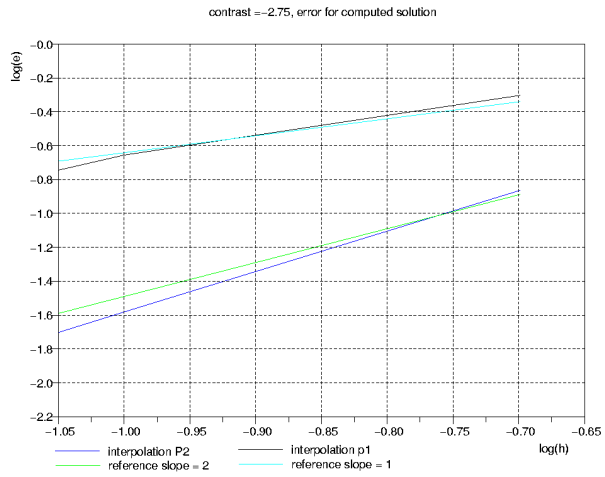

fig. 1

References

[1] M. Costabel, E. Stephan, “A direct boundary integral method for transmission problems”, *J. of Math. Anal. and Appl.*, **106**, 367-413, 1985.

[2] A.S. Bonnet-Ben Dhia, M. Dauge, K. Ramdani, “Analyse spectrale et singularités d’un problème de transmission non coercif”, *C. R. Acad. Sci. Paris, Ser. I*, **328**, 717-720, 1999.

[3] F. Cakoni, D. Colton, H. Haddar, “The linear sampling method for anisotropic media”, *J. Comput. Appl. Math.*, **146**, 285-299, 2002.

[4] A. S. Bonnet-Ben Dhia, P. Ciarlet Jr. and C. M. Zwolf, “Two- and three-field formulation for wave transmission between media with opposite sign dielectric constant”, J. of Comp. and App. Math., 2007.

[5] A. S. Bonnet-Ben Dhia, P. Ciarlet Jr. and C. M. Zwolf, “A new compactness result for electromagnetic waves. Application to the transmission problem between dielectrics and metamaterials”, submitted to Math. Mod. and Meth. in the Appl. Sci.

Bloch wave homogenisation for spectral asymptotic analysis of the periodic Maxwell operator

K. D. Cherednichenko[†,*], **S. Guenneau**[‡]
[†]School of Mathematics, Cardiff University, Senghennydd Road, Cardiff, CF24 4AG
[‡]Department of Mathematical Sciences, University of Liverpool, Peach Street, Liverpool, L69 3BX
[*]Email: cherednichenkokd@cardiff.ac.uk

Abstract

We study the asymptotic behaviour of the spectrum of the three-dimensional Maxwell operator in a bounded periodic heterogeneous dielectric medium $\mathbf{T} = [-T, T]^3$, $T > 0$, as the structure period η, such that $\eta^{-1}T$ is a positive integer, tends to 0. The domain $\mathbf{T}$ is extended periodically to the whole of $\mathbb{R}^3$, so that the original operator is understood as acting in a space of $\mathbf{T}$-periodic functions. We use the so-called Bloch wave homogenisation technique which, unlike the classical homogenisation method, is capable of characterising a renormalised limit of the spectrum (called the *Bloch spectrum*). The related procedure is concerned with sequences of eigenvalues Λ_η of the order of the square of the medium period, which correspond to the oscillations of high-frequencies of order η^{-1}. The Bloch-wave description is obtained via the notion of two-scale convergence for bounded self-adjoint operators, and a proof of the "completeness" of the limiting spectrum is provided.

Introduction

The problem of determining the effective properties of a composite periodic medium in the context of electrostatics is an old one, and has been studied extensively, starting with the paper [11] by Lorenz. However, when the electric fields exhibit time-dependence one moves into the area of electromagnetism, which is a less-developed subject, at least in the context of the effective response of periodic composite media. In this respect it may be helpful to recall that although practitioners often make use of the traditional static formulae in the dynamic regime, this technique, generally known as the "quasi-static limit", tacitly relies on a set of assumptions about the fields in the material; namely, that their wavelengths are long in comparison with the typical size of heterogeneity. In this respect it seems to be of interest to investigate the material response when the wavelengths and the average period of variations in the conducting properties become comparable, thus inducing significant scale interactions. Whether the material then supports the imposed oscillations, such as an externally applied electric signal, becomes a non-trivial question, requiring a new averaging procedure of some sort.

There are several recent examples of similar kind, where the limiting procedure has exhibited a strong dependence on the precise way in which the underlying length-scales become small, see *e.g.* [12], [14]. Most of them are due to some sort of contrast in the properties at different points of the composite, which makes it possible to have comparatively short waves in selected parts of the medium. It seems equally plausible to imagine, however, that the external frequency is high enough already to warrant the existence of scale interaction effects in the medium. Several works investigating this possibility have been written by Allaire and Conca, in the context of fluid-solid structures [2], [4], as well as for a scalar elliptic equation with Dirichlet boundary conditions [3]. The present paper deals with an analogous problem in the context of electromagnetic waves. In order to avoid technical complications unrelated to the aim of the present study, we restrict ourselves to the case of periodic boundary conditions, thus excluding a possibility of the emergence of a "boundary layer spectrum", see *e.g.* [3]. Throughout, we use bold type to denote various spaces of vector functions, such as $\mathbf{L}^2$, or $\mathbf{C}^\infty_{\rm per}$; the subscript "per" will refer to the respective spaces of periodic functions. We use the notation $\sigma(\mathcal{A})$ for the spectrum of an operator $\mathcal{A}$.

1 Formulation

Consider an isotropic dielectric medium occupying the domain $\mathbf{T} = [-T, T]^3 \subset \mathbb{R}^3$ of fixed period $2T > 0$, which is extended periodically to $\mathbb{R}^3$ and composed of $(\eta^{-1}2T)^3$ periodicity cells with a small period $\eta \in \Xi$, where the set Ξ is defined by $\Xi := \{\eta > 0 : \eta^{-1}T \in \mathbb{N}\}$. Such a composite medium can be a model of what is known as the photonic crystal [13]. The analysis of electromagnetic modes in such a medium amounts to looking for pairs[1] $(\Lambda_\eta, \boldsymbol{H}_\eta) \in \mathbb{R}^+ \times \mathcal{H}_{\rm per}(\mathbf{curl}, \mathbf{T})$, $\boldsymbol{H}_\eta \not\equiv \mathbf{0}$, such that

$$\mathbf{curl}\big(\varepsilon^{-1}(\boldsymbol{x}, \boldsymbol{x}/\eta)\mathbf{curl}\boldsymbol{H}_\eta\big) = \Lambda_\eta^{-1}\boldsymbol{H}_\eta, \qquad (1.1)$$

where $\varepsilon(\boldsymbol{x}, \boldsymbol{x}/\eta)$ is the (matrix) relative permittivity of the medium at the point $\boldsymbol{x}$. The set of all first el-

[1]The space $\mathcal{H}_{\rm per}(\mathbf{curl}, \mathbf{T})$ is defined as the closure of the set $\mathbf{C}^\infty_{\rm per}(\mathbf{T})$ of $\mathbf{T}$-periodic infinitely smooth vector functions $\boldsymbol{\varphi}$ with respect to the norm $\|\boldsymbol{\varphi}\|_{\mathbf{L}^2(\mathbf{T})} + \|\mathbf{curl}\boldsymbol{\varphi}\|_{\mathbf{L}^2(\mathbf{T})}$.

ements Λ_η in such pairs is referred to as the spectrum of (1.1), and we denote it by σ_η. We assume that $\varepsilon(\boldsymbol{x},\boldsymbol{y}) \in C_{\rm per}\big(\mathbf{T},[L^\infty(Y)]^9\big)$, where $Y := [0,1]^3$, and that $\varepsilon(\boldsymbol{x},\boldsymbol{y}) \geq I$ for a.e. $(\boldsymbol{x},\boldsymbol{y}) \in \mathbf{T}\times Y$, which, in the case when the medium is isotropic, means that $\varepsilon(\boldsymbol{x},\boldsymbol{y})$ is bounded below at almost every point by the permittivity of vacuum. If follows from the above two conditions that the operator in the left-hand side of (1.1) is uniformly elliptic (or "coercive"). The equation (1.1) is understood in the weak sense, *i.e.*

$$\int_{\mathbf{T}} \varepsilon^{-1}(\boldsymbol{x},\boldsymbol{x}/\eta)\mathbf{curl}\boldsymbol{H}_\eta(\boldsymbol{x})\cdot\mathbf{curl}\boldsymbol{\varphi}(\boldsymbol{x})\mathrm{d}\boldsymbol{x}$$

$$= \Lambda_\eta^{-1}\int_{\mathbf{T}} \boldsymbol{H}_\eta(\boldsymbol{x})\cdot\boldsymbol{\varphi}(\boldsymbol{x})\mathrm{d}\boldsymbol{x}$$

for any $\boldsymbol{\varphi}\in\mathbf{C}^\infty_{\rm per}(\mathbf{T})$. Note in particular that for any solution of (1.1) one has $\mathrm{div}\,\boldsymbol{H}_\eta = 0$.

2 Convergence of spectra

In order to study the spectrum of (1.1) for each $\eta\in\Xi$, consider the Green operator $\mathcal{G}_\eta$ in $\mathbf{L}^2(\mathbf{T})$ defined for every $\boldsymbol{f}\in\mathbf{L}^2(\mathbf{T})$ by $\mathcal{G}_\eta\boldsymbol{f} = \boldsymbol{u}_\eta$, where $\boldsymbol{u}_\eta$ is the unique solution (by the Lax-Milgram lemma, see *e.g.* [10]) in $\mathcal{H}_{\rm per}(\mathbf{curl},\mathbf{T})$ of the problem

$$\mathbf{curl}\big(\varepsilon^{-1}(\boldsymbol{x},\boldsymbol{x}/\eta)\mathbf{curl}\boldsymbol{u}_\eta\big) + \boldsymbol{u}_\eta = \boldsymbol{f}. \qquad (2.2)$$

Clearly, $\mathcal{G}_\eta$ is self-adjoint and it can also be shown that it is compact; we can thus write $\sigma(\mathcal{G}_\eta) = \{0,1\}\bigcup\{\tilde\Lambda^k_\eta\}_{k\geq1}$, where for each η the sequence $\tilde\Lambda^k_\eta$ converges to 0 as $k\to\infty$. In the above union we include every eigenvalue as many times as is its multiplicity, so that to each $\tilde\Lambda^k_\eta$ is associated a normalised eigenfunction[2] $\boldsymbol{u}^k_\eta\in\mathbf{L}^2_{\rm sol}(\mathbf{T})$ such that $\|\boldsymbol{u}^k_\eta\|_{\mathbf{L}^2(\mathbf{T})} = 1$ and the family $\{\boldsymbol{u}^k_\eta\}_{k\geq1}$ is an orthonormal basis of $\mathbf{L}^2_{\rm sol}(\mathbf{T})$. The eigenvalues $\tilde\Lambda^k_\eta$ are related to the eigenvalues of (1.1) by the formula $\tilde\Lambda^k_\eta = (\Lambda^k_\eta+1)^{-1}\Lambda^k_\eta$.

The aim of this paper is to study the asymptotic behaviour of the spectrum σ_η when the period η goes to zero along the set Ξ. It is known (see *e.g.* [9], [8]) that when $\boldsymbol{f}\in\mathbf{L}^2(\mathbf{T})$, the solutions $\boldsymbol{u}_\eta$ of (2.2) converge strongly in $\mathbf{L}^2(\mathbf{T})$ to a limit $\boldsymbol{u}_{\rm hom}$, which is a unique solution in $\mathcal{H}_{\rm per}(\mathbf{curl},\mathbf{T})$ of the homogenised problem:

$$\mathbf{curl}\big(\varepsilon^{-1}_{\rm hom}(\boldsymbol{x})\mathbf{curl}\boldsymbol{u}_{\rm hom}\big) + \boldsymbol{u}_{\rm hom} = \boldsymbol{f}, \qquad (2.3)$$

[2]The space $\mathbf{L}^2_{\rm sol}(\mathbf{T})$ is defined to consist of those functions in $\mathbf{L}^2(\mathbf{T})$ whose divergence vanishes, with the Hilbert structure induced from $\mathbf{L}^2(\mathbf{T})$. Denote by $H^1_{\rm per}(\mathbf{T})$ the closure of $C^\infty_{\rm per}(\mathbf{T})$ in the norm $\|\varphi\|_{L^2(\mathbf{T})}+\|\nabla\varphi\|_{\mathbf{L}^2(\mathbf{T})}$. Then the divergence $\mathrm{div}\boldsymbol{u}$ of a vector function $\boldsymbol{u}\in\mathbf{L}^2(\mathbf{T})$ is a functional on $H^1_{\rm per}(\mathbf{T})$ defined by the formula $\langle\mathrm{div}\boldsymbol{u},\varphi\rangle = -\int_{\mathbf{T}}\boldsymbol{u}(\boldsymbol{x})\cdot\nabla\varphi(\boldsymbol{x})\mathrm{d}\boldsymbol{x}$.

where the effective matrix $\varepsilon_{\rm hom}(\boldsymbol{x})$ is given by

$$\varepsilon_{\rm hom}(\boldsymbol{x})\boldsymbol{\xi}\cdot\boldsymbol{\xi}$$

$$= \inf_{\Phi\in H^1_{\rm per}(Y)}\int_Y \varepsilon(\boldsymbol{x},\boldsymbol{y})\big(\boldsymbol{\xi}+\bigtriangledown\Phi(\boldsymbol{y})\big)\cdot\big(\boldsymbol{\xi}+\bigtriangledown\Phi(\boldsymbol{y})\big)\mathrm{d}\boldsymbol{y} \qquad (2.4)$$

for any $\boldsymbol{\xi}\in\mathbb{R}^3$.

Further, as $\eta\to0$, the restrictions to $L^2_{\rm sol}(\mathbf{T})$ of the operators $\mathcal{G}_\eta$ converge in norm to the restriction to $L^2_{\rm sol}(\mathbf{T})$ of the limit operator $\mathcal{G}$ defined for every $\boldsymbol{f}\in\mathbf{L}^2(\mathbf{T})$ by $\mathcal{G}\boldsymbol{f} = \boldsymbol{u}_{\rm hom}$, where $\boldsymbol{u}_{\rm hom}$ is the solution of (2.3). This fact follows from the weak compactness of the unit ball in $\mathbf{L}^2(\mathbf{T})$ and the above mentioned result that when a sequence of $\boldsymbol{f}_\eta\in\mathbf{L}^2_{\rm sol}(\mathbf{T})$ weakly converges to $\boldsymbol{f}\in\mathbf{L}^2_{\rm sol}(\mathbf{T})$ one has the strong convergence in $\mathbf{L}^2(\mathbf{T})$ of $\mathcal{G}_\eta\boldsymbol{f}_\eta$ to $\mathcal{G}\boldsymbol{f}$. [The proof of an analogous statement can be found in [3, Theorem 2.2].] Clearly, $\mathcal{G}$ is a compact self-adjoint operator and for its spectrum one has $\sigma(\mathcal{G}) = \{0,1\}\bigcup\{\tilde\Lambda^k\}_{k\geq1}$, where the eigenvalues $\tilde\Lambda^k$ are listed in the decreasing order and $\lim_{k\to+\infty}\tilde\Lambda^k = 0$. The min-max principle implies that $|\tilde\Lambda^k_\eta - \tilde\Lambda^k| \leq \|\mathcal{G}_\eta-\mathcal{G}\|$. Therefore, the above convergence in norm yields the convergence of each individual eigenvalue $\tilde\Lambda^k_\eta$ labelled in the decreasing order, and therefore of each eigenvalue Λ^k_η of (1.1). In particular, when $\eta\to0$, the sets σ_η converge (in the Hausdorff sense[3]) to $\big\{(1-\Lambda)^{-1}\Lambda : \Lambda\in\sigma(\mathcal{G})\big\}$. However, this convergence result alone does not say anything about the asymptotic behaviour of sequences of eigenvalues $\Lambda^{k(\eta)}_\eta$ when $\eta\to0$, where $k(\eta)\to\infty$ (which corresponds to high frequencies Λ^{-1}_η), and this is the issue that we address in the present work. It turns out that the behaviour of the eigenvalues Λ_η as $\eta\to0$ depends on the way they are scaled with η. In particular, three different limiting operators can be constructed, depending on whether the limit of $\eta^{-2}\Lambda_\eta$ is finite, infinite, or zero. The first case, which is of greatest interest in applications, corresponds to a limiting operator with a band-gap spectrum.

3 Main results

We first recall the concept of two-scale convergence for sequences in $\mathbf{L}^2(\mathbf{T})$ and adapt it to sequences of bounded self-adjoint operators. This adaptation is then utilised to characterise the limit spectrum of the type $\lim_{\eta\to0}\eta^{-2}\sigma_\eta$. Via a change of variable, we look for pairs $(\mu_\eta,\boldsymbol{H}_\eta)\in\mathbb{R}^+\times\mathcal{H}_{\rm per}(\mathbf{curl},\mathbf{T})$, $\boldsymbol{H}_\eta\not\equiv0$, such that

$$\eta^2\mathbf{curl}\big(\varepsilon^{-1}(\boldsymbol{x},\boldsymbol{x}/\eta)\mathbf{curl}\boldsymbol{H}_\eta\big) + \boldsymbol{H}_\eta = \mu_\eta^{-1}\boldsymbol{H}_\eta. \qquad (3.5)$$

[3]We say that σ_η converge to σ in the Hausdorff sense if $\max\{\sup_{\lambda_1\in\sigma_\eta}\inf_{\lambda_2\in\sigma}|\lambda_1-\lambda_2|, \sup_{\lambda_2\in\sigma}\inf_{\lambda_1\in\sigma_\eta}|\lambda_1-\lambda_2|\}\to0$ as $\eta\to0$.

This transformation of (1.1) into (3.5) keeps unchanged the eigenfunctions and changes the eigenvalues Λ_η to $\mu_\eta = (\eta^2 + \Lambda_\eta)^{-1}\Lambda_\eta$, ensuring that $\mu_\eta \sim 1$ if $\Lambda_\eta \sim \eta^2$.

The problem (3.5) generates a bounded operator $\mathcal{S}_\eta$ defined for each $\boldsymbol{f} \in \mathbf{L}^2(\mathbf{T})$ by $\mathcal{S}_\eta \boldsymbol{f} = \boldsymbol{v}_\eta$, where $\boldsymbol{v}_\eta$ is the unique solution in $\mathcal{H}_{\rm per}(\mathbf{curl}, \mathbf{T})$ of the problem

$$\eta^2 \mathbf{curl}\big(\varepsilon^{-1}(\boldsymbol{x}, \boldsymbol{x}/\eta)\mathbf{curl}\boldsymbol{v}_\eta\big) + \boldsymbol{v}_\eta = \boldsymbol{f}.$$

It can be shown that $\mathcal{S}_\eta$ converge weakly to the identity operator, but this fact does not provide any information on the behaviour of the spectra of $\mathcal{S}_\eta$. The latter issue can be handled using the notion of two-scale convergence [1], whereby the limit operator $\mathcal{S}^K$ defined for every $K \in \mathbb{N}$ acts on the space $\mathbf{L}^2(\mathbf{T} \times KY.)$ The (renormalised) limit of σ_η will then be determined by studying the spectra $\sigma(\mathcal{S}^K)$, $K \in \mathbb{N}$, via the Bloch-wave decomposition. For this, we introduce a family of limit problems, whereby for every $(\boldsymbol{x}, \boldsymbol{\theta}) \in \mathbf{T} \times Y$, we look for pairs $(\mu(\boldsymbol{x}, \boldsymbol{\theta}), \boldsymbol{v}(\boldsymbol{y})) \in \mathbb{R} \times \mathcal{H}_{\rm per}(\mathbf{curl}, Y)$ that satisfy (in the weak sense) the equation

$$\mathbf{curl}_y\Big(\varepsilon^{-1}(\boldsymbol{x}, \boldsymbol{y})\mathbf{curl}_y\big(\boldsymbol{v}(\boldsymbol{y})e^{2\pi i \boldsymbol{\theta}\cdot\boldsymbol{y}}\big)\Big) + \boldsymbol{v}(\boldsymbol{y})e^{2\pi i \boldsymbol{\theta}\cdot\boldsymbol{y}}$$

$$= \mu(\boldsymbol{x}, \boldsymbol{\theta})^{-1}\boldsymbol{v}(\boldsymbol{y})e^{2\pi i \boldsymbol{\theta}\cdot\boldsymbol{y}}. \qquad (3.6)$$

Note that for the spectrum $\sigma(\boldsymbol{x}, \boldsymbol{\theta})$ of the problem (3.6) we have $\sigma(\boldsymbol{x}, \boldsymbol{\theta}) = \{0, 1\} \bigcup \{\mu^k(\boldsymbol{x}, \boldsymbol{\theta})\}_{k \geq 1}$, where the sequence $\mu^k(\boldsymbol{x}, \boldsymbol{\theta})$ converges to 0. It can be shown that for each fixed k, the eigenvalue $\mu^k(\boldsymbol{x}, \boldsymbol{\theta})$ is a continuous function of $(\boldsymbol{x}, \boldsymbol{\theta})$ (*cf.* [3]). We then define the Bloch spectrum (band spectrum) by

$$\sigma_{\rm Bloch} := \{0, 1\} \cup \bigcup_{k \geq 1} \Big[\min_{(x,\theta)} \mu^k(\boldsymbol{x}, \boldsymbol{\theta}), \max_{(x,\theta)} \mu^k(\boldsymbol{x}, \boldsymbol{\theta})\Big]$$

In order to show that $\lim_{\eta \to 0} \sigma(\mathcal{S}_\eta) \subset \sigma_{\rm Bloch}$ we: 1) Construct "approximate eigenfunctions" for the permittivity matrix $\varepsilon(\boldsymbol{x}, \boldsymbol{y})$ "frozen" at a certain value $\boldsymbol{x} = \boldsymbol{x}_0$, and then 2) Use the so-called "Bloch measure" technique (*cf.* [3]) to show that as $\eta \to 0$, the Bloch components of these approximate eigenfunctions correspond to Bloch eigenvalues concentrating near μ.

Finally, we characterise the limit spectrum for other scalings. An appropriate multi-scale generalisation of the two-scale convergence method [5] is used to study the spectra of the types $a_\eta^{-2}\sigma_\eta$, where $a_\eta \gg \eta$ or $a_\eta \ll \eta$. It tuns out that outside the scaling regime $a_\eta \sim \eta$ there is no interaction between the homogenisation scale η and the singular perturbation scale a_η. One of two things can happen instead: either η is much smaller than a_η in which case the homogenisation occurs first and the singular perturbation concerns the homogenised system; or η is larger than a_η and it turns out that the singular perturbation occurs first at a microscopic scale making the homogenisation irrelevant.

4 Further work

There are several possible directions in which our results could be developed. First, the issue of whether non-periodic boundary conditions could be treated in a similar way, which is of special importance in the electromagnetic context. Secondly, the high-frequency spectrum analysis can be considered in the context of high-contrast periodic composites, which has received considerable attention recently in the finite-frequency regime, see [14], [6]. Depending on the exact relationship between the contrast parameter δ, the period of oscillations η and the wavelength $a_{\delta,\eta}$, the limiting problem could possess some or other type of spectrum, possibly leading to a number of new effects in the limit of vanishing parameter values. The band-gap features of the "high-contrast high-frequency" case can then be exploited in creating localised modes in the spectrum by adding a compact perturbation to the limiting operator. This will translate in a suitably rescaled perturbation of the original composite with finite δ, η, which possesses the mentioned localisation properties in a controlled way as δ and η vary. These aspects of the high-frequency spectral asymptotics for periodic media will be studied elsewhere.

References

[1] Allaire, G. 1992 Homogenization and two-scale convergence, *SIAM J. Math. Anal.* **23**, 1482–1518

[2] Allaire, G., Conca C. 1996 Bloch wave homogenization for a spectral problem in fluid-solid structures, *Arch. Rational Mech. Anal.* **35**, No. 3, 197–257

[3] Allaire, G., Conca C. 1998 Boundary layers in the homogenization of a spectral problem in fluid-solid structures, *SIAM J. Math. Anal.* **29**, 343–379

[4] Allaire, G., Briane, M. 1996 Multiscale convergence and reiterated homogenization, *Proc. Roy. Soc. Edinburgh* **126 A**, 297–342

[5] Cherednichenko, K. D., Smyshlyaev V. P., Zhikov, V. V. 2006 Non-local homogenised limits for composite media with highly anisotropic periodic fibres, *Proc. Roy. Soc. Edinburgh* **136 A**, 87–114

[6] Conca, C., Planchard, J., Vanninathan, M. 1995 Fluids and periodic structures, RMA **38**, J. Wiley and Masson, Paris

[7] Guenneau, S. 2001 Homogénéisation des quasi-cristaux et analyse des modes dans des fibres optiques de type cristal photonique, PhD Thesis, Université de Provence

[8] Guenneau, S., Zolla, F. 2000 Homogenization of three-dimensional finite photonic crystals, *J. Elec. Waves and Appl.* **14**, 529–530

[9] Jikov, V. V., Kozlov, S. M., Oleinik, O. A. 1994 *Homogenization of differential operators and integral functionals*, Springer

[10] Lorenz. L. V. 1869 Experimentale og theoretiske undersøgelser over legemernes brydningsforhold, I, *K. Dan. Vidensk. Selsk. Forh.* **8**(5) 203–248

[11] Poulton, C. G., Botten, L. C., McPhedran, R. C., Nicorovici, N. A., Movchan, A. B. 2001 Noncommuting limits in electromagnetic scattering: asymptotic analysis for an array of highly conducting inclusions, *SIAM J. Appl. Math.* **61**(5), 1706–1730

[12] Yablonovitch, E. 2001 Photonic crystals: semiconductors of light, *Sci. Amer.* **285**, 34–41

[13] Zhikov, V. V. 2000 On an extension of the method of two-scale convergence and its applications, *Sb. Math.*, **191**(7), 973–1014

NEGATIVE REFRACTION FOR LINEAR SURFACE WATER WAVES

M. Farhat[†], S. Guenneau[†,‡,*], S. Enoch[†], G. Tayeb[†], A.B. Movchan[‡], N.V. Movchan[‡]
[†]Institut Fresnel-CNRS (UMR 6133), University of Aix-Marseille, 13397 Marseille cedex 20, France
[‡]Department of Mathematical Sciences, Peach Street, Liverpool L69 3BX, UK
[*]Email: guenneau@liv.ac.uk

Abstract

We analyse transport properties of linear water waves propagating within a square array of fixed square cylinders. The main focus is on achieving Negative Refraction thanks to anomalous dispersion in fluid filled periodic structures. In the limit case when the cylinders come close to touching, the array can be approximated by a lattice of thin water channels (for which dispersion curves are given in closed form and thus frequencies at which Negative Refraction occurs). Applications lie in water wave lenses through inverted Snell-Descartes law.

Introduction

In 1967, Victor Veselago proposed to use negative refraction to make a convergent flat lens [1]. In 2000, John Pendry further shown that this flat lens overcomes the diffraction limit through enhancement of evanescent waves via plasmon resonances occurring on the boundaries when its refractive index is close to -1 [2]. Using photonic crystals, it is possible to achieve such a negative refraction index [3]. Alike photonic crystals, negative refraction has been experimentally demonstrated for liquid water waves propagating within arrays of circular cylinders, also leading to lensing effects [4].

In this paper, we analyse focussing effects for water waves propagating in arrays of square cylinders with close to touching edges. We carry out a simple asymptotic analysis providing us with dispersion curves in close form. Our analytical estimates are in good agreement with finite element computations.

Set up of the spectral problem

Let us consider a water tank filled an array of fixed rigid circular cylinder. We look for harmonic liquid surface waves characterized by their velocity potential Φ:

$$\Phi(x_1,x_2,x_3,t) = \Re e\left(\phi(x_1,x_2)\cosh(\kappa x_3)e^{-i\omega t}\right) , \tag{1}$$

where t is the time variable, ω is the wave frequency and x_3 is the vertical coordinate which is perpendicular to the horizontal plane $(x_1 - x_2)$. For simplicity, $x_3 = 0$ corresponds to the bottom of the water tank within which surface waves are propagating. Furthermore, κ is a spectral parameter linked to the reduced potential ϕ through the Helmholtz equation

$$\nabla^2\phi + \kappa^2\phi = 0 , \tag{2}$$

where κ is the spectral parameter linked to the wave-frequency through the dispersion relation

$$\omega^2 = g\kappa(1 + d_c^2)\tanh(\kappa h) , \tag{3}$$

where d_c is the water capillarity, h the water depth and g the acceleration caused by gravity.

The Helmholtz equation (2) is supplied with a Neumann (no flow) boundary condition

$$\frac{\partial\phi}{\partial n} = 0 , \tag{4}$$

on each rigid cylinder with a fixed boundary S.

These water waves propagating in a periodic structure are sought in the form of Floquet-Bloch waves, hence ϕ are functions of finite energy in a basic $Y = [0;1]^2$ (repeated periodically) such that

$$\phi(x_1+1,x_2+1) = \phi(x_1,x_2)e^{i(k_1+k_2)} , \tag{5}$$

where the Bloch vector $\mathbf{k} = (k_1,k_2) \in Y^* = [0,\pi]^2$, where Y^* is the so-called first Brillouin zone. This square cell Y^* in reciprocal space can be further reduced to a square triangle ΓMX with vertices $\Gamma = (0,0)$, $X = (0,\pi)$ and $M = (\pi,\pi)$, as depicted on Figure 1(b) if the inclusion within the cell Y in physical space exhibits a four-fold symmetry.

Asymptotic estimates of dispersion curves

Using local coordinates, we have

$$\Pi_\varepsilon^j = \left\{(x_1,x_2) \,:\, a_j < x_1 < b_j \,,\mid x_2 \mid < \varepsilon h_j/2\right\} , \tag{6}$$

where ε is a small non-dimensional parameter, and a_j, b_j and h_j are given constants denoting respectively the end points and thickness of the j-th bridge.

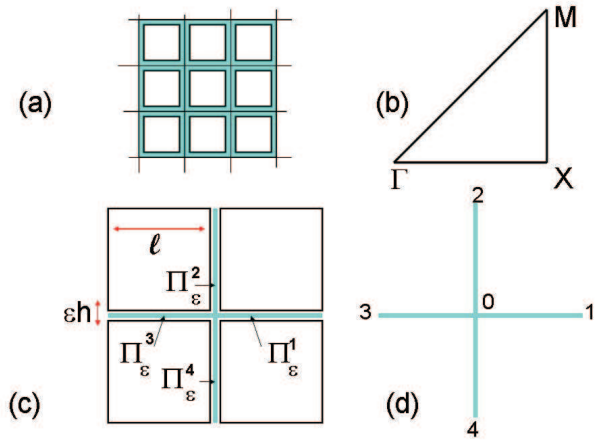

Figure 1: (a) Square array of square cylinders of pitch 1 where the blue region is filled with water; (b) Corresponding reduced Brillouin zone ΓXM; (c) Selected region of the square array showing four square cylinders separated by four thin bridges Π^j_ε within which water flows (blue region). (d) Corresponding lattice structure.

Let us introduce the scaled variable

$$\xi = \frac{x_2}{\varepsilon} \,, \tag{7}$$

The rescaled Helmholtz equation in Π^j_1 is

$$\left\{ \left(\frac{1}{\varepsilon^2} \frac{\partial^2}{\partial \xi^2} + \frac{\partial^2}{\partial x_1^2} \right) + \kappa^2 \right\} \phi_j = 0 \,. \tag{8}$$

The potential ϕ_j is approximated in the form

$$\phi_j \sim \phi_j^{(0)}(x_1, \xi) + \varepsilon^2 \phi_j^{(1)}(x_1, \xi) \,. \tag{9}$$

We derive that the leading order term in (9) satisfies

$$\frac{d^2 \phi_j^{(0)}}{dx_1^2} + \kappa^2 \phi_j^{(0)} = 0 \,,\ a_j < x_1 < b_j \,. \tag{10}$$

This equation is supplied with Floquet-Bloch boundary conditions at the endpoints $1, .., 4$ on Fig. 1 as well as an equilibrium condition at the central point 0 [5]:

$$0 \quad = \sum_{j=1}^{4} \frac{d^2 \phi_j^{(0)}}{dx_1^2} \mid_{x_1 = 0} \,. \tag{11}$$

This leads us to the asymptotic dispersion relation

$$\sin(\kappa l) \left(\cos(k_1 l) + \cos(k_2 l) - 2\cos(\kappa l) \right) = 0 \,. \tag{12}$$

For a wave propagating in the ΓX direction, $k_1 = k_2$, so that (12) reduces to $\kappa = k_1$. This has important practical consequences as it gives the frequency at which focusing of water waves occurs for a slab lens consisting of close to touching square cylinders.

Analysis of anomalous dispersion and lensing effect

To analyze the transport of water wave energy within the array of cylinders, we need to link the dispersion relation to that of propagation of energy. This can be done in a way similar to what was discussed for electromagnetism in [3] by noting that the group velocity of Floquet-Bloch water waves is defined as

$$\mathbf{V}_g = \nabla_{\mathbf{k}}(\omega) = \frac{\partial \omega}{\partial k_1} \mathbf{e}_1 + \frac{\partial \omega}{\partial k_2} \mathbf{e}_2 \,. \tag{13}$$

This group velocity corresponds to the speed at which the amplitude of the water wave propagates. This is easily seen to be equal to the average velocity (taken over the basic cell) of the energy flow.

The essential condition for the all angle negative refraction (AANR) effect is that the equifrequency surfaces (EFS) should become convex everywhere about some point in the reciprocal space, and the size of this EFS should shrink with increasing frequency. Further the EFS should be larger than the free space dispersion surface and the frequency should be within the first Bragg zone [3].

As can be seen in Figure 2, the analytical formula (12) compares very well with the finite elements computations for a filling fraction of 0.9. The starred curve on Figure 2 corresponds to this case for a depth of water of $h = 6mm$. Its intersection with the acoustic band provides us with the frequency at which negative refraction occurs. We note that this frequency is around $f_{lens1} = 2\pi$ Hz, which is a straightforward consequence of (3) and (12). We check in Figure 3 that the corresponding EFS satisfy the criteria for AANR and we observe on Figure 4 that for a harmonic source set at this frequency, there is indeed an image forming on the other side of the array.

Perspectives: experimental setup

We now want to check our numerical results against experimental values. In our experimental setup we consider a water tank that consists of a rectangular glass bottom covered by a thin layer of

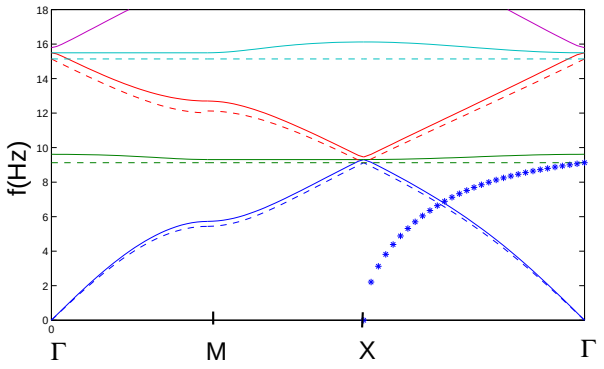

Figure 2: Comparison of FEM computations of dispersion curves (continuous curves) against analytical estimate (12)(dotted curves) for a filling fraction of cylinder in water of 0.9; Horizontal axis: projection of the Bloch vector on the first Brillouin zone ΓXM; Vertical axis: wave frequency $f = \omega/(2\pi)$ in Hertz; The starred curve corresponds to surface waves propagating in water along the ΓM direction, as given by equation (3). The depth of water is $h = 6mm$ and the capillarity $d_c = 0.109mm$.

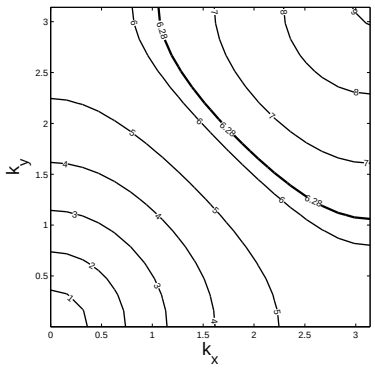

Figure 3: Isofrequencies corresponding to dispersion curves of diagram 2.

water surrounded by four absorbing sides (foam) acting as Perfectly Matched Layers. A flat rectangular slab of about 200 cylinders is placed in the middle of the vessel. A small vibrator serves as a point source generator. Both frequency and amplitude of the vibrator can be tuned by a signal generator. We then observe the vertical displacement of the liquid surface ξ which is related to the reduced potential ϕ by

$$\xi(x_1, x_2, t) = \Re e\left(-\frac{i\omega}{g}\phi(x_1, x_2)e^{-i\omega t}\right). \qquad (14)$$

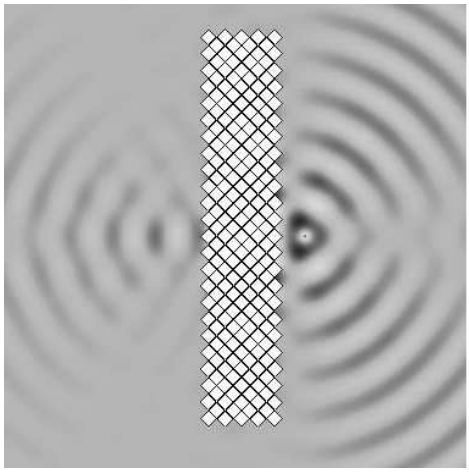

Figure 4: Water-wave lensing for one source at frequency $f_{lens1} = 6.28 \sim 2\pi$ Hz, through an array of 212 square cylinders of side length $9.5mm$. The pitch of the array is $10mm$, the depth of water is $h = 6mm$ and the capillarity $d_c = 0.109mm$.

Unlike electromagnetic waves in the micro-wave regime, ξ provides a readily observable evidence of negative refraction (inverted Snell-Descartes law).

References

[1] V.G. Veselago, "Properties of materials having simultaneaously negative values of dieletric (xi) and magnetic (mu) susceptibilities", Usp. Fiz. Nauk vol. 92, 517, 1967 & Sov. Phys.Usp., vol. 10, p. 509, 1968.

[2] J.B. Pendry,"Negative refraction makes a perfect lens", Phys. Rev. Lett., vol. 85, pp. 3966-3969, 2000.

[3] B. Gralak, S. Enoch, G. Tayeb, "Anomalous refractive properties of photonic crystals", J. Opt. Soc. Am. A 17, pp. 1012-1020, 2000.

[4] X. Hu, Y. Shu, X. Liu, R. Fu and J. Zi, "Superlensing effect in liquid surface waves", Phys. Rev. E, vol. 69, pp. 030201-030204, 2004.

[5] P.G. Martinsson and A.B. Movchan, " Vibrations of lattice structures and phononic band gaps", Q. Jl Mech. Appl. Math. 56, 45-65 (2002)

ADAPTIVE FINITE ELEMENT METHODS FOR PHOTONIC CRYSTAL FIBERS

S. Giani[†,*], **I. G. Graham**[†,‡]
[†]Department of Mathematical Sciences, University of Bath, Bath, BA2 7AY, UK
[*]Email: sg240@maths.bath.ac.uk
[‡]Email: I.G.Graham@bath.ac.uk

Abstract

In this talk we shall discuss the calculation of the spectra of PDEs arising in models of photonic crystal fibers (PCFs) in both periodic and non-periodic cases.
For periodic PCF problems, under the assumptions of TE and TM polarizations, we derive error estimators for approximated eigenvalues and eigenvectors, arising from discretization of a typical cell problem. We give numerical illustrations of how the adaptivity copes with internal interfaces in the device and with high contrast media.
We shall also give illustrations of the use of our error estimates in an adaptive procedure for finding spectral gaps and related trapped modes in devices with defects.

Introduction

We consider eigenvalue problems arising from the modelling of photonic crystal fibers (PCFs) and in particular we are interested in computing the first gaps in the spectrum of periodic structures and trapped modes arising in structures with defects. In order to locate the gaps we split the Maxwell's equations into the TE and TM modes. Then we apply the Bloch-Floquet transform obtaining two families of eigenvalue problems on a two-dimensional primitive cell P parameterized by the quasi-momentum κ.

In this talk we solve both families of problems using linear finite elements on triangular meshes and we propose a reliable and efficient a posteriori error estimate to drive mesh adaptivity. The a posteriori error estimator we use is based on residuals. This kind of estimate is quite common in finite element methods for partial differential equations, but there are relatively few results for eigenvalue problems, with some exceptions being [1], [2], [3], [4] and [5]. The approach presented in [4] and [5] is different because eigenvalue problems are treated as standard non linear problems. We are not aware so far of any a posteriori error estimates or mesh adaptivity for photonic eigenvalue problems.

A new a posteriori error estimator for PC

Let $\mathcal{T}_h$ be a conforming and shape regular mesh of triangles. We denote with $\mathcal{F}_h$ the set of all the edges of the elements of the mesh $\mathcal{T}_h$. We assume to have already chosen a preorientated unit normal vector $\vec{n}_F$ for each edge F. On the mesh $\mathcal{T}_h$ we define the piecewise constant function h_τ which assumes, at any point in the interior of any element τ, the value of the diameter of τ. Furthermore, we define on the edges $\mathcal{F}_h$ the function h_F, which assumes in the interior of each edge F the length of F.

The estimation of the error is a sum of local residuals coming from the interior of the elements and from the edges of the mesh. For a computed eigenpair (λ_h, u_h), we denote the residual contribution from the interior of the elements by $R_I(u_h, \lambda_h)$. In addition we define the residual from the edges of the elements for a computed eigenpair (λ_h, u_h) by the functional $R_F(u_h)$. The estimator η^{TE} for the TE mode is defined in the following way:

$$\eta^{TE} := \Big\{ \sum_{\tau\in\mathcal{T}_h} \frac{h_\tau^2}{M_\tau} \|R_I^{TE}(u_h,\lambda_h)\|_{0,\tau}^2 + \sum_{F\in\mathcal{F}_h} \frac{h_F}{M_F} \|R_F^{TE}(u_h)\|_{0,F}^2 \Big\}^{1/2}, \tag{1}$$

where M_τ is an element wise constant function depending on the dielectricity of the materials and M_F is an edge wise constant function also depending on the coefficients of the problem. Instead, the estimator η^{TM} for the TM mode is defined as:

$$\eta^{TM} := \Big\{ \sum_{\tau\in\mathcal{T}_h} h_\tau^2 \|R_I^{TM}(u_h,\lambda_h)\|_{0,\tau}^2 + \sum_{F\in\mathcal{F}_h} h_F \|R_F^{TM}(u_h)\|_{0,F}^2 \Big\}^{1/2}. \tag{2}$$

We have proved the reliability for both error estimators in the energy norms of the error and in the error for the eigenvalues. In the following theorems we have collected the two reliability results. Since eigenvalue problems are non-linear, we have the appearance of high order terms in the results of Theorem 1 and Theorem 2. If the computed eigenvalue is close enough to the true one, we have that these terms decay to 0 quicker than the leading term when

the size of the mesh shrinks to 0. In [6] there is a very insightful a priori analysis for eigenvalue problems. It is explained that when the mesh size is small enough, the computed eigenvalues cluster around the true ones and the number of computed eigenvalues in the clusters depend on the multiplicity of the true eigenvalues. In addition, when the mesh size goes to 0 the points in the clusters converge to the true eigenvalues and also the corresponding computed eigenfunctions converge to true eigenfunctions. So each computed eigenvalue λ_h converges to a unique true eigenvalue λ, when the mesh size shrinks to 0. Furthermore, for each computed eigenpair (λ_h, u_h) it is possible to uniquely identify a true eigenpair (λ, u) such that λ_h converges to λ and u is the eigenfunction of λ that minimize the distance to u_h for a chosen norm. We use the notation $\lesssim$ to hide a constant independent of the mesh diameter, provided the meshes are shape regular, and we denote by $|||\cdot|||_P$ the energy norm related to the considered problem.

Theorem 1 (Reliability for the TE mode)**.** *Let (λ_h, u_h) be an eigenpair of the TE mode problem computed on a mesh $\mathcal{T}_h$ for some value of the quasimomentum κ. Let (λ, u) be the corresponding true eigenpair of the continuous problem for the same value of κ. Then we have that the error estimator (1) bounds the error in the energy norm as:*

$$|||u - u_h|||_P^{TE} \lesssim \eta^{TE} + \textit{high order terms}.$$

Also, the error estimator (1) bounds the error for the eigenvalues as:

$$0 \leq \lambda_h - \lambda \lesssim (\eta^{TE})^2 + \textit{high order terms}.$$

Theorem 2 (Reliability for the TM mode)**.** *Let (λ_h, u_h) be an eigenpair of the TM mode problem computed on a mesh $\mathcal{T}_h$ for some value of the quasimomentum κ. Let (λ, u) be the corresponding true eigenpair of the continuous problem for the same value of κ. Then we have that the error estimator (2) bounds the error in the energy norm as:*

$$|||u - u_h|||_P^{TM} \lesssim \eta^{TM} + \textit{high order terms}.$$

Also, the error estimator (2) bounds the error for the eigenvalues as:

$$0 \leq \lambda_h - \lambda \lesssim (\eta^{TM})^2 + \textit{high order terms}.$$

In addition, we have also proved the global efficiency for the two error estimators. As for the reliability, also in the results for the global efficiency we have higher order terms coming from the non-linearity of the problems.

Theorem 3 (Global efficiency for the TE mode)**.** *Let (λ_h, u_h) be an eigenpair of the TE mode problem computed on a mesh $\mathcal{T}_h$ for some value of the quasimomentum κ. Let (λ, u) be the corresponding true eigenpair of the continuous problem for the same value of κ. Then we have that the error in the energy norm bounds the error estimator (1) as:*

$$\eta^{TE} \lesssim |||u - u_h|||_P^{TE} + \textit{high order terms}.$$

Theorem 4 (Global efficiency for the TM mode)**.** *Let (λ_h, u_h) be an eigenpair of the TM mode problem computed on a mesh $\mathcal{T}_h$ for some value of the quasimomentum κ. Let (λ, u) be the corresponding true eigenpair of the continuous problem for the same value of κ. Then we have that the error in the energy norm bounds the error estimator (2) as:*

$$\eta^{TM} \lesssim |||u - u_h|||_P^{TM} + \textit{high order terms}.$$

Finally, we have developed a computationally efficient way to calculate the bottom part of the spectrum in the periodic case. In order to be computationally efficient, our method exploits mesh adaptivity by solving a lot of eigenvalue problems for different values of the quasimomentum κ using the same properly refined mesh for all of them. Furthermore, in a separate piece of work, an adaptive procedure similar to the one used here has been proved to converge for simplified model elliptic eigenvalue problems. All our results are supported by numerical evidence showed at the end of the paper.

References

[1] M. G. Larson, "A Posteriori and a Priori Analysis for Finite Element Approximations of Self-Adjoint Elliptic Eigenvalue Problems", SIAM J. Numer. Anal, vol. 38, pp. 608-625, 2000.

[2] T. F. Walsh , G. M. Reese and U. L. Hetmaniuk, "Explicit a posteriori error estimates for eigenvalue analysis of heterogeneous elastic structures", Technical Report, Sandia National Laboratories, 2005.

[3] R. G. Duran, C. Padra and R. Rodriguez, "A posteriori error estimates for the finite element approximation of eigenvalue problems", Math. Mod. & Met.in Appl. Sc., vol 13, no 8, pp 1219-1229, 2003.

[4] R. Verfurth, "A posteriori error estimates for nonlinear problems. Finite element discretizations of elliptic equations", Math. Comp., vol. 62, no. 206, pp. 445-475, 1994.

[5] V. Heuveline and R. Rannacher , “A posteriori error control for finite element approximations of elliptic eigenvalue problems”, J. Adv. Comp. Math., vol. 15, pp. 107138, 2001.

[6] G. Strang, G. J. Fix, “An analysis of finite element method”, Prentice-Hall, 1973

ACOUSTIC BAND GAPS IN ARRAYS OF NEUTRAL INCLUSIONS

S. Guenneau[†,‡,*], **A.B. Movchan**[‡], **F. Zolla**[†], **N.V. Movchan**[‡], **A. Nicolet**[†]
[†]Institut Fresnel-CNRS (UMR 6133), University of Aix-Marseille, 13397 Marseille cedex 20, France
[‡]Department of Mathematical Sciences, Peach Street, Liverpool L69 3BX, UK
[*]Email: guenneau@liv.ac.uk

Abstract

We analyse numerically the acoustic stop band properties of an array of orthotropic coated cylinders. These coated cylinders behave either as neutral inclusions (leading to an invisible material) or local resonators (leading to a perfect mirror) depending upon the wave frequency range. We also give the eigenfield within the cloak in closed form for a frequency on the lower-edge of the first stop band.

Introduction

In 1994, McPhedran, Nicorovici and Milton [1] studied a coated cylinder within which the permittivity was complex with a negative real part (but the permeability was kept to 1). In 2006, the last two authors further proposed to cloak a countable set of line sources using anomalous resonance when it lies in the close neighborhood of a cylindrical coating filled with negative refractive index material [5]. A geometric route to cloaking was independently proposed the same year by Pendry, Shurig and Smith [6] and Ulf and Philbin [7] in the ray optics limit. A numerical proof of cloaking was subsequently provided in the intense near field limit (full electromagnetic wave simulation) in [9]. The elastodynamic counterpart of invisibility cloaks, known as neutral inclusions [2], was discussed by Milton *et al.* in [8]. We extend this latter work to a periodic array of cylindrical acoustic cloaks.

Governing equations

Let us consider a cylindrical elastic object we want to cloak located within a disk of radius R_1. We can use the same route to cloaking as that proposed in electromagnetism by Pendry *et al.* [6]. For this, we consider a geometric transformation which maps the field within the disk $r \leq R_2$ onto the annulus $R_1 \leq r \leq R_2$:

$$\begin{cases} r' = R_1 + r(R_2 - R_1)/R_2 \ , \ 0 \leq r \leq R_2 \\ \theta' = \theta \ , \ 0 < \theta \leq 2\pi \\ z' = z \ , \ z \in \mathbb{R}, \end{cases} \tag{1}$$

where r', θ' and z' are 'radially contracted cylindrical coordinates'. Moreover, this transformation maps the field for $r \geq R_2$ onto itself by the identity transformation.

In this paper, we focus on the case of anti-plane shear elastic waves.

This change of co-ordinates is characterized by the transformation of the differentials through the Jacobian:

$$\mathbf{J}_{rr'} = \frac{\partial(r,\theta,z)}{\partial(r',\theta',z')} = \begin{pmatrix} \frac{1}{\alpha} & 0 & 0 \\ 0 & 1 & 0 \\ 0 & 0 & 1 \end{pmatrix} . \tag{2}$$

where $\alpha = (R_2 - R_1)/R_2$ for $0 \leq r \leq R_2$ and $\alpha = 1$ for $r > R_2$.

The elastic properties of the transformed medium are described by the matrix

$$\mathbf{T} = \mathbf{J}^T \mathbf{J} / det(\mathbf{J}) \ , \tag{3}$$

which is a representation of the metric tensor, as recognized by Milton *et al.*[8]. The only thing to do in the transformed coordinates is to replace the materials (often homogeneous and isotropic) by equivalent ones that are inhomogeneous and orthotropic whose elastic parameters are given by

$$\mu' = \mu \mathbf{T}^{-1} \ , \quad \text{and} \quad \rho' = \rho \mathbf{T}^{-1} \ . \tag{4}$$

We note that there is no change in the wave-speed v of shear waves in the transformed medium:

$$(\mu' \rho'^{-1})^{1/2} = \sqrt{\frac{\mu}{\rho}} Id = v \ , \tag{5}$$

since the density ρ and the shear modulus μ suffer the same transformation. Here, Id denotes the 3×3 Identity matrix, and ρ' and μ' are 3×3 matrices.

In the transformed medium, the acoustic wave equation thus writes

$$\begin{aligned} &\frac{1}{r^2} \nabla_{r,\theta} \cdot \left(\mu \begin{bmatrix} \frac{r-R_1}{r} & 0 \\ 0 & \frac{r}{r-R_1} \end{bmatrix} \nabla_{r,\theta} \, u \right) \\ &+ \rho \frac{r - R_1}{\alpha^2 r} \omega^2 u = 0 \ , \end{aligned} \tag{6}$$

where $\nabla_{r,\theta} = (r\partial/\partial r, \partial/\partial\theta)$.

These acoustic waves propagating in a periodic structure are sought in the form of Floquet-Bloch waves, hence the out-of-plane displacement u is a function of finite energy in a basic cell $Y = [0,d]^2$ (repeated periodically) such that

$$u(x_1 + d, x_2 + d) = u(x_1, x_2)e^{i(k_1+k_2)d} , \qquad (7)$$

where $x_1 = r\cos\theta$, $x_2 = r\sin\theta$ and $\mathbf{k} = (k_1, k_2)$ is the Bloch vector which describes the first Brillouin zone $Y^* = [0, \pi/d]^2$. This square cell Y^* in reciprocal space is further reduced to a square triangle ΓMX with vertices $\Gamma = (0,0)$, $X = (0, \pi/d)$ and $M = (\pi/d, \pi/d)$ if the inclusion within the cell Y in physical space exhibits a four-fold symmetry (which is obviously the case for a coated circular inclusion).

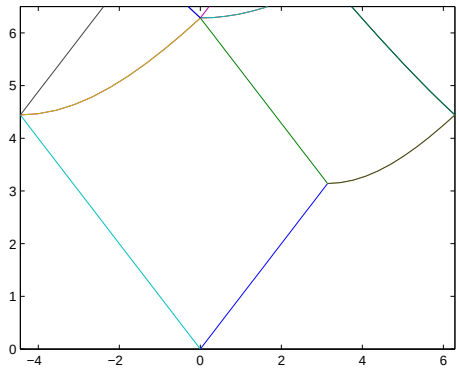

Figure 1: Dispersion curves for a homogeneous elastic medium (normalised elastic parameters $\mu = 1$ and density $\rho = 1$) with enforced Floquet-Bloch conditions on a square array of pitch d. We plot the normalised radian frequency $\omega d/v = 2$ (where v is the shear waves velocity as given by formula 5), versus $|\,\mathbf{k}\,|$ (when the Bloch vector $\mathbf{k}$ describes the first Brillouin zone ΓMX).

Analysis of stop bands

On figures 1 and 2 we compare computations for a homogeneous elastic medium ($\mu = \rho = 1$) with enforced Floquet-Bloch boundary conditions to that of an array of inclusions ($\mu = 2$, $\rho = 2$) or radius $R_1 = 0.2d$ surrounded by an "invisibility cloak" (μ' and ρ' as given by 4) of radius $R_2 = 0.2d$. As one would expect some of the corresponding dispersion curves reported on Figures 1 and 2 are indeed superimposed.

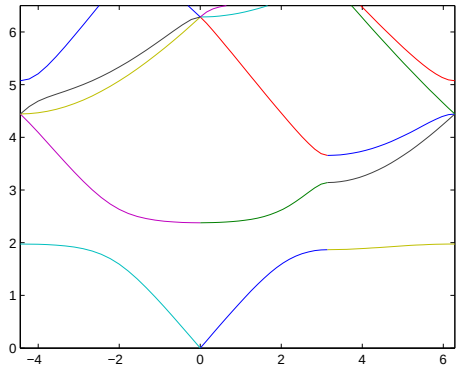

Figure 2: Same as Figure caption 1 for a square array (pitch d) of circular cylinders of radius $0.2d$ and normalised elastic parameters $\mu = 2$ and density $\rho = 2$, surrounded by a coating of inner and outer radii $R_1 = 0.2d$ and $R_2 = 0.4d$.

But surprisingly, we observe the appearance of a stop band around the normalised eigenfrequency 2 which is associated with a defect mode (see Figure 3). The split of the acoustic band of Figure 1 leading to the appearance of the stop band on figure 2 is typical for locally resonant structures such as arrays of coated inclusions [3] and split ring resonators which behave like Helmholtz resonators [4].

Frequency estimate for the first localised mode

Let us now assume that $u(r,\theta) = u(r)$ *i.e.* u is axi-symmetric. In this case, (6) reduces to

$$\mu\frac{d}{dr}u + \mu(r - R_1)\frac{d^2}{dr^2}u + \rho\frac{r - R_1}{\alpha^2}\omega^2 u = 0 , \qquad (8)$$

for $R_1 < r < R_2$.

The general solution of (8) is expressed in terms of Bessel functions of first and second kind:

$$u(r) = AJ_0\left(\frac{(r - R_1)\omega}{v\alpha}\right) + BY_0\left(\frac{(r - R_1)\omega}{v\alpha}\right) , \qquad (9)$$

where A and B are arbitrary constants. In the case of the first localised mode (axi-symmetric, see figure 2), we observe that the core of the inclusion moves freely whereas the outer boundary of the coating is clamped, hence we set $u'(R_1) = 0$ and $u(R_2) = 0$. The eigenfrequency should thus satisfy

$$Y_0(\omega R_2/v)/J_0(\omega R_2/v) = 0 . \qquad (10)$$

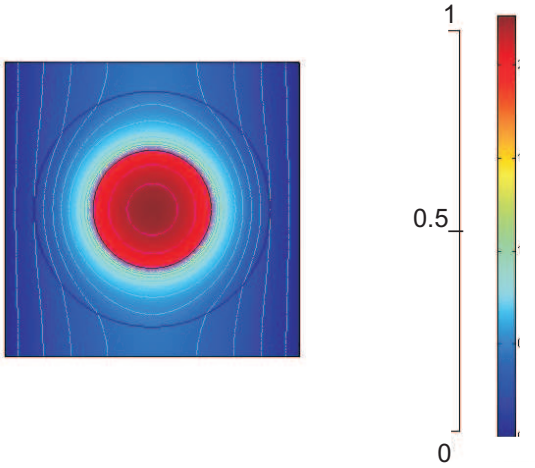

Figure 3: 2D plot of the first mode associated with the normalised eigenfrequency $\omega d/v = 1.95$ for a Bloch vector $\mathbf{k} = (\pi/d, \pi/d)$. The elastic and geometric parameters are those of Figure caption 2.

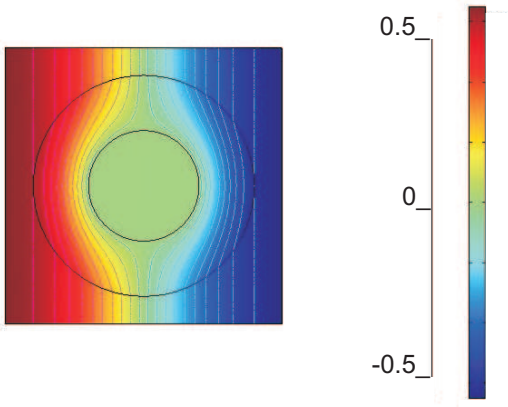

Figure 4: Same as figure caption 3 for the second mode which associated with the normalised eigenfrequency $\omega d/v = 4.44$. We note that the frequency of this mode corresponds to that of the first mode on Figure 1 (homogeneous medium).

For $R_2 = 0.4d$, this gives the normalised frequency estimate $\omega d/v \sim 2.22$ which is in reasonable agreement with the finite elements' solution $\omega d/v = 1.98$.

Conclusion and perspectives

The frequency estimate (10) provides us with the lower edge of the stop band of figure 2. An interesting feature of (9) is that the field is singular on the inner boundary of the coating ($r = R_1$). This was numerically observed in the case of transverse electromagnetic waves scattered by a cylindrical object surrounded by such a coating (known as invisibility cloak)[9]: the elastic parameters ρ and μ then play the role of the permittivity and/or permeability of the coating depending upon the light polarization.

References

[1] R.C. McPhedran, N.A. Nicorovici, G.W. Milton,"Optical and dielectric properties of partially resonant composites", Physical review B, vol. 49, pp. 8479 -8482, 1994.

[2] D. Bigoni, S.K. Serkov, M. Valentini, A.B. Movchan, "Asymptotic models of dilute composites with imperfectly bonded inclusions", Int. Jour. Sol. Struct., vol. 35, pp. 3239-3258, 1998.

[3] S.B. Platts and N.V. Movchan,"Low frequency band gaps and localised modes for arrays of coated inclusions", Proceedings of IUTAM Symposium on Asymptotic, Singularities and Homogenization in Problems of Mechanics, Kluwer Academic, Dordrecht, pp. 63-71, 2003.

[4] A.B. Movchan and S. Guenneau, "Split ring resonators and localized modes", Physical Review B 70, pp. 125116, 2004.

[5] G.W. Milton, N.A. Nicorovici, "On the cloaking effects associated with anomalous localised resonance", Proc. Roy. Lond. A, 462, pp. 3027, 2006.

[6] J.B. Pendry, D. Shurig, D.R. Smith,"Controlling electromagnetic fields", Science, vol. 312, pp. 1780, 2006.

[7] U. Leonhardt and T. G. Philbin, "General relativity in electrical engineering, New Journal of Physics", vol. 8, pp. 247, 2006.

[8] G.W. Milton, M. Briane and J.R. Willis, "On cloaking for elasticity and physical equations with a transformation invariant form", New Journal of Physics, vol. 8, pp. 248, 2006.

[9] F. Zolla, S. Guenneau, A. Nicolet and J.B. Pendry, "Electromagnetic analysis of cylindrical invisibility cloaks and the mirage effect", Optics Letters, vol. 32, pp. 1069, 2007.

LOCALIZATION AND PROPAGATION IN PHOTONIC FIBERS VIA HIGH-CONTRAST HOMOGENIZATION

I. Kamotski[†,*],
[†] Bath University, UK
[*]Email: i.v.kamotski@bath.ac.uk

Introduction

One of physical motivations for the reported study is wave localization in photonic crystal fibers (PCF). Those are optical materials representing geometrically a periodic medium (whose physical properties vary across the fiber but not along it), with the defect being its "core", which is a propagating "channel" or a waveguide: electromagnetic waves of certain frequencies (the "band gap" frequencies) fail to propagate in the surrounding periodic medium and hence remain localised inside the PCF, which allows for them to propagate along the core for long distances with little loss. Mathematically, the problem reduces to an appropriate spectral problem at the cross-section of the PCF. This is that of characterisation of localised modes or eigenfunction (whenever such exist) in the band gaps in the Floquet-Bloch spectrum for the Maxwell's operator in the surrounding periodic medium with a fixed "propagation constant" (the wave vector along the fiber). The latter cross-sectional geometry is a periodic medium "perturbed" by a big size heterogeneity (domain $\Omega^R = \{x : xR^{-1} \in \Omega$ see below). The problem is hence first in detecting the band gaps in the periodic medium without defects and then in finding, in the presence of a defect, the "extra point spectrum" in the gaps as well as the associated eigenfunctions, the localised states. In the present work we aim at detecting such localised modes in an asymptotically (with respect to size of defect and properly chosen wave number) explicit way due to defects periodic medium applying and appropriately developing further the tools of (high contrast) "non-classical" homogenization theory.

The problem

We consider Maxwell's equations,

$$\nabla \wedge \mathbf{H} = \epsilon \frac{\partial \mathbf{E}}{\partial t},$$

$$\nabla \wedge \mathbf{E} = -\mu \frac{\partial \mathbf{H}}{\partial t},$$

$$\nabla \cdot \epsilon \mathbf{E} = 0, \quad \nabla \cdot \mu \mathbf{H} = 0.$$

In what follows we assume that $\mu = 1$ and ϵ doesnot depend on x_3. We are interested in time harmonic fields with fixed dependence on third variable,

$$\mathbf{H}(t, x_1, x_2, x_3) = e^{i\omega(t+kx_3)} H(x_1, x_2),$$

$$\mathbf{E}(t, x_1, x_2, x_3) = e^{i\omega(t+kx_3)} E(x_1, x_2),$$

where k is a real parameter.

Then we arrive at scalar equations for TE and TM cases, see [1]:

$$\nabla \cdot (\epsilon - k^2)^{-1} \nabla H_3 + \omega^2 H_3 = 0,$$

$$\nabla \cdot \epsilon(\epsilon - k^2)^{-1} \nabla E_3 + \epsilon\omega^2 E_3 = 0.$$

Let $\square = (0,1) \times (0,1)$ be a reference unit cell and Q_0 domain with smooth boundary such that $\overline{Q_0} \subset \square$. We define periodic spreading $\widetilde{Q}_0$ of Q_0 i.e $\widetilde{Q}_0 = \{x = (x_1, x_2) : x + m \in Q_0, m \in \mathbb{Z}^2\}$ and define periodic electric permittivity: $\epsilon^p = \epsilon_0$, in $\widetilde{Q}_0$ and $\epsilon^p = \epsilon_1$, in $\mathbb{R}^2 \setminus \widetilde{Q}_0$ (we assume that $\epsilon_0 > \epsilon_2$). Let us introduce a "big" defect: we fix domain Ω and define defect: $\Omega^R = \{x : xR^{-1} \in \Omega, \}$, $R > 0$. Then $\epsilon^d = \epsilon_1$, in Ω^R and $\epsilon^d = \epsilon^p$ in $\mathbb{R}^2 \setminus \Omega^R$. We perform rescaling $x \to x/R$ and arrive at problem with finite size defect in media with small period:

$$A_R^{d,p}(k^2)u := -R^{-2}\nabla \cdot \Big((\epsilon^{d,p}(x/R) - k^2)^{-1}) \nabla u \Big) = \lambda u,$$

$$B_R^{d,p}(k^2)u := -R^{-2}\nabla \cdot \Big(\epsilon^{d,p}(x/R)(\epsilon^{d,p}(x/R) - k^2)^{-1}) \nabla u \Big)$$
$$= \epsilon^{d,p}(x/R)\lambda u,$$

which are spectral problems for self-adjoint operators $A_R^{d,p}(k^2)$ and $B_R^{d,p}(k^2)$. Properties of this operators are very similar and we consider only operator $A_R^{d,p}(k^2)$.

Homogenization

Spectral theory ensures that the "unperturbed" operator $A_R^p(k^2)$ ($\epsilon = \epsilon^p$) has a band structure, whose (essential) spectrum persists under the perturbation, so the only "extra" spectrum may be the point spectrum in the gaps, with corresponding eigenvalues exponentially decaying at infinity. If the size of the defect is much larger than that of the periodicity, one could hope to "homogenize" the periodicity when the underlying big parameter R tends to

infinity. However, the "classical" homogenization is of no use in the present context since the (constant coefficients) homogenized operator ceases having the band gap structure (effectively accounting only for the behaviour at the bottom of the spectrum of the original operator). We employ instead a *high contrast* ("non-classical") homogenization, introducing another small parameter of contrast $\delta = \epsilon_1 - k^2$. It is known, see [1] that if $\delta \to 0$ then gaps appear in spectrum of operator $A_R(k^2)$. But here we are going to apply different strategy based on homogenization approach which is now natural since we have small periodicity cells. The limit behavior then depends on the relation between δ and R, and one can see that there is only one "critical" scaling $\delta(R) \sim R^{-2}$, the so-called "double-porosity" scaling, when the phenomena at the micro and macro scales are coupled in a non-trivial way, see [2] for precise details.

It then appears that the "limit" problem (in contrast to the classical homogenization) is "two-scale", and recently developed techniques of *two-scale convergence* appear an appropriate tool, see e.g. [3] for recent developments and further references therein. In particular, one can well define the two-scale limit operator A_0, which is self-adjoint in a subspace of $L^2(\mathbb{R}^n \times Q)$ (Q in the periodicity cell in the "fast" variable y). The unperturbed part of the limit operator has an explicitly described band-gap structure, cf. [3], and we show that the perturbed limit operator may develop explicit extra point spectrum in the gaps [2]. We show that extra point spectrum converges to point spectrum of following spectral problem with nonlinear dependence on spectral parameter:

$$-\nabla \cdot a_1 \nabla u_0(x) = \lambda_0 u_0(x), \;\; x \in \Omega, \qquad (1)$$

$$-a_1 \nabla \cdot A^{\hom} \nabla u_0(x) = \beta(\lambda_0) u_0(x), \;\; x \in \mathbb{R}^n \backslash \Omega, \qquad (2)$$

$$(u_0)_- = (u_0)_+ ,$$

$$\left(\frac{\partial u_0}{\partial n}\right)_- = \left(A_{ij}^{\hom} \frac{\partial u_0}{\partial x_j} n_i\right)_+ , \; x \in \partial\Omega_2. \qquad (3)$$

Where A_{ij}^{hom} is a standard porous matrix for Laplacian in $\widetilde{Q}_1$, $a_1 = \lim R^{-2}(\epsilon_1 - k^2)^{-1}$ and $a_0 = (\epsilon_0 - \epsilon_1)^{-1}$ and finally

$$\beta(\lambda) := \lambda + \lambda^2 \sum_{j:\, \langle \varphi_j \rangle_y \neq 0} \frac{\langle \varphi_j \rangle_y^2}{\lambda_j - \lambda} \qquad (4)$$

is the function introduced by Zhikov [3], see Figure 1, λ_j and $\varphi_j(y)$ be the eigenvalues and the (normalized) eigenfunctions respectively of $-a_0 \Delta_y$ in Q_0 with Dirichlet boundary conditions on ∂Q_0 (Δ_y is the Laplace operator).

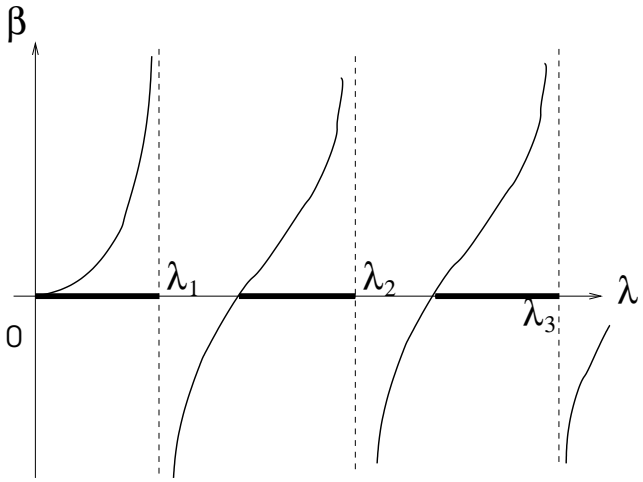

Figure 1: Function $\beta(\lambda)$

We then prove that, for big enough R, near every eigenvalue λ_0 there exists an eigenvalue $\lambda(R)$ of the original operator $A_R^d(k^2)$ ($\epsilon_1 - k^2 \sim R^{-2}$), with an error bound

$$|\lambda(R) - \lambda_0| \leq C\, R^{-1/2}.$$

The proof employs a Rayleigh-type variational principle, with appropriately modified formal asymptotic approximations serving as test functions, and the above error bound is an the effect of a boundary layer in the high-contrast homogenization, see [2] for details.

Let us notice that if Q_0 and Ω are balls then spectral problem (1)-(3) admits an explicit solution in terms of special functions.

References

[1] S.Soussi, "Modeling photonic crystal fibers", Adv. in Appl. Math. 36, no. 3, 288–317, 2006.

[2] I.V. Kamotski and V.P. Smyshlyaev, *Localised eigenstates due to defects in high contrast periodic media via homogenisation*. BICS preprint 3/06, http://www.bath.ac.uk/math-sci/bics/preprints/BICS06_3.pdf (2006)

[3] V.V. Zhikov, *On an extension of the method of two-scale convergence and its applications*, (Russian) Mat. Sb. **191** (2000), 31–72; English translation in Sb. Math. **191** (2000), 973–1014.

INVISIBILITY DEVICES: GENERAL RELATIVITY IN ELECTRICAL ENGINEERING

U. Leonhardt*, **T. G. Philbin**
School of Physics and Astronomy, University of St Andrews, St Andrews, UK
*Email: ulf@st-andrews.ac.uk

Abstract

The recent breakthroughs in invisibility devices are a result of advances in theoretical optics and in material science. On the theoretical side, invisibility devices are an example of *transformation media*—media that, as far as electromagnetism is concerned, perform active coordinate transformations. General relativity provides the theoretical tools for calculating the material properties required to achieve a given transformation. The development of electromagnetic metamaterials allows electrical engineers to implement the design recipes of transformation media.

Introduction

Recently, the first prototype of an invisibility device was made at Duke University, USA [1], inspired by theoretical work at Duke, Imperial College [2] and St Andrews [3] (see Fig. 1). So far, such a device operates for fixed frequencies in the microwave region of the electromagnetic spectrum, thus making objects invisible for specific microwave eyes only. Nevertheless, Science and Scientific American [5] regarded this demonstration as one of the major research and technology breakthroughs of 2006. This cloaking device vividly illustrates one of the recent advances in material science, namely the development of electromagnetic metamaterials [4], and it is also based on a new theoretical concept, transformation media [2], [3], [6]. A transformation medium performs an active coordinate transformation: electromagnetism in physical space, including the effect of the medium, is equivalent to electromagnetism in transformed coordinates where space appears to be empty. The sole function of the device is to facilitate such a transformation.

The theory of transformation media requires us to consider transformations between arbitrary coordinate systems, and the most efficient mathematical tools for dealing with arbitrary coordinates are provided by differential geometry, which also underpins Einsteins general relativity. Cloaking thus combines some highly abstract ideas that normally belong to the physics of curved space, general relativity, with one of the latest and most active trends in engineering. The practical use of general relativity in electrical engineering may seem surprisingly unorthodox:

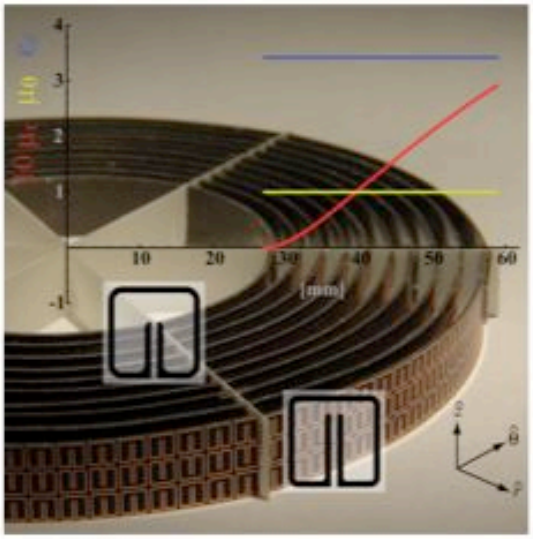

Figure 1: Duke cloaking device [1]. The picture shows the 2D microwave cloaking structure (background image) with a plot of the material parameters that are implemented. A metamaterial made of cells etched in circuit board guides microwave radiation around the interior of the cloak without causing significant distortions. Such devices turn out to represent applications of general relativity in electrical engineering [6].

relativity is associated with the physics of gravitation and cosmology, the physics of black holes or the expanding universe. Due to the development of transformation media, however, the theoretical tools for dealing with these exotic systems can also be used to design engineering devices.

Theory

An invisibility device is supposed to guide light around any object put inside it as if the object were not there. The recipe [2] for invisibility employs an optical medium that mimics a transformation from straight to curved coordinates. To understand why, imagine the following thought experiment: suppose one sends a grid of laser beams through a transparent material. The medium bends the light grid, but suppose this grid fits the lines of a curved coordinate system. Since light itself spans the coordi-

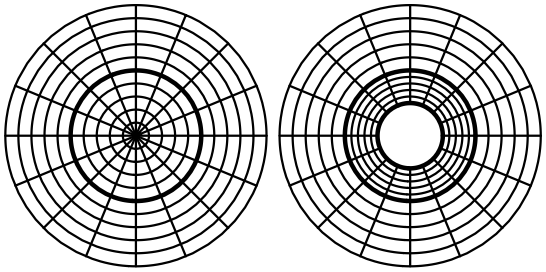

Figure 2: Two-dimensional invisibility device. The active coordinate transformation performed by the device; the transformation consists of blowing up the origin in the left grid into the hole seen on the right grid so that the grid inside the dark circle gets squeezed.

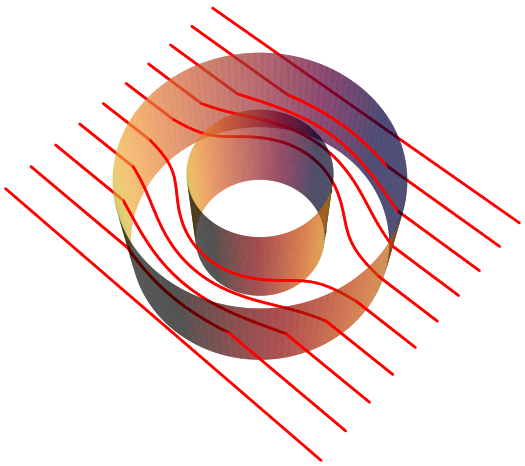

Figure 3: Two-dimensional invisibility device. The effect of the transformation of Fig. 2 on light rays; no light penetrates the inner cylinder.

nates, all light rays are straight lines here, relative to this system, regardless how curved they appear in physical space. All the medium does is a coordinate transformation from Cartesian coordinates. Now, if this transformation contains a hole, if real space is not fully covered, the medium acts as an invisibility device where everything inside is hidden. However, not all transparent media perform coordinate transformations. (Otherwise, invisibility would be commonplace.) A combination of Maxwells electromagnetism and Einsteins general relativity clarifies the precise recipes for invisibility devices [6]. Light is an electromagnetic wave subject to Maxwells equations for the electric field E, the displacement D, the magnetic induction B and the magnetic field H. Remarkably, Maxwells equations are the same in any coordinate system, no matter how curved. Einsteins general relativity supplements them with the constitutive equations that connect E and B to D and H [6]. If the medium is designed to fit the constitutive equations of transformed space, it performs the transformation [2], [3], [6]. Light follows the curved coordinate lines and they may be chosen to guide any light around a region of space. Anything placed there is invisible see Figs. 2 and 3.

Perfect invisibility devices such as that described in Figs. 2 and 3 require anisotropic media. For devices based on isotropic media invisibility can be perfect within the accuracy of geometrical optics [3]. A recipe for invisibility in this case is given by the theory of optical conformal mapping [3]. This theory is based on the fact that conformal transformations of the two-dimensional Helmholtz equation are equivalent to transforming the refractive-index profile: in this case the active coordinate transformation performed by the medium is a conformal mapping. Fig. 4 shows an example of a conformal invisibility device.

The practical demonstration of invisibility [1] requires the use of artificial metamaterials [4], because naturally occurring materials have not sufficiently strong electromagnetic properties. What are metamaterials? All materials consist of atoms, but usually an electromagnetic wave does not interact with them on an individual basis. The wave averages over volumes roughly the size of the wavelength cubed. The engineers of metamaterials create sub-wavelength structures in otherwise normal material, for example the cells in the ordinary circuit board shown in Fig. 1, designer structures that electromagnetic waves would not resolve; and so they make their very own electromagnetic atoms. In contrast to natural atoms, the artificial ones are controllable. This is easiest for electromagnetic waves with sizeable wavelengths, say a few centimetres, like the radio waves used by mobile phones or radar, but exotic metamaterials for visible light have been already demonstrated [8].

So far, electromagnetic cloaking [1] relies on highly dispersive metamaterials, because the theoretical recipes [2], [3] require the use of materials with anomalous phase-velocity dispersion [7], which limits the performance of cloaking devices to single frequencies. Cloaking devices or devices based on similar principles will first find applications in wireless technology, because currently the most-advanced metamaterials are those that respond to electromagnetic radiation with wavelengths of a few centimetres, commonly used by mobile phones, Bluetooth or radar. Applications for visual light are conceivable, because one could use modern nanotechnology

for scaling down the principal structures of microwave metamaterials to sizes below optical wavelengths. First advances in this field have been published already [8]. The tantalizing ideas of invisibility are likely to motivate significantly more research on optical metamaterials that, in combination with new theoretical concepts for avoiding dispersion, can pave the way towards optical cloaking.

References

[1] D. Schurig *et al.*, Science, vol. 314, p. 977, 2006.

[2] J.B. Pendry, D. Schurig and D.R. Smith, Science, vol. 312, p. 1780, 2006.

[3] U. Leonhardt, Science, vol. 312, p. 1777, 2006.

[4] D. R. Smith, J. B. Pendry and M. C. K. Wiltshire, Science, vol. 305, p. 788, 2004.

[5] http://www.sciencemag.org/sciext/btoy2006/; D. Musser, Sci. Am., p. 54, December 2006.

[6] U. Leonhardt and T. G. Philbin, New J. Phys., vol. 8, p. 247, 2006.

[7] M. Born and E. Wolf, Principles of Optics, Cambridge University Press, Cambridge, 1999.

[8] S. Zhang *et al.*, Phys. Rev. Lett., vol. 95, p. 137404, 2005; G. Dolling *et al.*, Opt. Lett., vol. 30, p. 3198, 2005; V. M. Shalaev *et al.*, Opt. Lett., vol. 30, p. 3356, 2005; A. N. Grigorenko *et al.*, Nature, vol. 438, p. 335, 2005.

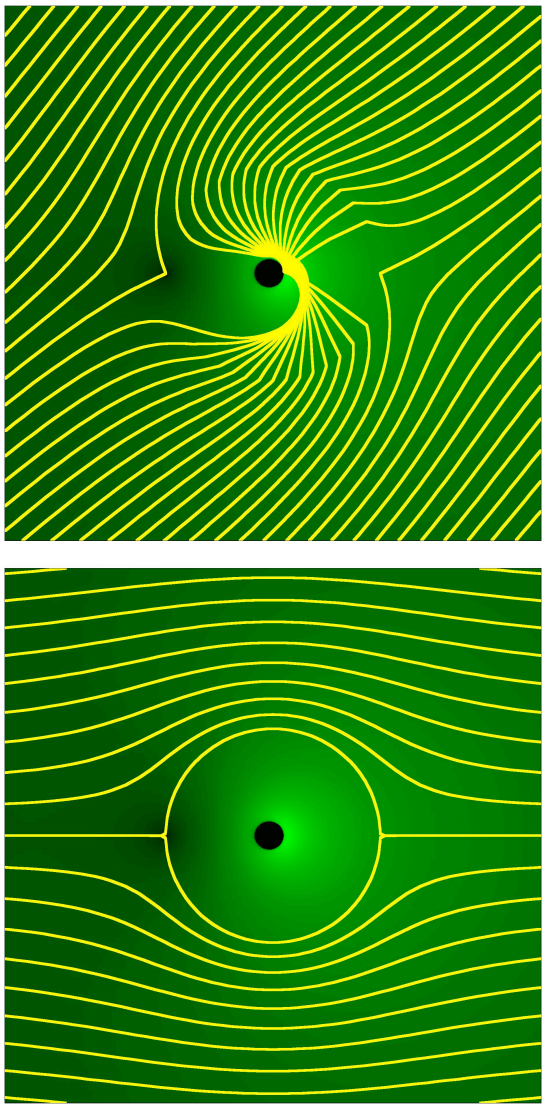

Figure 4: Light propagation in a conformal invisibility device. The device consists of an exterior and an interior layer with a clear boundary. The invisible region is the black disk in the centre. The top figure illustrates how light is refracted at the boundary between the two layers and guided around the invisible region. In the bottom figure light simply flows around the interior layer.

PLASMONICS THROUGHOUT THE SPECTRUM: SUB-WAVELENGTH ENERGY CONFINEMENT FOR WAVEGUIDING, SPECTROSCOPY AND SENSING

Stefan A. Maier[†,*]
[†]Centre for Photonics and Photonic Materials, Department of Physics, University of Bath, Bath, UK.
[*]Email: s.maier@bath.ac.uk

The confinement of electromagnetic energy to volumes below the diffraction limit leads to a concomitant field enhancement, enabling a wealth of opportunities for sensing and spectroscopy. One of the challenges is to create such confinement in a controlled manner, and to channel electromagnetic energy from conventional, wavelength-scale devices such as planar waveguides and optical fibres down to the nanoscale. The field of plasmonics holds the promise of achieving this via the excitation of electromagnetic surface modes at the interface between a conductor and a dielectric. Depending on the exact geometry and the frequency of the electromagnetic radiation, a deep sub-wavelength mode size is possible.

In the first part of the talk, we will present results for the controlled focusing of electromagnetic radiation at frequencies from the visible to the THz regime to sub-wavelength volumes, with a view to applications in biological sensing. While for visible and near-infrared frequencies conical metallic tips coupled to conventional optical waveguides are a convenient means for nanoscale focusing, at lower frequencies the situation is more challenging. Here, the frequency of excitation is far below the intrinsic plasma frequencies of metallic conductors, and surface plasmon polaritons acquire the character of delocalized Sommerfeld-Zenneck waves. Sub-wavelength energy localization can however be achieved periodic surface structuring, leading to designer electromagnetic surface modes termed spoof surface plasmon polaritons. While structured planar surfaces enable a new infrastructure for THz technology, corrugated cylindrical and conical structures show a high promise for the guiding and super-focusing of THz radiation (Figure). Analytical and numerical electromagnetic modelling of such structures will be discussed, and first implementations be presented.

In the second part of this talk, we will discuss various approaches for confining electromagnetic energy at visible and near-infrared frequencies using hybridized modes in designer cavities consisting of planar metallic structures with nanoscale gaps. Results from finite difference time domain simulation and near-field optical spectroscopy will be presented, and implications for biosensing discussed.

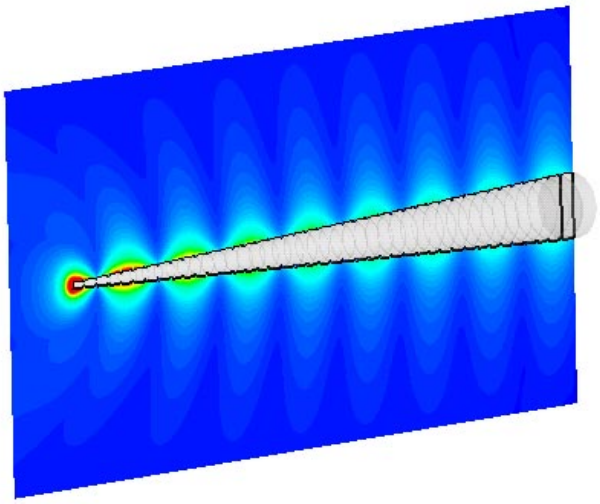

Figure 1: Focusing of electromagnetic radiation at 0.6THz on a corrugated conical taper via spoof surface plasmon polaritons.

ELECTROMAGNETIC CLOAKING THROUGH PLASMONIC RESONANCE

R. C. McPhedran[†,*], **G. W. Milton**[‡], **N. A. Nicorovici**[♯], **and L. C. Botten**[♯]
[†]CUDOS, School of Physics, University of Sydney, Sydney, NSW, Australia
[‡]Department of Mathematics, University of Utah, Salt Lake City, Utah, USA
[♯]Department of Mathematical Sciences, University of Technology Sydney, Sydney, NSW, Australia
[*]Email: Ross@physics.usyd.edu.au

Abstract

There is much current interest in electromagnetic cloaking of objects, by exploiting structured materials. One approach has been pioneered by J.B. Pendry [1] and U. Leonhardt [2], and exploits metamaterials to create electromagnetic guiding around the region to be shielded (internal cloaking). A second approach [3], [4] uses electromagnetic resonances in a coated cylinder, designed to have a resonant interaction between its coating and the surrounding material, to quench polarization responses in dipoles within an analytically-determined cloaking region surrounding the cylinder (external cloaking). We have extended the treatment of [4] to include interacting systems of polarizable dipoles or quadrupoles, and present animations illustrating that resonant cloaking still works for complicated assemblies of dipoles, or for higher order multipoles, and that the cloaking region does not depend on the details of the entity to be cloaked. We comment on the resolution inherent in the external cloaking process, which is linked to the material properties of the metamaterial composing the shell of the cloaking cylinder.

References

[1] J.B. Pendry, D. Schurig, and D.R. Smith, "Controlling Electromagnetic Fields", Science, vol. 312, 1780–1782, 2006.

[2] U. Leonhardt, "Notes on conformal invisibility devices", New J. Phys., 8, 118, 2006.

[3] N.A. Nicorovici, R.C. McPhedran, and G.W. Milton, "Optical and dielectric properties of partially resonant composites", Phys. Rev. B, 49, 8479, 1994.

[4] G.W. Milton, and N.A. Nicorovici, Proc. Roy. Soc. A, 462, 3027 (2006). G.W. Milton, and N.A. Nicorovici,"On the cloaking effects associated with anomalous localized resonance", Proc. Roy. Soc. A 462, 3027–3059, 2006.

BLOCH-FLOQUET WAVES IN PERIODIC STRUCTURES WITH COATED INCLUSIONS

N. V. Movchan
Department of Mathematical Sciences, University of Liverpool, Liverpool, UK
Email: nvm@liv.ac.uk

Abstract

We present a mathematical model describing propagation of elastic waves in a composite medium containing an array of two-phase inclusions. Each inclusion consists of a core and a finite width coating; the displacements and tractions are assumed to remain continuous across each interface. We consider two types of problems: transmission problems for waves interacting with a finite thickness composite slab, and spectral problems for doubly periodic arrays of inclusions. In the case when all the interface boundaries are circular, we derive series representations of the Rayleigh type for the components of the displacements and analyse transmission/dispersion diagrams. We look for stop bands, the intervals of frequencies corresponding to waves that cannot propagate through the structure. Numerical examples illustrate the effect of the material properties of the coating on the position and the width of stop bands.

Scattering problem for a finite stack of gratings

We first analyse the propagation of elastic waves in an elastic medium containing an array of two-phase circular cylindrical inclusions. The cylinders are of infinite length with their axes parallel to the z-axis; they are periodically spaced in the (horizontal) x-direction. The array is finite in the (vertical) y-direction, and the spacing between the cylinder axes is D. Each cylindrical inclusion is of radius r_c, and it consists of a core of radius r_1 surrounded by a coating of width $r_c - r_1$. All three phases - the core, the coating and the surrounding matrix - are isotropic and linearly elastic with the elastic moduli λ_i, μ_i and densities ρ_i (where $i = 0, 1, 2,$ is for the core, the coating and the elastic matrix, respectively); they are bonded in such a way that the displacements and tractions remain continuous across each interface.

We assume that the incident wave is a time-harmonic plane wave propagating in the xy-plane, and it excites reflected and transmitted plane waves respectively above and below the stack; the direction of the incident wave is characterised by the angle θ_i. Our objective is to study the scattering of such a wave by the stack and, in particular, to look for band gaps, the intervals of frequencies for which waves cannot propagate through the structure.

The vectors $\mathbf{u}^{(i)},\ i = 0, 1, 2,$ of the amplitudes of the elastic displacements satisfy the equation of motion in each phase

$$\mu_i \Delta \mathbf{u}^{(i)}(\mathbf{x}) + (\lambda_i + \mu_i)\nabla\nabla\cdot\mathbf{u}^{(i)}(\mathbf{x}) + \rho_i\omega^2\mathbf{u}^{(i)}(\mathbf{x}) = \mathbf{0}, \tag{1}$$

and the continuity conditions on the interface boundaries

$$[\boldsymbol{\sigma}\mathbf{n}] = \mathbf{0},\ \ [\mathbf{u}] = \mathbf{0}, \tag{2}$$

where $\boldsymbol{\sigma}$ denotes the stress tensor, and ω is the angular frequency.

Since we consider plane waves only, the problem can be de-coupled into two: out-of-plane shear (scalar) problem and in-plane (vector) problem. The out-of-plane shear problem (for the u_z-component) is formally identical to the problem of scattering of electromagnetic waves in the case where the magnetic field vectors of both incident and scattered fields are aligned with the z-axis (H_z polarisation), we do not discuss it here and refer the reader to [1], [2].

For the coupled in-plane problem, we use the scalar and vector potentials $\varphi^{(i)}$ and $\boldsymbol{\Psi}^{(i)} = (0, 0, \psi^{(i)})$ for dilatational and shear waves, such that

$$\mathbf{u}^{(i)} = \nabla\varphi^{(i)} + \nabla\times\boldsymbol{\Psi}^{(i)},\ \ i = 0, 1, 2.$$

These potentials satisfy the Helmholtz equations

$$(\Delta + k_d^{(i)2})\varphi^{(i)} = 0,\ \ (\Delta + k_s^{(i)2})\psi^{(i)} = 0, \tag{3}$$

where $k_d^{(i)} = \omega/v_d^{(i)}$, $k_s^{(i)} = \omega/v_s^{(i)}$, and v_d, v_s are the velocities of dilatational (type d) and shear (type s) waves respectively. The interface conditions couple the potentials:

$$\left[\frac{\partial\varphi}{\partial r} + \frac{1}{r}\frac{\partial\psi}{\partial\theta}\right] = 0,\ \ \left[\frac{1}{r}\frac{\partial\varphi}{\partial\theta} - \frac{\partial\psi}{\partial r}\right] = 0, \tag{4}$$

$$\left[\mu\left(-\frac{2}{r^2}\frac{\partial\varphi}{\partial\theta} + \frac{2}{r}\frac{\partial^2\varphi}{\partial\theta\partial r} + k_s^2\psi + \frac{2}{r}\frac{\partial\psi}{\partial r} + \frac{2}{r^2}\frac{\partial^2\psi}{\partial\theta^2}\right)\right] = 0, \tag{5}$$

$$\left[2\mu\left(\frac{1}{r}\frac{\partial^2\psi}{\partial\theta\partial r} - \frac{1}{r^2}\frac{\partial\psi}{\partial\theta} - \frac{1}{r}\frac{\partial\varphi}{\partial r} - \frac{1}{r^2}\frac{\partial^2\varphi}{\partial\theta^2}\right) - k_d^2(2\mu + \lambda)\varphi\right] = 0, \tag{6}$$

where (r, θ) are the polar coordinates associated with the centre of every inclusion. All potentials $\varphi^{(i)}$ and $\psi^{(j)}$ satisfy the quasi-periodicity conditions

$$\varphi^{(j)}(x + D, y) = \varphi^{(j)}(x, y)e^{ik_{0x}D}, \tag{7}$$

$$\psi^{(j)}(x + D, y) = \psi^{(j)}(x, y)e^{ik_{0x}D}, \tag{8}$$

where $\mathbf{k} = (k_{0x}, k_{0y})$ is the Bloch vector, and D is the spacing between the inclusions.

We first construct the solution of the scattering problem for a single grating by writing the multipole expansions for the potentials $\varphi^{(j)}$ and $\psi^{(j)}$:
• within the core ($j = 0,\ r < r_1$):

$$\varphi^{(0)} = \sum_{l=-\infty}^{\infty} C_l^d J_l(k_d r)e^{il\theta},\ \psi^{(0)} = \sum_{l=-\infty}^{\infty} C_l^s J_l(k_s r)e^{il\theta},$$

• within the coating ($j = 1,\ r_1 < r < r_c$) and the surrounding matrix ($j = 2,\ r > r_c$):

$$\varphi^{(j)} = \sum_{l=-\infty}^{\infty} [A_l^{(j,d)} J_l(k_d r) + B_l^{(j,d)} Y_l(k_d r)]e^{il\theta},$$

$$\psi^{(j)} = \sum_{l=-\infty}^{\infty} [A_l^{(j,s)} J_l(k_s r) + B_l^{(j,s)} Y_l(k_s r)]e^{il\theta},$$

where J_l and Y_l are the Bessel functions of the first and second kind respectively.

Using the interface conditions (4)-(6) we eliminate the coefficients C^d and C^s and couple the two sets of the multipole coefficients A and B. We then reduce the problem to finding the coefficients $B^{(2)}$ using the Rayleigh identity [2]. The system of equations for the multipole coefficients $B_l^{(2,d)}$ and $B_l^{(2,s)}$ has the form

$$iM_l^{(dd)} B_l^{(2,d)} + iM_l^{(ds)} B_l^{(2,s)} + \sum_{m=-\infty}^{\infty} S_{l-m}^d B_m^{(2,d)}$$

$$= -i\delta_d(-1)^l \frac{((\chi_{0d} + ik_{0x})/k_d)^{-l}}{\sqrt{\chi_{0d}}}, \tag{9}$$

$$iM_l^{(sd)} B_l^{(2,d)} + iM_l^{(ss)} B_l^{(2,s)} + \sum_{m=-\infty}^{\infty} S_{l-m}^s B_m^{(2,s)}$$

$$= -i\delta_s(-1)^l \frac{((\chi_{0s} + ik_{0x})/k_s)^{-l}}{\sqrt{\chi_{0s}}}, \tag{10}$$

where S^d, S^s are the lattice sums, the other notations are the same as in [2]. The expressions and numerical algorithms for calculation of the lattice sums are given in in [1]-[3].

The system (9), (10) is truncated prior to its numerical solution, so l is restricted to the range $[-L, L]$, with L typically exceeding $2k_s r_c$ to guarantee rapid convergence of results.

The reflection and transmission coefficients ρ_p^d, ρ_p^s and τ_p^d, τ_p^s, which form the reflection and transmission matrices R and T for a single grating, are evaluated from the reconstruction equations [2]. The scattering matrices for a single grating are then employed in a recurrence procedure [1], [2] to find the total reflection and transmission matrices for a stack of N gratings. The results of numerical calculations for normal incidence ($\theta_i = 0$) are given in the next section.

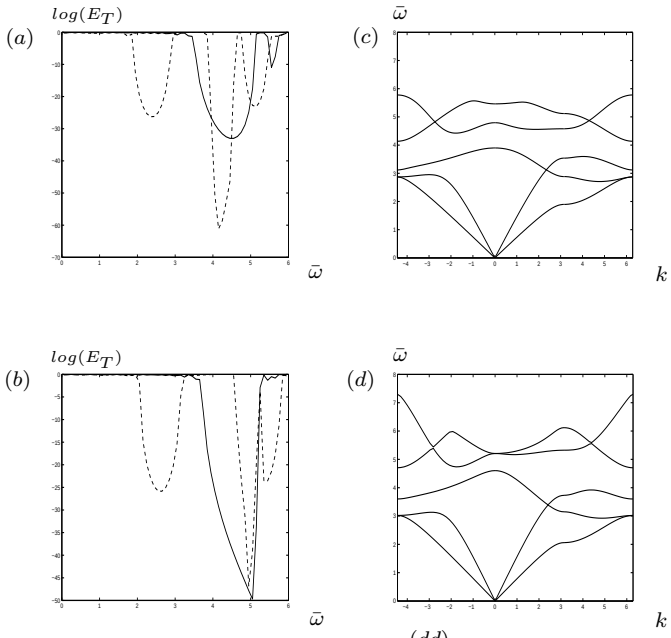

Figure 1: Transmittances $log(E_T^{(dd)})$ (solid line) and $log(E_T^{(ss)})$ (dashed line) versus $\bar{\omega} = \omega D/v_s$ for a stack of 20 gratings of coated inclusions of total radius $r_c = 0.3$ in Al matrix: (a) Cu circular core ($r_1 = 0.15$) and Ta coating ; (b) Ta circular core ($r_1 = 0.15$) and Cu coating. The dispersion diagrams (c) and (d) correspond to doubly periodic arrays of such inclusions.

Numerical examples and discussion

In Figs 1a and 1b we plot the total transmittances

$$E_T^{dd} = \sum_{p \in \Omega_d} |\tau_p^d|^2, \quad E_T^{ss} = \sum_{p \in \Omega_s} |\tau_p^s|^2$$

for a stack of 20 gratings. The dispersion diagrams 1d and 1c correspond to doubly periodic arrays; they were generated by solving a homogeneous system (9), (10) with the

lattice sums for a doubly periodic array of inclusions, and then verified by independent finite element computations (Comsol 3.2).

The diagrams 1a and 1c (for inclusions with Cu core and Ta coating) show a stop band for $\bar{\omega} \in [3.88, 4.11]$; the diagrams 1b and 1d (which correspond to inclusions with Ta core and Cu coating) exhibit a more narrow stop band in the range of frequencies $[4.58, 4.69]$. This example clearly shows the effect of the material arrangement within the inclusion on the position and the width of the stop band.

The other issue we want to address in this paper is standing waves or localised vibration modes which may form in arrays of high contrast coated inclusions [4]. In Fig. 2 we present results of finite element computations (Comsol 3.2) for doubly periodic arrays of two-phase inclusions with Ta core and Mg coating in Al matrix: the diagram 2a corresponds to the case of a circular core, and the diagram 2b is for an elliptical core of the same area. As both diagrams of Fig. 2 show, the amplitude of the elastic displacements is almost zero outside the inclusions, and it changes quite rapidly near the interface boundary: uniformly along the entire interface boundary for the circular core, and near the points of the largest curvature for the elliptical core.

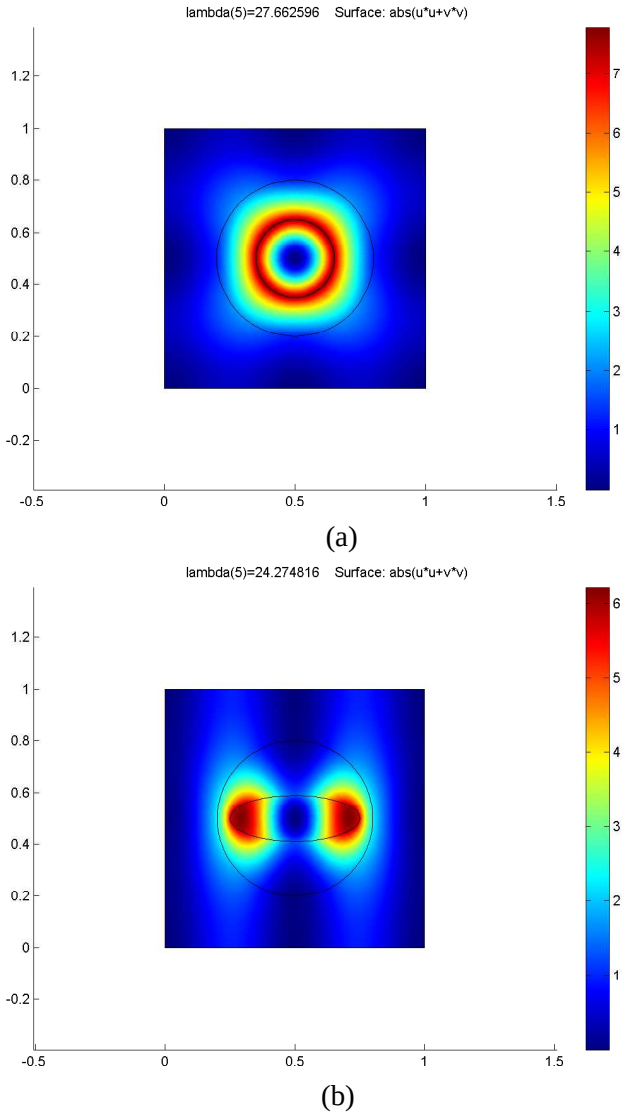

Figure 2: Localised vibration mode for a square array of (high contrast) coated inclusions of total radius $r_c = 0.3$ with Ta core (of radius $r_1 = 0.15$) and Mg coating in Al matrix; both diagrams show the amplitude of the elastic displacements:(a) circular core of radius $r_1 = 0.15$, (b) elliptical core of the same area as in (a) with $a = 0.25$, $b = 0.09$.

References

[1] L.C. Botten, N.A. Nicorovici, A.A. Asatryan, R.C. McPhedran, C.M. de Sterke and P.A. Robinson, "Formulation for electromagnetic scattering and propagation through grating stacks of metallic and dielectric cylinders for photonic crystal calculations", J. Opt. Soc. Am. A, vol. 17, Part I: pp. 2165-2176; Part II: pp. 2177-2190, 2002.

[2] S.B. Platts, N.V. Movchan, R.C. McPhedran and A.B. Movchan, "Two-dimensional phononic crystals and scattering of elastic waves by an array of voids", Proc. Roy. Soc. Lond. A, vol. 458, pp. 2327-2347, 2002.

[3] S.B. Platts, N.V. Movchan, R.C. McPhedran and A.B. Movchan, "Band gaps and elastic waves in disordered stacks: normal incidence", Proc. Roy. Soc. Lond. A, vol. 459, pp. 221-240, 2003.

[4] A.B. Movchan, N.V. Movchan and S. Haq, "Localised vibration modes and stop bands for continuous and discrete periodic structures", Materials Science and Engineering A, vol. 431, pp. 175-183, 2006.

CONVERGENCE ANALYSIS OF PLANEWAVE EXPANSION FOR BAND GAP COMPUTATIONS IN PHOTONIC CRYSTAL FIBRES

Richard A. Norton[†,*], **Robert Scheichl**[†]
[†]Department of Mathematical Sciences, University of Bath, Bath, UK
[*]Email: ran20@maths.bath.ac.uk

Abstract

In this paper we consider the numerical computation of band gaps in photonic crystal fibres. We approximate the solution to a variational eigenvalue problem using the planewave expansion method (spectral Galerkin method). As well as presenting implementation and error analysis results we consider solving a modified problem where the piecewise constant coefficient function is replaced with a smooth function. The error analysis for the smooth problem is also presented and we answer the question: Is smoothing worth it?

Introduction

Photonic crystal fibres (PCFs) [1] are optical fibres that have a core surrounded by cladding. The structure of a PCF is described by its refractive index n. n is constant along the length of the fibre (z-axis) and we write $n = n(x, y)$. The function $n(x, y)$ is a piecewise constant function representing the refractive index of two materials. Light will be described by its frequency ω and its propagation constant in the z-direction β.

For certain designs of cladding and fixed frequency ω, light propagation in the cladding may be forbidden for some values of β. These values of β are called *band gaps*. If light is forbidden in the cladding and is permitted in the core then we have a *defect mode*. We are interested in finding band gaps and defect modes by approximating the solution to Maxwell's equations.

We restrict ourselves to the case where $n = n(x)$. Physically, this is the case of a radially symmetric PCF or a planar PCF. Using time harmonic, source free Maxwell's equations for a non-magnetic material the problem decouples into two eigenvalue problems

$$\frac{d^2 h_x}{dx^2} + \gamma(x) h_x = \beta^2 h_x \quad \text{on } \mathbb{R} \qquad \text{(TE)}$$

$$\frac{d^2 h_y}{dx^2} + \gamma(x) h_y - \frac{d\eta(x)}{dx}\frac{dh_y}{dx} = \beta^2 h_y \quad \text{on } \mathbb{R}. \qquad \text{(TM)}$$

where $\gamma(x) := \frac{4\pi^2}{\lambda_0^2} n^2(x\Lambda)$, $\eta(x) := \log\left(n^2(x\Lambda)\right)$, h_x is the x-component of the magnetic field, h_y is the y-component of the magnetic field, Λ is the period of the microstucture in the cladding and λ_0 is the wavelength of light relative to Λ. The remaining components of the magnetic and electric fields are uniquely determined given β, h_x and h_y.

Here we will mainly concentrate on the TE (*transverse electric*) mode problem. To make the operator in (TE) positive definite we multiply it by -1 and shift it by a constant K (sufficiently large). We apply the supercell method [1], [2] with supercell width L followed by a Floquet transform. This reduces (TE) to a family of eigenproblems on the period cell $Q := [-\frac{L}{2}, \frac{L}{2}]$. The variational form of the reduced problem is: for fixed $\xi \in [-\frac{\pi}{L}, \frac{\pi}{L}]$, find eigenpairs (λ, u) where $\lambda \in \mathbb{C}$ and $u \in H^1_p(Q) := \{u \in H^1(Q) : u(\frac{L}{2}) = u(-\frac{L}{2})\}$ with $\|u\|_{H^1} = 1$ such that

$$a(u, v) = \lambda\, b(u, v) \qquad \forall v \in H^1_p(Q), \qquad (1)$$

$$a(u, v) := \int_Q \left(\tfrac{d}{dx} + i\xi\right) u \, \overline{\left(\tfrac{d}{dx} + i\xi\right) v} + (K - \gamma)\, u\overline{v}\, dx$$

$$b(u, v) := \int_Q u\overline{v}\, dx.$$

The operator associated with (1) is compact and has discrete spectrum. As functions of ξ the eigenvalues $\lambda(\xi)$ form bands which coincide with the continuous spectrum of the operator in (TE) [3]. The bands may overlap or have gaps (*band gaps*). To compute these bands it is sufficient to solve (1) for $\xi = 0$ and $\frac{\pi}{L}$ [3]. We are only interested in the low end of the spectrum of (TE) and thus in a few of the smallest eigenvalues of (1).

In this work we study two methods to solve (1). Method 1 applies the standard planewave expansion method [1], [4]. In Method 2 we modify the problem by (artificially) smoothing $\gamma(x)$ and then apply the planewave expansion method to the modified problem. This is a commonly used approach in Theoretical Physics to improve the convergence properties of the planewave expansion method [4], [5]. However, we show here that smoothing does not pay off and that the convergence rates to the exact solution are not improved. We present an error analysis for both methods and include some numerical results which confirm the sharpness of our theoretical results. We also include numerical results for the TM (*transverse magnetic*) mode problem. Unfortunately, due to the nonstandard "convective" term $\frac{d\eta(x)}{dx}\frac{dh_y}{dx}$ in (TM),

we have so far not been able to fully extend our convergence analysis to this case. For details and proofs of the implementation and error analysis please refer to [6].

In the following, $C \lesssim D$ (for two quantities C, D) means that C/D is bounded above independent of the discretisation parameters N, M and Δ (defined below).

Method 1 - discontinuous refractive index

We approximate (1) by using the planewave expansion (spectral Galerkin) method. We replace $H^1_p(Q)$ in (1) with $S_N := \operatorname{span}\{\mathrm{e}^{i2\pi nx/L} : |n| \leq N\} \subset H^1_p(Q)$ to get the following finite dimensional problem: for fixed $\xi \in [-\frac{\pi}{L}, \frac{\pi}{L}]$, find eigenpairs (λ_N, u_N) where $\lambda_N \in \mathbb{C}$ and $u_N \in S_N$ with $\|u_N\|_{H^1} = 1$ such that

$$a(u_N, v_N) = \lambda_N b(u_N, v_N) \qquad \forall v_N \in S_N. \quad (2)$$

This problem is equivalent to a $(2N+1) \times (2N+1)$ matrix eigenvalue problem $A\mathbf{u} = \lambda_N \mathbf{u}$ where $\mathbf{u}$ is the vector of Fourier coefficients of u_N. According to the definition of $a(\cdot,\cdot)$ we can write $A := D - V + KI$ where D is diagonal (derivative contributions from a), V is Toeplitz (Fourier coefficients of γ) and I is the identity matrix. The smallest few eigenvalues of A are found using a subspace iteration method, and we use the preconditioned conjugate gradient method (PCG) for the required linear system solves. Matrix-vector products with A can be computed in $\mathcal{O}(N \log N)$ operations using two Fast Fourier Transforms (FFTs). Moreover, we have an optimal preconditioner for A.

Theorem. *Let $C > 1$ and $D_A := \operatorname{diag}(A)$. Then there exists a K such that $\kappa(D_A^{-1}A) \leq C$.*

The following theorem gives a sharp convergence result in the case of the TE problem (with discontinuous γ).

Theorem. *Let (λ_N, u_N) be an eigenpair of* (2)*. Then there exists an eigenpair (λ, u) of* (1) *such that*

$$\|u - u_N\|_{H^1} \lesssim N^{-3/2} \quad \textit{and} \quad |\lambda - \lambda_N| \lesssim N^{-3}.$$

The above result uses exact Fourier coefficients of $\gamma(x)$. In practice we may need to approximate these coefficients. A method for approximating them is to compute a discrete Fourier transform of $\gamma(x)$ sampled on a uniform grid of M points (using one FFT). In this case there is an additional term in the error bounds.

Corollary. *Let $\gamma(x)$ be sampled at M points and let (λ_N, u_N) be an eigenpair of* (2)*. Then there exists an eigenpair (λ, u) of* (1) *such that*

$$\|u - u_N\|_{H^1} \lesssim N^{-3/2} + M^{-1}$$
$$|\lambda - \lambda_N| \lesssim N^{-3} + M^{-1}.$$

This shows that if we choose $M = \mathcal{O}(N)$ (as e.g. in [1], [5]), then we get suboptimal convergence. However, since this method only requires one extra FFT, we may choose $M = N^{3/2}$ at no significant extra cost to recover optimal convergence for the eigenfunction error. The eigenvalue error is still suboptimal in this case. Choosing larger M (e.g. $M = \mathcal{O}(N^3)$) becomes computationally infeasible.

Method 2 - smoothed refractive index

A standard way to smooth $\gamma(x)$ [5] is to replace it with $\widetilde{\gamma}(x) := G * \gamma(x)$ where $G(x)$ is the Gaussian $\frac{1}{\sqrt{2\pi}\Delta} \exp(-\frac{x^2}{2\Delta^2})$, $*$ represents convolution and Δ is a specified length scale. Larger values of Δ result in more smoothing. We carry out the error analysis by splitting the error into two parts: the error introduced by smoothing and the error introduced by using planewave expansion.

Theorem. *Let $(\widetilde{\lambda}_N, \widetilde{u}_N)$ be an eigenpair of* (2) *where γ has been replaced by $\widetilde{\gamma}$. Then there exists an eigenpair (λ, u) of* (1) *such that*

$$\begin{aligned} \|u - \widetilde{u}_N\|_{H^1} &\lesssim \Delta^{3/2} + \Delta^{-p} N^{-p-3/2} \\ |\lambda - \widetilde{\lambda}_N| &\lesssim \Delta^{3/2} + \Delta^{-2p} N^{-2p-3} \end{aligned} \qquad \forall p \in \mathbb{N} \cup \{0\}.$$

Although the eigenfunction error bound is sharp our numerical results (see Fig. 3) show that in practice $|\lambda - \widetilde{\lambda}_N| = \mathcal{O}(\Delta^2)$ for large N. Note that this is not the square of the eigenfunction error as one might expect.

We are still free to choose Δ. By balancing the two error terms for the eigenvalues in the above theorem, we see that the minima in the eigenfunction and in the eigenvalue error are attained for $\Delta = \mathcal{O}(N^{-2})$ and $p = 0$. The minima are $\mathcal{O}(N^{-3/2})$ and $\mathcal{O}(N^{-3})$, respectively. Thus, asymptotically, Method 2 converges no faster than Method 1 for any amount of smoothing. The numerical results below confirm this (see Fig. 4). The situation is the same, if the sharper eigenvalue error bound from our numerical computations is used (i.e. $\mathcal{O}(\Delta^2)$). In this case the minima are attained for $\Delta = \mathcal{O}(N^{-3/2})$.

Numerical Results

We finish by presenting a selection of numerical results that support our theoretical results in the previous section. We choose $\gamma(x)$ as in Figure 1 with $1.0 \leq n(x) \leq 1.4$ and $\lambda_0 := 0.5$. The reference solutions have been computed with $N = 2^{16} - 1$ and we plot the errors for the 1st and 12th eigenpairs as representative examples. Figures 2 and 4 show that our bounds from the previous sections are sharp with respect to N, while Figure 3 shows that our

bound on $|\lambda - \widetilde{\lambda}_N|$ is not sharp and that in practice it behaves like $\mathcal{O}(\Delta^2)$. The eigenfunction result is sharp in this case. Figure 5 demonstrates that the errors for the TM problem behave in a similar way to the TE problem except that the convergence rates are slower. This is expected because the eigenfunctions for the TM problem are only $C(Q)$, and not $C^1(Q)$.

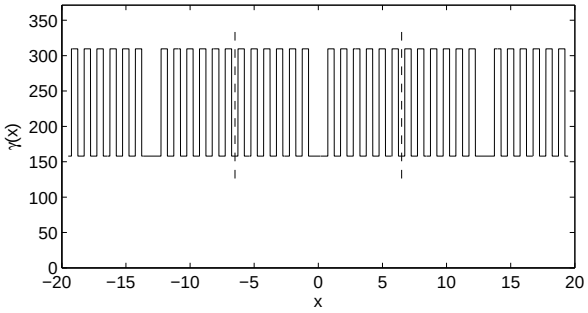

Figure 1: Plot of $\gamma(x)$ used in our computations.

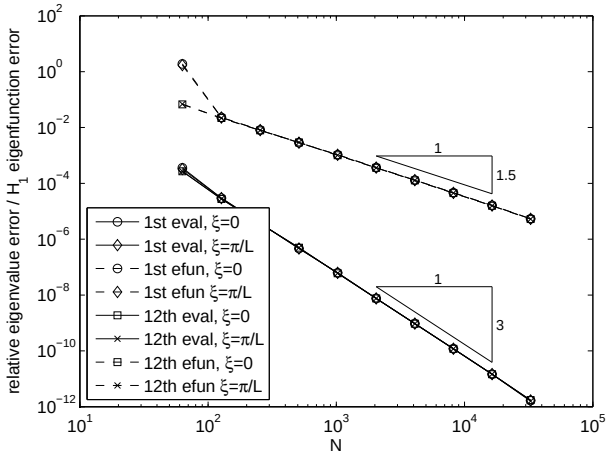

Figure 2: Plot of the errors for Method 1.

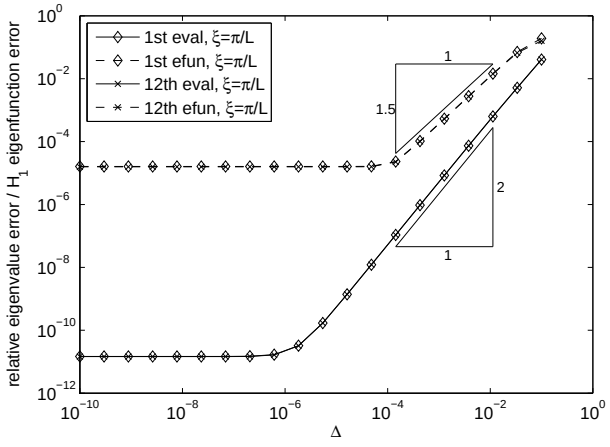

Figure 3: Plot of errors vs. Δ for Method 2.

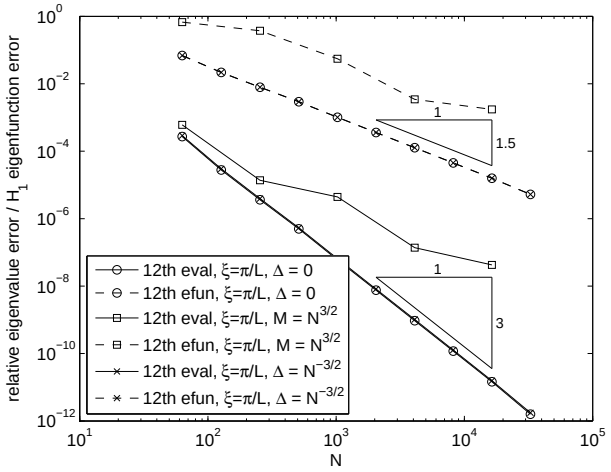

Figure 4: Errors for Method 1 and Method 2.

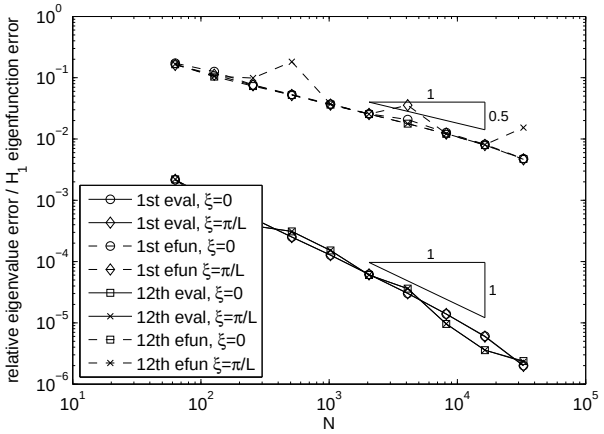

Figure 5: Errors for Method 1 applied to TM mode.

References

[1] J.M. Pottage, D.M. Bird, T.D. Hedley, T.A. Birks, J.C. Knight, P.St.J. Russell, Robust photonic band gaps for hollow core guidance in PCF made from high index glass, *Optics Express* **11**, pp. 2854-2861, 2003.

[2] S. Soussi, Convergence of the supercell method for defect modes calculations in photonic crystals, *SIAM J. Numer. Anal.* **43**, pp. 1175-1201, 2005.

[3] M. Reed & B. Simon, *Methods of Modern Mathematical Physics Vol. 4: Analysis of Operators*, Academic Press, New York, 1978.

[4] S.G. Johnson & J.D. Joannopoulos, Block-iterative frequency-domain methods for Maxwell's equations in a planewave basis, *Optics Express* **8**, pp. 173-190, 2001.

[5] G.J. Pearce, Plane-wave methods for modelling photonic crystal fibre, Ph.D. thesis, University of Bath, 2006.

[6] R.A. Norton & R. Scheichl, Numerical Computation of Band Gaps in Photonic Crystal Fibres, in preparation.

Design and fabrication of an ultra-compact photonic crystal directional coupler

T. P. White*, **D. M. Beggs and T. F. Krauss**
School of Physics and Astronomy, University of St Andrews, St Andrews, UK
*Email: tom.white@st-andrews.ac.uk

Abstract

Planar photonic crystals (PhCs) are a versatile platform for compact optical devices. The strong dispersive effects that can be obtained in such structures, and the ability to control these effects via structural tuning provide unique opportunities to control light propagation. Here we use structural tuning to design a compact directional coupler (DC) with a coupling length of less than $5\,\mu\mathrm{m}$. We consider also the issue of coupling light in and out of the device and demonstrate an efficient input/output coupler. Both experimental and numerical results are presented to verify the operation of the directional coupler.

Introduction

Switching and modulation of light are critical operations in photonic circuits. Switches based on the DC geometry can be used as passive wavelength-selective devices, or as active switches when dynamic tuning is incorporated into the design. When implemented in PhCs, directional couplers with coupling lengths below $10\,\mu\mathrm{m}$ can be achieved [1]–[4].

Recently, Yamamoto *et.al.* [4] reported a theoretical study of DCs and proposed an idealised bandstructure for obtaining short coupling lengths and wide bandwidths. A PhC directional coupler was designed such that the dispersion curves of the coupled modes approximated the ideal geometry, and 2D numerical results were presented. Here we present an alternative DC geometry using a similar design approach and analyse its coupling properties using 3D numerical techniques. In addition, we consider the issue of coupling light in and out of the structure and report on the fabrication and experimental demonstration of the device.

Directional coupler design

Directional couplers operate due to the mode splitting that occurs when two waveguides are placed close together, resulting in a pair of coupled modes with even and odd symmetry. The strength of the coupling is determined by the difference in propagation constants of the two modes, $\Delta k = |k_e - k_o|$, where k_e and k_o are the wavevectors of the even and odd modes respectively. Light input into one waveguide propagates through the DC as a superposition of the two modes, whose relative phase changes with distance L as $\Delta k L$. After propagating a length $L_c = \pi/\Delta k$, all of the incident light is coupled into the other waveguide. In practice, dispersion between the coupled modes means that the coupling length L_c is a function of frequency, and hence the bandwidth over which coupling occurs is limited. If the dispersion curves of the odd and even modes are parallel, then L_c remains constant, but this limits use of the DC as a switch. To overcome this, Yamamoto *et.al.* [4] proposed that the ideal DC design for wide bandwidth switching should have an abrupt change in L_c over a narrow frequency range, with L_c taking two different constant values on either side of this transition. By operating close to the transition frequency, a small change in the refractive index could induce a large change in L_c resulting in switching from one output waveguide to the other.

To obtain a practical PhC directional coupler design with dispersion properties close to the ideal ones described above requires considerable structural modification. The proposed design in Ref. [4] was obtained by starting with two coupled W1 waveguides then changing the radii and positions of several rows of holes. Here we use a similar approach, however we change only the radii, and not the position of the holes.

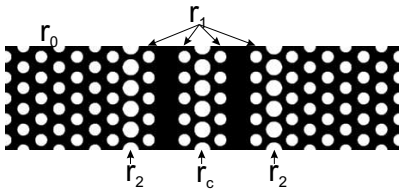

Figure 1: Diagram of the directional coupler geometry considered here. The dispersion curves are modified by varying the radii of several rows of holes.

Figure 1 illustrates the DC geometry that we consider. The PhC is taken to be a Si membrane of thickness $220\,\mathrm{nm}$ with air above and below, and the regular holes in the lattice have radius $r_0 = 0.33a$, where a is the lattice period. In the following results $a = 430\,\mathrm{nm}$. The dispersion curves are calculated using a freely-available 3D planewave method [2]. We consider first the dispersion properties of two coupled W1 waveguides with all holes of radius $r_0 = 0.33a$. The dispersion curves of the coupled modes are plotted as dashed-dotted curves in

Fig. 2(a), and the corresponding coupling length is shown in Fig. 2(b). Note that L_c changes smoothly with frequency and is only less than $10a$ for a narrow range of frequencies below $\omega a/2\pi c = 0.276$, and thus the dispersion properties are far from those required for wide bandwidth switching described above.

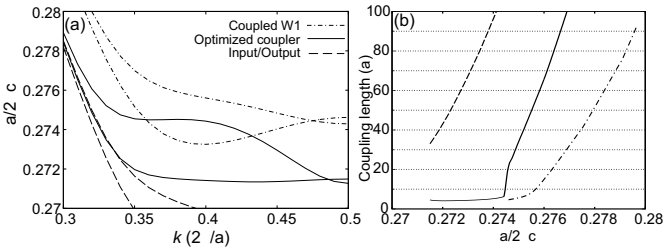

Figure 2: (a) Dispersion curves and (b) coupling length for the W1 and modified DCs and the input/output sections.

We modify dispersion curves by changing the size of the holes indicated in Fig. 1. The way in which the hole sizes change the dispersion curves is complex, however some intuition can be gained by considering the relative field distributions of odd and even modes [4]. For instance the odd mode has a nodal line half way between the two waveguides, so it is little affected by changes to r_c, whereas the even mode has a non-zero field in this region and is thus moved relative to the odd mode. Similar arguments can be used to understand the effects of the other holes, however it is not in the scope of this paper to detail these. Additional distortion to the dispersion curves can be induced by avoided crossings between the guided waveguide modes and modes in the photonic crystal cladding, an effect used by Petrov *et.al.* to obtain low group velocity modes in PhC waveguides [5].

The solid curves in Figs. 2(a) and (b) show the dispersion curves and corresponding coupling length for our modified directional coupler design with $r_1 = 0.29\,a$, $r_2 = 0.38\,a$ and $r_c = 0.39\,a$. Both figures show that the bandwidth in which $L_c < 10$ is significantly larger than for the unmodified W1 DC, and Fig. 2(b) shows that L_c changes rapidly at approximately $\omega a/2\pi c = 0.2745$. For frequencies below this, L_c changes only slowly with frequency, as desired for wide bandwidth coupling. At frequencies above the transition frequency, L_c changes rapidly, but provided the coupler length $L << L_c$ at these frequencies, light will not couple between the waveguides, so the change in L_c does not affect the overall operation of the DC.

The modified DC geometry presented above was designed without considering how to to couple light in and out of the waveguides. In general, coupling from a high-index dielectric waveguide to a standard W1 PhC waveguide is relatively efficient at frequencies well away from the W1 mode cutoff. Close to the cutoff frequency however, the group velocity of the W1 mode approaches zero and as a result the coupling losses increase rapidly [6]. This has consequences for the modified DC design, since the rapid change in L_c results from a low-group velocity region in the dispersion curve of the even mode, and the coupling losses can be significant [7]. Here we include a modified section of PhC at the front and rear of the DC that acts as a transition region between the ridge waveguide and the DC, as shown in Fig. 3. This input/output section is designed such that both modes both have relatively large group velocities and thus couple efficiently to the ridge waveguides. At the same time, the modes in the transition region couple into the DC section with relatively low losses. The dashed curves in Fig. 2(a) and (b) show the dispersion curves and L_c for the input and output sections with $r_1 = 0.29a$ and $r_2 = r_c = r_0$. Since the coupling length in these sections is more than ten times their total length, they do not contribute significantly to the directional coupling behaviour.

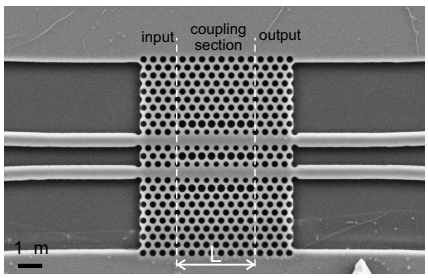

Figure 3: Scanning electron microscope image of a PhC DC fabricated in a Si membrane with input/output sections and coupling section of length L.

Simulation and experimental results

We consider first the transmission properties of the modified DC with the input and output sections on the front and rear. Figure 4 shows 3D finite-difference time-domain (FDTD) results calculated for DC lengths of $L = 4a$ and $L = 8a$ with $a = 430\,\mathrm{nm}$. Clear directional coupling behaviour is seen even for the DC of length $4a$, corresponding to a coupling length of less than $2\,\mu\mathrm{m}$. Note also that the peak in the $L = 4$ drop spectrum at $\lambda \approx 1573\,\mathrm{nm}$ corresponds closely to a peak in the through spectrum of the $L = 8$ device, indicating that there the input and output sections have little effect on the coupling behaviour as expected.

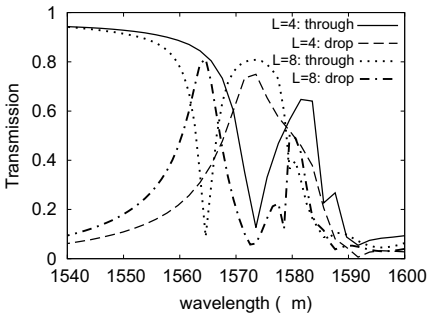

Figure 4: Calculated transmission spectra for directional couplers of length $L = 4$ and $L = 8$ with the parameters given in the text.

Directional couplers with both unmodified W1 waveguides and the modified design were fabricated in Si using e-beam lithography and reactive-ion etching, one of which is shown in Fig. 3. The through and drop transmissions were measured and compared to the 3D FDTD simulations. In the first set of fabricated devices, the hole sizes were somewhat larger than the designed size, so FDTD simulations were repeated for $r_0 = 0.34$ and the other holes were scaled accordingly. Figure 5(a) shows the measured and calculated spectra for the unmodified W1 coupler of length $L = 16a$. Directional coupling is clearly observed, and an extinction ratio of two orders of magnitude is measured for the first drop wavelength. The simulated and measured spectra show excellent agreement.

Figure 5(b) shows the spectra for the modified DC of length $L = 8a$. While the agreement with the simulated spectra is not as good as that for the W1 coupler, both spectra have common features. The discrepancy is thought to be due to variations in the relative hole sizes of the fabricated devices as the coupling properties are very sensitive to changes in these parameters. Further refinement in the fabrication process is expected to improve these results and enable us to fabricate a DC with the designed hole sizes.

Conclusions

We have proposed a modified directional coupler design for achieving short coupling lengths and wide bandwidths and demonstrated its operation both numerically and experimentally. Excellent agreement between simulation and experiment was found for the unmodified W1 coupler after the simulations were corrected to account for larger hole sizes than designed. These results are promising for future experimental demonstration of wide-bandwidth coupling in an ultra-compact directional coupler.

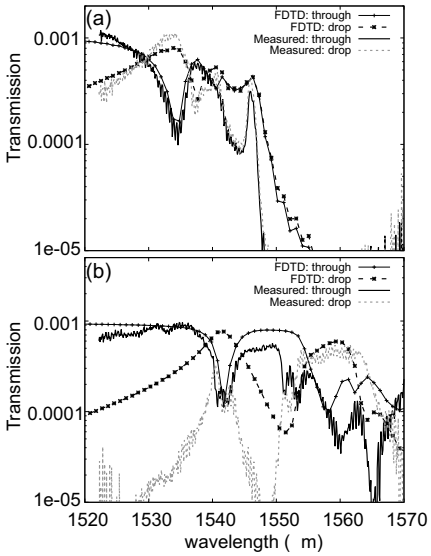

Figure 5: Comparison of measured and calculated transmission spectra for two DC geometries. (a) Unmodified W1 DC with all holes of the same radius $r_0 \approx 0.34$ and length $L = 16a$. (b) Modified DC geometry with $r_0 \approx 0.34$, $r_1 \approx 0.299$, $r_2 = r_c \approx 0.391$ and a coupling section of length $L = 8a$.

Acknowledgements

T. P. White is supported by an 1851 Royal Commission Research Fellowship. This research is partly supported under the European contract SPLASH of the 6th PCRD.

References

[1] A. Martinez, F. Cuesta, and J. Marti, IEEE Photonics Technl. Lett., vol. 15, pp. 694–696, 2003.

[2] S. G. Johnson and J. D. Joannopoulos, Opt. Express, vol. 8, pp. 173-190, 2001.

[3] Y. Tanaka, H. Nakamura, Y. Sugimito, N. Ikeda, K. Asakawa, and K. Inoue, IEEE J. Quantum Electron., vol. 41, pp. 76–84, 2005.

[4] N. Yamamoto, T. Ogawa, and K. Komori, Opt. Express, vol. 14, pp. 1223–1229, 2006.

[5] A. Yu. Petrov and M. Eich, Appl. Phys. Lett., vol. 85, pp. 4866–4868, 2003.

[6] Y. A. Vlasov and S. J. McNab, Opt. Lett., vol. 31, pp. 50–52, 2006.

[7] S-C. Huang, M. Kato, Eiichi Kuramochi, C-P. Lee, and M. Notomi, Opt. Express, vol. 15, pp. 3543–3549, 2007.

Minisymposium on Resonances and Trapped Modes

Organisers: Thorsten Hohage (Georg-August-Universität Göttingen) and Timo Weidl (Universität Stuttgart)

Sensitivity analysis of spectral properties of high contrast band gap materials

H. Ammari[†], H. Kang[‡], S. Soussi[§,*], H. Zribi[¶]
[†]Laboratoire Ondes et Acoustique, ESPCI, Paris, France
[‡]Department of Mathematics, Seoul National University, Seoul, Korea
[§]Institut für Numerische und Angewandte Mathematik, University of Göttingen, Göttingen, Germany
[¶]Impedance Imaging Research Center, Kyung Hee University, Seoul, Korea
[*]Email: soussi@math.uni-goettingen.de

Abstract

We investigate the band gap structure of the frequency spectrum for transverse electric (TE) polarized electromagnetic waves in a high-contrast two-component periodic dielectric medium made of a background medium with periodic inclusions. We perform a high-order sensitivity analysis with respect to the index ratio. Our method is based on integral equation formulations and analysis of meromorphic operator-valued functions based on generalized Rouché's theorem. We establish a connection between the band structures and the Dirichlet eigenvalue problem on one inclusion. The first-order term of the expansion is given explicitely by a simple variational formulation.

Introduction

Photonic crystals are structures of high dielectric contrast materials arranged in a periodic array. They have attracted enormous interest in the last decade because of their unique optical properties. Such structures have been found to exhibit interesting spectral properties with respect to classical wave propagation, including the appearance of band gaps [1], [2]. Incident electromagnetic waves with frequencies located in the band gaps are reflected by the photonic crystal and their magnitude decreases exponentially inside it.

Photonic crystals present then very interesting potential applications in waveguides and resonant cavities. In fact, because of the exponential localization, they can be used as cladding for waveguides and cavities within the band gap, where a cladding width of few wavelengths should sufficient to have an efficient localization [3].

However, it appears that there are only few results on the existence of spectral gaps for photonic crystals, and these are essentially based on one-dimensional calculations and separation of variables [4].

An important example of photonic crystals consists in a background medium with an array of arbitrary-shaped inclusions periodic along each of the two orthogonal coordinate axes in plane, the dielectric contrast between the background medium and the inclusions being high. In this paper, we adopt this specific model to demonstrate our technique and results. We give a full understanding of the relationship between variations in the index ratio and variations in the band gap structure of the photonic crystal. We provide an asymptotic expansion of the spectrum using integral approach and the generalized Rouché's theorem.

Carrying out a band structure calculation for a given photonic crystal involves a family of eigenvalue problems, as the quasi-momentum is varied over the first Brillouin zone. We show that these eigenvalues are the characteristic values of meromorphic operator-valued functions that are of Fredholm type with index 0. Then we proceed from the generalized Rouché's theorem to construct their complete asymptotic expressions as the index ratio goes to infinity.

Our results could be used to design a new tool based on a boundary integral perturbation theory for the optimal design problem in photonic crystals. Since the limiting situation reduces to the spectra of the Laplacian with Dirichlet boundary conditions and a related operator both in some canonical domains, say disks or ellipses, the idea would be to start with these easy-to-calculate spectra and compute the gradient of some target functionals using our asymptotic expansions with respect to the contrast and the shape of the inclusions. This method would be particularly suitable for optimizing photonic crystal waveguides [5].

Problem formulation

We consider a photonic crystal as specified in the introduction and we denote by k the dielectric contrast between the background medium and the inclusions. We assume that the structure has unit periodicity and define the periodic domain $Y = \mathbb{R}^2/\mathbb{Z}^2$, which can be identified with the unit square $[0,1]^2$. Let D be a bounded domain with a connected Lipschitz boundary strictly included in $[0,1]^2$ and representing the support of the intersection between the periodic inclusions and the unit cell $[0,1]^2$, see figure 1.

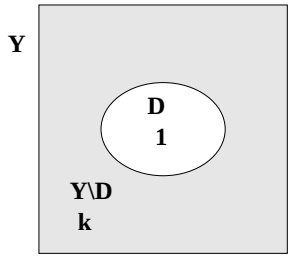

Figure 1: Unit cell

We seek eigenfunctions u_α of:

$$\begin{cases} k\Delta u_\alpha + \omega^2 u_\alpha = 0 & \text{in } Y \setminus \overline{D}, \\ \Delta u_\alpha + \omega^2 u_\alpha = 0 & \text{in } D, \\ u_\alpha|_+ = u_\alpha|_- & \text{on } \partial D, \\ k\frac{\partial u_\alpha}{\partial \nu}\Big|_+ = \frac{\partial u_\alpha}{\partial \nu}\Big|_- & \text{on } \partial D, \\ e^{-i\alpha.x}u_\alpha & \text{is } Y\text{-periodic.} \end{cases} \tag{1}$$

For each quasi-momentum variable α and k, let $\sigma_\alpha(D,k)$ be the (discrete) spectrum of (1). Then the spectral band of the photonic crystal is given by

$$\cup_{\alpha\in[0,2\pi]^2}\sigma_\alpha(D,k).$$

We shall investigate the behavior of $\sigma_\alpha(D,k)$ as $k \to +\infty$.

Integral representation

Let G^α_ω be the two-dimensional quasi-periodic Green's function satisfying

$$(\Delta+\omega^2)G^\alpha_\omega(x,y) = \sum_{n\in\mathbb{Z}^2}\delta(x-y-n)e^{in\cdot\alpha}, \tag{2}$$

and let $\mathcal{S}_D^{\alpha,\omega}$ be the quasi-periodic single layer potential associated to G^α_ω, that is, for a given density $\varphi \in L^2(D)$,

$$\mathcal{S}_D^{\alpha,\omega}\phi(x) = \int_{\partial D} G^\alpha_\omega(x,y)\varphi d\sigma(y), \quad x\in\mathbb{R}^2.$$

Then $\mathcal{S}_D^{\alpha,\omega}\phi(x)$ satisfies the Helmholtz equation in D and $Y\setminus D$ and the classical jump formulae on ∂D. It is also α-quasi-periodic in Y.

Using the quasi-periodic single layer potential, we show that solutions to (1) have an integral representation which will be useful for the asymptotical expansion of eigenvalues.

Theorem 1 *Suppose ω^2 is not an eigenvalue of $-\Delta$ in $Y\setminus\overline{D}$ with homogeneous Dirichlet condition on ∂D and α-quasi-periodic condition on ∂Y, and suppose that ω^2/k is not an eigenvalue of $-\Delta$ in D with homogeneous Dirichlet condition on ∂D.*

Then, any non trivial solution (ω^2,u) to problem (1) *can be represented as follows:*

$$u(x) = \begin{cases} \mathcal{S}_D^{\alpha,\omega}\phi(x), & x\in D, \\ \mathcal{S}_D^{\alpha,\frac{\omega}{\sqrt{k}}}\psi(x), & x\in Y\setminus\overline{D}, \end{cases} \tag{3}$$

where $(\phi,\psi)\in L^2(\partial D)\times L^2(\partial D)$ is solution to the integral equation system:

$$\begin{cases} \mathcal{S}_D^{\alpha,\omega}\phi - \mathcal{S}_D^{\alpha,\frac{\omega}{\sqrt{k}}}\psi = 0, & \text{on } \partial D, \\ \Big(-\frac{1}{2}I + (\mathcal{K}_D^{\alpha,\omega})^*\Big)\phi & \\ -k\Big(\frac{1}{2}I + (\mathcal{K}_D^{\alpha,\frac{\omega}{\sqrt{k}}})^*\Big)\psi = 0, & \text{on } \partial D. \end{cases} \tag{4}$$

This defines a bijection between the eigenvectors u of (1) *and the solutions (ϕ,ψ) to the system* (4)*.*

Here $(\mathcal{K}_D^{\alpha,\omega})^*\phi$ is given by

$$(\mathcal{K}_D^{\alpha,\omega})^*\phi = \text{p.v.}\int_{\partial D}\frac{\partial G^\alpha_\omega(x,y)}{\partial\nu_x}\phi(y)d\,\sigma(y).$$

This integral representation allows us to transform the eigenvalue problem into a characteristic value problem. To do so, we define the operator valued function $\mathcal{A}^\alpha_k(\omega)$, defined for $\omega\in\mathbb{C}$, by

$$\mathcal{A}^\alpha_k(\omega) := \begin{pmatrix} \mathcal{S}_D^{\alpha,\omega} & -\mathcal{S}_D^{\alpha,\frac{\omega}{\sqrt{k}}} \\ \frac{1}{k}\Big(\frac{1}{2}I - (\mathcal{K}_D^{\alpha,\omega})^*\Big) & \frac{1}{2}I + (\mathcal{K}_D^{\alpha,\frac{\omega}{\sqrt{k}}})^* \end{pmatrix}. \tag{5}$$

Actually, ω^2 is an eigenvalue of problem (1) if and only if ω is a characteristic value of $\mathcal{A}^{\alpha,k}$. The characteristic value definition can be found in [6], in our case it is equivalent to the values of ω for which $\mathcal{A}^{\alpha,k}(\omega)$ is not invertible.

We can show that $\mathcal{A}^\alpha_k$ is Fredholm analytic with index 0 in $\mathbb{C}\setminus i\mathbb{R}_-$ and hence the generalized Rouché's theorem, see [7], can be applied to $\mathcal{A}^\alpha_k$.

Suppose that $\alpha\neq 0$, then it has been proved in [8] that the n^{th} eigenvalue of problem (1) will converge to the n^{th} eigenvalue of the Dirichlet-Laplacian in D as $k\to+\infty$. As a consequence, the application of the generalized Rouché's theorem gives us the following result:

Proposition 1 *Suppose $\alpha\neq 0$ and let $\omega^2_{0,n}$ be the n^{th} eigenvalue (supposed single) of the Dirichlet-Laplacian in D. Let V be a tubular complex neighborhood of $]\omega_{0,n-1}+\eta,\omega_{0,n}+\eta[$. ($\eta$ is supposed small enough)*

Then, for k large enough, ω_k^α, the n^{th} eigenvalue of problem (1) *belongs to* $]\omega_{0,n-1}+\eta, \omega_{0,n}+\eta[$*, and satisfies:*

$$\omega_k^\alpha - \omega_{0,n} = \frac{1}{2i\pi}\mathrm{tr}\int_{\partial V}(\omega-\omega_{0,n})\left(\mathcal{A}_k^\alpha\right)^{-1}(\omega)\,\frac{d\mathcal{A}_k^\alpha}{d\omega}(\omega)\,d\omega.$$

Asymptotical expansion of characteristic values

Now, in order to get an expansion of the characteristic values, we operate an expansion of $\mathcal{A}_k^\alpha$ as $k \to +\infty$. Suppose $\alpha \neq 0$, then we have the following expansion as $\omega \to 0$

$$G_\omega^\alpha(x,y) = G_0^\alpha(x,y) - \sum_{l=1}^{+\infty}\underbrace{\omega^{2l}\sum_{n\in\mathcal{Z}^2}\frac{e^{i(2\pi n+\alpha)\cdot(x-y)}}{|2\pi n+\alpha|^{2(l+1)}}}_{:=-G_l^\alpha(x,y)}. \tag{6}$$

This expansion induces an expansion of $\mathcal{A}_k^\alpha$ in the form

$$\mathcal{A}_k^\alpha(\omega) = \mathcal{A}_0^\alpha(\omega) + \sum_{l=1}^{+\infty}\frac{1}{k^l}\mathcal{A}_l^\alpha(\omega). \tag{7}$$

Injecting this expansion into Proposition 1, we get the following result.

Theorem 2 *Suppose $\alpha \neq 0$. Let ω_0^2 be a single eigenvalue of the Dirichlet-Laplacian in D. Then, there exists a unique eigenvalue $(\omega_k^\alpha)^2$ of problem* (1)*, located in a tubular complex neighborhood V of $]\omega_{0,n-1}+\eta, \omega_{0,n}+\eta[$, and the following asymptotic expansion holds:*

$$\omega_k^\alpha - \omega_0 = \frac{1}{2i\pi}\sum_{p=1}^{+\infty}\frac{1}{p}\sum_{n=p}^{+\infty}\frac{1}{k^n}\,\mathrm{tr}\int_{\partial V}(\mathcal{A}_0^\alpha)^{-p}(\omega)B_{n,p}^\alpha(\omega)d\omega,$$

where

$$B_{n,p}^\alpha(\omega) = (-1)^p\sum_{\substack{n_1+\ldots+n_p=n\\ n_i\geq 1}}\mathcal{A}_{n_1}^\alpha(\omega)\ldots\mathcal{A}_{n_p}^\alpha(\omega),$$

$$(\mathcal{A}_0^\alpha)^{-1}(\omega) = \begin{pmatrix} (\mathcal{S}_D^{\alpha,\omega})^{-1} & (\mathcal{S}_D^{\alpha,\omega})^{-1}\mathcal{S}_{D,0}^\alpha(\frac{1}{2}I + (\mathcal{K}_{D,0}^\alpha)^*)^{-1} \\ 0 & (\frac{1}{2}I + (\mathcal{K}_{D,0}^\alpha)^*)^{-1}\end{pmatrix}.$$

Finally, we can get explicitely the first order term of the expansion. In fact, for $\alpha \neq 0$, if ω_0^2 is a single eigenvalue of the Dirichlet-Laplacian in D and u_0 is its associated eigenvalue. Suppose v is the α-quasi-periodic solution to the problem

$$\begin{cases}\Delta v_0 = 0 & \text{in } Y\setminus\overline{D},\\ \dfrac{\partial v_0}{\partial\nu}\Big|_+ = \dfrac{\partial u_0}{\partial\nu}\Big|_- & \text{on } \partial D,\end{cases}$$

then there is an eigenvalue $(\omega_k^\alpha)^2$ of problem (1) that will converge to ω_0^2 and we have

$$\omega_k^\alpha - \omega_0 = -\frac{1}{k}\frac{\int_{Y\setminus D}|\nabla v_0|^2dx}{2\omega_0\int_D|u_0|^2dx} + O(k^{-2}).$$

Similar results exist for the case $\alpha = 0$.

References

[1] E. Yablonovitch, "Inhibited spontaneous emission in solid-state physic and electronics", Phys. Rev. Lett., 58 (1987), pp. 2059-2062.

[2] S.G. Johnson and J.D. Joannopoulos, "Photonic Crystals: The Road from Theory to Practice", Kluwer Academic Publishers, 2002.

[3] H. Ammari and F. Santosa, "Guided waves in a photonic bandgap structure with a line defect", SIAM J. Appl. Math., 64 (2004), pp. 2018-2033.

[4] P. Kuchment, "The mathematics of photonic crystals, in Mathematical modeling in optical science", Frontiers Appl. Math. 22, SIAM, Philadelphia, PA, 2001.

[5] W. Crutchfield, H. Cheng, and L. Greengard, "Sensitivity analysis of photonic crystal fiber", Optics Express, 12, Issue 18, pp. 4220-4226.

[6] H. Ammari, H. Kang, S. Soussi, and H. Zribi "Layer potential techniques in spectral analysis. II. Sensitivity analysis of spectral properties of high contrast band-gap materials", Multiscale Model. Simul., 5 (2006), pp. 646-663.

[7] I.C. Gohberg and E.I. Sigal, "An operator generalization of the logarithmic residue theorem and Rouché's theorem", Mat. Sb. (N.S.), 84(126) (1971), pp. 607-629.

[8] R. Hempel and K. Lienau, "Spectral properties of periodic media in the large coupling limit", Comm. Partial Differential Equations 25 (2000), pp. 1445-1470.

ABSOLUTE CONTINUITY OF THE SPECTRUM FOR PERIODICALLY MODULATED LEAKY WIRES

Pavel Exner[†], **Rupert L. Frank**[‡,*]

[†]Department of Theoretical Physics, Nuclear Physics Institute, Academy of Sciences, Rez, Czech Republic
[‡] Department of Mathematics, Royal Institute of Technology, Stockholm, Sweden
[*]Email: rupert@math.kth.se

Abstract

We consider a model of leaky quantum wire in three dimensions. The Hamiltonian is a singular perturbation of the Laplacian supported by a line with the coupling which is bounded and periodically modulated along the line. We demonstrate that such a system has a purely absolutely continuous spectrum and its negative part has band structure with an at most finite number of gaps. This result is extended also to the situation when there is an infinite number of the lines supporting the perturbations arranged periodically in one direction.

Introduction and main results

The characteristic feature of Schrödinger operators which are periodic with respect to some, but not all space directions is the appearance of surface states, see [1] and the references in [7], [9]. On physical grounds one expects that these states are not bound but correspond to additional channels of scattering, i.e., that the spectrum of the corresponding operator is purely absolutely continuous. This question in different models was recently addressed in [4], [5], [6], [7] and [8].

In [2] we consider a model of a quantum wire described by a Hamiltonian with an interaction supported on a straight line in $\mathbb{R}^3$. In contrast to the case of a straight line in $\mathbb{R}^2$ where the Hamiltonian can be defined naturally through the associated quadratic form [6], now the operator has to be defined by means of boundary conditions involving generalized boundary values as, e.g., in [3]. We recall how to construct a self-adjoint operator H in $L_2(\mathbb{R}^3)$ which corresponds to the formal expression

$$H = -\Delta + \sigma(x)\delta(|y|).$$

Here σ is a bounded, real-valued and 2π-periodic function and coordinates in $\mathbb{R}^3$ are denoted by (x, y), $x \in \mathbb{R},\ y \in \mathbb{R}^2$. The operator H can be viewed as a Schrödinger-type operator with singular potential $\sigma(x)\delta(|y|)$ describing the interaction of a quantum-mechanical particle with a quantum wire $\Gamma := \mathbb{R} \times \{(0, 0)\}$. Our main result is

Theorem 1 *The spectrum of the operator H is purely absolutely continuous.*

We also investigate the scattering between H and H_0, the standard self-adjoint realization of $-\Delta$ in $\mathbb{R}^3$, and prove

Theorem 2 *The wave operators*

$$W_\pm := s - \lim_{t\to\pm\infty} \exp(itH)\exp(-itH_0).$$

exist, satisfy $\mathcal{R}(W_+) = \mathcal{R}(W_-)$ and are not *complete.*

The existence of the wave operators implies that the interval $\sigma_{ac}(H_0) = [0, \infty)$ is contained in the absolutely continuous spectrum of the operator H. Moreover, the identity $\mathcal{R}(W_+) = \mathcal{R}(W_-)$ implies the unitarity of the scattering matrix. The non-completeness of the wave operators is due to *guided states*, i.e., states that are localized near the wire Γ for all times. In particular, all states corresponding to the negative spectrum of H are guided states. We prove the following

Theorem 3 *The negative spectrum of the operator H is non-empty and has band structure with at most finitely many gaps.*

The existence of guided states with positive energy is an interesting, mostly open problem.

The results presented in Theorems 1–3 remain true if the operator H is replaced by the operator $-\Delta + \sum_{n\in\mathbb{Z}} \sigma(x)\delta(y_1 - 2\pi n)\delta(y_2)$ describing an infinite family of periodically arranged wires.

Ingredients of the proofs

We briefly explain some of the mathematical ideas involved in the proofs of Theorems 1–3. By means of Floquet theory the operator H can be represented as a direct integral

$$\int_{(-\frac{1}{2},\frac{1}{2})}^{\oplus} H(k)\,dk$$

of operators $H(k)$ acting in $L_2(\Pi)$ where $\Pi := (-\pi, \pi) \times \mathbb{R}^2$. The operators $H(k)$ correspond to the formal expression

$$H(k) = (-i\partial_x + k)^2 - \Delta_y + \sigma(x)\delta(|y|)$$

acting on functions in Π which are periodic with respect to the variable x. The investigation of the operator H reduces to the study of the fibers $H(k)$. Note that the fundamental domain Π is unbounded, so the operators $H(k)$ have non-empty continuous spectrum.

The absolutely continuous part of the spectrum of $H(k)$ can be studied by scattering theory. We prove that the resolvent difference $(H(k)+\gamma)^{-1} - (H_0(k)+\gamma)^{-1}$ for sufficiently large γ belongs to the trace class, which implies the existence of the fiber wave operators and the invariance of the absolutely continuous spectrum of the fiber operators.

We derive a limiting absorption principle for the operators $H(k)$, which implies the absence of singular continuous spectrum of the fiber operators.

The absolute continuity of the spectrum of the original operator H will be established by controlling the dependence of the eigenvalues of the fiber operators $H(k)$ on the quasi-momentum k. A particular difficulty to be overcome is the existence of eigenvalues which are embedded in the continuous spectrum. We "separate" them from the remaining spectrum by characterizing them, in the spirit of the Birman-Schwinger principle, as parameters λ for which a certain operator $A(\lambda, k)$ on the wire $(-\pi, \pi)$ has eigenvalue 0. The latter operator is of the form of a Schrödinger operator, $A(\lambda, k) = A_0(\lambda, k) + \sigma$, where σ enters as an electric potential and $A_0(\lambda, k)$ represents an effective kinetic energy, growing logarithmically in Fourier space. The operator $A(\lambda, k)$ has discrete spectrum and its eigenvalues depend, away from crossings, analytically on λ and k. Moreover, they are non-constant, as can be seen using Thomas' method of complexifying the quasi-momentum k [10]. These facts imply the absolute continuity of the spectrum of the original operator H, as claimed in Theorem 1.

The assertion of Theorem 3 concerning the negative spectrum of the operator H follows from the fact that the fiber operators $H(k)$ have, for any σ, at least one and at most a finite number of eigenvalue below their essential spectrum.

The existence of the wave operators $W_\pm$ on the whole plane and the equality of their ranges is a consequence of the existence and completeness of the wave operators for the fiber operators. Indeed, the wave operators $W_\pm$ turn out to be given by the direct integral of the wave operators for the fiber operators. The non-completeness of the wave operators $W_\pm$ is a consequence of Theorems 1 and 3, namely the existence of negative absolutely continuous spectrum. This concludes the proof of Theorem 2.

Finally, we remark that the above scheme of proof is applicable in the more general setting of partially periodic problems [8].

References

[1] E. B. Davies, B. Simon, *Scattering Theory for Systems with Different Spatial Asymptotics on the Left and Right*, Comm. Math. Phys. **63** (1978), 277-301.

[2] P. Exner, R. L. Frank, *Absolute continuity of the spectrum for periodically modulated leaky wires in* $\mathbb{R}^3$, Ann. Henri Poincaré **8** (2007), no. 2, 241 - 263.

[3] P. Exner, S. Kondej, *Curvature-induced bound states for a* δ *interaction supported by a curve in* $\mathbb{R}^3$, Ann. H. Poincaré **3** (2002), 967-981.

[4] N. Filonov, F. Klopp, *Absolute continuity of the spectrum of a Schrödinger operator with a potential which is periodic in some directions and decays in others*, Documenta Math. **9** (2004), 107-121; Erratum: ibd., 135-136.

[5] N. Filonov, F. Klopp, *Absolutely continuous spectrum for the isotropic Maxwell operator with coefficients that are periodic in some directions and decay in others*, Comm. Math. Phys. **258** (2005), no. 1, 75–85.

[6] R. L. Frank, *On the Laplacian in the halfspace with a periodic boundary condition*, Ark. Mat. **44** (2006), no. 2, 277 - 298.

[7] R. L. Frank, R. G. Shterenberg, *On the scattering theory of the Laplacian with a periodic boundary condition. II. Additional channels of scattering*, Documenta Math. **9** (2004), 57-77.

[8] R. L. Frank, R. G. Shterenberg, *On the spectrum of partially periodic operators*, in: Operator Theory, Analysis and Mathematical Physics, J. Janas, et al. (eds.), 35 – 50, Oper. Theory Adv. Appl. **174**, Birkhäuser, Basel, 2007.

[9] P. Kuchment, *On some spectral problems of mathematical physics*, Partial differential equations and inverse problems, 241–276, Contemp. Math., 362, Amer. Math. Soc., Providence, RI, 2004.

[10] L. Thomas, *Time dependent approach to scattering from impurities in a crystal*, Comm. Math. Phys. **33** (1973), 335–343.

ON THE EXISTENCE OF INFINITELY MANY TRAPPED MODES IN THREE-DIMENSIONAL ELASTIC PLATES

Clemens Förster[†,*]
[†]Institute for Analysis, Dynamics and Modelling, University Stuttgart, Stuttgart, Germany
[*]Email: foerster@mathematik.uni-stuttgart.de

Abstract

We consider a three-dimensional linear elastic plate with stress-free boundary conditions in the special case of zero Poisson's coefficient. Perturbing the plate by a local change of Young's modulus or by a hole in the material means perturbing the corresponding differential operator by additional second-order terms or additional stress-free boundary conditions. We show that under such perturbations infinitely many eigenvalues arise in the essential spectrum which accumulate to a non-zero threshold. Furthermore, we state estimates on the accumulation rates.

Introduction

We consider a homogeneous and isotropic linear elastic medium on the domain $G = \mathbb{R}^2 \times J$ with $J = (-\frac{\pi}{2}, \frac{\pi}{2})$. For functions $u \in H^1(G;\mathbb{C}^3)$ we set

$$\epsilon(u) = \tfrac{1}{2}(\nabla u + (\nabla u)^T). \tag{1}$$

Let $\langle \epsilon(u), \epsilon(u)\rangle_{\mathbb{C}^{3\times 3}} = \sum_{i,j=1}^3 \epsilon_{ij}(u)\,\overline{\epsilon_{ji}(u)}$. Then

$$a_0[u] = 2\int_G \langle \epsilon(u), \epsilon(u)\rangle_{\mathbb{C}^{3\times 3}}\,\mathrm{d}x,\ u \in H^1(G;\mathbb{C}^3) \tag{2}$$

is the quadratic form of the elasticity operator

$$A_0 = -\left(\Delta + \operatorname{grad}\operatorname{div}\right) \tag{3}$$

in $L^2(G;\mathbb{C}^3)$ for zero Poisson coefficient with stress-free (Neumann-type) boundary conditions. Here we have chosen a suitable set of units such that Young's modulus E fulfils $E = 2$.

Let $f \in L^\infty(\mathbb{R}^2;[0,1])$ be a function of compact support which is extended to G by $f(x) = f(x_1,x_2)$ for $x = (x_1,x_2,x_3) \in G$. The function f describes a local perturbation consisting in an area of reduced Young's modulus. For $\alpha \in (0,1)$ we consider the operator A_α corresponding to the quadratic form

$$a_\alpha[u] = 2\int_G (1-\alpha f)\langle \epsilon(u), \epsilon(u)\rangle_{\mathbb{C}^{3\times 3}}\,\mathrm{d}x \tag{4}$$

with $u \in H^1(G;\mathbb{C}^3)$.

On the other hand, we study holes in G of shape $\Omega = \Omega_0 \times J$, where $\Omega_0 \subset \mathbb{R}^2$ is a bounded, connected Lipschitz-domain. This corresponds to the investigation of the operator A_Ω being (3) on $G\backslash\overline{\Omega}$ with Neumann-type boundary conditions. In fact, this problem is investigated by studying the operator A_Γ, $\Gamma := \partial\Omega_0 \times J$, which is (3) on $G\backslash\Gamma$ with Neumann-type boundary conditions. The operators A_Ω and A_Γ are rigorously defined by suitable quadratic forms.

The perturbations give rise to local oscillations of the plate which are situated around the perturbation. These oscillations are called trapped modes and correspond to eigenvalues of A_α and A_Γ, respectively, which are embedded into their essential spectra. We show that there arise infinitely many eigenvalues $\nu_k, k \in \mathbb{N}$, for each of the two perturbation types. The eigenvalues accumulate at a finite threshold $\Lambda > 0$. We study the accumulation rate and show that

$$\ln(\Lambda - \nu_k) = -2k\ln k + o(k\ln k) \quad \text{as} \quad k \to \infty. \tag{5}$$

Symmetries and spectral structure

In order to distinct eigenvalues from the surrounding essential spectrum we make use of spatial and internal symmetries of the elasticity operator. Let

$$H_1 := \{u \in L^2(\mathbb{R}^2 \times J;\mathbb{C}^3) \mid u_{1/2} \text{ symmetric in } x_3,\ u_3 \text{ antisymmetric in } x_3\}$$

$$H_4 := \{u \in H_1 \mid \int_J u_{1/2}\,\mathrm{d}x_3 \equiv 0 \text{ in } L^2(\mathbb{R}^2;\mathbb{C})\}.$$

Then $H_4, H_4^\perp$ reduce A_α for $\alpha \in [0,1)$ and A_Γ. Note that this is valid only for the elasticity operator with zero Poisson's ratio. Let

$$A_\alpha^{(4)} := A_\alpha|_{D(A_\alpha)\cap H_4}, \quad A_\Gamma^{(4)} := A_\Gamma|_{D(A_\Gamma)\cap H_4}.$$

While $\sigma_e(A_\alpha) = \sigma_e(A_\Gamma) = [0,\infty)$ we have $\sigma_e(A_\alpha^{(4)}) = \sigma_e(A_\Gamma^{(4)}) = [\Lambda,\infty)$ for some $\Lambda > 0$. We study eigenvalues of $A_\alpha^{(4)}$ and $A_\Gamma^{(4)}$ below Λ which are also eigenvalues of A_α and A_Ω, respectively.

There is a close connection between the behaviour of the eigenvalues and the lower bound of the essential spectrum. For a closer look on $\sigma_e(A_0^{(4)})$ we apply the unitary

Fourier transform Φ in (x_1, x_2) and consider

$$\Phi A_0^{(4)} \Phi^* = \int_{\mathbb{R}^2}^{\oplus} A^{(4)}(\xi)\, \mathrm{d}\xi,$$

where $\xi \in \mathbb{R}^2$ is the Fourier coordinate with respect to (x_1, x_2). The operators $A^{(4)}(\xi)$ are self-adjoint in $L^2(J; \mathbb{C}^3)$ and have purely discrete spectrum. Let us denote by $\lambda_j(\xi)$ the infinite series of eigenvalues of $A(\xi)$ in non-decreasing order including multiplicities.

The crucial point is that the minimum Λ of the lowest branch $\lambda_1(\xi)$ is attained on the whole circle $\{\xi \in \mathbb{R}^2 : |\xi| = \varkappa\}$ for some $\varkappa > 0$. This corresponds to infinitely many wave functions $w_\xi(x) = \psi(\xi, x_3)\mathrm{e}^{i\xi\cdot\binom{x_1}{x_2}}$ with minimal kinetic energy. Here $\psi(\xi, \cdot)$ denotes the eigenfunction of $A(\xi)$ with respect to $\lambda_1(\xi)$. The infinite degeneration of the essential spectral minimum leads to infinitely many eigenvalues when a perturbation is applied.

Existence of eigenvalues

Let us consider the case of additive perturbation. The existence of infinitely many eigenvalues of $A_\alpha^{(4)}$ below Λ is proven by finding a suitable series of k-dimensional test spaces $\mathcal{E}_k \subset H^1(G; \mathbb{C}^3) \cap H_4$, such that

$$\sup_{u \in \mathcal{E}_k : \|u\| = 1} a_\alpha[u] < \Lambda \tag{6}$$

for all $k \in \mathbb{N}$. Then the existence result follows by applying Glazman's lemma which is an easy consequence of the variational principle [2, 10.2.2]. As basis of the test space $\mathcal{E}_k$ we choose k linearly independent wave functions w_{ξ^j} with $|\xi^j| = \varkappa$, $j = 1, \dots, k$, and apply a suitable cut-off function in order to obtain L^2-integrable test functions.

The operator $A_\Gamma^{(4)}$ with boundary perturbation Γ cannot be treated directly. Instead we consider its inverse which can be interpreted as an operator with bounded additive perturbation. Let $R := (A_0^{(4)})^{-1}$, $R_\Gamma := (A_\Gamma^{(4)})^{-1}$. Then $R_\Gamma = R + (R_\Gamma - R)$ and the existence result is obtained by finding k-dimensional test spaces $\mathcal{F}_k \subset H_4$ such that

$$\inf_{u \in \mathcal{F}_k : \|u\| = 1} \langle R_\Gamma u, u\rangle > \Lambda^{-1}. \tag{7}$$

The test spaces are constructed using functions $A_0(w_{\xi^j}\zeta)$ where $|\xi^j| = \varkappa$ and ζ are suitable cut-off functions.

Result on the accumulation rate

The existence of infinitely many trapped modes below Λ relies on the strong degeneration of the spectral minimum of $A_0^{(4)}$. To obtain results on the accumulation rate for eigenvalues at Λ we follow the approach of [3]. There two difficulties arise. On the one hand, we have to modify the method in such a way that it is applicable to differential operators with additive perturbations of the same differential order. On the other hand we need a refined analysis which deals with super-polynomial accumulation rates of eigenvalues as they occur for our problems. Note that this special behaviour rests on the combination of a compactly supported perturbation which is applied to a strongly degenerated operator.

The case of an additive perturbation

Let us consider the elasticity operator $A_\alpha^{(4)}$ with additive perturbation. The asymptotics for the eigenvalue accumulation at Λ can be obtained by studying the counting function $n_-(\tau, A_\alpha^{(4)})$ which denotes the number of eigenvalues below τ of $A_\alpha^{(4)}$. In order to obtain (5) it is sufficient to prove that

$$\lim_{\tau \to 0} \frac{n_-(\Lambda - \tau, A_\alpha^{(4)})}{w^{-1}(\tau)} = 1 \tag{8}$$

where $w(t) := t^{-2t}$. The first step in proving (8) is the application of a modified version of the Birman-Schwinger principle [1]. This allows to substitute the counting of eigenvalues of $A_\alpha^{(4)}$ by the counting of eigenvalues of some compact operator, the so-called Birman-Schwinger operator. In our case this operator is given by

$$\mathcal{Y}_\alpha(\tau) := \left(\frac{\Lambda - \tau}{A_0^{(4)} - \Lambda + \tau}\right)^{\frac{1}{2}} V_\alpha \left(\frac{\Lambda - \tau}{A_0^{(4)} - \Lambda + \tau}\right)^{\frac{1}{2}} \tag{9}$$

in H_4, where

$$V_\alpha = U^* \sqrt{\alpha f}(I - \alpha \sqrt{f}\, U U^* \sqrt{f})^{-1} \sqrt{\alpha f}\, U \tag{10}$$

and $Uv = \sqrt{2}\epsilon((A_0^{(4)})^{-1/2} v)$ for $v \in H_4$. Note that V_α is bounded for $\alpha \in (0, 1)$ since $f \in L^\infty(\mathbb{R}^2; [0, 1])$. Denoting by $n_+(1, \mathcal{Y}_\alpha(\tau))$ the number of eigenvalues of $\mathcal{Y}_\alpha(\tau)$ larger than one, our version of the Birman-Schwinger principle states that

$$n_-\left(\Lambda - \tau, A_\alpha^{(4)}\right) = n_+\left(1, \mathcal{Y}_\alpha(\tau)\right). \tag{11}$$

for $\tau \in (0, \Lambda)$ and $\alpha \in (0, 1)$. Thus, we have to study the spectrum of $\mathcal{Y}_\alpha(\tau)$ in more detail. It turns out that the main spectral asymptotics of $\mathcal{Y}_\alpha(\tau)$ can be obtained by considering the behaviour of $\mathcal{Y}_\alpha(\tau)$ on the wave functions in the strongly degenerated spectral minimum of $A_0^{(4)}$. Applying a suitable reduction argument it is possible to

relate the spectral asymptotics of $\mathcal{Y}_\alpha(\tau)$ to an integral operator K on $L^2(\{\xi \in \mathbb{R}^2 : |\xi| = \varkappa\})$ having the smooth kernel

$$k(\eta,\xi) = \frac{1}{(2\pi)^2}\int_G f(x)\,\mathrm{e}^{i(\eta-\xi)\cdot\binom{x_1}{x_2}}\times \\ \times\,\langle\varphi_1(\eta,x_3),\varphi_1(\xi,x_3)\rangle_{\mathbb{C}^{3\times 3}}\,\mathrm{d}x. \tag{12}$$

Here $\varphi_1(\xi,x_3) = \lambda_1(\xi)^{-1/2}\sqrt{2}\epsilon(w_\xi)(x)\mathrm{e}^{-i\binom{x_1}{x_2}\cdot\xi}$ for $x \in \mathbb{R}^2 \times J$. We obtain that

$$\lim_{\tau\to 0}\frac{n_+(1,\mathcal{Y}_\alpha(\tau))}{w^{-1}(\tau)} = \lim_{\tau\to 0}\frac{n_+(\tau,K)}{w^{-1}(\tau^2)}. \tag{13}$$

The eigenvalues of K can be estimated by a direct calculation which gives

$$\lim_{\tau\to 0}\frac{n_+(\tau,K)}{w^{-1}(\tau^2)} = 1. \tag{14}$$

Combining (11), (13) and (14) we obtain (8).

The case of a boundary perturbation

Let us consider the operator $A_\Gamma^{(4)}$. As for $A_\alpha^{(4)}$, the accumulation rate for the eigenvalues of $A_\Gamma^{(4)}$ at Λ is obtained by investigating the number of eigenvalues above one for a suitable compact Birman-Schwinger operator. In this case the Birman-Schwinger operator is given by

$$\mathcal{Y}(\tau) := \left(\frac{1}{(\Lambda-\tau)} - R\right)^{-\frac{1}{2}} B_\Gamma \left(\frac{1}{(\Lambda-\tau)} - R\right)^{-\frac{1}{2}} \tag{15}$$

in H_4 for $\tau \in (0,\Lambda)$. Here $R = (A_0^{(4)})^{-1}$ and $B_\Gamma = (A_\Gamma^{(4)})^{-1} - (A_0^{(4)})^{-1}$. As before, the main term in the eigenvalue asymptotics is obtained by restricting $\mathcal{Y}(\tau)$ to the wave functions in the spectral minimum of $A_0^{(4)}$. Especially the behaviour of the operator B_Γ has to be described. This is done using the terminology of elastic potential theory. As for the problem with additive perturbation, the reduction process leads to an integral operator on $L^2(\{\xi \in \mathbb{R}^2 : |\xi| = \varkappa\})$ with a smooth kernel. The kernel is much more difficult than for the case of additive perturbation. But it is still possible to obtain the desired asymptotics by direct estimates on the eigenvalues of this operator.

References

[1] M. S. Birman, "On the spectrum of singular boundary-value problems" (Russian), Mat. Sb. (N.S.), vol. 55, 125–174, 1961, translated in Amer. Math. Soc. Trans. (2), vol. 53, 23–80, 1966.

[2] M. S. Birman and M. Z. Solomjak, Spectral Theory of Self-Adjoint Operators in Hilbert Space, D. Reidel Publishing Company, 1987 (original: Leningrad University Press, 1980)

[3] A. Laptev, O. Safronov, and T. Weidl, "Bound states asymptotics for elliptic operators with strongly degenerating symbols", Nonlinear problems in mathematical physics and related topics, I, In Honor of Professor O. A. Ladyzhenskaya, Int. Math. Ser. 1, Kluwer/Plenum, New York, pp. 233–246, 2002.

[4] C. Förster and T. Weidl, "Trapped modes for an elastic strip with perturbation of the material properties", Q. Jl. Mech. Appl. Math., vol. 59, pp. 399–418, 2005.

[5] C. Förster, "Trapped modes for an elastic plate with a perturbation of Young's modulus", Preprint: Stuttgarter Mathematische Berichte 009, 2006.

Hardy space infinite elements for scattering and resonance problems

T. Hohage[†], **L. Nannen**[‡]
Institut für Numerische und Angewandte Mathematik, Georg-August-Universität Göttingen
[†]Email: hohage@math.uni-goettingen.de
[‡]Email: nannen@math.uni-goettingen.de

Abstract

We present a new method for solving Helmholtz-type scattering and resonance problems. Physical solutions are characterised by their Laplace transform in radial direction, which belong to the Hardy space of the negative complex half plane. After another transformation a symmetric variational formulation in the Hardy space of the complex unit disc is derived. Using a Galerkin method with respect to the monomial basis of this Hardy space we obtain super-algebraic convergence. Uniqueness and equivalence to usual characterisations of physical solutions can be proven.

Introduction

Let $K \subset \mathbb{R}^d$, $d = 2, 3$ be a smooth, closed subset of $B_a := \{x \in \mathbb{R}^d : |x| \leq a\}$. We consider two types of problems: First to find for some known $\kappa > 0$ and some boundary values $f \in H^{1/2}(\partial K)$ a solution u to the *scattering problem*

$$-\Delta u(x) - \kappa^2 u(x) = 0, \quad x \in \mathbb{R}^d \setminus K, \tag{1a}$$
$$u(x) = f(x), \quad x \in \partial K, \tag{1b}$$
$$r^{(d-1)/2}\left(\frac{\partial u}{\partial r}(x) - iku(x)\right) \to 0, \; r = |x| \to \infty. \tag{1c}$$

Second, we consider the corresponding *resonance problem* to find eigenpairs (κ^2, u) where κ is now a complex number with $\Re(\kappa) > 0$ and u a nontrivial solution to

$$-\Delta u(x) = \kappa^2 u(x), \quad x \in \mathbb{R}^d \setminus K, \tag{2a}$$
$$u(x) = 0, \quad x \in \partial K, \tag{2b}$$
$$u \text{ satisfies a radiation condition.} \tag{2c}$$

It can be shown with the help of Rellich's lemma that $\Im(\kappa) < 0$ for solutions to (2). It turns out that the Sommerfeld condition (1c) is *not* a valid characterisation of outgoing waves in this case since the resonance functions u grow exponentially at infinity. Alternative radiation conditions will be discussed below. All that follows also holds true for other boundary conditions on ∂K and other differential equations in $B_a \setminus K$.

Radiation conditions

We split the domain $\mathbb{R}^d \setminus K$ into a bounded interior domain $\Omega_{\text{int}} := B_a \setminus K$ and a unbounded exterior domain $\Omega_{\text{ext}} := \mathbb{R}^d \setminus B_a$. Radiation conditions for $\Im(\kappa) < 0$ can be formulated with the help of integral representations of the exterior solution using the outgoing fundamental solution of the free Helmholtz equation or with the help of series representations. The former conditions lead to FEM-BEM coupling methods, the latter to classical infinite elements. However, both approaches have the disadvantage that they destroy the eigenvalue structure of the resonance problem (2).

Therefore, we use the *pole condition* as an alternative radiation condition. A function $u : \mathbb{R}^d \setminus B_a \to \mathbb{C}$ satisfies the *pole condition* if its Laplace transform in radial direction

$$\hat{u}(s, \hat{x}) := \int_0^\infty e^{-sr} u\left(\frac{r+a}{a}\,\hat{x}\right) dr,$$

defined initially for $\Re(s) > 0$, has a holomorphic extension to the lower complex half plane $\mathbb{C}^- := \{s \in \mathbb{C} : \Im(s) < 0\}$ for each $\hat{x} \in \partial B_a$. It has been shown in [1] for $\kappa > 0$ that the pole condition is equivalent to (1c) (strictly speaking additional uniformity conditions w.r.t. $\hat{x}$ are required), and similar results can be shown for complex κ. Introducing the Hardy space $H^-(\mathbb{R})$ of L^2 boundary values of holomorphic functions in $\mathbb{C}^-$, we can formulate the radiation condition as

$$\hat{u}(\bullet, \hat{x}) \in H^-(\mathbb{R}) \qquad \text{for all } \hat{x} \in \partial B_a. \tag{3}$$

Note that the eigenvalue equation (2a) for the physical exterior solution translates into an eigenvalue equation for $\hat{u}$.

Hardy space infinite elements: idea

The idea of Hardy space infinite elements is to incorporate the radiation condition in the form (3) by a Galerkin method in the Hardy space $H^-(\mathbb{R})$. In the interior domain an arbitrary standard finite element space can be used. Due to the lack of a convenient basis of $H^-(\mathbb{R})$, we perform a further transformation to the Hardy space $H^+(S^1)$ of L^2-boundary values of holomorphic functions

in the unit disk $\{z \in \mathbb{C} : |z| < 1\}$. It can be shown that the Möbius function $M : \mathbb{R} \to S^1$, $M(s) := \frac{s+i\kappa_0}{s-i\kappa_0}$ induces a unitary mapping $\mathcal{M} : H^-(\mathbb{R}) \to H^+(S^1)$, $(\mathcal{M}\varphi)(z) := \varphi(M^{-1}(z))\frac{\sqrt{2i\kappa_0}}{z-1}$. The parameter κ_0 with $\Re(\kappa_0) > 0$ will act as a tuning parameter in the algorithms to be discussed below. Note that the monomials $(2\pi)^{-1/2}z^n$, $n = 0, 1, \ldots$ form a natural orthonormal basis of $H^+(S^1)$.

It is beyond the scope of this extended abstract to derive a variational formulation of the problems (1) and (2) in appropriate tensor product spaces involving $H^+(S^1)$ (see [2]). We start from a finite dimensional approximation of the exterior solution of the form

$$u\left(\frac{a+r}{a}\hat{x}\right) = \sum_{n=0}^{N} \frac{u_n(r)}{(r+a)^{(d-1)/2}}\varphi_n(\hat{x}), \qquad (4)$$

for $r > 0$ and $\hat{x} \in \partial B_a$ where the functions φ_n form a basis of the trace space corresponding to the finite element space in Ω_{int}, and the radial functions u_n are chosen such that $U_n := \mathcal{M}\mathcal{L}u_n$ belong to a finite dimensional subspace of $H^+(S^1)$. Here $\mathcal{L}u_n$ denotes the Laplace transform of u_n.

It remains to discuss the coupling of the interior and exterior spaces. Since $(\mathcal{L}u_n)(s) \sim u_n(0)s^{-1}$ as $|s| \to \infty$ and $M(\infty) = 1$, we have

$$u_n(0) = -\sqrt{-2i\kappa_0}U_n(1).$$

Therefore, the interior and the exterior domain can be coupled naturally by introducing the values of the solution on the coupling boundary, $u_{0,n} := \frac{u_n(0)}{a^{(d-1)/2}}$ as common degrees of freedom. More precisely, we choose U_n of the form

$$U_n(z) = c_0 u_{0,n} + (z-1)\widetilde{U}_n(z), \quad z \in S^1 \qquad (5)$$

with $c_0 := -\frac{a^{(d-1)/2}}{\sqrt{-2i\kappa_0}}$ and $\widetilde{U}_n$ as polynomial of degree $\leq m$ restricted to S^1.

Since $U_n \in H^+(S^1) \cap C^\infty(S^1)$ by virtue of results in [1], it follows that $\widetilde{U}_n \in H^+(S^1) \cap C^\infty(S^1)$. Therefore, by the approximation properties of trigonometric polynomials, we can expect super-algebraic convergence as $m \to \infty$, which is in fact shown in [2]. This convergence property holds true for the interior solution and for the transformed exterior solution in the Hardy space norm, but *not* for the exterior solution (4) in any reasonable norm.

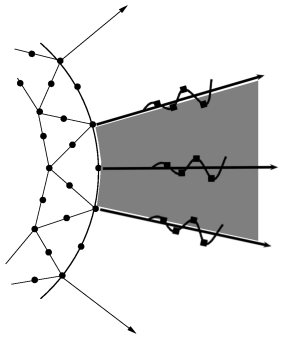

Figure 1: Example of an infinite element for nodal quadratic finite elements in the interior.

Local element matrices

Due to the ansatz (4) the local element matrices of the infinite elements (cf. Fig. 1) have a tensor (or Kronecker) product structure. More precisely, the local element matrices for the transformed bilinear form corresponding to the exterior Helmholtz equation (1a) have the form

$$M_{\text{el}}^{\hat{x}} \otimes M_{\text{el}}^{r} + S_{\text{el}}^{\hat{x}} \otimes S_{\text{el}}^{r} - \kappa^2\Big(M_{\text{el}}^{\hat{x}} \otimes M_{\kappa,\text{el}}^{r}\Big) \qquad (6)$$

where $M_{\text{el}}^{\hat{x}}$ denotes the local boundary element mass matrix corresponding to the bilinear form $\int_{\partial B_a} uv\,dx$, and $S_{\text{el}}^{\hat{x}}$ denotes the local boundary element stiffness matrix corresponding to the bilinear form $\int_{\partial B_a} \nabla_{\hat{x}} u \nabla_{\hat{x}} v\,dx$. In the second factors M_{el}^{r}, S_{el}^{r}, and $M_{\kappa,\text{el}}^{r}$, the first rows correspond to the values $u_{0,n}$, i.e. the degrees of freedom shared with the interior elements. These matrices are given by

$$M_{\text{el}}^{r} = \frac{d-1}{2a}\begin{pmatrix} 1 & \\ & \mathbf{0} \end{pmatrix} + \frac{1}{a^{d-1}}\widetilde{T}_+^\top\widetilde{T}_+ - \frac{C_d}{a^{d-1}}\widetilde{T}_-^\top\widetilde{D}_a^{-2}\widetilde{T}_-,$$

$$S_{\text{el}}^{r} = \frac{1}{a^{d-1}}\widetilde{T}_-^\top\widetilde{D}_a^{-2}\widetilde{T}_-, \quad M_{\kappa,\text{el}}^{r} = \frac{1}{a^{d-1}}\widetilde{T}_-^\top\widetilde{T}_-,$$

with $C_d := \frac{(1-d)(3-d)}{4}$,

$$\widetilde{T}_\pm := \begin{pmatrix} c_0 & \pm 1 & & \\ & 1 & \pm 1 & \\ & & \ddots & \ddots \end{pmatrix} \text{ and}$$

$$\widetilde{D}_a := a\,\mathrm{id} + \frac{1}{2i\kappa_0}\begin{pmatrix} -1 & 1 & & & \\ 1 & -3 & 2 & & \\ & 2 & -5 & 3 & \\ & & \ddots & \ddots & \ddots \end{pmatrix}.$$

Numerical examples

In a first example, we studied the scattering of plane incident waves with different wave numbers κ by a kite-

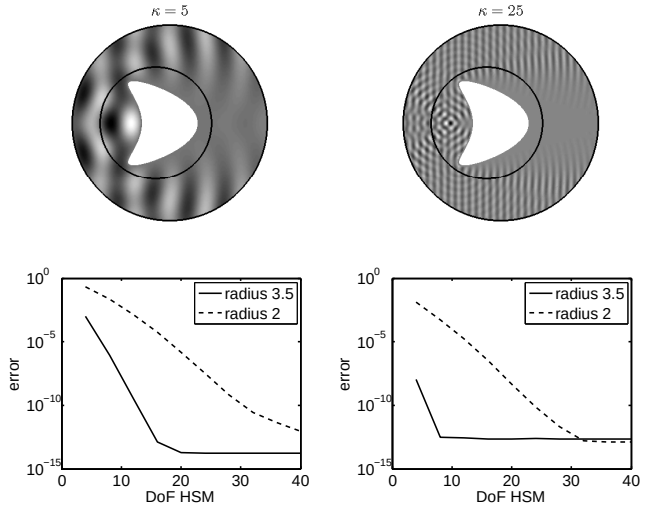

Figure 2: $H^{1/2}(\partial B_a)$ error in the Dirichlet data for different wave numbers and radii

shaped obstacle (see Fig. 2). First, a reference solution was computed by an integral equation method as described in [3, Section 3.5]). Then we used the computed Neumann data of the scattered wave on spheres of radius 2 and 3.5 as initial data for the the Hardy space infinite element method (HSM) and compared the Dirichlet data computed by the HSM with the data computed by the integral equation method. The error plot in Fig. 2 clearly exhibits fast convergence with respect to the degrees of freedom in the Hardy space $H^+(S^1)$. As for other methods (e.g. PML or standard infinite elements), the error for a fixed number of degrees of freedom in the exterior domain is the smaller the larger the distance of the coupling boundary to the scatterer. Surprisingly, we observed a smaller error for larger wave numbers.

As a second example we computed the resonances of a square with a small opening as shown in Fig. 3 using the HSM. The computations were done with the finite element solver NGSOLVE, an add-on of the mesh generator NETGEN [4]. In Fig. 3 three different eigenfunctions are plotted. The first two correspond to interior eigenvalues of the Laplace operator in a closed square and the third

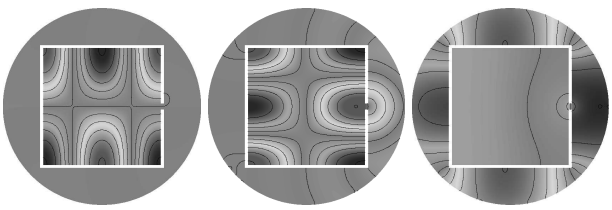

Figure 3: resonance functions of an open square

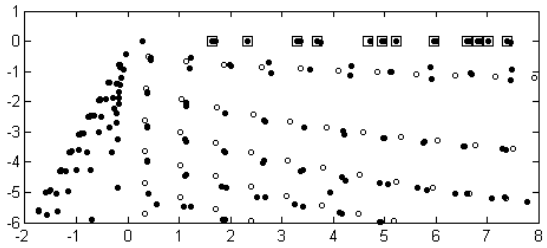

Figure 4: resonances of an open square;
●: resonances computed by the HSM;
□: exact eigenvalues of the closed square;
○: exterior resonances of a sphere with the same circumference as the closed square;

to an exterior resonance, which depends mainly on the circumference of the square (see also Fig. 4). The asymptotic behavior of these types of resonances has been studied intensively (see [5] and references therein). The resonances in the third quadrand are computational artifacts.

Acknowledgements:

The ideas presented here arose from discussions with Frank Schmidt and Lin Zschiedrich. Financial support of the DFG project Ho 2551/2-1 is gratefully acknowledged.

References

[1] T. Hohage, F. Schmidt, and L. Zschiedrich , "Solving time-harmonic scattering problems based on the pole condition. I. Theory", SIAM J. Math. Anal., 35 (2003), pp. 183–210 (electronic).

[2] T. Hohage, L. Nannen , "Hardy space infinite elements for scattering and resonance problems", in preparation.

[3] D. Colton, R. Kress , "Inverse acoustic and electromagnetic scattering theory", 2nd edition, Springer-Verlag, Berlin, 1998.

[4] J. Schöberl, "NETGEN - An Advancing Front 2D/ 3D-Mesh Generator Based On Abstract Rules", Comput.Visual.Sci, 1 (1997), pp. 41–52.

[5] M. Zworski, "Resonances in Physics and Geometry", Notices AMS, 46 (1999), p. 319–328.

ESTIMATES FOR TRAPPED MODES IN QUANTUM WAVEGUIDES AND LAYERS

H. Kovařík
Institute of Analysis, Dynamics and Modeling,
Universität Stuttgart, PF 80 11 40, D-70569 Stuttgart, Germany

Quantum waveguides

Consider the Dirichlet Laplacian $-\Delta_\Omega$ on straight tube $\Omega = \mathbb{R} \times \omega$, where $\omega \subset \mathbb{R}^{d-1}$ is a rather general cross-section. The spectrum of this operator is obviously purely absolutely continuous and covers the interval $[\lambda_1(\omega), \infty)$, where $\lambda_1(\omega)$ is the lowest eigenvalue of the Dirichlet Laplacian on ω. If $-\Delta_\Omega$ is perturbed by an attractive potential or by a local geometrical perturbation of the waveguide, eigenvalues below λ_1 might appear. The corresponding bound states, called *trapped modes*, are the main object of our interest.

Assume, for example, that a local potential perturbation V has been added. The corresponding Schrödinger operator

$$-\Delta_\Omega - V$$

has the essential spectrum $[\lambda_1(\omega), \infty)$. In addition, some discrete eigenvalues below λ_1, trapped modes, will appear. In [2] an upper bound on the sum of the moments of these eigenvalues has been obtained:

Theorem 1 (Exner, Weidl)**.** *For $x \in \Omega$ we write $x = (x', x_d)$. Let $\psi_1(x')$ be the eigenfunction associated with $\lambda_1(\omega)$. For any $\sigma \geq \frac{1}{2}$ we have*

$$\begin{aligned} tr(-\Delta_\Omega - \alpha V - \lambda_1)_-^\sigma \;\leq\; & \\ & c_1 \alpha^{\sigma+\frac{1}{2}} \int_{\mathbb{R}} \left(\int_\omega V(x', x_d) |\psi_1(x')|^2 dx' \right)^{\sigma+\frac{1}{2}} dx_d \\ & + c_2\, \alpha^{\sigma+\frac{d}{2}} \int_\Omega V^{\sigma+\frac{d}{2}} dx\,, \end{aligned} \tag{1}$$

where $(-\Delta_\Omega - \alpha V - \lambda_1)_-$ denotes the negative part of the operator $-\Delta_\Omega - \alpha V - \lambda_1$.

From the weak coupling asymptotics follows that (1) fails for any $\sigma < \frac{1}{2}$. In the borderline case $\sigma = \frac{1}{2}$, then (1) gives

$$\begin{aligned} \mathrm{tr}(-\Delta_\Omega - \alpha V - \lambda_1)_-^{\frac{1}{2}} \;\leq\; & \\ & c_1 \alpha \int_{\mathbb{R}} \left(\int_\omega V(x', x_d) |\psi_1(x')|^2 dx' \right)^{\sigma+\frac{1}{2}} dx_d \\ & + c_2\, \alpha^{\frac{d+1}{2}} \int_\Omega V^{\frac{d+1}{2}} dx. \end{aligned} \tag{2}$$

Note that this inequality has the optimal behaviour in α in the weak coupling regime, when $\alpha \to 0$, [5], as well as in the strong coupling regime, when $\alpha \to \infty$. Indeed, for small α the r.h.s. of (2) is dominated by the first term, which is linear in α. On the other hand, for α large the r.h.s. of (2) is dominated by the second term, which gives the correct Weyl asymptotic behaviour. Analogous estimates hold also for trapped modes induced by geometrical deformations, [1].

Quantum layers

Here we consider trapped modes in quantum layers, which concern a conducting plate $\Omega = \mathbb{R}^2 \times (0, d)$ with an electric potential V decaying at infinity. We will study the shifted Hamiltonian

$$H_\alpha = -\Delta_\Omega - \alpha V - \frac{\pi^2}{d^2} \quad \text{in} \quad L^2(\Omega)\,, \tag{3}$$

with Dirichlet boundary conditions at $\partial\Omega$. The essential spectrum of the operator H_α covers the half line $[0, \infty)$. Let us denote by $-\tilde{\lambda}_j$ the non decreasing sequence of negative eigenvalues of H_α. Our goal is to find an analog of inequality (2). Because of the different dimensionality of the system we have to replace the square root function on the l.h.s. of (2) by a different one. We introduce the family of functions $F_s : (0, \infty) \to (0, 1]$ such that

$$\forall\, s > 0 \quad F_s(t) := \begin{cases} |\ln ts^2|^{-1} & 0 < t \leq e^{-1} s^{-2}\,, \\ \\ 1 & t > e^{-1} s^{-2}\,. \end{cases} \tag{4}$$

In order to formulate our result we need some notation. The space $L^1(\mathbb{R}_+, L^p(\mathbb{S}^1))$ in polar coordinates (r, θ) in $\mathbb{R}^2$, is defined as the space of functions f such that

$$\|f\|_{L^1(\mathbb{R}_+, L^p(\mathbb{S}^1))} := \int_0^\infty \left(\int_0^{2\pi} |f(r,\theta)|^p \, d\theta \right)^{1/p} r \, dr < \infty\,. \tag{5}$$

Moreover, given $s > 0$ we denote $B(s) := \{x \in \mathbb{R}^2 : |x| < s\}$. We then have

Theorem 2 (Kovařík, Vugalter, Weidl)**.** *There exist positive constants C_1, C_2, C_3 such that*

$$\sum_j F_s(\tilde{\lambda}_j) \;\leq\; C_1\,\alpha\,\|\tilde{V}\ln(x_1^2+x_2^2)\|_{L^1(B(s))} + C_3\,\alpha\,\|\tilde{V}\|_{L^1(\mathbb{R}_+,L^p(\mathbb{S}^1))} + C_2\,\alpha^{3/2}\,\|V^{3/2}\|_{L^1(\Omega)}\,, \tag{6}$$

where

$$\tilde{V}(x_1,x_2) = \frac{2}{d}\int_0^d V(x_1,x_2,x_3)\,\sin^2\left(\frac{\pi\,x_3}{d}\right)\,dx_3\,.$$

Notice that (6) has the right asymptotic behaviour in both weak and strong coupling limits. Namely, in the weak coupling limit the r.h.s. is dominated by the term linear in α, while in the strong coupling limit prevails the term proportional to $\alpha^{3/2}$. Also here the result can be extended to the case of geometrically induced trapped modes, [4].

References

[1] P. Exner, H. Linde, T. Weidl: Lieb-Thirring inequalities for geometrically induced bound states, *Lett. Math. Phys.*, **70** (2004) 83–95.

[2] P. Exner, T. Weidl: Lieb-Thirring inequalities on trapped modes in quantum wires. In *Proc. XIII Internat. Congr. Math. Phys.*, (London 2000), International Press, Boston, 2001, pp. 437–443.

[3] H. Kovařík, S. Vugalter, T. Weidl: Spectral estimates for two-dimensional Schrdinger operators with application to quantum layers, To appear in *Commun. Math. Phys.* Preprint: math-ph/0612070.

[4] H. Kovařík, S. Vugalter: Estimates for trapped modes in deformed quantum layers. In preparation.

[5] B. Simon: The Bound State of Weakly Coupled Schrödinger Operators in One and Two Dimensions, *Ann. of Physics* **97** (1976) 279–288.

Evaluation of Rayleigh-Sommerfeld diffraction formula for PML solution

L. Zschiedrich[†,*], **F. Schmidt**[†]
[†]Zuse Institute, Takustrasse 7, 14195 Berlin, Germany
[*]Email: zschiedrich@zib.de

Abstract

The Rayleigh-Sommerfeld diffraction formula is commonly used for the evaluation of the scattered electromagnetic field outside the computational domain. However standard numerical methods lack the precise computation of the arising high–frequency integral with infinite integration domain. In this paper we propose a numerical method for the computation of the Rayleigh-Sommerfeld integral which is based on the computed near field data within the computational domain including the perfectly matched layer domain. In the presentation on the conference we will discuss the algorithm's application to the light beam characterization of a resonant optical device such as a laser cavity.

Introduction

The situation one typically encounters in optical simulations is as depicted in Figure 1. An optical device with a complex geometry is embedded in an inhomogeneous surrounding. Prominently, an integrated optical device, or an optical grating such as a phase shift lense is placed on a substrate which might consist of several glass layers. A pure near field simulation is of little practical interest. Instead, engineers are typically interested in field properties many wavelength away from the obstacle. In this paper we tackle the problem to compute the scattered field in the half space above the structure. This is commonly done by the evaluation of Rayleigh-Sommerfeld integral [1] which we will introduce in the next section. For a numerical evaluation we exploit complex continuation properties of the solution in combination with the Perfectly Matched Layer (PML) method. To keep the notation simple we will restrict ourself to the Helmholtz equation in 2D in this presentation. The obtained results are readily generalized to 3D and Maxwell's equations.

Rayleigh-Sommerfeld integral

The cartesian coordinates are denoted by (x, z). The scatterer is located in the lower half space $z < 0$. The material in the upper half space $z > 0$ has constant and isotropic optical properties. The permittivity and the permeability in the upper half space is denoted by ε_+ and μ_+. We aim to compute the scattered field in the upper half space $z > 0$ by means of the Rayleigh Sommerfeld integration formula which we formally derive here.

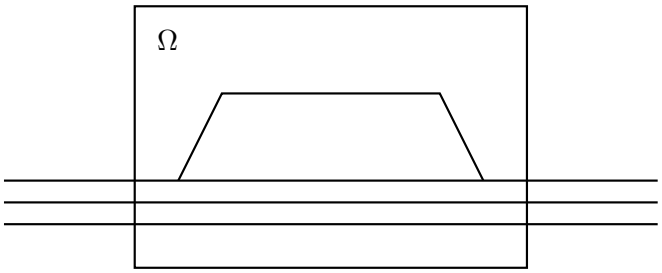

Figure 1: Typical mounting of an optical device. Ω denotes the computational domain.

In the homogeneous upper half space each field component E_x, E_y and E_z of the electric field satisfies the scalar Helmholtz equation

$$-\Delta u(x,z) - k_+^2 u(x,z) = 0$$

with $k_+ = \omega\sqrt{\varepsilon_+\mu_+}$. The Fourier transform on the hyper plane $z = 0$ is defined as

$$\widehat{u}(k_x) = \frac{1}{(2\pi)^{(d-1)/2}} \int_{\mathbb{R}^{d-1}} u(x',0) e^{-ik_x\cdot x'}\,\mathrm{d}x'.$$

Using the inverse Fourier transform and assuming that u is outward radiating in the upper half space one formally gets

$$\begin{aligned} u(x,z) &= \frac{1}{(2\pi)^{(d-1)/2}} \int_{\mathbb{R}^{d-1}} \widehat{u}(k_x) e^{ik_z z} e^{+ik_x\cdot x}\,\mathrm{d}k_x \\ &= \frac{1}{(2\pi)^{(d-1)/2}} \int_{\mathbb{R}^{d-1}} u(x',0) \frac{1}{(2\pi)^{(d-1)/2}} \\ &\quad \int_{\mathbb{R}^{d-1}} e^{ik_x\cdot(x-x')} e^{ik_z z}\,\mathrm{d}k_x\,\mathrm{d}x' \end{aligned}$$

with $k_z = \sqrt{k_+^2 - |k_x|^2}$. To evaluate the kernel

$$K(x') = \frac{1}{(2\pi)^{(d-1)/2}} \int_{\mathbb{R}^{d-1}} e^{ik_x\cdot(x-x')} e^{ik_z z}\,\mathrm{d}k_x$$

observe that $K(x')$ is equal to the inverse Fourier transform of the function $v(k_x) = \exp(ik_z z)$ at $(x - x')$. Therefore we must find the function whose Fourier transform is equal to $v(k_x)$. By Weyl's representation of a di-

verging spherical wave we have

$$\begin{aligned}\{\widehat{G_z(x')}\} &= \frac{i(2\pi)^{1/2}}{4\pi k_z}e^{ik_z z}, \quad \text{and hence}\\ \{\widehat{\partial_z G_z(x')}\} &= -\frac{(2\pi)^{1/2}}{4\pi}e^{ik_z z} = -\frac{(2\pi)^{1/2}}{4\pi}v(k_x),\end{aligned}$$

where G_z is the shifted Green function to the Helmholtz equation above,

$$-\Delta G_z(x',z') - k_+^2 G_z(x',z') = \delta(0,z'-z).$$

In the two dimensional case we have $G_z(x',z') = i/4H_0^{(1)}(k_+R)$ with $R = |(\vec{0},z) - (x',z'))|$ and with the zero order Hankel function $H_0^{(1)}$ of first kind.

Eventually one gets the first Rayleigh–Sommerfeld diffraction integral

$$u(x,z) = -2\int_{\mathbb{R}^{d-1}} u(x',0)\partial_z G_z(x-\vec{x'})\,\mathrm{d}x'. \qquad (1)$$

With $r_p = |(x,z) - (x',0)|$ and

$$\partial_z G_z(x-\vec{x'}) = -\frac{izk_+}{4r_p}H_1^{(1)}(k_+r_p)$$

and with the asymptotic behaviour of the Hankel function $|H_1^{(1)}(r)| \sim r^{-1/2}$ for large values r, one proves that the Rayleigh–Sommerfeld diffraction integral (1) is absolutely convergent,

$$\int_{-\infty}^{\infty} |u(x',0)\frac{iz}{4r_p}H_1^{(1)}(k_+r_p)| \le C\cdot z\int_1^{\infty} r^{-3/2} < \infty$$

for any bounded field $u(x',0)$.

PML: Evaluation of Rayleigh-Sommerfeld integral

The slow decay property of the Green function $G_z(x) \sim |x|^{-1/2}$ makes a direct numerical evaluation of the Rayleigh–Sommerfeld diffraction integral (1) prohibitively expensive. But as we will see a complex deformation of Rayleigh–Sommerfeld diffraction integral will yield an exponentially fast convergence to the true value with the size of the integration domain. Furthermore the arising integrand is available from the PML method. From the Rayleigh–Sommerfeld diffraction integral (1) one sees that for $z > 0$ the scattered field $u(x,z)$ possesses a complex extension in x to $s \in \mathbb{C}$ with $\Re s > a$ and $\Im s \ge 0$ for any $a > 0$. Hence after shifting the hyper plane $z = 0$ a bit we may assume that such a complex extension also exists for $z = 0$. Now we split the Rayleigh–Sommerfeld diffraction integral into three parts,

$$\begin{aligned}\int_{-\infty}^{\infty} u(x',0)\frac{iz}{4r_p}H_1^{(1)}(k_+r_p)\,\mathrm{d}x' &= \\ \int_{-\infty}^{-a} u(x',0)\frac{iz}{4r_p}H_1^{(1)}(k_+r_p)\,\mathrm{d}x' + \\ \int_{-a}^{a} u(x',0)\frac{iz}{4r_p}H_1^{(1)}(k_+r_p)\,\mathrm{d}x' + \\ \int_{a}^{\infty} u(x',0)\frac{iz}{4r_p}H_1^{(1)}(k_+r_p)\,\mathrm{d}x'.\end{aligned}$$

The second term is evaluated numerically. To evaluate the first or the third term we use Cauchy's contour integral theorem,

$$\begin{aligned}\int_{a}^{A} u(x',0)\frac{iz}{4r_p}H_1^{(1)}(k_+r_p)\,\mathrm{d}x' &= \\ \int_{a}^{A+i\sigma(A-a)} u(s,0)\frac{iz}{4r_p}H_1^{(1)}(k_+r_p)\,\mathrm{d}s + \\ \int_{A+i\sigma(A-a)}^{A} u(s,0)\frac{iz}{4r_p}H_1^{(1)}(k_+r_p)\,\mathrm{d}s.\end{aligned} \qquad (2)$$

We show that the second integral vanishs for $A \to \infty$. Due to the boundedness of $u(s,0)$ for $s \in \mathbb{C}_{+,A} = \{z \in \mathbb{C} : \Re z > A,\ \Im z \ge 0\}$ we have

$$\begin{aligned}|\int_{A+i\sigma(A-a)}^{A} u(s,0)\frac{1}{r_p}H_1^{(1)}(k_+r_p)\,\mathrm{d}s| &\le \\ CA\max_{s\in\mathbb{C}_{+,A}}\frac{1}{|r_p|}\cdot\max_{s\in\mathbb{C}_{+,A}}|H_1^{(1)}(k_+r_p)|.\end{aligned}$$

Recall that $r_p = \sqrt{(x-s)^2+z^2}$ so that $r_p \sim s$ for $\|s\| \to \infty$ and hence $|r_p| \ge CA$ for $s \in \mathbb{C}_{+,A}$ and A large enough. Together with the asymptotic behaviour of the Hankel functions this shows that the right hand side in the unequality above is zero in the limit $A \to \infty$.

For $A \to \infty$ the first integral term in Equation (2) can be cast into the form

$$\gamma\int_0^{\infty} u(a+\gamma\tau,0)\frac{iz}{4r_{p,\gamma}}H_1^{(1)}(k_+r_{p,\gamma})\,\mathrm{d}\tau$$

with $\gamma = 1 + i\sigma$ and $r_{p,\gamma} = \sqrt{(x-(a+\gamma\tau))^2+z^2}$. This integral has very favorable properties with respect to a numerical integration. The integrand is essentially the product of the complex continued solution field as it appears in the PML method and a Hankel function with complex arguments. Asymptotically both factors are exponentially decaying. But the Hankel function contribution might first increase exponentially for small values of

τ depending on the position of the evaluation point. However, typically the exponential decay of the PML solution over-compensates the growth of the second factor so that an exponential decay of the integrand is observed even for small values of τ. Thus the integration domain can be truncated with a controllable loss of accuracy.

Remarks

An adaptive PML method as proposed in our paper [2] is designed for an optimal convergence within the computational domain. It does not guarantee that the chosen discretization in the perfectly matched layer is appropriate for an accurate evaluation of the complex deformed Rayleigh-Sommerfeld integral. In our code we therefore do not use the PML data obtained from the near field simulation directly. Instead we recompute the complex deformed solution and use an adaptive method to guarantee convergence.

For 3D it is necessary to use a polar like coordinate system in the $z = 0$ hyperplane. Such a (ξ, η) coordinate system with a radial like variable ξ and angular like variable η was introduced in [3]. In the PML method only a complex deformation in the radial like $\xi-$direction is used. A deformed Rayleigh-Sommerfeld integral in polar coordinates can be derived.

Numerical example: Waveguide notch

As a numerical example we consider a notch in a waveguide, c.f. Figure 2. The waveguide has a width $w = 0.2\mu m$ and a permittivity of $\epsilon_{\mathrm{wg}} = 11.42\mu m$. The waveguide is buried $0.4\mu m$ deep in a substrate with permittivity $\epsilon_{\mathrm{sub}} = 10.05\mu m$. In our simulation the waveguide's fundamental mode enters the computational domain from the left and is scattered by an air filled defect of width $w_{\mathrm{N}} = 0.6\mu m$. We evaluated the exterior field above the structure at a distance of $\delta_z = 5\mu m$. In a first setting we used a rectangular computational domain with an vertical extension of $1\mu m$ above the structure. In horizontal direction we used a small slit of $2\mu m$ around the notch. The exterior field values were computed by the Rayleigh-Sommerfeld integral formula as proposed in the previous section. In a second setting we chose a computational domain sufficiently large to contain all evaluation points. The computed exterior domain data are given in Figure 3. The solid lines correspond to the first setting and the marks to the second setting. Both computed data are in a very good agreement. We will study the convergence of the proposed method in more detail in the presentation.

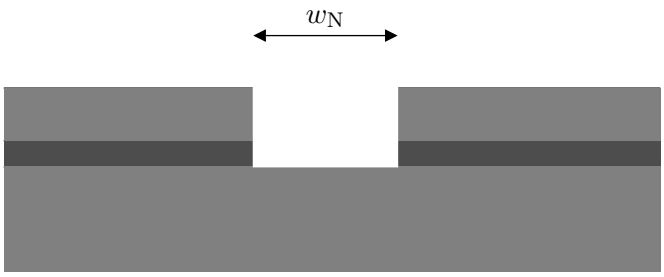

Figure 2: Waveguide notch. A dielectric integrated waveguide (dark gray) is disrupted by an air filled notch.

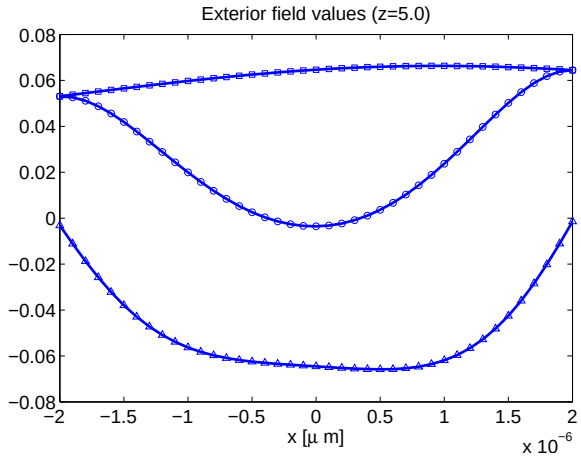

Figure 3: Exterior field values for waveguide notch problem. (real part: ○, imaginary part: △, absolute values: □).

References

[1] W. Singer, M. Totzeck, H. Gross, "Handbook of Optical Systems, Volume 2: Physical Image Formation", Wiley-VCH, Berlin, 2005

[2] L. Zschiedrich, S. Burger, B. Kettner, F. Schmidt "Advanced finite element method for nano-resonators", Proc. SPIE Vol. 6115, 2006

[3] F. Schmidt, "Solution of Interior-Exterior Helmholtz-Type Problems Based on the Pole Condition Concept: Theory and Algorithms", Free University Berlin, Fachbereich Mathematik und Informatik Habilitation thesis (2002)

Minisymposium on Time-Domain Methods

Organisers: Markus Grote (University of Basel) and Patrick Joly (INRIA)

INVESTIGATION OF IMPLICIT TIME STEPPING FOR GRID-INDUCED STIFFNESS IN DISCONTINUOUS GALERKIN TIME DOMAIN METHODS ON UNSTRUCTURED TRIANGULAR MESHES

A. Catella[†], V. Dolean[†,‡] and S. Lanteri[†,*]
[†]Caiman project-team, INRIA, 06902 Sophia Antipolis Cedex, France
[‡]J.A. Dieudonné Mathematics Laboratory, University of Nice-Sophia Antipolis, 06108 Nice Cedex, France
[*]Email: Stephane.Lanteri@irnia.fr

Abstract

Numerical methods for solving the time domain Maxwell equations most often rely on cartesian meshes and are variants of the finite difference time domain method originating in the seminal work of Yee[6]. However, in the recent years, there has been an increasing interest in discontinuous Galerkin time domain methods dealing with unstructured meshes since the latter are particularly well suited for the discretization of geometrical details that characterize applications of practical relevance. Similarly to Yee's finite difference time domain method, discontinuous Galerkin time domain methods generally rely on explicit time integration schemes and are therefore constrained by a stability condition that can be very restrictive on highly refined or unstructured meshes. An implicit time integration scheme is a natural way to obtain a time domain method which is unconditionally stable. The present study aims at investigating the applicability of an implicit time integration scheme in conjunction with a discontinuous Galerkin approximation method for solving the time domain Maxwell equations on unstructured triangular meshes.

Introduction

In the numerical treatment of the time domain Maxwell equations, finite difference time domain (FDTD) methods based on Yee's scheme[6] are still prominent because of their simplicity (a time explicit method defined on cartesian meshes) and their non-dissipative nature (they hold an energy conservation property which is an important ingredient in the numerical simulation of unsteady wave propagation problems). Unfortunately, when dealing with complex geometries, the FDTD method is not always the best choice since local refinements of the grid, albeit possible in the form of subgridding techniques [4], has an adverse effect on accuracy and efficiency. In particular, local refinement translates in a very restrictive time step in order to preserve the stability of the explicit leap-frog scheme used for time integration in the FDTD method. Finite element time domain (FETD) based on unstructured meshes can easily deal with complex geoemtries however they induce heavy computations or require accurate and efficient lumping of mass matrices. Finite volume time domain (FVTD) methods on unstructured meshes also appeared as an alternative to FDTD methods, but they suffer from numerical diffusion resulting from the use of upwind schemes, and their extension to high-order accuracy is a tedious task.

Discontinuous Galerkin time domain (DGTD) methods can handle unstructured meshes and deal with discontinuous coefficients and solutions [5]. They can be seen as generalizations of the FVTD methods, where the finite element approximation is piecewise constant inside elements. The different achievements of the FVTD methods are now being extended in the context of DGTD methods which enjoy a renewed favor nowadays and are used in a wide variety of applications [1] as people rediscover the abilities of these methods to handle complicated geometries, media and meshes, to achieve a high order of accuracy by simply choosing suitable basis functions, to allow long-range time integrations and, last but not least, to remain highly parallelizable [3]. However, DGTD methods suffer from the same limitation concerning the allowable time step on locally refined unstructured meshes. In this study, we investigate the applicability of an implicit time integration strategy in order to overcome the stability constraint that apply to explicit DGTD methods for solving the two-dimensional Maxwell equations on unstructured triangular meshes.

Implicit DGTD methods

The starting point of this study is the explicit DGTD method presented in [5]-[3] for solving the three-dimensional time domain Maxwell equations on unstructured tetrahedral meshes. Beside a standard discontinuous Galerkin formulation [1], this method is based on two basic ingredients: a centered approximation for the calculation of numerical fluxes at inter-element boundaries, and an explicit leap-frog time integration scheme. The implicit DGTD method proposed here differs from its explicit counterpart in the time integration scheme which is a Crank-Nicholson scheme. The resulting implicit

DGTD method is non-dissipative and unconditionally stable. This method requires the resolution of a sparse linear system at each time step but, for non-dispersive materials, the coefficient of this system are time independent, a feature that can be taken into account to minimize the additional computational overhead.

Sample of numerical results

We present here a sample of results aiming at a preliminary comparison between the explicit, leap-frog based DGTD method and the implicit, Crank-Nicholson based DGTD method. Both methods have been developed in the framework of high-order polynomial interpolation ($\mathbb{P}_p$ nodal basis for $p \geq 0$) on unstructured triangular meshes for the resolution of the two-dimensional transverse magnetic Maxwell equations. The implicit DGTD method proposed here requires the resolution of a sparse linear system at each time step however, for non-dispersive materials, the coefficient of this system are time independent, a feature that can be taken into account to minimize the additional computational overhead. Consequently, in this study, we decided to use a LU factorization method for sparse matrices more precisely, the MUMPS multifrontal sparse matrix solver [2]. The sparse matrix characterizing the implicit DGTD method has a block structure where the size of a block is $3n_p \times 3n_p$, n_p being the number of degrees of freedom associated to a nodal polynomial basis of the space $\mathbb{P}_p$ i.e $n_p = ((p+1)(p+2))/2$. This matrix is factored once for all before the time stepping loop. Then, each linear system inversion amounts to a forward and a backward solve using the triangular L and U factors.

The test case that we consider here is the propagation of an eigenmode in a unitary square cavity with perfectly conducting walls. This test case allows a direct comparison with an exact solution. Here, it will also be used to demonstrate that we cannot take advantage of the proposed implicit DGTD-$\mathbb{P}_p$ method if the underlying mesh is uniform (or quasi-uniform) while substantial reductions of the computing time can be achieved in the case of a non-uniform mesh. For this purpose, we make use of two triangular meshes:

- a uniform mesh consisting of 1681 vertices and 3200 triangles. The non-dimensioned time step corresponding to CFL-$\mathbb{P}_0$=1 is $(\Delta t)_u = 0.017678$ m (the physical time step is defined by $\overline{(\Delta t)_u} = (\Delta t)_u/3.10^8$ s). For the interpolation orders $p \geq 1$, the time step actually used is CFL-$\mathbb{P}_p \times (\Delta t)_u$ where CFL-$\mathbb{P}_p$ is the CFL number associated to the DGTD-$\mathbb{P}_p$ method.
- a non-uniform mesh consisting of 1400 vertices and 2742 triangles. The ratio between the largest and smallest edges of this mesh is 178. In this case, the minimum and maximum values of the time step are respectively given by $(\Delta t)_m = 0.000434$ m and $(\Delta t)_M = 0.070617$ m. The time step used in the simulations is CFL-$\mathbb{P}_p \times (\Delta t)_m$.

For the explicit DGTD-$\mathbb{P}_p$ method, CFL-$\mathbb{P}_p \leq 1$ and the actual value is dictated by stability issues while CFL-$\mathbb{P}_p$ can be set to an arbitrarily large value for the implicit DGTD-$\mathbb{P}_p$ method but is constrained in practice by accuracy issues. Results are given on Fig. 1 and Fig. 2 in the form of the time evolution of the L2 error between the numerical and exact solutions. The simulations were carried out for ten periods. Computing times are summarized in Tab. 1 and 2. It is clear from these results that a second order implicit time integration scheme is not a good option if the underlying mesh is uniform. Indeed, the numerical dispersion introduced by the Crank-Nicolson scheme notably degrades the overall accuracy of the calculation. However, if a non-uniform mesh is used then an implicit scheme becomes a viable strategy despite the computational overhead of the solution of a linear system at each time iteration. Taking into account the time behavior of the L2 error on Fig. 1 and 2, we see that a CFL value of 12.0 (respectively 4.0) for the implicit DGTD-$\mathbb{P}_1$ method (respectively DGTD-$\mathbb{P}_2$ method) yields an acceptable solution. For these values of the CFL, the gain in overall computing (CPU) times between the implicit and explicit methods is respectively equal to 3.3 and 2.2 (note that the given CPU times include the factorization times).

Time integration	Method	CFL-$\mathbb{P}_p$	CPU time
Explicit	DGTD-$\mathbb{P}_1$	0.3	15 sec
Implicit	-	1.0	44 sec
-	-	1.5	30 sec

Table 1: Eigenmode in a PEC cavity - Uniform mesh CPU times (AMD Opteron 2 GHz based workstation)

Time integration	Method	CFL-$\mathbb{P}_p$	CPU time
Explicit	DGTD-$\mathbb{P}_1$	0.3	443 sec
Implicit	-	12.0	133 sec
-	-	24.0	67 sec
Explicit	DGTD-$\mathbb{P}_2$	0.2	2057 sec
Implicit	-	2.0	1923 sec
-	-	4.0	938 sec
-	-	6.0	620 sec

Table 2: Eigenmode in a PEC cavity - Non-uniform mesh CPU times (AMD Opteron 2 GHz based workstation)

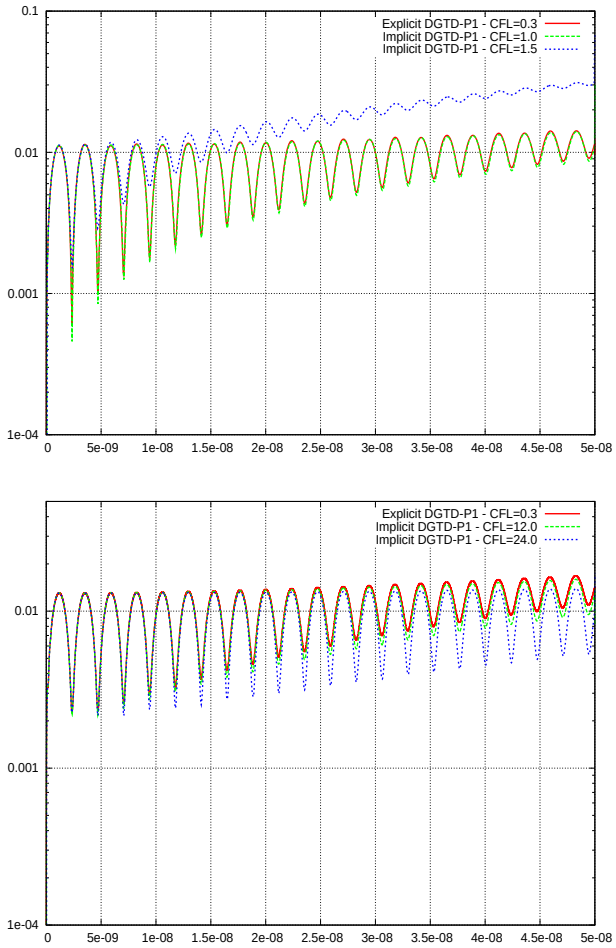

Figure 1: Eigenmode in a PEC cavity - DGTD-$\mathbb{P}_1$ method
L2 error versus time : uniform mesh (top) and non-uniform mesh (bottom)

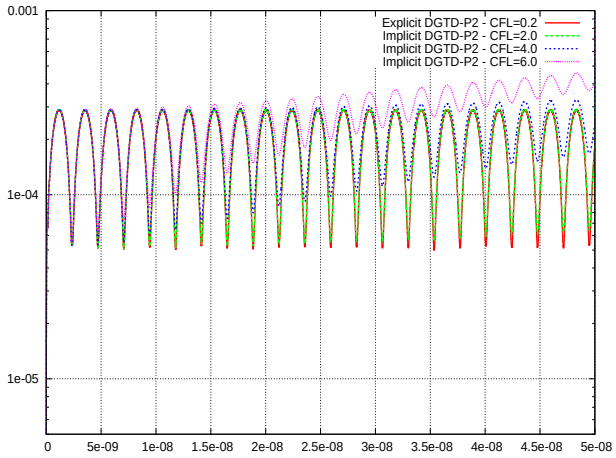

Figure 2: Eigenmode in a PEC cavity - Non-uniform mesh
DGTD-$\mathbb{P}_2$ method: L2 error versus time

Closure

We are investigating the potential benefits of using an implicit DGTD-$\mathbb{P}_p$ method for solving the time domain Maxwell equations on unstructured triangular meshes. This method is non-dissipative, second order accurate in time an $p+1$-th order accurate in space. For two-dimensional problems, a direct solver based on a LU factorization such as the one adopted in this study is generally considered as the optimal strategy, at least from the computing time point of view. Preliminary numerical results suggest that an implicit discontinuous Galerkin time domain is a viable numerical strategy for solving electromagnetic wave propagation problems on locally refined unstructured meshes. Ongoing works are concerned with the assessment of the proposed implicit DGTD-$\mathbb{P}_p$ method on test cases for which local refinement of the mesh is motivated by physical or/and geometrical features.

References

[1] Discontinuous Galerkin methods. Theory, computation and applications, Lecture Notes in Computational Science and Engineering, Vol. 11, Springer-Verlag, 2000.

[2] P.R. Amestoy, I.S. Duff and J.-Y. L'Excellent, "Multifrontal parallel distributed symmetric and unsymmetric solvers", Comput. Meth. App. Mech. Engng., Vol. 184, pp. 501-520, 2000.

[3] M. Bernacki and L. Fezoui and S. Lanteri and S. Piperno, "Parallel unstructured mesh solvers for heterogeneous wave propagation problems", Appl. Math. Model., Vol. 30, No. 8, pp. 744–763, 2006.

[4] S. Chaillou and J. Wiart and W. Tabbara, "A subgridding scheme based on mesh nesting for the FDTD method", Vol. 22, No. 3, pp. 211–214, 1999.

[5] L. Fezoui and S. Lanteri and S. Lohrengel and S. Piperno, "Convergence and stability of a discontinuous Galerkin time-domain method for the 3D heterogeneous Maxwell equations on unstructured meshes", M2AN, Vol. 39, No. 6, pp. 1149-1176, 2005.

[6] K.S. Yee, "Numerical solution of initial boundary value problems involving Maxwell's equations in isotropic media", IEEE Trans. Antennas and Propagation, Vol. 14, No. 3, pp. 302–307, 1966.

A HYBRID HIGH ORDER FINITE ELEMENT METHOD FOR THE TIME DOMAIN SOLUTION OF WAVE SCATTERING PROBLEMS

Richard W. Davies[†], **Ken Morgan, Oubay Hassan**
Civil & Computational Engineering Centre, University of Wales Swansea, Swansea, Wales
[†]Email: 175677@swan.ac.uk

Abstract

The motivation for a higher order solution procedure for wave scattering problems is explained and the development of a hybrid method is discussed. Details of the method are given to elucidate its properties and results of some simple wave scattering examples are presented for validation and to enable the possibilities offered by the approach to be assessed.

Introduction

To achieve fully developed solutions for practical time domain wave propagation and scattering problems, integration through a significant amount of time is often necessary. Consequently, approximation with low order spatial schemes can prove to be inappropriate, as results employing practical domain discretisation can be highly inaccurate. Since the first applications of higher order spatial schemes, much interest has been generated by the potential of these methods to exhibit exponential *p*-convergence. In this way, it is believed that the ultimate goal of a more efficient numerical scheme may be achieved.

Spectral element formulations have been shown to offer accurate and efficient solutions [1]. The approach employs a specific set of Gauss-Legendre-Lobatto (GLL) points to define the interpolation functions, with a corresponding quadrature method for integration. This leads to a diagonal mass matrix. However, at present, these properties can only be achieved on quadrilateral meshes. An alternative procedure for triangles has been proposed [2], but the use of Fekete points, and the corresponding inferior quadrature, results in lower solution accuracy.

Higher order discontinuous Galerkin methods applied to triangular meshes have numerous benefits. An element-wise variational statement enables the use of the consistent mass matrix, as inversion is on a local, element level. This avoids the computational expense associated with the requirement for assembly and inversion of a global mass matrix. Accurate reproduction of the complex surfaces often encountered in industrially interesting problems can be critical and is best achieved with an unstructured triangular mesh. However, the increase in nodal points, due to the discontinuous nature of the scheme, leads to more computational work.

For scattering simulations, which involve the interaction between an incident wave, generated by a source in the far field, and a scattering object, this naturally leads to the requirement for a hybrid method. A diagonal mass matrix spectral element method (SEM) will be applied to a structured quadrilateral mesh in the regular regions of the domain, while in the more geometrically complex regions surrounding the scatterer, a spectral discontinuous Galerkin (DG) method will be applied to an unstructured triangular mesh. An example of such a hybrid grid can be seen in Figure 1.

The purpose of this paper will be to provide a brief introduction to the method and offer an indication of the results which can be achieved.

Governing Equations

The governing equations considered here can be expressed as a single vector equation

$$\frac{\partial \mathbf{U}}{\partial t} + \frac{\partial \mathbf{F}}{\partial x} + \frac{\partial \mathbf{G}}{\partial y} = \mathbf{0} \tag{1}$$

where, for acoustic waves, $\mathbf{U} = [u^t, v^t, p^t]^T$, $\mathbf{F} = [p^t, 0, u^t]^T$, $\mathbf{G} = [0, p^t, v^t]^T$. Here p is the pressure and u and v are the velocities in the x and y directions respectively. However, the definition of the vectors as $\mathbf{U} = [E_y^t, -E_x^t, H_z^t]^T$, $\mathbf{F} = [H_z^t, 0, E_y^t]^T$, $\mathbf{G} = [0, H_z^t, -E_x^t]^T$ where E_x and E_y are the electric field intensities in the x and y directions respectively and H_z is the magnetic field intensity in the z direction, gives the governing equations for a transverse electric (TE^z) polarization of Maxwell's electromagnetic equations. Similarly, the definition $\mathbf{U} = [-H_y^t, H_x^t, E_z^t]^T$, $\mathbf{F} = [E_z^t, 0, -H_y^t]^T$, $\mathbf{G} = [0, E_z^t, H_x^t]^T$ produces the equations for a transverse magnetic (TM^z) polarization.

The linearity of the governing equations enables the total wave field, indicated by the superscript t, to be decomposed into its incident and scattered components. Therefore, as our interest lies mainly in the scattered wave field, (1) can be rewritten solely in terms of this component, thus enabling its direct calculation.

Solution Procedures

Previous research [3], examining the accuracy of various temporal discretisation schemes applied to wave propagation problems involving extended integration times, concluded in the recommendation that a Taylor-Galerkin scheme be used for temporal approximation. Applying an explicit one-step second order Taylor-Galerkin (TG2) scheme to (1) leads to a semi discrete form. Higher order schemes, such as the third order (TG3) and fourth order (TG4) Taylor Galerkin schemes, are available [4] but have not been implemented to date. From here, standard forms of the variational statements for the governing equation are obtained in the usual weighted residual manner for both the continuous SEM and the spctral DG parts of the domain.

For the structured quadrilateral elements, which constitute the SEM part of the domain, the interpolation functions are constructed from a tensor product of two one-dimensional interpolation functions $N(x,y) = P(x) \otimes Q(x)$, each of which is formed by Lagrange interpolation through Gauss-Legendre-Lobatto (GLL) points. The diagonal form of the mass matrix can then be achieved by utilising GLL quadrature for the evaluation of the mass matrix integral. As discussed in [5], the integration properties of GLL quadrature ensure that the accuracy of this approximation is maintained and the resulting solution is sufficiently close to that of the consistent mass form.

The triangular element interpolation functions are formed directly by performing Lagrange interpolation through the two-dimensional set of Fekete points [2]. These points were chosen because of their interpolation properties and as they coincide with GLL points along the boundaries of the elements. This simplifies the application of the coupling procedure, a standard Roe flux calculation, between both parts of the hybrid mesh. As noted previously, a corresponding diagonal treatment for the triangular element mass matrix results in a loss of accuracy. Therefore, using the alternative spectral DG formulation, the consistent form of the mass matrix can be used, for which integration is performed here using standard Gauss quadrature.

The infinite domains encountered in wave scattering problems must be truncated to enable the creation of practical computational models. Therefore, an appropriate treatment must be applied at these artificial boundaries. In this work, this is achieved by addition of a perfectly matched layer (PML) [6].

Results

Validation of the computational procedure was performed using a standard model of a circular perfectly electrically conducting (PEC) scatterer for which an exact analytical solution is available. Figure 1 shows the hybrid mesh used for this model and the H_z^s scattered wave field for a TE^z polarization of the EM wave equations, while Figure 2 illustrates the corresponding scattering width using varying element order. The electrical length of this model was 2λ. Convergence to the exact solution, as the polynomial order is increased on this mesh, is evident.

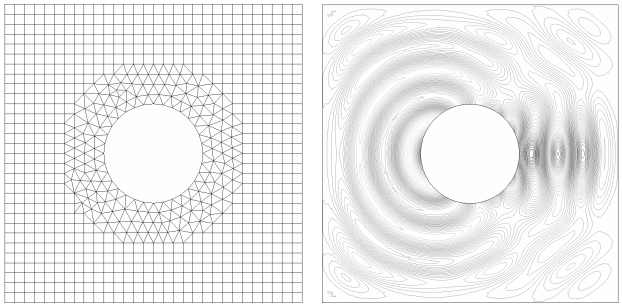

Figure 1: (a) Hybrid mesh and (b) H_z^s scattered wave field for a TE^z polarization of the EM wave equations

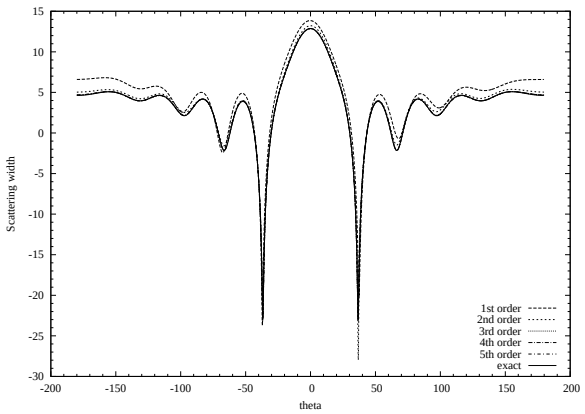

Figure 2: Scattering width for a circular scatterer of electrical length 2λ using varying element order

Further validation was achieved by increasing the complexity of the model and comparing the computational model with the exact solution for a scatterer of electrical length 15λ. Figure 3 shows that the numerical solution for the scattering width obtained using 5^{th} order elements is indistinguishable by visual inspection from the exact solution.

As an example of the use of the approach in a predictive mode, a TE^z model of a simple PEC dihedral scatterer is considered. For this model, the point of intersection of the legs of the dihedral is located at the origin with the

legs lying along the negative x-axis and the positive y-axis. Convergence of the scattering width with increasing element order, for an incident wave propagating in the positive x-direction (incident direction $\theta = 180^o$), can be seen in Figure 4. Scattered wave distributions of H_z^s for four different incident wave directions are presented in Figure 5.

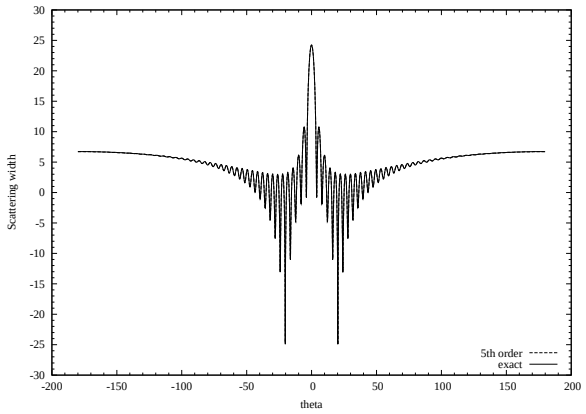

Figure 3: Scattering width for a circular scatterer of electrical length 15λ using 5^{th} order elements

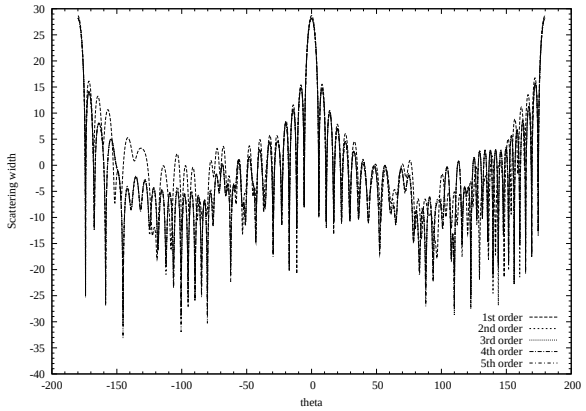

Figure 4: Scattering width for a dihedral scatterer using varying element order

Conclusion

A hybrid SEM / spectral DG method for wave scattering problems has been introduced and validated against an analytical solution. Subsequently, a further scattering example was presented to demonstrate the possible output of the method. Initial results seem promising, however, further work is needed to assess the relative computational advantages be be gained.

Acknowledgements

The authors would like to thank D.P. Rowse and D. Hoffman, BAE Systems plc, ATC (Sowerby), Filton, Bristol for suggesting the dihedral wave scattering example.

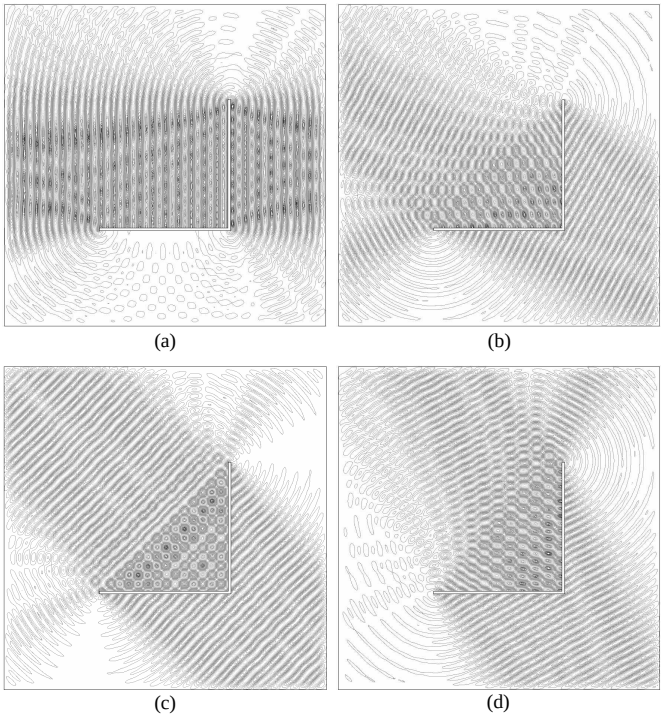

Figure 5: Scattering field distribution for various incident directions (a)-(d) $\theta = 180^o, 150^o, 135^o, 120^o$

References

[1] A.T. Patera, “A Spectral Element Method for Fluid Dynamics: Laminar Flow in a Channel Expansion”, Journal of Computational Physics, Vol 54 pp 468-488, 1984.

[2] M.A. Taylor, B.A. Wingate, “A Generalized Diagonal Mass Matrix Spectral Element Method for Non-quadrilateral Elements”, Applied Numerical Mathematics, Vol 33 pp 259-265, 2000.

[3] R.W. Davies, “Solution of Wave Scattering Problems using a SEM on 2D Quadrilateral Grids”, MRes Thesis, University of Wales Swansea, 2005.

[4] J. Donea, A. Huerta, Finite Element Methods for Flow Problems, Wiley, Chichester, England, 2003.

[5] R.W. Davies, K. Morgan, O. Hassan, “A Time Domain SEM for Acoustic Scattering Problems”, in Proceedings of the 14^{th} ACME Conference , Queen’s University, Belfast, 19-20 April 2006, pp. 91-94.

[6] F. Bonnet, F. Poupaud, “Berenger Absorbing Boundary Condition with Time Finite-Volume Scheme for Triangular Meshes”, Applied Numerical Mathematics, Vol 25 pp 333-354, 1997.

ENERGY CONSERVING EXPLICIT LOCAL TIME STEPPING FOR SECOND-ORDER WAVE EQUATIONS

J. Diaz[†,*], **M. Grote**[‡]
[†]Magique3D, Inria Futurs, Pau, France
[‡]Department of Mathematics, University of Basel, Basel, Switzerland.
[*]Email: julien.diaz@inria.fr

Abstract

We present a new local time-stepping method for the wave equation. The scheme is explicit, conserves a discrete energy and is stable under an optimal CFL condition. We illustrate the efficiency of the method and validate the theory with numerical results.

Introduction

Adaptivity and mesh refinement are certainly key for the efficient numerical solution of partial differential equations. However, locally refined meshes impose severe stability constraints on explicit time-stepping schemes, where the maximal time step allowed by a CFL condition is dictated by the smallest elements in the mesh. When mesh refinement is restricted to a small region, the use of implicit methods, or a very small time step in the entire computational domain, are very high a price to pay. To overcome that stability restriction, we propose local time-stepping schemes, which allow arbitrarily small time steps where small elements in the mesh are located. When combined with a symmetric finite element discretization in space with an essentially diagonal mass matrix, the resulting fully discrete scheme is explicit and exactly conserves a discrete energy. Starting from the standard second order "leap-frog" scheme, time integrators of arbitrary order of convergence are derived. Numerical experiments illustrate the efficiency of these methods and validate the theory.

1 Local time-stepping

We consider the scalar wave equation

$$u_{tt} - \nabla \cdot \left(c^2 \, \nabla u \right) = f \qquad \text{in } (0,T) \times \Omega, \qquad (1)$$

with appropriate initial and boundary conditions. Here Ω is a bounded domain in $\mathbb{R}^d$, $d = 2, 3$. The source term f lies in $L^2(0,T;L^2(\Omega))$ and we assume that the speed of propagation, $c(x)$, is piecewise smooth, bounded, and strictly positive.

Starting from the weak formulation of (1), we then consider either standard conforming finite elements with mass lumping [2] or a recent symmetric interior penalty discontinuous Galerkin (DG) formulation [1] for the spatial discretization of (1). Both eventually lead to a second-order system of ordinary differential equations of the form:

$$M \frac{d^2 y}{dt^2} + Ky = F, \qquad (2)$$

where both M, K are $m \times m$ symmetric positive definite (SPD) matrices, where m denotes the number of degrees of freedom in the discrete solution. Moreover, $M^{1/2}$ can be obtained at low cost, since M is (block-)diagonal. For $F = 0$ the energy

$$E[y](t) = \dot{y}^\top M \dot{y} + y^\top K y$$

is conserved in time. Hence, we now seek time discretizations of (2), which also conserve (a discrete version of) the energy.

We let $F = 0$ and multiply (2) by $M^{-1/2}$ to obtain

$$\frac{d^2 z}{dt^2} + M^{-1/2} K M^{-1/2} z = 0, \qquad (3)$$

with $z = M^{1/2} y$. Next, we set $A = M^{-1/2} K M^{-1/2}$, which is also symmetric positive definite, and thus rewrite (3) as

$$\frac{d^2 z}{dz^2} + Az = 0 \, . \qquad (4)$$

The (exact) solution $z(t)$ of (4) satisfies

$$\begin{aligned} &z(t+\Delta t) - 2z(t) + z(t-\Delta t) = \\ &-\Delta t^2 \int_{-1}^{1} (1-|\theta|) A z(t+\theta \Delta t) \, d\theta. \end{aligned} \qquad (5)$$

The integral on the right-hand side of (5) represents a weighted average of $Az(s)$ over the interval $(t-\Delta t, t+\Delta t)$, which needs to be approximated in any numerical algorithm. For instance, if we simply replace $Az(t+\theta\Delta t)$ by $Az(t)$ in (5) and evaluate the remaining θ-dependent integral, we obtain the well-known second order leap-frog scheme with time step Δt,

$$\frac{z_{m+1} - 2z_m + z_{m-1}}{\Delta t^2} = -Az_m, \qquad z_m \simeq z(t_m), \quad (6)$$

which, however, would require Δt to be comparable in size to the smallest elements in the mesh.

Instead, following [3], [4], we now split the vector $z(t)$ in two parts:

$$z(t) = (I-P)z(t) + Pz(t) = z^{[\text{coarse}]}(t) + z^{[\text{fine}]}(t)\ .$$

The projection matrix P is diagonal: its diagonal entries, equal to zero or one, identify the unknowns associated with the locally refined region, that is where smaller time steps are needed. To circumvent the severe CFL restriction on Δt in (6), we shall treat $z^{[\text{fine}]}(t)$ differently from $z^{[\text{coarse}]}(t)$ in

$$z(t+\Delta t) - 2z(t) + z(t-\Delta t) =$$
$$-\Delta t^2 \int_{-1}^{1} (1-|\theta|) A \left[z^{[\text{coarse}]}(t+\theta\Delta t) + z^{[\text{fine}]}(t+\theta\Delta t) \right] d\theta.$$

Thus, we replace

$$A\left[z^{[\text{coarse}]}(t+\theta\Delta t) + z^{[\text{fine}]}(t+\theta\Delta t) \right]$$

by

$$Az^{[\text{coarse}]}(t) + APq(\theta\Delta t),$$

where $q(\tau)$ solves the differential equation

$$\frac{d^2q}{d\tau^2}(\tau) = -A(I-P)z(t) - APq(\tau), \qquad (7)$$
$$q(0) = z(t), \qquad q'(0) = 0. \qquad (8)$$

Using Taylor expansions, we can show that the exact solution q of (7-8) satisfies $q(\Delta t) = q(-\Delta t)$ and

$$2(q(\Delta t) - q(0)) = \Delta t^2 Az(t) + O(\Delta t^4),$$

whereas the exact solution z of (4) satisfies

$$z(t+\Delta t) - 2z(t) + z(t-\Delta t) = \Delta t^2 Az(t) + O(\Delta t^4).$$

Then we obtain that :

$$z(t+\Delta t) - 2z(t) + z(t-\Delta t) = 2(q(\Delta t) - q(0)) + O(\Delta t^4). \qquad (9)$$

2 Algorithm

For each time step Δt, the algorithm to advance $z(t)$ from t to $t+\Delta t$ proceeds as follows :

1. We solve (7) with the leap-frog scheme using p time steps each of size $\Delta\tau = \Delta t/p$, $p \geq 1$, which yields $q(\Delta t)$;
2. We update $z(t+\Delta t)$ by using (9).

Here, a key observation in (7) is that the term $A(I-P)z(t)$ is independent of τ. For time step of size Δt, this algorithm therefore requires only one multiplication by $(I-P)A$ and p multiplications by PA. Those p multiplications, however, only affect the unknowns in the highly refined region where P is nonzero, and hence the additional work will be small if the refined region only occupies a fraction of the entire mesh.

3 Energy and stability

We have proved that the resulting overall algorithm is second-order accurate in time and is equivalent to

$$z(t+\Delta t) - 2z(t) + z(t-\Delta t) = -\Delta t^2 A_p z(t), \quad (10)$$

with

$$A_p = A - \frac{2}{p^2} \sum_{j=1}^{p-1} \left(\frac{\Delta t}{p} \right)^{2j} \alpha_j^p (AP)^j A.$$

The matrix A_p is symmetric and we can therefore deduce from (10) the conservation of the discrete energy

$$E^{n+1/2} = \frac{1}{2} \left\langle \left(I - \frac{\Delta t^2}{4} A_p \right) \frac{z_{n+1}-z_n}{\Delta t}, \frac{z_{n+1}-z_n}{\Delta t} \right\rangle + \frac{1}{2} \left\langle A_p \frac{z_{n+1}+z_n}{2}, \frac{z_{n+1}+z_n}{2} \right\rangle,$$

where the brackets denote the standard euclidean inner product on $\mathbb{R}^m$. This energy corresponds to the energy conserved by the leap-frog scheme with time step Δt with A_p replaced by A).

The above local time-stepping scheme will then be stable if and only if the matrices $I - \frac{\Delta t^2}{4} A_p$ and A_p are both positive definite. Because of the projection matrix P, it is not possible to easily deduce the eigenvalues of these two matrices from the eigenvalues of A and to obtain an analytical CFL condition of the new scheme. However, it is (experimentally) usually comparable to that of the standard leap-frog scheme without local refinement. If a small overlap across at most three elements is allowed into the coarse region immediately next to the refined region, the CFL condition is optimal, in the sense that the same time step can be used.

4 Numerical results

To illustrate the versatility of the method, we consider a computational domain that consists of two rectangles connected by a very narrow channel. We use the IP-DG formulation [1] with P^3 elements on a triangular mesh,

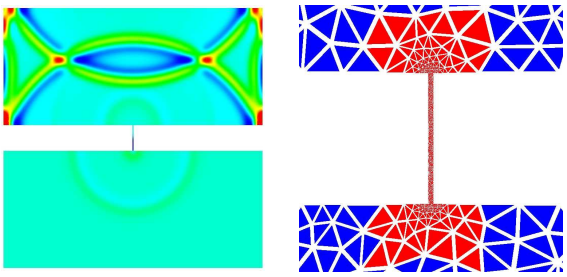

Figure 1: Left: The solution is shown at time $t = 0.2$. Right: the highly refined mesh inside the narrow channel.

which is highly refined inside the narrow region, as shown in the right frame of Fig. 1. Since the mesh size inside the refined region is about 17 times smaller than in the surrounding coarse region, we take $p = 17$ local time steps for every time step Δt.

As shown in Fig. 1, the wave is initiated by a pulse in the upper region, which propagates outward until it impinges on the boundaries. A fraction of the wave then penetrates the channel and generates a circular outgoing wave as it reaches the opposite lower region. Further reflections occur as the wave moves back and forth inside the channel, subsequently generating multiple circular waves in the upper and lower domains.

References

[1] M.J. Grote, A. Schneebeli, and D. Schötzau, *Discontinuous Galerkin finite element method for the wave equation*, SIAM Numer. Analysis **44** (2006), 2408–2431.

[2] G. Cohen, P. Joly, J.E. Roberts, and N. Tordjman, *Higher order triangular finite elements with mass lumping for the wave equation*, SIAM Numer. Analysis **38** (2001), 2047–2078.

[3] E. Hairer, C. Lubich, G. Wanner, *Geometric Numerical Integration*, 2nd edition, Springer-Verlag Berlin Heidelberg, 2006

[4] B. Leimkuhler and S. Reich, *Simulating Hamiltonian dynamics*, Cambridge Monographs on Applied and Computational Mathematics, 2004.

SPACE-TIME MESH REFINEMENT AND DISCONTINUOUS GALERKIN METHODS FOR SYMMETRIC FIRST ORDER HYPERBOLIC SYSTEMS

A. Ezziani[*], **P. Joly**[‡]
[*]LMA-Projet Magique 3D, I.P.R.A-Université de Pau, B.P 1155, 64013 Pau Cedex, France
[‡]Projet Poems, INRIA Rocquencourt, B.P 105, 78153 Le Chesnay Cedex, France
Email: Abdelaaziz.Ezziani@univ-pau.fr

Abstract

We present a new non conforming space-time mesh refinement method for symmetric first order hyperbolic system. This method is based on the use of a discontinuous Galerkin approximation and a discrete energy conservation.

Introduction

In this paper, we are interested in a non conforming space-time mesh refinement method for wave propagation in aeroacoustic, in the spirit of previous work in wave equation [3], [4], electromagnetism [5] and elastodynamics [1]. We develop a method which is applicable to zero order perturbations of symmetric hyperbolic systems in the sense of Friedrichs (Linearized Euler equations, Maxwell's equations and elastodynamics' equations are of this type). The method is based on the one hand on the use of a conservative higher order discontinuous Galerkin approximation for space discretization and a finite difference scheme in time, on the other hand on appropriate discrete transmission conditions between the grids. We use a discrete energy technique to drive the construction of the matching procedure between the grids and guarantee the stability condition. Moreover, under suitable geometrical conditions on the grids, this method is quasi explicit.

1 First order symmetric hyperbolic systems

Suppose Ω is a bounded and open domain in $\mathbb{R}^d$, $d \geq 1$, we consider a first order symmetric hyperbolic system in the sense of Friedrichs in $\Omega \times [0,T]$:

$$\begin{cases} \text{find } \mathbf{u} : \Omega \times [0,T] \mapsto \mathbb{R}^m \text{ such that:} \\ M\partial_t \mathbf{u} + \sum_{j=1}^{d} A_j \partial_{x_j} \mathbf{u} + B\mathbf{u} = \mathbf{f}, \quad \text{in } \Omega\times]0,T], \\ \mathbf{u}(x,0) = \mathbf{u}_0(x), \qquad\qquad \text{in } \Omega, \end{cases} \quad (1)$$

where M, A_j, $j = 1, \cdots, d$ and B are $m \times m$ matrices: $\Omega \mapsto \mathbb{R}^{m\times m}$, $\mathbf{f}$ is m vector: $\Omega \times [0,T] \mapsto \mathbb{R}^m$ and $\mathbf{u}_0$ is m vector. We assume that M is positive definite and A_j, $j = 1, \cdots, d$ are symmetric.
We complete the system (1) by the boundary condition:

$$(A(\mathbf{n}) - N)\mathbf{u} = 0 \quad \text{on } \Gamma\times]0,T]. \quad (2)$$

Here, Γ denotes the boundary of Ω, $\mathbf{n} = (n_1, \cdots, n_d)^t$ the unit outward normal to Γ, $A(\mathbf{n}) = \sum_{j=1}^{d} n_j A_j$ and N is a $m \times m$ matrix which satisfies:

$$\begin{cases} N + N^t \geq 0, \\ \ker(A(\mathbf{n}) - N) + \ker(A(\mathbf{n}) + N) = \mathbb{R}^m. \end{cases} \quad (3)$$

Under these assumptions and smoothness conditions Friedrichs [6] showed that (1)-(2) has a unique solution.

Energy identity

We denote by $(.,.)$ (resp. $<\cdot,\cdot>$) the inner product in $[L^2(\Omega)]^m$ (resp. $[L^2(\Gamma)]^m$) and $\mathbf{div}\, A = \sum_{j=1}^{d} \partial_{x_j} A_j$. If we define the energy of $\mathbf{u}$ at time t by: $E(t) = (M(x)\mathbf{u}, \mathbf{u})$, we can show that this quantity verifies:

Theorem 1

$$\begin{aligned} \frac{dE}{dt} &= (\mathbf{f}, \mathbf{u}) + \frac{1}{2}\left[(\mathbf{div}A\,\mathbf{u}, \mathbf{u}) - \left((B + B^t)\mathbf{u}, \mathbf{u}\right)\right] \\ &- \frac{1}{4} < (N + N^t)\mathbf{u}, \mathbf{u} > . \end{aligned}$$

We remark that, if $\mathbf{f} = 0$, we have an energy conservation (respectively dissipation) when $\frac{1}{2}\mathbf{div}A - B$ and N are antisymmetric (resp. $\mathbf{div}A - (B + B^t)$ is positive definite). In the general case we obtain the following L^2-estimation:

$$\|\mathbf{u}(t)\| \leq e^{\alpha t}\left(\|\mathbf{u}_0\| + \int_0^t e^{-\alpha s}\|\mathbf{f}(s)\|\, ds\right)^2,$$

where α is a positive constant depending on $\|\mathbf{div}A\|_\infty$ and $\|B\|_\infty$.

2 Conservative discontinuous Galerkin method

The method developed here is applicable in the general case, but to simplify this study we limit ourselves to the conservative case, in particular we consider the matrices A_j, $j = 1, \cdots, d$ are constants, $B = 0$, $\mathbf{f} = 0$ and $\Omega = \mathbb{R}^d$.

2.1 Space discretization

We consider a mesh $\mathcal{T}_h$ of our domain $\Omega = \cup_{K\in\mathcal{T}_h} K$, we denote by $\mathbf{n}_K$ the unit outward normal to ∂K and

$\Sigma_{KL} = \partial K \cap \partial L$ for all K, L in $\mathcal{T}_h$.
We introduce $\mathbb{V}_K$ the finite-dimensional sub-space of $[H^1(K)]^m$, $\mathbb{V}_K = [P_r(K)]^m$, where $[P_r(K)]^m$ is the set polynomials of maximum degree $\leq r$. We consider the conservative discontinuous Galerkin approximation, obtained by the usual Galerkin procedure with centered fluxes [2]:

$$\left\{ \begin{array}{l} \text{find } \mathbf{u}_h(t) : [0,T] \mapsto \mathbb{V}_h \text{ such that :} \\ \dfrac{d}{dt} m(\mathbf{u}_h, \mathbf{v}_h) + a_h(\mathbf{u}_h, \mathbf{v}_h) = 0, \quad \forall\, \mathbf{v}_h \in \mathbb{V}_h, \end{array} \right. \tag{4}$$

with $\mathbb{V}_h = [L^2(\Omega)]^m \cap \prod_{K \in \mathcal{T}_h} \mathbb{V}_k$, $\mathbf{u}_h = (\mathbf{u}_K)_K$, $\mathbf{v}_h = (\mathbf{v}_K)_K$ and the bilinear forms:

$$\left| \begin{array}{rcl} m(\mathbf{u}_h, \mathbf{v}_h) & = & \displaystyle\sum_K \int_K M(x) \mathbf{u}_K \cdot \mathbf{v}_K \, dx, \\ a_h(\mathbf{u}_h, \mathbf{v}_h) & = & \displaystyle -\sum_K \sum_j \int_K A_j \, \mathbf{u}_K \cdot \partial_{x_j} \mathbf{v}_K \, dx \\ & + & \displaystyle \sum_{K,L} \int_{\Sigma_{KL}} A(n_K) \frac{\mathbf{u}_K + \mathbf{u}_L}{2} \cdot \mathbf{v}_K \, d\sigma \end{array} \right.$$

We show that the bilinear form a_h is antisymmetric:

$$a_h(\mathbf{u}_h, \mathbf{v}_h) = -a_h(\mathbf{v}_h, \mathbf{u}_h) \;\; \forall\, \mathbf{u}_h, \mathbf{v}_h \in \mathbb{V}_h. \tag{5}$$

Remark 1 *We remark that using this last equality we can rewrite a_h in the form:*

$$\begin{aligned} a_h(\mathbf{u}_h, \mathbf{v}_h) &= \frac{1}{2} \left[a_h(\mathbf{u}_h, \mathbf{v}_h) - a_h(\mathbf{v}_h, \mathbf{u}_h) \right] \\ &= \frac{1}{2} \sum_{j,K} \int_K \left[A_j \, \partial_{x_j} \mathbf{u}_K \cdot \mathbf{v}_K - A_j \, \mathbf{u}_K \cdot \partial_{x_j} \mathbf{v}_K \right] \, dx \\ &+ \frac{1}{4} \sum_{K,L} \int_{\Sigma_{KL}} \left[A(\mathbf{n}_K) \, \mathbf{u}_L \cdot \mathbf{v}_K - A(\mathbf{n}_K) \, \mathbf{v}_L \cdot \mathbf{u}_K \right] \, d\sigma. \end{aligned}$$

The antisymmetric property of a_h allow us to obtain a semi-discrete energy conservation:

$$\frac{dE_h}{dt} = 0, \quad E_h(t) = m_h(\mathbf{u}_h, \mathbf{u}_h).$$

2.2 Time discretization and stability analysis

For the time discretization we construct a totally explicit centered finite difference scheme, by approximating the system (4) at $t^n = n\Delta t$ with the leap-frog scheme:

$$\left\{ \begin{array}{l} \text{find } \mathbf{u}_h^n \in \mathbb{V}_h, \text{ such that } \forall\, \mathbf{v}_h \in \mathbb{V}_h : \\ m_h\left(\dfrac{\mathbf{u}_h^{n+1} - \mathbf{u}_h^{n-1}}{2\Delta t}, \mathbf{v}_h\right) + a_h(\mathbf{u}_h^n, \mathbf{v}_h) = 0, \end{array} \right. \tag{6}$$

Using the antisymmetric property of a_h we have the identity:

$$\frac{E_h^{n+1/2} - E_h^{n-1/2}}{\Delta t} = 0,$$

where $E_h^{n+1/2}$ is the discrete energy at time $t^{n+1/2}$ defined by:

$$E_h^{n+1/2} = \frac{1}{2} \left[\|\mathbf{u}_h^{n+1}\|_{m_h}^2 + \|\mathbf{u}_h^n\|_{m_h}^2 \right] + 2\Delta t \, a_h(\mathbf{u}_h^{n+1}, \mathbf{u}_h^n),$$

where $\|\mathbf{u}_h\|_{m_h}^2 = m_h(\mathbf{u}_h, \mathbf{u}_h), \; \forall\, \mathbf{u}_h \in \mathbb{V}_h$.
In order to establish a sufficient stability condition, thanks to the energy discrete conservation, it suffices to show that the energy $E_h^{n+1/2}$ is a positive quadratic form. This is true if the following stability condition is satisfied:

$$\Delta t \|a_h\| \leq 1; \;\; \|a_h\| = \sup_{\mathbf{u}_h, \mathbf{v}_h \in \mathbb{V}_h \setminus \{0\}} \frac{a_h(\mathbf{u}_h, \mathbf{v}_h)}{\|\mathbf{u}_h\|_{m_h} \|\mathbf{v}_h\|_{m_h}}.$$

3 Space-time mesh refinement

3.1 Space mesh refinement

We suppose that Ω is a union of two domain Ω_c and Ω_f separated by a surface $\Sigma = \Omega_c \cap \Omega_f$, and we consider a mesh $\mathcal{T}_h^c$ (resp. $\mathcal{T}_h^f$) of Ω_c (resp. Ω_f). We introduce the following sets :

$$\begin{aligned} &\mathcal{I}_l = \{(K,L) \,/\, \Sigma_{KL} \subset \Omega_l\}, \;\; \forall\, l \in \{c, f\}, \\ &\mathcal{I} = \{(K,L) \,/\, \Sigma_{KL} \neq \emptyset, \; K \subset \Omega_c, \; L \subset \Omega_f\}. \end{aligned}$$

We denote $\mathbf{u}_{l,h} = \mathbf{u}_h|_{\Omega_l}$ and $\mathbb{V}_h^l = \mathbb{V}_h \cap [L^2(\Omega_l)]^m$, $\forall\, l \in \{c, f\}$. Thanks to the remark 1, we can rewrite the variational formulation (4) as follows:

$$\left\{ \begin{array}{l} \text{find } \mathbf{u}_{l,h}(t) : [0,T] \mapsto \mathbb{V}_h^l \text{ such that :} \\ \dfrac{d}{dt} m^c(\mathbf{u}_{c,h}, \mathbf{v}_{c,h}) + a_h^c(\mathbf{u}_{c,h}, \mathbf{v}_{c,h}) + b_h(\mathbf{u}_{f,h}, \mathbf{v}_{c,h}) = 0, \\ \dfrac{d}{dt} m^f(\mathbf{u}_{f,h}, \mathbf{v}_{f,h}) + a_h^f(\mathbf{u}_{f,h}, \mathbf{v}_{f,h}) - b_h(\mathbf{v}_{f,h}, \mathbf{u}_{c,h}) = 0, \\ \forall\, (\mathbf{v}_{c,h}, \mathbf{v}_{f,h}) \in \mathbb{V}_h^c \times \mathbb{V}_h^f, \end{array} \right. \tag{7}$$

where the bilinear forms b_h, and m_h^l, $\forall\, l \in \{c, f\}$ are defined by:

$$\left| \begin{array}{l} m^l(\mathbf{u}_h, \mathbf{v}_h) = \displaystyle\sum_{K \in \mathcal{T}_h^l} \int_K M(x) \, \mathbf{u}_K \cdot \mathbf{v}_K \, dx, \\ b_h(\mathbf{u}_{f,h}, \mathbf{u}_{c,h}) = \dfrac{1}{4} \displaystyle\sum_{(K,L) \in I} \int_{\Sigma_{KL}} A(\mathbf{n}_k) \mathbf{u}_L^f \cdot \mathbf{u}_K^c \, d\sigma. \end{array} \right.$$

and a_h^l is an antisymmetric bilinear form on $\mathbb{V}_h^l \times \mathbb{V}_h^l$, $\forall\, l \in \{c, f\}$:

$$\left|\begin{array}{l} a_h^l(\mathbf{u}_h, \mathbf{v}_h) = \\ \frac{1}{2} \sum\limits_{K \in \mathcal{T}_h^l} \sum\limits_j \int_K \left[A_j\, \partial_{x_j} \mathbf{u}_K \cdot \mathbf{v}_K - A_j\, \mathbf{u}_K \cdot \partial_{x_j} \mathbf{v}_K\right] dx + \\ \frac{1}{4} \sum\limits_{(K,L) \in I_l} \int_{\Sigma_{KL}} \left[A(\mathbf{n}_K)\, \mathbf{u}_L \cdot \mathbf{v}_K - A(\mathbf{n}_K)\, \mathbf{v}_L \cdot \mathbf{u}_K\right] d\sigma. \end{array}\right.$$

3.2 Time discretization and stability analysis

Our aim is to determine an explicit numerical scheme in the case of space-time mesh refinement, and for which we can establish the conservation of the discrete energy quantity. This will permit us to ensure the stability of the scheme.

We suppose that the fine mesh $\mathcal{T}_h^f$ of Ω_f is finer than the coarse mesh $\mathcal{T}_h^c$ of Ω_c, more precisely, the space step h_f of $\mathcal{T}_h^f$ is twice smaller than h_c of $\mathcal{T}_h^c$; $h_f = h_c/2$. We mention that we extended the method presented below to a general mesh refinement; $h_c = h/q_c$, $h_f = h/q_f$ with $q_c < q_f$.

For time discretization of the system (7), we use a centered scheme like in (6). Given that we want to keep the ratio time step over space step constant on all computational domain, we approach $\mathbf{u}_h$ at even times t^{2n} in coarse mesh, and at odd times $t^{2n+1/2}$ in fine mesh (see figure 1). In this way, after time discretization, the system (7) is rewritten in the form:

$$\left\{\begin{array}{l} m_h^c\left(\frac{\mathbf{u}_{c,h}^{2n+2} - \mathbf{u}_{c,h}^{2n-2}}{4\Delta t}, \mathbf{v}_{c,h}\right) + a_h^c(\mathbf{u}_{c,h}^{2n}, \mathbf{v}_{c,h}) \\ + b_h([\mathbf{u}_{f,h}]^{2n}, \mathbf{v}_{c,h}) = 0, \\ \\ m_h^f\left(\frac{\mathbf{u}_{f,h}^{2n+3/2} - \mathbf{u}_{f,h}^{2n-1/2}}{2\Delta t}, \mathbf{v}_{f,h}\right) + a_h^f(\mathbf{u}_{f,h}^{2n+1/2}, \mathbf{v}_{f,h}) \\ + b_h([\mathbf{u}_{c,h}]^{2n+1/2}, \mathbf{v}_{f,h}) = 0, \\ \\ m_h^f\left(\frac{\mathbf{u}_{f,h}^{2n+1/2} - \mathbf{u}_{f,h}^{2n-3/2}}{2\Delta t}, \mathbf{v}_{f,h}\right) + a_h^f(\mathbf{u}_{f,h}^{2n-1/2}, \mathbf{v}_{f,h}) \\ + b_h([\mathbf{u}_{c,h}]^{2n-1/2}, \mathbf{v}_{f,h}) = 0, \\ \forall\, (\mathbf{v}_{c,h}, \mathbf{v}_{f,h}) \in \mathbb{V}_h^c \times \mathbb{V}_h^f. \end{array}\right.$$

Here, $[\mathbf{u}_{f,h}]^{2n}$ (resp. $[\mathbf{u}_{c,h}]^{2n+1/2}$ and $[\mathbf{u}_{f,h}]^{2n-1/2}$) is an approximation of $\mathbf{u}_{f,h}$ (resp. $\mathbf{u}_{c,h}$) at time t^{2n} (resp. $t^{2n+1/2}$ and $t^{2n-1/2}$). Using the antisymmetric property of a_h^c and a_h^f, and if we take:

$$\begin{array}{rcl} [\mathbf{u}_{c,h}]^{2n+1/2} = [\mathbf{u}_{c,h}]^{2n-1/2} = \left(\mathbf{u}_{c,h}^{2n+2} + \mathbf{u}_{c,h}^{2n+2}\right)/2, \\ [\mathbf{u}_{f,h}]^{2n} &=& \left(\mathbf{u}_{f,h}^{2n+3/2} + \mathbf{u}_{f,h}^{2n+1/2}\right)/4 \\ &+& \left(\mathbf{u}_{f,h}^{2n-1/2} + \mathbf{u}_{f,h}^{2n-3/2}\right)/4, \end{array} \tag{8}$$

we show that the last numerical scheme has a conservative discrete energy:

$$\frac{\mathcal{E}_h^{2n+1} - \mathcal{E}_h^{2n-1}}{2\Delta t} = 0, \text{ with } \mathcal{E}_h^{2n+1} = E_{c,h}^{2n+1} + E_{f,h}^{2n+1},$$

where $E_{l,h}^{2n+1}$, $l \in \{c, f\}$ is the discrete energy of $\mathbf{u}_{l,h}$ in Ω_l:

$$\begin{array}{rcl} E_{c,h}^{2n+1} &=& \frac{1}{2}\left[\|\mathbf{u}_{c,h}^{2n+2}\|_{m_h^c}^2 + \|\mathbf{u}_{c,h}^{2n}\|_{m_h^c}^2\right] \\ &+& 2\Delta t\, a_h^c(\mathbf{u}_{c,h}^{2n+2}, \mathbf{u}_{c,h}^{2n}), \\ E_{f,h}^{2n+1} &=& \frac{1}{2}\left[\|\mathbf{u}_{f,h}^{2n+3/2}\|_{m_h^c}^2 + \|\mathbf{u}_{f,h}^{2n+1/2}\|_{m_h^f}^2\right] \\ &+& \Delta t\, a_h^f(\mathbf{u}_{f,h}^{2n+3/2}, \mathbf{u}_{f,h}^{2n+1/2}). \end{array}$$

The sufficient stability condition is assured thanks to:

$$\Delta t \|a_h^c\| \leq 1 \text{ and } \Delta t \|a_h^f\| \leq 2.$$

This implies that we have the same CFL stability condition in coarse and fine grid ($h_f = h_c/2$).

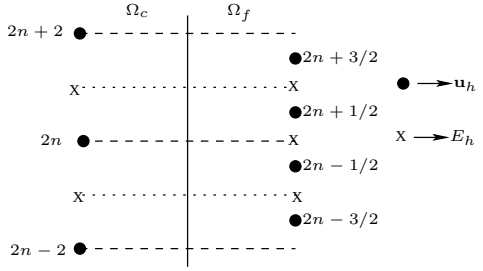

Figure 1: Time distribution of the unknowns and of the energy quantities

The matrix system associated to our numerical scheme is given by:

$$\left\{\begin{array}{l} M_h^c\, \frac{\mathbf{U}_c^{2n+2} - \mathbf{U}_c^{2n-2}}{4\Delta t} + A_h^c\, \mathbf{U}_{c,h}^{2n} \\ + B_h\, [\mathbf{U}_f]^{2n} = 0, \\ \\ M_h^f\, \frac{\mathbf{U}_f^{2n+3/2} - \mathbf{U}_f^{2n-1/2}}{2\Delta t} + A_h^f\, \mathbf{U}_f^{2n+1/2} \\ + B_h\, [U_c]^{2n+1/2} = 0, \\ \\ M_h^f\, \frac{\mathbf{U}_f^{2n+1/2} - \mathbf{U}_f^{2n-3/2}}{2\Delta t} + A_h^f\, \mathbf{U}_f^{2n-1/2} \\ + B_h\, [U_c]^{2n-1/2} = 0, \end{array}\right. \tag{9}$$

where $[\mathbf{U}_f]^{2n}$, $[U_c]^{2n+1/2}$ and $[U_c]^{2n-1/2}$ are given by (8), M_h^c and M_h^f are the local mass matrices, A_h^c and A_h^f are the local stiffness matrices, and B_h is the coupling stiffness matrix (transmission matrix).

The system (9) is quasi explicit under suitable geometrical conditions on the grids. The numerical simulations for Linearized Euler equations will be presented during the conference.

References

[1] E. Bécache, P. Joly and J. Rodríguez, "Space-time mesh refinement for elastodynamics. numerical results", J. Comp. Meth. Appl. Mech. Eng., vol. 194, pp. 355-366, 2005.

[2] B. Cockburn, G. E. Karniadakis and C.-W. Shu, editors, "Discontinuous Galerkin Methods: Theory, Compuration and Applications", Lecture notes in computational science and engineering, vol. 11, Springer, 2000.

[3] F. Collino, T. Fouquet and P. Joly "A conservative space-time mesh refinement method for the 1-D wave equation. I. Construction.", Numer. Math., vol. 95, pp. 197-221, 2003.

[4] F. Collino, T. Fouquet and P. Joly "A conservative space-time mesh refinement method for the 1-D wave equation. II. Analysis.", Numer. Math., vol. 95, pp. 223-251, 2003.

[5] F. Collino, T. Fouquet and P. Joly "Conservative space-time mesh refinement methods for the FDTD solution of Maxwell's equations", Journal Computational Physics, vol. 211, pp. 9-35, 2006.

[6] K. O. Friedrichs "Symmetric positive linear differential equations", Comm. Pure. Appl. Math., vol. 11, pp. 333-418, 1958.

HIGHER ORDER TIME STEPPING FOR SECOND ORDER HYPERBOLIC PROBLEMS AND OPTIMAL CFL CONDITIONS

J. Charles Gilbert[†,1], **Patrick Joly**[‡,1] **and Jerónimo Rodríguez**[‡,2]

[†]Projet Estime, INRIA-Rocquencourt
[‡]Laboratoire POEMS, UMR 2706 CNRS-ENSTA-INRIA

[1]INRIA-Rocquencourt, B.P. 105, F-75158, Le Chesnay, France
[2]ENSTA, 32, Boulevard Victor, 75739, Paris, Cedex 15, France

Jean-Charles.Gilbert@inria.fr
Patrick.Joly@inria.fr
Jeronimo.Rodriguez@ensta.fr

1 Abstract

We investigate explicit higher order time discretizations of linear second order hyperbolic problems. We study the even order ($2m$) schemes obtained by the modified equation method. We show that the corresponding CFL upper bound for the time step remains bounded when the order of the scheme increases. We propose variants of these schemes constructed to optimize the CFL condition. The corresponding optimization problem is analyzed in detail. The corresponding optimal schemes are constructed and their asymptotic complexity for large order is analyzed.

2 Introduction

We are concerned here with a very classical problem, namely the numerical approximation of second order hyperbolic problems, more precisely problems of the form

$$\frac{d^2u}{dt^2} + \mathcal{A}u = 0, \tag{1}$$

where $\mathcal{A}$ is a linear unbounded positive self-adjoint operator in some Hilbert space V. This appears to be the generic abstract form for a large class of wave propagation problems, with $\mathcal{A}$ is a second order differential operator in space, of elliptic nature. During the past 4 decades, a considerable literature has been devoted to the construction of numerical methods for the approximation of (1). The most recent research deals with the construction of higher order in space and energy preserving methods for the space semi-discretization of (1) (using finite differences, finite elements, discontinuous Galerkin methods - see for instance [3] and the references therein). These methods lead us to consider a family (indexed by $h > 0$, the approximation parameter which tends to 0 - typically the step size of the computational mesh) of problems of the form:

$$\frac{d^2u_h}{dt^2} + \mathcal{A}_h u_h = 0, \tag{2}$$

where the unknown u_h is a function of time with value in some Hilbert space V_h (whose norm will be denoted $\|\cdot\|$, even if it does depend on h) and $\mathcal{A}_h$ denotes a bounded self-adjoint and positive operator in V_h.

In what follows, we are interested in the time discretization of (2) by explicit finite difference schemes. More specifically, we are interested in the stability analysis of such schemes and its influence on the choice of the time step. The energy preserving nature of the continuous problem can be seen as a consequence of the time reversibility of this equation. That is why we shall favor centered finite difference schemes which preserve such a property at the discrete level.

The most well known scheme is the classical second order leap-frog scheme ($u_h^n \in V_h$ denotes an approximation of $u_h(t^n)$, $t^n = n\Delta t$)

$$\frac{u_h^{n+1} - 2u_h^n + u_h^{n-1}}{\Delta t^2} + \mathcal{A}_h u_h^n = 0. \tag{3}$$

which is stable under the condition.

$$\frac{\Delta t^2}{4} \|\mathcal{A}_h\| \leq 1. \tag{4}$$

Next we investigate one way to construct more accurate (in time) discretization schemes for (2). This is particularly relevant when $\mathcal{A}_h$ represents some $O(h^k)$ space approximation of $\mathcal{A}$ with $k > 2$: one would like to adapt the time accuracy to the space accuracy.

Most of the mathematical details and proofs of our results can be found in [5].

3 The modified equation approach

This approach [6], [2], [4], [1] consists at looking at the Taylor expansion of the truncation error of (3) and replac-

ing higher order time derivatives by powers of $\mathcal{A}_h$. One than obtain the scheme $(\mathcal{S}_m)$, of order $2m$:

$$\begin{aligned} &\frac{u_h^{n+1} - 2u_h^n + u_h^{n-1}}{\Delta t^2} + \mathcal{A}_h^{(m)}(\Delta t)\ u_h^n = 0, \\ &\mathcal{A}_h^{(m)}(\Delta t) = \mathcal{A}_h\ P_m(\Delta t^2 \mathcal{A}_h), \end{aligned} \tag{5}$$

where the polynomial $P_m(x)$ is defined by,

$$P_m(x) = 1 + 2\sum_{l=1}^{m-1}(-1)^l \frac{x^l}{(2l+2)!}. \tag{6}$$

This scheme remains energy preserving and explicit. Moreover, the computational cost for one time step of the scheme of order $2m$ is m times larger than the computational cost for one time step of the second order scheme. However, this additional cost could be counterbalanced if one would be able to choose the time step proportionally to m. Unfortunately, one has the following result

Theorem 3.1 *The stability condition of $\mathcal{S}_m$ (see (5)) is*

$$\Delta t^2\ \|\mathcal{A}_h\| \leq \alpha_m, \tag{7}$$

where

$$\alpha_m := \sup\{\ \alpha\ /\ \forall\ x \in [0,\alpha], 0 \leq xP_m(x) \leq 4\}.$$

We have that

$$\lim_{m\to+\infty} \alpha_{2m} = 4\pi^2, \quad \lim_{m\to+\infty} \alpha_{2m+1} = \pi^2. \tag{8}$$

Our goal, next, is to modify the scheme $\mathcal{S}_m$ in order to be able to use a much larger time step than the one allowed by (7), without increasing too much the cost per time step.

4 Modified schemes: an optimization approach

For an integer k, we denote by $\mathbf{P}_k$ the set of polynomials of degree less or equal to k. For a given $R \in \mathbf{P}_{k-1}$, we construct an explicit scheme $\mathcal{S}_m(R)$ of order $2m$ by:

$$\begin{aligned} &\frac{u_h^{n+1} - 2u_h^n + u_h^{n-1}}{\Delta t^2} + P_m(\Delta t^2 \mathcal{A}_h) u_h^n \\ &+ \Delta t^{2m}\ \mathcal{A}_h^m\ R(\Delta t^2 \mathcal{A}_h)\ \mathcal{A}_h u_h^n = 0, \end{aligned} \tag{9}$$

The cost per time step of $\mathcal{S}_m(R)$ is at most $(m+k)/m$ times larger than the one of $\mathcal{S}_m$. One can show that the stability condition of this new scheme is:

$$\Delta t^2\ \|\mathcal{A}_h\| \leq \alpha_m(R_k), \tag{10}$$

where we have defined,

$$\alpha_m(R) = \sup\ \{\ \alpha\ /\ \forall\ x \in\ [0,\alpha],\ 0 \leq Q_R(x) \leq 4\ \}. \tag{11}$$

with $Q_R(x) = x\ [\ P_m(x) + x^m\ R(x)\ ]$.

The natural idea, in some sense, to get an optimal scheme would be to solve the optimization problem:

$$\text{Find } R_{m,k}\ \in\ \mathbf{P}_{k-1}\ /\ \alpha_m(R_{m,k}) = \sup_{R\ \in\ \mathbf{P}_{k-1}} \alpha_m(R). \tag{12}$$

A priori, this is a difficult optimization problem since the function $R \mapsto \alpha_m(R)$ is discontinuous [5]. However one can show the following theorem:

Theorem 4.1 *For any $k \geq 1$, the optimization problem (12) admits a unique solution $R = R_{m,k}$, characterized by the following optimality condition: there exists k points*

$$0 < \tau_k < \cdots < \tau_1 < \tau_0 = \alpha_m(R) \tag{13}$$

such that, if $Q_R(x) = x\ [\ P_m(x) + x^m\ R(x)\ ]$

$$Q_R(\tau_j) + Q_R(\tau_{j+1}) = 4, \quad j = 0, \ldots, k-1. \tag{14}$$

>From the theoretical point of view, it is interesting to know the behavior of:

$$\alpha_{m,k} = \sup_{R\ \in\ \mathbf{P}_{k-1}} \alpha_m(R) \tag{15}$$

which fixes the maximum value of Δt for the *optimal scheme*. $\mathcal{S}_{m,k} := \mathcal{S}_m(R_{m,k})$. One first obtains an upper bound:

Theorem 4.2 *For $k \geq 0$,*

$$\begin{aligned} &\alpha_{1,k} = 4(k+1)^2, \\ &\alpha_{m,k} \leq 4\ (m+k)^2, \quad \textit{for } m \geq 2. \end{aligned} \tag{16}$$

More interesting is a lower bound. We consider the case $k = m$, for which the cost per time step is only twice the one of (3).

Theorem 4.3

$$\alpha_{m,m} \geq \beta_m = 2^{\frac{1}{m}}(2m)!^{\frac{1}{m}}, \quad \textit{with} \quad \beta_m \sim \frac{4m^2}{e^2} \tag{17}$$

This means that for the optimal schemes $\mathcal{S}_{m,m}$, Δt can be chosen proportionally to m. In other words, one can achieve the $2m^{th}$ order accuracy with a computational cost which remains bounded when m increases: the cost per time step is $2m$ times larger than the one for (3) but the time step can be chosen $Cste \times m$ larger.

5 Computational issues

It appears quite difficult to solve numerically the problem (12) with standard optimization algorithms.

Fortunately, exploiting the optimality condition, we have been able to design an *ad hoc* algorithm based on the parameterization of the polynomials R by the points τ_j satisfying (13, 14) coupled to a Newton's strategy [5].

We have been able to determine the optimal polynomials $R_{m,k}$ for $1 \leq k \leq 8$ and $1 \leq m \leq 8$ and to obtain the following tables for the coefficients $\alpha_{m,k}$.

Table 1: Computed values of the first $\alpha_{m,k}$'s, $k \leq 4$

	$k=0$	$k=1$	$k=2$	$k=3$	$k=4$
$m=1$	4.00	16.00	36.00	64.00	100.00
$m=2$	12.00	32.43	60.56	96.61	140.64
$m=3$	7.57	23.40	45.72	75.06	111.58
$m=4$	21.48	44.03	73.45	110.01	153.83
$m=5$	9.53	31.61	58.23	90.77	129.90
$m=6$	30.72	57.23	89.78	128.89	174.84
$m=7$	9.85	37.37	68.93	108.35	151.08
$m=8$	37.08	70.89	107.67	150.35	199.32

Table 2: Computed values of the first $\alpha_{m,k}$'s, $k \geq 5$

	$k=0$	$k=5$	$k=6$	$k=7$	$k=8$
$m=1$	4.00	144.00	196.00	256.00	324.00
$m=2$	12.00	192.66	252.67	320.68	396.69
$m=3$	7.57	155.38	206.51	265.04	331.00
$m=4$	21.48	204.98	263.51	329.49	402.92
$m=5$	9.53	175.84	228.71	288.59	355.23
$m=6$	30.72	227.71	287.61	354.59	428.71
$m=7$	9.85	199.56	255.61	317.90	357.95
$m=8$	37.08	254.89	317.22	386.35	462.27

6 Numerical experiments

The schemes $\mathcal{S}_{m,k}$ have been implemented for the case of the $2D$ wave equation, when a higher order discontinuous Galerkin method is used for the space discretization (see [7] for more details).

The corresponding numerical results will be presented at the conference and the actual efficiency of our new schemes will be discussed in terms of accuracy and computational cost.

References

[1] Laurent Anné, Patrick Joly, and Quang Huy Tran. Construction and analysis of higher order finite difference schemes for the 1D wave equation. *Comput. Geosci.*, 4(3):207–249, 2000.

[2] Romuald Carpentier, Armel de La Bourdonnaye, and Bernard Larrouturou. On the derivation of the modified equation for the analysis of linear numerical methods. *RAIRO Modél. Math. Anal. Numér.*, 31(4):459–470, 1997.

[3] Gary C. Cohen. *Higher-order numerical methods for transient wave equations*. Scientific Computation. Springer-Verlag, Berlin, 2002.

[4] M. A. Dablain. The application of high order differencing for the scalar wave equation. *Geophysics*, 51:54–56, 1986.

[5] Jean-Charles Gilbert and Patrick Joly. Higher order time stepping for second order hyperbolic problems and optimal CFL conditions. *"Numerical Analysis and Scientific Computing for PDEs and their Challenging Applications"*, To appear.

[6] Gregory R. Shubin and John B. Bell. A modified equation approach to constructing fourth-order methods for acoustic wave propagation. *SIAM J. Sci. Statist. Comput.*, 8(2):135–151, 1987.

[7] Lucas Wilcox. *Sledge++ Users' Guide*. Sandia National Laboratories, 2005.

TAMING THE CFL CONDITION FOR DISCONTINUOUS GALERKIN IN TWO-DIMENSIONS

T. Warburton[†,*], **Thomas Hagstrom**[‡]
[†]Department of Computational and Applied Mathematics, Rice University, Houston, TX 77005, USA
[‡] Department of Mathematics and Statistics, University of New Mexico, Albuquerque, NM 87131, USA.
[*]Email: timwar@rice.edu

Abstract

The discontinuous Galerkin method excels at solving time-dependent hyperbolic conservation laws. It is possible to use high-order explicit time-stepping methods and high-order spatial approximations without incurring heavy numerical linear algebra overheads. We demonstrate how it is possible to use a co-volume mesh based filter in 2D to improve the CFL condition for discontinuous Galerkin methods with limited impact on accuracy.

Introduction

The discontinuous Galerkin (DG) method, originally introduce for simulating neutron transport [1], has gained traction as a competitive method for solving time-dependent hyperbolic conservation laws in partial differential equation form. In [2] we showed how using DG with high-order polynomial approximation suffers from an undesirable time step size restriction, and that this may be overcome with a judicious application of a gradient filter. Specifically, we showed theoretical and experimental results indicating that adding a staggered grid based filter to the formulation increases the allowable time step size by a factor proportional to the order of the polynomials being used for approximation. This combination in fact yields time step sizes comparable to those allowable for typical finite difference based schemes. Furthermore, it was demonstrated that the filter does not appreciably reduce the order of accuracy achievable for sufficiently smooth solutions. The results in that paper were specific to one-dimensional and tensor-product one-dimensional computations.

In this paper we outline one possible way to extend the staggered mesh filter approach to meshes of unstructured triangles. The approach relies on the construction of a co-volume mesh, and the use of L_2 projection of the solution from the primal unstructured mesh of triangles onto the space of piecewise polynomial functions supported on the co-volume mesh of vertex centered polygons, and subsequent projection back to the primal mesh. We will show experimental results indicating that this filter does effect accuracy slightly, but not in a disastrous way. However, this is still a work in progress and we will also discuss some issues with the conditioning of the discrete projection operators.

Formulation

Given the two-dimensional TM Maxwell's equations

$$\frac{\partial H_x}{\partial t} = -\frac{\partial E_z}{\partial y}\,, \tag{1}$$
$$\frac{\partial H_y}{\partial t} = \frac{\partial E_z}{\partial x}\,, \tag{2}$$
$$\frac{\partial E_z}{\partial t} = \frac{\partial H_y}{\partial x} - \frac{\partial H_x}{\partial y}\,, \tag{3}$$

valid in a doubly periodic domain Ω we consider the following variational statement for the upwind discontinuous Galerkin method applied. Given a triangulation of K simplices covering the domain, $\Omega = \bigcup_{1\le k\le K} D^k$ we seek of a finite dimensional approximation to the magnetic and electrical fields, given by $(H_x, H_y, E_z) \in (V^h)^3$ that satisfies

$$\left(\phi, \frac{\partial H_x}{\partial t} + \frac{\partial E_z}{\partial y}\right)_{D^k} = (\phi, -n_y\,[R])_{\partial D^k}\,,$$
$$\left(\psi, \frac{\partial H_y}{\partial t} - \frac{\partial E_z}{\partial y}\right)_{D^k} = (\psi, n_x\,[R])_{\partial D^k}\,,$$
$$\left(\chi, \frac{\partial E_z}{\partial t} + \frac{\partial H_x}{\partial y} - \frac{\partial H_y}{\partial x}\right)_{D^k} = (\chi, -\,[R])_{\partial D^k}\,,$$

for all $(\phi, \psi, \chi) \in \left(V^h\right)^3$. The notation

$$R^- = -n_y^- H_x^- + n_x^- H_y^- + E_z^- \tag{4}$$
$$R^+ = -n_y^- H_x^+ + n_x^- H_y^+ + E_z^+ \tag{5}$$
$$[R] = \frac{R^+ - R^-}{2} \tag{6}$$

corresponds to the internal and external traces and jump of the incoming characteristic variable on an element face with outward facing normal (n_x, n_y). In what follows we assume a piecewise polynomial space $V^h = \cup_{1\le k\le K} P^n\left(D^k\right)$ (see [3] for further details).

In addition to the primal grid, we will require a co-volume mesh defined as the union of polygons formed by joining the centers of the element of all elements sharing each vertex (see example in Figure 1). We will

also associate a polynomial space to each vertex, using the lower triangular part tensor-product of M'th order one-dimensional Legendre polynomial spaces $W^h = \bigcup_{1\leq v\leq N_v} P^M(E^v)$ for polygonal co-volumes E^v given N_v mesh vertices. Expressing $Q = (H_x, H_y, E_z)^t$ the

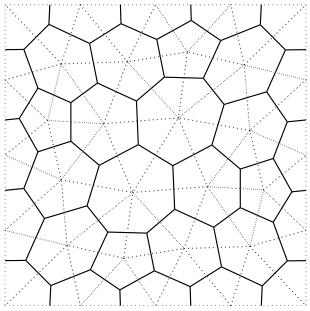

Figure 1: Example of doubly periodic primal mesh (dotted line) and covolume mesh (solid lines).

semidiscrete scheme reads

$$\frac{dQ}{dt} = DQ\ . \tag{7}$$

By a straight forward application of inverse inequalities for polynomials, we can estimate that after spatial discretization the discrete DG Maxwell's derivative operator, D, will have a spectral radius that grows in proportion to $\frac{n^2}{h}$. The goal of this paper is to outline the construction of a filter matrix F that we use to control the spectrum of D and we instead solve

$$\frac{dQ}{dt} = FDQ\ . \tag{8}$$

The filter matrix F is considered to be a 3×3 block matrix, with the same sub-matrix on each of the three diagonal blocks. The block filter is the product of two L^2 projection operators given by $\Pi^{p\to c} : V^h \to W^h$ that projects functions from primal mesh to a function supported by the co-volume mesh with $\Pi^{c\to p} : W^h \to V^h$ projecting in the reverse direction. The former is defined uniquely as the linear operator that satisfies

$$(\phi, \Pi^{p\to c}\psi)_\Omega = (\phi,\psi)_\Omega\ , \tag{9}$$

for all $\phi\in W^h$ and for all $\psi\in V^h$. A similar definition holds for $\Pi^{c\to p}$. After discretization the filter matrix $\mathbf{F}$ has structure

$$\mathbf{F} = \begin{pmatrix} \Pi^{c\to p}\Pi^{p\to c} & 0 & 0 \\ 0 & \Pi^{c\to p}\Pi^{p\to c} & 0 \\ 0 & 0 & \Pi^{c\to p}\Pi^{p\to c} \end{pmatrix}\ . \tag{10}$$

In the following results section we outline the impact of this filter matrix on the spectral radius of the new filtered DG derivative matrix, and also on the accuracy of the solution to a time-dependent simulation.

Results

To illustrate the quite dramatic impact of the co-volume based filter on the eigenspectrum of the DG spatial operator (based on polynomial orders $N = M = 7$ for the primal and co-volume mesh in Figure 1 we show the eigenvalues of

$$D^\alpha = (1-\alpha)\, D + \alpha FD\ , \tag{11}$$

for $\alpha = 0, 0.2, 0.4, 0.6, 0.8, 1.0$ in Figure 2. It is immedi-

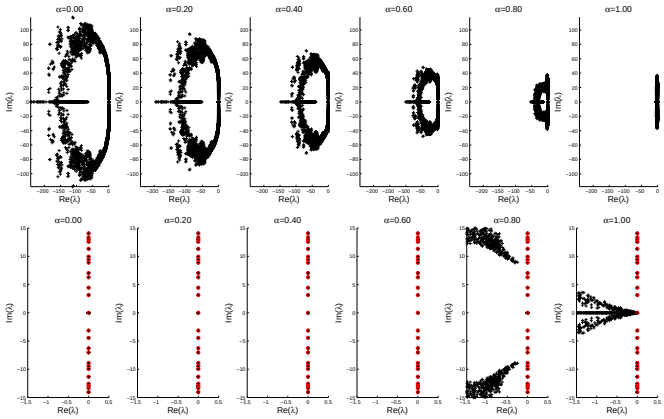

Figure 2: Top: eigenspectra of the discrete upwind DG Maxwell's operator D^α on a doubly periodic mesh with $K = 46$ triangular elements and polynomial order $N = 7$ for $\alpha = 0, 0.2, 0.4, 0.6, 0.8, 1.0$. Bottom: close up of the well resolved eigenvalues on the imaginary axis ('+') and exact eigenvalues ('o').

ately obvious that the eigenvalues of D^α are pushed into a smaller and smaller part of the complex plane as the amount of filtering used is increased, i.e. as α increases. At the same time a zoom of the complex plane near the origin and imaginary axis shows that well resolved, physical eigenvalues of the discrete operators are not visibly modified by the filtering. However, we do notice that as the amount of filtering is increased damped spurious modes from the unfiltered upwind DG spatial operator are pushed close to the origin and become much more slowly decaying spurious eigenvalues. Thus we recommend a compromise $\alpha = \frac{N-1}{N}$ in line with similar findings in [2]. In Table 1 we compare the spectral radii of D^0,$D^{(N-1)/N}$, and D^1. The latter two clearly grow more slowly than the former with increasing N. To address the impact of the filter on the accuracy of the numerical method, we computed the error in the well resolved

Table 1: Comparison of spectral radiii of filtered and unfiltered upwind DG Maxwell's operators $(M = N)$.

N	$\rho\left(D^0\right)$	$\rho\left(D^{(N-1)/N}\right)$	$\rho\left(D^1\right)$
1	30.49	30.49	6.76
2	52.39	26.33	11.08
3	78.90	28.74	15.47
4	110.84	29.10	20.47
5	149.22	32.12	25.73
6	190.73	33.84	31.30
7	242.27	39.14	36.75
8	294.58	42.82	42.11

physical eigenvalues for the cases $\alpha = 0, (N-1)/N$, and 1 with $N = M = 7$. It is clear that the filter does have an impact on the accuracy of the discrete resonances. In a further experiment we increased the polyno-

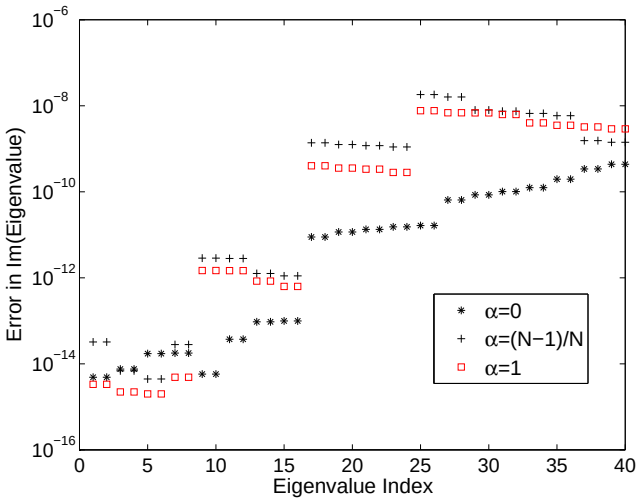

Figure 3: Error in the first forty eigenvalues of the unstabilized, and stabilized upwind DG Maxwell's operator D^α with $N = M = 7$.

mial order used for the co-volume mesh from $M = 7$ to $M = 8$. This time the errors in the discrete eigenvalues are closer to the errors of the unfiltered discrete eigenvalues, as shown in Figure 4 and the spectral radius of the filtered operators does not dramatically increase despite of the enhanced resolution on the co-volume mesh, as shown in Table 2.

Summary & Comments

Experiments have been presented to show the impact of a co-volume based filter on the symptotic growth of the spectral radius of DG based discrete derivative operators and the accuracy of their physically correct eigenvalues.

Table 2: Comparison of spectral radiii D^α for different polynomial orders on the primal and co-volume meshes $(M = N + 1)$.

N	$\rho\left(D^0\right)$	$\rho\left(D^{(N-1)/N}\right)$	$\rho\left(D^1\right)$
1	30.49	30.49	8.81
2	52.39	27.02	13.67
3	78.90	28.72	18.19
4	110.84	31.74	23.16
5	149.22	33.21	28.43
6	190.73	35.11	33.94
7	242.27	40.39	39.64
8	294.58	45.95	45.30

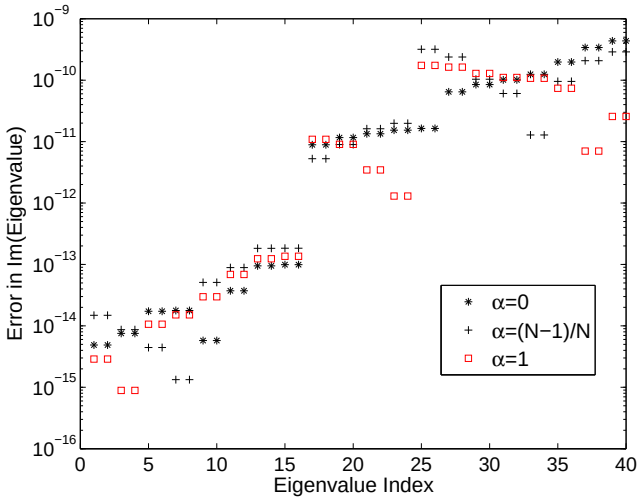

Figure 4: Error in the first forty eigenvalues of the unstabilized, and stabilized upwind DG Maxwell's operator D^α with $N = 7$ and $M = 8$.

We will address other issues including the need for a more robust construction of the filter operator, to improve the conditioning of the inter-grid projection operators.

References

[1] W. Reed and T. Hill, "Triangular mesh methods for the neutron transport equation", Technical report, Los Alamos, Los Alamos, NM, 1973.

[2] T. Warburton and Thomas Hagstrom, "Taming the CFL Number for Discontinuous Galerkin Methods on Structured Meshes", submitted to SINUM, 2006.

[3] J. S. Hesthaven and T. Warburton. High-order nodal methods on unstructured grids. i: Time-domain solution of Maxwell equations. *J. Comp. Phys.*, 181:186–221, 2002.

Absorbing Boundary Conditions

NEW *LOCAL* DtN-LIKE BOUNDARY CONDITIONS FOR EXTERIOR ELLIPTICAL SHAPED BOUNDARIES

H. Barucq[†], R.Djellouli[‡] and A.G. Saint-Guirons[†,*]
[†]LMA, CNRS UMR 5142, University of Pau and INRIA Futurs, Magique-3D team, IPRA, BP 1155, 64013 Pau, France
[‡]Department of Mathematics, California State University Northridge and INRIA Futurs, Associate team MAGIC, Northridge, CA 91330-8313, USA
[*]Email: anne-gaelle.saint-guirons@univ-pau.fr

Abstract

We construct a new class of absorbing boundary conditions for elliptical shaped boundaries to be used when solving acoustic scattering problems by elongated obstacles. These conditions result from a *local* approximation of the DtN operator expressed in Fourier series. Their main features are : (a) they are exact for the first n modes, and (b) they are easy to implement and parallelize, and (c) they retain the local structure of the computational scheme. We assess the computational efficiency of these conditions, with respect to the wavenumber and to the eccentricity of the artificial boundary, by conducting an analytical study as well as a numerical investigation. The analysis reveals that one may avoid excessive computational cost at low wavenumber for many practical applications. It also provides guidelines for satisfactory performance.

Introduction

Exterior Helmholtz problems are classical mathematical models for studying scattering problems arising in many applications such as as sonar, radar, geophysical exploration, nondestructive testing, etc... Despite their simplicity, this class of problems is not completely solved particularly from a numerical point of view. For example, the computation of the solutions of these problems requires first to limit it to a finite domain. This is often achieved by surrounding the given scatterer(s) (or radiator) by an artificial boundary that is located at some distance (measured in multiples of wavelength of interest) from its surface. A so-called "nonreflecting" boundary condition is then prescribed on the artificial boundary to represent the "far-field" behavior of the scattered field. The challenge here is the development of a simple but reliable as well as cost-effective computational procedure for representing the far-field behavior of the scattered. The quest for such conditions is ongoing. In 1982, Bayliss et al constructed a second order absorbing boundary conditions constructed we call here BGT2 that assumes however a circular or spherical artificial boundary. When applied for solving elongated scatterers, this condition often leads to larger than needed computational domains, which hampers computational efficiency. Moreover, the computational cost may become prohibitively expensive in the low frequency regime.

Our objective here is to construct approximate boundary conditions that can accommodate elliptical-shaped boundaries that are primary candidates for elongated scatterers and can be easily implemented in any finite element code. These conditions are Robin-type boundary conditions. We construct them by approximating the Dirichlet-to Neumann (DtN) operator represented in Fourier series in terms of Mathieu functions (for 2D problems) and prolate spheroidal functions (for 3D problems). The key requirement in the construction process of these conditions is that they are exact for the first modes. We then investigate mathematically and numerically the performance of these conditions with respect to the wavenumber and to the eccentricity of the artificial boundary. The mathematical analysis is conducted analytically in the OSRC context. Because of space limitation, we consider in this abstract the two-dimensional case and only a summary of these results are reported.

Second-order local DtN boundary conditions in elliptical coordinates

We restrict the presentation to the case of two-dimensional Helmholtz problems. Then, in the elliptical coordinates (ξ, θ), it is possible to approximate the DtN operator, through suitable algebraic manipulations only, and construct a class of Robin-type boundary conditions that are exact for the first n cylindrical modes. Example of such absorbing boundary conditions is the following second order local DtN boundary condition:

$$\frac{\partial u}{\partial \xi} = \frac{\sqrt{1-e^2}}{e(a_0 - a_1)} \left[(a_0\alpha_1 - a_1\alpha_0)u + (\alpha_1 - \alpha_0)\Delta_\theta u \right] \tag{1}$$

where Δ_θ is the following second order differential operator:

$$\Delta_\theta = \frac{\partial^2}{\partial \theta^2} - \frac{(eka)^2}{2} \cos 2\theta \mathrm{I} \tag{2}$$

The constants a_0 and a_1 are the characteristic numbers of

the periodic Mathieu functions [1], and the constants α_0 and α_1 are given by:

$$\alpha_n = \frac{\mathrm{Re}_n^{(3)'}(eka, e^{-1})}{\mathrm{Re}_n^{(3)}(eka, e^{-1})} \tag{3}$$

where $Re_n^{(3)}$ is the even radial Mathieu function of third type [1], k is the wavenumber, a the semi-major of the considered elliptical boundary, e its eccentricity.

The local boundary condition (1) is called a second order absorbing boundary condition because this condition is exact for the first two even modes. More examples of such absorbing boundary conditions can be found in [2].

Mathematical analysis

In order to investigate analytically the performance of the second order local DtN boundary condition (1), we use the specific impedance which is a practical tool for measuring the efficiency of absorbing boundary conditions in the context of on-surface radiation conditions (OSRC). This non-dimensional quantity measures the effect of the truncated medium in physical terms. It provides a convenient indicator of the performance of a given approximate representation. In the elliptical coordinates system, the specific impedance can be expressed as follows:

$$Z = \frac{ieka\, U(\xi_0, \theta)}{\frac{\partial U(\xi, \theta)}{\partial \xi}|_{\xi=\xi_0}} \tag{4}$$

where ξ_0 defines the boundary of the elliptical obstacle (radiator or scatterer).

Therefore, the specific impedances of the n^{th} elliptic cylindrical *even* mode on the surface of an elliptical cylinder at $\xi = \xi_0$ are:

- The exact specific impedance (z_n^{exact2e}):

$$z_n^{\mathrm{exact2e}} = ieka \frac{Re_n^{(3)}(eka, e^{-1})}{\frac{\partial Re_n^{(3)}}{\partial \xi}(eka, e^{-1})}, n \geq 0$$

- The approximate specific impedance (z_n^{DtN2e}) corresponding to the second order DtN boundary condition (1):

$$z_n^{\mathrm{DtN2e}} = \frac{ika\,(a_0 - a1)\sqrt{1-e^2}}{\underbrace{(a_0\alpha_1 - a_1\alpha_0)}_{A_e} - c_n \underbrace{(\alpha_1 - \alpha_0)}_{B_e}}$$

Similarly, the exact specific impedance $Z_\theta^{\mathrm{exact2}}$ corresponding to the two-dimensional sound-soft scattered field u, by an incident plane wave with an incident angle θ_0, can be computed easily in terms of Mathieu functions using the Fourier series representation of u [2]-[3], while the corresponding approximate specific impedance $Z_\theta^{\mathrm{DtN2e}}$ is given by:

$$Z_\theta^{\mathrm{DtN2e}} = \frac{ika\sqrt{1-e^2}\,(a_0 - a_1)}{A_e - B_e\left(ika\lambda + (ka)^2\left(\frac{\partial \lambda}{\partial \theta}\right)^2 + \frac{(eka)^2}{2}\cos 2\theta\right)} \tag{5}$$

where $\lambda = \cos\theta\cos\theta_0 + \sqrt{1-e^2}\sin\theta\sin\theta_0$.

The following result states the asymptotic behavior of the specific impedances as $ka \to 0$.

Theorem

- The asymptotic behavior of the specific impedances of the n^{th} elliptic cylindrical mode as $ka \to 0$ is given by:

$$z_n^{\mathrm{exact2e}} \sim \frac{4\pi}{(n!)^2}\left(\frac{ka}{2}\right)^{2n+1} - i\frac{ka}{n}\ ;\ n \geq 2 \tag{6}$$

$$z_n^{\mathrm{DtN2e}} \sim \frac{\pi}{2n^2}(ka)^3 - i\frac{ka}{n^2} \text{ if } n \geq 2 \tag{7}$$

- The asymptotic behavior of the specific impedances of the scattered field on the surface of an elliptical cylinder as $ka \to 0$ is given by:

$$Z_\theta^{\mathrm{exact2}} \sim Z_\theta^{\mathrm{DtN2e}} \sim 1 - i\frac{1}{2ka} \tag{8}$$

The previous theorem reveals that the asymptotic behavior of both the exact and the DtN2e specific impedances are identical in the case of scattering problems. However, for radiator problems the situation is different since it depends on the order of the modes. More specifically, the theorem states that for higher modes, the real part of z_n^{exact2e} tend to zero faster for very low wavenumber ka than the corresponding part of z_n^{DtN2e}, while the imaginary part of z_n^{exact2e} tend to zero slower than the corresponding part of z_n^{DtN2e}. This indicates that, for higher modes n, DtN2e will perform poorly and therefore may not be appropriate.

Numerical investigation

We have performed several numerical experiments to investigate the effect of the wavenumber ka and the eccentricity e on the performance of the DtN2e condition. Such investigation includes a performance comparison with the exact specific impedances as well as with the approximate specific impedances Z^{BGT2} corresponding to the second order Bayliss-Gunzburger-Turkel condition (BGT2) [4]. The results depicted in Fig. 1 and Fig. 2. are obtained for $ka = 0.1, 1, 10$ in the case of a boundary with a mild eccentricity $e = 0.4$ and a very elongated boundary $e = 0.9$. The results obtained in the

case of scattering problems indicate, as predicted analytically, that the range of satisfactory performance of the DtN2e condition extends to relatively low wavenumbers ($ka = 0.1$) for all values of eccentricity.

Illustrations

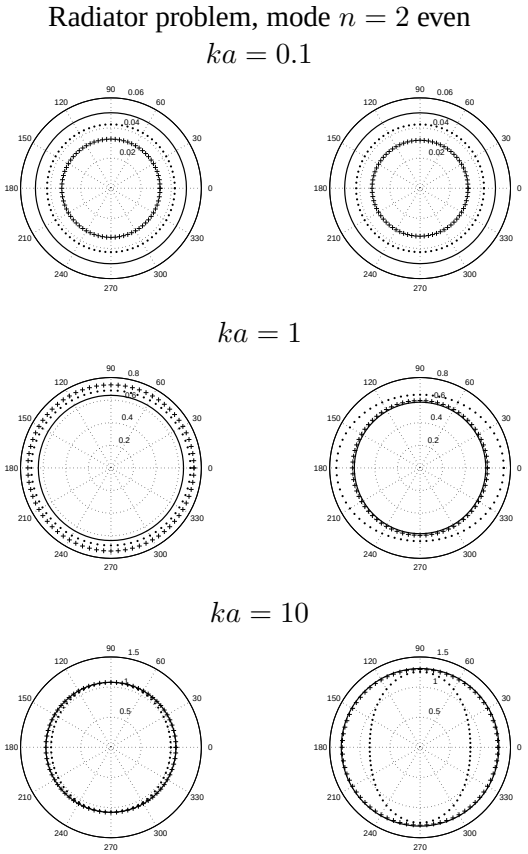

Figure 1: Absolute value of the specific impedance for the second even elliptic cylindrical mode for the exact (—), the even DtN2 (+ + +) and the BGT2 (**. . .**) for $e = 0.4$ (left) and $e = 0.9$ (right).

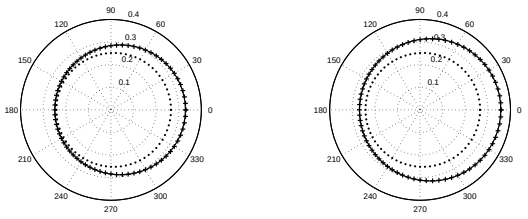

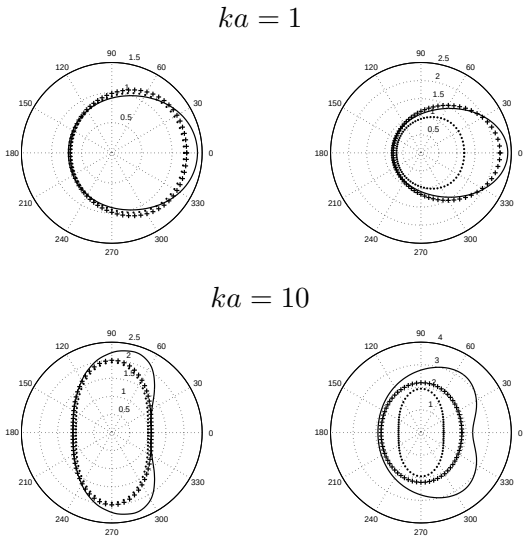

Figure 2: Absolute value of the specific impedance for the exact (—), the even DtN2 (+ + +) and the BGT2 (**. . .**) for $e = 0.4$ (left) and $e = 0.9$ (right).

Aknowledgement

The authors acknowledge the support by INRIA/CSUN Associate Team Program.

References

[1] M. Abramovitz, I. Stegun, Handbook of Mathematical Functions with Formulas, Graphs and Mathematical Tables, Dover Publications, New York, 1972.

[2] H. Barucq, R. Djellouli, A.G. Saint-Guirons, Construction and performance assesment of local Dirichlet-to-Neumann elliptical boundary operators for scalar acoustic scattering problems, INRIA research report, (in preparation).

[3] J.J. Bowman, T.B.A. Senior, P.L.E. Uslenghi, Electromagnetic and Acoustic Scatttering by Simple Shapes, Hemisphere Publishing Corporation, New York, NY, 1987.

[4] R.C. Reiner, R. Djellouli, I. Harari, The performance of local absorbing boundary conditions for acoustic scattering from elliptical shapes, Comput. Methods Appl. Mech. Engrg, 195, 3622-3665, 2006.

ACCURACY AND ROBUSTNESS OF A FINITE ELEMENT METHOD BASED ON AN EXACT PML TECHNIQUE IN TIME-HARMONIC SCATTERING PROBLEMS

A. Bermúdez[†], L. M. Hervella-Nieto[‡], A. Prieto[†,*], R. Rodríguez[§]
[†]Departamento de Matemática Aplicada, Universidade de Santiago de Compostela, 15782 Santiago de Compostela, Spain.
[‡]Departamento de Matemáticas, Universidade da Coruña, 15707 A Coruña, Spain.
[§]GI[2]MA Departamento de Ingeniería Matemática, Universidad de Concepción, Concepción, Chile.
[*]Email: maprieto@usc.es

Abstract

We consider the numerical solution of a two-dimensional dissipative acoustic vibration problem in an unbounded domain, under the assumption of time-harmonic dependence. With this aim, we implement a standard finite element method combined with an exact PML technique with finite thickness, which allows recovering the solution of the scattering problem stated in the original unbounded domain. In its construction, this exact PML technique overcomes the dependence of parameters for the discrete problem. Taking into account different meshes, formed by triangles or quadrilaterals, the numerical accuracy of our method and the robustness of the numerical solution used in the discretization are illustrated with some numerical tests, where we consider acoustic fluids and rigid porous media.

Introduction

We focus our attention on a time-harmonic dissipative acoustic scattering problem in two dimensions: computing the fluid pressure field scattered by a rigid obstacle surrounded by an acoustic fluid or a rigid porous medium, filling the whole space.

We denote by Ω the domain occupied by the rigid obstacle and g the Neumann data on its boundary $\partial\Omega$. We consider the following Neumann boundary value problem for the Helmholtz equation, which models the wave propagation for frequency $\omega > 0$ and a complex wave number $k(\omega)$ with $\mathrm{Re}(k(\omega)) > 0$:

$$\begin{aligned} -\Delta u - k(\omega)^2 u &= 0 && \text{in } \mathbb{R}^2 \setminus \overline{\Omega}, \\ \frac{\partial u}{\partial \boldsymbol{n}} &= g && \text{on } \partial\Omega, \\ \lim_{r\to\infty} \sqrt{r}\left(\frac{\partial u}{\partial r} - iku\right) &= 0, \end{aligned}$$

where u is the pressure field and the last equation is the Sommerfeld radiation condition. Classically, for linear acoustic problems $k(\omega) = \omega/c > 0$, being c the fluid sound speed. However if rigid porous materials are taken into account, then the wave number is complex and satisfies $\mathrm{Re}(k(\omega)) > 0$ (see for instance [1]). For instance, in Darcy like porous model [2], $k(\omega) = \sqrt{(\rho\omega^2 + is)/c^2}$, being ρ the fluid mass density at rest and s the flux resistivity of the porous medium.

The first problem to be tackled for the numerical solution is to truncate the computational domain and, consequently, to reduce the original scattering domain to a bounded domain where we focus our interest.

An exact PML technique

To truncate the computational domain we use the PML technique, introduced by Bérenger in [3]. As it is well known, this technique is based on introducing damping terms in a layer surrounding the domain of interest. These terms depend on a absorbing function σ, which plays a key role on the construction of the PML. Classically, σ is positive and it is chosen constant or quadratic (see for instance [3]).

Moreover, the governing equations in the PML domain can be formally obtained by means of a complex stretching of variables from the standard Helmholtz equation. For instance, if the PML is written in Cartesian coordinates for the x-direction, and this layer is placed between $x = L$ and $x = L^*$, the complex stretching of variable $\hat{x}$ is defined by

$$\hat{x} = x + i\int_L^x \sigma(\xi)\,\mathrm{d}\xi,$$

where $\sigma(s)$ is an absorbing function; for instance, a typical choice is the quadratic function

$$\sigma(\xi) = \frac{\sigma^*}{\omega}(L - \xi)^2, \tag{1}$$

with $\sigma^* > 0$.

Instead, we use the exact PML studied in [4] and [5], which is based on an absorbing function σ with

unbounded integral, for instance,

$$\sigma(\xi) = \frac{1}{k(\omega)} \frac{1}{L^* - \xi}. \qquad (2)$$

With this kind of choice, it has been proved for $k(\omega)$ real and positive that the exact solution is theoretically recovered, even though the thickness of the PML is finite [4]. In spite of the use of non-integrable absorbing functions, the resulting discrete problem is well posed and no numerical drawbacks arise in its implementation [5].

Let us remark that if the wave number is complex, then the absorbing function is complex valued as well. In fact, by using a plane wave analysis, it is easy to check that if $\mathrm{Im}(k(\omega)) \neq 0$, then it is necessary to chose a complex absorbing function σ to recover the theoretical accuracy results with the PML technique. Moreover, if σ were positive and $k(\omega)$ complex, then spurious reflections would arise from the outer boundary of the PML for any absorbing function.

Numerical accuracy and robustness

The associated coupled fluid/PML weak problem leads to a complex-symmetric (non-Hermitian) pressure formulation, which we discretize with standard finite elements. We use a triangular mesh and linear finite elements in the fluid domain.

It has been shown in [5] that if bilinear elements on a structured quadrilateral mesh are used inside the PML domain and a non-integrable absorbing function like (1) is considered, then the accuracy of this method improves that of the same discrete problem with quadratic absorbing functions.

In spite of the fact that the absorbing function is not integrable, for quadrilateral meshes and bilinear elements, all the coefficients in the element matrices are bounded and this discretization leads to a well posed finite element problem. Moreover, the use of unbounded absorbing functions overcomes the problem of tuning optimal parameters for the PML.

The use of structured quadrilateral meshes in the PML domain could become a drawback, since matching meshes on the fluid should be created separately. Moreover, triangular meshes in the fluid domain turn out useful to fit more precisely the shape of the scatterer.

One of the aims of this work is to study the influence of using triangular meshes inside the PML. More precisely, instead of the quadrilateral meshes used typically for Cartesian PML, which are aligned with the Cartesian directions, we consider unstructured quasi-uniform regular triangular meshes. We compare their accuracy and robustness with respect to those formed by quadrilaterals.

Analogously to the discrete problem with quadrilateral meshes and bilinear elements, if we use triangular meshes and linear elements in the PML domain, then all the coefficients in the element matrices are bounded and we compute them with standard quadrature formulas.

To illustrate the performance of our method, we consider that the obstacle Ω is the unit circle centered at the origin and the Neumann data is

$$g(x,y) = \frac{i}{4} \mathrm{H}_0^{(1)} \left(k(\omega) \sqrt{(x-0.5)^2 + y^2} \right),$$

where $\mathrm{H}_0^{(1)}$ is the Hankel function of first kind and order zero and $k(\omega) = \omega/c$.

We have used uniform refinements of the mesh shown in Figure 1. The number N of elements through the thickness of the PML is used to label each mesh.

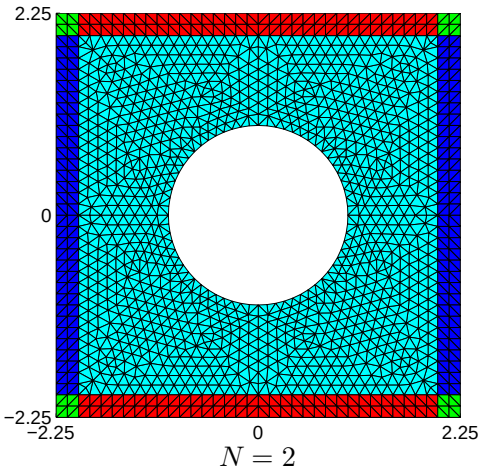

Figure 1: Structured triangular mesh in the scattering problem.

Table 1 shows the relative errors obtained using a structured triangular mesh in the PML domain with 0.25 m of thickness (see Figure 1). When the quadratic absorbing function is used, the parameter σ^* has been computed to minimize the error. We check that also in the case of the triangular meshes, the use of unbounded functions improves the accuracy of the method.

Table 1: Comparison of PML methods with unbounded and quadratic absorbing functions for $\omega = 250$ rad/s and $c = 340$ m/s.

	Unbounded (1)	Quadratic (2)	
Mesh	Error(%)	σ^*	Error(%)
$N = 2$	2.7233	$20.53\,c$	18.3060
$N = 4$	0.6757	$28.94\,c$	4.7286
$N = 8$	0.2826	$37.57\,c$	1.3783

Numerical results show the accuracy and the robustness of the exact PML technique for the above mentioned two-dimensional discrete scattering problems involving acoustic fluids and rigid porous media, as well.

References

[1] J.-F. Allard, Y. Champoux, "New empirical equations for sound propagation in rigid frame fibrous materials", J. Acoust. Soc. Am., vol. 91, pp. 3346–3353, 1992.

[2] A. Bermúdez, J.L. Ferrín, A. Prieto, "A finite element solution of acoustic propagation in rigid porous media", Int. J. Numer. Meth. Engng., vol. 62, n. 10, pp. 1295-1314, 2005.

[3] J.P. Berenger, "A perfectly matched layer for the absorption of electromagnetics waves", J. Comput. Phys., vol. 114, pp. 185-200, 1994.

[4] A. Bermúdez, L.M. Hervella-Nieto, A. Prieto, R. Rodríguez, "An exact bounded PML for the Helmholtz equation", C. R. Acad. Sci. Paris, Ser. I., vol. 339, pp. 803–808, 2004.

[5] A. Bermúdez, L.M. Hervella-Nieto, A. Prieto, R. Rodríguez, "An optimal perfectly matched layer with unbounded absorbing function for time-harmonic acoustic scattering problems", J. Comput. Phys., vol. 223, pp. 469-488, 2007.

LOCAL NONREFLECTING BOUNDARY CONDITIONS FOR TIME-DEPENDENT MULTIPLE SCATTERING

Marcus J. Grote[†], **Imbo Sim**[‡]
Department of Mathematics, University of Basel,
Rheinsprung 21, CH-4051 Basel, Switzerland
Email:[†] Marcus.Grote@unibas.ch, [‡] Imbo.Sim@unibas.ch

Abstract

In [4], [5] a nonreflecting boundary condition(NBC) for time-dependent multiple scattering was derived, which is local in time but nonlocal in space. Here, based on a high-order *local* nonreflecting boundary condition (NBC) for single scattering [6], we seek a local NBC for time-dependent multiple scattering, which is completely *local both in space and time*. To do so, we first develop a high order representation formula for a purely outgoing wave field, given its values and those of certain auxiliary functions needed for the artificial boundary condition. By combining that representation formula with a decomposition of the total scattered field into purely outgoing contributions, we obtain the first exact, completely local, NBC for time-dependent multiple scattering. The accuracy and stability of this local NBC is evaluated by coupling it to standard finite element and finite difference methods.

1 Local NBC for single scattering

We wish to calculate numerically the time dependent field u scattered from a bounded scattering region in three-dimensional space. In this region, there may be one or more scatterers, and the equation for u may have variable coefficients and source terms. As usual, we surround the scattering region by an artificial boundary B, and confine the computation to the region Ω bounded by B – see Fig. 1. Then, a nonreflecting boundary condition (NBC) is needed at B, which guarantees that the solution of the problem in Ω coincides with the solution of the original problem in the unbounded region.

We let B be the sphere of radius R and assume that u satisfies the homogeneous wave equation,

$$u_{tt} - c^2 \Delta u = 0, \tag{1}$$

outside B. Then, Hagstrom and Hariharan [6] derived the following exact NBC in three space dimensions:

$$\Big(\frac{1}{c}\frac{\partial}{\partial t} + \frac{\partial}{\partial r} + \frac{1}{r}\Big)u = w_1, \tag{2}$$
$$\Big(\frac{1}{c}\frac{\partial}{\partial t} + \frac{k}{r}\Big)w_k = \frac{1}{4R^2}\Big(k(k-1) + \Delta_S\Big)w_{k-1} + w_{k+1},$$

for $k = 1, 2, \ldots$, and $w_0 = 2u$. Here, Δ_S denotes the Laplace-Beltrami operator in spherical coordinates (r, θ, ϕ),

$$\Delta_S = \frac{1}{\sin\theta}\frac{\partial}{\partial\theta}\Big(\sin\theta\frac{\partial}{\partial\theta}\Big) + \frac{1}{\sin^2\theta}\frac{\partial^2}{\partial\phi^2}. \tag{3}$$

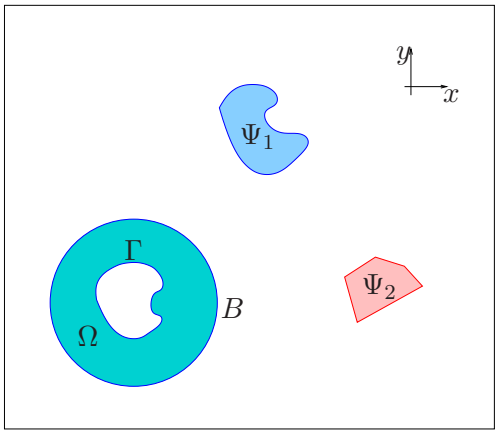

Figure 1: Wave scattering from an obstacle Γ. The computational domain, Ω, is bounded by the artificial boundary B, where the local NBC (2) is imposed. Subsequent evaluation of the solution in other sub-domains, $\Psi_{1,2}$ is possible via (4) by using past values of u and w_k at B.

In two dimensions, a similar expansion is available; however, it is no longer exact but only asymptotic in inverse powers of R. The boundary condition (2) is *local in space and time* and does not involve high-order derivatives, but instead an infinite sequence of auxiliary variables w_k defined on B. In practice, only a finite number, P, of auxiliary variables is used. Then, the boundary condition remains exact for any combination of spherical harmonics up to order P, while the error introduced at B generally behaves like R^{-2P-1}. Hence, P can always be chosen large enough to reduce the error introduced at B below the discretization error inside the computational domain, at any fixed R. Because it does not involve high-order derivatives, this local boundary condition is easily combined with standard numerical methods and enables

arbitrarily high order implementations. Recently, it was extended to the time dependent Maxwell equations [2].

When the solution consists of a finite sum of spherical harmonics up to order P, the local NBC (2) with $k = 0, \ldots, P$ becomes exact. Then, the past values of u and the auxiliary functions w_k at $r = R$ determine the solution *everywhere outside* Ω through the following exact (analytical) representation:

$$u^{[P]}(r,\theta,\phi,t) \qquad (4)$$
$$= \frac{R}{r}\sum_{k=0}^{P}\frac{2^{k-1}}{k!}\Big(R\Big(1-\frac{R}{r}\Big)\Big)^k w_k(R,\theta,\phi,t-\tfrac{r-R}{c}).$$

For a general wave field, equation (4) yields an approximate evaluation formula for u in the exterior region, whose accuracy improves with increasing P (or R).

2 Local NBC for multiple scattering

When the scatterer consists of several obstacles, which are well separated from each other, the use of a single artificial boundary to enclose the entire scattering region becomes too expensive. Instead it is preferable to enclose every sub-scatterer by a separate artificial boundary B_i. Then we seek an exact boundary condition on $B = \bigcup B_i$, where each B_i surrounds a single computational sub-domain Ω_i. This boundary condition must not only let outgoing waves leave Ω_i without spurious reflection from B_i, but also propagate the outgoing wave from Ω_i to all other sub-domains, which it may reenter subsequently. To derive such an exact boundary condition, an analytic representation of the solution everywhere in the exterior region is needed, as in (4).

For simplicity, we consider a scattering problem with two bounded disjoint scatterers, each surrounded by a sphere B_i of radius, R_i $i = 1, 2$. Hence, the entire artificial boundary $B = B_1 \cup B_2$ and the computational domain $\Omega = \Omega_1 \cup \Omega_2$. In contrast to the situation of single scattering above, we cannot simply expand u outside B as a superposition of purely outgoing wave fields. In fact, since part of the scattered field leaving Ω_1 will reenter Ω_2 at later times, and vice versa, u is not outgoing ouside Ω. Thus, the boundary condition we seek at B must not only let outgoing waves leave Ω_1 without spurious reflection from B_1, but also propagate those waves to Ω_2, and so forth, without introducing any spurious reflections.

Following [5], we first decompose the scattered field u in two wave fields, $u = u_1 + u_2$, where u_i is purely outgoing as seen from Ω_i. The two wave fields u_1 and u_2 both solve the homogeneous wave equation (1) outside Ω, and their sum coincides with u. The outgoing field u_1^{out}, as seen from Ω_1, is fully determined by its boundary values on B_1, while the incoming field u_{12}^{in} is fully determined by its boundary values on B_2. Hence,

$$\begin{aligned} u_1^{out} + u_{12}^{in} &= u|_{B_1}, \\ u_2^{out} + u_{21}^{in} &= u|_{B_2}, \end{aligned} \qquad (5)$$

where u_i^{out} is the outgoing wave field from Ω_i and u_{ij}^{in} is the incoming wave propagating from Ω_j to Ω_i.

Next, we apply $c^{-1}\partial_t + \partial_{r_i} + R_i^{-1}$ in local spherical coordinates (r_i, θ_i, ϕ_i) to u on each artificial boundary component B_i, $i = 1, 2$. This yields the following exact local NBC for multiple scattering:

$$\begin{aligned} \mathcal{B}_1 u|_{B_1} &= \Big(\frac{1}{c}\frac{\partial}{\partial t} + \frac{\partial}{\partial r_1} + \frac{1}{R_1}\Big)u|_{B_1} \\ &= \mathcal{B}_1 u_1^{out} + \mathcal{B}_1 u_{12}^{in} \qquad \text{on } B_1, \\ \mathcal{B}_2 u|_{B_2} &= \Big(\frac{1}{c}\frac{\partial}{\partial t} + \frac{\partial}{\partial r_2} + \frac{1}{R_2}\Big)u|_{B_2} \\ &= \mathcal{B}_2 u_2^{out} + \mathcal{B}_2 u_{21}^{in} \qquad \text{on } B_2. \end{aligned} \qquad (6)$$

To evaluate $\mathcal{B}_1 u_1^{out}$ we use (2) at B_1, whereas to evaluate $\mathcal{B}_1 u_{12}^{in}$ we use (4) for u_2 on B_1. The needed past values of w_k are stored on each B_i at regular time and angular intervals and calculated, as needed, via local spline interpolation [1]. Because those values are time-retarded, they are already known, so that the entire scheme remains explicit in time. Remarkably, the information transfer (of time retarded values) between sub-domains occurs only across those parts of the artificial boundary, where outgoing rays intersect neighboring sub-domains, i.e. typically only across a fraction of the artificial boundary.

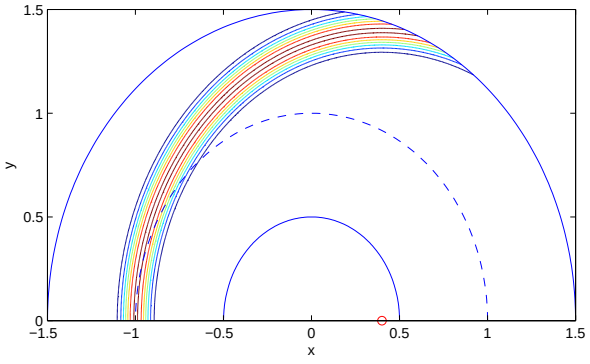

Figure 2: Contour lines across B obtained either from the numerical solution for $0.5 \le r \le 1$ or the evaluation formula (4) for $r > 1$; the source is located at $(0.4, 0)$.

3 Numerical Experiments

We shall now illustrate the accuracy of the local NBC (2) and the evaluation formula (4). To do so, we consider an outgoing spherical wave generated by a Gaussian point source located at distance $d = 0.4$ from the origin. Its time dependence is determined by

$$g(t) = e^{-(t-\alpha)^2/\sigma^2}, \quad \alpha = 0.3, \quad \sigma = \frac{\alpha}{7\log 10} \qquad (7)$$

and vanishes outside the time window $[0, 0.6]$. This exact solution is used to initialize the numerical solution inside the computational domain $\Omega = \{(r,\theta)\,|\,r \in [0.5, 1], \theta \in [0, \pi]\}$ and we impose (2) for varying P on the artificial boudary located at $R = 1$.

Inside Ω we use standard second-order finite differences on a regular polar grid. The auxiliary functions w_k in (2) are advanced concurrently with u as in [6]. Outside the computational domain in the region $\Omega^{ext} = \{(r,\theta)\,|\,r \in [1.0, 1.5], \theta \in [0, \pi]\}$ directly adjacent to it, the solution is evaluated using (4). As shown in Fig. 2, the contour lines across B are smooth.

In Fig. 3 we compare the numerical solution along a ray at a fixed time for varying P with the exact solution. Next, the total L^2-error inside Ω vs. the mesh size h is shown in Fig. 4. For $P = 4$ we observe the expected global second-order convergence up to the finest mesh chosen here. Further mesh refinement generally requires increasing the value of P.

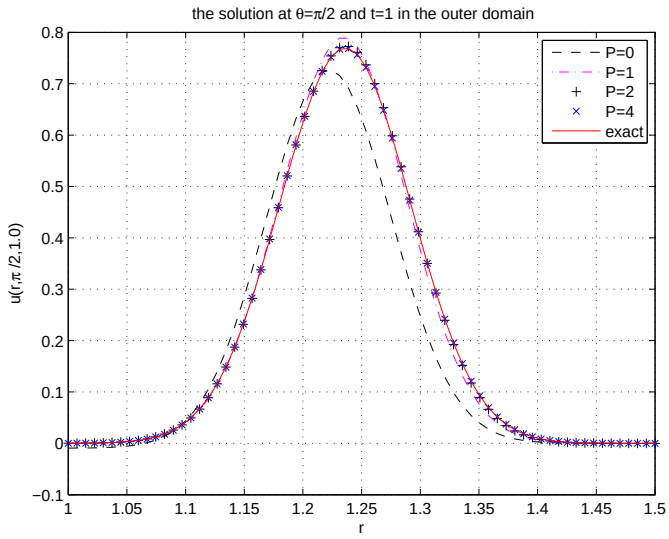

Figure 3: Evaluation of the solution at $\theta = \pi/2$ and $t = 1$ for varying P.

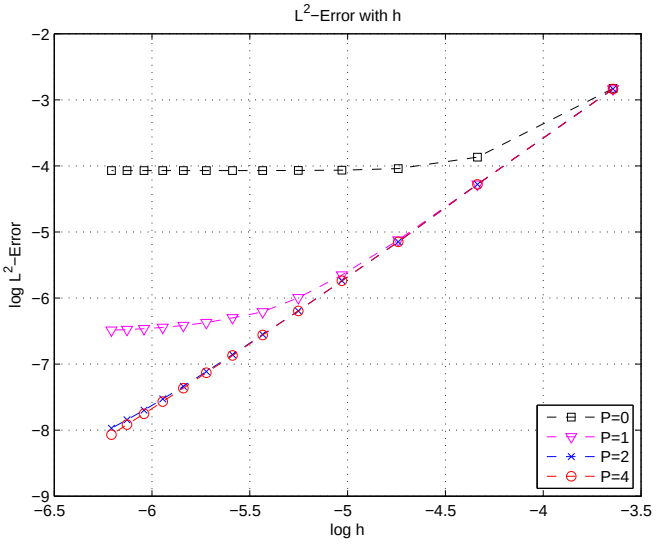

Figure 4: The total L^2-error is shown vs. the mesh size h for varying P.

References

[1] H. Akima: "A new method of interpolation and smooth curve fitting based on local procedures", J. of the ACM **17**(4), pp. 589–602, 1970

[2] M.J. Grote: "Local nonreflecting boundary condition for Maxwell's equations", Comput. Methods Appl. Mech. Engrg. **195**, pp. 3691–3708, 2006

[3] M.J. Grote, C. Kirsch: "Far-field evaluation via nonreflecting boundary conditions. In Hyperbolic Problems: Theory, Numerics, Applications", Proc. 9th Internat. Conf. on Hyperbolic Problems, HYP 2002, Eds. T. Y. Hou, E. Tadmor, Springer, pp. 195–204, 2003

[4] M.J. Grote, C. Kirsch: "Dirichlet-to-Neumann boundary conditions for multiple scattering problems", J. Comp. Phys, **201**(2), pp. 630–650, 2004

[5] M.J. Grote, C. Kirsch: "Nonreflecting boundary conditions for time-dependent multiple Scattering", J. Comp. Phys, **221**(1), pp. 41–62, 2007

[6] T. Hagstrom, S.I. Hariharan: "A formulation of asymptotic and exact boundary conditions using local operators", Appl. Numer. Math. **27**(4), pp. 403–416, 1998

PERFECTLY MATCHED LAYERS AND ABSORBING BOUNDARY CONDITIONS: UNIFICATION OF CONCEPTS

Murthy N. Guddati
North Carolina State University, Raleigh, NC 27560, USA
Email: mnguddat@ncsu.edu

Abstract

Techniques to simulate unbounded domains are typically classified into three categories: (a) exact global absorbing boundary conditions (global ABCs), (b) approximate local absorbing boundary conditions (local ABCs), and (c) perfectly matched layers (PML). While there exist links between global and local ABCs, PML has always been thought of as a conceptually disparate technique. We have recently shown that there is a simple but illuminating link between local ABCs and PML. This link, which is based on continued fraction ideas, has led to a new ABC called the perfectly matched discrete layers (PMDL), which is superior to the PML as well as the local and global ABCs.

Introduction

Domain truncation techniques are of paramount importance in accurate modeling of wave propagation in unbounded domains. The primary goal of these methods is to accurately simulate the effect of the truncated exterior. Many methods, developed in the past thirty years, can be classified into three categories that have their respective advantages and disadvantages:

(a) Global ABCs (e.g. [1]), which attempt to exactly capture the effect of the exterior through Green's functions. The obvious advantage is their accuracy. However, these methods render the computation global in both space and time and are often prohibitively expensive.

(b) Local ABCs (e.g. [2,3]), which approximate the Green's functions with the goal of local computation. Their main advantage is the computational efficiency. The disadvantage is that the extension to corner regions and evanescent waves are not well-developed. Furthermore, the treatment of more complex elastic wave equation is not well established.

(c) PML [4], which is based on the ideas of material damping. PML is very effective because of its ability to attenuate waves while avoiding any interface reflections by perfectly matching the impedance. The power of PML lies in its flexibility. The disadvantage is that, a PML, when discretized, loses its perfect-matching property and tends to be less efficient than local ABCs.

The above classes of boundary conditions, especially the PML, are considered conceptually disparate by many researchers. In this talk, we present a new boundary condition that links the three types of boundary conditions. Specifically, a simple yet powerful discretization method is presented for the PML, which preserves the perfect-matching property of the impedance even after discretization. Due to this property, the method is named perfectly matched discrete layers (PMDL). Originally named the continued-fraction ABC (CFABC), this boundary condition combines the accuracy of global ABCs, efficiency of local ABCs, and the flexibility of PML [6]. The rest of the abstract contains a brief summary of the underlying ideas.

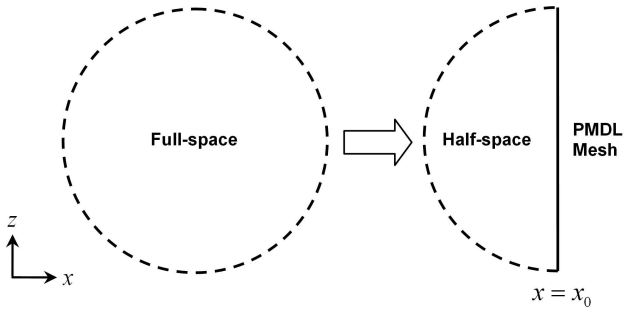

Figure 1: Model problem

Perfectly Matched Discrete Layers (PMDL)

Consider the model problem of replacing a full space with a left half-space representing the interior, and an absorbing boundary codition representing the exterior on the right (see Figure 1). An option for the absorbing boundary condition is the PML. The PML can either be viewed as an attenuating medium or as stretching the domain into complex space. While both versions are equivalent, we consider the complex-stretching version for the purposes of discussion. When the complex-stretching PML is discretized with the help of finite elements or finite differences, the resulting mesh could be viewed as a regular mesh modified with complex element lengths. The complex-length finite element mesh contains discretization errors, and accurate solution typically requires

small elements.

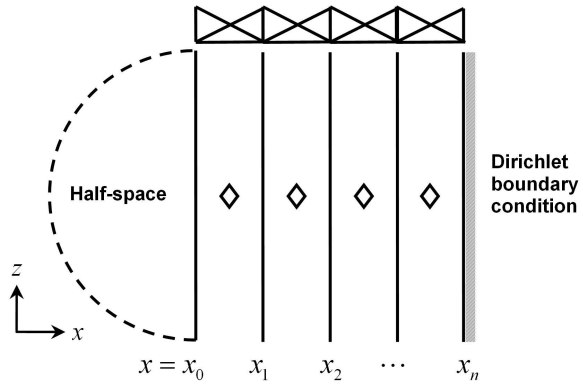

Figure 2: PMDL mesh is almost similar to PML, but midpoint integration is performed in conjunction with linear finite element discretization

The key idea of PMDL is to eliminate the discretization error with the help of modified integration, thus facilitating the use of large elements. Specifically, we showed that *if midpoint integration rule is used in conjunction with linear finite element interpolation (Figure 2), the discretization error in the impedance disappears*; the integration error completely cancels the error due to discretization. Since perfect matching is achieved even after discretization, we call this modification perfectly matched discrete layers (PMDL). It is also shown in [6] that PMDL presents a continued-fraction approximation of the exterior Greens function and hence it is formerly named continued-fraction ABC (CFABC). The PML/CFABC inherits the flexibility of PML, and as explained below, it can be made as accuate as global ABCs, and as efficient as local ABCs.

Reflection coefficient

Reflection coefficient is the ratio of the amplitude of artificial reflections to that of the incident wave, and is often used as the error measure of ABCs. The reflection coefficient for the PMDL can be derived as [6]:

$$R = \prod_{j=1}^{n} \left| \frac{k - 2i/L_j}{k + 2i/L_j} \right|^2, \qquad (1)$$

where k is the wavenumber in the direction normal to the boundary and L_j are the lengths of PMDL/CFABC layers. Due to the complex stretching of PML, PMDL/CFABC layers have complex or imaginary lengths and the reflection coefficient is less than unity for real k, indicating the effectiveness for propagating waves. Furthermore, it is easy to see that the reflection coefficient exponentially converges to zero with respect to the number of PMDL/CFABC layers. This is in contrast with the conventionally discretized PML, which is polluted with discretization errors that have polynomial dependence on the element size. PMDL/CFABC does not have this error, and the only error is from the truncation of the number of layers.

Treatment of Evanescent Waves

Typically, many local ABCs neglect special treatment of evanescent waves with the argument that the computational boundaries can be placed far enough so that the evanescent waves decay by the time they reach the boundary. However, in situations where the waves decay very slowly, the ABCs are to be placed very far from the scatterer, making the computation very expensive. PML does treat evanescent waves to some extent, but still requires a rather large number of layers to simultaneously treat evanescent waves of varying rates of decay. Global ABCs, as they are exact, treat evanescent waves, but are extremely expensive.

PMDL/CFABC can be made to accurately treat evanescent waves by a simple modification. By examining the expression for the reflection coefficient, making PMDL/CFABC lengths L_j real, one can make the reflection coefficient less than unity for evanescent waves (complex k). We call this real-length PMDL region the padding region. The difference between PMDL padding and regular (real) finite element mesh is that PMDL padding attains exponential convergence, facilitated by the use of midpoint integration. Many times, in situations where slowly decaying evanescent waves exist, the solution accuracy is significantly improved by using just one or two PMDL padding elements. When both evanescent and propagating waves are to be absorbed, the padding region is simply laced with regular PMDL/CFABC, resulting in so-called padded PMDL [7].

PMDL for more Complex Waves (e.g. elastic waves)

The basic ideas of PMDL, namely imaginary stretching and midpoint integration resulting in exponential convergence, extend to more complex equations such as the elastic wave equation. In fact, it is shown in [5] that the ideas of PMDL/CFABC are applicable to problems where the governing equation is linear and second-order in space.

Representative Numerical Example

PMDL/CFABC has been tested for a wide range of problems including acoustic wave equation, dispersive acoustics, and elastic wave equations, for various geo-

metrics including full space, half-space and wave guide. Figure 3 contains an example result that illustrates the effectiveness of PMDL/CFABC.

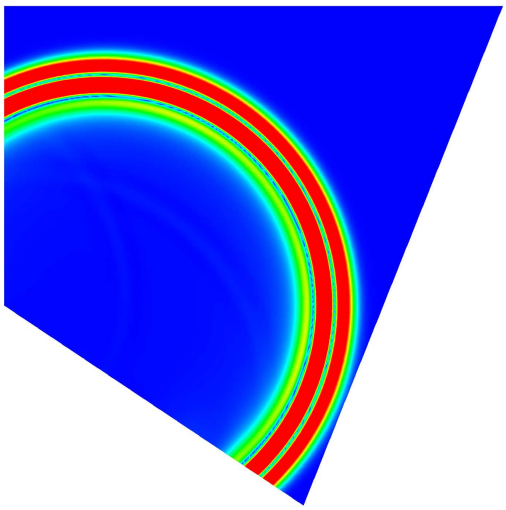

Figure 3: An illustrative result for PMDL: a polygonal computational domain is laced with three PMDL layers all around the boundary to simulate full space. Clearly, the wave front is well-absorbed with just three layers, indicating the effectiveness of PMDL

Discussion

The discretization of the PML presented above, namely linear finite elements with midpoint integration, while simple, has significant implications. Essentially the integration error eliminates the discretization error, thus preserving the perfect-matching property even after discretization. The resulting PMDL/CFABC preserves the perfect matching of the impedance and high accuracy can be achieved with just three to five discrete layers. Typically, regular discretization of the PML requires much larger mesh.

The PMDL/CFABC is linked closely to Engquist-Majda boundary conditions as it is closely linked to the continued fraction approximation of the exterior Green's function [8,9]. The reflection coefficient of the PMDL is very similar to that of Higdon's multi-directional absorbers. Since Engquist-Majda and Higon's boundary conditions have already been linked to existing local ABCs by other researchers, PMDL can be considered a local ABC, thus inheriting their effectiveness in approximating the Green's function.

Finally, since padded PMDL/CFABC can be efficient in treating propagating as well as evanescent waves, it is similar to global ABCs in thier accuracy.

In conclusion, by unifying the concepts underlying various boundary conditions, PMDL/CFABC combines the accuracy of the global ABCs, efficiency of local ABCs and the flexibilty of PML. This talk would present further details of the ideas and performance of PMDL/CFABC.

References

[1] E.Kausel and J.L.Tassoulas, "Transmitting boundaries a closed form comparison", Bulletin of Seismological Society of America, v.71, pp.143-159, 1981.

[2] B.Engquist, and A.Majda, "Absorbing boundary-conditions for numerical simulation of waves", Mathematics of Computation, v.31, pp.629-651, 1977.

[3] R.L.Higdon, "Numerical absorbing boundary conditions for the wave equations", Mathematics of Computation, v.49, pp.65-90, 1987.

[4] J.P.Berenger, "A Perfectly Matched Layer for the absorption of electromagnetic waves", Journal of Computational Physics, v.114, pp.185-200, 1994.

[5] M.N.Guddati, "Arbitrarily Wide Angle Wave Equations for Complex Media", Computer Methods in Applied Mechanics and Engineering, v.195, pp.65-93, 2006.

[6] M.N.Guddati and K.W.Lim, "Continued Fraction Absorbing Boundary Conditions for Convex Polygonal Domains", International Journal for Numerical Methods in Engineering, v. 66, pp. 949-977, 2006.

[7] M.A.Zahid and M.N.Guddati, "Padded Continued Fraction Absorbing Boundaries for Dispersive Waves", Computer Methods in Applied Mechanics and Engineering, in press.

[8] S.Asvadurov, V.Druskin, M.N.Guddati and L.Knizhnerman, "On Optimal Finite-Difference Approximation of PML", SIAM Journal on Numerical Analysis, v.41, pp.287-305, 2003.

[9] M.N.Guddati and J.L.Tassoulas, "Continued Fraction Absorbing Boundary Conditions for the Wave Equation", Journal of Computational Acoustics, v.8, pp.139-156, 2000.

PERFECTLY MATCHED LAYERS FOR THE STATIONARY SCHRÖDINGER EQUATION IN A PERIODIC STRUCTURE

V. Kalvin[†,*]
[†]Department of Mathematical Information Technology, University of Jyväskylä, Jyväskylä, Finland
[*]Email: vkalvin@it.jyu.fi

Abstract

The Perfectly Matched Layers (PML) method, introduced in [1], attracted much attention. This method is in common use for a numerical analysis of a wide class of problems. For some problems the convergence of the method has been proved mathematicaly, see e.g. [2–5].

In this work, we introduce the PML method for the stationary Schrödinger equation in a "half-plane" with periodic boundary and Dirichlet or Neumann boundary conditions. Under rather weak assumptions on the potential, we construct the PML of infinite length for the original problem supplied with special radiation conditions. Under more restrictive assumptions on the potential, the special radiation conditions are equivalent to the classical ones. Solving the problem with the PML of finite length, we obtain an approximation for the solution of the original problem with radiation conditions in the computational domain. We prove that the error of this approximation tends to zero with an exponential rate as the length of PML tends to infinity.

Statement of the problem and preliminaries

Let $\mathcal{P}$ be an upper "half-plane" in $\mathbb{R}^2$ with smooth 2π-periodic boundary $\partial\mathcal{P}$. Let $\mathcal{E} = \{(y,t) \in \mathcal{P} : |y| < \pi\}$ be the periodicity cell of $\mathcal{P}$. We set $\Upsilon^{\pm} = \{(y,t) \in \mathcal{P} : y = \pm\pi\}$ and $\Upsilon^0 = \partial\mathcal{E} \setminus \{\Upsilon^+ \cup \Upsilon^-\}$. As it usually is, the problem in $\mathcal{P}$ reduces to a quasi-periodic boundary value problem in the periodicity cell $\mathcal{E}$. We consider the stationary Schrödinger equation

$$(\Delta + k^2 + q(y,t))u(y,t) = \mathcal{F}(y,t),\ (y,t) \in \mathcal{E}, \quad (1)$$

with the quasi-periodicity conditions

$$\partial_y^j u(\pi,t) = e^{2\pi i\alpha}\partial_y^j u(-\pi,t), j = 0,1, \quad (2)$$

where $(\pm\pi,t) \in \Upsilon^{\pm}$, and Dirichlet (or Neumann) boundary conditions

$$u(y,t) = 0 \text{ (or } \partial_\nu u(y,t) = 0),\ (y,t) \in \Upsilon^0. \quad (3)$$

Here $\alpha \in [0,1)$, $\partial_y = \partial/\partial y$, $\partial_\nu = \partial/\partial\nu$, and ν is the outward normal to Υ^0. The parameter k is a fixed real number that does not coincide with a threshold value, i.e. $k^2 \neq (n+\alpha)^2$ for all $n \in \mathbb{Z}$. In this section we assume that the potential q is a smooth real-valued function in $\overline{\mathcal{P}}$, $q(y,t) = q(y+2\pi,t)$ for all $(y,t) \in \overline{\mathcal{P}}$, and $q(y,t) \to 0$ as $t \to +\infty$ uniformly in $y \in [-\pi,\pi]$.

For all $n \in \mathbb{Z}$ we set $\lambda_n^{\pm} = \mp\sqrt{k^2-(n+\alpha)^2}$, where we choose the main branch of the square root. Let $\mathfrak{N} = \{n \in \mathbb{Z} : |n+\alpha| < |k|\}$. To the problem (1–3) with $q \equiv 0$ there correspond incoming waves w_n^+ and outgoing waves w_n^-, where

$$w_n^{\pm}(y,t) = \exp(i\lambda_n^{\pm}t + i(n+\alpha)y),\ n \in \mathfrak{N},$$

$$\mathfrak{N} = \{n \in \mathbb{Z} : |n+\alpha| < |k|\}.$$

Let $\Pi = \{(y,t) : |y| < \pi, t \in \mathbb{R}\}$. We denote by $H^{\ell}_{\beta}(\Pi)$ the space with norm $\|e_{\beta\cdot}; H^{\ell}(\Pi)\|$, where $H^{\ell}(\Pi)$ is the Sobolew space, $e_\beta : (y,t) \mapsto \exp\beta t$, and $\beta \in \mathbb{R}$. Let $H^{\ell}_{\beta,\alpha}(\Pi)$ denote the subspace in $H^{\ell}_{\beta}(\Pi)$ of all functions satisfying the quasi-periodicity conditions (2) on the boundary $\partial\Pi$ of Π. As is known (e.g., see [6]), the map $A_\beta = \{\Delta + k^2\} : H^2_{\beta,\alpha}(\Pi) \to H^0_{\beta}(\Pi)$ is an isomorphism if $\beta \neq \Im\lambda_n^{\pm}$ for all $n \in \mathbb{Z}$. Let $q^T(y,t) = q(y,t)$ for $t \geq T$ and $q^T(y,t) = 0$ for $t < T$, $y \in [-\pi,\pi]$. Let β be such that $0 < \beta < |\Im\lambda_n^{\pm}|$ for all $n \in \mathbb{Z} \setminus \mathfrak{N}$. We set

$$\mathsf{w}_n^{\pm,T} = w_n^{\pm} + \sum_{m=1}^{\infty}\left((A_{-\beta})^{-1}q^T\right)^m w_n^{\pm},\ n \in \mathfrak{N}, \quad (4)$$

where T is a large number such that the series $\sum(A_{-\beta}^{-1}q^T)^m w_n^{\pm}$ converges with respect to the norm in the space $H^2_{-\beta}(\Pi)$. The functions (4) do not depend on the choice of β, satisfy the quasi-periodicity conditions (2) on $\partial\Pi$ and the equation

$$\left(\Delta + k^2 + q^T(y,t)\right)u(y,t) = 0,\ (y,t) \in \Pi. \quad (5)$$

The relation $\mathsf{w}_n^{\pm,T} = w_n^{\pm} \mod H^2_{\beta,\alpha}(\Pi)$ holds. We define

$$\mathfrak{F}(u) = -\lim_{R\to+\infty}\Im\int_{-\pi}^{\pi} u(y,t)\overline{(du(y,t)/dt)}dy|_{t=R}.$$

The value $\mathfrak{F}(u)$ is the flow of the energy that a wave u transmits to the infinity; e.g. $-\mathfrak{F}(w_n^+) = \mathfrak{F}(w_n^-) > 0$. For the functions (4) we have $\mathfrak{F}(\mathsf{w}_n^{\pm,T}) = \mathfrak{F}(w_n^{\pm})$.

We denote by $H^\ell_\beta(\mathcal{E})$ the weighted Sobolev space with norm $\|e_{\beta\cdot}; H^\ell(\mathcal{E})\|$.

Theorem 1. (see e.g. [6]) *Let β and T be the same as in (4) and let $\mathcal{F} \in H^0_\beta(\mathcal{E})$. Then for a solution $u \in H^2_{-\beta}(\mathcal{E})$ to the problem (1–3) the inclusion*

$$u - \sum_{n\in\mathfrak{N}} (a_n(T)\mathsf{w}_n^{-,T} + b_n(T)\mathsf{w}_n^{+,T}) \in H^2_\beta(\mathcal{E}) \qquad (6)$$

is valid for some coefficients $a_n(T) \in \mathbb{C}$ and $b_n(T) \in \mathbb{C}$; moreover,

$$\mathfrak{F}(u) = \sum_{n\in\mathfrak{N}} \big(|a_n(T)|^2\mathfrak{F}(w_n^-) + |b_n(T)|^2\mathfrak{F}(w_n^+)\big).$$

Complex scaling and radiation conditions

Here, for simlicity, we assume that the right hand side $\mathcal{F}$ of the equation (1) has a compact support. Denote

$$\mathbb{K}^T_\phi = \{z \in \mathbb{C} : z = T + e^{i\psi}t, 0 \le \psi \le \phi, t \ge 0\}.$$

In addition to the previous assumptions, we suppose that for some $T_0 > 0$ and $\phi > 0$ the potential q can be continued to a function $\mathbb{R} \times \mathbb{K}^{T_0}_\phi \ni (y, z) \mapsto q(y, z) \in \mathbb{C}$, which is analytic in z, smooth 2π-periodic in y, and uniformly tends to zero as $|z| \to +\infty$, $z \in \mathbb{K}^{T_0}_\phi$. Let $\mathcal{E}^T = \{(y, t) \in \mathcal{E} : t < T\}$. By applying the complex scaling $t \to T + e^{i\phi}(t - T)$ for $t \ge T$ (complex change of variables) to the original problem (1–3), we obtain the problem

$$\big(\Delta + k^2 + q(y, t)\big)v^T(y, t) = \mathcal{F}(y, t),\ (y, t) \in \mathcal{E}^T, \quad (7)$$

$$\Big(\partial_y^2 + e^{-2i\phi}\partial_t^2 + q\big(y, T + e^{i\phi}(t - T)\big) + k^2\Big)v^T(y, t) = 0,\ (y, t) \in \mathcal{E} \setminus \overline{\mathcal{E}^T}, \quad (8)$$

$$\partial_y^j v^T|_{\Upsilon^+} = e^{2\pi i\alpha}\partial_y^j v^T|_{\Upsilon^-},\ \ j = 0, 1, \qquad (9)$$

$$v^T = 0 \text{ (or } \partial_\nu v^T = 0) \quad \text{on } \Upsilon^0 \qquad (10)$$

with the contact conditions

$$\partial_t^j v^T(y, T-) = e^{i\phi j}\partial_t^j v^T(y, T+),\ j = 0, 1, |y| \le \pi. \qquad (11)$$

Here $\partial_t^j v^T(y, T-)$ and $\partial_t^j v^T(y, T+)$ denote the limits of $\partial_t^j v^T(y, t)$ as t tends to T from the left and from the right side correspondingly.

Theorem 2. *Assume that for all $\gamma > 0$ there is no non-trivial solution to the homogeneous problem (1-3) in the space $H^2_\gamma(\mathcal{E})$. Let T be a sufficiently large positive number and let $\phi < \pi/2$. Then the following assertions hold.*

(i) There exists a unique solution $v^T \in H^1(\mathcal{E})$ to the problem (7-10). This solution is in the space $H^1_\gamma(\mathcal{E})$ if

$$|\gamma| < \min_{n\in\mathbb{Z}}\{\Im(e^{i\phi}\lambda_n^-)\}.$$

(ii) Let $U^T(y, T + e^{i\phi}(t - T)) = v^T(y, t)$ for $(y, t) \in \mathcal{E} \setminus \overline{\mathcal{E}^T}$. Then U^T can be continued to an analytic in z function $(-\pi, \pi) \times \mathbb{K}^T_\phi \ni (y, z) \mapsto U^T(y, z) \in \mathbb{C}$.

(iii) Let $u^T(y, t) = v^T(y, t)$ for $(y, t) \in \mathcal{E}^T$ and $u^T(y, t) = U^T(y, t)$ for $(y, t) \in \mathcal{E} \setminus \overline{\mathcal{E}^T}$. Then u^T is a solution to the problem (1-3) from the space $H^2_{-\beta}(\mathcal{E})$. The inclusion

$$u^T - \sum_{n\in\mathfrak{N}} c_n(T)\Big(\mathsf{w}_n^{-,T} + \sum_{m\in\mathfrak{N}} d_m^n(T)\mathsf{w}_m^{+,T}\Big) \in H^2_\beta(\mathcal{E}) \qquad (12)$$

holds with some $c_n(T) \in \mathbb{C}$ and $d_m^n(T) \in \mathbb{C}$. The coefficients $c_n(T)$ depend on the right hand side F, the parameter T, and the potential q, while the coefficients $d_m^n(T)$ depend on the parameter T and the potential q only, $|d_m^n(T)| \to 0$ as $T \to +\infty$.

(iv) Let $d_m^n(T)$ $(n, m \in \mathfrak{N})$ be arbitrary complex coefficients with sufficiently small modules. Then for every $\mathcal{F} \in H^0_\beta(\mathcal{E})$ there exists a unique solution u^T to the problem (1-3) such that the inclusion (12) is satisfied for some coefficients $c_n(T) \in \mathbb{C}$.

Theorem 2 shows that there exists a unique solution u^T of the original problem (1–3) satisfying the inclusion (12) for some $c_n(T) \in \mathbb{C}$. This solution is related to a unique solution $v^T \in H^1(\mathcal{E})$ of the problem (7–10) by the complex scaling. From the inclusion (12) it follows the equality $\mathfrak{F}(u^T) = \sum |c_n(T)|^2(\mathfrak{F}(w_n^-) + \sum |d_n^m(T)|^2\mathfrak{F}(w_n^+))$, the flux $\mathfrak{F}(u^T)$ is negative. We call the inclusion (12) *radiation conditions*. In the case of sufficiently rapid decay (say, with exponential rate) of the potential q as $|t| \to \infty$, $t \in \mathbb{K}^T_\phi$, we are able to get the asymptotics of the functions $\mathsf{w}_n^{\pm,T}(y, t)$ as $t \to +\infty$ in terms of the waves $w_n^\pm(y, t)$. Then the radiation conditions (12) take the well known form, the solution u^T satisfies the radiation conditions

$$|u^T(y, t) - \sum_{n\in\mathfrak{N}} C_n w_n^-(y, t)| = o(1),\ t \to +\infty, \quad (13)$$

with some coefficients $C_n \in \mathbb{C}$. Moreover, it turns out that u^T is independent of T, the coefficients $d_m^n(T)$ tend to zero and $c_n(T)$ tend to C_n as $T \to +\infty$ with the same rate as $q(y, t)$ goes to zero as $t \to +\infty$. In particular, if the potential q has a compact support, then for some large

T we have $q^T = 0$, $\mathsf{w}_n^{\pm,T} \equiv w_n^{\pm}$, and $d_n^m(T) \equiv 0$. In this case the coefficiens in (12) are independent of T, from (12) we get (13) with $C_n \equiv c_n$.

The assertion (*iv*) of Theorem 2 shows the well-posedness of the statement of the problem (1–3) with radiation conditions (12) in the general case.

Perfectly Matched Layer method

We search for an approximation of a solution u^T to the problem (1–3) with radiation conditions (12) in some bounded domain $\mathcal{E}^L$, $0 < L < T$. Since a solution $v^T \in H^1(\mathcal{E})$ to the problem (7–11) and u^T are coincident on $\mathcal{E}^T$ (see Theorem 2), one can search for an approximation of v^T instead of an approximation of u^T. The advantage is that v^T is in the space $H^1_\gamma(\mathcal{E})$, $0 < \gamma < \min\{\Im(e^{i\phi}\lambda_n^-)\}$, of functions "exponentially decreasing" at infinity , while $u^T \notin H^1(\mathcal{E})$. It is clear that v^T has these properties because of the *perfecly matched* equation (8). In other words, the equation (8) describes a *perfectly matched layer* (PML) of infinite length.

We truncate the domain $\mathcal{E}$ at a finite distance R. By Υ^R we denote the boundary of truncation, $\Upsilon^R = \partial\mathcal{E}^R \setminus \partial\mathcal{E}$. Let us also set $\Upsilon^{\pm,R} = \{(y,t) \in \Upsilon^{\pm} : t < R\}$. With the aim of approximating v^T by a solution $v^{T,R}$ to some problem in the bounded domain $\mathcal{E}^R$, we introduce the problem

$$\big(\Delta + k^2 + q\big)v^{T,R} = \mathcal{F} \text{ in } \mathcal{E}^T, \tag{14}$$

$$\Big(\partial_y^2 + e^{2i\phi}\partial_t^2 + q\big(y, T + e^{i\phi}(t-T)\big) + k^2\Big)v^{T,R}(y,t) = 0,\ (y,t) \in \mathcal{E}^R \setminus \overline{\mathcal{E}^T}, \tag{15}$$

$$\partial_y^j v^{T,R}|_{\Upsilon^{+,R}} = e^{2\pi i\alpha}\partial_y^j v^{T,R}|_{\Upsilon^{-,R}},\ \ j = 0, 1, \tag{16}$$

$$v^{T,R} = 0 \text{ (or } \partial_\nu v^{T,R} = 0) \ \ \textit{on } \Upsilon^0, \tag{17}$$

$$\partial_t^j v^{T,R}(y, T-) = e^{i\phi j}\partial_t^j v^{T,R}(y, T+),\ j = 0, 1, \tag{18}$$

$$v^{T,R} = 0 \text{ (or } \partial_\nu v^{T,R} = 0) \ \ \textit{on } \Upsilon^R, \tag{19}$$

where as artifitial boundary conditions on Υ^R we take Dirichlet (or Neumann) boundary conditions. The equation (15) describes a PML of the finite length $R - T$.

Theorem 3. *Let the assumptions of Theorem 2 be fulfilled. There exists $R_0 > T$ such that for all $R > R_0$ the problem (14-19) admits a unique solution $v^{T,R} \in H^1(\mathcal{E}^R)$. This solution $v^{T,R}$ converges to the solution $v^T \in H^1(\mathcal{E})$ of the problem (7–11) in the sence that*

$$\|v^{T,R} - v^T; H^1(\mathcal{E}^R)\| \le Ce^{-\gamma(R-T)},\ R > R_0, \tag{20}$$

where $0 < \gamma < \min_n\{\Im(e^{i\phi}\lambda_n^-)\}$.

Corollary 4. *From (20) it follows the estimate*

$$\|u^T - v^{T,R}; H^1(\mathcal{E}^L)\| \le Ce^{-\gamma(R-T)} \tag{21}$$

for the error of approximation of a solution u^T to the problem (1–3) with radiation conditions (12) by a solution $v^{T,R}$ to the problem (14–19) with PML.

This shows that under a rather weak assumptions on the potential the PML method is exponentially convergent, it gives a close approximation of a solution u^T to the original problem (1–3) with radiation conditions (12). Some more restrictive assumptions on the potential q allow us to rewrite the radiation conditions (12) in the well known form (13).

Acknowledgment.

This work was funded by grant number 108898 awarded by the Academy of Finland.

References

[1] J.P. Bérenger, "A perfectly matched layer for the absorption of electromagnetic waves", J. Comp. Phys., vol. 114, pp. 185–200, 1994.

[2] M. Lassas, E. Somersalo, "Analysis of the PML equations in general convex geometry", Proc. Roy. Soc. Edinburgh Sect. A, vol. 131, pp. 1183–1207, 2001.

[3] T. Hohage, F. Schmidt, L. Zschiedrich, "Solving time-harmonic scattering problems based on the pole condition II. Convergence of the PML method", SIAM J. Math. Anal., vol. 35 pp. 547–560, 2003.

[4] E. Becache, A.-S. Bonnet-Ben Dhia, G. Legendre, "Perfectly matched layers for the convected Helmholtz equation", SIAM J. Numer. Anal., vol. 42, pp. 409–433, 2004

[5] E. Becache, A.-S. Bonnet-Ben Dhia, G. Legendre, "Perfectly matched layers for time-harmonic acoustics in the presence of a uniform flow", SIAM J. Numer. Anal., vol. 44, pp. 1191–1217, 2006.

[6] V. Maz'ya, B. Plamenevskii, "Estimates in L_p and Hölder classes and the Miranda-Agmon maximum principle for solutions of elliptic boundary value problems in domains with singular points on the boundary", Amer. Math. Soc. Trans., vol. 123, pp. 1–56, 1984.

ONE-WAY MODEL-NESTING USING HIGH-ORDER ABSORBING BOUNDARY CONDITIONS

Assaf Mar - Or[†], **Dan Givoli**[‡,*]
[†]Inter-Departmental program for Applied Mathematics, Technion – Israel Institute of Technology, Haifa 3200, Israel.
[‡]Department of Aerospace Engineering, Technion – Israel Institute of Technology, Haifa 3200, Israel
[*]Email: givolid@technion.ac.il

Abstract

The problem of global-regional model interaction (sometimes referred to in the literature as "model nesting") is considered. Following the introduction, Carpenter's lateral boundary scheme [1] and its relation to Sommerfeld's absorbing boundary condition is presented and analyzed in the context of the scalar wave equation. Carpenter's boundary scheme is then compared with other possible boundary conditions and is shown to yield better results. In the third part, the shortcomings of Carpenter's lateral boundary scheme are demonstrated in the case of a two dimensional model problem and a new lateral boundary scheme, which is based on the Hagstrom-Warburton (H-W) family of high-order absorbing boundary conditions [2], is presented. This lateral boundary scheme is then extended further and investigated using a two-dimensional model problem with wave-guide geometry.

1 Introduction

The use of artificial boundaries to enclose a region of interest in a much larger, or unbounded, domain is a common practice. It is well known in the context of wave problems that if one is not careful, waves that impinge on an artificial boundary from within the computational domain may give rise to spurious reflections that might pollute the numerical solution inside the region. Most of the problems discussed in the literature are concerned with the development and use of Absorbing Boundary Conditions (ABCs), which eliminate or significantly reduce the spurious reflections from the boundary of the computational domain (see, for example, the reviews in [3], [4], [5] and references therein). In Numerical Weather Prediction (NWP), for example, a commonly used ABC is the one developed by Orlanski [6].

In this talk, however, a somewhat different setup is considered. This setup, which is sometimes called 'nesting,' arises in NWP as well as in other fields involving waves in very large domains [7]. In this setup (an illustration of which is shown in Fig. 1), one distinguishes between a Global Model (GM), in which the atmospheric equations are solved over the entire spherical surface of the globe, occupying the domain Ω_G, and a regional or Limited-Area Model (LAM), in which the solution is sought in a relatively small region Ω_L bounded by an artificial boundary Γ_{E}. The GM captures the large-scale atmospheric phenomena and is based on a coarse grid (about 100km resolution), whereas the LAM captures the mesoscale phenomena and is based on a finer grid (typically 10-20km resolution). The common practice, which is referred to as "one-way nesting", is first to solve the global problem (via the GM) by a certain numerical method, and then to solve the regional problem (via the LAM), usually using an entirely different numerical method while taking into account the relevant GM results. The question that arises in this context is how to incorporate the GM data into the LAM model. In constructing such a method two conflicting requirements have to be addressed – waves originating from within the LAM domain, Ω_L, should be allowed to depart it with minimal reflections (this requirement implies the use of an ABC of some sort) but also waves originating from outside the LAM domain would be allowed to enter it with minimal distortion (which calls for the use of the global data for the incoming waves).

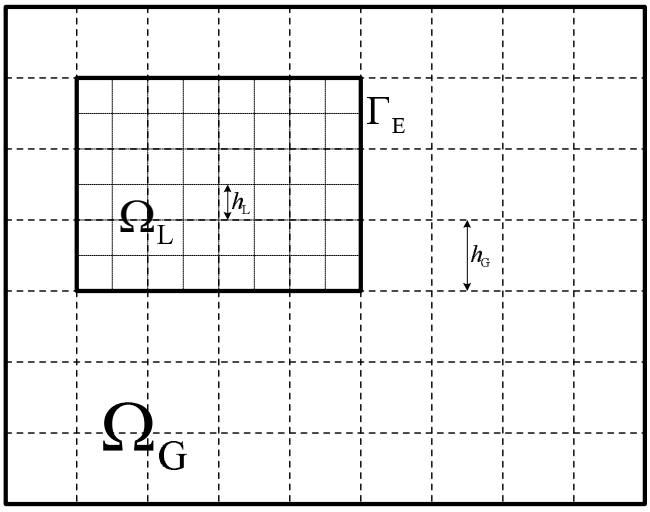

Figure 1: A typical setup for the GM-LAM nesting problem

2 Carpenter's boundary scheme for the scalar wave equation

Consider the following wave equation in Ω:

$$\partial_t^2 u - c^2 \nabla^2 u = 0 \quad \text{in } \Omega,\ t > 0, \tag{1}$$

where $c > 0$ is the constant wave speed in the domain. In 1982, Carpenter [1] proposed a simple open boundary condition to be used on the boundary Γ of a LAM, which extends the Sommerfeld-like ABC (see [4])

$$\mathcal{S}u \equiv \partial_t u + c\partial_n u = 0 \quad \text{on } \Gamma. \tag{2}$$

Whereas Sommerfled's ABC handles only outgoing waves, the Carpenter condition is supposed to absorb waves outgoing from the LAM while at the same time admitting incoming waves generated by the GM.

Following is a derivation of the Carpenter scheme. The solution of the GM is assumed to be known, and is denoted u_G. The solution of the LAM is sought, and is denoted u_L. Carpenter writes both solutions as sums of incoming and outgoing waves on Γ, at all times:

$$u_G = u_G^{\text{in}} + u_G^{\text{out}} \quad \text{on } \Gamma \tag{3}$$
$$u_L = u_L^{\text{in}} + u_L^{\text{out}} \quad \text{on } \Gamma. \tag{4}$$

The following assumptions are made. First, it is assumed that the incoming components of the GM and LAM solutions agree on Γ:

$$u_L^{\text{in}} = u_G^{\text{in}} \quad \text{on } \Gamma \tag{5}$$

Second, it is assumed that the outgoing components of both the GM and LAM solutions satisfy the Sommerfeld-like condition (2) on Γ:

$$\partial_t u_L^{\text{out}} + c\partial_n u_L^{\text{out}} = 0 \quad \text{on } \Gamma \tag{6}$$
$$\partial_t u_G^{\text{out}} + c\partial_n u_G^{\text{out}} = 0 \quad \text{on } \Gamma. \tag{7}$$

It should be noted that the Sommerfeld-like condition $\mathcal{S}u = 0$ perfectly absorbs outgoing waves only in one dimension. In higher dimensions this ABC is approximate, and is in fact quite crude. From (3)–(7) one finally obtains after simple algebra

$$(\partial_t + c\partial_n)\, u_L = (\partial_t + c\partial_n)\, u_G \qquad \text{on } \Gamma \tag{8}$$

This is the Carpenter lateral boundary condition. Using the notation $\mathcal{S}$ for the Sommerfeld operator defined in (2), (8) can written as

$$\mathcal{S}u_L = \mathcal{S}u_G \qquad \text{on } \Gamma. \tag{9}$$

The performance of Carpenter's lateral boundary scheme will be analyzed and studied for incoming and outgoing waves using a one-dimensional model problem (for which an analytical solution can be found). Particular attention will be paid to the influence of errors (both in the prescribed GM data and in the LAM itself) on the resulting computation of the LAM solution (see [8] for further details).

3 The H-W/Carpenter lateral boundary scheme

Whereas Carpenter's lateral boundary scheme is based on Sommerfeld's ABC, it is possible, building on (9), to construct other boundary schemes using high-order ABCs. This course is pursued since Sommerfeld's ABC, while being exact for the one-dimensional non-dispersive wave equation, performs poorly in multi-dimensional situations. For this purpose, the Hagstrom-Warburton (H-W) family of high-order ABCs [2] will be used. Following the description of the H-W boundary conditions and their basic properties, the corresponding H-W/Carpenter lateral boundary scheme is derived and analyzed.

3.1 The Hagstrom-Warburton (H-W) family of high-order ABCs

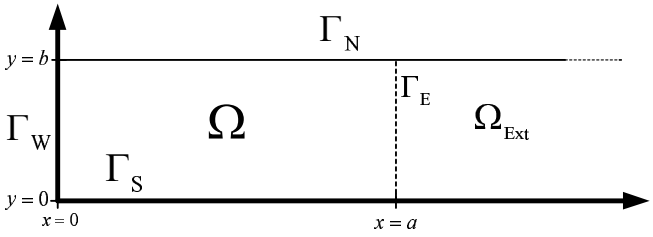

Figure 2: A two-dimensional wave-guide set-up

Consider the following wave problem defined in a two-dimensional waveguide domain, $\Omega_{\text{WG}} = [0, \infty] \times [0, b]$, as shown in Fig. 2. Along the domain's boundary a non-homogeneous Dirichlet boundary condition is imposed on Γ_{W} and an homogeneous Neumann boundary condition is imposed on Γ_{S} and Γ_{N}.

$$\partial_t^2 u - c^2 \nabla^2 u = 0 \quad \text{in } \Omega_{\text{WG}},\ t > 0 \tag{10}$$
$$u = g \quad \text{On } \Gamma_{\text{W}} \tag{11}$$
$$\partial_n u = 0 \qquad \text{On } \Gamma_{\text{S}}, \Gamma_{\text{N}} \tag{12}$$
$$u(\mathbf{x}, 0) = u_0(\mathbf{x}) \quad \text{in } \Omega_{\text{WG}} \tag{13}$$
$$\partial_t u(\mathbf{x}, 0) = v_0(\mathbf{x}) \quad \text{in } \Omega_{\text{WG}} \tag{14}$$

where c is the wave speed, g the Dirichlet data on Γ_{W} and u_0, v_0 the initial displacement and velocity. In or-

der to solve the problem numerically, an artificial boundary, $\Gamma_{\rm E}$, is introduced, dividing $\Omega_{\rm WG}$ into a finite domain, $\Omega = [0,a] \times [0,b]$ (it is assumed that the both u_0 and v_0 vanish outside Ω) and an external domain, $\Omega_{\rm Ext} = [a,\infty) \times [0,b]$. Using a set of auxiliary functions, $\varphi^{(j)},\ j = 1 \ldots P$, defined on $\Omega_{\rm Ext}$, a set of recurrence relations for the auxiliary functions, (15)-(17), is imposed on $\Gamma_{\rm E}$.

$$(a_0\partial_t + c\partial_n)u = \partial_t\varphi^{(1)} \tag{15}$$

$$(a_j\partial_t + c\partial_n)\varphi^{(j)} = (a_j\partial_t - c\partial_n)\varphi^{(j+1)}\ j = 1..P \tag{16}$$

$$\varphi^{(P+1)} = 0. \tag{17}$$

Where $0 < a_j \leq 1$, $j = 0 \ldots P$, are some given constants. From (15)-(17) it follows (see [2]) that the auxiliary functions, $\varphi^{(j)}$, satisfy the following wave problem in the external domain, $\Omega_{\rm Ext}$:

$$\partial_t^2\varphi^{(j)} - c^2\nabla^2\varphi^{(j)} = 0 \qquad \text{in } \Omega_{\rm Ext} \tag{18}$$

$$\partial_n\varphi^{(j)} = 0 \quad \text{On } \Gamma_{\rm S}, \Gamma_{\rm N} \tag{19}$$

$$\varphi^{(j)}(x,y,0) = \partial_t\varphi^{(j)}(x,y,0) = 0. \tag{20}$$

Using the process detailed in [2] it is possible to derive a set of P second-order equations for the auxiliary functions, involving only derivatives w.r.t. t and y, which is equivalent to the recursive first-order set, (15)–(17). This set can be written in matrix form as:

$$\mathbf{L}\partial_t^2\mathbf{\Phi} - \mathbf{M}\partial_y^2\mathbf{\Phi} = \mathbf{F}, \tag{21}$$

where $\mathbf{L}$ and $\mathbf{M}$ are two $P \times P$ real matrices (whose entries are known), $\mathbf{\Phi} = \{\varphi^{(1)}, \ldots, \varphi^{(P)}\}^{\rm T}$, and $\mathbf{F}$ is a vector whose only nonzero entry is the first one, which depends on u and its derivatives. The Hagstrom-Warbutron (H-W) ABC comprises, then, the system (21) and (15).

3.2 The H-W/Carpenter lateral boundary scheme

If we examine the last $(P-1)$ equations of (21), which define an under-determined system of $(P-1)$ equations in P unknowns, it is possible to express $\varphi^{(1)}$, or, better yet, $-\partial_t\varphi^{(1)}$, in terms of the remaining $P-1$ auxiliary functions:

$$-\partial_t\varphi^{(1)}(y,t) = \mathcal{F}\Big(\varphi^{(2)}, \ldots, \varphi^{(P)}\Big)(y,t). \tag{22}$$

Since, according to (21), all the auxiliary functions depend only on u, (22) could be written, in fact, as:

$$-\partial_t\varphi^{(1)}(y,t) \equiv \mathcal{M}_P[u] \tag{23}$$

where $\mathcal{M}_P$ is some operator, which will not be calculated explicitly. Using this expression for $\partial_t\varphi^{(1)}$, it is possible to write the H-W ABC in operator form:

$$\mathcal{S}_{\text{H-W}}[u] \equiv [a_0\partial_t + c\partial_n + \mathcal{M}_P]\,u = 0 \tag{24}$$

Note that if $a_0 = 1$, then the first two terms in (24) are, in fact, Sommerfeld's operator, (2). Using this form of the H-W boundary operator enables it to be used, in (9) instead of Sommerfeld's operator, thus producing the H-W/Carpenter lateral boundary scheme which will be analyzed for several problems.

References

[1] K. M. Carpenter, "Note on 'Radiation Conditions for Lateral Boundaries of Limited-Area Models' by M. J. Miller and A. J. Thorpe", Quart. J. R. Met. Soc., vol. 108, 717–719, 1982.

[2] T. Hagstrom, T. Warburton, "A new auxiliary variable formulation of high-order local radiation boundary conditions: corner compatibility conditions and extensions to first-order system", Wave Motion, vol. 39, 327–338, 2004.

[3] S.V. Tsynkov, "Numerical Solution of Problems on Unbounded Domains, A Review", Appl. Numer. Math., vol. 27, 465–532, 1998.

[4] D. Givoli, Numerical Methods for Problems in Infinite Domains, Elsevier, Amsterdam, 1992.

[5] T. Hagstrom, "Radiation Boundary Conditions for the Numerical Simulation of Waves", Acta Numerica, vol. 8, 47–106, 1999.

[6] I. Orlanski, "A Simple Boundary Condition for Unbounded Hyperbolic Flows", J. Comp. Phys., vol. 21, 251–269, 1976.

[7] R. D. Durran, Numerical Methods for Wave Equations in Geophysical Fluid Dynamic, Springer, New-York, 1998.

[8] A. Mar - Or, D. Givoli, "The Global-Regional Model Interaction Problem: Analysis of Carpenter's Scheme and Related Issues", Int. J. for Multiscale Comp. Engng., vol. 4(5-6), 617–645, 2006.

Local Absorbing Boundary Conditions for Elliptical Shaped Boundaries

M. Medvinsky and E. Turkel*
School of Mathematical Sciences, Tel-Aviv University, Tel-Aviv, Israel
***Email: turkel@post.tau.ac.il**

Abstract

We compare several local absorbing boundary conditions for solving the Helmholtz equation exterior to an ellipse. We also introduce a new boundary condition based on a modal expansion.

Introduction

When computing wave scattering about a body either in the time domain or the frequency domain one needs to truncate the unbounded domain and introduce an artificial surface with a boundary condition to prevent reflections of outgoing waves into the domain. We consider local absorbing boundary conditions (ABC) that link only nearby neighbors of a boundary point. We shall consider the Helmholtz equation in frequency space. Bayliss and Turkel [2] and later Gunzburger (BGT) [3] constructed a sequence of absorbing boundary conditions, for the wave equation, based on matching terms in the series based on the inverse radius $\frac{1}{R}$. Since the condition is written in polar coordinates it is most convenient when the outer surface is a circle or sphere. The most popular is BGT-2 which contains a first order normal derivative and a second order tangential derivative and can be easily implemented in both finite differences and linear finite elements. Preferably the outer artificial surface should have a shape reasonably close to the scatterer. Many attempts have been made to generalize BGT to more general shapes. The series developed where either in some generalized radius, or the inverse wave number or else a modal expansion and also an approximation to the DtN method. Remarkably, all these approaches reduced to the BGT condition for a circle or sphere, at least through second order. However, they differ in the boundary condition constructed for other outer shapes. We consider scattering about an ellipse for which the exact solution is known. We compare several approaches both for an On Surface Radiation Condition (OSRC) and as the outer boundary condition for a finite difference approximation in elliptical coordinates. The boundary conditions we compare are those of Reiner et.al [8], Kriegsmann et.al [6], Jones et.al [4], Kallivokas et.al [5] and Antoine et.al [1].

The BGT condition was developed from a series in $\frac{1}{R}$. For scattering about a circle an alternative is to use a modal expansion in Hankel functions [7]. For ka large this gives results similar to the BGT approach. However, for small wavenumbers it is significantly better [9]. For scattering about an ellipse we consider a modal expansion in Mathieu functions. The resultant ABC has the same structure as before but the coefficients involve Mathieu functions. We compare this new ABC for an outer ellipse with the other boundary conditions.

New Absorbing Boundary Condition

Assume an expansion in arbitrary functions [7]

$$w = \alpha_0\psi_0(k\xi) + \alpha_1\psi_1(k\xi) \tag{1a}$$

$$\frac{\partial w}{\partial \xi} = k\alpha_0\psi_0'(k\xi) + k\alpha_1\psi_1'(k\xi) \tag{1b}$$

$$\frac{\partial^2 w}{\partial \xi^2} = k^2\alpha_0\psi_0''(k\xi) + k^2\alpha_1\psi_1''(k\xi) \tag{1c}$$

Solving for α_0 and α_1 from the first two equations we get

$$\alpha_0 = \frac{k\psi_1' w - \psi_1 \frac{\partial w}{\partial \xi}}{k\left(\psi_0\psi_1' - \psi_0'\psi_1\right)}$$

$$\alpha_1 = -\frac{k\psi_0' w - \psi_0 \frac{\partial w}{\partial \xi}}{k\left(\psi_0\psi_1' - \psi_0'\psi_1\right)}$$

substituting in (1c)

$$\frac{\partial^2 w}{\partial \xi^2} + k\frac{(\psi_1\psi_0'' - \psi_0\psi_1'')}{\psi_0\psi_1' - \psi_0'\psi_1}\frac{\partial w}{\partial \xi} + k^2\frac{(-\psi_1'\psi_0'' + \psi_0'\psi_1'')}{\psi_0\psi_1' - \psi_0'\psi_1}w = 0$$

Introduce elliptical coordinates

$$x = f\cosh(u)\cos(v) \qquad y = f\sinh(u)\sin(v)$$
$$\xi = \cosh(u) \qquad \eta = cos(v)$$

The Helmholtz equation is given by

$$\frac{\partial^2 w}{\partial u^2} + \frac{\partial^2 w}{\partial v^2} + \frac{k^2 f^2}{2}(\cosh(2u) - \cos(2v))w = 0 \tag{2}$$

Assume $w = F(u)G(v)$. Then

$$\frac{d^2F}{du^2} + \left(\frac{k^2 f^2}{2}\cosh(2u) - a\right)F = 0$$

$$q = \frac{f^2k^2}{4} = \frac{k^2}{4}\left(A^2 - B^2\right) \tag{3}$$

"a" is separation constant determined so $G(v)$ is periodic which leads to either even or odd solutions with eigenvalues $a_r(q)$ for r even. Choose $\psi_j \quad j=1,2$ as the first two even Mathieu-Hankel functions, M_0, M_1 with the corresponding characteristic values a_0, a_1. Define

$$\frac{-D}{M_0 M_1} = \frac{M_0}{M_0'} - \frac{M_1}{M_1'}$$

Then we get

$$\frac{\partial^2 w}{\partial u^2} - \frac{(a_1 - a_0)\, M_0 M_1}{D} \frac{\partial w}{\partial u} - \left(a_0 - 2q\cosh(2u) - \frac{(a_1 - a_0)\, M_0' M_1}{D} \right) w = 0 \tag{4}$$

We use the Helmholtz equation to eliminate $\frac{\partial^2 w}{\partial \xi^2}$ in terms of $\frac{\partial^2 w}{\partial \eta^2}$. Subtracting (2) from (4) we get

$$(a_1 - a_0)\frac{\partial w}{\partial u} = \frac{-D}{M_0 M_1}\frac{\partial^2 w}{\partial v^2} + \left(\frac{-D}{M_0 M_1}(a_0 - 2q\cos(2v)) + \frac{(a_1 - a_0)\, M_0'}{M_0} \right) w \tag{5}$$

Results

We first consider several boundary conditions imposed directly on the scattering ellipse (OSRC). The physical boundary condition is a Dirichlet condition for the scattered wave. The ABC then gives the normal derivative on the scatterer which we compare to the exact one. In all cases the angle of the incident plane wave is 0, the major axis is 1 and we vary the minor axis. In figure 1 we compare several methods with the exact solution for $k=1$ and an aspect ratio of 2. The error between the approximate OSRC solutions and the exact normal derivative is given in the legend. In figure 2 we consider $k = 1$ but aspect ratio 5. In figure 3 we consider the aspect ratio of 2 but with $k = 5$. In all cases the solution at 180° (i.e. behind the ellipse in the shadow region) is quite poor. For $k=1$ the ABC of Reiner et.al works best among the standard ABCs. For higher k the various methods get closer though now Kriegsmann et.al followed by Reiner et.al are the best. However, it is clear that the new method based on Mathieu functions is far superior especially for low and intermediate frequencies.

We next consider the same problem but exterior to the ellipse and solved with a finite difference method. The scatterer and outer artificial surface are concentric ellipses with semi-major axis 1 for the scatterer and approximately 1.5 for the outer surface. We consider the same three cases as with the OSRC. The new ABC based on a modal expansion in Mathieu functions, (5) is again the best. For an ABC based on expansions the ABC of Jones et.al is next best. For higher wavenumbers most of the boundary conditions yield similar accuracy and the easiest to implement is that of Kriegsmann et.al.

The new modal based boundary condition (5) is superior to the those based on expansions both as an OSRC and as an ABC. It remains accurate for low frequencies and high angles of attack (not shown).

References

[1] X. Antoine, H. Barucq and A. Bendali, *Bayliss-Turkel like Radiation Conditions on Surfaces of Arbitrary Shape*, J. Math. Anal. Appl. 229, 184-211, 1999.

[2] A. Bayliss and E. Turkel, *Radiation Boundary Conditions for Wave-Like Equations*, Comm. Pure Appl. Math. 33, 707-725, 1980.

[3] A. Bayliss, M. Gunzburger and E. Turkel, *Boundary Conditions for the Numerical Solution of Elliptic Equations in Exterior Regions*, Siam J. Appl. Math. 42, 430-45l, 1982.

[4] D.S. Jones and G.A. Kriegsmann, *Note on Surface Radiation Conditions*, Siam J. Appl. Math. 50, 559-568, 1990.

[5] L.F. Kallivokas and S. Lee, *Local Absorbing Boundaries of Elliptical Shape for Scalar Waves*, Comput. Meth. Appl. Mech. Engng. 193, 4979-5015, 2004.

[6] G.A. Kriegsmann, A. Taflove and K.R. Umashankar, *A New Formulation of Electromagnetic Scattering Using on Surface Radiation Condition Approach*, IEEE Trans. Ant. Prop. AP35, 153-161, 1987.

[7] Y. Li and Z.J. Cendes, *Modal Expansion Absorbing Boundary Conditions for Two-Dimensional Electromagnetic Scattering*, IEEE Trans. Magnetics 29, 1835-1838, 1993.

[8] R.C. Reiner, R. Djellouli and I. Harari, *The Performance of Local Absorbing Boundary Conditions For Acoustic Scattering from Elliptical Shapes*, Comput. Methods Appl. Mech. Engng. 195, 3622-3665, 2006.

[9] E. Turkel, C. Farhat and U. Hetmaniuk, *Improved Accuracy for the Helmholtz Equation in Unbounded Domains*, IJNME 59:1963-1988, 2004.

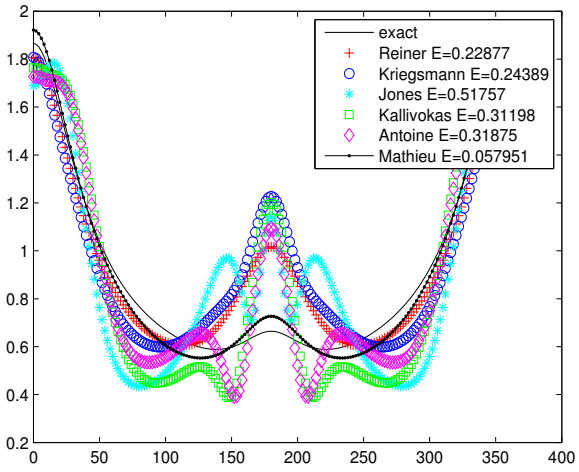

Figure 1: OSRC, $k=1$, AR=2

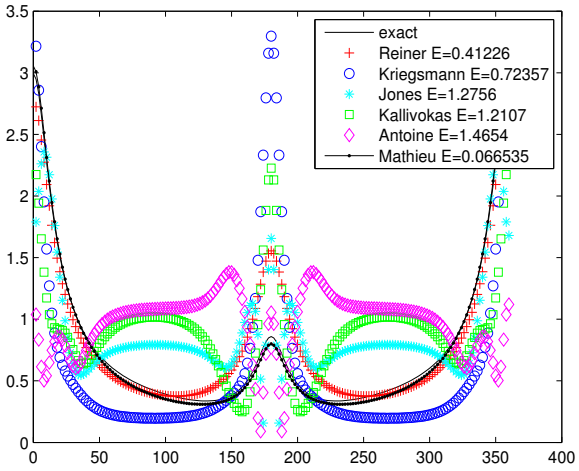

Figure 2: OSRC, $k=1$, AR=5

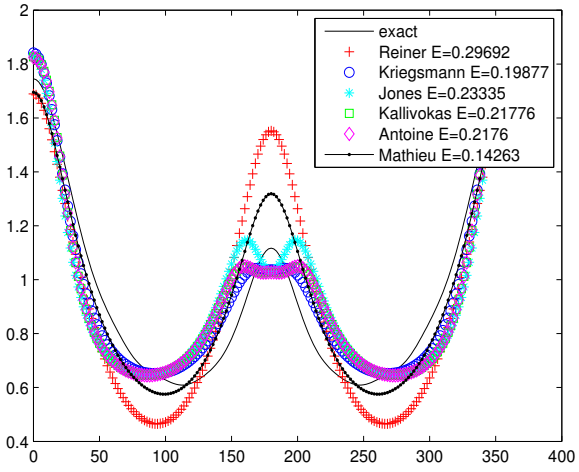

Figure 3: OSRC, $k=4$, AR=2

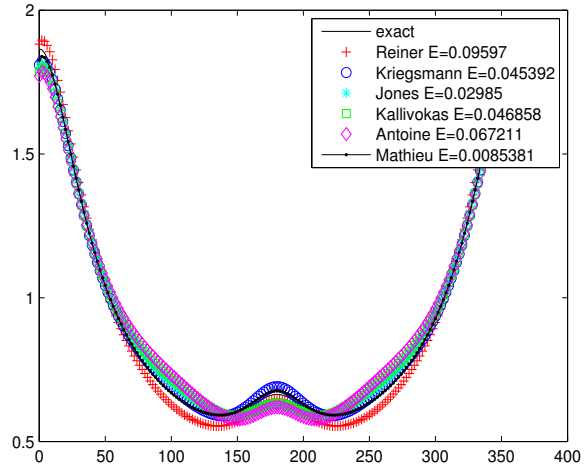

Figure 4: FD, $k=1$, AR=2

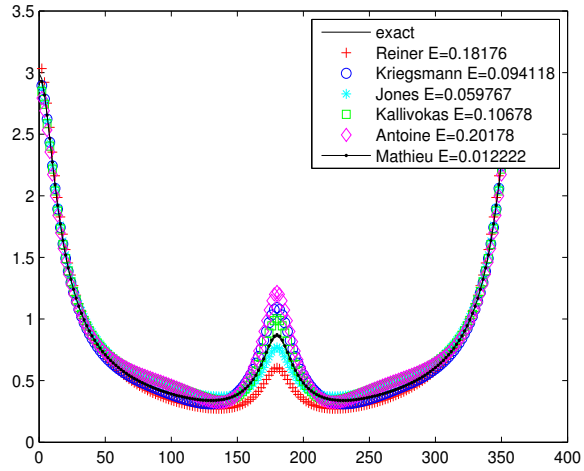

Figure 5: FD, $k=1$, AR=5

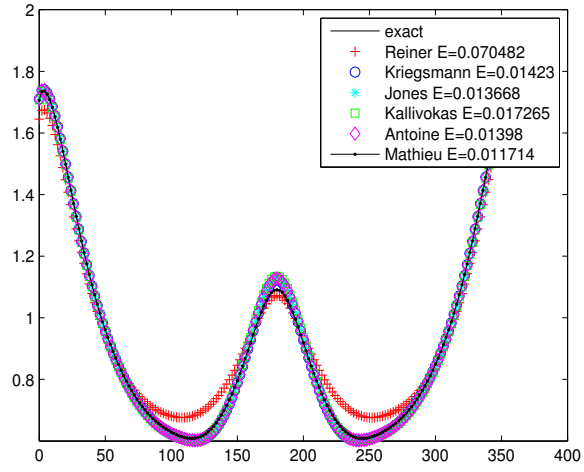

Figure 6: FD, $k=4$, AR=2

LACUNAE BASED STABILIZATION OF PMLs

H. Qasimov[†] and S. Tsynkov[†,*]

[†]Department of Mathematics, North Carolina State University, Box 8205, Raleigh, NC 27695, USA
[*]Email: tsynkov@math.ncsu.edu

Abstract

Perfectly matched layers (PMLs) are used for the numerical solution of wave propagation problems on unbounded regions. They surround the finite computational domain (obtained by truncation) and are designed to attenuate and completely absorb all the outgoing waves while producing no reflections from the interface between the domain and the layer. PMLs have demonstrated excellent performance for many applications. However, they have also been found prone to long-time instabilities. Hereafter, we propose a modification that stabilizes any PML applied to a hyperbolic partial differential equation/system that satisfies the Huygens' principle. The modification makes use of the presence of lacunae and allows us to rigorously prove a temporally uniform error bound for arbitrarily long time intervals.

Introduction

Numerical solution of infinite-domain problems requires truncation of the unbounded domain for the purpose of constructing a finite-dimensional discretization. Then, one needs to set some artificial boundary conditions (ABCs) at the outer boundary of the computational domain. They should provide a closure for the truncated formulation and guarantee that its solution will not differ much from the corresponding fragment of the original infinite-domain solution (ideally, will coincide with it).

For the problems of propagation of electromagnetic waves, a very efficient closure mechanism was introduced by Bérenger [1], [2]. He proposed to surround the computational domain by a layer of artificial material capable of rapidly damping all the outgoing waves while generating no reflections from the interface between the domain and the layer. It was called a perfectly matched layer (PML). The PML capabilities were attained in work [1], [2] by splitting the field components, i.e., introducing additional unknowns and equations in the layer, and then using the resulting extra degrees of freedom for the development of an efficient waves' attenuation strategy.

It has also been noticed [3], however, that the Bérenger's split transforms the strongly hyperbolic (symmetric) Maxwell's equations into a weakly hyperbolic system, which, in turn, implies transition from strong well-posedness to weak well-posedness of the Cauchy problem. A weakly well-posed system can become ill-posed under a low order perturbation, and an example of such a perturbation for the Bérenger's equations was given in [3]. Even though it has later been shown [4] that the actual form of the Bérenger's system does not lead to ill-posedness, the system still remains only weakly well-posed, and a linear growth of the split field components inside the PML is possible. This behavior may lead to an instability of the discretization, and it has indeed been demonstrated in [3] for the very popular Yee scheme.

In spite of the excellent performance of PML [1], [2] in many applications, concerns about its stability have prompted development of other types of PMLs [5], [6], [7]. These alternative strategies do not require splitting of the field components, although they still introduce additional unknowns inside the layer. Later, however, the unsplit PMLs have also been found susceptible to gradually developing instabilities [8]. A remedy has been proposed in [8] for unsplit PMLs based on changing the governing equations in the layer. It has been experimentally shown to work well, but theoretically it is unclear whether the modified layer remains perfectly matched and absorbing.

Lacunae-based methods for the numerical integration of hyperbolic equations and systems have been developed quite independently. They apply to the equations that satisfy the Huygens' principle [9] and guarantee a temporally uniform grid convergence for any consistent and stable scheme applied to the problem of radiation of waves by a known source [10]. The basic idea of lacunae-based methods is that once the domain of interest falls completely into the lacuna of the solution [11], the integration does not need to be continued any further. The presence of the lacunae can also be efficiently exploited for the construction of exact ABCs for various wave propagation problems [12], [13], [14]. These ABCs have only a fixed and limited extent of temporal nonlocality.

In this paper, we use the idea of lacunae-based integration for stabilizing the PMLs. Our key result, Theorem 1, says that for a finite computational domain lacunae-based integration guarantees that the PML-induced errors will remain uniformly bounded for all times.

Work supported by the US AFOSR, Grant No. FA9550-04-1-0118.

Main Theorem

Consider a Cauchy problem:

$$\begin{aligned} \frac{\partial \boldsymbol{w}}{\partial t} + \boldsymbol{L}\boldsymbol{w} = \boldsymbol{f}(\boldsymbol{x},t), \quad \boldsymbol{x} \in \mathbb{R}^3, \quad t > 0, \\ \boldsymbol{w}(\boldsymbol{x},0) = \boldsymbol{\varphi}(\boldsymbol{x}), \quad \boldsymbol{x} \in \mathbb{R}^3, \end{aligned} \tag{1}$$

where the operator $\boldsymbol{L}$ is linear, $\mathrm{supp}\boldsymbol{f} \subseteq \Omega \times [0,+\infty)$ & $\mathrm{supp}\boldsymbol{\varphi} \subseteq \Omega$, and $\Omega \subset \mathbb{R}^3$ is bounded. We require that the operator $\partial/\partial t + \boldsymbol{L}$ of (1) satisfies the Huygens' principle. Mathematically, this means that the waves due to a compactly supported source (in space-time) have sharp aft fronts. In other words, at any fixed location of the observer these waves come and pass, and the solution becomes identically zero after a finite time. This time is no greater than the maximum distance between the observer and the source divided by the wave propagation speed c.

Let $\mathrm{diam}\Omega = d$, denote by $T = d/c$ the characteristic time, which is required for the waves to cross the domain Ω, and let $T_1 > 0$. We partition the RHS $\boldsymbol{f}(\boldsymbol{x},t)$ of (1):

$$\begin{aligned} \boldsymbol{f}(\boldsymbol{x},t) &= \sum_{m=0}^{\infty} \boldsymbol{f}_m(\boldsymbol{x},t), \\ \boldsymbol{f}_m(\boldsymbol{x},t) &= \begin{cases} \boldsymbol{f}(\boldsymbol{x},t), & t_m \le t < t_{m+1}, \\ \boldsymbol{0}, & \text{otherwise}, \end{cases} \end{aligned} \tag{2}$$

where $t_m = mT_1$, and consider the Cauchy problems:

$$\begin{aligned} \frac{\partial \boldsymbol{w}_m}{\partial t} + \boldsymbol{L}\boldsymbol{w}_m = \boldsymbol{f}_m(\boldsymbol{x},t), \quad \boldsymbol{x} \in \mathbb{R}^3, \quad t > t_m, \\ \boldsymbol{w}_m(\boldsymbol{x},t_m) = \begin{cases} \boldsymbol{\varphi}, & m = 0, \\ \boldsymbol{0}, & m > 0, \end{cases} \quad \boldsymbol{x} \in \mathbb{R}^3. \end{aligned} \tag{3}$$

Each problem (3) is Huygens', and hence its solution $\boldsymbol{w}_m(\boldsymbol{x},t)$ becomes zero on Ω after the time $T_1 + T$ elapses, i.e., for $t \ge t_m + T_1 + T$. Therefore,

$$\boldsymbol{w}(\boldsymbol{x},t) = \sum_{m=M_0}^{M} \boldsymbol{w}_m(\boldsymbol{x},t), \quad \boldsymbol{x} \in \Omega, \quad t \ge 0, \tag{4}$$

where $M_0 \stackrel{\text{def}}{=} [(t-T)/T_1]$, $M \stackrel{\text{def}}{=} \lceil t/T_1 \rceil - 1$, $[\alpha]$ is the integer part, and $\lceil \alpha \rceil$ is the smallest integer $\ge \alpha$. As such, formula (4) represents the solution $\boldsymbol{w}(\boldsymbol{x},t)$ of problem (1) as *the sum of a finite non-increasing number of components $\boldsymbol{w}_m(\boldsymbol{x},t)$ that each has a finite non-increasing "lifespan" $T_1 + T$ on Ω* (until Ω falls into the lacuna).

In reality we are not solving problem (1) directly. Instead, we are solving a combined formulation that involves the PML outside Ω:

$$\begin{aligned} \frac{\partial \boldsymbol{w}^{(\Omega)}}{\partial t} + \boldsymbol{L}\boldsymbol{w}^{(\Omega)} = \boldsymbol{f}(\boldsymbol{x},t), \quad \boldsymbol{x} \in \Omega, \quad t > 0, \\ \boldsymbol{w}^{(\Omega)}(\boldsymbol{x},0) = \boldsymbol{\varphi}, \quad \boldsymbol{x} \in \Omega, \end{aligned} \tag{5a}$$

$$\begin{aligned} \frac{\partial \boldsymbol{w}^{(\mathrm{PML})}}{\partial t} + \boldsymbol{L}^{(\mathrm{PML})}\boldsymbol{w}^{(\mathrm{PML})} = \boldsymbol{0}, \ \boldsymbol{x} \in \mathrm{PML}, \ t > 0, \\ \boldsymbol{w}^{(\mathrm{PML})}(\boldsymbol{x},0) = \boldsymbol{0}, \ \boldsymbol{x} \in \mathrm{PML}, \end{aligned} \tag{5b}$$

A PML is designed to guarantee that

$$\boldsymbol{w}^{(\Omega)}(\boldsymbol{x},t) \equiv \boldsymbol{w}(\boldsymbol{x},t), \quad \boldsymbol{x} \in \Omega, \quad t \ge 0. \tag{6}$$

In reality, however, a PML can amplify small perturbations $\boldsymbol{\xi}$ of the initial data:

$$\|\tilde{\boldsymbol{w}}^{(\Omega)}(\,\cdot\,,t) - \boldsymbol{w}^{(\Omega)}(\,\cdot\,,t)\| \le \mu(t)\|\boldsymbol{\xi}\|', \tag{7a}$$

$$\|\tilde{\boldsymbol{w}}^{(\mathrm{PML})}(\,\cdot\,,t) - \boldsymbol{w}^{(\mathrm{PML})}(\,\cdot\,,t)\| \le \mu(t)\|\boldsymbol{\xi}\|'. \tag{7b}$$

In formulae (7), $\tilde{\boldsymbol{w}}^{(\Omega)}$ is the solution of the perturbed problem (5a), and $\tilde{\boldsymbol{w}}^{(\mathrm{PML})}$ is the solution of the perturbed problem (5b). The rate of growth $\mu(t)$ is either linear or quadratic for standard PMLs, see [3], [8], [4]. In actual computations, the perturbations $\boldsymbol{\xi}$ originate from the truncation error, and estimates (7) indicate that for long simulation times the accuracy of the solution can be ruined.

If, however, instead of (5) we consider individual problems (3) supplemented by the PML, then estimates (7) will immediately transform into:

$$\|\tilde{\boldsymbol{w}}_m^{(\Omega)}(\,\cdot\,,t) - \boldsymbol{w}_m^{(\Omega)}(\,\cdot\,,t)\| \le C\|\boldsymbol{\xi}\|', \tag{8a}$$

$$\|\tilde{\boldsymbol{w}}_m^{(\mathrm{PML})}(\,\cdot\,,t) - \boldsymbol{w}_m^{(\mathrm{PML})}(\,\cdot\,,t)\| \le C\|\boldsymbol{\xi}\|', \tag{8b}$$

where $C = \mu(T_1 + T)$ is a constant. Combining estimate (8a) with formula (4), we obtain:

$$\|\tilde{\boldsymbol{w}}^{(\Omega)}(\,\cdot\,,t) - \boldsymbol{w}^{(\Omega)}(\,\cdot\,,t)\| \le C_0\|\boldsymbol{\xi}\|', \tag{9a}$$

where $C_0 = C\cdot(M - M_0 + 1)$. In contradistinction to (7a), estimate (9a) implies that even if the PML errors contaminate Ω, *the resulting error on Ω will remain uniformly bounded for all times.* Thus, with relation (6) taken into account, we have proved:

Theorem 1 *Let $\Omega \subset \mathbb{R}^3$ be a bounded domain, and let problem (1) be solved using a PML around Ω combined with the lacunae-based algorithm, see (2), (3), (4) and (5). Then, the error on Ω due to the perturbations $\boldsymbol{\xi}$ in the PML will remain uniformly bounded for all times:*

$$\|\tilde{\boldsymbol{w}}^{(\Omega)}(\,\cdot\,,t) - \boldsymbol{w}(\,\cdot\,,t)\|_{\Omega} \le C_0\|\boldsymbol{\xi}\|'. \tag{9b}$$

The error growth inside the PML is also uniformly bounded, but the estimate should be written differently:

$$\Big\| \sum_{m=M_0}^{M} \tilde{\boldsymbol{w}}_m^{(\mathrm{PML})}(\,\cdot\,,t) - \sum_{m=M_0}^{M} \boldsymbol{w}_m^{(\mathrm{PML})}(\,\cdot\,,t) \Big\| \le C_0\|\boldsymbol{\xi}\|'. \tag{9c}$$

The first and second terms on the left-hand side of (9c) are solutions in the PML with and without perturbations, respectively. They are left in the form of the sums because the lossy equations of the PML shall not be expected to be Huygens', and equality (4) typically won't hold. In other words, since the solution is represented as a finite sum of terms with finite lifespan, the uniform bound (9c) is guaranteed. However, unlike on Ω, the solutions obtained in the PML with and without lacunae are not the same.

Discussion

Unlike in the approach proposed in [8], the PML equations never get modified by lacunae-based integration, and for each individual problem after the partition (2) the layer remains perfectly matched and absorbing.

Our analysis imposes no constraints on the rate of growth $\mu(t)$, see (7), and C_0 in inequality (9b) is a constant in any event. The actual value of this constant $C_0 = \mu(T_1+T)\cdot(M-M_0+1)$, however, may or may not be acceptable in a particular context. If $\mu(t)$ is a slowly increasing function, then C_0 will not be large.

In practice, the lacunae-based algorithm is implemented in a continuous framework [10], [12]. Namely, formula (4) implies that at every moment of time t we need to know solutions of $M - M_0 + 1 \equiv \lceil t/T_1 \rceil - \lfloor (t - T)/T_1 \rfloor$ individual problems that form the "active set." As the overall solution evolves, new problems are added to this set while the "expired" problems (for which Ω is already in the lacuna) are dropped. The total number of problems in the set never exceeds a certain maximum (2 for $T_1 \geq T$). Of course, the computational cost increases compared to the standard time marching. If, say, $T_1 = T$, then every moment of time t needs to be passed twice during the integration. As, however, the individual problems are independent, they can be solved concurrently on a parallel computer. In addition, the overhead can sometimes be reduced. If $T_1 > T$, the average number of integration passes through a given t is $1 < (T_1 + T)/T_1 < 2$, which is close to 1 for $T_1 \gg T$. The constant $C_0 \sim \mu(T_1+T)$ in this case will increase, but this, again, is not necessarily a limitation because according to [8] μ is large only for very long times. In the limit $T_1 \to \infty$, we are back to the conventional time marching with no use of lacunae.

The original problem may involve a more sophisticated mechanism of waves' generation than the source terms of (1). There may be radiation, scattering, variable coefficients in the governing equations, etc. As long as all these phenomena are confined to Ω, and the operator $\partial/\partial t + \boldsymbol{L}$ remains Huygens' on $\mathbb{R}^3 \setminus \Omega$, the lacunae-based methodology will still apply. In this case, the problem needs to be split into the interior and auxiliary sub-problems as when setting the ABCs [12], [13], [14]. In doing so, the auxiliary sub-problem will be precisely of type (1).

References

[1] Jean-Pierre Bérenger. A perfectly matched layer for the absorption of electromagnetic waves. *J. Comput. Phys.*, 114(2):185–200, 1994.

[2] Jean-Pierre Bérenger. Three-dimensional perfectly matched layer for the absorption of electromagnetic waves. *J. Comput. Phys.*, 127(2):363–379, 1996.

[3] S. Abarbanel and D. Gottlieb. A mathematical analysis of the PML method. *J. Comput. Phys.*, 134(2):357–363, 1997.

[4] E. Bécache and P. Joly. On the analysis of Bérenger's perfectly matched layers for Maxwell's equations. *M2AN Math. Model. Numer. Anal.*, 36(1):87–119, 2002.

[5] S. D. Gedney. An anisotropic perfectly matched layer-absorbing medium for the truncation of FDTD lattices. *IEEE Trans. Antennas Propagat.*, 44(12):1630–1639, 1996.

[6] R. W. Ziolkowski. Time-derivative Lorenz material model based absorbing boundary conditions. *IEEE Trans. Antennas Propagat.*, 45(10):1530–1535, 1997.

[7] S. Abarbanel and D. Gottlieb. On the construction and analysis of absorbing layers in CEM. *Appl. Numer. Math.*, 27(4):331–340, 1998.

[8] S. Abarbanel, D. Gottlieb, and J. S. Hesthaven. Long time behavior of the perfectly matched layer equations in computational electromagnetics. *J. Sci. Comput.*, 17(1-4):405–422, 2002.

[9] R. Courant and D. Hilbert. *Methods of Mathematical Physics. Volume II*. Wiley, New York, 1962.

[10] V. S. Ryaben'kii, S. V. Tsynkov, and V. I. Turchaninov. Long-time numerical computation of wave-type solutions driven by moving sources. *Appl. Numer. Math.*, 38:187–222, 2001.

[11] I. Petrowsky. On the diffusion of waves and the lacunas for hyperbolic equations. *Matematicheskii Sbornik (Recueil Mathématique)*, 17 (59)(3):289–370, 1945.

[12] V. S. Ryaben'kii, S. V. Tsynkov, and V. I. Turchaninov. Global discrete artificial boundary conditions for time-dependent wave propagation. *J. Comput. Phys.*, 174(2):712–758, 2001.

[13] S. V. Tsynkov. Artificial boundary conditions for the numerical simulation of unsteady acoustic waves. *J. Comput. Phys.*, 189(2):626–650, August 2003.

[14] S. V. Tsynkov. On the application of lacunae-based methods to Maxwell's equations. *J. Comput. Phys.*, 199(1):126–149, September 2004.

TRANSPARENT BOUNDARY CONDITIONS – THE POLE CONDITION APPROACH

A. Schädle[◦,*], **D. Ruprecht**[◦], **F. Schmidt**[◦]
[◦]Zuse Institute, Berlin, Germany.
[*]Email: schaedle@zib.de

Abstract

A new approach to derive transparent boundary conditions (TBCs) for wave, Schrödinger and drift-diffusion equations is presented. It relies on the pole condition approach and distinguishes physical reasonable and unreasonable solutions by the location of the singularities of the spatial Laplace transform U of the exterior solution. By the condition that U is analytic in some region TBCs are established. To realize the pole condition numerically, a Möbius transform is used to map the region of analyticity to the unit disc. There the Laplace transform is expanded in a power series. The equations coupling the coefficients of the power series with the interior provide the TBC. Numerical result for the damped wave equation show that the error introduced by truncating the power series decays exponentially in the number of coefficients.

Introduction

Transparent boundary conditions are a key ingredient for the simulation of wave propagation on unbounded domains. In this talk work in progress is presented.

Prototypes of the governing equations under consideration are the wave, drift-diffusion and Schrödinger equations on the real line for $t > 0$ given by

$$\partial_{tt} u = \partial_{xx} u - k^2 u, \quad (1)$$
$$\partial_t u = \partial_{xx} u + 2d\partial_x u, \quad (2)$$
$$i\partial_t u = \partial_{xx} u - k^2 u. \quad (3)$$

All of these have to complemented by appropriate initial values. To treat (1) - (3) simultaneously the symbol $p(\partial_t)$ is introduced. Hence the generic equation is

$$p(\partial_t) u = \partial_{xx} u + 2d\partial_x u - k^2 u. \quad (4)$$

For the procedure to derive exact non-local transparent boundary conditions we refer to the recent review articles [1]. The pole condition approach is an alternative and as we hope to show a more flexible way of deriving transparent boundary conditions. Almost immediately the pole condition approach yields an algorithm to implement approximate local transparent boundary conditions. The pole condition for time-harmonic problems is studied in [2], where it is shown that it coincides with the Sommerfeld radiation condition.

Alternative derivation of TBCs

Suppose we are only interested in the solution u restricted to the interval $[-a, a]$. Furthermore suppose that the initial value(s) are compactly supported in $[-a, a]$. To truncate the computational domain TBCs are needed. The exact TBCs are in general convolution in time, i.e. they are non-local.

Variational formulation

Multiplying (4) by a test function and integrating over the real line yields

$$\int p(\partial_t) uv \, dx = \int -\partial_x u \partial_x v + 2d\partial_x uv - k^2 uv \, dx. \quad (5)$$

As test functions we chose $v(x) = \mathrm{e}^{-s(x-a)}$ for $x > a$ and $v(x) = \mathrm{e}^{s(x+a)}$ for $x < -a$ with a complex parameter s with $\Re s > 0$. The integral over the real line is split into three parts: an integral from $-\infty$ to $-a$, from $-a$ to a and from a to ∞. Defining

$$U^{(r)}(t, s) := \int_0^\infty u(t, x + a)\mathrm{e}^{-sx},$$

which is the Laplace transform of the solution u in the right exterior, and similar $U^{(l)}$ one obtains after some simple manipulations

$$\begin{aligned}\int_{-a}^{a} p(\partial_t) uv \, dx + p(\partial_t) U^{(r)} + p(\partial_t) U^{(l)} = \\ \int_{-a}^{a} -\partial_x u \partial_x v + 2d\partial_x uv - k^2 uv \, dx \\ + s(sU^{(l)} - u_{-a}) - 2d(s(U^{(l)} - u_{-a})) - k^2 U^{(l)} \\ + s(sU^{(r)} - u_a) + 2d(s(U^{(r)} - u_a)) - k^2 U^{(r)},\end{aligned}$$

where $u_{\pm a}$ are the boundary values of u at the left and right boundary.

Pole Condition

Consider the equation for the right exterior only, suppose for the moment that u is given on $[-a, a]$ and set

$$u' := \int_{-a}^{a} p(\partial_t) uv \, dx + \partial_x u \partial_x v - 2d\partial_x uv + k^2 uv \, dx.$$

Then the equation for $U^{(r)}$ is given by

$$s(sU^{(r)} - u_a) + 2d(sU^{(r)} - u_a) - k^2 U^{(r)} - p(\partial_t) U^{(r)} = u' .$$

Taking a Laplace transform in time with dual variable ω, $p(\partial_t)$ corresponds to a multiplication with $p(\omega) = \omega$, $p(\omega) = i\omega$ or $p(\omega) = \omega^2$ depending on the type of equation. Solving for $U^{(r)}(s)$ one obtains

$$U^{(r)}(s) = (s^2 + 2ds - k^2 - p(\omega))^{-1}(u' + su_a + 2du_a).$$

Clearly $U^{(r)}(s)$ is analytic in s except for two poles (or more generally for several singularities). If s_- and s_+ are the roots of $(s^2 + 2ds - k^2 - p(\omega))$ one can write by Cauchy's integral formula

$$\begin{aligned} U^{(r)}(s) &= \frac{1}{2\pi}\oint_{\gamma_-} \frac{(\sigma^2 + 2d\sigma - k^2 - p(\omega))^{-1}}{\sigma - s} d\sigma \\ &\quad + \frac{1}{2\pi}\oint_{\gamma_+} \frac{(\sigma^2 + 2d\sigma - k^2 - p(\omega))^{-1}}{\sigma - s} d\sigma \end{aligned}$$

where $\gamma_\pm$ are paths enclosing $s_\pm$. In this simple setting this is equivalent to a partial-fraction decomposition.

$$U^{(r)}(s) = \frac{r_+(s, u', u_a)}{s_+ - s} + \frac{r_-(s, u', u_a)}{s_- - s},$$

with $r_\pm = 1/2(u_a \pm (u' + 2du_a)/\sqrt{p(\omega) + k^2 + d^2})$. Transforming back to space domain we have the correspondence

$$\frac{1}{s_- - s} \leftrightarrow \mathrm{e}^{s_- x} \quad \text{and} \quad \frac{1}{s_+ - s} \leftrightarrow \mathrm{e}^{s_+ x}.$$

Suppose that we can identify $\mathrm{e}^{s_+ x}$ as an incoming wave or a exponentially increasing solution. Thus depending on the location of the poles $s_\pm$ we can now distinguish incoming/exponentially increasing waves from outgoing/exponentially decreasing waves. So we are in the position to formulate TBCs as a *condition on* $U^{(r)}(s)$. The pole condition states: A wave is outgoing if $U^{(r)}(s)$ is an analytic function in the half plane E of possible locations of s_+. This is equivalent to the condition that $r_+ = 0$, which yields the classical transparent boundary condition.

Pole Condition in Hardy space

How to handle the pole condition numerically? Analytic functions can be expanded into power serieses, which convergence in some ball, yet the pole condition is a condition set on a complex half plane. The Möbius transform is a conformal transformation that transforms a half plane to the unit ball. The Möbius transform is thus the key ingredient to make our algorithm fly. Let $s \mapsto \tilde{s} = M(s)$ be the Möbius transform that maps the half plane E to the unit ball. We can now reformulate the pole condition: A wave is outgoing if $U^{(r)}(\tilde{s})$ is analytic in the unit ball. Expanding

$$U^{(r)}(\tilde{s}) = \sum_{\ell=0}^{\infty} a_\ell \tilde{s}^\ell \tag{6}$$

one has to deduce equations for the a_ℓ. Then simply truncating the series expansion by setting $a_\ell = 0$ for $\ell > L$ an algorithm is obtained, that realizes TBCs.

The details are as follows. The Möbius transform

$$s \mapsto \tilde{s} = M(s) := \frac{s + s_0}{s - s_0}$$

maps the half plane $\{z : \Re(-z/s_0) < 0\}$ onto the unit disk. (e.g. for positive real s_0 the left half plane is mapped onto the unit ball; the imaginary axis is mapped to the unit circle; $-s_0$ is mapped to 0; and 0 is mapped to -1.) The inverse is again a Möbius transform

$$\tilde{s} \mapsto s = M^{-1}(\tilde{s}) := s_0 \frac{\tilde{s} + 1}{\tilde{s} - 1}.$$

Space discretization

For the sake of clearness we consider the case $d = 0$ only. Space discretization is done using third order finite elements resulting in the standard local mass and stiffness matrices, that are assemble to a global system. At the right boundary (and similar for the left boundary) we use the special *exp*-element as test function

$$v_s(x) = \begin{cases} \mathrm{e}^{-s(x-a)} & x \geq a \\ \frac{x-(a-h)}{h} & a - h \leq x \leq a \end{cases}$$

and obtain

$$\begin{aligned} &p(\omega)U^{(r)} + p(\omega)u_a^{(0)} = u_a^{(2)} - k^2 u_a^{(0)} + \\ &s_0 \frac{\tilde{s} + 1}{\tilde{s} - 1}\left(s_0 \frac{\tilde{s} + 1}{\tilde{s} - 1} U^{(r)} - u_a\right) - k^2 U^{(r)}, \end{aligned} \tag{7}$$

where $u_a^{(0)}$ and $u_a^{(2)}$ are the boundary contributions

$$u_a^{(0)} = \sum_j \int_{a-h}^{a} u_j \phi_j v_s \, dx \,;\; u_a^{(2)} = \sum_j \int_{a-h}^{a} u_j \phi_j' v_s \, dx$$

Setting $u_a' = (p(\omega) + k^2)u_a^{(0)} - u^{(2)}$, multiplying (7) by $(\tilde{s} - 1)^2$ and rearranging terms yields

$$\begin{aligned} &\left(s_0^2(\tilde{s} + 1)^2 - (\tilde{s} - 1)^2(p(\omega) + k^2)\right) U^{(r)} \\ &\qquad = (\tilde{s} - 1)^2 u_a' + s_0(\tilde{s}^2 - 1)u_a. \end{aligned}$$

Inserting the power series (6), sorting for powers of $\tilde{s}$ and comparing coefficients yields equations for the a_j:

$$\left(s_0^2 - p - k^2\right) a_0 = u_a' - s_0 u_a, \tag{8}$$

$$2\left(s_0^2 + p + k^2\right) a_0 + \left(s_0^2 - p - k^2\right) a_1 = -2u_a', \tag{9}$$

$$\begin{aligned}\left(s_0^2 - p - k^2\right) a_0 + 2\left(s_0^2 + p + k^2\right) a_1 \\ + \left(s_0^2 - p - k^2\right) a_2 = u_a' + s_0 u_a,\end{aligned} \tag{10}$$

$$\begin{aligned}\left(s_0^2 - p - k^2\right) a_{\ell-1} + 2\left(s_0^2 + p + k^2\right) a_\ell \\ + \left(s_0^2 - p - k^2\right) a_{\ell+1} = 0, \quad \ell = 1, \ldots, L\end{aligned} \tag{11}$$

with $a_{L+1} = 0$. Similar equations hold for the left boundary. Transforming back to time-domain equations (8) to (11) yield a system of ordinary differential equations for the coefficients a_j for $j = 1, \ldots, L$.

Take a closer look at (8). If one would choose $s_0 = \sqrt{p(\omega) + k^2}$ then (8) is the well-known exact non-local TBC; equations (8) to (11) decouple and all a_ℓ vanish for $\ell \geq 2$. Choosing s_0 to be constant gives local approximate TBCs.

In case of the wave equation (i.e. $p(\omega) = \omega^2$) choosing $s_0 = \omega$ gives local TBCs. In case $k = 0$ this choice gives the exact TBCs.

Numerical results

The numerical results for the wave equation (1) integrated from $t = 0, \ldots, 20$ with an extremely small stepsize of $\Delta t = 10^{-4}$ using the trapezoidal rule are shown below. The computational domain is $[-5, 5]$, $k = 5$, the initial value is a Gaußian $u(x, 0) = \exp(-x^2)$ and the initial velocity is set to zero. Space discretization is done by third order finite elements on an equidistant grid with $\Delta x = 0.002$. The reference solution is calculated on a domain $[-15, 15]$; this way the dominating error component should be the truncation error in the power series representation. Figure 1 shows the evolution of the error in energy norm for different L. Figure 2 shows the error in energy-norm vs. the number of coefficients L in the power series, idicating a supergeometric convergence in L.

Extensions and future work

The concepct is easily extended to systems

$$Mp(\partial_t)u = A\partial_{xx}u + 2D\partial_x u - Ku.$$

with matrices M, A, D and K. These type of systems arise for example for two dimensional problems on a strip $\{(x, y), |y| < b, \infty < x < \infty\}$ after a discretisation of the y component. The extension to general two or three dimensional problems is currently under investigation.

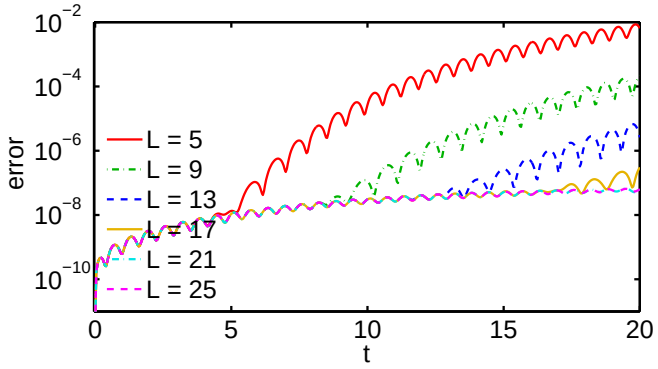

Figure 1: Evolution of the error for different L.

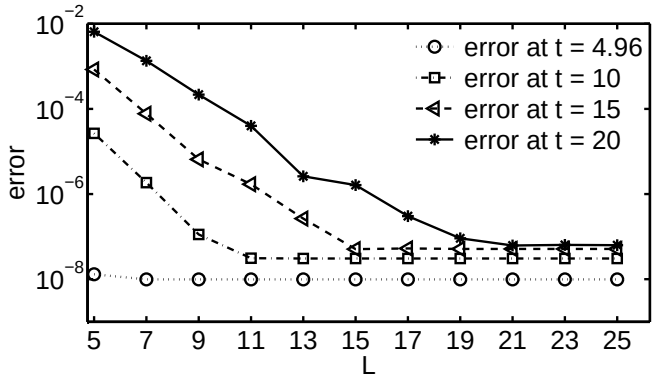

Figure 2: Error vs. L at different t.

References

[1] T. Hagstrom, "Radiation boundary conditions for numerical simulation of waves", Acta Numerica, vol. 8, pp. 47–106, 1999.

[2] T. Hohage, F. Schmidt, and L. Zschiedrich, "Solving Time-Harmonic Scattering Problems Based on the Pole Condition I: Theory", SIAM J. Math. Anal., vol. 35, pp. 183–210, 2003.

TRANSPARENT BOUNDARY CONDITIONS FOR ELASTODYNAMICS IN A VTI MEDIUM LAYER

Ivan L. Sofronov[†,*], **Nikolai A. Zaitsev**[†]
[†]Keldysh Institute of Applied Mathematics RAS, Moscow, Russia
[*]Email: sofronov@spp.keldysh.ru

Abstract

We propose transparent boundary conditions for the dynamic equations of elasticity in the vertical transverse isotropy medium. The conditions are generated numerically for the side surface of a cylinder, the open boundary of a computational domain. The correspondent operator is non-local in both space and time: the finite Fourier series is used at the surface to treat a necessary number of space harmonics of the solution while for the convolutions with respect to time the kernels are represented by sums-of-exponentials. Preliminary test calculations show high accuracy, efficiency, and stability of the proposed non-reflecting conditions.

Acknowledgement: The work is supported by RFBR grant No. 07-01-00476 and CRDF grant No. RUM1-1605-MO-05. The authors are grateful to Alexander N. Daryin and Olga I. Voskoboinikova for the help in algorithmic implementation.

Introduction

The model of Vertical Transverse Isotropy medium, a special case of anisotropy, has wide application in seismoelasticity. The problem of the construction of non-reflecting boundary conditions on the open boundaries of computational domains for such media is crucial both for practical simulations of the propagation of waves and for the methods of computational mathematics, since the known analytical approaches no longer work. Also the popular PML approach can fail in anisotropic media, see [1], [2].

In order to provide non-reflecting and stable conditions for long-time simulations, we develop the concept of *transparent boundary conditions* (TBCs) that are based on the Green's function of governing equations in the external unbounded domain. Recently advantages of the method have been demonstrated for the case of azimuthal anisotropy: see in [3] description of the approach as well as numerical results for different variants of the anisotropy including those considered in [1].

Here we develop the approach for generating *quasi-analytic* TBCs on the side surface of a cylinder $C : \{r \le R_0\}$ for the equations of the transverse-isotropic medium:

$$\begin{cases} \rho\frac{\partial^2 u}{\partial t^2} = A_{11}\frac{\partial}{\partial r}\left(\frac{1}{r}\left(\frac{\partial (ru)}{\partial r}\right)\right) + \frac{\partial}{\partial z}\left(A_{44}\left(\frac{\partial u}{\partial z} + \frac{\partial w}{\partial r}\right)\right) \\ \qquad\qquad + A_{13}\frac{\partial^2 w}{\partial r \partial z} \\ \rho\frac{\partial^2 w}{\partial t^2} = \frac{1}{r}\frac{\partial}{\partial r}\left(r\left(A_{44}\left(\frac{\partial w}{\partial r} + \frac{\partial u}{\partial z}\right) + \frac{\partial}{\partial z}\left(A_{13}u\right)\right)\right) \\ \qquad\qquad + \frac{\partial}{\partial z}(A_{33}\frac{\partial w}{\partial z}), \end{cases}$$

u, w are radial and axial displacements in $(r, z)-$geometry; $A_{11}(z)$, ..., $A_{44}(z)$ are the elastic parameters of VTI medium that may depend on z.

We consider hereafter the conditions of the mirror symmetry at the top and bottom of the cylinder $Z_{min} \le z \le Z_{max}$ for simplicity. A typical aspect ratio $(Z_{max} - Z_{min})/R_0$ in our numerical tests is several dozens.

Derivation of the TBCs operator

The procedure of generating TBCs operator on the boundary $\Gamma : \{r = R_0\}$ is described by several main stages. Let us use the above original VTI system written in the operator form:

$$\frac{\partial^2 f}{\partial t^2} - Lf = 0, \quad f = (u, w). \tag{1}$$

Stage 1. Denote by $\{\varphi^m(z)\}_{m=0}^{\infty}$ the orthonormal basis functions for expansion $f(t, r, z)$ with respect to z. They are constructed from $\{\sin mz, \cos mz\}$ by a natural way satisfying the mirror symmetry condition for f at $z = Z_{min}$, $z = Z_{max}$. Consider the set with respect to $m = 0, 1, ...$ of auxiliary external initial boundary-valued problems at $r \ge R_0$:

$$\begin{cases} \mathcal{E}^m_{tt} - L\mathcal{E}^m &= 0 \quad \text{in } R^2/C \\ \mathcal{E}^m|_{t=0} &= 0 \\ \mathcal{E}^m|_{\Gamma} &= \delta(t)\varphi^m(z) \end{cases}$$

where $\delta(t)$ is Dirac's delta function. (Function $\mathcal{E}^m$ is usually called *Green's function of the Dirichlet problem.*)

Making Laplace transform we pass to elliptic boundary-valued problems parameterized by s:

$$\begin{cases} s^2\hat{\mathcal{E}}^m - L\hat{\mathcal{E}}^m &= 0 \quad \text{in } R^2/C \\ \hat{\mathcal{E}}^m|_{t=0} &= 0 \\ \hat{\mathcal{E}}^m|_{\Gamma} &= \varphi^m(z). \end{cases} \tag{2}$$

Stage 2. We take a finite interval $[0, S_{\max}]$ and form set of points $\{s_j\}_{j=1}^{J} \in [0, S_{\max}]$, J is an integer, using distribution law of Chebyshev's grid nodes. Then we solve numerically $J \times (M+1)$ problems (2) – for each $s = s_j$ with a desired amount $M+1$ of basis functions ($m = 0, 1, ..., M$), and evaluate $\psi^m \equiv \frac{\partial}{\partial n}\hat{\mathcal{E}}^m$ on Γ. Thus the Neumann data ψ of basis functions are obtained as function of two indices (j, m):

$$\{\varphi^m(z), s_j\} \mapsto \{\psi^m(z, s_j)\}.$$

Taking now arbitrary Dirichlet data on Γ, $\hat{f}(s,z) = \sum\limits_m \hat{c}^m(s)\varphi^m(z)$, we write the representation of correspondent Neumann data $N[\hat{f}]$ by using the expansion in terms of the basis $\{\varphi^m(z)\}$:

$$N[\hat{f}(s,z)] = \sum_m \hat{c}^m(s)\psi^m(z,s)$$

$$= \sum_m \hat{c}^m(s) \sum_n P_n^m(s)\varphi^n(z).$$

Thus we obtain the Poincaré-Steklov operator on the Fourier coefficients space:

$$\hat{d}^n(s) \ = \sum_n \hat{P}_n^m(s)\hat{c}^m(s)$$

or, in matrix form:

$$\hat{\mathbf{d}}(s) \ = \hat{\mathbf{P}}(s)\hat{\mathbf{c}}(s) \qquad (3)$$

with

$$\hat{\mathbf{c}} \equiv \left\{\hat{c}^0,\ \hat{c}^1,\ ...\right\}^{\mathrm{T}}, \quad \hat{\mathbf{d}} \equiv \left\{\hat{d}^0,\ \hat{d}^1,\ ...\right\}^{\mathrm{T}},$$

$$\frac{\partial}{\partial n}\hat{f}(s,z) \equiv \sum_m \hat{d}^m(s)\varphi^m(z,s).$$

Stage 3. We make inverse Laplace transform for the Poincaré-Steklov operator (3) as follows. First, the matrix $\hat{\mathbf{P}}(s)$ is represented by sum of three matrices to take into account asymptotics as $s \to \infty$:

$$\hat{\mathbf{P}}(s) = \mathbf{P}_1 s + \mathbf{P}_0 + \hat{\mathbf{K}}(s); \quad \mathbf{P}_1, \mathbf{P}_0 \text{ are } \textit{consts},$$

$$\hat{\mathbf{K}}(s) = o(1).$$

These constant matrices $\mathbf{P}_1$, $\mathbf{P}_0$ are estimated from rational approximations

$$R_n^m(s_j) \ \approx \hat{P}_n^m(s_j)$$

that are evaluated by using Chebyshev-Padé algorithm on the interval $[0, S_{\max}]$.

Then we calculate rational approximations of each entry in $\hat{\mathbf{K}}(s)$ so that all poles have negative real parts, i.e.

$$\hat{K}_n^m(s) \approx \hat{\tilde{K}}_n^m(s) \equiv \sum_{l=1}^{L_n^m} \frac{\alpha_{n\,l}^m}{s - \beta_{n\,l}^m}, \quad \mathrm{Re}(\beta_{n\,l}^m) < 0$$

where L_n^m is a number of poles (it exerts significant influence on accuracy of the approximation). Again the Chebyshev-Padé algorithm on the interval $[0, S_{\max}]$ is the main tool for the approximations.

Finally, the inverse Laplace transform of (3) gives:

$$\mathbf{d}(t) \ \approx \mathbf{P}_1 \frac{\partial \mathbf{c}(t)}{\partial t} + \mathbf{P}_0\mathbf{c}(t) + \tilde{\mathbf{K}}(t) * \mathbf{c}(t). \qquad (4)$$

Important property of (4) is that kernels $\tilde{K}_n^m(t)$ having the explicit form

$$\tilde{K}_n^m(t) = \sum_{l=1}^{L_n^m} \alpha_{n\,l}^m \exp(\beta_{n\,l}^m t), \qquad \mathrm{Re}(\beta_{n\,l}^m) < 0$$

permit to treat convolutions by *stable recurrent* formulas.

Stage 4. Denote by $\mathbf{Q}$, $\mathbf{Q}^{-1}$ operators of Fourier expansion with respect to basis $\{\varphi^m(z)\}_{m=0}^M$, i.e.

$$\mathbf{Q} : f(t,z)|_{r=R_0} \to \{c^m(t)\}, \qquad \mathbf{Q}^{-1} : \{c^m(t)\} \to f.$$

Ignoring an approximate character of the relationship (4) we are in position to write out the desired operator of TBC in the physical space:

$$\mathbf{Q^{-1}P}_1\mathbf{Q}\frac{\partial f}{\partial t} \ - \ \frac{\partial f}{\partial r} \ + \ \mathbf{Q^{-1}P}_0\mathbf{Q}f$$

$$+ \ \mathbf{Q}^{-1}\left\{\tilde{\mathbf{K}}(t)*\right\}\mathbf{Q}f \ = \ 0. \qquad (5)$$

Actually, the scheme of generating (5) looks very similar to [4], [5] where analytical derivation of TBC operator for the wave equation is proposed; the discrimination is that all *analytical* stages are now replaced by *numerical* counterparts (Stages 2,3).

It is worth to emphasize that numerical algorithm solving the elliptic problems (2) finds the functions with a maximally possible accuracy in order to provide the numerically stable inverse Laplace transformation (4). In particular, for the VTI case we develop a highly-accurate elliptic solver using the Galerkin method with basis functions $\{\varphi^m(z)\}_{m=0}^M$.

Test calculation

Accuracy and stability of the proposed transparent boundary conditions are demonstrated on several numerical tests. We describe one of them.

Geometry of the computational domain $[R_{\min}, R_0] \times [Z_{\min}, Z_{\max}]$ is given by $R_{\min} = 0.1$, $R_0 = 0.3$, $Z_{\min} = 0$, $Z_{\max} = \pi$.

Initial displacements are generated at the boundary $r = R_{\min}$. This is a finite pulse in both space, $0.5 < z < 2.5$ and time, $0 < t < 0.1$. TBCs boundary is $r = R_0$.

Parameters of the VTI medium are described via the Thomsen's parameters:

$$A_{11} = V_{P0}^2(1+2\varepsilon),\ \ A_{33} = V_{P0}^2,\ \ A_{44} = V_{S0}^2,$$
$$A_{13} = \sqrt{(A_{33}-A_{44})^2 + 2\delta A_{33}\,(A_{33}-A_{44})} - A_{44}$$

where $V_{P0} = 3.3$, $V_{S0} = 1.8$, $\delta = -0.22$, $\varepsilon = 0.2$.

We consider three uniform grids with treble numbers of intervals in the computational domain: Grid1 $Nr = 16,\ Nz = 64$, Grid2 $Nr = 47,\ Nz = 190$, and Grid3 $Nr = 140,\ Nz = 568$ (each coarser grid is a subgrid of the fine grid).

Governing equations (see Introduction) are approximated by explicit central-difference second-order scheme. A reference solution is calculated in the extended domain $[R_{\min},\, R_{\max}]$, $R_{\max} \approx 3$ on the finest grid. Number of basis functions of the TBCs operator is defined by $M = 24$.

Figure 1 shows history of difference with reference solution (relative $C-$norm over the computational domain). One can observe that 1) test solutions have the second order of accuracy; 2) approximation error of the difference scheme and error of TBCs reflections are approximatively the same for Grid3 – about 0.2% (i.e. TBCs are too accurate for coarser grids).

Figure 2 shows long-time stability of calculations with TBCs.

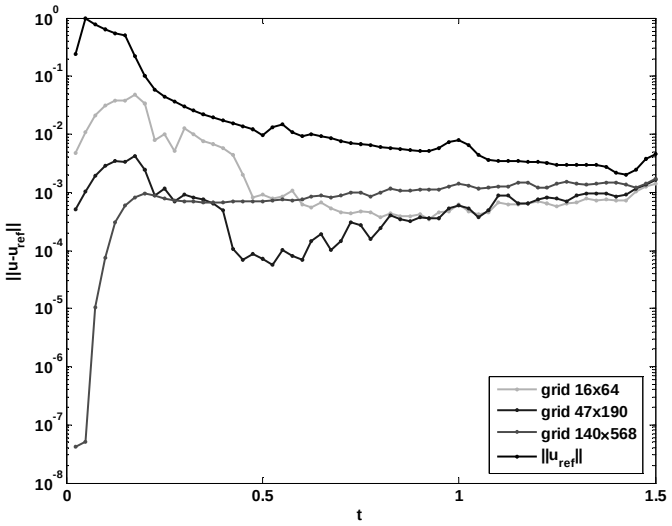

Figure 1: Norm of reference solution (top curve), Norms of difference with reference solution for Grid1, Grid2, and Grid3

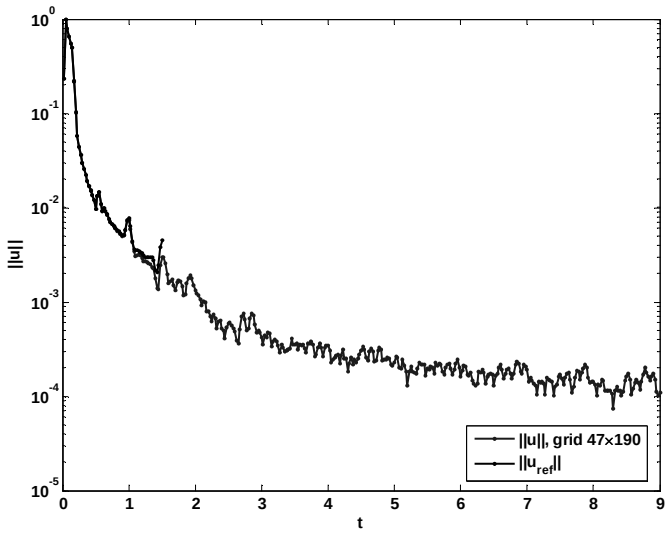

Figure 2: Norm of solution for long-time calculations

References

[1] E. Becache, S. Fauqueux, and P. Joly, "Stability of perfectly matched layers group velocities and anisotropic waves", Journal of Computational Physics, vol. 188, pp. 399–433, 2003.

[2] D. Appelo, G. Kreiss, "A new absorbing layer for elastic waves", Journal of Computational Physics, vol. 215, pp. 642–660, 2006.

[3] I. Sofronov, N. Zaitsev, "Transparent boundary conditions for the elastic waves in anisotropic media", in Proceedings of Eleventh International Conference on Hyperbolic Problems Theory, Numerics, Applications. Ecole Normale Superieure de Lyon, Lyon, France, 17-21 July 2006. Accepted for publication.

[4] I. Sofronov, "Conditions for complete transparency on the sphere for the three-dimensional wave equation", Russian Acad. Sci. Dokl. Math. vol. 46, pp. 397–401, 1993.

[5] I. Sofronov, "Artificial boundary conditions of absolute transparency for two- and three-dimensional external time-dependent scattering problems", Euro. J. Appl. Math., vol. 9, No.6, pp. 561–588, 1998.

Absorbing boundary conditions in quantum scattering calculations for breakup problems with multiple particles

W. Vanroose[1,*], **D. A. Horner** [2], **F. Martín** [3], **T. N. Rescigno** [4] **and C. W. McCurdy** [4,5]
[1] Department Wiskunde-Informatica, Universiteit Antwerpen, Middelheimlaan 1, 2020 Antwerpen, Belgium
[2] Los Alamos National Laboratory, Theoretical Division, Los Alamos, NM 87545, USA.
[3] Departamento de Qumica C-9, Universidad Autnoma de Madrid, 28049 Madrid, Spain
[4] Lawrence Berkeley National Laboratory, Chemical Sciences, Berkeley, California 94720, USA
[5] Departments of Applied Science and Chemistry, University of California, Davis, California 95616, USA
[*]Email: wim.vanroose@ua.ac.be

Introduction

In physics and chemistry, the scattering of multiple charged particles is research topic that is getting a lot of attention recently. Modern experimental detectors such as the "reaction microscopes" can detect, in coincidence, the directions and momenta of all the particles that emerge from a breakup reaction. This has resulted in a wealth of experimental information that still needs to be explained theoretically [1].

In this talk we present some of the computational and mathematical challenges that make these kind of problems hard to solve.

One particle Schrödinger equation

The Schrödinger equation is a wave equation that describes the dynamics of particles such as electrons and nuclei at the level of a molecule. For example, the equation for one particle with a mass m and an energy E in the potential field $V(\mathbf{r})$ is

$$-\frac{\hbar^2}{2m}\Delta\psi(\mathbf{r}) + V(\mathbf{r})\psi(\mathbf{r}) - E\psi(\mathbf{r}) = 0, \qquad (1)$$

where $\hbar$ is the constant of Planck. As usually we will use atomic units such that $m = 1$ and $\hbar = 1$. For $E > 0$, this equation can be interpreted as a Helmholtz equation $\Delta u + k^2(\mathbf{r})u = 0$ with a position dependent wave number

$$k(\mathbf{r}) = \sqrt{2(E - V(\mathbf{r}))}.$$

The simplest system is the hydrogen atom that consists out of a electron and proton. The dynamics of the negatively charged electron in the field of a positively charged proton is governed by the Coulomb interaction caused by their mutual attraction. The field is $-1/|\mathbf{r}|$ where $\mathbf{r}$ is the vector that starts at the position of the proton and ends at the position of the electron.

As the electron and the proton come close together this results in a very large effective wave number. As the proton and electron are very far apart, in the asymptotic region, one would expect that the wave number becomes

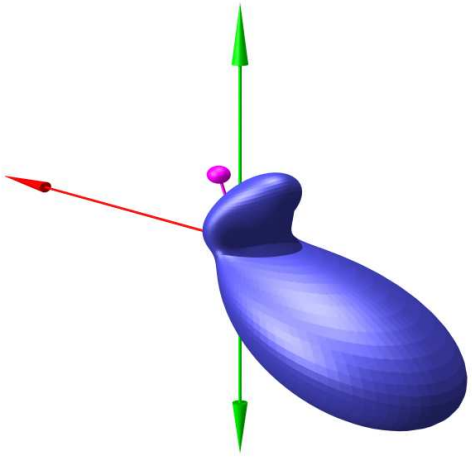

Figure 1: For the reaction $\hbar\omega + \mathrm{H}_2 \rightarrow e^- + e^- + p + p$, where a single photon breaks the molecule op in two electrons and two protons, we calculate distribution of direction in which the second electron espace. The molecule (purple) is aligned 20° with the polarisation of the photon field (green). The first electron escapes in a fixed direction (red arrow) and takes away 90% of the available energy. The impact photon has an energy of 55eV.

$\sqrt{2E}$ and the solution u becomes a linear combination of plane waves. But, this is not the case. It has been known for almost a century that the long-range Coulomb interaction still has a influence asymptotically and the solutions become a linear combination of

$$\sum_{lm} \sin(kr - \eta \ln 2kr - l\frac{\pi}{2} + \sigma_l)Y_{lm}(\hat{r}) \qquad (2)$$

and

$$\sum_{lm} \cos(kr - \eta \ln 2kr - l\frac{\pi}{2} + \sigma_l)Y_{lm}(\hat{r}), \qquad (3)$$

where $\eta = -1/k$ and σ_l is the *Coulomb phase* that is expressed with the complex gamma function

$$\sigma_l = \arg[\Gamma(l + 1 + i\eta)]. \qquad (4)$$

Because of the logarithmic phase the asymptotic wave never really becomes a pure sine or cosine. This is standard text book quantum mechanics.

Many particle Schrödinger equation

The scattering problem becomes notoriously more complicated when more than one particle is involved. Let us take a look at the hydrogen molecule H_2, the simplest molecular system, that consists out of two protons and two electrons. In the assumption that the electrons move much faster than the protons, we can look at the Schrödinger equation for the two electrons with the two protons remain fixed. Such a assumption is valid in the case of double photo-ionization, a fundamental proces where a single photon ionizes simultaneously the two electrons as a result the two proton are also free to escape. We can write this as the reaction $\hbar\omega + \mathrm{H}_2 \rightarrow e^- + e^- + p + p$. This proces is incredibly fast and it is valid to assume that the protons remain fixed during the ionization of the electron proces. Once the electrons are remove the to bare protons are left behind that start to repel each other. See [1] for description of the reaction.

The Schrödinger equation is then

$$(E_0 + \omega - H)\psi(\mathbf{r}_1, \mathbf{r}_2) = \epsilon \cdot (\nabla_{\mathbf{r}_1} + \nabla_{\mathbf{r}_2})\, \phi(\mathbf{r}_1, \mathbf{r}_2)$$

where $\phi(\mathbf{r}_1, \mathbf{r}_2)$ is the groundstate eigenfunction with eigenvalue E_0 of Hamiltonian H, defined below. The frequency ω is the energy of the photon and $\psi(\mathbf{r}_1, \mathbf{r}_2)$ is the six dimensional wavefunction describing the scattered motion of the two electrons. The vector ϵ denotes the polarization of the photon and $\nabla_{\mathbf{r}_1} + \nabla_{\mathbf{r}_2}$ the dipole operator that works on the electronic groundstate. The Hamiltoniaan H for this problem is

$$H = -\frac{1}{2}\Delta_{\mathbf{r_1}} - \frac{1}{2}\Delta_{\mathbf{r_2}} - \frac{1}{|\mathbf{r}_1 - \mathbf{R}_1|} - \frac{1}{|\mathbf{r}_2 - \mathbf{R}_1|} - \frac{1}{|\mathbf{r}_1 - \mathbf{R}_2|} - \frac{1}{|\mathbf{r}_2 - \mathbf{R}_2|} + \frac{1}{|\mathbf{r}_1 - \mathbf{r}_2|} \quad (5)$$

where we recognise the differential operators that correspond to the kinetic energy and several Coulomb potential interactions. We have the attraction of the first electron at $\mathbf{r}_1$ with the two protons respectively positioned at $\mathbf{R}_1$ and $\mathbf{R}_2$. Similarly, we have the attraction of the second electron r_2 with the two protons. Finally. there is the Coulomb repulsion between the two positively charged electrons.

Again we can write it as an effective Helmholtz equation for the wavefunction $u(\mathbf{x}, \mathbf{x}) = \psi(\mathbf{r}_1, \mathbf{r}_2)$. It is a six-dimensional equation

$$\Delta u(\mathbf{x}, \mathbf{y}) + k^2(\mathbf{x}, \mathbf{y}; \mathbf{R}_1, \mathbf{R}_2)u(\mathbf{x}, \mathbf{y}) = \mathbf{f}(\mathbf{x}, \mathbf{y}), \quad (6)$$

where the wave number now depends parametrically on the position fo the two protons.

In contrast to the one-particle problems, the asymptotic scattered wave for multiple charged particles is notoriously complicated and cannot be written in the form of (2) and (3) or any other simple analytical form. This finds its origin in the effective Coulomb interaction that in the asymptotic region depends sensitively to the relative positions of the charged particles.

Methods

To avoid that we have to know asymptotic wave at the boundary, we use an absorbing boundary condition known in the physics and chemistry community as *Exterior Complex Scaling* (ECS). It was introduced by B. Simon [2] and rotates the coordinates, from a certain hyperradius on, into the complex plane. The transformation is

$$r \rightarrow \begin{cases} r & \text{for} \quad r \leq R_0 \\ R_0 + (r - R_0)e^{i\eta} & \text{for} \quad r > R_0 \end{cases}, \quad (7)$$

where η is the complex rotation angle. The result is that all outgoing waves start to decay from this radius on and zero boundary conditions can be applied. This circumvents the application of the complicated boundary conditions based on the asymptotic Coulomb wave. A review can be found in [4].

The exterior complex scaling absorbing boundary conditions are very similar to the perfectly matched layers boundary condition [3].

The resulting equation is discretized and results in a large linear system $Ax = b$. It is solved with a preconditioned iterative Krylov subspace method [6].

Once the solution is found, the wavefunction is analyzed and information about the directions in which the particles escape after the reaction can be extracted. The results are then compared with experimental observations with the reaction microscopes.

Results and Conclusions

We have solved these equations for the double photoionization reaction in the hydrogen molecule and we have solved the problem at various distances between the two protons and have shown that the pattern of escaping electrons depends sensitively on this internuclear distance [5], [6], [7].

In figure 1, we reproduce the results of [7], where we have calculated the probability distribution of escaping electrons for a particular angle between the molecule and polarization direction of the photon. These probabilities are extracted from a six-dimensional wave function.

To conclude, since recently it has become possible to predict quantum mechanical breakup problems and solve the Schrödinger equations exactly for multiple charged particles. Until now only the simplest systems have been considered and many computational and mathematical challenges need to be solved before we can develop scalable methods that can solve these problems in more complex system of interest.

References

[1] T. Weber et al. *Nature* (London) 431, 437 (2004)

[2] B. Simon, *Phys. Lett. A*, **71**, 221 (1979).

[3] J. P. Berenger, *J. Comp. Phys.*, vol. 114, pp. 185-200, Oct. 1994.

[4] C. W. McCurdy, M. Baertschy, and T. N. Rescigno, *J. Phys. B***37**, R137 (2004).

[5] W. Vanroose, F. Martín, T. N. Rescigno, and C. W. McCurdy, *Science* **310**, 1787 (2005).,

[6] W. Vanroose, F. Martín, T. N. Rescigno, and C. W. McCurdy, *Phys. Rev. A* **74**, 052702 (2006).

[7] D. A. Horner *et al*, *Phys. Rev. Lett.* **98** 073001 (2007).

Acoustic Waves in Moving Media

A LOW MACH MODEL FOR TIME HARMONIC ACOUSTICS IN ARBITRARY FLOWS

A. S. Bonnet-Ben Dhia[†,*], **J. F. Mercier**[†], **F. Millot**[‡], **S. Pernet**[‡]
[†]POEMS, UMR 2706 CNRS-INRIA-ENSTA, Paris, France
[‡]CERFACS, Toulouse, France
[*]Email: anne-sophie.bonnet-bendhia@ensta.fr

Abstract

The reduction of noise in aeronautics motivates an intensive research in aeroacoustics. In particular, there is a need for efficient numerical tools to simulate acoustic propagation in a mean flow. We are interested here by solving the problem in the frequency domain, by a finite element method able to take into account general geometries and flows. Up to our knowledge, only the potential case (when the flow and the source are irrotational) has been completely handled. Recently, a more general approach has been developed and validated in the case of a parallel shear flow [1]: this method relies on a finite elements discretization combined with PMLs of a so-called regularized formulation of Galbrun's equation. We will show here how to extend this approach to the case of a non parallel flow. For simplicity, we restrict ourselves to the two-dimensional case.

1 Derivation of the modified Galbrun equation

1.1 Galbrun's equation

Consider a stationary subsonic flow of a perfect compressible fluid satisfying Euler's equations, characterized by the non uniform fields of velocity $\mathbf{v}_0$, density ρ_0, pressure p_0 and sound velocity c_0, and a time harmonic harmonic perturbation (with an $e^{-i\omega t}$ time dependence). Galbrun's equation, whose unknown is the perturbation of displacement $\mathbf{u}$, is obtained by a linearization process (see for example [2] or [3]). It reads as follows :

$$\rho_0 \frac{D^2\mathbf{u}}{Dt^2} - \nabla(\rho_0 c_0^2 \mathrm{div}\,\mathbf{u}) + \mathrm{div}\,\mathbf{u}\nabla p_0 - {}^t\nabla\mathbf{u}\cdot\nabla p_0 = 0 \quad (1)$$

where $\dfrac{D\mathbf{u}}{Dt} = -i\omega\mathbf{u} + \nabla\mathbf{u}\cdot\mathbf{v}_0$.

Notice that in the particular case of a parallel shear flow, ρ_0, p_0 and c_0 are uniform and Galbrun's equation reduces to:

$$\frac{D^2\mathbf{u}}{Dt^2} - c_0^2\nabla(\mathrm{div}\,\mathbf{u}) = 0. \quad (2)$$

It has been observed that a direct finite element resolution of (2) (using Lagrange elements) leads to a polluted result, due to a lack of H^1 coerciveness. A way to restore coerciveness is to consider the following "regularized" (or "augmented") formulation of (2) [4]:

$$\frac{D^2\mathbf{u}}{Dt^2} - c_0^2\nabla(\mathrm{div}\,\mathbf{u}) + c_0^2\mathbf{curl}(\mathrm{curl}\mathbf{u} - \psi) = 0$$

where the new unknown $\psi = \mathrm{curl}\mathbf{u}$ (the "vorticity") is introduced. We will extend this regularization technique to the general equation (1). Then a "hydrodynamic" relation between ψ and $\mathbf{u}$ will be derived and solved in the low Mach approximation.

1.2 Regularization

Let s_0 be a positive real function. The regularized equation associated to (1) is given by:

$$\begin{aligned}&\rho_0\frac{D^2\mathbf{u}}{Dt^2} - \nabla(\rho_0 c_0^2\mathrm{div}\,\mathbf{u}) + \mathbf{curl}(\rho_0 s_0(\mathrm{curl}\mathbf{u} - \psi))\\ &+\mathrm{div}\,\mathbf{u}\nabla p_0 - {}^t\nabla\mathbf{u}\cdot\nabla p_0 = 0\end{aligned} \quad (3)$$

The hydrodynamic equation is then derived by taking the curl of (1), which gives:

$$\mathrm{curl}\left(\rho_0\frac{D^2\mathbf{u}}{Dt^2} + \mathrm{div}\,\mathbf{u}\nabla p_0 - {}^t\nabla\mathbf{u}\cdot\nabla p_0\right) = 0$$

and after some calculations:

$$\frac{D^2\psi}{Dt^2} = -2\frac{D}{Dt}(\mathcal{B}\mathbf{u}) - \mathcal{C}\mathbf{u} \quad (4)$$

with $\mathcal{B}\mathbf{u} = \displaystyle\sum_{j=1}^{2}\nabla\mathbf{v}_{0,j}\wedge\frac{\partial\mathbf{u}}{\partial x_j}$ and

$$\begin{aligned}\mathcal{C}\mathbf{u} = &\sum_{j,k=1}^{2}\left(\frac{\partial\mathbf{v}_{0,k}}{\partial x_j}\nabla\mathbf{v}_{0,j}\wedge\frac{\partial\mathbf{u}}{\partial x_k} - \mathbf{v}_{0,j}\nabla\frac{\partial\mathbf{v}_{0,k}}{\partial x_j}\wedge\frac{\partial\mathbf{u}}{\partial x_k}\right)\\ &+\frac{1}{\rho_0}\sum_{j=1}^{2}\left(\frac{1}{\rho_0 c_0^2}\frac{\partial p_0}{\partial x_j}\nabla p_0 - \nabla\left(\frac{\partial p_0}{\partial x_j}\right)\right)\wedge\nabla u_j.\end{aligned}$$

Notice that for a shear flow, $\mathcal{C}\mathbf{u} = 0$.

1.3 Low Mach approximation

In the case of a shear flow, it was possible to derive an exact expression of ψ versus $\mathbf{u}$ as a convolution integral along the stream lines. It is not straightforward to extend this approach in the general case. However, under suitable hypotheses, simple approximations of ψ can be obtained. For instance, if we suppose that the flow is slow

and has slow variations (compared to the wavelength), we can neglect the contribution $\mathcal{C}\mathbf{u}$ in (4). Then if the mean flow does not present recirculations (closed streamlines), (4) is equivalent to $\frac{D\psi}{Dt} = -2\mathcal{B}\mathbf{u}$ whose solution has the following low Mach approximation:

$$\psi \approx \frac{2}{i\omega}\mathcal{B}\mathbf{u}. \tag{5}$$

Finally, using (3) and (5), we get the modified Galbrun equation which will be solved in practice:

$$\mathcal{G}^{LM}\mathbf{u} \stackrel{def}{=} \rho_0 \frac{D^2\mathbf{u}}{Dt^2} - \nabla(\rho_0 c_0^2 \mathrm{div}\,\mathbf{u}) + \mathrm{div}\,\mathbf{u}\nabla p_0$$
$$-{}^t\nabla\mathbf{u}\cdot\nabla p_0 + \mathbf{curl}\left(\rho_0 s_0\left(\mathrm{curl}\mathbf{u} - \frac{2}{i\omega}\mathcal{B}\mathbf{u}\right)\right) = 0$$

2 Setting of the diffraction problem

Let us now consider a particular diffraction problem which will be solved by using the previous model.

2.1 Geometry and incident wave

Let $\mathcal{O}$ be a bounded domain of $\mathbb{R}^2$ occupied by a rigid obstacle. The mean flow $(\mathbf{v}_0, \rho_0, p_0, c_0)$ is defined in $\mathbb{R}^2\backslash\mathcal{O}$ and is supposed to be almost uniform far from the obstacle :

$$\exists R > 0/ \text{ for } |x| > R,$$
$$\mathbf{v}_0(x) = v_\infty \mathbf{e}_1,\ (\rho_0(x), p_0(x), c_0(x)) = (\rho_\infty, p_\infty, c_\infty).$$

The regularization function s_0 is then chosen such that $s_0(x) = c_\infty^2$ for $|x| > R$. Then we can consider an incident wave which is for instance a downstream plane wave of this uniform medium $\mathbf{u}_{inc}(x) = e^{ik_\infty x_1}\mathbf{e}_1$ with $k_\infty = \frac{\omega}{c_\infty + v_\infty}$ and the diffraction problem is the following: Find $\mathbf{u} \in H^1_{loc}(\mathbb{R}^2\backslash\mathcal{O})$ such that:

$$\begin{array}{lll} \mathcal{G}^{LM}\mathbf{u} = 0 & \text{in} & \mathbb{R}^2\backslash\mathcal{O} \\ \mathbf{u}.\mathbf{n} = 0 & \text{on} & \partial\mathcal{O} \\ \mathrm{curl}\mathbf{u} - \dfrac{2}{i\omega}\mathcal{B}\mathbf{u} = 0 & \text{on} & \partial\mathcal{O} \\ \mathbf{u}_{dif} = \mathbf{u} - \mathbf{u}_{inc} \text{ is outgoing .} & & \end{array} \tag{6}$$

This radiation condition is precised in the next paragraph.

2.2 Radiation condition and PMLs

The hypothesis of uniformity of the flow far from the obstacle implies that:

$$\forall \mathbf{u} \in H^1_{loc}(\mathbb{R}^2\backslash\mathcal{O}), \quad \mathcal{B}\mathbf{u}(x) = 0 \text{ for } |x| > R.$$

As a consequence, for every solution $\mathbf{u}$ of (6), $\varphi = \mathrm{div}\,\mathbf{u}_{dif}$ and $\varphi = \mathrm{curl}\mathbf{u}_{dif}$ satisfy the convected Helmholtz equation far from the obstacle:

$$\frac{D_\infty^2\varphi}{Dt^2} - c_\infty^2\Delta\varphi = 0 \text{ for } |x| > R,$$

where $\frac{D_\infty}{Dt} = -i\omega + v_\infty\frac{\partial}{\partial x_1}$. It is well known that this equation is equivalent to a classical Helmholtz equation for $\tilde{\varphi}$ defined by:

$$\tilde{\varphi}(x_1/\tau_\infty, x_2) = \varphi(x_1, x_2)e^{ik\nu_\infty x_1}$$

with $\tau_\infty = 1 - \frac{v_\infty^2}{c_\infty^2}$ and $\nu_\infty = \frac{v_\infty}{\tau_\infty c_\infty}$. Then we say that φ is outgoing if $\tilde{\varphi}$ is outgoing (in the classical sense) and we say that $\mathbf{u}_{dif}$ is outgoing if $\mathrm{div}\,\mathbf{u}_{dif}$ and $\mathrm{curl}\mathbf{u}_{dif}$ are outgoing.

In practice, we use PMLs to select this outgoing solution (other methods like a coupling with an integral representation could also be used). The computational domain is defined by $\Omega_L = B_L\backslash\mathcal{O}$ where

$$B_L = \{(x_1, x_2)/|x_1| < R + L \text{ and } |x_2| < R + L\}$$

where L denotes the width of the absorbing layers. The model in the PMLs involves a complex parameter α such that $\Re e(\alpha) > 0$ and $\Im m(\alpha) < 0$. Finally, the problem that we solve is the following: find $\mathbf{u}_{dif} \in H^1_{loc}(\Omega_L)$ such that:

$$\begin{array}{lll} \mathcal{G}^{LM}_\alpha\mathbf{u}_{dif} = \mathbf{f}_{inc} & \text{in} & \Omega_L \\ \mathbf{u}_{dif}.\mathbf{n} = 0 & \text{on} & \partial\mathcal{O} \\ \mathrm{curl}_\alpha\mathbf{u}_{dif} - \dfrac{2}{i\omega}\mathcal{B}_\alpha\mathbf{u}_{dif} = 0 & \text{on} & \partial\mathcal{O} \\ \mathbf{u}_{dif} = 0 & \text{on} & \partial B_L \end{array} \tag{7}$$

where $\mathbf{f}_{inc}$ is a source term coming from the incident wave and where the index α means that the corresponding operator has been modified according to the following substitution:

$$\frac{\partial}{\partial x_i} \to \alpha_i(x)\frac{\partial}{\partial x_i}$$

with α_i defined by:

$$\alpha_i(x) = \left\{ \begin{array}{lll} 1 & \text{if} & |x_i| < R \\ \alpha & \text{if} & |x_i| > R. \end{array} \right.$$

2.3 Well-posedness

To prove well-posedness of problem (7), we derive its variational form ($\mathbf{u}_{dif}$ is denoted $\mathbf{u}$ for simplicity):

$$\begin{array}{l} \text{Find } \mathbf{u} \in V \text{ such that } \forall \mathbf{v} \in V \\ a(\mathbf{u}, \mathbf{v}) + b(\mathbf{u}, \mathbf{v}) + c(\mathbf{u}, \mathbf{v}) = \ell(\mathbf{v}) \end{array} \tag{8}$$

where

$$V = \{\mathbf{u} \in H^1(\Omega_L)^2; \mathbf{u}.\mathbf{n}_{|\partial\mathcal{O}} = 0 \text{ and } \mathbf{u}_{|\partial B_L} = 0\},$$

$$a(\mathbf{u},\mathbf{v}) = \big(\rho_0 c_0^2 \mathrm{div}_{\,\alpha}\mathbf{u}, \mathrm{div}_{\,\alpha}\mathbf{v}\big) + \big(\rho_0 s_0 \mathrm{curl}_\alpha \mathbf{u}, \mathrm{curl}_\alpha \mathbf{v}\big) - \big((\mathbf{v}_0\cdot\nabla_\alpha)\mathbf{u}, (\mathbf{v}_0\cdot\nabla_\alpha)\mathbf{v}\big),$$

$$b(\mathbf{u},\mathbf{v}) = -\frac{2}{i\omega}\big(\rho_0 s_0 \mathcal{B}_\alpha \mathbf{u}, \mathrm{curl}_\alpha \mathbf{v}\big)$$

and $c(\mathbf{u},\mathbf{v})$ contains the compact perturbation. To prove coerciveness, we first use Costabel's inequality [5] and establish the following Garding inequality:
if $|\mathbf{v}_0|^2 < s_0 \leq c_0^2$ $\quad a.e.$ there exists $\beta_1 > 0$ and $\beta_2 > 0$ such that:

$$|a(\mathbf{u},\mathbf{u})| \geq \beta_1 \|\mathbf{u}\|^2_{H^1(\Omega_L)} - \beta_2 \|\mathbf{u}\|^2_{L^2(\Omega_L)} \quad \forall \mathbf{u} \in V.$$

Then, we prove that the hydrodynamic term $b(\mathbf{u},\mathbf{u})$ is controlled if $\nabla \mathbf{v}_0$ is not too large (compared to ω), so that finally, the problem is of Fredholm type.

3 Numerical results

We consider the diffraction case by a circle of center $(0,0)$ and with radius r. If one assumes that the fluid is incompressible and the flow is potential (ie $\mathbf{v}_0 = \nabla\varphi_0$), the characteristics of the mean flow can be analytically derived . In particular, $\varphi_0 = v_\infty x_1 \left(1 + r^2/(x_1^2+x_2^2)\right)$. Since the scatterer is illuminated by an incident plane wave, the perturbed flow is still potential and this problem can be solved. We have considered a finite element discretization of the problem: Find $\varphi_a \in H^1_{loc}(\mathbb{R}^2\backslash\mathcal{O})$ (φ_a is the perturbed potential) such that:

$$\begin{aligned}
&\mathrm{div}\,(\rho_0(I - {}^tM_0M_0)\nabla\varphi_a) + \rho_0 k_0^2 \varphi_a + \\
&ik_0\rho_0 M_0\cdot\nabla\varphi_a + \mathrm{div}\,(ik_0\rho_0\varphi_a M_0) = 0 \text{ in } \mathbb{R}^2\backslash\mathcal{O} \\
&\frac{\partial\varphi_a}{\partial\mathbf{n}} = 0 \text{ on } \partial\mathcal{O} \\
&\varphi_a - \varphi_{a,inc} \text{ is outgoing}
\end{aligned}$$

where $M_0 = \mathbf{v}_0/c_0$ and $k_0 = \omega/c_0$. Consequently, numerical results of this potential model can be compared with those obtained from the low Mach model (8). The perturbation of the Euler speed $\mathbf{v}_a$ [3] is computed with the relation $\mathbf{v}_a = \nabla\varphi_a = \dfrac{D\mathbf{u}}{Dt} - \nabla\mathbf{v}_0\cdot\mathbf{u}$ and can be compared. Numerical results are done with the finite element library MÉLINA [6] and are given for $\omega = 5$, $r = 1.25$ and $v_\infty = 0.1$. Fig. 1 shows the speed components of the mean flow. A mean variation of the speed near the circle can be seen. In particular, the maximum of $\mathbf{v}_{0x}$ is $2v_\infty$. This simple test case contains the main difficulties which we want to treat. Fig. 2 shows the component $\mathbf{v}_{ax}$ of the perturbation of the Euler speed. The two methods clearly simulate the same phenomena.

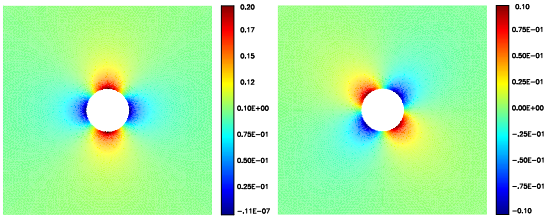

Figure 1: $\mathbf{v}_{0x}$ (left) and $\mathbf{v}_{0y}$ (right)

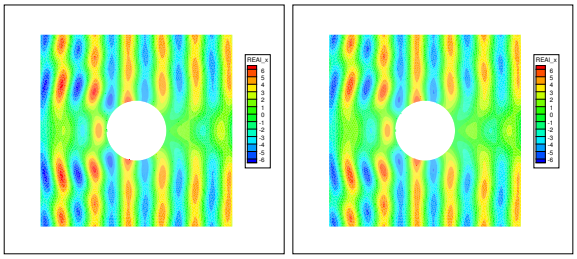

Figure 2: $\mathbf{v}_{ax}$(potential case (left) and low Mach model (right))

References

[1] A. S. Bonnet-BenDhia, E. M. Duclairoir and J. F. Mercier, "Acoustic propagation in a flow: numerical simulation of the time-harmonic regime". Proceedings du CANUM 2006, à paraître dans ESAIM Procs.

[2] B. Poirée, "Les équations de l'acoustique linéaire et non linéaire dans un écoulement de fluide parfait", Acustica, 57, pp. 5–25, 1985.

[3] G. Legendre, "Rayonnement acoustique dans un fluide en écoulement : analyse mathématique et numérique de l'équation de Galbrun", Thèse de l'Université Paris VI, 2003.

[4] A. S. Bonnet-BenDhia, E. M. Duclairoir, G. Legendre and J. F. Mercier, "Time-harmonic acoustic propagation in the presence of a shear flow", J. of Comp. and App. Math., 2007.

[5] M. Costabel, "A coercive bilinear form for Maxwell's equations", J. Math. Anal. Appl., 157, pp. 527-541, 1991.

[6] D. Martin, "On line documentation of MÉLINA", http://perso.univ-rennes1.fr/daniel.martin/melina/.

HYDRODYNAMICS INSTABILITIES IN THE ACOUSTIC WAVE SYSTEM

O. Lafitte[†,*], **R. Poncet**[‡,*]
[†]Institut Galilée, Université de Paris 13, F-93 430 Villetaneuse, France
[‡]IRMAR, ENS Cachan Bretagne, av. R. Schuman, F-35 170 Bruz, France
[*]Email: olivier.lafitte@mines.org, poncet@bretagne.ens-cachan.fr

Abstract

We study the system of 2D isentropic Euler equations with a gravity term in the neighborhood of a null velocity profile and a given density profile. We perform the classical (see [3]) high frequency analysis as well as the stability analysis. The linear system admits high frequency approximate solutions associated with the acoustic wave equation. However, we prove the existence of unstable normal modes similar to the Rayleigh unstable modes for the incompressible model ([1], [2]).

Introduction and physical model

We consider a Newtonian nonviscous fluid subjected to a gravity force $(g, 0)$, which follows the first principle of thermodynamics (which means that the entropy S is solution of the conservation law $\partial_t S + \nabla\cdot(S\vec{u}) = 0$). The equations of motion are the compressible Euler equations:

$$\begin{aligned}
&\partial_t \rho + \nabla\cdot(\rho\vec{u}) = 0,\\
&\partial_t(\rho\vec{u}) + \nabla\cdot(\rho\vec{u}\otimes\vec{u} + p\,\mathrm{Id}) = \rho\vec{g},\\
&\partial_t E + \nabla\cdot\big((E+p)\vec{u}\big) = \rho\vec{u}\cdot\vec{g},\\
&\partial_t S + \nabla\cdot(S\vec{u}) = 0,
\end{aligned}$$

where $E = \frac{1}{2}\rho|\vec{u}|^2 + \rho e$, p being the pressure of the fluid, e being the internal energy of the fluid, solutions of $\partial_t e + \vec{u}\cdot\nabla e + \frac{p}{\rho}\nabla\cdot\vec{u} = 0$, $\partial_t p + \vec{u}\cdot\nabla p + \rho c^2\nabla\cdot\vec{u} = 0$, c denoting the sound speed. The previous system rewrites:

$$\begin{aligned}
&\partial_t \rho + \nabla\cdot(\rho\vec{u}) = 0,\\
&\partial_t p + \vec{u}\cdot\nabla p + \rho c^2\nabla\cdot\vec{u} = 0,\\
&\partial_t(\rho\vec{u}) + \nabla\cdot(\rho\vec{u}\otimes\vec{u} + p\,\mathrm{Id}) = \rho\vec{g},\\
&\partial_t s + \vec{u}\cdot\nabla s = 0,
\end{aligned} \tag{1}$$

where $s = S/\rho$ is the specific entropy.

The first step is to linearize the Euler equations around a given steady state of the form $(\rho_0, p_0, 0, 0, s_0)$. Note that this steady state depends only on x thanks to $\vec{g} = (g, 0)$. One obtains:

$$\begin{aligned}
&\partial_t \rho + \nabla\cdot(\rho_0\vec{u}) = 0,\\
&\partial_t p + \vec{u}\cdot\nabla p_0 + \rho_0 c_0^2\nabla\cdot\vec{u} = 0,\\
&\partial_t(\rho_0\vec{u}) + \nabla p = \rho\vec{g},\\
&\partial_t s + \vec{u}\cdot\nabla s_0 = 0.
\end{aligned} \tag{2}$$

In a first section, we study the high frequency asymptotic analysis of this system. Writing each quantity as $h_1 e^{ik\phi(x,y,t)}$, one deduces that the waves decompose into travelling waves of phase ϕ solution of the classical eikonal equation for the waves $(\partial_t\phi)^2 = c_0^2|\nabla\phi|^2$, and steady waves of phase ϕ independent of t.

In a second section, we prove that there is a limiting (exponential) growth rate in time Λ for any solution of the linear system. The value of Λ is linked with $\nabla p_0.\nabla\rho_0$ (characterizing in the physical literature a Rayleigh-Taylor instability) and $\frac{g^2}{c_0^2}$.

In a third section, in order to identify unstable modes, we perform a normal mode analysis, that is we write all the quantities h in this system as $h(x, y, t) = \tilde{h}(x)e^{iky+\gamma t}$. Since the steady state depends only on x, we denote by c_0', ρ_0', and p_0' the derivatives of c_0, ρ_0 and p_0 (hence, for example, $\nabla p_0 = (p_0', 0)$). We obtain an equation on $\tilde{u}$, and prove that γ satisfies

$$0 \in \mathrm{Sp}\big(-\frac{1}{k^2}\frac{\mathrm{d}^2}{\mathrm{d}x^2} + \tilde{q}_0(x, \gamma, k)\big), \tag{3}$$

the function $\tilde{q}_0$ being given below by (8).

We then prove that, for k large enough, there is at least one value of $\gamma > 0$ satisfying (3), as in [2].

In conclusion, in system (2), we have asymptotic high frequency propagating waves, and unstable solutions generated by the steady asymptotic waves.

High frequency analysis

We consider an asymptotic solution

$$(\rho, p, u, v, s)^t = (\rho_1, p_1, u_1, v_1, s_1)^t e^{ik\phi(x,y,t)},$$

where all quantities f_1 admit an asymptotic expansion in k of the form $f_1(x, y, t, k) = \sum_{j=0}^{\infty} f_{1,j}(x, y, t)(ik)^{-j}$.

System (2) rewrites:

$$ik\begin{pmatrix} \partial_t\phi & 0 & \rho_0\partial_x\phi & \rho_0\partial_y\phi & 0 \\ 0 & \partial_t\phi & \rho_0c_0^2\partial_x\phi & \rho_0c_0^2\partial_y\phi & 0 \\ 0 & \partial_x\phi & \rho_0\partial_t\phi & 0 & 0 \\ 0 & \partial_y\phi & 0 & \rho_0\partial_t\phi & 0 \\ 0 & 0 & 0 & 0 & \partial_t\phi \end{pmatrix}\begin{pmatrix} \rho_1 \\ p_1 \\ u_1 \\ v_1 \\ s_1 \end{pmatrix} = -\begin{pmatrix} \partial_t\rho_1 + \nabla.(\rho_0\vec{u}_1) \\ \partial_t p_1 + p_0'u_1 + \rho_0c_0^2\nabla.\vec{u}_1 \\ \rho_0\partial_t u_1 + \partial_x p_1 - \rho_1 g \\ \rho_0\partial_t v_1 + \partial_y p_1 \\ s_0'u_1 \end{pmatrix}. \tag{4}$$

We derive the **eikonal** equation and prove that we can apply the projection method (see [4]).

The eikonal equation is obtained by considering a nonzero solution $U = (\rho_{1,0}, p_{1,0}, u_{1,0}, v_{1,0}, s_{1,0})^t$ of (4). Hence, its matrix $M(x, y, \partial_t\phi, \nabla\phi)$ has a null determinant, and:

$$(\partial_t\phi)^3\big((\partial_t\phi)^2 - c_0^2(\nabla\phi)^2\big) = 0. \tag{5}$$

Notice that if $\partial_t\phi = 0$, the dimension of the kernel K_0 of $M(x, y, \partial_t\phi, \nabla\phi)$ is 3, and it is characterized by the two equations $p_{1,0} = 0$, $\partial_x\phi u_{10} + \partial_y\phi v_{1,0} = 0$.

If we consider a solution of the eikonal equation which does not satisfy $\partial_t\phi = 0$, one deduces that ϕ is solution of $(\partial_t\phi)^2 = c_0^2(\nabla\phi)^2$ — it is the eikonal equation for the acoustic wave equation $\partial^2_{t^2}p = c_0^2\Delta p$.

Introducing $\pi_\pm$ the projection on the kernel of M along the range of M when ϕ satisfies $\partial_t\phi \pm c_0|\nabla\phi| = 0$, the compatibility condition writes $\pi_\pm U = U$, the transport equation writes $\pi_\pm M(x, y, \partial_t, \partial_x, \partial_y)\pi_\pm U + \mu_\pm(x, y, t)\pi_\pm U = 0$, where $\mu_p m$ is the group velocity associated with the equation $\partial_t\phi \pm c_0|\nabla\phi| = 0$. Hence we obtain the classical asymptotic solutions associated with the acoustic forward and backward waves. It is not our purpose here to describe these solutions ; it is enough to notice that the hyperbolic behavior can be analyzed even if we cannot extract a natural scalar wave equation of order two from the Euler system with a Rayleigh-Taylor term. For more details and related studies, see [3], [4].

We may finally notice that the eigenvector associated with the eikonal equation $\partial_t\phi = c_0|\nabla\phi|$ is

$$\big(\rho_0, \rho_0c_0^2, -\rho_0\frac{\partial_x\phi}{|\nabla\phi|}, \rho_0\frac{\partial_y\phi}{|\nabla\phi|}, 0\big),$$

which gives the polarization of the forward high frequency acoustic wave.

In the next sections, we derive unstable in time solutions associated with this system. These solutions correspond to a Rayleigh-Taylor instability.

Universal growth rate

We notice that system (2) implies

$$\rho_0\partial_t^2\vec{u} + \mathcal{L}\vec{u} = 0,$$

where $\mathcal{L}$ is a symmetric operator (e.g. $\int \mathcal{L}\vec{u}\cdot\vec{v}\,dxdy = \int \mathcal{L}\vec{v}\cdot\vec{u}\,dxdy$). This implies that $\frac{\mathrm{d}}{\mathrm{d}t}\frac{1}{2}\int \mathcal{L}\vec{u}\cdot\vec{u}\,dxdy = \int \mathcal{L}\vec{u}\cdot\partial_t\vec{u}\,dxdy$.

From this equality, we deduce the identity

$$\forall t \geq 0, \quad \frac{1}{2}\int \rho_0|\partial_t\vec{u}|^2\,dxdy + \frac{1}{2}\int \mathcal{L}\vec{u}\cdot\vec{u}\,dxdy = A_0.$$

Under the assumption $\vec{g}\wedge\nabla\rho_0 = 0$, and using identity

$$\int \mathcal{L}\vec{u}\cdot\vec{u}\,dxdy = \int \rho_0\big(c_0\nabla\cdot\vec{u} + \frac{1}{c_0}\vec{g}\cdot\vec{u}\big)^2dxdy + \int \rho_0(\vec{g}.\vec{u})^2\big(\frac{\vec{g}\cdot\nabla\rho_0}{g^2} - \frac{1}{c_0^2}\big)dxdy,$$

one deduces

$$\int \rho_0|\partial_t\vec{u}|^2dxdy \leq 2A_0 + \Lambda^2\int \rho_0|\vec{u}|^2dxdy,$$

where $\Lambda = (\max(0, \max(\frac{g^2}{c_0^2} - g\frac{\rho_0'}{\rho_0}))^{\frac{1}{2}}$. Note that Λ is strictly positive when we have a Rayleigh-Taylor instability, that is $g\rho_0' = \rho_0^{-1}\nabla p_0\cdot\nabla\rho_0 < 0$. It may also be positive even in the case $\nabla p_0\cdot\nabla\rho_0 > 0$, hence leading to an instability generated with the sound velocity. This implies the following inequality:

$$\Big(\int \rho_0|\vec{u}|^2\Big)^{\frac{1}{2}} \leq \frac{\sqrt{2A_0}}{\Lambda}\sinh\big(\theta(0) + \frac{\Lambda}{\sqrt{2A_0}}t\big), \tag{6}$$

$\theta(0)$ being given by $\Lambda(\int \rho_0|\vec{u}|^2)^{\frac{1}{2}} = \sqrt{2A_0}\sinh\big(\theta(0)\big)$.

Normal modes solutions

In this section, we prove that the instability growth rate Λ appearing in the previous section may correspond to unstable modes. For a normal mode solution, (2) rewrites:

$$\begin{aligned} &\gamma\rho + \rho_0'u + \rho_0\frac{\mathrm{d}u}{\mathrm{d}x} + ik\rho_0v = 0, \\ &\gamma p + p_0'u + \rho_0c_0^2\big(\frac{\mathrm{d}u}{\mathrm{d}x} + ikv\big) = 0, \\ &\gamma\rho_0u + \frac{\mathrm{d}p}{\mathrm{d}x} = \rho g, \\ &\gamma\rho_0v + ikp = 0, \\ &\gamma s + s_0'u = 0. \end{aligned}$$

We deduce from the second and the fourth equalities of this system that v is given by

$$v = \frac{ik}{\gamma^2 + k^2 c_0^2}\big(gu + c_0^2 \frac{\mathrm{d}u}{\mathrm{d}x}\big).$$

Hence, γp and $\gamma\rho$ are given, thanks to the first and the second equation of the system, in terms of u. We thus deduce, from identity $\gamma^2\rho_0 u + \frac{\mathrm{d}}{\mathrm{d}x}(\gamma p) = \gamma\rho_0 g$, the following equation:

$$\rho_0\gamma^2 u - \frac{\mathrm{d}}{\mathrm{d}x}\big(\rho_0 c_0^2 \frac{\mathrm{d}u}{\mathrm{d}x}\big) - \frac{k^2\rho_0 g}{\gamma^2 + k^2 c_0^2}\big(gu + c_0^2\frac{\mathrm{d}u}{\mathrm{d}x}\big) + \frac{\mathrm{d}}{\mathrm{d}x}\big(\frac{k^2 c_0^2\rho_0}{\gamma^2 + k^2 c_0^2}(gu + c_0^2\frac{\mathrm{d}u}{\mathrm{d}x})\big) = 0. \quad (7)$$

Notice that, multiplying this equation by $\bar{u}$ and integrating, one deduces that γ^2 is real, which implies that the growth rate γ is either real, or purely imaginary. Using the new unknown $\omega = c_0\gamma\sqrt{\frac{\rho_0}{\gamma^2 + c_0^2 k^2}}u = a_0^{1/2}u$, equation (7) yields:

$$\Big[1 - \frac{1}{\gamma^2}\big(-g\frac{\rho_0'}{\rho_0} + \frac{g^2}{c_0^2}\big) + \frac{1}{k^2}\big(\gamma^2 + 2g\frac{c_0'}{c_0}\frac{k^2c_0^2}{\gamma^2 + k^2c_0^2} + \frac{(\sqrt{a_0})''}{\sqrt{a_0}}\big)\Big]\omega = \frac{1}{k^2}\frac{\mathrm{d}^2\omega}{\mathrm{d}x^2}.$$

Introducing

$$\tilde{q}_0(x,\gamma,k) = \frac{1}{k^2}\big(\gamma^2 + 2g\frac{c_0'}{c_0}\frac{k^2c_0^2}{\gamma^2 + k^2c_0^2} + \frac{(\sqrt{a_0})''}{\sqrt{a_0}}\big) + 1 - \frac{1}{\gamma^2}\big(-g\frac{\rho_0'}{\rho_0} + \frac{g^2}{c_0^2}\big), \quad (8)$$

the Rayleigh equation (7) is equivalent to the Schrödinger equation

$$Q\omega = -\frac{1}{k^2}\frac{\mathrm{d}^2\omega}{\mathrm{d}x^2} + \tilde{q}_0(x,\gamma,k)\omega = 0.$$

Hence, it has a solution if and only if 0 is in the spectrum of the operator Q.

Consider the additional hypothesis that the maximum Λ^2 of $-g\frac{\rho_0'}{\rho_0} + \frac{g^2}{c_0^2}$ is non degenerate. Using the methods of [2], one deduces that the spectrum of Q contains points of the form $1 - \frac{\Lambda^2}{\gamma^2} + o(k^{-1})$. Hence, equality $1 - \frac{\Lambda^2}{\gamma^2} + o(k^{-1}) = 0$, that is $\gamma = \Lambda + o(k^{-1})$, leads to a null eigenvalue for Q.

Note finally that the eigenvector, in the normal mode hypothesis, for $\gamma > 0$, is given by:

$$\Big(\frac{\rho_0}{\gamma}\big(\frac{gk^2}{\gamma^2 + k^2c_0^2} - \frac{\rho_0'}{\rho_0}\big)\hat{u} - \frac{\rho_0\gamma}{\gamma^2 + k^2c_0^2}\frac{\mathrm{d}\hat{u}}{\mathrm{d}x}, -\frac{\rho_0\gamma}{\gamma^2 + k^2c_0^2}\big(g\hat{u} + c_0^2\frac{\mathrm{d}\hat{u}}{\mathrm{d}x}\big), \hat{u}, \frac{ik}{\gamma^2 + k^2c_0^2}(g\hat{u} + c_0^2\frac{\mathrm{d}\hat{u}}{\mathrm{d}x}), -\frac{s_0'}{\gamma}\hat{u}\Big),$$

where $\hat{u}$ is solution of the Rayleigh equation (7). It does not belong to K_0.

Remark. The existence of an unstable mode can also be deduced from the existence of a variational equality in the system, as in [2], [6].

References

[1] H.-J. Hwang, Y. Guo, *On the dynamical Rayleigh-Taylor instability*, Arch. Rat. Mech. Anal. **167** , no. 3, 235–253 (2003).

[2] B. Helffer, and O. Lafitte, *Asymptotic growth rate for the linearized Rayleigh equation for the Rayleigh-Taylor instability*, Asymptotic Analysis **33**, 189–235 (2003)

[3] J.L. Joly, G. Métivier, J. Rauch, *Generic rigorous asymptotic expansions for weakly nonlinear multidimensional osillatory waves*, Duke Math J., **70**, 373–404 (1993)

[4] O. Lafitte, Y. Noumir, *High frequency asymptotics for the Euler aeroacoustics system*, Journal of Computational and Applied Mathematics 204 , 537–548 (2007)

[5] O. Lafitte, R. Poncet, *The Rayleigh-Taylor instability for compressible fluids*, in preparation

[6] C. Besse, P. Degond, H.-J. Hwang, R. Poncet, *Nonlinear instability of the two-dimensional striation model about smooth steady states*, accepted for publication in Comm. P. D. E. (2007)

Complex Materials

A NON LOCAL SCHRÖDINGER MODEL FOR THE PROPAGATION OF WAVES IN A PHOTOREFRACTIVE MEDIUM

B. Bidégaray-Fesquet[†,*]

[†]Laboratoire Jean-Kuntzmann, CNRS UMR 5224, B.P. 53, 38041 Grenoble Cedex 9, France
[*]Email: Brigitte.Bidegaray@imag.fr

Abstract

We present various mathematical results (Cauchy problem, solitary waves) for the Zozulya–Anderson model which describes the propagation of an optical wave through a photorefractive medium. This is a joint work with Jean-Claude Saut.

1 Introduction

Photorefractive media are optical material, highly anisotropic, with memory effects. They are commonly used to realize optically induced gratings or for holographic applications.

The propagation of an optical wave in insulating or semi-insulating electrooptical crystals induces a charge transfer. The new distribution of charges ρ induces in turn an electric field $\mathbf{E}$, with $\nabla \cdot (\widehat{\varepsilon}\mathbf{E}) = \rho$. This field derives from a potential φ and produces a variation δn of the refraction index in the main direction of the photovoltaic effect (which we choose here to be x): $\delta n \propto \partial_x \varphi$. The main characteristics of this effect are the following: 1- Sensibility to energy (and not to the electric field). This recalls the Kerr effect and the cubic nonlinear Schrödinger equation. 2- Nonlocal effect (charge distributions and the electric field are not located at the same position). 3- Inertia (charges need a certain time to move). We will not take this into account here. 4- Memory and reversibility (in the dark the space charge, and therefore the index variation, is persistent but an uniform light redistributes uniformly all charges — this yields applications to holography). We will also neglect this effect here, reducing our study to material where only electrons are moving.

2 Mathematical setting

A complete mesoscopic model for the modeling of photo-refractive media is the Kukhtarev model [6]. In the case when the charges that contribute to the photorefractive effect are only electrons (insulating media), an asymptotic study allows to derive a macroscopic model, the Zozulya–Anderson model. The complete assumptions and approximations made are precisely described in [2].

The description of the propagation of a laser through the photorefractive material is given by a Schrödinger equation using paraxial and envelope approximations. The propagation axis is chosen to be z and all constants are taken to be 1, which can be justified rigorously using dimensionless variables (see [2]). One obtains

$$\left[\partial_z - \frac{i}{2}\nabla_\perp^2\right] A = -iA\partial_x\varphi.$$

If we specify a material (e.g. $LiNbO_3$) and therefore symmetries of the tensor $\widehat{\varepsilon}$, we can write an equation for φ which reads

$$\nabla_\perp^2\varphi + \nabla_\perp \ln(1+|A|^2)\cdot\nabla_\perp\varphi = \partial_x \ln(1+|A|^2).$$

These are the Zozulya–Anderson equations [10].

If we look at a wider class of materials we may have different signs for the nonlinearity (in reference to the cubic nonlinear Schrödinger equation, the case $a = 1$ is classically called the focusing case, and $a = -1$ the defocusing case). Besides mathematicians are more accustomed to use t as the evolution variable. Finally logarithms are difficult to handle in the mathematical analysis (although natural if we look at 1D solitary waves, see below), we therefore rewrite also the equation for φ. We finally impose an initial data A_0 in some convenient (see below) functional space and obtain the system

$$\text{(ZA)} \left\{ \begin{array}{rcl} i\partial_t A + \Delta A &=& -aA\partial_x\varphi, \\ \operatorname{div}\left((1+|A|^2)\nabla\varphi\right) &=& \partial_x(|A|^2), \\ A(\cdot,0) &=& A_0. \end{array} \right.$$

The main effects take place in the t (propagation) and the x directions. It is therefore natural to study the equations with no dependence in the y variable. In the one dimensional case, since we assume furthermore that no external field is applied, we can immediately infer that $\partial_x\varphi = |A|^2/(1+|A|^2)$. We therefore consider the saturated non linear Schrödinger equation

$$\text{(SNLS)} \left\{ \begin{array}{rcl} i\partial_t A + \Delta A &=& -a\dfrac{|A|^2 A}{1+|A|^2}, \\ A(\mathbf{x},0) &=& A_0(\mathbf{x}), \end{array} \right.$$

where $a = \pm 1$, $A = A(\mathbf{x},t)$ and $\mathbf{x} \in \mathbb{R}^d$. We have derived this equation for $d = 1$, but give here results for a

general d, which also arises in other contexts, such as the propagation of a laser beam in gas vapors [9].

In the two-dimensional case (ZA) can be viewed as a saturated version of a Davey–Stewartson system. Namely, replacing $1 + |A|^2$ by 1 in the left hand-side of (ZA) we obtain a Davey–Stewartson system of the elliptic–elliptic type (see Ghidaglia and Saut [4]).

3 The Cauchy problem

3.1 The generalized saturated NLS equation

Theorem 1 *(i) Let $A_0 \in L^2(\mathbb{R}^d)$. Then there exists a unique solution $A \in \mathcal{C}(\mathbb{R}; L^2(\mathbb{R}^d))$ of (SNLS) which satisfies furthermore $\mathcal{E}(t) = \mathcal{E}(0)$ for all $t \in \mathbb{R}$, where*

$$\mathcal{E}(t) \equiv \int_{\mathbb{R}^d} |A(t)|^2 d\mathbf{x}.$$

(ii) Let $A_0 \in H^1(\mathbb{R}^d)$. Then the solution above satisfies $A \in \mathcal{C}(\mathbb{R}; H^1(\mathbb{R}^d))$ and $\mathcal{H}(t) = \mathcal{H}(0)$ for all $t \in \mathbb{R}$, where

$$\mathcal{H}(t) \equiv \int_{\mathbb{R}^d} \left[|\nabla A(t)|^2 d\mathbf{x} + a \ln(1 + |A(t)|^2) \right] d\mathbf{x}.$$

The proof follows the usual steps for nonlinear Schrödinger equations. Contrarily to the context of the usual nonlinear cubic Schrödinger equation, the solution is global in time, whatever the sign of a. Saturation prevents from blowing up.

We would like to mimic this proof to treat (ZA). To this aim we would like to express A in terms of φ for say $A \in L^2(\mathbb{R}^2)$. With such a data A, we indeed have a unique φ in some convenient space but no Lipschitz regularity for the mapping $A \mapsto \varphi$, which is required to perform some fixed point procedure. To ensure this we will have to assume $A \in H^2(\mathbb{R}^2)$.

Theorem 2 *Let $A_0 \in H^2(\mathbb{R}^2)$. Then there exists $T_0 > 0$ and a unique solution $(A, \nabla\varphi)$ of (ZA) such that $A \in \mathcal{C}([0, T_0]; H^2(\mathbb{R}^2))$ and $\nabla\varphi \in \mathcal{C}([0, T_0]; H^2(\mathbb{R}^2))$. Moreover for all $0 \le t \le T_0$*

$$\|A(t)\|_{L^2(\mathbb{R}^2)} = \|A_0\|_{L^2(\mathbb{R}^2)}$$

and

$$\int_{\mathbb{R}^2} (1 + \frac{1}{2}(t)|A|^2)|\nabla\varphi(t)|^2 d\mathbf{x} \le \frac{1}{2} \int_{\mathbb{R}^2} |A_0|^2 d\mathbf{x}.$$

The proof of this result necessitates many steps. Uniqueness results follows from simple energy estimates. Then we derive a H^2 *a priori* estimate of the solution of (ZA). We introduced an approximate system for which the well-posedness stems from classical fixed point arguments and the convergence towards (ZA) is first obtained in $L^\infty(0, T; H^2(\mathbb{R}^2))$ using the Aubin–Lions compactness lemma [7]. The final existence result in $\mathcal{C}([0, T]; H^2(\mathbb{R}^2))$ follows from the Bona–Smith approximation [3]. We do not have any hint on whether this local solution is global or not.

4 Solitary waves

4.1 First integrals for 1D solitary waves

1D bright solitary waves are sought for in the form $A(x, t) = e^{i\omega t}u(x)$ (see [8]), where A is a solution to (SNLS). The function u is supposed to have a maximum at $x = 0$ ($u(0) = u_m > 0$ and $u'(0) = 0$). We furthermore want that for $x \to \infty$, $u(x) \to 0$ and $u'(x) \to 0$. This yields a unique possible frequency for the solitary wave, namely

$$\omega = a \left(1 - \frac{\ln(1 + u_m^2)}{u_m^2} \right)$$

and imposes $a = 1$ (focusing case). The bright solitary wave is solution to the first order equation

$$u'(x) = -\text{sign}(x) \sqrt{\ln(1 + u^2) - \frac{u^2}{u_m^2} \ln(1 + u_m^2)}.$$

4.2 Non existence of solitary waves for (SNLS) and (ZA)

Consider now the (bright) solitary wave solutions of (SNLS) of the type $A(\mathbf{x}, t) = e^{i\omega t}U(\mathbf{x})$, where $U \in H^1(\mathbb{R}^d)$. It is solution to the elliptic equation

$$-\Delta U + \omega U = a \frac{|U|^2 U}{1 + |U|^2}, \qquad U \in H^1(\mathbb{R}^d).$$

Proposition 3 *No non-trivial ($U \not\equiv 0$) solitary wave of (SNLS) exists when*
(i) $a = -1$ (defocusing case), for $\omega \ge 0$. (ii) $a = 1$ (focusing case) and $\omega \ge 1$. (iii) $a = \pm 1$ if $\omega < 0$ provided $|U|^2/(1 + |U|^2) = O(1/|\mathbf{x}|^{1+\varepsilon})$, $\varepsilon > 0$ as $|\mathbf{x}| \to +\infty$.

We now look for solitary wave solutions of (ZA), that is solutions of the form $(e^{i\omega t}U(x), \phi(x))$ with $x \in \mathbb{R}^d$, $\omega \in \mathbb{R}$, $U \in H^1(\mathbb{R}^d)$ and $\phi \in H$. Thus (U, ϕ) should satisfy the system

$$\text{(RSW)} \quad \left\{ \begin{array}{rcl} -\Delta U + \omega U & = & aU\partial_x\phi, \\ \text{div}((1 + |U|^2)\nabla\phi) & = & \partial_x(|U|^2). \end{array} \right.$$

The existence of non-trivial solutions of (SW) is an open problem. Note that (SW) does not seem to be the Euler–Lagrange equation associated to a variational problem. We have however:

Proposition 4 *(i) Let $a = -1$ (defocusing case). Then no non-trivial solution of (SW) exists for $\omega \geq 0$.*
(ii) Let $a = 1$ (focusing case). No non-trivial solution of (SW) exists for $\omega \geq 1$.
(iii) Let $a = \pm 1$. No non-trivial solution of (SW) exists if $\omega < 0$ provided $\partial_x \phi = O(1/|\mathbf{x}|^{1+\varepsilon})$, $\varepsilon > 0$ as $|\mathbf{x}| \to +\infty$.

In both propositions, (i) and (ii) follow from simple energy estimates and (iii) from the classical result of Kato [5] on the absence of embedded eigenvalues.

4.3 Existence of solitary waves for (SNLS)

We now turn to the existence of non-trivial H^2 solutions of

$$-\Delta U + \omega U = \frac{|U|^2 U}{1 + |U|^2}$$

when $0 < \omega < 1$. We will look for real radial solutions $U(\mathbf{x}) = u(|\mathbf{x}|) \equiv u(r)$ and thus consider the ODE problem

$$\text{(RSW)} \quad \begin{cases} -u'' - \dfrac{d-1}{r} u' + \omega u = \dfrac{u^3}{1+u^2}, \\ u \in H^2(]0,\infty[), \qquad u'(0) = 0. \end{cases}$$

Theorem 5 *If $a = 1$ and $0 < \omega < 1$, there exists a non-trivial positive solution of (RSW).*

This a consequence of a classical result of Berestycki, Lions and Peletier [1].

5 Conclusion

We have derived from the Kukhtarev equations an asymptotic model for the propagation of light in a photorefractive medium.

The 1D asymptotic model is a saturated nonlinear Schrödinger equation the Cauchy problem of which is studied (in any space dimension) in L^2 and H^1. We also prove the existence of solitary waves in 1 and higher dimensions. An interesting and open issue would be to study the transverse stability of the 1D solitary waves in the framework of the asymptotic model.

For the 2D asymptotic model (the Zozulya–Anderson model) we also have studied the Cauchy problem and the non-existence of solitary waves. The question of imposing other boundary conditions, not vanishing in one space direction, should also be addressed to treat a wider range of experimental applications. We are already able to find first integrals of (dark) solitary waves in this context.

Memory effects also certainly lead to interesting equations from the mathematical point of view. This necessitates however a new full derivation, which is a difficult and tedious task.

References

[1] H. Berestycki, P.-L. Lions, and L.A. Peletier, "An ODE approach to the existence of positive solutions for semilinear problems in $\mathbb{R}^N$", Indiana University Mathematics Journal, vol. 30, pp. 141-157, 1981.

[2] B. Bidégaray-Fesquet and J.-C. Saut, "On the propagation of an optical wave in a photorefractive medium", to appear in Mathematical Models and Methods in Applied Sciences, 2007. `http://fr.arxiv.org/abs/math.AP/0703223`

[3] J.L. Bona and R. Smith, "The initial value problem for the Korteweg-de Vries equation" Philos. Trans. Royal. Soc. London A, vol. 278, pp. 555-601, 1975.

[4] J.-M. Ghidaglia and J.-C. Saut, "On the initial value problem for the Davey–Stewartson systems", Nonlinearity, vol. 3, pp. 475-506, 1990.

[5] T. Kato, "Growth properties of solutions of the reduced wave equation with a variable coefficient", Communications in Pure and Applied Mathematics, vol. 12, pp. 403-425, 1959.

[6] N.V. Kukhtarev, V.B. Markow, S.G. Odoluv, M.S. Soskin, and V.L. Vinetskii, "Holographic storage in electrooptic crystals", Ferroelectrics, vol. 22, pp. 949-960, 1979.

[7] J.-L. Lions, Quelques méthodes de résolution des problèmes aux limites non linéaires, Dunod, Paris, 1969.

[8] A.V. Mamaev, M. Saffman, and A.A. Zozulya, "Break-up of two-dimensional bright spatial solitons due to transverse modulational instability", Europhysics Letters, vol. 35, pp. 25-30, 1996.

[9] V. Tikhonenko, J. Christou, and B. Luther-Davies, "Three-dimensional bright spatial soliton collision and fusion in a saturable nonlinear medium", Physical Review Letters, vol. 76, pp. 2698-2701, 1996.

[10] A.A. Zozulya and D.Z. Anderson, "Propagation of an optical beam in a photorefractive medium in the presence of a photogalvanic nonlinearity or an externally applied electric field", Physics Review A, vol. 51, pp. 1520-1531, 1995.

3D Numerical Simulation of Sonic Log for Viscoelastic Media

V. Kostin[†] **G. Reshetova**[†*] **V. Tcheverda**[†**]
† ZAO "Intel A/O" 6a, prosp. Lavrentiev, 630090, Novosibirsk, Russia
[†*]Institute of Numerical Mathematics and Mathematical Geophysics SB RAS, 6, prosp. Lavrentiev, 630090, Novosibirsk, Russia
[†*] Trofimuk Institute of Petroleum Geology and Geophysics SB RAS, 3, prosp. Koptyug, 630090, Novosibirsk, Russia
† Email: victor.i.kostin@intel.com
[†*]Email: kgv@nmsf.sscc.ru
[†**]Email: chev@uiggm.nsc.ru

Finite-difference (FD) method for 3D simulation of sonic waves propagation in a borehole and surrounding 3D heterogeneous viscoelastic medium is presented. It is based on explicit second-order staggered grid FD scheme that solves the first-order viscoelastic wave equations (velocity-stress formulation) in cylindrical coordinates. Attenuation is implemented via Generalize Standard Linear Solid model. In order to provide desired Quality Factors τ-method is applied (Blanch et al., 1995). In order to bound area of computations special modification of Perfectly Matched Layer for cylindrical coordinate system is developed and implemented (Kostin et al., 2006). Essential 3D nature of the waves processes for realistic models claims necessity to use parallel computations. Parallelization is performed on the base of domain decomposition and implemented under Message Passing Interface. Results of numerical experiments are presented and discussed.

1 Introduction

Sonic logs are very important borehole measurements providing knowledge about physical properties of surrounding rocks. In order to be able to recover physical properties of surrounding rocks by sonic data one should fully appreciate key peculiarities of elastic waves propagating through and around borehole imbedded within 3D heterogeneous elastic formations. We believe that the most effective way to do that is to use 3D numerical simulation. This follows necessity to develop numerical methods and corresponding software providing a possibility to perform a range of numerical experiments for a variety of models and a range of different source positions. Most of the previous 3D FD studies are done for Cartesian coordinates. But, the use of these coordinates leads to saw-like representation of the sharpest interface of the problem - interface between fluid-filled borehole and enclosing rocks. In its own turn this provokes generation of rather strong artifacts known as "numerical scattering". We believe one should take special care to avoid this artifact because for the first of all correct simulation of sonic log should provide one with correct simulation of head P- and S-waves. These waves are of first arrivals and possess very important information about desired elastic property of borehole vicinity. In particular we would like to pay attention that the use of eccentric sources inevitably leads to spiral-like propagation path of head waves along cylindrical interface well/surrounding medium followed by their intensive numerical scattering on mentioned above saw-like structures. The same spiral-like propagation of head waves should be expected for media with azimuth heterogeneities. So, we believe that the use of cylindrical coordinates is mandatory in order to get the proper results of numerical simulation of sonic log for 3D heterogeneous media.

2 Statement of the Problem

Waves propagation in heterogeneous viscoelastic media is governed by initial-boundary value problem for t-hyperbolic first-order system of partial differential equations in cylindrical coordinates for velocity vector, stress components and memory variables (Groby and Tsogka, 2004). In order to provide the desired value of Quality Factor we use τ-method described in (Blanch, 1995). Its main advantage is in essential memory savings following significant reduction of computer resources needed for modeling. In the finite-difference implementation the system of partial differential equations is approximated by Virieux-like difference scheme on staggered grids.

The main trouble the person faces on when dealing with FD scheme in cylindrical coordinate system is linear inflation of azimuth face of grid cells with radius increase. In order to compensate this inflation we perform periodical refinement of azimuth sampling. On the Fig.2 one can see mutual disposition of coarse and fine grids. It is easy to recognize that in order to couple both these grids one should interpolate components of velocity and stress vectors with respect to azimuth at some specific points. Our choice was to use advantage providing by

2π-periodicity of velocity and stress vectors with respect to azimuth and to use interpolation on the base of Fourier Transform. This interpolation possesses exponential accuracy and its Fast Fourier Transform (FFT) version is extremely fast. In order to incorporate in the model objects of rather small scale (for example, it could be necessity to take into account completion of the well) the person needs in local refinement of radial step as well. Our approach consists in the use of some scaling factor providing smooth increase/decrease of this step. In order to choose this factor the series of numerical experiments was implemented.

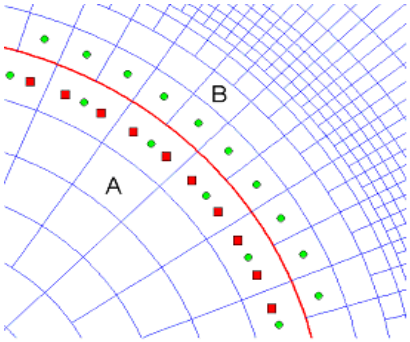

Figure 1: Coupling of coarse (A) and fine (B) grids. Red diamonds placed at positions where one should perform interpolation from red circles.

3 Perfectly Matched Layers (PML) for Cylindrical Coordinates

For numerical simulation of elastic wave propagation one has to truncate infinite physical domain to finite computational one. The most widespread approach to do that is surrounding of a computational domain by a special layer with intrinsic attenuation introduced in a special way that provides extremely low reflections on both interior and exterior interfaces. We used here our own development described in (Kostin et al., 2002).

4 Parallel Implementation

For implementation of parallel computations we use approach based on domain decomposition of the target area. The total 3D model is sliced into a number of disc-like subdomains Ω_i. Each of these subdomains is assigned to a separate Processor Units (PU). Finite difference scheme assumes communication between neighboring processors (Fig.2) requiring them to exchange function values on the interfaces between slices. This communication is arranged with a help of Message Passing Interface library. The very important peculiarity of the problem under consideration, besides its essential 3D nature, is comparatively small amount of data for processors to exchange.

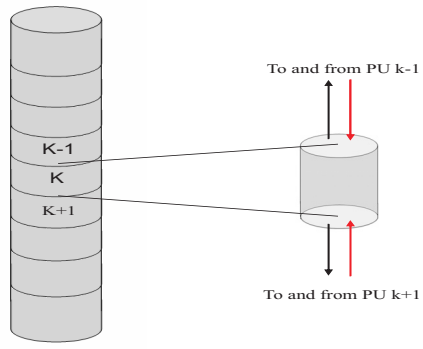

Figure 2: Domain decomposition and data flow between neighbor PU.

5 Numerical Experiments

The series of numerical experiments have been implemented for a range of source frequencies, positions and models of well completion and surrounding elastic media. For illustration let us consider the model with well completion and vertical crack presented on the Fig.3. The main purpose of this numerical experiment is to analyze if one can reveal the fracture by sonic waves within well with completion.

Detailed structure of the model is as following (numbers coincide with presented on the Fig.3a):

1. Vertical borehole with radius 0.1 m is filled with mud with V_p=1500 m/s, $\varrho = 1000$ kg/m^3 and Quality factor $Q = 65$;

2. There is a steel tube encircling borehole; its width is equal to 0.01 m, wave propagation velocities $V_p = 5600$ m/s, $V_s = 3270$ m/s, ϱ=7830 kg/m^3 and Quality factor Q=100;

3. There is a casing around steel tube; its width is equal to 0.04 m, its elastic parameters are the following: V_p=4200 m/s, V_s=2425 m/s, ϱ=2400 kg/m^3 and Quality factor Q=80;

4. Background - homogeneous viscoelastic layer (yellow) with wave propagation velocities V_p=4989 m/s, V_s=2605 m/s, ϱ=2400 kg/m^3 and Quality factor Q=100;

5. Background - homogeneous viscoelastic layer (blue) with wave propagation velocities V_p=3208

m/s, V_s=1604 m/s, ϱ=2400 kg/m^3 and Quality factor Q=60;

6. Background - homogeneous viscoelastic layer (green) with wave propagation velocities V_p=2650 m/s, V_s=1219 m/s, ϱ =2400 kg/m^3 and Quality factor Q=15;

7. Vertical crack through all background (from r=0.18 m to r=0.55 m and 0.02 m in width (see images b) and c)) filled with mud with parameters V_p=1500 m/s, ϱ=1000 kg/m^3 and Quality factor Q=65.

Results one can see on the Fig.4.

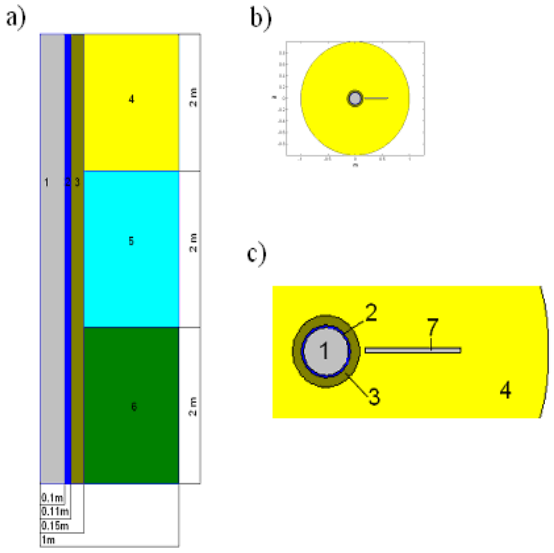

Figure 3: a) Vertical cross-section of the model; b)Horizontal cross-section of the model; c)Zoomed version of horizontal cross-section.

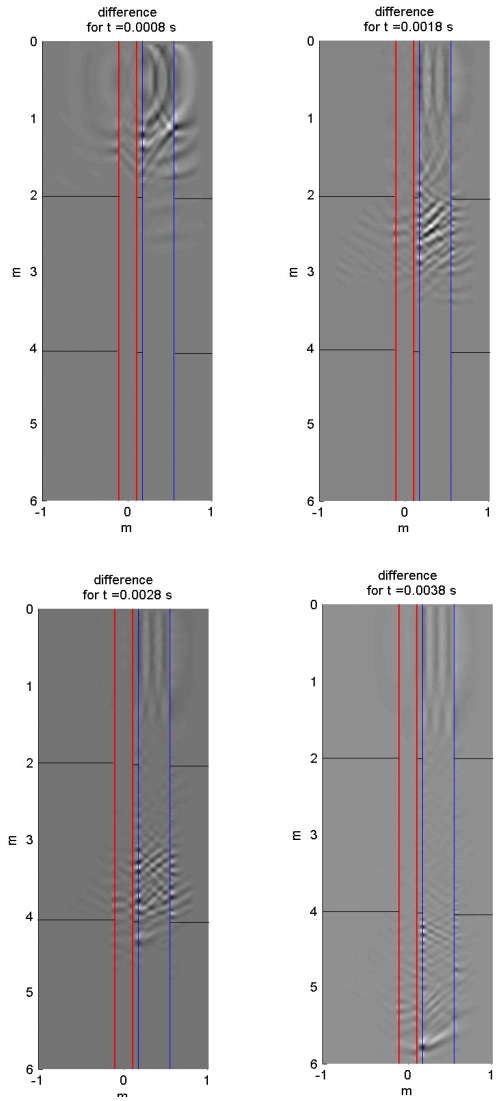

Figure 4: Snapshots of propagation through the model difference of σ_{rr} for the models with and without of crack. One can clear see influence of the crack. Red lines - borehole projection, black lines - interface of the layers, blue lines - projection of the crack.

Aknowledgement Research described in this presentation was done together with Schlumberger Moscow Research and partially supported from RFBR, grants 05-05-64277, 06-05-64748 and 07-05-00538.

References

[1] Blanch J.O., Robertsson J.O.A., Symes W.W. Modeling of a constant Q: Methodology and algorithm for an efficient and optimally inexpensive viscoelastic technique. *Geophysics*, **60**(1), 176 - 184.

[2] Groby J.-P., Tsogka C. A time domain method for modeling viscoelastic wave propagation. *Journal of Computational Acoustics*, **5**(19), 1 - 35.

[3] Kostin V.I., Tcheverda V.A., Vishnevsky D.M. Radiation of seismic waves by source located within fluid-filled borehole. *Fizicheskaja Mezomehanika (in Russian)*, **5** (2002) 85 - 92.

[4] Liu K.H., Sinha B.K. A 3D cylindrical PML/FDTD method for elastic waves in fluid-filled pressurized boreholes in triaxially stresed formations. *Geophysics*, **68**, n.5 (2003), 1731 -1743.

MATHEMATICAL PROBLEMS FOR PIEZOELECTRIC-METALLIC COMPOSITES: EXISTENCE AND STRESS SINGULARITY ANALYSIS

D. Natroshvili, T. Buchukuri, O. Chkadua
Department of Mathematics, Georgian Technical University, 77 M.Kostava, Tbilisi 0175, Georgia
Email: natrosh@hotmail.com

Abstract

We study mixed three-dimensional transmission problems for composites consisting of a piezoelectric matrix with metallic inclusions (electrodes). We derive a linear model with regard to thermal stress effects for the interaction of the thermoelastic and electrical fields and perform a rigorous mathematical analysis by the potential method. We reduce the initial transmission problem to the equivalent strongly elliptic system of pseudodifferential equations on manifold with boundary. The solvability and regularity of solutions to the resulting boundary integral equations and the original transmission problem are analyzed in Sobolev-Slobodetski H^s_p and Besov $B^s_{p,t}$ spaces. We investigate the stress singularities which appear near zones, where the boundary conditions change and where the interfaces meet the exterior boundary. We analyse also the stress singularities of solutions at the interior and interface crack edges. We show that the stress singularity exponents cam be efficiently calculated by means of the eigenvalues of the symbol matrices of the corresponding pseudodifferential operators and study their dependence on the material parameters.

Description of the problem and main results

The paper deals with mixed type boundary transmission problems arising in the theory of multi-structural composites consisting of piezoelectric matrix with metallic inclusions (electrodes) when thermal effects are taken into consideration. Modern industrial and technological processes apply widely such type composite materials. Therefore investigation of the mathematical models for such composite materials and analysis of the corresponding mechanical, thermal and electric fields became very actual and important for both fundamental research and practical applications. We remark here that during last years more then 1000 scientific works have been published annually (see, e.g., [1], [2] and the references therein).

Let Ω_m and Ω be bounded, non-intersecting three-dimensional domains with C^∞-smooth boundaries $\partial\Omega$ and $\partial\Omega_m$, respectively. Moreover, let $\partial\Omega$ and $\partial\Omega_m$ have a nonempty intersection $\overline{\Gamma}_m = \partial\Omega \cap \partial\Omega_m$ with positive measure.

We set $S_m := \partial\Omega_m \setminus \overline{\Gamma}_m$ and $S_2^* := \partial\Omega \setminus \overline{\Gamma}_m$. Further, we denote by Γ some open, nonempty, proper submanifold of S_2^* and let $S := S_2^* \setminus \overline{\Gamma}$. Thus, we have the following decomposition of the boundary surfaces

$$\partial\Omega = \overline{\Gamma}_m \cup \overline{S} \cup \overline{\Gamma}, \quad \partial\Omega_m = \overline{\Gamma}_m \cup \overline{S}_m.$$

We assume that $\partial\Omega_m$, $\partial\Omega$, ∂S_m, $\partial\Gamma_m$, $\partial\Gamma$, $\partial S \in C^\infty$, and $\partial\Omega_m \cap \overline{\Gamma} = \emptyset$.

Let Ω_m be occupied by an anisotropic homogeneous elastic medium (metallic inclusion) and Ω be filled by an anisotropic homogeneous piezoelectric medium (ceramic matrix). These two bodies interact to each other along the interface surface Γ_m.

We apply the Voigt's linear model in the piezoelectric part and the usual classical model of thermoelasticity in the metallic part to write the corresponding coupled systems of governing partial differential equations. As a result, in the metallic part the unknown field is described by a 4-component vector $U^{(m)} := (u_1^{(m)}, u_2^{(m)}, u_3^{(m)}, \vartheta^{(m)})^\top$ (three components of the displacement vector $u_j^{(m)}$, $j = 1, 2, 3$, and the temperature distribution $\vartheta^{(m)}$), while in the piezoceramic part the unknown field is represented by a 5-component vector $U = (u_1, u_2, u_3, \vartheta, \varphi)$ (three components of the displacement vector u_j, $j = 1, 2, 3$, the temperature distribution ϑ and the electric potential function φ). The situation becomes complicated since we have to find boundary and transmission conditions for the physical fields possessing different dimensions in adjacent domains. The main difficulty in modelling is to find appropriate boundary and transmission conditions for the composed body and to formulate them in an efficient way.

The physical problem under consideration is described by strongly elliptic systems of linear partial differential equations in the corresponding elastic and piezoelastic domains with appropriate mixed boundary and transmission conditions on S, S_m, Γ, and Γ_m: on S and S_m the mechanical stress vector and temperature flux are prescribed, on Γ the Dirichlet condition is given for U, and on Γ_m we have appropriate transmission conditions along with the Dirichlet boundary condition for the electric potential function φ (for details see [2]).

Solutions to this kind of mixed boundary value problems and related mechanical and electrical characteristics usually have singularities in a neighbourhood of curves where the boundary conditions change (e.g., $\partial\Gamma$) or where the interface intersects the exterior boundary of the composite body (e.g., $\partial\Gamma_m$). If the composite body under consideration contains interior or interface cracks, then stress singularities appear at the crack edges as well.

Our goal is to study the solvability of the mixed boundary transmission problem in appropriate function spaces and analyse regularity properties of solutions. In particular, we describe dependence of the stress singularity exponents on the material parameters.

In the metallic part of the composite we have the system of differential equations

$$A^{(m)}(\partial,\tau)\,U^{(m)}(x)+\tilde{X}^{(m)}(x)=0 \qquad (1)$$

with $A^{(m)}(\partial,\tau)=[\,A^{(m)}_{jk}(\partial,\tau)\,]_{4\times4}$, and

$$\begin{aligned}
A^{(m)}_{jk}(\partial,\tau)&=c^{(m)}_{ijlk}\,\partial_i\,\partial_l-\varrho^{(m)}\,\tau^2\,\delta_{jk},\\
A^{(m)}_{4k}(\partial,\tau)&=-\tau\,T^{(m)}_0\,\gamma^{(m)}_{kl}\,\partial_l,\\
A^{(m)}_{j4}(\partial,\tau)&=-\gamma^{(m)}_{ij}\,\partial_i,\quad k,j=1,2,3,\\
A^{(m)}_{44}(\partial,\tau)&=\kappa^{(m)}_{il}\,\partial_i\,\partial_l-\alpha^{(m)}\,\tau,
\end{aligned}$$

where $U^{(m)}:=(u^{(m)},\vartheta^{(m)})^\top$ is the sought vector, $\tilde{X}^{(m)}=(X^{(m)}_1,X^{(m)}_2,X^{(m)}_3,X^{(m)}_4)^\top$, $X^{(m)}=(X^{(m)}_1,X^{(m)}_2,X^{(m)}_3)^\top$ is a given mass force density, $X^{(m)}_4$ is a given heat source density, δ_{jk} is the Kronecker delta, $A^{(m)}(\partial,\tau)$ is the nonselfadjoint matrix differential operator generated by the thermoelastic field equations, $\partial_j:=\partial/\partial_j$, the superscript $\top$ denotes transposition. Here and in what follows we employ the Einstein summation convention.

Analogously, in the piezo-ceramic part we have the following system of partial differential equations

$$A(\partial,\tau)\,U(x)+\widetilde{X}(x)=0\ \text{ in }\ \Omega \qquad (2)$$

with $A(\partial,\tau)=[A_{jk}(\partial,\tau)]_{5\times5}$ and

$$\begin{aligned}
A_{jk}(\partial,\tau)&=c_{ijlk}\,\partial_i\,\partial_l-\varrho\,\tau^2\,\delta_{jk},\\
A_{j4}(\partial,\tau)&=-\gamma_{ij}\,\partial_i,\quad A_{j5}(\partial,\tau)=e_{lij}\partial_l\partial_i,\\
A_{4k}(\partial,\tau)&=-\tau\,T_0\,\gamma_{kl}\,\partial_l,\quad j,k=1,2,3,\\
A_{44}(\partial,\tau)&=\kappa_{il}\,\partial_i\,\partial_l-\alpha\,\tau,\\
A_{45}(\partial,\tau)&=\tau\,T_0\,g_i\,\partial_i,\quad A_{5k}(\partial,\tau)=-e_{ikl}\,\partial_i\partial_l,\\
A_{54}(\partial,\tau)&=-g_i\partial_i,\quad A_{55}(\partial,\tau)=\varepsilon_{il}\,\partial_i\partial_l,
\end{aligned}$$

where $U:=(u,\vartheta,\varphi)^\top$ is the sought vector, $\widetilde{X}=(X_1,X_2,X_3,X_4,X_5)^\top$, $X=(X_1,X_2,X_3)^\top$ is a given mass force density, X_4 is a given heat source density, X_5 is a given charge density, $A(\partial,\tau)$ is the nonselfadjoint matrix differential operator generated by the piezothermoelastic field equations.

The material constants involved in the above equations are: ϱ, $\varrho^{(m)}$ – mass densities; c_{ijkl}, $c^{(m)}_{ijkl}$ – elastic constants; e_{kij} – piezoelectric constants; ε_{kj} – dielectric (permittivity) constants; γ_{kj}, $\gamma^{(m)}_{kj}$ – thermal strain constants; κ_{kj}, $\kappa^{(m)}_{kj}$, – thermal conductivity constants; $\widetilde{c}$, $\widetilde{c}^{(m)}$– specific heat per unit mass; T_0, $T^{(m)}_0$ – initial reference temperature, that is the temperature in the natural state in the absence of deformation and electromagnetic fields; $\alpha:=\varrho\,\widetilde{c}$, $\alpha^{(m)}:=\varrho^{(m)}\,\widetilde{c}^{(m)}$ – thermal material constants; g_i $(i=1,2,3)$ – constants characterizing the relation between thermodynamic processes and piezoelectric effect (pyroelectric constants).

These equations are obtained from the corresponding dynamic field equations by the Laplace transform with respect to the time variable. If $\tau=\sigma+i\omega$ is a complex parameter, we have the *pseudo-oscillation equations*. If $\tau=i\omega$ is a pure imaginary number, with a real frequency parameter ω, we obtain the *steady state oscillation equations*. Finally, if $\tau=0$ we get the *equations of statics*.

In this paper we apply potential method and look for solutions as layer potentials in the ceramic and metallic parts with unknown densities. The densities are to determine in such a way, that the transmission and boundary conditions are satisfied. This reduces the original transmission problem to the system of pseudodifferential equations involving boundary operators acting on the interface $\Gamma^{(m)}$ and the Dirichlet part Γ of the exterior boundary:

$$\mathcal{A}_\tau:[\widetilde{B}^{r-1}_{p,t}(\Gamma)]^5\to[B^r_{p,t}(\Gamma)]^5, \qquad (3)$$

$$[\mathcal{A}_\tau+\mathcal{B}^{(m)}_\tau]:[\widetilde{B}^{s-1}_{p,t}(\Gamma^{(m)})]^5\to[B^s_{p,t}(\Gamma^{(m)})]^5, \qquad (4)$$

where $\mathcal{A}_\tau$ and $\mathcal{A}_\tau+\mathcal{B}^{(m)}_\tau$ are strongly elliptic pseudodifferential operators of order -1 (Steklov-Poincaré type operators). Here $\widetilde{B}^r_{p,t}$ and $B^r_{p,t}$ are Besov function spaces.

Let $\widetilde{\sigma}_1(x,\xi_1,\xi_2)$ be the principal symbol matrix of the operator $\mathcal{A}_\tau$ and $\lambda^{(1)}_j(x)$ $(j=\overline{1,5})$ be the eigenvalues of the matrix $[\widetilde{\sigma}_1(x,0,+1)]^{-1}\,\widetilde{\sigma}_1(x,0,-1)$ for $x\in\partial\Gamma$.

Similarly, let $\widetilde{\sigma}_2(x,\xi_1,\xi_2)$ be the principal symbol matrix of the operator $\mathcal{A}_\tau+\mathcal{B}^{(m)}_\tau$ and $\lambda^{(2)}_j(x)$ $(j=\overline{1,5})$ be the eigenvalues of the corresponding matrix $[\widetilde{\sigma}_2(x,0,+1)]^{-1}\,\widetilde{\sigma}_2(x,0,-1)$ for $x\in\partial\Gamma^{(m)}$.

Further, let

$$\gamma_1{}' := \inf_{x\in\partial\Gamma,\,1\le j\le 5} \frac{1}{2\pi}\ \arg\ \lambda_j^{(1)}(x),$$
$$\gamma_1{}'' := \sup_{x\in\partial\Gamma,\,1\le j\le 5} \frac{1}{2\pi}\ \arg\ \lambda_j^{(1)}(x),$$
$$\gamma_2{}' := \inf_{x\in\partial\Gamma^{(m)},\,1\le j\le 5} \frac{1}{2\pi}\ \arg\ \lambda_j^{(2)}(x),$$
$$\gamma_2{}'' := \sup_{x\in\partial\Gamma^{(m)},\,1\le j\le 5} \frac{1}{2\pi}\ \arg\ \lambda_j^{(2)}(x).$$

Note that $\gamma_j{}'$ and $\gamma_j{}''$ $(j = 1, 2)$ depend on the material parameters, in general, and belong to the interval $(-\frac{1}{2},\ \frac{1}{2})$. We put

$$\gamma' := \min\{\gamma_1{}',\ \gamma_2^{'}\},\quad \gamma'' := \max\{\gamma_1{}'',\ \gamma_2^{''}\}.$$

We prove that if the parameters s, r, $1 < p < \infty$, and $1 \le t \le \infty$, satisfy the conditions

$$\frac{1}{p} - \frac{1}{2} + \gamma_1{}'' < r < \frac{1}{p} + \frac{1}{2} + \gamma_1{}',$$
$$\frac{1}{p} - \frac{1}{2} + \gamma_2{}'' < s < \frac{1}{p} + \frac{1}{2} + \gamma_2{}',$$

then the operators (3) and (4) are Fredholm operators with index zero. These results along with the uniqueness theorem for the initial mixed transmission problem lead then to the existence of the solution pair $(U^{(m)}, U) \in [W_p^1(\Omega_m)]^4 \times [W_p^1(\Omega)]^5$ with $\frac{4}{3-2\gamma''} < p < \frac{4}{1-2\gamma'}$. Moreover, $U^{(m)}$ and U are represented by potential type surface integrals.

Further, we show the global C^α-regularity results with some $\alpha \in (0,\ \frac{1}{2})$. For sufficiently smooth data we have, $(U^{(m)}, U) \in [C^\alpha(\overline{\Omega_m})]^4 \times [C^\alpha(\overline{\Omega})]^5$ with $\alpha < \frac{1}{2} + \gamma'$.

In general, the above eigenvalues $\lambda_j^{(l)}(x)$ $(j = \overline{1,5}$, $l = 1, 2)$ and $\gamma' \le 0$ depend on the material parameters and actually they define the singularity exponents for the first order derivatives of solutions (stress singularity exponents). For particular composites, with the piezoelectric materials $BaTiO_3$ (the crystal symmetry of the class **4mm**), PZT-4 and PZT-5A (the crystal symmetry of the class **6mm**) and metallic inclusion *silver-palladium alloy*, we compute these complex-valued stress singularity exponents and demonstrate their dependence on the material parameters.

Detailed analysis based on the asymptotic expansions of solutions shows that for sufficiently smooth boundary data (e.g., C^∞-smooth data say) the principal singular terms of the solution vectors $U^{(m)}$ and U near the curves $\partial\Gamma^{(m)}$ and $\partial\Gamma$ can be represented as a product of a "good" vector-function and a singular factor of the form $[\ln \varrho(x)]^{m_j-1}[\varrho(x)]^{\alpha_j+i\beta_j}$. Here $\varrho(x)$ is the distance from a reference point x to the curves $\partial\Gamma^{(m)}$ or $\partial\Gamma$. Therefore, near these curves the dominant singular terms of the corresponding generalized stress vectors are represented as a product of a "good" vector-function and the factor $[\ln \varrho(x)]^{m_j-1}[\varrho(x)]^{-1+\alpha_j+i\beta_j}$. The numbers β_j are different from zero, in general, and describe the *oscillating character* of the stress singularities.

The exponents $\alpha_j + i\,\beta_j$ are related to the above eigenvalues by the equalities

$$\alpha_j = \frac{1}{2} + \frac{\arg\ \lambda_j}{2\pi}\,,\quad \beta_j = -\frac{\ln\ |\lambda_j|}{2\pi}\,.$$

Here $\lambda_j \in \{\lambda_1^{(1)}(x), \cdots, \lambda_5^{(1)}(x)\}$ for $x \in \partial\Gamma$, and $\lambda_j \in \{\lambda_1^{(2)}(x), \cdots, \lambda_5^{(2)}(x)\}$ for $x \in \partial\Gamma^{(m)}$. In the above expressions the parameter m_j denotes the multiplicity of the eigenvalue λ_j.

We establish that near the curves $\partial\Gamma^{(m)}$ and $\partial\Gamma$ the components of the generalized stress vector behave like $\mathcal{O}\left([\ln \varrho(x)]^{m_0-1}[\varrho(x)]^{-\frac{1}{2}+\gamma'}\right)$, where m_0 denotes the maximal multiplicity of the eigenvalues. This is a global singularity effect for the first order derivatives of the vectors $U^{(m)}$ and U. In contrast to the classical pure elasticity case (where $\gamma' = \gamma'' = 0$), here γ' and γ'' depend on the material parameters and are different from zero, in general. This is related to the fact that our transmission problem and, consequently, the corresponding strongly elliptic matrix pseudodifferential operator are not selfadjoint. This implies that the eigenvalues $\lambda_j^{(k)}$ are complex numbers, in general.

Similar analysis is done for the stress singularity exponents near the interior and interface crack edges.

The results of the calculations for particular composites are presented in the form of graphs and tables.

References

[1] S. Lang, "Guide to the Literature of Piezoelectricity and Pyroelectricity", Ferroelectrics, vol. 24, No. 322, pp. 115-210, 2005.

[2] T. Buchukuri, O.Chkadua, D. Natroshvili, "Mathematical modelling and analysis of interaction problems for metallic-piezoelectric structures with regard to thermal stresses", University of Stuttgart, IANS, Preprint 2006/008, pp. 1-64, 2006 (Electronic version can be found at the address: WWW: http://preprints.ians.uni-stuttgart.de).

NUMERICAL ANALYSIS OF ELASTIC WAVES PROPAGATION IN COSSERAT CONTINUUM

Oxana V. Sadovskaya[†,*], **Vladimir M. Sadovsky**[†]

[†]Institute of Computational Modelling SB RAS, Krasnoyarsk, Russia, 660036
[*]Email: o_sadov@icm.krasn.ru

Abstract

Parallel computational algorithm is worked out for the analysis of two-dimensional dynamic problems within the framework of mathematical model of Cosserat continuum, in which independent rotations of particles are considered as well as translational degrees of freedom of the particles motion, and two asymmetric tensors (the tensor of stresses and the tensor of moments) are used for the description of stressed state. This algorithm is realized as a parallel program system for multiprocessor supercomputers of MVS series. Some computations are carried out to demonstrate an oscillatory character of the angular velocity changing on fronts of transversal waves in moment elastic materials.

Introduction

Mathematical model of Cosserat theory of elasticity [1], taking into account the microstructure of materials, is applicable to the description of stress-strained state of composites, powder and granular materials, and also to the special models constructing for thin-walled elements, e.g. rods, plates and shells. In addition to translational motion, which is characterized by the velocity vector v, the independent rotations of particles, describable by means of the angular velocity vector ω, are considered in this model, and besides the asymmetric stress tensor σ the asymmetric tensor of couple stresses m is introduced, too.

A total system of equations of the model consists of motion equations, kinematic relationships and generalized elastic law [2]:

$$\rho\,\dot v = \nabla\sigma + f, \quad j\,\dot\omega = \nabla m - 2\,\sigma^a + q,$$
$$\dot\Lambda = \nabla v + \omega, \quad \dot M = \nabla\omega,$$
$$\sigma = (k - 2\,\mu/3)\,(\delta : \Lambda^s)\,\delta + 2\,\mu\,\Lambda^s + 2\,\alpha\,\Lambda^a,$$
$$m = \beta\,(\delta : M^s)\,\delta + 2\,\gamma\,M^s + 2\,\varepsilon\,M^a.$$

Here ρ is the material density, f and q are given vectors of volumetric forces and moments, Λ and M are the strain tensor and the curvature tensor, which are equal to zero in normal (stress-free) state, j is a special dynamic characteristic of material, equals to the product of the moment of inertia with respect to axis, passing through the focal point of any particle, by the particle number in a volume unit, δ is the Kronecker delta, k, μ, α, β, γ, ε are the phenomenological coefficients of elasticity in isotropic case. Superscripts s and a denote symmetric and antisymmetric parts of tensors. The antisymmetric part is identified with corresponding vector, if it's necessary. In particular, the vector of the tensor $\sigma^a = (\sigma - \sigma^*)/2$ is included in motion equations.

If material particles of microstructure are regular spheres of the radius r_0 and the mass m_0 then coefficient j can be calculated as $j = 2\,r_0\,m_0^2\,N/5$ (N is a particle number per unit volume). The density of material, taking into account the porosity, is $\rho = m_0\,N$, hence

$$j = 2\,\rho\,r_0^2/5, \quad r_0 = \sqrt{5j/(2\,\rho)}.$$

The principal distinction of Cosserat model from the classical elasticity theory is that a small parameter implicitly presents in it, which has the measure of length. Therefore the stress fields are able to change appreciably at a range of order r_0. So, it is necessary to solve dynamic problems for Cosserat continuum numerically only on sufficiently small grids, which mesh size is appreciably less than r_0, otherwise the accuracy of numerical solution may be insufficient to analyze some delicate small-scale effects.

Equations of 2D model

In the case of plane strained state the model describes a behavior of material consisting of particles of cylindrical form with axis, directed along the axis x_3. The angular velocity vector has only one nonzero projection ω_3. A total system of equations in plane case takes the next form:

$$\rho\,\dot v_1 = \sigma_{11,1} + \sigma_{21,2}, \quad \rho\,\dot v_2 = \sigma_{12,1} + \sigma_{22,2},$$
$$\dot\sigma_{11} = (k + 4\,\mu/3)\,v_{1,1} + (k - 2\,\mu/3)\,v_{2,2},$$
$$\dot\sigma_{22} = (k - 2\,\mu/3)\,v_{1,1} + (k + 4\,\mu/3)\,v_{2,2},$$
$$\dot\sigma_{33} = (k - 2\,\mu/3)\,(v_{1,1} + v_{2,2}),$$
$$\dot\sigma_{12} = (\mu - \alpha)\,v_{1,2} + (\mu + \alpha)\,v_{2,1} - 2\,\alpha\,\omega_3,$$
$$\dot\sigma_{21} = (\mu + \alpha)\,v_{1,2} + (\mu - \alpha)\,v_{2,1} + 2\,\alpha\,\omega_3,$$
$$j\,\dot\omega_3 = m_{13,1} + m_{23,2} + \sigma_{12} - \sigma_{21},$$
$$\dot m_{23} = (\gamma + \varepsilon)\,\omega_{3,2}, \quad \dot m_{32} = (\gamma - \varepsilon)\,\omega_{3,2},$$
$$\dot m_{31} = (\gamma - \varepsilon)\,\omega_{3,1}, \quad \dot m_{13} = (\gamma + \varepsilon)\,\omega_{3,1}.$$

This system is reduced to symmetric form

$$A\,U_t = B^1 U_{x_1} + B^2 U_{x_2} + Q\,U + G,$$

recorded with respect to the vector–function $U =$

$$\big(v_1, v_2, \sigma_{11}, \sigma_{22}, \sigma_{33}, \sigma_{12}, \sigma_{21}, \omega_3, m_{23}, m_{32}, m_{31}, m_{13}\big).$$

The matrix–coefficients A, B^1 and B^2 of this system are symmetric, and Q is antisymmetric. Furthermore, the matrix A is positively defined if k, μ, α, $\gamma + \varepsilon > 0$, so the system is hyperbolic by Friderix. In two-dimensional case it determines three types of elastic waves in boundless continuum – longitudinal and transverse waves, propagating with the velocities $c_p = \sqrt{(k + 4\,\mu)/\rho}$ and $c_s = \sqrt{(\mu + \alpha)/\rho}$, as well as the waves of rotational motion with the velocity $c_\omega = \sqrt{(\gamma + \varepsilon)/j}$.

Numerical algorithm

Parallel computational algorithm is worked out for the analysis of two-dimensional dynamic problems within the framework of considering mathematical model. Numerical realization of this model is carried out by means of the bicyclical space-variable decomposition method on each step by time. For the solution of one-dimensional systems in space directions the monotone essentially nonoscillatory finite-difference scheme with limit reconstruction of the second degree of accuracy is used. A parallel program system for multiprocessor computers is created on the basis of SPMD (Single Program – Multiple Data) technology in Fortran-95 with the use of MPI (Massage Passing Interface) library. The parallelization is accomplished due to 1D or 2D division of computational domain. Program system allows to simulate the propagation of elastic waves produced by mechanical impacts in a body, aggregated of heterogeneous blocks with curvilinear boundaries. It may be applied for the solution of direct seismic problems taking into account complicated mechanical properties of geomaterials.

The system consists of the front-end processor program, the main program of velocities and stresses computation, the subprograms for realization of boundary conditions and pasting together conditions in interior boundaries, and the back-end processor program. The front-end processor is intended to prepare initial data in the packed form and to distribute them uniformly between parallel computational nodes. It also constructs the curvilinear grids in blocks by the Hermite cubic splines. The back-end processor performs special resampling down of data bulks to lower time of traffic along the global network and time of the results graphic processing with the help of personal computer software. The blocks of high dimensionality covered with small grid are distributed (cut on vertical zones) among some computational nodes. If the grid dimensionality of one or more blocks is less than an average dimensionality per node then they are processed by one node. On each node of cluster the main program makes a similar computations consisting of mutually coordinated step-by-step realization of the space-variable decomposition method. The solution of one-dimensional systems in vertical direction is occurred independently. In horizontal direction the interchange of data between processes is carried out at the stage of the limit reconstruction of solution. The standard technology of contour meshes is used. To minimize calculating time the number of interchanges is varied by combined solution of some one-dimensional systems.

Results of computations

To demonstrate an effect of scale parameter in the model of Cosserat continuum let us consider an exact solution of the problem about simple shearing strain in x_1, x_2 plane with constant shear rate $\dot\chi > 0$. In this problem the projection $v_2 = \dot\chi\, x_1$ of the velocity vector is nonzero, and the angular velocity of particles depends only on time variable. Due to the vanishing of normal stresses σ_{ii} and all moments the total system of equations, being under consideration, gives

$$j\,\dot\omega_3 = \sigma_{12} - \sigma_{21}, \quad \dot\sigma_{12} = (\mu + \alpha)\,\dot\chi - 2\,\alpha\,\omega_3,$$
$$\dot\sigma_{21} = (\mu - \alpha)\,\dot\chi + 2\,\alpha\,\omega_3.$$

The rest of equations of the system become identities. From this as a result of time differentiation it follows that

$$j\,\ddot\omega_3 = 2\,\alpha\,\dot\chi - 4\,\alpha\,\omega_3.$$

The solution of such equation, satisfying the initial condition $\omega_3(0) = 0$, is

$$\omega_3(t) = \dot\chi\,\sin^2\sqrt{\frac{\alpha}{j}}\;t.$$

It shows that the self-excited oscillations of angular velocity in the shift domain may be observed. The period of self-oscillations $T = \pi\sqrt{j/\alpha}$ depends on α and tends to infinity under $\alpha \to 0$. If j decreases when the microstructure parameter r_0 tends to zero, then the frequency of oscillations becomes higher.

The stress-strained state, close to simple shear, appears behind the front of transverse wave, if tangential stress, generating it, changes monotonously with time. Graph

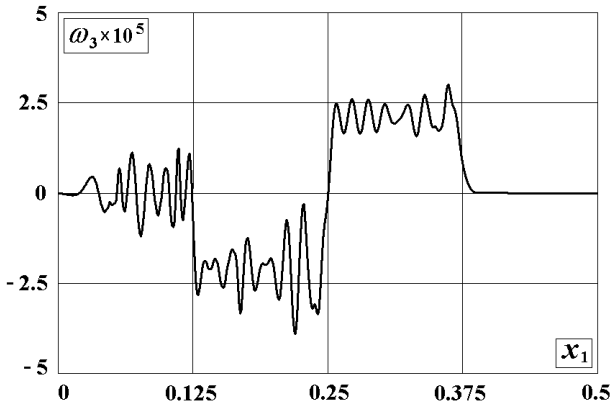

Figure 1: Dependence of ω_3 on x_1 coordinate

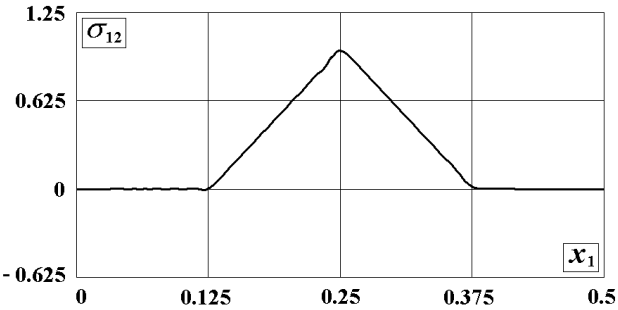

Figure 2: Dependence of σ_{12} on x_1 coordinate

of the dependence of angular velocity ω_3 on longitudinal coordinate x_1 in the case of Λ–like impulse of tangential stress on the boundary $x_1 = 0$ is represented in Fig. 1. The boundary stress increases by linear law during the time interval t_0 and then decreases during the same time. Graph of the dependence of tangential stress σ_{12} on x_1 is shown in Fig. 2. These results are obtained by means of numerical solution within the framework of the model of one-dimensional motion with plane waves. In Fig. 3 and Fig. 4 one can see the level curves of angular velocity and tangential stress in two-dimensional problem, obtained on the grid from 1000×1000 meshes. Three waves of loading and three waves of unloading propagate in the material under action of three impulses on the boundary (Fig. 4). Phenomenological coefficients of the material are taken from [3] for polyurethane, the step of spacial grid is set in accordance with typical scale of the microstructure. The results show the same effect – the oscillations of rotational motion (see Fig. 3) are observed on the fronts of transverse waves.

Acknowledgements

This work was supported by the Complex Program of the Presidium of RAS no. 14 “Fundamental Problems of Informatics and Informational Technologies” and the Russian Science Support Foundation.

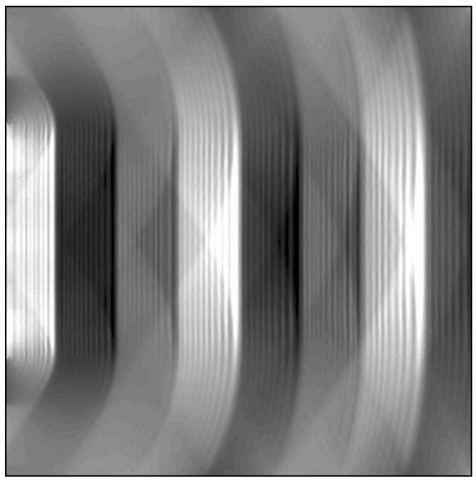

Figure 3: Level curves of angular velocity ω_3

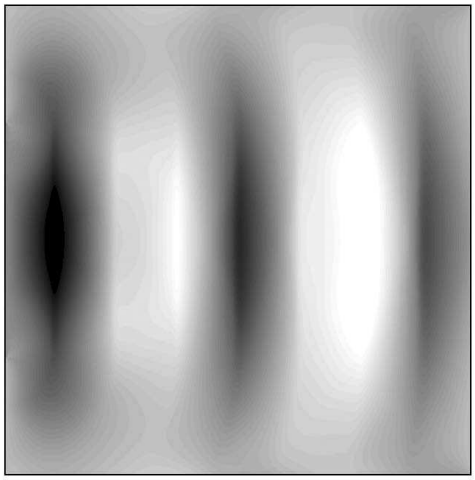

Figure 4: Level curves of tangential stress σ_{12}

References

[1] E. et F. Cosserat, Theorie des Corps Deformables, Librarie Scientifique a Hermann et Fils., Paris, 1909.

[2] V.A. Palmov, “Basic Equations of the Theory of Asymmetrical Elasticity”, Appl. Math. & Mech., vol. 28, pp. 401-408, 1964.

[3] R. Lakes, “Experimental Methods for Study of Cosserat Elastic Solids and Other Generalized Elastic Contiua”, in Continuum Models for Materials with Micro-Structure (Ed. by H. Mühlhaus, J. Wiley), New York, 1995, pp. 1-22.

Elastic Waves

A STABLE FINITE DIFFERENCE METHOD FOR THE ELASTIC WAVE EQUATION ON COMPLEX DOMAINS WITH FREE SURFACE BOUNDARY CONDITIONS

D. Appelö[†,*], **S. Nilsson, N. A. Petersson**[†,*], **B. Sjögreen**[†,*]

[†] CASC, Lawrence Livermore National Laboratory, Livermore, Ca 94551, USA
[*]Email: {appelo2,nilsson2,andersp,sjogreen2}@llnl.gov

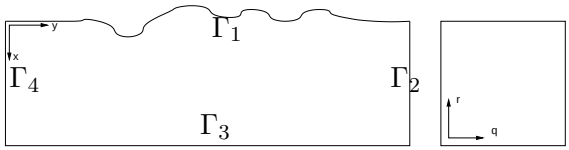

Figure 1: The Geometry. The surface is mapped onto to $q = 0$ and $y = 0$ is mapped onto $r = 0$.

Introduction

We consider elastic wave propagation on complex domains simulated by centered finite difference discretization of the elastic wave equation on second order form. Such discretizations are highly efficient but their use has been limited due to two major difficulties: Stable discretization of the free surface boundary condition and the handling of complex geometries needed for topography. A remedy to the first problem was recently presented in [1] were a stable discretization of the free surface boundary conditions on a Cartesian grid were derived. Here we generalize the results in [1] to curvilinear grids, providing a solution to the second difficulty.

In curvilinear coordinates the elastic wave equation is (on conservative form)

$$J\rho\ddot{u} = \Big[Jq_x\big[\,(2\mu+\lambda)\,\mathcal{D}^x u + \lambda\mathcal{D}^y v\big] + Jq_y\big[\mu(\mathcal{D}^x v + \mathcal{D}^y u)\big]\Big]_q \tag{1}$$
$$+\Big[Jr_x\big[\,(2\mu+\lambda)\,\mathcal{D}^x u + \lambda\mathcal{D}^y v\big] + Jr_y\big[\mu(\mathcal{D}^x v + \mathcal{D}^y u)\big]\Big]_r,$$
$$J\rho\ddot{v} = \Big[Jq_x\big[\mu(\mathcal{D}^x v + \mathcal{D}^y u)\big] + Jq_y\big[\,(2\mu+\lambda)\,\mathcal{D}^y v + \lambda\mathcal{D}^x u\big]\Big]_q \tag{2}$$
$$+\Big[Jr_y\big[(2\mu+\lambda)\mathcal{D}^y v + \lambda\mathcal{D}^x u\big] + Jr_x\big[\mu(\mathcal{D}^x v + \mathcal{D}^y u)\big]\Big]_r.$$

Here $\mathcal{D}^z w = (q_z w_q + r_z w_r)$, $z \in \{x, y\}$. We are interested in a domain (see Figure 1) with free surface boundary condition on Γ_1

$$q_x\left[(2\mu+\lambda)\mathcal{D}^x u + \lambda\mathcal{D}^y v\right] + q_y\mu(\mathcal{D}^x v + \mathcal{D}^y u) = 0, \tag{3}$$
$$q_y\left[(2\mu+\lambda)\mathcal{D}^x v + \lambda\mathcal{D}^y u\right] + q_x\mu(\mathcal{D}^x v + \mathcal{D}^y u) = 0, \tag{4}$$

periodic on Γ_2 and Γ_4 and homogeneous Dirichlet on Γ_3.

This work was performed under the auspices of the U.S. Department of Energy by University of California, Lawrence Livermore National Laboratory under Contract W-7405-Eng-48.

Spatial Discretization

Let the mapping from the unit square to the physical domain be given by

$$x(q,r), y(q,r), \;\; (q,r) \in [0,1]^2,$$

and let the grid in (q, r) space be defined by

$$q_i = (i-1)h_q, i = 0, \ldots, N_q, h_q = 1/(N_q - 1),$$
$$r_j = (j-1)h_r, j = 0, \ldots, N_r, h_r = 1/(N_r - 1).$$

Denote the grid functions $[u_{i,j}, v_{i,j}]$. The standard second order accurate difference operators are

$$h_r D_+^r u_{i,j} = u_{i,j+1} - u_{i,j}, \;\; D_-^r u_{i,j} = D_+^r u_{i,j-1},$$
$$h_q D_+^q u_{i,j} = u_{i+1,j} - u_{i,j}, \;\; D_-^q u_{i,j} = D_+^q u_{i-1,j},$$
$$2D_0^r u_{i,j} = D_+^r u_{i,j} + D_-^r u_{i,j},\; 2D_0^q u_{i,j} = D_+^q u_{i,j} + D_-^q u_{i,j}.$$

We will also use the one sided operator and averaging operators

$$\widetilde{D_0^q} u_{i,j} = \begin{cases} D_+^q u_{i,j}, & i = 1, \\ D_0^q u_{i,j}, & i \geq 2, \end{cases}$$
$$2E_{1/2}^q(\sigma_{i,j}) = \sigma_{i+1,j} + \sigma_{i,j}, \;\; 2E_{1/2}^r(\sigma_{i,j}) = \sigma_{i,j+1} + \sigma_{i,j},$$

to discretize (1) and (2). The spatial approximation is

$$\begin{aligned} J\rho\ddot{u} = {} & D_-^q E_{1/2}^q(Jq_xq_x(2\mu+\lambda))D_+^q u + \widetilde{D_0^q}(Jq_xr_x(2\mu+\lambda))D_0^r u \\ & + D_-^q E_{1/2}^q(Jq_xq_y\lambda)D_+^q v + \widetilde{D_0^q}(Jq_xr_y\lambda)D_0^r v + D_-^q E_{1/2}^q(Jq_yq_x\mu)D_+^q v \\ & + \widetilde{D_0^q}(Jq_yr_x\mu)D_0^r v + D_-^q E_{1/2}^q(Jq_yq_y\mu)D_+^q u + \widetilde{D_0^q}(Jq_yr_y\mu)D_0^r u \\ & + D_0^r(Jr_xq_x(2\mu+\lambda))\widetilde{D_0^q} u + D_-^r E_{1/2}^r(Jr_xr_x(2\mu+\lambda))D_+^r u \\ & + D_0^r(Jr_xq_y\lambda)\widetilde{D_0^q} v + D_-^r E_{1/2}^r(Jr_xr_y\lambda)D_+^r v + D_0^r(Jr_yq_x\mu)\widetilde{D_0^q} v \\ & + D_-^r E_{1/2}^r(Jr_yr_x\mu)D_+^r v + D_0^r(Jr_yq_y\mu)\widetilde{D_0^q} u + D_-^r E_{1/2}^r(Jr_yr_y\mu)D_+^r u \\ & \equiv L^{(u)}(u,v). \end{aligned} \tag{5}$$

$$\begin{aligned} J\rho\ddot{v} = {} & D_-^q E_{1/2}^q(Jq_xq_x\mu)D_+^q v + \widetilde{D_0^q}(Jq_xr_x\mu)D_0^r v + D_-^q E_{1/2}^q(Jq_xq_y\mu)D_+^q u \\ & + \widetilde{D_0^q}(Jq_xr_y\mu)D_0^r u + D_-^q E_{1/2}^q(Jq_yq_x\lambda)D_+^q u + \widetilde{D_0^q}(Jq_yr_x\lambda)D_0^r u \\ & + D_-^q E_{1/2}^q(Jq_yq_y(2\mu+\lambda))D_+^q v + \widetilde{D_0^q}(Jq_yr_y(2\mu+\lambda))D_0^r v + D_0^r(Jr_xq_x\mu)\widetilde{D_0^q} v \\ & + D_-^r E_{1/2}^r(Jr_xr_x\mu)D_+^r v + D_0^r(Jr_xq_y\mu)\widetilde{D_0^q} u + D_-^r E_{1/2}^r(Jr_xr_y\mu)D_+^r u \\ & + D_0^r(Jr_yq_x\lambda)\widetilde{D_0^q} u + D_-^r E_{1/2}^r(Jr_yr_x\lambda)D_+^r u \\ & + D_0^r(Jr_yq_y(2\mu+\lambda))\widetilde{D_0^q} v + D_-^r E_{1/2}^r(Jr_yr_y(2\mu+\lambda))D_+^r v \\ & \equiv L^{(v)}(u,v). \end{aligned} \tag{6}$$

The discrete boundary conditions on Γ_3 and Γ_2, Γ_4 are

$$u_{N_q,j} = v_{N_q,j} = 0, \tag{7}$$

$$u_{i,1} = u_{i,N_r}, \;\; u_{i,0} = u_{i,N_r-1} \tag{8}$$

$$v_{i,1} = v_{i,N_r}, v_{i,0} = v_{i,N_r-1}. \tag{9}$$

Finally, in order to obtain a stable method we approximate the boundary conditions (3), (4) by

$$\begin{aligned}
&\tfrac{1}{2}\left((Jq_xq_x(2\mu+\lambda))_{3/2,j}D_+^q u^1_{1,j} + (Jq_xq_x(2\mu+\lambda))_{1/2,j}D_+^q u^1_{0,j}\right)\\
&+(Jq_xr_x(2\mu+\lambda))_{1,j}D_0^r u^1_{1,j} + \tfrac{1}{2}\left((Jq_xq_y\lambda)_{3/2,j}D_+^q v^1_{1,j} + (Jq_xq_y\lambda)_{1/2,j}D_+^q v^1_{0,j}\right)\\
&+(Jq_xr_y\lambda)_{1,j}D_0^r v^1_{1,j} + \tfrac{1}{2}\left((Jq_yq_x\mu)_{3/2,j}D_+^q v^1_{1,j} + (Jq_yq_x\mu)_{1/2,j}D_+^q v^1_{0,j}\right)\\
&+(Jq_yr_x\mu)_{1,j}D_0^r v^1_{1,j} + (Jq_yr_y\mu)_{1,j}D_0^r u^1_{1,j}\\
&+\tfrac{1}{2}\left((Jq_yq_y\mu)_{3/2,j}D_+^q u^1_{1,j} + (Jq_yq_y\mu)_{1/2,j}D_+^q u^1_{0,j}\right) = 0,
\end{aligned} \tag{10}$$

$$\begin{aligned}
&\tfrac{1}{2}\left((Jq_xq_x\mu)_{3/2,j}D_+^q v^1_{1,j} + (Jq_xq_x\mu)_{1/2,j}D_+^q v^1_{0,j}\right)+\left((Jq_xr_x\mu)_{1,j}D_0^r v^1_{1,j}\right)\\
&+\tfrac{1}{2}\left((Jq_xq_y\mu)_{3/2,j}D_+^q u^1_{1,j} + (Jq_xq_y\mu)_{1/2,j}D_+^q u^1_{0,j}\right)+\left((Jq_xr_y\mu)_{1,j}D_0^r u^1_{1,j}\right)\\
&+\tfrac{1}{2}\left((Jq_yq_y(2\mu+\lambda))_{3/2,j}D_+^q v^1_{1,j} + (Jq_yq_y(2\mu+\lambda))_{1/2,j}D_+^q v^1_{0,j}\right)\\
&+\left((Jq_yr_y(2\mu+\lambda))_{1,j}D_0^r v^1_{1,j}\right) + \left((Jq_yr_x\lambda)_{1,j}D_0^r u^1_{1,j}\right)\\
&+\tfrac{1}{2}\left((Jq_yq_x\lambda)_{3/2,j}D_+^q u^1_{1,j} + (Jq_yq_x\lambda)_{1/2,j}D_+^q u^1_{0,j}\right) = 0.
\end{aligned} \tag{11}$$

Introducing the discrete scalar products

$$(w,u)_h = \sum_{j=1}^{N_r-1}\frac{h_qh_r}{2}w_{1,j}u_{1,j} + \sum_{i=2}^{N_q-1}h_qh_rw_{i,j}u_{i,j},$$

$$(w,u)_{hr} = \sum_{j=1}^{N_r-1}\sum_{i=2}^{N_q-1}h_qh_rw_{i,j}u_{i,j},$$

where u and v are real valued functions, with corresponding norms $\|w\|_h^2 = (w,w)_h$, $\|w\|_{hr}^2 = (w,w)_{hr}$, we can prove the following

Lemma 1 (self adjoint spatial discretization). *For all real-valued grid functions (u^0,v^0), (u^1,v^1) satisfying the discrete boundary conditions (7), (8), (9), (10), (11), the spatial operator $(L^{(u)},L^{(v)})$ is self-adjoint, i.e.*

$$\begin{aligned}
&(u^0, L^{(u)}(u^1,v^1))_h + (v^0, L^{(v)}(u^1,v^1))_h =\\
&(u^1, L^{(u)}(u^0,v^0))_h + (v^1, L^{(v)}(u^0,v^0))_h.
\end{aligned} \tag{12}$$

From lemma 1 it follows that.

Corollary 1 (conservation of energy). *All real-valued solutions (u,v) to the equations (5), (6) with boundary conditions (7), (8), (9), (10) and (11), satisfy*

$$\begin{aligned}
&\|\sqrt{J\rho}\,u_t\|_h^2 + \|\sqrt{J\rho}\,v_t\|_h^2\\
&-(u, L^{(u)}(u,v))_h - (v, L^{(v)}(u,v))_h = C.
\end{aligned} \tag{13}$$

Here C is a constant depending only on the initial data.

We can also use the following lemma to establish that the conserved quantity (13) is a norm.

Lemma 2 (ellipticity). *For all real-valued grid functions (u,v) satisfying the discrete boundary conditions (7), (8), (9), (10), (11), the spatial operator the spatial operators $L^{(u)}(u,v), L^{(v)}(u,v)$ satisfy the following equality*

$$\begin{aligned}
&-(u, L^{(u)}(u,v))_h - (v, L^{(v)}(u,v))_h =\\
&\mathcal{P}_1 + \mathcal{P}_2 + \mathcal{P}_3 + \mathcal{P}_4,\\
&\mathcal{P}_1 \geq 0, \;\; \mathcal{P}_2 \geq 0, \;\; \mathcal{P}_3 \geq 0, \;\; \mathcal{P}_4 \geq 0.
\end{aligned} \tag{14}$$

Where

$$\begin{aligned}
\mathcal{P}_1 &= \|\sqrt{J\lambda}(q_x\widetilde{D_0^q}u + r_xD_0^ru + q_y\widetilde{D_0^q}v + r_yD_0^rv)\|_h^2 + \|\sqrt{J2\mu}(q_x\widetilde{D_0^q}u + r_xD_0^ru)\|_h^2\\
&+\|\sqrt{J2\mu}(q_y\widetilde{D_0^q}v + r_yD_0^rv)\|_h^2 + \|\sqrt{J\mu}(q_y\widetilde{D_0^q}u + r_yD_0^ru + q_x\widetilde{D_0^q}v + r_xD_0^rv)\|_h^2,\\
\mathcal{P}_2 &= \frac{h_r^2}{4}\left(\|\sqrt{J2\mu}r_xD_+^rD_-^ru\|_h^2 + \|\sqrt{J2\mu}r_yD_+^rD_-^rv\|_h^2\right)\\
&+\frac{h_q^2}{4}\left(\|\sqrt{J2\mu}q_xD_+^qD_-^qu\|_{hr}^2 + \|\sqrt{J2\mu}q_yD_+^qD_-^qv\|_{hr}^2\right)\\
&+\frac{h_r^2}{4}\|\sqrt{J\lambda}(r_xD_+^rD_-^ru + r_yD_+^rD_-^rv)\|_h^2 + \frac{h_q^2}{4}\|\sqrt{J\lambda}(q_xD_+^qD_-^qu + q_yD_+^qD_-^qv)\|_{hr}^2\\
&\frac{h_r^2}{4}\|\sqrt{J\mu}(r_xD_+^rD_-^rv + r_yD_+^rD_-^ru)\|_h^2 + \frac{h_q^2}{4}\|\sqrt{J\mu}(q_xD_+^qD_-^qv + q_yD_+^qD_-^qu)\|_{hr}^2,\\
\mathcal{P}_3 &= \frac{h_r}{2}\sum_{j=1}^{N_r-1}\left((J\lambda)_{N_q,j}((q_x)_{N_q,j}u_{N_q-1,j} + (q_y)_{N_q,j}v_{N_q-1,j})^2\right.\\
&\left.+(J\mu)_{N_q,j}((q_x)_{N_q,j}v_{N_q-1,j} + (q_y)_{N_q,j}u_{N_q-1,j})^2\right),\\
\mathcal{P}_4 &= \frac{h_qh_r}{2}\sum_{j=1}^{N_r-1}\left((J\lambda)_{3/2,j}((q_x)_{3/2,j}D_+^qu_{1,j} + (q_y)_{3/2,j}D_+^qv_{1,j})^2\right.\\
&+(J\mu)_{3/2,j}((q_x)_{3/2,j}D_+^qv_{1,j} + (q_y)_{3/2,j}D_+^qu_{1,j})^2\\
&\left.+(J2\mu)_{3/2,j}(((q_x)_{3/2,j}D_+^qu_{1,j})^2 + ((q_y)_{3/2,j}D_+^qv_{1,j})^2)\right).
\end{aligned}$$

Temporal Discretization

In time we discretize using standard Leap-Frog, i.e. the fully discrete equations are

$$\begin{aligned}
u^{n+1} - 2u^n + u^{n-1} &= (\rho J)^{-1}k^2L^{(u)}(u^n,v^n),\\
v^{n+1} - 2v^n + v^{n-1} &= (\rho J)^{-1}k^2L^{(v)}(u^n,v^n).
\end{aligned}$$

For this time discretization it can be proved that the discrete quantity

$$\begin{aligned}
C_e(t_{n+1}) &= \|D_+^tu^n\|_\rho^2 + \|D_+^tv^n\|_\rho^2 -\\
&(u^{n+1}, (\rho J)^{-1}L^{(u)}(u^n,v^n))_{\rho J}\\
&-(v^{n+1}, (\rho J)^{-1}L^{(v)}(u^n,v^n))_{\rho J},
\end{aligned}$$

is conserved. That is, $C_e(t_{n+1}) = C_e(t_n)$. Here $(f, g/(\rho J))_{\rho J} = (f,g)_h$ is a weighted scalar product.

Computations

To verify the order of accuracy we determined forcing functions in the equations and boundary conditions such

N	maxerr u	maxerr v	e_i/e_{i+1}, u	e_i/e_{i+1}, v
80	0.16533	0.15609		
160	0.04245	0.03912	3.89	3.99
320	0.01071	0.00971	3.96	4.03
640	0.00269	0.00240	3.98	4.04

Table 1: Order of accuracy with method of manufactured solution.

that the solution is given by

$$u = \sin(6.2(x - 1.3t))\sin(6.2y),$$
$$v = \sin(6.2(x - 1.2t))\sin(6.2y).$$

We computed the solution on the grid defined by

$$x = x' + 0.05\sin(y'),\ y = y' + 0.05\sin(x'),$$
$$(x', y') \in [-\pi, \pi]^2.$$

We choose $\lambda = \mu = 1$ and advanced the solution up to time $\pi/5$ with a time step $k = 0.1h$, $h = \pi/N, N = 80, 160, 320, 640$ and computed the maximum error in the final solution. The results, showing the second order convergence, are displayed in Table 1.

Computations on a single grid

In Figure 2 we present a computation with initial data consisting of a pure pressure pulse centered in $(x, y) = (0.1, 1)$ which we advance up to time 0.2. The computation is performed for a material with $\rho = 1, \mu = 1, \lambda = 7$. As the pulse hits the free surface the P-wave transforms into reflected P and S-waves and surface waves traveling along the surface, see Figure 2. For this computation we

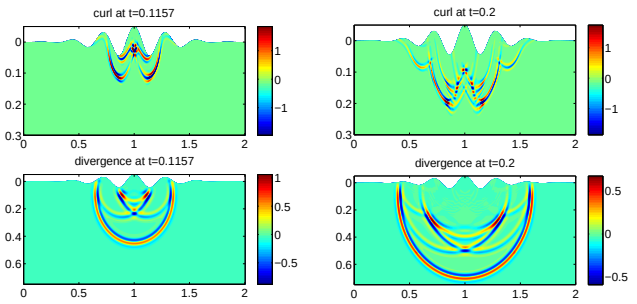

Figure 2: Divergence and Curl at two times. The initial data consisted of a pure pressure wave, thus there is no S-wave corresponding to the lowermost P-wave. The free surface boundary condition converts the P-wave into S-waves and surface waves.

monitored the quantity $C_e(t_{n+1}) - C_e(t_n)$ and as can be seen in Figure 3 it is conserved to machine precision.

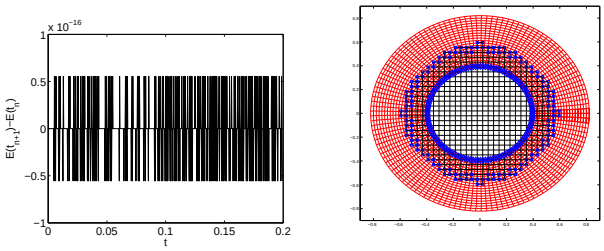

Figure 3: Left: Difference in the discrete energy, $C_e(t_{n+1}) - C_e(t_n)$, for subsequent time steps. Right: An overset grid.

Computations on an overset grid

Finally we present a computation on an overset grid of the type displayed in Figure 3. On the Cartesian grid we use the discretization from [1] and on the curvilinear grid we use the proposed discretization. To suppress weak instabilities triggered by the interpolation we add a small dissipative term, $\alpha h^3(D_+D_-)^2$, to both equations in both directions on both grids. Here we chose $\lambda = 0.005, \mu = 0.001$ and force the solution in $(x, y) = (-0.7, 0)$ with a Gaussian pressure pulse with support up to time 1.6. Again, the reflection of the free surface generates a S-wave and a P-wave while the primary P-wave traveling to the right in the interior remains solitary, see Figure 4.

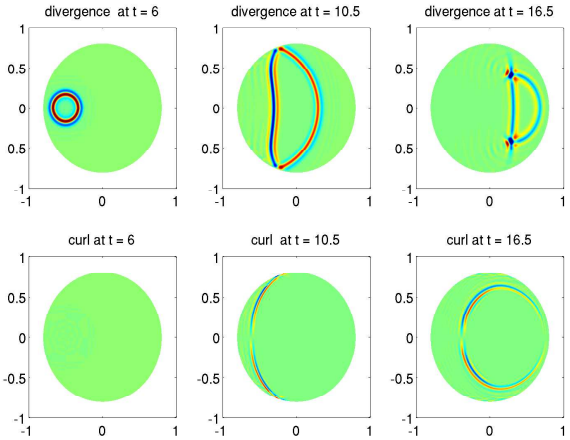

Figure 4: P and S-wave at three different times.

References

[1] Nilsson, Petersson, Sjogreen and Kreiss, "Stable difference approximations for the elastic wave equation in second order formulation", submitted to SINUM.

DISPERSION OF ELASTIC WAVES IN THE CONTACT-IMPACT PROBLEM OF A LONG CYLINDER

D. Gabriel[†,*], **J. Plešek**[†], **R. Kolman**[†], **and F. Valeš**[†]
[†]Institute of Thermomechanics, Academy of Sciences, Praha, Czech Republic
[*]Email: gabriel@it.cas.cz

Abstract

The numerical dispersion of two-dimensional finite elements was studied. The outcome of this dispersion study was verified by the numerical and analytical solutions to the longitudinal impact of two long cylindrical bars. In accordance with the results of the dispersion analysis it was proved that the quadratic elements showed better accuracy than the linear ones.

Introduction

Spatial discretization of a continuum by means of the finite element method (FEM) introduces dispersion error to a numerical solution of wave propagation. Despite of many papers published on the subject, little attention has been paid so far to higher-order elements. Belytschko and Mullen [1] were the first to extend the dispersion analysis to quadratic one-dimensional finite elements. The dispersion study of the three-dimensional second-order Helmholtz equation was carried out by Abboud and Pinsky [2] for 20-node elements. However, the dispersion analysis of a standard solid mechanics problem has not yet been performed.

In this work, recent results accomplished by authors are summarized, specifically the extension of dispersion analysis to the eight-node serendipity finite elements [3], [4]. The outcome of this dispersion study is verified by the numerical and analytical solutions to the longitudinal impact of two long cylindrical bars [5].

Numerical dispersion analysis

In dispersion analysis two dimensional bilinear and serendipity finite element meshes were used. Since the meshes were regular and uniform only the characteristic patches containing 2×2 elements were considered—see Fig. 1. Furthemore, in bilinear mesh, all the nodes possess the same sub-matrices in the final assembly and, thus, only one characteristic set of equations corresponding to, say, node $\{m, n\}$ have to be assembled. Likewise, one corner node $\{m, n\}$ and two mid-side nodes $\{m + 1, n\}$ and $\{m, n + 1\}$ must be taken into account when dealing with the serendipity mesh.

Suppose that the origin of the coordinate system is located at the node $\{m, n\}$. Thus, for the bilinear mesh holds

$$x_{m+k} = kH_x, \;\; y_{n+l} = lH_y, \;\; \text{for} \;\; k, l = \pm 0, 1 \qquad (1)$$

and for the serendipity mesh

$$x_{m+k} = kH_x/2, \;\; y_{n+l} = lH_y/2, \;\; \text{for} \;\; k, l = \pm 0, 1, 2 \qquad (2)$$

where H_x and H_y denote the size of rectangular element (Fig. 1).

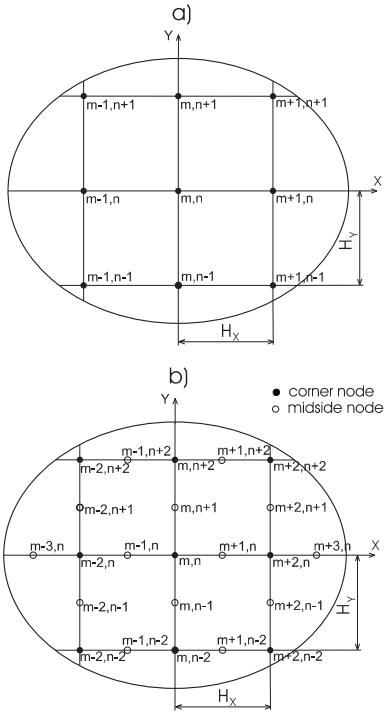

Figure 1: Two dimensional a) bilinear b) serendipity regular finite element mesh.

The system of differential equation derived for the nodes of the considered patch can be written as

$$\mathbf{M}_c \ddot{\mathbf{u}}_c + \mathbf{K}_c \mathbf{u}_c = \mathbf{0} \qquad (3)$$

where the local consistent mass matrix $\mathbf{M}_c$ and the local stiffness matrix $\mathbf{K}_c$ are of a rectangular form 2×18 and 6×42 for the bilinear and serendipity elements, respectively.

Next, the classic Fourier analysis follows when the prescribed nodal harmonic solution in the form

$$u_{ij} = U_{ij} \exp(\mathrm{i}\frac{2\pi}{\lambda}(p_x x_i + p_y y_j - ct)) \qquad (4)$$
$$v_{ij} = V_{ij} \exp(\mathrm{i}\frac{2\pi}{\lambda}(p_x x_i + p_y y_j - ct))$$

is substituted to the differential equilibrium equations (3). In Eqn. (4) $\mathrm{i} = \sqrt{-1}$ is the imaginary unit, λ is the wavelength , c is the phase velocity, t is time and U_{ij}, V_{ij} are unknown amplitudes defining the shape of the deformation mode. The components of the unit normal to the wave front $\mathbf{p}$ may be expressed as

$$p_x = \cos\theta, \qquad p_y = \sin\theta \tag{5}$$

where θ is the direction of the plane wave propagation throw the finite element grid. The described approach leads to the solution of a generalized eigenvalue problem and the desired dispersion relationships in the form $c = f(\lambda, \theta)$ are obtained.

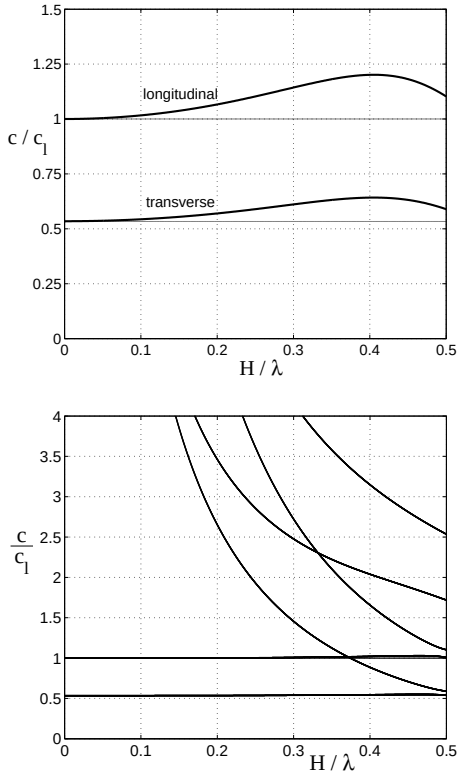

Figure 2: Wave speed versus wave length for bilinear (upper) and serendipity (lower) elements.

Comparison of dispersion properties for bilinear and serendipity elements is shown in Fig. 2, where the normalized wave speed c/c_1 versus the normalized wave length H/λ is drawn for the worst case in terms of dispersion $\theta = 0$. Fig. 2 clearly shows the advantage of quadratic elements over linear ones. There is virtually no dispersion up to the resolution limit $H/\lambda = 0.5$ for quadratic elements. Furthermore, there are four additional spurious solutions, called the optical modes, which are connected with the discrete structures only. In contrast to the acoustic modes (longitudinal and transversal waves) they do not really exist in a perfect continuum. Note that the optical modes are not eigenvectors so that they do not affect the numerical stability.

Impact of two long elastic cylinders

The longitudinal impact of two long elastic cylinders was studied, for which the analytical solution was available [5]. The cylinders dimensions were $\varnothing 5 \times 6.25$ mm. Young's modulus, Poisson's ratio and density were $E = 2.1 \times 10^5$ MPa, $\nu = 0.3$, $\rho = 7800\,\mathrm{kg/m^3}$, respectively. The cylinders made contact with initial velocity $v_0 = 1$ m/s prescribed at time $t = 0$ s. Using this problem, symmetric properties of the contact algorithm based on the pre-discretization penalty method [6] were tested simultaneously.

The analytical solution [5] utilizing the Laplace transform is rather complex. The distributions of displacements and stresses are cast in the form of infinite series of improper integrals which are evaluated numerically. For illustration, theoretical positions of wave fronts for time $c_1 t/a = 2$ are plotted in Fig. 3, where r, z denote cylindrical coordinates, a the radius of the cylinder and t time, respectively.

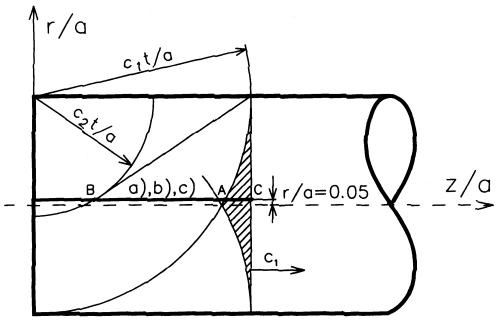

Figure 3: Theoretical position of wave fronts for $c_1 t/a = 2$ after [5].

The primary wave front propagates with the speed of longitudinal waves c_1. Furthermore, the wave fronts of longitudinal and transversal waves generated by the reflection from boundaries can be observed. The unloading (rarefaction) wave fronts of shear waves propagate with the speed c_2. The hatched part corresponds to the state of stress encountered in the impact of two half-spaces.

The problem was treated as axisymmetric one, each cylinder discretized by 100×250 four-node linear elements and 50×125 eight-node serendipity elements. The linear mesh was obtained by regular refinement bisecting the quadratic elements at the mid-side nodes. Thus, the total number of degrees of freedom `NDOF` is greater for

the linear mesh ($\mathsf{NDOF} = 50702$) than for the quadratic one ($\mathsf{NDOF} = 38202$). The Newmark integration scheme with the consistent mass matrix was employed. In order to diminish the influence of numerical integration the time step was chosen very small. It was set to $\Delta t = 1.038174 \cdot 10^{-9}$ s, which corresponds to the dimensionless Courant number $Co = 0.25$ for linear elements and 0.125 for quadratic elements.

Comparison of accuracy for both discretization patterns follows from Fig. 4, where the normalized axial stress distribution $\sigma_z^* = \sigma_z c_1/\lambda v_0$ along the cylinders axis z/a is drawn. The results are plotted for time $c_1 t/a = 2$ at a short distance from the axis $r/a = 0.05$ (see Fig. 3). In addition, the analytical solution is plotted in Fig. 4.

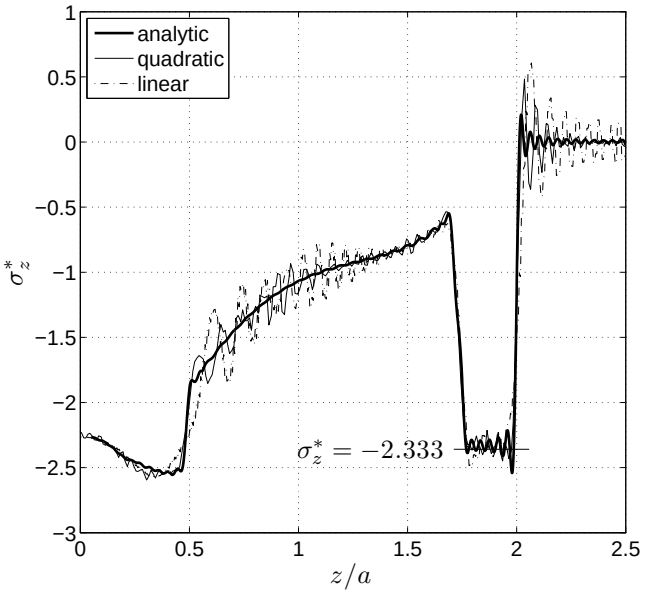

Figure 4: Axial stress distribution along axial coordinate for $c_1 t/a = 2$ and $r/a = 0.05$.

It is interesting to note the way the response is influenced by wave fronts of unloading waves (see points A and B). In the region between points A and C the value of axial stress should be identical to the constant value $\sigma_z^* = -2.333$ corresponding to the half-space impact problem. At point C the stress should undergo a step change from $\sigma_z^* = -2.333$ to zero. It should be pointed out that the accuracy of analytical solution is strongly influenced by the number of terms included in the series of improper integrals [5]. The analytical solution plotted in this paper was derived from the summation of the first 150 terms of this series. However, the value of axial stress significantly oscillates in the region of the "should have been" constant stress. This effect will reduce provided a greater number of terms have been used.

It is obvious that the quadratic elements exhibit better accuracy than the linear ones using even less number of degrees of freedom. In addition, the linear solution shows more "ragged" distribution. This is especially apparent behind the primary wave front corresponding to the state of zero stress. In this pre-front zone, the decay of undesired oscillation is slower than for the quadratic mesh. This example nicely demonstrates capabilities of the two element types and evokes similar conclusions as those drawn from the dispersion distributions compared in Fig. 2.

Acknoledgements

This work was supported by the Grant Agency of the Czech Republic under grant numbers 101/07/1471, 101/06/0914 and 101/06/0213 in the framework of AV0Z 20760514.

References

[1] T. Belytschko, R. Mullen, "On dispersive properties of finite element solutions", in Modern Problems in Elastic Wave Propagation, Wiley, New York, 1978, pp. 67-82.

[2] N.N. Abboud, P.M. Pinsky, "Finite element dispersion analysis for the three-dimensional second-order scalar wave equation", International Journal for Numerical Methods in Engineering, vol. 35, pp. 1183-1218, 1992.

[3] J. Plešek, R. Kolman, M. Okrouhlík, "Numerical dispersion of quadratic finite element meshes", in WCCM VII, University of California, Los Angeles, 16-22 July 2006, CDROM.

[4] J. Plešek, R. Kolman, M. Okrouhlík, "On the occurrence of spurious optical modes in transient finite element analysis", in Mechanics & Materials in Design, University of Porto, Porto, Portugal, 24-26 July 2006, pp. 189-190.

[5] F. Valeš, Š. Morávka, R. Brepta, J. Červ, "Wave propagation in a thick cylindrical bar due to longitudinal impact", JSME Int. J., Ser.A, vol. 39(1), pp. 60-70, 1996.

[6] D. Gabriel, J. Plešek, M. Ulbin, "Symmetry preserving algorithm for large displacement frictionless contact by the pre-discretization penalty method", International Journal for Numerical Methods in Engineering, vol. 61, pp. 2615-2638, 2004.

TRUNCATION OF TARGET AREA IN NUMERICAL SIMULATION OF ELASTIC WAVES BASED ON OPTIMAL GRIDS

V. Lisitsa[†,*]
[†]Institute of Petroleum Geology & Geophysics SB RAS, Novosibirsk, Russia
[*]Email: vlisitsa@uiggm.nsc.ru

Abstract

This paper presents an efficient way of domain truncation for isotropic and anisotropic elastic problems based on the Optimal Grids (OG) technique. In case of isotropic elasticity the optimal discretization of the Perfectly Matched Layer (PML) allows one to use as few as three points to achieve desired reduction of artificial reflections. It is well known that PML for elastic anisotropic media could be unstable. The domain distension with use of OG is proposed for these problems. OG provides extremely high level of accuracy so one can use a few grid points per wavelength in this extension and to reduce the computational cost of this approach to acceptable level in comparison with regular PML.

Introduction

The commonly used approaches to truncate the target area are Absorbing Boundary Conditions (ABC) [5] and PML [4]. The main idea of ABC is to cut off incoming solutions. In a spectral domain it is equivalent to boundary condition $u_x = -\sqrt{\Lambda}u$ for scalar problems. In physical domain this condition leads to nonlocal operator which is hard to discretize efficiently. In order to have local spatial operator one should use rational approximation of the square root [5]. This approach is efficient and low cost but complicated for implementation especially for elastic wave equations. PML is surrounding the target area with some artificial medium with attenuation. PML is simpler in implementation but it increases the size of the problem essentially. In order to reduce its claims we introduce the Optimal PML discretization proposed for the wave equation in [1]. Within this PML one performs pure imaginary change of variables $i\omega x = \tilde{x}$ transforming the propagative modes to evanescent ones. The solution on the interface $x = 0$ is under investigation and it can be represented as action of the Neumann to Dirichlet (NtD) map on Neumann data $u = \frac{-1}{\sqrt{\Lambda}}u_x$. On the other hand finite-difference (f-d) NtD map is rational function of the spectral parameter depending on grid steps [1]. So the problem of optimal discretization of the PML is equivalent to the rational approximation of the square root and consequently to construction of ABC. The main difference between Optimal PML and ABC is a representation of rational function in physical domain which is simpler in terms of grid steps as it was done for PML. We are presenting the expansion of this approach on elasticity problems.

For anisotropy elastic media one can not construct PML being stable for any values of parameters (see for example [3]). We prove that the domain distension allows one to avoid this problem. The main idea of this method is a surrounding of the computational area by the rather thick elastic layer with the same properties as target area. This approach is computationally expensive if equidistant grids are used. On the other hand implementation of the Optimal Grids allows one to reach more then exponential convergence of the f-d solution at the interface [6] and essentially reduce the size of f-d problem.

Optimal PML for Isotropic Elasticity

Let us consider the system of equations:

$$\begin{cases} \rho\dfrac{\partial u}{\partial t} = \nabla\cdot\sigma \\ \dfrac{\partial \sigma}{\partial t} = C\dfrac{1}{2}\left(\nabla u + \nabla u^T\right) \end{cases} \tag{1}$$

where ρ is a density, u is a velocity vector, σ is a stress tensor and C is a fourth order tensor of media parameters.

Assume the PML in x direction needs to be constructed. Following [1] let us implement pure imaginary coordinate transform in spectral domain and obtain the system:

$$\begin{pmatrix} 0 & A \\ A^T & 0 \end{pmatrix}\frac{d}{dx}\begin{pmatrix} w_1 \\ w_2 \end{pmatrix} - \begin{pmatrix} B_1 & 0 \\ 0 & B_2 \end{pmatrix}\begin{pmatrix} w_1 \\ w_2 \end{pmatrix} = 0, \tag{2}$$

where matrix A is constant, matrices B_1 and B_2 are symmetric depending on media parameters, time and spatial frequencies. Unknowns are $w_1 = (u_x, \sigma_{xz})$ and $w_2 = (\sigma_{xx}, u_z, \sigma_{zz})$.

Let us introduce boundary conditions:

$$w_1 \to 0|_{x\to\infty}, \quad Aw_2 = w^0|_{x=0}.$$

The solution of the problem on the interface can be uniquely represented as an action of the Neumann to Dirichlet (NtD) map on the input data. So

$$w_1(0) = \left[R^p\sqrt{\Lambda_p}^{-1} + R^s\sqrt{\Lambda_s}^{-1}\right]w^0,$$

where matrices R^p and R^s are the functions of frequencies and they are bounded, parameters are

$$\Lambda_{p,s} = v_{p,s}^{-2}\cos^2(\alpha) \in [0, v_{p,s}^{-2}] \subseteq [0, v_s^{-2}],$$

where α is an incident angle.

Finite-difference problem approximating (2) on some staggered grid with boundary conditions has unique solution. This solution can be computed explicitly at the interface:

$$(w_1^k)_1 = \left[R^p f^k(\Lambda_p) + R^s f^k(\Lambda_s)\right] w^0,$$

where matrices R^p and R^s coincide with ones appeared in solution of the differential problem. Function $f^k(\Lambda)$ with k being the total number of points within PML is rational and depends on grid steps. Moreover if the rational approximation of a square root was done then according to [1] the grid steps for Optimal PML can be recovered uniquely.

Anisotropic Problems

Let us consider the system (1). In case of arbitrary anisotropic problems the tensor of media parameters is no longer block-diagonal so the Virieux scheme [7] can not be used. As it was shown in [2] Lebedev scheme(LS) on both optimal and equidistant is applicable for these elastic media. This fact will be used to construct a domain distension for anisotropy.

Let us implement the domain distension in x direction for $x > 0$. The artificial layer should be added for $0 < x < L$ where L is defined by the model parameters. Use of LS leads to transformation of system (1) in spectral domain to the following one

$$\begin{pmatrix} 0 & A \\ A^T & 0 \end{pmatrix} \frac{d}{dx} \begin{pmatrix} w_1 \\ w_2 \end{pmatrix} - \begin{pmatrix} B & 0 \\ 0 & B \end{pmatrix} \begin{pmatrix} w_1 \\ w_2 \end{pmatrix} = 0, \tag{3}$$

where matrix A is constant, matrix B is symmetric depending on frequencies. The vectors w_1 and w_2 are no longer physical variables so we skip their explicit representation. Let us add boundary conditions:

$$w_1 = 0|_{x=L}, \quad Aw_2 = w^0|_{x=0}.$$

The solution of this problem at the interface $x = 0$ can be found analytically and it is result of an action of the NtD map on Neumann data:

$$w_1(0) = \sum_j R_j f(\Lambda_j) w^0,$$

where summation is performed over all modes, $-\infty < \Lambda^0 v_j^{-2} \leq \Lambda_j \leq 0$ is spectral parameter, left boundary of the spectral interval Λ^0 is defined by the source function, normalizing parameter v_j is a phase velocity of corresponding mode. Meromorphic function $f(\Lambda)$ coincides with one for wave equation with unitary velocity.

The solution of the corresponding f-d problem on Lebedev scheme can also be represented as action of the f-d NtD map on Neumann data:

$$(w_1^k)_1 = \sum_j R_j f^k(\Lambda_j) w^0,$$

where matrices R_j coincide with ones appeared in true NtD map and they are bounded as functions of frequencies. Rational function $f^k(\Lambda)$ depends on grid steps and has the same form as one for PML so grid steps can be recovered if rational function was constructed. The rate of convergence of f-d solution is defined the convergence of the rational approximation. As it was shown in [6] use of Pade-Tchebichev approximation for this problem allows one to archive more then exponential convergence. So Optimal Grids for allows to compute high order f-d solution at the interface using as few as three points per minimal wavelength.

Numerical Experiments

Optimal PML

The goal of the numerical experiments for Optimal PML was to investigate dependence of the reflection coefficients on number of grid points inside the PML. The discretization of the PML was done for true velocities i.e. for ones corresponding to the differential problem. Due to numerical dispersion appearing in f-d solution the velocities on the scheme differ from the true ones so the reflection coefficients do not converge to zero anymore. These coefficients the same as velocities on f-d scheme depend on number of points per wavelength (ppw) inside the target area, Courant ratio and propagation angle. Figure 1 represents the reflection coefficients as functions of number of grid points inside the PML zone for different incident angles. The ppw was 40 and Courant ratio 0.6 for S-wave. Figure 2 represents the same experiment for ppw equals to 20. Solid lines correspond to incident angle $\alpha = 0$, dash-dotted ones are $\pi/6$, dotted ones are $\pi/3$ and dash ones are $5\pi/12$. One can see that the reflection coefficients converge exponentially to their asymptotes defined by the discretization of target area.

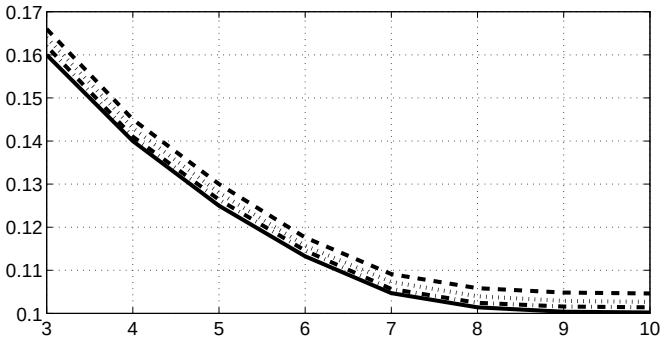

Figure 1: Reflection coefficients in percents over number of points in PML for 40 ppw in target area.

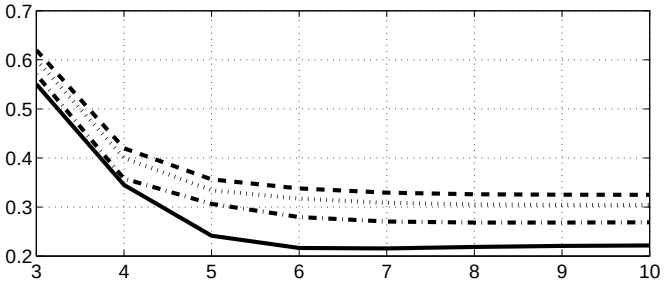

Figure 2: Reflection coefficients in percents over number of points in PML for 20 ppw in target area.

Anisotropy

A checkered-board model was used to perform a numerical experiment for anisotropy. The geometry of the domain and media parameters were chosen not to satisfy necessary stability conditions for PML [3]. To avoid reflections from the outer boundaries the target area was surrounded by the layer twice as thick as size of the area. The OG were used inside this layer with about 5 ppw in average and equidistant ones with 40 ppw inside the target area. So the size of the domain was 1200×800 points, the thickness of additional layer 200 points. Figure 3 represents the wavefield on free surface. One can see neither reflections no unstability appeared.

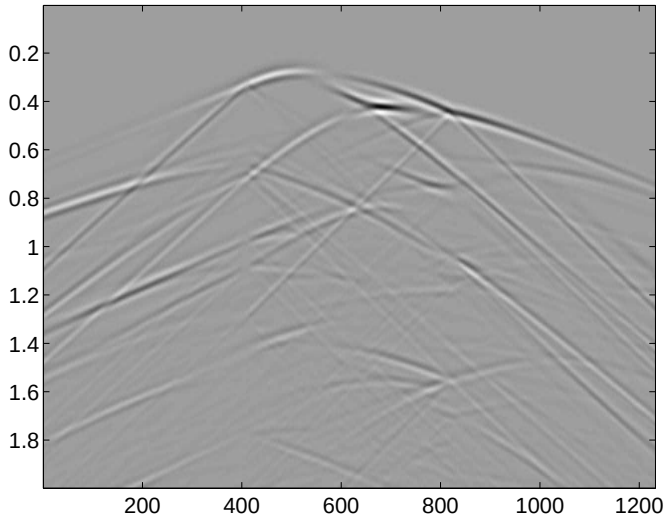

Figure 3: Wavefield on free surface. Vertical axis represents time in seconds, horizontal presents the coordinate in points.

Acknowledgments

Author is grateful to V.Druskin, V. Kostin and V.Tcheverda for useful discussions. This research is sponsored by Schlumberger Moscow Research and partially supported by RFBR grants #05-05-64277, #07-05-00538 and Lavrentev grant of SB RAS.

References

[1] Asvadurov S., Druskin V., Guddati M.N., Knizhnerman L. “On optimal finite-difference approximation of PML”, SAIM J. on Num. Analysis, 2003, n.41, pp.287-305.

[2] Asvadurov S., Druskin V. and Moskow S. “Optimal Grids for Anisotropic Problems” ETNA, to appear.

[3] E. Becache, S. Fauqueux, P. Joly, “Stability of perfectly patched payers, group velocities and anisotropic waves” J. of Comp. Phys, 188, pp. 399-433, 2003.

[4] Berenger J.-P. “Perfectly matched layer for the absorption of electromagnetic waves” J. Comput. Phys., v.114, pp.185-200, 1994.

[5] Engquist B., Majda A. “Radiation boundary conditions for acoustic and elastic wave calculations” Comm. Pure Appl. Math., vol.32, pp. 313-357, 1979.

[6] Lisitsa V.V. “Optimal Grids for Solution of Wave Equation with Variable Coefficients” Sib.J. of Comp.Math., vol. 8, pp.219-229, 2005, in Russian

[7] Virieux J. “P-SV wave propagation in heterogeneous media: Velocity-stress finite-difference method” Geophysics, v.51, pp.889-901, 1986.

RUNNING TWO-DIMENSIONAL WAVE PACKETS IN A THIN NON-UNIFORM CYLINDRICAL SHELL

G. I. Mikhasev
Department of Applied Mathematics and Mechanics, Vitebsk State University, Vitebsk, Belarus
Email: mikhasev@vsu.by

Abstract

The initial-value problem for the differential equations describing motion of a thin, infinitely long cylindrical shell is studied. Thickness, Young's modulus and density of the shell are considered as functions of curvelinear co-ordinates on the shell surface. The shell is supposed to experience external static or slowly varying dynamic forces which may be non-uniform in the circumferential and axial directions. Using the complex WKB method the asymptotic solution of the governing equations is constructed in the form of localized families of bending waves (wave packets) with the centers in points moving over the shell surface. The dependence of frequencies, group velocities, amplitudes upon variable geometrical and physical parameters of the shell is analyzed.

Introduction

Thin cylindrical shells are used as elements of hight-speed vehicles, underwater objects and other thin-walled engineering structures experiencing dynamic loading. Non-stationary vibrations or waves running in thin shells caused by the transient dynamic forces and/or the initial conditions (displacements and velocities) on the shell surface are especially complicated for analysis. Numerous numerical methods applied for examining these problems do not reveal any mechanical effects which are inherent to the transitional wave processes in thin shells. However, in cases when a shell is subjected to local perturbations which may be treated as the initial conditions localized near some lines or points on its surface, the asymptotic methods are found the most affective [1], [2]. So, transient bending vibrations of a thin non-circular medium-length cylinder with the oblique edges have been studied in Ref. [1], where by using the complex WKB method, solutions of the governing equations have been found in the form of packets of short bending waves with the centers at generators running in the circumferential direction. In Ref. [2], this method has been applied to studying the packets of bending, longitudinal and torsional waves with the centers at some parallel running in the axial direction in an infinitely long cylindrical shell including the effect of initial tensions due to non-uniform static internal pressure.

In this paper, the asymptotic solution of the governing equations is found in the form of two-dimensional wave packets with the centers in points moving over the surface of the non-uniform cylindrical shell subjected to non-uniform, static or dynamic, external forces.

Setting the problem

Consider an elastic thin infinitely long cylindrical shell. Let $h^*(s,\varphi)$ be the shell thickness, $\rho^*(s,\varphi)$ be the density, $E^*(s,\varphi)$ be Young's modulus, and $\nu^*(s,\varphi)$ be Poisson ratio of the material, where Rs and$R\varphi$ are the axial and circumferential coordinates, respectively, and R is the radius of the neutral surface of the cylinder. Let the shell be under the non-uniform, dynamic force $\mathbf{F}$. It is assumed that $\mathbf{F}$ is slowly varying vector function with respect to both co-ordinates and the time so that the dynamic stress state of the shell due to the load may be specified only by the axial, hoop and shear stresses

$$T_i^* = -\mu^2 E_0 h_0 T_i(s,\varphi,t), \quad i = 1,2,3, \qquad (1)$$

which are easily found from the equations of the membrane shell theory. In Eq. (1), $\mu^4 = h_0^2(12R^2)^{-1}$ is a small parameter, and h_0, E_0, ρ_0 are the characteristic magnitudes of h^*, E^*, ρ^* respectively, $t = t^*/t_c$ is dimensionless time, and $t_c^2 = \mu^{-2}R^2\rho_0 E_0^{-1}$ is the characteristic time.

For analysis of the short waves running in the shell the following system of equations [3], including the effect of the initial stresses, and written in a dimensionless form, may be used:

$$\begin{gathered}\mu^2\Delta(d\Delta w) + \tfrac{\partial^2\Phi}{\partial s^2} + \Delta_T w + \gamma\tfrac{\partial^2 w}{\partial t^2} = 0,\\ \mu^2\Delta(g\Delta\Phi) - \tfrac{\partial^2 w}{\partial s^2} = 0,\end{gathered} \qquad (2)$$

where

$$\begin{gathered}\Delta = \tfrac{\partial^2}{\partial s^2} + \tfrac{\partial^2}{\partial\varphi^2}, \quad \Delta_T w = \tfrac{\partial}{\partial\varphi}(T_2\tfrac{\partial w}{\partial\varphi}) +\\ \tfrac{\partial}{\partial s}(T_3\tfrac{\partial w}{\partial\varphi}) + \tfrac{\partial}{\partial\varphi}(T_3\tfrac{\partial w}{\partial s}) + \tfrac{\partial}{\partial s}(T_1\tfrac{\partial w}{\partial s}),\\ d = \tfrac{Eh^3}{1-\nu^2}, \quad g = \tfrac{1}{Eh}, \quad \gamma = \rho h,\\ E(s,\varphi) = \tfrac{E^*}{E_0}, \quad h(s,\varphi) = \tfrac{h^*}{h_0}, \quad \rho(s,\varphi) = \tfrac{\rho^*}{\rho_0}.\end{gathered} \qquad (3)$$

In Eq. (2), $w = \mu^2 w^*/R$, $\Phi = \Phi^*/(E_0 h_0 R^2)$ are the dimensionless normal deflection and stress function respectively.

Let us consider the initial conditions

$$w|_{t=0} = w^\circ(\zeta_1,\zeta_2)\exp\{i\mu^{-1}S^\circ(s,\varphi)\},$$
$$\dot{w}|_{t=0} = i\mu^{-1}\vartheta^\circ(\zeta_1,\zeta_2)\exp\{i\mu^{-1}S^\circ(s,\varphi)\}, \quad (4)$$
$$S^\circ = \mathbf{p}^\circ\mathbf{\Lambda}^T + \tfrac{1}{2}\mathbf{\Lambda}\mathbf{B}^\circ\mathbf{\Lambda}^T,$$

where $\zeta_1 = \mu^{-1/2}s, \quad \zeta_2 = \mu^{-1/2}\varphi, \quad k = 1,2$, $\mathbf{\Lambda} = (s,\varphi)$, $\mathbf{p}^\circ = (p_1^\circ, p_2^\circ)$ are the 2-vectors, w°, ϑ° are polynomials in ζ_1, ζ_2 with complex coefficients, and $\mathbf{B}^\circ$ is the 2×2 symmetric complex matrix with the positive defined imaginary part.

The real and imaginary parts of functions (4) define the two initial wave packets localized near the point $s = 0, \varphi = 0$. The general goal of the present paper is to study the wave forms of motion caused by the initial localized perturbations (4).

The approach

Let $s = q_1(t)$, $\varphi = q_2(t)$ be the packet center of the bending waves, where $q_k(t)$ are twice differentiable functions. In view of the local character of the solution, it is convenient to introduce a local co-ordinate system connected with the center $q_k(t)$: $s = q_1(t) + \mu^{1/2}\xi_1$, $\varphi = q_2(t) + \mu^{1/2}\xi_2$. All the functions contained in Eqs. (2) are expanded into series in a neighborhood of the center $q_k(t)$.

Upon taking into account Eqs. (4), the solution of system (2) is assumed to be of the form

$$w = \sum_{j=0}^{\infty}\mu^{j/2}w_j(\xi_1,\xi_2,t)\exp\{i\mu^{-1}S[\xi_1,\xi_2,t,\mu]\},$$

$$S = \int_0^t \omega(\tau)d\tau + \mu^{1/2}\mathbf{p}(t)\mathbf{\Xi} + \frac{1}{2}\mu\mathbf{\Xi}^T\mathbf{B}(t)\mathbf{\Xi}. \quad (5)$$

The function Φ is constructed in the same form (5). In Eqs.(5), $\mathbf{p}(t) = (p_1(t), p_2(t))$, $\mathbf{\Xi} = (\xi_1,\xi_2)^T$, w_j are polynomials in ξ_j, $p_j(t)$ are the wave numbers, $\mathbf{B}(t)$ is the 2×2 complex matrix such that $\mathrm{I}m\mathbf{B}(t) > 0$ for any $t \geq 0$. The last inequality guarantees attenuation of wave amplitudes within the packet.

The substitution of Eqs. (5) into Eqs. (2) produces the sequence of equations

$$\sum_{j=0}^{m}\mathbf{L}_j\mathbf{X}_{m-j} = \mathbf{0}, \quad m = 0,1,2,\ldots \quad (6)$$

where $\mathbf{X}_j = (w_j, \Phi_j)^T$ are the 2-vector, and $\mathbf{L}_j$ are the 2×2 matrix.

In the zeroth order approximation $(m = 0)$, one has the homogeneous system of algebraic equations $\mathbf{L}_0\mathbf{X}_0 = \mathbf{0}$. For a non-trivial solution of this system, the determinant of their coefficients is set equal to zero yielding the relation

$$\omega = \dot{q}_1p_1 + \dot{q}_2p_2 \mp H(p_1,p_2,q_1,q_2,t), \quad (7)$$

where H is Hamiltonian functions. The signs $\mp$ in Eq. (7) indicate the availability of two branches of the solutions.

In the first order approximation $(m = 1)$, the condition for solution of the non-homogeneous system (6) gives Hamiltonian system

$$\dot{\mathbf{q}} = H_{\mathbf{p}}, \quad \dot{\mathbf{p}} = -H_{\mathbf{q}} \quad (8)$$

with respect to $p_k(t), q_k(t)$, $k = 1,2$.

For $m = 2$, the compatibility condition for the non-homogeneous system (7) yields the Riccati equation

$$\dot{\mathbf{B}} + \mathbf{B}H_{\mathbf{pp}}\mathbf{B} + H_{\mathbf{qp}}\mathbf{B} + \mathbf{B}H_{\mathbf{qp}}^T + H_{\mathbf{qq}} = \mathbf{0} \quad (9)$$

with respect to the matrix $\mathbf{B}$ and the amplitude equation for finding the polynomials w_0, Φ_0. To determine the polynomials w_m, Φ_m for $m \geq 2$, one must consider responding system (7) in the $(m+2)$nd approximation.

The properties of the obtained solution depend strongly on the geometrical and physical parameters of the shell, the character of loading, and the initial conditions as well. As an example, the cylindrical shell with the thickness $h(s)$ depending on the axial co-ordinate has been considered. Analysis of the solution has showed that the initial wave packet (4) splits into two packets running in the opposite directions, with the tracks of the packet centers being helixes. Furthermore, the packet running in the direction of thickness increasing can be reflected from some parallel, this reflection being accompanied by strong focusing and growing amplitudes.

References

[1] G.I. Mikhasev, Localized Families of Bending Waves in a Thin Medium-Length Cylindrical Shell under Pressure, Journal of Sound and Vibration, 2002, vol.253, No.4, pp.833—857.

[2] G.I. Mikhasev, Travelling wave packets in an infinite thin cylindrical shell under internal pressure, Journal of Sound and Vibration, 1998, vol.209, No.4, pp.543—559.

[3] P.E. Tovstik, A.L. Smirnov, Asymptotic Methods in the Buckling Theory of Elastic Shells, World Scientific, Singapore, New Jersey, London, Hong Kong, 2001.

TIME-HARMONIC SOLUTION FOR LINEAR ELASTIC WAVE EQUATION WITH CONTROLLABILITY AND HIGHER-ORDER DISCRETIZATIONS

Sanna Mönkölä
Department of Mathematical Information Technology,
University of Jyväskylä, Jyväskylä, Finland
Email: sanna.monkola@jyu.fi

Abstract

The typical way of solving the time-harmonic linear elastic wave problem is to discretize the equations with finite elements or finite differences. This approach leads to large-scale complex-valued linear systems. For this kind of systems, it is difficult to construct efficient iterative solution methods. That is why we use an alternative approach and solve the time-harmonic problem by controlling the solution of the corresponding time-dependent wave equation.

Introduction

In an elastic, homogeneous, and isotropic domain Ω, the propagation of time-harmonic waves is governed by the Navier equation (see e.g. [1], [5], [7]). Since the typical procedure of solving the Navier equation leads to a large scale indefinite linear systems, for which it is difficult to construct efficient iterative solution techniques, we return to the time-dependent problem

$$\rho\frac{\partial^2\mathbf{u}}{\partial t^2} - \nabla\cdot\sigma(\mathbf{u}) = \mathbf{0}, \qquad \text{in } \Omega\times[0,T], \quad (1)$$

$$\mathbf{u} = \mathbf{0}, \qquad \text{on } \Gamma_0\times[0,T], \quad (2)$$

$$\mathbf{B}\frac{\partial\mathbf{u}}{\partial t} + \sigma(\mathbf{u})\mathbf{n}_s = \mathbf{g}, \qquad \text{on } \Gamma_{\mathrm{e}}\times[0,T], \quad (3)$$

where ρ is the density, length of the time interval is marked as T, $\mathbf{u} = (u_1(\mathbf{x}), u_2(\mathbf{x}))^T$ is the displacement field, and $\mathbf{g}$ is the source function. The stress tensor is expressed as $\sigma(\mathbf{u})$, and $\mathbf{n}_s = (n_1, n_2)^T$ is the outward pointing normal vector on Γ_{e}. The boundary Γ_0 is assumed to be rigid, whereas on the artificial boundary Γ_{e} we impose the conventional first order absorbing boundary condition [4], [11], where $\mathbf{B}$ is a symmetric positive definite 2×2-matrix

$$\mathbf{B} = \begin{pmatrix} n_1 & n_2 \\ n_2 & -n_1 \end{pmatrix}\begin{pmatrix} c_p & 0 \\ 0 & c_s \end{pmatrix}\begin{pmatrix} n_1 & n_2 \\ n_2 & -n_1 \end{pmatrix},$$

with elements c_p and c_s representing the speed of the pressure waves and the speed of the shear waves, respectively. In addition to the system (1)-(3), we take into account the initial conditions

$$\mathbf{u}(\mathbf{x},0) = \mathbf{e}_0, \quad \frac{\partial\mathbf{u}(\mathbf{x},0)}{\partial t} = \mathbf{e}_1, \quad \text{in } \Omega. \quad (4)$$

Exact controllability formulation

We formulate the exact controllability problem (see e.g. [2], [8]) as follows: Find initial conditions $\mathbf{e} = (\mathbf{e}_0, \mathbf{e}_1)^T$ such that equations (1)-(4) hold with the terminal conditions

$$\mathbf{u}(\mathbf{x},T) = \mathbf{e}_0, \quad \frac{\partial\mathbf{u}(\mathbf{x},T)}{\partial t} = \mathbf{e}_1. \quad (5)$$

The time period corresponding to the angular frequency ω is given by $T = \frac{2\pi}{\omega}$, and the T-periodic solution can be achieved by controlling the initial conditions such that the terminal conditions (5) are equal to the initial conditions (4) at the end of the computation.

Discretization

The wave equation is discretized in space domain with the spectral element method [3], [9]. The basis functions are higher-order Lagrange interpolation polynomials, and the nodes of these functions are placed at Gauss-Lobatto collocation points. The integrals in the weak form of the equation are evaluated with the corresponding Gauss-Lobatto quadrature formulas.

After spectral element discretization, the semi-discretized equation can be rewritten in the matrix form

$$\mathcal{M}\frac{\partial^2\mathbf{U}}{\partial t^2} + \mathcal{S}\frac{\partial\mathbf{U}}{\partial t} + \mathcal{K}\mathbf{U} = \mathcal{F},$$

where $\mathbf{U}$ is the global block vector containing the values of the displacement $\mathbf{u}(\mathbf{x},t)$ at the Gauss-Lobatto points of the quadrilateral mesh, $\mathcal{M}$ is the mass matrix, $\mathcal{S}$ is the matrix arising from the absorbing boundary condition, $\mathcal{K}$ is the stiffness matrix, and $\mathcal{F}$ is the vector due to the source function $\mathbf{g}$. In the next section, we use a short notation $\mathcal{L}$ for the block-diagonal matrix containing the matrices $\mathcal{K}$ and $\mathcal{M}$ such that

$$\mathcal{L} = \begin{pmatrix} \mathcal{K} & 0 \\ 0 & \mathcal{M} \end{pmatrix}.$$

For time discretization we use the fourth order Runge-Kutta method (see e.g. [8]). Because of the diagonality of the mass and the boundary matrices, only matrix-vector multiplications are needed in time stepping. This makes the time simulation efficient.

Conjugate gradient algorithm

Essentially the solution procedure of the exact controllability problem is similar to that presented for the scalar wave equation in [8]. After discretization, the exact controllability problem is reformulated as a least-squares optimization problem,

$$\min \left(\begin{pmatrix} \mathbf{U}(T) - \mathbf{e}_0 \\ \frac{\partial \mathbf{U}(T)}{\partial t} - \mathbf{e}_1 \end{pmatrix}^T \mathcal{L} \begin{pmatrix} \mathbf{U}(T) - \mathbf{e}_0 \\ \frac{\partial \mathbf{U}(T)}{\partial t} - \mathbf{e}_1 \end{pmatrix} \right), \quad (6)$$

which is solved with a preconditioned conjugate gradient algorithm. Each conjugate gradient iteration requires computation of the gradient of the discretized least-squares functional, solution of a linear system with the block-diagonal preconditioner $\mathcal{L}$, and some matrix-vector operations. Computation of the gradient is an essential point of the method, and we have done it with the adjoint state technique.

The algebraic multigrid (AMG) method [10] (see also [8]) is chosen for preconditioning the conjugate gradient algorithm. As a smoother for the AMG we use the Gauss-Seidel (GS) method. One iteration of the GS is used as pre- and post-smoothing. Additionally, in the beginning of every multigrid iteration, four iterations of the GS are used to smooth the solution initially. So called W-cycle [6] is utilized as a multigrid iteration until the residual norm of the solution is smaller than 10^{-6}.

Numerical example

We consider the scattering problem in an isotropic homogeneous elastic medium with $\rho = 2.70$, $c_p = 1.96$ and $c_s = 0.99$. The boundary Γ_e coincides with a rectangle with the lower left corner at the point $(0.0, 0.0)$ and the upper right corner at the point $(4.0, 4.0)$. In the center of this rectangle, we have a rigid square obstacle, with side length 2, surrounded by the boundary Γ_0. The propagation direction is chosen to be $\vec{\omega} = (\omega_1, \omega_2) = \left(-\frac{1}{\sqrt{2}}, \frac{1}{\sqrt{2}}\right)$, and angular frequency is $\omega = 2\pi$. In these experiments $\mathbf{g} = \mathbf{B}\frac{\partial \mathbf{u}_{\text{inc}}}{\partial t} + \sigma(\mathbf{u}_{\text{inc}})\mathbf{n}$, where the incident plane wave $\mathbf{u}_{\text{inc}}$ is

$$\mathbf{u}_{\text{inc}} = \begin{pmatrix} \omega_1 \cos(\omega t - \frac{\omega}{c_p}\mathbf{x}\cdot\vec{\omega}) + \omega_2 \cos(\omega t - \frac{\omega}{c_s}\mathbf{x}\cdot\vec{\omega}) \\ \omega_2 \cos(\omega t - \frac{\omega}{c_p}\mathbf{x}\cdot\vec{\omega}) - \omega_1 \cos(\omega t - \frac{\omega}{c_s}\mathbf{x}\cdot\vec{\omega}) \end{pmatrix}.$$

Order of elements r	1	2	3	4	5
Number of timesteps	50	60	80	90	210
Mesh stepsize	20	10	7	5	4

Table 1: Number of timesteps and mesh stepsize for different spectral orders r.

r	DOF	CG iter	AMG cf	AMG iter	CG time	AMG time
1	10080	30	0.10	8	56.33	4.41
2	10080	42	0.14	10	144.18	14.73
3	11088	38	0.45	22	256.20	33.57
4	10080	42	0.36	17	400.37	36.89
5	10080	33	0.37	17	765.62	30.10

Table 2: Order of elements r, number of degrees of freedom (DOF), number of conjugate gradient iterations (CG iter), convergence factor (cf), number of AMG cycles (AMG iter), CPU time in seconds for the algorithm (CG time), and CPU time in seconds for AMG cycles during the algorithm (AMG time).

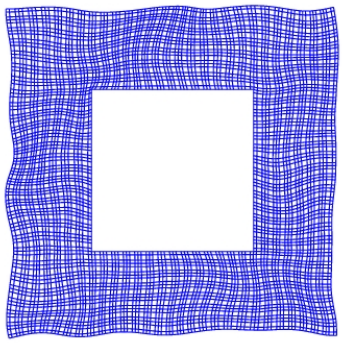

Figure 1: Solution of the elastic displacement $\mathbf{e}_0$ at the Gauss-Lobatto points of the quadrilateral mesh with stepsize $h = 1/7$ and order of the elements $r = 3$.

Computations have been carried out on an HP ProLiant DL585 with an AMD Opteron 885 CPU at 2.6 GHz, and the mesh stepsize is chosen such that the resolution of the spatial discretization is approximately constant (see Table 1). The number of conjugate gradient iterations and CPU time needed to solve the control problem, i.e. to reduce the relative euclidean norm of the gradient of the functional to be minimized in (6) below 10^{-4}, are given in Table 2. Table 2 shows also the number of degrees of freedom (DOF) in the spectral element mesh, convergence factor and the number of AMG cycles in the first

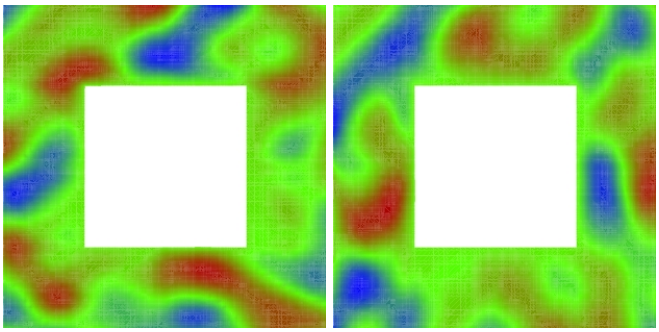

(a) Re($u_1(\mathbf{x})$) (b) Re($u_2(\mathbf{x})$)

Figure 2: Solution contours of the components of the elastic displacement $\mathbf{e}_0$ which is equal to the real part of the time harmonic wave $\mathbf{u} = (u_1(\mathbf{x}), u_2(\mathbf{x}))^T$. Mesh stepsize is $h = 1/5$ and order of elements is $r = 4$.

CG iteration, and CPU time for AMG cycles during the algorithm. The number of iterations is not dependent on the order of elements. This simulation result shows also that only a small proportion of CPU time is consumed for AMG cycles, which makes AMG solver a feasible preconditioner. Real parts of the time-harmonic solution are illustrated in Figures 1 and 2.

Conclusions

Simulation results show that the number of iterations required to attain the stopping criterion is independent of the element order and the AMG solver is working as an efficient preconditioner for higher-order elements.

Acknowledgements

The author thanks Prof. Tuomo Rossi and Dr. Erkki Heikkola for guidance and stimulating discussions and MSc. Anssi Pennanen and Dr. Janne Martikainen for providing the AMG solver.

References

[1] D. S. Bindel and S. Govindjee. Elastic PMLs for resonator anchor loss simulation. *International Journal for Numerical Methods in Engineering*, 64(6):789–818, 2005.

[2] M. O. Bristeau, R. Glowinski, and J. Périaux. Controllability methods for the computation of time-periodic solutions; application to scattering. *Journal of Computational Physics*, 147(2):265–292, 1998.

[3] G. Cohen. *Higher-Order Numerical Methods for Transient Wave Equations*. Springer Verlag, 2001.

[4] B. Engquist and A. Majda. Radiation boundary conditions for acoustic and elastic wave calculations. *Communications on Pure and Applied Mathematics*, 32:313–357, 1979.

[5] G. K. Gächter and M. J. Grote. Dirichlet-to-Neumann map for three-dimensional elastic waves. *Wave Motion*, 37(3):293–311, 2003.

[6] W. Hackbusch. *Multigrid Methods and Applications*. Springer-Verlag, Berlin, Germany, 1985.

[7] I. Harari and U. Albocher. Studies of FE/PML for exterior problems of time-harmonic elastic waves. *Computer Methods in Applied Mechanics and Engineering*, 195(29-32):3854–3879, 2006.

[8] E. Heikkola, S. Mönkölä, A Pennanen, and T. Rossi. Controllability method for the Helmholtz equation with higher order discretizations. *Journal of Computational Physics*, 2007.

[9] D. Komatitsch, C. Barnes, and J. Tromp. Wave propagation near a fluid-solid interface: A spectral-element approach. *Geophysics*, 65(2):623–631, 2000.

[10] J. Martikainen, A. Pennanen, and T. Rossi. Application of an algebraic multigrid method to incompressible flow problems. Reports of the Department of Mathematical Information Technology, Series B. Scientific Computing, B 2/2006, Department of Mathematical Information Technology, University of Jyväskylä, 2006.

[11] A. Quarteroni, T. Tagliani, and E. Zampieri. Generalized Galerkin approximations of elastic waves with absorbing boundary conditions. *Computer methods in applied mechanics and engineering*, 163:323–341, 1998.

DFT MODAL ANALYSIS OF SPECTRAL ELEMENT METHODS FOR THE 2D ELASTIC WAVE EQUATION

S. P. Oliveira, G. Seriani
Department of Geophysics of the Lithosphere, Istituto Nazionale di Oceanografia e Geofisica Sperimentale, Italy.
Email: spomponet@inogs.it,gseriani@inogs.it

Abstract

We perform a modal analysis of spectral element methods for the 2D isotropic elastic wave equation in the discrete Fourier transform domain sampled in the mesh nodes. We employ a Rayleigh quotient approximation of the eigenvalue problem that characterizes the dispersion relation, taking full advantage of the tensor product representation of the spectral element matrices. We compute dispersion graphs that show the dependence of dispersion errors on the grid resolution and the polynomial degree with both Gauss-Lobatto-Chebyshev and Gauss-Lobatto-Legendre collocation points.

Introduction

The spectral element method for elastic wave propagation is well established for quadrilateral meshes and Chebyshev [4] or Legendre [1] orthogonal polynomials. We study the numerical dispersion of spectral elements for the isotropic elastic wave equation, which is given by

$$\rho\frac{\partial^2 \boldsymbol{u}}{\partial t^2} - (\lambda+\mu)\nabla(\nabla\cdot\boldsymbol{u}) - \mu\nabla\cdot\nabla\boldsymbol{u} = 0, \quad (1)$$

where $\lambda, \mu > 0$ are the Lamé coefficients and $\rho > 0$ is the density. The elastic modulus is $E := \lambda + 2\mu$ and the Poisson's ratio is $\nu := \lambda/2(\lambda+\mu)$. For solutions in the form of harmonic plane waves $\boldsymbol{R}\exp[-\mathrm{i}\,(\omega t - \boldsymbol{\kappa}\cdot\boldsymbol{x})]$, we find the dispersion relations $\omega_P = \kappa c_P$ and $\omega_S = \kappa c_S$, where $\kappa := |\boldsymbol{\kappa}|$, $c_P := \sqrt{(\lambda+2\mu)/\rho}$, and $C_S := \sqrt{\mu/\rho}$.

In general, the numerical dispersion relation is expressed by an eigenvalue problem whose solution provides the approximate angular frequencies. Mulder [3] proposes a modal analysis in the discrete Fourier transform (DFT) space of the nodal values, which is well suited for high-order operators. The main difficulty of Mulder's strategy is the identification problem: the eigenvalues of the spatial operator must be properly ordered to assure eigenpair matching. It is not trivial to find such an ordering for 2D or 3D problems.

We circumvent the identification problem by introducing a new approach that matches each wave number with the Rayleigh quotient of the corresponding plane wave with respect to the spatial operator [5]. The Rayleigh quotient provides an estimate of the wave velocity generated by a numerical method, indicating how many grid points per wavelength are needed for practical computations.

Spectral element approximation

Let us partition the interval $[0,1]$ into N^{II} elements of size $h := 1/N^{II}$ subdivided into N^I interior subintervals. The total number of nodes is $\mathcal{N} := N^I N^{II}$.

This one-dimensional grid is described by the *local index* $p^I \in \langle N^I\rangle := \{0,\ldots,N^I-1\}$ and the *element index* $p^{II} \in \langle N^{II}\rangle$. These two indices provide a global ordering of all grid nodes, $p := p^I + p^{II}N^I \in \langle\mathcal{N}\rangle$. The mesh node position $x[p]$ is $(p^{II} + \zeta_{p^I})h$, where ζ_i is the $i-th$ *collocation point* in the interval $[0,1]$.

Two standard sets of collocation points are the Gauss-Lobatto-Legendre (GLL) and Gauss-Lobatto-Chebyshev (GLC) points. The GLL points can be found by numerically solving the equation $(1-\xi^2)P'_N(\xi) = 0$, where P_N denotes the Legendre polynomial of degree N [1]. The GLC points are $\zeta_i := (1-\cos(\pi i/N^I))/2$.

The grid over the domain $\Omega := [0,1]\times[0,1]$ is defined by $N_1^{II}\times N_2^{II}$ rectangular elements with $N_1^I \times N_2^I$ interior nodes. The coordinates of the nodes are $(x_1[p_1], x_2[p_2])$,

$$x_\alpha[p_\alpha] := (p_\alpha^{II} + \zeta_{p_\alpha^I})h_\alpha = \frac{p_\alpha^{II} + \zeta_{p_\alpha^I}}{N_\alpha^{II}}, \quad \alpha\in\{1,2\}.$$

Let $p := p_1 + p_2\mathcal{N}_1$. the spectral element approximation of (1) in the mesh defined above can be written as

$$\begin{cases} \rho\boldsymbol{M}\frac{\partial^2\boldsymbol{u}_1^*}{\partial t^2}(t) + \boldsymbol{K}_1\boldsymbol{u}_1^*(t) + \boldsymbol{K}_2\boldsymbol{u}_2^*(t) = \boldsymbol{0} \\ \rho\boldsymbol{M}\frac{\partial^2\boldsymbol{u}_2^*}{\partial t^2}(t) + \boldsymbol{K}_2^T\boldsymbol{u}_1^*(t) + \boldsymbol{K}_3\boldsymbol{u}_2^*(t) = \boldsymbol{0}. \end{cases} \quad (2)$$

The unknowns of the system (2) are the vectors $\boldsymbol{u}_1^*(t)$ and $\boldsymbol{u}_2^*(t)$ such that $(\boldsymbol{u}_\alpha^*)_p(t) \approx u_\alpha(\boldsymbol{x}[p],t)$, while $\boldsymbol{M}$ and $\boldsymbol{K}_i$ $(i=1,2,3)$ are assembled from the local matrices

$$\begin{aligned} \boldsymbol{M}^e &:= (h_1h_2/4)\boldsymbol{A}_2\otimes\boldsymbol{A}_1, \\ \boldsymbol{K}_1^e &:= E(h_2/h_1)\boldsymbol{A}_2\otimes\boldsymbol{C}_1 + \mu(h_1/h_2)\boldsymbol{C}_2\otimes\boldsymbol{A}_1, \\ \boldsymbol{K}_2^e &:= \lambda(\boldsymbol{B}_2)^T\otimes\boldsymbol{B}_1 + \mu\boldsymbol{B}_2\otimes(\boldsymbol{B}_1)^T, \\ \boldsymbol{K}_3^e &:= \mu(h_2/h_1)\boldsymbol{A}_2\otimes\boldsymbol{C}_1 + E(h_1/h_2)\boldsymbol{C}_2\otimes\boldsymbol{A}_1. \end{aligned}$$

The *Kronecker product* $\boldsymbol{C} := \boldsymbol{A}\otimes\boldsymbol{B}$ is defined as $C_{p_1+p_2M_1,q_1+q_2M_2} := A_{p_2,q_2}B_{p_1,q_1}$, where M_1, M_2 are the dimensions of $\boldsymbol{B}$. We have from [2] that

$$(\boldsymbol{A}\otimes\boldsymbol{C})(\boldsymbol{B}\otimes\boldsymbol{D}) = \boldsymbol{AB}\otimes\boldsymbol{CD}. \quad (3)$$

The matrices $\boldsymbol{A}_\alpha$, $\boldsymbol{B}_\alpha$, and $\boldsymbol{C}_\alpha$ are defined as

$$
\begin{aligned}
(A_\alpha)_{p^I,q^I} &:= \int_{-1}^{1} \varphi_{q^I}(z)\varphi_{p^I}(z)\,dz,\\
(B_\alpha)_{p^I,q^I} &:= \int_{-1}^{1} \varphi_{q^I}(z)\tfrac{\partial \varphi_{p^I}}{\partial z}(z)\,dz,\\
(C_\alpha)_{p^I,q^I} &:= \int_{-1}^{1} \tfrac{\partial \varphi_{q^I}}{\partial z}(z)\tfrac{\partial \varphi_{p^I}}{\partial z}(z)\,dz,
\end{aligned}
$$

where $p^I, q^I \in \langle N_\alpha^I + 1\rangle$. The functions $\varphi_i(z)$ form the Lagrangian interpolant basis of degree N^I. If $\boldsymbol{A}_\alpha^G$, $\boldsymbol{B}_\alpha^G$, and $\boldsymbol{C}_\alpha^G$ are the global matrices found from the assembly of the matrices $\boldsymbol{A}_\alpha$, $\boldsymbol{B}_\alpha$, and $\boldsymbol{C}_\alpha$, then

$$
\begin{aligned}
\boldsymbol{M} &= (h_1h_2/4)\boldsymbol{A}_2^G \otimes \boldsymbol{A}_1^G,\\
\boldsymbol{K}_1 &= E(h_2/h_1)\boldsymbol{A}_2^G \otimes \boldsymbol{C}_1^G + \mu(h_1/h_2)\boldsymbol{C}_2^G \otimes \boldsymbol{A}_1^G,\\
\boldsymbol{K}_2 &= \lambda(\boldsymbol{B}_2^G)^T \otimes \boldsymbol{B}_1^G + \mu\boldsymbol{B}_2^G \otimes (\boldsymbol{B}_1^G)^T,\\
\boldsymbol{K}_3 &= \mu(h_2/h_1)\boldsymbol{A}_2^G \otimes \boldsymbol{C}_1^G + E(h_1/h_2)\boldsymbol{C}_2^G \otimes \boldsymbol{A}_1^G.
\end{aligned}
$$

DFT modal analysis

The discrete Fourier transform (DFT) of a vector $\boldsymbol{v}$ is

$$
\hat{\boldsymbol{v}} = \boldsymbol{F}[\mathcal{N}]\boldsymbol{v}, \quad F[\mathcal{N}]_{n,p} := \frac{1}{\mathcal{N}} \exp\left(\mathsf{i}\,\frac{-2\pi}{\mathcal{N}} np\right).
$$

The two-dimensional DFT of $\boldsymbol{W}$ can be written as $\hat{\boldsymbol{W}} = \boldsymbol{F}[\mathcal{N}_1]\boldsymbol{W}\boldsymbol{F}[\mathcal{N}_2]^T$. Let $\boldsymbol{w} := \mathrm{Vec}\,\boldsymbol{W}$ defined by $W[p_1, p_2] = w[p_1 + p_2\mathcal{N}_1]$. We have $\hat{\boldsymbol{w}} = \boldsymbol{F}[\boldsymbol{\mathcal{N}}]\mathrm{Vec}\,\hat{\boldsymbol{W}}$, where $\boldsymbol{F}[\boldsymbol{\mathcal{N}}] := \boldsymbol{F}[\mathcal{N}_2] \otimes \boldsymbol{F}[\mathcal{N}_1]$. In particular,

$$
\boldsymbol{F}[\boldsymbol{\mathcal{N}}](\boldsymbol{v} \otimes \boldsymbol{u}) = \hat{\boldsymbol{v}} \otimes \hat{\boldsymbol{u}}. \tag{4}
$$

Let us write $\boldsymbol{u}^*(t)$ as a harmonic plane wave:

$$
\begin{aligned}
(u_\alpha^*)_p(t) &= R_\alpha^* e^{\mathsf{i}\,(2\pi \boldsymbol{k}\cdot\boldsymbol{x}[p] - \omega^*[\boldsymbol{k}]t)}\\
\boldsymbol{u}_\alpha^*(t) &= R_\alpha^* e^{-\mathsf{i}\,\omega^*[\boldsymbol{k}]t}\boldsymbol{v}[k_2] \otimes \boldsymbol{v}[k_1],
\end{aligned} \tag{5}
$$

where $v_p[k_\alpha] := \exp(\mathsf{i}\,2\pi k_\alpha x_\alpha[p_\alpha])$. Let $\chi := (\omega^*[\boldsymbol{k}])^2$. Substituting (5) into the first equation of (2), we find:

$$
\begin{aligned}
-R_1^*\chi\rho\boldsymbol{M}(\boldsymbol{v}[k_2] \otimes \boldsymbol{v}[k_1]) + R_1^*\boldsymbol{K}_1(\boldsymbol{v}[k_2] \otimes \boldsymbol{v}[k_1])\\
+R_2^*\boldsymbol{K}_2(\boldsymbol{v}[k_2] \otimes \boldsymbol{v}[k_1]) = \boldsymbol{0}.
\end{aligned}
$$

We substitute the Kronecker-product representations of $\boldsymbol{M}$, $\boldsymbol{K}_1$ and $\boldsymbol{K}_2$, write $\boldsymbol{v}[k_\alpha] = \boldsymbol{F}[\mathcal{N}_\alpha]\hat{\boldsymbol{v}}[k_\alpha]$, and premultiply the equation above by $\boldsymbol{F}[\boldsymbol{\mathcal{N}}]$, using the properties (3) and (4):

$$
\begin{aligned}
-R_1^*\chi\rho(h_1h_2/4)(\hat{\boldsymbol{A}}_2\hat{\boldsymbol{v}}[k_2]) \otimes (\hat{\boldsymbol{A}}_1\hat{\boldsymbol{v}}[k_1]) &+\\
R_1^*E(h_2/h_1)(\hat{\boldsymbol{A}}_2\hat{\boldsymbol{v}}[k_2]) \otimes (\hat{\boldsymbol{C}}_1\hat{\boldsymbol{v}}[k_1]) &+\\
R_1^*\mu(h_1/h_2)(\hat{\boldsymbol{C}}_2\hat{\boldsymbol{v}}[k_2]) \otimes (\hat{\boldsymbol{A}}_1\hat{\boldsymbol{v}}[k_1]) &+\\
R_2^*\lambda(\widehat{(\boldsymbol{B}_2{}^T)}\hat{\boldsymbol{v}}[k_2]) \otimes (\hat{\boldsymbol{B}}_1\hat{\boldsymbol{v}}[k_1]) &+\\
R_2^*\mu(\hat{\boldsymbol{B}}_2\hat{\boldsymbol{v}}[k_2]) \otimes ((\widehat{\boldsymbol{B}_1{}^T})\hat{\boldsymbol{v}}[k_1]) &= \boldsymbol{0},
\end{aligned}
$$

where $\hat{\boldsymbol{A}}_\alpha := \boldsymbol{F}[\mathcal{N}_\alpha]\boldsymbol{A}_\alpha^G\boldsymbol{F}^{-1}[\mathcal{N}_\alpha]$ (similarly for $\hat{\boldsymbol{B}}_\alpha$ and $\hat{\boldsymbol{C}}_\alpha$). Introducing $\hat{\boldsymbol{v}}[\boldsymbol{k}] := \hat{\boldsymbol{v}}[k_2] \otimes \hat{\boldsymbol{v}}[k_1]$, we find

$$
\begin{aligned}
-\chi R_1^*\rho(h_1h_2/4)(\hat{\boldsymbol{A}}_2 \otimes \hat{\boldsymbol{A}}_1)\hat{\boldsymbol{v}}[\boldsymbol{k}] +\\
R_1^*\left(E(h_2/h_1)\hat{\boldsymbol{A}}_2 \otimes \hat{\boldsymbol{C}}_1 + \mu(h_1/h_2)\hat{\boldsymbol{C}}_2 \otimes \hat{\boldsymbol{A}}_1\right)\hat{\boldsymbol{v}}[\boldsymbol{k}]\\
-R_2^*(\lambda+\mu)(\hat{\boldsymbol{B}}_2 \otimes \hat{\boldsymbol{B}}_1)\hat{\boldsymbol{v}}[\boldsymbol{k}] = \boldsymbol{0}.
\end{aligned}
$$

The same argument holds to the second row of (2):

$$
\begin{aligned}
-\chi R_2^*\rho(h_1h_2/4)(\hat{\boldsymbol{A}}_2 \otimes \hat{\boldsymbol{A}}_1)\hat{\boldsymbol{v}}[\boldsymbol{k}] +\\
R_2^*\left(\mu(h_2/h_1)\hat{\boldsymbol{A}}_2 \otimes \hat{\boldsymbol{C}}_1 + E(h_1/h_2)\hat{\boldsymbol{C}}_2 \otimes \hat{\boldsymbol{A}}_1\right)\hat{\boldsymbol{v}}[\boldsymbol{k}]\\
-R_1^*(\lambda+\mu)(\hat{\boldsymbol{B}}_2 \otimes \hat{\boldsymbol{B}}_1)\hat{\boldsymbol{v}}[\boldsymbol{k}] = \boldsymbol{0}.
\end{aligned}
$$

The transformed variables above are found as in [3], [5] and are block-diagonal. For instance,

$$
\hat{v}_{n'}[k'_\alpha] = \begin{cases} 0 & \text{if } n^{I\!I} \neq k_\alpha^{I\!I},\\ \frac{1}{N_\alpha^I}\sum_{p^I \in \langle N_\alpha^I+1\rangle} \cos\sigma & \text{if } n^{I\!I} = k_\alpha^{I\!I}, \end{cases}
$$

$$
\sigma := 2\pi\left(\frac{k_\alpha^{I\!I}}{N_\alpha^{I\!I}}\left(\zeta_{p^I} - \frac{p^I}{N_\alpha^I}\right) + \left(k_\alpha^I\zeta_{p^I} - n^I\frac{p^I}{N_\alpha^I}\right)\right),
$$

where $n \in \langle \mathcal{N}_\alpha\rangle$ and the prime accent denotes a reordering of the local and element indices; that is, $n' := n^{I\!I} + n^I N_\alpha^{I\!I}$, $n^I \in \langle N_\alpha^I\rangle$, $n^{I\!I} \in \langle N_\alpha^{I\!I}\rangle$.

We write the transformed linear system as a block eigenvalue problem $\boldsymbol{X}\boldsymbol{y} = \chi\boldsymbol{Z}\boldsymbol{y}$,

$$
\begin{aligned}
\boldsymbol{X} &:= \begin{bmatrix} \boldsymbol{D}_1 & \boldsymbol{D}_2 \\ \boldsymbol{D}_2 & \boldsymbol{D}_3 \end{bmatrix}, \quad \boldsymbol{y} := \begin{bmatrix} R_1^*\hat{\boldsymbol{v}}[\boldsymbol{k}] \\ R_2^*\hat{\boldsymbol{v}}[\boldsymbol{k}] \end{bmatrix},\\
\boldsymbol{Z} &:= \begin{bmatrix} \hat{\boldsymbol{A}}_2 \otimes \hat{\boldsymbol{A}}_1 & 0 \\ 0 & \hat{\boldsymbol{A}}_2 \otimes \hat{\boldsymbol{A}}_1 \end{bmatrix},
\end{aligned} \tag{6}
$$

$$
\begin{aligned}
\boldsymbol{D}_1 &:= \tfrac{E}{\rho}\tfrac{4}{h_1^2}\hat{\boldsymbol{A}}_2 \otimes \hat{\boldsymbol{C}}_1 + \tfrac{\mu}{\rho}\tfrac{4}{h_2^2}\hat{\boldsymbol{C}}_2 \otimes \hat{\boldsymbol{A}}_1,\\
\boldsymbol{D}_2 &:= -\tfrac{\lambda+\mu}{\rho}\tfrac{4}{h_1h_2}\hat{\boldsymbol{B}}_2 \otimes \hat{\boldsymbol{B}}_1,\\
\boldsymbol{D}_3 &:= \tfrac{\mu}{\rho}\tfrac{4}{h_2^2}\hat{\boldsymbol{A}}_2 \otimes \hat{\boldsymbol{C}}_1 + \tfrac{E}{\rho}\tfrac{4}{h_1^2}\hat{\boldsymbol{C}}_2 \otimes \hat{\boldsymbol{A}}_1.
\end{aligned}
$$

The solution χ exists only if $\boldsymbol{y}$ is an eigenvector of $\boldsymbol{X}\boldsymbol{y} = \chi\boldsymbol{Z}\boldsymbol{y}$, which is not true in general. We compute the best approximation of χ in the sense that the residual $(\boldsymbol{X} - \chi\boldsymbol{Z})\boldsymbol{y}$ is orthogonal to $\boldsymbol{y}$, i.e., the Rayleigh quotient $\chi_{OPT} = (\boldsymbol{y}^T\boldsymbol{X}\boldsymbol{y})/(\boldsymbol{y}^T\boldsymbol{Z}\boldsymbol{y})$. χ_{OPT} can be found by solving $\tilde{\boldsymbol{X}}\boldsymbol{R}^* = \chi_{OPT}\boldsymbol{R}^*$,

$$
\tilde{\boldsymbol{X}} = \begin{bmatrix} d_1 & d_2 \\ d_2 & d_3 \end{bmatrix}, \quad d_i := \frac{\hat{\boldsymbol{v}}[\boldsymbol{k}]^T\boldsymbol{D}_i\hat{\boldsymbol{v}}[\boldsymbol{k}]}{\hat{\boldsymbol{v}}[\boldsymbol{k}]^T\hat{\boldsymbol{A}}_2 \otimes \hat{\boldsymbol{A}}_1\hat{\boldsymbol{v}}[\boldsymbol{k}]}. \tag{7}
$$

We set $\omega_P^*[\boldsymbol{k}] = (\chi_{OPT}^+)^{1/2}$ and $\omega_S^*[\boldsymbol{k}] = (\chi_{OPT}^-)^{1/2}$,

$$
\chi_{OPT}^{\pm} = \frac{d_1+d_3}{2} \pm \sqrt{\left(\frac{d_1-d_3}{2}\right)^2 + d_2^2}. \tag{8}
$$

The coefficients d_1, d_2, d_3 reduce to Rayleigh quotients of 1D matrices. For instance,

$$
d_1 = \frac{E}{\rho}\frac{4}{h_1^2}\frac{\hat{\boldsymbol{v}}[k_1]^T\hat{\boldsymbol{C}}_1\hat{\boldsymbol{v}}[k_1]}{\hat{\boldsymbol{v}}[k_1]^T\hat{\boldsymbol{A}}_1\hat{\boldsymbol{v}}[k_1]} + \frac{\mu}{\rho}\frac{4}{h_2^2}\frac{\hat{\boldsymbol{v}}[k_2]^T\hat{\boldsymbol{C}}_2\hat{\boldsymbol{v}}[k_2]}{\hat{\boldsymbol{v}}[k_2]^T\hat{\boldsymbol{A}}_2\hat{\boldsymbol{v}}[k_2]}.
$$

Results and discussion

We use the same element length and polynomial degree in both x and y directions, set $\mathcal{N}_1 = \mathcal{N}_2 = 120$, $\rho = \lambda = 1$ and compute μ from the Poisson ratio ν. Given $\boldsymbol{k} = k(cos(\theta), \sin(\theta))$, we measure the grid resolution by the number of grid points per wavelength $G := \mathcal{N}/k$ or the normalized spatial frequency $H := k/\mathcal{N}$.

From the numerical angular frequency $\omega_P^*[\boldsymbol{k}]$ we compute the numerical phase velocity $c_P^* = \omega_P^*[\boldsymbol{k}]/k$. We interpolate $\omega_P^*[\boldsymbol{k}]$ when the argument $\boldsymbol{k}$ is non-integer. Analogously, c_S^* is evaluated from $\omega_S^*[\boldsymbol{k}]$. We compute the following dispersion errors:

$$\varepsilon_P := \frac{{c_P}^* - c_P}{c_P}, \quad \varepsilon_S := \frac{{c_S}^* - c_S}{c_S}.$$

Fig. 1 illustrates the dependence of the dispersion error with the polynomial degree for waves propagating in the horizontal direction. The approximate phase velocities of the spectral element methods with GLL and GLC points are similar, although GLL produces lagging phase error, which is related to the use of reduced integration to compute the mass matrix [1].

Fig. 2 presents polar plots of $1+20\varepsilon_S$ for several values of ν. The values of ε_P do not significantly change with ν. The method with GLL collocation points has a smaller error in the horizontal direction, but is more sensitive to the Poisson's ratio, specially in the directions that make an angle of about 30^o with the axes.

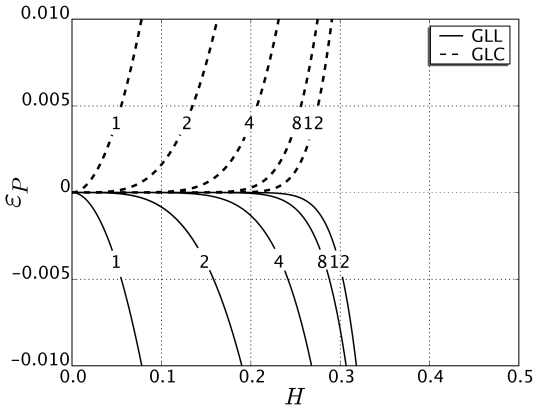

Figure 1: Phase velocity errors of spectral element methods with GLC and GLL collocation points ($N^I = 1, \ldots, 12$ and $\theta = 0^o$).

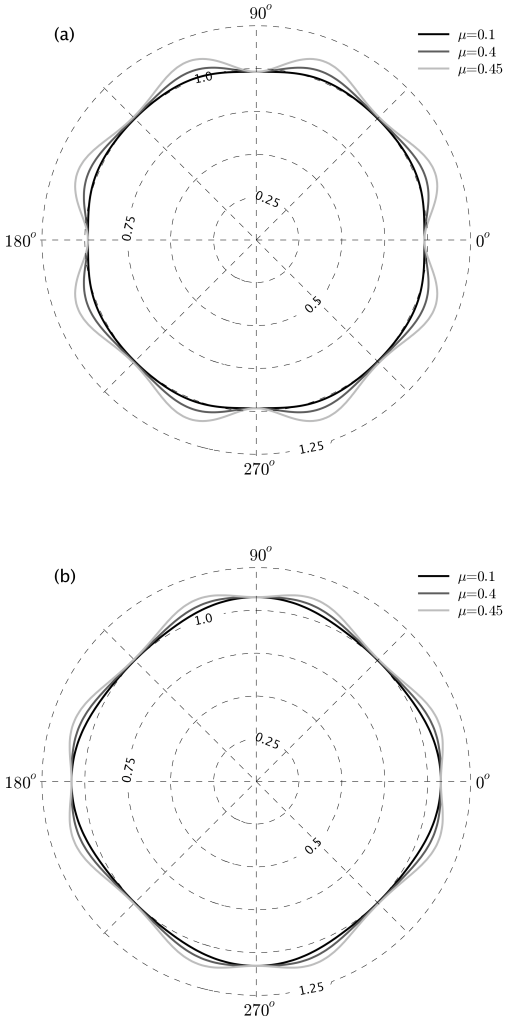

Figure 2: Normalized shear velocity dispersion ($G = 4$) of the eighth-degree spectral element method with GLL (a) and GLC (b) collocation points.

References

[1] D. Komatitsch and J. Tromp, "Introduction to the spectral-element method for 3-D seismic wave propagation", Geophys. J. Int., vol. 139, pp. 806-822, 1999.

[2] H. Lütkepohl, Handbook of Matrices, John Wiley & Sons, Chichester, 1996.

[3] W. Mulder, "Spurious modes in finite-element discretizations of the wave equation may not be all that bad", Appl. Numer. Math., vol. 30, pp. 425-445, 1999.

[4] E. Priolo, J. Carcione, and G. Seriani, "Numerical simulation of interface waves by high-order spectral modeling techniques", J. Acoust. Soc. Am., vol. 95, pp. 681-693, 1994.

[5] G. Seriani and S. Oliveira, "Dispersion analysis of spectral element methods for acoustic wave propagation", submitted to J. Comput. Acoust.

MATHEMATICAL MODELING OF SEISMIC AND ACOUSTO-GRAVITY WAVES IN A HETEROGENEOUS EARTH-ATMOSPHERE MODEL

G. Reshetova[†,*], **B. Mikhailenko**[†,*]
[†]Laboratory of Numerical Modeling of Seismic Fields , Institute of Computational Mathematics and Mathematical Geophysics, Novosibirsk, Russia
[*]Email: kgv@nmsf.sscc.ru

Abstract

A numerical-analytical solution for seismic and acoustic-gravitational waves propagation problem is applied to a heterogeneous Earth-Atmosphere model. Seismic wave propagation in an elastic half-space is described by a system of first order dynamic equations of the elasticity theory. The propagation of acoustic-gravitational waves in the atmosphere is described by the linearized Navier-Stokes equations. The proposed algorithm is based on the integral Laguerre transform with respect to time, the finite integral Bessel transform along the radial coordinate with a finite difference solution of the reduced problem along the vertical coordinate. The algorithm is numerically tested for the heterogeneous Earth-Atmosphere model for different source locations.

Introduction

The problem of the propagation of acoustic-gravitational waves in a heterogeneous atmosphere has long been known. The first publications concerning the impact of the gravitational field on the wave processes in the atmosphere and the ocean appeared at the end of the last century [9]. Martyn [10] and Hines [7] indicated to an important role of acoustic-gravitational waves for understanding and interpretation of numerous physical processes in the atmosphere. Starting in the 50-s, an increasing interest to studying the generation and propagation of the acoustic-gravitational waves in the real atmosphere is associated with the development of the infrasonic method of monitoring the nuclear explosions in the atmosphere. A review on studying the basic characteristics of the acoustic-gravitational waves in the atmosphere can be found in [4-6]. Recently, the methods of observations of the state of the atmosphere have been improved, the models of media in theoretical calculations becoming more complicated. The methods and algorithms for the simulation of the acoustic-gravitational waves propagation in the atmosphere are being upgraded. The fact is, in many theoretical studies, the Earth-Atmosphere interface is considered to be absolutely reflecting, the effects, related to the excitation of seismic waves in the Earth's crust and their interaction with the acoustic-gravitational waves in the atmosphere being neglected. Theoretical and experimental studies in the course of the recent decades have shown a close relation between lithospheric and atmospheric wave motions. Alekseev et al.[1] discovered the effect of acoustic-seismic induction, in which an acoustic wave from a powerful vibrator induced intense surface seismic waves at a distance of tens of kilometers due to the atmospheric refraction.

Our approach is an analogue to the frequency-domain forward modeling, where instead of the temporal frequency we have number p - the degree of the Laguerre polynomials. We apply this numerical-analytical method to study the wave propagation in a heterogeneous Earth-Atmosphere model. The algorithm combines the Bessel integral transform along the radial coordinate and the integral Laguerre transform with respect to time with the FD solution along the vertical coordinate. Such an approach to the problem of seismic wave propagation in the heterogeneous elastic half-space was developed in [8,11].

Method

0.1 Statement of the problem

A specific feature of the numerical modeling of wave fields for a heterogeneous Earth-Atmosphere model is a considerable difference in velocities of seismic and acoustic waves. In this case, the use of explicit finite difference schemes brings about serious restrictions on the time step of a finite difference scheme and results in large computer costs. Another way of overcoming such difficulties is application of the Fourier transform with respect to the time coordinate (the frequency domain modeling). In this case, after employing finite difference (FD) methods with respect to spatial coordinates, we deal with an extremely large matrix to be implicitly solved for a great number of temporal frequencies. This difficulty can be avoided if the Fourier transform with respect to time is replaced by the Laguerre transform when simulating the acoustic-gravitational waves propagation in heterogeneous media.

0.2 Solution algorithm

The algorithm combines the Bessel integral transform along the radial coordinate and the integral Laguerre transform with respect to time with the FD solution along the vertical coordinate.

At the first step, we reduce the dimension of our problem with the help of Fourier-Bessel transform , then we apply the integral Laguerre transform with respect to time to the reduced system [11].

As a result, we obtain a system of algebraic equations, whose matrix is independent of the parameter p - the degree of the Laguerre polynomials. Only the right-hand side of the system has a recurrent dependence on the parameter p. The system of algebraic equations can be solved for a great number of the right-hand sides using fast solutions, such as the Cholesky decomposition.

0.3 Perfectly Matched Layers (PML)

To avoid reflections from artificial boundaries, we use the PML technique that was originally introduced for the Maxwell equations in [2] and later generalized to elasticity [3]. Our version of PML is a combination of the Laguerre transform with respect to time and the original version of PML. This modification of PML does not claim doubling/tripling of unknown functions within the PML areas and provides the possibility of creating a very effective software for the numerical simulation [12].

0.4 Parallel implementation

The algorithm of solution to the problem was parallelized for carrying out calculations on a cluster system. The parallelization was in solving an independent system of linear algebraic equations for each k-th harmonic of the Fourier-Bessel transform on a separate processor. With such an approach, there is no need in data communication among processors, which essentially decreases computer costs. In fact, all processors do independent calculations, and the desired solution is obtained by weighted summation of calculated data received from each processor.

Illustrations and References

Consider a numerical example illustrating the case of a high-frequency seismic exploration bandwidth and a model of an explosive source in the atmosphere $10m$ above the Earth-Atmosphere interface with the dominant frequency of f_0 - $20Hz$. Let us introduce an elastic half-space that borders on the atmosphere, where the sound velocity is constant and density decreases exponentially with height. The wave propagation velocities in the elastic half-space are $v_p = 3000m/s$, $v_s = 1760m/s$ and the density is $\rho_0 = 2.3g/sm^3$. The velocity of acoustic waves in the atmosphere is $c_0 = 340m/s$ and the density is $\rho_0 = 0.001225g/sm^3$ (at $z = 0$). To the elastic half-space we add an elastic $20\ m$ thick layer that borders on the atmosphere with wave propagation velocities being lower than in the atmosphere: $v_P = 250m/s$, $c_s = 150m/s$, and $\rho_0 = 1.7g/sm^3$. This case is common for seismic exploration in the presence of a low-velocity zone.

A snapshot at the time $t = 2.5\ s$ for the stress component and the atmospheric pressure P (Fig.1) images the non-geometrical waves PP* and PS* and the conical P and S waves in the elastic half-space. They form a wave pattern if the elastic half-space with its P and S velocities is higher than in the atmosphere and in the low-velocity zone. The snapshot in Fig.2 is for the vertical displacement velocity components at t = 1.6 s. Fig.3 shows synthetic seismograms of the displacement velocity at the Earth-Atmosphere interface.

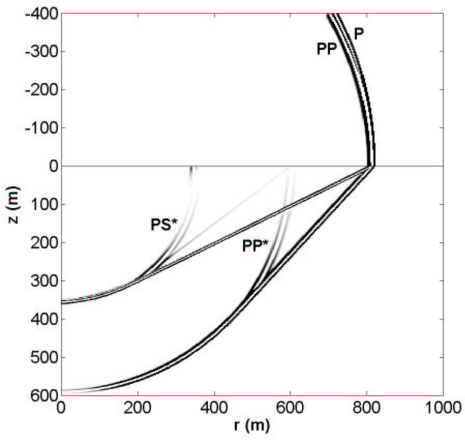

Figure 1: A snapshot at the time $t = 2.5\ s$ for the stress component in the elastic half-space and the atmospheric pressure P.

Conclusion

We offer a numerical-analytical algorithm applied to simulate propagation of seismic and acoustic-gravitational waves within the limits of a heterogeneous Earth-Atmosphere model and test it in numerical experiments for simple models. The study was supported by grants 06-05-64149, 07-05-00538 from the Russian Foundation for Basic Research.

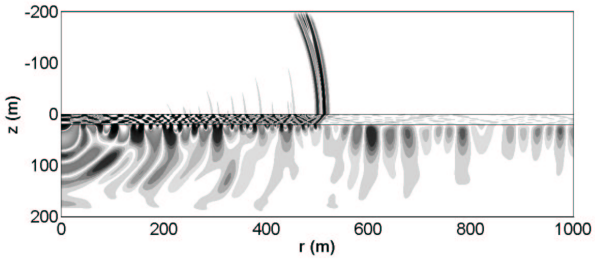

Figure 2: A snapshot at the time $t = 1.6\ s$ for the vertical displacement velocity component in an elastic half-space, a low-velocity zone and in the Atmosphere.

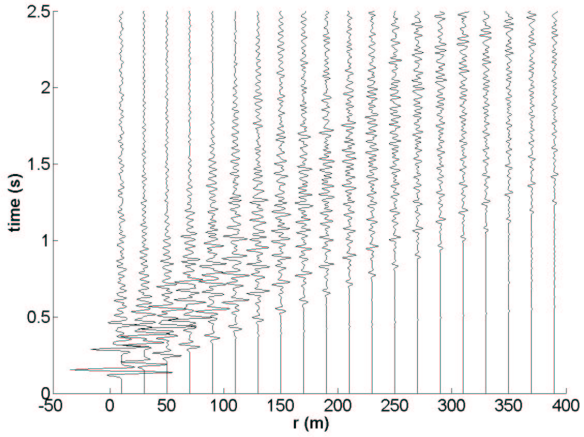

Figure 3: Synthetic seismograms of the vertical displacement velocity component at the Earth-Atmosphere interface, for different distances at every $20\ m$ from $10\ m$.

References

[1] Alekseev, A.S., Glinsky B. M., Dryakhlov S. and et al., “The effect of acoustic-seismic induction in vibroseismic soundings”, Dokl. RAN [in Russian], vol. 346, 5, pp. 664-667, 1996.

[2] Berenger, J.P., “ A perfectly matched layer for the absorption of electromagnetic waves”, J. Comput. Phys., vol. 114, pp. 185-200, 1994.

[3] Collino, F. and Tsogka, C., “Application of PML absorbing layer model to the linear elastodynamic problem in anisotropic heterogeneous media”, Geophysics, vol. 66, pp. 294-307, 2001.

[4] Francis, S.H., “Global propagation of atmospheric gravity waves: A review”, J. Atmos. and Terr. Phys., vol. 37, pp. 1011-1054, 1975.

[5] Gossard, E.E. and Hooken, W. H., Waves in the atmosphere. Elsevier Scientific Publishing Company, 1975.

[6] Grigoriev, G. I., “Acoustic-gravitational waves in the Earth’s atmosphere (review)”, Izv. Vnzov Radiofizika, XLII, vol. 1, pp. 3-25, 1999.

[7] Hines, C. O., “Internal atmospheric gravity waves at ionospheric heights”, Can. J. Phys., vol. 38, pp. 1441-1481, 1960.

[8] Konyukh G.V., Mikhailenko B.G. and Mikhailov A.A, “Application of the integral Laguerre transforms for forward seismic modeling”, Journal of Computational Acoustics, vol. 9, 3, pp. 1-19, 2001.

[9] Lamb, H., “ Hydrodynamics Dover publications”. Ins., New York, 1945.

[10] Martyn, D. F., “Cellular atmospheric waves”, Proc. R. Soc. London, A**201**, pp. 216-234, 1950.

[11] Mikhailenko, B.G., Mikhailov, A. A. and Reshetova, G. V., “Numerical modeling of transient seismic fields in viscoelastic media based on the Laguerre spectral method”, Pure Appl. Geophys., vol. 160,pp. 1207-1224, 2003.

[12] Mikhailenko, B.G., and Reshetova, G. V., “The perfectly matched layer technique in 3D seismic modeling”. Proc. Intern. Symp. on Mathematical Modeling of Dynamic Processes in Atmosphere, Ocean and Solid Earth, Novosibirsk, pp. 91-97,2004.

RESULTS OF NUMERICAL MODELING OF SEISMIC WAVE PROPAGATION IN NOLINEARLY ELASTIC FRACTURED MEDIA

G.M.Woskoboynikova[†,*],

[†]Institute of Computational Mathematics and Mathematical Geophysics SB RAS, prospect Akademika Lavrentjeva, 6, Novosibirsk, 630090, Russia.

[*]Email: gulya@opg.sscc.ru

Abstract

Relations of nonlinear processes of seismic wave radiation by a ground-based vibrational source and their accumulation during the propagation of waves in the medium are considered. Results of numerical modeling of the dependence of the parameters of seismic wave field nonlinearity on the characteristics of mediums inhomogeneity are presented. Fluid-saturated fractured media with different parameters of physical elasticity are considered as examples.

Methods

A homogeneous and isotropic body is taken as a model of the medium. The body has elasticity modules K_1 and μ_1 and density ρ_1, and voids of spheroidal shape are scattered uniformly and oriented chaotically in it. The shape of the voids is determined by the parameter α, which is equal to the ratio between the length of the rotation axis of the spheroid and the length of its second axis. The relative volume distribution of the voids along the shape parameter between its minimal α_{min} and maximal α_{max} values is described by the function $\varphi(\alpha)$.

For the case of propagation, in the medium being modeled, of plane monochromatic elastic waves along the axis OX when there are only longitudinal motions in the medium ($u_x \neq 0, u_y = u_z = 0$), the equation of propagation has the following form:

$$\rho_0 \frac{\partial^2 u_x}{\partial t^2} - M_0 \frac{\partial^2 u_x}{\partial x^2} = B \frac{\partial u_x}{\partial x} \cdot \frac{\partial^2 u_x}{\partial x^2} \qquad (1)$$

At the boundary condition $u_x(0,t) = U_x \sin \omega t$ the solution to the equation in a second approximation has the form [2]

$$u_x = U_x \sin \omega \left(t \mp \tfrac{x}{c_p}\right) - \left(\tfrac{U_x}{2}\right)^2 \tfrac{B}{M_0} k_p^2 x \cos 2\left(\omega t \mp k_p x\right), \qquad (2)$$

where

$$k_p = \omega / c_p, \;\; M_0 = k_0 + \frac{4}{3}\mu_0$$

$$B = -3\varphi \frac{k_0}{p_0}\left(a\frac{k_0^2}{k_1} + \frac{4}{3} b \frac{\mu_0^2}{\mu_1}\right) f(\alpha_0).$$

The following relations for effective elasticity modules of the medium with spheroidal voids have been obtained:

$$\begin{aligned} K_{(1)} &\approx K_0 \left[1 - \varphi_{rel} a \tfrac{K_0^2}{p_0 K_1} f(\alpha_0)\, u_{ll}\right], \\ \mu_{(1)} &\approx \mu_0 \left[1 - \varphi_{rel} b \tfrac{K_0 \mu_0}{p_0 \mu_1} f(\alpha_0)\, u_{ll}\right], \end{aligned} \qquad (3)$$

where

$$K_0 \approx K_1 (1 + \varphi_{rel} a F)^{-1}, \;\; \mu_0 \approx \mu_1 (1 + \varphi_{rel} b F)^{-1},$$

$$a = \frac{4\left(1-\nu_1^2\right)}{3\pi(1-2\nu_1)}, \;\; b = \frac{8(1-\nu_1)\cdot(5-\nu_1)}{15\pi(2-\nu_1)},$$

$$f(\alpha_0) = \frac{\varphi(\alpha)}{\varphi_{rel}}, \;\; \varphi_{rel} = \int_0^{\alpha_{\max}} \varphi(\alpha)\, d\alpha,$$

$$F = \int_{\alpha_0}^{\alpha_{\max}} f(\alpha)/\alpha \; d\alpha;$$

p_0 is the static pressure, ν_1 is the Poisson coefficient, K_0 is the effective modulus of all-round compression of an unperturbed microfractured medium, u_{ll} is the sum of diagonal components of the dynamic deformation tensor, and φ_{rel} is the initial value of the fractured porous medium.

It follows from (2) that in the fractured medium there appear harmonics of doubled frequency. Their level is determined by the coefficient B, which depends on the character of the fractured medium and the length of the wave travel path x. In the latter case, the level of the second harmonic increases as the distance x from the source increases. This phenomenon was observed earlier as accumulating nonlinearity in a nonlinearly elastic medium. Taking into account (2), the nonlinearity coefficient of the monochromatic wave shape determined by the ratio between the amplitude of the second harmonic and the first harmonic is

$$\frac{u_2}{u_1} = \frac{1}{8}\frac{U_x B k_p^2 x}{M_0} \qquad (4)$$

Equation (4) relates the parameters of wave field nonlinearity in the source zone to the character of the medium's fracturing. The fracturing is determined by the parameter B, which depends on the size of fractures, their

density distribution, and the densities and elasticity modules of the medium. Taking into account this dependence, it seems that the dynamic parameters of wave field nonlinearity can be successfully used as a prognostic quantitative parameter characterizing the process of source development [1].

In accordance with equation (4), we performed an analysis of the dependence between the wave field nonlinearity and the characteristics of medium's fracturing, the amplitude of oscillation velocity of medium's particles U_x, and the distance x. Water-saturated fractured granite was taken as the medium. Its elasticity parameters were as follows: Young modulus $E = 2.216 \cdot 10^9$ Pa, Poisson coefficient $\nu = 0.44296$, static pressure $p_0 = 103$ Pa, frequency $f = 10$ Hz, and propagation speed of longitudinal wave in granite $C_p = 2500$ m/s. The following three variation domains of the geometrical parameters of fractures (in meters) were taken: $0.001 \div 0.01$, $0.012 \div 0.05$, and $0.052 \div 0.015$. The distribution density of fractures in the volume is described by the uniform distribution function.

Figure 1 shows the nonlinearity coefficient of monochromatic wave shape versus the ratio between the ellipsoid axes describing an elementary fracture for the selected parameters.

Plots for the nonlinearity coefficient of monochromatic wave shape versus the wave travel path x (in meters) in fluid-saturated granite with $c_p = 2500$ m/s, $c_s = 800$ m/s and uniform distribution of fractures in the medium are given in Fig. 2. The plots correspond to different geometrical sizes of fractures given at the bottom of the figure.

It follows from an analysis of Figs. 1 and 2 that the nonlinearity coefficient increases

- as the sizes of fractures and the amplitude of oscillation speed U_x increase. At $U_x = 2.7 \cdot 10^{-8}$, u_2/u_1 varies from 0.05 to 0.17 and at $U_x = 70 \cdot 10^{-8}$ from 0.2 to 0.45 in the 10-km travel path of oscillations (Fig.1).

- as the wave travel path increases. It follows from the plots in Fig.2 that in a fractured medium depending on the geometrical parameters of fractures the nonlinearity coefficient can increase from 0 to 0.7 at the travel length =100 km.

Another relation for the "accumulation" of the nonlinear effect in media with dissipation and absorption is determined by the dependence of the amplitude of the second harmonic on the distance, which is described by [3]

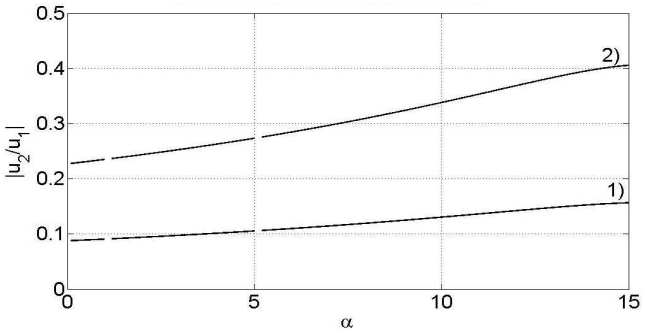

Figure 1: Wave travel path x = 10 km, oscillation speed. 1) $U_x = 2.7 \cdot 10^{-8}$ m/s; 2) $U_x = 70 \cdot 10^{-8}$ m/s

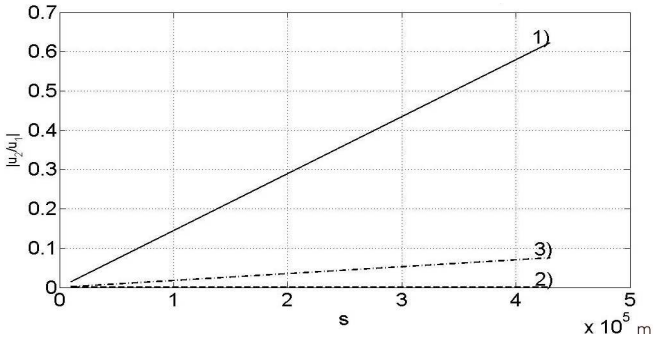

Figure 2: Wave travel path x = 10 km, oscillation speed. 1) $\alpha_{min} = 0.0067, \alpha_{max} = 0.067$; 2) $\alpha_{min} = 0.06, \alpha_{max} = 0.5$ 3) $\alpha_{min} = 0.48, \alpha_{max} = 0.8$

$$a_2 = \frac{K_c r \omega^2 a_1^2}{8 c_{p,s}^2} \tag{5}$$

Here r is the wave travel path, K_c is the nonlinearity coefficient of the medium. It is determined by the expression $K_c \approx \rho\nu(\Delta\nu/\Delta p) \approx (\Delta\nu/\nu)\Delta\theta$, where ρ is the density, $\Delta\theta$ is the volume deformation variation, Δp is the pressure variation, a_1 is the amplitude of the first harmonic, and $c_{p,s}$ is the velocity of longitudinal and transverse waves. The value $K_c \approx 10^3$. As an illustration, Figs.3a and 3b show a family of plots, which demonstrate the "accumulation" of the nonlinear effect versus the distance in the "source-receiver" distance range of $0.3 \div 355$ km. Cases of a longitudinal and transverse wave in the medium are considered.

The parameters of wave field nonlinearity in the far zone are subject to the influence of the nonlinearity effect of radiation by the vibrator itself [5]. In this case, the initial ratios between the second and first harmonics a_{01}/a_{02} observed in the source zone versus the distance

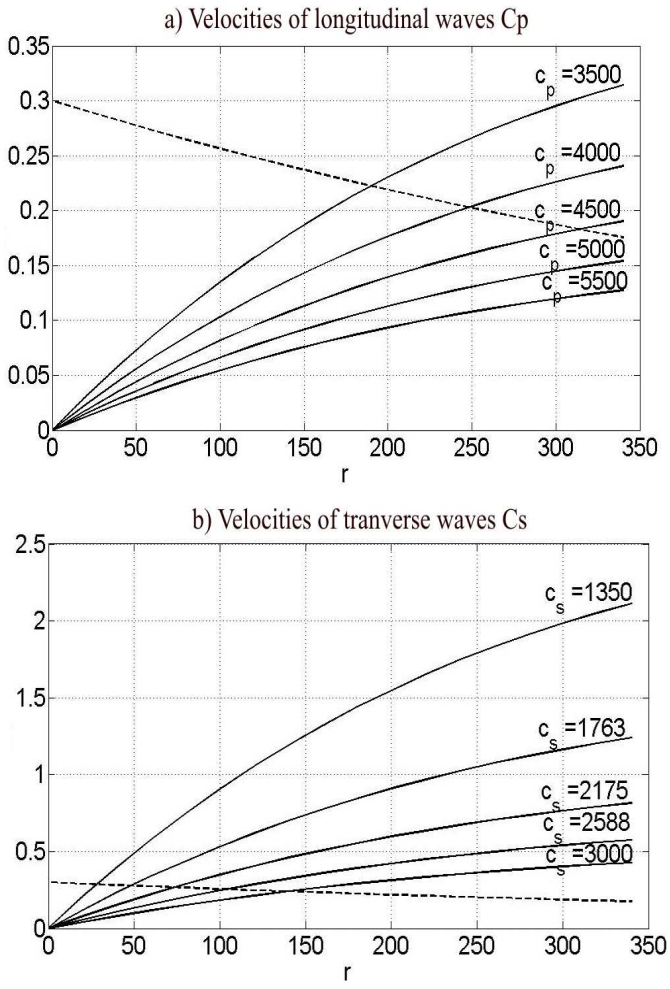

Figure 3: Coefficient of nonlinear distortions versus the distance at different seismic velocities

decrease in accordance with the following law:

$$\frac{a_{f2}(r)}{a_{f1}(r)} = \frac{a_{02}}{a_{01}} \exp\left[-(\alpha_2 - \alpha_1)(r - r_0)\right], \qquad (6)$$

where a_{01} and a_{02} are the amplitudes of both oscillations near the source at the boundary of a sphere of radius r_0; a_{f1} and a_{f2} are the amplitudes of the second and first harmonics at the distance r from the boundary of a sphere of radius r_0; and $\alpha_{1,2} \approx 2.5 \cdot 10^{-4} f_{1,2}$(1/km) are the absorption coefficients for the frequency oscillations f_1 and f_2. The dashed lines in Figs. 3a and 3b show exponential plots for the ratios between the second and first harmonics versus the distance, in accordance with equation (6). The plots are monotonically decreasing within $0.3 \div 0.18$ versus the distance ($0.3 \div 355$ km). The sphere radius $r_0 = 0.3$ km; the basic sounding frequency of the monochromatic signal $f_1 = 6.3$ Hz, and its second harmonic $f_2 = 12.6$ Hz.

The "accumulation" of the nonlinear effect in media with inhomogeneities has been detected in some experiments on Earth's vibrational sounding at "source-receiver" distances of hundreds of km [1].

References

[1] M.S. Khairetdinov, "The Nonlinear Wave Effects in Vibroseismics", Bull. Nov. Comp. Center, Math. Model. in Geoph., No.8, pp. 59-69, 2003.

[2] T.Z. Verbitskii, "Peculiarities of Elastic Wave Propagation in Nonlinearly Elastic Porous Media", Problems of Nonlinear Seismics, Nauka, Moscow, 1987, pp. 94-103.

[3] L.K. Zarembo, V.A. Krasilnikov, Introduction to Nonlinear Acoustics, Nauka, Moscow, 1966.

[4] A.V. Nikolayev,. Development of Nontraditional Methods in Geophysics, Coll. of Scientific Papers: Physical Fundamentals of the Seismic Method. Nauka, Moscow.

[5] B.M. Glinsky, M.S. Khairetdinov, V.V. Kovalevsky, "Nonlinear Wave in the Powerful Seismic Vibrators Zones", Nonlinear Acoustics at the Beginning of the 21st Century (Faculty of Physics, MSU, Moscow, 2002) vol.1, pp 327-330.

Finite Element Methods for the Helmholtz Equation and Maxwell System

AN ALGEBRAIC MULTIGRID BASED SHIFTED-LAPLACIAN PRECONDITIONER FOR THE HELMHOLTZ EQUATION

T. Airaksinen[†,*], **E. Heikkola**[‡], **A. Pennanen**[†], **J. Toivanen**[γ]
[†]Department of Mathematical Information Technology, University of Jyväskylä,
P.O. Box 35 (Agora), FI-40014 University of Jyväskylä, Finland
[‡]Numerola Oy, P.O. Box 126, FI-40101 Jyväskylä, Finland
[γ]Institute for Computational and Mathematical Engineering,
Building 500, Stanford University, Stanford, CA 94305, USA
[*]Email: tuomas.airaksinen@jyu.fi

Abstract

A preconditioner defined by an algebraic multigrid cycle for a damped Helmholtz operator is proposed for the Helmholtz equation. This approach is well-suited for acoustic scattering problems in complicated computational domains and with varying material properties. The spectral properties of the preconditioned systems and the convergence of the GMRES method are studied with linear, quadratic, and cubic finite element discretizations. The most important results are reviewed here briefly, for complete analysis, see [1]. Numerical results are presented for two-dimensional acoustic scattering problems in a cross section of a car cabin. Asymptotically the number of iterations grows linearly with respect to the frequency while for lower frequencies the growth is milder. The proposed preconditioner is particularly effective for low-frequency and mid-frequency problems.

Introduction

Acoustic scattering problems can be typically modeled using wave equation and often it is sufficient to consider time-harmonic solutions which are described by the Helmholtz equation

$$-\boldsymbol{\nabla}\cdot\frac{1}{\rho}\boldsymbol{\nabla}u-\frac{k^2}{\rho}u \;=\; 0, \qquad (1)$$

where $u(\mathbf{x})$ is time-harmonic pressure field, $\rho(\mathbf{x})$ is the density of the material $k(\mathbf{x})=\omega/c(\mathbf{x})$ is the wave number. The equations can be discretized using the finite element method, for example. Solving the resulting systems of linear equations can be a computationally challenging problem.

The resulting systems of linear equations from the discretization of the Helmholtz equation are non-Hermitian and indefinite. Furthermore, for mid-frequency and high-frequency problems, the systems can be extremely large. Hence, it is a necessity to use iterative methods such as the GMRES method. However, these methods require a good preconditioner for the discretized Helmholtz equations in order to have reasonably fast convergence.

In this paper, we consider shifted-Laplacian preconditioners which are obtained from the Helmholtz operator by adding damping. This is based on the work described in [2], [3]. The preconditioner used here [1] applies an algebraic multigrid (AMG) method. Multigrid has also been used efficiently for the Helmholtz problem in [4].

Iterative solution and preconditioning

For medium- and large-scale scattering problems, the system of equations $\mathbf{Au}=\mathbf{f}$ is badly conditioned, which leads to a very slow convergence of Krylov subspace methods when applied directly to the system. To improve the speed of convergence, we use a right preconditioner denoted by $\mathbf{B}$. This leads to a preconditioned system $\mathbf{AB}^{-1}\tilde{\mathbf{u}}=\mathbf{f}$. Once $\tilde{\mathbf{u}}$ is solved from this system, the solution $\mathbf{u}$ is obtained as $\mathbf{u}=\mathbf{B}^{-1}\tilde{\mathbf{u}}$.

In 2004, it was suggested in [2] to construct a preconditioner $\mathbf{B}_{SL}$ by discretizing a shifted-Laplace operator

$$\mathcal{B}_{SL}=-\boldsymbol{\nabla}\cdot\frac{1}{\rho}\boldsymbol{\nabla}-(\beta_1+\beta_2 i)\,\frac{k^2}{\rho}. \qquad (2)$$

By choosing $\beta_1=1$ and β_2 to be positive, $\mathcal{B}_{SL}$ is the original Helmholtz operator with additional damping. Such damping leads to good conditioning of $\mathbf{AB}_{SL}^{-1}$ and it is easier to solve systems with $\mathbf{B}_{SL}$ than with $\mathbf{A}$.

Later in 2006 in [3], the inverse of the shifted-Laplacian preconditioner $\mathbf{B}_{SL}$ was approximated by using one cycle of a geometric multigrid method, which we denote by $\mathbf{B}_{MG}$; see [5], for example. This leads to a good conditioning of $\mathbf{AB}_{MG}^{-1}$ for low-frequency problems. In this paper, we replace the geometric multigrid method with a more generic algebraic multigrid method.

For the GMRES method, convergence estimates can be derived based on the spectrum of a matrix and its non-normality. Similarly to [2], [3], we study numerically the spectrum of the preconditioned matrices. For small problems, it is possible to compute the spectrum, while for

larger problems we can only approximate it. The GMRES method forms the basis for a Krylov subspace using the Arnoldi iteration. After m iterations it has generated an $m \times m$ upper Hessenberg matrix which is usually denoted by $\mathbf{H}_m$. The eigenvalues of $\mathbf{H}_m$ approximate the eigenvalues of the system matrix.

Algebraic multigrid method

For preconditioning we use an AMG method introduced by Kickinger in [6] with modifications proposed in [7]. This method uses a graph based on the system matrix to construct coarse spaces. Furthermore, it eliminates the degrees of freedom associated to the Dirichlet boundaries after forming the matrices for the coarse spaces. Under these choices, the AMG method can be constructed in such a way that the coarse problems coincide with the ones obtained using a geometric multigrid method on a hierarchical linear finite element mesh.

Numerical results

We perform numerical experiments with the AMG preconditioner on a cross section of a car cabin. Figure 1 shows a typical solution of the Helmholtz equation on this geometry. The height of the car cabin is 1.5 m and its width is 3 m. The noise source is modeled as the Dirichlet boundary condition $u = 1$ on the wall behind pedals and other partially absorbing walls are modelled using the impedance boundary condition $\frac{\partial u}{\partial \mathbf{n}} = i\gamma k u$ with $\gamma = 0.2$.

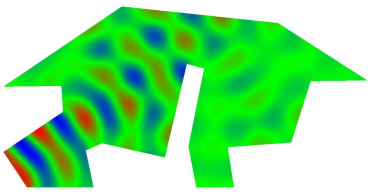

Figure 1: A solution for the car cabin problem with wave number $k = 18.3$ which corresponds to the frequency $f \approx 1$ kHz.

Eigenvalue study

We study the eigenvalues of the preconditioned linear system by computing both the full spectrum and Arnoldi approximations discussed in the end of the previous section. We always have $\beta_1 = 1$ while for β_2 we use the values 0.5 and 1.0. The preconditioner performs one W-cycle with one presmoothing and postsmoothing iteration using the underrelaxed Jacobi with the relaxation parameter given in Table 1. The plots of eigenvalues for the car cabin problem with $k = 15$ in Figure 2 give an indication of the quality of the preconditioner $\mathbf{B}_{MG}^{-1}$.

Table 1: The choice of the Jacobi relaxation parameter ω minimizing the overall solution time for different finite elements and different values of β_2.

β_2	ω		
	linear	quadratic	cubic
0.5	0.4	0.4	0.4
1.0	0.8	0.7	0.7

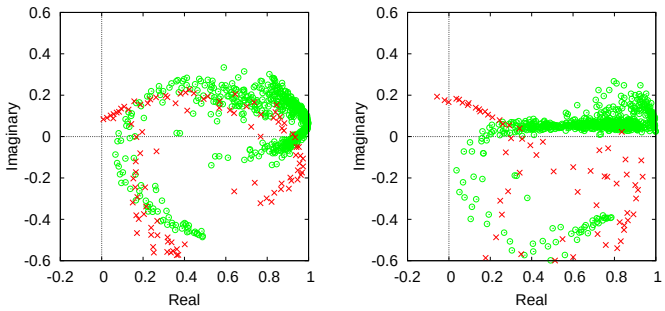

Figure 2: For the car cabin problem discretized with linear elements the eigenvalues of $\mathbf{A}\mathbf{B}_{MG}^{-1}$ marked with ○ and their Arnoldi approximations marked with ×. The left and right plots are based on $\beta_2 = 1.0$ and $\beta_2 = 0.5$, respectively.

Performance analysis

The car cabin problem is used here to study the performance of the iterative solver. The preconditioner $\mathbf{B}_{MG}^{-1}$ is defined by one algebraic multigrid cycle as we have described. Our aim is to choose the parameters defining the preconditioner in such a way that the overall solution time is optimal. Here we show the results only for the choice $\beta_2 = 0.5$ as it leads to much better results than $\beta_2 = 1.0$, especially on higher wave numbers.

The convergence results for the car cabin problem are presented in Table 2. The wave number doubles from a row to the next and the mesh step size h is halved from a column to the next. This leads to a constant number of nodes per wavelength on each diagonal. Along them, we can observe that for higher frequencies, the number of iterations roughly doubles when the wave number is doubled. The lower triangles of the tables correspond to discretizations which do not have sufficiently high number of nodes per wavelength to capture the oscillatory behavior of solutions. This shows up as unusually high number of iterations.

Table 2: For the car cabin problem discretized with linear, quadratic and cubic elements, the number of GMRES iterations required to reduce the norm of the residual by the factor 10^{-6} as a function of the number of refinements n_r and the wave number k.

	Linear elements						
k/n_r	0	1	2	3	4	5	6
2	**8**	12	13	13	13	12	12
4	13	**14**	15	15	15	14	14
8	20	25	**22**	21	21	21	20
16	32	58	52	**43**	35	34	35
32	7	144	172	124	**91**	75	73
64	4	13	433	408	279	**194**	148
	Quadratic elements						
2	**11**	11	12	12	11	11	11
4	13	**13**	14	14	13	12	12
8	26	21	**20**	20	20	19	18
16	59	52	40	**34**	35	34	32
32	158	175	122	85	**72**	69	67
64	15	452	425	271	181	**164**	167
	Cubic elements						
2	**16**	15	15	15	15	15	15
4	20	**17**	17	16	16	16	16
8	33	25	**23**	22	22	21	21
16	77	56	46	**37**	36	38	34
32	193	195	123	87	**70**	70	69
64	250	>500	459	234	161	**149**	137

Conclusions

We have studied a preconditioner defined by an algebraic multigrid (AMG) approximation of the inverse of a shifted-Laplacian for the Helmholtz equation. With finite element discretizations and the AMG preconditioner we can solve problems in complicated domains and with varying wave numbers. The numerical results in here and in [1] demonstrated the efficiency of this approach. Furthermore, the preconditioner was shown to be effective with linear, quadratic, and cubic finite elements.

A big advantage of the AMG method is that the solver does not need hierarchical meshes nor operators discretized on different meshes. The proposed approach is especially well-suited for low-frequency and mid-frequency problems while for high-frequency problems the number of iterations roughly doubles when the frequency is doubled. The same behavior was also observed in [3].

Acknowledgments

The research was supported by the Academy of Finland grant #207089 and the U.S. Office of Naval Research grant N00014-06-1-0067.

References

[1] T. Airaksinen, E. Heikkola, A. Pennanen, J. Toivanen, An algebraic multigrid based shifted-Laplacian preconditioner for the Helmholtz equation, J. Comput. Phys. (2007), to appear.

[2] Y. A. Erlangga, C. Vuik, C. W. Oosterlee, On a class of preconditioners for solving the Helmholtz equation, Appl. Numer. Math. 50 (3-4) (2004) 409–425.

[3] Y. A. Erlangga, C. W. Oosterlee, C. Vuik, A novel multigrid based preconditioner for heterogeneous Helmholtz problems, SIAM J. Sci. Comput. 27 (4) (2006) 1471–1492.

[4] H. C. Elman, O. G. Ernst, D. P. O'Leary, A multigrid method enhanced by Krylov subspace iteration for discrete Helmholtz equations, SIAM J. Sci. Comput. 23 (4) (2001) 1291–1315.

[5] W. L. Briggs, V. E. Henson, S. F. McCormick, A multigrid tutorial, 2nd Edition, Society for Industrial and Applied Mathematics (SIAM), Philadelphia, PA, 2000.

[6] F. Kickinger, Algebraic multi-grid for discrete elliptic second-order problems, in: Multigrid methods V (Stuttgart, 1996), Springer, Berlin, 1998, pp. 157–172.

[7] J. Martikainen, A. Pennanen, T. Rossi, Application of an algebraic multigrid method to incompressible flow problems, Tech. Rep. B2/2006, Department of Mathematical Information Technology, University of Jyväskylä, Jyväskylä, Finland (2006).

GENERATION OF HIGH-ORDER POLYNOMIAL BASES OF NÉDÉLEC H(CURL) FINITE ELEMENTS FOR MAXWELL'S EQUATIONS

M. Bergot[*], **P. Lacoste**[**]
[*]MATMECA, Université Bordeaux I, 351 Cours de la Libération, 33405 Talence, FRANCE
[**]CESTA/DEV/SIS, Commissariat à l'Énergie Atomique, Le Barp, 33114, FRANCE
[**]Email: lacoste.patrick@cea.fr

Abstract

The purpose of this study is the construction of a vectorial polynomial base for Nédélec mixed finite elements [3]. We also aim to build automatically a code written in fortran90 for elementary mass and stiffness matrices. To that end, it is essential to use a symbolic calculus tool (in this case, Maple), so that the input data for the development of such a finite elements of order k, are the number k itself and the k-order mesh made of triangles or tetrahedra. In particular, the main motive is to generate finite elements automatically, without the expression of the polynomial basis functions, attached to the symbolic calculus: **the representation of basis functions has no practical interest**.

Introduction

This article is addresses with the need to increase the order of finite element methods in electromagnetism [1],[2],[5]. The aim here is to determine polynomial basis functions of triangular and tetrahedral elements for any order k. For that purpose, we need first to express the polynomial space of start R^k for any order k, then to give the mathematical expression of the degrees of freedom, and finally to solve the unisolvance system. For all those steps, a symbolic mathematical program is used.

1 Higher-order finite elements of order of $H(curl)$ Finite elements of order k in $\mathbb{R}^3$ on tetrahedra

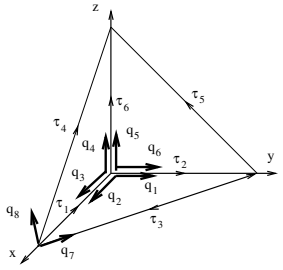

Figure 1: Reference tetrahedron

We recall notations of some polynomial spaces used to define Nédélec finite elements:
$\mathbb{P}_k$ linear space of polynomials of degree $\leq k$,
$\tilde{\mathbb{P}}_k$ linear space of homogeneous polynomials of degree k,
$S^k = \{u \in (\tilde{\mathbb{P}}_k)^3, u_1 x + u_2 y + u_3 z = 0\}$,
$R^k = (\mathbb{P}_{k-1})^3 \oplus S^k$ linear space of polynomials for finite elements of order k and class $H(curl)$.

2 Space of polynomials and degrees of freedom of k-order $H(curl)$ finite elements

Our interest is the k-order finite element built on a tetrahedron (see figure 1). In the sequel we use classical notations of finite elements: $\hat{K}$ is the reference tetrahedron with nodes $(0,0,0),(1,0,0),(0,1,0),(0,0,1)$, K is any tetrahedron of the mesh, $\hat{f}$ a face of $\hat{K}$, f a face of K, etc.

2.1 Characterizing and determining S^k

To built R^k, we first need to determine explicitly S^k. We prove that S^k is entirely described by the following:

$$\begin{array}{l} 1 \leq m \leq k \\ 0 \leq n \leq k-1 \end{array} \quad \begin{pmatrix} \hat{x}^{m-1}\hat{y}^n\hat{z}^{k-m-n+1} \\ 0 \\ -\hat{x}^m\hat{y}^n\hat{z}^{k-m-n} \end{pmatrix} \tag{1}$$

$$\begin{array}{l} 0 \leq m \leq k-1 \\ 1 \leq n \leq k \end{array} \quad \begin{pmatrix} 0 \\ \hat{x}^m\hat{y}^{n-1}\hat{z}^{k-m-n+1} \\ -\hat{x}^m\hat{y}^n\hat{z}^{k-m-n} \end{pmatrix} \tag{2}$$

$$\begin{array}{l} m+n = k+1 \\ m \neq 0, n \neq 0 \end{array} \quad \begin{pmatrix} \hat{x}^{m-1}\hat{y}^n \\ -\hat{x}^m\hat{y}^{n-1} \\ 0 \end{pmatrix} \tag{3}$$

2.2 Definition of the degrees of freedom

Let:

$$\overrightarrow{\hat{p}} = \begin{pmatrix} \hat{p}_1(\hat{x},\hat{y},\hat{z}) \\ \hat{p}_2(\hat{x},\hat{y},\hat{z}) \\ \hat{p}_3(\hat{x},\hat{y},\hat{z}) \end{pmatrix}.$$

Degrees of freedom of edge type $\int_\Gamma \overrightarrow{p} \cdot \overrightarrow{\tau} d\gamma$

If k is the order of the element, the number of edge degrees of freedom is $n_e = 6k$ and they are:
for $m = 1, k$

$$\int_0^1 -\hat{p}_1(1-\hat{x},0,0)\hat{x}^{m-1}d\hat{x} \tag{4}$$

$$\int_0^1 \hat{p}_2(0,\hat{y},0)\hat{y}^{m-1}d\hat{y} \quad (5)$$

$$\int_0^1 (\hat{p}_1(\hat{x},1-\hat{x},0)-\hat{p}_2(\hat{x},1-\hat{x},0))\hat{x}^{m-1}d\hat{x} \quad (6)$$

$$\int_0^1 (-\hat{p}_1(1-\hat{x},0,\hat{x})+\hat{p}_3(1-\hat{x},0,\hat{x}))\hat{x}^{m-1}d\hat{x} \quad (7)$$

$$\int_0^1 (\hat{p}_2(0,\hat{y},1-\hat{y})-\hat{p}_3(0,\hat{y},1-\hat{y}))\hat{y}^{m-1}d\hat{y} \quad (8)$$

$$\int_0^1 \hat{p}_3(0,0,\hat{z})\hat{z}^{m-1}d\hat{z} \quad (9)$$

Volume type degrees of freedom

For k the element order, the number of volume degrees of freedom is $n_v = k(k-1)(k-2)/2$ and they are:
for $m+n+l \leq k-3$,

$$\int_0^1\int_0^{1-\hat{x}}\int_0^{1-\hat{x}-\hat{y}} \hat{p}_1(\hat{x},\hat{y},\hat{z})\hat{x}^m\hat{y}^n\hat{z}^l d\hat{x}d\hat{y}d\hat{z} \quad (10)$$

$$\int_0^1\int_0^{1-\hat{x}}\int_0^{1-\hat{x}-\hat{y}} \hat{p}_2(\hat{x},\hat{y},\hat{z})\hat{x}^m\hat{y}^n\hat{z}^l d\hat{x}d\hat{y}d\hat{z} \quad (11)$$

$$\int_0^1\int_0^{1-\hat{x}}\int_0^{1-\hat{x}-\hat{y}} \hat{p}_3(\hat{x},\hat{y},\hat{z})\hat{x}^m\hat{y}^n\hat{z}^l d\hat{x}d\hat{y}d\hat{z} \quad (12)$$

Face type degrees of freedom

To define them, the following eight vectors are used:

$$\hat{q}_1 = \hat{q}_6 = \begin{pmatrix} 0 \\ 1 \\ 0 \end{pmatrix}, \hat{q}_2 = \hat{q}_3 = \begin{pmatrix} 1 \\ 0 \\ 0 \end{pmatrix}$$

$$\hat{q}_4 = \hat{q}_5 = \begin{pmatrix} 0 \\ 0 \\ 1 \end{pmatrix}, \hat{q}_7 = \begin{pmatrix} -1 \\ 1 \\ 0 \end{pmatrix}, \hat{q}_8 = \begin{pmatrix} -1 \\ -1 \\ 2 \end{pmatrix}.$$

If k is the order of the element, the number of faces degrees of freedom is $n_f = 4k(k-1)$ and they are:
for $m+n \leq k-2$,

$$\int_0^1\int_0^{1-\hat{x}} ((\overrightarrow{\hat{p}} \wedge \overrightarrow{\hat{n}})\cdot\overrightarrow{\hat{q}_1})(\hat{x},\hat{y},0)\hat{x}^m\hat{y}^n d\hat{x}d\hat{y} \quad (13)$$

$$\int_0^1\int_0^{1-\hat{x}} ((\overrightarrow{\hat{p}} \wedge \overrightarrow{\hat{n}})\cdot\overrightarrow{\hat{q}_2})(\hat{x},\hat{y},0)\hat{x}^m\hat{y}^n d\hat{x}d\hat{y} \quad (14)$$

$$\int_0^1\int_0^{1-\hat{x}} ((\overrightarrow{\hat{p}} \wedge \overrightarrow{\hat{n}})\cdot\overrightarrow{\hat{q}_3})(\hat{x},0,\hat{z})\hat{x}^m\hat{z}^n d\hat{x}d\hat{z} \quad (15)$$

$$\int_0^1\int_0^{1-\hat{x}} ((\overrightarrow{\hat{p}} \wedge \overrightarrow{\hat{n}})\cdot\overrightarrow{\hat{q}_4})(\hat{x},0,\hat{z})\hat{x}^m\hat{z}^n d\hat{x}d\hat{z} \quad (16)$$

$$\int_0^1\int_0^{1-\hat{y}} ((\overrightarrow{\hat{p}} \wedge \overrightarrow{\hat{n}})\cdot\overrightarrow{\hat{q}_5})(0,\hat{y},\hat{z})\hat{y}^m\hat{z}^n d\hat{y}d\hat{z} \quad (17)$$

$$\int_0^1\int_0^{1-\hat{y}} ((\overrightarrow{\hat{p}} \wedge \overrightarrow{\hat{n}})\cdot\overrightarrow{\hat{q}_6})(0,\hat{y},\hat{z})\hat{y}^m\hat{z}^n d\hat{y}d\hat{z} \quad (18)$$

$$\int_0^1\int_0^{1-\hat{x}} ((\overrightarrow{\hat{p}} \wedge \overrightarrow{\hat{n}})\cdot\overrightarrow{\hat{q}_7})(\hat{x},\hat{y},1-\hat{x}-\hat{y})\hat{x}^m\hat{y}^n d\hat{x}d\hat{y} \quad (19)$$

$$\int_0^1\int_0^{1-\hat{x}} ((\overrightarrow{\hat{p}} \wedge \overrightarrow{\hat{n}})\cdot\overrightarrow{\hat{q}_8})(\hat{x},\hat{y},1-\hat{x}-\hat{y})\hat{x}^m\hat{y}^n d\hat{x}d\hat{y} \quad (20)$$

3 Change of bases for the degrees of freedom to preserve $H(curl)$ continuity

As the $H(curl)$ finite elements are invariant by affine transformation if we use - for a given (3×3) matrice B:

$$\overrightarrow{p} = B^{*-1}\overrightarrow{\hat{p}}$$

we can define affine equivalent finite elements [2],[3].

3.1 Change of bases for edge degree of freedom

For all number i of an edge $\hat{\Gamma}$, we impose to find $\overrightarrow{\hat{p}}_j$, such that $\hat{\sigma}_i(\overrightarrow{\hat{p}}_j) = \delta_{ij}$, where δ_{ij} is the kronecker symbol and where for these degrees of freedom, for $i = 1, k$:

$$\hat{\sigma}_i(\overrightarrow{\hat{p}}_j) = \int_{\hat{\Gamma}} \overrightarrow{\hat{p}_j}\cdot\overrightarrow{\hat{\tau}}\,\hat{s}^{i-1}d\hat{\gamma}$$

We define:

$$\overrightarrow{\tilde{p}_j} = B^{*-1}\overrightarrow{\hat{p}_j}$$

We suppose that the degrees of freedom for each edge Γ of a tetrahedron K are, for $i = 1, k$:

$$\tilde{\sigma}_i(\overrightarrow{\tilde{p}}_j) = \int_{\Gamma} \overrightarrow{\tilde{p}_j}\cdot\overrightarrow{\tau}\,s^{i-1}d\gamma$$

Then $\tilde{\sigma}_i$ verifies: $\tilde{\sigma}_i(\overrightarrow{\tilde{p}}_j) = \hat{\sigma}_i(\overrightarrow{\hat{p}}_j) = \delta_{ij}$.
We define: $\sigma_i(\overrightarrow{p}) = \tilde{\sigma}_i(\overrightarrow{p})$ when the edge Γ is covered in the same way as $\hat{\Gamma}$. If this edge is covered in the opposite way, we define, refering to a parametrization of Γ on the interval $[0,1]$:

$$\sigma_i(\overrightarrow{p}) = -\int_{\Gamma} \overrightarrow{p}\cdot\overrightarrow{\tau}(1-s)^{i-1}d\gamma$$

Then we formally define the matrice: $A_e = (a^e_{il})$, where $a^e_{il} = (-1)^{l+1}\begin{pmatrix} i-1 \\ l \end{pmatrix}$, if $(i-1) \geq l$ and $a^e_{il} = 0$ if not. We have:

$$\begin{pmatrix} \sigma_1 \\ \dots \\ \sigma_i \\ \dots \\ \sigma_k \end{pmatrix} = A_e \begin{pmatrix} \tilde{\sigma}_1 \\ \dots \\ \tilde{\sigma}_i \\ \dots \\ \tilde{\sigma}_k \end{pmatrix} \quad (21)$$

Then we must choose as $H(curl)$ compatible basis $\mathrm{Span}\{\overrightarrow{\tilde{p}}_i\}$ related to edges:

$$\begin{pmatrix} \overrightarrow{p}_1 \\ ... \\ \overrightarrow{p}_i \\ ... \\ \overrightarrow{p}_k \end{pmatrix} =^t A_e \begin{pmatrix} \overrightarrow{\tilde{p}}_1 \\ ... \\ \overrightarrow{\tilde{p}}_i \\ ... \\ \overrightarrow{\tilde{p}}_k \end{pmatrix}. \tag{22}$$

3.2 Change of bases for faces degree of freedom

As for the edges, the $H(curl)$ continuity at the faces interfaces has to be formulated. This study is restricted to the 2nd-order case; the k-order general case will be presented in a paper to be published.

For all number i of a face $\hat{f}$, we impose to find $\overrightarrow{\hat{p}}_j$, such that $\hat{\sigma}_i(\overrightarrow{\hat{p}}_j) = \delta_{ij}$ where for these degrees of freedom:

$$\hat{\sigma}_i(\overrightarrow{\hat{p}}_j) = \frac{1}{|\hat{f}|}\int_{\hat{f}} (\overrightarrow{\hat{p}}_j \wedge \overrightarrow{\hat{n}}) \cdot \overrightarrow{\hat{q}_i} d\hat{\gamma}$$

This gives:

$$\hat{\sigma}_i(\overrightarrow{\hat{p}}_j) = \tilde{\sigma}_i(\overrightarrow{\tilde{p}}_j) = \frac{1}{|f|}\int_f (\overrightarrow{\tilde{p}_j} \wedge \overrightarrow{n}) \cdot \overrightarrow{u_i} d\gamma$$

where: $\overrightarrow{\tilde{p}_j} = B^{*-1}\overrightarrow{\hat{p}}_j$ and $\overrightarrow{u_i} = B(\overrightarrow{\hat{n}} \wedge \overrightarrow{\hat{q}_i}) \wedge \overrightarrow{n}$. We define the degree of freedom for a face f in the mesh by:

$$\sigma_i(\overrightarrow{p}) = \frac{1}{|f|}\int_f (\overrightarrow{p} \wedge \overrightarrow{n}) \cdot \overrightarrow{q_i} d\gamma$$

where $\overrightarrow{q}_i = \frac{B\overrightarrow{\hat{q}_i}}{|B\overrightarrow{\hat{q}_i}|}$ and $\overrightarrow{q_{i+1}} = \overrightarrow{q_i}^{\perp}, \overrightarrow{q_{i+1}} \subset f$, for $i \in \{1,3,5,7\}$. Then we look for basis functions $\overrightarrow{p}_j$ related to faces verifying:

$$\sigma_i(\overrightarrow{p_j}) = \tilde{\sigma}_i(B^{*-1}\overrightarrow{\hat{p}}_j) = \delta_{ij}$$

To that end, we decompose - following the figure - the $\overrightarrow{u}_i$ on each orthonormal vector base face $(\overrightarrow{q}_i, \overrightarrow{q}_{i+1})$, so that:

$$\overrightarrow{u}_i = \alpha_i \overrightarrow{q}_i + \beta_i \overrightarrow{q}_{i+1}$$

$$\overrightarrow{u}_{i+1} = \alpha_{i+1} \overrightarrow{q}_i + \beta_{i+1} \overrightarrow{q}_{i+1}$$

For the degrees of freedom, we have:

$$\tilde{\sigma}_i = \alpha_i \sigma_i + \beta_i \sigma_{i+1}$$

$$\tilde{\sigma}_{i+1} = \alpha_{i+1} \sigma_i + \beta_{i+1} \sigma_{i+1}$$

or with the (2×2) matrix $A_f = \begin{pmatrix} \alpha_i & \beta_i \\ \alpha_{i+1} & \beta_{i+1} \end{pmatrix}$.

$$\begin{pmatrix} \sigma_i \\ \sigma_{i+1} \end{pmatrix} = A_f^{-1} \begin{pmatrix} \tilde{\sigma}_i \\ \tilde{\sigma}_{i+1} \end{pmatrix} \tag{23}$$

finally the effective vectorial basis on face f is taken to be:

$$\begin{pmatrix} \overrightarrow{p}_j \\ \overrightarrow{p}_{j+1} \end{pmatrix} =^t A_f \begin{pmatrix} \overrightarrow{\tilde{p}}_j \\ \overrightarrow{\tilde{p}}_{j+1} \end{pmatrix}. \tag{24}$$

4 Obtention of mass and stiffness matrices

Then we determine the mass and stiffness matrices:

$$M = (m_{ij})$$

$$K = (k_{ij})$$

where

$$m_{ij} = \int_K \overrightarrow{p}_i \cdot \overrightarrow{p}_j \, dxdydz \tag{25}$$

$$k_{ij} = \int_K curl\,\overrightarrow{p}_i \cdot curl\,\overrightarrow{p}_j \, dxdydz \tag{26}$$

For that purpose, we use a symbolic program to make an exact integration of these integrals with a simplification by the 6 factors of the symmetric matrix $(B^*B)^{-1}$.

Conclusion

The systems $\hat{\sigma}_i(\overrightarrow{\hat{p}}_j) = \delta_{ij}$ with relations (1) to (20) and equations (25)-(26), are solved with symbolic calculus. Although polynomial vector bases are effectively produced by these equations, their contents never appear. The main effort will then be devoted to the $H(curl)$ compatibility equations (21) to (24) which are to be processed with a small but not easy to handle program.

This method can be extended to the $H(div)$ conforming finite elements [4], and more generally to any mixed finite elements using such degrees of freedom.

References

[1] G. Cohen, Higher-Order Numerical Methods for Transcient Wave Equation, Springer Verlag, 2002.

[2] P. Monk, Finite Element Methods for Maxwell's Equations, Oxford University Press, 2003.

[3] J.C. Nédélec, Mixed Finite Elements in $\mathbb{R}^3$, Numer. Math. 35 (1980) 315-341.

[4] P.-A. Raviart, J.-M. Thomas, A Mixed Finite Element Method for Second Order Elliptic Problems, Springer Verlag, 1977.

[5] P. Šolín, K. Segeth, I. Doleźel, Higher-Order Finite Element Methods, Chapman & Hall/CRC, 2003.

SOLVING THE MAXWELL EIGENPROBLEM IN NON-SMOOTH DOMAINS

P. Ciarlet, Jr.[†], **G. Hechme**[†,*]
[†]POEMS, UMR 2706 CNRS-ENSTA-INRIA, 32 boulevard Victor, 75739 Paris Cedex, France
[*]Email: hechme@ensta.fr

Abstract

Costabel and Dauge proposed a variational setting to solve numerically the time-harmonic Maxwell equations in $3D$ polyhedral geometries, with a continuous approximation of the electromagnetic field. In order to remove spurious eigenmodes, three computational strategies are then possible. The original method, which requires a parameterization of the variational formulation. The second method, which is based on an *a posteriori* filtering of the computed eigenmodes. And the third method, which uses a mixed variational setting so that all spurious modes are removed *a priori*. In this talk, the three approaches are compared.

Introduction

In a recent paper [6], Costabel and Dauge proposed a method, which allowed to discretize the electromagnetic field with a continuous approximation, in $3D$, convex or non-convex, polyhedra. In a way, they generalized the method earlier developed by Heintzé *et al* [1], which relied also on a continuous approximation of the field, but worked only in $3D$, convex polyhedra. As it is well-known, when solving the Maxwell equations in a non-convex polyhedron with a continuous and conforming discretization, the discretized spaces are always included in a closed, strict subspace – sometimes called the subspace of *regular fields* – of the space of all possible fields. In other words, one cannot hope to approximate the part of the field which belongs to the orthogonal of the subspace of regular fields. Over the past decade, several methods have been devised to address this problem. We refer to [5] and References therein for an extended discussion on this topic. In [6] the authors propose to recover density of the discretized spaces by measuring the electromagnetic fields in *weighted Sobolev spaces*.

In order to solve the time-harmonic Maxwell equations, Costabel and Dauge proceeded by adding a *regularization term*, with a parameter s: this resulted in the *parameterized weighted regularization method*. Using this technique, one has to discriminate between two sequences of eigenpairs: one is correct and the other is *spurious*. The spurious eigenvalues vary with the parameter s, whereas the correct ones don't. To remove the spurious modes, one has to repeat the computations for various values of the parameter s. This makes the method computationally costly, and its study is omitted here.

To get around this difficulty, we propose two possible solutions. The *filter method* (alluded to in [7]), discriminates between the eigenpairs by examining *a posteriori* the divergence of fields. The *mixed method* [5], [4] imposes *a priori* the divergence free constraint, and spurious modes are automatically excluded. Both methods lead in the end to the correct pairs, however with the second method, it is expected that the constraint on the divergence of the fields is better taken into account.

Computational methods

We consider the case of a resonator cavity Ω, bounded by a perfect conductor. The domain $\Omega \subset \mathbb{R}^3$ is a bounded, simply connected, open polyhedron with a Lipschitz, connected, boundary $\partial\Omega$. Let $\mathbf{n}$ be the unit outward normal to $\partial\Omega$. The electric eigenvalue problem, referred to as (PE), resulting from the time-harmonic Maxwell equations is:
Find $\mathcal{E}$ and ω such that

$$\begin{aligned} c^2 \mathbf{curl}\,\mathbf{curl}\,\mathcal{E} &= \omega^2 \mathcal{E} \text{ in } \Omega, \\ \operatorname{div}\mathcal{E} &= 0 \text{ in } \Omega, \\ \mathcal{E}\times\mathbf{n} &= 0 \text{ on } \partial\Omega, \end{aligned}$$

with c the light velocity, $\mathcal{E}$ the electric field, and ω the time-frequency.

First we introduce the functional spaces needed to deal with variational formulations associated to (PE). Let $L^2(\Omega)$, with norm $\|\cdot\|_0$, be the usual Lebesgue space of measurable and square integrable functions over Ω. Then, $H^1(\Omega)$ denotes the space of $L^2(\Omega)$ functions with gradients in $L^2(\Omega)^3$, and $\mathcal{H}_0(\mathbf{curl}\,,\Omega)$ the space below

$$\{\mathcal{F}\in L^2(\Omega)^3 \,|\, \mathbf{curl}\,\mathcal{F}\in L^2(\Omega)^3, \mathcal{F}\times\mathbf{n}_{|\partial\Omega}=0\}.$$

Let d denote the distance to the set of reentrant edges E of Ω: $d(\mathbf{x}) = dist(\mathbf{x}, \cup_{e\in E}\bar{e})$. We introduce the following weighted spaces:

$$L^2_\gamma(\Omega) := \{v\in L^2_{\rm loc}(\Omega)\,|\, d^\gamma\, v\in L^2(\Omega)\},$$

with norm $||v||_{0,\gamma} := ||d^\gamma\, v||_0$, and

$$\mathcal{X}_\gamma := \{\mathcal{F}\in\mathcal{H}_0(\mathbf{curl}\,,\Omega)\,|\,\operatorname{div}\mathcal{F}\in L^2_\gamma(\Omega)\},$$

with the semi-norm $|\!|\mathcal{F}|\!|_{\mathcal{X}_\gamma} := \left(|\!|\mathbf{curl}\,\mathcal{F}|\!|_0^2 + |\!|\mathrm{div}\,\mathcal{F}|\!|_{0,\gamma}^2\right)^{\frac{1}{2}}$.

Costabel and Dauge in [6] proved that for all $\gamma \in]1/2, 1[$, the graph norm and the semi-norm are equivalent norms on $\mathcal{X}_\gamma$, and moreover $\mathcal{X}_\gamma \cap H^1(\Omega)^3$ is dense in $\mathcal{X}_\gamma$. Let $(\cdot,\cdot)_{\mathcal{X}_\gamma}$ be the scalar product associated to $||\cdot||_{\mathcal{X}_\gamma}$.

Set $\lambda = \omega^2/c^2$. Since the electric field belongs naturally to

$$\mathcal{K}_\gamma := \{\mathcal{F} \in \mathcal{X}_\gamma \,|\, \mathrm{div}\,\mathcal{F} = 0\},$$

an equivalent variational formulation of (PE) is
Find $(\mathcal{E}, \lambda) \in \mathcal{K}_\gamma \times \mathbb{R}^+$ *such that*

$$(\mathbf{curl}\,\mathcal{E}, \mathbf{curl}\,\mathcal{F})_0 = \lambda(\mathcal{E}, \mathcal{F})_0,\ \forall \mathcal{F} \in \mathcal{K}_\gamma.$$

Building a conforming discretization in $\mathcal{K}_\gamma$ is very difficult due to the divergence free condition imposed to the discrete fields. In practice, the electric field is measured in $\mathcal{H}_0(\mathbf{curl}\,, \Omega)$, or in $\mathcal{X}_\gamma$ here.

In this work, we are interested in conforming discretizations with nodal finite elements. Such discretizations cannot be applied to the standard variational formulation above, and we deal with augmented variational formulations instead.

For the *filter method*, we consider the following weighted augmented variational formulation:
Find $(\mathcal{E}, \lambda) \in \mathcal{X}_\gamma \times \mathbb{R}^+$ *such that*

$$(\mathcal{E}, \mathcal{F})_{\mathcal{X}_\gamma} = \lambda(\mathcal{E}, \mathcal{F})_0,\ \forall \mathcal{F} \in \mathcal{X}_\gamma.$$

As for the *parameterized weighted regularisation method*, the spectrum of the eigenproblem spans two families of eigenpairs. The problem is then discretized with P_k Lagrange finite elements. According to the standard theory for Galerkin approximations [2], we have convergence of the discrete eigenpairs towards the Maxwell and the spurious pairs. Hence, when the discrete eigenproblem is solved, eigenpairs in both families are computed. The filter method retains only Maxwell pairs by monitoring *a posteriori* the value of the *filter ratio*:

$$\frac{\|\mathrm{div}\ \mathcal{E}_h\|_{0,\gamma}}{\|\mathbf{curl}\ \mathcal{E}_h\|_0}.$$

This value is small for Maxwell eigenpairs since the divergence part of the eigenvector is small and large for spurious ones since the $\mathbf{curl}$ part is small [7]. However, when a multiple eigenvalue is encountered an additional step must be carried out. Indeed, for a multiple eigenvalue the corresponding eigenvectors are possibly linear combinations of vectors in both families. Hence, the eigenspace should be projected onto the subspace of vectors with a null divergence in order to obtain correct values of the filter ratio before filtering.

The idea of the *mixed method* is to avoid *a priori* all spurious eigenpairs in the spectrum of the considered eigenproblem. For this purpose, we impose the constraint on the divergence of fields by taking a weighted *mixed* augmented *formulation* of the problem, based on a Lagrange multiplier as follows:
Find $(\mathcal{E}, p, \lambda) \in \mathcal{X}_\gamma \times L^2_\gamma(\Omega) \times \mathbb{R}^+$ *such that*

$$\begin{cases} (\mathcal{E}, \mathcal{F})_{\mathcal{X}_\gamma} + (p, \mathrm{div}\,\mathcal{F})_{0,\gamma} = \lambda(\mathcal{E}, \mathcal{F})_0\ \forall \mathcal{F} \in \mathcal{X}_\gamma \\ (q, \mathrm{div}\,\mathcal{E})_{0,\gamma} = 0,\ \forall q \in L^2_\gamma(\Omega). \end{cases}$$

This mixed formulation is equivalent to (PE), as one finds $p = 0$. In [4] the convergence theory for this mixed variational setting is analyzed, within the abstract framework of [3].

The mixed formulation is discretized with Taylor-Hood $P_{k+1} - P_k$ finite elements ($k \geq 1$). As a result, the wanted Maxwell pairs can be computed by solving a generalized symmetric eigenproblem.

Numerical experiments

In this section, we illustrate the two methods with some numerical results. We consider (PE) in the "Fichera corner" domain, which is the cube $[-1,1]\times[-1,1]\times[-1,1]$ minus the cube $[-1,0]\times[-1,0]\times[-1,0]$. The first eight Maxwell eigenmodes given in [8] are listed in Table 1.

Table 1: Conjectured eigenvalues

λ_1	3.2	λ_5	10.694
λ_2	5.88	λ_6	10.7
λ_3	5.88	λ_7	12.32
λ_4	10.694	λ_8	12.32

Computations were performed on a mesh made of 2688 tetrahedra and 665 vertices, refined towards the reentrant edges and corner. The relative errors on the computed eigenmodes, $r_k = |\lambda_{h,k} - \lambda_h|/|\lambda_k|$, are reported in Tables 2 and 3. Filter ratios for the associated eigenvectors are depicted in figures 1, 2 and 3.

We can see that the filter method gives slightly better relative errors. Nevertheless, the mixed method consistently provides better results on the divergence of eigenvectors (see Fig. 1 and 3). Furthermore, the approximation is improved when higher order finite elements are considered, which is not always the case of the filter method (cf. Fig. 2), since the constraint is not explicitly enforced.

Table 2: Filter method

F E	P_2	P_3
r_1	1.9×10^{-1}	2.3×10^{-3}
r_2	8.1×10^{-3}	3.8×10^{-3}
r_3	8.1×10^{-3}	3.8×10^{-3}
r_4	6.3×10^{-3}	1.3×10^{-3}
r_5	6.3×10^{-3}	1.3×10^{-3}
r_6	2.8×10^{-2}	8.8×10^{-3}
r_7	2.8×10^{-3}	9.2×10^{-3}
r_8	2.8×10^{-3}	9.2×10^{-3}

Table 3: Mixed method

F E	$P_2 - P_1$	$P_3 - P_2$
r_1	1.4×10^{-1}	9.8×10^{-2}
r_2	9.2×10^{-3}	4.2×10^{-3}
r_3	9.2×10^{-3}	4.2×10^{-3}
r_4	7.7×10^{-3}	2.5×10^{-3}
r_5	7.7×10^{-3}	2.5×10^{-3}
r_6	1.5×10^{-3}	2.8×10^{-3}
r_7	5.3×10^{-3}	6.0×10^{-3}
r_8	5.3×10^{-3}	6.0×10^{-3}

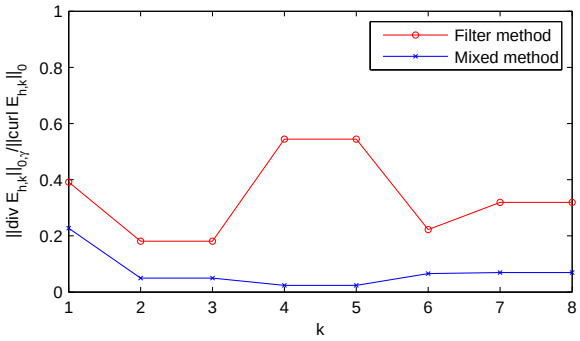

Figure 1: Filter ratios for both methods, P_3 FE.

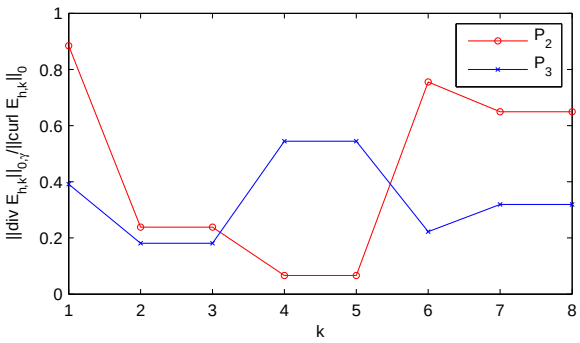

Figure 2: Filter ratios for the filter method.

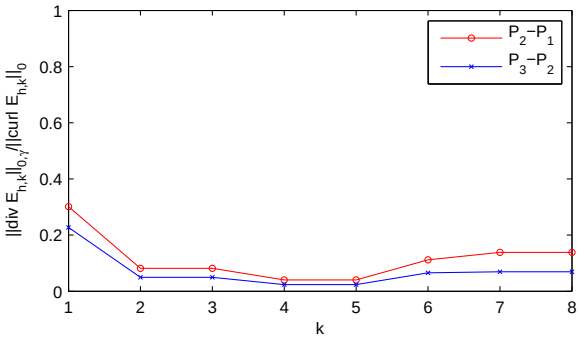

Figure 3: Filter ratios for the mixed method.

References

[1] F. Assous, P. Degond, E. Heintzé, P.-A. Raviart, J. Segré, "On a finite element method for solving the three-dimensional Maxwell equations", J. Comput. Phys., **109**, pp. 222-237 (1993).

[2] I. Babuska, J. E. Osborn, "Eigenvalue problems", in Handbook of Numerical Analysis, Volume II, North Holland, pp. 641-787 (1991).

[3] D. Boffi, F. Brezzi, L. Gastaldi, On the convergence of eigenvalues for mixed formulations. Annali Sc. Norm. Sup. Pisa Cl. Sci., **25**, pp. 131-154 (1997).

[4] A. Buffa, P. Ciarlet, Jr., E. Jamelot, "Solving electromagnetic eigenvalue problems in polyhedral domains", submitted.

[5] P. Ciarlet, Jr., "Augmented formulations for solving Maxwell equations", Comp. Meth. Appl. Mech. and Eng., **194**, pp. 559-586 (2005).

[6] M. Costabel, M. Dauge, "Weighted regularization of Maxwell equations in polyhedral domains", Numer. Math., **93**, pp. 239-277 (2002).

[7] M. Costabel, M. Dauge, "Computation of resonance frequencies for Maxwell equations in non smooth domains", In Computational methods for wave propagation in direct scattering, Lecture Notes in Comp. Sc. and Eng., **31** (2003).

[8] M. Dauge, "Benchmark computations for Maxwell equations for the approximation of highly singular solutions" `http://perso.univ-rennes1.fr/monique.dauge/core/index.html` (2004-2007).

Efficient Resolution of 3-D Maxwell's Equations in Frequency Domain, with Higher-Order Finite Element Methods

Gary Cohen[†,*], **Marc Duruflé**[†]

[†]Inria Rocquencourt, Domaine de Voluceau, 78153 Le Chesnay, FRANCE
[*]Email: gary.cohen@inria.fr

Abstract

The edge elements are well suited for the approximation of time-harmonic Maxwell's equations. For Nedelec's second family on quadrilaterals, we can use a mass lumping technique, which induces a fast matrix-vector product. Such a technique is very suitable for an iterative resolution in frequency domain. Unfortunately, we observe some "spurious" modes on distorted meshes [Cohen et Durufle, 2007]. The Nedelec's first family doesn't have these problems. For this family, we describe a new algorithm, which leads to a fast matrix-vector product, then compare these elements with classical Nedelec's first family on tetrahedral elements. Two types of preconditioning techniques are proposed, they are based on the damped Maxwell's equations. Some 3-D numerical experiments show the efficiency of the method.

1 The 3-D Model Problem

Let $\Omega \subset \mathbb{R}^3$ be a domain with an exterior boundary Σ and an interior boundary Γ, in which we solve the hetereogeneous Maxwell's equations. Γ represents a perfectly metallic scatterer and a Silver-Müller condition is set on Σ. Ω is a homogeneous or heterogeneous medium whose permittivity and permeability are ε and μ respectively. Moreover, we suppose that the medium is homogeneous at infinity and its indices are ε_0 and μ_0. The scattered field is then solution of

$$\begin{aligned} -k^2\varepsilon_r\vec{E} + \mathrm{curl}(\frac{1}{\mu_r}\mathrm{curl}(E)) &= k^2(\varepsilon_r-\varepsilon_0)E^i \\ &\quad +\mathrm{curl}[(\frac{1}{\mu_r}-\frac{1}{\mu_0})\mathrm{curl}(E^i)] \\ \nu\times\vec{E}(x) &= -\nu\times\vec{E}^i(x) \quad x\in\Gamma, \\ (\nabla\times\vec{E})\times\nu &= ik(\nu\times\vec{E})\times\nu \quad x\in\Sigma, \end{aligned} \tag{1}$$

where $\vec{E}$ is the electric field, $k=\omega(c_0)^{-1}$ and $c_0^2=(\varepsilon_0\mu_0)^{-1}$. $\vec{E}^i$ is the incident electric field

$$\vec{E}^i = E^0\exp(ikx)$$

ε_r and μ_r are the relative permittivity and permeability.

2 First Class of Edge Elements

We use the first class of edge elements described in [Nédélec, 1980]. If F_i is the transformation from unit cube $\hat{K}$ onto any hexahedral K_i and DF_i the jacobian matrix, the approximate space is equal to

$$\begin{aligned} V_h &= \{\vec{u}_h\in H_0(\mathrm{curl},\Omega) \text{ such that} \\ &\quad DF_i^t\vec{u}_h\circ\vec{F}_i\in Q_{r-1,r,r}\times Q_{r,r-1,r}\times Q_{r,r,r-1}\} \end{aligned}$$

Then, the basis functions satisfy the following property

$$\vec{\varphi}_i\circ\vec{F}_i = DF_i^{-t}\vec{\hat{\varphi}}_i \tag{2}$$

The basis functions on $\hat{K}$ are defined as in [Cohen et Monk, 1998]:

$$\vec{\hat{\varphi}}^1_{i,j,k} = \hat{\varphi}^G_i(x)\hat{\varphi}^{GL}_j(y)\hat{\varphi}^{GL}_k(z)\vec{e}_x \quad 1\le i\le r \quad 1\le j,k\le r+1,$$

$$\vec{\hat{\varphi}}^2_{i,j,k} = \hat{\varphi}^{GL}_i(x)\hat{\varphi}^G_j(y)\hat{\varphi}^{GL}_k(z)\vec{e}_y \quad 1\le i,k\le r+1 \quad 1\le j\le r.$$

$$\vec{\hat{\varphi}}^3_{i,j,k} = \hat{\varphi}^{GL}_i(x)\hat{\varphi}^{GL}_j(y)\hat{\varphi}^G_k(z)\vec{e}_z \quad 1\le i,j\le r+1 \quad 1\le k\le r.$$

$\hat{\varphi}^G_i$ is the Lagrange function associated to the ith Gauss quadrature point, $\hat{\varphi}^{GL}_i$, the Lagrange function associated to the ith Gauss-Lobatto quadrature point, $\vec{e}_x=(1,0)^T$ and $\vec{e}_y=(0,1)^T$.

3 A Fast matrix vector product

The main drawback of the first class of edge element versus the second class is that we cannot get mass-lumping on non orthogonal meshes [Cohen et Monk, 1998].

3.1 Main statement

This drawback leads a priori, to a slow algorithm for iterative methods. However, the use of the basis functions previously defined provides a fast algorithm for computing the matrix-vector product. We use the Gauss-Lobatto quadrature formulas to evaluate the integrals. we get the following linear system:

$$-\omega^2 M_h E_h + K_h E_h = F_h. \tag{3}$$

After a change of variables, the elementary matrices are computed over the unit cube $\hat{K}$ as follows

$$(M_h)_{j,k} = \int_{\hat{K}} J_i DF_i^{-1}\varepsilon_r DF_i^{-t}\hat{\varphi}_j\cdot\hat{\varphi}_k,$$

$$(K_h)_{j,k} = \int_{\hat{K}} \frac{1}{J_i} DF_i^* \mu_r^{-1} DF_i \hat{\nabla} \times \hat{\varphi}_j \cdot \hat{\nabla} \times \hat{\varphi}_k.$$

We have supposed here that the jacobian J_i is always positive.

These two matrices are computed by using Gauss-Lobatto quadrature rules. We need then to compute the following 3×3 symmetric matrices $(A_h)_{k,k}$ and $(B_h)_{k,k}$ at each quadrature point ξ_k^{GL}:

$$(A_h)_{k,k} = \omega_k^{GL} J_i DF_i^{-1} \varepsilon_r DF_i^{-t}(\hat{\xi}_k^{GL})$$

$$(B_h)_{k,k} = \frac{\omega_k^{GL}}{J_i} DF_i^* \mu_r^{-1} DF_i(\hat{\xi}_k^{GL})$$

Matrices A_h and B_h are block-diagonal matrices, with 3×3 symmetric blocks. An "interpolation" operator $\hat{C}$ is defined by

$$\hat{C}_{j,k} = \hat{\varphi}_j(\hat{\xi}_k^{GL})$$

In the same way, a discrete "curl" $\hat{R}$ operator is defined by

$$\hat{R}_{j,k} = \hat{\nabla} \times \hat{\varphi}_j^{GL}(\hat{\xi}_k^{GL}),$$

where functions $\hat{\varphi}_j^{GL}$ are basis functions associated to Gauss-Lobatto points. The reader can notice that matrix $\hat{R}$ is the same as the stiffness matrix introduced for the mixed formulation.

Theorem 1 *With the previous notations, we get the following factorizations:*

$$M_h = \hat{C} A_h \hat{C}^*,$$
$$K_h = \hat{C} \hat{R} B_h \hat{R}^* \hat{C}^*.$$

3.2 Complexity of the matrix vector product

The complexity of this fast matrix-vector product $(-\omega^2 M_h + K_h)X_h$ is in $O(r^4)$. Moreover, the number of operations is equal to : $((r+1)^3[24(r+1) + 12r + 30])N_e$, where N_e represents the number of hexahedra of the mesh. The required storage is equal to $12(r+1)^3 N_e$ coefficients, which is equivalent to four vectors if r is large enough. In order to compare the different orders of approximation, we compute the quantity :

$$\frac{\text{Computational cost}}{\text{Number of d.o.f.s}}$$

This quantity is displayed in Fig. 1 As we can see in this figure, the fast matrix-vector product is more efficient than standard matrix-vector product for order greater or equal to 3, and also leads to a lower storage than the standard method for order greater or equal to 2.

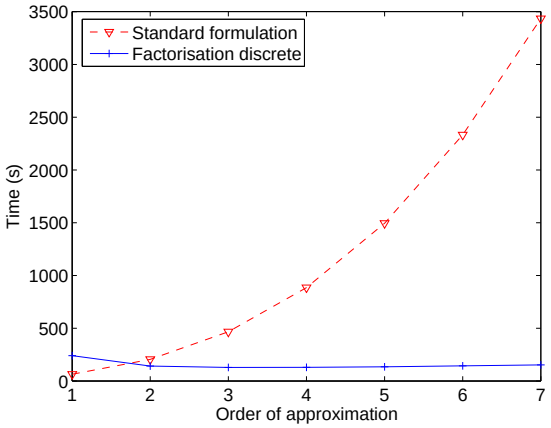

Figure 1: Computational time according to the order of approximation. A standard matrix-vector product (by storing the full matrix) and the fast matrix-vector are compared

Remark: The factorization is also true if an almost-"exact" integration is used ($k+1$ Gauss points instead of $k+1$ Gauss-Lobatto points). In this case, $\hat{R}$ has the same sparsity pattern, but $\hat{C}$ is a full matrix. Fortunatelaty, thanks to tensorization of basis functions on the hexahedron, the triple sum induced by the matrix-vector product $\hat{C}X$ can be decomposed into three single sums. By doing that, we use an implicit factorization: $\hat{C} = \hat{C}_1 \hat{C}_2 \hat{C}_3$, where the intermediaries matrices $\hat{C}_1, \hat{C}_2$ and $\hat{C}_3$ are sparse. A fast matrix-vector is obtained, but it is slower than the fast matrix-vector product obtained with approximate integration. More precisely, it is 67 % slower, if we use exact integration with no improvement in accuracy. This difference was confirmed numerically.

3.3 Cost of the Matrix-Vector Product. Comparison with Tetrahedra

In this section, we numerically compare hexahedral and tetrahedral elements for the first family. The results are summarized in Fig. 2. The **mesh** and the matrix are main components of the storage requirement. For Q_1 and R_1, the mesh represents the main part. The hexahedral elements provide a matrix-vector product which becomes faster than for tetrahedral elements for an order of approximation greater or equal to 3. In practice, the use of high order for tetrahedra of the first family is quite difficult because of a need of high storage.

4 Preconditioning Technique

The iterative solver used is an iterative solver which only works for complex symmetric matrices. It is

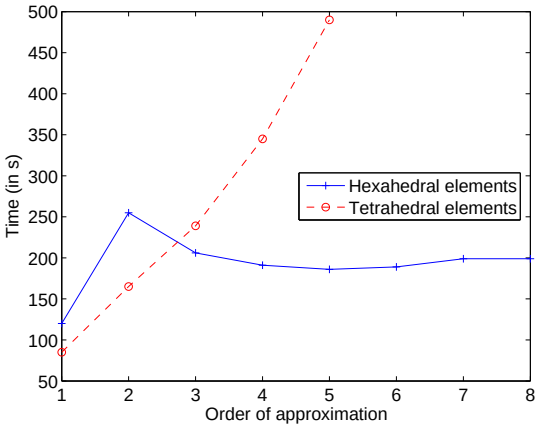

Figure 2: Time for 1 000 iterations of COCG on a test-case of 200 000 d.o.f.s.

called BICGCR (BIConjugate Gradient Conjugate Residual method) and is described in [Clemens et Weiland, 2002].

The main idea of the preconditioning technique used in this article, is to consider damped Maxwell equations by taking ε' complex of the form:

$$\varepsilon' = \varepsilon(\theta + i\eta).$$

Damping is obtained under the assumption $\eta > 0$. The preconditioner is constructed on the damped Maxwell equations, while non-damped Maxwell equations are solved.

4.1 Incomplete Factorization

The effect of damping is to "localize" the inverse of the matrix so that the incomplete factorization works fine. In Table 1, we put the number of iterations of BICGCR preconditioned by ILUT, according to η and different values of the threshold. The incomplete factorization is a classical ILUT, but we only store the U factor, considering that the L factor can be recovered by symmetry. We can see that, if you don't use damping, the incomplete factorization crashes very fast, and there is no gain in storage. The gain in storage increases with damping, but also the number of iterations. The parameters choosen will be equal to $(1,1)$ for all other numerical experiments of the paper.

Threshold	$1e-3$	0.01	0.05
$\theta = 1\,\eta = 0$	$\infty/350\,Mo$	$\infty/340\,Mo$	$\infty/326\,Mo$
$\theta = 1\,\eta = 0.5$	$55/242\,Mo$	$55/149\,Mo$	$82/74\,Mo$
$\theta = 1\,\eta = 1$	$97/197\,Mo$	$99/108\,Mo$	$110/53\,Mo$

Table 1: Number of iterations of BICGCR for a perfectly conducting sphere, and memory used for factorization. The preconditioning used is incomplete factorization on the finite element matrix Q_1

In order to have a low storage, we use a subdivided a $Q1$ mesh to compute a $Q1$ matrix. There is an exact matching between degrees of freedom (d.o.f.s) of the high-order mesh and d.o.f.s of low-order provided a diagonal scaling. This diagonal scaling is due to the transform DF_i^{*-1} incorporated in the definition of the basis functions.

4.2 Multigrid

Several papers propose a multigrid approach as a preconditioning technique [Hiptmair, 1998], [Gopalakrishnan *et al.*, 2004], on low-order edge finite elements. We use a multigrid iteration for the subdived Q1 mesh, with damping. The smoother used is the same than the smoother used in [Hiptmair, 1998].

References

CLEMENS, M. et WEILAND, T. (2002). Iterative methods for the solution of very large complex symmetric linear systems of equations in electrodynamics. Fachbereich 18 elektrische nachrichtentechnik, Technische Hochschule Darmstadt.

COHEN, G. et DURUFLE, M. (2007). Non spurious spectral-like element methods for Maxwell's equations. *Journal of Computational Mathematics*. to appear.

COHEN, G. et MONK, P. (1998). Gauss point mass lumping schemes for Maxwell's equations. *NMPDE Journal*, 14(1):63–88.

GOPALAKRISHNAN, J., PASCIAK, J. E. et DEMKOWICZ, L. F. (2004). Analysis of a multigrid algorithm for time-harmonic Maxwell equations. *SIAM Journal on Numerical Analysis*, 42:90–108.

HIPTMAIR, R. (1998). Multigrid method for Maxwell's equations. *SIAM Journal on Numerical Analysis*, 36:204–225.

NÉDÉLEC, J. C. (1980). Mixed finite elements in $\mathbb{R}^3$. *Numer. Math.*, 35(3):315–341.

CURL CONFORMING ELEMENTS ON HEXAHEDRA

R.S. Falk[†], P. Gatto[‡], and P. Monk[§,*]
[†] Department of Mathematics, Rutgers University, Piscataway, NJ 08854-8019, USA
[‡] Dipartimento di Matematica, Universitá di Paria, Via Ferrata 1, 27100 Paria, Italy
[§*] Department of Mathematical Sciences, University of Delaware, Newark, DE 19716, USA
[*] E-mail: monk@math.udel.edu

Abstract

Edge elements on hexahedral grids are often used to approximate Maxwell's equations. On all but the most trivial domains the elements are obtained by mapping from a reference element to each hexahedron in the grid. This mapping modifies the basis functions and can affect the order of convergence of the resulting method. We examine this problem for the lowest order edge elements of Nédélec and show that in $\mathbf{L}^2(\Omega)$ these elements are first order convergent, but that in $\mathbf{H}(\text{curl};\Omega)$ they do not, in general, provide good approximation. We propose a modified basis that restores convergence.

1 Introduction

Suppose we wish to approximate the electric field $\boldsymbol{E}$ that satisfies Maxwell's equations

$$\nabla \times \nabla \times \boldsymbol{E} - k^2 \boldsymbol{E} = \boldsymbol{f}$$

in a bounded polyhedral domain Ω where the wavenumber $k > 0$ and $\boldsymbol{f} \in \boldsymbol{L}^2(\Omega)$ are given data (here $\boldsymbol{L}^2(\Omega) = (L^2(\Omega))^3$, and in a general bold face quantities are associated with vectors in this paper). The field $\boldsymbol{E}$ must also be subject to a suitable boundary condition, for example $\boldsymbol{n} \times \boldsymbol{E} = 0$ on $\partial\Omega$ where $\boldsymbol{n}$ is the unit outward normal to Ω. A popular finite element method for this problem is to use the edge elements of Nédélec [6] to build a conforming subspace of

$$H(\text{curl};\Omega) = \left\{ \boldsymbol{u} \in \boldsymbol{L}^2(\Omega) \mid \nabla \times \boldsymbol{u} \in \boldsymbol{L}^2(\Omega) \right\}.$$

In particular we shall consider the use of edge elements on a hexahedral mesh. We assume that Ω is covered by a regular mesh of hexahedra. Each element K in the mesh has maximum diameter h and is assumed to be obtained by applying a trilinear map $F_K(\hat{\boldsymbol{x}}) \in Q^3_{1,1,1}$, $\hat{\boldsymbol{x}} = (\hat{x}, \hat{y}, \hat{z})^T$, to the reference element $\hat{K} = [0,1]^3$. Here

$$Q_{\ell,m,n} = \{\text{polynomials of degree at most } \ell \text{ in } \hat{x}, m \text{ in } \hat{y} \text{ and } n \text{ in } \hat{z}\}.$$

On the reference element $\hat{K}$, Nédélec uses the basis

$$\hat{\boldsymbol{P}} = Q_{0,1,1} \times Q_{1,0,1} \times Q_{1,1,0}$$

with degrees of freedom on the edges $\hat{e}$ of $\hat{K}$ having unit tangent vector $\boldsymbol{\tau}_{\hat{e}}$ given by

$$\hat{\Sigma} = \left\{ \int_{\hat{e}} \hat{\boldsymbol{u}} \cdot \boldsymbol{\tau}_{\hat{e}} \, d\hat{s}, \quad \hat{e} \text{ an edge of } \hat{K} \right\}.$$

To preserve the degrees of freedom and curl conformance, it is necessary to obtain the finite element functions $\boldsymbol{u}$ on an element K in the mapped mesh by using the transformation

$$\boldsymbol{u}\left(\boldsymbol{F}_K(\hat{\boldsymbol{x}})\right) = \left(DF_K(\hat{\boldsymbol{x}})\right)^{-T} \hat{\boldsymbol{u}}(\hat{\boldsymbol{x}}) \tag{1}$$

where DF_K is the Jacobian matrix for F_K. This mapping results in basis functions on K that are rational functions and hence the approximation properties of the mapped functions are not immediately obvious.

In 2D, where hexahedra are replaced by quadrilaterals obtained by mapping from a reference square, the question of approximation under mapping has been examined in [2], [1], [3]. In particular, in [3], it is shown that the lowest order Raviart-Thomas divergence conforming elements can achieve first order convergence in $\boldsymbol{L}^2(\Omega)$ using mapped grids. However the elements may not converge in $H(\text{div};\Omega)$ in general.

In this paper we shall carry out a similar program of study for the lowest order $H(\text{curl};\Omega)$ conforming elements of Nédélec in three dimensions. This element is linked with compatible elements for $H^1(\Omega)$, $H(\text{div};\Omega)$ and $L^2(\Omega)$ by the discrete de Rhan diagram [5]. We have also examined the use of mapped hexchedral elements for these spaces in [4]. We provide a new family of elements for $H(\text{div};\Omega)$ that verifies the discrete de Rham diagram when used with the elements discussed in this paper.

2 The Curl Conforming Element

The analysis of convergence of finite elements using basis functions obtained by mapping is considered in [2], [1], [3]. Here it is shown that for general families of regular grids, first order convergence is only assured if the appropriate piecewise constant functions or vectors are contained in the basis on the mapped element K. Rewriting the transformation we obtain (1)

$$\hat{\boldsymbol{u}}(\hat{\boldsymbol{x}}) = \left(DF_K\left(\hat{\boldsymbol{x}}\right)\right)^T \boldsymbol{u}(\boldsymbol{x}).$$

If we require that $\boldsymbol{u}$ can be any constant vector so that $\boldsymbol{u} = \boldsymbol{e}_1 = (1,0,0)^T$, $\boldsymbol{u} = \boldsymbol{e}_2 = (0,1,0)^T$ or $\boldsymbol{u} = \boldsymbol{e}_3 = (0,0,1)^T$ we see that in order to obtain first order convergence in $\boldsymbol{L}^2(K)$, the basis in $\hat{\boldsymbol{P}}$ must contain the columns of $(DF_K)^T$. By writing $\boldsymbol{F}_K(\hat{\boldsymbol{x}}) = (F_1(\hat{\boldsymbol{x}}), F_2(\hat{\boldsymbol{x}}), F_3(\hat{\boldsymbol{x}}))$ where

$$\begin{aligned} F_1 &= a_1 + b_1\hat{x} + c_1\hat{y} + d_1\hat{z} + e_1\hat{x}\hat{y} + f_1\hat{y}\hat{z} \\ &\quad + g_1\hat{z}\hat{x} + h_1\hat{x}\hat{y}\hat{z}, \\ F_2 &= a_2 + b_2\hat{x} + c_2\hat{y} + d_2\hat{z} + e_2\hat{x}\hat{y} + f_2\hat{y}\hat{z} \\ &\quad + g_2\hat{z}\hat{x} + h_2\hat{x}\hat{y}\hat{z}, \\ F_3 &= a_3 + b_3\hat{x} + c_3\hat{y} + d_3\hat{z} + e_3\hat{x}\hat{y} + f_3\hat{y}\hat{z} \\ &\quad + g_3\hat{z}\hat{x} + h_3\hat{x}\hat{y}\hat{z}. \end{aligned}$$

and computing the Jacobian matrix

$$DF_K = \begin{pmatrix} \mathbf{dF}_1^T \\ \mathbf{dF}_2^T \\ \mathbf{dF}_3^T \end{pmatrix}.$$

where

$$\begin{aligned} \mathbf{dF}_1 &= \begin{pmatrix} b_1 + e_1\hat{y} + g_1\hat{z} + h_1\hat{y}\hat{z} \\ c_1 + e_1\hat{x} + f_1\hat{z} + h_1\hat{x}\hat{z} \\ d_1 + f_1\hat{y} + g_1\hat{x} + h_1\hat{x}\hat{y} \end{pmatrix}, \\ \mathbf{dF}_2 &= \begin{pmatrix} b_2 + e_2\hat{y} + g_2\hat{z} + h_2\hat{y}\hat{z} \\ c_2 + e_2\hat{x} + f_2\hat{z} + h_2\hat{x}\hat{z} \\ d_2 + f_2\hat{y} + g_2\hat{x} + h_2\hat{x}\hat{y} \end{pmatrix} \end{aligned}$$

and

$$\mathbf{dF}_3 = \begin{pmatrix} b_3 + e_3\hat{y} + g_3\hat{z} + h_3\hat{y}\hat{z} \\ c_3 + e_3\hat{x} + f_3\hat{z} + h_3\hat{x}\hat{z} \\ d_3 + f_3\hat{y} + g_3\hat{x} + h_3\hat{x}\hat{y} \end{pmatrix}.$$

we see that each column of $(DF_K)^T$ is indeed contained in $\hat{P}$. Hence first order convergence in $\boldsymbol{L}^2(\Omega)$ is indeed possible.

Turning to convergence in the $H(\mathrm{curl};\Omega)$ norm we note that if (1) is used then curls are related by

$$\hat{\nabla} \times \hat{\boldsymbol{u}}(\hat{\boldsymbol{x}}) = J_K(\hat{\boldsymbol{x}}) \left(DF_K(\hat{\boldsymbol{x}})\right)^{-1} (\nabla \times \boldsymbol{u}) \left(F_K(\hat{\boldsymbol{x}})\right),$$

where $J_K(\hat{\boldsymbol{x}})$ denotes the determinant of DF_K. Choosing successively $\nabla \times \boldsymbol{u} = \boldsymbol{e}_1, \boldsymbol{e}_2, \boldsymbol{e}_3$ we can see that first order convergence of the curl is possible only if the columns of $J_K(\hat{\boldsymbol{x}}) \left(DF_K(\hat{\boldsymbol{x}})\right)^{-1}$ are contained in $\nabla \times \hat{\boldsymbol{P}}$. For lowest order edge elements and a general trilinear map this is not the case and so there are mesh families on which edge elements will not converge in the $H(\mathrm{curl};\Omega)$ norm.

We propose to extend the standard Nédélec basis $\hat{\boldsymbol{P}}$ (consisting of 12 vectors) by an additional 15 basis vectors

$$\begin{gathered} \begin{pmatrix} 0 \\ (1-\hat{z})\hat{x}(1-\hat{x}) \\ 0 \end{pmatrix}, \begin{pmatrix} 0 \\ 0 \\ (1-\hat{y})\hat{x}(1-\hat{x}) \end{pmatrix}, \\ \begin{pmatrix} (1-\hat{z})\hat{y}(1-\hat{y}) \\ 0 \\ 0 \end{pmatrix}, \begin{pmatrix} 0 \\ 0 \\ (1-\hat{x})\hat{y}(1-\hat{y}) \end{pmatrix}, \\ \begin{pmatrix} 0 \\ (1-\hat{x})\hat{z}(1-\hat{z}) \\ 0 \end{pmatrix}, \begin{pmatrix} (1-\hat{y})\hat{z}(1-\hat{z}) \\ 0 \\ 0 \end{pmatrix}, \\ \begin{pmatrix} 0 \\ \hat{x}(1-\hat{x})\hat{z} \\ 0 \end{pmatrix}, \begin{pmatrix} 0 \\ 0 \\ \hat{x}(1-\hat{x})\hat{y} \end{pmatrix}, \begin{pmatrix} \hat{z}(1-\hat{z})\hat{y} \\ 0 \\ 0 \end{pmatrix}, \\ \begin{pmatrix} 0 \\ \hat{z}(1-\hat{z})\hat{x} \\ 0 \end{pmatrix}, \begin{pmatrix} 0 \\ 0 \\ \hat{y}(1-\hat{y})\hat{x} \end{pmatrix}, \begin{pmatrix} \hat{y}(1-\hat{y})\hat{z} \\ 0 \\ 0 \end{pmatrix}, \\ \begin{pmatrix} 0 \\ 0 \\ \hat{y}(1-\hat{y})\hat{x}(1-\hat{x}) \end{pmatrix}, \begin{pmatrix} 0 \\ \hat{z}(1-\hat{z})\hat{x}(1-\hat{x}) \\ 0 \end{pmatrix}, \\ \begin{pmatrix} \hat{y}(1-\hat{y})\hat{z}(1-\hat{z}) \\ 0 \\ 0 \end{pmatrix}. \end{gathered}$$

The resulting 27 basis vectors are determined by specifying the degrees of freedom

- $\int_{\hat{e}} \hat{\boldsymbol{u}} \cdot \boldsymbol{\tau}_{\hat{e}}\, d\hat{s}$ on each edge $\hat{e}$ of $\hat{K}$,
- $\int_{\hat{f}} \hat{\nabla} \times \hat{\boldsymbol{u}} \cdot \boldsymbol{n}_{\hat{f}}\, p\, d\hat{A}$ for all $p \in \mathbb{P}_1 \backslash \mathbb{P}_0$ and each face $\hat{f}$ of $\hat{K}$,
- $\int_{\hat{K}} (\hat{\nabla} \times \hat{\boldsymbol{u}}) \cdot \hat{\boldsymbol{r}}\, d\hat{V}$ for all $\hat{\boldsymbol{r}} \in \hat{\boldsymbol{R}}$,

where $\boldsymbol{n}_{\hat{f}}$ is the unit normal to $\hat{f}$, $\mathbb{P}_k$ is the space of polynomials of degree k in two variables and $\hat{\boldsymbol{R}}_K$ is spanned by

$$\left\{ \begin{pmatrix} \frac{1}{2} - \hat{y} \\ \hat{x} - \frac{1}{2} \\ 0 \end{pmatrix}, \begin{pmatrix} \frac{1}{2} - \hat{z} \\ 0 \\ \hat{x} - \frac{1}{2} \end{pmatrix}, \begin{pmatrix} 0 \\ \frac{1}{2} - \hat{z} \\ \hat{y} - \frac{1}{2} \end{pmatrix} \right\}.$$

The resulting element is curl conforming and unisolvent. For sufficiently smooth vector functions, the interpolent will converge at first order in the $\boldsymbol{L}^2(\Omega)$ and $H(\mathrm{curl};\Omega)$ norms.

3 Conclusion

We have shown how to modify the lowest order edge elements of Nédélec to make possible first order convergence on regular grids obtained by general trilinear mappings of the reference element. This construction can be extended to obtain a full discrete de Rham complex [4].

We note that many practical mesh families may exhibit convergence without our construction. For example, if the elements asymptotically become right hexehedra as $h \to 0$, or if the mesh is obtained by a global h independent mapping standard Nédélec elements will have first order convergence. However for arbitrary regular grid families, care must be taken to ensure convergence of mapped hexahedral edge elements. We hope to obtain numerical results for these elements in the future.

References

[1] D. ARNOLD, D. BOFFI, R. FALK, AND L. GASTALDI, *Finite element approximation on quadrilateral meshes*, Commun. Numer. Meth. Eng., 17 (2001), pp. 805–12.

[2] D. N. ARNOLD, D. BOFFI, AND R. S. FALK, *Approximation by quadrilateral finite elements*, Math. Comput., 71 (2002), pp. 909–22.

[3] ——, *Quadrilateral $h(div)$ finite elements*, SIAM J. Numer. Anal., 42 (2005), pp. 2429–51.

[4] R. FALK, P. GATTO, AND P. MONK, *Hexahedral $h(div)$ and $h(curl)$ finite elements*. in preparation, 2007.

[5] P. MONK, *Finite Element Methods for Maxwell's Equations*, Oxford University Press, Oxford, 2003.

[6] J. NÉDÉLEC, *Mixed finite elements in $\mathbb{R}^3$*, Numer. Math., 35 (1980), pp. 315–41.

A DOMAIN DECOMPOSITION METHOD FOR A CLASS OF DISCONTINUOUS GALERKIN DISCRETIZATIONS OF HELMHOLTZ PROBLEMS

C. Farhat, R. Tezaur, J. Toivanen
Institute for Computational and Mathematical Engineering, Stanford University, Stanford, CA 94305, USA
Email: cfarhat@stanford.edu, rtezaur@stanford.edu, toivanen@stanford.edu

Abstract

Recently, a discontinuous Galerkin finite element method with plane wave basis functions was introduced for the efficient solution of Helmholtz problems. The method uses Lagrange multipliers to enforce a weak continuity of the solution at the element interfaces. Here, a preconditioned iterative solution procedure based on a domain decomposition is proposed for the resulting systems of linear equations. Numerical experiments study the iterative solution of a two-dimensional model problem.

Introduction

The oscillatory behavior of mid and high frequency scattering problems necessitates a fine discretization of the governing PDE like the Helmholtz equation considered in this paper. The discretization leads to a very large system of linear equations which is not easy to solve efficiently. During the last decade plane wave based discretizations have become more popular as they offer a way to reduce the system size. The partition of unity method [5], the ultra weak variational formulation [1], and a discontinuous Galerkin method with Lagrange multipliers [3] can employ plane waves. These discretizations lead to ill-conditioned linear systems which have been so far solved with direct solvers. Here, a domain decomposition method is proposed for solving iteratively the systems resulting from the discontinuous Galerkin discretization with Lagrange multipliers.

Formulation

The solution $u \in H^1(\quad)$ of a Helmholtz problem in satisfies the equations

$$\begin{aligned} -\quad u - k^2 u &= 0 && \text{in} \\ \left(\alpha + \quad \frac{\partial}{\partial \boldsymbol{\nu}}\right) u &= -\left(\alpha + \quad \frac{\partial}{\partial \boldsymbol{\nu}}\right) g && \text{on } \Sigma_1 \\ \frac{\partial u}{\partial \boldsymbol{\nu}} &= iku && \text{on } \Sigma_2, \end{aligned} \tag{1}$$

where k is the wavenumber, Σ_1 is the boundary of a scatterer, Σ_2 is the far-field boundary, and $\boldsymbol{\nu}$ denotes the unit outward normal. The function g gives the incident field. The parameters α and define the type of scatterer.

The computational domain is partitioned into elements $_e$ in such a way that:

$$^- = \bigcup_{e=1}^{n_e} {}^-{}_e \quad \text{and} \quad \bigcap_{e=1}^{n_e} {}_e = \emptyset.$$

Let a space $\mathcal{V}$ for the primal variable u and a space $\mathcal{W}$ for Lagrange multiplier be

$$\mathcal{V} = \left\{ v \in L^2(\tilde{}\,) \;:\; v|_{\Omega_e} \in H^1(\quad_e) \right\} \qquad \text{and}$$
$$\mathcal{W} = \prod_e \prod_{e'<e} H^{-1/2}(\Gamma_{e,e'}),$$

where the following notations have been used

$$\tilde{} = \bigcup_{e=1}^{n_e} \quad_e \quad \text{and} \quad \Gamma_{e,e'} = \partial \quad_e \cap \partial \quad_{e'}.$$

The considered discontinuous Galerkin method is based on the following hybrid variational formulation:

Find $(u, \quad) \in \mathcal{V} \times \mathcal{W}$ such that

$$\begin{aligned} a(u,v) + b(\quad, v) &= r(v) && \forall v \in \mathcal{V} \\ b(\mu, u) &= s(\mu) && \forall \mu \in \mathcal{W}, \end{aligned} \tag{2}$$

where the bilinear forms a on $\mathcal{V} \times \mathcal{V}$ and b on $\mathcal{W} \times \mathcal{V}$ are defined as

$$a(u,v) = \int_{\widetilde{\Omega}} (\nabla u \quad \nabla v - k^2 uv)\, d \quad - \int_{\Sigma_2} ikuv \, d\Gamma$$
$$\text{and} \quad b(\quad, v) = \sum_e \sum_{e'<e} \int_{e,e'} \quad (v|_{e'} - v|_e)\, d\Gamma,$$

and the linear forms r on $\mathcal{V}$ and s on $\mathcal{W}$ are defined as

$$r(v) = - \quad \int_{\Sigma_1} \frac{\partial g}{\partial \boldsymbol{\nu}} \, v \, d\Gamma \quad \text{and} \quad s(\mu) = -\alpha \int_{\Sigma_1} g \, \mu \, d\Gamma.$$

The space $\mathcal{V}$ is discretized using its subspace

$$\mathcal{V}_{n_\theta} = \left\{ u \in \mathcal{V} \;:\; u(\mathbf{x}) = \sum_{p=1}^{n_\theta} e^{ik\boldsymbol{\theta}_p \cdot \mathbf{x}} u_{e,p}, \right.$$
$$\left. \mathbf{x} \in \quad_e, \;\; u_{e,p} \in \mathbb{C} \right\},$$

where the wave propagation directions $\boldsymbol{\theta}_p$ are defined by

$$\boldsymbol{\theta}_p = \begin{pmatrix} \cos(2 \ (p-1)/n \ ) \\ \sin(2 \ (p-1)/n \ ) \end{pmatrix}, \quad p = 1, \ldots, n \ .$$

The space $\mathcal{W}$ is discretized using its subspace

$$\mathcal{W}_{n_\lambda} = \Bigg\{ \quad \in \mathcal{W} \ : \quad (\mathbf{x}) = \sum_{p=1}^{n_\lambda} e^{ik\eta_p \boldsymbol{\tau}_{e,e'} \ \mathbf{x}} \quad _{e,e',p}, \\ \mathbf{x} \in \Gamma_{e,e'}, \quad _{e,e',p} \in \mathbb{C} \Bigg\},$$

where $\boldsymbol{\tau}_{e,e'}$ is a unit tangent vector. In [3], [4], the set of values of $\ _p$ for $n_\lambda = 2, 4$ are proposed to be $\{ \ \ 0.5\}$ and $\{ \ \ 0.2, \ \ 0.75\}$, respectively. The name Q-n -n_λ is used for quadrilateral elements with n and n_λ plane waves for the primal variable and Lagrange multiplier, respectively.

Domain decomposition and modified formulation

The elements e are divided into n_d subdomains and the set of elements belonging into the dth subdomain is denoted by E^d. The closure of the dth subdomain is

$$^- \ ^d = \bigcup_{e \in E^d} \ ^- \ _e.$$

In subdomains away from the absorbing boundary Σ_2, the subdomain problem defined by the variational formulation (2) can be singular. To avoid this the regularization described in [2] is adopted which adds a boundary term to the subdomain problems. In the subdomain $\ ^d$, the term corresponds to a Robin boundary condition

$$\frac{\partial u}{\partial \boldsymbol{\nu}} = i\gamma s^d k u \quad \text{on} \ \ \Gamma_d = \partial \ \ ^d \setminus (\Sigma_1 \cup \Sigma_2), \qquad (3)$$

where γ is a regularization parameter and s^d is a sign chosen for $\ ^d$. The signs are assigned in such a way that two subdomains with a common edge have opposite signs. Typically, s^d is assigned in a checkerboard manner if possible while with more general domain decompositions, it might be necessary to set s^d to be zero on a part of the boundary [2].

The additional subdomain boundary term can be incorporated to the variational form (2) by modifying the bilinear form a as follows:

$$\tilde{a}(u,v) = a(u,v) + i\gamma \sum_d \sum_{d' \neq d} \int_{\ _{d,d'}} s^d k u v \, d\Gamma,$$

where $\Gamma^{d,d'} = \partial \ \ ^d \cap \partial \ \ ^{d'}$.

Linear systems and condensations

The discretization leads to a saddle point problem

$$\begin{pmatrix} \mathbf{A} & \mathbf{B}^T \\ \mathbf{B} & \mathbf{0} \end{pmatrix} \begin{pmatrix} \mathbf{u} \\ \boldsymbol{\lambda} \end{pmatrix} = \begin{pmatrix} \mathbf{f} \\ \mathbf{0} \end{pmatrix}$$

The condensation of the primal variable leads to a Schur complement system

$$\mathbf{F}\boldsymbol{\lambda} = \mathbf{B}\mathbf{A}^{-1}\mathbf{B}^T\boldsymbol{\lambda} = \mathbf{B}\mathbf{A}^{-1}\mathbf{f} = \mathbf{b}.$$

This system has a block form

$$\mathbf{F}\boldsymbol{\lambda} = \begin{pmatrix} \mathbf{F}_{II} & \mathbf{F}_{IB} \\ \mathbf{F}_{BI} & \mathbf{F}_{BB} \end{pmatrix} \begin{pmatrix} \boldsymbol{\lambda}_I \\ \boldsymbol{\lambda}_B \end{pmatrix} = \begin{pmatrix} \mathbf{b}_I \\ \mathbf{b}_B \end{pmatrix},$$

where I refers to the Lagrange multipliers in the interior of the subdomains and B refers to the Lagrange multipliers on the interfaces between the subdomains.

The condensation of the interior Lagrange multipliers leads to a Schur complement system

$$\mathbf{F}_S\boldsymbol{\lambda}_B = \mathbf{b}_S, \qquad (4)$$

where $\mathbf{F}_S = \mathbf{F}_{BB} - \mathbf{F}_{BI}\mathbf{F}_{II}^{-1}\mathbf{F}_{IB}$ and $\mathbf{b}_S = \mathbf{b}_B - \mathbf{F}_{BI}\mathbf{F}_{II}^{-1}\mathbf{b}_I$. Once the interface Lagrange multipliers $\boldsymbol{\lambda}_B$ have been solved from this system, the interior ones are given by $\boldsymbol{\lambda}_I = \mathbf{F}_{II}^{-1}(\mathbf{b}_I - \mathbf{F}_{IB}\boldsymbol{\lambda}_B)$.

Iterative solution

Following the idea of two-level FETI, a coarse space is formed and the linear system (4) is solved iteratively on its orthogonal complement. Let the columns of a matrix $\mathbf{Q}$ span the coarse space. A projector to the orthogonal complement of $\mathbf{Q}$ is defined as

$$\mathbf{P} = \mathbf{I} - \mathbf{Q}(\mathbf{Q}^T\mathbf{F}_S\mathbf{Q})^{-1}\mathbf{Q}^T\mathbf{F}_S.$$

Then it can be shown [2] that the solution of (4) has the form $\boldsymbol{\lambda}_B = \boldsymbol{\lambda}_B^0 + \mathbf{P}\boldsymbol{\lambda}_B^1$, where $\boldsymbol{\lambda}_B^0 = \mathbf{Q}(\mathbf{Q}^T\mathbf{F}_S\mathbf{Q})^{-1}\mathbf{Q}^T\mathbf{b}_B$ and $\boldsymbol{\lambda}_B^1$ satisfies the system

$$\mathbf{P}^T\mathbf{F}_S\mathbf{P}\boldsymbol{\lambda}_B^1 = \mathbf{P}^T\mathbf{b}_S.$$

A natural idea is to use plane waves in the construction of the coarse space. Similarly to FETI-H in [2], each subdomain corresponds to a block of $\mathbf{Q}$ given by the products of plane waves and Lagrange multiplier basis functions. Here the number of plane waves in a subdomain is the same as in the discretization of primal variable. The components of $\mathbf{Q}$ are given by

$$\mathbf{Q}_{j,(d-1)n_\theta+p} = \int_{\ _d} \mu_j e^{ik\boldsymbol{\theta}_p \ \mathbf{x}} \, d\Gamma,$$

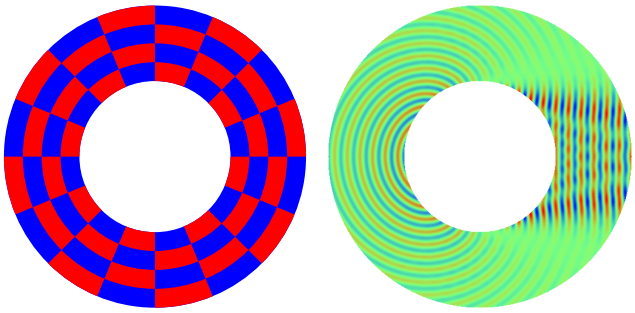

Figure 1: The 16×4 domain decomposition and the real part of the exact solution with $k = 12$.

where μ_j is the jth basis function of $\mathcal{W}_{n_\lambda}$ living on the interfaces between the subdomains.

Plane wave bases can have very poor orthogonality which leads to ill-conditioned systems. A preconditioner based on the Lagrange multiplier mass matrix

$$\mathbf{M} = \begin{pmatrix} \mathbf{M}_{II} & \mathbf{0} \\ \mathbf{0} & \mathbf{M}_{BB} \end{pmatrix}$$

is employed to improve the conditioning. The mass matrix is obtained by discretizing the bilinear form

$$m(\ \ ,\mu) = \sum_{e} \sum_{e'<e} \int_{e,e'} \ \mu \, d\Gamma$$

on $\mathcal{W} \times \mathcal{W}$. Now, the preconditioned system reads

$$\mathbf{P}\mathbf{M}_{BB}^{-1}\mathbf{P}^T\mathbf{F}_S\mathbf{P}\boldsymbol{\lambda}_B^1 = \mathbf{P}\mathbf{M}_{BB}^{-1}\mathbf{P}^T\mathbf{b}_S. \qquad (5)$$

Numerical results

The scatterer is circular and sound-hard, that is, $\alpha = 0$ and $\ = 1$ in (1). The computational domain is $\ = \{\mathbf{x} \in \mathbb{R}^2 \ : \ 1 < \|\mathbf{x}\| < 2\}$ and the incident field is $g = e^{ikx_1}$ in (1). The finest domain decomposition and the exact solution of (1) are shown in Figure 1. The regularization parameter is $\gamma = 0.1$ in (3). The linear systems (4) and (5) are solved using the GMRES method. The iteration counts required to reduce the norm of the residual by the factor 10^{-7} and relative discretization errors at the nodal points in l_2-norm are reported in Table 1.

Conclusions

The presented results and preliminary results with three-dimensional problems show the iterative domain decomposition method to be effective for systems resulting from the discontinuous Galerkin finite element discretizations of the Helmholtz equation. The convergence rate can improved by increasing the number of plane waves in the construction of the coarse space and by introducing a local subdomain preconditioner.

Table 1: The number of iterations without a preconditioner it_1, with the preconditioner it_2, and the relative discretization error with respect to the wavenumber k, element type, mesh, and the number of subdomains n_d.

k	element	mesh	n_d	it_1	it_2	error
6π	Q-8-2	96×8	4×1	53	35	$5.4e{-3}$
6π	Q-8-2	96×8	8×2	214	57	$5.4e{-3}$
6π	Q-8-2	96×8	16×4	537	52	$5.4e{-3}$
6π	Q-16-4	48×4	4×1	53	25	$6.9e{-4}$
6π	Q-16-4	48×4	8×2	252	29	$6.8e{-4}$
6π	Q-16-4	48×4	16×4	660	4	$6.9e{-4}$
12π	Q-8-2	192×16	4×1	85	56	$5.8e{-3}$
12π	Q-8-2	192×16	8×2	370	137	$5.8e{-3}$
12π	Q-8-2	192×16	16×4	909	195	$5.8e{-3}$
12π	Q-16-4	96×8	4×1	103	52	$5.0e{-4}$
12π	Q-16-4	96×8	8×2	473	115	$5.0e{-4}$
12π	Q-16-4	96×8	16×4	> 1000	113	$5.0e{-4}$

Acknowledgments

The research was supported by the U.S. Office of Naval Research grant N00014-05-1-0204-1.

References

[1] O. Cessenat, B. Despres, "Application of an Ultra Weak Variational Formulation of Elliptic PDEs to the Two-dimensional Helmholtz Problem", SIAM J. Numer. Anal., vol. 35, pp. 255–299, 1998.

[2] C. Farhat, A. Macedo, M. Lesoinne, F.-X. Roux, F. Magoulés, A. de La Bourdonnaie, "Two-level Domain Decomposition Methods with Lagrange Multipliers for the Fast Iterative Solution of Acoustic Scattering Problems", Comput. Methods Appl. Mech. Engrg., vol. 184, pp. 213–239, 2000.

[3] C. Farhat, I. Harari, U. Hetmaniuk, "A Discontinuous Galerkin Method with Lagrange Multipliers for the Solution of Helmholtz Problems in the Mid-frequency Regime", Comput. Methods Appl. Mech. Engrg., vol. 192, pp. 1389–1419, 2003.

[4] C. Farhat, R. Tezaur, P. Weidemann-Goiran, "Higher-order Extensions of a Discontinuous Galerkin Method for Mid-frequency Helmholtz Problems", Internat. J. Numer. Methods Engrg., vol. 61, pp. 1938–1956, 2004.

[5] J.M. Melenk, I. Babuška, "The Partition of Unity Finite Element Method: Basic Theory and Applications", Comput. Methods Appl. Mech. Engrg., vol. 139, pp. 289–314, 1996.

Fluid-Structure Interaction

PROPERTIES OF AEROELASTIC MODES AND MODE SHAPES FOR AIRCRAFT WING MODEL (SUBSONIC CASE)

Marianna A. Shubov
Department of Mathematics, University of New Hampshire, Durham, NH 03824, USA
E-mail: marianna.shubov@euclid.unh.edu

Abstract

The paper deals with an aircraft wing model in an inviscid subsonic airflow. It has been developed in the Flight Systems Research Center of the University of California at Los Angeles in collaboration with NASA Dryden Flight Research Center. The model has been successfully tested in a series of flight experiments at Edwards Airforce Base, CA, and has been extensively studied numerically. The model is governed by a system of two coupled integro–differential equations and a two parameter family of boundary conditions modeling the action of self–straining actuators. The system of equations is equivalent to a single operator evolution–convolution equation in the energy space. The Laplace transform of the solution of this equation can be represented in terms of the so-called generalized resolvent operator, which is a finite–meromorphic operator–valued function of the spectral parameter. Its poles are precisely the aeroelastic modes.

Introduction and Statement of Problem.

An ultimate goal of an aircraft wing modeling is to design flutter control mechanism. Flutter is a structural dynamical instability, which consists of violent vibrations of a solid structure with rapidly increasing amplitude when the structure interacts with gas or fluid flow. It usually results either in a serious damage of the structure or in its complete destruction. Flutter occurs when the parameters characterizing fluid–structure interaction reach certain critical values.

Flutter is an extremely complex physical phenomenon, whose complete theoretical explanation is an open problem. At the present moment, there exist only a few models of fluid–structure interaction involving flutter development for which precise mathematical formulations are available. We believe that analytical treatment of flutter problem is an important component of research. Such treatment can provide insights not available from purely computational or experimental results.

To describe mathematical model, let us introduce the dynamical variables [1,5-8]

$$X(x,t) = \begin{pmatrix} h(x,t) \\ \\ \alpha(x,t) \end{pmatrix}, \quad -L \le x \le 0, \ t \ge 0, \quad (1)$$

where $h(x,t)$ is bending and $\alpha(x,t)$ is torsion angle. The model, is described by the following linear system:

$$(M_s - M_a)X_{tt} - uD_aX_t + (K_s - u^2K_a)X = [f_1, f_2]^T. \quad (2)$$

We use the subscripts "s" and "a" to distinguish the structural and aerodynamical parameters respectively. All 2×2 matrices in Eq.(2) are given by the following formulas:

$$M_s = \begin{bmatrix} m & S \\ S & I \end{bmatrix}, \quad M_a = (-\pi\rho)\begin{bmatrix} 1 & -a \\ -a & (a^2+1/8) \end{bmatrix}, \quad (3)$$

where m is density of the structure, S is mass moment, I is moment of inertia, ρ is density of air, u is the stream speed, a is a relative distance between the elastic axis of a wing and its line of center of gravity, $-1 \le a \le 1$; $D_a = (-\pi\rho)\ codiag\{1,-1\}$, and

$$K_s = \begin{bmatrix} E\frac{\partial^4}{\partial x^4} & 0 \\ 0 & -G\frac{\partial^2}{\partial x^2} \end{bmatrix}, \quad K_a = (-\pi\rho)\begin{bmatrix} 0 & 0 \\ 0 & -1 \end{bmatrix}, \quad (4)$$

where E is bending stiffness, G is torsion stiffness. The right–hand side of system (2) can be represented as the following system of two convolution–type integral operations:

$$f_1(x,t) = \int_0^t \tilde{C}_1(t-\sigma)g(x,\sigma)d\sigma, \quad (5)$$

$$f_2(x,t) = \int_0^t \tilde{C}_2(t-\sigma)g(x,\sigma)d\sigma, \quad (6)$$

$$g(x,t) = u\dot{\alpha}(x,t) + \ddot{h}(x,t) + (1/2-a)\ddot{\alpha}(x,t). \quad (7)$$

Here $\tilde{C}_1(t)$ and $\tilde{C}_2(t)$ are known functions, whose precise formulas can be found in [1,5,7]. It is known that the self–straining control actuator action can be modeled by the following boundary conditions [1,7,9]:

$$Eh''(0,t) + \beta h_t'(0,t) = 0, \quad h'''(0,t) = 0, \quad (8)$$

$$G\alpha'(0,t) + \delta\alpha_t(0,t) = 0, \quad \beta,\delta > 0. \quad (9)$$

The boundary conditions at $x = -L$ are

$$h(-L,t) = h'(-L,t) = \alpha(-L,t) = 0. \quad (10)$$

The initial state is standard: $h(x,0) = h_0(x)$, $h_t(x,0) = h_1(x)$, $\alpha(x,0) = \alpha_0(x)$, $\alpha_t(x,0) = \alpha_1(x)$.

Additionally we assume that the parameters satisfy the following two conditions: (a) $mI > S^2$ and (b) $0 < u \leq \sqrt{2G/(L^2\pi\rho)}$.

Condition (b) means that the flow speed must be below the "divergence" or static aeroelastic instability speed for the system [3]. Now we describe the energy space. Let $\mathcal{H}$ be the set of 4-component vector–valued functions $\Psi = (h, h_t, \alpha, \alpha_t)^T \equiv (\psi_0, \psi_1, \psi_2, \psi_3)^T$ obtained as a closure of smooth functions satisfying the boundary conditions $\psi_0(-L) = \psi_0'(-L) = \psi_2(-L) = 0$ in the following energy norm:

$$\|\Psi\|_{\mathcal{H}}^2 = \frac{1}{2}\int_{-L}^{0} \Big[E|\psi_0''|^2 + G|\psi_2'|^2 + \tilde{m}|\psi_1|^2 + \tilde{I}|\psi_3|^2 + \tilde{S}(\psi_3\bar{\psi}_1 + \bar{\psi}_3\psi_1) - \pi\rho u^2|\psi_2|^2\Big]\, dx, \tag{11}$$

where $\tilde{m} = m + \pi\rho$, $\tilde{S} = S - a\pi\rho$, $\tilde{I} = I + \pi\rho(a^2 + 1/8)$, $\Delta = \tilde{m}\tilde{I} - \tilde{S}^2$. The problem defined by (2) and (8)-(10) can be represented in the form ($\Psi = (\psi_0, \psi_1, \psi_2, \psi_3)^T$):

$$\Psi_t = i\mathcal{L}_{\beta\delta}\Psi + \tilde{\mathcal{F}}\Psi_t, \quad \Psi|_{t=0} = \Psi_0. \tag{12}$$

$\mathcal{L}_{\beta\delta}$ is the following matrix differential operator in $\mathcal{H}$:

$$-i\mathcal{L}_{\beta\delta} = \begin{bmatrix} 0 & 1 & 0 & 0 \\ -\frac{E\tilde{I}}{\Delta}\frac{d^4}{dx^4} & -\frac{\pi\rho u\tilde{S}}{\Delta} & -\frac{\tilde{S}}{\Delta}\left(G\frac{d^2}{dx^2} + \pi\rho u^2\right) & -\frac{\pi\rho u\tilde{I}}{\Delta} \\ 0 & 0 & 0 & 1 \\ \frac{E\tilde{S}}{\Delta}\frac{d^4}{dx^4} & \frac{\pi\rho u\tilde{m}}{\Delta} & \frac{\tilde{m}}{\Delta}\left(G\frac{d^2}{dx^2} + \pi\rho u^2\right) & \frac{\pi\rho u\tilde{S}}{\Delta} \end{bmatrix} \tag{13}$$

defined on the domain

$$\mathcal{D}(\mathcal{L}_{\beta\delta}) = \{\Psi \in \mathcal{H}: \quad \mathcal{L}_{\beta\delta}\Psi \in \mathcal{H}; \\ \psi_1(-L) = \psi_1'(-L) = \psi_3(-L) = 0; \ \ \psi_0'''(0) = 0; \\ E\psi_0''(0) + \beta\psi_1'(0) = 0, \ \ G\psi_2'(0) + \delta\psi_3(0) = 0\}. \tag{14}$$

$\tilde{\mathcal{F}}$ is a linear integral operator in $\mathcal{H}$ given by the formula

$$\tilde{\mathcal{F}} = \frac{1}{\Delta}\begin{bmatrix} 1 & 0 & 0 & 0 \\ 0 & T_1 & uT_1 & (1/2 - a)T_1 \\ 0 & 0 & 1 & 0 \\ 0 & T_2 & uT_2 & (1/2 - a)T_2 \end{bmatrix},$$

where $T_1 = [\tilde{I}(\tilde{C}_1 *) - \tilde{S}(\tilde{C}_2 *)]$, $T_2 = [-\tilde{S}(\tilde{C}_1 *) + \tilde{m}(\tilde{C}_2 *)]$, and the star "*" stands for the convolution.

Important Remark. We emphasize that (12) is not an *evolution equation*. It does not have a dynamics generator and does not define any semigroup in the standard sense. However, the notion of the spectral analysis is well–understood. Our aircraft wing model can be described by the evolution–convolution equation

$$\Psi_t(t) = i\,A\,\Psi(t) + \int_0^t F(t-\tau)\Psi_\tau(\tau)d\tau. \tag{15}$$

Ψ is a 4-component vector–valued function, $A (A = \mathcal{L}_{\beta\delta})$ is a matrix differential operator, and $F(t)$ is a matrix–valued function. The formal solution in the Laplace representation can be given by the formula

$$\hat{\Psi}(\lambda) = \Big(\lambda I - iA - \lambda\hat{F}(\lambda)\Big)^{-1}\Big(I - \hat{F}(\lambda)\Big)\,\Psi_0, \tag{16}$$

where Ψ_0 is the initial state, i.e., $\Psi(0) = \Psi_0$, and the symbol "$\hat{}$" is used to denote the Laplace transform. It is an extremely nontrivial problem "to calculate" the inverse Laplace transform of (16) in order to have the representation of the solution in the space–time domain. To do this, it is necessary to investigate the "generalized resolvent operator"

$$\mathcal{R}(\lambda) = \Big(\lambda I - iA - \lambda\hat{F}(\lambda)\Big)^{-1}, \tag{17}$$

which is an operator–valued meromorphic function on the complex plane with a branch–cut along the negative real semi–axis. The poles of $\mathcal{R}(\lambda)$ are called *the aeroelastic modes*. The branch–cut corresponds to the continuous spectrum. The Laplace transform representation for the solution of problem (12), corresponding to (17), has the following form:

$$\hat{\Psi}(\lambda) = \Big(\lambda I - i\mathcal{L}_{\beta\delta} - \lambda\hat{\mathfrak{F}}(\lambda)\Big)^{-1}\Big(I - \hat{\mathfrak{F}}(\lambda)\Big)\,\Psi_0. \tag{18}$$

Our ultimate goal is to find the solution of the problem in the space–time domain. To this end, we have "to calculate" the inverse Laplace transform of $\hat{\Psi}$. It will be done by accomplishing the contour integration in the complex λ-plane. In this connection, the properties of the "generalized resolvent operator"

$$\mathcal{R}(\lambda) = \Big(\lambda I - i\mathcal{L}_{\beta\delta} - \lambda\hat{\mathfrak{F}}(\lambda)\Big)^{-1} \tag{19}$$

are of special importance for us. In our works (see [6] and references therein) it has been shown (1) that the aeroelastic modes are asymptotically close to the discrete spectrum of the operator $i\mathcal{L}_{\beta\delta}$; (2) that there may be only a finite number of the aeroelastic modes having positive real parts, which means that for a given stream speed u, there exists at most a finite number of *unstable aeroelastic mode shapes*; (3) that the set of mode shapes forms a nonorthogonal basis in the energy space.

Statement of main results

Asymptotic properties of aeroelastic modes.

Theorem 1. *a) Problem (16) has a countable set of the complex aeroelastic modes. If*

$$\delta \neq \sqrt{G\tilde{I}}, \tag{20}$$

then this set asymptotically splits into two different subsets. We call them the β–branch and the δ–branch and denote these branches by $\{\lambda_n^\beta\}_{n\in\mathbb{Z}}$ and $\{\lambda_n^\delta\}_{n\in\mathbb{Z}}$ respectively. If $\Re\ \beta \geq 0$ and $\Re\ \delta > 0$, then each branch is asymptotically close to its own horizontal line in the closed upper half–plane. If $\Re\ \beta > 0$ and $\Re\ \delta = 0$, then both horizontal lines coincide with the real axis. If $\Re\ \beta = \Re\ \delta = 0$, then the set of the aeroelastic modes is asymptotically real. The entire set may have only two points of accumulation: $+\infty$ and $-\infty$ in the sense that $\Re\ \lambda_n^{\beta(\delta)} \longrightarrow \pm\infty$ and $|\Im\ \lambda_n^{\beta(\delta)}| \leq const$ as $n \longrightarrow \pm\infty$.

b) The following asymptotical representation is valid for the β–branch as $|n| \longrightarrow \infty$:

$$\lambda_n^\beta = (sgn\ n)(\pi^2/L^2)\sqrt{E\tilde{I}/\Delta}\ (|n| - 1/4)^2 + \xi_n(\omega), \tag{21}$$

where $\omega = |\delta|^{-1} + |\beta|^{-1}$. A complex–valued sequence $\{\xi_n\}$ is bounded above in the following sense: $\sup_{n\in\mathbb{Z}}\{|\xi_n(\omega)|\} = C(\omega)$, $C(\omega) \longrightarrow 0$ as $\omega \longrightarrow 0$.

c) The following asymptotical representation is valid for the δ–branch of the spectrum as $|n| \longrightarrow \infty$:

$$\lambda_n^\delta = \frac{\pi n}{L\sqrt{\tilde{I}/G}} + \frac{i}{2L\sqrt{\tilde{I}/G}}\ \ln\ \frac{\delta + \sqrt{G\tilde{I}}}{\delta - \sqrt{G\tilde{I}}} + O(|n|^{-1/2}). \tag{22}$$

In (22), "ln" means the principal value of the logarithm.

d) There may be only a finite number of multiple aeroelastic modes of a finite multiplicity each. Therefore, only a finite number of the associate mode shapes may exist.

We recall that a basis in a Hilbert space is a *Riesz basis* if it is a linear isomorphic image of an orthonormal basis, i.e., if it is obtained from an orthonormal basis by means of a bounded and boundedly invertible operator [4].

Finally, we formulate the main result, which will be crucial for the "calculation" of the inverse Laplace transform of the solution. The solution of problem (15) can be represented in the form of a sum of an infinite series and an improper integral. The absolute convergence of the integral can be easily seen. The aforementioned infinite series represents a series with respect to the mode shapes. Its unconditional convergence is guaranteed by the result formulated below.

Theorem 2. *The set of the mode shapes forms a Riesz basis in the energy space $\mathcal{H}$.*

Acknowledgement.

Partial support by the National Science Foundation Grant DMS # 0604842 is highly appreciated.

References

[1] Balakrishnan A. V., Subsonic flutter suppression using self-straining acutators, *Journal of the Franklin Institute*, Special Issue on Control, Udwadia F.,Ed., **338**, (2/3), (2001), p.149–170.

[2] Balakrishnan A. V., Control of structures with self-straining actuators: coupled Euler/ Timoshenko model, *Nonlinear Problems in Aviation and Aerospace*, Gordon and Breach Sci. Publ., Reading, United Kingdom, (1998).

[3] Bisplinghoff R. L., Ashley H., and Halfman R. L., *Aeroelasticity*, Dover Publ. Inc., New York, (1996).

[4] Gohberg I. Ts. and Krein M.G., *Introduction to the Theory of Linear Nonselfadjoint Operators*, Trans. of Math. Monogr., **18**, AMS, Providence, RI, (1996).

[5] Shubov M.A., Mathematical analysis of aircraft wing model in subsonic airflow, *IMA Journal of Applied Math.*, **66**, (2001), p.319–356.

[6] Shubov M.A., Riesz basis property of mode shapes for aircraft wing model (subsonic case), *Proc. Royal Soc.A*, **462**, (2006), p.607-646.

[7] Shubov M.A., Asymptotics of the aeroelastic modes and basis property of mode shapes for aircraft wing model, *J. Fraklin Inst.*, **338**, (2/3), (2001), p.171–186.

[8] Shubov M. A. and Peterson C.A., Asymptotic distribution of eigenfrequencies for coupled Euler–Bernoulli/Timoshenko beam model, *NASA Technical Publication, NASA/CR–2003–212022; November, 2003 (NASA Dryden Center)*; p.1–78.

[9] Yang S. M., and Lee Y. J., Modal analysis of stepped beams with piezoelectric materials, *J. Sound Vibr.*, **176**, (1994), p.289-300.

THE PROCEDURE FOR INVESTIGATION OF IMPACTS AND WAVES PROPAGATION IN ROTORS DAMPED BY LONG CAVITATED FLUID FILM BEARINGS

J. Zapomel[*], P. Ferfecki[#]
*Department of Mechanics, VSB-Technical University of Ostrava, Ostrava, Czech Republic
[#]Centre of Advanced and Innovative Technologies, VSB-TU of Ostrava, Ostrava, Czech Republic
E-mail : *jaroslav.zapomel@vsb.cz, [#]petr.ferfecki@vsb.cz

Abstract

A rotor system consists of a rotor and of a stationary part and fluid film bearings are often used as coupling elements. As the clearance between the discs and the casing is usually very small, excessive lateral vibration of the rotor can cause impacts between the discs and the housing. In mathematical models both the bearings and the impacts are implemented by nonlinear force couplings. The induced mechanical waves propagate via the shaft and the bearings into the rotor stationary part. To determine components of the impact forces a Hertz theory is applied. Components of the hydraulic forces are calculated by integration of the pressure distribution in the oil film around the circumference and along the length of the bearing. In the non-cavitated part of the lubricant layer the pressure distribution is governed by a Reynolds equation and in the cavitated region the pressure remains constant. For the solution of the equation of motion a modified Newmark method is adopted.

Introduction

A rotor system consists of a rotor and of a stationary part and fluid film bearings are often used as coupling elements. To ensure efficient performance of rotating machinery the clearance between the discs and the casing is usually very narrow. Therefore excessive lateral vibration of the rotor can cause impacts between the discs and the housing. The induced mechanical waves propagate via the shaft into the rotor casing and the hydrodynamic bearings contribute to their damping. Up to now the fluid film bearings and the impacts have been investigated separately. Therefore it is desirable to develope a procedure that would make possible to analyze their mutual interaction and influence on the rotor behaviour.

An important tool for such investigations is a computer modelling method. Usually both the fluid film bearings and the impacts are implemented into the mathematical models by means of nonlinear force couplings.

The simplest approach to a mathematical description of impacts is based on application of the theories of Newton and Hertz [1].

The length to diameter ratio of many fluid film bearings used in real rotating machinery is often between 0.5 and 1.0 and it allows to consider them as long. To determine components of the bearing forces it is necessary to know a pressure distribution in the oil layer. As the bearing clearance is very narrow the pressure distribution in the full oil film is governed by a Reynolds equation. At locations where the pressure drops to a critical level a vapour cavitation takes place. The observations carried out by Zeidan and Vance showed that pressure of the medium in such areas remained approximately constant [2].

Pressure distribution in long cavitated bearings

A pressure distribution in the full oil film is described by a Reynolds equation modified for the case of long bearings. Application of a finite difference method for its solution requires to divide the bearing circumference by nodes into the periods of the same angular length. Then the Reynolds equation is solved using the Dirichlet boundary conditions (magnitude of pressure under which the oil is supplied into the bearing) for all portions of the bearing circumference between two adjacent oil inlets. If pressure minimum at some location drops to a critical level, a vapour cavitation occurs.

To determine the inflow edge of the cavitated area the nodes are succesively chosen from the node of the pressure minimum in the direction opposite to the journal rotation. Then the Reynolds equation is solved over the portion of the bearing circumference between the node corresponding to the oil inlet before the cavitated region and the selected node. A zero pressure gradient is assigned to the latter. This process is repeated until the pressure in the selected node is equal or greater than the pressure in the cavitated area. This node is then considered to be the inlet edge of the cavitated region.

To determine the outlet border of the cavitated area the nodes are succesively selected from the node of the pressure minimum in the direction of the journal rotation. The Reynolds equation is then solved between the selected node and the node correesponding to the oil inlet behind the cavitated area and the Dirichlet boundary conditions are applied. This manipulation is repeated until the difference between the flow rate in the selected node and in the node corresponding to the inlet edge of the cavitated region is minimum. This node is then considered to be the outlet edge of the cavitated area.

These manipulations are repeated for all portions of the bearing circumference situated between two adjacent oil inlets. Components of the hydraulic forces are then calculated by integration of the pressure around the bearing circumference.

Pressure distribution in long cavitated bearings

To calculate components of the impact forces it is assumed that the stationary part and the discs are absolutely rigid except a small neighbourhood of the contact point, friction in the contact area is of a Coulomb type, direction and orientation of the friction force depends only on the sense of the rotor turning, and the impacts does not influence the angular speed of the rotor rotation.

The contact force consists of two components, of the normal and tangential ones. The normal component is produced by the contact stiffness and damping in material in the neighbourhood of the contact point. Therefore it depends on the displacement and velocity of the disc centre relative to the stationary part in the radial direction. The contact stiffness is determined by means of a Hertz theory and the coefficient of contact damping is considered to be proportional to the contact stiffness. The normal component of the impact force can be only compressive and it can act only if the displacement of the disc centre in the radial direction is greater than is the width of the clearance between the rotor and the stationary part.

The tangential component is a friction force. Its magnitude is given by the Coulomb's law.

Equation of motion

Lateral vibration of rotors supported by fluid film bearings is governed by a nonlinear equation of motion and by the relationship for the boundary conditions. Its solution by a Newmark method [3] arrives at each integration step at solving a set of algebraic equations that are nonlinear due to the bearing forces. To avoid this operation the hydraulic forces at time $t+\Delta t$ are determined by means of their expansion into a Taylor series in the neighbourhood of time t. Taking into account only the linear portion of this expansion arrives at the modified equation of motion that has the form required by the basic Newmark algorithm.

It is assumed that the time increment Δt is very short. Therefore magnitudes of the components of the impact forces related to time $t+\Delta t$ can be determined utilizing kinematic parameters of the rotor system calculated at time t.

Example

Rotor of the investigated rotor system (Fig.1) has a disc that is placed in a cylindrical hole in the casing. The rotor rotates at constant angular speed and is loaded by its weight. In addition the system is excited by centrifugal forces caused by imbalance of both discs. The task was to analyze a propagation of mechanical waves produced by the impacts between the disc and the housing and their transmission to the stationary part by the bearings.

The steady state trajectory of the disc D2 centre is evident from Fig.2. The orbit is periodic or close to periodic. Time histories of the impact and bearing forces are drawn in Fig.3 and 4. The individual impacts last between 400 and 500 μs.

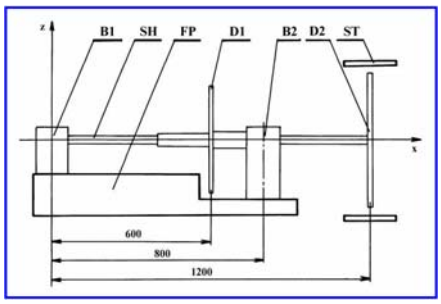

Figure 1 : Scheme of the investigated rotor

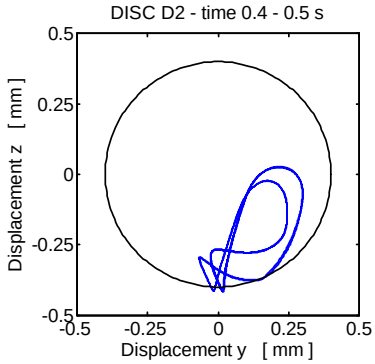

Figure 2 : Steady state orbit (disc D2 centre)

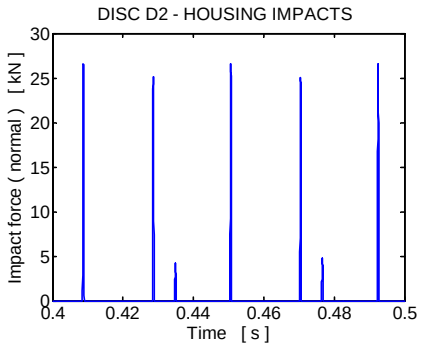

Figure 3 : Impact force (normal component)

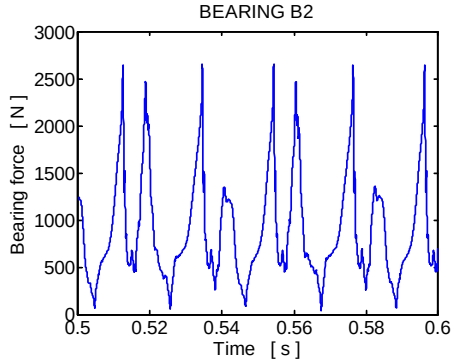

Figure 4 : Hydraulic force in bearing B2

Conclusions

The described approach represents a numerical method for investigation of a transient response of rotors supported by long hydrodynamic bearings and carrying discs that are placed in holes in the stationary part.

The procedure is intended for investigation of the impact forces, propagation of mechanical waves through the shaft, and their transmission by the bearings into the stationary part.

The results of computer simulations show that action of the hydrodynamic bearings and the impacts on the rotor can be analyzed together and that the procedure proposed for solving the equation of motion is numerically stable. The length of the integration step is governed more by the requirements put on calculation of the impact forces than of the forces acting in the bearings.

Acknowledgement

This research work has been supported by the grant projects GA101/06/0063 and MSM 6198910027. The support is gratefully acknowledged.

References

[1] B. Brogliato, Impacts in Mechanical Systems, Springer, Berlin, Heidelberg, 2000

[2] F.Y. Zeidan, J.M. Vance "Cavitation regimes in squeeze film dampers and their effect on the pressure distribution", STLE Tribology Transactions, vol.33, 1990, pp. 447-453.

[3] J. Zapoměl , E. Malenovský, "Approaches to numerical investigation of the character and stability of forced and and self-excited vibration of flexible rotors with non-linear supports", Proceedings of the 7th International. Conference on Rotating Machinery (IMechE Conference Transactions), Nottingham, England, 2000, pp.691-699

Half-Space and Rough Surface Scattering Problems

COMPUTATION OF THE GREEN'S FUNCTION ASSOCIATED WITH THE ELASTICITY SYSTEM IN A HALF-PLANE WITH IMPEDANCE BOUNDARY CONDITION

M. Durán[†,*], **E. Godoy**[†,‡,**], **J.-C. Nédélec**[‡,**]

[†] Facultad de Ingeniería, Pontificia Universidad Católica de Chile, Casilla 306, Santiago 22, Chile
[‡]CMAP, Ecole Polytechnique, 91128 Palaiseau, France
*Email: mduran@ing.puc.cl **Email: egodoy@ing.puc.cl ***Email: nedelec@cmapx.polytechnique.fr

Abstract

An effective numerical analytical method for calculating the Green's function associated with the time-harmonic elasticity system in a half-plane is presented, where an impedance boundary condition is imposed. The need to calculate arises when studying resonant states in underground mining and seismological engineering. The proposed method is based on the work done by Durán, Muga and Nédélec [5] for the Helmholtz's equation. The desired Green's function is expressed as a sum of two terms, namely, the first one associated with the whole plane and the second one taking into account the half-plane's boundary. The poles of this last term are related to surface waves and they are numerically determined. We have found that in addition to the well-known Rayleigh wave, under certain conditions another surface wave appears. Indeed, there exists a case where the associated pole is real and it can be analytically computed.

Basic mathematical model

Let us consider $\mathbb{R}^2_+ = \{\boldsymbol{x} = (x,y) \in \mathbb{R}^2 / \ y > 0\}$ the upper half-plane, whose boundary is denoted by Γ. Let $\boldsymbol{x} = (x_0, y_0)$, $\boldsymbol{y} = (x,y) \in \mathbb{R}^2_+$ be the source and variable points, respectively. The Green's function of the time-harmonic elasticity system in $\mathbb{R}^2_+$, denoted by $G = G(\boldsymbol{x}, \boldsymbol{y})$, is a 2×2 matrix function with complex values, whose column vectors are denoted by $\boldsymbol{g}_j = \boldsymbol{g}_j(\boldsymbol{x}, \boldsymbol{y})$, where $j = 1, 2$. For a fixed $\boldsymbol{x}$, these vectors are obtained as solution of the next differential system in $\boldsymbol{y}$:

$$\begin{aligned} \rho\,\omega^2 \boldsymbol{g}_j + \operatorname{div}\sigma(\boldsymbol{g}_j) &= -\delta_{\boldsymbol{x}} \boldsymbol{e}_j \qquad \text{in } \mathbb{R}^2_+, \\ \sigma(\boldsymbol{g}_j)\boldsymbol{n}\cdot\boldsymbol{n} &= 0 \qquad \text{on } \Gamma, \\ \big(\sigma(\boldsymbol{g}_j)\boldsymbol{n} - Z\boldsymbol{g}_j\big)\cdot\boldsymbol{t} &= 0 \qquad \text{on } \Gamma, \end{aligned}$$

$+$*Outgoing radiation conditions at infinity*,

where ρ is the elastic solid density, $\omega > 0$ is the pulsation, $\delta_{\boldsymbol{x}}$ is the Dirac mass centered at $\boldsymbol{x}$, $\boldsymbol{e}_j$ is the j^{th} canonic vector of $\mathbb{R}^2$, $\boldsymbol{n}$ and $\boldsymbol{t}$ are the external normal and tangential unit vectors on Γ, Z is the impedance and σ is the stress tensor, which evaluated at a displacement field $\boldsymbol{u}$ is given by the classic Hooke's law:

$$\sigma(\boldsymbol{u}) = \lambda(\operatorname{div}\boldsymbol{u})I + \mu\left(\nabla\boldsymbol{u} + (\nabla\boldsymbol{u})^T\right),$$

where λ and μ are the Lamé constants and I is the 2×2 identity matrix. The transversal and longitudinal slowness of the elastic medium are defined as follows, respectively:

$$s_T = \sqrt{\frac{\rho}{\mu}}, \qquad s_L = \sqrt{\frac{\rho}{\lambda+2\mu}}.$$

Note that the impedance boundary condition corresponds to a proportionality relation between sheer stresses and tangential displacements on Γ. As the normal stresses are null, when $Z = 0$, the well-known free boundary condition is retrieved. On the other hand, radiation conditions at infinity have to be imposed to obtain outgoing solutions. For a broader framework about Green's functions and their use in integral equations for time-harmonic problems, see Nédélec [7], Bonnet [3] and Linkov [6].

Spectral Green's function

The differential system for $\boldsymbol{g}_j(\boldsymbol{x}, \cdot)$ is solved by applying the following partial Fourier transform in x:

$$\widehat{\boldsymbol{g}}_j(\boldsymbol{x}, s, y) = \frac{1}{\sqrt{2\pi}} \int_{-\infty}^{\infty} \boldsymbol{g}_j(\boldsymbol{x}, \boldsymbol{y})\, e^{-i\,\omega s(x-x_0)}\,\mathrm{d}x,$$

where for reasons of convenience, a Fourier variable s normalized by ω has been considered instead of the standard one. An ODE matrix system in y with constant coefficients is obtained, with s regarded as a parameter. The Fourier transform of G, denoted by $\widehat{G} = \widehat{G}(\boldsymbol{x}, s, y)$, is the so-called spectral Green's function, which is calculated by solving this system. The expression achieved for $\widehat{G}$ can be separated as a sum of two terms:

$$\widehat{G} = \widehat{G}^{\infty} + \widehat{G}^{\Gamma},$$

where $\widehat{G}^{\infty} = \widehat{G}^{\infty}(\boldsymbol{x}, s, y)$ is a symmetric matrix associated with the whole plane $\mathbb{R}^2$ and $\widehat{G}^{\Gamma} = \widehat{G}^{\Gamma}(\boldsymbol{x}, s, y)$ is a non-symmetric matrix which takes into account the boundary conditions imposed on Γ.

Effective computation of Green's function

In order to make an effective computation of the Green's function $G(\boldsymbol{x}, \boldsymbol{y})$, an accurate calculation of the inverse Fourier transform of $\widehat{G}$ is necessary. The expression as a sum of two terms suggests dealing separately with terms $\widehat{G}^{\infty}$ and $\widehat{G}^{\Gamma}$. Their respective inverse Fourier transforms are denoted by $G^{\infty}(\boldsymbol{x}, \boldsymbol{y})$ and $G^{\Gamma}(\boldsymbol{x}, \boldsymbol{y})$.

In the first case, the inverse Fourier transform of $\widehat{G}^{\infty}$ is analytically calculated by means of integral formulas taken from Bateman [1]. As obtained by Durán, Muga and Nédélec in [5] for the Helmholtz's equation, we obtain that $G^{\infty}(\boldsymbol{x}, \boldsymbol{y})$ corresponds to the Green's function of the time -harmonic elasticity system in $\mathbb{R}^2$ (cf. [4]).

In the second case, the inverse Fourier transform of $\widehat{G}^{\Gamma}$ is computed by combining analytical and numerical techniques. For the sake of accuracy, it is necessary to carefully take into account each singularity present in this term when computing its inverse transform. Hence we separate $\widehat{G}^{\Gamma}$ as the following sum:

$$\widehat{G}^{\Gamma} = \widehat{G}^{\Gamma,\,\mathrm{r}} + \widehat{G}^{\Gamma,\,\mathrm{sp}} + \widehat{G}^{\Gamma,\,\mathrm{p}},$$

where $\widehat{G}^{\Gamma,\,\mathrm{r}}$ corresponds to a regular part, $\widehat{G}^{\Gamma,\,\mathrm{sp}}$ is a part containing pseudo-poles and $\widehat{G}^{\Gamma,\,\mathrm{p}}$ is a part containing poles. These three terms arise in the analysis of $\widehat{G}^{\Gamma}$.

The pseudo-poles appear in the diagonal components of $\widehat{G}^{\Gamma}$. Specifically, there are factors $(s^2 - s_T^2)^{-1/2}$ and $(s^2 - s_L^2)^{-1/2}$ in these components. In order to remove these singularities, an appropriate diagonal matrix $\widehat{G}^{\Gamma,\,\mathrm{sp}}$ is subtracted from $\widehat{G}^{\Gamma}$. The matrix obtained $\left(\widehat{G}^{\Gamma} - \widehat{G}^{\Gamma,\,\mathrm{sp}}\right)$ has poles only, and the inverse Fourier transform of term $\widehat{G}^{\Gamma,\,\mathrm{sp}}$, denoted by $G^{\Gamma,\,\mathrm{sp}}(\boldsymbol{x}, \boldsymbol{y})$, is analytically computed with formulas obtained from [1].

The poles of $\left(\widehat{G}^{\Gamma} - \widehat{G}^{\Gamma,\,\mathrm{sp}}\right)$ come from a common denominator that appears in all its components, given by:

$$\begin{aligned} f_z(s) =& \left(s_T^2 - 2s^2\right)^2 - 4s^2\sqrt{s^2 - s_T^2}\sqrt{s^2 - s_L^2} \\ &+ \eta\, z\sqrt{s^2 - s_T^2}, \end{aligned}$$

where $\eta = \rho/\mu^2$ and $z = Z/\omega$ is the impedance normalized by the pulsation. The definition of the complex square roots is taken assuming special branches in $\mathbb{C}$ (see [5] for details). The poles are determined as solutions of equation $f_z(s) = 0$, which is non-trivial to solve (this matter is discussed in the next section). However, as in $f_z(s)$ only appear terms in s^2, it is possible to assure a priori that the solutions are pairs symmetrically located with respect to the origin, namely, $s = \pm s_0$, where $s_0 > 0$. The term $\left(\widehat{G}^{\Gamma} - \widehat{G}^{\Gamma,\,\mathrm{sp}}\right)$ is assumed to have two simple poles at these locations, which are removed by subtracting a matrix $\widehat{G}^{\Gamma,\,\mathrm{p}}$ given by:

$$\widehat{G}^{\Gamma,\,\mathrm{p}}(\boldsymbol{x}, s, y) = \left(\frac{1}{s - s_0}\right) A^{+} + \left(\frac{1}{s + s_0}\right) A^{-},$$

where A^{+}, A^{-} are constants matrices containing the residues associated with the poles at $s = \pm s_0$. The inverse Fourier transform of $\widehat{G}^{\Gamma,\,\mathrm{p}}$, denoted by $G^{\Gamma,\,\mathrm{p}}(\boldsymbol{x}, \boldsymbol{y})$, is analytically computed by an integration along an appropriate contour in the complex plane and application of the Cauchy's residues theorem (cf. [5]).

Once the terms associated with pseudo-poles and poles of $\widehat{G}^{\Gamma}$ have been subtracted, the obtained term, denoted by $\widehat{G}^{\Gamma,\,\mathrm{r}}$, is regular, because its singularities have been removed. Moreover, it is possible to verify that $\widehat{G}^{\Gamma,\,\mathrm{r}}$ decreases fast at infinity. Its inverse Fourier transform, denoted by $G^{\Gamma,\,\mathrm{r}}(\boldsymbol{x}, \boldsymbol{y})$, is numerically approximated within a bounded area by an FFT algorithm.

Numerical computation of poles

As above mentioned, the poles are determined by solving the equation $f_z(s) = 0$. In general, this equation has to be solved by numerical procedures. Nevertheless, when $z = 0$ an analytical solution is possible, because the equation can be led to a third degree polynomial equation in s^2 and the well-known explicit formulas for their roots are used. In the general case $z \in \mathbb{R}$, the equation can only be led to a sixth degree polynomial equation in s^2 and in order to compute their roots, the use of numerical techniques is necessary. In both cases, not all the roots of the polynomial equations are associated with solutions of the original equation. In order to find true solutions, we evaluate $f_z(s)$ in each root and we keep those for which we obtain the smallest relative errors.

Realistic numerical values for the physical parameters are assumed in the calculations. The considered elastic medium is limestone, a sedimentary rock whose physical constants are approximately: $\rho = 2.400$ [Kg/m^3], $\lambda = 40,3846$ [GPa], and $\mu = 26,9231$ [GPa]. The longitudinal and transversal slownesses are $s_T = 2.9857 \times 10^{-4}$ [s/m] and $s_L = 1.5959 \times 10^{-4}$ [s/m].

We have found that for all $z \in \mathbb{R}$ the polynomial equation has a positive root yielding two real poles at $s = \pm s_R$, where $s_R > 0$ is the so-called Rayleigh slowness. The numerical procedure shows that s_R is an increasing function of z. In particular, in the free boundary case we have obtained $s_R = 3,2194 \times 10^{-4}$ [s/m].

Moreover, the numerical evidence shows that there exists another root of the polynomial equation (in general

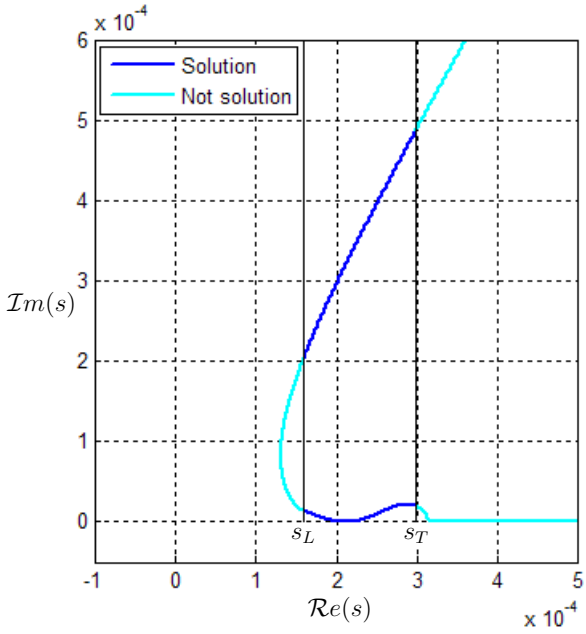

Figure 1: Additional pole behavior in the complex plane as a function of z.

complex), which for certain values of z yields two additional poles at $s = \pm(s_A + i\delta_A)$, where s_A, $\delta_A \geq 0$. The whole curve described by the positive pole as a function of z in the complex plane is shown in Fig. 1, where the zones corresponding to true poles of the spectral Green's function have been emphasized. Notice that these poles are only located in the area $s_L < \mathfrak{Re}(s) < s_T$. This is due to the assumed definition of complex square roots. From this graph we observe that there exists a unique value $z = z^* > 0$ for which the imaginary part δ_A becomes null. Consequently, the corresponding real part s_A is an additional slowness associated with another surface wave. The values of s_A and z^* can be directly calculated from the equation $f_z(s) = 0$ and imposing $s_L < s_A < s_T$:

$$s_A = \sqrt{\frac{\rho}{2\mu}}, \qquad z^* = \sqrt{\frac{2\,\rho\,\lambda\,\mu}{\lambda + 2\mu}}.$$

Note that both parameters depend only on physical constants of elastic medium. Replacing the numerical values of ρ, λ, and μ, we obtain $s_A = 2,1112 \times 10^{-4}$ [s/m] and $z^* = 7,4421$ [MPa/m].

A numerical result

Next, a numerical result of the Green's function is shown. The physical constants of limestone are assumed, and a pulsation $\omega = 2\pi \cdot 5$ [Hz] $= 31.4159$ [Rad/s] is considered. The source point is taken at $(x_0, y_0) = (0, 500$ [m]). A normalized impedance $z = z^*$ is assumed. Fig. 2 shows a contour plot in (x, y) of the component $G_{12}(\boldsymbol{x}, \cdot)$ (real part). Note that surface waves can be observed at $y = 0$.

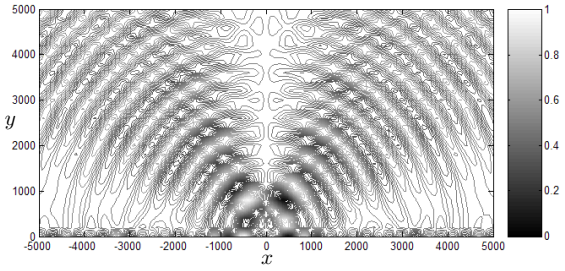

Figure 2: Real part of G_{12}.

Acknowledgements

This work was supported by the Proyecto ACT30 ANILLO de Investigación del Programa Bicentenario en Ciencia y Tecnología de CONICYT/World Bank (Chile) and the PUC fellowship for doctoral students. The authors want to thank I. Muga for his support of this work.

References

[1] H. Bateman, *Tables of Integral Transformations, Volume I*, McGraw-Hill Book Company, Inc., 1954.

[2] W.W. Bell, *Special Functions for Scientists and Engineers*, Dover Publications, Inc., New York, 1968.

[3] M. Bonnet, *Boundary Integral Equation Methods for Solids and Fluids*, John Wiley & Sons Ltd., Chichester, 1995.

[4] J. Dompierre, *Équations Intégrals en Axisymétrie Généralisée, Application à la Sismique Entre Puits*, Thesis, École Centrale de Paris, 1993.

[5] M. Durán, I. Muga & J.-C. Nédélec, *The Helmholtz Equation in a Locally Perturbed Half-plane with Passive Boundary*, IMA Journal of Applied Mathematics, 71, pp. 853-876, 2006.

[6] A.M. Linkov, *Boundary Integral Equations in Elasticity Theory*, Kluwer Academic Publishers, Dordrecht, Boston, 2002.

[7] J.-C. Nédélec, *Acoustic and Electromagnetic Equations. Integral Representations for Harmonic Problems*, Springer, Berlin, 2001.

COMPUTING NUMERICALLY THE GREEN'S FUNCTION OF THE HALF-PLANE HELMHOLTZ EQUATION WITH IMPEDANCE BOUNDARY CONDITIONS

M. Durán[†,*], **R. Hein**[†,‡,**], **J.-C. Nédélec**[‡,***]
[†]Facultad de Ingeniería, Pontificia Universidad Católica de Chile, Casilla 306, Santiago 22, Chile
[‡]Centre de Mathématiques Appliquées, École Polytechnique, 91128 Palaiseau, Cedex, France
[*]Email: mduran@ing.puc.cl [**]Email: rhein@puc.cl [***]Email: nedelec@cmapx.polytechnique.fr

Abstract

The Green's function of the half-plane Helmholtz equation with impedance boundary conditions is computed numerically. A compactly perturbed half-plane Helmholtz problem is presented to motivate this calculation, which is treated through integral equation techniques, leading to a boundary element discretization. The Green's function is computed using an inverse Fourier transform, applying an inverse FFT for the regular part, and removing the singularities analytically.

Introduction

In this work we are interested in the development of numerical tools which permit to treat complex wave propagation phenomena involving infinite half-planes and impedance boundary conditions.

For this purpose, we study a classical two-dimensional model of time-harmonic waves, based on the Helmholtz equation, which describes a wide range of different wave propagation phenomena acting in the linear range. The understanding of these phenomena for a relatively simple model allows to study them later for more complex and specific cases. In these models, we are interested in studying the appearance of resonant states and surface waves, by imposing impedance boundary conditions.

Since unbounded exterior domains are involved, we treat this problem numerically using an integral equation and the boundary element method. This treatment requires the knowledge of the half-plane Green's function, which is calculated explicitly in a numerical manner, as an inverse Fourier transform of its spectral counterpart. The singularities of the spectral Green's function are calculated analytically, while the remaining regular part is then computed with the help of an inverse fast Fourier transform (IFFT). The same procedure is performed for the calculation of the gradient of the Green's function.

Some related previous works can be found in the numerous existing literature. Proofs of existence and uniqueness for the model problem treated here, as well as the radiation condition, can be found in [1], whereas further related studies and references can be found in [2], [3], [4], [5], [6], [7], [8].

Perturbed half-plane Helmholtz problem

We consider the direct scattering problem of time-harmonic waves on a perturbed half-plane $\Omega_e \subset \mathbb{R}^2$, and a known incident field u_i. The goal is to find the scattered field u as a solution to the Helmholtz equation in Ω_e, satisfying an outgoing radiation condition, and such that the total field u_t, decomposed as $u_t = u_i + u$, satisfies a homogeneous impedance boundary condition on the regular boundary $\Gamma = \Gamma_p \cup \Gamma_\infty$. The exterior domain Ω_e is composed by the half-plane $\mathbb{R}^2_+ = \{(x_1, x_2) \in \mathbb{R}^2 \,|\, x_2 > 0\}$ with a compact perturbation near the origin, as shown in Figure 1. The perturbed boundary is denoted by Γ_p, while Γ_∞ denotes the remaining unperturbed boundary of $\mathbb{R}^2_+$, which extends to infinity on both sides. The unit normal $\boldsymbol{n}$ is taken outwardly oriented of Ω_e.

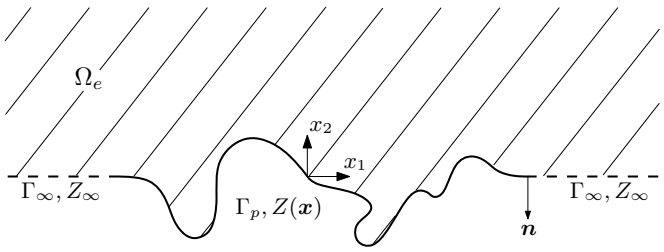

Figure 1: Problem domain.

The direct scattering problem of the perturbed half-plane with impedance boundary conditions, for a given wave number $k \in \mathbb{R}$, is thus given by: Find $u : \Omega_e \to \mathbb{C}$ such that

$$\begin{cases} \Delta u + k^2 u = 0 \quad \text{in } \Omega_e, \\ -\dfrac{\partial u}{\partial n} + Zu = f_z \quad \text{on } \Gamma, \\ \text{+ Outgoing radiation condition as } |\boldsymbol{x}| \to \infty. \end{cases} \tag{1}$$

The impedance is decomposed as $Z(\boldsymbol{x}) = Z_\infty + Z_p(\boldsymbol{x})$, where $Z_p(\cdot)$ is a regular function having its support contained in Γ_p, and $Z_\infty \geq 0$ is constant throughout Γ. The function $f_z : \Gamma \to \mathbb{C}$ is known, has its support contained in Γ_p, and is given by $f_z = \frac{\partial u_i}{\partial n} - Zu_i$.

Plane waves

Two different kinds of independent plane wave solutions exist for the unperturbed half-plane Helmholtz problem ($\Omega_e = \mathbb{R}^2_+$, $Z = Z_\infty$, $f_z = 0$, and without the radiation condition). The volume waves solution is

$$u(\boldsymbol{x}) = e^{i(k_1 x_1 + k_2 x_2)} - \left(\frac{Z_\infty + ik_2}{Z_\infty - ik_2}\right) e^{i(k_1 x_1 - k_2 x_2)},$$

where $i = \sqrt{-1}$, and $\boldsymbol{k} = (k_1, k_2) \in \mathbb{R}^2$ is the wave propagation vector, being $(\boldsymbol{k} \cdot \boldsymbol{k}) = k^2$. The other kind, the surface waves solution, is

$$u(\boldsymbol{x}) = Z_\infty e^{\pm i\sqrt{k^2 + Z_\infty^2} x_1} e^{-Z_\infty x_2}.$$

Half-plane Green's function

The Green's function G_{k,Z_∞} associated with the half-plane $\mathbb{R}^2_+$ is obtained as the solution of the boundary value problem: Find $G_{k,Z_\infty}(\boldsymbol{x}, \cdot) : \mathbb{R}^2_+ \to \mathbb{C}$ such that

$$\begin{cases} \Delta_{\boldsymbol{y}} G_{k,Z_\infty} + k^2 G_{k,Z_\infty} = \delta_{\boldsymbol{x}}, \quad \boldsymbol{y} \in \mathbb{R}^2_+, \\ \dfrac{\partial G_{k,Z_\infty}}{\partial y_2} + Z_\infty G_{k,Z_\infty} = 0, \quad y_2 = 0, \\ + \text{Outgoing radiation condition as } |\boldsymbol{y}| \to \infty, \end{cases}$$

where $\delta_{\boldsymbol{x}}$ is a Dirac mass at the source point $\boldsymbol{x} \in \mathbb{R}^2_+$.

Taking a one-dimensional Fourier transform on the horizontal y_1-axis, and solving the resulting ordinary differential equation for the given boundary values, yields the following representation of the Green's function as an inverse Fourier transform [1]

$$G_{k,Z_\infty}(\boldsymbol{x}, \boldsymbol{y}) = \frac{1}{4\pi} \int_{-\infty}^{\infty} \left(- \frac{e^{-\sqrt{\xi^2 - k^2}\,|y_2 - x_2|}}{\sqrt{\xi^2 - k^2}} + \frac{Z_\infty + \sqrt{\xi^2 - k^2}}{Z_\infty - \sqrt{\xi^2 - k^2}} \frac{e^{-\sqrt{\xi^2 - k^2}\,(y_2 + x_2)}}{\sqrt{\xi^2 - k^2}} \right) e^{i(y_1 - x_1)\xi} \mathrm{d}\xi \,.$$

To compute this expression numerically, the appearing singularities in the spectral domain are treated analytically, while the remaining regular part is calculated using an IFFT.

The spectral Green's function presents a slow decrease at infinity when $y_2 = x_2$, associated with the first term under the integral sign, which occurs due the essential singularity of logarithmic type that appears in the spatial origin for the full-plane Green's function of the Helmholtz equation. The associated term can be derived, e.g., from [10], and is given by

$$G_\infty(\boldsymbol{x}, \boldsymbol{y}) = -\frac{i}{4} H_0^{(1)}\left(k\,|\boldsymbol{y} - \boldsymbol{x}|\right),$$

where $H_0^{(1)}$ denotes the zeroth order Hankel function of the first kind (cf. [9]).

Two pseudo-poles (i.e., poles of half order) appear at $\xi = k$ and $\xi = -k$, linked to the image of the full-plane Green's function, located in the lower half-plane and associated with a negative Dirac mass. Again, from [10], we can derive the associated term, yielding

$$G_s(\boldsymbol{x}, \boldsymbol{y}) = \frac{i}{4} H_0^{(1)}\left(k\,|\boldsymbol{y} - \bar{\boldsymbol{x}}|\right),$$

where $\bar{x} = (x_1, -x_2)$ is the image point of $\boldsymbol{x}$.

The spectral Green's function has two simple poles at $\xi = \xi_p$ and $\xi = -\xi_p$, where $\xi_p = \sqrt{Z_\infty^2 + k^2}$. The calculation of the associated part is performed by means of the residue theorem in complex analysis, using the frame of the limit absorption principle, as done in [1]. The part of the poles is thus given by

$$G_p(\boldsymbol{x}, \boldsymbol{y}) = \frac{Z_\infty}{i\xi_p} e^{-Z_\infty(y_2 + x_2)} e^{i\xi_p |y_1 - x_1|}.$$

The regular part is calculated using an IFFT, therefore

$$G_r(\boldsymbol{x}, \boldsymbol{y}) = \text{IFFT}\left[\frac{1}{\sqrt{2\pi}} \frac{e^{-\sqrt{\xi^2 - k^2}\,(y_2 + x_2)}}{Z_\infty - \sqrt{\xi^2 - k^2}} - \frac{Z_\infty e^{-Z_\infty(y_2 + x_2)}}{\sqrt{2\pi}\,\xi_p} \left(\frac{1}{\xi + \xi_p} - \frac{1}{\xi - \xi_p} \right) \right] \{y_1 - x_1\}.$$

The desired numerically calculated half-plane Green's function is finally given by

$$G_{k,Z_\infty} = G_\infty + G_s + G_p + G_r \,.$$

The gradient of the Green's function is calculated in the same manner. The slow decrease at infinity part yields

$$\nabla G_\infty(\boldsymbol{x}, \boldsymbol{y}) = \frac{ik}{4} H_1^{(1)}\left(k\,|\boldsymbol{y} - \boldsymbol{x}|\right) \frac{\boldsymbol{y} - \boldsymbol{x}}{|\boldsymbol{y} - \boldsymbol{x}|},$$

where $H_1^{(1)}$ denotes the first order Hankel function of the first kind (cf. [9]).

The pseudo-poles part is given by

$$\nabla G_s(\boldsymbol{x}, \boldsymbol{y}) = -\frac{ik}{4} H_1^{(1)}\left(k\,|\boldsymbol{y} - \bar{\boldsymbol{x}}|\right) \frac{\boldsymbol{y} - \bar{\boldsymbol{x}}}{|\boldsymbol{y} - \bar{\boldsymbol{x}}|}.$$

The derivative for the horizontal variable y_1 of the poles part yields

$$\frac{\partial G_p}{\partial y_1}(\boldsymbol{x}, \boldsymbol{y}) = Z_\infty \text{sign}(y_1 - x_1) e^{-Z_\infty(y_2 + x_2)} e^{i\xi_p |y_1 - x_1|}.$$

The derivative for y_1 of the regular part is given by

$$\frac{\partial G_r}{\partial y_1}(\boldsymbol{x},\boldsymbol{y}) = \text{IFFT}\left[\frac{i\xi}{\sqrt{2\pi}}\,\frac{e^{-\sqrt{\xi^2-k^2}\,(y_2+x_2)}}{Z_\infty-\sqrt{\xi^2-k^2}} - \frac{Z_\infty e^{-Z_\infty(y_2+x_2)}}{\sqrt{2\pi}\,\xi_p}\left(\frac{i\xi}{\xi+\xi_p}-\frac{i\xi}{\xi-\xi_p}\right)\right]\{y_1-x_1\}.$$

The derivative for the vertical variable y_2 considers

$$\frac{\partial G_{pr}}{\partial y_2}(\boldsymbol{x},\boldsymbol{y}) = \frac{ik}{2}H_1^{(1)}\left(k\,|\boldsymbol{y}-\bar{\boldsymbol{x}}|\right)\frac{(y_2+x_2)}{|\boldsymbol{y}-\bar{\boldsymbol{x}}|} - Z_\infty\left(G_r(\boldsymbol{x},\boldsymbol{y})+G_p(\boldsymbol{x},\boldsymbol{y})\right).$$

The desired numerically calculated gradient of the half-plane Green's function is finally given by

$$\nabla G_{k,Z_\infty} = \nabla G_\infty + \nabla G_s + \left(\frac{\partial G_p}{\partial y_1}+\frac{\partial G_r}{\partial y_1},\frac{\partial G_{pr}}{\partial y_2}\right).$$

Integral equation

The solution u of the direct scattering problem (1) admits the following integral representation for $\boldsymbol{x}\in\Omega_e$:

$$u(\boldsymbol{x}) = \int_{\Gamma_p} f_z(\boldsymbol{y})\,G_{k,Z_\infty}(\boldsymbol{x},\boldsymbol{y})\,\mathrm{d}\gamma(\boldsymbol{y}) + \int_{\Gamma_p}\left(\frac{\partial G_{k,Z_\infty}}{\partial n_{\boldsymbol{y}}}(\boldsymbol{x},\boldsymbol{y}) - Z(\boldsymbol{y})G_{k,Z_\infty}(\boldsymbol{x},\boldsymbol{y})\right)u(\boldsymbol{y})\,\mathrm{d}\gamma(\boldsymbol{y}).$$

An integral equation can be derived for $\boldsymbol{x}\in\Gamma_p$, given by

$$\int_{\Gamma_p}\left(-\frac{\partial G_{k,Z_\infty}}{\partial n_{\boldsymbol{y}}}(\boldsymbol{x},\boldsymbol{y})+Z(\boldsymbol{y})G_{k,Z_\infty}(\boldsymbol{x},\boldsymbol{y})\right)u(\boldsymbol{y})\,\mathrm{d}\gamma(\boldsymbol{y}) + \frac{u(\boldsymbol{x})}{2} = \int_{\Gamma_p} f_z(\boldsymbol{y})\,G_{k,Z_\infty}(\boldsymbol{x},\boldsymbol{y})\,\mathrm{d}\gamma(\boldsymbol{y}). \quad (2)$$

Numerical discretization

The solution of the direct scattering problem (1) is found by applying the boundary element method on the variational or weak formulation of the integral equation (2), using on the boundary curve Γ_p Lagrange finite elements of type $\mathbb{P}_1$ (piecewise linear functions). Thus Γ_p is approximated by the discrete curve Γ_p^h, composed by I rectilinear segments T_j, sequentially ordered for $1\le j\le I$, such that the length $|T_j|<h$ for some $h>0$.

This discretization leads to the linear matrix system

$$M_{k,Z}\boldsymbol{u} = \boldsymbol{b}_{k,Z},$$

where $\boldsymbol{u}\in\mathbb{C}^{I+1}$ is the vector of unknowns, $M_{k,Z}$ is a full, complex, non-symmetric $(I+1)\times(I+1)$ matrix, and $\boldsymbol{b}_{k,Z}\in\mathbb{C}^{I+1}$ is a known vector related to the incident field u_i.

Acknowledgements

The authors gratefully acknowledge the support of this work by the Research Proyect ACT30 ANILLO of the Bicentenary Program for Science and Technology of CONICYT/World Bank (Chile), and the CONICYT fellowship for doctorate students.

References

[1] M. Durán, I. Muga & J.-C. Nédélec, "The Helmholtz Equation in a Locally Perturbed Half-plane with Passive Boundary", IMA Journal of Applied Mathematics 71, 853–876, 2006.

[2] P. Barton & A. Rawlins, "Acoustic Diffraction by a Semi-Infinite Plane with Different Face Impedances", Q. J. Mech. Appl. Math. 52 (3), 469–487, 1999.

[3] S. Chandler-Wilde, "The Impedance Boundary Value Problem for the Helmholtz Equation in a Half-Plane", Math. Meth. Appl. Sci. 20, 813–840, 1997.

[4] S. Chandler-Wilde & A. Peplow, "A Boundary Integral Equation Formulation for the Helmholtz Equation in a Locally Perturbed Half-Plane", Z. Angew. Math. Mech. 85, No. 2, 79–88, 2005.

[5] M. Durán, I. Muga & J.-C. Nédélec, "The Helmholtz Equation with Impedance in a Half-Space". C. R. Acad. Sci. Paris, Ser. I 341, 561–566, 2005.

[6] D. Natroshvili, T. Arens & S. Chandler-Wilde, "Uniqueness, Existence, and Integral Equation Formulations for Interface Scattering Problems", Memoirs on Differential Equations and Mathematical Physics 30, Georgian Academy of Sciences, 105–146, 2003.

[7] J.-C. Nédélec, "Acoustic and Electromagnetic Equations: Integral Representations for Harmonic Problems", Springer, Berlin, 2001.

[8] A. Peplow & S. Chandler-Wilde, "Noise Propagation from a Cutting of Arbitrary Cross-Section and Impedance", J. Sound Vib. 223, 355–378, 1999.

[9] M. Abramowitz & I.A. Stegun, "Handbook of Mathematical Functions with Formulas, Graphs, and Mathematical Tables", Dover, New York, 1965.

[10] I.S. Gradshteyn & I.M. Ryzhik, "Table of Integrals, Series and Products", Academic Press, New York, 1980.

RADIATION CONDITION FOR A CLASS OF TIME-HARMONIC ACOUSTIC AND ELASTIC WAVE PROBLEMS ARISING IN HALF-SPACES

M. Durán[†,*], **I. Muga**[‡,**], **J.-C. Nédélec**[§,***]

[†]Facultad de Ingeniería, Pontificia Universidad Católica de Chile, Casilla 306, Santiago 22, Chile
[‡]Instituto de Matemáticas, Pontificia Universidad Católica de Valparaíso, Valparaíso, Chile
[§]Centre de Mathématiques Apliquées, École Polytechnique, 91128 Palaiseau Cedex, France
[*]Email: mduran@ing.puc.cl [**]Email: ignacio.muga@ucv.cl [***]Email: nedelec@cmap.polytechnique.fr

Abstract

In this work we establish original radiation conditions able to describe outgoing wave propagation phenomena in half-spaces, including surface waves propagating towards infinity. We focus our intention in two time-harmonic model problems: the direct scattering problem of acoustic waves in (locally perturbed) half-spaces with passive boundary, and the direct scattering problem of elastic waves in (locally perturbed) half-spaces with free boundary condition.

Introduction

The problem of scattering by unbounded surfaces has become very important due to vast applications where more complex models are needed. As examples, in acoustics we found the problem of outdoor sound propagation over ground surfaces, or the harbour resonance problem in coastal engineering. On the other hand, in elasticity we can mention non-destructive testing, isolation from ground borne vibrations, or predictions in underground drilling and blasting mining processes.

Dealing with half-spaces and surface acoustic waves propagating near the unbounded boundary, we observe that the well known Sommerfeld radiation condition does not describe outgoing surface wave behaviour. In fact, surface waves propagate with a wave-number different from volume waves. The same situation holds in the elastic case for Rayleigh waves and the Kupradze radiation condition [6].

In relation to scattering by unbounded surfaces, we found in literature some radiation conditions like the *upward propagating radiation condition* or the *Rayleigh expansion radiation condition*. We refer to Chandler-Wilde [2] or Chandler-Wilde and Bo Zhang [3] for the acoustic case, while for the elastic case we can mention the work of Arens [1]. Despite, as far as we know, those radiation conditions do not cover the case of surface wave propagation guided by the boundary.

In the articles [4] or [5] we have proposed an original radiation condition able to prove uniqueness and existence results for the Helmholtz equation in half-spaces with passive boundary (the case where induced surface waves propagate). This radiation condition is fulfilled by an appropriate half-space Green's function. Indeed, we constructed an integral representation of the solution in terms of this Green's function and boundary data. These results can be directly extended to the elastic case for half-spaces with free boundary condition.

The half-space acoustic problem

We consider the half-space :

$$\mathbb{R}^n_+ := \{\mathbf{x} = (x_1, \ldots, x_n) \in \mathbb{R}^n : x_n > 0\},\ n = 2 \text{ or } 3.$$

Our first objective will be to set the correct mathematical formulation that allows only one outgoing solution for the problem :

$$\begin{cases} \Delta u + k^2\, u = 0 & \text{in} \quad \mathbb{R}^n_+, \\ -\dfrac{\partial u}{\partial \mathbf{n}} + zu = f & \text{on} \quad \{x_n = 0\}. \end{cases} \tag{1}$$

The given wave number k will be a positive constant. The impedance parameter $z > 0$ needs to be thought as $z = ik\beta$ for a given constant acoustic admittance β such that $\Re e(\beta) = 0$ and $\Im m(\beta) < 0$. Along this work, $\mathbf{n}$ will denote the outward unit normal vector field along the surfaces. In this first part, $\partial u/\partial \mathbf{n}$ becomes $-\partial u/\partial x_n$. For the scattering problem with passive boundary, the function f represents a source given by an incident wave u_i, i.e.

$$f = \frac{\partial u_i}{\partial \mathbf{n}} - zu_i. \tag{2}$$

In general, it will be sufficient to consider a piecewise continuous function f with compact support in $\mathbb{R}^{n-1}$.

It is well-known that in order to get the uniqueness of the solution of the problem (1), we need to specify the behaviour that we want for u in the far field. Hence, an outgoing wave condition needs to be imposed. As we can see in [4] or [5], a solution of (1) can be represented as a single layer potential by means of the boundary data f and a specific Green's function G. This fact implies that

the far field behaviour of this integral representation, has to be the same as that of its associated Green's function in the $\mathbf{x}$-variable. Having this in mind, the radiation condition for problem (1) will be extracted from an asymptotic study of G.

The half-space Green's function

We denote by δ the usual Dirac's delta distribution in $I\!R^n$. With a fixed source point $\mathbf{y} = (y_1, \ldots, y_n) \in I\!R^n_+$, our Green's function G will be a distribution satisfying the boundary value PDE :

$$\begin{cases} \Delta_{\mathbf{x}} G(\mathbf{x},\mathbf{y}) + k^2 G(\mathbf{x},\mathbf{y}) = \delta(\mathbf{x}-\mathbf{y}) \ \text{ in } I\!R^n_+, \\ \dfrac{\partial G}{\partial x_n} + zG = 0 \quad \text{over } \{x_n = 0\}. \end{cases} \tag{3}$$

Solving (3), we get the following representation of G as an inverse Fourier transform :

$$G(\mathbf{x},\mathbf{y}) = \frac{\pi}{(2\pi)^n} \int_{I\!R^{n-1}} \left(-\frac{e^{-\sqrt{\xi^2-k^2}\,|x_n-y_n|}}{\sqrt{\xi^2-k^2}} \right. \tag{4}$$
$$\left. + \frac{z+\sqrt{\xi^2-k^2}}{z-\sqrt{\xi^2-k^2}} \frac{e^{-\sqrt{\xi^2-k^2}\,(x_n+y_n)}}{\sqrt{\xi^2-k^2}} \right) e^{-i(\tilde{\mathbf{x}}-\tilde{\mathbf{y}})\cdot\xi} d\xi,$$

where $\xi = (\xi_i)_{i=1}^{n-1}$ is the Fourier variable, $\tilde{\mathbf{x}} = (x_i)_{i=1}^{n-1}$, $\tilde{\mathbf{y}} = (y_i)_{i=1}^{n-1}$ and $\xi^2 = \sum_{i=1}^{n-1} \xi_i^2$.

The radiation condition

Given $\alpha \in (0,1)$, we define the domains :

$$I\!R^n_+(\alpha+) := \left\{ \mathbf{x} \in I\!R^n_+ / x_n > r^\alpha \right\},$$
$$I\!R^n_+(\alpha-) := \left\{ \mathbf{x} \in I\!R^n_+ / 0 \le x_n < r^\alpha \right\},$$

where $r > 0$ denotes the euclidean norm of $\mathbf{x}$. The asymptotic analysis of the Green's function (4) shows two types of outgoing wave behaviour, each one with its own velocity. The wave behaviour associated with volume waves is dominant in regions like $I\!R^n_+(\alpha+)$, while the surface wave behaviour is dominant in regions like $I\!R^n_+(\alpha-)$. Summarising, for $n = 2$, we observe that the Green's function (4) satisfies the following radiation condition :

$$\begin{cases} \left| \dfrac{\partial u}{\partial r} - iku \right| < \dfrac{c}{r^{1-\alpha}} \quad \text{in } I\!R^2_+(\alpha+) \\ \\ \text{and} \\ \\ \left| \dfrac{\partial u}{\partial r} - i\sqrt{k^2+z^2}\, u \right| < \dfrac{c}{r^{1-\alpha}} \quad \text{in } I\!R^2_+(\alpha-), \\ \\ \text{when } r \to +\infty \text{ and for any } \alpha \in \left(0, \frac{1}{2}\right). \end{cases} \tag{5}$$

While for $n = 3$, Green's function (4) satisfies:

$$\begin{cases} \left| \dfrac{\partial u}{\partial r} - iku \right| < \dfrac{C}{r^{\left(2\alpha+\frac{1}{2}\right)}} \ \text{ in } I\!R^3_+(\alpha+) \\ \\ \text{and} \\ \\ \left| \dfrac{\partial u}{\partial r} - i\sqrt{k^2+z^2}\, u \right| < \dfrac{C}{r^{\left(\frac{3}{2}-\alpha\right)}} \ \text{ in } I\!R^3_+(\alpha-), \\ \\ \text{when } r \to +\infty \text{ and for any } \alpha \in \left(\frac{1}{4}, \frac{1}{2}\right). \end{cases} \tag{6}$$

In the articles [4] and [5] we prove that the only one solution satisfying the boundary value problem (1) and the radiation condition (5) or (6) (depending if n is two or three) has the representation :

$$u(\mathbf{x}) = \int_{I\!R^{n-1}} G\left(\mathbf{x}, (\tilde{\mathbf{y}}, 0)\right) f(\tilde{\mathbf{y}})\, d\tilde{\mathbf{y}}. \tag{7}$$

Moreover, the existence and uniqueness results can be extended to the case of locally perturbed half-spaces.

The half-space elastic problem

Consider an isotropic elastic media filling the whole half-space :

$$I\!R^3_+ := \{ \mathbf{x} = (x_1, x_2, x_3) \in I\!R^3 / x_2 > 0 \}. \tag{8}$$

We are interested to find in this domain, an outgoing solution of the time-harmonic elastic wave equation when the source is given by a local normal stress excitation at the surface :

$$\Gamma := \{ \mathbf{x} = (x_1, x_2, x_3) \in I\!R^3 / x_2 = 0 \}. \tag{9}$$

The problem can be written in the following way using vectorial notation: find a mechanical displacement field $\mathbf{u} : I\!R^3_+ \longrightarrow \mathbb{C}^3$, such that :

$$\begin{cases} \rho\omega^2 \mathbf{u} + \mu \Delta \mathbf{u} + (\lambda+\mu) \nabla(\ \text{div}\ \mathbf{u}) = \mathbf{0} \ \text{ in } I\!R^3_+ \\ \\ \sigma(\mathbf{u})\, \mathbf{n}^{\mathbf{t}} = \mathbf{f} \ \text{ on } \Gamma, \end{cases} \tag{10}$$

where σ is the stress tensor and $\mathbf{n} = (0, -1, 0)$ is the outwardly directed normal vector. The Lamé coefficients μ and λ are positive constants related to the characteristics of the elastic material, and so on the density ρ. The source function $\mathbf{f} = (f_1, f_2, f_3)$ must have compact support in Γ.

We remark that problem (10) is not well posed yet. In order to have an uniqueness result, we need to specify the behaviour that we want for $\mathbf{u}$ in the far field. An outgoing radiation condition needs to be imposed. Analogous to

the acoustic case, the information of the correct radiation condition will be obtained from an asymptotic study of the Green's function associated with problem (10).

Usually in linear elasticity theory, we can represent a solution $\mathbf{u}$ of the linear elastic equations as the sum :

$$\mathbf{u} = \mathbf{u}^{(P)} + \mathbf{u}^{(S)}, \tag{11}$$

where $\mathbf{u}^{(P)}$ is the vector field associated with pressure waves and $\mathbf{u}^{(S)}$ is the vector field associated with shearing waves. Each one of these two elastic waves propagates with its own velocity, so they have different wave numbers between them. These wave numbers are respectively :

$$k_P := \omega\sqrt{\frac{\rho}{\lambda+2\mu}} \quad \text{and} \quad k_S := \omega\sqrt{\frac{\rho}{\mu}}. \tag{12}$$

The expressions for $\mathbf{u}^{(P)}$ and $\mathbf{u}^{(S)}$ can be easily obtained using the projection formulae [6] :

$$\begin{cases} \mathbf{u}^{(P)} = \dfrac{1}{k_S^2 - k_P^2}(\Delta + k_S^2)\mathbf{u} \\ \text{and} \\ \mathbf{u}^{(S)} = \dfrac{1}{k_P^2 - k_S^2}(\Delta + k_P^2)\mathbf{u}\,. \end{cases} \tag{13}$$

Moreover, $\mathbf{u}^{(P)}$ and $\mathbf{u}^{(S)}$ satisfy the conditions :

$$\begin{cases} (\Delta + k_P^2)\mathbf{u}^{(P)} = 0, \quad \text{curl } \mathbf{u}^{(P)} = 0 \\ \text{and} \\ (\Delta + k_S^2)\mathbf{u}^{(S)} = 0, \quad \text{div } \mathbf{u}^{(S)} = 0. \end{cases} \tag{14}$$

Now, we can restrict ourselves to the Helmholtz analysis done for the acoustic problem. The idea is, once we have an expression for the Green's function matrix $G(\mathbf{x},\mathbf{y})$ associated with (10), we use the decomposition (11) and we analyse the asymptotic of each one of the components :

$$\begin{cases} G^{(P)}(\mathbf{x},\mathbf{y}) := \dfrac{1}{k_S^2 - k_P^2}(\Delta_{\mathbf{x}} + k_S^2)\, G(\mathbf{x},\mathbf{y}) \\ \text{and} \\ G^{(S)}(\mathbf{x},\mathbf{y}) := \dfrac{1}{k_P^2 - k_S^2}(\Delta_{\mathbf{x}} + k_P^2)\, G(\mathbf{x},\mathbf{y})\,, \end{cases} \tag{15}$$

as we did for the acoustic situation.

As we hoped, for each component in (15) we obtain two types of outgoing wave behaviour, each one with its own velocity. For $G^{(P)}$ we have observed an outgoing pressure wave behaviour associated with volume waves with wave number k_P, and an outgoing surface wave behaviour with a different wave number. Analogously, for $G^{(S)}$ we have observed an outgoing shearing wave behaviour associated with volume waves with wave number k_S, and an outgoing surface wave behaviour with a different wave number. Surprisingly, the wave number of the surface wave behaviour in both cases is the same, which means that the Rayleigh wave has both, shearing and pressure components, propagating at the same velocity.

As for the Helmholtz case, the wave behaviour associated with volume waves is dominant in regions like $\mathbb{R}^n_+(\alpha+)$, while the surface wave behaviour is dominant in regions like $\mathbb{R}^n_+(\alpha-)$.

Acknowledgements

The authors gratefully acknowledge the support of the project: *ACT30 ANILLO de Investigación del Programa Bicentenario en Ciencia y Tecnología de CONICYT/World Bank (Chile)*. Ignacio Muga wants to thank the support of *Pontificia Universidad Católica de Valparaíso* (Research Project #124.710/2007).

References

[1] T. Arens, "Uniqueness for Elastic Wave Scattering by Rough Surfaces", SIAM J. Math. Anal., 33 (2), pp. 461-476, 2001.

[2] S.N. Chandler-Wilde, "The Impedance Boundary Value Problem for the Helmholtz Equation in a Half-Plane", Math. Meth. Appl. Sci., vol. 20, pp. 813-840, 1997.

[3] S.N. Chandler-Wilde & Bo Zhang, "A Uniqueness Result for Scattering by Infinite Rough Surfaces", SIAM J. on Appl. Math., Vol. 58, No. 6 (Dec., 1998), pp. 1774-1790.

[4] M. Durán, I. Muga & J.-C. Nédélec, "The Helmholtz Equation in a Locally Perturbed Half-Plane with Passive Boundary", IMA J. of Appl. Math., 71 (6), pp. 853-876, 2006.

[5] M. Durán, I. Muga & J.-C. Nédélec, "The Helmholtz Equation with Impedance in a Half-Space" C. R. Acad. Sci. Paris, Ser. I 341 (9), pp. 561-566, 2005.

[6] V.D. Kupradze, Three-Dimensional Problems of the Mathematical Theory of Elasticity and Thermoelasticity, North-Holland Series in Applied Mathematics and Mechanics, Vol. 25, 1979.

THE MULTI-SECTION METHOD: WHY RECTANGLES ARE SOMETIMES BETTER THAN SQUARES.

E. Heinemeyer[†], **M. Lindner**[*], **R. Potthast**[*]
[†] Institut für Numerische und Angewandte Mathematik, Universität Göttingen, Göttingen, Germany
[*] Department of Mathematics, University of Reading, Reading, UK

Abstract

We introduce a novel method, the so-called *multi-section method*, for the approximate solution of integral equations on unbounded domains and other operator equations in similar settings. The idea is to truncate the operator to a finite domain, as is usually done with the so-called *finite section method*, but in a slightly different way that was designed to overcome difficulties one sometimes runs into when applying the finite section method.

Introduction

Let A be a bounded and linear operator on a function space over a (discrete or continuous) unbounded domain. For simplicity, let us restrict ourselves to the one-dimensional domains $\mathbb{Z}$ and $\mathbb{R}$ here, although this is not required by the method. The function spaces we are talking about are, for example, spaces of the form $E = \ell^p(\mathbb{Z})$ or $E = L^p(\mathbb{R})$, respectively, and A acts boundedly on E. In the discrete case, we can think of A as a two-sided infinite matrix $(a_{ij})_{i,j\in\mathbb{Z}}$. In the L^p case we will take integral operators

$$(Au)(x) \;=\; \int_{\mathbb{R}} k(x,y)\,u(y)\,dy, \qquad y \in \mathbb{R}$$

as our model case, where $k(\cdot,\cdot)$ is a suitable function on $\mathbb{R}\times\mathbb{R}$.

Finite Section Method. Suppose we know that the operator $A : E \to E$ is invertible. Then the equation

$$Au \;=\; b \tag{1}$$

has a unique solution $u \in E$ for every given right-hand side $b \in E$. How do we find u? What's usually done is to take a large (whatever that means) positive number r, truncate the right-hand side b to the interval $[-r,r]$ and look for a function $\tilde{u}_r$ that also is only supported in $[-r,r]$ and solves the following truncated version of (1):

$$P_rAP_r\,\tilde{u} \;=\; P_rb, \tag{2}$$

where P_r is the operator that takes an element of E and zeros all its values outside $[-r,r]$.

We say that the finite section method is *applicable* if the unique solvability of (1) implies that of (2) for all large r, and if the unique solution $\tilde{u}$ of (2) tends to the unique solution u of (1) in an appropriate sense as $r\to\infty$. If this is the case, then we can take a large $r>0$ and solve equation (2) on the computer (possibly after a suitable discretization, if we are in the case $E = L^p(\mathbb{R})$). Here we will not worry about this discretization step but only about the truncation step that brings us from (1) to (2).

Essentially, what is happening as we pass from (1) to (2) is that, for the discrete case, we replace the infinite matrix $(a_{ij})_{i,j\in\mathbb{Z}}$ by the finite quadratic section $(a_{ij})_{i,j\in\{-r,\dots,r\}}$ – hence the name 'finite section method'. For the integral operator in the L^p case, something very similar happens: The kernel function $k(\cdot,\cdot)$ is truncated from $\mathbb{R}\times\mathbb{R}$ to the finite square $[-r,r]\times[-r,r]$.

There are sufficient and necessary criteria [5], [6], [1], [3], [4] for when the finite section method is applicable to a given operator A. These criteria involve calculations of local representatives (so-called limit operators) of A and they also need A to be in a suitable class of operators.

Multi-Section Method. It is not surprising that, in general, the finite section method fails to be applicable, as already very simple examples like the shift operator $(Au)(x) = u(x-1)$ demonstrate. In this example, the truncated operator P_rAP_r is never invertible on its corresponding subspace of E, which is why (2) is never uniquely solvable, however large r is chosen.

In [2], the authors suggested a modified version of the finite section method. We make the reasonable assumption that, for every fixed $r>0$,

$$\|(I-P_R)AP_r\| \;\to\; 0 \quad \text{as} \quad R\to\infty, \tag{3}$$

which, by the way, is much weaker than the assumptions made on A in the theorems about the finite section method. This implies that $AP_r\tilde{u}$ is well-approximated by $P_RAP_r\tilde{u}$ if $R \ge r > 0$ are chosen accordingly. We now replace the left-hand side of (2) by $P_RAP_r\tilde{u}$ and the right-hand side by P_Rb to get

$$P_RAP_r\,\tilde{u} \;=\; P_Rb. \tag{4}$$

In the sense as discussed above, (4) corresponds to a linear system with rectangular matrix $(a_{ij})_{i\in\{-R,R\},j\in\{-r,r\}}$ or an integral equation with kernel function $k(\cdot,\cdot)$ on

$[-R,R] \times [-r,r]$. Because of this generally overdetermined nature, it is not sensible to expect that (4) even has solutions. We therefore, roughly speaking, replace the ' $=$' sign by a ' $\approx$' sign. Precisely, for a given precision $\delta > 0$ and sufficiently large cut-off parameters $r, R > 0$, we are looking for solutions $\tilde{u} \in E$ of

$$\|P_R A P_r \, \tilde{u} \; - \; P_R b\| \; < \; \delta. \tag{5}$$

Without loss of generality, we can suppose that $\tilde{u}$ is supported in $[-r,r]$ only. This is what we call the multisection method.

Results

Let E be a function space as described, where $P_r \to I$ pointwise as $r \to \infty$, and let $A : E \to E$ be bounded, linear, invertible, and subject to (3).

- For every precision $\delta > 0$, there is a $r_0 > 0$ such that (5) is solvable for all $R \geq r > r_0$.
- For every $\varepsilon > 0$, there are parameters $\delta, r, R > 0$ such that every solution $\tilde{u}$ of (5) is a norm approximation

  $$\|\tilde{u} \; - \; u\|_E \; < \; \varepsilon$$

  to the unique solution u of the original problem (1).

In [2], we have successfully used this method to numerically solve the Brakhage-Werner integral equation corresponding to a 3D rough surface acoustic scattering problem.

Questions

1. Under which additional conditions on A can we choose $r = R$ (i.e. work with approximate solutions $\tilde{u}$ of the *finite* section method (2)) and still have the above results?

2. We are still experimenting with the optimal coupling of the two cut-off parameters. For example, depending on the operator A, is it better to keep the ratio R/r or the difference $R-r$ fixed as both R and r go to infinity?

References

[1] S. N. CHANDLER-WILDE and M. LINDNER: Boundary integral equations on unbounded rough surfaces: Fredholmness and the Finite Section Method, accepted at *J. Integral Eq. and Appl.*, 2006.

[2] E. HEINEMEYER, M. LINDNER and R. POTTHAST: Convergence and numerics of a multisection method for scattering by three-dimensional rough surfaces, (preprint: *Numerical Analysis Report 12/2006, University of Reading*), accepted at *SIAM J. Numerical Analysis*, 2007.

[3] M. LINDNER: The Finite Section Method in the Space of Essentially Bounded Functions: An Approach Using Limit Operators., *Numerical Functional Analysis and Optimization* **24** (2003), no. 7&8, 863–893.

[4] M. LINDNER: *Infinite Matrices and their Finite Sections: An Introduction to the Limit Operator Method*, Frontiers in Mathematics, Birkhäuser 2006.

[5] V. S. RABINOVICH, S. ROCH and B. SILBERMANN: *Limit Operators and Their Applications in Operator Theory*, Birkhäuser 2004.

[6] S. ROCH: Finite sections of band-dominated operators, *Preprint Nr. 2355, Technical University Darmstadt*, 2004 (to appear in *Memoirs AMS*, 2006).

Fast evaluation of potentials and potential-operators arising from 3D acoustic rough surface scattering problems

E. Heinemeyer[†,*], **R. Potthast**[‡], **S.N. Chandler-Wilde**[‡]

[†]Institute for Numerical and Applied Mathematics, Georg-August University of Göttingen, Germany
[‡]University of Reading, Department of Mathematics, Whiteknights, PO Box 220, Berkshire, RG6 6AX, UK
[*]Email: heinemey@math.uni-goettingen.de

Abstract

We present a new method for the fast evaluation of boundary layer potential operators arising in 3D rough surface scattering problems. The main ingredients are the use of high order approximations for the Dirac delta distribution to encode the information on the scattering surface and the use of FFT methods to compute the corresponding potential inside a box containing the surface patch of interest.

Introduction

Rough surface scattering problems arise in applications for acoustic and electromagnetic waves and there is an increasing interest in simulations ranging from outdoor sound propagation, optical scattering in nano-technology to remote sensing of ocean and soil. The simulation is a challenging problem in scientific computing. From a computational point of view the main difficulties are the need to discretise very large surface patches, very often of the size of several hundred wavelength. As a rule of thumb one should use at least 5 discretisation points per wavelength. Using boundary integral equation methods and Nyström discretisation techniques a dense unstructured linear system for several hundred-thousands of unknowns has to be solved. Thus the use of direct solvers is prohibitive on standard desktop machines with up to 4 GB RAM. Instead the method of choice will be to employ some iterative solver like the GMRES. In this case the limiting factor is not the computers memory but the computation time needed for one matrix vector multiplication. It is therefore inevitable to have a fast matrix vector multiplication that reduces the overall cost from a standard $O(N^2)$ algorithm where N denotes the total number of unknowns.

The integral equation formulation

In [1] the authors treat the case of a two-dimensional sound soft rough surface Γ and analysed the scattering of an incident wave that was due to a point source situated above the scatterer, see Figure 1. They derived the following integral equation

$$\varphi(x) + \int_\Gamma K(x,y)\varphi(y)\, ds(y) = g(x), \quad x \in \Gamma, \quad (1)$$

in the case where the scatterer is the simplest example of a rough surface, namely it is given as graph of a bounded continuous function $f : \mathbb{R}^2 \to \mathbb{R}$, i.e. $\Gamma := \{(\boldsymbol{x}, f(\boldsymbol{x})) \in \mathbb{R}^3 : \boldsymbol{x} := (x_1, x_2) \in \mathbb{R}^2\}$. The kernel in (1) is given by $K(x,y) := 2\frac{\partial G(x,y)}{\partial \nu(y)} - i\eta 2G(x,y)$ where $G(x,y) := \Phi(x,y) - \Phi(x,y')$ denotes the Dirichlet Greens function for the half-space and $\Phi(x,y) := \frac{e^{i\kappa|x-y|}}{4\pi|x-y|}, x \neq y$ the free space Greens function to the Helmholtz equation in $\mathbb{R}^3$. Throughout this text we denote the reflection of a point $z = (z_1, z_2, z_3) \in \mathbb{R}^3$ onto the plane $\Gamma_0 := \{x \in \mathbb{R}^3 : x_3 = 0\}$ by $z' := (z_1, z_2 - z_3)$. We further define the perturbed half-space $D := \{x = (\boldsymbol{x}, x_3) : x_3 > f(\boldsymbol{x})\}$ above the scatterer Γ and the *combined double- and single-layer potential*

$$V(x) := \frac{1}{2}\int_\Gamma K(x,y)\varphi(y)\, ds(y), \quad x \in D. \quad (2)$$

It can be shown that for a given incident field $u^i = \Phi(\cdot, z), z \in D$, the scattered field can be represented as

$$u^s(x) = V(x) - \Phi(x, z'), \quad x \in D, \quad (3)$$

where φ solves (1) for right hand side $-2G(\cdot, z)$, see [1] and [2] for more details.

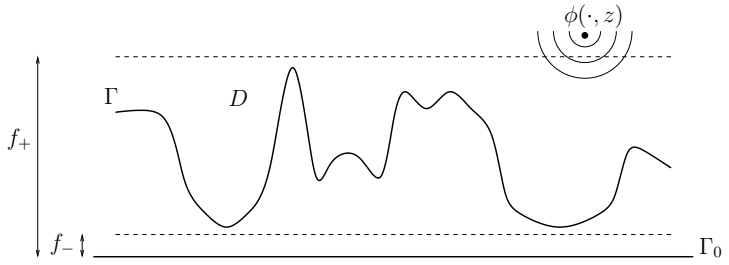

Figure 1: Geometrical setting of the scattering problem.

Finite-Section methods

To get an approximate solution to (1) we apply a *finite section method*, i.e. we replace the unbounded scattering surface Γ by some finite section $\Gamma_R := \{(\boldsymbol{x}, f(\boldsymbol{x})) :$

$\boldsymbol{x} \in R\}$, where $R := [a_1, b_1] \times [a_2, b_2]^2 \subset \mathbb{R}^2$ denotes the supporting rectangle of the surface patch Γ_R. Using the parametrisation of Γ as introduced above and setting $\psi(\boldsymbol{x}) := \varphi(\boldsymbol{x}, f(\boldsymbol{x}))$ and $\tilde{g}(\boldsymbol{x}) := g(\boldsymbol{x}, f(\boldsymbol{x})), \boldsymbol{x} \in R$, we have to find an approximate solution to the truncated integral equation

$$(I + W)\psi = \tilde{g} \quad \text{on } R, \tag{4}$$

where W is the integral operator

$$(W\psi)(\boldsymbol{x}) := \int_R K(\boldsymbol{x}, \boldsymbol{y}) J(\boldsymbol{y}) \psi(\boldsymbol{y})\, d\boldsymbol{y}, \quad \boldsymbol{x} \in R,$$

with kernel $K(\boldsymbol{x}, \boldsymbol{y}) := 2(\partial G(x, y)/\partial \nu(y) - i\eta G(x, y))$ for $x = (\boldsymbol{x}, f(\boldsymbol{x})),\ y = (\boldsymbol{y}, f(\boldsymbol{y}))$. The function $J(\boldsymbol{y}) = \sqrt{1 + \|\nabla f(\boldsymbol{y})\|^2}$ denotes the surface area element.

We note that up to now it is not known whether this truncated equation is solvable. Despite this gap in the theory we discretise the equation by applying a Nyström method to get some approximate solution to the truncated equation. An actual implementation shows a stable and numerically well posed system and therefore empirically justifies this step. At the moment more research is done to close this gap. A promising new scheme is a generalisation of the finite section method in what has been titled *multi-section method* see [3]. Within this framework one can show the existence of a minimum norm least square solution that approximates the solution to the untruncated equation arbitrary well.

Nyström discretisation

Due to the weak singularity of the integral kernel we can not apply the Nyström discretisation immediately. Hence we split the kernel into a regular smooth part and a weakly singular part. The idea is to discretise the regular part by a standard quadrature and to use some local spectral scheme for the singular part.

We introduce a smooth cut-off function $\chi : \mathbb{R} \to [0, 1]$ for a fixed positive real parameter R_{cut} such that $\chi(r) = 1$ for $|r| \leq R_{\text{cut}}/2$ and $\chi(r) = 0$ for $|r| \geq R_{\text{cut}}$. Thus we can write $K(\boldsymbol{x}, \boldsymbol{y}) = K_1(\boldsymbol{x}, \boldsymbol{y}) + K_2(\boldsymbol{x}, \boldsymbol{y})$ with $K_1(\boldsymbol{x}, \boldsymbol{y}) := K_{\text{reg}}(\boldsymbol{x}, \boldsymbol{y}) + (1 - \chi(|\boldsymbol{x} - \boldsymbol{y}|))K_{\text{sing}}(\boldsymbol{x}, \boldsymbol{y})$ and $K_2(\boldsymbol{x}, \boldsymbol{y}) := \chi(|\boldsymbol{x} - \boldsymbol{y}|)K_{\text{sing}}(\boldsymbol{x}, \boldsymbol{y})$. To obtain a discrete representation of the operator W we replace the integral by the trapezoidal rule, i.e.

$$(W\psi)(\boldsymbol{x}) \approx h^2 \sum_{j \in I} K_1(\boldsymbol{x}, \boldsymbol{x}_j) J(\boldsymbol{x}_j) \psi(\boldsymbol{x}_j) + \sum_{j \in I} \beta_j(\boldsymbol{x}) \psi(\boldsymbol{x}_j), \quad \boldsymbol{x} \in R,$$

where $\{\boldsymbol{x}_j = (hx_{j_1}, hx_{j_2}) \in R : j \in I \subset \mathbb{Z}^2\}$ denotes an equidistantly spaced grid of integration points in R with stepsize h and $\beta_j(\boldsymbol{x})$ denotes the weights for the high order local spectral scheme that have to be determined by numerical integration. So we approximate the solution of equation (4) by the solution of the equation

$$\psi(\boldsymbol{x}) + \sum_{j \in I} [h^2 K(\boldsymbol{x}, \boldsymbol{x}_j) J(\boldsymbol{x}_j) + \beta_j(\boldsymbol{x})] \psi(\boldsymbol{x}_j) = \tilde{g}(\boldsymbol{x}),$$

$\boldsymbol{x} \in R$, which reduces to solve the finite-dimensional system

$$\psi(\boldsymbol{x}_i) + \sum_{j \in I} [h^2 K(\boldsymbol{x}_i, \boldsymbol{x}_j) J(\boldsymbol{x}_j) + \beta_j(\boldsymbol{x}_i)] \psi(\boldsymbol{x}_j) = \tilde{g}(\boldsymbol{x}_i),$$

$i \in I$. Please note that the function $\beta(\boldsymbol{x})$ has support in $B(\boldsymbol{x}, R_{\text{cut}}) := \{\boldsymbol{y} \in R : |\boldsymbol{x} - \boldsymbol{y}| \leq R_{\text{cut}}\}$, thus the singular part is represented by a sparse matrix with $O(N)$ nonzero entries with band structure. For this type of matrix the matrix vector multiplication can be done with $O(N)$ operations.

Fast matrix vector product

The prototype of the operators we are interested in can be written as

$$(A\psi)(\boldsymbol{x}) = \int_R k((\boldsymbol{x}, f(\boldsymbol{x})) - (\boldsymbol{y}, f(\boldsymbol{y})))\psi(\boldsymbol{y}) J(\boldsymbol{y}) d\boldsymbol{y} \tag{5}$$

for $\boldsymbol{x}$ in R, with a smooth kernel of difference type.

For such an operator we introduce the associated *box potential*. For this purpose let a_3 and b_3 be real constants such that $a_3 < f(\boldsymbol{x}) < b_3$ for all $\boldsymbol{x} \in R$. Then we denote by Q the cube $R \times T := R \times [a_3, b_3] \subset \mathbb{R}^3$ that contains the surface patch Γ_R with supporting rectangle R. The associated box potential to the integral operator is given through

$$(\mathcal{A}\psi)(x) = \int_R k(x - (\boldsymbol{y}, f(\boldsymbol{y})))\psi(\boldsymbol{y}) J(\boldsymbol{y}) d\boldsymbol{y}$$

for x in Q and defines a smooth function in Q. Thus we have the relation

$$(\mathcal{A}\psi)(\boldsymbol{x}, f(\boldsymbol{x})) = (A\psi)(\boldsymbol{x}), \quad \boldsymbol{x} \in R. \tag{6}$$

The main idea of our method is the following:

Step 1: We write the box potential as a convolution of the smooth difference kernel with a weighted approximation of a Dirac delta distribution. The delta distribution encodes the information on the scattering surface. Now we approximate the box potential on a regular spaced grid

in Q. This can be done by the use of the FFT. So we have a fast method to compute the left hand side of (6) on a regular grid in Q.

Step 2: The approximation to the delta distribution are chosen in a way, to yield high order interpolation operators when discretised. Thus we can transfer the information from the regular grid in Q to the correct surface points on the discretised boundary Γ. This yields an approximation to the discretised right hand side of (6).

Step 1

We define a weighted Dirac delta sequence $\psi_{h_3} : Q \to \mathbb{C}, (\boldsymbol{y}, y_3) \mapsto \psi(\boldsymbol{y})J(\boldsymbol{y})\delta_{h_3}(f(\boldsymbol{y}) - y_3)$. Thus we get an approximation to the box potential that we can write

$$\begin{aligned}(\mathcal{A}\psi_{h_3})(x) &\approx \int_R \int_T k(x - (\boldsymbol{y}, y_3))\psi_{h_3}(\boldsymbol{y}, y_3)\, dy_3\, d\boldsymbol{y} \\ &= \int_Q k(x - y)\psi_{h_3}(y)\, dy. \end{aligned} \tag{7}$$

In order to regard (7) as a convolution the kernel and the density must have the same domain of definition. Without loss of generality we can restrict ourselves to the case that $Q = \times_{j=1}^3 [0, b_j - a_j]$. The kernel is defined on the cube $\times_{j=1}^3 [-(b_j - a_j), b_j - a_j]$ and has a uniquely determined periodic extension onto $\mathbb{R}^3$ that we denote by k_p. Thus we extend ψ_{h_3} by zero onto $Q^* := \times_{j=1}^3 [0, 2(b_j - a_j)] \subset \mathbb{R}^3$, i.e. we define

$$\Psi_{h_3} : Q^* \to \mathbb{C} : x \mapsto \begin{cases} \psi_{h_3}(x), & x \in Q, \\ 0, & x \in Q^* \setminus Q. \end{cases}$$

The periodic extension of Ψ_{h_3} to a periodic function onto $\mathbb{R}^3$ is denoted by $\Psi_{h_3,p}$. Now we see that we can rewrite (7) as

$$\begin{aligned}(\mathcal{A}\psi_{h_3})(x) &\approx (k_p * \Psi_{h_3,p})(x) \\ &= |Q^*|\, \mathcal{F}_3^{-1}(\mathcal{F}_3(k_p) \cdot \mathcal{F}_3(\Psi_{h_3,p}))(x)\end{aligned}$$

for $x \in Q$. Let $\{x_{j,l} := (\boldsymbol{x}_j, x_l) : x_l = h_3 l, j \in I, l = 1, \ldots, M\}$ denote a regular spaced grid in Q with M levels. Then we can calculate $(\mathcal{A}\psi_{h_3})(x_{j,l})$ efficiently with 3 three-dimensional FFT's in $O(3 \cdot 8NM \log(8NM))$ operations.

Step 2

Once we know the box potential on the regular grid we get an approximation to our desired matrix vector multiplication through

$$\begin{aligned}(A\psi)(\boldsymbol{x}_j) &\approx (A\psi_{h_3})(\boldsymbol{x}_j) \\ &= (\mathcal{A}\psi_{h_3})(\boldsymbol{x}, f(\boldsymbol{x}_j)) \\ &\approx \sum_{l=1}^{M} h_3 (\mathcal{A}\psi_h)(\boldsymbol{x}_j, x_l)\delta_h(f(\boldsymbol{x}_j) - x_l).\end{aligned}$$

This can be done in $O(NM)$ operations.

On the choice of δ_h

The regularised versions of the Dirac delta distribution are based on the following Lemma, see [4].

Lemma 1. *Assume that $f \in C^p([\alpha - Lh, \alpha + Lh])$. If δ_h satisfies $\delta_h(x) = 0$ for $|x| > Lh$ and the* discrete moment condition

$$h \sum_l (x_l - \alpha)^m \delta_h(x_l - \alpha) = \delta_{m,0} \tag{8}$$

for $m = 0, \ldots, p - 1$, then

$$f(\alpha) - h \sum_l f(x_l)\delta_h(x_l - \alpha) = O(h^p), \quad h \to 0.$$

First numerical computations show the expected rate of convergence. About 20 levels with an eight order approximation yield a relative L2 error of about 10^{-4}.

References

[1] S. N. Chandler-Wilde, E. Heinemeyer and R. Potthast, *Acoustic scattering by mildly rough unbounded surfaces in three dimensions*, SIAM J. Appl. Math., Vol. 66 (3), pp. 1002-1026, 2006.

[2] S. N. Chandler-Wilde, E. Heinemeyer and R. Potthast, *A well-posed integral equation formulation for three-dimensional rough surface scattering*, Proc. R. Soc. A, Vol. 462, pp. 3683-3705, 2006.

[3] E. Heinemeyer, M. Lindner and R. Potthast, *Convergence and numerics of a multi-section method for scattering by three-dimensional rough surfaces*, SIAM Journal on Numerical Analysis, submitted 2007

[4] R.P. Beyer and R.J. Leveque, *Analysis of a One-Dimensional Model for the Immersed Boundary Method*, SIAM Journal on Numerical Analysis, Vol. 29, No.2 ,pp. 332-364, 1992

SUITABLE SPACES FOR THE DIRICHLET-TO-NEUMANN AND CALDERÓN OPERATORS ON AN INFINITE FLAT SURFACE

S. Ritterbusch
Institut für Algebra und Geometrie,
Universität Karlsruhe, Germany
Email: ritterbusch@math.uni-karlsruhe.de

Abstract

The Calderón Operator and the Neumann-to-Dirichlet Mapping on an infinite plane expose singular behavior in a setup of a two-layered space with both an non-dissipative and a dissipative medium. The mapping properties of both operators are characterized by weighted Sobolev Spaces based on an extended class of generalized functions.

Introduction

To solve the time harmonic Maxwell System in 3D for a bounded scatterer in homogeneous space via finite element methods, [2] proposed to transform the problem to a bounded domain with non-local boundary conditions using the exterior Calderón operator. In the setup of a two layered medium, as thoroughly discussed in [1], we explore the feasibility of using the interface between the half-spaces as a natural, albeit unbounded, choice of the boundary for the Calderón operator, when the lower half-space is dissipative.

Setup

The considered geometry is a two-layered space, where the upper half-space is an homogeneous non-dissipative medium, the lower half-space an homogeneous dissipative medium around an impenetrable obstacle. As in [1], we consider a Silver-Müller radiation condition in the upper half-space. This setup can be seen as a model for air and an metallic object within the soil. The proposed Ansatz reduces the problem to a scattering problem in the lower half-space, which is feasible in traditional fractional Sobolev spaces for TE and TM modes, but the extension to full Maxwell's equations is unclear and needs careful analysis.

Procedure

In the situation of a domain $\Omega \subset \mathbb{R}^3$ with sufficiently smooth boundary $\partial\Omega$, we have the following well known function spaces, cf. [3]:

Definition 1

$$H^s(\mathrm{Div};\partial\Omega) := \Big\{ u \in \big(H^s(\partial\Omega)\big)^3 : u\cdot\hat{x} \overset{a.e.}{=} 0 \text{ and } \mathrm{Div}_{\partial\Omega} u \in H^s(\partial\Omega) \Big\}$$

Where $\mathrm{Div}_{\partial\Omega}$ *denotes the surface divergence at* $\partial\Omega$*,* $\hat{x}$ *the normal vector at* $\partial\Omega$ *and* H^s *Sobolev-spaces for* $s \in \mathbb{R}$*.*

Then, the E to H Calderón operator G_e for a bounded domain Ω has the following known properties:

Lemma 2 *The Calderón operator is linear and bounded*

$$\begin{aligned} G_e :\ H^{-1/2}(\mathrm{Div};\partial\Omega) &\to H^{-1/2}(\mathrm{Div};\partial\Omega) \\ \lambda &\mapsto \hat{x}\times H_{|\partial\Omega}\,, \end{aligned}$$

where $\lambda = \hat{x}\times E_{|\partial\Omega}$ *and* H *is the* H*-Field of the unique* (E,H) *solution of the outer time harmonic Maxwell system in* $\mathbb{R}^3\backslash\overline{\Omega}$ *with tangential boundary data* $\hat{x}\times E$ *at* $\partial\Omega$ *and a radiation condition.*

In the regarded geometry $\Omega = \mathbb{R}^2\times(-\infty,0)$ with the infinite boundary plane $\partial\Omega = \mathbb{R}^2\times\{0\}$, we consider the following explicit representation for the Calderón operator for radiating solutions of upper half space problems:

Lemma 3 *Assume a radiating solution* (E,H) *of the time harmonic Maxwell system in the half space* $\mathbb{R}^2\times(0,\infty)$*. Then* $G_e\lambda = \hat{x}\times H_{|\partial\Omega}$ *for* $\lambda = \hat{x}\times E_{|\partial\Omega}$ *and*

$$G_e := \frac{1}{\omega\mu}\,\mathcal{F}_{\partial\Omega}^{-1}\,M_k\,\mathcal{F}_{\partial\Omega}$$

with Fourier multiplier

$$M_k := \frac{1}{\sqrt{k^2-|\xi|^2}}\begin{pmatrix} \xi_1\xi_2 & -k^2+\xi_2^2 \\ k^2-\xi_1^2 & -\xi_1\xi_2 \end{pmatrix},$$

where $\mathcal{F}_{\partial\Omega}$ *denotes the two dimensional Fourier transform at* $\partial\Omega$ *with spectral variables* ξ_1,ξ_2 *and constant wave number* $k>0$ *in the upper half space.*

Here, the operator G_e exhibits singular spectral properties at frequencies around $|\xi| = k$, thus the precise mapping properties are yet unclear. Reduction of the problem to the TE or the TM mode leads to two dimensional problems with a Dirichlet-to-Neumann operator on a one dimensional boundary. This operator or, more specifically, its inverse– the Neumann-to-Dirichlet operator, exposes similar singular spectral properties:

Lemma 4 *The Dirichlet-to-Neumann mapping for $k > 0$*

$$\begin{aligned} \Lambda : H^s(\mathbb{R}) &\to H^{s-1}(\mathbb{R}) \\ \lambda &\mapsto i\,\mathcal{F}^{-1}\,D_k\,\mathcal{F}\,\lambda \end{aligned}$$

with Fourier transform $\mathcal{F}$ and multiplier

$$D_k = \begin{cases} \sqrt{k^2-\xi^2} & \text{for} \quad |k| \le |\xi| \\ i\sqrt{\xi^2-k^2} & \text{for} \quad |k| > |\xi| \end{cases}$$

is a bounded linear operator, but is not surjective.

The inverse Neumann-to-Dirichlet operator is characterized by the reciprocal Fourier multiplier, by which it is only defined on the image of Λ. For $s < 1$, the image set is embedded in the concept of generalized functions which are solely defined by their test function spaces. It turns out that then even here, the definition of the image space of Λ is improper if the test function space remains unchanged.

In relation to the structure of the Neumann-to-Dirichlet operator, an adapted space of rapidly decreasing Schwartz test functions is introduced, leading to an enlarged dual space of generalized functions:

Definition 5 *For $k > 0$ and $\varrho_k(\xi) := \left|k^2 - |\xi|^2\right|^{-1/2}$, let*

$$\begin{aligned} S_k(\mathbb{R}) &:= \{u \in S(\mathbb{R}) :\ \varrho_k\,\mathcal{F}\,u \in S(\mathbb{R})\}\,, \\ S_k^*(\mathbb{R}) &:= \{\varphi : S_k(\mathbb{R}) \to \mathbb{C} :\ \varphi \textit{ linear and bounded}\}\,, \end{aligned}$$

where $S(\mathbb{R})$ represents the Schwartz space of rapidly decreasing functions.

Theorem 6 *For $s \in \mathbb{R}$ and $k > 0$, the Bessel k-Potential*

$$\begin{aligned} \mathcal{J}_k^s &:= \mathcal{F}^{-1}\,\psi_{s,k}\,\mathcal{F}\,, \\ \psi_{s,k} &:= \frac{\left(1+|\xi|^2\right)^{\frac{s+1}{2}}}{|k^2-|\xi|^2|^{1/2}} \end{aligned}$$

is invertible bounded linear map $S_k(\mathbb{R}) \to S_k(\mathbb{R})$.

Based on these structures on $\mathbb{R}$ and on higher dimensions, wave-number dependent weighted Sobolev spaces of fractional order on $\mathbb{R}$ and $\mathbb{R}^n$ are introduced:

Definition 7 *For $s \in \mathbb{R}$, $k > 0$ and $n \in \mathbb{N}$, let*

$$H_k^s(\mathbb{R}^n) := \{\varphi \in S_k^*(\mathbb{R}^n) :\ \mathcal{J}_k^s\,\varphi \in L^2(\mathbb{R}^n)\}\,.$$

Results

The traditional fractional order Sobolev spaces commonly used at bounded interfaces will be shown to be inadequate. Besides some additional properties, the introduced test function spaces, generalized function spaces and weighted Sobolev spaces are found to be well-defined and complete, the weighted Sobolev-spaces are embedded in the usual Sobolev-spaces.

The new Sobolev spaces accurately characterize the image of the Dirichlet-to-Neumann operator as desired, and are well suited for the Neumann-to-Dirichlet operator:

Lemma 8 *The Dirichlet-to-Neumann operator is a linear and bounded mapping $\Lambda : H^s(\mathbb{R}) \to H_k^{s-1}(\mathbb{R})$ with bounded inverse.*

Finally, the mapping properties of the Calderón boundary operator at an infinite plane for the full 3D Maxwell's equations based on above functions spaces are stated:

Theorem 9 *The E to H Calderón operator G_e is a linear bounded mapping*

$$G_e :\ H_k^s(\mathrm{Div};\mathbb{R}^2) \to H_k^s(\mathrm{Div};\mathbb{R}^2)\,,$$

where

$$\begin{aligned} H_k^s(\mathrm{Div};\mathbb{R}^2) &:= \{u \in \left(H^s(\mathbb{R}^2)\right)^2 :\ \mathrm{Div}\,u \in H^s(\mathbb{R}^2)\,, \\ &\qquad \mathrm{Curl}\,u \in H_k^{s-1}(\mathbb{R}^2)\} \end{aligned}$$

and Curl *represents the surface curl on the interface.*

A suitable decomposition of the Calderón operator will illustrate its strong relation to the above Dirichlet-to-Neumann and Neumann-to-Dirichlet mappings.

References

[1] P.-M. Cutzach and C. Hazard: Existence, uniqueness and analyticity properties for electromagnetic scattering in a two-layered medium, Math. Meth. Appl. Sci. **21** (1998), 433-461

[2] A. Kirsch and P. Monk: A finite element/spectral method for approximating the time harmonic Maxwell system in $\mathbb{R}^3$, SIAM J. Appl. Math., **55** (1995), 1324-1344.

[3] P. Monk: Finite Element Methods for Maxwell's Equations. Oxford Science, 2003.

Integral Equation Methods

CONVERGENCE OF KRYLOV SUBSPACE SOLVERS FOR FINITE ELEMENTS-INTEGRAL REPRESENTATION COUPLING

F. Ben Belgacem [†], **N. Gmati**[‡,*], **F. Jelassi** [⋆,‡], **B. Philippe** [⋆⋆]
[†]UTC/LMAC, Centre de Recherches de Royallieu, BP 20 529, 60 205 Compiègne cedex, FRANCE.
[‡]LAMSIN/ENIT, BP 37, Le belvédère 1002 Tunis, TUNISIE
[⋆]FSB, Jarzouna 7021, Bizerte, TUNISIE.
[⋆⋆]IRISA/INRIA-Rennes Campus de Beaulieu, 35042 Rennes cedex, France FRANCE
[*] Email: nabil.gmati@ipein.rnu.tn

Abstract

The method coupling finite elements and integral representation (cf.[4]) allows to solve exterior problems, thanks to an exact boundary condition on a fictitious boundary, which delimitate the computational domain. This boundary condition is non local, the associated algebraic system is then not sparse and ill-conditioned. We study the convergence of an iterative method based on a Krylov subspace method to solve the Steklov-Poincaré interface equation. We prove the convergence of the algorithm, and we compare it to the resolution of the initial algebraic system, where the Schwarz algorithm is used as a preconditioner.

Coupling finite elements and integral representation

Let Ω_i be a bounded obstacle (in R^3) with a regular boundary Γ and Ω_e be its unbounded complementary. The Helmholtz problem is a fair modeling of a scattered acoustic wave propagating through Ω_e; it consists in *finding u such that*

$$\Delta u + \kappa^2 u = 0 \text{ in } \Omega_e, \qquad \partial_n u = f \text{ on } \Gamma, \quad (1)$$

$$(\frac{x}{|x|}.\nabla - i\kappa)u = e^{i\kappa|x|}O(\frac{1}{|x|^2}) \qquad \|x\| \to \infty, \quad (2)$$

where κ is the wave number. The last condition represents the Sommerfeld radiation condition. To make the boundary value problem (1)-(2) accessible to scientific computing, we may resort to the integral equation method (eventually coupled to finite element method for nonconstant coefficients). The efficicency of these methods has been investigated by several authors (cf.[6], [3]). An alternative consists in using a coupled method which combines finite elements and integral representations (cf.[4]). This approach avoids the singularities of the Green kernel. The idea simply amounts to introducing a fictitious boundary Σ surrounding the obstacle. The Helmholtz problem is posed in the truncated domain Ω_c (delimited by Γ and Σ) with a non-standard outgoing condition using the integral formula is prescribed on Σ,

$$\begin{aligned} \Delta u + \kappa^2 u &= 0 \text{ in } \Omega_c, \partial_n u = f \text{ on } \Gamma, & (3)\\ (\partial_n - i\kappa)u(x) &= D_\Gamma(u)(x) - S_\Gamma(f)(x), \forall x \in \Sigma, & (4)\end{aligned}$$

where D_Γ and $S_\Gamma(f)$ denote respectively the double and simple layer, such that

$$\begin{aligned} D_\Gamma(u)(x) &= \int_\Gamma u(y)\partial_n K(x-y)\mathrm{d}\gamma,\\ S_\Gamma(f)(x) &= \int_\Gamma f(y)K(x-y)\mathrm{d}\gamma,\end{aligned}$$

and $K(x) = (\frac{x}{|x|}.\nabla - i\kappa)G_\kappa(x)$. G_κ is the Green function defined by $G_\kappa(x) = -\frac{1}{4\pi}\frac{e^{i\kappa|x|}}{|x|}$. Observe that the integral representation is used only in Σ which avoids occurrences of any singularities. We suppose that this problem is discretized by a Lagrange finite element method. Let N_Ω be the total number of degrees of freedom on Ω_c and N_Σ (resp. N_Γ) be the number of degrees of freedom on Σ (resp. Γ). The shape function associated with a node x_α is denoted w_α. Let u_α be the approximation of the solution u at x_α and $U = (u_\alpha)_\alpha$.

The linear system can be formulated as follows:

$$(A - C)U = F^\Gamma - F^\Sigma \quad (5)$$

where

$$\begin{aligned} A_{\alpha,\beta} &= \int_{\Omega_c} \left(\nabla w_\alpha(x)\nabla\overline{w}_\beta(x) - \kappa^2 w_\alpha(x)\overline{w}_\beta(x)\right) dx\\ &\qquad -i\kappa\int_\Sigma w_\alpha(x)\overline{w}_\beta(x)d\sigma(x)\\ C_{\alpha,\beta} &= \int_\Sigma D_\Gamma(w_\alpha)(x)\overline{w}_\beta(x)\ d\sigma(x)\\ F^\Gamma_\alpha &= \int_\Gamma f(x)\overline{w}_\alpha(x)d\gamma(x)\\ F^\Sigma_\alpha &= \int_\Sigma S_\Gamma(f)(x)\overline{w}_\alpha(x)\ d\sigma(x)\end{aligned}$$

The non-local coupling enforced by the integral term generates some difficulties in its numerical treatment because it perturbs the sparse structure of the stiffness matrix (around the degrees of freedom located on the artifical boundary). Indeed, in system (5), the matrix is complex, non Hermitian and ill-conditioned. Numerical re-

sults show the convergence of the BICG algorithm applied to system (5) with a Schwarz preconditioner. In other words, the linear system is formulated as follow:

$$(I_{N_\Omega} - A^{-1}C)U = A^{-1}(F^\Gamma - F^\Sigma) \qquad (6)$$

There is no theorical proofs of the convergence of the BICG method for a complex matrix. We propose in this work, to explore different ways to solve this problem and prove the convergence of the iterative algorithm.

The Steklov-Poincaré interface equation

We propose to establish the Steklov-Poincaré interface equation, in order to reduce the number of degrees of freedom of the linear system. Let us introduce :

$$\lambda(x) = D_\Gamma(u)(x) - S_\Gamma(f)(x), \forall x \in \Sigma. \qquad (7)$$

defined on Σ. In the problem solved by u, the last equation becomes:

$$(\partial_n - i\kappa)u(x) = \lambda(x), \qquad \forall x \in \Sigma. \qquad (8)$$

Let Λ be the finite element approximation of λ, $P_\Sigma \in M_{N_\Sigma,N_\Omega}(R)$ (resp. $P_\Gamma \in M_{N_\Gamma,N_\Omega}(R)$) the restriction matrix on Σ (resp. Γ) and M_Σ the mass matrix on Σ. The finite element discretization leads to the following linear system :

$$AU - P_\Sigma^t M_\Sigma \Lambda = F^\Gamma \qquad (9)$$

while by a finite element interpolation, equation (7) becomes :

$$\Lambda = G_n M_\Gamma P_\Gamma U - H. \qquad (10)$$

where H is the finite element approximation of $\int_\Gamma f(y)K(x-y)\mathrm{d}\gamma(y)$, and $G_n \in M_{N_\Sigma,N_\Gamma}(C)$ is the matrix defined by: $(G_n)_{\alpha,\beta} = \partial_n K(x_\alpha - y_\beta)$, for each couple of nodes $(x_\alpha, y_\beta) \in \Sigma \times \Gamma$. Equations (9-10) leads to the Steklov-Poincaré interface equation:

$$(I_{N_\Sigma} - B_2B_1)\Lambda = B_2A^{-1}F^\Gamma - H \qquad (11)$$

where $B_1 = A^{-1}P_\Sigma^t M_\Sigma$ and $B_2 = G_n M_\Gamma P_\Gamma$. When the distance between Σ and Γ is sufficiently large, the spectrum of B_2B_1 is included in the unit disk. In this case, a Richardson method can be used to solve (11), and it corresponds to an alternating Schwarz method ([1], [2]). In the general case B_2B_1 have at least a few eigenvalues out of the unit disk, and the convergence of a Krylov subspace method can be achieved as in [7]. We show that it can be also obtained by a generalisation of the proof of [8] for the conjugate gradient method. Numerical results show that the convergence of the GMRES algorithm applied to equation (11) is comparable to the convergence of GMRES applied to (6). Indeed, we can easily check that $A^{-1}C = B_1B_2$. Consequently, except eventually for the eigenvalue 0, $A^{-1}C$ and B_2B_1 have the same eignenvalues, with the same multiplicities. The matrices involved in systems (11) and (6) are the same, and the application of B_1B_2 or B_2B_1 have the same computation cost. All the difference lies in the storage size of the Arnoldi basis for GMRES algorithm.

References

[1] F. Ben Belgacem, M. Fournié, N. Gmati and F. Jelassi, “Comment traiter des conditions aux limites à l’infini pour quelques problèmes extérieurs par la méthode de Schwartz alternée”, C. R. Acad. Sci. Paris, Ser. I 336 , pp. 277-282, 2003.

[2] F. Jelassi, “Calcul des courants de Foucault harmoniques dans des domaines non bornés par un algorithme de point fixe de Cauchy”, Revue Africaine de la Recherche en Informatique et Mathématiques Appliquées (ARIMA), vol. 5, pp. 168-182, 2006.

[3] C. Johnson, J.-C. Nédélec, “On the coupling of boundary integral and finite element methods”. Math. Comp. Vol. 35 , N.152, pp.1063–1079, 1980.

[4] A. Jami and M. Lenoir, “ A new numerical method for solving exterior linear elliptic problems”, Lecture Notes in Phys., vol. 90, Springer, pp. 292-298, 1979.

[5] J. Liu, J.–M. Jin, “A Highly effective preconditioner for solving the finite element-boundary integral matrix equation of 3-D scattering”, IEEE transactions on antennas and propagation, vol. 50, pp. 1212-1221, 2002.

[6] J.-C. Nédélec, “Acoustic and electromagnetic equations Integral Representations for Harmonic Problems”, Applied Mathematical Sciences, vol 144, Springer-Verlag, New-York, 2001.

[7] I. Moret, “A note on the superlinear convergence of GMRES”, SIAM Journal of numerical analysis, vol. 34, N.2, pp. 513-516, april 1997.

[8] R. Winther, “Some superlinear convergence results for the conjugate gradient method”, SIAM Journal of numerical analysis, vol. 17, N.1, pp. 14-17, february 1980.

On a Galerkin wave boundary element formulation for scattering by non smooth obstacles

H. Bériot, E. Perrey-Debain*, M. Ben Tahar, C. Vayssade
Laboratoire Roberval, Université de Technologie de Compiègne
60205 Compiègne BP 20529 France
*Email: emmanuel.perrey-debain@utc.fr

Abstract

We consider the problem of scattering of a time-harmonic acoustic incident wave by a hard obstacle. The numerical solution to this problem is found using a Galerkin wave boundary integral formulation whereby the functional space is built as the product of conventional low order piecewise polynomials with a set of plane waves propagating in various directions. We show a practical use of the method for dealing with irregular meshes and corners.

Introduction

It is well known that the use of discrete (frequency domain) numerical methods for the solution of the Helmholtz equation is limited to problems in which the wavelength under consideration is not small in comparison with the domain size. The limitation arises because conventional elements, based on polynomial shape functions require around ten variables per full wavelength. Following earlier predictions of de La Bourdonnaye [1], it has been found that drastic progress can be made by including a plane wave basis in a collocation boundary element formulation [2], [3]. However all the studies previously published involved regularly meshed and analytically described smooth scatterers. Furthermore, the method depends strongly on the number and locations of the collocation points [2] and this is particularly relevant for 3D obstacles for which the number of points must largely exceed the number of variables [3]. We present in this paper an improvement of the method (i) by considering a Galerkin formulation that allows to reliably circumvent the non uniqueness problem and avoids overdetermined systems and (ii) by using an adaptive scheme to deal with irregular meshes.

Problem statement and integral formulation

We consider the scattering of an time-harmonic acoustic incident wave ϕ^i by a bounded obstacle Ω' in a bidimensional homogeneous propagative medium Ω of characteristic sound speed c_0. Let $\kappa = \omega/c_0$ denote the associated wavenumber; we aim at finding the scattered wave field ϕ^s satisfying ($\mathrm{e}^{-\mathrm{i}\omega t}$ time-dependence)

$$\Delta\phi^s + \kappa^2\phi^s = 0 \quad \text{in} \quad \Omega\,, \tag{1}$$

as well as the usual radiation condition,

$$\lim_{|x|\to\infty} \sqrt{|x|}\left(\frac{\partial\phi^s}{\partial|x|} - \mathrm{i}\kappa\phi^s\right) = 0. \tag{2}$$

In this work, we shall consider Neumann type conditions on the surface of the scatterer $\Gamma = \partial\Omega'$, i.e., the total field $\phi = \phi^i + \phi^s$ must satisfy

$$\frac{\partial\phi}{\partial n}(x) = \nu(x), \quad x \in \Gamma. \tag{3}$$

Using a direct combined integral representation, the unknown field $\phi(x)$ on Γ is found to be the unique solution of the second kind integral equation [4]

$$L\phi = \left(\frac{1}{2} + D + \beta H\right)\phi = g \quad \text{on } \Gamma\backslash\{\mathcal{C}\} \tag{4}$$

where $\{\mathcal{C}\}$ is the set of corners of Ω' and g stems for the incident field and the radiation term ν,

$$g = \phi^i + \beta\frac{\partial\phi^i}{\partial n} + \left(S + \beta D^* - \frac{\beta}{2}\right)\nu \tag{5}$$

and S, D, D^* and H stand respectively for the usual single layer potential operator

$$S\phi(x) = \int_\Gamma G(x,y)\phi(y)\mathrm{d}\gamma_y\,, \tag{6}$$

the double layer potential operator

$$D\phi(x) = \int_\Gamma \frac{\partial G(x,y)}{\partial n_y}\phi(y)\mathrm{d}\gamma_y\,, \tag{7}$$

its adjoint operator

$$D^*\phi(x) = \frac{\partial}{\partial n_x}\int_\Gamma G(x,y)\phi(y)\mathrm{d}\gamma_y\,, \tag{8}$$

and the hypersingular operator

$$H\phi(x) = \frac{\partial}{\partial n_x}\int_\Gamma \frac{\partial G(x,y)}{\partial n_y}\phi(y)\mathrm{d}\gamma_y. \tag{9}$$

The kernel G stands for the free-space Green function $G(x,y) = \mathrm{i}/4H_0^1(\kappa|x-y|)$ and n_y (resp. n_x) is the inward normal unit vector at point y (resp. x). H_0^1 denotes the Hankel function of the first kind of zero order. The coupling coefficient β must have a non-zero imaginary part to ensure the uniqueness of the solution. As we are not dealing with very low frequency applications, we shall take $\beta = \mathrm{i}/\kappa$.

A Galerkin wave boundary element formulation

The integral equation (4) can be conveniently solved using standard variational procedure, i.e, find ϕ such that

$$\langle L\phi, \varphi\rangle = \langle g, \varphi\rangle, \quad \forall\varphi \in \mathcal{V}, \tag{10}$$

where $\mathcal{V}$ is an appropriate functional space and we note $\langle\cdot,\cdot\rangle$ the usual hermitian product on Γ. The discretization of (10) starts with the introduction of a set of N nodes located on Γ, $\{\mathcal{N}\} = \{x_{n=1,N} \in \Gamma\}$. These points must coincide with the corners of Ω' so that $\{\mathcal{C}\} \subset \{\mathcal{N}\}$. We assume that the geometry of the scatterer Γ_n between two consecutive nodes x_n and x_{n+1} is known analytically, or can be simulated by appropriate approximation methods (via Lagrange interpolation for instance), i.e., there exists a regular function γ_n defined on the reference interval $[-1,1]$ such that $\Gamma_n = \{\gamma_n(\eta),\ \eta \in [-1,1], x_n = \gamma_n(-1), x_{n+1} = \gamma_n(1)\}$ with the convention that $x_{N+1} = x_1$. We introduce a set of M_n plane wave directions 'attached' to each node x_n. In this work, these direction are chosen to be regularly distributed as

$$\theta_m^n = \begin{pmatrix} \cos(m2\pi/M_n + \delta\theta^n) \\ \sin(m2\pi/M_n + \delta\theta^n) \end{pmatrix}, \tag{11}$$

where $m = 1,\ldots,M_n$ and the parameter $\delta\theta^n$ is introduced to define a tilt in the wave basis directions. On each element Γ_n, the potential ϕ is approximated as the following plane wave expansion

$$\begin{aligned} \phi(x)|_{x\in\Gamma_n} &= (\eta+1)\sum_{m=1}^{M_n}\phi_m^n w(\theta_m^n;x) \\ &+ (\eta-1)\sum_{m=1}^{M_{n+1}}\phi_m^{n+1} w(\theta_m^{n+1};x) \end{aligned} \tag{12}$$

where the function $w(\theta;x) = \mathrm{e}^{\mathrm{i}\kappa\theta\cdot x}$ denotes a propagative plane wave traveling in the θ-direction and the unknown coefficients ϕ_m^n can be interpreted as the amplitudes of the associated plane waves. The double integration in (10) is performed using Duffy-like transformations [5] and the hypersingular integral is transformed into a weakly singular one via a regularization procedure [6].

An adaptative approach for irregular meshes

Through numerical and theoretical results [2], [7] it is found that the plane wave approximation error essentially behaves with respect to the discretization level τ (i.e. the number of variable per wavelength) and the relative wavenumber κh where h is a characteristic length of the boundary domain. For the specific case of a regularly meshed rigid circular scatterer, numerical experiments show that the overall error on the boundary is kept constant as long as the number of variables is chosen so that

$$\tau \approx C(\kappa h)^{-1/2} + 2, \tag{13}$$

where h is the length of a boundary element and C is a constant. To deal with non-smooth obstacles and irregular meshes, we consider the empirical rule of thumb (13) *locally*, i.e. we define the local discretization level τ_n associated with the element Γ_n as

$$\tau_n = \frac{M_n + M_{n+1}}{2}\frac{\lambda}{h_n}, \tag{14}$$

where $\lambda = 2\pi/\kappa$ is the wavelength and $h_n = \int_{\Gamma_n}\mathrm{d}\gamma_y$ is the length of the element Γ_n. Inverting (14) together with the condition (13) yields the following system

$$\mathsf{AM} = \mathsf{L}\,, \text{with} \quad \mathsf{A} = \begin{bmatrix} 1 & 1 & 0 & \ldots & 0 \\ 0 & 1 & 1 & & 0 \\ \vdots & \ddots & \ddots & \ddots & \vdots \\ \vdots & & 0 & 1 & 1 \\ 1 & 0 & \ldots & 0 & 1 \end{bmatrix}. \tag{15}$$

The vector L contains the number of variables required per element and $\mathsf{M} = (M_1, M_2, \ldots, M_n)^T$. The connectivity matrix A is always singular when N is even and $\det\mathsf{A} = 2$ otherwise. In this work, the optimal combination $\mathsf{M}_{\mathrm{opt}}$ is found via the minimization procedure:

$$Find \quad \min_{2\le M_1,M_2,\ldots,M_n\le M_{\max}} \|\mathsf{D}^{-1}\mathsf{AM} - \mathsf{e}\|, \tag{16}$$

where D is the diagonal matrix containing the vector L and $\mathsf{e} = (1,1,\ldots,1)^T$. This is achieved by using standard evolutionary algorithms with uniform crossover (see for instance [8]). The method is applied to the rigid scatterer displayed in Fig. 1. In order to give an accurate measurement of the error, we first consider the artificial radiating problem by imposing $\nu(x) = \partial G(x,x_0)/\partial n_x$ with a source located inside Ω'. Results are conveniently displayed in Fig. 2 (the overall error is defined as the L_2 norm relative error on Γ). The straight line corresponds to

the standard quadratic interpolation scheme ($p = 2$) and the reference GWBE stands for 'Galerkin Wave Boundary Element'. These results clearly demonstrate the advantage of considering an adaptative scheme. Even in the presence of a very small cavity (a/b=40), a global discretization level of $\tau = 3.3$ provides a good precision ($\sim 0.1\%$) and a very high convergence rate is still observed when compared to the standard quadratic interpolation. Figure 3 shows the total potential ϕ on the boundary of the hard obstacle (with $a/b = 20$) due to the scattering of an incident plane wave of incidence $\theta^i = \pi/4$ at $\kappa a = 17$. Here again, the good agreement between our formulation and the standard quadratic discretization scheme shows the potentiality of the GWBE method.

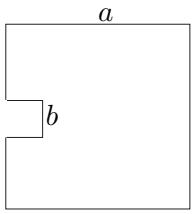

Figure 1: Square scatterer with a cavity.

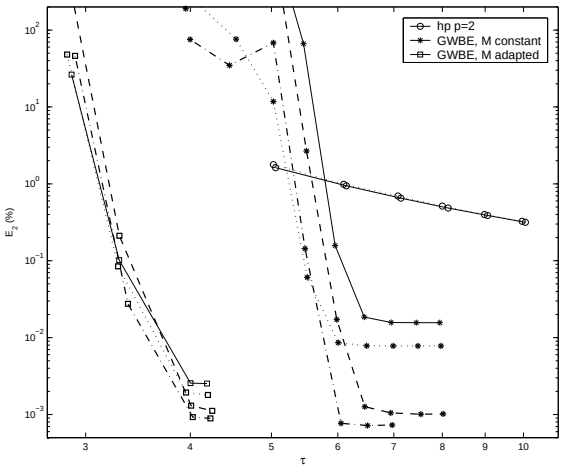

Figure 2: Convergence rates for a radiating problem, $\kappa a = 25$. Solide line: $b = a/40$; dashed line: $b = a/20$; dotted line: $b = a/10$; dash-dotted line: $b = a/5$.

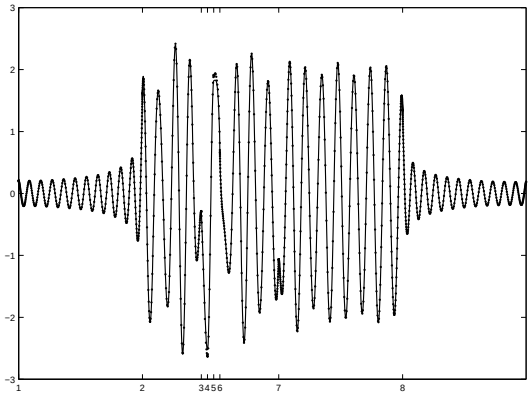

Figure 3: Potential (real part) on the scattering obstacle. Solide line: quadratic interpolation with $\tau = 30$; dotted line: the GWBE solution (dots) with $\tau = 3$.

References

[1] A. de La Bourdonnaye, "A microlocal discretization method and its utilization for a scattering problem", C.R. Acad. Sci., Série I, vol. 318, pp. 385-88, 1994.

[2] E. Perrey-Debain, J. Trevelyan, P. Bettess, "Use of wave boundary elements for acoustic computations", J. Comp. Acou., vol. 11, pp. 305-321, 2003.

[3] E. Perrey-Debain, O. Laghrouche, P. Bettess, J. Trevelyan, "Plane wave basis finite elements and boundary elements for three dimensional wave scattering", Proc. Roy. Soc. A, vol. 362, pp. 561-577, 2004.

[4] A.J. Burton, G.F. Miller, "The application of integral equation methods to the numerical solution of some exterior boundary-value problems", Proc. Roy. Soc. A, vol. 323, pp. 201-210, 1971.

[5] M. Bonnet, M. Guiggiani, "Galerkin BEM with direct evaluation of hypersingular integrals", Elect. J. Bound. Elem., vol. 1, pp 95-111, 2003.

[6] M.A. Hamdi, "A integral equation variational formulation for the resolution of the Helmholtz equation including mixed boundary conditions", C.R. Acad. Sci., vol. 292, pp.17-20, 1981.

[7] E. Perrey-Debain, "Plane wave decomposition in the unit disc: convergence estimates and computational aspects." J. Comp. App. Math., vol. 193, pp. 140-156, 2006.

[8] Z. Michalewicz, Genetic Algorithms + Data Structures = Evolution Programs, Springer-Verlag, Berlin, 1996.

THEORETICAL JUSTIFICATION OF POCKLINGTON'S EQUATION FOR DIFFRACTION BY THIN WIRES

X. Claeys[†,*]

[†] Project POems INRIA, Domaine de Voluceau 78153 Le Chesnay, FRANCE
[*]Email : xavier.claeys@inria.fr

Introduction

Pocklington in [1] proposed a simplified one-dimensional integral equation relating the current at the surface of a straight finite wire to the tangential trace of an incident electromagnetic field. This equation has been derived assuming that the current is constant across any section of the wire. At least for the model problem of a finite, straight and cylindrical wire, this simplified equation has been proved to be well posed, see [2],[3] or [6]. Moreover, many results have been established for the regularity of the solutions of this equation, see [4] and [5]. However, to our knowledge, there has been no rigorous study of the error between the solution of the exact integral equation and the solution of Pocklington's equation. We address this problem for the model case of acoustics in a smooth geometry.

Pocklington's equation

Denote Γ^ε the boundary of a thin wire with thickness ε small with respect to a wavelength $\lambda = 2\pi/k$. Denote u^ε the unique outgoing radiating function satisfying $\Delta u^\varepsilon + k^2 u^\varepsilon = f$ in $\mathbb{R}^3 \setminus \Gamma^\varepsilon$ with an homogeneous Dirichlet boundary condition on Γ^ε. We suppose $f \in L^2(\mathbb{R}^3)$ such that $\text{supp} f \cap \Gamma^\varepsilon = \emptyset$ for ε small enough. We first consider the usual geometry where $\Gamma^\varepsilon = \{\mathbf{x} \in \mathbb{R}^3 \,|\, \max(z^2, \frac{x^2+y^2}{\varepsilon^2}) = 1\}$ and its limit $J = \{\mathbf{x} \in \mathbb{R}^2 \,|\, x = y = 0\,,\ |z| \leq 1\}$.

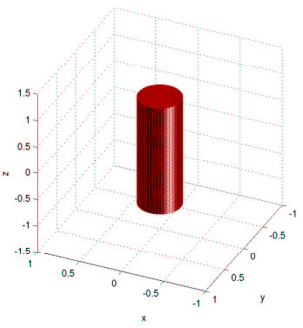

Figure 1: Usual wire geometry

According to Pocklington's model (adapted to acoustics) the jump of the normal derivative $p^\varepsilon = [\frac{\partial u^\varepsilon}{\partial n}]_{|\Gamma^\varepsilon} = \frac{\partial u^\varepsilon}{\partial n_e}{}_{|\Gamma^\varepsilon_+} + \frac{\partial u^\varepsilon}{\partial n_i}{}_{|\Gamma^\varepsilon_-}$ has approximately no transversal dependancy $p^\varepsilon(\mathbf{x}) \simeq \mathfrak{p}^\varepsilon(z)/2\pi\varepsilon$ and satisfies the integral equation

$$\int_{-1}^{+1} K_p(z,z')\,\mathfrak{p}^\varepsilon(z')dz' = -u_0(z)\,,\ z \in [-1,1]$$

where $u_0(z)$ refers to the trace on J of the unique outgoing radiating function satisfying $\Delta u_0 + k^2 u_0 = f$ in $\mathbb{R}^3$. The integral kernel is given by

$$K_p(z,z') = \frac{1}{2\pi}\int_0^{2\pi} \frac{e^{ik\sqrt{(z-z')^2+\varepsilon^2 4\sin^2(\varphi/2)}}}{4\pi\sqrt{(z-z')^2+\varepsilon^2 4\sin^2(\varphi/2)}}d\varphi.$$

For a smoother geometry, we propose to rigorously derive a one dimensional integral equation similar to the preceding one, and estimate the difference $|p^\varepsilon - \mathfrak{p}^\varepsilon/2\pi\varepsilon|_{-1/2,\Gamma^\varepsilon}$, the norm $|\quad|_{-1/2,\Gamma^\varepsilon}$ being well chosen.

Ellipsoidal coordinates

Instead of the classical geometry, we wish to consider a family of C^∞-surfaces $(\Gamma^\varepsilon)_{\varepsilon>0}$ shrinking to the limit segment $\Gamma^\varepsilon \to J$. For this purpose we introduce ellipsoidal coordinates (ξ,ν,φ) related to cartesian coordinates by

$$\left\{\begin{array}{ll} x = \sqrt{\xi^2-1}\sqrt{1-\nu^2}\cos\varphi\,, & \xi \in [1,+\infty[\\ y = \sqrt{\xi^2-1}\sqrt{1-\nu^2}\sin\varphi\,, & \nu \in [-1,1] \\ z = \xi\nu\,, & \varphi \in [0,2\pi] \end{array}\right.$$

Then we consider surfaces described by the equation $(\Gamma^\varepsilon)\,:\,\xi^2 = 1+\varepsilon^2\Phi^2(\nu)$ (for simplicity sake we suppose it to have the symmetry of revolution) where Φ is a C^∞-function strictly positive on $[-1,1]$. Such a surface looks like a perturbed ellipsoid (see figure 2). If we define $\Omega^R = B(0,R)$ and the bilinear form $a(u,v) = \int_{\Omega^R}\nabla u\cdot\nabla\overline{v} - k^2 u\overline{v} + \int_{\partial\Omega^R}\overline{v}T_R u$ where T_R is the usual DtN map for Helmholtz problems in spherical coordinates, we are interested in $(u^\varepsilon,p^\varepsilon) \in H^1(\Omega^R)\times H^{-1/2}(\Gamma^\varepsilon)$ satisfying

$$\left\{\begin{array}{ll} a(u^\varepsilon,\overline{v}) + \int_{\Gamma^\varepsilon} p^\varepsilon\overline{v} = \int_{\Omega^R} f\overline{v}\,, & \forall v \in H^1(\Omega^R) \\ \int_{\Gamma^\varepsilon} q\overline{u}^\varepsilon = 0\,, & \forall q \in H^{-1/2}(\Gamma^\varepsilon). \end{array}\right.$$

The norm we consider on $H^1(\Omega^R)$ is classical $\|u\|^2_{H^1(\Omega^R)} = \|u\|^2_{L^2(\Omega^R)} + \|\nabla u\|^2_{L^2(\Omega^R)}$. On the other hand, for this problem to have good stability properties (with respect to ε), we have to be careful about the definition of the norm $|\ |_{1/2,\Gamma^\varepsilon}$ on $H^{1/2}(\Gamma^\varepsilon)$. If we consider the geometrical transformation given in spheroidal coordinates $\mathcal{G}(\xi,\nu,\varphi) = (\sqrt{1+\frac{\xi^2-1}{\varepsilon^2}},\nu,\varphi)$, then the surface $\Gamma = \mathcal{G}(\Gamma^\varepsilon)$ is described by the equation $\xi^2 = 1+\Phi^2(\nu)$ independantly of ε. We define $|u|_{1/2,\Gamma^\varepsilon} = |u\circ\mathcal{G}^{-1}|_{1/2,\Gamma}$, and $|u|_{-1/2,\Gamma^\varepsilon} = \sup_{v\in H^{1/2}(\Gamma^\varepsilon)} \int_{\Gamma^\varepsilon} u\, v / |v|_{1/2,\Gamma^\varepsilon}$.

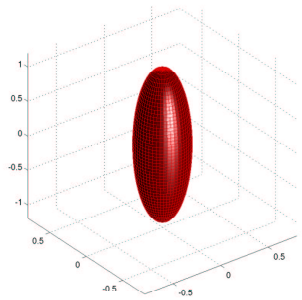

Figure 2: Ellipsoid of equation $\xi = \xi_0$

Analysis by matched asymptotics

In order to obtain a simplified problem that would lead to Pocklington's equation, we study the behavior of $(u^\varepsilon, p^\varepsilon)$ when $\varepsilon \to 0$ using matched asymptotic expansions. This study is close to previous works achieved by Fedoryuk in [7] (see also [8],[9]). We are led to an approximate field

$$\widetilde{u}^\varepsilon(\mathbf{x}) = (1-\chi^\varepsilon(\mathbf{x}))\big(u_0(\mathbf{x}) + u_1^\varepsilon(\mathbf{x})\big) + \chi^\varepsilon U_1^\varepsilon(\mathbf{x}).$$

In this expression χ^ε is a smooth cut-off function equal to 1 for $\xi^2 - 1 < \varepsilon/2$ and equal to 0 for $\xi^2 - 1 > \varepsilon$. Note that the set $\varepsilon/2 < \xi^2 - 1 < \varepsilon$ is an ellipsoidal shell surrounding Γ^ε. The definitions of the other terms $U_1^\varepsilon(\mathbf{x}) = -\frac{a^\varepsilon(\nu)}{4\pi}\ln\big(\frac{\xi^2-1}{\varepsilon^2\Phi^2(\nu)}\big)$ and $u_1^\varepsilon(\mathbf{x}) = \int_J a^\varepsilon(\mathbf{x}')e^{ik|\mathbf{x}-\mathbf{x}'|}/4\pi|\mathbf{x}-\mathbf{x}'|d\mathbf{x}'$ involve a 1D-function $a^\varepsilon \in C^\infty(J)$ that depends on ε and has to be chosen in order to satisfy a matching principle. With this definition, we find that $\widetilde{p}^\varepsilon = [\frac{\partial\widetilde{u}^\varepsilon}{\partial n}]_{|\Gamma^\varepsilon}$ does not depend on the variable φ. This is an interesting property that we will take into account in a modified formulation of our acoustic problem. Moreover we have the estimates (for suitable constants κ_i, $i=1,2,3$)

$$\|u^\varepsilon - \widetilde{u}^\varepsilon\|_{H^1(\Omega^R)} + |p^\varepsilon - \widetilde{p}^\varepsilon|_{-1/2,\Gamma^\varepsilon} \leqslant \kappa_1\varepsilon^{1/2}\ln 1/\varepsilon$$

$$\frac{\kappa_2}{\ln 1/\varepsilon} \leqslant |\widetilde{p}^\varepsilon|_{-1/2,\Gamma^\varepsilon} \leqslant \frac{\kappa_3}{\ln 1/\varepsilon}$$

which means that $(\widetilde{u}^\varepsilon, \widetilde{p}^\varepsilon)$ is a relevant approximation of $(u^\varepsilon, p^\varepsilon)$, and provides in addition the behavior of p^ε when $\varepsilon \to 0$.

Simplified problem

This result suggests to get interested in a simplified problem. We introduce the averaging operator $\mu^\varepsilon : H^{1/2}(\Gamma^\varepsilon) \to L^2(I)$ defined by

$$\mu^\varepsilon(u)(\nu) = \frac{1}{2\pi}\int_0^{2\pi} u(\nu,\varphi)d\varphi.$$

We also introduce the one dimensional spaces $E^r(I)$ of elements $u = \sum_n u_n P_n$ such that $\|u\|^2_{E^r(I)} = \sum_n (1+n^2)^{r-1/2}|u_n|^2 < +\infty$, where $(P_n)_{n\in\mathbb{N}}$ is the orthogonal basis of Legendre polynomials (note that $L^2(I) = E^0(I)$ due to the L^2-norm of P_n). We can prove that $E^{1/2}(I) = \mathrm{Im}\,\mu^\varepsilon$, and that μ^ε is continuous for the norms $\|\ \|_{E^{1/2}(I)}$ and $|\ |_{1/2,\Gamma^\varepsilon}$. We will consider the transpose operator (with respect to the usual L^2 scalar products) ${}^t\mu^\varepsilon : E^{-1/2}(I) \to H^{-1/2}(\Gamma^\varepsilon)$ that is explicitly given by ${}^t\mu^\varepsilon(q)(\nu) = (\varepsilon^2+1-\nu^2)^{-1/2}\, q(\nu)/2\pi\varepsilon$. This operator enables to consider a problem with a reduced space of Lagrange multipliers : find $(\mathfrak{u}^\varepsilon, \mathfrak{p}^\varepsilon) \in H^1(\Omega^R)\times E^{-1/2}(I)$ such that

$$\begin{cases} a(\mathfrak{u}^\varepsilon, \overline{v}) + \int_{\Gamma^\varepsilon} {}^t\mu^\varepsilon(\mathfrak{p}^\varepsilon)\overline{v} = \int_{\Omega^R} f\overline{v}\,, & \forall v \in H^1(\Omega^R) \\ \int_{\Gamma^\varepsilon} {}^t\mu^\varepsilon(q)\overline{\mathfrak{u}^\varepsilon} = 0\,, & \forall q \in E^{-1/2}(I) \end{cases}$$

We say that this problem is simplified because the space of Lagrange multipliers has been reduced, it is now a one dimensional functional space instead of a two dimensional one. We can prove with usual techniques that this problem is well posed and also prove the following estimates

$$\|u^\varepsilon - \mathfrak{u}^\varepsilon\|_{H^1(\Omega^R)} + |p^\varepsilon - {}^t\mu^\varepsilon(\mathfrak{p}^\varepsilon)|_{-1/2,\Gamma^\varepsilon} \leqslant \kappa_1\varepsilon^{1/2}\ln 1/\varepsilon.$$

In fact using stability arguments and the regularity of the data, it is even possible to prove

$$|p^\varepsilon - {}^t\mu^\varepsilon(\mathfrak{p}^\varepsilon)|_{-1/2,\Gamma^\varepsilon} \leqslant \kappa_1\,\varepsilon.$$

According to the behavior of p^ε, this means that p^ε and ${}^t\mu^\varepsilon(\mathfrak{p}^\varepsilon)$ are asymptotically equivalent. Finally we show that $\mathfrak{p}^\varepsilon$ is solution to a one dimensional integral equation of the same nature as Pocklington's equation. Indeed the

simplified problem caracterizing $(\mathfrak{u}^\varepsilon, \mathfrak{p}^\varepsilon)$ leads to the integral equation

$$\int_{-1}^{+1} K_p(\nu,\nu')\mathfrak{p}^\varepsilon(\nu')d\nu' = \frac{-1}{2\pi}\int_0^{2\pi} u_{0|\Gamma^\varepsilon}(\nu,\varphi)d\varphi$$

where the integral kernel is given by

$$K_p(\nu,\nu') = \frac{1}{2\pi}\int_0^{2\pi} \frac{e^{ik|\mathbf{x}(\nu,\varphi)-\mathbf{x}(\nu',\varphi')|}}{4\pi|\mathbf{x}(\nu,\varphi)-\mathbf{x}(\nu',\varphi')|}d\varphi'.$$

In this expression, $\mathbf{x}(\nu,\varphi)$ refers to the point of Γ^ε with ellipsoidal coordinates ν and φ. It is easy, using symmetry of revolution, to see that this kernel does not depend on φ. This integral equation appears to be close to the original Pocklington's equation since $\frac{1}{2\pi}\int_0^{2\pi} u_{0|\Gamma^\varepsilon}(\nu,\varphi)d\varphi \simeq u_0(z)$ because of the regularity of this function ($u_0(z)$ being the trace on J of u_0) and the expression of K_p has the same form as the original K_p, but with ellipsoidal instead of cylindrical coordinates. Moreover, the preceding error estimates provide a justification of this final integral equation.

References

[1] H.C. Pocklington, "Electrical Oscillations in wires" in Pro. of the Cambridge Philosophical Society, 1897.

[2] D.S. Jones,"Note on the integral equation for a straight wire antenna " in IEE Proc. n.128, 114-16, 1981.

[3] B.P. Rynne,"The well-posedness of the integral equations for thin wire antennas" in IMA Journal of Applied Mathematics, 1992.

[4] B.P. Rynne, "On the well-posedness of Pocklington's equation for a straight wire antenna and convergence of numerical solutions" in Journal of Electromagnetic Waves and Applications, 2000.

[5] O.P. Bruno and M.C. Haslam, "Regularity theory and super-algebraic solvers for wire antennas problems", submitted.

[6] A. Mazari,"Détermination par une méthode d'équations intégrales du champ électromagnétique rayonné par une structure filiforme", PhD thesis Universit'e Paris VI, 1991.

[7] M.V. Fedoryuk, "The Dirichlet problem for the Laplace operator in the exterior of a thin body of revolution", in Theory of Cubature Formulas and the Application of Functionnal Analysis to Problems of Mathematical Physics, AMS Translations 126, 1985.

[8] F. Rogier, "Problèmes mathématiques et numériques lies à l'approximation de la géométrie d'un corps diffractant dans les équations de l'électromagnétisme", PhD thesis Universit'e Paris VI, 1989.

[9] V. Maz'ya, S. Nazarov and B. Plamenevskii, "Asymptotic theory of elliptic boundary value problems in singularly perturbed domains. Vol II", Birkhäuser Verlag 111, 2000.

VOLUME AND SURFACE INTEGRAL EQUATIONS FOR ELECTROMAGNETIC SCATTERING BY A DIELECTRIC BODY

M. Costabel[†], E. Darrigrand[†], and E. H. Koné[†,*]
[†]IRMAR, Université de Rennes 1, Campus de Beaulieu, 35042 Rennes, FRANCE
[*]Email: el-hadji.kone@univ-rennes1.fr

Abstract

We analyze two integral formulations for the electromagnetic scattering by a dielectric object. The one is a volume integral equation (VIE) having a strongly singular kernel and the other is a coupled surface-volume system of integral equations with a weakly singular kernel.

Introduction

We are concerned with solving an electromagnetic scattering problem by a dielectric, with integral equations. The scientific literature is abundant on the theoretical and numerical analysis of surface integral equations related to scattering problems. Conversely, the volume integral equation (VIE) has been till now, the subject of only few studies, namely [1], [2] and [7] where the VIE is numerically solved with scheme based on the method of moments (MoM). In [4], the VIE is combined with a multilevel fast multipole algorithm, to analyze antenna radiation in the presence of dielectric radomes. The spectrum of the volume integral operator is numerically studied in [3] and [11], with an analysis in [3], under hypothesis of Hölder continuity of constitutive parameters in the whole space. Furthermore, the VIE is introduced and analyzed in [5], for a scattering problem in a medium with a refractive index uniformly Hölder continuously differentiable, with exponent $0 < \alpha < 1$ ($C^{1,\alpha}$), in the whole space $\mathbf{R}^3$. The VIE is also introduced in [1], for the scattering by a dielectric with discontinuities in the electric permittivity and the magnetic permeability of the medium.

We introduce a theoretical analysis of the scattering by a dielectric, with a piecewise regular electric permittivity which is discontinuous across the boundary (to be more realistic). More precisely, in a well-defined functional framework, we establish two integral formulations. The one being the VIE and the other, being a coupled surface-volume system of integral equations. We then justify equivalence between the scattering problem and the two integral formulations, and next we prove that the problem is well posed in the functional framework.

The work was built around references presented at the end of the paper, using a number of results namely, Stratton-Chu integral representation theorem [5], started point of integral formulations to the problem, results of density of smooth functions space in some non standard Sobolev spaces [6], allowing us to extend integral representations. We also used the unique continuation principle [8] and [10].

The problem

Let Ω^- be a bounded domain of $\mathbf{R}^3$ (Ω^- stands for the dielectric). The boundary Γ of Ω^- is supposed to be regular enough ($C^k, k \geq 2$). Let us note $\Omega^+ = \mathbf{R}^3 \setminus \overline{\Omega^-}$. The electric permittivity ε is a spatially varying function such that $\varepsilon > 0$, $\varepsilon_{|_{\Omega^-}} \in C^1(\Omega^-) \cap C^0(\overline{\Omega^-})$, $\varepsilon_{|_{\Omega^+}} = \varepsilon_0$ and ε is discontinuous across Γ. Let us note $\varepsilon_r = \frac{\varepsilon}{\varepsilon_0}$. The electric conductivity σ vanishes everywhere in the space ($\sigma \equiv 0$). The magnetic permeability μ is everywhere equal to one of the vacuum ($\mu \equiv \mu_0$). ω is the frequency and $\kappa = \omega\sqrt{\varepsilon_0\mu_0}$ is the wave number (with $\kappa > 0$). $\mathbf{n}$ is the unit outward normal vector to Ω^-.
We introduce the function spaces:

$$H(\mathrm{curl}, \Omega^-) = \{\mathbf{u} \in (L^2(\Omega^-))^3; \nabla \times \mathbf{u} \in (L^2(\Omega^-))^3\}$$

$H(\mathrm{div}, \Omega^-)$ and $H(\mathrm{div}, \Omega^+)$ are defined in the same way, with $\nabla \times \mathbf{u}$ replaced by $\nabla \cdot \mathbf{u}$

$$\begin{aligned} H(\mathrm{curl}, \mathrm{div}, \Omega^-) = &\quad H(\mathrm{curl}, \Omega^-) \cap H(\mathrm{div}, \Omega^-) \\ H_{loc}(\mathrm{curl}, (\overline{\Omega^+})) = &\quad \{\mathbf{u} \in (L^2_{loc}(\Omega^+))^3; \\ &\quad \nabla \times \mathbf{u} \in (L^2_{loc}(\Omega^+))^3\} \end{aligned}$$

$H_{loc}(\mathrm{div}, (\overline{\Omega^+}))$ is defined in the same way, with $\nabla \times \mathbf{u}$ replaced by $\nabla \cdot \mathbf{u}$

$$\begin{aligned} H_{loc}(\mathrm{curl}, \mathrm{div}, (\overline{\Omega^+})) = &\quad H_{loc}(\mathrm{curl}, (\overline{\Omega^+})) \\ &\quad \cap H_{loc}(\mathrm{div}, (\overline{\Omega^+})) \end{aligned}$$

Let $\mathbf{F} \in H(\mathrm{div}, \Omega^+)$ be a field with a compact support contained in Ω^+.

The scattering problem ($\mathcal{P}$) we want to solve can be written as follows:

Find $\mathbf{E}$, $\mathbf{H}$ such that $\mathbf{E}_i \in H(\mathrm{curl}, \mathrm{div}, \Omega^-)$, $\mathbf{E}_e \in H_{loc}(\mathrm{curl}, \mathrm{div}, \overline{\Omega^+})$, $\mathbf{H}_i \in H(\mathrm{curl}, \Omega^-)$,

$\mathbf{H}_e \in H_{loc}(\mathrm{curl}, \overline{\Omega^+})$, with $\mathbf{E}_i = \mathbf{E}_{|_{\Omega^-}}$,$\mathbf{H}_i = \mathbf{H}_{|_{\Omega^-}}$, $\mathbf{E}_e = \mathbf{E}_{|_{\Omega^+}}$ and $\mathbf{H}_e = \mathbf{H}_{|_{\Omega^+}}$, satisfying the equations:

$$(\mathcal{P}) \begin{cases} \nabla \times \mathbf{E}_i - i\kappa\, \mathbf{H}_i = 0 & \text{in } \Omega^- \\ \nabla \times \mathbf{H}_i + i\kappa\varepsilon_r\, \mathbf{E}_i = 0 & \text{in } \Omega^- \\ \nabla \times \mathbf{E}_e - i\kappa\, \mathbf{H}_e = 0 & \text{in } \Omega^+ \\ \nabla \times \mathbf{H}_e + i\kappa\, \mathbf{E}_e = \mathbf{F} & \text{in } \Omega^+ \\ \\ \mathbf{n} \times \mathbf{H}_e = \mathbf{n} \times \mathbf{H}_i \ \text{ and } \mathbf{n} \cdot \mathbf{H}_e = \mathbf{n} \cdot \mathbf{H}_i & \text{on } \Gamma \\ \mathbf{n} \times \mathbf{E}_e = \mathbf{n} \times \mathbf{E}_i \ \text{ and } \mathbf{n} \cdot \mathbf{E}_e = \mathbf{n} \cdot \varepsilon_r\, \mathbf{E}_i & \text{on } \Gamma \\ \\ \mathbf{H}_e \times \hat{x} - \mathbf{E}_e = \mathcal{O}\left(\frac{1}{r^2}\right);\ r \to +\infty \end{cases}$$

Integral equations and well-posedness

As a first step in the derivation of the integral equations, we extend the Stratton-Chu integral representation [5] to fields $(\mathbf{E}, \mathbf{H})$ in $H(\mathrm{curl}, \mathrm{div}, \Omega^-) \times H(\mathrm{curl}, \Omega^-)$, using arguments of density of $C^\infty(\overline{\Omega^-})$ in $H(\mathrm{curl}, \mathrm{div}, \Omega^-)$ and in $H(\mathrm{curl}, \Omega^-)$ [6]. From this, we obtain both the VIE and a coupled surface-volume system of integral equations, involving the electric field $\mathbf{E}$.

Introducing the following operators:

For $x \in \Omega^-$,

$$\mathcal{L}f(x) = \int_\Gamma (1 - \varepsilon_r(y))\, G(\kappa, |x-y|)\, f(y)\, d\gamma(y)$$

$$\mathcal{Q}\mathbf{u}(x) = \int_{\Omega^-} G(\kappa, |x-y|) \frac{1}{\varepsilon_r(y)}\, \nabla\varepsilon_r(y) \cdot \mathbf{u}(y)\, dy$$

$$\mathcal{N}\mathbf{u}(x) = \int_{\Omega^-} (1 - \varepsilon_r(y))\, G(\kappa, |x-y|)\, \mathbf{u}(y)\, dy$$

$$\mathcal{M}\mathbf{u}(x) = \int_{\Omega^-} (1 - \varepsilon_r(y)) \nabla_y G(\kappa, |x-y|) \cdot \mathbf{u}(y)\, dy$$

f and $\mathbf{u}$ are respectively scalar and vector fields defined on Ω^-.

$G(\kappa, |x-y|) = \frac{1}{4\pi} \frac{e^{i\kappa|x-y|}}{|x-y|}$, is the fundamental solution of Helmholtz equation.

$\gamma_0^\pm g := g^\pm_{|\Gamma}; \quad \gamma_1^\pm g := (\partial_n g^\pm)_{|\Gamma}$ and $\gamma_n^\pm \mathbf{v} := (\mathbf{n} \cdot \mathbf{v}^\pm)_{|\Gamma}$

For g and $\mathbf{v}$ respectively scalar and vector fields defined on $\mathbf{R}^3$ with $g^\pm := g_{|\Omega^\pm}$ and $\mathbf{v}^\pm := \mathbf{v}_{|\Omega^\pm}$.

Noting then :

$$\mathbf{F}_1(x) = \int_{\Omega^+} G(\kappa, |x-y|)\, \mathbf{F}(y)\, dy \qquad (x \in \Omega^-)$$

$$f_1(x) = \int_{\Omega^+} \mathrm{div}\mathbf{F}(y) G(\kappa, |x-y|)\, dy \qquad (x \in \Omega^-)$$

The coupled surface-volume system of integral equations is given by the problem $(\mathcal{E}_1)$ defined as follows:

$$(\mathcal{E}_1) \begin{cases} \text{Find } (\mathbf{E}_i, e_i) \in (L^2(\Omega^-))^3 \times H^{-\frac{1}{2}}(\Gamma) \text{ such that:} \\ \\ \begin{pmatrix} 1 - \nabla\mathcal{Q} + \kappa^2\mathcal{N} & -\nabla\mathcal{L} \\ \kappa^2\gamma_n^- \circ \mathcal{N} - \gamma_1^- \circ \mathcal{Q} & 1 - \gamma_1^- \circ \mathcal{L} \end{pmatrix} \begin{pmatrix} \mathbf{E}_i \\ e_i \end{pmatrix} \\ \\ = \begin{pmatrix} i\kappa\, \mathbf{F}_1 - \frac{1}{i\kappa} \nabla f_1 \\ i\kappa\, \gamma_n^-(\mathbf{F}_1) - \frac{1}{i\kappa}\, \gamma_1^- f_1 \end{pmatrix} \end{cases}$$

And the VIE is given by the problem $(\mathcal{E}_2)$ defined as follows:

$$(\mathcal{E}_2) \begin{cases} \text{Find } \mathbf{E}_i \in (L^2(\Omega^-))^3 \text{ such that:} \\ \\ \left(1 - \nabla\mathcal{M} + \kappa^2\mathcal{N}\right) \mathbf{E}_i = i\kappa\, \mathbf{F}_1 - \frac{1}{i\kappa} \nabla f_1 \end{cases}$$

As a first result, we justify equivalence between these integral equations and the problem $(\mathcal{P})$. Indeed, using integral representations, we prove that:

If $(\mathbf{E}, \mathbf{H})$ ***is a solution of the problem*** $(\mathcal{P})$***, then*** $(\mathbf{E}_i, \mathbf{n} \cdot \mathbf{E}_i)$ ***is a solution of the problem*** $(\mathcal{E}_1)$**.**

Reciprocally, using straightforward calculations and the unique continuation principle [8] and [10], we prove that:

If $(\mathbf{E}_i, e_i) \in (L^2(\Omega^-))^3 \times H^{-\frac{1}{2}}(\Gamma)$ ***is a solution of the problem*** $(\mathcal{E}_1)$***, then we have a solution*** $(\mathbf{E}, \mathbf{H})$ ***of the problem*** $(\mathcal{P})$***, this solution is defined by :***

$$\mathbf{E}_{|_{\Omega^-}} = \mathbf{E}_i \qquad \textbf{\textit{and}} \qquad \mathbf{E}_{|_{\Omega^+}} = \mathbf{E}_e$$

with

$$\begin{aligned} \mathbf{E}_e(x) = & \nabla \int_\Gamma (1 - \varepsilon_r(y)) G(\kappa, |x-y|) \mathbf{n}(y) \cdot \mathbf{E}_i(y)\, ds(y) \\ & - \nabla \int_{\Omega^-} G(\kappa, |x-y|) \nabla \cdot \mathbf{E}_i(y)\, dy \\ & - \kappa^2 \int_{\Omega^-} (1 - \varepsilon_r(y)) G(\kappa, |x-y|) \mathbf{E}_i(y)\, dy \\ & + i\kappa \int_{\Omega^+} G(\kappa, |x-y|) \mathbf{F}(y)\, dy \\ & - \tfrac{1}{i\kappa} \nabla \int_{\Omega^+} \nabla \cdot \mathbf{F}(y) G(\kappa, |x-y|)\, dy \end{aligned}$$

$$\mathbf{H}_{|_{\Omega^-}} = \frac{1}{i\kappa} \nabla \times \mathbf{E}_i := \mathbf{H}_i$$

and $\mathbf{H}_{|_{\Omega^+}} = \frac{1}{i\kappa} \nabla \times \mathbf{E}_e := \mathbf{H}_e.$

We establish thereafter that:

(i) If $(\mathbf{E}_i, e_i)$ ***is a solution of the problem*** $(\mathcal{E}_1)$***, then*** $\mathbf{E}_i$ ***is a solution of the problem*** $(\mathcal{E}_2)$**.**

(ii) If $\mathbf{E}_i$ ***is a solution of the probem*** $(\mathcal{E}_2)$***, then defining*** $e_i = \mathbf{n} \cdot \mathbf{E}_i$ ***on*** Γ**,** $(\mathbf{E}_i, e_i)$ ***is a solution of the probem*** $(\mathcal{E}_1)$ **.**

In addition of the equivalence results, we conclude that the scattering problem $(\mathcal{P})$ is well-posed by showing uniqueness for the problem $(\mathcal{P})$ and that:

The matrix operator of the problem $(\mathcal{E}_1)$

$$\mathrm{D} = \begin{pmatrix} 1 - \nabla \circ \mathcal{Q} + \kappa^2 \mathcal{N} & -\nabla \circ \mathcal{L} \\ \\ \kappa^2 \gamma_n^- \circ \mathcal{N} - \gamma_1^- \circ \mathcal{Q} & 1 - \gamma_1^- \circ \mathcal{L} \end{pmatrix}$$

from $(L^2(\Omega^-))^3 \times H^{-\frac{1}{2}}(\Gamma)$ ***to*** $(L^2(\Omega^-))^3 \times H^{-\frac{1}{2}}(\Gamma)$ ***is Fredholm of index zero.***

The well-posedness property is obviously satistfied by problems $(\mathcal{E}_1)$ and $(\mathcal{E}_2)$.

Conclusion and perspectives

Under more realistic hypothesis of discontinuity of the electric permittivity across the boundary of a dielectric, we justified equivalence between the electromagnetic scattering problem , the VIE and a coupled surface-volume system of integral equations. The last one has only been used to analyze the problem and to prove its well-posedness. As for the VIE, it will be used for the numerical study of the problem, making us free of the discretization of the boundary and the unit normal vector, on the numerical approximation of the solution.

We expect a numerical implementation based on a Finite Differences-Finite Elements discretization, which could be combined with a Fast Multipole Method (FMM). Results obtained by this scheme could then be compared with those obtained by other methods, namely those based on method of moments which is widely used on numerical solving of the VIE.

References

[1] M. I. Sancer, K. Sertel, J. L. Volakis, and P. V. Alstine, "On Volume Integral Equations", IEEE Trans. Antennas Propag., vol. 54(5), pp. 1488-1495, 2006.

[2] M. M. Botha, "Solving the Volume Integral Equations of Electromagnetic Scattering", J. Comput. Phys., vol. 128, pp. 141-158, 2006.

[3] N. V. Budko, and A. B. Samokhin, "On the eigenvalues of the volume integral operator of electromagnetic scattering", SIAM J. Sci. Comput., vol. 28(2), pp. 682-700, 2006.

[4] C. C. Lu, "A fast algorithm based on volume integral equation for analysis of arbitrarily shaped dielectric radomes", IEEE Trans. Antennas Propag., vol. 51, pp. 606-612, 2003.

[5] D. Colton and R. Kress, Inverse Acoustic and Electromagnetic Scattering Theory, Springer-Verlag, 1998.

[6] V. Giraud and P. A. Raviart, Finite Element Methods for the Navier-Stokes Equations, Theory and Algorithms, Springer Series in Computat. Math. 5, Springer-Verlag, Berlin, 1996.

[7] J. P. Kottmann, and O. J. F. Martin, "Accurate solution of the volume integral equation for high-permittivity scatterers", IEEE Trans. Antennas Propag., vol. 48, pp. 1719-1726, 2000.

[8] R. Leis, Initial Boundary Value Problems in Mathematical Physics, John Wiley, New York, 1986.

[9] J. C. Nédélec, Acoustic and Electromagnetic Equations, Integral Representations for Harmonic Problems, Springer-Verlag, New York, 2000.

[10] M. H. Protter, "Unique continuation for elliptic equations", Trans. Amer. Math. Soc., vol.95(1), pp. 81-91, 1960.

[11] J. Rahola, "Spectrum of the volume integral operator of electromagnetic scattering", SIAM J. Sci. Comput., vol. 21(5), pp. 1740-1754, 2000.

A surface integral algorithm for T-matrix computations in three dimensional electromagnetic scattering

M. Ganesh[†,*], **S. C. Hawkins**[‡]
[†]Department of Mathematical and Computer Sciences, Colorado School of Mines, Golden, USA.
[‡]School of Mathematics and Statistics, University of New South Wales, Sydney, Australia.
[*]Email: mganesh@mines.edu

Abstract

The infinite T-matrix method is a powerful tool for electromagnetic scattering simulations, particularly when one is interested in changes in orientation of the scatterer with respect to the incident wave or changes of configuration of multiple scatterers and random particles, because it avoids the need to solve the fully reconfigured systems. The truncated T-matrix is often computed using the null-field method. The main disadvantage of the null-field based T-matrix computation is its numerical instability for particles that deviate from a sphere. For large and/or highly non-spherical particles the null-field method based truncated T-matrix computations can become slowly convergent or even divergent. In this work we describe an efficient surface integral equation based algorithm for computing the T-matrix that avoids the numerical instability.

Introduction

In electromagnetic simulations by a three dimensional obstacle, the transition matrix (T-matrix) method is based on the series expansion of the incident field in vector spherical (or spheroidal or ellipsoidal) wave functions and similar expansion of the scattered field outside a circumscribing sphere (or spheroid or ellipsoid) of the scatterer. Using the linearity of the Maxwell equations, these coefficients are connected by an infinite matrix, known as the T-matrix. The T-matrix is independent of the incident wave and it characterizes the scattering properties of the obstacle.

Hence the infinite T-matrix method is a useful technique for electromagnetic scattering simulation to study the effect of changes in orientation of the scatterer with respect to the incident wave. In multiple scattering, by building the T-matrix of each obstacle in the configuration, the T-matrix method is a powerful tool to investigate the effect of changes in the original configuration of the particles because it avoids the need to solve the fully reconfigured/dynamic systems.

In practice, only truncated versions of the T-matrix can be computed (by starting with truncated series expansions of the incident and scattered fields) and it is essential to have numerical stability and convergence in the truncated T-matrix computations. Analysis of effective changes in the scattered field due to incident field or configuration changes critically depends on the accuracy and numerical stability of the truncated T-matrix.

The truncated T-matrix is often computed using the null-field method. The null-field and T-matrix methods were devised for single obstacle electromagnetic scattering by Waterman [12] and were extended for arbitrary number of scatterers by Peterson and Ström [11]. There is a vast literature on the T-matrix computations as described in recent books [3], [8], [9] and references therein.

The null-field method based T-matrix computations suffer from numerical instability and round-off errors become very significant if the size of the T-matrix is required to be large. Consequently, such computations can even become divergent for large and/or highly non-spherical particles [10, Page 543]. There are several approaches to tackle this problem (see [10], [3], [8], [9] and references therein) such as expansions obtained using spheroidal or ellipsoidal functions for high-aspect ratio convex obstacles, and computations using slow extended precision arithmetic to minimize the effect of round-off errors.

Although it is known [8, Section 7.9.4] that numerical instability involved in the null field method can be avoided by using a boundary integral equation (BIE) method to compute the T-matrix, the connection between the BIE and T-matrix methods has not been (computationally) exploited [8, Page 272] and it should be [7, Page 777], using efficient computational BIE algorithms. The analytical derivation of the connections between BIEs and the T-matrix for acoustic scattering in [7] and [8] is based on the realization of the idea of using a BIE to obtain the T-matrix by Gurel and Chew [6]. The approach in [6] is for electromagnetic scattering by thin strips and similar observations for the need to exploit the connections were remarked in [6]. Both BIE and T-matrix methods have a long pedigree and computational bridging of the two for electromagnetic scattering in three dimensions, which is overdue, is the aim of this work.

The only disadvantage of using a BIE to compute the T-matrix is that this approach requires solving a large number of (boundary integral) linear systems with a fixed scattering matrix (obtained by discretizing the associated

boundary integral operator) but different right hand sides (corresponding to each wave function used in expanding the incident and scattered field). Consequently, it is crucial to use a scattering algorithm that allows LU-factorization of the scattering matrix. In particular, this is not practically possible for three dimensional scattering problems using low order schemes such as the standard boundary element methods. The industrial standard algorithms for three dimensional electromagnetic scattering such as FISC [1] are based on BIEs solved using the method of moments, accelerated using the fast multipole method (FMM). The FMM is necessary because medium frequency simulations using FISC require solution of dense complex systems with millions of unknowns. Such large systems require iterative solvers to avoid setting up and storing the scattering matrix.

Spectrally accurate high-order algorithms for three dimensional electromagnetic scattering have been developed recently by the authors in [4] and [5]. By taking advantage of the spectrally accurate nature of these algorithms, medium frequency scattering simulations can be performed using the LU-factorization of the scattering matrix. This capability is demonstrated for a range of perfect conducting scatterers in [4], [5]. Availability of such three dimensional spectrally accurate algorithms opens the way to efficient and stable T-matrix computations through an electromagnetic scattering BIE. In this work, we apply a variant of algorithms in [4], [5] for computational realization of the bridging of the T-matrix and BIE for a class of convex, non-convex, and random particles.

We conclude this short preview presentation by formulating the T-matrix and BIE problem for electromagnetic scattering by a single three dimensional obstacle (and the corresponding multiple obstacle case follows from derivations in [11]).

Problem Formulation

The time harmonic electromagnetic field scattered by a perfect three dimensional conductor D, with surface ∂D having unit outward normal $\boldsymbol{n}$, comprises an electric field $\boldsymbol{E}$ and a magnetic field $\boldsymbol{H} = (1/ik)\ \mathbf{curl}\ \boldsymbol{E}$, where $k = 2\pi/\lambda$ is the wavenumber and λ is the wavelength. The divergence free electric field satisfies the Maxwell equation in the form

$$\mathbf{curl}\ \mathbf{curl}\ \boldsymbol{E}(\boldsymbol{x}) - k^2\boldsymbol{E}(\boldsymbol{x}) = \mathbf{0}, \quad \boldsymbol{x} \in \mathbb{R}^3 \setminus \overline{D}, \quad (1)$$

subject to the Silver-Müller radiation condition

$$\lim_{|\boldsymbol{x}|\to\infty} [\mathbf{curl}\ \boldsymbol{E}(\boldsymbol{x}) \times \boldsymbol{x} - ik|\boldsymbol{x}|\boldsymbol{E}(\boldsymbol{x})] = \mathbf{0}. \quad (2)$$

and the perfect conductor boundary condition

$$\boldsymbol{n}(\boldsymbol{x}) \times [\boldsymbol{E}(\boldsymbol{x}) + \boldsymbol{E}^i(\boldsymbol{x})] = \mathbf{0}, \quad \boldsymbol{x} \in \partial D, \quad (3)$$

where the scattered field $[\boldsymbol{E}, \boldsymbol{H}]$ is induced by the incident field $[\boldsymbol{E}^{\mathrm{i}}, \boldsymbol{H}^{\mathrm{i}}]$. A requirement for T-matrix derivation (see [11], [12]) is that there must exist a point inside D which is a suitable origin for a spherical coordinate system, so that the radius r to a point on D is a continuous function $r(\theta, \phi)$ of the spherical angles θ, ϕ. Also, D must be piecewise-smooth. (For multiple scattering, one origin must be chosen for each obstacle in the configuration [11].) Vector spherical wave functions that satisfy the exterior vector Helmholtz equation with wave number k can be expressed in terms of

$$\begin{aligned} \boldsymbol{e}_{lj}(\boldsymbol{x}) &= \boldsymbol{x} h_l^{(1)}(k|\boldsymbol{x}|) Y_{lj}(\widehat{\boldsymbol{x}}), \\ \widetilde{\boldsymbol{e}}_{lj}(\boldsymbol{x}) &= \boldsymbol{x} j_l(k|\boldsymbol{x}|) Y_{lj}(\widehat{\boldsymbol{x}}), \end{aligned}$$

for $l \geq 1$, $|j| \leq l$ and $\widehat{\boldsymbol{x}} = \boldsymbol{x}/|\boldsymbol{x}|$ for $\boldsymbol{x} \in \mathbb{R}^3 \setminus \overline{D}$, where j_l and $h_l^{(1)}$ are spherical Bessel and Hankel functions of degree l respectively,

$$Y_{l,j}(\widehat{\boldsymbol{x}}) = (-1)^{(j+|j|)/2} \sqrt{\frac{2l+1}{4\pi} \frac{(l-|j|)!}{(l+|j|)!}} P_l^{|j|}(\cos\theta) e^{ij\phi}, \quad (4)$$

for $0 \leq l \leq n,\ |j| \leq l$, and $P_l^{|j|}$ is an associated Legendre function. In (4) we have used the spherical polar coordinates $\widehat{\boldsymbol{x}} = (\sin\theta\cos\phi, \sin\theta\sin\phi, \cos\theta)^T$. Hence the divergence free vector spherical wave functions

$$\begin{aligned} \boldsymbol{M}_{lj} &= \mathbf{curl}\ \boldsymbol{e}_{lj}, \qquad \boldsymbol{N}_{lj} = \frac{1}{ik}\mathbf{curl}\ \mathbf{curl}\ \boldsymbol{e}_{lj}, \\ \widetilde{\boldsymbol{M}}_{lj} &= \mathbf{curl}\ \widetilde{\boldsymbol{e}}_{lj}, \qquad \widetilde{\boldsymbol{N}}_{lj} = \frac{1}{ik}\mathbf{curl}\ \mathbf{curl}\ \widetilde{\boldsymbol{e}}_{lj}, \end{aligned}$$

are solutions of the Maxwell equation (1) [2, Theorem 6.4]. $\boldsymbol{M}_{lj}$ and $\boldsymbol{N}_{lj}$ additionally satisfy the radiation condition (2).

The incident field is assumed to be a linear combination of the spherical wave functions:

$$\boldsymbol{E}^{\mathrm{i}} = \sum_{l=1}^{\infty} \sum_{|j|\leq l} \left[p_{lj}\widetilde{\boldsymbol{M}}_{lj} + q_{lj}\widetilde{\boldsymbol{N}}_{lj} \right] = \begin{bmatrix} \widetilde{\boldsymbol{M}} \\ \widetilde{\boldsymbol{N}} \end{bmatrix} \cdot \begin{bmatrix} \boldsymbol{p} \\ \boldsymbol{q} \end{bmatrix}. \quad (5)$$

where $\widetilde{\boldsymbol{M}}$, $\widetilde{\boldsymbol{N}}$ and $\boldsymbol{p}$, $\boldsymbol{q}$ denote column vectors in the natural way. The coefficients p_{lj}, q_{lj} are given analytically when $\boldsymbol{E}^{\mathrm{i}}$ is a plane wave. The T-matrix derivation is based on similar expansion of the scattered field $\boldsymbol{E}$:

$$\boldsymbol{E} = \sum_{l=1}^{\infty} \sum_{|j|\leq l} [a_{lj}\boldsymbol{M}_{lj} + b_{lj}\boldsymbol{N}_{lj}] = \begin{bmatrix} \boldsymbol{M} \\ \boldsymbol{N} \end{bmatrix} \cdot \begin{bmatrix} \boldsymbol{a} \\ \boldsymbol{b} \end{bmatrix}. \quad (6)$$

Since the Maxwell equation (connecting the incident and scattered fields) is linear, the coefficients $\boldsymbol{a}$, $\boldsymbol{b}$ for the scattered field $\boldsymbol{E}$ can be represented as

$$\begin{bmatrix} \boldsymbol{a} \\ \boldsymbol{b} \end{bmatrix} = T \begin{bmatrix} \boldsymbol{p} \\ \boldsymbol{q} \end{bmatrix} \tag{7}$$

where T is a matrix, called the T-matrix, that transforms the expansion coefficients of the incident field into those of the scattered field.

In practice, we replace the infinite series (5) and (6) by finite sums

$$\boldsymbol{E}^{\mathrm{i}} = \sum_{l=1}^{n_t} \sum_{|j|\le l} \left[p_{lj} \widetilde{\boldsymbol{M}}_{lj} + q_{lj} \widetilde{\boldsymbol{N}}_{lj} \right], \tag{8}$$

$$\boldsymbol{E} = \sum_{l=1}^{n_t} \sum_{|j|\le l} \left[a_{lj} \boldsymbol{M}_{lj} + b_{lj} \boldsymbol{N}_{lj} \right], \tag{9}$$

which leads to a truncated T-matrix in (7).

BIE based T-matrix computations

For a given field $\boldsymbol{u}$, the radiation of the field at large distances from D is described by the far field $\boldsymbol{u}^\infty$ of $\boldsymbol{u}$:

$$\boldsymbol{u}^\infty(\widehat{\boldsymbol{x}}) = \lim_{|\boldsymbol{x}|\to\infty} |\boldsymbol{x}| e^{-ik|\boldsymbol{x}|} \boldsymbol{u}(\boldsymbol{x}), \quad \widehat{\boldsymbol{x}} = \frac{\boldsymbol{x}}{|\boldsymbol{x}|}. \tag{10}$$

Denote by S the mapping

$$S : C(\mathbb{R}^3 \setminus \overline{D}) \to C(\partial B), \quad S\boldsymbol{f} := \boldsymbol{u}^\infty,$$

where $\boldsymbol{u}$ solves (1) and (2) subject to the boundary condition $\boldsymbol{n} \times \boldsymbol{u} = -\boldsymbol{n} \times \boldsymbol{f}$ on ∂D, and $\boldsymbol{u}^\infty$ is the far field of $\boldsymbol{u}$. For a given $\boldsymbol{f} \in C(\mathbb{R}^3 \setminus \overline{D})$, $S\boldsymbol{f}$ can be expressed as a surface integral on ∂D [2, Theorem 6.8] and evaluation of the integrand in the representation requires computational solutions of an electric or magnetic or combined field BIE [2, Chapter 6].

It can be shown that the far fields of the spherical wave functions $\boldsymbol{M}_{lj}$ and $\boldsymbol{N}_{lj}$ are orthogonal on the sphere. Thus the entries in the T-matrix can be computed from the far fields $S\widetilde{\boldsymbol{M}}_{lj}$ and $S\widetilde{\boldsymbol{N}}_{lj}$ induced by the fields $\widetilde{\boldsymbol{M}}_{lj}$ and $\widetilde{\boldsymbol{N}}_{lj}$ interacting with D. Consequently, the T-matrix entries can be computed provided an algorithm is available to compute solutions of the BIE. Since one such far-field computation is required for each field $\widetilde{\boldsymbol{M}}_{lj}$ and $\widetilde{\boldsymbol{N}}_{lj}$, it is critical that this algorithm be efficient. The spectrally accurate algorithms [4], [5], (and their variants, retaining spectral accuracy) are ideal because they have been demonstrated for efficient simulation of medium frequency electromagnetic scattering by a range of three dimensional convex, non-convex, and random obstacles with just a few thousands of unknowns, using LU-factorization to solve the linear systems.

Acknowledgments

Support of the Australian Research Council is gratefully acknowledged.

References

[1] W. C. Chew, J. M. Jin, E. Michielssen, and J. Song. *Fast and Efficient Algorithms in Computational Electromagnetics*. Artech House, 2001.

[2] D. Colton and R. Kress. *Inverse Acoustic and Electromagnetic Scattering Theory*. Springer, 1998.

[3] A. Doicu, T. Wriedt, and Y. Eremin. *Light Scattering by Systems of Particles. Null-Field Method with Discrete Sources - Theory and Programs*. Springer Verlag, 2006.

[4] M. Ganesh and S. C. Hawkins. A spectrally accurate algorithm for electromagnetic scattering in three dimensions. *Numer. Algorithms*, 43:25–60, 2006.

[5] M. Ganesh and S. C. Hawkins. A hybrid high-order algorithm for radar cross section computations. *SIAM J. Sci. Comput.*, *to appear*, 2007.

[6] L. Gurel and W. C. Chew. On the connection of T matrices and integral equations. *IEEE Antennas and Propagation Society Symposium Digest*, pages 1624–1625, 1991.

[7] P. A. Martin. On connections between boundary integral equations and T-matrix methods. *Eng. Anal. Boundary Elem.*, 27:771–777, 2003.

[8] P. A. Martin. *Multiple Scattering: Interaction of Time-Harmonic Waves with N Obstacles*. Cambridge University Press, 2006.

[9] M. I. Mishchenko, L. D. Travis, and A. A. Lacis. *Multiple Scattering of Light by Particles: Radiative Transfer and Coherent Backscattering*. Cambridge University Press, 2006.

[10] M. I. Mishchenko, L. D. Travis, and D. W. Mackowski. T-matrix computations of light scattering by nonspherical particles: A review. *J. Quant. Spectrosc. Radiat. Transfer*, 55:535–575, 1996.

[11] B. Peterson and S. Ström. T matrix formulation of acoustic scattering from an arbitrary number of scatterers and representations of E(3). *Physical Review D*, 41:3661–3678, 1973.

[12] P. C. Waterman. Matrix formulation of electromagnetic scattering. *Proc. IEEE*, 53:805–812, 1965.

A MULTIGRID ALGORITHM FOR THE ACOUSTIC SINGLE LAYER EQUATION

S. Gemmrich[†,*], **J. Gopalakrishnan**[‡], **N. Nigam**[†]
[†]Dept. of Mathematics and Statistics, McGill University, Montréal Canada.
[‡] Dept. of Mathematics, University of Florida, Gainesville Florida.
[*]Email: gemmrich@math.mcgill.ca

Abstract

In this paper, we present a multigrid algorithm for integral equations of the first kind arising in acoustic scattering, and present some numerical results. Our method combines the ideas of [1] and [2] and is suitable to study scattering from obstacles or screens. The multigrid strategy works well both as a solution strategy, and as a preconditioner.

Introduction

Boundary integral equations, and their numerical approximations, form a popular framework for studying the scattering of time-harmonic waves from bounded obstacles. When studying such scattering problems, one is lead naturally to the Helmholtz equation as a PDE model in the exterior of the scatterer, with appropriate growth conditions on the scattered field. A reformulation in terms of integral equations on the surface of the scattering object may be achieved by a layer ansatz or by a direct method. Depending on the nature of the obstacle, one is then lead to an integral equation of the first or second kind. Our focus in this paper is on integral equations of the first kind. The integral operators involved may be viewed as pseudodifferential operators of order minus one.

Fichera, Hsiao and MacCamy and others have observed some of the advantages of using integral equations of the first kind. For example, these techniques generalize readily to higher-order differential equations. Also, first-kind integral equations seem particularly well-suited to the situation when the scattering object is very thin, or indeed reduces to an arc or a screen.

Boundary integral equations typically lead to dense linear systems upon discretization. Though one needs to mesh on a surface of co-dimension one, the matrix fill-in corresponding to the integral operators is significant. Without some form of preconditioning or acceleration, these methods then become prohibitively expensive. There has been considerable work in this direction in recent years, e.g [6], or the work of Bruno and co-workers. Stephan et. al. developed multilevel algorithms for such equations based on Haar bases, [7]. We present a multigrid strategy for integral equations of the first kind, for acoustics.

The use of multigrid strategies for positive-definite, negative-order pseudodifferential operators was first described in [1]. Since the spectra of these operators link highly oscillatory eigenfunctions to the small magnitude eigenvalues, the use of standard smoothing methods is not appropriate. Key for multigrid methods in this context is the use of weaker Sobolev norms in order to modify the spectral behavior, while avoiding the inversion of the resulting Gram matrix. Discretizations of integral equations for acoustics suffer from similar lack of definiteness as the associated PDE discretizations. Accordingly, we modify the strategy presented in [1] for an indefinite negative-order operator. The analysis of multigrid methods hence require pertubation arguments such as in [2] and [4].

Model problem and notation

Let Γ be a polygonal closed curve in the plane, and let Ω^+ denote its exterior domain. We consider the Dirichlet problem with data $g \in \mathrm{H}^{\frac{1}{2}}(\Gamma)$ and wave-number $\kappa \in \mathbb{R}$:

$$-\Delta u - \kappa^2 u = 0 \text{ in } \Omega^+, \qquad u = g \text{ on } \Gamma \qquad (1)$$

along with the Sommerfeld radiation condition at infinity, $\lim_{r\to\infty} r^{\frac{1}{2}}(\frac{\partial u}{\partial r} - i\kappa u) = 0$. We assume that κ^2 is not an interior eigenvalue for $-\Delta$ in order to guarantee unique solvability.

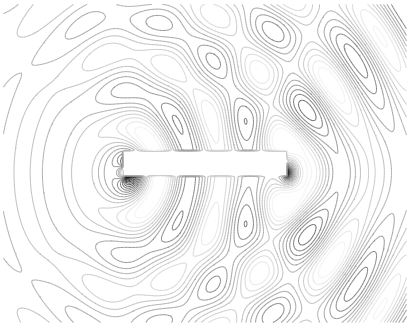

Figure 1: Plane-wave acoustic scattering from a rectangular obstacle. We show $\Re$(scattered wave), computed using a multigrid method for (2).

There are various ways to solve (1) with given boundary data and radiation conditions, in terms of boundary

integral operators. We follow the direct approach which leads to the acoustic single layer equation for the unknown Neumann data $\sigma \in \mathrm{H}^{-\frac{1}{2}}(\Gamma)$:

$$V\,\sigma = (-\frac{1}{2}Id + K)\,g =: F \in \mathrm{H}^{\frac{1}{2}}(\Gamma). \qquad (2)$$

Here, the single layer operator

$$V\sigma(x) = \int_\Gamma \frac{i}{4}\mathrm{H}_0^{(1)}(\kappa|x-y|)\,\sigma(y)ds_y \quad \text{for } x \in \Gamma \quad (3)$$

is to be understood as a weakly singular integral. K is the acoustic double-layer operator. The L^2 duality pairing $\langle \cdot\,,\,\cdot \rangle$ between $H^{\frac{1}{2}}(\Gamma)$ and $H^{-\frac{1}{2}}(\Gamma)$ allows us to state equation (2) in its weak form as follows: *Given* $F \in \mathrm{H}^{\frac{1}{2}}(\Gamma)$, *find* $\sigma \in \mathrm{H}^{-\frac{1}{2}}(\Gamma)$ *such that:*

$$\mathcal{V}(\sigma,\mu) = F(\mu) \quad \text{for all } \mu \in \mathrm{H}^{-\frac{1}{2}}(\Gamma), \qquad (4)$$

where $\mathcal{V} : H^{-1/2}(\Gamma) \times H^{-1/2}(\Gamma) \to \mathbb{C}$ is the continuous sesquilinear form defined by $\mathcal{V}(\sigma,\mu) := \langle V\sigma, \mu\rangle$. Note that V can be decomposed into a sum of operators

$$V\,\sigma = \Lambda\,\sigma + D\,\sigma,$$

where Λ represents the single layer operator corresponding to Laplace's equation and hence (modulo rescaling) is positive definite. The difference operator $D = (V - \Lambda)$ is compact, and has no singularity in its kernel. We denote by $\Lambda(\cdot,\cdot)$ the coercive sesquilinear form induced by Λ.

Methods

Suppose we are given a sequence of finite dimensional approximation spaces $\mathcal{M}_1 \subset \ldots \subset \mathcal{M}_J \subset H^{-1/2}(\Gamma)$. We now review and adopt the multigrid algorithm devised in [1] for the indefinite equation (4). The discrete operators $\mathbf{V_k} : \mathcal{M}_k \to \mathcal{M}_k$ are defined via the relation

$$(\mathbf{V_k}\sigma,\mu)_{-1} = \mathcal{V}(\sigma,\mu) \quad \text{for all } \sigma,\mu \in \mathcal{M}_k.$$

Analogously, we let $\mathbf{f_k} \in \mathcal{M}_k$ satisfy

$$(\mathbf{f_k},\mu)_{-1} = F(\mu) \quad \text{for all } \mu \in \mathcal{M}_k.$$

On every level k we can then write the equation of interest in operator form as $\mathbf{V_k}\,\sigma_k = \mathbf{f_k}$. Further, we introduce the projections $\mathbf{Q_k} : H^{-1}(\Gamma) \to \mathcal{M}_k$ defined by

$$(\mathbf{Q_k}\sigma,\mu)_{-1} = (\sigma,\mu)_{-1} \quad \text{for all } \mu \in \mathcal{M}_k.$$

The smoothing operators $\mathbf{R_k} : \mathcal{M}_k \to \mathcal{M}_k$ are defined in terms of additional discrete inner products $[\cdot\,,\,\cdot]_k$ on $\mathcal{M}_k$. These discrete inner products are defined through certain differencing operators in such a way that they are equivalent to the $(\cdot,\cdot)_{-1}$ inner product uniformly for all levels. A simple Richardson smoother is then given by

$$[\mathbf{R}_k\sigma,\theta]_k = \frac{1}{\bar{\lambda}_k}(\sigma,\theta)_{-1}.$$

Here, $\bar{\lambda}_k$ is an upper bound for the eigenvalue of the definite sesquilinear form $\Lambda(\cdot\,,\,\cdot)$ which corresponds to the principal part of the operator, $\bar{\lambda}_k = \sup_{\theta\in\mathcal{M}_k} \frac{\Lambda(\theta,\theta)}{[\theta,\theta]_k}$. Given an initial guess $\sigma_0 \in \mathcal{M}_J$, Algorithm 1 computes a sequence of approximate solutions to (4) using an iteration of the form

$$\sigma_{i+1} = \mathbf{Mg_J}(\sigma_i, \mathbf{f_J}),$$

where $\mathbf{Mg_J}(\cdot\,,\cdot)$ as a mapping of $\mathcal{M}_J \times \mathcal{M}_J$ into $\mathcal{M}_J$ is defined recursively.

Algorithm 1. *Set* $\mathbf{Mg_1}(\sigma,f) = \mathbf{V_1}^{-1} f$. *If* $k > 1$ *we define* $\mathbf{Mg}_k(\sigma,f)$ *as follows:*

$$\sigma_1 = \sigma + \mathbf{R_k}(f - \mathbf{V_k}\sigma)$$
$$\mathbf{Mg_k}(\sigma,f) = \sigma_1 + \mathbf{Mg_{k-1}}(0, \mathbf{Q_{k-1}}(f - \mathbf{V_k}\sigma_1))$$

The implementation of Algorithm 1 is done in a similar fashion to [3]. Using ideas from [2] and [4], we are able to prove following convergence result for the error reduction operator $E = E_J = \mathbf{Mg}_J(\cdot\,,0)$:

Theorem 1. *There exists an* $H > 0$ *such that whenever* $h_1 \le H$

$$\Lambda(E\theta\,,\,E\theta) \le \delta^2\,\Lambda(\theta\,,\,\theta) \quad \text{for all } \theta \in \mathcal{M}_J$$

with $\delta = \hat{\delta} + ch_1$. *Here,* $0 < \hat{\delta} < 1$ *is an upper bound for the error reduction operator of the definite problem, which is independent of the level* J.

The proof uses standard strategies, and will be presented in a forthcoming work.

Some numerical experiments and results

We now present some numerical experiments demonstrating the effectiveness of the multigrid strategy outlined above. We consider the plane-wave scattering problem from a thin rectangle, whose ratio of side lengths is $\frac{1}{32}$, for wave numbers $\kappa = 2.1$ and 10.2, leading to the discretized linear system $V_h\,\sigma_h = f_h$. We used regular (uniform) meshes to discretize the curve Γ. Tables 1 and 2 show the iteration counts for the multigrid method when

used as a linear solver for two different wave numbers. Iterations were stopped after the relative residual norm had reached the value 10^{-6}, i.e. $||f_h - V_h\sigma_h^i|| < 10^{-6}\,||f_h||$. We also show the iteration counts for the unpreconditioned GMRES needed to achieve the same behaviour in the residual as well as the preconditioned GMRES iterations needed to achieve a relative residual norm of 10^{-6} of the preconditioned system, i.e. $||B_h f_h - B_h V_h \sigma_h^i|| < 10^{-6}\,||B_h f_h||$, where B_h denotes the matrix version of the multigrid preconditioner. We did not restart the GMRES in these experiments.

It is worth drawing attention to the behaviour of the GMRES iteration counts, where we precondition with the multigrid implementation described. For both wave numbers, the iteration counts remain nearly constant over several levels of refinement. More importantly, this number remains independent of wave-number. The effect of the wave number is seen in the choice of coarse-grid size, H.

Table 1: Iteration counts with $\kappa = 2.1$, scattering from a rectangle. Coarsest grid $H = 1/2$. DoF denotes the number of degrees of freedom, MG the no. of multigrid iterations, MG+GMRES the number of GMRES iterations required with multigrid preconditioning

h	DoF	MG	GMRES	MG+GMRES
1/4	72	15	27	7
1/8	144	17	41	9
1/16	288	18	51	9
1/32	576	18	58	10
1/64	1152	19	65	10
1/128	2304	19	70	10

Table 2: Iteration counts with $\kappa = 10.2$, scattering from a rectangle. Coarsest grid $H = 1/8$.

h	DoF	MG	GMRES	MG+GMRES
1/16	288	16	100	7
1/32	576	16	110	9
1/64	1152	17	119	10
1/128	2304	18	127	10

These numerical results establish the effectiveness of the multigrid as both a solver and a preconditioner for the first-kind integral equation for acoustics. Future work includes the extension of this preconditioning strategy to screen problems, and to coupled FEM-BEM systems. For a screen problem one would need to use a graded mesh, or account for the singularities as in [5]. One could still implement the proposed multigrid algorithm, albeit with much more care in the differencing operators used to define the discrete inner products $[\cdot,\cdot]_k$. A careful investigation of this situation is currently under progress.

Acknowledgments

The authors wish to thank Prof. Olaf Steinbach for helpful discussions on this problem. NN's research was partially supported by NSERC and FQRNT. JG acknowledges support from NSF grants 0619080 and 0410030.

References

[1] J.H. Bramble, Z. Leyk and J.E. Pasciak, "The analysis of multigrid algorithms for pseudodifferential operators of order minus one", Math. Comp., 63, pp. 461–478, 1994.

[2] J.H. Bramble, D.Y. Kwak and J.E. Pasciak, "Uniform convergence of multigrid V-cycle iterations for indefinite and nonsymmetric problems", SIAM J. Numer. Anal., 31, pp. 1746–1763, 1994.

[3] S.A. Funken and E.P. Stephan, "The BPX preconditioner for the single layer potential operator", Appl. Anal, 67, pp. 327–340, 1997.

[4] J. Gopalakrishnan, J.E. Pasciak and L.F. Demkowicz,'Analysis of a multigrid algorithm for time harmonic Maxwell equations' SIAM J. Numer. Anal., 42, pp. 90–108 (el.), 2004.

[5] H. Holm, M. Maischak and E.P. Stephan, "The hp-version of the boundary element method for Helmholtz screen problems." Computing 57 (1996), no. 2, 105–134.

[6] M. Maischak, P. Mund and E.P. Stephan, "Adaptive multilevel BEM for acoustic scattering." Comput. Methods Appl. Mech. Engrg. 150 (1997), no. 1-4, 351–367.

[7] E.P. Stephan and T. Tran, "Domain decomposition algorithms for indefinite weakly singular integral equations: the h and p versions." IMA J. Numer. Anal. 20 (2000), no. 1, 1–24.

HYBRID GALERKIN BASES FOR SURFACE ACOUSTIC WAVES DEVICE MODELLING

Carlos F. Jerez-Hanckes[†,‡,◇,*], **Jean-Claude Nédélec**[†], **Vincent Laude**[‡], **Raphael Lardat**[◇]
[†]Centre de Mathématiques Appliquées, École Polytechnique, 91128 Palaiseau, France
[‡]Département LPMO, Institut FEMTO-ST, 25044 Besançon, France
[◇]Temex, Sophia-Antipolis, France
[*]Email: carlos.jerez@polytechnique.edu

Abstract

We present promising results for the three-dimensional modelling of surface acoustic waves (SAW) interdigital (IDT) filters using the boundary element method. We have taken into account the singular behavior of the electrical charges at corners and edges of the electrode-bus system for defining *ad hoc* Galerkin bases used in the associated singular integral equation. Large length-to-width ratio structures are modelled while keeping the number of variables at a practical level. We show results for the non-periodic and periodic electrostatic term under flat massless electrodes.

Introduction

Surface Acoustic Waves (SAW) devices can be found in a plethora of applications: they are ubiquitous in mobile telecommunications, RADAR and SONAR systems, and pervade many novel applications in emerging areas such as non-destructive testing and wireless sensing.

A typical SAW device consists of a piezoelectric anisotropic substrate on top of which sets of interdigital transducers (IDTs) are placed (see Figure 1). Each IDT comprises a large number of electrodes with alternating voltages which, under certain geometric and material conditions, originate mechanical Rayleigh waves. As the wave propagates, chiefly along x_1, a second set of IDT electrically picks up the filtered signal. Acoustic beam focusing is achieved by a large electrode' length-to-width ratio (> 100).

Traditional models for SAW IDTs have avoided dealing with such elongated structures by only considering the sagittal plane ($x_3 = 0$), using a FEM/BEM formulation [1]. However, stringent requirements on miniaturization and power consumption demand for smaller electrodes, and consequently, the neglected transversal effects come into play. In particular, acoustic diffraction and inhomogeneous capacitances at the corners and edges of the metallized areas account for energy losses and poor performance. In what follows, we present a Galerkin approach using hybrid bases to fully model the electrode-bus system which mimic the singular edge-corner behaviors.

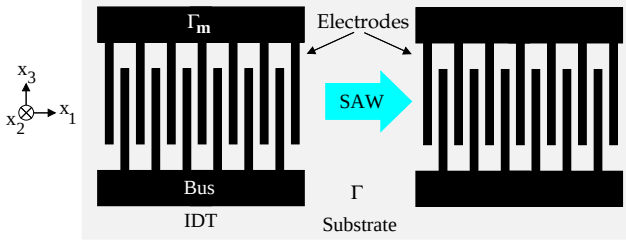

Figure 1: SAW IDT diagram and coordinate definition.

1 Problem statement

Let us decompose $\mathbb{R}^3$ in the following subdomains:

$$\begin{aligned}\mathbb{R}^3_+ &= \{\mathbf{x} \in \mathbb{R}^3 : x_2 > 0\}\\ \mathbb{R}^3_- &= \{\mathbf{x} \in \mathbb{R}^3 : x_2 < 0\}\\ \Gamma &= \{\mathbf{x} \in \mathbb{R}^3 : x_2 = 0\}\end{aligned}$$

with $\Gamma_m \subset \Gamma$ and $\Gamma_{free} = \Gamma \setminus \bar{\Gamma}_m$, being the metallized and metal-free areas, respectively. Let $\mathbb{R}^3_-$ be the vacuum over the device, with constant permittivity ϵ_0, and $\mathbb{R}^3_+$ the anisotropic substrate described by the tensors: C^E_{ijkl}, elasticity for constant electric field; e_{kij}, piezoelectricity; ϵ^S_{ik}, permittivity for constant strain; and ρ, density of piezoelectric material. If we denote $\mathbf{u} \in [H^1_{loc}(\mathbb{R}^3)]^3$ the mechanical displacement and $\phi \in H^1_{loc}(\mathbb{R}^3)$ the electric potential, we can define the stress tensor field and electric displacement vector as:

$$\begin{aligned}T_{ij}(\mathbf{u},\phi) &= \sum_{k=1}^{3}\left[\sum_{l=1}^{3} C^E_{ijkl}\frac{\partial u_l}{\partial x_k} + e_{kij}\frac{\partial \phi}{\partial x_k}\right]\\ D_i(\mathbf{u},\phi) &= \sum_{k=1}^{3}\left[\sum_{l=1}^{3} e_{ikl}\frac{\partial u_l}{\partial x_k} - \epsilon^S_{ik}\frac{\partial \phi}{\partial x_k}\right]\end{aligned}$$

respectively. Neglecting the electrodes, the complete problem can be stated into two separate ones coupled at Γ: (i) a linear anisotropic piezoelectric problem in $\mathbb{R}^3_+$; and (ii) an isotropic electrostatic problem in $\mathbb{R}^3_-$, each under adequate radiation conditions. At Γ, normal stresses are zero and the electric Neumann and Dirichlet traces are continuous.

1.1 *Green's dyad and integral equation for G_{44}*

If a time harmonic dependence $e^{\imath\omega t}$ is assumed, the entire solution is provided by the 4×4 spatial surface Green dyad $\mathsf{G}(\mathbf{x},\mathbf{x}';\omega)$ [2], via the integral representation:

$$(\mathbf{u}(\mathbf{x})\,,\,\phi(\mathbf{x}))^t \;=\; \int_\Gamma \mathsf{G}(\mathbf{x},\mathbf{x}';\omega)\sigma d\Gamma \qquad (3)$$

where $\sigma_i = \mathbf{T}_i(\mathbf{u},\phi)\cdot\mathbf{n}$, $i=1,2,3$, represent the mechanical surface tensions and $\sigma_4 = [\mathbf{D}(\mathbf{u},\phi)+\epsilon_0\nabla\phi]\cdot\mathbf{n}$ the surface electrical charge distribution. We will further assume: a piecewise constant applied potential $\phi_a \in L^\infty(\Gamma_m)$; massless flat electrodes and buses, i.e., $\sigma_i(\Gamma) = 0$, $i=1,2,3$; and no free surface charges, $\sigma_4(\Gamma_{free}) = 0$. Thus, we arrive at the following singular integral equation in σ_4,

$$\phi_a(\mathbf{x}) \;=\; (\mathcal{G}_{44}\sigma_4)(\mathbf{x}) \;=\; \int_{\Gamma_m} G_{44}(\mathbf{x},\mathbf{x}')\sigma_4(\mathbf{x}')d\Gamma \quad (4)$$

provided that σ_4 has zero average. The mechanical displacements u_i can be retrieved by replacing the found σ_4 in the integral representation (3). Let us define the space $H_{av}^{-1/2}(\Gamma_m) = \left\{ f\in H^{-1/2}(\Gamma_m) \,:\, \int_{\Gamma_m} f d\Gamma = 0 \right\}$. With this we solve (4) variationally:
Find $\sigma \in H_{av}^{-1/2}(\Gamma_m)$ such that

$$\mathcal{A}_m(\sigma,\sigma^t) \;=\; \langle \mathcal{G}_{44}\sigma, \sigma^t\rangle_{\Gamma_m} \;=\; \langle \phi_a, \sigma^t\rangle_{\Gamma_m} \qquad (5)$$

for all $\sigma^t \in H_{av}^{-1/2}(\Gamma_m)$. Since the interesting cases arrive for singular part of G_{44}, $G_{44}^s \sim 1/r$, we will concentrate on this term only from now on. If periodic, the singularity also has a logarithm term.

2 Hybrid Galerkin bases and solution method

2.1 *Singularities at corners and edges*

Since Γ_m is a flat non-smooth Lipschitz domain, σ is singular at $\partial\Gamma_m$. Let $\partial\Gamma_m^C$ and $\partial\Gamma_m^E$ denote the set of corners and edges, respectively, in $\partial\Gamma_m$. If r_j is the smallest distance between $\mathbf{x}$ and the elements in the sets $\partial\Gamma_m^j$, $j=E,C$, then the following asymptotics hold [4]:

- As r_E vanishes while $r_C \gg r_E$ is fixed, the singularity order is as $r_E^{-1/2}$.
- If r_C goes to zero, the singularity order depends on the reentrant or salient nature of the corner. In the former case, the singular order is smaller than $1/2$, whereas for the latter, the singularity is greater than $1/2$.

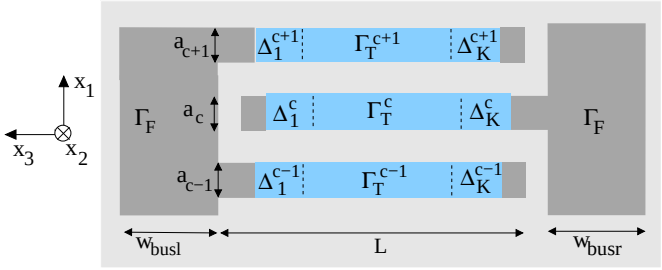

Figure 2: Domain decomposition Γ_T, Γ_F and parameters.

Thus, at corners, the use of cartesian variables as a practical basis is not possible [5]. However, first-order polynomials can yield plausible solutions if the surrounding area is finely meshed. Unluckily, for a typical geometry Γ_m, a standard $\mathbb{P}_1$ basis yields a number of matrix terms ($\sim 10^8$) [3] unbearable for any practical use.

2.2 *Numerical method*

Considering the above, we split Γ_m in two subdomains (see Figure 2):

- Γ_T, which takes most of the electrodes' areas and only presents edge singularities along x_1 for each electrode c. If Γ_T^c is the c-electrode's corner-free area, we can state
$$\Gamma_T = \bigcup_c \Gamma_T^c \quad\text{and}\quad \Gamma_T^c = \bigcup_k \Delta_k^c$$
where Δ_k^c are small rectangles in each Γ_T^c.
- $\Gamma_F = \Gamma_m \setminus \bar{\Gamma}_T$ which accounts for buses and corner areas coming from the bus-electrode joints.

Let the μ_c be the weight function

$$\mu_c(x_1) \;=\; \left[1-\left(\frac{x_1-x_1^c}{a_c}\right)^2\right]^{-1/2} \quad,\; |x_1-x_1^c| < a_c$$

where a_c and x_1^c are the c-electrode's width and center x_1-coordinate. We define the space with weight:

$$Q_{c,N_T}^T = \left\{ f_{N_T} \,:\, \mu_c\tilde{f}_{N_T} = \mu_c \sum_{n=0}^{N_T} d_n T_n\left[\frac{x_1-x_1^c}{a_c}\right]\right\}$$

where T_n is the Tchebychev polynomial of first order [6]. We can approximate σ in Γ_T for each electrode c by the tensorial basis product:

$$\sigma\big|_{\Gamma_T^c} \;\approx\; \sigma_{T^c} \;=\; \sum_k \sigma_T^{ck}\;,\quad \sigma_T^{ck} \in Q_{c,N_T}^T \otimes \mathbb{P}_0 \qquad (6)$$

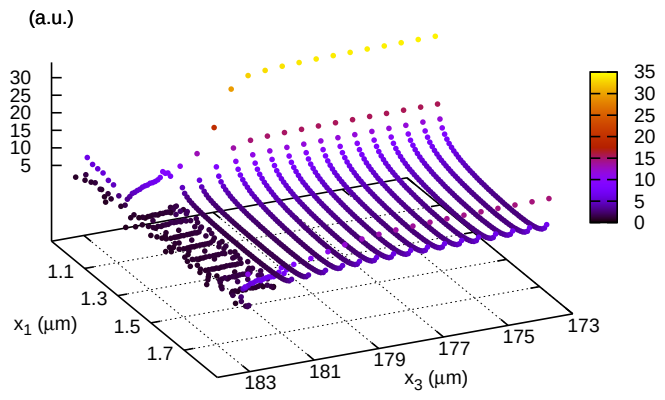

Figure 3: Charge distribution at an electrode-bus joint. Two-electrodes case.

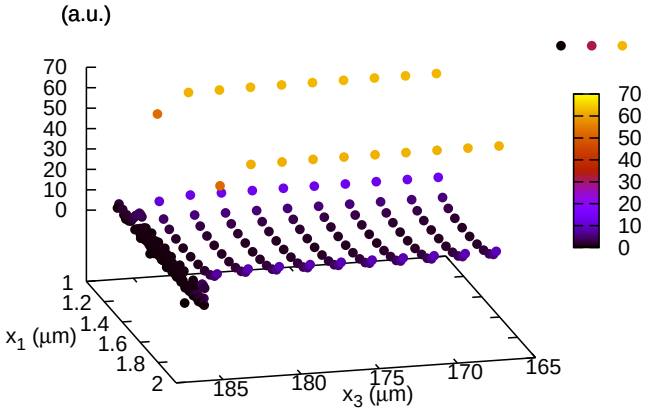

Figure 4: Charge distribution at an electrode-bus joint. Periodic case.

The choice of constant piecewise functions along the electrodes' length is justified by the fact that the edge charges distribute in a regular fashion. Nonetheless, other basis could be equally implemented.

In Γ_F, we approximate σ with classic $\mathbb{P}_1$ polynomials for a triangular mesh Γ_F^h wisely refined at the corners:

$$\sigma\big|_{\Gamma_F} \approx \sigma_F = \sum_{e=1}^{N_F} \sum_{j=1}^{3} \sigma_j^e N_j^e \quad \text{with} \quad N_j^e \in \mathbb{P}_1 \quad (7)$$

where N_F is the total number of elements in Γ_F. A discrete system is built by replacing the test function in (5) by the different elements in the bases (6) and (7). Computation time can be reduced by acknowledging that the resulting matrix is Hermitian and that semi-analytic routines can be used. No matching conditions are required at $\bar{\Gamma}_F \cap \bar{\Gamma}_T$ as they occur naturally. Nonetheless, zero average condition must be enforced.

3 Results

Figure 3 shows the electrode-bus joint for the non-periodic G_{44}^s for an electrode length and width of 80λ and 0.35λ, respectively. It reveals the smooth matching at the frontier between Γ_F and Γ_T. Since the basis over σ_T accurately describes the electrical charges' singular behavior, the number of terms required is very small (~ 3). The lack of symmetry observed in the x_1 direction recovered in Figure 4, where the periodic case is shown. It also reveals continuity along x_1 at the buses.

4 Conclusions

We provide an accurate and practical method for solving the integral representation for the G_{44} behavior of SAW IDTs. Further development includes full piezoelectric representation; optimization of matrix elements computation; and inclusion of mechanical corner and edge singularities.

References

[1] V. Plessky and T. Thorvaldsson, "Periodic green's function analysis of SAW and leaky SAW propagation in a periodic system of electrodes on a piezoelectric crystal," IEEE Trans. on Ultrason. Ferroelect. Freq. Cont., vol. 42, no. 2, pp. 280–293, 1995.

[2] V. Laude, C. Jerez-Hanckes, and S. Ballandras, "Surface Green's function of a piezoelectric halfspace," IEEE Trans. Ultrason., Ferroelec., Freq. Control, vol. 53, no. 2, pp. 420–428, 2006.

[3] C. Jerez-Hanckes, V. Laude, J.-C. Nédélec, and R. Lardat, "3D charge distributions along edges and corners of electrodes in SAW transducers", IEEE Internation Ultrasonics Symposium 2006.

[4] J. Keller, "Singularities at the tip of a plane angular sector," Journal of Mathematical Physics, vol. 40, no. 2, pp. 1087–1092, 1999.

[5] M. Costabel and M. Dauge, "Singularities of electromagnetic fields in polyhedral domains," Archive for Rational Mechanics and Analysis, vol. 151, pp. 221–276, 2000.

[6] J. Ribbe, On the Coupling of Integral Equations and Finite Elements for the Simulation of Piezoelectric Surface Acoustic Wave components. PhD thesis, Centre de Mathématiques Appliquées, École Polytechnique, Palaiseau, 2002.

Inverse Problems and Optimisation

High-order multi-step one-way modeling

C. Baldassari[†,*], **H. Barucq**[†,*], **D. Komatitsch**[‡,*], **N. Le Goff**[†,*], **R. Martin**[‡,*]
[†]Magique-3D Team INRIA Futurs, LMA UMR 5142, Pau University, BP 1155, 64013 Pau, FRANCE
[‡]Magique-3D Team INRIA Futurs, MIGP UMR 5212, Pau University, BP 1155, 64013 Pau, FRANCE.
[*]Email: caroline.baldassari@etud.univ-pau.fr

Abstract

This work concerns numerical aspects of a one-way formulation of the acoustic wave equation. We focus our study on a system of coupled one-way equations which generalizes the multi-step one-way modelling proposed by Kiyashchenko, Plessix and Kashtan. We show how the performance of the numerical method can be improved by developping a fast numerical algorithm whose efficiency is illustrated by some numerical experiments.

Introduction

The Reverse Time Migration (RTM) is an efficient method for depth imaging. RTM is based upon successive solutions of the wave equation and it obviously depends on the accuracy of the numerical solution of the wave equation but also on the computational burden which must be the lowest as possible to be applied to 3D problems in heterogeneous media. The migration process uses sismograms which involve two quantities: the arrival times and the amplitudes of the reflected waves which respectively represent the kinematics and the dynamics of the propagation medium. Solving one-way equations provide a fast solution for the acoustic wave equation which allows one to reproduce the kinematics but the amplitudes of the wave fields are generally erroneous because the one-way model neglects coupling terms modeling the transmission effects between the different materials constituting the propagation medium. Zhang et al. [6] have proposed an approximate formulation including an additional term to correct the amplitude of the solution. More recently, Kiyashchenko et al. [4] have proposed a multi-step one-way modelling which is equivalent to the wave equation. Herein we focus our attention on a first-order formulation which has been derived by M.V. De Hoop [2] in the framework of micro-local analysis.

The complete first-order formulation of the acoustic wave equation

The wave equation can be written as a first-order system of coupled equations after the time variable has been supressed by using a Laplace transform. The principal part of the system can be diagonalized and the reduced system involves then pseudo-differential operators. In practice, the numerical solution is obtained by solving an approximation of the reduced system in which the pseudo-differential operators have been replaced by their principal part. This is the system we consider and describe below.

Let x, y, z be the cartesian coordinates. Let us consider a domain Ω in $z > 0$ whose surface is given by the set $z = 0$. Then the first-order wave equation system reads as:

$$\left(\mathbf{D}_z + i\omega\Lambda\right)\mathbf{V} = R\mathbf{V} + P\mathbf{F} \text{ in } \Omega \tag{1}$$

where Λ is diagonal with $\Lambda = diag(\Gamma, -\Gamma)$ and Γ is a pseudo-differential operator whose symbol γ is given by:

$$\gamma = \left(\frac{1}{c^2\left(\vec{x}\right)} - \frac{\left|\vec{k}'\right|^2}{\omega^2} \right)^{1/2} . \tag{2}$$

Operator R represents the coupling terms describing the reflexion and transmission phenomena and has the form:

$$R = \begin{pmatrix} T & R_{du} \\ R_{ud} & T \end{pmatrix} \tag{3}$$

The vector F is defined from the source S, for instance S is a Ricker function acting at $z = 0$. The unknown $\mathbf{V}$ has two components respectively denoted by V_d and V_u which respectively propagate in the direction $z > 0$ and in the opposite sense. Hence V_d is the downward part of the wave field while V_u is its upward part. The operator P is supposed to be invertible and allows one to construct the solution $\mathbf{U}$ to the wave equation from the relation $\mathbf{V} = P\mathbf{U}$. Moreover, P can be chosen such that $T = -R_{du} = -R_{ud}$. The operator T represents the transmission effects while R_{du} and R_{ud} correspond to the reflections. The transmission operator is defined as the principal part of $-\frac{1}{2}\Gamma^{-1}\frac{\partial T}{\partial z}$ which means that the symbol of T is given by:

$$\sigma\left(T\right) = \frac{\omega^2}{2c^3\gamma^2}\frac{\partial c}{\partial z} \tag{4}$$

The above formula shows that when the medium is homogeneous, T is the null operator since the velocity c does

not vary. Thus in that case, the two components of $\mathbf{V}$ are uncoupled and satisfy a one-way system, involving the square-root of the Helmholtz operator in Γ. In the general case, the two components are coupled through R_{du} and R_{ud} and since the symbol of T is real-valued, T affects the amplitude of each component of $\mathbf{V}$. Hence if T is neglected, the dynamics is erroneous.

Numerical scheme

System 1 can be solved by using different approaches. Here we choose to expand the solution $\mathbf{V}$ as a Neumann series and to compare our method to the one formerly proposed by [4]. Assume that the inverse G of $\mathbf{D}_z + i\omega\Lambda$ is known. Then V is given by:

$$(I - GR)\, V = GF \tag{5}$$

Next the formal inverse of $I - GR$ is represented by a Neumann series and we have:

$$\mathbf{V} = \textstyle\sum_{j\geq 0} \mathbf{V}_j \mathbf{V}_0 = GF \text{ and } \mathbf{V}_j = GR\mathbf{V}_{j-1} \tag{6}$$

The first iterate $\mathbf{V}_0$ is obtained by solving two uncoupled one-way equations and models the propagation of the source F. The iterate $\mathbf{V}_1$ corrects $\mathbf{V}_0$ by accounting for the reflection and transmission terms. It is solution to :

$$(\mathbf{D}_z + i\omega\Lambda)\, \mathbf{V}_1 = R\mathbf{V}_0 \tag{7}$$

and the iterate $\mathbf{V}_j, j \geq 2$ is obtained by solving the same problem as above with $\mathbf{V}_j$ in place of $\mathbf{V}_1$ and $\mathbf{V}_{j-1}$ in place of $\mathbf{V}_0$.

The numerical approximation of $\mathbf{V}$ is defined by computing a finite number of iterates $\mathbf{V}_j$ and according to [5], the performances of the numerical algorithm can be improved by using an assembling process allowing one to compute two iterates in the same time. In [5], both G and R are represented by Fourier integrals and to limit the computational burden, their respective symbol are approximated by a class of functions where k' and (x, y) are separate. Then the number of required Fourier transforms decreases considerably.

In practice, the number of iterates is fixed at the beginning and it is not necessary to compute a lot of terms to obtain a high degree of accuracy.

Here we assume the upward part of $\mathbf{V}_0$ is null which means the region $z < 0$ behaves like the free space. Hence the propagation of the source involves the first one-way equation only. To compute the next terms, it is necessary to solve the two one-way equations after the right-hand side has been computed. Any entry of R is equal to $\pm T$ and T involves $\partial_z \Gamma$. By definition of Γ, we have:

$$\partial_z \Gamma = \frac{\omega^2 \partial_z c}{2c^3} \Gamma^{-1} \tag{8}$$

which implies that T acts like the principal part of

$$\frac{\omega^2 \partial_z c}{2c^3} \Gamma^{-2} \tag{9}$$

We can then observe that T involves the inverse of the Helmholtz equation.

We now compare our approach to the one proposed by Kiyashchenko *et al.* [4] for solving the scalar wave equation. To get the same type of numerical scheme, it is necessary to include the diagonal entries of R into the system of one-way equations and thus, the left-hand side of the system involves the extra terms of R only. We then get the same type of numerical scheme than in [4] by changing Γ into the identity and T by its Padé approximation at high-frequency. To replace Γ by the identity amounts to consider the simplest high-frequency approximation. Hence we can say that the numerical scheme in [4] corresponds to a high-frequency approximation of our scheme. Moreover, the solution computed in [4] corresponds to the sum of $\mathbf{V}_0$ and $\mathbf{V}_1$ only while we can consider high-order terms which do not require a high computational cost by using the assembling process suggested in [5]. This is why we claim that we generalize the approach in [4].

Illustrations

In that section, we intend to illustrate the performance of our numerical scheme by considering a synthetic 2D velocity model, the so-called GXT model. We represent the arrival times and we compare our results with the ones obtained by a finite element method. We use the SPECFEM2D software.

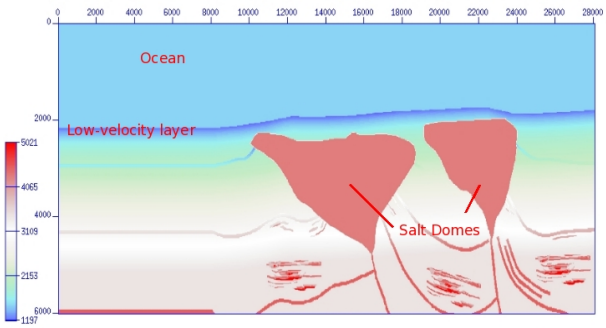

Figure 1: Velocity model GXT

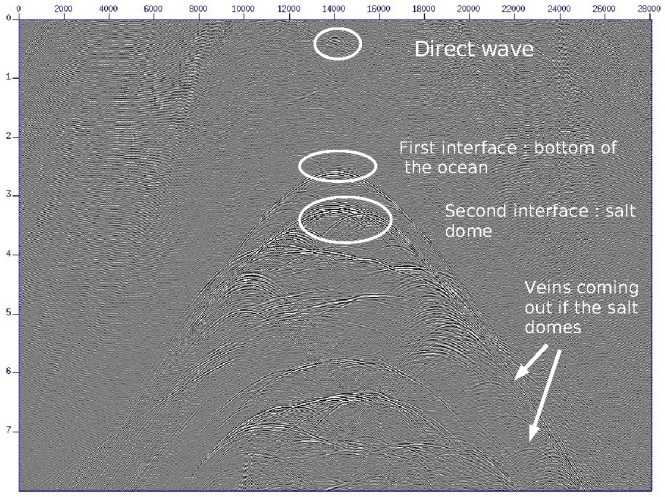

Figure 2: Sismogram obtained with the multi-step one-way system

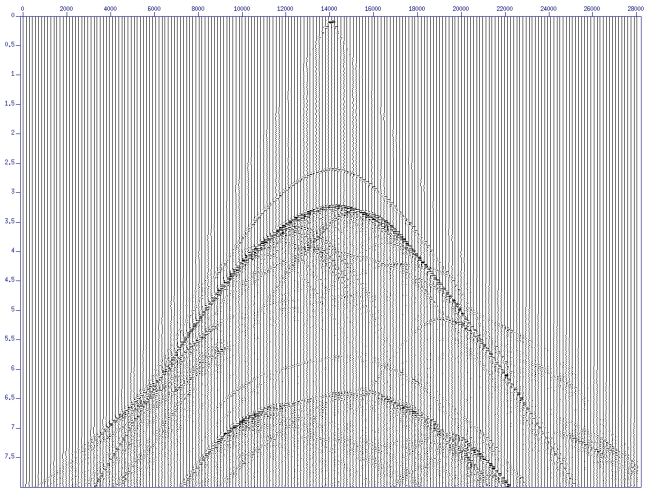

Figure 3: Sismogram obtained with the specfem2D software

The model is composed of a top layer with relatively low-velocity (water), a low-velocity layer (bottom of the ocean), and two salt domes. There is a velocity gradient, increasing as it goes deeper. The model is 28 x 6 kilometers, the source time function is a Ricker centered at 30 Hz, located at the middle of the top of the model, and the receivers, located along the top of the model, recorded 8 seconds. We focus our attention on the kinematics because we intend to apply migrations techniques. We can then observe that the sismograms are in good agreement and that the main interfaces such as the bottom of the ocean, and the first salt dome can be identified.

The next step of investigation concerns the application of migration techniques based on our solver for the wave equation. At present time, we are considering different methods which will be presented and compared to complete this work.

References

[1] H. Barucq, B. Duquet, F. Prat, "'True-amplitude formulation of a one-way model for seismic imaging"', submitted

[2] M.V. De Hoop, "Generalizing of the Bremmer coupling series", J. Math. Phys., vol. 37, pp. 3246-3282, 1996.

[3] H. Bremmer, "The W.K.B. approximation as the first term of a geometrical-optical series', Comm. Pure Appl. Math., vol. 4, pp. 105-115, 1951.

[4] D. Kiyashchenko, R.E. Plessix, B. Kashtan, "'Improved amplitude multi-step one-way modelling"', EAGE 66th Conference and Exhibition, Paris, France, 2004.

[5] F. Prat, "'Analyse du Generalized Screen Propagator"', Ph.D. Thesis, University of Pau, 2005, in french.

[6] Yu. Zhang, G. Zhang, N. Bleistein, Wave equation migration arising from true amplitude one-way equations, Inverse Problems, 19, 1113-1138, 2005

RCS ASSESSMENT IN THE LOW FREQUENCY DOMAIN

A. Cognault, F. Collino, S. Morvan, O. Vacus[†,*]
[†]CESTA, CEA, 33114 Le Barp, FRANCE
[*]Email: olivier.vacus@cea.fr

Abstract

Radar Cross Section (RCS) measurements cannot be entirely and accurately obtained because of experimental constraints in the low frequency domain. Since it is easy to make accurate computations in this frequency bandwidth, the aim of this paper is to present a filtering method based on a decomposition of the computed Perturbation Operator: the Characteristic Current Decomposition. This approach allows to project the RCS measurements onto a basis particularly suited to the target under test, allowing thus to optimally filter unwanted contributions affecting the measurements.

Introduction

Radar Cross Section (RCS) is a description of how an object reflects an incident electromagnetic wave. Quantitatively, RCS is the effective surface area that intercepts the incident wave and isotropically scatters the energy.

The RCS σ of an arbitrary object of size L is highly dependent on several parameters: frequency f (or wavelength $\lambda = c/f$, where c is the speed of light), incident angles (θ_i, ϕ_i), polarization p_i of the incident wave, observation angles (θ_s, ϕ_s) and polarization p_s of the scattered wave: $\sigma(f, \theta_i, \phi_i, \theta_s, \phi_s, p_s)$.

In this paper, we focus on RCS in the low frequency domain.
On the one hand, when $L \leq \lambda$, the measured RCS σ^{meas} is often an unsatisfactory approximation of σ:

- The RCS cannot be accurately measured: the illumination is not plane, the anechoic chamber is too small, the absorbers are not efficient enough;
- The RCS cannot be entirely measured on the whole unit sphere: only a few data are reachable.

On the other hand, the computed RCS σ^{num} is always available with a good precision because numerical systems to be inverted are of limited size.

As illustrated in [1] or [2], the Characteristic Current Decomposition (CCD) gives a relevant model of σ^{th} through σ_n^{th} modes : $\sigma^{th} = \sum_{n=1}^{\infty} a_n \sigma_n^{th}$.
An interesting issue is to find a way to improve the quality of RCS measurements σ^{meas} by using the CCD theory. More than that, this theory gives tools allowing to extrapolate accurately the few measured data.

EM scattering and Perturbation Operator

Let $\mathcal{O}$ be an open bounded subset of $\mathbb{R}^3$ with regular boundary Γ, and $\Omega = \mathbb{R}^3 \backslash \overline{\mathcal{O}}$ its exterior unbounded domain. The obstacle $\mathcal{O}$ is assumed to be Perfectly Electrically Conducting (PEC), and the surrounding medium (i.e. Ω) to be the vacuum. We denote by k the wavenumber of the wave and by Z_0 the vacuum impedance.

Let $\hat{s}$ be some direction of the unit sphere Σ and p some polarization vector. The incident plane wave of direction $\hat{s}$ and polarization p is $(E^i(x; \hat{s}, p), H^i(x; \hat{s}, p))$.
We denote by (E, H) the elementary fields solution to the harmonic Maxwell equations, and (E^∞, H^∞) the associated far field patterns. It is known, [3], that e.g. for E^∞:

$$E^\infty(\hat{x}; \hat{s}, p) = \frac{ikZ_0}{4\pi} \hat{x} \times \int_\Gamma (J \times \hat{x}) e^{-iky \cdot \hat{x}} ds \quad (1)$$

where $J(y; \hat{s}, p) = \nu(y) \times H(y; \hat{s}, p)$ is the electric current on Γ.

We introduce the space of tangential fields on the sphere Σ whose squared modulus is integrable:

$$T^2(\Sigma) = \left\{ g : \Sigma \to \mathbf{C}^3;\ g \in L^2(\Sigma),\ g(\hat{s}) \cdot \hat{s} = 0 \right\}$$

with g a vector field on Σ. In this space, we have :

$$E^\infty(x; \hat{s}, p) = \int_\Sigma E^\infty(x; \hat{s}, g(\hat{s})) d\sigma$$

Let us now introduce the Perturbation Operator (PO):

$$\begin{aligned} F : T^2(\Sigma) &\longrightarrow T^2(\Sigma) \\ g \qquad &\longmapsto Fg(\hat{x}) = \int_\Sigma E^\infty(\hat{x}; \hat{s}, g(\hat{s})) d\sigma \end{aligned}$$

It is important to notice that since F is intimately related to the Scattering Operator S by the relation $S = I + 2F$ [1], it contains the whole information on the RCS σ.
It is shown in the Colton Kress's monograph, [3], that F is an injective compact operator with dense range if and only if k is not a resonant wavenumber for the interior problem. Besides, the F operator is normal and such that:

$$F^* F = F F^* = -\frac{1}{2}(F + F^*). \quad (2)$$

The weak form of the Electromagnetic Field Integral Equation (EFIE) is: for all test current $J^t(x)$, find $J(x)$ such that $\left(E_i, \overline{J^t}\right)_\Gamma = iz(J, J^t)$ where

$$z(J, J^t) = Z_0 \int_\Gamma \int_\Gamma G \left(kJ \cdot \overline{J^t} - \frac{1}{k} \nabla J \nabla \overline{J^t} \right) dxdy$$

Let Z be the linear operator associated to the bilinear form z defined above; for all real non negative s, Z is shown to be an isomorphism between the spaces $H^s(\mathrm{Div})$ and $H^s(\mathrm{Rot})$ when k is not a resonant wavenumber, [4]. The special case $s = -\frac{1}{2}$ is interesting since V', the dual of $V = H^{-\frac{1}{2}}(\mathrm{Div})$, can be identified with $H^{-\frac{1}{2}}(\mathrm{Rot})$, [5]. In that case, z extends to a bilinear continuous form in $V \times V$ and Z is linear continuous onto V', [6]:
$Z : V \longrightarrow V'$ and $< ZJ, J' >= z(J, J')$ for all $J' \in V$.

Let A^∞ be the Bistatic Far Field Operator and $(A^\infty)^\star$ its adjoint. The equation relating J to g is:
$iZJ = \frac{1}{Z_0} (A^\infty)^\star g$, whence the Perturbation Operator reads : $Fg = A^\infty J = -iA^\infty (Z_0 Z)^{-1} (A^\infty)^\star g$.

Let us introduce the hermitian splitting of the operator Z: $< ZJ, J^t >=< Z_r J, J^t > + i < Z_i J, J^t >$.

Let z_r and z_i be the bilinear form associated respectively to Z_r and Z_i. We have, [7]:

$$z_i(J, J^t) = \frac{1}{Z_0} \int_\Sigma A^\infty(J)(\hat{s}) \cdot \overline{A^\infty(J^t)(\hat{s})} d\sigma$$

that is: $Z_0 Z_i = (A^\infty)^\star A^\infty$, and consequently:

$$Fg = -iA^\infty \left(Z_0 Z_r + i (A^\infty)^\star A^\infty \right)^{-1} (A^\infty)^\star g \quad (3)$$

Spectral decomposition

We can state the theorem:

Theorem 1 *Assume that k is not a resonant frequency for the interior problem, then there exists a complete family $(e_n)_{n\geq 1}$ of tangential fields orthonormal in $T^2(\Sigma)$ and a sequence of complex numbers $(\lambda_n)_{n\geq 1}$ lying on the circle of radius $\frac{1}{2}$ and center $-\frac{1}{2}$ (see Figure 1) such that*

$$Fe_n = \lambda_n e_n \text{ and } \lim_{n\to\infty} \lambda_n = 0.$$

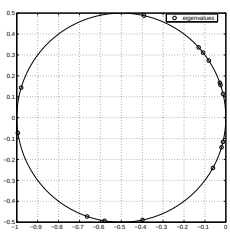

Figure 1: Computed eigenvalues λ_n

The outline of the proof are described below.
Let α be some complex number, we define

$$\begin{aligned} \tilde{F}(\alpha) &= A^\infty \left(Z_0 Z_r + \alpha (A^\infty)^\star A^\infty \right)^{-1} (A^\infty)^\star \\ &:= A^\infty Z_\alpha^{-1} (A^\infty)^\star \end{aligned}$$

so that $F = -i\tilde{F}(i)$.
We introduce D, a discrete subset of the complex plane $D = D(\alpha, k)$, such that Z_α^{-1} exists for all α in $\mathbf{C}\backslash D$. Let us pick some real α outside D, it is proved that $\tilde{F}(\alpha)$ is a compact self adjoint operator, and its spectral decomposition can be used to construct the spectral decomposition of F. Indeed, there is a sequence $(e_n, \lambda_n)_{n\geq 0}$ of pairs of tangential fields in $T^2(\Sigma)$ and real numbers, such that $(e_n)_{n\geq 0}$ forms a complete family of orthonormal vector fields in $T^2(\Sigma)$ and e_n is an eigenvector of $\tilde{F}(\alpha)$ with eigenvalue λ_n, i.e. $\tilde{F}(\alpha)e_n = \lambda_n e_n$. With [1] and [2] we define the characteristic currents $J_n^\alpha = Z_\alpha^{-1} (A^\infty)^\star e_n$, with $J_n^\alpha \in V$, and we check that $A^\infty J_n^\alpha = \lambda_n e_n$.
Let β be a complex number outside D, we obtain:

$$\tilde{F}(\beta)e_n = \frac{1}{\frac{1}{\lambda_n} - \alpha + \beta} e_n.$$

This proves that e_n diagonalizes $\tilde{F}(\beta)$ for all β in $\mathbf{C}\backslash D$. Since complex number i is not in D,we obtain that:

$$Fe_n = \lambda_n e_n.$$

The discrete Perturbation Operator

In this section, we study the discrete Perturbation Operator F_h to get a tractable eigendecomposition.

We start from a mesh $\mathcal{T}_h$ of Γ by some triangular elements (the generic symbol h is related to the size of the elements). Figure 2 shows the mesh of the Nasa-Almond, a generic 3-D object. Raviart Thomas's finite elements space V_h on $\mathcal{T}_h$ to approximate the currents flowing on Γ; space V_h is a finite dimensional approximation subspace of V.Then we substitute V_h for V in the continuous problem. Finally, we need some suitable quadrature rules to evaluate the integrals over Γ.

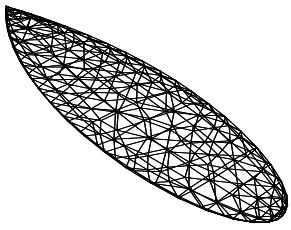

Figure 2: Mesh of the Nasa-Almond

This leads to a discrete Perturbation Operator F_h, that can be assimilated to σ^{num}.

RCS measurements filtering and extrapolation

The main properties of F are still true for its discrete version: F_h is normal so it can be diagonalized in an orthonormal basis: $F_h = \Sigma^{num} D (\Sigma^{num})^*$. Let M be the size of F_h and let us choose $P < M$ so that $[\sigma_1^{num} \cdots \sigma_P^{num}]$ are the first eigenvectors of F_h associated with the P largest eigenvalues. P can be chosen so that $\tilde{\sigma}^{num} = \sum_{n=1}^{P} b_n \sigma_n^{num}$ is a rank P approximation of σ^{num} with a given precision. We denote $[\sigma_1^{num} \cdots \sigma_P^{num}]$ the Signal subspace Si and $[\sigma_{P+1}^{num} \cdots \sigma_M^{num}]$ the Noise subspace N, according to [8].

By projecting σ^{meas} onto Si it is possible to filter the electromagnetic components of the measurements that do not belong to the scattering mechanism of the target, and to get a better measurement of the RCS target. Figure 3 illustrates this filtering process on the Nasa-Almond, where the crosses represent the errors on the raw measurements with respect to the theoretical RCS of the target ($\pm 25\%$, eg $\pm 1 dB$), and the dots show the errors obtained after filtering the measurements ($\pm 10\%$, eg $0.4 dB$).

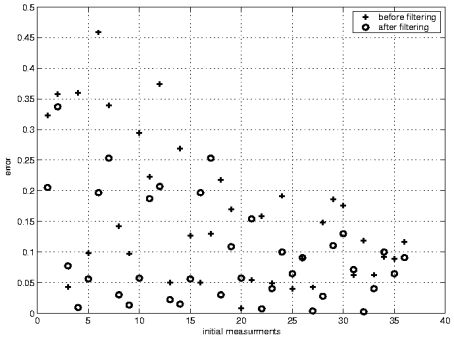

Figure 3: Error before and after filtering

Moreover, we know each σ_n^{num} on the whole unit sphere. So it is possible to extrapolate the measurements out of the measurement range, which is shown on the Figure 4. The crosses are the few true measurement points, the dashed line is the theoretical RCS of the target versus azimuth and the strong line is the extrapolated version of our measurements, which is clearely a very good approximation of σ^{th}.

This section can be summerized with this schema:

$$\begin{array}{ccccc} Si & = & \sigma & \stackrel{?}{\longleftarrow} & \sigma^{th} = \sum_{n=1}^{\infty} a_n \sigma_n^{th} \\ & & \uparrow & & \downarrow \\ Si + N & = & \sigma^{meas} & \longleftarrow & \sigma^{num} = \sum_{n=1}^{M} b_n \sigma_n^{num} \end{array}$$

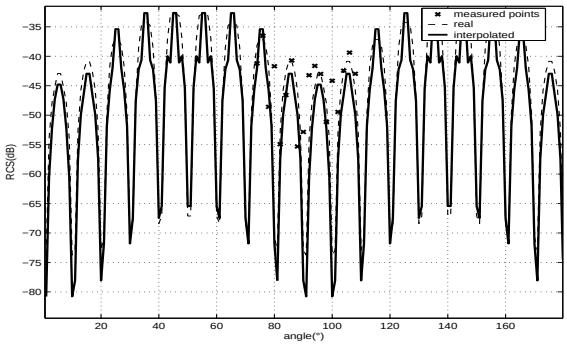

Figure 4: RCS Measurements and Interpolation

with $Si = \sum_{n=1}^{P} b_n^{'} \sigma_n^{num}$ and $N = \sum_{n=P+1}^{M} b_n^{'} \sigma_n^{num}$.

References

[1] R.F. Harrington and J.R. Mautz, "Theory of characteristic modes for conducting bodies", IEEE Trans. Antennas and Propag., vol. AP-19, number 5, 1971.

[2] D. Bouche, F. Collino, Y. Morel, O. Vacus, "Characteristic current decomposition and RCS analysis: scattering by conducting bodies", submitted to JCAM, 2006.

[3] D. Colton and R. Kress, Inverse Acoustic and Electromagnetic Scattering Theory, Applied Mathematical Sciences, vol. 93, Springer-Verlag, 1992.

[4] J.C. Nédelec, Acoustic and Electromagnetic Equations: Integral Representations for Harmonic Problems, Applied Mathematical Sciences, Springer-Verlag, Berlin, 2001.

[5] L. Paquet, "Problèmes mixtes pour le système de Maxwell", Anal. Fac. Sci. Toulouse Math, vol. 5, number 4, pp. 103-141, 1982.

[6] G.C. Hsiao and R.F. Kleinman, "Mathematical foundations for error estimations in numerical solutions of integral equations in electromagnetism", IEEE Trans. Antennas and Propag., vol. 45, number 3, pp. 316-328, 1997.

[7] F. Collino and B. Despres, "Integral Equation via saddle point problems for time-harmonic Maxwell's Equations", J. of Comput. and App. Math., vol. 150, pp. 157-192, 2003.

[8] Y. Morel, S. Morvan, O. Vacus,"Music 3D Bistatic High-Resolution Imaging: a Theoretical Point of View", AMTA 2005.

REDUCED BASIS OUTPUT BOUNDS FOR HARMONIC WAVE PROPAGATION PROBLEMS

Jan S. Hesthaven[1], **Yvon Maday**[1,2] **and Jerónimo Rodríguez**[3]

[1]Division of Applied Mathematics, Brown University, 182 George Street, Providence, RI 02912, USA
[2]Laboratoire Jacques-Louis Lions, UMR 7598, Université Paris6, B.C. 187, Paris, F-75005, France
[3]Laboratoire POEMS, UMR 2706, 32, Boulevard Victor, 75739, Paris, Cedex 15, France

jan_hesthaven@brown.edu
maday@ann.jussieu.fr
jeronimo.rodriguez@ensta.fr

1 Abstract

We combine a Galerkin approach with a reduced basis method for the evaluation of outputs of interest implicitly depending on a given input via the resolution of a PDE issue from a harmonic wave propagation problem. The main features of the method are: i) rapid convergence on the entire set of parameters, ii) a posteriori error estimators for the output and iii) an off-line (parameter independent) on-line (very fast) computational strategy. In the present paper we allow the use of different approximation spaces for solving the primal and dual *truth approximation* problems reducing the off-line computational effort.

2 Introduction

We are interested on the *rapid*, *accurate* and *reliable* resolution of the following problem [1]

$$\left|\begin{array}{l} \text{For an input } \mu \in \mathcal{D} \in \mathbb{R}^p \text{ evaluate the output} \\ \qquad s^e(\mu) := l(u^e(\mu)) \in \mathbb{C}, \\ \text{where } u^e(\mu) \in X^e \text{ is the solution of the PDE} \\ \qquad a(u^e(\mu), v; \mu) \;\; = \;\; f(v), \quad \forall v \in X^e. \end{array}\right. \tag{1}$$

Note that the output can be also obtained by adjoint techniques: if $\psi^e(\mu) \in X^e$ is the solution of the dual problem

$$a(\phi, \psi^e(\mu); \mu) \;\; = \;\; l(\phi), \quad \forall \phi \in X^e, \tag{2}$$

then $s^e(\mu) = f(\psi^e(\mu))$. This kind of problem often arises from applications related to optimization, control and material design. Examples of this implicit relation between the output and the input through the resolution of a PDE can be found in many situations: i) the *radar cross section* for an incident plane wave with a given *wave vector* in the case of a scattering problem by an object, ii) the *electromagnetic energy* on a region for some specific *properties* or *shape* of a component,...

The approach we follow is based on the *reduced basis method*. This method recognizes that the parameter dependent solution $u^e(\mu)$ is not some arbitrary member of the space X, but it *evolves* on a much lower-dimensional manifold induced by the μ-dependence. In this way, we might expect that, in many instances, there exist coefficients $c_i^N(\mu)$ such that the finite sum $\sum_{i=1}^N c_i^N(\mu) u^e(\mu_i)$ is very close to $u^e(\mu)$ for any $\mu \in \mathcal{D}$ for some well chosen parameters $\mu_i \in \mathcal{D}$.

The reduced basis method has been introduced in the 70's for nonlinear structural analysis [1]. More recently, [3], [5], [2] the method has been improved and extended to many other applications including the treatment of elliptic, parabolic and (in more recent works) non-coercive PDE's and nonlinear problems.

In the present work, the reduced basis approach is used for the evaluation of outputs related to the harmonic Maxwell's equations under parameter variations. We give the possibility of approximating problems (1) and (2) with different Galerkin spaces well adapted to each problem reducing the computational effort of the method. The feasibility and efficiency of the method will be shown during the presentation through several numerical experiments.

3 Presentation of the method

The method we apply combines a Galerkin approximation of the problems (1) and (2) (providing the accuracy) and a reduced basis approach to drastically reduce the dimension of the approximation spaces (giving the efficiency). The reliability is obtained via the construction of a posteriori error estimators.

3.1 The truth approximation

Let X^p (resp. X^d) be an approximation space well adapted to the primal problem (1) (resp. to the dual problem (2)) and let X^{pd} be a third approximation space satisfying $X^p \subset X^{pd}$, $X^d \subset X^{pd}$. We assume that $f(\cdot)$ and $l(\cdot)$ are continuous linear forms and that $a(\cdot, \cdot; \mu)$ is a bilinear form, continuous uniformly on $\mu \in \mathcal{D}$ satisfying

[1]The script "e" stands for *exact*. It will disappear on the next section once we've discretized the equations.

$\forall\, \mu \in \mathcal{D},\ m \in \{p, pd\},\ n \in \{d, pd\},$

$$\begin{aligned} 0 < \beta_0^{p,m} \le \beta^{p,m}(\mu) &:= \inf_{v \in X^m} \sup_{w \in X^m} \frac{a(v, w; \mu)}{\|v\|\, \|w\|}, \\ 0 < \beta_0^{d,n} \le \beta^{d,n}(\mu) &:= \inf_{\phi \in X^n} \sup_{\eta \in X^n} \frac{a(\eta, \phi; \mu)}{\|\eta\|\, \|\phi\|}. \end{aligned} \tag{3}$$

We introduce the approximate primal and dual problems

$$\left| \begin{array}{l} \text{Find } u^l(\mu) \in X^l \text{ such that } (l \in \{p, pd\}) \\ a(u^l(\mu), v; \mu) \;=\; f(v), \quad \forall\, v \in X^l, \end{array} \right. \tag{4}$$

$$\left| \begin{array}{l} \text{Find } \psi^l(\mu) \in X^l \text{ such that } (l \in \{d, pd\}) \\ a(\phi, \psi^l(\mu); \mu) \;=\; l(\phi), \quad \forall\, \phi \in X^l. \end{array} \right. \tag{5}$$

The approximation of the output is thus computed by the expression

$$s^{pd}(\mu) \;=\; l(u^{pd}(\mu)) \;=\; f(\psi^{pd}(\mu)). \tag{6}$$

We will assume that the approximation spaces have been chosen in such a way that $\forall\, l \in \{p, pd\}, n \in \{d, pd\}$

$$\|u^l - u^e\| \;\le\; \varepsilon, \qquad \|\psi^n - \psi^e\| \;\le\; \varepsilon,\ \forall\, \mu \in \mathcal{D}. \tag{7}$$

The solutions of the problems (4)–(5) and the output given by (6) will be called the *truth approximations* and they will be considered the reference solutions.

3.2 The reduced basis method

We introduce nested sets of samples

$$\left| \begin{array}{l} \mathcal{S}_N^p = \{\mu_i^p \in \mathcal{D},\ 1 \le i \le N\},\ N \le N_{max}, \\ \mathcal{S}_M^d = \{\mu_j^d \in \mathcal{D},\ 1 \le j \le M\},\ M \le M_{max}, \end{array} \right.$$

and associated Lagrangian reduced basis spaces

$$\left| \begin{array}{l} X_N^p = \text{span}\{u^p(\mu_i^p),\ 1 \le i \le N\},\ N \le N_{max}, \\ X_M^d = \text{span}\{\psi^d(\mu_j^d),\ 1 \le j \le M\},\ M \le M_{max}. \end{array} \right.$$

Solving the primal and dual reduced basis problems

$$\left| \begin{array}{l} \text{Find } u_N(\mu) \in X_N^p \text{ such that} \\ a(u_N(\mu), v; \mu) \;=\; f(v), \quad \forall\, v \in X_N^p, \end{array} \right. \tag{8}$$

$$\left| \begin{array}{l} \text{Find } \psi_M(\mu) \in X_M^d \text{ such that} \\ a(\phi, \psi_M(\mu); \mu) \;=\; l(\phi), \quad \forall\, \phi \in X_M^d, \end{array} \right. \tag{9}$$

we define the reduced basis approximation of the output by [4]

$$s_{N,M} \;=\; l(u_N) - a(u_N, \psi_M) + f(\psi_M). \tag{10}$$

where the dependence on μ has been omitted. We observe numerically that

$$|s^{pd}(\mu) - s_{N,M}(\mu)| \approx e^{-\alpha N - \beta M}, \quad \alpha, \beta > 0, \tag{11}$$

which implies, in general, that N and M can be taken very small.

4 The affine assumption: An off-line on-line computational strategy

Our ultimate goal is to build a method whose computational cost for the evaluation of the output is independent on $\dim X^m,\ m \in \{p, d, pd\}$ (only depending on N and M). Unfortunately, this is not possible in general. When the bilinear functional satisfies the so-called *affine assumption* (a variable separation property)

$$a(u, v; \mu) = \sum_{q=1}^{Q_a} \Theta_q(\mu)\, a_q(u, v), \tag{12}$$

we can apply an off-line on-line computational strategy: the off-line part is μ independent and can be thus done once and for all; the on-line part has a computational cost independent on $\dim X^m$ (see [5] for further details). A technique recovering this efficient off-line on-line strategy in presence of nonaffine parameter dependence has been introduced in [2].

5 The reliability: A posteriori estimators

On this section we provide *a posteriori error estimators* that certify the reduced basis approximation with respect to the truth approximation. This will allow us to determine whether the reduced basis is chosen appropriately, i.e., with enough elements in the basis to represent the solution adequately without overresolving at too high computational cost. Under the assumption (12) this estimators can be computed following a strategy such that the computational cost of the μ-dependent (on-line) part will only depend on N, M and Q_a, being thus very fast.

5.1 Some assumptions and notation

We define the residuals for the primal and dual problems by

$$\left| \begin{array}{rcl} R_N^p(v; \mu) &=& f(v) - a(u_N(\mu), v; \mu), \quad \forall\, v \in X^{pd}, \\ R_M^d(\phi; \mu) &=& l(\phi) - a(\phi, \psi_M(\mu); \mu), \quad \forall\, \phi \in X^{pd}, \end{array} \right.$$

and for $(n, L) \in \{(p, N), (d, M)\}$ we introduce their dual norms on $(X^m)',\ m \in \{p, d, pd\}$

$$\varepsilon_L^{n,m}(\mu) \;:=\; \sup_{v \in X^m} \frac{|R_L^n(v; \mu)|}{\|v\|_{X^m}}. \tag{13}$$

We assume that we can build a *lower bound for the inf-sup parameters* (3) denoted by $\overline{\beta}^{p,m}(\mu),\ m \in \{p, pd\}$ and $\overline{\beta}^{d,m}(\mu),\ m \in \{d, pd\}$ such that

$$\left| \begin{array}{rcccl} 0 &<& \overline{\beta}_0^{p,m} &\le& \overline{\beta}^{p,m}(\mu) \;\le\; \beta^{p,m}(\mu), \quad \forall\, \mu \in \mathcal{D}, \\ 0 &<& \overline{\beta}_0^{d,m} &\le& \overline{\beta}^{d,m}(\mu) \;\le\; \beta^{d,m}(\mu), \quad \forall\, \mu \in \mathcal{D}, \end{array} \right.$$

with a (low) on-line computational cost independent on the dimX^m (see [5] for its construction).

5.2 Estimators for the primal and dual solutions

Defining the primal estimator by

$$\Delta_N^p(\mu) := \frac{\varepsilon_N^{p,p}(\mu)}{\overline{\beta}^{p,p}(\mu)}, \tag{14}$$

one can easily show that

$$1 \quad \leq \quad \frac{\Delta_N^p(\mu)}{\|u_N(\mu) - u^p(\mu)\|} \quad \leq \quad \frac{\gamma(\mu)}{\overline{\beta}^{p,p}(\mu)}; \quad \forall\, \mu \in \mathcal{D},$$

where $\gamma(\mu)$ is the continuity constant of the operator $a(\cdot,\cdot;\mu)$. This shows that (14) provides an optimal rigorous upper bound for $\|u_N(\mu) - u^p(\mu)\|$. Similar results for the dual solution can be also obtained.

5.3 Estimators for the reduced basis output

The next theorem allow us to build a posteriori error estimators for the error between $s_{N,M}$ and s:

Theorem 1 *The following inequalities are satisfied*

$$\begin{aligned} |s^{pd} - s_{N,M}| \quad &\leq \quad \frac{\varepsilon_N^{p,pd}(\mu)\, \varepsilon_M^{d,pd}(\mu)}{\overline{\beta}^{p,pd}(\mu)}, \qquad (a) \\ |s^{pd} - s_{N,M}| \quad &\leq \quad \frac{\varepsilon_N^{p,p}(\mu)\, \varepsilon_M^{d,p}(\mu)}{\overline{\beta}^{p,p}(\mu)} \; + \qquad (b) \\ & \qquad \varepsilon_M^{d,pd}(\mu)\, \|u^{pd}(\mu) - u^p(\mu)\|. \end{aligned} \tag{15}$$

The right hand side of (15).(a) can be used as a rigorous upper bound of the error on the output. Note that the off-line computational cost might be rather expensive as it involves the resolution of linear systems (computation of $\varepsilon^{m,pd}(\mu)$) and, mainly, the resolution of eigenvalue problems (construction of $\overline{\beta}^{p,pd}(\mu)$) of size dim$X^{pd}$ (see [5] for further details).

In the application shown in figure 1 related to the 2D harmonic Maxwell's equations under variation of the material coefficients on a part of the domain, we have considered $X^p \neq X^d$ due to the singularities on the primal and the dual truth approximations. In this case dimX^{pd} is slightly larger than dimX^m, $m \in \{p, d\}$. Bounding $\|u^{pd} - u^p\|$ by 2ε (see (7)), the expression on (15).(b) can be also used as an estimator. In this way, the off-line computational effort is reduced as the eigenvalue problems needed for the construction of $\overline{\beta}^{p,p}(\mu))$ are set on the space X^p.

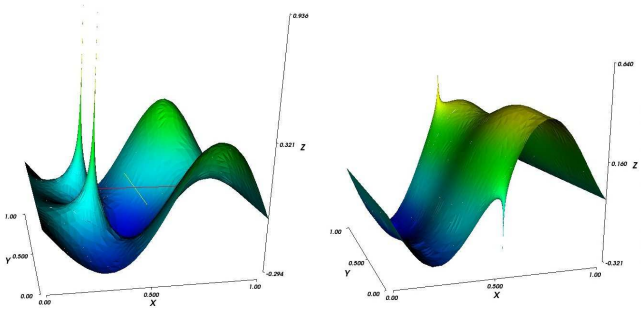

Figure 1: Primal (left) and dual (right) truth approximations for a given μ related to a harmonic 2D Maxwell application.

6 Conclusions

During the presentation we shall discuss the fundamental issues associated to the reduced basis method applied to harmonic Maxwell's equations. More precisely, we will exhibit the problems linked with the parameter variations through resonances (where the inf-sup parameter vanishes) as well as the treatment of non-affine functionals. Some techniques allowing to overcome these difficulties will be presented. Finally we will show some numerical experiments illustrating the performance of the approach.

References

[1] B.O. Almroth, P. Stern, and F.A. Brogan. Automatic choice of global shape functions in structural analysis. *AIAA Journal*, 16:525–528, May 1978.

[2] M. Barrault, N. C. Nguyen, Y. Maday, and A.T. Patera. An "empirical interpolation" method: Application to efficient reduced-basis discretization of partial differential equations. *C. R. Acad. Sci. Paris, Série I*, 339:667–672, 2004.

[3] Y. Maday, L. Machiels, A.T. Patera, and D. Rovas. Blackbox reduced-basis output bound methods for shape optimization, 2000.

[4] Niles A. Pierce and Michael B. Giles. Adjoint recovery of superconvergent functionals from PDE approximations. *SIAM Review*, 42(2):247–264, 2000.

[5] K. Veroy, C. Prud'homme, D.V. Rovas, and A.T. Patera. A posteriori error bounds for reduced-basis approximation of parametrized noncoercive and nonlinear elliptic partial differential equations. *AIAA*, 2003.

ELECTROMAGNETIC IMAGING METHODS FOR OBJECTS DETECTION

D. Ia[†,‡,*], **P. Millot**[‡], **X. Ferrieres**[‡], **M. Masmoudi**[†], **N. Maaref**[‡]
[†]Department of Electromagnetic and Radar, ONERA, Toulouse, France.
[‡]Institute of Mathematics of Toulouse, University Paul Sabatier, Toulouse, France.
[*]Email: davuth.ia@gmail.com

Abstract

This paper presents some methods to localize and to characterize buried dielectric objects in applications like tumor detection or through the wall detection of people. Two fast localization approaches using time reversal and the topological gradient methods are given. To estimate dielectric properties of the objects, a Gauss-Newton method is developed. Some numerical examples are given to illustrate these different methods.

Introduction

This work deals with an inverse scattering problem. A set of dielectric objects is buried in a background medium that is not exactly known. Several receiving antennas are located outside the domain which is illuminated by several sources. In this paper we are interested by problems where not only the localization but also the characterization of the dielectric properties of the objects is necessary. We study two kinds of problems in particular : a biological application for the detection of tumors and a security application where we want to detect through the wall people inside a room. For these applications, by using the recorded measured scattered field on some receivers, we first localize the buried objects by using time reversal or topological gradient methods. Next inside the detected areas, by using a Gauss-Newton method, we search the dielectric properties of the objects.

In the first section we give a general mathematical formulation of the inverse problem, in the second section, we present the basic principles and the application of time reversal and topological gradient methods to localize the buried objects. Some examples are given to illustrate these methods. In the third section, we present the Gauss-Newton method used to determine the dielectric properties of the objects. We give then some numerical examples.

Formulation of the inverse problem

Let's consider the electromagnetic problem given by the Maxwell equations :

$$\left\{ \begin{array}{rcl} -\varepsilon \frac{\partial E}{\partial t} + \text{curl } H & = & \sigma E, \\ \mu \frac{\partial H}{\partial t} + \text{curl } E & = & 0, \end{array} \right.$$

where the objects are represented by the dielectric parameters (ε, σ). The boundary conditions at infinity are given by the Sommerfeld condition :

$$\lim_{r \to \infty} \left(\sqrt{\mu} H^s \times \vec{r} - r \sqrt{\varepsilon} E^s \right) = 0.$$

The problem is to find, from the knowledge of the scattered field on the receivers, the buried objects (ε, σ). Figure 1 shows an experimental setting where the object to find is a bottle filled with salted water. Here the receivers are an array of 8 ETSA antennas. The inverse problem can be written as an optimization problem in which the following discretized cost function has to be minimized :

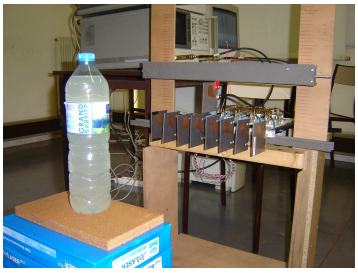

Figure 1: Experimental setting, the target is a salted water filled bottle, a 8 antennas array is used.

$$j(c) = \frac{1}{2} \sum_{t \in [0,T]} \sum_{s \in S} \| L u_c - u^{\text{meas}} \|^2 ,$$

where the unknown $c = (\varepsilon, \sigma)$, L is an operator which maps the field on all the points of the mesh to the measurements points, u_c is the computed field and u^{meas} the measured scattered field on the receivers.

Localization methods

We search for methods whith good localisation accuracy and low computation time. The chosen methods satisfying these constraints are the time reversal method and the topological gradient method. For both methods, the first step of the process can be considered as the localization of the objects.

The time reversal method

The time reversal method has been introduced in acoustics [1], [2]. It uses the reciprocity principle : considering

the field scattered by a set of objects on a surface which encloses them. If the time is reversed and the receivers are used as sources, where the recorded field is transmitted in the inverse sense of the time, the wave will focalize at the objects.

In the electromagnetic problem, the time reversed field $(\tilde{E}(x,t), \tilde{H}(x,t)) = (E(x,-t), H(x,-t))$ satisfies the following equation ;

$$\left\{ \begin{array}{rcl} \varepsilon \frac{\partial \tilde{E}}{\partial t} + \text{curl } \tilde{H} & = & \sigma \tilde{E}, \\ -\mu \frac{\partial \tilde{H}}{\partial t} + \text{curl } \tilde{E} & = & 0, \end{array} \right.$$

In practice, in the measured field on a receiver we have a contribution of the field scattered by the objects and a contribution of the field scattered by the others receivers. The first step consists in separating the field scattered by the objects from the total signal by evaluating fields without objects in the domain. Next, the resulting signal is applied on the receivers and the L^∞-norm is plotted on the domain. The point where the value of the norm is maximum defines the positions of the objects. In the case where we do not have losses in the domain, the time reversed field is equivalent to the solution of the adjoint Maxwell equations.

The topological gradient method

The topological gradient method [4] has been introduced for optimal design problems written as the minimization of a cost function $j(\Omega)$ depending on the domain to optimize. The method was introduced to allow topology changes during the optimization process. The variation of the cost function with respect to the insertion of an infinitesimal dielectric ball is computed as an asymptotic expansion :

$$j(\Omega \backslash \overline{B(x,\varepsilon)}) - j(\Omega) = f(\varepsilon) g(x) + o(f(\varepsilon)),$$

where $g(x)$ can be approached by the real part of the product of the direct state (solution of Maxwell equation) of and the conjugate of the adjoint state (solution of the adjoint Maxwell equation). We plot this function g on all point of Ω and material has to be removed where the cost function go down the most (where the topological gradient is the most negative). The localization problem can be viewed as an optimal design problem in which the final design is domain with the scatterers, it could be formulated as find the best localization of the scatterer to minimize the cost function.

Parameter identification

The Gauss-Newton method is now used in areas found by localization methods. The main difficulty in solving inverse problems is their ill-posedness, a small error on the measurements leads to a huge error on the solution. Then it is important to add information about the solution by using regularization methods[3].

The Gauss-Newton method is commonly used for solving inverse problems. It is based on the Newton method for minimizing the cost function

$$j(c) = \frac{1}{2} \|F(c)\|^2 + \alpha R(c),$$

where F is the difference between the computed field and the measured field on the receivers and $R(c)$ a regularization term. An iterate of the Newton method is written, we are looking for d such that :

$$D^2 j(c_k) d_k = -Dj(c_k),$$

Neglecting the second derivative term, leads to solve the problem :

$$\begin{array}{l} (DF(c_k)^T DF(c_k) + \alpha D^2 R(c)) d = \\ \qquad\qquad - (DF(c_k)^T F(c_k) + \alpha DR(c)), \end{array}$$

and

$$c_{k+1} = c_k + \beta_k d_k,$$

where β_k may be chosen with a line search or trust-region method. The main difficulty of the method is the evaluation of the derivative $DF(c_k)$. Different possibilities exist, for example the evaluation of the adjoint or the use of approximative derivative (Broyden formulas). When we have a very important number of unknowns, because the size of the Jacobian matrix, the adjoint solution with gradient method to evaluate the least-square problem is more appropriate. For the moment, in our case, we consider only homogeneous material and then by using a FDTD approach to evaluate the field, we prefer use a Broyden formula to approximate the derivative. This solution is more interesting in terms of cpu-time.

Numerical experiments

To illustrate the different presented methods, we consider a problem where the receivers are located around the objects to find. We put a source on a side of the domain and by using the field recorded on the receivers, we try to localize the objects and to identify their dielectric properties. The studied source is a 1 to 6 ghz, the domain is a $20cm \times 20cm$ squared domain and the searched default has a size of $1cm$. Figure 2 shows the position of the objects, figure 3 shows the position of the objects obtained by the time reversal method and by the topological

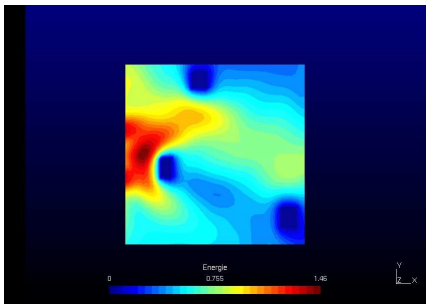

Figure 2: Objects position.

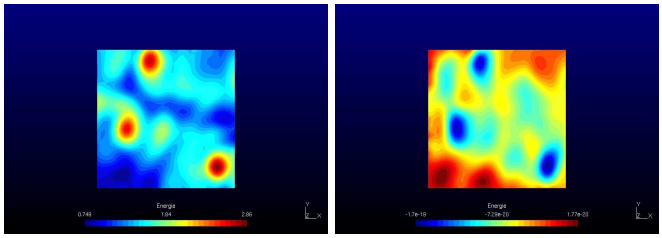

Figure 3: Localization by the time reversal method (left) and by the topological gradient method (right).

gradient. These computations took several minutes on a desktop computer.

To illustrate the Gauss-Newton method used to find dielectric properties when we assume known the localization of the objects, we have computed the field on the receivers for the previous configuration. For this computations we took homogeneous dieletric properties of $(\varepsilon = 40, \sigma = 0)$. Next by using the computed value and by taking the initial guess $(\varepsilon = 1, \sigma = 0)$, after 40 iterations, we retrieved the solution. For this example we didn't take any regularization. Figure 4 and 5 represents the evolution of the cost function and of the solution during the optimization process. This example is not completely demonstrative of the efficiency of the method because of the fact that we have committed the inverse crime. Some other development are currently in progress.

Conclusion

For some applications, the localization but also dielectric value of the target are necessary. In this paper we have presented some localization and characterization methods. We give interesting results. However, the methods are studied separately, their combined use, hasn't been studied yet. This study will be the subject of a future work.

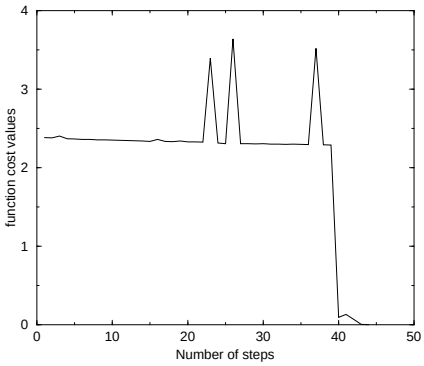

Figure 4: Evolution of the cost function.

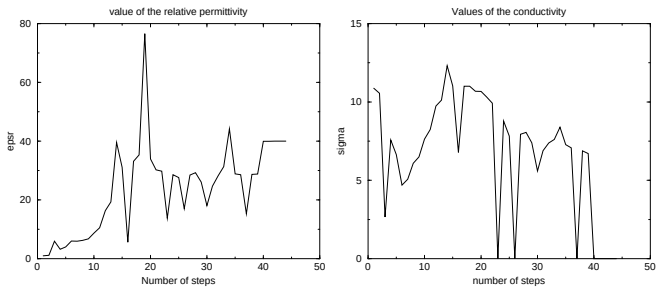

Figure 5: Evolution of the dielectric parameters.

References

[1] M. Fink, "Time reversal of ultrasonic fields part I : basic principles", IEEE Transactions on ultrasonics ferroelectrics and frequency control, vol. 39, pp. 555-566, 1992.

[2] C. Prada, S. Manneville, D. Spoliansky and M. Fink, "Decomposition of the time reversal operator : detection and selective focusing on two scatterers", Journal of acoustical society of America, vol. 99(4), 1996.

[3] Andreas Kirsch, An introduction to the mathematical theory of inverse problems, Springer, 1996.

[4] M. Masmoudi, J. Pommier and B. Samet, "The topological asymptotic expansion for the Maxwell equations and some applications", Inverse problems, vol. 21, pp. 547-564, 2005.

OPTIMAL DESIGN OF THE SUPPORT OF THE CONTROL FOR THE 2D WAVE EQUATION

Arnaud MÜNCH[†,*],
[†]Laboratoire de Mathématiques de Besançon, UMR CNRS 6623, 16, route de Gray, 25030 Besançon, FRANCE
[*]Email: arnaud.munch@univ-fcomte.fr

Abstract

We consider the 2-D wave equation defined on $\Omega \subset \mathbb{R}^2$. Using the HUM method, one may associate to any fixe subset $\omega \subset \Omega$, the control v_ω of minimal $L^2(\omega \times (0,T))$-norm which drives to rest the system at a time $T > 0$ large enough. We address the question of the optimal position of ω which minimize the functional $J : \omega \to ||v_\omega||_{L^2(\omega\times(0,T))}$. Assuming $\omega \in C^1(\Omega)$, we express the shape derivative of J as a curvilinear integral on $\partial\omega \times (0,T)$ independently of any adjoint solution. This expression leads to a descent direction and permits to define a gradient algorithm. The numerical approximation of the problem is discussed and numerical experiments are presented in the framework of the level set approach.

Introduction - Statement problem

Let us consider a Lipschitzian bounded domain $\Omega \subset \mathbb{R}^2$, two functions $(y^0, y^1) \in H_0^1(\Omega) \times L^2(\Omega)$ and a real $T > 0$. In the context of the exact distributed controllability, one may determine a subset ω of positive Lebesgue measure for which the following property holds (see [2], [5]) : there exists a control function $v_\omega \in L^2(\omega \times (0,T))$ such that the unique solution $y \in C([0,T]; H_0^1(\Omega)) \cap C^1([0,T]; L^2(\Omega))$ of

$$\begin{cases} y_{tt} - \Delta y = v_\omega \mathcal{X}_\omega, & \Omega \times (0,T), \\ y = 0, & \partial\Omega \times (0,T), \\ (y(\cdot,0), y_t(\cdot,0)) = (y^0, y^1), & \Omega, \end{cases} \quad (1)$$

satisfies

$$y(.,T) = y_t(.,T) = 0, \quad \text{on} \quad \Omega. \quad (2)$$

We introduce the set

$$V(y^0, y^1, T) = \{\omega \subset \Omega \text{ such that } (2) \text{ holds}\} \quad (3)$$

which contains in particular Ω. Moreover, from [2] assuming $\Omega \in C^\infty$, any subset ω satisfying the geometric control condition in Ω (*Every ray of geometric optics that propagates in Ω and is reflected on its boundary enters ω in time less than T*) belongs to $V(y^0, y^1, T)$. The controllability property may be obtained using the Hilbert Uniqueness Method (HUM) introduced by J.-L. Lions in [5], which reduces the problem to an optimal control one. Precisely, for any $\omega \in V(y^0, y^1, T)$, the unique HUM control v_ω of minimal L^2-norm may be obtained by minimizing the functional $\mathcal{J} : L^2(\Omega) \times H^{-1}(\Omega) \to \mathbb{R}$ defined by

$$\mathcal{J}(\phi^0,\phi^1) = \frac{1}{2}\int_\omega \int_0^T \phi^2 dt dx + < \phi_t(\cdot,0), y^0 >_{H^{-1}(\Omega),H_0^1(\Omega)} - \int_\Omega y^1 \phi(\cdot,0) dx, \quad (4)$$

where ϕ denotes the solution of the adjoint homogeneous system

$$\begin{cases} \phi_{tt} - \Delta\phi = 0, & \Omega \times (0,T), \\ \phi = 0, & \partial\Omega \times (0,T), \\ (\phi(\cdot,T), \phi_t(\cdot,T)) = (\phi^0, \phi^1), & \Omega. \end{cases} \quad (5)$$

This provides the following characterization of the HUM-control (see [5], chapter 7).

THEOREM 0.1 *Given any $(y^0, y^1) \in H_0^1(\Omega) \times L^2(\Omega)$, $T > 0$ and $\omega \in V(y^0, y^1, T)$, the functional $\mathcal{J}$ has a unique minimizer $(\hat\phi_0, \hat\phi_1) \in L^2(\Omega) \times H^{-1}(\Omega)$. If $\hat\phi$ is the corresponding solution of (5) with initial data $(\hat\phi^0, \hat\phi^1)$ then $v = -\hat\phi\mathcal{X}_\omega$ is the control of (1) with minimal L^2-norm.*

Related to the controllability problem (1)-(2), we consider for any $(y^0, y^1) \in H_0^1(\Omega) \times L^2(\Omega)$ and $T > 0$ fixed, the following problem :

$$(\mathcal{P}_\omega) : \inf_{\omega \subset V_L(y^0,y^1,T)} J(\mathcal{X}_\omega) = \frac{1}{2}||v_\omega||^2_{L^2(\omega\times(0,T))}, \quad (6)$$

and $V_L(y^0, y^1, T) = \{\omega \in V(y^0, y^1, T); |\omega| = L|\Omega|\}$ for some $L \in (0,1)$, which consists in finding the optimal location of ω in order to minimize the L^2-norm of the corresponding HUM-control v_ω. Note that this optimal shape design problem may be not well-posed in the sense that there is no solution in the class of characteristic function (we refer to [4] for a description in the static case).

We numerically solve the problem $(\mathcal{P}_\omega)$ and proceed as in [8] where the author considers a damped wave equation and optimizes the position of the damping zone in order

to minimize the energy of the system. Since the control associated to the optimal solution ω is *a fortiori* a HUM control (that is of minimal $L^2(0,T)$ norm), $(\mathcal{P}_\omega)$ is reduced to find the optimal HUM control with respect to ω. In this way, we make use of the explicit characterization of v_ω in term of the solution ϕ of (5). To the knowledge of the author, the problem $(\mathcal{P}_\omega)$ has never been studied so far. In the similar context of the boundary controllability, it is worth to mention the work of Asch-Lebeau [1]. In order to take into account the size restriction, we introduce a positive multiplier λ and then consider the functional $J_\lambda(\mathcal{X}_\omega) = J(\mathcal{X}_\omega) + \lambda(||\mathcal{X}_\omega||_{L^1(\Omega)} - L|\Omega|)$.

Shape and topological derivative of J_λ

In order to solve the problem $(\mathcal{P}_\omega)$ with a gradient descent procedure, let us compute an explicit expression of the derivative of the functional J_λ with respect to smooth variations of ω (the so-called shape derivative). In this respect, we assume that $\omega \in C^1(\Omega)$, Ω being fixed in $\mathbb{R}^2$. Let a vector field $\boldsymbol{\theta} \in (W^{1,\infty}(\Omega,\mathbb{R}^2))^2$, $\boldsymbol{\theta}_{|\partial\Omega} = 0$ and not vanishing on a neighborhood of $\partial\omega$. It is worth to mention that the initial condition (y^0, y^1) is independent of ω and that the field $\boldsymbol{\theta}$ is time independent (since ω is time independent). We refer the reader to [4] for the methodology to compute the shape derivative in the $\boldsymbol{\theta}$-direction.

THEOREM 0.2 *Let $\omega \in V(y^0, y^1, T)$, v_ω the HUM control for (1) and $\boldsymbol{\nu}$ be the unit normal vector oriented toward the exterior of ω. If ω is of class $C^1(\Omega)$ and if $(y^0, y^1) \in (H^2(\Omega) \cap H_0^1(\Omega)) \times H_0^1(\Omega)$, then the derivative of J_λ with respect to ω is given by the following expression :*

$$\frac{\partial J_\lambda(\mathcal{X}_\omega)}{\partial \omega} \cdot \boldsymbol{\theta} = \int_{\partial\omega} \left(-\frac{1}{2} \int_0^T v_\omega^2(\boldsymbol{x}, t) dt + \lambda \right) \boldsymbol{\theta} \cdot \boldsymbol{\nu} \, d\sigma \tag{7}$$

Remark 1

- *The shape derivative (7) is expressed independently of any adjoint solution. This is due to the minimal $L^2(0,T)$-norm property of the HUM control v_ω.*
- *It results from the relation (7) that the inclusion $\omega_1 \subset \omega_2 \subset \Omega$ implies $J_0(\omega_2) \leq J_0(\omega_1)$. In particular, for $\lambda = 0$, the optimal domain is $\omega = \Omega \in V(y^0, y^1, T)$. This justifies the introduction of the subset $V_L(y^0, y^1, T)$ in the formulation of $(\mathcal{P}_\omega)$.*

In a very similar way, one may obtain easily the so-called topological derivative associated to J_λ :

THEOREM 0.3 *For any $\boldsymbol{x_0} \in \Omega$ and ρ such that $D(\boldsymbol{x_0}, \rho) \equiv \{\boldsymbol{x} \in \mathbb{R}^2, dist(\boldsymbol{x}, \boldsymbol{x_0}) \leq \rho\} \subset \Omega$, the functional J_λ associated to $\Omega \backslash D(\boldsymbol{x_0}, \rho)$ may be expressed as follows :*

$$J_\lambda(\mathcal{X}_{\Omega\backslash D(\boldsymbol{x_0},\rho)}) = J_\lambda(\mathcal{X}_\Omega) + \pi\rho^2 \left(\frac{1}{2} \int_0^T v_\Omega^2(\boldsymbol{x_0}, t) dt - \lambda \right) + o(\rho^2) \tag{8}$$

in term only of the HUM control v_Ω associated to (1) with $\omega = \Omega$.

Descent algorithm

Relation (7) permits to build a decreasing sequence $(\omega^{(k)})_{(k\geq 0)}$ of domains in $V_L(y^0, y^1, T)$ for J_λ, efficiently initialized using the relation (8) by $\omega^{(0)} = \{\boldsymbol{x} \in \Omega, \frac{1}{2}\int_0^T v_\Omega^2(\boldsymbol{x}, t) - \lambda > 0\}$ where λ is chosen so that $|\omega| = L|\Omega|$. For $k > 0$, we define $\omega^{(k+1)} = (I + \eta\boldsymbol{\theta^{(k)}})\omega^{(k)}$ with

$$\boldsymbol{\theta^{(k)}}(\boldsymbol{x}) = \left(\frac{1}{2} \int_0^T v_{\omega^{(k)}}^2(\boldsymbol{x}, t) dt - \lambda^{(k)} \right) \boldsymbol{\nu^{(k)}}, \ \forall \boldsymbol{x} \in \Omega \tag{9}$$

and

$$\lambda^{(k)} = \frac{1}{2} \frac{\int_{\omega^{(k)}} div\left(\int_0^T v_{\omega^{(k)}}^2(\boldsymbol{x}, t) dt \, \boldsymbol{\nu^{(k)}} \right) dx}{\int_{\omega^{(k)}} div(\boldsymbol{\nu^{(k)}}) dx}. \tag{10}$$

Remark 2 *If $\omega^{(k)} \in V_L(y^0, y^1, T)$ then $\omega^{(k+1)} \in V_L(y^0, y^1, T)$ because $J(\mathcal{X}_{\omega^{(k+1)}}) \leq J(\mathcal{X}_{\omega^{(k)}}) < +\infty$.*

Uniformly controllable scheme

Since the pioneering work of R. Glowinski in the nineties, the numerical approximation of the HUM control is known to be extremely sensitive with respect to the parameters of approximations (we refer to [10] for a review). Any standard consistant finite element approximation of the wave equation may lead to exponentially divergent approximation v_h of the HUM control v. This non commuting property between exact controllability and numerical approximation is due to the spurious high frequency oscillations generated by discrete dynamics. In order to restore the uniform convergence of the discrete control, it is necessary to bound by below uniformly in h the group velocity of the high frequencies component. Efficient remedies recently introduced in ([3],[7]) consist in considering the finite element approximation of the so-called viscous wave equation

$$(I + \frac{h^2}{4}\partial_x^2)(I + \frac{h^2}{4}\partial_y^2) y_{tt} - \Delta y = v\mathcal{X}_\omega, \quad \Omega \times (0,T), \tag{11}$$

We refer to [6] for convergence analysis using Fourier series

Numerical experiments

We present some numerical experiments on the unit square $\Omega = (0,1)^2$ with the initial position $y^0(\boldsymbol{x}) = \exp^{-100(x_1-0.3)^2-100(x_2-0.3)^2}\,\mathcal{X}_\Omega(\boldsymbol{x})$ concentrated on $(0.3, 0.3)$ and velocity $y^1(\boldsymbol{x}) = 0$. Figures represents the optimal position of the support of the control for $T = 0.5, T = 1$ and $T = 3$ respectively. For fulls details, we refer to [9].

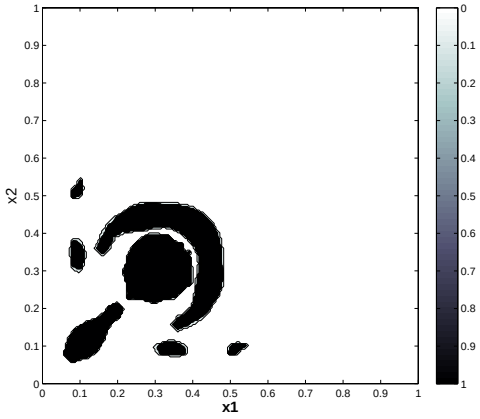

Figure 1: Optimal position (black zone) of the support of the control for $T = 0.5$

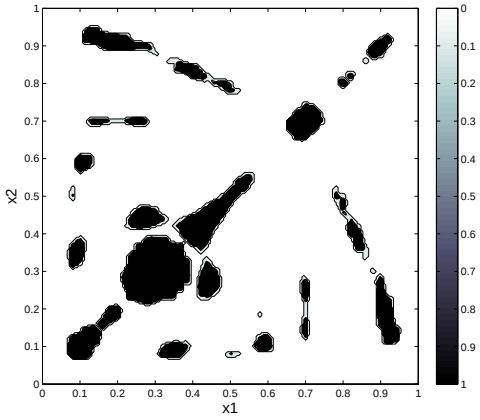

Figure 2: Optimal position for $T = 1$

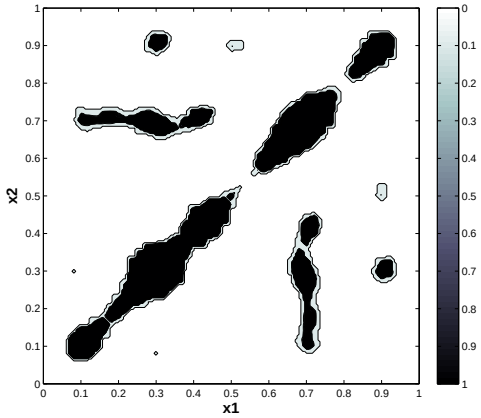

Figure 3: Optimal position for $T = 3$

References

[1] Asch M., Lebeau G., *Geometrical aspects of exact controllability for the wave equation - A numerical study*, Esaim : Cocv, **3**, 163-212 (1998).

[2] Bardos C., Lebeau G., Rauch J., *Sharp sufficient conditions for the observation, control and stabilization from the boundary*, SIAM J. Control and Opt., **30**, 1024-1065 (1992).

[3] Castro C., Micu S., Münch A., *Numerical approximation of the boundary control of the 2-D wave equation with mixed finite elements.*, Submitted to IMA Numerical Analysis.

[4] Delfour M.C., Zolesio J.P., *Shapes and Geometries*, Advances in Design and Control, Siam, (2001).

[5] Lions J.L., *Contrôlabilité exacte, stabilisation et perturbations de systèmes distribués, Tome 1*, Masson, RMA 8, Paris (1988).

[6] Münch A., *A uniformly controllable and implicit scheme for the 1-D wave equation*, Mathematical Modelling and Numerical Analysis **39(2)**, 377-418, (2005).

[7] Münch A., *An implicit scheme uniformly controllable for the 2-D wave equation*, To appear in J. Sci. Comput.

[8] Münch A., Pedregal P., Periago F., *Optimal design of the damping set for the stabilization of the wave equation*, J. Diff. Equations **231**, 331-358, (2006).

[9] Münch A., *Optimal design of the support of the control for the wave equation*, To appear in Int. J. Numer. Math. Model.

[10] Zuazua E., *Propagation, Observation, Control and Numerical Approximation of Waves approximated by finite difference methods*, SIAM Review, **47(2)**, 197-243, (2005).

QUASI INVERSION OF MULTISHOT - MULTIOFFSET SEISMIC DATA ON THE BASE OF GAUSSIAN BEAMS DECOMPOSITION

M. Protasov[†,*], **V. Tcheverda**[†,**]
[†] Tro£muk Institute of Petroleum Geology and Geophysics SB RAS, 3, prosp. Koptyug, 630090, Novosibirsk, Russia
[*]Email: pmi702@uiggm.nsc.ru
[**]Email: chev@uiggm.nsc.ru

Abstract.

The paper is devoted to recovery of local rapid perturbations (scatterers/re¤ectors) of *a priori* known macrovelocity background by means of linearized asymptotic inversion of multi-shot multi-offset seismic data. Inversion procedure is done via application of some speci£c integral transform to input data with respect to source/receiver positions and time frequency. Result of this transform is represented as an asymptotic series with leading term being superposition of some speci£c spatial Fourier constituents of desired local perturbations. Composition of these constituents is totally determined by range of time frequencies and geometry of acquisition system. The approach is tested on Sigsbee2A synthetic data set. Numerical results are presented and discussed.

Introduction.

Inversion procedure presented below is destined for imaging of rapid variations of the earth velocities embedded within background with *a priori* known macrovelocity model. It should be noted that besides necessity to recover proper geometry of these structures it is very important to provide their "true amplitude" imaging. As true amplitude imaging we mean images being free from in¤uence of geometrical spreading produced by macro-velocity background. Currently the most popular approaches for this are based on Kirchhoff method (Kirchhoff migration, Kirchhoff-based inversion). Origin of these approaches can be traced to the paper *Beylkin (1985)*. Their principal limitations are introduced by the use of high-frequency asymptotic entailing assumption that response at point $\vec{r}$ to a point source at $\vec{r}'$ can be represented as

$$G(\vec{r},\vec{r}';\omega) \approx A(\vec{r},\vec{r}')exp\left[i\omega T(\vec{r},\vec{r}')\right] \qquad (1)$$

with frequency-independent traveltime and amplitude. If this assumption is valid there is possible to integral transform (summation weights for discrete statement) providing one with a leading-order, high-frequency asymptotic inversion operator, that is with true amplitude quasi inversion procedure.

Representation (1) is inadequate for descriptions of some exploration seismic re¤ection data, but, besides, there are troubles connected with multivalued nature of travel time $T(\vec{r},\vec{r}')$ because of multipathing of the seismic energy. Retaining all the arrivals is dif£cult to achieve in a practical depth migration implementation, but even if these dif£culties are overcome, there remains the problem with behavior of amplitude function within the area where the traveltimes are multivalued. These troubles could be overcome by Gaussian beam migration *(Hill, 2001)*, when Green's function $G(\vec{r},\vec{r}';\omega)$ is computed by means of Gaussian beams superposition. Global regularity of GB provides a possibility to handle properly all singularities of ray £elds and to get an uniform high frequency approximation of Green's function. But at the moment there are only a few attempts to develop preserving amplitude version of Gaussian beam prestack migration.

Method

Statement

Let us suppose that a medium we are dealing with possesses *a priori* known macrovelocity constituent $c_0(x,z)$ and we are searching for its rapid perturbation $c_1(x,z)$.

Under some reasonable assumptions scattered/re¤ected wave £eld on the free surface (input multishot/multioffset data) can be represented as the following (Born's approximation):

$$\phi(x_r,x_s;\omega) = 2\omega^2 \int\int_X \frac{1}{c_0^2(\xi,\eta)} \cdot$$
$$\cdot\frac{c_1(\xi,\eta)}{c_0(\xi,\eta)} G_0(\xi,\eta;x_s,0;\omega)G_0(x_r,0;\xi,\eta;\omega)d\xi\eta. \qquad (2)$$

Here $(x_r,0)$, $(x_s,0)$ are receiver and source positions respectively and $G_0(\xi,\eta;x,z;\omega)$ - is Green's function for macro-velocity model.

Input data:

$$\phi(x_r,x_s,\omega) = u_{sc}(x_r,0;x_s,0;\omega) : 0<\omega_1\le\omega\le\omega_2;$$

$$X_{0s}\le x_s\le X_{1s}; \quad X_{0r}\le x_r\le X_{1r}. \qquad (3)$$

The problem is to resolve linear integral equation (2) with respect to function $\frac{c_1}{c_0}$ for given macro-velocity model c_0 and seismic data (3).

Asymptotic inversion

Let us £x some interior point $\overline{x} = (x_i, z_i)$ and shoot a couple of Gaussian beams - later referred as left and right (Fig. 1) - towards acquisition system. Twice application of Green's and reciprocity theorems leads to the following integral equation:

$$2\omega^2 \int\limits_X K(\overline{x};\overline{y};\omega)\frac{c_1(\overline{y})}{c_0(\overline{y})}dy =$$

$$= \int\limits_{x_s}\int\limits_{x_r} \tau_s^{(gb)}(x_s;\omega)\tau_r^{(gb)}(x_r;\omega)\phi(x_r;x_s;\omega)dx_s dx_r. \quad (4)$$

The kernel of integral operator in the left-hand side of this equation is product of a couple of mentioned above Gaussian beams:

$$K(y,\overline{x};\alpha,\beta;\omega) = u_s^{(gb)}(y;\overline{x};\alpha,\beta;\omega)u_r^{(gb)}(y;\overline{x};\alpha,\beta;\omega);$$

while integral transform of input multishot/multioffset data is de£ned by the following functions:

$$\tau_{s(r)}^{(gb)}(x_{s(r)};\omega) = \left.\frac{\partial u_{s(r)}^{(gb)}(x_{s(r)},z;\overline{x};x_{0s(0r)};\omega)}{\partial z}\right|_{z=0}.$$

Let us now apply Fourier transform with respect to time frequency ω to both sides of integral equation (4) and compute it for time $t(\overline{x};\alpha,\beta) = \tau_s(\overline{x};\alpha,\beta)+\tau_r(\overline{x};\alpha,\beta)$. Here $\tau_s(\overline{x};\alpha,\beta)$ and $\tau_r(\overline{x};\alpha,\beta)$ are travel-times from $\overline{x}$ to free surface computed for a priori known macrovelocity model along left and right rays respectively. For the next step we apply integration with respect to dip angle α under £xed opening angle β. These transformations lead to the linear integral operator M^β in the left-hand side which can be represented as the series of pseudodifferential ones:

$$M^\beta = T_0^\beta + T_1^\beta + T_2^\beta + T_3^\beta + ...$$

It should be noted that operator T_n^β acts from C^k to C^{k+n}. As we are interested in sharp perturbations of macrovelocity only, we can neglect all terms of this series except of the very £rst one and consider left-hand side as application of the following simple transform to desired perturbation:

$$M^\beta < \frac{c_1}{c_0} > (\overline{x}) \approx T_0^\beta < \frac{c_1}{c_0} > (\overline{x}) = \int\limits_{X_{par}(\overline{x})}\int d\overline{p}\cdot$$

$$\cdot \int\limits_X\int \exp\{i\cdot\overline{p}\cdot\overline{x}\}\exp\{-i\cdot\overline{p}\cdot\overline{y}\}\cdot\frac{c_1(\overline{y})}{c_0(\overline{y})}d\overline{y}. \quad (5)$$

The £rst integration in the right hand side of (5) is performed over domain X_{par} :

$$X_{par}(x_i,z_i) = \left\{ \begin{array}{c} \overline{p} : \omega_1 \le \dfrac{|\overline{p}|c_0(\overline{x})}{2\cos(\beta)} \le \omega_2; \\ \alpha_1 \le \arctan -\frac{p_x}{p_z} \le \alpha_2 \end{array} \right\}.$$

One can easy see that operator T_0^β is superposition of forward and quasi-inverse two-dimensional Fourier transform of the function $\frac{c_1}{c_0}$. We call it *quasiinverse* because it is performed not over the whole spectral space, but over it subspace X_{par} only. That is, we will image properly only constituents of re¤ectors/scatterers which possess spatial spectrum within speci£c set of partial reconstruction (6).

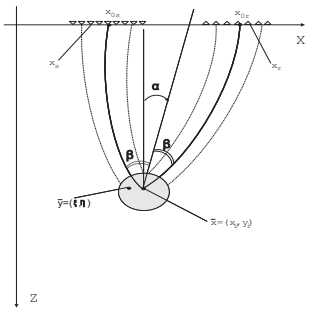

Figure 1: Geometry of true amplitude Gaussian beam imaging.

Numerical examples

Presented above procedure of true amplitude imaging was used on synthetic data set Sigsbee2a calculated by SMAART Joint Venture. The total stratigraphic model is presented on the Fig.2. True amplitude images are presented on the Fig.3 for target area out of salt body and on the Fig.4 for target area under salt intrusion. We would like to pay attention on the quite well recovery of faults for both target areas. One can estimate that intensity of images are proportional to the real distribution of re¤ectivity as well(real model possesses intensity of re¤ectors proportional to fast velocity perturbation).

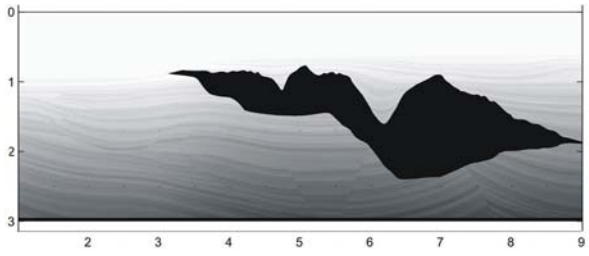

Figure 2: Total stratigraphic model Sigsbee2A model. Horizontal and vertical axes - distance in feets$\times 10^4$

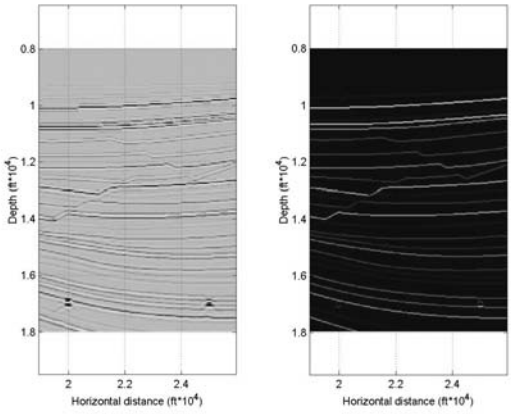

Figure 3: Recovered (left) and real (right) images of target area out of salt intrusion.

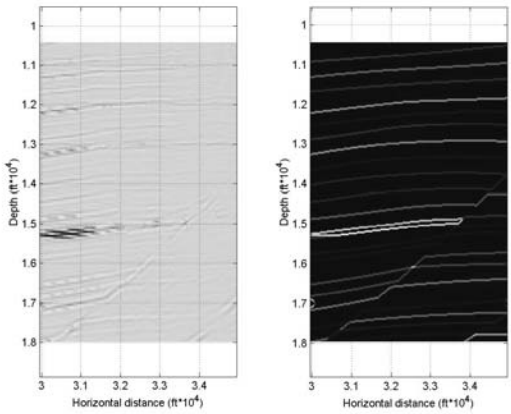

Figure 4: Recovered (left) and real (right) images of subsalt target area.

Conclusion

It should be noted that proposed imaging procedure provides so called ”selective image”. Their main features are as follows:

- If spatial spectrum of re¤ector/scatterer component lies within a set of partial reconstruction this perturbation is totally recovered ;
- If spatial spectrum of a local object is out of a set of partial reconstruction, it happens to be totally ”invisible”;
- If spatial spectrum of a local object possesses nonempty intersection with a set of partial reconstruction selective image will be made from linear projection of desired perturbation onto the image of a set of partial reconstruction.

This follows very useful property - any singular object like diffractor/scatterer, crack, fault, pinch and so on possesses rather wide spatial spectrum and, so, will be presented for a range of selective images. On the contrast, any regular interface possesses rather narrow spatial spectrum and, so, one can easy choose dip and open angles providing the set of partial reconstruction being far away from this spatial spectrum. This opens a possibility to get reliable image of low contrast singular objects of subseismic scale.

Acknowledgements.

The research described in this publication was done in cooperation with Schlumberger Moscow Research and was also supported by RFBR Grants 05-05-64277-a, 07-05-00538. We thank also our colleague V.I. Kostin fore very useful discussions and comments.

References

[1] Beylkin, G., 1985, Imaging of discontinuous in the inverse scattering problem by inversion of causual generalized Radon transform, *J. Math. Phys.*, **v.26(1)**, pp.99 - 108.

[2] Bleistein N., 1987, On the imaging of re¤ectors in the Earth, *Geophysics*, **52**, 931 - 942.

[3] Cerveny, V., & Popov, M.M., & Psencik, I., 1982, Computation of wave £elds in inhomogeneous media. Gaussian beam approach *Geoph. J. R. Astr. Soc.*, **v.70**, pp. 109-128.

[4] Shubin M.A., 1978, Pseudodifferential operators and spectral theory, Moscow,”Nauka”.(in Russian)

WAVELET MOMENT METHOD FOR CAUCHY PROBLEM FOR THE HELMHOLTZ EQUATION

T. Regińska[†,*], **A. Wakulicz**[†]

[†]Institute of Mathematics, Polish Academy of Sciences, Warsaw, Poland
[*]Email: reginska@impan.gov.pl

Abstract

The paper concerns with a problem of reconstruction of acoustic or electromagnetic field from unexact data given on an open part of a boundary of a given domain. A regularization concept is presented for the ill-posed moment problem equivalent to a Cauchy problem for the Helmholtz equation. A method of regularization by projection with application of Meyer wavelet subspaces is introduced and analyzed. The derived formula, describing the projection level in terms of the error bound of unexact Cauchy data, allows to prove convergence and stability of the method.

Introduction

Let Ω be a simply connected domain in R^d, $d = 2, 3$ with a sufficiently regular boundary $\partial\Omega$ and, moreover, let $\Gamma \subset \partial\Omega$ be an open and connected part of the boundary. We consider the problem of reconstruction of acoustic or electromagnetic field from unexact data given on Γ. Let u denote a certain component of the considered vector field. Let us assume further that the field is harmonic with the constant wave number k. In this case the scalar function u satisfies in Ω the Helmholtz equation. With respect to applications we have some freedom in the choice of domain Ω: namely, only the part Γ of the boundary $\partial\Omega$ is given a priori (indicated by measurement possibilities), and in particular we may assume the same regularity of $\partial\Omega$ as that of Γ.

Direct problems connected with the Helmholtz equation are typically defined by Dirichlet or Neumann conditions on $\partial\Omega$, or by Dirichlet conditions on a one part of boundary (i.e. Γ) and Neumann conditions on the second one. The inverse problem considered in this paper consists in solving the Helmholtz equation under both the Dirichlet and the Neumann conditions posed on the same part Γ of the boundary $\partial\Omega$. That means that we deal with the following Cauchy problem

$$Lu := \Delta u + k^2 u = 0, \text{ on } \Omega \qquad (1)$$

$$u|_\Gamma = f \quad u_\nu|_\Gamma = g$$

where u_ν is the outer normal derivative of u on $\partial\Omega$. We assume that $f \in H^1(\Gamma)$ and $g \in L^2(\Gamma)$ are such that there exists the unique solution $u \in H^{3/2}(\Omega)$. It is known that the Cauchy problem for elliptic equations is ill-posed, which means that the solutions do not depend continuously on Cauchy data, see e.g. [1], [2]. This implies serious numerical difficulties in solving problems of this type, especially in the case of perturbed data. However, just this case is important from the point of view of real applications to acoustic and electromagnetic fields (cf. [3], [2]) where the exact Cauchy data are approximated by their measurement values.

For a stable solving ill-posed problems, regularization techniques are required. Numerical analysis of the Cauchy problem for the Laplace equation is a topic of several papers where different regularization methods were proposed. Unfortunately, their application to Helmholtz equation requires some modifications and additional analysis because of essential differences between these two problems.

In this paper developed is the idea of a numerical method based on a transformation of the Cauchy problem to a generalized moment problem: find $\varphi \in L^2(\partial\Omega \setminus \Gamma)$ such that

$$\int_{\partial\Omega\setminus\Gamma} \varphi v d\sigma = \mu(v) \qquad \forall v \in V(\Omega), \qquad (2)$$

where $V(\Omega)$ is a certain subspace of $L^2(\Omega)$ and μ a linear functional on $V(\Omega)$ which will be defined later. This idea was proposed by J. Cheng et al. in [5] for the Cauchy problem for Laplace's equation.

Generalized moment problem

General case $\Omega \subset R^3$

Let the test space $V(\Omega) = V$ be defined as follows

$$V := \left\{ v \in H^{3/2}(\Omega) : Lv = 0 \text{ on } \Omega,\ v_\nu|_{\partial\Omega\setminus\Gamma} = 0 \right\}. \qquad (3)$$

Moreover, for $v \in V(\Omega)$

$$\mu(v) := \int_\Gamma [f v_\nu - g v]\, d\sigma. \qquad (4)$$

Going into lines of Cheng et al. reasoning [5] we prove that (1) is equivalent to the moment problem (2) with (3) and (4) in the following sense:

THEOREM 1 Let $\partial\Omega \in C^{1+\epsilon}$, $g \in L^2(\Gamma)$, $f \in H^{1/2}(\Gamma)$ and let k^2 does not be an eigenvalue of the Neumann problem for $-\Delta$. Then $\varphi \in L^2(\partial\Omega\backslash\Gamma)$ is a solution to the moment problem (2) with (3) and (4) if and only if there exists a solution u to the Cauchy problem (1) such that $u_\nu \in L^2(\partial\Omega \setminus \Gamma)$ and $u_\nu = \varphi$.

Model problem in R^2

Now, our consideration is restricted to the case $\Omega \subset R^2$. Without lost of generality we may assume that

$$\partial\Omega \setminus \Gamma = \{(x_1, x_2) : x_1 \in [0,1], x_2 = 0\} \tag{5}$$

and $\Gamma \subset R \times R^+$ is a sufficiently regular curve which connects the two points $(0,0)$ and $(1,0)$. Let

$$\gamma = max\{x_2 : (x_1, x_2) \in \Gamma\}. \tag{6}$$

THEOREM 2 Let U denote the set of functions

$$\left\{\beta \in L^2(R) : \widehat{\beta}(\xi)\xi^2 \cosh(\gamma\sqrt{\xi^2 - k^2}) \in L^2(R)\right\} \tag{7}$$

where $\widehat{\beta}$ denotes the Fourier transform of β, and $\forall\beta \in U$ let us define $w_\beta(x_1, x_2)$ equal to

$$\frac{1}{\sqrt{2\pi}} \int_R \widehat{\beta}(\xi) \cosh(x_2\sqrt{\xi^2 - k^2}) e^{i\xi x_1} d\xi, \tag{8}$$

The set of functions $\{w_\beta : \beta \in U\}$ is dense in $V(\Omega)$.

Moment problem with Meyer wavelets

The Meyer wavelet ψ is a function from $C^\infty(R)$ defined by its Fourier transform as follows

$$\widehat{\psi}(\xi) = e^{i\frac{\xi}{2}} b(\xi),$$

where for $\frac{2\pi}{3} \le |\xi| \le \frac{4\pi}{3}$

$$b(\xi) = \frac{1}{\sqrt{2\pi}} \sin\left[\frac{\pi}{2}\zeta\left(\frac{3}{2\pi}|\xi| - 1\right)\right],$$

for $\frac{4\pi}{3} \le |\xi| \le \frac{8\pi}{3}$

$$b(\xi) = \frac{1}{\sqrt{2\pi}} \cos\left[\frac{\pi}{2}\zeta\left(\frac{3}{4\pi}|\xi| - 1\right)\right],$$

and otherwise $b(\xi) = 0$. The function $\zeta(x)$ equals 0 if $x \le 0$, equals 1 if $x \ge 1$, and $\zeta(x) + \zeta(1-x) = 1$. Then

$$\psi_{jl}(x) := 2^{\frac{j}{2}}\psi(2^j x - l) \quad j, l \in Z$$

form the orthonormal basis of $L^2(R)$ and $\psi_{jl} \in U$, since

$$\text{supp}(\widehat{\psi}_{jl}) = \{\xi; \frac{2}{3}\pi 2^j \le |\xi| \le \frac{8}{3}\pi 2^j\}.$$

REMARK 1 Due to Theorem 2, the moment problem (2) with (3) and (4) can be now formulated as follows: find $\varphi \in L^2(0,1)$ such that $\forall j, k \in Z$

$$\int_0^1 \varphi(x)\psi_{j,l}(x)dx = \eta_{j,l}, \tag{9}$$

where

$$\eta_{j,l} := \mu(w_{\psi_{j,l}}).$$

From this it follows that

$$\sum_{j,l\in Z} \eta_{j,l}\psi_{j,l}(x) = \varphi(x) \text{ for } x \in (0,1)$$

and this sum is equal to 0 for $x \in R \setminus (0,1)$

Perturbed data

Let f_δ, and g_δ be perturbed boundary value functions on Γ such that

$$\|f_\delta - f\|_{L^2(\Gamma)} \le \delta,\ \|g_\delta - g\|_{L^2(\Gamma)} \le \delta, \tag{10}$$

$\delta \in (0,1)$.For

$$\eta^\delta_{j,l} := \int_\Gamma \left[f_\delta \frac{\partial w_{\psi_{j,l}}}{\partial\nu} - g_\delta w_{\psi_{j,l}}\right] d\sigma, \tag{11}$$

we prove

THEOREM 3 If $j_0 := max\{0, E[\log_2 \frac{3k}{8\pi}]\}$, then

$$\sum_{l\in Z} |\eta_{j,l} - \eta^\delta_{j,l}|^2 \le C\delta^2 2^j \text{ as } j \le j_0,$$

$$\sum_{l\in Z} |\eta_{j,l} - \eta^\delta_{j,l}|^2 \le C_1\delta^2 2^{3j} e^{\frac{4}{3}\pi 2^J\gamma} \text{ as } j > j_0.$$

Regularization by wavelet-projection

Let $\widetilde{\varphi} \in L^2(R)$ be equal to φ for $x \in (0,1)$ and 0 elsewhere. As the regularized (approximate) solution let us take the orthogonal projection of $\widetilde{\varphi}$ onto

$$V_J = \overline{\text{span}\{\psi_{j,l}\}}_{j<J, l\in Z},$$

i.e.:

$$\varphi_J(x) = \sum_{j<J, l\in Z} \eta_{j,l}\psi_{j,l}(x). \tag{12}$$

Similarly, the regularized solution for the perturbed data is given by

$$\varphi^\delta_J(x) = \sum_{j<J, l\in Z} \eta^\delta_{j,l}\psi_{j,l}(x). \tag{13}$$

It is clear that

$$\|\varphi_J - \varphi\|_{L^2(0,1)} \leq \|\varphi_J - \widetilde{\varphi}\|_{L^2(R)} \longrightarrow 0 \text{ as } J \longrightarrow \infty.$$

A rate of convergence can be obtained under an additional assumption on the smoothness. Let $B^s_{p,q}$, for $p, q \geq 1$, $0 < s < 1$ denote the Besov space, i.e.

$$B^s_{p,q}(R) = \{f \in L^p(R) : \{2^{sj}\omega_p(f, 2^{-j})\}_{j\geq 0} \in l_q\}, \tag{14}$$

where $\omega_p(f,t)$ is the L^p modulus of smoothness of f.

LEMMA 1 If $\varphi \in H^1(0,1)$ then $\widetilde{\varphi} \in B^s_{2,q}$ for $s \in (0, \frac{1}{2})$ and $0 < q \leq \infty$, and

$$\|\varphi_J - \widetilde{\varphi}\|_{L^2(R)} \leq C2^{-sJ}.$$

On the other hand, from Theorem 3 we get the following stability result:

LEMMA 2 If (10) holds, then there exist a constant C depending on the wave number k such that

$$\|\varphi_J - \varphi^\delta_J\|_{L^2(R)} \leq C\delta\lambda(J),$$

where

$$\lambda(J) = 2^{\frac{1}{2}J} \text{ as } J \leq j_0,$$
$$\lambda(J) = 2^{\frac{3}{2}J} e^{\frac{4}{3}\pi 2^J \gamma} \text{ as } J > j_0.$$

Thus, from Lemmas 1 and 2 it follows that

$$\|\varphi - \varphi^\delta_J\|_{L^2(0,1)} \leq C[2^{-sJ} + \delta\lambda(J)]. \tag{15}$$

Looking for a proper value of the parameter of regularization J as a function of δ (such that it implies the convergence when $\delta \to 0$) we get the following result with an a priori choice of J.

THEOREM 4 Let α be a fixed constant such that $0 < \alpha < \frac{1}{\gamma}$ for γ given by (6) and let $c_0 = \frac{3\alpha}{4\pi}$. If the assumptions of Lemmas 1 and 2 are satisfied and

$$J(\delta) := E\left[\log_2\left(c_0 \ln\frac{1}{\delta}\right)\right], \tag{16}$$

then for $\delta \leq (\frac{8\pi}{3k})^{1/2+s}$

$$\|\varphi - \varphi^\delta_{J(\delta)}\|_{L^2(0,1)} \leq C\left(\frac{1}{-\ln\delta}\right)^s.$$

Let us consider the model problem (1) in the domain $\Omega \subset R^2$. Let φ^δ_J (13) be the regularized solution of the moment problem described in Remark 1. For the given perturbed boundary value functions f_δ, g_δ we define the regularized solution u^δ_J as a solution of the well posed Neumann problem (for $\partial\Omega$ sufficiently smooth)

$$\Delta u^\delta_J + k^2 u^\delta_J = 0, \text{ on } \Omega \tag{17}$$
$$\frac{\partial u^\delta_J}{\partial \nu} = \varphi^\delta_J \text{ on } \partial\Omega \setminus \Gamma,$$
$$\frac{\partial u^\delta_J}{\partial \nu} = g_\delta \text{ on } \Gamma,$$

with additional condition

$$\int_\Gamma (u^\delta_J - f_\delta) d\sigma = 0. \tag{18}$$

Finally, from Theorem 4 and from the continuous dependence of the solution of the problem (17), (18) on the boundary conditions, we get an asymptotic convergence of the regularized solution

$$\|u - u^\delta_{J(\delta)}\|_{H^1(\Omega)} \longrightarrow 0 \text{ as } \delta \longrightarrow 0.$$

Conclusion

We proved that the wavelet projection method applied to the moment problem has a regularization property. However, the order of convergence is rather small. It would be desirable to add an additional regularization procedure for the moment problem on V_J. It will be a subject of a future work.

References

[1] L. Eldén and F. Berntsson, "A stability estimate for Cauchy problem for an elliptic partial differential equations", Inverse Problems, 21(5), pp.1643-1653, 2005.

[2] T. Hrycak and V Isakov, "Increased stability in the continuation of solutions to the Helmholtz equation", Inverse Problems, 20, pp. 697-712, 2004.

[3] T. Regińska and K. Regiński, "Approximate solution of a Cauchy problem for the Helmholtz equation", Inverse Problems 22, pp. 975-989, 2006.

[4] H.W. Engl, M. Hanke, and A. Neubauer, Regularization of Inverse Problems, Kluwer Academic Publishers, 1996.

[5] J. Cheng, Y.C. Hon, T. Wei, and M. Yamamoto, "Numerical computation of a Cauchy problem for Laplace's equation", ZAMM Z. Angew. Math. Mech., 81(10), pp. 665-674, 2001.

Reconstruction of periodic media by the Factorization Method in a vectorial scattering problem

K. Sandfort
Graduiertenkolleg 1294,
Universität Karlsruhe (TH), Germany
Email: sandfort@math.uni-karlsruhe.de

Abstract

We study the time-harmonic scattering problem where (quasi-)periodic incident fields generated by magnetic dipoles are scattered by a periodic medium with space dependent permittivity and conductivity. To solve the corresponding inverse problem, we adapt the Factorization Method by Kirsch to reconstruct the boundary of the medium from field measurements on a surface.

Introduction

We consider the scattering of time-harmonic, (quasi-)periodic electromagnetic fields generated by a collocation of magnetic dipoles at a periodic medium in a homogeneous, isotropic background medium in 3D. We denote the medium by Ω and assume it to be 2π-periodic in the directions given by the x_1- and x_2-coordinate axes and to be bounded in the x_3-direction. Let $\Pi := (-\pi,\pi) \times (-\pi,\pi) \times \mathbb{R}$ be the unit cell, and define the complex permittivity $\hat{\varepsilon} := \varepsilon + i\sigma/\omega$ as well as the relative permittivity $\varepsilon_r := \hat{\varepsilon}/\varepsilon_0$, where $\sigma = \sigma(x)$ is a space dependent conductivity, ω is the frequency of the radiation, and $\varepsilon_0 \in \mathbb{R}$ is the real permittivity of the background medium. Let the permeability μ be constant $\equiv \mu_0 \in \mathbb{R}$ throughout the whole space $\mathbb{R}^3$, $\mu_r = \mu/\mu_0 = 1$. We call $k := \sqrt{\varepsilon_r}k_0 := \sqrt{\varepsilon_r}\omega\sqrt{\varepsilon_0\mu_0} \in \mathbb{C}$ the wave number. Moreover, we define

$$\begin{aligned}
&\Gamma := \partial\Omega, \quad \Gamma_\pm := \{x \in \mathbb{R}^3 \mid x_3 = m_\pm\},\\
&\Omega_\pm := \{x \in \mathbb{R}^3 \mid x \text{ is p.w.c. to } y \in \Gamma_\pm \text{ in } \mathbb{R}^3\backslash\overline{\Omega}\},\\
&R_\pm := \{x \in \mathbb{R}^3 \mid x_3 \gtrless m_\pm\},
\end{aligned}$$

where $m_+ > sup\{x_3 \mid x \in \Omega\}$, $m_- < inf\{x_3 \mid x \in \Omega\}$, and "p.w.c." means pathwise-connected.

We will make the following assumptions: Ω is open with $\partial\Omega \in C^2$ and $\{x \in \mathbb{R}^3 \mid x_3 = 0\} \subset \Omega$. The permittivity $\hat{\varepsilon} \in L^\infty(\mathbb{R}^3, \mathbb{C})$ is constant $\equiv \varepsilon_0 \in \mathbb{R}$ in $\Omega_+ \cup \Omega_-$. In addition, $Re(\varepsilon_r) \geq 0$ and $Im(\varepsilon_r) \geq 0$ in Ω, and there is a constant $c_0 > 0$ such that $Re(\varepsilon_r) + Im(\varepsilon_r) \geq c_0$.

Definition 1 *A function $f : \mathbb{R}^3 \to \mathbb{C}^3$ of the form $f(x + 2\pi(1,1,0)) = e^{i\alpha\cdot 2\pi(1,1,0)}f(x)$ with $\alpha \in \mathbb{R}^3$, $\alpha_3 = 0$, is called α-quasi-periodic.*
For any α-quasi-periodic f, let $f_p(x) := e^{-i\alpha\cdot x}f(x)$ denote its 2π-(bi)periodic counterpart.

For convenient work with (α-quasi-)periodic functions, we use the modified differential operators

$$grad_\alpha := grad + i\alpha, curl_\alpha := grad_\alpha \times, div_\alpha := grad_\alpha \cdot .$$

Integral equation formulation of the direct problem

We start with the formulation of the direct problem. From the time-harmonic Maxwell equations for some α-quasi-periodic incident (E^i, H^i) and scattered (E^s,H^s) electric and magnetic fields we derive the equation

$$curl\left(\frac{1}{\varepsilon_r}\, curl\, H^s\right) - k_0^2 H^s = curl\,(q\, curl\, H^i) \quad \text{in } \mathbb{R}^3$$

where q is the contrast given by $q := 1 - 1/\varepsilon_r$. For later application of our factorization method, we replace $q\, curl\, H^i$ by a general α-quasi-periodic source $f \in L^2(\mathbb{R}^3, \mathbb{C}^3)$ with support in $\overline{\Omega}$. From now on, we identify all 2π-periodic functions with their restrictions to the unit cell Π and let $D := \Omega \cap \Pi$. With the notation introduced above, we reformulate the above equation for $v = H_p^s$ on the reduced domain Π and obtain

$$curl_\alpha\left(\frac{1}{\varepsilon_r} curl_\alpha v\right) - k_0^2 v = curl_\alpha f_p \quad \text{in } \Pi. \tag{1}$$

The solution v is searched for in $H_{\text{loc}}(curl_\alpha, \Pi)$ and has to be understood in the variational sense, i.e. here

$$\begin{aligned}
&\int_\Pi \frac{1}{\varepsilon_r} curl_\alpha v \cdot curl_{-\alpha}\psi - k_0^2 v \cdot \psi dx\\
= &\int_D f_p \cdot curl_{-\alpha}\psi dx
\end{aligned} \tag{2}$$

for all $\psi \in H(curl_\alpha, \Pi)$ with compact support.
To complete the problem description, we have to impose a radiation condition on v. In our case, this has the form

$$v(x) = \sum_{z\in Z} curl_\alpha\left(v_z^\pm e^{i(z\cdot x \pm \beta_z x_3)}\right) \quad \text{in } R_\pm \tag{3}$$

where $\beta_z = \sqrt{k_0^2 - |\alpha + z|^2}$, $Z := \mathbb{Z}^2 \times \{0\}$, and the series is required to converge uniformly on compact subsets of $\overline{R_\pm}$. The coefficients $v_z^\pm \in \mathbb{C}^3$, $z \in Z$, are called Rayleigh coefficients.

We define the (magnetic) 2π-periodic Green's tensor $\mathfrak{G} = \mathfrak{G}(x,y)$ by

$$\mathfrak{G} := G\,\mathrm{id}_{3\times 3} + k_0^{-2} grad_{\alpha,x} div_{\alpha,x}(G\,\mathrm{id}_{3\times 3})$$

with $x \neq y$, where $G = G(x,y)$ is the scalar 2π-periodic Green's function

$$G(x,y) := \frac{i}{8\pi^2} \sum_{z\in Z} \frac{1}{\beta_z} e^{i(z\cdot(x-y)+\beta_z|x_3-y_3|)}$$

and the operators are meant columnwise. As our central result for the direct problem we establish

Theorem 2 *Let the assumptions be fulfilled which are given in the introduction. Then there hold:*

(i) The equation (2) satisfies the Fredholm alternative, i.e. there exists a unique radiating solution $v \in H_{loc}(curl_\alpha, \Pi)$ for every $f_p \in L^2(D,\mathbb{C}^3)$ provided uniqueness holds. For v, we have the integro-differential equation

$$v(x) = \int_D curl_{\alpha,x}\mathfrak{G}(x,y)(f_p(y) + q(y) curl_\alpha v(y))dy$$

for $x \in \Pi$.

(ii) Let $\Gamma \cap \{x \in \mathbb{R}^3 \mid x_3 \gtrless 0\}$ be graphs of functions. Further, let $Im(\varepsilon_r) > 0$ a.e. on D or $\varepsilon_r \in C^{1,\gamma}(D)$. Then uniqueness holds, i.e. also existence by part (i).

Setting up of the F.M. for the inverse problem

We now consider the inverse problem of reconstructing the periodic scattering medium or, equivalently, the support of the contrast q by means of (here magnetic) field measurements. For this, we let the incident field H^i be generated by magnetic dipoles located on a smooth and 2π-periodic surface Γ_i contained in $\overline{R_+}$. We then take measurements on another surface Γ_s in $\overline{R_+}$, which we simply assume to be part of the plane Γ_+ and to have nonempty relative interior. Furthermore, we restrict the assumptions on ε_r to $Im(\varepsilon_r) \geq c_0$ in Ω for some constant $c_0 > 0$.

Precisely, we suppose the incident field $v^i = H_p^i$ to be

$$v^i(x) := k_0^2 \int_{\Gamma_i\cap\Pi} \mathfrak{G}(y,x)\phi_p(y)ds(y), \qquad x \in \Pi\backslash\Gamma_i,$$

where $\phi_p(y)$ is the 2π-periodic moment of the dipole at y. This gives rise to the scattered field

$$v(x) = k_0^2 \int_{\Gamma_i\cap\Pi} v_{\mathfrak{G}}(x,y)\phi_p(y)ds(y), \qquad x \in \Pi\backslash\overline{D},$$

where $v_{\mathfrak{G}}(\cdot,y)$ is the scattered field corresponding to the incident field $\mathfrak{G}(y,\cdot)$ (column by column). Now, define the integral operator $\mathcal{M} : L^2(\Gamma_i\cap\Pi,\mathbb{C}^3) \to L^2(\Gamma_s\cap\Pi,\mathbb{C}^3)$ by

$$(\mathcal{M}\phi_p)(x) := k_0^2 \int_{\Gamma_i\cap\Pi} v_{\mathfrak{G}}(x,y)\phi_p(y)ds(y)$$

for $x \in \Gamma_s \cap \Pi$. It is the aim to recover the support of q from the knowledge of this operator, and so its analysis is the essential matter of the Factorization Method. We assume that all three components of $v_{\mathfrak{G}}(\cdot,y)$ for all polarizations of the dipole at y are available to us.
For some surface $\tilde{\Gamma} \subset \overline{R_+}$, set $\mathcal{H}_{\tilde{\Gamma}} : L^2(\tilde{\Gamma}\cap\Pi,\mathbb{C}^3) \to L^2(D,\mathbb{C}^3)$ as

$$(\mathcal{H}_{\tilde{\Gamma}}\phi_p)(x) := k_0^2 curl_\alpha \int_{\tilde{\Gamma}\cap\Pi} \mathfrak{G}(y,x)\phi_p(y)ds(y), \qquad x \in D.$$

Moreover, let $\hat{f}_p$ be such that $f_p = q\hat{f}_p$, and define the operator $\mathcal{G} : L^2(D,\mathbb{C}^3) \to L^2(\Gamma_s\cap\Pi,\mathbb{C}^3)$ by

$$\mathcal{G}\hat{f}_p := v|_{\Gamma_s\cap\Pi}$$

where v solves (2). Inspecting the definitions, it gets clear that $\mathcal{M} = \mathcal{G}\mathcal{H}_{\Gamma_i}$.
The transpose $\mathcal{H}_{\tilde{\Gamma}}^t$ of $\mathcal{H}_{\tilde{\Gamma}}$ with respect to the bilinear forms

$$\langle\varphi,\chi\rangle = \int_{\tilde{\Gamma}\cap\Pi} \varphi\cdot\chi ds \qquad \langle g,h\rangle = \int_D g\cdot h dx,$$

respectively, is given by

$$(\mathcal{H}_{\tilde{\Gamma}}^t\vartheta)(x) = k_0^2 \int_D curl_{\alpha,x}\mathfrak{G}(x,y)\vartheta(y)dy, \qquad x \in \tilde{\Gamma}\cap\Pi.$$

An easy calculation with equation (2) reveals that $\mathcal{H}_{\Gamma_s}^t(q/k_0^2(curl_\alpha v|_D + \hat{f}_p)) = \mathcal{G}\hat{f}_p$, where v solves (2). Hence, we arrive at the factorization

$$\mathcal{M} = \mathcal{H}_{\Gamma_s}^t \mathcal{T} \mathcal{H}_{\Gamma_i}$$

with $\mathcal{T} : L^2(D,\mathbb{C}^3) \to L^2(D,\mathbb{C}^3)$ specified by

$$\mathcal{T}\hat{f}_p := \frac{q}{k_0^2}(curl_\alpha v|_D + \hat{f}_p).$$

The following positivity property of $\mathcal{T}$ completes the ground for the application of the Factorization Method:

Theorem 3 *The operator $Im(\mathcal{T}) = (\mathcal{T} - \mathcal{T}^*)/(2i)$ is coercive, i.e. there exists a constant $c > 0$ such that*

$$Im\langle\mathcal{T}\hat{f}_p, \hat{f}_p\rangle_{L^2(D)} \geq c\|\hat{f}_p\|^2_{L^2(D)}$$

for all $\hat{f}_p \in L^2(D,\mathbb{C}^3)$.

In order to characterize now the unknown medium Ω (or, equivalently, D) by means of the known, factorized operator $\mathcal{M}$, as the final step we can employ a method similar to the one discussed in [1].

References

[1] A. Kirsch. An integral equation for Maxwell's equations in a layered medium with an application to the Factorization Method. submitted to *J. Int. Equ. Appl.*, 2006.

NONSTATIONARY PROBLEM OF ACTIVE SOUND CONTROL IN BOUNDED DOMAINS

S.V. Utyuzhnikov
School of Mechanical Aerospace and Civil Engineering, University of Manchester,
P.O. Box 88, Manchester, M60 1QD, U.K.
Email: s.utyuzhnikov@manchester.ac.uk

Abstract

The nonstationary problem of active shielding of some domain from the effect of the sources distributed in another domain is considered.The active shielding is realized via the implementation of additional sources in such a way that the total contribution of all sources leads to the desirable effect. Along with undesirable field (noise) to be shielded the presence of a desirable component is accepted in the analysis. The solution of the problem requires only the knowledge of the total field on the perimeter of the shielded domain. It can be obtained via the Calderon-Ryaben'kii potentials. A few new very important aspects of the problem are addressed in the paper for the first time. The general nontstationary formulation is considered in the paper. In bounded domains the resonance regimes are analysed. The diffraction effect of the secondary sources is also studied in the paper.

Introduction

The active shielding (AS) of some domains from the effect of the field (noise) generated in other domains is realized via the implementation of additional sources in such a way that the total contribution of all sources leads to the desirable effect. The comprehensive reviews of the theoretical and experimental methods related to these subjects can be found in [1], [2], [3]. Most theoretical approaches assume some quite detailed information about the undesirable sources and the properties of the medium. The JMC method [4], [3], based on the Huygens' construction, requires only the information on the undesirable field on the perimeter of the shielded domain. Yet this method is not used in the case if a desirable field ("friendly sound"), generated in the shielded domain, has to be taken into account. In addition, the JMC method was only used to tackle the problems formulated in unbounded domains.

A principally new solution can be reached via the application of the Difference Potential Method (DPM) [5], [6]. The solution obtained in a finite–difference formulation requires only the knowledge of the total field (both desirable and undesirable) at the grid boundary of the shielded domain. Any other information on the sources and medium is not required. It is possible to say that the solution demands, in some sense, minimal information which is *a priori* available. A comprehensive study of the general solution [6] in the application to the Helmholtz equation including its optimization can be found in [7], [8], [9]. In [10] the problem of AS in composite domains is formulated for the first time and its general finite–difference solution is provided. The DPM–based solution was extended to arbitrary hyperbolic systems of equations including acoustic Euler equations with constant and variable coefficients in our paper [11]. In [12] it is shown that the control sources are capable not to disturb even the echo of the "friendly" sound component if the AS problem is considered in bounded domains. For the acoustic Euler equations in continuous spaces, the AS solution was first obtained in our paper [13] for time–harmonic waves under quite general assumptions. It is shown the equivalence between the DPM–based discrete solution and the obtained solution if the space step vanishes. In the current paper, the general formulation of essentially nonstationary problems (non time–harmonic waves) is addressed. The effect on the secondary sources on the input data (diffraction) and the resonance regime are studied for the first time.

General formulation of the AS problem

The AS problem can be formulated as follows. Let us assume that some field (sound) U is described by the following correct BVP in a domain $D \subseteq \mathbb{R}^m$:

$$LU = f, \tag{1}$$

$$U \in \Xi(D). \tag{2}$$

Here, the operator L is a linear differential operator, $\Xi(D)$ is some functional space specified further. In particular, the operator L can correspond to the acoustic Euler equations.

We assume that $f \in F(D)$, where $F(D) \subset L_2^{loc}(D)$ is a linear space of functions f for which the solution of BVP (1), (2) exists and unique.

Consider some bounded domain D^+: $\overline{D^+} \subset D$. It is assumed that the domain D^+ has a smooth boundary Γ. The sources on the right–hand side can be distributed both

on D^+ and outside D^+:

$$f = f^+ + f^-, \quad \operatorname{supp} f^+ \subset D^+, \quad \operatorname{supp} f^- \subset D^- \stackrel{def}{=} D \setminus \overline{D^+}. \tag{3}$$

Here, $f^+ \in F(D)$ is the source of a "friendly" field (sound), while f^- is the source of an "adverse" field (noise).

Suppose that we know the trace of the function U on the boundary Γ of the domain D^+. It is to be noted that only this information is assumed to be available. In particular, the distribution of the sources f on the right-hand side is unknown. The AS problem is reduced to seeking additional sources G in $\overline{D^-}$ such that the solution of the following BVP

$$LU' = f + G, \quad \operatorname{supp} G \subset \overline{D^-}, \quad U' \in \Xi(D) \tag{4}$$

coincides on the domain D^+ with the solution of BVP (1), (2) if $f^- \equiv 0$:

$$LU^+ = f^+, \quad U^+ \in \Xi(D). \tag{5}$$

Thus, we seek a source term G such that on the domain D^+ the functions U and U' coincide with each other:

$$U'_{D^+} = U^+_{D^+}. \tag{6}$$

Nonstationary AS problem

Suppose that field U is described by a correct initial–boundary value problem (IBVP) in the cylinder $K_\infty = D \times (0, \infty)$:

$$LU \stackrel{def}{=} \frac{\partial U}{\partial t} + \sum_1^m A^i \frac{\partial U}{\partial x^i} = f, \tag{7}$$

$$l_{\partial D} U = 0, \tag{8}$$

$$U(\mathbf{x}, 0) = U_0(\mathbf{x}), \tag{9}$$

$$f = f^- + f^+, \quad \operatorname{supp} f^+ \subset D^+, \ \ \operatorname{supp} f^- \subset D^-,$$

where $\left\{x^i\right\}$ $(i = 1, ..., m)$ is a Cartesian coordinate system; U and F are vector–functions taking values in $\mathbb{R}^p$; A^i is $p \times p$ matrices such that $A^i(\mathbf{x}) \in C^\infty(D)$ $(i = 1, ..., m)$.

Consider the solution of BVP (7), (8), (9) in the generalized sense [14]. For this purpose we introduce the space of basic functions $\Phi \in C_0^\infty(D)$. Equality (1) is then considered in the weak sense:

$$< LU, \Phi > = < f, \Phi >, \tag{10}$$

where $< LU, \Phi >$ and $< f, \Phi >$ mean linear distributions determined on the space of the basic functions $C_0^\infty(D)$:

$$< f, \Phi > = \int_0^\infty \int_D (f, \Phi) d\mathbf{x} dt. \tag{11}$$

We define the functional space $\Xi(D)$ in such a way that the weak solution of BVP (7), (8), (9) coincides almost everywhere with the classical solution of this problem. Thus, we require that the functions from $\Xi(D)$ are piece–wise smooth and satisfy the initial and boundary conditions (8), (9). Hence, we suppose that $\Xi(D) \subset H^s(D)$, where $H^s(D)$ is the Sobolev space of functions, determined on D, with $s > 1 + m/2$. We also assume the boundary conditions are such that if $W \in \Xi(D)$, then $W(\partial D) \in H^{s-1/2}(\partial D)$.

Calderon–Ryaben'kii potentials

The general solution of the active shielding problem can be represented via the theory of the Calderon–Ryaben'kii potentials [5].

It is possible to introduce a potential as follows [5]:

$$P_{D^+} V_{D^+}(\mathbf{x}) \stackrel{def}{=} V_{D^+} - \int_{D^+} Gr(\mathbf{x}, \mathbf{y}) LV(\mathbf{y}) d\mathbf{y}$$

Here, V_{D^+} is the value of some function $V(D) \in \Xi(D)$ on $\overline{D^+}$; Gr is Green's function of BVP (7), (8), (9).

In [5], it is introduced the notion of a clear trace $\operatorname{Tr}_\Gamma U_D$ in such a way that:

$$\operatorname{Tr}_\Gamma V_{D^+} = \operatorname{Tr}_\Gamma W_{D^+} \Rightarrow P_{D^+} V_{D^+} = P_{D^+} W_{D^+}. \tag{12}$$

Thus, it is possible to introduce the potential with a density ξ_Γ:

$$P_{D^+\Gamma} \xi_\Gamma \stackrel{def}{=} P_{D^+} V_{D^+} \tag{13}$$

where $\xi_\Gamma = \operatorname{Tr}_\Gamma V$.

For elliptic equations potential (13) coincides with the Calderon projector [5].

General solution of AS problem

It is possible to show that the annihilating field W_D is given by [13]:

$$W_{D^+} = -P_{D^+\Gamma} U_\Gamma = \left[Gr A_n U_\Gamma \delta(\Gamma) \right]_{D^+}, \tag{14}$$

where $U_\Gamma \stackrel{def}{=} U(\Gamma)$; $A_n \stackrel{def}{=} \sum_1^m n_i A^i$, n_i are the coordinates of the unit vector of the external normal **n** to the boundary ∂D^+.

Hence, we obtain

$$G \equiv G_0 = A_n U_\Gamma \delta(\Gamma), \tag{15}$$

where δ is the Dirac delta–function.

The AS solution is not unique. Any function g_a such that $\operatorname{supp} g_a \in D^-$ can be added to g_0.

The realization of the source (15) is based on the knowledge (measurement) of U_Γ. Once the AS source is implemented, the field both in the shielded domain D and outside is changed. Moreover, the field U becomes a piece–wise function having a discontinuity on the boundary ∂D^+. Thus, the implementation of the AS source in the nonstationary case leads to some uncertainty.

It is proved that the AS source term is given by

$$G \equiv G_0 = A_n P_\Gamma U_\Gamma^- \delta(\Gamma). \tag{16}$$

Here, $P_\Gamma \stackrel{def}{=} \operatorname{Tr}_\Gamma P_{D\Gamma}$, $U_\Gamma^- = \operatorname{Tr}_\Gamma U(\mathbf{x})$ if $\mathbf{x} \in D^-$.

Thus, the measurements should be done on the external boundary and the realization requires the solution of some BVP in the domain D.

Conclusion

The solution of the AS problem is obtained in the general nonstationary formulation. The solution only requires the knowledge of the total field (desirable and undesirable) on the perimeter of the shielded domain. It does not use any additional information on either the characteristics of the undesirable sources or the surrounding medium. The knowledge of the Green's function of the problem is not required either. The influence of the secondary source on the input data is taken into account. It is shown that some BVP is to be solved in this case. It is demonstrated that the solution is applicable to resonance regimes.

Acknowledgment

This research was supported by the Engineering and Physics Sciences Research Council (EPSRC) under grant GR/T26832/01. The author is grateful to Professor Victor S. Ryaben'kii for useful discussions.

References

[1] Nelson, P.A., Elliott, S.J., Active control of sound, Academic Press, San Diego, CA, USA, 1992.

[2] Fuller, C.R., Nelson, P.A., Elliott, S.J., Active control of vibration, Academic Press, 1996.

[3] Uosukainen, S., Välimäki, V., JMC actuators and their applications in active attenuation of noise in ducts, VTT Publications, 341, VTT Building Technology, ESPOO, 1998, 100p.

[4] Jessel, M.J., "Some evidences for a general theory of active noise sound absorption", Proceedings of Inter–Noise 79, Warzaw, 1979, pp. 169–174.

[5] Ryaben'kii, V.S., Method of difference potentials and its applications, Berlin, Springer-Verlag, 2002.

[6] Ryaben'kii, V.S., "A difference shielding problem. Functional Analysis and Applications", V29, pp. 70–71, 1995.

[7] Lončarić, J., Ryaben'kii, V. S., Tsynkov, S.V., "Active shielding and control of noise", SIAM J. Appl. Math., V62, 2, pp. 563–596, 2001.

[8] Lončarić, J., Tsynkov, S.V., "Optimization of acoustic sources strength in the problems of active noise control", SIAM J. Appl. Math., V63, pp. 1141–1183, 2003.

[9] Lončarić, J., Tsynkov, S.V., "Quadratic optimization in the problems of active control of sound", J. Applied Numerical Mathematics, V52, N4, pp. 381–400, 2005.

[10] Ryaben'kii, V.S., Tsynkov, S.V., Utyuzhnikov, S.V., "Inverse source problem and active shielding for composite domains", J. Applied Mathematics Letters, 2006, to appear.

[11] Ryaben'kii, V.S., Utyuzhnikov, S.V., "Active shielding model for hyperbolic equations", IMA Journal of Applied Mathematics, V71, N6, pp. 924–939, 2006.

[12] Ryaben'kii, V.S., Utyuzhnikov, S.V., Turan, A.A., "On the Application of Difference Potential Theory to Active Noise Control", J. Advances in Applied Mathematics, V20, N5, pp. 511–515, 2007.

[13] Ryaben'kii, V.S., Utyuzhnikov, S.V., "Differential and finite-difference problems of active shielding", Applied Numerical Mathematics, Vol. 57, N4, pp. 374–382, 2007.

[14] Vladimirov, V.S., Equations of Mathematical Physics, Dekker, New York, 1971.

Tsunami waveform inversion by a truncated SVD approach

T.A.Voronina [†,*]
[†]Institute of Computational Mathematics and Mathematical Geophysics SB RAS, Novosibirsk 630090, Russia
[*]Email: vta@omzg.sscc.ru

Abstract

The inversion problem to determine the initial sea perturbation is considered as the usually ill-posed problem of the hydrodynamic inversion of tsunami tide-gage records. The wave propagation is described by the linear shallow-water equations when the depth is assumed as an arbitrary function of two variables. The direct problem is approximated by the explicit-implicit finite difference scheme. The ill-posed inverse restoration problem is regularized by means of the least square inversion using the truncated SVD approach.

Introduction

During the past few years, the tsunami events that occurred in the Pacific and the Indian Oceans had caused to turn to on the inverse tsunami problem. Mathematically, the initial tsunami waveform problem is formulated as inverse problem of mathematical physics for restoration of the initial water displacement in the source area by the water level oscillations observed on a number of points distributed in the ocean. It is well known that the above-formulated problem is an ill-posed one. The mathematical description of the direct problem of the wave propagation consists in the linear shallow-water system of differential equations in the rectangular coordinates. This system is approximated by the explicit-implicit finite difference scheme on a uniform rectangular grid, so the system of the linear algebraic equations is obtained. The ill-posed inverse problem of the reconstruction is regularized by means of the least square inversion, using truncated SVD approach - in this method the inverse operator is regularized with the help of its restriction on the subspace spanned on a finite sample of the first right singular vectors (see [2]). So-called r-solution (see [1]) is a result of the numerical process. The quality of the solution obtained is evaluated as relative errors (in L_2-norm) in restoration of the source function. The results are fairly satisfactory, if the receivers have a good azimuthal coverage with respect to source area.

1 Statement of the problem

We neglect the curvature of the Earth and we assume that z-axis be directed downwards with depth. Since the tsunami wave in the ocean is a long gravitational low-amplitude wave, its propagation can be described by the shallow water equation:

$$W_{tt} = \mathrm{div}\,(\mathrm{h(x,y)grad\,W}) + \mathrm{f_{tt}(t,x,y)} \qquad (1)$$

with the initial and the boundary conditions

$$W_{|t=0} = 0; \quad W_{t|t=0} = 0 \quad (2); \quad \left.\frac{\partial W}{\partial n}\right|_L = 0 \quad (3),$$

where $W(x,y,t)$ is a water elevation over the undisturbed state, $h(x,y)$ is the depth of the ocean, $f(x,y,t)$ describes the movement of the bottom in the tsunami area. Here we consider run ups as normal vectors arrivals (on coast line L). The velocity of the tsunami wave propagation is also described as $c(x,y) = \sqrt{gh}$. We solve the problem in the domain with piecewise-linear inner and outer boundaries. An unique solution exists only when the function of the source allows factorization, i.e., the function $f(x,y,t)$ can be factorized as $f(x,y,t) = \varepsilon(t) \cdot \varphi(x,y)$, where $\varepsilon(t)$ is the Heavyside function, $\varphi(x,y)$ is the bottom movement in the tsunami center (subdomain Ω). The unknown function $\varphi(x,y)$ will be sought in the form of a series of spatial harmonics with the unknown coefficients in Ω, when the given data is the water elevation $W_0(x_i,y_i,t)$ in a certain set of the receivers, disposed on the line Γ. The algorithm used in this way and substantiation of using this approach are described in detail in [2]. The system of equations (1)-(3) is approximated by the explicit-implicit finite difference scheme on the uniform rectangular grid based on the 4-point pattern. The scheme is of second order of accuracy with respect to spatial variables and of the first order with the respect to time.

2 Numerical experiments and conclusion

Numerical experiments are presented for the model bottom relief having some basic morphological features typical for the island arc regions, with inner and outer boundaries of the target domain. As a model of initial water displacement we used displacement representing the bottom deformation due to the typical tsunamigenic earthquakes with reverse dip-slip or low-angle trust mechanisms. A series of calculations was carried out by the method proposed and were aimed at recovering the unknown function $\varphi(x,y)$. The observed data concerning the form of the arrived wave were simulated as a result of solution to direct problem (1)-(3), perturbed by

the background noise, i.e., a high-frequency disturbance rate of 5% of a maximum amplitude of a signal over all the receivers. It is necessary to recognize that the results obtained strongly depend on the presence of disturbance due to the ill-posedness of the problem. However, since a tsunami wave is considered to be of essentially lower frequency as compared to the background noise, it is reasonable enough to apply the frequency filtration of the observed signal. We have shown that to attain a reasonable quality of the source restoration in this case we need, at least seven records distributed over the space domain and their azimuthal coverage plays the key role in obtaining the satisfactory results of inversion.

References

[1] Cheverda V. A., Kostin V.I.: 'r-pseudoinverse for compact operators in Hilbert space: existence and stability'. In: *J. Inverse and Ill-Posed Problems*, 1995, V.3, N.2, pp. 131-148.

[2] T.A.Voronina :' Reconstruction of initial tsunami waveform by the coastal observations invertion'. In: *Bull.NCC, Math.Model.in Geoph.*, 7(2002), p.89-100.

HIGH CONTRAST MICROWAVE TOMOGRAPHY USING TOPOLOGY OPTIMIZATION TECHNIQUES

E. Wadbro, M. Berggren
Division of Scientific Computing, Uppsala University, Uppsala, Sweden
Email: Eddie.Wadbro@it.uu.se

Abstract

Microwave tomography for medical applications leads to a difficult reconstruction problem for the dielectric properties due to strongly diffracting waves in combination with large dielectric contrasts. We apply the material distribution technique used in topology optimization for elastic structures to solve the nonlinear least-squares problem underlying the reconstruction problem and show successful results using simulated numerical data.

Introduction

Microwave tomography, as a diffraction based imaging technique for medical applications, has been subject to intense research during the last decades. The high contrast dielectric properties of biological tissue in the microwave regime have high medical significance [1]. Moreover, microwave radiation is non-ionizing, and the tomography equipment is inexpensive and portable. Even so, due to the difficult reconstruction problem, microwave tomography is not yet in clinical practice.

For medical applications, the details being reconstructed are comparable in size to the wavelength of the illuminating microwaves. Thus the fast ray-theory based algorithms for x-ray and ultrasound tomography cannot be expected to give satisfactory results. Kak and Slaney [2] review classical straight-ray as well as fast diffraction tomography methods. The latter are applicable to the present case of long wavelengths, but only for low contrasts. The high contrasts of biological tissue turns the mathematical problem into a nonlinear least-squares problem, which we attack with methods developed for topology optimization.

Topology optimization has its origin in structural optimization and concerns the optimal placement of material within a given domain. During the last decade researchers have started to apply similar ideas to problems in other disciplines. Recently, Wadbro and Berggren [3] applied topology optimization techniques for microwave tomography. Here, the suggested approach is further studied and explored using multiple frequencies and simulated data.

Problem Statement

Our aim is to reconstruct the dielectric properties of unknown objects located inside a hexagonal metallic container with side length 16 cm. The objects are located in the region $\Omega_?$ (Figure 1) and embedded in a saline solution with dielectric properties ε_{s}. Attached to each side of the container is a 2.2 cm wide waveguide filled with a low-loss material with dielectric properties $\varepsilon_{\mathrm{wg}}$. At the end of each waveguide there is a device able to radiate microwaves as well as measure the electric field. The container, the waveguides, and the objects infinitely extend in the direction normal to the plane.

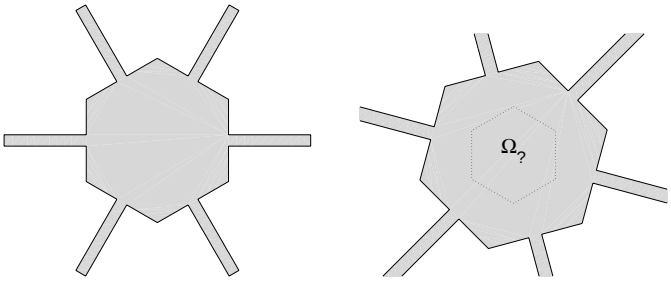

Figure 1: The problem consists of finding the dielectric properties of unknown objects. Left: A set of microwave transmitters and receivers are located at the ends of the waveguides. Right: the container can be rotated with respect to the region $\Omega_?$, in which the unknown objects are located.

We let σ and ϵ denote the conductivity and permittivity and assume that the permeability μ_0 is constant. The electric field E is governed by the Maxwell equations and is assumed to be polarized normal to the plane. We seek time harmonic solutions to the governing Maxwell equations using the ansatz $E = \Re\{(0,0,u)\mathrm{e}^{\mathrm{i}\omega t}\}$ and find that the complex amplitude function u satisfies the Helmholtz equation $\Delta u + \varepsilon k_0^2 u = 0$, where

$$\varepsilon = \epsilon_r - \mathrm{i}\sqrt{\frac{\mu_0}{\epsilon_0}}\frac{\sigma}{k_0}$$

is the complex permittivity, ϵ_0 the free space permittivity, $\epsilon_r = \epsilon/\epsilon_0$ the relative permittivity, $k_0 = \omega/c$ the free space wavenumber, and c the speed of light.

The computational domain Ω is illustrated to the left in Figure 1. The outer ends of the waveguides are denoted $\Gamma_{\mathrm{in}}^{(n)}$, $n = 1, 2, \ldots, 6$, and their union Γ_{in}. The sides of the container and the waveguides consists of perfectly conducting material, hence $u = 0$ on $\partial\Omega - \Gamma_{\mathrm{in}}$. The devices at the end of the waveguides are simulated

with a Sommerfeld approximation by prescribing the amplitudes of the incoming wave modes while assuring that the outgoing waves are perfectly absorbed.

Letting $\mathcal{V} = \{v \in H^1(\Omega) \mid v = 0 \text{ on } \partial\Omega - \Gamma_{\text{in}}\}$, the variational form of the wave propagation problem with a source located at waveguide m is:

$$\begin{aligned} &\text{Find } u \in \mathcal{V} \text{ such that} \\ &\int_\Omega \nabla u \cdot \nabla v - k_0^2 \int_\Omega \varepsilon u v + \mathrm{i}\widehat{k} \int_{\Gamma_{\text{in}}} uv \\ &\qquad = 2\mathrm{i}\widehat{k} C_m \int_{\Gamma_{\text{in}}^{(m)}} \sin\left(\frac{x \cdot t_m \pi}{d}\right) v, \quad \forall\, v \in \mathcal{V}, \end{aligned} \tag{1}$$

where t_m is the tangential vector on $\Gamma_{\text{in}}^{(m)}$, and C_m a constant used to set the amplitude of the incoming lowest wave mode at $\Gamma_{\text{in}}^{(m)}$.

To obtain a larger number of observations, the container is rotated, as illustrated to the right in Figure 1, at angles $\theta \in [0^\circ, 60^\circ)$ with respect to $\Omega_?$. For each fixed rotation angle θ_l and frequency ω_k, the devices at the end of the waveguides one at a time radiate the objects, and the resulting electrical field is measured by all the devices. In order to minimize systematic errors in the experiments, we observe the differences in mean complex amplitude between an empty (no unknown objects present) container and the container where the objects are present.

We let $u_n^{k,l}(\varepsilon)$ denote the solution to equation (1) for the case when the unknown objects are present in $\Omega_?$ to indicate that the source is located at $\Gamma_{\text{in}}^{(n)}$, at rotation angle θ_l, and at frequency ω_k. Similarly $w_n^{k,l}$ denotes the solution to equation (1) when there is only the saline solution in the container. Letting $\delta_{n,m}^{k,l}$ denote the observed mean complex difference at $\Gamma_{\text{in}}^{(m)}$, for source location $\Gamma_{\text{in}}^{(n)}$, at frequency ω_k, and at rotation angle θ_l, the problem of reconstructing the dielectric properties of the unknown objects may be formulated as

$$\min_{\varepsilon \in \mathcal{U}} \sum_{k=1}^{K} \sum_{l=1}^{L} \sum_{m,n=1}^{6} \left| \langle u_n^{k,l}(\varepsilon) \rangle_m - \langle w_n^{k,l} \rangle_m - \delta_{n,m}^{k,l} \right|^2, \tag{2}$$

where $\langle \cdot \rangle_m$ corresponds to an averaging over $\Gamma_{\text{in}}^{(m)}$, and $\mathcal{U}$ is the set of admissible permittivities defined by

$$\mathcal{U} = \left\{ \varepsilon \in L^\infty(\Omega) \;\middle|\; \begin{array}{l} \varepsilon = \varepsilon_{\text{wg}} \text{ in the waveguides} \\ 0 < \underline{\alpha} \le \Re\{\varepsilon\} \le \overline{\alpha} \text{ in } \Omega_? \\ \underline{\beta} \le \Im\{\varepsilon\} \le \overline{\beta} < 0 \text{ in } \Omega_? \\ \varepsilon = \varepsilon_{\text{s}} \text{ otherwise} \end{array} \right\},$$

where $\underline{\alpha}$, $\overline{\alpha}$, $\underline{\beta}$, and $\overline{\beta}$ are real constants.

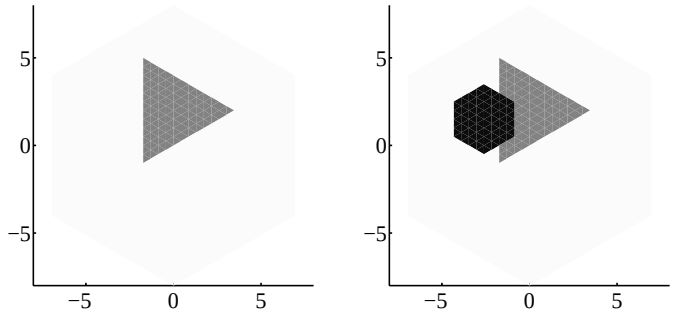

Figure 2: The sum of the real and imaginary part ($\Re\{\varepsilon\} + \Im\{\varepsilon\}$) for the dielectric properties for the phantoms used in the numerical experiments. Left: $\mathcal{P}_{\mathcal{I}}$, right: $\mathcal{P}_{\mathcal{II}}$. The scales on the axes are in centimeters.

Discrete Setup

The finite element method solves variational problem (1) numerically using second order Lagrangian elements. The inner region $\Omega_?$ is triangulated using equilateral triangles, and the rest of the container is, for each rotation, filled with an unstructured triangular mesh. The complex permittivity ε is approximated with a function being constant on each element.

The numerical experiments use frequencies in the range 870–930 MHz and aim to reconstruct the dielectric properties at 900 MHz of the two phantoms, $\mathcal{P}_{\mathcal{I}}$ and $\mathcal{P}_{\mathcal{II}}$, depicted in Figure 2. In the frequency range of study, there is only a weak frequency dependence of the materials comprising the phantoms. For each of these materials and at any frequency in the range 870–930 MHz, the relative permittivity difference compared with the 900 MHz case is less than one per cent. The dielectric properties of the phantoms are computed using the parametric formulae given by Gabriel et al. [4]. The triangular object in both phantoms has side length 6 cm and dielectric properties corresponding to those of a human muscle ($\varepsilon \approx 55 - 19\mathrm{i}$), and the hexagonal object in $\mathcal{P}_{\mathcal{II}}$ has side length 2 cm and dielectric properties corresponding to those of fat ($\varepsilon \approx 5 - \mathrm{i}$). The wavelengths at 900 MHz are about 3.7 cm in the saline solution, 4.4 cm in muscle tissue, and 14.9 cm in fat. The target differences in mean complex amplitude $\delta_{n,m}^{k,l}$ are computed using two different resolutions, one on a fine and one on a coarse mesh—the edge length in the structured region is 5 mm in the coarse mesh and 1.25 mm in the fine mesh. The reconstruction of the unknown objects is performed on the coarse mesh, attempting to fit the differences at the end of the waveguides with the precomputed target differences on either the fine or the coarse mesh.

We use the Method of Moving Asymptotes (MMA) [5] to numerically solve optimization problem (2). A sen-

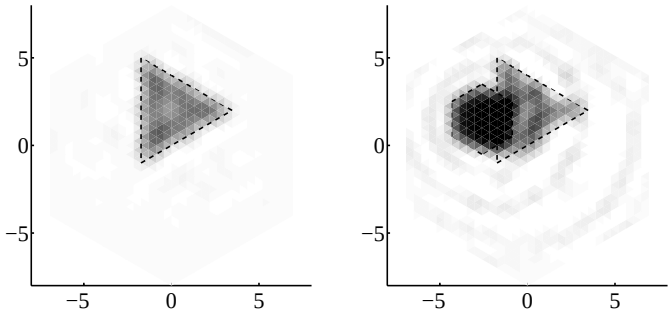

Figure 3: Phantoms reconstructed using exact numerical data, a frequency of 900 MHz, and 96 irradiation positions. The dashed lines indicates the contour of the objects. Left: $\mathcal{P}_{\mathcal{I}}$, right: $\mathcal{P}_{\mathcal{II}}$.

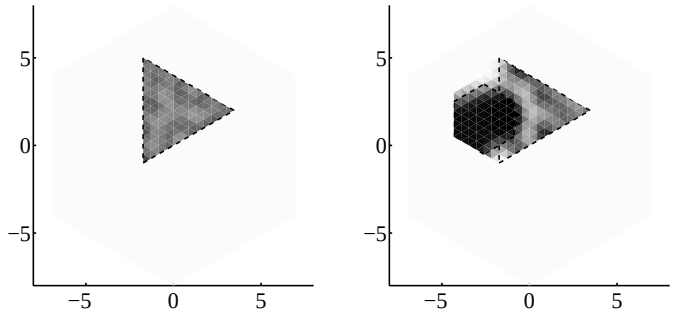

Figure 4: Phantoms reconstructed using information about the convex hull, filtering, inexact numerical data, the frequencies 870, 890, 910, and 930 MHz, and 24 irradiation positions. The dashed lines indicates the contour of the objects. Left: $\mathcal{P}_{\mathcal{I}}$, right: $\mathcal{P}_{\mathcal{II}}$.

sitivity analysis and a proof of existence of solutions to problem (2) are given by Wadbro and Berggren [3]. It is possible to argue, similar to Dobson [6], that the optimal admissible solution attains at least one of the bound constraints whenever there is no admissible complex permittivity such that the objective function is zero—a likely scenario when performing real experiments or using multiple frequencies in the reconstruction. This effect will manifest itself as noise in the optimal permittivity distribution. To combat such noise, we introduce a filter in the form of a local averaging. Note that the filter is not needed as a regularization to ensure existence of solutions to optimization problem (2).

Results

The first experiment aims to find the complex permittivity of the phantoms using data computed on the same mesh as used for the reconstruction. In this case we use a single frequency of 900 MHz, in order not to pollute the noiseless data. Figure 3 illustrates the dielectric properties of the phantoms reconstructed using 96 irradiation positions, resulting in 576 complex observations. The size, shape, and location of the triangular object are properly reconstructed in both phantoms. The reconstructed hexagonal object in $\mathcal{P}_{\mathcal{II}}$ is somewhat too small and centered slightly to the right of its correct center position.

In many cases the convex hull of the unknown object is known or can easily be obtained, through for example laser measurements. On the other hand, when performing real experiments, the obtained data is polluted with noise, decreasing the quality of the reconstruction. Figure 4 illustrates the dielectric properties of the phantoms reconstructed on the coarse mesh using the frequencies 870, 890, 910, and 930 MHz, 24 irradiation positions, and data computed on the fine mesh. The sizes and locations of the unknown objects are clearly visible in both phantoms and the reconstructed dielectric properties are close to the correct.

Acknowledgement Funding for the research has been provided by the Swedish Research Council.

References

[1] S. Y. Semenov, A. E. Bulyshev, A. Abubakar, V. G. Posukh, A. E. Souvorov, P. M. van den Berg, and T. C. Williams, "Microwave-Tomographic Imaging of the High Dielectric-Contrast Object Using Different Image-Reconstruction Approaches", IEEE Transactions on Microwave Theory and Techniques, vol. 53, pp. 2284–2294, 2005.

[2] A. C. Kak and M. Slaney, Principles of Computerized Tomographic Imaging, SIAM, Philadelphia, 2001.

[3] E. Wadbro and M. Berggren, "Microwave Tomography Using Topology Optimization Techniques", In review, 2007.

[4] S. Gabriel, R. W. Lau and C. Gabriel, "The dielectric properties of biological tissues: I–III", Physics in Medicine and Biology, vol. 41, pp. 2231–2293, 1996.

[5] K. Svanberg, "The method of moving asymptotes—a new method for structural optimization", International Journal for Numerical Methods in Engineering, vol. 24, pp. 359–373, 1987.

[6] D. C. Dobson, "Optimal Mode Coupling in Simple Planar Waveguides", in IUTAM Symposium on Topological Design Optimization of Structures, Machines and Materials, Springer 2006, pp. 311–320.

SHAPE AND TOPOLOGY OPTIMIZATION OF AN ACOUSTIC HORN–LENS COMBINATION

E. Wadbro, R. Udawalpola, M. Berggren
Division of Scientific Computing, Uppsala University, Uppsala, Sweden
Email: Martin.Berggren@it.uu.se

Abstract

Using gradient-based optimization combined with numerical solutions of the Helmholtz equation, we design an acoustic device with high transmission efficiency and even directivity throughout a two-octave-wide frequency range. The device consists of a horn, whose flare shape is subject to optimization, together with an area in front of the horn where solid material arbitrarily can be distributed using topology optimization techniques, effectively creating an acoustic lens.

Introduction

The two main characteristics of an acoustic horn are its transmission efficiency and directivity properties. For a horn operating as a part of a loudspeaker it is desired to control these characteristics for a range of frequencies. The setup we are interested in modeling and optimizing is illustrated in Figure 1. The geometry is assumed to be infinite in the direction normal to the plane. The device consists of a waveguide with a conical termination (the horn) and a lens located in front of the horn. The width of the waveguide (the throat of the horn) is 10 cm, the length of the horn is 50 cm, and the width of the mouth is 60 cm. The lens area is located 15 cm in front of the horn and is 25 cm wide and 100 cm high. We impose a right-going planar wave with amplitude A in the waveguide. The horn and the lens will aid in the transmission of the wave into free space, but parts of the wave will also be reflected back into the waveguide. The device is said to be efficient if a large portion of the incoming wave is transmitted into free space.

Bängtsson et al. [1] attacked the problem of designing an efficient horn using boundary shape optimization. Admissible horn flare shapes were given by functions β, prescribing the normal deflection from a straight horn (Figure 1). Wadbro and Berggren [2], [3] instead applied topology optimization, allowing an arbitrary material distribution in the interior of the horn, to design an efficient horn with requirements on the directivity. Recently, Udawalpola and Berggren [4] performed boundary shape optimization as above to study the tradeoff between high efficiency and directivity requirements. Their results suggest that manipulating the horn flare shape is sufficient to design highly efficient devices. However, these horns

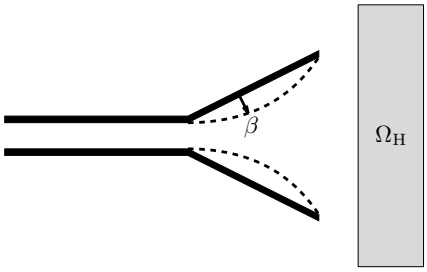

Figure 1: The walls of the horn are displaced and material is placed in the region Ω_{H} to improve the radiation properties.

exhibit a marked beaming effect, that is, the directional pattern narrows as the frequency increases. Breaking the beaming behavior using only modifications of the flare shape comes with a substantial penalty on efficiency, at least when restricting attention to 2D planar or cylindrical symmetry. Here, we use both shape and topology optimization to design an efficient horn–lens combination with even directivity for a wide range of frequencies.

Problem Statement

We assume that the wave propagation is governed by the linear wave equation for fluctuations P' in the acoustical pressure. We seek time harmonic solutions for a single angular frequency ω using the ansatz $P'(x,t) = \Re\{p(x)e^{\mathrm{i}\omega t}\}$ and find that the complex amplitude function p satisfies the Helmholtz equation

$$\Delta p + k^2 p = 0, \tag{1}$$

where $k = \omega/c$ is the wavenumber. Further, we stipulate that p satisfies the Sommerfeld radiation condition, specifying that all waves are outgoing in the far field.

The wave propagation in the waveguide can be expressed as a superposition of modal components satisfying the Helmholtz equation (1) together with the boundary condition

$$\frac{\partial p}{\partial n} = 0, \tag{2}$$

along the sound hard walls. If the width of the waveguide is sufficiently small compared to the wavelength, the nonplanar modes are evanescent.

We solve wave propagation problem (1) numerically using the finite element method on the computational do-

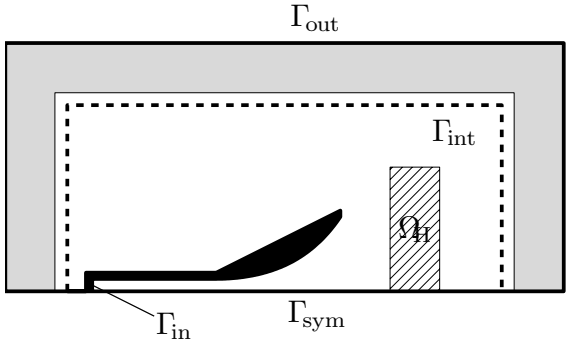

Figure 2: The computational domain.

main illustrated in Figure 2. A perfectly matched layer (PML) [5], [6] handles the outgoing wave property, modifying the governing equation in the region marked gray in Figure 2. The dashed interior boundary Γ_{int} is used in the computation of the far-field pattern, as detailed by Wadbro [7]. The left boundary of the truncated waveguide is denoted Γ_{in}. The boundary condition

$$\mathrm{i}\omega p + c\frac{\partial p}{\partial n} = 2\mathrm{i}\omega A \ \text{ on } \Gamma_{\text{in}}$$

imposes a right-going wave with amplitude A and absorbs any left-going wave. The boundary condition (2) is used for the the boundaries corresponding to the sound hard walls of the waveguide and the horn, as well as for the symmetry boundary Γ_{sym}.

We optimize the horn–lens combination presented in Figure 1 allowing the horn flare to deflect normal to the reference funnel shape and allowing an arbitrary distribution of sound hard material in Ω_{H}. Following Bängtsson et al. [1], we define the displacement function β as the solution to $\beta'' = -\eta$, with $\beta = 0$ at the throat and mouth of the horn. The design variable η roughly corresponds to the curvature of the horn. We denote by Ω^η the computational domain illustrated in Figure 2. The placement of material in Ω_{H} is modeled using a material indicator function $\alpha : \mathbb{R}^2 \to \{0, 1\}$, defined such that $\alpha(x) = 0$ if x is a solid point and 1 otherwise.

The variational form of the wave propagation problem is given by

Find $p \in H^1(\Omega^\eta)$ such that

$$c^2 \int_{\Omega^\eta} \alpha \nabla q \cdot (D\nabla p) - \omega^2 \int_{\Omega^\eta} \alpha\sigma qp + \mathrm{i}\omega c \int_{\Gamma_{\text{in}}} qp = 2\mathrm{i}\omega cA \int_{\Gamma_{\text{in}}} q, \ \ \forall q \in H^1(\Omega^\eta), \tag{3}$$

where D and σ corresponds to the changes in the equation due to the PML. In order to obtain a unique solution of problem (3) we redefine α such that $\alpha(x) \in \{\varepsilon, 1\}$ for all $x \in \Omega_{\text{H}}$, where ε is a small positive number.

The efficiency for a certain frequency ω can be measured by observing the mean complex amplitude $\langle p \rangle_{\text{in}}$ on Γ_{in}. The mean complex amplitude of the reflected wave at Γ_{in} is given by $\langle p \rangle_{\text{in}} - A$.

In the far-field, the complex amplitude function is essentially the product of a function of the distance to the device and a function of the direction. More precisely, let $\widehat{x}(\theta)$ be a point on the unit sphere, where θ denotes the polar argument of $\widehat{x}$; then

$$p(\widehat{x}(\theta)\rho) = \frac{\mathrm{e}^{\mathrm{i}k\rho}}{\sqrt{\rho}} \left\{ p_\infty(\theta) + O\left(\frac{1}{\rho}\right) \right\} \text{ as } \rho \to \infty,$$

where ρ represents the distance from the horn. The function $p_\infty(\theta)$ is called the far-field pattern.

We are interested in designing an efficient device with an even directivity pattern and thus state our general optimization problem as

$$\min_{\alpha,\eta} \sum_{\omega_j} \left(\left| \langle p^{(\omega_j)} \rangle_{\text{in}} - A \right|^2 + \tau \sum_{\vartheta_k} \left| p_\infty^{(\omega_j)}(\vartheta_k) \right|^2 + \upsilon \sum_{\theta_l} \left| \left| p_\infty^{(\omega_j)}(\theta_l) \right|^2 - \left| p_\infty^{(\omega_j)}(\theta_0) \right|^2 \right|^2 \right), \tag{4}$$

where ω_j are the frequencies for which we optimize the behavior, θ_l are the angles where we aim for even radiation (θ_0 corresponds to the horn axis), and the angles ϑ_k are introduced as a way to minimize the back scattering. The constants τ and υ are used set the relative weights of our different objectives.

Numerical Experiments

We solve optimization problem (4) numerically using the Method of Moving Asymptotes (MMA) [8] allowing α to attain values in the continuum $[\varepsilon, 1]$. The values ε and 1 are promoted through the addition of a penalty term in cooperation with a filtering procedure. Note that the addition of a penalty term without use of filtering may result in mesh dependent designs for the topology optimized portion; these issues are discussed in detail by Wadbro and Berggren [2]. Moreover, to promote a non oscillatory horn flare shape we apply Tichonov regularization [4]. For sensitivity analyses with respect to the different parts we refer to our earlier works [2], [4].

We optimize the device for even directivity at the angles $0^\circ, \pm 10^\circ, \ldots, \pm 50^\circ$ with respect to the horn axis for frequencies in the range 250–1000 Hz, exponentially

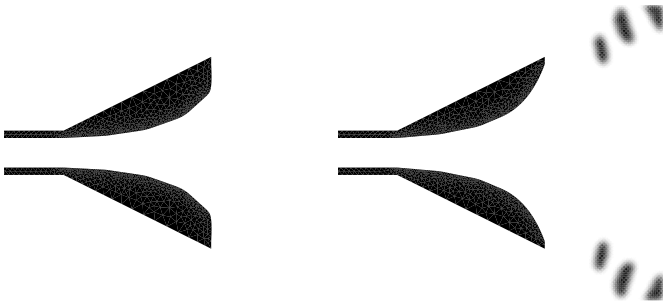

Figure 3: Left: horn without lens optimized for high efficiency and even directivity using only modifications of the horn flare boundary. Right: horn with lens optimized for high efficiency and even directivity using boundary movements of the horn and topology optimization of the lens in front of the horn.

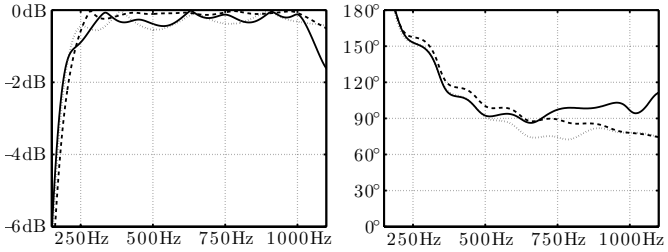

Figure 4: The transmission loss (left) in dB and the beamwidth (right) as functions of frequency for the two optimized devices. The dashed line corresponds to the optimized horn without a lens (left in Figure 3). The solid line corresponds to the horn–lens combination (right in Figure 3), and the dotted line corresponds to this horn functioning without a lens.

spaced with 12 frequencies per octave. The angles 90° and 180° were used to minimize the back scattering.

Figure 3 shows two devices: one designed using only shape optimization of the horn flare, and one designed simultaneously using shape optimization of the horn flare and topology optimization for the lens in front of the horn. The grayness in the lens area is due to the filtering. There are postprocessing methods that remove the gray while attending the design objective [2]. Both devices are very efficient throughout the frequency range subject to the optimization, with a maximum loss of 0.6 dB, and 0.9 dB for the horn without respectively with lens, as shown in Figure 4. This figure also presents the beamwidth—the angle between the -6 dB points on the far-field pattern—for the two devices. The beamwidth for the device without lens demonstrates a decreasing trend throughout the frequency range and is less than 80° at 1000 Hz. The beamwidth for the device with lens is well controlled and stays above 90°, except for a small frequency band around 650 Hz.

The dotted lines in Figure 4 illustrates the transmission loss and the beamwidth of the horn to the right in Figure 3, but with the lens removed. The influence of the lens can be seen by comparing the dotted and the solid lines in Figure 4. These results suggests that the addition of a lens only has a minor influence on the transmission efficiency, while it successfully breaks the beaming behavior of the horn.

Acknowledgement Funding for the research has been provided by the Swedish Research Council.

References

[1] E. Bängtsson, D. Noreland and M. Berggren, "Shape Optimization of an acoustic horn", Computer Methods in Applied Mechanics and Engineering, vol. 192, pp 1533–1571, 2003

[2] E. Wadbro and M. Berggren, "Topology Optimization of an Acoustic Horn", Computer Methods in Applied Mechanics and Engineering, vol. 196, pp 420–436, 2006

[3] E. Wadbro and M. Berggren, "Topology Optimization of Wave Transducers", in IUTAM Symposium on Topological Design Optimization of Structures, Machines and Materials, Springer, pp 301–310, 2006.

[4] R. Udawalpola and M. Berggren, "Optimization of an acoustic horn with respect to efficiency and directivity", In review, 2007

[5] J.-P. Berenger, "A Perfectly Matched Layer for the Absorption of Electromagnetic Waves", Journal of Computational Physics, vol. 114, pp. 185–200, 1994

[6] I. Harari, M. Slavutin and E. Turkel, "Analytical and Numerical Studies of a Finite Element PML for the Helmholtz Equation", Journal of Computational Acoustics, vol. 8, pp. 121–137, 2000

[7] E. Wadbro, "On the far-field properties of an acoustic horn", Technical Report 2006-042, Department of Information Technology, Uppsala University, 2006

[8] K. Svanberg, "The method of moving asymptotes—a new method for structural optimization", International Journal for Numerical Methods in Engineering, vol. 24, pp. 359–373, 1987

Nonlinear Waves

HIGH-ORDER NUMERICAL SOLUTION OF THE NONLINEAR HELMHOLTZ EQUATION WITH MATERIAL DISCONTINUITIES

G. Baruch[†], G. Fibich[†], and S. Tsynkov[‡,*]

[†]School of Mathematical Sciences, Tel Aviv University, Ramat Aviv, Tel Aviv 69978, Israel
[‡]Department of Mathematics, North Carolina State University, Box 8205, Raleigh, NC 27695, USA
[*]Email: tsynkov@math.ncsu.edu

Abstract

The nonlinear Helmholtz equation (NLH) models the propagation of electromagnetic waves in Kerr media and describes a range of important phenomena in optics and in other areas. In our previous work, we have built a fourth order method for its numerical solution that enables a direct simulation of nonlinear self-focusing in the non-paraxial regime, and provides a capability for the quantitative prediction of backscattering. Recently, we have also introduced a compact finite volume discretization for the analysis of material discontinuities, and a Newton-type nonlinear solver. Newton's linearization for the NLH is nontrivial since the Kerr nonlinearity contains absolute values of the field and is Frechét non-differentiable for complex-valued solutions. Hence, the NLH has to be recast as a system of two real equations, in which case Newton's method converges rapidly and enables computations for very high levels of nonlinearity, up to and beyond the limits of material breakdown.

Formulation of the Problem

We are considering the propagation of linearly polarized monochromatic laser light in an inhomogeneous lossless (i.e., optically transparent) medium. We are assuming that the parameters of the medium, which are given, as well as the intensity of the electric field E, which is the unknown quantity, may only vary along one spatial direction that coincides with the direction of propagation z. Then, the general three-dimensional NLH reduces to the following ordinary differential equation:

$$\frac{d^2E(z)}{dz^2} + k_0^2\left(\nu(z) + \epsilon(z)\left|E\right|^2\right)E = 0, \qquad (1)$$

where k_0 is the wavenumber outside the Kerr medium, $\nu = \nu(z)$ controls the variation of the linear refraction index inside the medium, and $\epsilon = \epsilon(z)$, which is the scaled Kerr coefficient, controls the nonlinearity, see, e.g., [1]. All these parameters are assumed real, whereas the solution to the NLH (1) is normally considered complex so that to properly account for the variation of phase in a time-harmonic setting.

Work of the third author supported by the US NSF, Grant No. DMS-0509695 and US AFOSR, Grant No. FA9550-04-1-0118.

The Kerr medium occupies the interval $[0, z_{\max}]$ of the variable z. The material coefficients $\nu(z)$ and $\epsilon(z)$ are, generally speaking, discontinuous at both outer boundaries, $z = 0$ and $z = z_{\max}$. As far as the interior, we are assuming that the material is either homogeneous, i.e., $\nu(z) \equiv \nu^{\text{int}}$, $\epsilon(z) \equiv \epsilon^{\text{int}}$, or layered. In the latter case, the variation of material properties is piecewise-constant so that for some given partition:

$$0 = \tilde{z}_1 < \cdots < \tilde{z}_l < \cdots < \tilde{z}_L = z_{\max}, \qquad (2a)$$

we have:

$$\nu(z) \equiv \tilde{\nu}_l, \quad \epsilon(z) \equiv \tilde{\epsilon}_l, \quad \text{for} \quad z \in (\tilde{z}_l, \tilde{z}_{l+1})\,. \qquad (2b)$$

At the interfaces $\tilde{z}_l$, the Maxwell's equations imply continuity of the field $E(z)$ and of its first derivative $\frac{dE}{dz}$. This continuity at $z = 0$ and $z = z_{\max}$, along with the assumption that the field outside the Kerr medium consists of the unknown scattered component and the impinging wave $E^0_{\text{inc}}e^{ik_0z}$ that comes from the left, yields:

$$\left(\frac{d}{dz} + ik_0\right)E\Big|_{z=0} = 2ik_0E^0_{\text{inc}}, \qquad (3a)$$

$$\left(\frac{d}{dz} - ik_0\right)E\Big|_{z=z_{\max}} = 0. \qquad (3b)$$

Relation (3a) is a two-way boundary condition for the NLH (1) at the left endpoint, and relation (3b) is a radiation boundary condition at the right endpoint.

Exact solutions of problem (1)-(3) were obtained by Chen and Mills for both homogeneous and layered materials, see [2], [3]. For sufficiently high input powers, it was shown that those solutions maybe not unique. Numerically, the homogeneous multidimensional NLH was solved with forth order accuracy in our previous work [4], [1]. A key element of the method was the nonlocal two-way artificial boundary conditions (ABCs) that generalized (3). The ABCs facilitated the reflectionless propagation of all the outgoing waves and also guaranteed a

full transmission of the given incoming field at the boundaries of the computational domain. However, the method of [4], [1] did not allow to solve the NLH for high input powers. In [5], [6], Suryanto, et al. used a finite element scheme for the one-dimensional NLH (1) with material discontinuities. The numerical approximation in [5], [6] was of a mixed order: fourth for the linear terms of (1) and second for the nonlinear terms.

Numerical Method

The goal of the current paper is to build a genuine high order numerical approximation of the NLH (1) that would allow for both the discontinuities in the material coefficients and the solution for high input powers.

At the points where the material coefficients ν and/or ϵ undergo discontinuities, the second derivative of the solution $E(z)$ also becomes discontinuous. The new fourth order discretization of the NLH (1) that we are presenting is based on a *compact approximation of finite volume type*. The use of integration over the grid cells allows us to correctly account for the discontinuities in $\nu(z)$ and $\epsilon(z)$ at the outer boundaries, as well as inside the domain. A fourth order accuracy is attained on the compact three node stencil by using the differential equation (1) itself to eliminate the leading terms of the truncation error.

Let $a,\, b \in [0, Z_{\max}]$, $a < b$, and let us integrate equation (1) between the points a and b with respect to z. Since $\frac{dE}{dz}$ is continuous everywhere, we obtain:

$$\frac{dE(b)}{dz} - \frac{dE(a)}{dz} + k_0^2 \int_a^b \left(\nu(z) + \epsilon(z)\,|E|^2\right) E\, dz = 0. \tag{4}$$

Equation (4) can be interpreted as the integral conservation law that corresponds to the NLH (1). It is easy to see that for sufficiently smooth solutions the two formulations are equivalent. Indeed, if we require that the integral relation (4) hold *for any pair of points* a and b, then at every point z_0 where $\frac{d^2E}{dz^2}$ exists the NLH (1) can be reconstructed from the conservation law (4) by a straightforward passage to the limit: $a \to z_0 - 0$, $b \to z_0 + 0$. However, the integral formulation (4) makes sense even when the differential equation per se loses its validity because of insufficient regularity of the solution, in particular, when the material coefficients undergo jumps and the second derivative $\frac{d^2E}{dz^2}$ becomes discontinuous.

The discretization of the NLH (1) is built by approximating equation (4) on a uniform grid with size h. In doing so, for every node $z_j = jh$ of the grid, $j = 0, 1, \ldots, M$, we take $a = x_j - h/2$ and $b = x_j + h/2$. Besides, we only allow the material discontinuities to occur at the grid nodes, which presents no loss of generality. The first derivatives (fluxes) at the cell centers a and b in (4) are approximated using central differences. Then, the leading term in the truncation error, which is proportional to the third derivative, is annihilated by approximating the latter as $E'''_{j+1/2} = (E''_{j+1} - E''_j)/h + \mathcal{O}(h^2)$, where the appropriate one-sided second derivatives are obtained through equation (1) itself. This yields the fourth order for the flux difference. To guarantee the overall fourth order accuracy, the integral term in (4) needs to be approximated carefully. Recall, inside every grid cell the material coefficients are constant and consequently, the solution $E(z)$ is infinitely differentiable. Therefore, on each of the two half-cells, $[z_{j-1/2}, z_j]$ and $[z_j, z_{j+1/2}]$, we can approximate it to fourth order using the appropriate Hermite-Birkhoff cubic interpolating polynomial [7] built using the nodal values of E and those of the one-sided second derivatives (re-written via the equation). Then, by integrating the interpolant and assembling all the terms, we obtain a fourth order accurate scheme for the NLH.

As far as the boundary conditions, relation (3a) facilitates the propagation of the outgoing waves through the interface $z = 0$ and at the same time prescribes the given incoming signal. This means that the solution to equation (1) for $z \le 0$ is to be composed of a given incoming wave and the outgoing wave, which is not known ahead of time. Since for $z \le 0$ the material is a homogeneous linear dielectric, $\nu \equiv 1$ and $\epsilon \equiv 0$, we have:

$$E(z) = E^0_{\text{inc}} e^{ik_0 z} + R e^{-ik_0 z}, \quad z \le 0, \tag{5}$$

and the boundary condition is derived from the continuity of E and E' at $z = 0$. To construct a boundary condition for the scheme we approximate (5) using the closed form solutions of the corresponding constant coefficient difference equation. This provides the value of the solution at the ghost node E_{-1} in terms of that at the boundary node E_0 and the incoming beam E^0_{inc}. Then, E_{-1} can be eliminated from the finite-difference equation. A discrete counterpart of boundary condition (3b) is obtained similarly. Details of the approach can be found in [4], [1].

The discrete approximation that we obtain for problem (1)-(3) is a system of nonlinear algebraic equations. In our work [4], [1], we solved similar systems by a straightforward iteration scheme based on freezing the nonlinearity in the NLH. In doing so, we have observed that the convergence of iterations was limited to relatively low incoming energies, i.e., weak nonlinearities. A similar iteration scheme was used by Suryanto, et al., see [5], [6].

In this paper, we develop a more capable and more efficient iteration scheme for solving the NLH (1); it is

based on Newton's method. Newton's method, however, cannot be applied to equation (1) directly, because $|E|$ is not differentiable in the Cauchy-Riemann sense and hence the entire operator is not differentiable in the sense of Frechét. Therefore, we recast the NLH as a system of two equations with real unknowns and then perform Newton's linearization using real variables. Newton's method is also known to be sensitive to the choice of the initial guess. To choose the initial guess for a particular strength of nonlinearity (value of ϵ), we employ a continuations strategy, i.e., increase ϵ in small increments from 0 to the desired value and use the solution for the previous value of ϵ as the initial guess for the next value of ϵ. Our computations show that the use of Newton's iterations leads to a very considerable improvement in performance over the previous iterative method [4], [1]. It enables robust numerical solution of the NLH for strong nonlinearities. In fact, solutions can be computed for nonlinearities that exceed the threshold of mathematical non-uniqueness, and even for the nonlinearities that are beyond the level of material breakdown in an actual physical setting. Note that in the latter case the Kerr model itself no longer applies.

Numerical Results

We have conducted a large number of numerical experiments aimed at testing the new method. We have also compared the results against those obtained using the original methodology of [4], [1] (when the latter converged). Our experiments fully corroborate the theoretical design properties of the new method, i.e., its fourth order grid convergence and its capability to obtain solutions for high levels of nonlinearity. Below, we only report on a particular set of results that demonstrate a fourth order convergence to the exact solutions of [2] for one case with weak nonlinearity and one case with strong nonlinearity.

Table 1: Examples of grid convergence for weak nonlinearity ($\epsilon = 0.01$) and for strong nonlinearity ($\epsilon = 0.845$).

Normalized grid size, hk_0	Weak nonlinearity, $\|\cdot\|_\infty$ error	Strong nonlinearity, $\|\cdot\|_\infty$ error
0.8	0.121	no convergence
$8 \cdot 10^{-1.5}$	$1.29 \cdot 10^{-3}$	$8.16 \cdot 10^{-2}$
$8 \cdot 10^{-2}$	$1.28 \cdot 10^{-5}$	$9.12 \cdot 10^{-5}$
$8 \cdot 10^{-2.5}$	$1.28 \cdot 10^{-7}$	$9.13 \cdot 10^{-7}$
$8 \cdot 10^{-3}$	$1.33 \cdot 10^{-9}$	$9.16 \cdot 10^{-9}$

For the case of a strong nonlinearity shown in Table 1, the initial guess for Newton's iterations was chosen by continuation in ϵ. The lack of iterations' convergence in this case on a very coarse grid is not surprising, because the sharp variations of the solution cannot be adequately resolved.

Conclusions

A new method for the numerical solution of the NLH has been developed that correctly accounts for the discontinuities of material properties and enables computations for high nonlinearities. The performance of the method was tested by comparing the results of computations with the exact solutions available for one-dimensional settings. In the future, we plan to construct a method with comparable capabilities for the multidimensional NLH.

References

[1] G. Fibich and S. V. Tsynkov. Numerical solution of the nonlinear Helmholtz equation using nonorthogonal expansions. *J. Comput. Phys.*, 210(1):183–224, 2005.

[2] W. Chen and D. L. Mills. Optical response fo a nonlinear dielectric film. *Phys. Rev. B*, 35:524–532, 1987.

[3] W. Chen and D. L. Mills. Optical response of nonlinear multilayer structures: Bilayers and superlattices. *Phys. Rev. B*, 36:6269–6278, 1987.

[4] G. Fibich and S. V. Tsynkov. High-order two-way artificial boundary conditions for nonlinear wave propagation with backscattering. *J. Comput. Phys.*, 171:632–677, 2001.

[5] A. Suryanto, E. van Groesen, M. Hammer, and H. J. W. M. Hoekstra. A finite element scheme to study the nonlinear optical response of a finite grating with out and with defect. *Opt. and Quant. Elec.*, 35:313–332, 2002.

[6] A. Suryanto, E. van Groesen, and M. Hammer. Finite element analysis of optical bistability in one-dimensional nonlinear photonic band gap structures with a defect. *J. Nonlinear Opt. Phys. and Materials*, 12:187–204, 2003.

[7] G. G. Lorentz, K. Jetter, and S. D. Riemenschneider. *Birkhoff Interpolation*. Cambridge University Press, 2004.

Semiline Solutions of a Nonlinear Heat Conduction Problem

S. De Lillo[†], G. Lupo[†,*] and M. Sommacal[‡]

[†]Dipartimento di Matematica e Informatica, Universitá degli Studi di Perugia, Via Vanvitelli 1, 06123 Perugia, Italy
Istituto Nazionale di Fisica Nucleare, Sezione di Perugia, Perugia, Italy
[‡]Laboratoire J.-L. Lions, Université Pierre et Marie Curie, Paris VI, France
[*]Email: gaia.lupo@pg.infn.it

Nonlinear evolution equations of diffusive type have been the subject of several investigations in the past, due to their applicative relevance [1]. In particular the nonlinear diffusion equation

$$u_t = \left(\frac{u_x}{u^2}\right)_x , \qquad u \equiv u(x,t) \tag{1}$$

was extensively studied in the literature as a mathematical model to describe heat conduction in high polymer systems [2] and in Storm type [3] materials.

In [4] we focused our attention on an initial/boundary value problem on the semiline for equation (1), with a prescribed constant thermal conductivity at the origin.

We generalize the results obtained in [4], by reporting the solution of the Cauchy problem in the case when the thermal conductivity at the boundary is time dependent.

Namely we consider for equation (1) the initial/boundary value problem on the semiline $0 \le x < \infty$ characterized by the following initial and boundary data

$$u(x,0) = u_0(x) , \qquad 0 \le x < \infty \tag{2a}$$

$$u(\infty,t) = \gamma , \qquad u_x(\infty,t) = 0 , \qquad t \ge 0 \tag{2b}$$

$$\frac{u_x(0,t)}{u^2(0,t)} = f(t) , \qquad t \ge 0 \tag{2c}$$

where γ is a positive constant and $f(t)$ is an integrable function. The boundary condition (2c) represents a given thermal conductivity at the origin (see [4]).

We introduce the hodograph transform

$$u(x,t) = [v(z,t)]^{-1} , \tag{3a}$$

with

$$\frac{\partial z}{\partial x} = u(x,t) , \tag{3b}$$

$$\frac{\partial z}{\partial t} = -\left(\frac{1}{u(x,t)}\right)_x , \tag{3c}$$

whose compatibility $\frac{\partial^2 z}{\partial x \partial t} = \frac{\partial^2 z}{\partial t \partial x}$ is guaranteed by (1).

By using the above transformation, equation (1) is mapped into the linear heat equation

$$v_t = v_{zz} \tag{4}$$

over the domain $F(t) \le z < \infty$, $F(t)$ satisfying the relation

$$F(t) = \int_0^t f(t')\, dt' . \tag{5}$$

Via the hodograph transform we associate to equation (4) the initial datum

$$v(z,0) \equiv v_0(z_0) = [u_0(x)]^{-1} \tag{6a}$$

where, in virtue of (3b) and (3c), z_0 is given by

$$z_0 \equiv z_0(x) = \int_0^x u_0(x')\, dx' , \tag{6b}$$

and the boundary conditions

$$v(\infty,t) = \frac{1}{\gamma} , \qquad v_z(\infty,t) = 0 \tag{7a}$$

$$f(t)\, v(F(t),t) + v_z(F(t),t) = 0 . \tag{7b}$$

The initial/boundary value problem for the nonlinear diffusion equation (1) with the initial datum (2a) and the boundary conditions (2b), (2c) is then mapped into the linear heat equation (4) over a domain with a moving boundary, characterized by the initial condition (6a) and the boundary conditions (7a), (7b).

In order to solve the linear problem we introduce the fundamental kernel of the heat equation

$$K(z-\xi, t-t') = \frac{1}{2\sqrt{\pi}} \frac{1}{\sqrt{t-t'}} \exp\left[-\frac{1}{4}\frac{(z-\xi)^2}{(t-t')}\right] \tag{8}$$

and integrate Green's identity for the heat equation

$$\frac{\partial}{\partial \xi}\left(K\,\frac{\partial v}{\partial \xi} - v\,\frac{\partial K}{\partial \xi}\right) - \frac{\partial}{\partial t'}\,(Kv) = 0 \tag{9}$$

over the domain $F(t') < \xi < \infty$, $\varepsilon < t' < t - \varepsilon$ and let $\varepsilon \to 0$. Using the condition (7b) and the fact that $K(z-\xi, 0) = \delta(z-\xi)$, we obtain

$$\begin{aligned} v(z,t) &= \int_0^t K_\xi(z - F(t'), t - t')\, v(F(t'), t')\, dt' \\ &+ \int_{F(0)}^{+\infty} K(z-\xi, t)\, v_0(\xi)\, d\xi. \end{aligned} \tag{10}$$

From (10) it is clear that $v(z,t)$ can be determined once the boundary value $v(F(t),t)$ is known; it is therefore convenient to evaluate (10) at $z = F(t)$. We put $w(t) = v(F(t),t)$ and we obtain

$$w(t) = G(t) + \lambda \int_0^t R(t,t')\, w(t')\, dt' , \tag{11a}$$

with

$$G(t) = \int_{F(0)}^{+\infty} K(F(t) - \xi, t)\, v_0(\xi)\, d\xi \tag{11b}$$

and

$$R(t,t') = \frac{1}{\lambda}\, K_\xi(F(t) - F(t'), t - t') , \quad \lambda = \frac{1}{4\sqrt{\pi}} . \tag{11c}$$

Equation (11a) is a linear Volterra integral equation of II type with a singular kernel $R(t,t')$. A suitable choice of the function $f(t)$ allows, via (5), to obtain a mildly singular kernel. Then the linear Volterra equation (11a) admits a unique solution under the assumption that $G(t)$ is an integrable and bounded function of its argument [5]. By using Picard's process of successive approximations [5] the solution of (11a) can be written as

$$w(t) = G(t) + \lambda \int_0^t H(t,t';\lambda)\, G(t')\, dt' , \tag{12}$$

where $H(t,t';\lambda)$ is the $resolvent\ kernel$ given by the series

$$H(t,t';\lambda) = \sum_{n=0}^{\infty} \lambda^n\, R_{n+1}(t,t') \tag{13a}$$

with

$$R_{n+1}(t,t') = \int_0^t R(t,t'')\, R_n(t'',t')\, dt'', \quad n = 1, 2, \ldots \tag{13b}$$

$$R_1(t,t') = R(t,t') . \tag{13c}$$

In the following we study numerically four examples that correspond to two different choices of the function $f(t)$, see (2c): a first case when $f(t)$ is a constant, and a second case when $f(t)$ is a linear function of time

$$f(t) = \alpha , \qquad \alpha \in \mathcal{R} , \tag{14a}$$

$$f(t) = a\, t + b , \qquad a,\, b \in \mathcal{R} , \tag{14b}$$

It is clear that by using (5), $F(t)$ is respectively a linear and a quadratic function of time. We also note that the choice (14a) corresponds to the case treated analytically in [4]. In both the cases we consider an initial datum $u_0(x)$ compatible with the asymptotic condition (2b), corresponding first to the function

$$u_0(x) = \beta - (\beta - \gamma)\, \vartheta(x - \eta) , \qquad \beta,\, \eta \in \mathcal{R} , \tag{15a}$$

where $\vartheta(x)$ is the usual unit step function, and then to the function

$$u_0(x) = \frac{\gamma}{1 + W\left(c\, \gamma\, e^{-\gamma\,(\kappa\, x - c)}\right)} , \qquad \kappa, c \in \mathcal{R} , \tag{15b}$$

where $W(x)$ is the Lambert-W function, implicitly defined by the relation $f(W) = W\, e^W$.

In the first case, (14a), the strategy is to proceed with a direct computation of the function $v(z,t)$ through the explicit solution, as displayed in [4]. Then we compute the function $v(z,t)$ according to (10), and finally obtain the solution $u(x,t)$ by inverting the hodograph transform (3a-3c). At fixed time $t = t^*$, via (3a) and (3b) we get

$$x(z)|_{t^*} = \int_0^z v(z', t^*)\, dz' \ . \tag{16}$$

From (16) we then obtain the inverse function $z(x)|_{t^*}$ and finally compute the solution of the original problem

$$u(x, t^*) = [v(z(x)|_{t^*}, t^*)]^{-1} \tag{17}$$

as implied by (3a).

When $F(t)$ is given by (14b), the Volterra integral equation (11a) is not solvable by quadratures as in the previous case but has to be solved numerically. The solution $v(z,t)$ of the linear problem is obtained via (10), but of course the computational charge of the algorithm is much heavier than in the previous case. The numerical

integration of the Volterra integral equation (11a) carries out using a non-uniform fixed mesh method, in order to avoid the problems due to the presence of a mildly singular Kernel (see, for example, [6]). As explained before, once obtained the function $v(z,t)$, by inverting the hodograph transform we get the solution $u(x,t)$ of the nonlinear problem (see (16) and (17)).

In the following we give a detailed description of the examples analyzed and we interpret the numerical results providing several graphics. We want to underline that in all the plots, each line represents the function $u(x,t)$ at a fixed time. As expected, for large x, the solution of the nonlinear problem $u(x,t)$ asymptotically approaches the value γ.

$1^{\mathbf{st}}$ *Case* $u_0(x)$ is given by (15a) and $f(t)$ by (14a), with $\alpha = 1$, $\beta = \frac{1}{3}$, $\eta = 3$ and $\gamma = \frac{1}{2}$. We then get

$$u_0(x) = \frac{1}{6}\left[2 + \vartheta(x-3)\right], \qquad f(t) = 1\,. \quad (18)$$

We observe that the discontinuity of the solution $u(x,t)$ in the x variable, due to the choice of the step function $\vartheta(x)$ in the initial datum $u_0(x)$, moves backward to the origin along the x axis, as $0 < t < 1$.

$2^{\mathbf{nd}}$ *Case* $u_0(x)$ is given by (15a) and $f(t)$ by (14b), with $a = 2$, $b = 0$, $\beta = \frac{1}{3}$, $\eta = 3$ and $\gamma = \frac{1}{2}$. We obtain

$$u_0(x) = \frac{1}{6}\left[2 + \vartheta(x-3)\right], \qquad f(t) = 2\,t\,. \quad (19)$$

Comparing this result with the previous one, we observe that the choice (14b) (namely, $F(t)$ is quadratic in time) seems to entail a faster approach in time of the solution $u(x,t)$ to the constant function $\hat{u}(x,t) = \gamma$.

$3^{\mathbf{rd}}$ *Case* $u_0(x)$ is given by (15b) and $f(t)$ by (14a), with $\alpha = 1$, $c = 1$, $\kappa = \frac{2}{3}$ and $\gamma = \frac{1}{2}$. We then obtain

$$u_0(x) = \frac{1}{2}\left[1 + W\left(\frac{1}{2}\,e^{-\frac{x}{3}+\frac{1}{2}}\right)\right]^{-1}, \quad f(t) = 1\,. \quad (20)$$

It is worth noting that in this case, from (20), via (6a) and (6b), we get

$$\begin{aligned} v_0(z) &= \frac{1}{\gamma} + c\,e^{-\kappa z} \\ &= 2 + e^{-\frac{2}{3}z}\,. \end{aligned} \quad (21)$$

$4^{\mathbf{th}}$ *Case* $u_0(x)$ is given by (15b) and $f(t)$ by (14b), with $\alpha = 1$, $c = 1$, $\kappa = \frac{2}{3}$ and $\gamma = \frac{1}{2}$:

$$u_0(x) = \frac{1}{2}\left[1 + W\left(\frac{1}{2}\,e^{-\frac{x}{3}+\frac{1}{2}}\right)\right]^{-1}, \quad f(t) = 2\,t\,. \quad (22)$$

Comparing this result with the previous one, we observe that the choice (14b) (namely, $F(t)$ is quadratic in time) seems to entail a faster approach in time of the solution $u(x,t)$ to the constant function $\hat{u}(x,t) = \gamma$.

References

[1] P. L. Sachdev, Nonlinear diffusive waves, Cambridge University Press, Cambridge, 1987, and references therein.

[2] G. Bluman and S. Kumei, "J. Math. Phys.", vol. 21, pp. 1019, 1989.

[3] M. L. Storm, "J. Appl. Phys.", vol. 22, pp. 940, 1951.

[4] S. De Lillo, G. Lupo and G. Sanchini, "J. Phys. A: Math. Gen.", vol. 39, pp. 7299, 2006.

[5] F. G. Tricomi, Integral Equations, Dover Publications, New York, 1985.

[6] W. H. Press, B. P. Flannery, S. A. Teukolsky and W. T. Vetterling, Numerical Recipes in Fortran, Cambridge University Press, Cambridge, 1992, and references therein.

NONDEGENERACY, FROM THE PROSPECT OF WAVE-WAVE REGULAR INTERACTIONS OF A GASDYNAMIC TYPE

L.F. Dinu[†,*], **M. I. Dinu**[‡,*]
[†]Institute of Mathematics of the Romanian Academy, P.O.Box 1-764, Bucharest, RO-014700, Romania,
[‡]Polytechnical University of Bucharest, Faculty of Applied Sciences, Dept of Math, Bucharest, Romania.
[*]Email: liviu.dinu@imar.ro

Abstract

An *analogue* of the *genuinely nonlinear* character of an one-dimensional simple waves solution is identified and *essentially* used in the construction of some *multi-dimensional extensions* (simple waves solutions, regular interactions of simple waves solutions). A *class* of exact multidimensional gasdynamic solutions is constructed whose interactive elements are regular. Some *specific* aspects of Burnat's multidimensional "algebraic" description [which uses a *dual* connection between the hodograph and physical characteristic details] are identified and classified with an admissibility criterion – selecting a "genuinely nonlinear" type where other ("hybrid") types are formally possible. A *parallel* is constructed between Burnat's "algebraic" approach and Martin's "differential" approach [centered on a Monge–Ampère type representation] regarding their contribution to describing some nondegenerate one-dimensional gasdynamic regular interaction solutions. The present approach parallels, from a *local* prospect, some details of the two-dimensional *global* approach of [7].

Introduction

For the multidimensional first order hyperbolic system of a gasdynamic type [whose coefficients only depend on u]

$$\sum_{j=1}^{n}\sum_{k=0}^{m} a_{ijk}(u)\frac{\partial u_j}{\partial x_k}=0, \quad 1\le i\le n \qquad (1)$$

the "algebraic" approach (Burnat [1]) starts with identifying *dual* pairs of directions $\vec{\beta},\vec{\kappa}$ [we write $\vec{\kappa}\rightharpoonup\vec{\beta}$] connecting [via their duality relation] the hodograph [= in the hodograph space H of the entities u] and physical [= in the physical space E of the independent variables] characteristic details. The duality relation at $u^*\in H$ has the form:

$$\sum_{j=1}^{n}\sum_{k=0}^{m} a_{ijk}(u^*)\beta_k\kappa_j=0, \quad 1\le i\le n. \qquad (2)$$

Here $\vec{\beta}$ is an *exceptional* direction [= orthogonal in the physical space E to a characteristic character]. A direction $\vec{\kappa}$ dual to an exceptional direction $\vec{\beta}$ is said to be a *hodograph characteristic* direction.

EXAMPLE 1. For the *one-dimensional* strictly hyperbolic version of system (1) a *finite* number n of dual pairs $\vec{\kappa}_i\rightharpoonup\vec{\beta}_i$ consisting in $\vec{\kappa}_i=\vec{R}_i$ and $\vec{\beta}_i=\Theta_i(u)[-\lambda_i(u),1]$, where $\vec{R}_i$ is a right eigenvector of the $n\times n$ matrix a and λ_i is an eigenvalue of a, are available ($i=1,...,n$). Each dual pair associates in this case, at each $u^*\in\mathcal{R}$ [for a suitable $\mathcal{R}\subset H$], to a vector $\vec{\kappa}$ a *single* dual vector $\vec{\beta}$.

EXAMPLE 2 (Peradzyński [5]). For the *two-dimensional* version (3) of (1), corresponding to an isentropic description (in usual notations: c is the sound velocity, v_x, v_y are fluid velocities)

$$\begin{cases} \dfrac{\partial c}{\partial t}+v_x\dfrac{\partial c}{\partial x}+v_y\dfrac{\partial c}{\partial y}+\dfrac{\gamma-1}{2}c\left(\dfrac{\partial v_x}{\partial x}+\dfrac{\partial v_y}{\partial y}\right)=0 \\ \dfrac{\partial v_x}{\partial t}+v_x\dfrac{\partial v_x}{\partial x}+v_y\dfrac{\partial v_x}{\partial y}+\dfrac{2}{\gamma-1}c\dfrac{\partial c}{\partial x}=0 \\ \dfrac{\partial v_y}{\partial t}+v_x\dfrac{\partial v_y}{\partial x}+v_y\dfrac{\partial v_y}{\partial y}+\dfrac{2}{\gamma-1}c\dfrac{\partial c}{\partial y}=0\,, \end{cases} \qquad (3)$$

an *infinite* number of dual pairs are available at each $u^*\in H$. Each dual pair associates, at the mentioned u^*, to a vector $\vec{\kappa}$ a *single* dual vector $\vec{\beta}$.

EXAMPLE 3 (Peradzyński [6]). For the *three-dimensional* version of (3) an *infinite* number of dual pairs are available at each $u^*\in H$. Each dual pair associates, at the mentioned u^*, to a vector $\vec{\kappa}$ a *finite* [constant, $\neq 1$] number of k independent exceptional dual vectors $\vec{\beta}_j$, $1\le j\le k$; and therefore has the structure $\vec{\kappa}\rightharpoonup(\vec{\beta}_1,...,\vec{\beta}_k)$.

DEFINITION 4 (Burnat [1]). A curve $\mathcal{C}\subset H$ is said to be *characteristic* if it is tangent at each point of it to a characteristic direction $\vec{\kappa}$. A hypersurface $\mathcal{S}\subset H$ is said to be *characteristic* if it possesses at least a characteristic system of coordinates.

Genuine nonlinearity. Simple waves solution. Regular interaction of simple waves solutions

REMARK 5. As it is well-known, in case of an one-dimensional strictly hyperbolic version of (1) any hodograph characteristic curve $\mathcal{C}\subset\mathcal{R}\subset H$, of index i, is said to be *genuinely nonlinear (gnl)* if the dual constructive pair $\vec{\kappa}_i\rightharpoonup\vec{\beta}_i$ is restricted by $\vec{\kappa}_i(u)\diamond\vec{\beta}_i(u)\equiv\vec{R}_i(u)\cdot\mathrm{grad}_u\lambda_i(u)\neq 0$ in $\mathcal{R}$; see Example 1. This condition transcribes the requirement $\frac{\mathrm{d}\vec{\beta}}{\mathrm{d}\alpha}\neq 0$ along $\mathcal{C}$.

DEFINITION 6. We naturally extend the *gnl* character of a hodograph curve to the cases corresponding to Examples 2 and 3, by requiring along $\mathcal{C}$

$$\left|\frac{\mathrm{d}\vec{\beta}}{\mathrm{d}\alpha}\right|\neq 0 \tag{4}$$

and, respectively,

$$\sum_{\mu=1}^{k}\left|\frac{\mathrm{d}\vec{\beta}_{\mu}}{\mathrm{d}\alpha}\right|\neq 0. \tag{5}$$

DEFINITION 7. A solution of (1) whose hodograph is laid along a *gnl* characteristic curve is said to be a *simple waves solution (sws)*. A solution of (1) whose hodograph is laid on a characteristic hypersurface is said to be a *regular interaction of sws* if its hodograph possesses a *gnl* system of coordinates.

A class of solutions of the system (1).
Wave-wave "algebraic" regular interactions

• Let $R_1,\ldots,R_p$ be characteristic coordinates on a given p-dimensional characteristic region $\mathcal{R}$ of a hodograph hypersurface $\mathcal{S}$. Solutions of the system

$$\frac{\partial u_l}{\partial x_s}=\sum_{k=1}^{p}\eta_k\kappa_{kl}(u)\beta_{ks}(u),\ u\in\mathcal{R};\ 1\leq l\leq n,\ 0\leq s\leq m \tag{6}$$

appear to concurrently satisfy the system (1). This indicates an "algebraic" importance of the concept of dual pair [see (2)]. We formally call these solutions *wave-wave regular interactions*.

• If a set of *Riemann−Burnat invariants* $R(x)$ exists, structuring the dependence on x of the solution u in the class above by a *regular* interaction representation

$$u_l=u_l[R_1(x_0,...,x_m),...,R_p(x_0,...,x_m)],\ 1\leq l\leq n, \tag{7}$$

it is easy to see that $R_i(x)$ must fulfil an (overdetermined and Pfaff) system

$$\frac{\partial R_k}{\partial x_s}=\eta_k\beta_{ks}[u(R)],\ \ 1\leq k\leq p,\ 0\leq s\leq m. \tag{8}$$

• Sufficient restrictions for solving (8) are proposed in [4]−[6]. Also see [2].

A class of exact solutions of the system (3).
Nondegeneracy. Linear degeneracy

A class of (local) exact solutions of (3) of the form

$$c=c(\xi,\eta),\ \ v_x=v_x(\xi,\eta),\ \ v_y=v_y(\xi,\eta), \tag{9}$$

where

$$\xi=\frac{x-x_0}{t-t_0},\quad \eta=\frac{y-y_0}{t-t_0} \tag{10}$$

is exhaustively presented in the contributed talk associated with this extended abstract (also see [2]). The interactive elements of this class appear to correspond to some *regular* interactions. Two highly nontrivial and very suggestive regular interaction elements in the mentioned class are considered in our contributing talk in every detail.

The hodograph associated to the first of these elements is shown to possess three *gnl* characteristic systems of coordinates; such an element puts together three distinct representations of regular interactions of multidimensional *sws*. Our talk also presents the physical details of each of these three representations.

The hodograph associated to the second of these mentioned elements also possesses three characteristic systems of coordinates; still, in this case two of these three systems of coordinates are proven to be [partially] *linearly degenerate (ldg)*. Again, three *distinct* and *multidimensionally coherent* [regular interaction] representations are concurrently present; only one of them would correspond to a *sws* interaction yet.

REMARK 8. A regular interaction of *sws* reflects the *nondegenerate* nature of the *gnl* hodographs of the interacting *sws*. The "algebraic" characterization of a regular interaction of *sws* will be regarded to correspond to a case of ["algebraic"] nondegeneracy. The second example above also includes a case of "algebraic" degeneracy ([2]). We therefore notice that representation (7) is not made of *sws* generally. We need a *criterion* to select the nondegenerate regular interaction solutions (see [2]).

An example of one-dimensional "differential" [and "nonalgebraic"] nondegenerate regular interaction

Next, we consider the gasdynamic system

$$\begin{cases}\dfrac{\partial\rho}{\partial t}+\dfrac{\partial(\rho v_x)}{\partial x}=0\\[2ex] \dfrac{\partial(\rho v_x)}{\partial t}+\dfrac{\partial}{\partial x}\left(\rho v_x^2+p\right)=0\\[2ex] \dfrac{\partial(\rho S)}{\partial t}+\dfrac{\partial(\rho v_x S)}{\partial x}=0\ ,\ \ S=S(p,\rho)\ ,\end{cases} \tag{11}$$

in usual notations, and use, to begin with, the first two equations $(11)_{1,2}$ to introduce (following Martin; see [3]), the functions $\psi,\tilde{\xi}$ and ξ cf.

$$\rho=\frac{\partial\psi}{\partial x},\ \rho v_x=-\frac{\partial\psi}{\partial t};\ \rho v_x=\frac{\partial\tilde{\xi}}{\partial x},\ \rho v_x^2+p=-\frac{\partial\tilde{\xi}}{\partial t};\ \xi=\tilde{\xi}+pt. \tag{12}$$

We get

$$\mathrm{d}x=\frac{1}{\rho}\mathrm{d}\psi+v_x\mathrm{d}t,\ \ \mathrm{d}\tilde{\xi}=v_x\mathrm{d}\psi-\rho\mathrm{d}t,\ \ \mathrm{d}\xi=v_x\mathrm{d}\psi+t\mathrm{d}p. \tag{13}$$

Then, we concretize (12), (13) to the case of a continuous [smooth] strictly adiabatic [anisentropic] flow for which in $(11)_3$ entropy $S(p,\rho)$ is a function of ψ alone, $F(\psi)$. Such a flow results behind a shock discontinuity of non-constant continuous [smooth] velocity which penetrates into a region of uniform flow. Prescription of F [as determined by the shock conditions] provides an algebraic relation between p, ρ, ψ throughout the adiabatic flow region. We select [Martin] p and ψ as new independent variables in place of x and t and compute from (13)

$$\frac{\partial x}{\partial \psi}=v_x\frac{\partial t}{\partial \psi}+\frac{1}{\rho},\ \frac{\partial x}{\partial p}=v_x\frac{\partial t}{\partial p},\ v_x=\frac{\partial \xi}{\partial \psi},\ t=\frac{\partial \xi}{\partial p}. \quad (14)$$

On eliminating x from $(14)_{1,2}$ and taking $(14)_{3,4}$ into account it results that ξ must fulfil the hyperbolic Monge–Ampère equation

$$\frac{\partial^2 \xi}{\partial p^2}\frac{\partial^2 \xi}{\partial \psi^2}-\left(\frac{\partial^2 \xi}{\partial p\partial \psi}\right)^2=-\zeta^2(p,\psi)\equiv-\frac{\partial}{\partial p}\left(\frac{1}{\rho}\right). \quad (15)$$

Finally, we compute from (14)

$$x=\int\left(\frac{\partial \xi}{\partial \psi}\frac{\partial^2 \xi}{\partial p\partial \psi}+\frac{1}{\rho}\right)\mathrm{d}\psi+\left(\frac{\partial \xi}{\partial \psi}\frac{\partial^2 \xi}{\partial p^2}\right)\mathrm{d}p. \quad (16)$$

REMARK 9. For *any* smooth solution $\xi(p,\psi)$ of (15) we get from (14), (16)

$$v_x=v_x(p,\psi),\ x=x(p,\psi),\ t=t(p,\psi). \quad (17)$$

On reversing $(17)_{2,3}$ into $p=p(x,t)$, $\psi=\psi(x,t)$ and carrying this into $(17)_1$ we get a form $p(x,t)$, $v_x(x,t)$, $\psi(x,t)$ of the corresponding anisentropic solution of (11).

- On prescribing F we will not find the streamlines as characteristics of (11). The two families of characteristics $\overline{\mathcal{C}}_\pm$ of (15) in the plane p,ψ appear to correspond to the two families of sound characteristics in the plane x,t.
- Next, we restrict the general Remark 9 to a *particular construction* − useful for identifying solutions of (15). To

$$\zeta=\frac{\psi^{\nu-1}}{p^{\nu+1}}\quad(\nu\neq 0) \quad (18)$$

in (15) we associate [Martin] two intermediate integrals

$$\mathcal{F}_\pm\equiv p\frac{\partial \xi}{\partial p}+\psi\frac{\partial \xi}{\partial \psi}-\xi\pm\frac{1}{\nu}\left(\frac{\psi}{p}\right)^\nu$$

for which $\mathcal{F}_\pm$=constant$_\pm$=$R_\pm$ along a characteristic $\overline{\mathcal{C}}_\pm$.

- We have to distiguish then between the cases (*a*) when $R_\pm$ depend on the charateristic $\overline{\mathcal{C}}_\pm$, and (*b*) when R_+ or R_- are overall constants.
- In the case (*a*) we may use (Martin; see [3]) $R_\pm$ as new independent variables. It can be shown in this case (Martin; see [3]) that the entities p^{-1}, v_x, ψ^{-1}, t, x fulfil various Euler−Poisson−Darboux *linear* equations

$$\frac{\partial^2 w}{R_+\partial R_-}-\frac{\nu}{R_+-R_-}\left(\frac{\partial w}{\partial R_+}-\frac{\partial w}{\partial R_-}\right)=0,\ \text{ constant } \nu$$

to which well-known representations are associated; we omit the details and present these representations by

$$p=p(R_+,R_-),\ \psi=\psi(R_+,R_-),\ v_x=v_x(R_+,R_-),\ t=t(R_+,R_-),\ x=x(R_+,R_-). \quad (19)$$

Reversing $(19)_2$ into $R_\pm=R_\pm(x,t)$ will induce a form of solution (19), parallel to (7) [as $R_\pm$ have a characteristic nature]. We call $R_\pm(x,t)$ *Riemann−Martin invariants*.

- In the case (*b*) we notice that a solution $\xi(p,\psi)$ of the *linear* equation $\mathcal{F}_+\equiv R_+$ or $\mathcal{F}_-\equiv R_-$ will automatically fulfil (15). We have to follow, in this case, Remark 9 to describe a solution of (11); we call such a solution *pseudo simple waves solution*. We notice ([3]) that [in contrast with a *sws*] a *pseudo sws* has a two-dimensional hodograph and for it none of the characteristic fields in the physical plane x,t is made of straightlines generally.
- The cases (*a*) and (*b*) appear to correspond to a *Martin linearization* strictly associated to (18).
- For the anisentropic "differential" construction above
  - we notice that solution (19) might be regarded as *pseudo nondegenerate* [a formal regular interaction of *pseudo sws*] and,
  - we show, via a comparison with Burnat's approach, that representation (19) is *strictly "nonalgebraic"*.

References

[1] M. Burnat, "The method of characteristics and Riemann's invariants for multidimensional hyperbolic systems", Sibirsk. Math J, vol. 11, pp. 279-309, 1970.

[2] L.F. Dinu, "Multidimensional wave-wave regular interactions and genuine nonlinearity: some remarks", Preprint Series of Newton Institute for Math. Sci., Cambridge UK, No. 29, 2006.

[3] L.F. Dinu, Mathematical concepts in nonlinear gas dynamics, CRC Press, to appear.

[4] E.V. Ferapontov and K.R. Khusnutdinova, "On integrability of (2+1)-dimensional quasilinear systems", Commun. Math. Phys., vol. 248, pp. 187-206, 2004.

[5] Z. Peradzyński, "Nonlinear plane k-waves and Riemann invariants", Bull. Acad. Polon. Sci., Ser. Sci. Tech., vol. 19, pp. 625-631, 1971.

[6] Z. Peradzyński, "Riemann invariants for the nonplanar k-waves", Bull. Acad. Polon. Sci., Ser. Sci. Tech., vol. 19, pp. 717-724, 1971.

[7] T. Zhang and Y.-X. Zheng, "Conjecture on structure of solutions of Riemann problem for two-dimensional gas dynamics", SIAM J. Math. Anal., vol. 21, pp. 593–630, 1990.

On novel wave front problems for reaction-advection-mixing systems

Peter Grindrod[†,*], **Elias Tuma**[‡]
[†]Mathematics Department, University of Reading, Reading, UK
[‡]Mathematics Department, Universidad Tecnica Federico Santa Maria, Valparaiso, Chile
[*]Email: p.grindrod@reading.ac.uk

Abstract

We consider a class of reaction, advection and mixing systems. These arise within situations where a large scale dispersive effect is achieved though a combination of a localised microscopic mixing (or exchange) of mass between "phases" and a concurrent phase-dependent advection process, rather than via either a microscopic diffusion process or the modelling assumption of a macroscopic dispersion term. Such processes generalise velocity jump models and multi-phase models. Coupled with a bistable nonlinear reaction term, the result is a nonlinear transport equation acting over a suitable space, describing the localised distribution of mass with respect to discrete, or a continuum of, phases. Like the reaction-diffusion counterpart we anticipate that such systems will exhibit stable travelling waves.

Introduction

We consider a class of semilinear reaction, advection and mixing systems that give rise to an asymptotic type of dispersion equivalent to a Fickian process. We augment such processes discussed in [1] with a nonlinear reaction term so as to model the dispersal of species in ecology, or reactive species within ecology, chemistry, physiology or geochemistry subject to such advection and mixing within the host environment.

Let X denote a Hilbert space, equipped with inner product denoted by $<.,.>$. Let $A : D(A) \subset X \to X$ denote an operator densely defined on X, We will assume further that the spectrum of A satisfies the following: A has a simple isolated eigenvalue at $\mu_0 = 0$; there exists some value of $\theta \in (0, \pi/2)$ such that any remaining spectrum of A lies within the sector

$$\{z | \pi/2 + \theta < Arg(z - \mu_0) < 3\pi/2 - \theta\}$$

(A is a sectorial operator), and is strictly bounded away from μ_0.

Let $B : X \to X$ denote a bounded linear self adjoint operator defined on X. Let $f : X \to X$ denote a nonlinear mapping, that is Lipschitz continuous.

For $\Omega \subseteq \mathbb{R}$, we let $C^1(\Omega \times \mathbb{R}^+, X)$ denote the space of continuously differentiable functions defined on $\Omega \times \mathbb{R}^+$ taking values in X. For $u \in C^1(\Omega \times \mathbb{R}^+, X)$ $u(x,t)$ denotes the X-value of u at any (x,t) in $\Omega \times \mathbb{R}^+$.

We will interpret functions $u \in C^1(\Omega \times \mathbb{R}^+, X)$ as time dependent density functions for the distribution of some substance, or particles, or population of individual *units*, of interest. To do so we assume there is an element $w_0^* \in X$, such that $\tilde{u}(x,t) =< w_0^*, u(x,t) >$ is the evolving real valued mass density function induced by u for real x in Ω. Then for any subset $\Omega' \subseteq \Omega$, $\int_{\Omega'} \tilde{u}(x,t)dx$ denotes the total mass held within Ω' at time t. In physical applications we would of course additionally require $\tilde{u}(x,t)$ to be nonegative.

If A is a mixing operator, then *conservation of mass* implies that the adjoint operator, A^* say, must satisfy $A^* w_0^* = 0$, hence w_0^* must be the eigenfunction of the adjoint A^* corresponding to the eigenvalue $\mu_0 = 0$.

Consider the following problem, where B maps u onto the corresponding local advective flux, also in X, and A described some (translation invariant), mass conserving, mixing process, and f denotes any state dependent source or sink processes:

$$u \in C^1(\Omega \times \mathbb{R}^+, X), \quad \frac{\partial u}{\partial t} + \frac{\partial (Bu)}{\partial x} = Au + f(u). \quad (1)$$

Of special interest are travelling wave solutions, where some fixed profile for u moves at some speed through the x domain. The interest in such waves is analogous to that for reaction diffusion problems [2].

In [1] the author considers (1) with the nonlinearity, f, absent. Let w_0 denote the eigenfunction for A corresponding to the eigenvalue at the origin, and assume henceforth that $< w_0^*, w_0 >= 1$. Let $\omega =< w_0^*, Bw_0 >$, and $D^* = - < w_0^*, (B - \omega I)A^\dagger (B - \omega I)w_0 >$, where $A^\dagger$ denotes the pseudo inverse for A obtained by restricting A to the orthogonal complement of the subspace spanned by w_0. Let $u(x,t)$ be the solution to the Cauchy problem for (1) (with $f \equiv 0$), defined for all $x \in \mathbb{R}$ and $t > 0$, say. Then in

[1] it is shown that if D^* exists and is strictly positive then there exists a real valued solution $\hat{u}(x,t)$, of the one dimensional equation,

$$\frac{\partial \hat{u}}{\partial t} = D^* \frac{\partial^2 \hat{u}}{\partial x^2} - \omega^* \frac{\partial \hat{u}}{\partial x},$$

such that $||u(x,t) - \hat{u}(x,t)w_0||_X \leq O(1/t)$. Furthermore, if A is self adjoint then D^* is real and positive. Hence there is a direct link between the microscopic advection and mixing processes and a macroscopic Fickian dispersion process.

Example: equations with n distinct phases

Here X is n dimensional Euclidean space. Assuming $u(x,t) = U(z)$ where $z = x - ct$ for some wave speed c, we obtain a system of n ordinary differential equations:

$$(B - cI)U' = AU + f(U).$$

This last may have one or more travelling wave solutions (each determined exactly up to a translation in z) for some discrete values of c. Hence we have a nonlinear eigenproblem for the pair (c, U).

Example: velocity jump models

In [3] and [4] the authors introduce velocity jump models for a population or distribution of particles (or ions, or individuals). A similar notion was employed in [5].

Consider a time, t, dependent population $u(x,v,t)$ of particles evolving a space, parameterised by location x and velocity $v \in [v_{min}, v_{max}]$. It is assumed that a particle moving with velocity $\tilde{v}$, jumps according to a Poisson process of intensity $\lambda(\tilde{v})$. For particles having prior velocity $\tilde{v}$, we introduce the kernel $T(v,\tilde{v})$ to represents the distribution for its possible velocities, v, post-jump. Conservation of mass demands

$$1 = \int_{v_{min}}^{v_{max}} T(v,\tilde{v}))dv \quad \text{for all } \tilde{v}.$$

Then the population is subject to :

$$\frac{\partial u}{\partial t} + v\frac{\partial u}{\partial x} = -\lambda(v)u + \int_{v_{min}}^{v_{max}} T(v,\tilde{v})\lambda(\tilde{v})u(x,\tilde{v},t)d\tilde{v}. \tag{2}$$

Here $X = L^2[(v_{min}, v_{max})]$. Firstly v_{min} and v_{max} should be finite so that B, the act of multiplication by v, is bounded. Secondly A has the form

$$Aw = G.H.w$$

where H and G are linear mappings: $H.w(v) = \lambda(v)w(v)$, $G.y(v) = -y(v) + \int_{v_{min}}^{v_{max}} T(v,\tilde{v})y(\tilde{v})d\tilde{v}$. Zero is an eigenvalue for G, but if $\lambda(v)$ vanishes in $[v_{min}, v_{max}]$ then the inverse of H is unbounded. Hence in general zero may not be an eigenvalue for A in that case. On the other hand if $\lambda(v)^{-1}$ is bounded it will be so.

Now we may wish to determine wave like solutions that occur when we add a nonlinear reaction term to the above transport equation.

Tavelling wave fronts

Our long term aim is to investigate travelling front solutions for systems over general spaces, X, with suitable mappings $f : X \to X$. In this paper we will focus on an exemplar problem, when X is simple.

Here $X = \mathbb{R}^2$ and $u(x,t)$ repesents a distribution over two distinct phases. We consider the system

$$u\frac{\partial u}{\partial t} + \frac{\partial (Bu)}{\partial x} = Au + f(u),$$

$$A = \begin{pmatrix} -a_1 & a_2 \\ a_1 & -a_2 \end{pmatrix},\ B = \begin{pmatrix} b_1 & 0 \\ 0 & b_2 \end{pmatrix}$$

where, a_1 and a_2 represent the nonnegative switching rates; and $b_1 \neq b_2$ are constants representing the phase dependent advection rates. Note $w_0^* = (1,1)^T$ satisfies $A^T.w_0^* = 0$. A has eigenvalues at 0 and -$(a_1 + a_2)$, which is negative.

Without loss of generality (we can rescale, and possibly reflect, the x variable so that) we have $b_1 = 2 + b_2$, and then introducing the travelling coordinate $z = x - (c + b_1 - 1)t$, and writing $u = U(z)$, we obtain

$$\begin{pmatrix} 1-c & 0 \\ 0 & -1-c \end{pmatrix} U' = AU + f(U),$$

Let us write $U = (U_1, U_2)^T$, and assume that $f(U) = (F(U_1), 0)^T$ so that only the first phase is subject to a raection process: the other phase is completely passive.

Then we have

$$(1-c)U_1' = a_2U_2 - a_1U_1 + F(U_1), \tag{3}$$

$$(-1-c)U_2' = a_1U_1 - a_2U_2. \tag{4}$$

Adding (3) and (4) (equivalent premultiplying the system by w_0^{*T}) we have

$$(1-c)U_1' - (1+c)U_2' = F(U_1). \tag{5}$$

Differentiating (3) we may substitute for U_2' in (5) and obtain

$$0 = \frac{1}{a_2}(1-c^2)U_1'' + \tag{6}$$
$$U_1'\left(\frac{c(a_1+a_2)+a_1-a_2}{a_2} - \frac{1}{a_2}(1+c)F_U(U_1)\right)$$
$$+F(U_1).$$

Here F_U denotes dF/dU.

Equation (6) is similar to the travelling front problem obtained for the scalar reaction diffusion problems

$$w_t = w_{xx} + F(w),$$

where writing $w = W(\zeta)$ with $\zeta = x - \eta t$, for some wave speed η, we have

$$0 = W'' + \eta W' + F(W). \tag{7}$$

This must be solved for the profile , W, and the wave speed, η: a nonlinear eigenproblem.

Let us be more specific about F. We assume this is *bistable*, with two roots, one at zero and one at unity, such that both equilibria are locally stable solutions of the ordinary differential equation $w_t = F(w)$.

Let us assume that $\alpha \in (0,1)$ is a constant and $F(w) = w(w-\alpha)(1-w)$. Then (7) has a monotically increasing travelling front solution [2] satisfying $W \to 0$ as $\zeta \to -\infty$, $W \to 1$ as $\zeta \to +\infty$, and unique wave speed $\eta = \sqrt{2}(1/2 - \alpha)$.

Now for such a choice of F we ask whether the same proposition is true of (6). We consider travelling front solutions $(U_1(z), c)$ such that $U_1 \to 0$ as $z \to -\infty$, $U_1 \to 1$ as $z \to +\infty$. In the special; case that $a_1 = a_2$ (symmetrical mixing) we obtain

$$0 = 2(1-c^2)U_1'' + U_1'(2c - 2(1+c)F_U(U_1)) + F(U_1). \tag{8}$$

Now let us assume that the unknown wave speed c lies between the extremes (± 1), representing the advection rates for each phase, then we may introduce a rescaled travelling varaible $y = z/\sqrt{2(1-c^2)}$, and abusing our notation to write $U_1 = U_1(y)$, we have

$$0 = U_1'' + U_1'\frac{(2c - 2(1+c)F_U(U_1))}{\sqrt{2(1-c^2)}} + F(U_1). \tag{9}$$

Then the following is true.

Proposition. If $F(w) = w(w-\alpha)(1-w)$ equation (9) has a monotonic travelling front $U_1(y)$, for a unique value of the wave speed, $-1 < c < 1$; satisfying $U_1 \to 0$ as $y \to -\infty$, $U_1 \to 1$ as $y \to +\infty$..

This in turn provides a solution to the original problem, changing variable from y back to z, and using (4) to obtainn $U = (U_1, U_2)$.

Summary

The class of equations presented here are parabolic only asymptotically, over large space and large time. Yet when coupling dispersion, via mixing and advection processes, with a reaction term, we anticipate that they can support wave fronts similar to those of reaction diffusion systems. In this paper we have ilustrated this phenomenon for a simple example.

Diffusion like terms are often the modeller's *first resort* (Occams' razor!) when incorporating transport and spatial dependence over nonlinear reaction systems. However their provenance is far from trivial. Advective systems, with waves driven by the advective supply of populations or species to reaction zones or reaction fronts, abound within biochemistry, physiology and geochemoistry. Therefore we suggest that this class of models and the novel mathematical challenges inherent in analysing them are highly relevent to many multidisciplinary research programmes over the next few years.

References

[1] P. Grindrod, On models of mispersion at macroscopic scales, BICS preprint, University of Bath, http://www.bath.ac.uk/math-sci/BICS/preprints/BICS06_15.pdf, 2007.

[2] P. Grindrod, Patterns and Waves: The Theory and Applications of Reaction-Diffusion Equations, Second Edition, OUP (1995).

[3] H. Othmer, S. Dunbar, and W. Alt, Models of dispersal in biological systems, Journal of Mathematical Biology, 26 (1988), 263–298.

[4] T. Hillen and H. Othmer, The diffusion limit of transport equation derived from velocity-jump processes, Siam J. Appl. Math., 61 (2000), 751–775.

[5] M.S. Edwards and P. Grindrod, A channel network model for chemical migration in subsurface media, Math. Models and Methods in Applied Science, 5, No 5 (1995) 641-657.

WHAT CHIRP-FREE NLSE SOLITONS CAN STAY ALIVE IN A REAL OPTICAL MEDIUM WITH GAIN AND LOSSES?

N. V. Ostrovskaya, M. N. Zhuravlev
Moscow State Institute of Electronic Technology,
Solnechnaya Alleya, 5, Zelenograd, Moscow, 124498, Russian Federation
Email: ost-miet@yandex.ru

Abstract

The perturbation of the nonlinear Scrödinger equation that transforms it to the form of quintic Ginzburg–Landau equation with the classical soliton as an initial condition is investigated. To average the last equation, the generalized moment method is applied. The derived ordinary differential equations are analyzed on the base of qualitative theory of differential equations. This technique permits to find the new chirp-free soliton branch bifurcating from the initial one. The results of qualitative analysis are compared with those obtained by direct numerical solution of the Ginzburg–Landau equation.

Introduction

The classical nonlinear Scrödinger equation (NLSE) belongs to the class of conservative, fully integrable systems, which extremely seldom realize in nature. The real situation must be described, at least, with processes of gain and losses taken into account. So, the natural questions arise: what will happen with the wellknown NLSE soliton in a real medium? How long is its time of life? At what conditions it can save its magic nondispersivity and stability properties?

To answer these questions let us perturb the NLSE with the function $R[\psi]$:

$$i\psi_t + \sigma\psi_{xx} + \eta|\psi|^2\psi = R[\psi], \tag{1}$$

where $R = i\delta\psi + i\epsilon|\psi|^2\psi + i\beta\psi_{xx} + i\mu|\psi|^4\psi - \nu|\psi|^4\psi$ with σ, η, δ, β, ϵ, μ ν being real constants. In the special case of optical fiber, these quantities are interpreted as follows: ψ is the complex envelope of an electromagnetic field; the parameters δ, ϵ, μ characterize pumping or energy dissipation (depending on their signs); β is a filtering coefficient; ν is the coefficient of a quadratic correction to a nonlinear refractive index. The parameter σ characterizes second-order dispersion ($\sigma = +1/2$ and $\sigma = -1/2$ correspond to anomalous and normal dispersion, respectively), and $\eta = 1$. If $R[\psi]$ is zero, then we have the conventional NLSE with cubic nonlinearity. Thereafter, the perturbed equation takes the form of the Ginzburg–Landau equation, one of the most significant equations in physics.

As a trial function for the theory of perturbation we take the soliton solution of the NSE

$$\psi(x,t) = \frac{A}{\mathrm{ch}[B^{-1}(x-x_c)]}\exp i[\varphi(t) + C(x-x_c)], \tag{2}$$

where A is the soliton amplitude, B is the soliton width, x_c is the center-of mass coordinate, and C is the wavenumber. When $R \equiv 0$, the parameter A in (2) has an arbitrary value, and the other two are related to it as follows:

$$A = B^{-1}, \quad \varphi(t) = A^2 t/2.$$

For the stationary NLSE soliton with center of mass lying on the axis passing through the origin, it holds that $C = 0$ and $x_c = 0$.

Dynamical system

To average the CGLE for further studies of soliton evolution under the perturbations we applied the generalized moment method [1], which can be used to perform a separate analysis of the dynamics both amplitude and width of a soliton solution to the unperturbed problem. The resulting dynamical system for five parameters of the initial condition is as follows [2]:

$$A' = -A\beta\left(\frac{1}{3B^2} + \frac{4}{\pi^2 B^2} + C^2\right) + A\delta + \\ + 2\epsilon A^3\left(\frac{1}{3} + \frac{1}{\pi^2}\right) + 2\mu A^5\left(\frac{4}{15} + \frac{1}{\pi^2}\right), \tag{3}$$

$$B' = \frac{4}{\pi^2}B\left(2\beta\frac{1}{B^2} - \epsilon A^2 - \mu A^4\right), \tag{4}$$

$$C' = -\frac{4}{3}\frac{1}{B^2}\beta C, \tag{5}$$

$$x_c' = 2\sigma C, \tag{6}$$

$$\varphi' = \sigma C^2 - \sigma\frac{1}{3B^2} + \frac{2}{3}\eta A^2 + \frac{8}{15}\nu A^4 - \beta\frac{C}{B}. \tag{7}$$

The equations (3)–(6) do not contain φ, and the system can be analyzed without taking (7) into account. In our

work, the ordinary differential equations were studied on the base of qualitative theory of differential equations [3], thereat the conditions for equilibria existence are of the first importance. As it follows directly from (5), (6), the equilibria exist only if $C = 0$ and $x_c = const$. Thus, it is sufficient to analyze only the equations for the soliton amplitude and width. Introducing the new variables $u = A^2$ and $v = B^2$, we obtain the second-order dynamical system

$$u' = -2\beta a_0 \frac{u}{v} + 2u(\delta + 2\epsilon a_1 u + \mu a_2 u^2), \qquad (8)$$

$$v' = 4\beta b - 2buv(\epsilon + \mu u), \qquad (9)$$

where

$$a_0 = \frac{1}{3} + \frac{4}{\pi^2}, \qquad a_1 = \frac{1}{3} + \frac{1}{\pi^2}, \qquad (10)$$

$$a_2 = 2\left(\frac{4}{15} + \frac{1}{\pi^2}\right), \qquad b = \frac{4}{\pi^2}. \qquad (11)$$

As it was shown in [2], the localized states of the field in (8)–(9) can exist as in the unfiltered problem, so and filtered one, but only when $\mu \neq 0$: at $\mu < 0$ they are stable, while at $\mu > 0$ unstable in both cases.

Unfiltered problem ($\beta = 0$)

The equilibria of the system are found by setting to zero the functions

$$P_1(u) = \mu a_2 u^2 + 2\epsilon a_1 u + \delta, \qquad (12)$$

and

$$Q_1(u) = \epsilon + \mu u. \qquad (13)$$

simultaneously. In [2] it was revealed that the stable localized states of the field relate to the singular line $u = -\epsilon/\mu$. Direct numerical solution of (1) confirmed this conclusion (fig.1). Moreover, the soliton exists in a more wide rang of parameters (ϵ, μ) then it is predicted by the qualitative theory for the dynamical system (8)–(9). In the figure the chronogram of the phase function is shown. It is featured with a flat part in the middle, where the amplitude is far from zero, and nonplanar parts along the edges, where the amplitude is very small. So, whether this soliton can be consider as a chirp-free one is a question. Probably, it can be refer to the class of composite solitons due to a very specific form of its phase function.

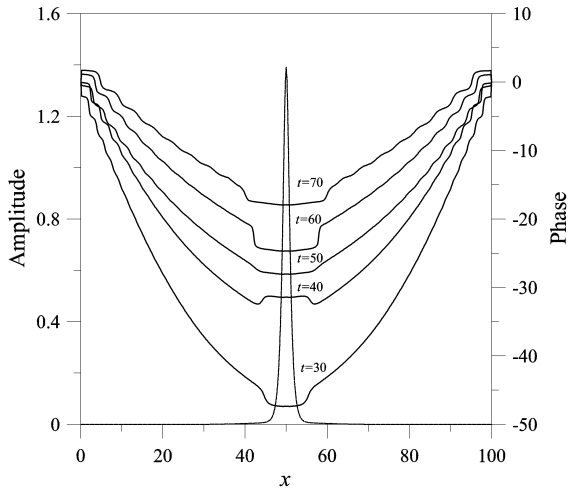

Figure 1: Amplitude and phase of a soliton at several instants for $\beta = 0$, $\delta = -0.1$, $\epsilon = 0.38722$, $\mu = -0.2$, $\nu = 0$.

Filtered problem ($\beta \neq 0$)

In this case the singular points are the roots of the expressions

$$P_2 = -2\beta a_0 \frac{u}{v} + 2u(\delta + 2\epsilon a_1 u + \mu a_2 u^2), \qquad (14)$$

$$Q_2 = 4\beta b - 2buv(\epsilon + \mu u), \qquad (15)$$

namely,

$$u_\pm = \frac{-15\epsilon \pm \Delta_2^{1/2}}{22\mu}, \qquad v_\pm = \frac{2\beta}{u_\pm(\epsilon + \mu u_\pm)}, \qquad (16)$$

where $\Delta_2 = (15\epsilon)^2 - 1320\mu\delta$. Therefore, singular points exist if

$$v_\pm > 0, \quad u_\pm > 0, \qquad u_\pm \neq \epsilon/\mu, \qquad \Delta_2 > 0.$$

By the condition $\Delta_2 > 0$ the elliptic cone $15\epsilon^2 - 88\delta\mu = 0$ divides the three-dimensional parameter space (δ, ϵ, μ) into an exterior set, which contain singular points, and an interior one, which does not. For any particular $\delta <= 0$, the distribution of singular points in the (ϵ, μ) plane, intersecting the cone, for the most important case $\delta < 0$, $\beta > 0$ is presented in the fig. 2. Here, curve *I* (parabola $\mu = 15\epsilon^2/88\delta$) is the intersection of the conic surface and the plane $\delta =$const, and curve *II* (parabola $\mu = 2\epsilon^2/15\delta$) is the locus of points where either v_+ or v_- changes sign. In the upper half-plane the system has one saddle-type singular point $T_+(u_+, v_+)$. If $\delta\mu < 0$ then in the gap between parabolas the system

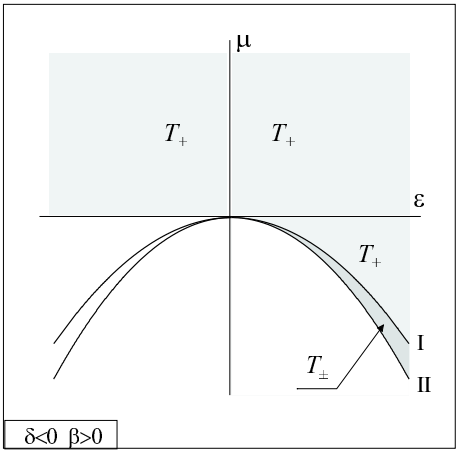

Figure 2: Bifurcation diagram for $\beta \neq 0$.

has two singular points $T_+(u_+, v_+)$ and $T_-(u_-, v_-)$ (dark-gray), namely, saddle and stable node.

The corresponding phase portrait is presented in the fig.3). Dashed curve S in the figure is curve of initial conditions (the amplitude–width curve of the NLSE soliton); asterisks represent the limit values of initial conditions that lead to the formation of a soliton. It is the node that corresponds to the localize soliton of the CGLE (fig.4).

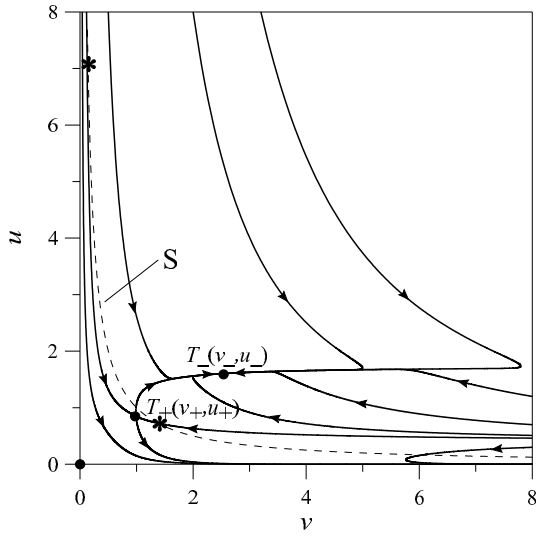

Figure 3: Phase portrait of the system with a saddle point T_+ and a node T_- at $\beta = 0.05$, $\delta = -0.1$, $\epsilon = 0.36$, $\mu = -02$.

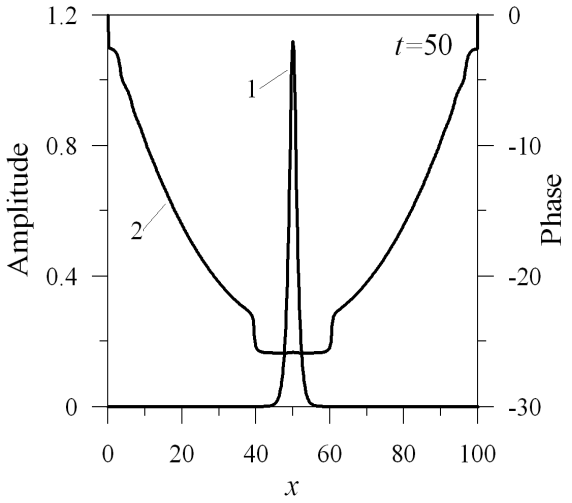

Figure 4: Amplitude (1) and phase (2) of a stable soliton in the filtered problem (below curve II) at $\delta = -0.1$, $\epsilon = 0.36$, $\mu = -0.2$, $\beta = 0.08$

Conclusion

Thus, the qualitative analysis of the dynamical system, which is a result of averaging of the complex nonlinear partial differential equation, gives the answer on the question, formulated in the title of the paper. But not only. It gives the possibility for classification of main types of dynamics of the NLSE soliton in the real physical media ([2]) and permits to purposively look for solutions featured with prescribed properties by analysis of the singular points of the short-cut dynamical system.

References

[1] A.I. Maimistov, "The evolution of solitary waves that are close to NSE solitons", Zh. Eksp. Teor. Fiz., vol. 104, pp. 3620–3625 (1993).

[2] M.N. Zhuravlev, N.V. Ostrovskaya "Dynamics od NSE solitons governed by the cubic–quintic Ginzburg–Landau equation", Zh. Eksp. Teor. Fiz., vol. 126, pp. 483–501 (2004).

[3] N.N. Bautin and E.A. Leontovich, Methods and Techniques for Qualitative Investigations of Dynamic Systems on a Plane, Nauka, Moscow, 1990 [in Russian].

[4] N.N. Akhmediev and A. Ankievich, Solitons: Nonlinear Pulses and Beams, Chapman & Hall, London, 1997; Fizmatlit, Moscow, 2003.

CAPTURING NONLINEAR SURFACE WAVES USING THE MOVING CONTROL VOLUME METHOD

B. Perot[†,*], **D. Schmidt**[‡,*]
[†]Department of Mechanical and Industrial Engineering, University of Massachusetts Amherst, MA 01003, USA
[*]Email: perot@ecs.umass.edu

Abstract

The ability to predict complex, highly nonlinear free-surface physics with accuracy is demonstrated. A moving-mesh approach is used to predict free-surface wave motions. The method uses an unstructured staggered-mesh approach to solve the incompressible Navier-Stokes equations. The method is fully conservative (including kinetic energy and vorticity/circulation). It does not have spurious pressure modes and it retains high mesh resolution of the free-surface at all times.

Introduction

The critical physics in many surface wave problems is essentially controlled by the moving free-surface. In numerical solutions, these critical free-surfaces are often represented by level sets, reconstruction methods like volume of fluids, immersed boundary methods, or combinations of these techniques. However, all these approaches smear the density interface in order to allow it to move through the mesh. They place large approximations and errors in the most critical part of the solution. The alternative approach is to have meshes that move with the free-surface always maintaining the sharp interface between liquid and gas phases. These methods tend to capture the physics well but they also tend to be highly theoretical. For example, boundary element techniques must assume Stokes or potential flow (no vorticity) so that the problem is fully elliptic. Other techniques use mathematical transformations (mappings) that work only for small deformations in a 2D setting. In this work, a general moving-mesh technique (based loosely on [1][2]) is described for computing large surface deformations and highly nonlinear surface waves.

The numerical method is a generalization of the staggered-mesh approach to fully unstructered meshes. It uses the Discrete Calculus approach [3] to exactly discretize the equations. The discrete operators result in a number of local conservation statements and also allow an exact projection scheme [4] to be implemented. Surface tension forces are based on the discrete surface representation itself, not a smooth approximation to the surface. The result is local conservation and exact surface force calculations on spheres and cylinders of finite resolution.

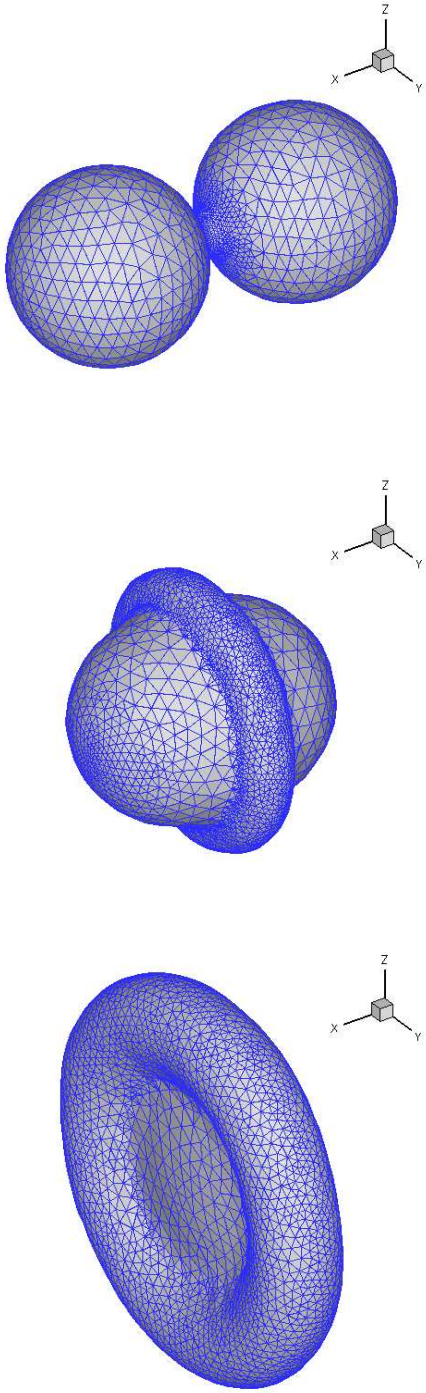

Figure 1: Collision of two liquid droplets.

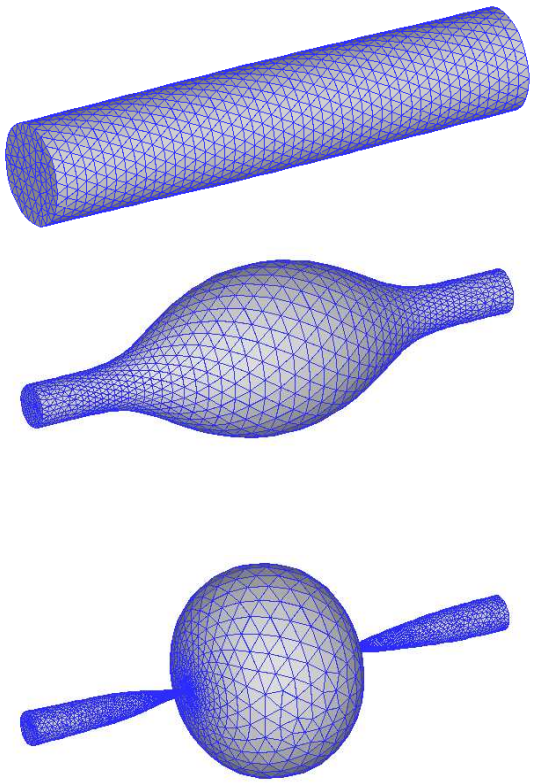

Figure 2: Surface tension instability.

Results

An example calculation is shown in Figure 1, which shows the head-on collision of two liquid droplets and their subsequent deformation. While the surface points move in a Lagrangian manner tracking the surface movement and maintaining very high accuracy near the surface, the interior mesh points do not. They move so that high mesh quality is always maintained. This means that internal vortical fluid motions do not tangle the mesh. The solution method is not an Arbitrary Lagrangian-Eularian (ALE) approach that has a highly diffusive remap stage where solution is mapped from one mesh to another. Instead, the numerical method is based directly on the moving/deforming control volume equations of fluid dynamics.

The placement of interior mesh vertices it determined by solving a generalized spring analogy. This is an elliptic equation for the vertex positions that optimizes a global measure of the mesh quality. In two dimensions this is equivalent to treating the edges between vertices as springs with large spring constants that have timescales much shorter than the fluid motion. In 3D, classical springs do not eliminate sliver cells (with very small volume), but our generalized spring approach can be proven to continue to generate an optimal mesh. For large deformations, such as that shown in figure 1 or 2, the internal mesh connectivity must be dynamically changed. We maintain optimal Delaunay connectivity via a 3D mesh flipping technique [5]. This approach is highly parallel, low cost (10-20 flips per time step), and can be implemented using only two flipping operators if the algorithms is correctly structured [6].

The ability of this approach to accurately compute large deformation waves is shown in Figure 2 where the evolution of a capillary wave (surface tension wave) on a cylinder is shown. The amplitude growth as a function of time is shown in figure 3 and compared to the linearized theory of Rayleigh [7] (good at small times) and quasi-linear theories of Weber [8] and Bogy [9].

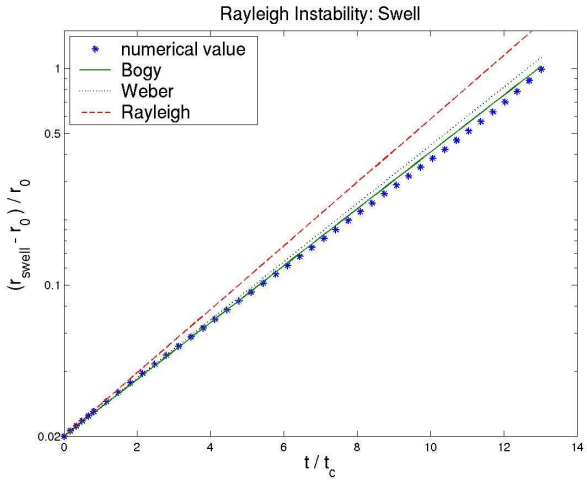

Figure 3: Comparison with theory.

References

[1] J. B. Perot, “Conservation Properties of Unstructured Staggered Mesh Schemes”, J. Comput. Phys., vol. 159, pp. 58-89, 2000.

[2] J. B. Perot and R. Nallapati, ”A Moving Unstructured Staggered Mesh Method for the Simulation of Incompressible Free-Surface Flows”, J. Comput. Phys., vol. 184, pp. 192-214, 2003.

[3] J. B. Perot and V. Subramanian, ”Discrete Calculus Methods for Diffusion”, J. Comput. Phys, vol. 224 (1), pp. 59-81, 2007.

[4] W. Chang, F. Giraldo and J. B. Perot, ”Analysis of an Exact Fractional Step Method”, J. Comput. Phys., vol. 179, 1-17, 2002.

[5] J. B. Perot and R. Nallapati, ”A Moving Unstructured Staggered Mesh Method for the Simulation of Incompressible Free-Surface Flows”, J. Comput. Phys., vol. 184, pp. 192-214, 2003.

[6] R. Nallapati and J. B. Perot, “Numerical simulation of free surface flows using a moving mesh”, Proceeedings of the 2000 ASME Fluids Engineering Summer Conference, 2000.

[7] L. Rayleigh, “On the instability of cylindrical fluid surfaces”, Scientific Papers, vol. 3, pp. 585-593, Cambridge University Press, 1982.

[8] C. Weber, “On the breakdown of a fluid jet”, ZAMM, vol. 1, pp. 136, 1931.

[9] D. B. Bogy, “Drop formation in a circular liquid jet”, A. Rev. Fluid Mech., vol. 11, pp. 207-228, 1979.

Inverse scattering for the nonlinear Schrödinger equation with the Yukawa potential

Hironobu Sasaki[†,*]
[†]Department of Mathematics, Osaka University, 560-0043, Japan
[*]Email: hisasaki1979@gmail.com

Abstract

We study the inverse scattering problem for the three dimensional nonlinear Schrödinger equation with the Yukawa potential. The nonlinearity of the equation is nonlocal. We reconstruct the potential and the nonlinearity by the knowledge of the scattering states.

Introduction

We consider the inverse scattering problem for the three dimensional nonlinear Schrödinger equation

$$i\partial_t u+\Delta u+Q_0\frac{e^{-\mu r}}{r}u-\left(Q_1\frac{e^{-\mu r}}{r}*|u|^2\right)u=0 \quad \text{(NLS)}$$

in $\mathbb{R}\times\mathbb{R}^3$. Here, u is a complex-valued unknown function of $(t,x)\in\mathbb{R}\times\mathbb{R}^3$, $\partial_t=\partial/\partial t$, Δ is the Laplacian in $\mathbb{R}^3$, $r=|x|$, $Q_0,Q_1\in\mathbb{R}^3$, $\mu>0$ and $*$ is the convolution in the space variables.

The equation (NLS) is approximately derived from the generalization of the electronic Hamiltonian for an N-electron atom in a plasma

$$-\frac{1}{2}\sum_{j=1}^{N}\Delta_j-\sum_{j=1}^{N}\frac{Ze^{-\mu|x^j|}}{|x^j|}+\sum_{j>k}^{N}\frac{e^{-\mu|x^j-x^k|}}{|x^j-x^k|}$$

where $x^j\in\mathbb{R}^3$ is the space variables for the j-th particle, Δ_j is the Laplacian with respect to x_j, Z is the nuclear charge and μ is a parameter depending on the density and the temperature of the plasma (see, e.g., Mukherjee–Karwowski–Diercksen [1]).

Scattering

In order to mention the inverse scattering problem, we introduce the definition of the scattering operator for the nonlinear evolution equation

$$i\partial_t v(t)+J(v(t))=f(v(t)),\quad t\in\mathbb{R}, \tag{1}$$

where v is a complex-valued function on the Hilbert space X, J is a self-adjoint operator on X and f is a mapping on some subspace of X. Let $B(\delta;X)$ be the set of all $\phi\in X$ with $\|\phi\|_X\le\delta$. *The scattering operator* S is defined by the mapping

$$S:B(\delta;X)\ni\phi_-\mapsto\phi_+\in X$$

if the following condition holds for some $\delta>0$ and some $Z\subset C(\mathbf{R};X)$:

For any $\phi_-\in B(\delta;X)$, there uniquely exists $v\in Z$ such that v is a time-global solution to (1) and satisfies

$$\lim_{t\to-\infty}\|v(t)-e^{itJ}\phi_-\|_X=0.$$

Furthermore, there uniquely exists $\phi_+\in X$ such that

$$\lim_{t\to\infty}\|v(t)-e^{itJ}\phi_+\|_X=0.$$

We remark that $e^{itJ}\phi$ is a solution to the Cauchy problem for

$$\begin{cases} i\partial_t v(t)+J(v(t))=0, & t\in\mathbb{R},\\ v(0)=\phi. \end{cases}$$

Inverse Scattering

The inverse scattering problem for the equation (1) is to recover the perturbed term f by applying the knowledge of the scattering operator S. Before we treat (NLS), we first review the inverse scattering problem for the Schrödinger equation with power nonlinearity briefly. Strauss [6] considered the nonlinear Schrödinger equation

$$i\partial_t u+\Delta u=V(x)|u|^{p-1}u,\quad (t,x)\in\mathbb{R}\times\mathbb{R}^n.$$

Suppose that p is an integer satisfying

$$\begin{cases} p>4 & \text{if } n=1,\\ p>3 & \text{if } n=2,\\ p\ge 3 & \text{if } n\ge 3, \end{cases}$$

and $V(x)$ is real-valued continuous and bounded, whose derivatives up to order $l>3n/4$ are bounded. Then the scattering operator S is well-defined. It was shown that $V(x)$ is recovered from the scattering operator by the following way: For $s\in\mathbb{R}^n$, let $H^s(\mathbb{R}^n)$ be the Sobolev space $(1-\Delta)^{-s/2}L^2(\mathbb{R}^n)$. For any $\phi\in H^1(\mathbb{R}^n)\cap L^{1+1/p}(\mathbb{R}^n)$, we have

$$V(x_0)=\frac{\lim_{\alpha\to0}\alpha^{-(n+2)}I[\phi_{\alpha,x_0}]}{\displaystyle\int_{\mathbb{R}}\int_{\mathbb{R}^n}|e^{it\Delta}\phi(x)|^{p+1}dxdt}, \tag{2}$$

where $\phi_{\alpha,x_0}(x) = \phi(\alpha^{-1}(x-x_0))$, $x, x_0 \in \mathbb{R}^n$ and

$$I[\phi] = \lim_{\varepsilon\to 0} \frac{i}{\varepsilon^p}\big\langle (S-id)(\varepsilon\phi), \phi\big\rangle_{L^2(\mathbb{R}^n)}.$$

The above limit is called the small amplitude limit.

Unfortunately, the above method to obtain the reconstruction formula (2) is not applicable to the case (NLS) with $Q_0 = 0$. The essential point to prove the formula (2) is the change of variables in the following integral:

$$I[\phi] = \int_{\mathbb{R}}\int_{\mathbb{R}^n} V(x)|e^{it\Delta}\phi(x)|^{p+1}dxdt.$$

By changing variable x by $\alpha^{-1}(x-x_0)$, we have

$$I[\phi_{\alpha,x_0}] = \alpha^{n+2}\int_{\mathbb{R}}\int_{\mathbb{R}^n} V(x_0+\alpha x)|e^{it\Delta}\phi(x)|^{p+1}dxdt.$$

Therefore, as $\alpha \to 0$, we can take the value $V(x_0)$ from the inside integral. Applying the same method to (NLS) with $Q_0 = 0$, we obtain

$$\begin{aligned} &I[\phi_{\alpha,x_0}] \\ &= \int_{\mathbb{R}}\int_{\mathbb{R}^n} \big(V * |e^{it\Delta}\phi_{\alpha,x_0}(x)|^2\big)|e^{it\Delta}\phi_{\alpha,x_0}(x)|^2 dxdt \\ &= \alpha^{2n+2}\int_{\mathbb{R}}\int_{\mathbb{R}^n} \big(V(\alpha\cdot) * |e^{it\Delta}\phi(x)|^2\big)|e^{it\Delta}\phi(x)|^2 dxdt, \end{aligned}$$

where $V(x) = Q_1\dfrac{e^{-\mu r}}{r}$. Since the integral

$$\int_{\mathbb{R}}\int_{\mathbb{R}^n} \big(V(0) * |e^{it\Delta}\phi(x)|^2\big)|e^{it\Delta}\phi(x)|^2 dxdt$$

does not converge, we can not make α tend to infinity.

We next review the inverse scattering problem for the nonlinear Schrödinger equation with a cubic convolution

$$i\partial_t u + \Delta u + \widetilde{V}(x)u = F^\sigma(u), \quad (t,x) \in \mathbb{R}\times\mathbb{R}^n. \tag{3}$$

Here, $\widetilde{V} : \mathbb{R}^3 \to \mathbb{C}$ is measurable and satisfies some suitable condition,

$$F^\sigma(u) \quad = \lambda(x)(|\cdot|^{-\sigma} * |u|^2)u$$

and $\lambda \in C^1(\mathbf{R}^n)\cap W^1_\infty(\mathbf{R}^n)$. It was proved by Watanabe [7] that if σ is a given number, then we can reconstruct V and λ by the knowledge of the scattering operator. Watanabe [8] determined σ of the term F^σ if $\widetilde{V} \equiv 0$ and $\lambda(x)$ is a non-zero constant function. Under the condition $\widetilde{V} \equiv 0$, Sasaki [5] proved that σ of F^σ can be determined even if λ_j is not a constant. In fact, σ is given by

$$\sigma = 2n+2 - \lim_{\alpha\to 0}\ln\frac{|T[\phi_{e\alpha}]|}{|T[\phi_\alpha]| + \alpha^{2n+2}}, \tag{4}$$

$$T[\phi] = \lim_{\varepsilon\to 0}\frac{i}{\varepsilon^3}\big\langle (S-id)(\varepsilon\phi), \phi\big\rangle_{L^2(\mathbb{R}^n)},$$

where e is the base of the natural logarithm, $\phi \in H^1(\mathbb{R}^n)\setminus\{0\}$, $\phi_\alpha = \phi_{\alpha,0}$ and S is the scattering operator.

As we mention before, we study the inverse scattering problem for (NLS). Remark that we can not directly apply the known results to recovering the terms $V_j := -Q_j\dfrac{e^{-\mu r}}{r}u$, $j = 1, 2$.

Main Results

Our goal is to give a formula for determining the parameter Q_0, Q_1 and μ by using the knowledge of the scattering operator for (NLS) given by Theorem 0.1 below.

We now define some notation which will be used later. We put $L^2(\mathbb{R}^3) = \mathcal{H}$. We denote the norm and the inner product of $\mathcal{H}$ by $\|\cdot\|$ and $\langle\cdot,\cdot\rangle$, respectively. For $1 \le p, q \le \infty$, $\|\cdot\|_q$ and $\|\cdot\|_{(p,q)}$ denote $\|\cdot\|_{L^q(\mathbb{R}^3)}$ and $\|\cdot\|_{L^p(\mathbb{R};L^q(\mathbb{R}^3))}$, respectively. We set $F(u) = -(V_1 * |u|^2)u$. Let H be an unbounded operator on $\mathcal{H}$ defined by

$$D(H) = H^2(\mathbb{R}^3), \quad H = -\Delta + V_0.$$

The Kato-Rellich theorem implies that H is self-adjoint on $D(H)$ (for the detail, see Theorem X.15 in [2]). Therefore, we see that $e^{-itH} : \mathcal{H} \to \mathcal{H}$ is a unitary operator. That is, we have

$$\|e^{-itH}\phi\| = \|\phi\| \tag{5}$$

for any $\phi \in \mathcal{H}$. For a measurable function $V : \mathbb{R}^3 \to \mathbb{C}$, we set

$$\|V\|_R = \sqrt{\int_{\mathbb{R}^{3+3}} \frac{|V(x)V(y)|}{|x-y|^2}d(x,y)},$$

$$\|V\|_{\mathcal{K}} = \sup_{x\in\mathbb{R}^3}\int_{\mathbb{R}^3}\frac{|V(y)|}{|x-y|}dy.$$

The norm $\|\cdot\|_R$ is said to be the Rollnik norm. Our first result is concerned with the direct scattering problem for (NLS).

Theorem 0.1. *Assume that*

$$\frac{|Q_0|}{\mu} < 4\pi\min\left\{\left\|\frac{e^{-r}}{r}\right\|_R^{-1}, \left\|\frac{e^{-r}}{r}\right\|_{\mathcal{K}}^{-1}\right\}. \tag{6}$$

Let $Y_1 = L^3(\mathbb{R};L^{18/7}(\mathbb{R}^3))$ and $Z_1 = C(\mathbb{R};\mathcal{H})\cap Y_1$. Then there exists some $\delta > 0$ such that if $\phi_- \in B(\delta;\mathcal{H})$, then there uniquely exists $u \in Z_1$ such that u is a time-global solution to (1) and satisfies

$$u(t) = e^{-itH}\phi_- + \frac{1}{i}\int_{-\infty}^t e^{-i(t-\tau)H}F(u(\tau))d\tau, \tag{7}$$

$$\lim_{t\to-\infty}\|u(t) - e^{-it\Delta}\phi_-\| = 0. \tag{8}$$

Furthermore, there exists a unique $\phi_+ \in \mathcal{H}$ such that

$$\lim_{t\to\infty} \|u(t) - e^{-it\Delta}\phi_+\| = 0. \tag{9}$$

Therefore, the scattering operator for (NLS)

$$S_1 : B(\delta;\mathcal{H}) \ni \phi_- \mapsto \phi_+ \in \mathcal{H}$$

is well-defined.

It is well-known that the wave operators

$$\Omega_\pm = s - \lim_{t\to\pm\infty} e^{itH}e^{it\Delta} : \mathcal{H} \to \mathcal{H}$$

and the inverse wave operators

$$\Omega_\pm^* = s - \lim_{t\to\pm\infty} e^{-it\Delta}e^{-itH}P_{ac} : \mathcal{H} \to \mathcal{H}$$

are well-defined (see Theorem XI.30 in [3]). Here, P_{ac} means the projection onto the absolutely continuous subspace of H. If we have $\|V_0\|_R < 4\pi$, then P_{ac} becomes identity (see the proof of Theorem XIII.21,(a) in [4]). We define a mapping S_{V_0} by

$$S_{V_0} = \Omega_+^*\Omega_- : \mathcal{H} \to \mathcal{H}.$$

The operator S_{V_0} is the scattering operator for (1) with $J = -\Delta$ and $f(u) = -V_0 u$.

Using the method of [7], we see that S_{V_0} can be determined from the knowledge of S_1.

Theorem 0.2. *([7]) Assume that (6) holds. For any $\phi \in \mathcal{H}\setminus\{0\}$, we have*

$$\lim_{\varepsilon\to 0}\frac{1}{\varepsilon}S_1(\varepsilon\phi) = S_{V_0}(\phi) \quad \text{in } \mathcal{H}. \tag{10}$$

Once we have determined S_{V_0}, we can reconstruct V_0, $e^{\pm itH}$, $\Omega_\pm$, $\Omega_\pm^*$ by Enss and Weder [9]. Therefore, we can see the exact value of Q_0, and of μ if $Q_0 \neq 0$. If $Q_0 = 0$, then we see that $H = H_0$, but μ is still unknown. The remained unknown numbers are determined by the following result:

Theorem 0.3. *Assume that (6) holds.*

(i) If $Q_0 \neq 0$, then we have for any $\phi \in \mathcal{H}\setminus\{0\}$,

$$Q_1 = \frac{\lim_{\varepsilon\to 0}\frac{i}{\varepsilon^3}\Big\langle(\Omega_+S_1\Omega_-^* - id)(\varepsilon\phi),\phi\Big\rangle}{\left\|\left(\frac{e^{-\mu r}}{r} * |e^{-itH}\phi|^2\right)|e^{-itH}\phi|^2\right\|_{(1,1)}}. \tag{11}$$

(ii) If $Q_0 = 0$, then we have for any $\phi \in H^{1/4}(\mathbb{R}^3)\setminus\{0\}$,

$$\frac{Q_1}{\mu^2} = \frac{\lim_{\lambda\to\infty} i\lambda^4\Big\langle(S_1 - id)(\lambda^{-3}\phi_\lambda),\phi_\lambda\Big\rangle}{\left\|\frac{e^{-r}}{r}\right\|_1 \|e^{it\Delta}\phi\|_{(4,4)}^4}, \tag{12}$$

$$\frac{Q_1}{\mu} = \frac{\displaystyle\int_0^\infty \lambda^{-7}\lim_{\varepsilon\to 0}\frac{i}{\varepsilon^3}\Big\langle(S_1 - id)(\varepsilon\phi_\lambda),\phi_\lambda\Big\rangle d\lambda}{\left\|\left(r^{-2} * |e^{it\Delta}\phi|^2\right)|e^{it\Delta}\phi|^2\right\|_{(1,1)}}. \tag{13}$$

References

[1] P. Mukherjee, J. Karwowski and G. Diercksen, On the influence of the Debye screening on the spectra of two-electron atoms, Chem. Phys. Lett. 363 (2002), 323–327.

[2] M. Reed and B. Simon, Methods of modern mathematical physics II, Academic Press 1975.

[3] M. Reed and B. Simon, Methods of modern mathematical physics III, Academic Press 1978.

[4] M. Reed and B. Simon, Methods of modern mathematical physics IV, Academic Press 1977.

[5] H. Sasaki, The inverse scattering problem for Schrödinger and Klein-Gordon equations with a nonlocal nonlinearity, Nonlinear Analysis, Theory, Methods & Applications 66 (2007), 1770–1781.

[6] W. Strauss, Non linear scattering theory, in "Scattering Theory in Mathematical Physics", pp. 53–78. J. A. Lavita and J.-P. Marchand, editors, D. Reidel, Dordrecht-Holland / Boston 1974.

[7] M. Watanabe, Inverse scattering for the nonlinear Schrödinger equation with cubic convolution nonlinearity, Tokyo J. Math. 24 (2001), 59–67.

[8] M. Watanabe, Reconstruction of the Hartree-type nonlinearity, Inverse Problems 18 (2002), 1477–1481.

[9] V. Enss and R. Weder, The geometrical approach to multidimensional inverse scattering, J. Math. Phys. 36 (1995), 3902–3921.

DISCRETE NONLINEAR SOLITARY WAVES : SIMULATION OF LINEAR WAVE EQUATIONS

J. Steinhoff[†,*], **S. Chitta**[‡,*]
[†]MAES Department, University of Tennessee Space Institute, Tullahoma, TN 37388, USA
[‡]Graduate Research Assistant, UTSI
[*]Email:jsteinho@utsi.edu

Abstract

A new method is described to compute thin pulse solutions to the multidimensional wave equation that can propagate over long distances. Unlike conventional numerical solutions, these waves remain narrow, several grid cells (h) in width, and never spread due to discretization error. These "pulses" represent a travelling wave front as a codimension 1 surface in the limit $h \Rightarrow 0$. The wave has two conserved quantities as it transverses a grid point : total amplitude and centroid speed.

Introduction

A *nonlinear* method is described to economically represent the solution to a *linear* wave equation. This is different from most work on solitary waves which involves *linear* methods to solve *nonlinear* wave equations. The reason that this offers an attractive means of simulating waves is that conventional Eulerian computational methods typically rapidly degrade the solution over distances even if complex higher order numerical methods are used [1]. Also, unlike Lagrangian "Ray Tracing"[2], which attempts to solve similar problems, the solitary waves are Eulerian and represent intrinsically codimension 1 surfaces rather than collections of marker coordinates.

Methodology

A simple example of this concept in one dimension involves the convection or wave equation for a passive scalar that is concentrated in a small region. The goal then, is to ensure that it remains compact and non-oscillatory - essentially spread over a small number of cells, and that it preserves the important properties of the linear convection/wave equation. Only a few important properties are considered since the pulse width is only a few grid cells. The method is related to another - "Vorticity Confinement" for solving fluid flows with thin vortical regions [3].

We start with a simple convective difference method, centered in space and explicit, first order Euler in time.

$$\phi_j^{n+1} = \phi_j^n - \frac{1}{2}\left(\nu_{j+1}\phi_{j+1}^n - \nu_{j-1}\phi_{j-1}^n\right) + E_j^n \qquad (1)$$

where j is the spatial grid index, the time is nΔt, c_j is the convection speed, and $\nu_j = \frac{c_j \Delta t}{j}$. We introduce a "Confinement" term, E_j^n. $E_j^n = 0$ would result in an unstable centered scheme, and any diffusion added for stability would make it dissipative and spread over time. However, a nonlinear term can be added to maintain stability and in addition, keep the pulse close to its desired, compact shape. The term acts like a "forward backward" heat equation in the frame propagating with the pulse.
For the convection equation, a simple form, $E_j^n = \delta_j^2 F_j^n$ conserves the total amplitude and centroid speed, since $\sum_j E_j = 0$ and $\sum_j jE_j = 0$. Here, δ_j^2 is a discrete second difference operator and F_j^n is a function of ϕ and its differences which vanish in the far field. A preliminary version of the method was presented in [4].

For accurate simulations, F_j^n must be homogeneous of degree 1 in ϕ, as the other terms in the linear pde, so that there is no dependence on the amplitude, or scale of ϕ. Also, $\delta_j^2 F_j^n$ must represent a negative diffusion for long wavelengths, contracting the pulse. To prevent instabilities from negative diffusion, it is then required to use a nonlinear form for F_j^n. For short wavelengths, $\delta_j^2 F_j^n$ must be positive, spreading the pulse and relaxing it to a desired shape.

A simple formulation that satisfies the above requirement is $F_j^n = \mu\phi_j^n - \epsilon\Phi_j^n$ where μ and ε are constants, and Φ_j^n is a nonlinear mean (there are many other forms) given by

$$\Phi_j^n = 3\left[\sum_{j-1}^{j+1}(\phi_l^n)^{-1}\right]^{-1} \qquad (2)$$

The exact "sampled" pulse height at any given time step depends on the centroid position, as if an approximately fixed pulse shape were "moved" through the grid at a weighted average velocity. In the small Δt "semidiscrete" limit, for constant c, ϕ satisfies $\delta_j^2(\mu\phi_j^n - \epsilon\Phi_j^n) = 0$ for which the solution is given by

$$\phi_j^n = A\,sech\left(\gamma\left(x - x_0 - ct\right)\right) \qquad (3)$$

where A is the initial amplitude, x_0 is the initial centroid position and $\cosh(\gamma) = \left(\frac{3\epsilon}{\mu} - 1\right)/2$. A depends periodically (slightly) on position in each cell.

For the discrete wave equation, the "Confinement" term involves a time derivative:

$$\phi_j^{n+1} = 2\phi_j^n - \phi_j^{n-1} + \delta_j^2 \nu_j^2 \phi_j^n + \delta_n^- E_j^n \qquad (4)$$

where $\delta_n^- E_j^n = E_j^n - E_j^{n-1}$
In 2-D, we have the same behaviour for a straight line pulse: $\phi_{ij}^n = Asech\left(\gamma\left(z - z_0 - ct\right)\right)$ and $\frac{\epsilon}{\mu} = [1 + 2cosh(\gamma\cos\theta) + 2cosh(\gamma\sin\theta)]/5$. Here, the width of the pulse, γ^{-1} will depend on the orientation of the line - θ. However, the centroid propagation speed in the normal direction is independent of θ, so that in the small cell limit, it accurately represents the wavefront of an isotropic wave equation. A dependence on angle was also seen in [5]. An important point is that there is no effect on the amplitude and centroid after the solitary waves pass through each other.

Continuum case

As an example, we consider a scalar (ϕ) advecting at a speed *c* that, in the continuum case, would satisfy the pde

$$\partial_t \phi = -\partial_x c\phi \qquad (5)$$

Our basic point is that there will be errors when we discretize equation 5, and when we confine the pulse solution to ∼2-3 grid cells, these "errors" will be large. However, corresponding to the small number of grid points within in the pulse, there will be only a small number of quantities that we can conserve (for a continuum pulse solution of equation 5, there are an infinite number of conserved quantities): By integrating equation 5 or premultiplying by x and then integrating, it is easy to see that adding a term $E = \partial_x^2 F(\{\phi\})$, that vanishes at the boundaries, along with derivatives, will not affect the conservation of the total amplitude

$$A = \int \phi dx \qquad (6)$$

or the speed of the centroid, *V*, where the centroid is

$$< x >= \int x\phi dx/A \qquad (7)$$

and

$$V = \frac{d < x >}{dt} = \int \phi c(x) dx/A \qquad (8)$$

To satisfy these conditions, and to keep the essential physics of equation 5 for a short convecting pulse, we want *E* to satisfy a set of conditions described above. In the convecting frame of the pulse, the pde becomes the heat equation $\partial_t \phi = E$. If we take

$$E = \partial_x^2(\mu\phi - \epsilon\Phi) \qquad (9)$$

where Φ is a nonlinear function of ϕ, then at convergence, $\mu\phi_0(s) = \epsilon\Phi(\phi_0(s))$. For the discrete case, $\phi(s)$ will stay close to $\phi_0(s)$. The discrete form given in equation 1, which involves a harmonic mean, when Taylor expanded on a grid with cell size *h*, using equation 9 for E, gives

$$\partial_t\phi + c\partial_x\phi = -\beta h^2 \partial_x^2 \phi - \frac{\epsilon h^2}{3}\partial_x^2\left(\partial_x^2\phi - 2\frac{\left(\partial_x\phi\right)^2}{\phi}\right) \qquad (10)$$

where $\epsilon = \mu + \beta h^2$ and ($\epsilon > \mu$). The pulse then relaxes to the form given by equation 3. It is interesting that the role of the second order term in equation 10 is different from most popular nonlinear pde's, such as KdV, that harbor solitary waves: In these, the linear (diffusion or dispersion) term is the "expansion" term, and the "contraction", or "steepener" term is the nonlinear Burgers-like convection: $(\partial_x\phi^2/2)$. Here, the linear diffusion term acts to contract and prevents ϕ from changing sign, and it is the nonlinear term that expands. Also, the $\frac{1}{\phi}$ term there increases the expansion as the pulse contracts, until a balance is reached.

Results

The solution of the discretized wave equation in 1-D is presented in Fig.1, for a conventional discretization, and with the Confinement term which results in a solitary wave. Periodic boundary conditions were used. The conventional solution and the solitary wave had passed through the grid 15 times. In Fig.2, contours are presented for the 2-D solitary wave solution with periodic boundary conditions. In Fig.3, a solitary wave solution is shown as in Fig.2, but in 3-D. The solutions of Figs.1-4 involve constant index of refraction. The 2-D solution of Fig.4 involves a non-constant index of refraction. As validation, Lagrangian markers which follow the correct paths, as in Ray Tracing methods [2], were superimposed on the computed solitary wave amplitude contours. In Fig.5, an elliptical pulse is shown that converges to a focus and then diverges. Despite lack of grid resolution at the focus, the final result is correct, since the method enforces correct motion for second order moments. As in Fig.4, Lagrangian markers are superimposed for validation.

Acknowledgement

This work was sponsored by AFOSR.

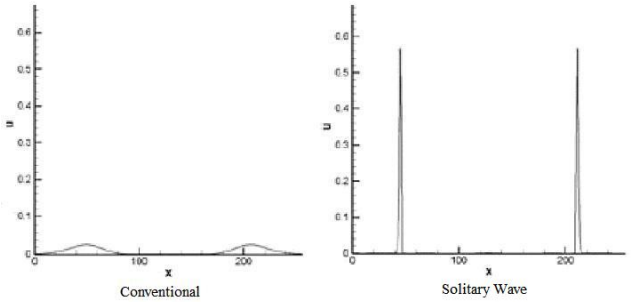

Figure 1: 1D Wave Equation

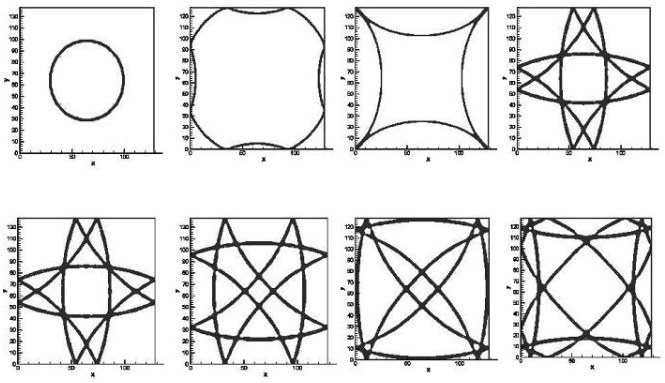

Figure 2: 2D Wavefront Propagation

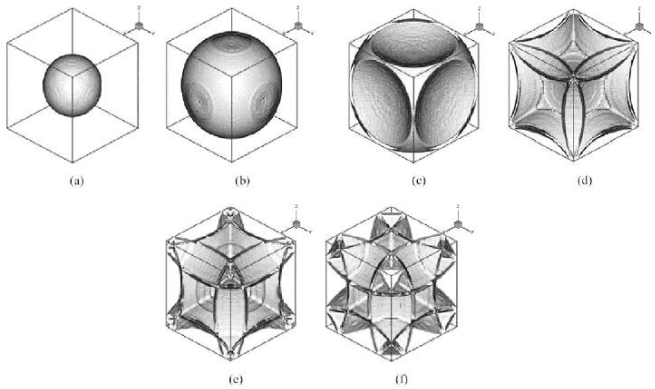

Figure 3: 3D Wavefront Propagation

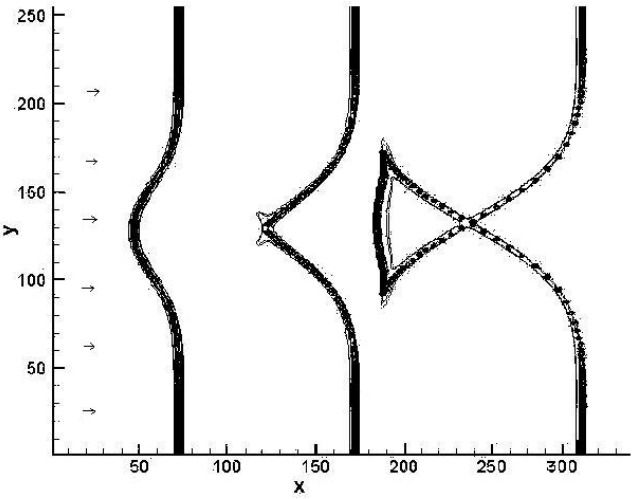

Figure 4: Variable Index of Refraction

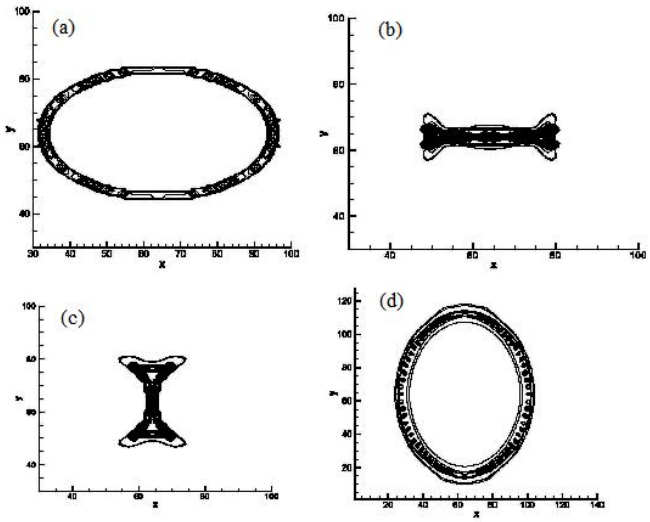

Figure 5: Focussing Elliptical Wavefront

References

[1] D.V. Gaitonde, J.S. Shang, J.L. Young, "Practical Aspects of Higher-Order Numerical Schemes for Wave Propagation Phenomena",International J. of Numerical Methods in Engineering, vol. 45, pp. 1849-1869, 1999.

[2] V. Vinje, E. Iversen, H. Gjoystdal, "Traveltime and amplitude estimation using wavefront construction", Geophyics, vol. 58, no. 8, pp. 1157-1166, 1993.

[3] J. Steinhoff *et al.*, "Large Eddy Simulation Using Vorticity Confinement" ,Chapter 4 in Implicit Large Eddy Simulation: Computing Turbulent Flow Dynamics, Edited by F. F. Grinstein, L. G. Margolin, and W. J. Rider, Cambridge University Press, 2006.

[4] M. Fan, L. Wang, J. Steinhoff, W. Dietz, "Convection of concentrated vortices and passive scalars as solitary waves", Journal of Scientific Computing, December, 2003.

[5] O.A. Druzhinin, L.A. Ostrovskii, "Solitons in discrete lattices",Physics Letters A, vol. 160, no. 4, pp. 357-362, November, 1991.

RESONANT SOLUTIONS OF THE PERIODICALLY FORCED eKdVB EQUATION

Philippe Trinh[†], **David E. Amundsen**[†,*]
[†]School of Mathematics and Statistics, Carleton University, Ottawa, ON, Canada
[*]Email: dave@math.carleton.ca

Introduction

We consider the steady (long time) periodic solutions of a class of damped extended Korteweg-de Vries equations with Burger's damping (eKdVB) and with periodic forcing. In particular we consider equations of the form

$$u_t - \gamma u_{xxx} + \Delta u_x + \alpha u u_x + \beta u^2 u_x - \mu u_{xx} = f(x), \quad (1)$$

on the domain $x \in [0, 2L]$ where $f(x)$ corresponds to an arbitrary forcing with period $2L$. The parameter γ provides a measure of the linear dispersive effects, μ the diffusive effects, and α, β the nonlinear effects. Finally Δ may be seen as a measure of detuning from resonance.

While model equations of this type arise in a number of physical scenarios, analysis depends crucially on the relative magnitude of the various parameters. In some cases either one or both of the nonlinear terms may be considered weak, or forcing effects may be considered weak, and in others they cannot. In the case where both nonlinear and forcing effects are strong it is known that a rich array of steady solutions emerge. While analytic studies in this regime have been performed, for instance [1], [2], they remain limited in terms of their scope. Recently Amundsen, Cox and Mortell [3] developed a general framework based on singular perturbation and asymptotic matching in the context of the forced KdV equation ($\beta = 0$). We now extend this to the more general eKdV case, and in doing so will not only characterize and illustrate the much wider class of solutions, but also further develop the methodology and illuminate its features and limitations.

Analytic Approximation of Steady Solutions

We return to (1) and where in order to ensure boundedness of the long-time solutions it is assumed that the periodic forcing, $f(x)$ has zero mean. This often corresponds physically to a global constraint such as mass conservation. Consequently enforcing periodicity in x for u we may assume without loss of generality that u satisfies the global condition

$$\int_0^{2L} u(x,t)dx = 0. \quad (2)$$

While the question of non-steady solutions is also interesting and indeed while there are some cases where aperiodic and even chaotic behaviour is observed, [4], we restrict our focus to cases where the dissipative effects render the solution steady in the limit $t \to \infty$. Thus (1) reduces to the ODE

$$-\gamma u_{xx} + \Delta u + \frac{\alpha}{2}u^2 + \frac{\beta}{3}u^3 - \mu u_x = F(x) + C, \quad (3)$$

where $F(x)$ is taken as the anti-derivative of $f(x)$ also having zero mean. Consequently we see immediately through (2) that the integration constant

$$C = \frac{1}{2L}\int_0^{2L} \alpha\frac{u^2}{2} + \beta\frac{u^3}{3}dx.$$

In the present context, as noted above, we consider the case where the dissipative effects are small $\gamma \ll 1$, the diffusive parameter $\mu = O(\gamma) = \nu\gamma$ and all other parameters, and the forcing are assumed order unity. We now seek to obtain approximate solutions, asymptotically valid in the limit that $\gamma \to 0$. First if we apply a simple perturbation expansion $u = u_0 + \sqrt{\gamma}u_1 + \ldots$ then to leading order we see that

$$\Delta u_0 + \alpha\frac{u_0^2}{2} + \beta\frac{u_0^3}{3} = F(x) + C.$$

Using standard formulas for roots of cubic polynomials, the solutions u_0 may be determined. For example in the case where $\alpha = 0$ (mKdV)

$$u_{0_k} = \frac{\rho^{1/3}}{2\beta}e^{2\pi ik} - \frac{2\Delta}{\rho^{1/3}}e^{-2\pi ik}, \qquad k = 0, 1, 2$$

$$\rho = \left(12[F(x)+C] + 4\sqrt{M}\right)\beta^2, M = \frac{4\Delta^3 + 9\beta[F(x)+C]^2}{\beta}.$$

However not all such solutions may satisfy (2) for all values of C and indeed it is not assured that at all points these solutions are either real or differentiable. In this case we note that there exist two critical values $\Delta = 0$, and $\Delta = \Delta_M$ where $M = 0$ corresponding to when roots transition from being complex to real and vice versa. It can be seen that for intermediate values of Δ the non-dispersive solutions may be real for certain values of x, but not over the entire interval, whereas outside this "resonant band" one non-dispersive solution is entirely real and also satisfies (2) for some value of C. Therefore,

for parameter values within this resonant range, we must modify our approach and allow for dispersive effects to play a role. Therefore we introduce a layer at $x = \delta$ where dispersive effects cannot be neglected at leading order. Within this layer we introduce a new coordinate

$$X = \frac{\omega_1(x)}{\sqrt{\gamma}} + \omega_2(x) + \sqrt{\gamma}\omega_3(x) + \ldots, \qquad (4)$$

so that the solutions $u = u(x, X)$ are now assumed to vary on both the slow and fast coordinate scale. Thus applying a perturbative approach $u(x, X) = u_0(x, X) + \sqrt{\gamma}u_1(x, X) + \gamma u_2(x, X) + \ldots$ it can be seen that to leading order,

$$-(\omega_1')^2 u_{0XX} + \frac{\alpha}{2}u_0^2 + \frac{\beta}{3}u_0^3 + \Delta u_0 = (F(x) + C), \quad (5)$$

which upon integrating once becomes

$$\omega_1'^2 u_{0X}^2 = \frac{\alpha}{3}u_0^3 + \frac{\beta}{6}u_0^4 + \Delta u_0^2 - 2(F(x) + C)u_0 + E, \quad (6)$$

where $E = E(x)$ is a further constant of integration. Now by integrating once more, we can obtain the solutions by way of an inverse elliptic integral. However, if it is assumed that the roots of the quartic polynomial are real and distinct then we can write the solution in an explicit form

$$u_0(x, X) = \frac{-(b-d)c + \mathrm{sn}^2(B(X-\delta), m)(b-c)d}{-(b-d) + \mathrm{sn}^2(B(X-\delta), m)(b-c)}, \qquad (7)$$

$$B = \frac{\sqrt{(a-c)(b-d)}}{2\omega_1'}, \qquad m = \frac{(b-c)(a-d)}{(a-c)(b-d)},$$

and $a \le b \le c \le d$ are the roots of the quartic polynomial in (6), which in turn depend on the slow varying x coordinate through the variation of the forcing.

In order to account for and determine the nature of the slow variation of the parameters we investigate the secularities arising at subsequent orders. First, as noted by Luke [5], we must ensure that the periodicity of the solutions in a problem such as this is constant with respect to the slow variation. Consequently

$$T = \frac{2K(m)}{B} = \frac{2K(m)}{\sqrt{(a-c)(b-d)}}\omega_1',$$

where T is an arbitrary constant associated with the period in X. Choosing $T = 2$ we now obtain an expression for the leading order variation of the dispersive layer coordinate

$$\omega_1'(x) = \frac{\sqrt{(a-c)(b-d)}}{K(m)}. \qquad (8)$$

Now we consider the equation which arises at $O(\sqrt{\gamma})$

$$\begin{aligned} -\omega_1^2 u_{1XX} + \Delta u_1 + \alpha u_0 u_1 + \beta u_0^2 u_1 &= 2\omega_1'\omega_2' u_{0XX} \\ +2\omega_1' u_{0xX} + \omega_1'' u_{0X} &+ \nu\omega_1' u_{0X}. \quad (9) \end{aligned}$$

The solution of the homogeneous self-adjoint problem is u_{0_X}, so that by taking the standard functional inner product and applying periodicity it can be shown that the solubility condition reduces to

$$\frac{d}{dx}\omega_1' \int_0^T u_{0X}^2 \, dX - \nu\omega_1' \int_0^T u_{0X}^2 \, dX = 0. \qquad (10)$$

Then this equation is easily integrated and using the expression for u_0 an explicit algebraic equation emerges relating the variation of the solution parameters to that of the forcing. While for the pure KdV case it is possible to obtain an explicit expression, [3], this criterion may also be evaluated and solved numerically. Then by applying matching criteria that on either side of the layer the solutions within the dispersive layer match solutions outside the layer we obtain a framework for generation of a broad class of solutions.

Discussion and Comparisons

The matching procedure is perhaps best understood in terms of the associated phase plane configuration. Equation (5) has an associated phase plane in (u_0, u_{0X}), as shown in Figure 1, where the non-dispersive solutions of

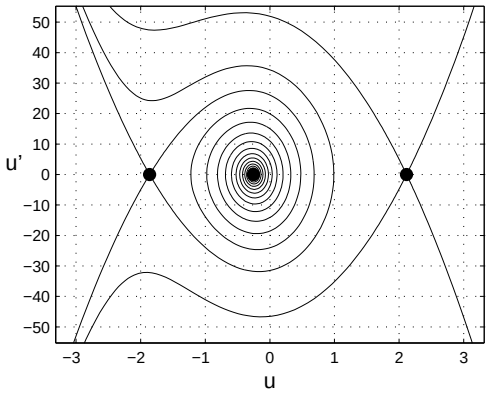

Figure 1: Phase plane configuration eKdVB

(3) correspond to fixed points which move slowly in response to the variation of the forcing. Consequently the solutions within the dispersive layer correspond to trajectories in this non-autonomous phase-space beginning and ending at a fixed point. Thus the matching is such that, for example with the solutions (7), that the modulus of the elliptic functions $m(x) \to 1$ in the matching region,

ensuring that the solutions transition smoothly from the dispersive to non-dispersive regions. This matching criteria then also supplies the possible layer locations δ once $m(x)$ is determined through (10). For example in the undamped KdV case it was found that layers must be located around the local extrema of $F(x)$. Similar results follow for the more general nonlinearities, however for example with the undamped mKdV the layer locations are seen to lie at the inflection points of $F(x)$.

In the end a range of possible leading order matched asymptotic solutions emerge, corresponding to solutions starting at one of the saddle points, orbiting the centre, and then matching to one of the two saddles. However once the global condition on the mean (2) is applied only a limited set of these solutions remain. For example, Figure 2 shows a solution which arises for the case

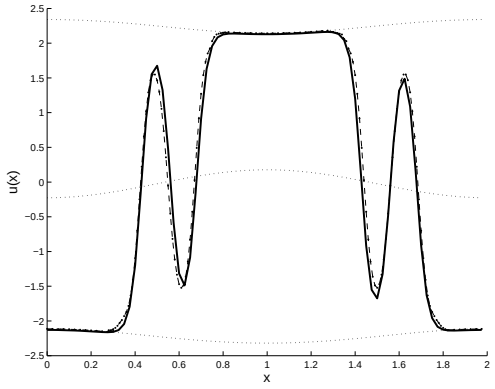

Figure 2: Numerical (solid) and approximate (dashed) solutions, with non-dispersive solutions (dotted)

$\gamma = .005$, $\Delta = -5$, $\alpha = 0$, $\beta = 3$, $\mu = .0015$, $L = 1$ $f(x) = -\pi \sin \pi x$. The trajectory transitions between the saddle points and during the transition it orbits the nodal solution one and a half times. In this way the full range of solutions across the resonant band may be captured.

It is also interesting not only to consider variation of Δ, but also in the relative magnitude of the nonlinear terms. In this way a connection can then be drawn between resonant solutions for the KdV ($\beta = 0$) and mKdV($\alpha = 0$) equations, manifested geometrically by the presence and influence of the additional saddle point. In particular Figure 3 depicts the full range of resonant solutions which emerge for the case where $\gamma = .005, \mu = .0015,$ $\alpha = 2, L = 1, f(x) = \pi \sin \pi x$ and $\beta = 0, .1, .1037$. We see that as the effect of the cubic nonlinearity increases, a bifurcation occurs and additional resonant solutions emerge, corresponding analytically to solutions which transition from one steady solution to the other (as in Figure 2).

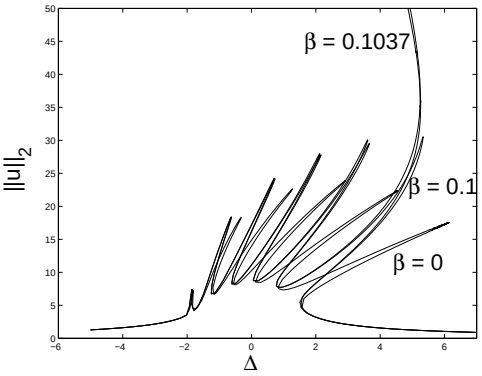

Figure 3: Resonant response over full resonant band

This methodology provides a framework for understanding and constructing steady resonant solutions of (1) across the resonant band. Moreover we gain insight into the many connections, yet distinctions between resonant solutions of the KdV, mKdV and the general eKdV in the presence of forcing. The approach, however, remains local in nature as each dispersive layer is assumed to be independent. Therefore care must be taken in cases where layers separate or merge. In addition it was seen that due to the second saddle point associated with the higher nonlinearity, there also appear certain cases where even in the limit that $\gamma \to 0$ transitions occur but no clear distinction may be drawn between the dispersive and non-dispersive regimes. In such cases a more global approach may be required.

References

[1] H. Ockendon, J.R. Ockendon, & A.D. Johnson, "Resonant sloshing in shallow water" J. Fluid Mech., 167, pp. 465-479, 1986.

[2] J.G.B. Byatt-Smith, "Resonant oscillations in shallow water with small mean-square disturbances" J. Fluid Mech., 193, 369-390, 1988.

[3] D.E. Amundsen, E.A. Cox, & M.P. Mortell, "Asymptotic solutions for resonant sloshing of shallow water in a tank". Zeitschrift fur Angewandte Mathematik und Physik(ZAMP), To appear, 2007.

[4] E.A. Cox, M. P. Mortell, A.V. Pokrovskii, & O. Rasskazov, "On chaotic wave patterns in periodically forced steady-state KdVV and extended KdVB equations" Proc. Roy. Soc. A, 461, pp. 2857-2885, 2005.

[5] J.C. Luke, "A perturbation method for nonlinear dispersive wave problems." Proc. Roy. Soc. London, A292, pp. 403-412, 1966.

DEEP WATER PERIODIC WAVES AS HAMILTONIAN RELATIVE EQUILIBRIA

E. van Groesen[†,*], **L. She Liam, I. Lakhturov, Andonowati**[†,‡]
Applied Mathematics, University of Twente, Netherlands
[†] & LabMath-Indonesia, Bandung Indonesia
[‡]& Mathematics, Institut Teknologi Bandung, Indonesia
[*]Email: groesen@math.utwente.nl

Abstract

We use a recently derived KdV-type of equation for waves on deep water to study Stokes waves as relative equilibria. Special attention is given to investigate the cornered Stokes-120 degree wave as a singular solution in the class of smooth steady wave profiles.

Introduction

Surface waves on a layer of incompressible, inviscid fluid in irrotational motion, are described by Luke's variational principle. The formulation of the dynamics as a Hamiltonian system was found by Zakharov '68, Broer '74 and Miles '77. This Hamiltonian formulation is helpful to study basic properties of surface waves. The conservation of energy (which is the Hamiltonian H) is accompanied by conservation of horizontal momentum M when the case of a flat bottom or the case of infinitely deep water is considered. These two integrals are independent and Poisson commute. As is the case for any Hamiltonian system with additional integrals, relative equilibria (RE) can be considered; in this case these are the extremizers of the Hamiltonian on level sets of the momentum. An extremizer provides a surface profile η and corresponding velocity potential ϕ that satisfy the Lagrange multiplier rule: $\delta H = \mu \delta M$ for some multiplier μ. The action of the M flow is a shift in time at a constant velocity which is precisely the multiplier μ, provides a steadily propagating wave as dynamic solution of the Hamiltonian system.

Looking for the existence and shape of steady waves was an important motivation for research in the nineteenth century (wave of elevation) and continued in the twentieth century. The main motivation in the 1895 paper of Korteweg and de Vries was to investigate this existence matter. The existence and explicit formulation of steady finite energy solutions (later called solitons) and periodic (cnoidal) waves was their contribution to this issue, providing a positive answer about existence. All this in the approximation of the one-way directional KdV equation that they derived. Existence of periodic waves (for the full wave equation) has been investigated in the twentieth century by many scientists, among which Levi-Civita, Toland, while approximations of the periodic wave shapes using expansion methods (in amplitude, Fourier modes, etc,) have been derived to a high degree of accuracy, for instance by Rienecker & Fenton [1]. It is to be noted that as far as we are aware of, none of the approximations uses directly the Hamiltonian RE-description.

Among the steady periodic solutions, one is exceptional. It occurs on infinitely deep water, and, while the other profiles are smooth, this special one, referred to as S120 in the following, is a Stokes wave with a profile that has a corner of 120 degrees in the crest. It was shown recently by Rainey & Longuet-Higgens [2] that in a good approximation, S120 has actually the profile of a catenary, i.e. can be written as a hyperbolic cosine curve in between two successive crests. The appearance of a cornered profile indicates a certain singularity in the governing description, since any non-smoothness in an initial profile will be resolved by dispersion in regular dispersive nonlinear equations with differential operators.

In this paper we contribute to the steady wave issue on infinitely deep water from the point of view of considering these steady profiles as Hamiltonian RE. However, instead of the exact surface wave formulation, we use a KdV-type of equation, called the AB-equation, that was recently derived. This equation is exact up to and including quadratic nonlinear terms, and can be taken to have exact linear dispersive properties; the dispersion enters the nonlinear terms in a nontrivial way, correcting substantially inaccuracies in the nonlinear propagation properties. Moreover, this equation, unlike other KdV-type of equations, can also describe waves on infinitely deep water. The equation, and in particular the Hamiltonian and Momentum integrals, is given in section 2.

We formulate the RE-problem of this equation in section 3, and show in section 4 how close the RE are to the set of Rienecker & Fenton solutions, and, especially, how the cornered S120-wave can be approximated. All these results confirm that, at least for these steady solutions, the approximate Hamiltonian and Momentum must be rather accurate, providing relatively simple approximations of these integrals of the full surface wave problem. The explicit expresssion may make these integrals also useful for further advanced functional analytic investigations.

1 AB equation

The AB equation as derived in [3], specialised for the case of infinitely deep water, uses skew-symmetric and symmetric pseudo-differential operators A and B with symbols $\hat{A} := i.sign(k)\sqrt{|k|}$ and $\hat{B} = \sqrt{|k|}$. The Hamiltonian is given by

$$H_{AB}(\eta) = g\int\left[\eta^2 + \frac{1}{2}\eta\left\{(B\eta)^2 - (A\eta)^2\right\}\right]dx \quad (1)$$

and the horizontal Momentum integral by $M(\eta) = \sqrt{g}\int \eta B\eta$. The AB-equation is then given by the Hamiltonian system

$$\partial_t\eta = -\frac{A}{2\sqrt{g}}\delta H_{AB}(\eta), \quad (2)$$

which may also be written in the way of Benjamin [4] as $\partial_t\delta M(\eta) = -\partial_x\delta H(\eta)$; hence solutions have a constant center-of mass velocity. Note that the non-rational pseudo-differential operators A, B cannot be easily approximated with ordinary differential operators.

2 Periodic waves

In the following we consider periodic waves of fundamental period 2π and zero average $\int \eta dx = 0$. Taking the crest at $x = 0 mod(2\pi)$, we look for solutions of the RE equation in the form of a truncated Fourier series. With a an amplitude parameter, we look for solutions as

$$\eta_N = a\cos x + a^2\left[\Sigma_{k=2}^N \beta_k \cos(kx)\right].$$

Restricting the hamiltonian and momentum to this set, we arrive at functions H_N and M_N of $p = (a, \beta_2, ..., \beta_N)$ and the RE equation becomes

$$\nabla_p H_N = \mu_N \nabla_p M_N,$$

which corresponds to the Galerkin projected equation $\delta H = \mu\delta M$.

Splitting the Hamiltonian in a quadratic and cubic part, $H = H^{(2)} + H^{(3)}$ it is remarkable to observe that $H^{(3)}(\alpha\cos(kx)) = 0$, which implies that the energy for Fourier expansions as above does not contain terms of third order $H\left(a\cos x + a^2 v\right)/g = \frac{1}{2}a^2 + O\left(a^4\right)$. Also, since $\delta H^{(3)}(\alpha\cos(kx)) = \frac{1}{2}g\alpha^2\cos(2kx)$, the second order Stokes contribution appears immediately: $\delta H(a\cos x)/g = 2a\cos x + \frac{1}{2}a^2\cos(2x)$.

3 Illustrations

In Figs. 1,2 we show in the Momentum-Hamiltonian plane the curves parameterized by the first-order amplitude parameter a for various approximations of Stokes waves. The tangent at a point to a curve correspond to the propagation speed of the wave at that point, see Fig.3,4. The small deviation from a straight line (obtained for the first order mode only), indicates that increase in velocity with amplitude is rather small, in agreement with the vanishing of third order contribution in the Hamiltonian. The one-term approximation of the highest Stokes wave is indicated by a dot; for this solution $ak = 0.36$. Shown are the results for the Rienecker& Fenton (RF) solutions with 64 Fourier modes (solid line), and the AB relative equilibria with 2, 4 and 16 modes. The dot corresponds to the Rainey & Longuet-Higgins one-term approximation.

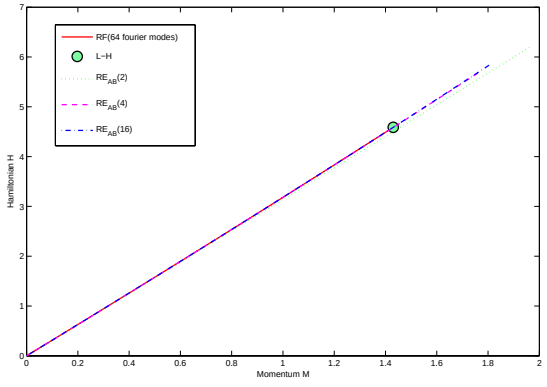

Figure 1: Values of Momentum and Hamiltonian for approximations of Stokes waves.

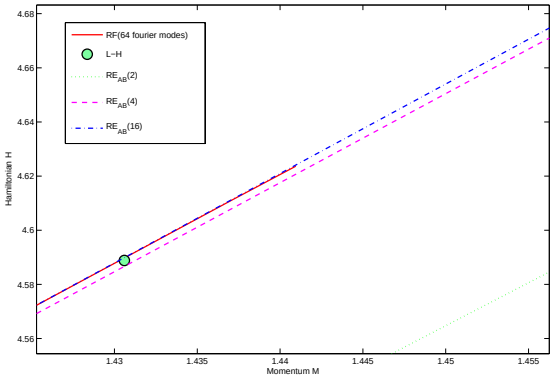

Figure 2: As Fig.1 zoomed in near the highest Stokes wave.

In Fig.5 the profiles are shown of the waves with the same momentum as the highest Stokes wave. Besides the cornered one-term approximation by Rainey & Longuet-Higgens, the Rienecker & Fenton 64-mode approximation and the 2 and 16-mode AB relative equilibria are plotted. Fig.6 shows a zoom-in near the crest.

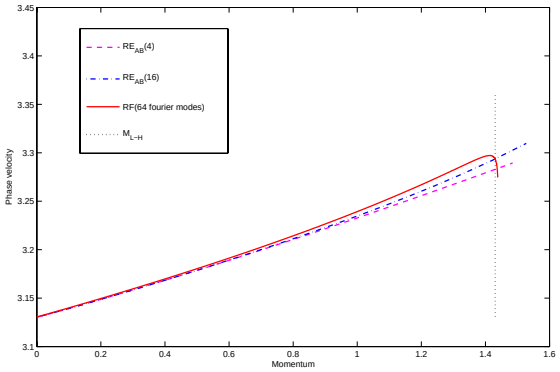

Figure 3: Plots of the phase speed corresponding to the curves in Fig.1.

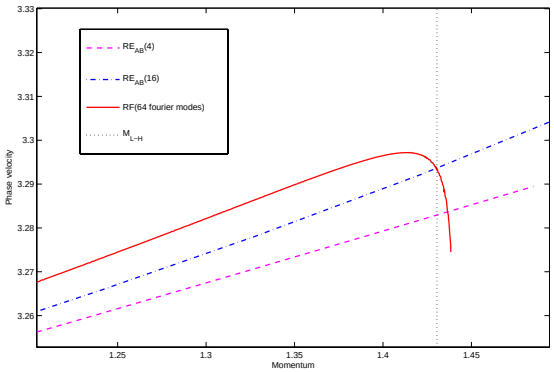

Figure 4: Zoom-in of Fig.3.

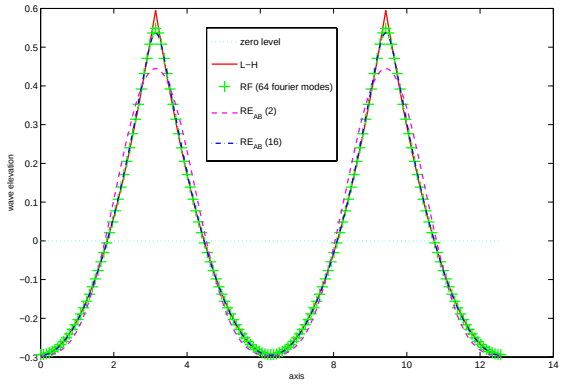

Figure 5: Approximations of the highest Stokes wave.

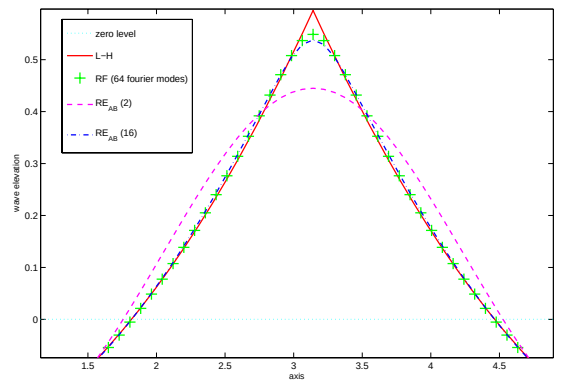

Figure 6: As Fig.5, zoome-in near the crest.

4 Numerical simulations

Calculations have been performed with a high-order (256 or 1024) pseudo-spectral implementation, for calculations over more than 100 wavelengths. As expected, all AB-RE travel virtually undisturbed at constant speed for RE's approximated with at least 6 modes. Also the highest Stokes wave travels with only a small breathing undisturbed in shape. The speeds of these solutions are equal: the tops remain in a small neighbourhood of eachother, with small periodic oscillations.

Acknowledgement

Use of the code of Gert Klopman to calculate the RF-solutions is acknowledged. This research is part of Netherlands Science Foundation NWO-STW, TWI-7216.

References

[1] M.M. Rienecker & J.D. Fenton, A Fourier Approximation Method for Steady Water Wave, Journal of Fluid Mechanics, 104(1981)119-137.

[2] R.C.T. Rainey & M.S. Longuet-Higgins, A close one-term approximation to the highest Stokes Wave on deep water, Ocean Engineering 33(2006) 2012-2024.

[3] E. van Groesen & Andonowati, Variational derivation of KdV-type of models for surface water waves, Physics Letters A, Feb 2007; http://dx.doi.org/10.1016/j.physleta.2007.02.031

[4] T.B. Benjamin, Lectures on nonlinear wave motion, in: Nonlinear Wave Motion, Lectures in Applied Mathematics, vol.15, AMS, Providence, 1974.

ELECTROMAGNETIC WAVE BACKSCATTERING BY NONLINEAR LOADED ANTENNAS WITH MAGNETODIELECTRIC CORE

T. M. Zaboronkova
Department of VLF electrodynamics, Radiophysical Research Institute, Nizhny Novgorod, Russia;
E-mail: zabr@nirfi.sci-nnov.ru

Abstract

The electromagnetic wave scattering by a metallic loop with a lumped nonlinear load and a spherical core has been studied in the approximation of weak nonlinearity. There has been given the problem solution procedure and numerical calculation results of a nonlinear scattered signal for different parameters of the antenna and the core.

Introduction

Nonlinear load antennas have long attracted the attention of researchers. The area of practical application of nonlinear electromagnetic wave scattering effects is wide enough. For example, nonlinear radars which heart is a nonlinear load antenna permit remote location of mines, radio-controlled field charges, revelation of hidden defects in buildings (flaw detection) [1], concealed marking of materials and equipment. They are used to search people in building ruins [2, 3]. Small diode-loaded buit-in probes are used in non-invasive electric stimulation [4]. Nonlinear electromagnetic wave scattering by systems of loop and vibrator scatterers placed in the uniform space or in the presence of planar interfaces has been studied in [5, 6]. Of particular interest is the scattering by nonlinearly loaded antennas with a dielectric core [7]. We present here the problem solution on the electromagnetic wave scattering by a thin circular metallic loop with a spherical dielectric core made in the approximation of weak nonlinearity permitting adequate interpretation of experimental data in many cases (see, for example, [7]). The antenna may be placed into a medium with arbitrary values of dielectric conductivity and permittivity.

The nonlinearly scattered signal is studied for steady-state conditions that allows one to account a finite number of sounding signal (SS) harmonics in the spectral approximation. We consider here the case of a local nonlinear load [7]. The voltage-current characteristic of the nonlinear element is assumed to be described by a second- or third-degree polynomial.

Methods

The following algorithm is suggested to determine the field scattered on SS harmonics:

1. First we consider the problem of electromagnetic wave diffraction over a magnetodielectric sphere with permittivity and permeability $\varepsilon_1 = \varepsilon_1' - i\varepsilon_1''$ and $\mu_1 = \mu_1' - i\mu_1''$ located in the uniform space.

2. Then we solve the antenna problem and determine the loop current distribution at the SS frequency in the presence of a magnetodielectric core.

3. The currents at high SS harmonics are excited due a presence of a lumped EMF caused by the local nonlinear load [5, 6].

4. Finally, for the given current distribution, we determine the electromagnetic field components radiated by the antenna with the magnetodielectric core at the frequency of a corresponding harmonic of SS.

Current distribution in antenna with dielectric core

Let a plane electromagnetic wave be incident on the dielectric sphere of radius b. We shall solve the problem in the spherical coordinate system (r, θ, φ). The electrical constitutive complex parameters are ε_1, μ_1 for the sphere and ε_2, μ_2 for the surrounding medium. The circular loop is placed at a distance $b\cos\beta$ from the center of a sphere. The thin loop is constructed from perfectly conducting wire of radius a ($a \ll c = b\sin\beta$, $a \ll \lambda$; where c is the loop radius, λ is the wave length in the medium). The current has one azimuth component in the case of thin loop. The current at the fundamental frequency ω induced by incident plane electromagnetic wave (defining by the angles θ_0, φ_0) is expressed as a Fourier series

$$I_\omega(\varphi) = \frac{2E_0}{\zeta_1} \sum_{m=-\infty}^{+\infty} \frac{\beta_m}{[a_m + b_m]}\, e^{-im(\varphi-\varphi_0)}, \quad (1)$$

here $\zeta_1 = \sqrt{\dfrac{\mu_0\mu_1}{\varepsilon_0\varepsilon_1}}$ is wave impedance, E_0 is the amplitude of incident wave; β_m can be presented as

$$\beta_m = \sum_{n=|m|}^{\infty} \gamma(m,n)\, i^n \Delta \times$$
$$\times \left[\frac{m^2}{k_2 b} \frac{\varepsilon_2}{\varepsilon_1} \frac{d_{1\psi}}{\Delta_\varepsilon} \frac{P_n^m(\cos\theta_0)}{\sin\theta_0} \frac{P_n^m(\cos\theta)}{\sin\theta} + \right.$$
$$\left. + \; i \frac{\psi_n(k_1 b)}{\Delta_\mu} \frac{\partial P_n^m(\cos\theta_0)}{\partial\theta_0} \frac{\partial P_n^m(\cos\theta)}{\partial\theta} \right],$$

$$\Delta = \xi_n^{(2)}(k_2 b) d_{2\psi} - \psi_n(k_2 b) d_{2\xi},$$

$$\Delta_\varepsilon = \frac{\varepsilon_2}{\varepsilon_1}\,\xi_n^{(2)}(k_2 b) d_{1\psi} - \psi_n(k_1 b) d_{2\xi},$$

$$\Delta_\mu = \frac{\mu_2}{\mu_1}\,\xi_n^{(2)}(k_2 b) d_{1\psi} - \psi_n(k_1 b) d_{2\xi},$$

$$d_{1,2\psi} = \psi_n(k_{1,2} b) + k_{1,2} b \dot{\psi}_n(k_{1,2} b),$$

$$d_{1,2\xi} = \xi_n^{(2)}(k_{1,2} b) + k_{1,2} b \dot{\xi}_n^{(2)}(k_{1,2} b),$$

$\gamma(m,n) = \dfrac{2n+1}{n(n+1)}\,\dfrac{(n-m)!}{(n+m)!}$; $k_{1,2} = \omega\sqrt{\varepsilon_0\mu_0\varepsilon_{1,2}\mu_{1,2}}$; $\psi_n(x)$ and $\xi_n^{(2)}(x)$ are the first and third order spherical Bessel functions ($\dot{\psi}_n(x)$ and $\dot{\xi}_n^{(2)}$ are their derivation); $P_n^m(\cos\theta)$ is the associated Legendre function. The expressions for coefficients a_m and b_m one can find in [8].

We restrict ourselves to the approximation of a weak nonlinearity. The current voltage characteristic of the local nonlinear load is described by a second- or third-degree polynomial. The current at higher harmonics of SS is excited due to the lumped electromotive force caused by the presence of nonlinear element (see more details in [6]). The current distribution ($I_{N\omega}(\varphi)$) at the higher harmonics $N\omega$ ($N = 2; 3$) of SS in the indicated above approximation is given as

$$I_{N\omega}(\varphi) = \sum_{m=1}^{+\infty} h(m) I_m^{(N\omega)} \cos[m(\varphi - \varphi_n)];$$

$$I_m^{(N\omega)} = \frac{-i\alpha_N\,|I_\omega|^N R_0^N}{2^{N-1}\pi\zeta_1[a_{N,m} + b_{N,m}]}\,, \qquad (2)$$

where $h(0) = 1$ and $h(m) = 2$ if $m \neq 0$; α_N is the coefficient of nonlinearity; the angular coordinate φ_n is determined the location of the nonlinear element; I_ω is the current at fundamental frequency at the point of nonlinear load location; a_{Nm} and b_{Nm} are determined by the similar expressions as the coefficients a_m and b_m but at the frequency $N\omega$; R_0 is the initial resistance of the antenna load.

Radiation of antenna at the harmonics of sounding signal

Below we give the expression only for the angular components of the electric field excited by the current (2) at the harmonics $N\omega$ in the surrounding medium ($r > b$). Obviously that the radial component of the electric field is negligibly small for the considering polarization of an incident wave. The θ- and φ-components of the field at the frequencies $N\omega$ may be expressed as follows

$$E_\theta^{(N\omega)}(r,\theta,\varphi) = -\frac{i\zeta_1}{r\sin\theta}\sum_{m=1}^{+\infty} I_m^{(N\omega)} G_{\theta m} \sin m[\varphi - \varphi_n],$$

$$E_\varphi^{(N\omega)}(r,\theta,\varphi) = -\frac{i\zeta_1}{2r\sin\theta}\times$$

$$\times\left[\sum_{m=1}^{+\infty} h(m) I_m^{(N\omega)} G_{\varphi m}\cos m[\varphi - \varphi_n]\right]. \qquad (3)$$

The functions $G_{\theta m}$ and $G_{\varphi m}$ are determined at the frequency $N\omega$ by the expressions

$$G_{\theta m} = \sum_{n=m}^{+\infty} m\gamma(m,n)\times$$

$$\times\left\{\frac{d_{1\psi} d_{r\xi}}{k_1 b \Delta_{\xi\psi}^{\varepsilon\mu}}\sin\theta\, P_n^m(\cos\beta)\,\frac{\partial P_n^m(\cos\theta)}{\partial\theta} - \right.$$

$$-\sqrt{\frac{\varepsilon_1}{\varepsilon_2}}\,\frac{k_2 r \xi_n^{(2)}(k_2 r)\,\psi_n(k_1 b)}{\Delta_{\xi\psi}}\times$$

$$\left.\times\sin\beta\,\frac{\partial P_n^m(\cos\beta)}{\partial\beta}\,P_n^m(\cos\theta)\right\},$$

$$G_{\varphi m} = \sum_{n=m}^{+\infty} m\gamma(m,n)\times$$

$$\times\left\{\frac{m^2}{\Delta_{\xi\psi}^{\varepsilon\mu}}\,\frac{d_{1\psi} d_{r\xi}}{k_1 b}\,P_n^m(\cos\beta)\,P_n^m(\cos\theta) - \right.$$

$$-\sqrt{\frac{\varepsilon_1}{\varepsilon_2}}\,\frac{k_2 r\xi_n^{(2)}(k_2 r)\,\psi_n(k_1 b)}{\Delta_{\xi\psi}}\,\frac{\partial P_n^m(\cos\beta)}{\partial\beta}\times$$

$$\left.\times\,\frac{\partial P_n^m(\cos\theta)}{\partial\theta}\,\sin\beta\sin\theta\right\};$$

$$d_{r\xi} = \xi_n^{(2)}(k_2 r) + k_2 r\dot{\xi}_n^{(2)}(k_2 r),$$

$$\Delta_{\xi\psi}^{\varepsilon\mu} = \frac{\varepsilon_2}{\varepsilon_1}\,\frac{\mu_2}{\mu_1}\,\xi_n^{(2)}(k_2 b) d_{1\psi} - \psi_n(k_1 b) d_{2\psi},$$

$$\Delta_{\xi\psi} = \xi_n^{(2)}(k_2 b) d_{1\psi} - \psi_n(k_1 b) d_{2\psi},$$

here $k_0 = N\omega\sqrt{\mu_0\varepsilon_0}$, $k_{1,2} = k_0\sqrt{\varepsilon_{1,2}\mu_{1,2}}$.

Conclusion

We have thus obtained the expressions for the electric field (3) allowing to estimate the influence of the dielectric core on the backscattering field produced by the antenna with a nonlinear local load at the second or third harmonic of the sounding signal. The numerical calculations have been performed in the decimeter — wavelength range at the second harmonic of the sounding signal. In particular, the calculations have shown that the

presence of a dielectric core may lead to a significant increase in the signal scattered at higher harmonics for a certain range of the core electric size due to resonance reflection of the waves inside the core.

This work was supported by the grant of Leading Scientific School (NSh-1087.2006.2).

References

[1] A. S. Kuznetsov, G. I. Kutin, "The method of the investigation of the effect of nonlinear scattering of electromagnetic waves", Zarubezhnaya Electronica, No 4, pp. 41–53, 1985. [Russian]

[2] M. Bouthcnon, J. Gavan, F. Zadworny, 10th Europ. Microwave Conf., Warsaw, 1980, p. 65.

[3] H.-R. Chuang, Y.-F. Chen, K-M. Chen, "Automatic clutter-canceller for microwave life-detection systems", IEEE Trans. Instrum. And Meas., vol-IM.40. No 4, p. 747, 1991.

[4] Nonlinea Electromagnetics. Ed. by Piergiorgio L. E. Uslenghi, Academic Press, London, 1980.

[5] A. A. Gorbachev, T. M. Zaboronkova, A. A. Vasenkov, "Electromagnetic wave scattering from antennas with nonlinear load", Journal of Electromagnetic Waves and Applications, vol. 13, pp. 807–809, 1999.

[6] A. A. Gorbachev, T. M. Zaboronkova, S. P. Tarakankov, "Scattering of electromagnetic waves by nonlinear antennas under presence of a two media boundary", Journal of Electromagnetic Waves and Applications, vol. 9, No 10, pp. 1285–1299, 1995.

[7] A. A. Gorbachev, T. M. Zaboronkova, A. A. Vasenkov, E. A. Shorokhova, "Scattering of electromagnetic waves by nonlinear loaded loop with dielectric core", Nonlinear Mir, No 5, 2007.

[8] L. N. An, G. S. Smith, "The horizontal circular loop antenna near a planar interface", Radio science, vol. 17, No 3, pp. 483–502, 1982.

Periodic and Random Media

WAVES RUNNING ALONG A PERIODIC SET OF INHOMOGENEITIES IN FLUID LOADED THIN ELASTIC PLATE

I. V. Andronov
St.Petersburg State University, Russia
Email: iva---@list.ru

Abstract

Waves running along a periodic set of pointwise inhomogeneities in fluid loaded thin elastic plate are studied. Two types of inhomogeneities are considered: attached masses and small circular holes. Boundary conditions in the points of attached masses are classical. Conditions that simulate holes of asymptotically small radius are formulated using the approach of zero-range potentials. Dispersion equations for concentrated waves are written in explicit form involving exponentially converging integrals. These equations are solved numerically.

Introduction

Waves concentrated along a periodic set of inhomogeneities in an elastic plate are considered. The plate is supposed to be thin and only its flexure vibrations are taken into account and are studied by using Kirchoff approximation. The analysis of physical effects is the most simple one if the problem allows analytic solution to be constructed. Such solutions are in particular possible if the inhomogeneities are pointwise. In two-dimensional problems the set of pointwise inhomogeneities that can be formulated by classical boundary conditions is sufficiently large. However in three-dimensional case there is only the model of attached point-wise mass. Some examples see e.g. in [1], [2].

Periodic set of attached masses

First, a periodic set of pointwise masses attached to fluid-loaded thin elastic plate is considered. The problem for acoustic pressure U and flexure displacements of the plate w can be written as [3]

$$\left(\Delta - k^2\right) U(x,y,z) = 0, \qquad z > 0, \tag{1}$$

$$\left(\Delta^2 - k_0^4\right) w(x,y) = U(x,y,0) \tag{2}$$

$$+\frac{\omega^2 M}{D} w(0,0) \sum_{j=-\infty}^{+\infty} \delta(x, y - jd),$$

$$w(x,y) = \frac{1}{\varrho_0 \omega^2} \frac{\partial U(x,y,0)}{\partial z}. \tag{3}$$

Here ω is frequency, time factor $e^{-i\omega t}$ is dropped, k is the wave number in acoustic media $\{z > 0\}$, $k_0 = (\varrho\omega^2/D)^{1/4}$ is the wave number of flexure waves in isolated plate (ϱ is surface density, D is bending stiffness), M is attached pointwise mass, ϱ_0 is the density of fluid.

Analysis of that problem allows to conclude that specific wave may run along the set of masses. The dispersion equation for the parameter α of these waves can be written in explicit form

$$1 - \frac{\omega^2 M}{D} \sum_j e^{i\alpha j} g_p(0,0;0,jd) = 0, \tag{4}$$

where

$$g_p(x,y;x_0,y_0) = -\frac{N}{4\pi^2} \times$$

$$\times \iint \frac{e^{i\lambda(x-x_0)+i\mu(y-y_0)-\sqrt{\lambda^2+\mu^2-k^2}z}}{\left(\left(\lambda^2+\mu^2\right)^2 - k_0^4\right)\sqrt{\lambda^2+\mu^2-k^2} - N} d\lambda d\mu$$

is the Green function (flexure displacements excited by a point force applied to the plate), $N = \omega^2\varrho_0/D$. The sum in (4) can be reduced to exponentially converging integral. For that one calculates the integral by λ, then changes the order of summation and integration by μ and calculates the sum. Finally the path of integration is deformed into loops around the cuts of the square roots in the upper half plane

$$\sum_j \ldots = \frac{i}{\pi} \sum_s{}' Q_s \int_{\kappa_s}^{k} \Phi(\mu d, \alpha) \frac{d\mu}{\sqrt{\kappa_s^2 - \mu^2}}$$

$$+ \frac{i}{2\pi} \int_k^{k+i\infty} \Phi(\mu d, \alpha) \left(\sum_{s=0}^{4} \frac{Q_s}{\sqrt{\kappa_s^2 - \mu^2}} \right) d\mu, \tag{5}$$

where κ_s are zeros of the dispersion equation for waves in thin fluid loaded elastic plate, $Q_s = (\kappa_s^2 - k^2)/(5\kappa_s^4 - 4\kappa_s^2 k^2 - k_0^4)$ and

$$\Phi(\mu d, \alpha) = \frac{1}{e^{-i\alpha - i\mu d} - 1} + \frac{1}{e^{i\alpha - i\mu d} - 1}.$$

The dispersion equation (4) is analyzed numerically. For example, parameters α for waves in 1 cm steel plate in water are presented on Fig. 1. Waves

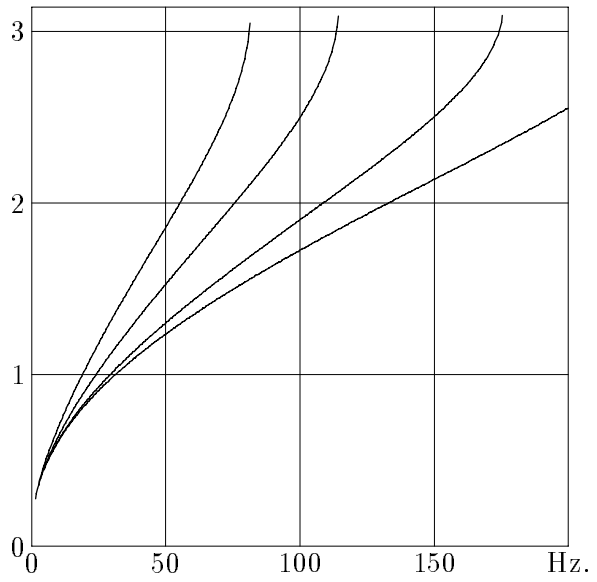

Figure 1: Parameter α for waves running along the set of point masses of 100 kg, 50 kg, 20 kg and 10 kg placed with the period of 20 cm.

concentrated near the masses are possible if the frequency is lower than some cut-off frequency, its dependence on mass is presented on Fig. 2. Thin curve corresponds to the case of isolated plate.

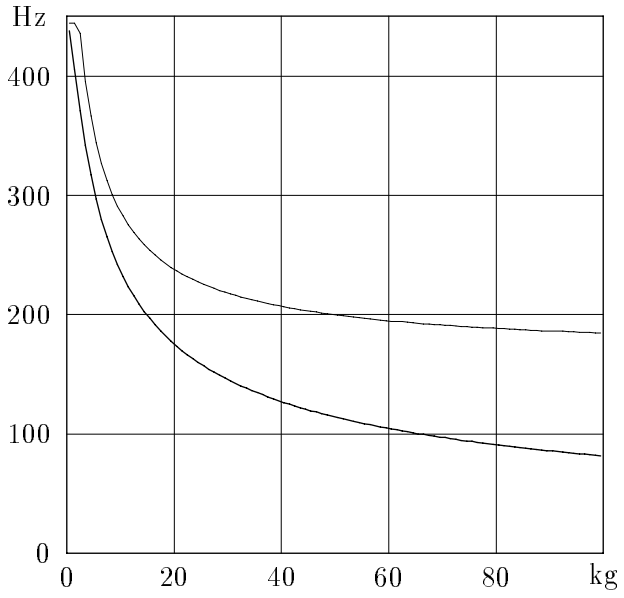

Figure 2: Cut-off frequency dependence on mass.

Model of a small hole

Pointwise model of a hole can not be formulated as the usual condition in the point. However one can extend the class of point-wise models by using the theory of zero-range potentials [4]. That results in the following. One considers local asymptotics of arbitrary square-integrable solution of the equations (1), (2) and (3) that are satisfied everywhere except the origin. This asymptotics have the form

$$U \sim c_0 \frac{1}{2\pi r} + b_0 + o(1), \qquad r \to 0, \tag{6}$$

$$\begin{aligned} w \;\sim\; & \frac{c_1}{2}\rho^2 \ln\rho + c_2 x \ln\rho + c_3 y \ln\rho \\ & + c_4\Big(\ln\rho + \cos^2\varphi\Big) + \frac{c_5}{2}\sin(2\varphi) \\ & + c_6\Big(\ln\rho + \sin^2\varphi\Big) + b_1 + b_2 x + b_3 y \\ & + b_4\frac{x^2}{2} + b_5 xy + b_6\frac{y^2}{2} + o(\rho^2), \quad \rho \to 0. \end{aligned} \tag{7}$$

(Here we use spherical radius r, and polar coordinates (ρ, φ) on the plate.) Analysis of energy fluxes allow to conclude that if coefficients c_ℓ of singular terms are proportional to the coefficients b_ℓ of regular terms with some Hermitian matrix A, i.e.

$$(c_0, c_1, \ldots, c_6)^T = A(b_0, b_1, \ldots, b_6)^T, \tag{8}$$

then the field U can be interpreted as the field of passive sources. The matrix A characterizes that passive source. We choose it in such a way that the far field amplitude of the solution U coincides with the principal order term in the asymptotic decomposition of the far field amplitude in the problem of scattering by a small circular hole [5]. The asymptotics (6) and (7) with the coefficients satisfying relations (8) with the chosen matrix A can be written in the form

$$U \sim c_0\left(\frac{1}{2\pi r} - \frac{1}{2a}\right) + o(1), \tag{9}$$

$$w \sim -\frac{2\sigma a^2}{1-\sigma}\Big(b_4 + b_6\Big)\,(\ln(\rho/a) + 1) + b_1 + b_2 x + \\ + b_3 y + b_4 x^2 + b_5 xy + b_6 y^2 + o(\rho^2) \tag{10}$$

where c_0 and b_n are arbitrary.

The asymptotics (9), (10) play the role of "boundary" conditions in the point that simulate scattering by a circular hole of small radius a.

Concentrated waves

The problem of waves propagation in the fluid loaded thin elastic plate with a periodic set of small holes is formulated as follows: The pressure U and the displacements w satisfy the equations (1), (2), (3) everywhere except the points $x = 0$, $y = jd$, $j \in \mathbb{Z}$. In a vicinity of every of these points the field has the asymptotics (9) and (10) with arbitrary coefficients.

The dispersion equation for waves that run along y direction in that system can be written in explicit form involving exponentially converging integrals of the type (5). Its numerical analysis shows that the properties of waves running along the set of holes appear significantly different from that in the case of isolated plate when there is an equivalence

$$\frac{\omega^2 M}{k_0^2 D} \longleftrightarrow 2\pi \frac{\sigma}{1-\sigma}(k_0 a)^2$$

of holes and masses.

In particular, besides the upper cut-off frequency (as in the case of masses) there is also a lower cut-off frequency. With the increase of fluid density these cut-off frequencies approach to each other and therefore nonattenuated waves are possible only if the density of acoustic media is not to large. The upper and the lower cut-off frequencies as functions of fluid density are presented on Fig. 3. The upper cut-off frequency corresponds to the condition $\kappa d = \pi$, where κ is the wave number of surface wave in fluid loaded plate. Thus it depends significantly on the period d. On the contrary, the lower cut-off frequency is almost independent of d. Its explanation is yet not sufficiently understood.

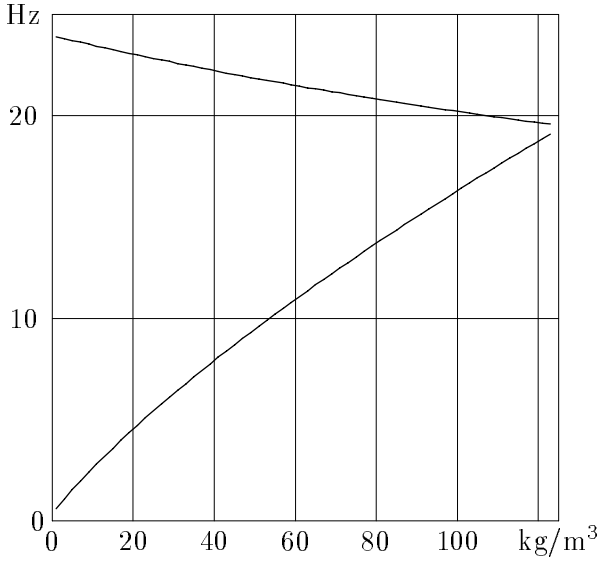

Figure 3: Lower and upper cut-off frequencies dependence on fluid density for 1 cm steel plate with holes of radius 10 cm placed with the period $d = 1$ m (sound speed assumed equal to 1500 m/c).

References

[1] G. I. Usoskin, "Scattering of bending waves by the system of point-wise obstacles", Soviet Phys. Acoust., vol. 13, 1967.

[2] M. S. Howe, "Diffraction of bending waves", Sound and Vibration, vol. 22, No 4, 1972.

[3] D. P. Kouzov, V. D. Lukyanov, "On the transparency to sound of thin elastic plate supported in a discrete set of points", Soviet Physics Acoustics, vol. 22, No. 1, 1976.

[4] S. Albeverio, P. Kurasov, Singular perturbations of differential operators. Solvable Schrödinger type operators. London Math. Soc. Lecture Notes Ser., 271, Cambridge Univ. Press, 2000.

[5] I. Andronov, Generalized point models in structural mechanics, World Scientific, Singapore, 2002.

NUMERICAL METHODS FOR MULTIPLE SCATTERING OF ULTRASOUNDS IN RANDOM MEDIA

M. Chekroun[*,†], **L. Le Marrec**[**], **B. Lombard**[***], **J. Piraux**[***], **O. Abraham**[****]
[*]Laboratoire Central des Ponts et Chaussées (LCPC) - Electricité De France (EDF R&D), Nantes, France
[**]Institut de Recherche Mathématique de Rennes (IRMAR), Rennes, France
[***]Laboratoire de Mécanique et d'Acoustique (LMA), Marseille, France.
[****]Laboratoire Central des Ponts et Chaussées (LCPC), Nantes, France
[†]Email: mathieu.chekroun@lcpc.fr

Abstract

The mathematical basis of theories for studying multiple scattering is well understood. However, the real domain of validity of these methods is still not clearly established. This paper presents the frame for a numerical validation of a classical method, the Independent Scattering Approximation, detailing specific implementation and signal processing used to obtain the parameters of an equivalent homogeneous medium. The setup is illustrated with a problem already well studied in an experimental way, but presenting strong difficulties for the numerical simulation.

Introduction

Let us consider the propagation of ultrasounds in an heterogeneous medium, where the wavelength and the size of heterogeneities are similar. In this case, the wave field is considered as the superposition of a coherent field and of an incoherent field. The coherent field resists to the averaging on disorder, and it can be interpreted as waves propagating in an equivalent homogeneous effective medium. Moreover, the coherent field is progressively dispersed and attenuated, even if the propagation media have no intrinsic dispersion and attenuation.

The aim of the treatment of multiple scattering is to define an equivalent homogeneous effective medium to the real heterogeneous medium. If the heterogeneities are statistically homogeneous and do not depend on the incident wave vector, the effective wavenumber satisfies $k_{eff}^2(\omega) = k_0^2 - \Sigma(\omega)$, where k_0 denotes the wavenumber of the host medium, ω is the angular frequency, and $\Sigma(\omega)$ contains all information about multiple scattering and must be determined.

The *Independent Scattering Approximation* (ISA) is a classical method to determine the parameters of the equivalent homogeneous medium. It takes into account the single scattering [1]: for each scatterer, the surrounding field is considered as not perturbed by the other scatterers, and there is no correlation between the scatterers. Then, Σ follows from physical and geometrical features of the scatterers, and also from the density n of scatterers in the host medium. To respect the hypotheses of ISA, the scatterers have to be far one from the others (n has to be low), and the impedance contrast between scatterers and the host medium must be weak. When one of these hypotheses is relaxed, the ISA may still provide accurate results. For instance, it has been experimentally shown to describe well cases of steel rods embedded in water [2]: the surface concentration of scatterers did not exceed 15%, but the impedance contrast between steel and water was high.

The goal of our work is to examine the precision of the ISA, especially outside its theoretical domain of validity. To our knowledge, no systematic study has been dedicated to this subject. Our methodology is purely numerical, based on direct numerical simulations and on signal-processing tools. This methodology avoids the limitations of the ISA. It is much faster and less expensive than real experiments, allowing also much finer measures.

Direct numerical simulations

Numerical methods

The aforementionned configuration, studied experimentally in a two-dimensional (2D) setup [2], is chosen to illustrate our approach. The 2D computations are performed on uniform Cartesian grids with spatial mesh size $\Delta x = \Delta y$. A velocity-stress formulation of acoustics (in fluid) and elastodynamics (in solid) is followed. The linear first-order hyperbolic systems so-obtained are integrated by the classical second-order Lax-Wendroff scheme. The main source of numerical dispersion and numerical diffusion follows from the numerical propagation in the fluid. A plane-wave analysis bounds these artefacts by their theoretical values in the homogeneous fluid medium in 1D (see section Results).

To couple the computations done on the fluid matrix and on the solid inclusions, one uses an interface method [5]. This numerical method describes accurately the geometry of interfaces, avoiding the spurious diffractions induced by a naive stair-step description of interfaces. Moreover, the fluid-solid boundary conditions are strongly enforced. Lastly, it maintains the global pre-

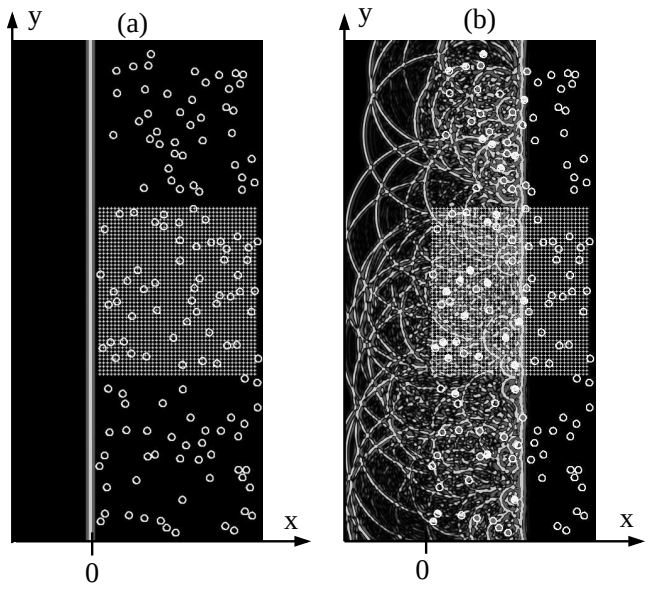

Figure 1: Snapshots of the acoustic pressure at the initial instant (a) and after 10000 steps (b), for a concentration of scatterers of 0.12 rods/mm^2. The regular grid denotes the location of receivers.

cision of the scheme of integration, despite the non-smoothness of solutions across interfaces.

Numerical setup

The heterogeneous medium under study is made of circular rods of steel randomly embedded in water. The intrinsic attenuation of the media are not taken into account. The size of the computational domain is respectively 3 cm along x and 6 cm along y. The mesh size is $\Delta x = 7.5\,\mu$m. The 0.4 mm radius rods are randomly distributed on a 2 cm-wide subdomain (i.e around 3 mean free path). An exclusion length of $4\,\Delta x$ between each inclusion is ensured. This correlation between scatterers, contradicting one hypothesis of the ISA, is not too penalizing [2]. For each simulation, the right-going incident plane wave is a Ricker centred at 2 MHz (wavelength in water: $\lambda_0 = 0.75$ mm). The CFL number is 0.6 in the steel; for stability reasons, the CFL is not optimal in water.

A regular array of receivers with 45 lines and 42 columns is put on the domain every $\Delta x_R = \Delta y_R = 0.45$ mm $> \lambda_0/2$. The receivers are sufficiently far from the boundaries of the computational domain to avoid spurious reflections (Figure 1). At each receiver and at each time step, the component of the velocity along x is recorded. Each line corresponds to a particular realization of a random process. Three simulations with different distributions of inclusions provide 135 independent realizations of disorder, ensuring the convergence of the post-processing methods.

At the initial instant, the plane wave lies at $x = 0$ (Figure 1-a). The simulations are stopped after 20000 time steps, when the incident wave has crossed the inclusions. On a Pentium PC at 3 GHz, a time step takes roughly 12 s. Consequently, each simulation takes roughly 66 hours, and it requires 2 Go of RAM.

Post-processing

Coherent field

The discrete coherent field s is obtained by spatially averaging the recorded data through the numerous equivalent realizations of disorder; since ISA considers heterogeneities as discrete scatterers, only receivers located in water are taken into account. The host medium is water, hence the coherent field is acoustic. The coherent field, expressed in the Fourier domain $s(\omega, d_i)$, corresponds to the propagation of a wave in an equivalent homogeneous medium at $N = 42$ regular offsets denoted by $d_i = i\,\Delta x_R$, with $i = 0, ..., N-1$. Phase velocity and attenuation are now extracted from s.

Phase velocity

The phase velocity $c(\omega)$ is computed using the $p-\omega$ transform. This one differs from the spatial Fourier transform by using the slowness $p_0(\omega) = 1/c(\omega)$ as a parameter, which reduces signal-processing errors for the evaluation of phase velocity [3]. The coherent field $s(\omega, d_i)$ is

$$s(\omega, d_i) \;=\; A(\omega, d_i)\mathrm{e}^{-i\omega p_0(\omega) d_i}, \qquad (1)$$

where $A(\omega, d_i)$ is the amplitude spectrum at d_i. The discrete $p-\omega$ stack $\hat{s}(\omega, p)$ is

$$\hat{s}(\omega, p) = \sum_{i=1}^{N} A(\omega, d_i) e^{i\omega(p - p_0(\omega))d_i}. \qquad (2)$$

The computation of $\hat{s}(\omega, p)$ is performed for several values of p. Given ω, the maximum of $|\hat{s}(\omega, p)|$ is reached for $p = p_0(\omega)$, leading to $c(\omega)$.

Damping factor

In the frequency domain, the amplitude spectrum in (1)-(2) can be written as $A(\omega, d_i) \;=\; A_0(\omega)\mathrm{e}^{-\alpha(\omega) d_i}$, where $A_0(\omega)$ is the amplitude of s at the first receiver. The damping parameter $\alpha(\omega)$ is determined by the slope of a least-square linear fit of $\ln(A(\omega, d_i))$. For an incident plane wave, no geometric damping has to be considered.

Results

The comparison between the numerical results and ISA are presented for a density of scatterers of 0.12 rods/mm^2 (surface concentration $6\,\%$), as shown in Figure 1.

Figure 2 presents the ratio $c(\omega)/c_0$, where c_0 is the celerity of waves in water. The theoretical numerical dispersion in water, computed for a 1D mesh, is also plotted. For frequencies lower than 3 MHz, the theoretical phase velocity within ISA and the numerical results are in good agreement. The differences in the higher frequencies may be due to the numerical dispersion. On the whole frequency range, $c(\omega)$ is very close to c_0 [2]. The results for the damping are plotted in figure 3. They are in good agreement, and the differences do not seem to increase with the frequency. The theoretical numerical damping is negligible.

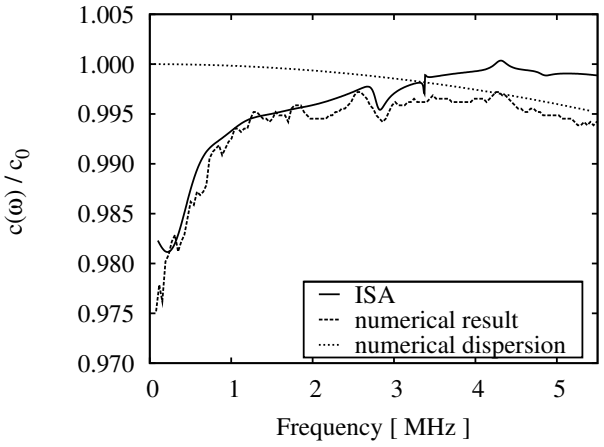

Figure 2: Results for the phase velocity

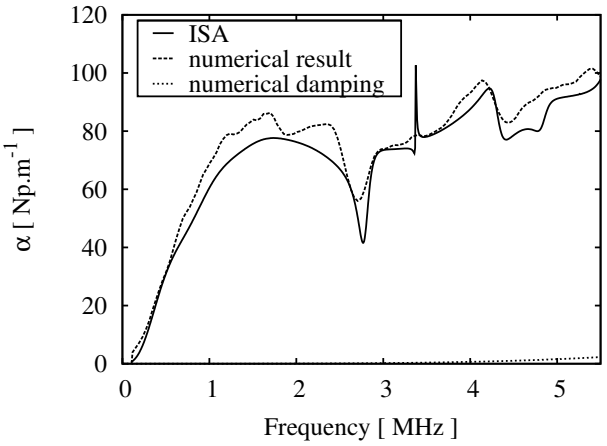

Figure 3: Results for the damping factor

Conclusion and perspectives

The preliminary results proposed here have shown that a numerical methodology allows to recover quite precisely the theoretical behavior predicted by the ISA. Up to now, we cannot clearly state about the small differences observed between both approaches. Are they induced by the approximations underlying the ISA, are they due to an error of protocol, or lastly do they follow from the numerical discretization ? To eliminate with certainty the last hypothesis, we foresee to use more sophisticated schemes (such as fourth-order ADER), and also to compute the solution on a finer grid. For reasons of computational memory, such a convergence study requires the parallelization of the algorithms, which is currently in progress.

An application of the methodology proposed here concerns the concrete. It is a very heterogeneous medium, and it can be considered as aggregates embedded in a cement paste matrix (mortar). Multiple scattering is important, and it is possible to extract a coherent and an incoherent part from measurements [5]. Before using ISA for non-destructive evaluation of concrete, one has to determine whether the hypotheses underlying ISA are satisfied: since aggregates represent 50 % in volume, the medium cannot be considered as dilute. However, the impedance contrast between the aggregates and the mortar is very low. The numerical tools provides a mean to decide whether ISA is still valid or not in that case.

References

[1] A. Derode, A. Tourin and M. Fink, “Random multiple scattering of ultrasound. I. Coherent and ballistic waves”, Phys. Rev. E 64, 036605, 2001.

[2] A. Derode, V. Mamou and A. Tourin, “Influence of correlations between scatterers on the attenuation of the coherent waves in random medium”, Phys. Rev. E 74, 036606, 2006.

[3] T.A. Mokhtar, R.B. Herrmann and D.R. Russel, “Seismic velocity and Q model for the shallow structure of the arabian shield from short-period Rayleigh waves”, Geophysics 53 (11), 1988, pp. 1379-1387.

[4] B. Lombard and J.Piraux, “Numerical treatment of two-dimensional interfaces for acoustic and elastic waves”, J. Comput. Phys. 195, 2004, pp. 90-116.

[5] M. Chekroun, *et al.*, “Multiple scattering of ultrasonic propagation for non destructive evaluation of concrete; first experiment”. Proceedings of NDT-CE Conference (St Louis, USA), 2006, pp. 365-370.

EXACT BOUNDARY CONDITIONS FOR LOCALLY PERTURBED 2D- PERIODIC PLANE

S. Fliss[†,*], **P. Joly**[†], **J. R. Li**[†]
[†]POEMS - INRIA Rocquencourt
[*]Email: sonia.fliss@inria.fr

Abstract
Locally perturbed periodic media play a major role in applications, in particular in optics for micro and nano technology, because they exhibit interesting properties, such as allowed modes in the spectral band gaps of the non perturbed periodic media. Of course there is a need for efficient numerical methods for computing the propagation of waves inside such structures. For a complete, mathematically oriented presentation, we refer the reader to [2, 3].

We are interested in propagation media which are a local perturbation of an infinite periodic medium and investigate the question of finding artificial boundary conditions to reduce the actual numerical computations to a neighborhood of this perturbation. We consider the situation of a 2D periodic media and propose a method for construction DtN operators on the artificial boundary by solving a family of waveguide problems.

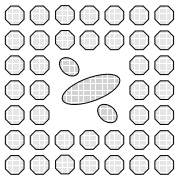

Figure 1: The domain of propagation

1 Description of the problem

The propagation model we consider is a simple 2D ($\mathbf{x} = (x,y)$) scalar model:

$$n(\mathbf{x})^2 \frac{\partial^2 U}{\partial t^2} - \Delta U = F.$$

We assume that the source term is time harmonic with frequency $\omega > 0$, ($F(\mathbf{x},t) = f(\mathbf{x})\, e^{i\omega t}$) and look for the time harmonic solution $U(\mathbf{x},t) = u(\mathbf{x})\, e^{i\omega t}$ where u satisfies the Helmholtz equation:

$$-\Delta u - n(\mathbf{x})^2\, \omega^2\, u = f. \qquad (1)$$

In order to solve this problem using the limiting absorption principle, we will concentrate, here, on the case with small absorption ($\varepsilon > 0$) and so solve the following problem:

$$-\Delta u - n(\mathbf{x})^2\, (\omega^2 + i\varepsilon)\, u = f. \qquad (\mathcal{P})$$

Before defining the domain and the parameters of the problem, we want to remark that, for simplicity, we will restrict ourselves to the case where the periodicity cell is a square which has double symmetry [defined below], which is often the case in the applications.

Definition 1 *S_α is the symmetry with respect to the line $y = \alpha x$.*
A subset $\mathcal{C}$ of $\mathbb{R}^2$ has a double symmetry if it is invariant with respect to S_1 and S_{-1}.
A function $n : \mathcal{C} \mapsto \mathbb{C}$ has double symmetry if:

$$n(S_1\mathbf{x}) \;=\; n(S_{-1}\mathbf{x}) \;=\; n(\mathbf{x}).$$

Proposition 1 *Let $\mathcal{C}$ be a domain with double symmetry and $V(\mathcal{C})$ a space of functions from $\mathcal{C}$ into $\mathbb{C}$.*
One has the decomposition :

$$V(\mathcal{C}) = \sum_{(i,j)\in\{0,1\}} V_{i,j}(\mathcal{C})$$

where

$$V_{i,j}(\mathcal{C}) = \{v \in V(\mathcal{C}), v(\mathbf{x}) = (-1)^i v(S_1\mathbf{x}) = (-1)^j v(S_{-1}\mathbf{x})\}$$

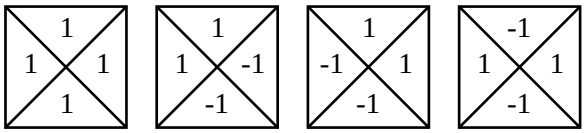

Figure 2: Examples of functions of $V_{i,j}(\mathcal{C})$ with $\mathcal{C} = [-1,1]^2$

See figure 2, for an example.
The domain of propagation Ω is infinite in the two directions, its geometry is periodic outside a bounded region Ω^i, in $\Omega^e = \Omega \setminus \Omega^i$, and the periodicity cell $\mathcal{C}_{00}$ has a double symmetry (in particular that implies that it is a square) (see figures 1 and 3). The function n is periodic as well, in Ω^e, with the same periodicity than the geometry and in $\mathcal{C}_{00}$ is with double symmetry.
Let us suppose for simplicity that the period is 1.
Ω^i is a square, which contains the defect (support of f, compact perturbation of n and geometrical defects) and

whose side is a multiple of the size of the periodicity cell, let' say N cells. For simplicity, we will suppose that $N = 1$.

Our objective is to characterize the restriction of u to Ω^i

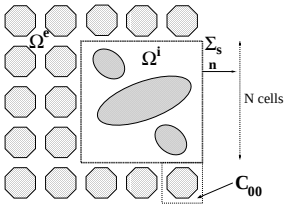

Figure 3: Some Notations

as the solution of $(\mathcal{P})$ in Ω^i and satisfying a condition of the form:

$$\frac{\partial u}{\partial \mathbf{n}} + \Lambda u = 0, \quad \text{on } \Sigma_S \tag{2}$$

where Σ_S is the boundary of the square Ω^i. The DtN operator is defined on Σ_S (which is an original situation, even in the constant coefficient case).

Definition 2 *Definition of the DtN operator*

$$\begin{array}{rcl} \Lambda \ : H^{1/2}(\Sigma_S) & \to & H^{-1/2}(\Sigma_S) \\ \varphi & \mapsto & \dfrac{\partial}{\partial \mathbf{n}} u^e(\varphi) \end{array}$$

where $u^e(\varphi)$ is the unique H^1 solution of the problem:

$$\begin{cases} -\Delta u^e(\varphi) - n(\mathbf{x})^2 \, (\omega^2 + i\varepsilon) \, u^e(\varphi) = 0, \quad \text{in } \Omega^e \\ u^e(\varphi) = \varphi, \quad \text{on } \Sigma_S \end{cases} \tag{$\mathcal{P}^e_\varphi$}$$

Proposition 2 *One has the block diagonal decomposition:*

$$\Lambda = \bigoplus_{i,j} \Lambda_{i,j}, \quad \Lambda_{i,j} \in \mathcal{L}\left(H^{1/2}_{i,j}(\Sigma_S).H^{-1/2}_{i,j}(\Sigma_S)\right)$$

in the sense that, refering to proposition 1:

$$\varphi = \sum_{i,j} \varphi_{i,j} \ \Rightarrow \ \Lambda\varphi = \sum_{i,j} \Lambda_{i,j}\varphi_{i,j}$$

Remark 1 *Each $H^{\pm 1/2}_{i,j}(\Sigma_S)$ is isomorphic to $H^{\pm 1/2}_{i,j}(\Sigma_0)$ where Σ_0 is one of the side of the square Σ_S.*

2 Factorization of the DtN map $\Lambda_{i,j}$

Theorem 1

$$\Lambda_{i,j} = \chi_{\Sigma_0} \circ \Lambda^H \circ D_{i,j}$$

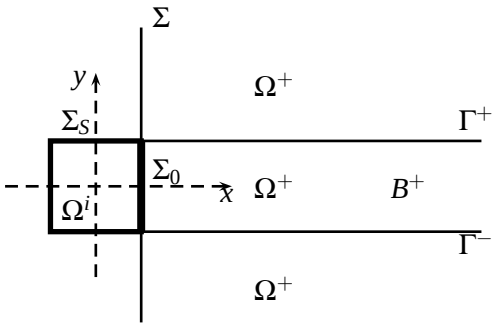

Figure 4: More notations

where :

• *$D_{i,j}$ is a Dirichlet-to-Dirichlet operator defined by:*

$$\begin{array}{rcl} D_{i,j} \ : H^{1/2}_{i,j}(\Sigma_S) & \to & H^{1/2}(\Sigma) \\ \varphi & \mapsto & u^e(\varphi)|_\Sigma \end{array}$$

where $u^e(\phi)$ is the solution of the problem $(\mathcal{P}^e_\varphi)$.

• *Λ^H is the halfspace DtN operator defined by:*

$$\begin{array}{rcl} \Lambda^H \ : H^{1/2}(\Sigma) & \to & H^{-1/2}(\Sigma) \\ \psi & \mapsto & \dfrac{\partial}{\partial \mathbf{n}} v^+(\psi)|_\Sigma \end{array}$$

where $v^+(\psi)$ is the solution of the problem $(\mathcal{P}^+_\psi)$:

$$\begin{cases} -\Delta v^+(\psi) - n(\mathbf{x})^2 \, (\omega^2 + i\varepsilon) \, v^+(\psi) = 0, \quad \text{in } \Omega^+ \\ v^+(\psi) = \psi, \quad \text{on } \Sigma \end{cases} \tag{$\mathcal{P}^+_\psi$}$$

and Ω^+ is the halfspace at the right of Σ.

• *χ_{Σ_0} is the restriction operator defined from $H^{-1/2}(\Sigma)$ to $H^{-1/2}(\Sigma_0)$.*

see figure 4 for some notations.

2.1 Characterization of Λ^H

Definition 3 *The Floquet-Bloch (FB) Transform of period 1 is defined by (see [4]):*

$$\begin{array}{rcl} \mathcal{F} \ : L^2(\mathbb{R}) & \to & L^2(R_0 = [-\frac{1}{2}; \frac{1}{2}] \times [-\pi, \pi]) \\ \psi(y) & \mapsto & \mathcal{F}\,\psi(y,k) = \dfrac{1}{\sqrt{2\pi}} \displaystyle\sum_{n \in \mathbb{Z}} \psi(y+n) e^{-ink} \end{array}$$

Moreover we have the inversion formula:

$$\forall y \in [0,1], \quad \psi(y+n) = \frac{1}{2\pi} \int_{-\pi}^{\pi} \mathcal{F}\,\psi(y,k) e^{ink} dk$$

We note $\mathcal{F}_y$ the FB Tranform applied in the y-direction to a function of $\mathbb{R}^2$.

Let $v^+(\psi)$ be the solution of the problem $(\mathcal{P}^+_\psi)$, then using the periodicity of the problem, for every k in $[-\pi, \pi]$,

$\mathcal{F}_y v^+(\psi)(\cdot,k)$ is the solution of the waveguide problem:

$$\begin{cases} \left[-\Delta \mathcal{F}_y v^+(\psi) - n^2(\omega^2+i\varepsilon)\,\mathcal{F}_y v^+(\psi)\right](\cdot,k) = 0, \quad \text{in } B^+ \\ \mathcal{F}_y v^+(\psi)(\cdot,k)|_{\Sigma_0} = \mathcal{F}_y\psi(y,k), \\ \mathcal{F}_y v^+(\psi)(\cdot,k)|_{\Gamma^+} = e^{ik}\mathcal{F}_y v^+(\psi)(\cdot,k)|_{\Gamma^-} \\ \partial_y \mathcal{F}_y v^+(\psi)(\cdot,k)|_{\Gamma^+} = e^{ik}\partial_y \mathcal{F}_y v^+(\psi)(\cdot,k)|_{\Gamma^-} \end{cases}$$

where B^+ is the region bounded by Γ^-, Γ^+ and Σ_0, (see figure 4).

Using the method developed in [1], we can characterize and compute, for every $k \in [-\pi,\pi]$, the corresponding waveguide DtN operator $\Lambda^H(k)$, defined by:

$$\begin{array}{rccc} \Lambda^H(k) & : H^{1/2}(\Sigma_0) & \to & H^{-1/2}(\Sigma_0) \\ & \mathcal{F}_y\psi & \mapsto & \dfrac{\partial}{\partial \mathbf{n}} \mathcal{F}_y v^+(\psi)(\cdot,k)|_{\Sigma_0} \end{array}$$

Proposition 3 *Λ^H is described in terms of a family of waveguide DtN operators $\Lambda^H(k)$*

$$\Lambda^H = \int^{\oplus} \Lambda^H(k)\, dk. \tag{3}$$

Remark 2 *The method in [1] contains also the determination of $\mathcal{F}_y v^+(\psi)(\cdot,k)$, for every k. We can then construct semi-analytically, using the inversion formula, $v^+(\psi)$ for any Dirichlet condition ψ.*

2.2 Characterization of $D_{i,j}$

For simplicity, we will develop just the construction of $D_{0,0}$ defined on $H^{1/2}_{0,0}(\Sigma_S)$, we can generalize easily to the other operators $D_{i,j}$.

Proposition 4 *$D_{0,0}$ is in the affine space:*

$$\mathcal{L}_{\Sigma_0} = \left\{ L \in \mathcal{L}\left(H^{1/2}_{0,0}(\Sigma_s), H^{1/2}(\Sigma)\right), \quad \forall \varphi,\, L\varphi|_{\Sigma_0} = \varphi|_{\Sigma_0} \right\}$$

To characterize $D_{0,0}$, we have to define some aditionnals objects. Let $\Sigma = \Sigma^- \cup \Sigma_0 \cup \Sigma^+$ where Σ^- and Σ^+ are respectively the lower and the upper part of Σ. We will call Γ the set $\Gamma^- \cup \Sigma_0 \cup \Gamma^+$. We can see easily that Γ (resp. Γ^- and Γ^+) is isomorphic to Σ (resp. Σ^- and Σ^+). See figure 4.

Let D be the Dirichlet-to-Dirichlet operator defined by:

$$\begin{array}{rccc} D & : H^{1/2}(\Sigma) & \to & H^{1/2}(\Sigma) \\ & \psi & \mapsto & \left| \begin{array}{rcl} D\psi|_{\Sigma^+} & = & v^+(\psi)|_{\Gamma^+} \\ D\psi|_{\Sigma_0} & = & v^+(\psi)|_{\Sigma_0} \\ D\psi|_{\Sigma^-} & = & v^+(\psi)|_{\Gamma^-} \end{array} \right. \end{array}$$

Because $v^+(\psi)$ can be computed semi-analitycally, D can be computed too.

Theorem 2 *$D_{0,0}$ is the unique solution in $\mathcal{L}_{\Sigma_0}$ of the affine equation:*

$$D_{0,0} = D \circ D_{0,0} \tag{$\mathcal{E}_{0,0}$}$$

The proof relies on symmetry arguments together with uniqueness results for quarter-plane problems.

Remark 3 *The resolution of this equation is not as simple as it seems. Actually, the equation has to be solved successively for every function in $\varphi \in H^{1/2}(\Sigma_0)$ to find a function,$D_{0,0}\varphi \in H^{1/2}(\Sigma) \sim H^{1/2}(\mathbb{R})$. Actually the formulation in terms of FB-variables in this problem is more natural and for any φ we have to solve an integral equation with a constraint (contained in "$\mathcal{L}_{\Sigma_0}$"), and we will find a function ($\mathcal{F}_y D_{0,0}\varphi \in H^{1/2}(R_0)$.*

Algorithm of computation

- Computation of Λ^H
  - For each $k \in [-\pi,\pi]$, computation of $\Lambda^H(k)$
  - Computation of Λ^H by recomposition
- Computation of $\Lambda_{i,j}$ for each $(i,j) \in \{0,1\}$
  - Computation of $D_{i,j}$ by resolution of $\mathcal{E}_{i,j}$,
  - $\Lambda_{i,j} = \chi_{\Sigma_0} \circ \Lambda^H \circ D_{i,j}$

Generalization and some conclusions

Numerical results will be shown during the presentation.

The method is valid for fewer symmetries, but the four operators $D_{i,j}$ are coupled.

References

[1] P. Joly, J.-R. Li and S. Fliss, "Exact boundary conditions for periodic waveguides containing a local perturbation", in Communications in Computational Physics, vol.1(6), pp. 945-973, 2006.

[2] P. Kuchment, "On some spectral problems of mathematical physics", Partial differential equations and inverse problems,volume 362 of Contemp. Math., Amer.Math.Soc., Providence, pp.241-276, 2004.

[3] P. Kuchment, "The mathematics of photonics crystals" (chapter 7), Mathematical Modelling in optical science , vol. 22 of Frontiers in applied Mathematics. SIAM, Philadelphia, 2001.

[4] P. Kuchment, "Floquet theory for Partial differential Equations", Operator Theory : Advances and applications, vol. 60, Birkhäuser Verlag, Basel, 1993.

TRANSMISSION THROUGH A RANDOMLY PERTURBED PERIODIC MEDIUM

Yu. A. Godin[†,*], **S. Molchanov**[†], **B. Vainberg**[†]
[†]Department of Mathematics and Statistics, University of North Carolina at Charlotte, Charlotte, NC 28223, USA
[*]Email: ygodin@uncc.edu

Abstract

We study the variance of the transfer matrix of a periodic 1D Schrödinger operator perturbed by the white noise. It is shown that if the frequency of propagation lies inside the band, then the total variance is proportional to $N\sigma^2$, where σ is the intensity of the white noise and N is the number of periods. However, if the wave frequency is close to the band edge, the resulting variance is proportional to $N\sigma^{2/3}$. Thus, propagation becomes highly sensitive to random perturbations.

Numerical simulations reveal that even small noise in periodic potential can suppress transmission near the band edges and make it strongly irregular inside the band. Further increase of the noise amplitude leads to intermittent behaviour of the transmission coefficient, and makes transmission possible only for few random frequencies in the band.

Introduction

Let H be a Schrödinger operator on $L^2(\mathbb{R})$ with a potential $q = q(x)$ supported on an interval $(0, \ell)$

$$H\psi = -\frac{d^2\psi}{dx^2} + q(x)\,\psi(x), \tag{1}$$

and let ψ be the scattering solution for H, i.e. (1) holds and

$$\psi(x) = \begin{cases} e^{i\omega x} + r(\omega)\, e^{-i\omega x}, & x < 0; \\ t(\omega)\, e^{i\omega x}, & x > \ell. \end{cases} \tag{2}$$

Suppose that the transfer matrix $\mathbf{M}_\omega$ through each period $[(n-1)L, nL]$, $n = 1, 2, \ldots, N$, contains some noise (defects, absorption, etc.), i.e. the corresponding propagator $\mathbf{M}_{\omega,n}$ through the period is a small random perturbation of the transfer matrix. Then the transmission coefficient has the following form

$$|t_N(\omega)|^2 = \frac{4}{\left\|\prod_{n=1}^{N} \mathbf{M}_{\omega,n}\right\|_2^2 + 2}. \tag{3}$$

Here $\mathbf{\Pi}_N = \prod_{n=1}^{N} \mathbf{M}_{\omega,n}$ is the transfer matrix on the support interval $[0, NL]$ of the potential $q(x)$. This matrix will be the main object of our studies.

With the advance of applications of periodic structures to different electromagnetic devices (optical waveguides, photonic crystals), more emphasis is placed on the analysis of effects due to disorder in periodic materials [1]-[3]. The effects of randomness of the refractive index and geometry of photonic crystals on their transmission properties have been studied mostly numerically (see [4]-[5] and references therein). One of the essential consequences of the disorder is the appearance of the localized states in the gaps similar to the impurity states outside the spectrum of the periodic Schrödinger operator. The unperturbed transfer matrix $\mathbf{M}_\omega$ is unimodular $\det \mathbf{M}_\omega = 1$. However, after a random perturbation of its entries this property may not hold anymore. In terms of the operator (1) it corresponds to the case when potential $q(x)$ becomes complex-valued or terms with first derivative appear in (1) as a result of the perturbation.

Additive and Multiplicative Perturbations

We will consider two models where the perturbation of $\mathbf{M}_\omega$ is either additive or multiplicative. In the first case, the propagator $\mathbf{M}_{\omega,n}$ has the form

$$\mathbf{M}_{\omega,n} = \mathbf{M}_\omega + \sigma \mathbf{W}_n, \tag{4}$$

where σ is a small parameter, and $\mathbf{W}_n = \begin{bmatrix} \xi_n & \eta_n \\ \zeta_n & \mu_n \end{bmatrix}$. Here ξ_n, η_n, ζ_n, μ_n are independent (for all n) $\mathcal{N}(0,1)$ random variables depending only on ω. In the multiplicative case we assume that

$$\mathbf{M}_{\omega,n} = \mathbf{M}_\omega\,(\mathbf{I} + \sigma \mathbf{V}_n), \tag{5}$$

where σ is a small parameter, $\mathbf{V}_n = \begin{bmatrix} \xi_n & \eta_n \\ \zeta_n & -\xi_n \end{bmatrix}$, and ξ_n, η_n, ζ_n are random variables which are not necessary independent, but have a joint Gaussian distribution with the covariance

$$\mathbf{B} = [b_{i,j}] = \mathsf{E} \begin{bmatrix} \xi_n^2 & \xi_n\eta_n & \xi_n\zeta_n \\ \xi_n\eta_n & \eta_n^2 & \eta_n\zeta_n \\ \xi_n\zeta_n & \eta_n\zeta_n & \zeta_n^2 \end{bmatrix}. \tag{6}$$

Clearly matrix (4) can be written in the form (5) and vice versa. The difference between the additive and multiplicative perturbations is in the assumptions of the random variables. In the first case we assume that the entries

of the perturbation matrix are independent identically distributed random variables (isotropic case). As a result,

$$\det \mathbf{M}_{\omega,n} = 1 + O(\sigma),\ \sigma \to 0.$$

In the multiplicative case, three entries of the matrix $\mathbf{V}_n$ are independent and the fourth is chosen in such a way that the trace of $\mathbf{V}_n$ would be zero. This leads to the fact that

$$\det \mathbf{M}_{\omega,n} = 1 + O(\sigma^2),\ \sigma \to 0.$$

The problem under investigation depends on two parameters: $\sigma \to 0$ and N. We assume that N is bounded or grows not very fast: $\sigma^h N < C < \infty$, where $h > 0$ will be defined in Theorem 1. Our goal is to find the error in the transfer matrix over N periods,

$$\mathbf{\Pi}_N = \prod_{n=1}^{N} \mathbf{M}_{\omega,n}, \tag{7}$$

due to a random perturbation of the matrix over each period.

Variance of the Transfer Matrix

The expectation of matrix $\mathbf{\Pi}_N$ is clearly equals $(\mathbf{M}_\omega)^N$. The scalar variance of $\mathbf{\Pi}_N$ due to additive perturbation is estimated by

Theorem 1. *The variance D_N has the following asymptotic behavior when ω is fixed, $\sigma \to 0$, and N is bounded or growing not very fast.*

If ω is an interior point of a band and $\sigma^2 N < C < \infty$, then

$$D_N = c(\omega)\sigma^2 N(1 + o(1)). \tag{8}$$

If ω is inside a band and close to the band edge ω_0 such that $\omega - \omega_0 = o(\sigma^{2/3})$ and $\sigma^{2/3} N < C < \infty$, then

$$D_N = c(\omega_0)\sigma^{2/3} N(1 + o(1)). \tag{9}$$

Similar theorem is true in the case of multiplicative perturbations.

Theorem 2. *If ω is an interior point of a spectral band, then the first statement (8) of Theorem 1 holds. If ω is close to a spectral band edge ω_0 such that $\omega - \omega_0 = o(\sigma^{2/3})$, then the second statement (9) of Theorem 1 is valid provided that the correlation matrix $\mathbf{B}(\omega)$ is nondegenerate at that frequency.*

Numerical example

As an example we consider perturbation of a periodic delta-function potential

$$V(x) = A \sum_n \delta(x - nL), \tag{10}$$

where $A > 0$ is a constant.

The sensitivity of the scalar variance D of the transfer matrix over one period on the propagating frequency ω is shown in figure 1 for $L = 1$ and $A = 6$. If $\omega = 2.6$ is close to the middle of the band, then the variance of the transfer matrix is increasing linearly with σ^2 having the same order (lower curve). If, however, $\omega = 1.977$ is close to the band edge then the variance undergoes drastic changes with σ^2 (cf. (8)-(9)).

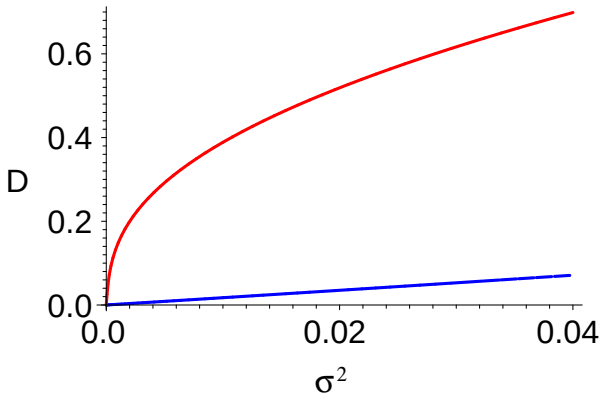

Figure 1: Dependence of the scalar variance D of the transfer matrix over one period on the perturbation variance σ^2 for $L = 1$ and $A = 6$. The lower curve corresponds to the frequency $\omega = 2.6$ in the middle of the first band, while the upper one matches $\omega = 1.977$ near the left edge of the first band.

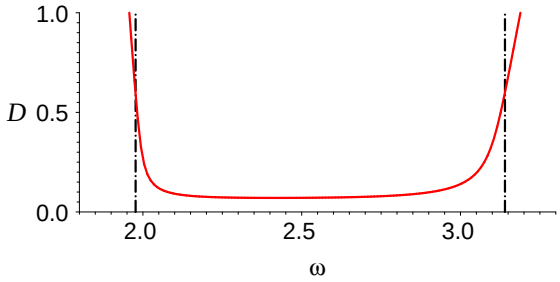

Figure 2: Dependence of the scalar variance D of the transfer matrix over one period on the frequency ω for the perturbation variance $\sigma^2 = 0.04$, $L = 1$, and $A = 6$. The band is confined between vertical lines.

Figure 2 illustrates dependence of the variance of the transfer matrix D over one period on the frequency ω for

perturbation variance $\sigma^2 = 0.04$ and $L = 1$, $A = 6$. The area in the center of the band is the least sensitive to the noise. As the frequency approaches the band edges, the variance of the transfer matrix increases dramatically.

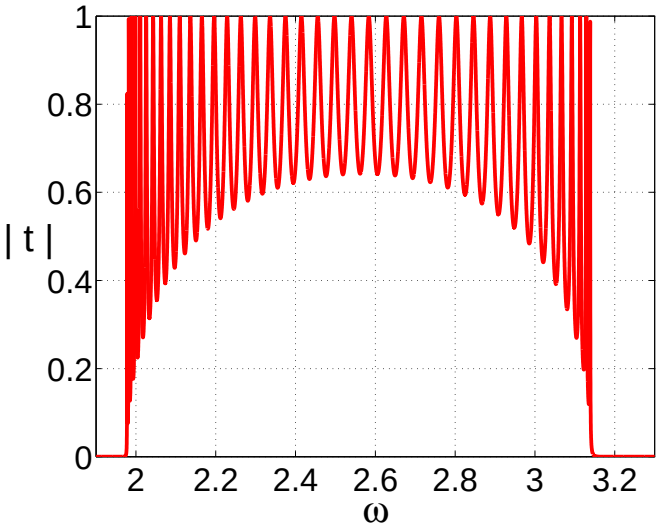

Figure 3: Transmission $|t|$ of unperturbed periodic waveguide ($\sigma = 0$) with $A = 6$ and $L = 1$.

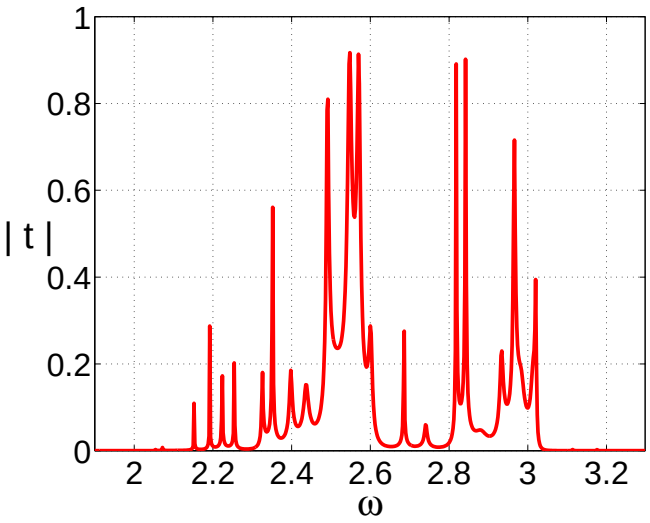

Figure 4: Same as in figure 3 with white noise of intensity $\sigma = 0.8$.

Dependence of the transmission coefficient $|t|$ on frequency over 40 periods of delta-function potential (10) with $A = 6$ and $L = 1$ is shown in figures 3-5. Figure 3 corresponds to the noiseless transmission and indicates regular periodic behavior within the band. Addition of a small noise with $\sigma = 0.4$ drops transmission to zero near the band edges and destroys completely the periodic character of transmission (not shown). Further growth of the noise amplitude to $\sigma = 0.8$ in figure 4 decreases the band width and leads to the appearance of the intervals inside the band where transmission is suppressed. Finally, in figure 5, for $\sigma = 1.2$ transmission becomes highly intermittent and is possible only for few frequencies.

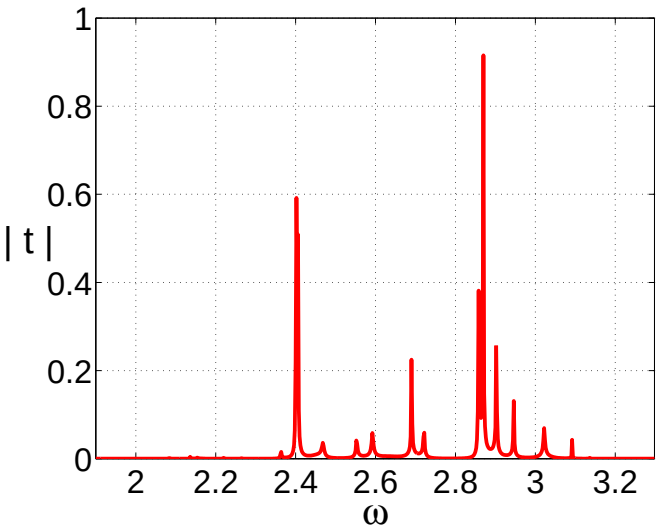

Figure 5: Same as in figure 3 with white noise of intensity $\sigma = 1.2$.

Acknowledgment

The work of S. Molchanov and B. Vainberg was supported in part by NSF grant DMS-0405927.

References

[1] A. Yariv, Y. Xu, R. K. Lee, A. Scherer, "Coupled-resonator optical waveguide: a proposal and analysis", Optics Letters, vol. 24, pp. 711-713, 2002.

[2] J. E. Heebner, R. W. Boyd , "'Slow' and 'fast' light in resonator-coupled waveguides", Journal of Modern Optics, vol. 49, pp. 2629-2636, 2002.

[3] A. Figotin, I. Vitebskiy, "Slow light in photonic crystals", Waves in Random and Complex Media, vol. 16, pp. 293-382, 2006.

[4] M. M.Sigalas, C. M. Soukoulis, C. T. Chan, R. Biswas, K. M.Ho, "Effect of disorder on photonic band gaps", Physical Review B, vol. 59, pp. 12767-12770, 1999.

[5] A. A. Asatryan et al., "Effects of disorder on wave propagation in two-dimensional photonic crystals", Physical Review E, vol. 60, pp. 6118-6127, 1999.

Efficient calculation of Green's functions for the two-dimensional Helmholtz equation in periodic domains

H. Kurkcu[†,*], **F. Reitich**[‡,*]
[†]School of Mathematics, University of Minnesota, Minneapolis, Mn 55455, USA
[*]Email: kurkcu@math.umn.edu

Abstract

A difficulty that arises in the context of infinite, $d-$periodic rough-surface scattering relates to the effective numerical evaluation of the corresponding "quasi-periodic Green function" G_d. Due to its relevance in a variety of applications, this problem has generated significant interest over the last thirty years, and a variety of numerical methods have been devised for this purpose. None of these methods to evaluate G_d however, were designed for high-frequency calculations. As a result, in this regime, these methods become prohibitively expensive and/or unstable. Here we present a novel scheme that can be shown to outperform every alternative numerical evaluation procedure, and is especially effective for high-frequency calculations. Our new algorithm is based on the use of some exact integrals that arise on judicious manipulation of the integral representation of G_d and which reduce the overall problem to that of evaluation of a sequence of simpler integrals that can be effectively handled by standard quadrature formulas. We include a variety of numerical results that confirm that, indeed, our algorithm compares favorably with alternative methods.

Introduction

Even though there are many efficient methods for the evaluation of the Green's function (G_d) [1] for the numerical solution of electromagnetic and acoustic scattering by infinite periodic rough surfaces at small to moderate frequencies the design of methods for high frequency problems remains a substantial challenge. Indeed, a variety of techniques have been devised over the past thirty years to accelerate the numerical evaluation of G_d including, most notably, those based on spectral or integral representations, Kummer transforms, lattice sums and Ewald's method (see e.g. [1] for a recent review of these and their relative merits). None of the existing methods however, were designed for high-frequency calculations and, as a result, these methods become prohibitively expensive and/or unstable in this regime

In what follows we present an alternative scheme that allows for the efficient evaluation of G_d at high frequencies. Briefly, the method begins with the integral representation of the fundamental solution wherein G_d is represented as an integral of an exponentially decaying function f over $[0,\infty)$. At high frequencies the integrand f displays large and rapid oscillations which cancel out to produce a significantly smaller integrated value. For this reason classical quadratures tend to be unstable and unable to accurately determine the values of G_d. To overcome these difficulties our scheme is based on polynomial expansion of quotients of f and suitably chosen functions that allow for explicit evaluations. Moreover, the procedure further relies on judicious integration by parts to minimize cost and ill-conditioning. We present numerical results that confirm that this approach delivers a method that significantly outperforms every alternative procedure and that it enables accurate simulations at very high frequencies.

The integral representation of G_d

For a fixed incidence angle θ, the integral representation of G_d is given by [1]:

$$G_d(x,y) = -\frac{i}{4}H_0(kr) - \frac{1}{\pi}I \tag{1}$$

where k is the wave number of the incident plane wave, $\beta = k\sin(\theta)$, $r=\sqrt{x^2+y^2}$ and

$$I = \int_0^\infty \left[\frac{e^{kx(u^2-i)}}{e^{-i\beta d+kd(u^2-i)}-1}\frac{\cos(ikyu\sqrt{u^2-2i})}{\sqrt{u^2-2i}} + \frac{e^{-kx(u^2-i)}}{e^{i\beta d+kd(u^2-i)}-1}\frac{\cos(ikyu\sqrt{u^2-2i})}{\sqrt{u^2-2i}}\right] du, \tag{2}$$

The integral in (2) can be rewritten as $I = I_+ + I_-$ where

$$I_+ = \int_0^\infty \left(\frac{e^{ikyu\sqrt{u^2-2i}+kx(u^2-i)}}{2(e^{-i\beta d}e^{kd(u^2-i)}-1)(\sqrt{u^2-2i})} + \frac{e^{ikyu\sqrt{u^2-2i}-kx(u^2-i)}}{2(e^{i\beta d}e^{kd(u^2-i)}-1)(\sqrt{u^2-2i})}\right) du, \tag{3}$$

$$I_- = \int_0^\infty \left(\frac{e^{-ikyu\sqrt{u^2-2i}+kx(u^2-i)}}{2(e^{-i\beta d}e^{kd(u^2-i)}-1)(\sqrt{u^2-2i})} + \frac{e^{-ikyu\sqrt{u^2-2i}-kx(u^2-i)}}{2(e^{i\beta d}e^{kd(u^2-i)}-1)(\sqrt{u^2-2i})}\right) du. \tag{4}$$

The Algorithm

To simplify the presentation of our procedure, we shall assume that $\theta = 0$ (normal incidence) and $x = 0$; the arguments for the most general case follow largely along the same lines. To clearly reveal the exponential decay of the integrands, using the relation $\sqrt{u^2-2i} \sim 1-i$ for $u \sim 0$, it follows that

$$f_+ = \frac{e^{iky u\sqrt{u^2-2i}}}{(e^{kd(u^2-i)}-1)(\sqrt{u^2-2i})} \sim g_+ = \frac{e^{kyu(1+i)}}{e^{kd(u^2-i)}},$$
$$f_- = \frac{e^{-iky u\sqrt{u^2-2i}}}{(e^{kd(u^2-i)}-1)(\sqrt{u^2-2i})} \sim g_- = \frac{e^{-kyu(1+i)}}{e^{kd(u^2-i)}}.$$

As we mentioned, a main difficulty that arises in the evaluation of the integrals in (3) and (4) relates to the fact that, for large values for large values of y ($y > \sqrt{\frac{1}{kd}}$), and at high frequencies integrand f_+ in (3) displays large and fast oscillations ($|f_+| \gg 1$ and $|f_+'| \gg 1$) which cancel out to produce a significantly smaller integral. More precisely, we have

$$\max|f_+| \sim e^{\frac{ky^2}{2d}} \gg 1 \quad \text{and} \quad \left|\int_0^\infty f_+ du\right| \sim \frac{1}{\sqrt{k}} \ll 1.$$

Our algorithm relies on further manipulation of the integrals in (3) and (4) in a manner so as to reduce the integration problem to one where the application of classical quadrature formulas becomes simultaneously stable and efficient. To begin we note that

$$\begin{aligned}
&\int_0^\infty f_+ du = \int_0^\infty \frac{f_+}{g_+} g_+ du \\
&= \int_0^\infty \left(\frac{e^{iky u\sqrt{u^2-2i}-kyu(1+i)}}{(1-e^{-kd(u^2-i)})\sqrt{u^2-2i}}\right) g_+ du \\
&= \int_0^\infty \left(\sum_{n=0}^\infty a_n u^n\right) \frac{1}{(1-e^{-kd(u^2-i)})} g_+ du \\
&= \int_0^\infty \left(\sum_{n=0}^\infty a_n u^n\right)\left(\sum_{j=0}^m \frac{1}{e^{jkd(u^2-i)}}\right) g_+ du \\
&+ \int_0^\infty \left(\sum_{n=0}^\infty a_n u^n\right) \frac{1}{e^{mkd(u^2-i)} - e^{(m-1)kd(u^2-i)}} g_+ du \\
&= \sum_{n=0}^\infty a_n \left(\sum_{j=1}^m I_{nj}\right) \\
&+ \int_0^\infty \frac{e^{iky u\sqrt{u^2-2i}}}{(e^{(m+1)kd(u^2-i)} - e^{mkd(u^2-i)})\sqrt{u^2-2i}} du
\end{aligned} \tag{5}$$

where

$$I_{nj} = \int_0^\infty \frac{u^n g_+}{e^{k(j-1)du^2}} du = \int_0^\infty u^n \frac{e^{kyu(1+i)}}{e^{kjdu^2}} du, \tag{6}$$

and

$$h(u) = \frac{e^{iky u\sqrt{u^2-2i}-kyu(1+i)}}{\sqrt{u^2-2i}} = \sum_{n=0}^\infty a_n u^n. \tag{7}$$

The evaluation of the integrals I_{nj} in (6) is clearly preferable to that in (3), on account of the diminishing values and faster decay of the former as n and j increase. For small values of these parameters, however, a further manipulation is necessary to attain similar characteristics. In more detail, we first note that [2, Equations 4.146.1 and 4.146.2] can be used to derive the following

$$I_{0j} = \int_0^\infty \frac{e^{kyu(1+i)}}{e^{kjdu^2}} = -\int_0^\infty \frac{e^{-kyu(1+i)}}{e^{kjdu^2}} du + A_j \tag{8}$$

where $A_j = \sqrt{\frac{\pi}{kjd}} e^{i\frac{ky^2}{2jd}}$.

After integration by parts n times, the following recursive formula can be derived.

$$I_{nj} = -\int_0^\infty (-u)^n \frac{e^{-kyu(1+i)}}{e^{kjdu^2}} + v_{nj} \tag{9}$$

with, $w_j = \frac{2dj}{y(1+i)}$, $v_{0j} = A_j$, $v_{1j} = \frac{A_j}{w_j}$, $s = ky(1+i)$, $v_{nj} = \frac{v_{n-1,j}}{w_j} + \frac{(n-1)v_{n-2,j}}{w_j s}$.

Even though the integrals on the right hand side of (9) can be calculated in a fast and efficient way using classical quadratures, a further simplification can be obtained using the symmetry of $h(u)$. Indeed we have

$$\sum_{n=0}^\infty a_n (-u)^n = \frac{e^{-iky u\sqrt{u^2-2i}+kyu(1+i)}}{\sqrt{u^2-2i}}, \tag{10}$$

and using this in (5) we obtain,

$$\begin{aligned}
&\sum_n^\infty a_n \sum_{j=1}^m I_{nj} = \\
&= -\int_0^\infty \left(\sum_{n=0}^\infty a_n (-u)^n\right) \frac{e^{-kyu(1+i)}}{e^{mkd(u^2-i)}} du + \sum_n^\infty a_n \sum_j^m v_{nj} \\
&= -\int_0^\infty \frac{e^{-iky u\sqrt{u^2-2i}}}{e^{kd(u^2-i)}\sqrt{u^2-2i}} du + \sum_n^\infty a_n \sum_j^m v_{nj} \\
&+ \int_0^\infty \frac{e^{-iky u\sqrt{u^2-2i}}}{(e^{(m+1)kd(u^2-i)} - e^{mkd(u^2-i)})\sqrt{u^2-2i}} du.
\end{aligned} \tag{11}$$

Note that I_- appears already in the (11). Finally the Green function can be rewritten as:

$$G_d(x,y) = -\frac{i}{4}H_0(kr) - \frac{2}{\pi}S - \frac{1}{\pi}I_{new}, \qquad (12)$$

where

$$S = \sum_{n=0}^{\infty} a_n(\sum_{j=1}^{m} v_{nj}), \qquad (13)$$

$$I_{new} = \int_0^{\infty} \frac{e^{ikyu\sqrt{u^2-2i}} + e^{-ikyu\sqrt{u^2-2i}}}{(e^{(m+1)kd(u^2-i)} - (e^{mkd(u^2-i)})(\sqrt{u^2-2i})} du. \qquad (14)$$

At this point we note that with the choice $m = O(\frac{ky^2}{d})$, the integral can be truncated to $[0, C_{new}]$ where $C_{new} = \frac{y+\sqrt{y^2-\frac{4md\log(\epsilon)}{k}}}{2md} \sim \frac{1}{k}$. Since the integrand does not oscillate, rapidly within this range, a canonical quadrature can be applied to evaluate it accurately.

The overall problem then reduces to calculating the series S, in a fast and stable way. Even though, for small y, the direct calculation of S via (13) works efficiently, as y increases ($\frac{ky^4}{d^3} > C$) the algorithm becomes unstable due to cancellations, arising from the alternating values of $a_n \sim \frac{(-\frac{(1-i)ky}{4})^n}{n!}$. To avoid this unstability the following "diagonal decomposition" is applied to improve stability and reduce computational cost.

$$S = \sum_{n}^{\infty} a_n(\sum_{j=1}^{m} v_{nj}) = \sum_{j=1}^{m}(\sum_{n}^{\infty} \frac{f_w^{2n}(1)}{n!}(\frac{w_j}{2ky(1+i)})^n), \qquad (15)$$

where $f_w(u) = \frac{e^{\frac{ikyu}{w_j}\sqrt{\frac{u^2}{w_j^2}-2i} - \frac{kyu(1+i)}{w_j}}}{\sqrt{\frac{u^2}{w_j^2}-2i}}$.

Numerical Examples

Here we provide three numerical experiments comparing the values of G_d obtained from an implementation of new algorithm and the classical spectral representation method. Specifically we consider examples with $d = 2\pi$, $\theta = 0$ and $x = 0$ for $y = 0.001, y = 0.01$ and $y = 0.1$. For the calculation of S, we use (13) for $y = 0.001, y = 0.01$ and (15) for $y = 0.1$. For comparison purposes, and to ensure the accuracy of both representations, all calculations were performed in quadruple precision arithmetic. The tables display the values of G_d at those points exact to 16 digits. As the tables show, significant improvements are attained by the scheme presented here for values of the wave number and spatial variables spanning several orders of magnitude.

Table 1: $k = 10^j + 0.2, y = 0.001, x = 0$

j	$Re(G_d)$	$Im(G_d)$	t_{SM}	t_{NA}
3	2.628688433907873e-2	-1.931709214516594e-1	6s	0.8s
4	1.522921154252366e-2	6.0888120714261587e-2	6s	0.8s
5	-1.888899645476105e-2	-5.186820874700445e-3	11s	0.8s
6	1.320719689032495e-3	-6.246830904346455e-3	87s	0.8s
7	9.675804564485829e-4	1.7939201404409735e-3	871s	0.8s
8	4.707091871365607e-4	4.1506677934769309e-4	8711s	0.8s
9	-1.852452152048772e-4	-8.295346774005824e-5	87100s	0.8s

Table 2: $k = 10^j + 0.2, y = 0.01, x = 0$

j	$Re(G_d)$	$Im(G_d)$	t_{SM}	t_{NA}
3	1.800341805729301e-2	5.964066204467009e-2	1s	0.8s
4	-1.789585869078290e-2	-5.538978697501209e-3	1s	0.8s
5	1.751207333507672e-3	-5.997317465685739e-3	8s	0.8s
6	9.994378477643144e-4	1.6276014923110622e-3	88s	0.8s
7	4.231349592437124e-4	4.291612136180172e-4	875s	0.8s
8	-1.837569041951388e-4	-7.921502500918968e-5	8755s	0.8s
9	5.476706509738081e-5	2.462038876030244e-5	87500s	0.8s

Table 3: $k = 10^j + 0.2, y = 0.1, x = 0$

j	$Re(G_d)$	$Im(G_d)$	t_{SM}	t_{NA}
3	-1.360795993008191e-2	-3.41097397114758e-4	0.2s	0.8s
4	2.213299101443911e-3	-7.65486217303957e-3	1.6s	0.8s
5	4.996867808830845e-4	1.778896007853010e-3	8s	0.8s
6	4.307177862473456e-4	4.862936472948697e-4	87s	0.8s
7	-1.977769511467323e-4	-5.03991366521495e-5	874s	1.5s
8	4.020872995782040e-5	5.290100535833349e-5	8734s	7s
9	3.202404057788981e-5	-1.40490522531367e-5	87400s	66s

References

[1] Linton C.M., The Green's Function for the two-dimensional Helmholtz Equation in Periodic Domain, Journal of Engineering Mathematics 33, (1998), 377-402.

[2] Gradshteyn I.S., Ryzhik I.M., Tables of Integrals, Series, and Products, Academic Press, New York, (1980) 522p .

Propagation through point scatterers: effect of correlations

A. Maurel[†,*], **V. Pagneux**[‡]
[†] LOA, ESPCI, 10 rue Vauquelin, Paris – France
[‡] LAUM, Univ. du Maine, Av. Olivier Messiaen, Le Mans – France.
[*]Email: agnes.maurel@espci.fr

Abstract

The propagation of a wave through point scatterers is under consideration. When the scatterer positions is random, in a sense that has to be made precise, an effective medium can be defined as the medium averaged over all realizations of random distributions. We restrict the study to small scattering strength, so that the effective medium can be characterized by deriving the effective wavenumber solving the Dyson equation. We refer to 2 typical configurations, where (1) the scatterers have a random distribution and are uncorrelated and (2) the scatterers have a periodic distribution, the whole lattice being allowed to translate. This latter case corresponds to strong correlation between scatterers and it is shown to have the same effective wavenumber as a single realization of periodic distribution. As a perturbation to the periodic case, the scatterers are allowed to randomly move around their periodic position with amplitude η (introducing another type of correlation). The different cases are exemplified with numerical results.

1 Introduction

The problem of wave propagation in randomly distributed scatterers has been widely studied and a large part of the literature is devoted to the derivation of the index of the so-called effective medium. This medium corresponds to the homogeneous dissipative medium felt by the "mean" acoustic wave when it propagates, the "mean" wave being the wave averaged over all realizations of the scatterer configurations, such as their positions and their characteristics. These studies have encountered a great success because of their practical applications from at least two domains: the geophysics literature seeks to understand the effect of inhomogeneities within the Earth crust on seismic waves [1] and the non-destructive evaluation literature seeks to gauge the effect that flaws in elastic materials have on elastic waves [2].

The characterization of the effective medium has been studied *via* mainly three theoretical approaches: 1) The first comes from the pioneering works of Foldy [3]. The goal is to derive an integral equation for the mean acoustical wave, which is achieved with the use of a heuristic approximation that gives a closure equation. The simplest closure equation is given by Foldy and referred to as the effective medium approximation (EFA). The quasicrystalline approximation (QCA) is an improvement at second order due to Lax [4]. 2) The second approach is based on the resolution of the so called Dyson equation. It consists in deriving an equation for the Green function of the effective medium, which can be done easily by expanding the Green function in the -assumed small- scattering strength. At leading order, this corresponds to the first Born approximation and at second order, to the first-order smoothing approximation (FOSA) or Keller approximation [5]. 3) Finally, in the low frequency limit, methods inspired from homogenization, as the Coherent Potential Approximation (CPA), are used. In these cases, the problem is reduced to the resolution in a single cell containing one scatterer [6].

We consider the propagation of a wave in one dimension through point scatterers, the effect of one scatterer being encapsulated in a potential $V(x) = v_0 k \delta(x)$ in the wave equation $(\Delta + k^2)u(x) = -V(x)u(x)$. We adopt the Dyson approach, where the scattering strength v_0 is assumed to be small. Two reference distributions of scatterers is taken: (1) the full randomly distributed scatterers, that is the scatterers are uncorrelated and have all the whole space as accessible space, and (2) the periodic distribution, where the first scatterer has the whole space as accessible space afterwards all other scatterers are placed at distance ja of the first scatterer (with $-\infty < j < \infty$ and a the lattice spacing). In between these two configurations, and following the idea of Parnell & Abrahams [7], an intermediate distribution (3) is considered, where each scatterer is allowed to move with amplitude $\eta < a$ around its mean (periodic) position. Numerical calculations of the mean configurations exemplify the theoretical results (the numerical method is detailed in [8]). The periodic case (2) is found to be a limit of the configuration (3) for $\eta \to 0$ but the fully random configuration (1) can not be recovered because of the correlation that has been introduced in (2-3).

2 The effective medium solving the Dyson equation

One way to find the effective wavenumber K is to solve the so called Dyson equation. The Dyson equa-

tion links the modified Green function $\langle G \rangle$ for the effective medium to the Green function G^0 of the space free of scatterer through the mass operator Σ: $\langle G \rangle = [{G^0}^{-1} - \Sigma]^{-1}$. For weak scattering, Σ can be expanded in powers of the potential V and, at second order, $\Sigma = \langle V \rangle - \langle V G^0 V \rangle + \langle V \rangle G^0 \langle V \rangle$. The resulting explicit expression for $\langle G \rangle(k)$ can be easily solved in the spectral space when the medium is invariant by translation and $K^2 \simeq k^2 + \Sigma(k)$ (K is expected to be close to k). When the potential is the sum of the potentials of $2N+1$ individual scatterers in a space of length L (afterwards, we take the limit $L, N \to 0$): $V(x) = \sum_j V_j(x)$, the mass operator can be simplified and we get $\Sigma = \Sigma_1 + \Sigma_2$

$$\begin{aligned}
&\Sigma_1(k) = n \int dx dx_1 p(x_1) e^{ikx} V_1(x) e^{-ikx}, \\
&\Sigma_2(k) = -n \int dx dx' dx_1 p(x_1) e^{ikx} V_1(x) G^0(x-x') \times \\
&V_1(x') e^{-ikx'} + \frac{N(N-1)}{L^2} \int dx dx' dx_1 dx_2 p(x_1) \times \\
&\left[p(x_2) - p(x_2|x_1)\right] e^{ikx} V_1(x) G^0(x-x') V_2(x') e^{-ikx'},
\end{aligned} \tag{1}$$

where $n = (2N+1)/L$ is the density of scatterers, $p(x_1)$ is the probability function of a single scatterer (say the first scatterer to be fixed up) and $p(x_2|x_1)$ is the pair correlation function, that is the probability function of the second scatterer to be fixed up, the first one be placed at x_1 position. In the considered cases (1-3), we have $p(x_1) = 1/L$, which means that the first scatterer has the whole space as accessible space. We also define $a = 1/n$ the mean distance between two scatterers.

3 Uncorrelated scatterers randomly placed

This case is the simplest one: with $p(x_2|x_1) = p(x_2)$, the modified wavenumber is

$$K^2 = k^2 + v_0 k/a + i v_0^2 k/(2a) + O(v_0^3). \tag{2}$$

It corresponds to the well-known result for uncorrelated scatterers $K^2 = k^2 + nf(0)$, with f the scattering function. It is written here with f expanded at second order in v_0.

It is easy to see that this result for uncorrelated scatterers randomly placed does not involve multiple scattering process (for instance, all terms in n^2, n^3 vanishes in the expansion). Let us consider a unique point scatterer at x_1 position randomly moving in the interval $[0, L]$. For an incident wave e^{ikx}, the transmission and reflexion coefficients are $T = (1 - iv_0/2)^{-1}$ and $R = iv_0/(2(1-iv_0/2))e^{2ikx_1}$. The Fig. 1 illustrates the random process and the resulting attenuation: at a given x-position, the field $u(x) = (1+T)e^{ikx}$ for a realization $x_1 \leq x$ and it is Re^{-ikx} otherwise. Over all possible

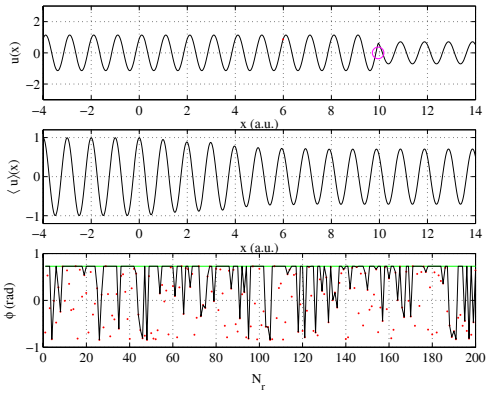

Figure 1: A unique scatterer moves in the interval $[0, L]$. Here $v_0 = 2$, $k = 2\pi$, $L = 10$. (a) example of the field $u(x)$ (here $x_1 = 9.7$ in pink circle). The red circle indicated the position where the phase on (c) is recorded, (b) mean field $\langle u \rangle(x)$ obtained for $N_r = 200$ realizations (200 x_1-positions) and (c) phase recorded at $x = 6$ position at each realization, the dotted line shows the phase of $(1+T)e^{ikx}$ (independent of x_1) and the red points give the phase of $R(x_1)e^{-ikx}$. The phase indeed recorded at the x-position fluctuates between the two values depending on whether $x < x_1$ or $x > x_1$. Only the realizations $x > x_1$ gives a coherent (constant) phase (the realizations $x < x_1$ gives random phase values).

realizations of the x_1-positions, those that correspond to $x_1 \leq x$ yield to the same phase for $u(x)$ while the latter cases yield to phase values that randomly fluctuate. It results that the realisations $u(x < x_1)$ are "incoherent", in the sense that their mean value vanishes while the realisation $u(x > x_1)$ are "coherent" in the sense that they are insensitive to a change in the disorder: the resulting mean field $\langle u \rangle(x)$ experiences a decrease in amplitude because of the loss of all incoherent realisations $x < x_1$.

4 The periodic case

The periodic case (1) is defined by $p(x_2|x_1) = \sum_{j \neq 0} \delta(x_2 - x_1 - ja)/(2N)$. This means that each realization consists of a periodic lattice with constant spacing a but two realizations differ by a translation since the first scatterer is allowed to move ($-L/2 \leq x_1 \leq L/2$). The effective wavenumber is obtained

$$(Ka)^2 = (ka)^2 + v_0 ka + v_0^2 \left[1 - ka \operatorname{cotan}(ka)\right]/4 + O(v_0^3). \tag{3}$$

It can be noticed that no attenuation occurs in that case. In fact, the above wavenumber corresponds to the wavenumber of the Floquet mode (for one realization of the periodic medium) expanded at second order in v_0 [from the dispersion relation $\cos Ka = \cos ka - v_0/2 \sin ka$].

This is illustrated on Fig. 2: the field $u(x)$ for one position of the periodic lattice has roughly the same aspect as the mean field $\langle u\rangle(x)$ except some fluctuations that are smoothed in the average process. Notably, the phase recorded at a given position appears to be constant, which explains why no attenuation occurs.

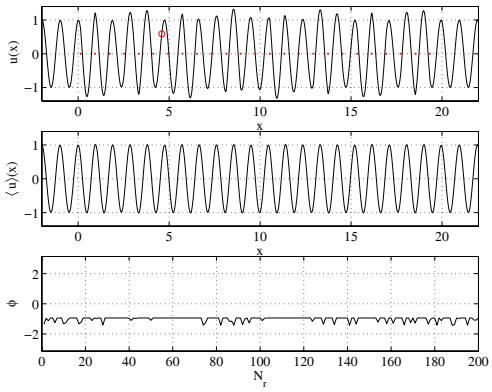

Figure 2: Illustration of the periodic case. Here, $v_0 = 0.5$, $k = 2\pi$, $a = 0.8$, the lattice of 25 scatterers is placed in $[0, 20]$. (a) $u(x)$ for a given position of the lattice. The scatterers are indicated with pink points, the red points give the phase recorded on (c). (b) Mean field $\langle u\rangle(x)$ averaged over 200 realizations of the lattice position in $[0, 20]$ and (c) phase recorded at $x \simeq 4.7$ at each realization.

5 Perturbation of the periodic case

Following the idea of Ref. [7], we consider the case where the scatterers are allowed to move around their periodic position with amplitude η. It follows that $p(x_2|x_1) = \sum_j \Pi_\eta(x_2 - x_1)/(2N\eta)$, with $\Pi_\eta(x) = 0$ for $|x| > \eta/2$ and $= 1$ for $|x| \leq \eta/2$. We obtain

$$(Ka)^2 = (ka)^2 + v_0 ka + v_0^2 \left[1 - P(\eta) ka \mathrm{cotan} ka\right]/4 + i[1 - P(\eta)] v_0^2 ka/4 + O(v_0^3), \tag{4}$$

with $P(\eta) \equiv \sin(k\eta)/(k\eta)$. The random perturbation introduced here has two effects, at second order in v_0: a modification in the effective wavelength and an imaginary part in K that holds a manifestation that attenuation has appeared. As expected, as $\eta \to 0$, the periodic case (2) is recovered. To the opposite, as $\eta = a$, which means that the set of scatterers covers the whole space over all realizations of disorder, the full random case (1) is not recovered. This is because all configurations of the disorder in the case (1) are not recovered in the present case: the configurations where two or more scatterers are in the same cell of length a. Note that this suggests that the approaches of CPA-type always consider correlation between scatterers and that they cannot tackle the full random case (1).

The law for K can be numerically checked with reasonable agreement, as illustrated on Fig. 3.

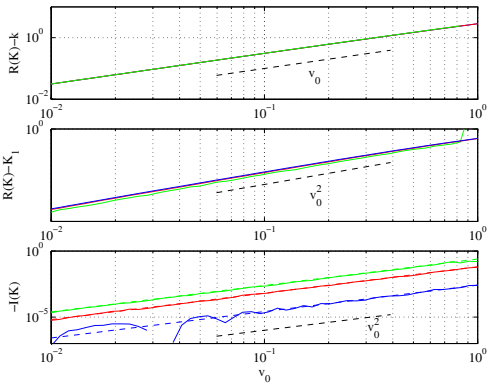

Figure 3: Effective wavenumber as a function of v_0 in the case (3) [$k = 2\pi$, $a = 1/2\pi$ and 61 scatterers]. $\eta = a/10$ (blue), $\eta = a/2$ (red) and $\eta = a$ (green). (a) First order correction $R(K) - k$ numerically obtained compared with the theoretical value $K_1 - k$, $K_1 = k[1 + v_0/(2ka)]$ (the curves are indistinguishable), (b) second order correction $-R(K) + K_1$ numerically obtained. In dotted line, the theoretical value $-P(\eta)\mathrm{cotan}ka/8a$. (c) Imaginary part $I(K)$ numerically obtained, in dotted line the corresponding theoretical value.

References

[1] T. Yamashita, Pure Appl. Geophys. **132**, 545-568 (1990).

[2] J.E. Gubernatis, E. Domany & J.A. Krumhansl, J. Appl. Phys. **48**, 2804-2811 (1977).

[3] L.L. Foldy, Phys. Rev. **67**(3,4), 107-119 (1945).

[4] M. Lax, Rev. Mod. Phys. **23**(4), 287-310 (1951).

[5] F.C. Karal & J.B. Keller, J. Math. Phys. **5**, 537-546 (1964).

[6] D. Torrent & J. Sánchez-Dehesa, Phys. Rev. B **74**, 224305 (2006).

[7] W.J. Parnell & I.D. Abrahams, to appear in IMA J. Appl. Maths (2007).

[8] A. Maurel, submitted to J. Am. Soc. Acoust. (2007).

On a Periodic FMM for Time-harmonic Wave Problems

Y. Otani[†,*], **N. Nishimura**[†]
[†]Graduate School of Informatics, Kyoto University, Kyoto, Japan
[*]Email: otani@mbox.kudpc.kyoto-u.ac.jp

Abstract

An FMM (Fast Multipole Method) [1], [2] for wave problems with periodic boundary conditions [3] is developed. We apply the proposed method to Helmholtz' and Maxwell's equations. In the case of Helmholtz' equation, we deal with scattering problems with periodic array of cracks and plot the energy transmittance versus wave numbers. The stopband and related phenomena are observed clearly.

Introduction

Solution of periodic boundary value problems for Helmholtz' and Maxwell's equations are interesting subject because of various applications in engineering. Typical applications of this type include photonic crystals and meta materials, which attract increased attention these days. Since one often has to solve high frequency problems in complicated domains in such applications, one is naturally lead to solutions of large scale problems. The Fast Multipole Methods (FMM) seem to provide good approaches for solving such problems.

As a matter of fact, the use of FMM in periodic boundary value problems in statics has been investigated since the beginning of the development of this method[1]. In dynamics, however, not much has been done except in a few works including the recent investigation by the present authors[3]. In view of important applications of periodic boundary value problems in dynamics, we present FMM formulations for Helmholtz' equation in 2D and Maxwell's equations in 3D, together with numerical examples, in the present paper.

Helmholtz' Equation in 2D

Statement of the problem

In this section, we consider periodic problems in 2 dimensional Helmholtz' equation.

Let D be a two-dimensional domain defined by $D = \mathbb{R} \times (-\frac{1}{2}, \frac{1}{2})$. Also, let S_c be a union of smooth non-self-intersecting line segments, which represents cracks physically (See Figure 1). Our problem is to find a solution u of Helmholtz' equation

$$\Delta u + k^2 u = 0$$

subject to the periodic boundary condition

$$u(x_1, 1/2) = e^{i\beta} u(x_1, -1/2)$$
$$\frac{\partial u}{\partial n}(x_1, 1/2) = -e^{i\beta} \frac{\partial u}{\partial n}(x_1, -1/2)$$

for $\forall x_1$, boundary condition on the cracks S_c given by

$$\frac{\partial u}{\partial n} = 0 \quad \text{on } S_c$$

and the radiation condition for the scattered wave given by $u - u^I$, where k is the wave number which satisfies

$$k \neq 2n\pi \pm \beta, \quad n \in \mathbb{Z},$$

u^I is the plane incident wave given by

$$u^I(x) = C_{\text{int}} e^{ik\boldsymbol{v}\cdot\boldsymbol{x}}$$

with $\boldsymbol{v} = (\cos\bar{v}, \sin\bar{v})$, and $\bar{v}$ is the incident angle. The quantity β is related to $\bar{v}$ *via*

$$\beta = k \sin\bar{v}.$$

The solution to the problem defined above is written as

$$u(x) = u^I(x) + \int_{S_c} \frac{\partial G^p}{\partial n_y}(\boldsymbol{x} - \boldsymbol{y})\phi(y) dS_y,$$

where G^p is the periodic Green function, and ϕ is the crack opening displacement which is the solution to the following integral equation:

$$0 = \frac{\partial u^I}{\partial n}(\boldsymbol{x}) + \text{⨍}_{Sc} \frac{\partial^2 G^p}{\partial n_x \partial n_y}(\boldsymbol{x} - \boldsymbol{y})\phi(\boldsymbol{y}) dS_y,$$

where the integral of the RHS is taken in the sense of the finite part.

Fast Multipole Method

In this section we briefly discuss the formulation of the FMM for ordinary boundary value problems, leaving aside the periodicity for a while.

As indicated in Figure 2, we take the cells with the centres O and O' in a way that $|\overrightarrow{O'x}| < |\overrightarrow{OO'}|$ and $|\overrightarrow{Oy}| < |\overrightarrow{OO'}|$ hold. The fundamental solution for Helmholtz'

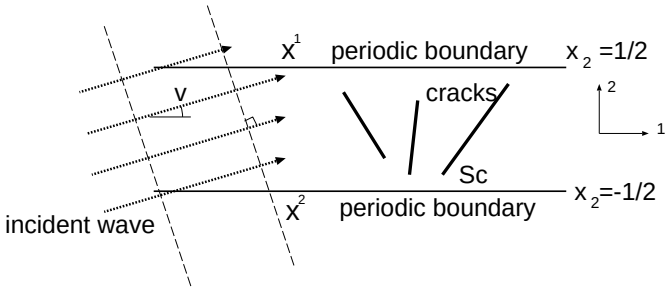

Figure 1: Problem under consideration

equation in 2D can be written in the form of the multipole expansion as

$$G(\boldsymbol{x}-\boldsymbol{y}) = \frac{i}{4}\sum_n\sum_\nu (-1)^n I^n(\overrightarrow{O'x}) O^{-n-\nu}(\overrightarrow{OO'}) I^n(\overrightarrow{Oy})$$

where O^n and I^n are functions defined as follows:

$$O^n(\overrightarrow{Ox}) = i^n H_n^{(1)}(kr)e^{in\theta}$$
$$I^n(\overrightarrow{Ox}) = (-i)^n J_n(kr)e^{in\theta}.$$

Let S_0 be the part of the boundary included in the cell whose centre is O. We obtain the multipole moment M_n and the coefficient of the local expansion L_n as follows:

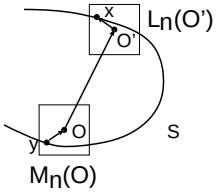

$$M_n(O) = \int_{S_0} I^n(\overrightarrow{Oy})\phi(\boldsymbol{y})dS_y$$
$$L_n(O') = \sum_\nu O^{n-\nu}(\overrightarrow{OO'})M_\nu(O).$$

Figure 2: Cells

With L_n, the single-layer potential computed over S_0 is expanded into the following local expansion:

$$\int_{S_0} G(\boldsymbol{x}-\boldsymbol{y})\phi(\boldsymbol{y})dS_y = \frac{i}{4}\sum_n (-1)^n I^n(\overrightarrow{O'x}) L_n(O').$$

One can also obtain a similar expansion for the double-layer potential and its normal derivative.

One can use these expansions to formulate a multilevel FMM. The reader is referred to [1], [2] for details.

Periodic FMM

We now present the outline of the periodic FMM. The details are found in Otani and Nishimura [3]. The periodic Green function G^p can be written as the following

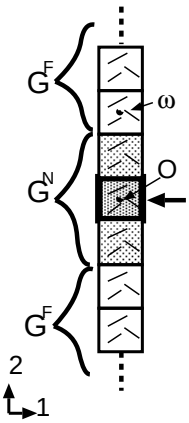

$$G^p(\boldsymbol{x}-\boldsymbol{y}) = G^N(\boldsymbol{x}-\boldsymbol{y}) + G^F(\boldsymbol{x}-\boldsymbol{y})$$
$$G^N(\boldsymbol{x}-\boldsymbol{y}) = \sum_{l=-1}^{1} G(\boldsymbol{x}-\boldsymbol{y}-l\boldsymbol{e}_2)e^{i\beta l}$$
$$G^F(\boldsymbol{x}-\boldsymbol{y}) = \sum_{|l|\geq 2} G(\boldsymbol{x}-\boldsymbol{y}-l\boldsymbol{e}_2)e^{i\beta l}$$

Figure 3: Replica cells

lattice sum of the fundamental solution:

$$G^p = \sum_l G(\boldsymbol{x}-\boldsymbol{y}-l\boldsymbol{e}_2)e^{il\beta} \quad (1)$$
$$= \frac{i}{4}\sum_\omega H_0^{(1)}(\boldsymbol{x}-\boldsymbol{y}-l\boldsymbol{e}_2)e^{il\beta},$$

which is very slowly convergent because $H^{(1)}(r) \sim \frac{1}{\sqrt{r}}$ with oscillation. We take the the unit cell whose vertices are given by $(\pm\frac{1}{2},\pm\frac{1}{2})$. The unit cell is taken as the level 0 cell for the FMM. As is seen from Eq. (1), the periodic boundary condition can be satisfied as we carry out FMM assuming that the replicas of the original unit cell are placed infinitely in the x_2 direction aligned with the original one (See Figure 3).

We split G^p into the sum of the contribution from nearby replicas denoted by G^N and those from far replicas denoted by G^F. The evaluation of the contribution of G^N can be done with tools for ordinary FMM. For the evaluation of the contribution of G^F, we use the "periodic M2L formula" given as in the following formula:

$$L_n(O) = \sum_\nu \left(\sum_{|l|\geq 2} O^{n-\nu}(-l\boldsymbol{e}_2)e^{il\beta}\right) M_\nu(O),$$

where $M_n(O)$ and $L_n(O)$ are the multipole moment and the coefficient of the local expansion for the level 0 cell (the unit cell). We evaluate $\sum_{l\geq 2} O^n(-l\boldsymbol{e}_2)e^{il\beta}$ with Fourier analysis as follows:

$$\sum_{|l|\geq 2} O^n(-l\boldsymbol{e}2)e^{il\beta} = \frac{1}{\pi i k^n}\left[\int_{-\infty}^{\infty}\frac{e^{-2i\beta-2p}(\xi-p)^n}{p(1-e^{-i\beta-p})}d\xi + \int_{-\infty}^{\infty}\frac{e^{2i\beta-2p}(\xi+p)^n}{p(1-e^{i\beta-p})}d\xi\right].$$

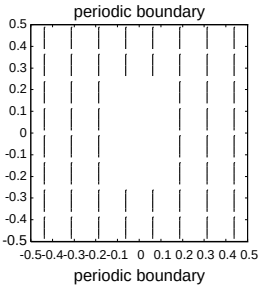

Figure 4: Unit structure

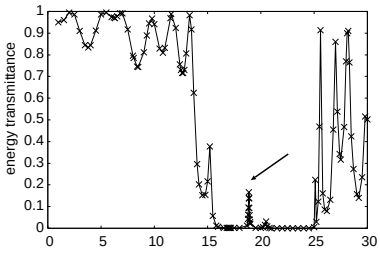

Figure 5: Energy transmittance versus wave number

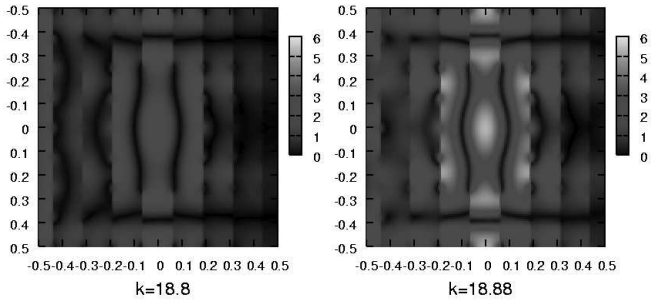

Figure 6: Distribution of $|u|$ for $k = 18.8$ and for $k = 18.88$

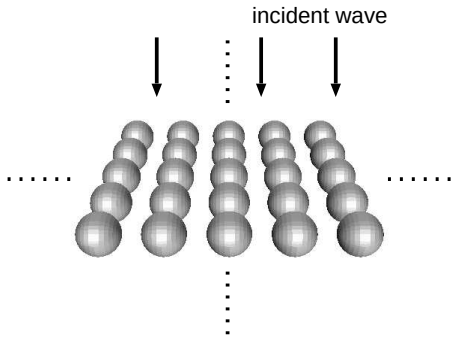

Figure 7: 2 dimensional arrays of spherical dielectrics

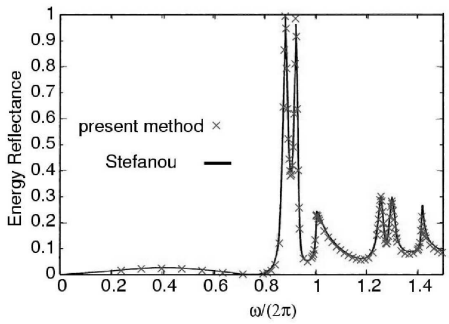

Figure 8: Energy reflectance versus frequency

Numerical results

Consider the unit structure indicated in Figure 4. For this structure, the energy transmittance is plotted versus wave numbers in Figure 5. In this figure, we clearly see not only a stopband, but also a narrow passband near $k = 18.88$. To understand the mechanism of this behaviour, we plot the magnitude of $|u|$ for $k = 18.8$ and 18.88 in Figure 6. These results indicate that there exists a mode localised near the 'hole' (the part where there exist no cracks). This phenomenon is considered to be similar to the so-called localised modes in photonic crystals.

Maxwell's Equations in 3D

The idea presented so far can be applied to Maxwell's equations as well. In this section, we focus on doubly periodic problems in 3D. We show only the numerical results because of the limitations of the space.

We here consider the 2 dimensional periodic arrays of spherical dielectrics shown in Figure 7, which is a model of the slab photonic crystal. For the present model, the period is 1, the radius of the spheres is 0.35 and the relative permittivity is 1.6^2. We consider the case of the normal incidence and plot the energy reflectances (x-marks) for frequencies in Figure 8. The same problem has been investigated numerically by Stefanou and Modinos [4], whose results are also plotted in Figure 8. As this figure indicates, these results agree quite well.

References

[1] L. Greengard and V. Rokhlin, "A fast algorithm for particle simulations", Journal of Computational Physics, Vol. 73, pp.325–348, 1987

[2] N. Nishimura, "Fast multipole accelerated boundary integral equation methods", Applied Mechanics Reviews, Vol. 55, pp.299–324, 2002

[3] Y. Otani and N. Nishimura, "An FMM for periodic boundary value problems for cracks for Helmholtz' equation in two dimensions", International Journal for Numerical Methods in Engineering, DOI: 10.1002/nme.2077

[4] N. Stefanou and A. Modinos, "Scattering of light from a two-dimensional array of spherical particles on a substrate", Journal of Physics Condensed Matter, Vol. 3, pp.8135–8148, 1991

HOMOGENIZATION OF THE ACOUSTIC TRANSMISSION THROUGH PERFORATED LAYER

E. Rohan[†,*], **V. Lukeš**[‡]
[†,‡]Dept. of Mechanics, University of West Bohemia, Pilsen, Czech Republic
[*]Email: rohan@kme.zcu.cz

Abstract

The paper deals with transmission conditions imposed on the interface plane separating two halfspaces occupied by the acoustic medium. The conditions are obtained as the two-scale homogenization limit of the standard acoustic problem imposed in the layer with the perforated periodic structure embedded inside. Both the characteristic scale of the perforations and the layer thickness are parameterized by $\varepsilon \to 0$. The limit model involving some homogenized coefficients governs the interface discontinuity of the acoustic pressure associated with the two halfspaces and the magnitude of the fictitious transversal acoustic velocity. This novel approach presents a new alternative to the usual description of the acoustic impedance, which relies on a rough averaging the quasi-experimental data.

Introduction

The purpose of the paper is to present the homogenization approach employed to derive a proper model of the acoustic transmission through perforated planar structure. We consider the acoustic medium occupying domain Ω which is subdivided by perforated plane Γ_0 in two disjoint subdomains Ω^+ and Ω^-, so that $\Omega = \Omega^+ \cup \Omega^- \cup \Gamma_0$. Denoting by p^+ and p^- the acoustic pressures in Ω^+ and Ω^-, respectively, in a case of no convection flow the usual transmission conditions are given by

$$\frac{\partial p^+}{\partial n^+} = -\mathrm{i}\frac{\omega\rho}{Z}(p^+ - p^-), \quad \frac{\partial p^-}{\partial n^-} = -\mathrm{i}\frac{\omega\rho}{Z}(p^- - p^+)\ , \tag{1}$$

where n^+ and n^- are the outward unit normals to Ω^+ and Ω^-, respectively, ω is the frequency, ρ is the density and Z is the *transmission impedance*; this complex number is characterized by features of the actual perforation considered and is determined using experiments in the acoustic laboratories, see e.g. [1].

We suggest a more refined mathematical treatment of such transmission problem, which results in constraints involving several *homogenized coefficients* computed directly for a specified shape of perforation. As an advantage, with such modelling approach one can think of *inverse problems* aimed at optimal design of the perforated structure to obtain a desired acoustic response.

Problem formulation

Here we briefly introduce the acoustic problem in the layer containing the periodically perforated structure. By indices $^\varepsilon$ we denote dependence of variables on scale parameter $\varepsilon > 0$; similar convention is adhered in the explicit reference to the layer thickness $\delta > 0$. By the Greek indices we refer to the coordinate index 1 or 2, so that $(x_\alpha, x_3) \in \mathbb{R}^3$.

Geometry

Let $\Omega_\delta \subset \mathbb{R}^3$ be an open domain shaped as a layer bounded by $\partial\Omega_\delta$ which is split as follows

$$\partial\Omega_\delta = \Gamma_\delta^+ \cup \Gamma_\delta^- \cup \partial\Omega_\delta^\infty\ , \tag{2}$$

where $\delta > 0$ is the layer thickness, see Fig. 1. The acoustic medium occupies domain $\Omega_\delta^\varepsilon \setminus S_\delta^\varepsilon$, where S_δ^ε is the solid obstacle which in a simple layout has a form of the periodically perforated sheet; thus, S_δ^ε is obtained by the usual *periodic lattice* extension of the solid unit structure.

For homogenization technique, it is important to have a fixed domain, therefore the *dilatation* is considered, cf. [2]; let Γ_0 be the plane spanned by coordinates $1, 2$ and containing the origin. Further let Γ_δ^+ and Γ_δ^- be equidistant to Γ_0 with the distance $\delta/2 = \mathrm{dist}(\Gamma_0, \Gamma_\delta^+) = \mathrm{dist}(\Gamma_0, \Gamma_\delta^-)$. Therefore, $x_3 \in]-\delta/2, \delta/2[$ and we introduce the rescaling $x_3 = z\delta$ so that one has $z \equiv y_3 \in]-1/2, +1/2[$.

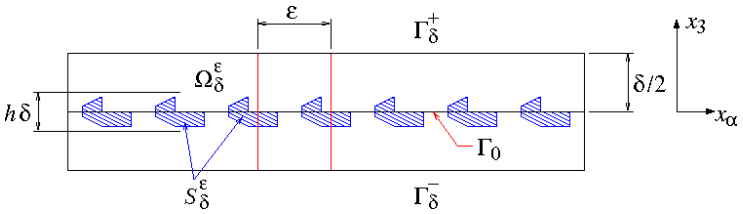

Figure 1: The layer Ω_δ of the acoustic medium with periodic "solid perforations" S_δ^ε situated within the layer $x_3 \in]-h\delta/2, +h\delta/2[$, where $h < 1$. The reference periodic cell spans the whole thickness of the layer.

Boundary value problem

The problem of acoustics is defined in $\Omega_\delta^\varepsilon$. We assume a monochrome stationary incident wave with the frequency

ω and no convection velocity of the medium, so that

$$\begin{aligned} c^2\nabla^2 p^{\varepsilon\delta} + \omega^2 p^{\varepsilon\delta} &= 0 \quad \text{in } \Omega_\delta^\varepsilon \,, \\ c^2 \frac{\partial p^{\varepsilon\delta}}{\partial n^\delta} &= -\mathrm{i}\omega g^{\varepsilon\delta\pm} \quad \text{on } \Gamma_\delta^\pm \\ \frac{\partial p^{\varepsilon\delta}}{\partial n^\delta} &= 0 \text{ on } \partial\Omega_\delta^\infty \,, \end{aligned} \tag{3}$$

where $c = \omega/k$ is the speed of sound propagation, $g^{\varepsilon\delta\pm}k^2$ is the interface normal acoustic velocity; by n^δ we denote the normal vector outward to Ω_δ, so that due to the special choice of the coordinate system:

$$\frac{\partial}{\partial n^\delta} = \frac{\partial}{\partial x_3} = \frac{1}{\delta}\frac{\partial}{\partial z} \,.$$

After the thickness dilatation $x_3 = \delta z$, the problem is transformed in domain Ω^ε with the unit (constant) thickness. The weak formulation of (3) then reads as follows: find $p^\varepsilon \in H^1(\Omega^\varepsilon)$ such that

$$\begin{aligned} c^2 \int_{\Omega^\varepsilon} \left(\partial_\alpha p^\varepsilon \partial_\alpha q^* + \frac{1}{\delta^2} \partial_z p^\varepsilon \partial_z q^* \right) - \omega^2 \int_{\Omega^\varepsilon} p^\varepsilon q^* = \\ -\mathrm{i}\omega \frac{1}{\delta} \left(\int_{\Gamma^+} g^{\varepsilon\delta+} q^* \, dS + \int_{\Gamma^-} g^{\varepsilon\delta-} q^* \, dS \right) \end{aligned} \tag{4}$$

for all $q \in H^1(\Omega^\varepsilon)$.

Homogenization

For passing to the limit $\varepsilon \to 0$ we consider a proportional scaling between the period length and the thickness, so that $\delta = \varkappa\varepsilon$, for a fixed $\varkappa > 0$. Further, we need a convenient prepositions on the problem data involved in (3). Note that $g^{\varepsilon\delta\pm}$ is defined on Γ_0, which is equidistant to $\Gamma^\pm$; we assume

$$g^{\varepsilon\delta+} \rightharpoonup g^{0+}, \quad g^{\varepsilon\delta-} \rightharpoonup g^{0-}, \quad \frac{1}{\delta}\left(g^{\varepsilon\delta+} + g^{\varepsilon\delta-} \right) \rightharpoonup 0 \,,$$

weakly in $L^2(\Gamma_0)$, which yields

$$g^{0\pm} \equiv g^{0+} = -g^{0-} \,. \tag{5}$$

The homogenized coefficients are introduced using so called corrector functions computed for the reference periodic cell $Y =]0,1[^2 \times]-1/2,+1/2[\subset \mathbb{R}^3$ which is perforated by the solid (rigid) obstacle T, so that the acoustic medium occupies domain $Y^* = Y \setminus T$. For clarity we use notation $I_y =]0,1[^2$ and $I_z =]-1/2,+1/2[$. Further we refer to the upper and lower boundaries of Y by $I_y^+ = \{y \in \partial Y : \; z = 1/2\}$ and $I_y^- = \{y \in \partial Y : \; z = -1/2\}$.

The limit (homogenized) problem is obtained by the *periodic unfolding* method, see e.g. [3], applied to (4). We employ a specific form of the unfolding operator $\mathcal{T}_\varepsilon(\cdot)$ adapted to the present geometrical situation. Since $|I_z| = 1$, for $\mathcal{T}_\varepsilon(f) = F$ the integration formula reads as

$$\int_\Omega \mathcal{T}_\varepsilon(f^\varepsilon(x_\alpha, z)) dV_x = \frac{1}{|Y|} \int_{\Gamma_0 \times Y} F(x_\alpha, y_\alpha, z) dS_x dS_y dz,$$

where $dV_x = dS_x dz$ and $dS_y dz$ are the volume elements associated with domains Ω and Y, respectively, whereas dS_x and dS_y are the surface elements associated with planes $(x_\alpha, 0)$ and $(y_\alpha, 0)$, respectively. By $H^1_{\#(1,2)}(Y)$ we denote the space of $H^1(Y)$ functions which are "1-periodic" in y_α, $\alpha = 1, 2$. There are the limit fields $p^0 \in H^1(\Gamma_0)$, $p^1 \in L^2(\Gamma_0; H^1_{\#(1,2)}(Y^*))$, such that

$$\begin{aligned} \mathcal{T}_\varepsilon(p^\varepsilon) &\rightharpoonup p^0 \quad \text{weakly in } L^2(\Gamma_0 \times Y) \\ \mathcal{T}_\varepsilon(\partial_\alpha p^\varepsilon) &\rightharpoonup \partial^x_\alpha p^0 + \partial^y_\alpha p^1 \quad \text{weakly in } L^2(\Gamma_0 \times Y) \\ (\varkappa\varepsilon)^{-1} \mathcal{T}_\varepsilon(\partial_z p^\varepsilon) &\rightharpoonup \varkappa^{-1} \partial_z p^1 \quad \text{weakly in } L^2(\Gamma_0 \times Y) \,. \end{aligned}$$

Limit model – Microscopic subproblems

The microscopic and macroscopic problems are introduced by virtue of the following decomposition

$$p^1(x_\alpha, y) = \pi^\beta(y) \partial_\beta p^0(x_\alpha) + \mathrm{i}\omega \xi^\pm(y) g^{0\pm}(x_\alpha), \tag{6}$$

where $\pi^\beta, \xi^\pm \in H^1_{\#(1,2)}(Y)/\mathbb{R}$, $\beta = 1, 2$ are solutions of the local microscopic problems:

$$\begin{aligned} \int_{Y^*} \left[\partial^y_\alpha \xi^\pm \, \partial^y_\alpha q + \frac{1}{\varkappa^2} \partial_z \xi^\pm \partial_z q \right] \\ + \frac{|Y|}{c^2 \varkappa} \left(\int_{I_y^+} q - \int_{I_y^-} q \right) = 0 \end{aligned} \tag{7}$$

for all $q \in H^1_{\#(1,2)}(Y)/\mathbb{R}$, and

$$\int_{Y^*} \partial^y_\alpha (y^\beta + \pi^\beta) \, \partial^y_\alpha q + \frac{1}{\varkappa^2} \int_{Y^*} \partial_z \pi^\beta \partial_z q = 0 \tag{8}$$

for all $q \in H^1_{\#(1,2)}(Y)/\mathbb{R}$, $\beta = 1, 2$.

Limit macroscopic problem in transmission layer

Homogenized transmission behaviour is expressed in terms of *interface mean acoustic pressure* $p^0 \in H^1(\Gamma_0)$, and *fictitious acoustic velocity* $g^{0\pm} L^2(\Gamma_0)$ which satisfy the interface probe (to hold for all $q \in H^1(\Gamma_0)$ and $\psi \in L^2(\Gamma_0)$)

$$\begin{aligned} \int_{\Gamma_0} A_{\alpha\beta} \partial^x_\beta p^0 \partial^x_\alpha q - \frac{|Y^*|}{|Y|} \omega^2 \int_{\Gamma_0} p^0 q = -\mathrm{i}\omega \int_{\Gamma_0} B_\alpha \partial^x_\alpha q \, g^{0\pm} \\ \int_{\Gamma_0} (p^+ - p^-)\psi - \int_{\Gamma_0} D_\beta \partial^x_\beta p^0 \psi = \mathrm{i}\omega \int_{\Gamma_0} F^\pm g^{0\pm} \psi \,, \end{aligned} \tag{9}$$

where the homogenized equations are expressed in terms of the local corrector functions π^β and $\xi^\pm$:

$$A_{\alpha\beta} = \frac{c^2}{|Y|}\int_{Y^*} \partial^y_\gamma(y^\beta+\pi^\beta)\,\partial^y_\gamma(y^\alpha+\pi^\alpha) + \frac{c^2}{|Y|\varkappa^2}\int_{Y^*}\partial_z\pi^\beta\partial_z\pi^\alpha\,, \quad (10)$$

$$B_\alpha = \frac{c^2}{|Y|}\int_{Y^*}\partial^y_\alpha\xi^\pm\,, \quad (11)$$

$$D_\alpha = \frac{1}{|I_y|}\left(\int_{I_y^+}\pi^\alpha - \int_{I_y^-}\pi^\alpha\right)\,, \quad (12)$$

$$F^\pm = \frac{1}{|I_y|}\left(\int_{I_y^+}\xi^\pm - \int_{I_y^-}\xi^\pm\right)\,. \quad (13)$$

We remark that while $(9)_1$ results as the homogenization limit of (4), eq. $(9)_2$ is derived specially as the constraint of the interface discontinuity between p^+ and p^-.

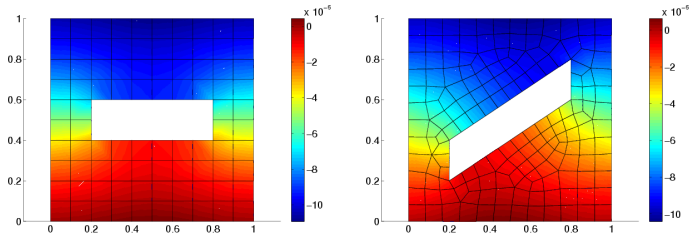

Figure 2: Distribution of $\xi^\pm$ in Y^* for two shapes of perforations.

For illustration, in Fig. 2 the corrector functions are displayed for 2D examples of two different shapes of the perforations.

Interface conditions of acoustic wave transmission

We consider the acoustic waves propagating in $\Omega = \Omega^+ \cup \Omega^- \cup \Gamma_0$, as declared in the introduction. In the differential form the problem for unknown acoustic pressures p^+, p^- reads as follows:

$$\begin{aligned} c^2\nabla^2 p^+ + \omega^2 p^+ = 0 \quad &\text{in } \Omega^+\,,\\ c^2\nabla^2 p^- + \omega^2 p^- = 0 \quad &\text{in } \Omega^-\,,\\ + \text{ boundary conditions} \quad &\text{on } \partial\Omega\,, \end{aligned} \quad (14)$$

supplemented by the transmission conditions on interface Γ_0; these are defined in terms of p^0 and $g^{0\pm}$:

$$\begin{aligned} c^2\frac{\partial p^+}{\partial n^+} &= \mathrm{i}\omega g^{0\pm} \text{ on } \Gamma_0\,,\\ c^2\frac{\partial p^-}{\partial n^-} &= -\mathrm{i}\omega g^{0\pm} \text{ on } \Gamma_0\,, \end{aligned} \quad (15)$$

Interface problem (9) for p^0 and $g^{0\pm}$ is satisfied ,

where n^+ and n^- are defined as in (1).

Conclusion

We derived the transmission conditions involving homogenized parameters (10)-(13) which reflect specific features of the periodic perforation. The separating structures can be quite general, thus not only flat plates with holes may be considered. Moreover, even the "no-obstacle" situation is treated by the present model, when $Y = Y^*$ and $\varkappa \to +\infty$. Then $\pi^\beta = \xi^\pm \equiv 0$, therefore both $F^\pm$ and D_β vanish, so that $(9)_2$ yields continuity $p^+ = p^-$ on Γ_0.

We emphasize that this modelling tool allows for formulation and treatment of the "optimal perforation design", which can be an extension of structural optimization in acoustics, see e.g. [4], [5]. In numerical studies (not included here, presented at the conference) we shall demonstrate the sensitivity of the acoustic transmission coefficients on the shape of perforations.

Acknowledgment

The research and publication was supported by projects GAČR 101/07/1471 and MŠMT 1M06031 of the Czech Republic.

References

[1] R. Kirby, A. Cummings, "The impedance of perforated plates subjected to grazing gas flow and backed by porous media", J. Sound and Vibration, vol 217(4), pp. 619-636, 1998.

[2] D. Cioranescu, J. Saint Jean Paulin, Homogenization of Reticulated Structures, Springer, Appl. Math. Ser. 136, New York, 1999.

[3] D. Cioranescu, A. Damlamian, G. Griso, "Periodic unfolding and homogenization", C. R. Acad. Sci. Paris, Ser. I 335 pp. 99-104, 2002.

[4] E. Bangtsson, D. Noreland, M. Berggren, "Shape optimization of an acoustic horn", Comput. Methods Appl. Mech. Engrg. vol. 192 pp. 1533-1571, 2003.

[5] E. Wadbro, M. Berggren, "Topology optimization of an acoustic horn", Comput. Methods Appl. Mech. Engrg. vol. 196, pp. 420-436, 2006.

[6] E. Rohan, B. Miara, "Sensitivity analysis of acoustic wave propagation in strongly heterogeneous piezoelectric composite", in: Topics on Mathematics for Smart Systems, World Sci. Publ., pp. 139-207, 2006.

Time-Domain Numerical Modelling

ACOUSTIC SCATTERING APPROXIMATIONS ON ELLIPTIC GRIDS WITH ADAPTIVE CONTROL FUNCTIONS

Sebastian Acosta[†,*], **Vianey Villamizar**[‡,**]

[†]Department of Mechanical Engineering, Brigham Young University, Provo, UT 84602, USA
[‡]Department of Mathematics, Brigham Young University, Provo, UT 84602, USA
[*]Email: sebastian@byu.net [**]Email: vianey@math.byu.edu

Abstract

An explicit two-dimensional finite difference method to obtain numerical approximations of acoustic scattering problems is developed. The method employs novel elliptic grids with adaptive control functions. In contrast with other elliptic grid generators, the control functions are held as dependent variables. They obey Poisson's type equations forced by the rate of changes of the jacobian in the curvilinear coordinate directions. As a consequence, the cell areas of the resulting grids converge to an average cell area over the entire domain. Numerical experiments show that the smoothness and the cell area uniformity of the new grids enhance the stability condition and the convergence rate of the acoustic scattering numerical method.

Grid Generator with Adaptive Control Functions

The governing equations for the novel grid generation method are an extension of the familiar quasilinear elliptic system of partial differential equations [5], [3] for the generalized curvilinear coordinates $(x(\xi,\eta), y(\xi,\eta))$ given by

$$\alpha x_{\xi\xi} - 2\beta x_{\xi\eta} + \gamma x_{\eta\eta} = -\alpha\psi\, x_\xi - \gamma\phi\, x_\eta, \quad (1)$$
$$\alpha y_{\xi\xi} - 2\beta y_{\xi\eta} + \gamma y_{\eta\eta} = -\alpha\psi\, y_\xi - \gamma\phi\, y_\eta, \quad (2)$$

The independent variables ξ and η vary in a rectangular domain $\mathcal{D}'$ called the computational domain. The grid generation method can be thought as a transformation T from the computational domain $\mathcal{D}'$ with coordinates (ξ,η) to the physical domain $\mathcal{D}$ with coordinates$(x(\xi,\eta), y(\xi,\eta))$. The symbols α, β and γ represent the scale metric factors of the transformation T. They are defined as $\alpha = x_\eta^2 + y_\eta^2$, $\beta = x_\xi x_\eta + y_\xi y_\eta$, $\gamma = x_\xi^2 + y_\xi^2$.

The functions ψ and ϕ are known as control functions of the grid generation method. Their appropriate definition has been a subject of intensive research [2], [5]. In reference [5], [6], their definitions is based solely on the initial distribution of nodes along the boundaries of the physical domain and a branch cut of the transformation T. Once they are defined their values are maintained through all the grid generation process. These functions ϕ and ψ allow to have some control on the spacing between grid lines and produce stretching or clustering of grid points at specific regions of the physical domain.

The focus of this work is to create smooth grids with almost uniform cell areas and use them to improve acoustic scattering numerical simulations. To begin, a uniformly spaced rectangular grid with step sizes $\Delta\xi = 1$ and $\Delta\eta = 1$ is defined on the computational domain $\mathcal{D}'$. The discrete values for ξ and η are represented by $\xi_i = (i-1)\Delta\xi$ and $\eta_j = (j-1)\Delta\eta$, for $i = 1,\dots N_2$ and $j = 1,\dots N_1$, respectively. Also, $x_{i,j}$ and $y_{i,j}$ correspond to the discrete values of $x(\xi_i,\eta_j) = x(i,j)$ and $y(\xi_i,\eta_j) = y(i,j)$, respectively. Discrete approximations for the other dependent variables are denoted accordingly. Regarding the cell areas, they can be approximated, at each grid point, by $|x_\xi y_\eta - x_\eta y_\xi|\Delta\xi\Delta\eta = |J|$ where J is the jacobian of the jacobian matrix, $\mathcal{J}$, of T [1].

Formulation of the Grid Generation Model with Adaptive Control Functions

In [4], a study of the effects that changes of the control function values have over the distribution of the grid lines was conducted. It was found that an increment of the ϕ value at a given grid point produces a local displacement of the corresponding η-curves (η = constant) in the positive direction (outward). Similarly, a decrement of ϕ values brings the grid lines inwards (negative direction). Moreover, the displacement of the η-curves is proportional to the magnitude of the change experienced by ϕ. The relationship between changes of ψ values and displacement of ξ-curves (ξ = constant) is analogous. This relationship between grid line displacements and the values of the control functions is illustrated in Fig. 1. The left grid cells correspond to a set of control functions ϕ_{old} and ψ_{old}. The intermediate cells are obtained by increasing the value of ϕ at the point (ξ_i,η_j) ($\phi_{new}(\xi_i,\eta_j) > \phi_{old}(\xi_i,\eta_j)$). The final grid cells are obtained from the intermediate one after increasing the control function ψ, *i.e*, $\psi_{new}(\xi_i,\eta_j) > \psi_{old}(\xi_i,\eta_j)$. The above observations motivated us to formulate a new ellip-

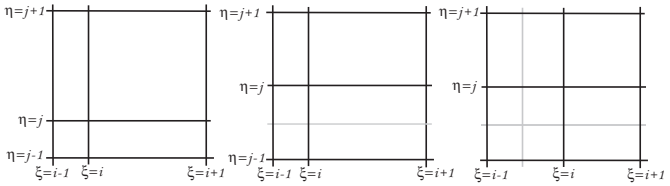

Figure 1: (a) ϕ_{old}, ψ_{old} (b) $\phi_{new} > \phi_{old}$ (c) $\psi_{new} > \psi_{old}$.

tic grid generation mathematical model that includes the control functions as unknown functions. The new model seeks to create grids with rather uniform cell areas. Since the jacobian's value is an approximation of the cell area at each grid point, uniform cell area meshes can be obtained by equalizing the jacobian's values at all nodes. We achieve this goal by adding two new Poisson's type equations to the original quasilinear elliptic system (1)-(2).

As a starting point in the derivation of the new equations, we consider the following discrete equations,

$$\phi_{new}(i,j) = \phi_{old}(i,j) + k_1 J_\eta(i,j), \quad (3)$$
$$\psi_{new}(i,j) = \psi_{old}(i,j) + k_2 J_\xi(i,j), \quad (4)$$

where $k_1 > 0$ and $k_2 > 0$ are real constants. If equations (3)-(4) were added to the grid generation model governed by (1)-(2), then the area of all the cells would gradually tend to a constant value. This is because J_η and J_ξ act as regulatory terms of the grid line displacements. In fact, the direction of the grid line displacements depends on the signs of J_η and J_ξ. Eventually, all the grid cell areas will approximate a constant value as the gradient of the jacobian J converges to zero everywhere.

A key idea in the derivation is to notice that the equations (3)-(4) lead to continuous differential equations if the terms $\phi_{old}(i,j)$ and $\psi_{old}(i,j)$ are replaced by the average values of ϕ and ψ about the four neighboring points of (ξ_i, η_j), respectively. More precisely, the equation (3) is replaced by

$$\phi^k_{i,j} = \frac{\phi^{k-1}_{i+1,j} + \phi^{k-1}_{i-1,j} + \phi^{k-1}_{i,j+1} + \phi^{k-1}_{i,j-1}}{4} + k_1 J_{\eta i,j}, \quad (5)$$

where $\phi^k_{i,j}$ corresponds to $\phi_{new}(i,j)$ and $\phi^{k-1}_{i,j}$ corresponds to $\phi_{old}(i,j)$. Now, by noticing that the term at the left and the first term at the right of (5) correspond to a central difference approximation of $\nabla^2_{\xi,\eta}\phi = 0$ written in iterative form, equation (5) can be written in continuous form as $\nabla^2_{\xi,\eta}\phi = -k_1 J_\eta$. A continuous version of (4) can be analogously obtained . By adding these two equations to the original quasilinear system, we obtain our new set of equations modelling the grid generation method,

$$\alpha x_{\xi\xi} - 2\beta x_{\xi\eta} + \gamma x_{\eta\eta} = -\alpha\psi\, x_\xi - \gamma\phi\, x_\eta, \quad (6)$$
$$\alpha y_{\xi\xi} - 2\beta y_{\xi\eta} + \gamma y_{\eta\eta} = -\alpha\psi\, y_\xi - \gamma\phi\, y_\eta, \quad (7)$$
$$\phi_{\xi\xi} + \phi_{\eta\eta} = -k_1 J_\eta, \quad (8)$$
$$\psi_{\xi\xi} + \psi_{\eta\eta} = -k_2 J_\xi, \quad (9)$$

For multiply connected domains such as the one in Fig. 2, a boundary value problem (BVP), including the four equations above, is obtained by defining Dirichlet boundary conditions on the physical boundaries and a conveniently chosen branch cut in the interior. This BVP is numerically solved by approximating the partial derivative terms present in the equations using centered differences. This is followed by an application of point SOR iteration to the discrete system of equations that results. The grid generation process requires the definition of an initial grid and the implementation of a smoothing technique such as the one introduced in [5]. The constants k_1 and k_2 should be conveniently chosen to ensure convergence of the method.

Comparison Against Other Structured Grids

The advantages of the new grids, obtained with adaptive control functions, can be observed by comparing them against grids obtained from the standard Winslow elliptic grid generation approach without control functions [1]. Table 1 contains a comparison of the minimum, maximum, and average jacobian between both grids. The domain chosen has a central hole bounded by an astroid curve which presents severe singularities on the four cusps. The Winslow grid has the tendency to cluster its nodes inward. It results in very small cells in the vicinity of the astroid's cusps. Moreover, the cells close to the outer boundary are relatively large. This anomalous behavior can be fixed by the application of our method with adaptive control functions. As shown in Fig. 2 (right), the η-curves of the new grid conform to the astroid's boundary with relatively large cells around it. The numerical experiments reported in Table 1 show that, in the case of

Table 1: Grid quality comparison

Size	121×121		241×241	
	Winslow	Adaptive	Winslow	Adaptive
J_{min}	8.02e-6	3.50e-3	5.03e-7	3.22e-4
J_{max}	8.01e-2	2.57e-2	2.07e-2	6.43e-3
J_{ave}	2.21e-2	2.21e-2	5.41e-3	5.41e-3

a Winslow grid, J_{max} is over 10^{-4} times larger than J_{min}. Instead, with the adaptive control function grid, J_{max} and J_{min} differ by only one order of magnitude.

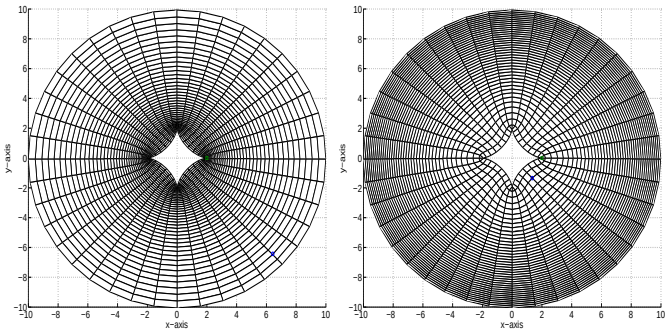

Figure 2: 41×41 Winslow Grid (left), Adaptive Grid (right)

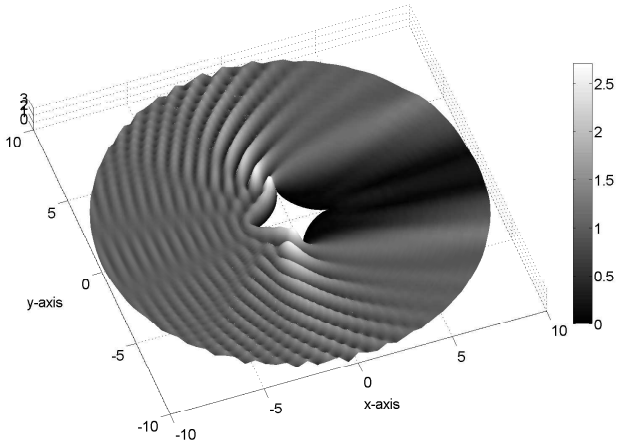

Figure 3: Amplitude of total pressure field

Table 2: Simulation for 20,000 time steps with $\Delta t = 10^{-3}$.

Grid size	121×121		241×241	
	Winslow	Adaptive	Winslow	Adaptive
Max Avg. Error	9.93e-4	2.03e-4	div	2.98e-4
Min Avg. Error	5.77e-4	4.26e-5	div	1.08e-4
Final Avg. Error	6.87e-4	4.26e-5	div	1.09e-4

Acoustic Scattering from Complexly Shaped Obstacles

Both of the previous grids were employed to obtain numerical solutions for an acoustic scattering problem over the complex domain illustrated in Fig. 2. The initial boundary value problem in the new curvilinear coordinates is given by

$$(p_{sc})_{tt} = \frac{c^2}{J^2}\Big(\alpha(p_{sc})_{\xi\xi} - 2\beta(p_{sc})_{\xi\eta} + \gamma(p_{sc})_{\eta\eta} + \alpha\psi\,(p_{sc})_{\xi} + \gamma\phi\,(p_{sc})_{\eta}\Big), \quad (\xi,\eta) \in \mathcal{D}', \quad t > 0, \tag{10}$$

$$p_{sc}(\xi, 1, t) = -e^{ik\left(x(\xi,1)\cos\delta + y(\xi,1)\sin\delta\right)} e^{-iwt}, \tag{11}$$

$$p_{sc}(\xi,\eta,0) = 0,\ (p_{sc})_t(\xi,\eta,0) = 0,\ (\xi,\eta) \in \mathcal{D}' \tag{12}$$

$$(p_{sc})_t + \frac{c}{rJ}\Big((xy_\eta - yx_\eta)(p_{sc})_\xi + (yx_\xi - xy_\xi)(p_{sc})_\eta\Big) + \frac{c\,p_{sc}}{2r} \to 0, \qquad \text{when } r \to r_\infty. \tag{13}$$

An explicit leap-frog finite difference method, based on Winslow and adaptive control function grids, was employed until a harmonic steady state was reached. For a time step $\Delta t = 10^{-3}$ and a 121×121 grid size the results for both grids are similar with a better rate of convergence for the adaptive control functions method. In contrast for a 241×241 grid size the simulation based on a Winslow grid is divergent because the stability condition of the leap-frog method is violated by the cells close to the obstacle. Instead, the simulation based on the novel grids, introduced in this work, is stable and converges (see Table 2). In Fig. 3, a numerical approximation for the amplitude of the pressure field computed over a adaptive control function grid 241×241 is shown. A more complete analysis and study will be presented in a forthcoming extended paper.

References

[1] P. Knupp and S. Steinberg. *Fundamentals of Grid Generation*. CRC Press, 1993.

[2] S. P. Spekreijse. Elliptic grid generation based on laplace equations and algebraic transformations. *J. Comput Phys.*, 118:38–61, 1995.

[3] J. F. Thompson, B. K. Soni, and N. G. Weatherill. *Handbook of Grid Generation*. CRC Press, 1999.

[4] V. Villamizar and S. Acosta. Generation of smooth grids with line control for scattering from multiple obstacles. *Math. Comput. Simul.*, submitted.

[5] V. Villamizar, O. Rojas, and J. Mabey. Generation of curvilinear coordinates on multiply connected regions with boundary singularities. *J. Comput. Phys.*, 223:571–588, 2007.

[6] V. Villamizar and M. Weber. Boundary-conforming coordinates with grid line control for acoustic scattering from complexly shaped obstacles. *Numer. Meth. Part. Differ. Equ.*, (2007), DOI:10.1002/num.20235. Available online on March 2007.

2D HIGH-RESOLUTION SIMULATION OF SHOCK STRUCTURES IN CHARGED-PARTICLE FLUIDS UNDER ELECTROMAGNETIC FIELDS

S. Baboolal[†,*], **D. Naidoo**[†,*]
[†]School of Computer Science, University of KwaZulu-Natal, Westville Campus, Private Bag X54001, Durban 4000, South Africa
[*]Email: baboolals@ukzn.ac.za

Abstract

In this work we show how the full set of governing equations for the dynamics of charged-particle fluids in an electromagnetic field may be solved numerically for nonlinear wave structures propagating in two dimensions. The algorithm employed is a source-term adaptation and two-fluid extension of a recent second-order high-resolution central scheme developed by Balbas *et al.* ["Non-Oscillatory Central Schemes for One- and Two-Dimensional Equations I.", J. Comput. Phys. vol. 201, pp. 261-285, 2004]. In addition, in order to obtain stable wave structures over prolonged modelling times, we show how suitable boundary conditions may be chosen. Illustrative results are presented depicting the evolution of shock-like structures related to the magnetosonic mode.

Introduction

Recently, Balbas *et al.*[1] presented a two-dimensional high-resolution Riemann-solver-free central-difference scheme for staggered grids which they employed in the simulation of magnetosonic shock-like structures. In their model, they considered an ideal single-fluid plasma interacting with a magnetic field B, say. Following this and Shumlak and Loverich [2], a two-fluid plasma model allowing for three dimensional variation in the fluid dynamical and electric (E) and magnetic (B) field variables but allowing for wave variations in one space direction (x) only was employed to simulate magnetosonic shock and soliton structures [3].

In this work we generalize these approaches to the extent that we employ an ideal-gas two-fluid plasma, allow for source terms in the governing equations, and admit three-dimensional variation in the dynamical and field variables but consider two-dimensional variation in the wave structures. Results depicting a two-dimensional magnetosonic shock wave propagating in a two-fluid three-dimensional-field plasma are given.

Numerical method

In order to make a numerical study of such phenomena, we first write the system of equations in the conservative form,

$$\frac{\partial U}{\partial t}+\frac{\partial F(U)}{\partial x}+\frac{\partial G(U)}{\partial y}=S(U). \tag{1}$$

Here $U(x,y,z,t)$ is the unknown (m-dimensional) vector, $F(U)$ is the x-flux vector, $G(U)$ is the y-flux vector and $S(U)$ is a source vector function, with x and y the only two spatial coordinates considered (for no variation in the z direction) and t is the time coordinate.

For this system, we follow through the derivation given in [1] but now include a source term. Then the following modified scheme in terms of *cell averages* is obtained:

$$\begin{aligned}\bar{U}^{n+1}_{j+\frac{1}{2},k+\frac{1}{2}} &= \frac{1}{4}\left[\bar{U}^{n}_{jk}+\bar{U}^{n}_{j+1,k}+\bar{U}^{n}_{j,k+1}+\bar{U}^{n}_{j+1,k+1}\right]\\ &+\frac{1}{16}\left[U^{n}_{x,j,k}-U^{n}_{x,j+1,k}+U^{n}_{x,j,k+1}-U^{n}_{x,j+1,k+1}\right]\\ &+\frac{1}{16}\left[U^{n}_{y,j,k}-U^{n}_{y,j,k+1}+U^{n}_{y,j+1,k}-U^{n}_{y,j+1,k+1}\right]\\ &-\frac{\Delta t}{2\Delta x}\left[F^{n+\frac{1}{2}}_{j+1,k}-F^{n+\frac{1}{2}}_{j,k}+F^{n+\frac{1}{2}}_{j+1,k+1}-F^{n+\frac{1}{2}}_{j,k+1}\right]\\ &-\frac{\Delta t}{2\Delta y}\left[G^{n+\frac{1}{2}}_{j,k+1}-G^{n+\frac{1}{2}}_{j,k}+G^{n+\frac{1}{2}}_{j+1,k+1}-G^{n+\frac{1}{2}}_{j+1,k}\right]\\ &+\frac{\Delta t}{4}\left[S^{n+\frac{1}{2}}_{j+1,k+1}+S^{n+\frac{1}{2}}_{j+1,k}+S^{n+\frac{1}{2}}_{j,k+1}+S^{n+\frac{1}{2}}_{j,k}\right].\end{aligned} \tag{2}$$

This scheme advances the cell average vectors $\bar{U}^{n}_{j,k}$ (see [1]) where j,k are the spatial discretization indices with grid spacings Δx and Δy in the respective directions and n is the time level index, with time spacing Δt, and it is used in conjunction with non-oscillatory approximations ([1],[4]) for the derivative arrays (U_x and U_y) .

The boundary conditions employed in all variables were outflow conditions: we simply use quadratic extrapolations of the nearest inner point-values to compute the value at a boundary point.

Charged particle fluids in an electromagnetic field

The model equations employed are those for the electromagnetic fields (E,B), the current density (J), and the ideal-gas collisionless-plasma equations for the electrons

(e) and ions (i). In the latter (with species $s = e, i$) the $n_s, V_s, p_s, \gamma_s, m_s$ are the respective component number densities, flow velocities, partial pressures, adiabatic indices and particle masses with particle charges taken as $-e$ (electrons) and $+e$ (ions). The complete governing equations then are ([2],[3],[5]):-

Maxwell's equations in *vacuo*:

$$\frac{\partial B}{\partial t} = -\nabla \times E \tag{3}$$

$$\frac{\partial E}{\partial t} = \frac{1}{\epsilon_0 \mu_0} \nabla \times B - \frac{1}{\epsilon_0} J \tag{4}$$

$$\nabla \cdot E = \frac{1}{\epsilon_0} e(n_i - n_e) \tag{5}$$

$$\nabla \cdot B = 0 \tag{6}$$

The plasma fluid equations:

$$\frac{\partial n_e}{\partial t} + \nabla \cdot [n_e V_e] = 0 \tag{7}$$

$$\frac{\partial n_i}{\partial t} + \nabla \cdot [n_i V_i] = 0 \tag{8}$$

$$m_e n_e \left[\frac{\partial V_e}{\partial t} + (V_e \cdot \nabla) V_e \right] = -\nabla p_e - n_e e \left[E + V_e \times B \right] \tag{9}$$

$$m_i n_i \left[\frac{\partial V_i}{\partial t} + (V_i \cdot \nabla) V_i \right] = -\nabla p_i + n_i e \left[E + V_i \times B \right] \tag{10}$$

The energy equations:

$$\frac{\partial \varepsilon_e}{\partial t} + \nabla \cdot [(\varepsilon_e + p_e) V_e] = -e n_e V_e \cdot E \tag{11}$$

$$\frac{\partial \varepsilon_i}{\partial t} + \nabla \cdot [(\varepsilon_i + p_i) V_i] = e n_i V_i \cdot E \tag{12}$$

where,

$$\varepsilon_e \equiv \frac{n_e k_B T_e}{\gamma - 1} + \frac{1}{2} m_e n_e |V_e|^2 = \frac{p_e}{\gamma - 1} + \frac{1}{2} m_e n_e |V_e|^2 \tag{13}$$

$$\varepsilon_i \equiv \frac{n_i k_B T_i}{\gamma - 1} + \frac{1}{2} m_i n_i |V_i|^2 = \frac{p_i}{\gamma - 1} + \frac{1}{2} m_i n_i |V_i|^2 \tag{14}$$

Here, we take $\gamma_e = \gamma_i = \gamma = C_p/C_v$ as the common ratio of specific heat capacities, $p_e = n_e k_B T_e$ and $p_i = n_i k_B T_i$ are the respective electron and ion partial pressures for ideal gases, with their temperatures given as $T_e = m_e V_{Te}^2 / k_B$ and $T_i = m_i V_{Ti}^2 / k_B$ where V_{Te} and V_{Ti} denote the root-mean-square thermal speeds for each species.

For wave structures varying in two dimensions we employ the operation $\partial/\partial z \equiv 0$ and then normalize (see the Appendix) the set of equations to time and spatial scales appropriate for the study of magnetosonic waves as before [3] and finally render them into component forms. Now with,

$$w_e = n_e |V_e|^2 + 3 n_e V_{Te}^2, w_i = n_i |V_i|^2 + 3 n_i V_{Ti}^2 \tag{15}$$

and the notation

$$\begin{aligned} U = [&u_1, u_2, u_3, u_4, u_5, u_6, u_7, u_8, u_9, \\ &u_{10}, u_{11}, u_{12}, u_{13}, u_{14}, u_{15}, u_{16}]^T \\ \equiv [&n_e, n_i, n_e v_{ex}, n_e v_{ey}, n_e v_{ez}, n_i v_{ix}, n_i v_{iy}, n_i v_{iz}, \\ &w_e, w_i, E_x, E_y, E_z, B_x, B_y, B_z]^T, \end{aligned} \tag{16}$$

in normalized variables and with consequential forms for $F(U)$, $G(U)$ and $S(U)$ the equations above reduce to the form (1). For the numerical integration we employ a system of size 10×10 in Debye lengths (see the Appendix) with correspondingly 201×201 grid points giving giving $\Delta x = 0.05$ and $\Delta y = 0.05$, and we take $\Delta t = 0.0025$, an artificial ion-to-electron mass ratio of 10:1, and an ion-to-electron temperature ratio of 1:10.

Application

Magnetosonic shocks

The magnetosonic mode arises when wave propagation observed in a direction, say x, is driven by a transverse magnetic field in a direction, say, y coupled with a transverse electric field component in the other direction, z. This causes the plasma to undergo rarefactions and compressions in the x direction owing to the "$E \times B$ drift" [5].

Here we employ the initial conditions

$$\begin{cases} n_e = 4, n_i = 4, V_e = 0, V_i = 0, w_e = 3 n_e V_{Te0}^2, \\ w_i = 3 n_i V_{Ti0}^2, E_x = 0, E_y = 0, E_z = 0, \\ B_x = 0, B_y = 1, B_z = 0; \quad x \le x_c. \\ n_e = 1, n_i = 1, V_e = 0, V_i = 0, w_e = 3 n_e V_{Te0}^2, \\ w_i = 3 n_i V_{Ti0}^2, E_x = 0, E_y = 0, E_z = 0, \\ B_x = 0, B_y = 1, B_z = 0; \quad x > x_c. \end{cases}$$

corresponding to a Riemann (shock-tube or two-state plasma) problem with a discontinuity at the system centre x_c in the x direction, with no variation in the y direction. Also we use the normalized value $c = 10$, corresponding to a 'hot' -to-'very-hot' plasma (see [3]).

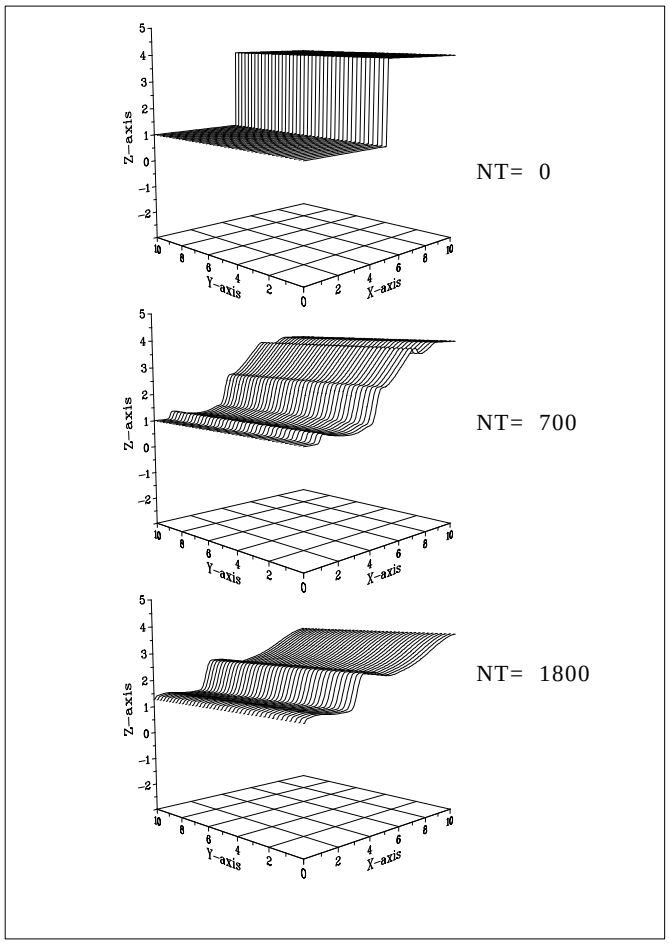

Figure 1: Computed magnetosonic shock structure in the electron density at time steps NT = 0, 700 and 1800.

A typical computed result is shown in the figure. Such results extend the previous two-fluid one-dimensional treatments of [2] and [3] and of the source-free one-fluid two-dimensional treatment of [1].

Conclusion

We have shown how the high-resolution staggered difference scheme of Balbas, Tadmor and Wu [1] may be adapted to handle a two-fluid plasma with source terms modelled by the ideal-gas fluid-dynamical equations and Maxwell equations for the electromagnetic field. The model is fully three-dimensional except that wave variation is restricted to two-dimensions. As an illustration we have shown how a magnetosonic shock wave may subsequently evolve through the system. The numerical procedure employed should be useful for studying nonlinear wave propagation of varying types in different charged particle fluid systems and may be extended to fully three-dimensional situations.

Appendix: Normalizations

Here, the electron and ion densities are given in terms of n_0 their common equilibrium density, lengths (x) are in units of the electron Debye length $\lambda_{de} = \sqrt{\epsilon_0 k_B T_{e0}/n_0 e^2} = \sqrt{\epsilon_0 m_e V_{Te0}^2/n_0 e^2}$ where ϵ_0 is the electric permittivity in free space and T_{e0} is the equilibrium electron temperature, temperatures are given in terms of T_{e0}, particle charges in terms of $e > 0$ the electronic charge, time (t) is in units of the inverse of the inverse of the ion plasma frequency $\omega_{pi} = \sqrt{n_0 e^2/\epsilon_0 m_i}$, velocities are in terms of the ion sound speed at equilibrium, $\sqrt{m_e V_{Te0}^2/m_i}$, and we take $\gamma = 5/3$ for adiabatic fluids. Components of the electric field are in units of $E_0 = \sqrt{m_e n_0 V_{Te0}^2/\epsilon_0}$, those of the magnetic field are in units of $B_0 = E_0/c$ where c is the unnormalized speed of light, and we take m_e/m_s as the mass electron/ion mass ratio and σ_s as the normalized charge (= -1 for electrons, +1 for ions). The normalized energy-per-mass terms then are $w_s = n_s|V_s|^2 + 3n_s V_{Ts}^2$.

Acknowledgments

The authors are grateful to Jorge Balbas for guidance in the development of their computer code as an extension of that given in [1]. They also thank Helmut Michels (Max Planck Institute for Solar System Research) for free use of his DISLIN 3D graphics package.

References

[1] J. Balbas, E. Tadmor, C.C. Wu, "Non-Oscillatory Central Schemes for One- and Two-Dimensional Equations I.", J. Comput. Phys. vol. 201, pp. 261-285, 2004.

[2] U. Shumlak, J. Loverich, "Approximate Riemann solver for the two-fluid plasma model", J. Comput. Phys., vol. 187, pp. 620-638, 2003.

[3] S. Baboolal, R. Bharuthram, "Two-scale numerical solution of the electromagnetic two-fluid plasma-Maxwell equations: Shock and soliton simulation", Math. Comput. Simul., doi:10.1016/j.matcom.2007.01.004, 2007.

[4] H. Nessyahu, E. Tadmor, "Non-oscillatory central differencing for hyperbolic conservation laws", J. Comput. Phys. vol. 87, pp. 408-463, 1990.

[5] F. Chen, Introduction to Plasma Physics, Plenum Press, New York, London, 1974.

A NUMERICAL SCHEME FOR AN IMPROVED MODEL OF BOUSSINESQ TYPE EQUATIONS

A. G. Bratsos* **and I. Th. Famelis***
Department of Mathematics,
Technological Educational Institution (T.E.I.) of Athens,
122 10 Egaleo, Athens, Greece
*E-mail: bratsos@teiath.gr and ifamelis@teiath.gr

Abstract

This paper presents a parametric finite-difference scheme concerning the numerical solution of the one-dimensional Boussinesq-type set of equations, as they were introduced by Beji and Nadaoka [2] in the case of waves relatively long with small amplitudes in water of varying depth. The proposed method, which can be considered as a generalization of the Crank-Nickolson method, aims to investigate alternative approaches in order to improve the accuracy of analogous methods known from the bibliography. The resulting linear finite-difference scheme has been applied successfully to the bathymetry used by Beji and Battjes [1] as well as in an analogous one known in the bibliography as the Ohyama's experiment [5] giving numerical results which are in agreement with the corresponding results given by MIKE 21 BW [4] developed by DHI Software.

Introduction

Beji and Nadaoka [2] following Peregrine's [6] assumption have proposed the following set of *improved* Boussinesq-type equations to describe the relatively long, small amplitude waves propagating in water of varying depth in $2+1$ dimensions

$$\frac{\partial \eta}{\partial t} + \boldsymbol{\nabla} \cdot [(h+\eta)\,\mathbf{u}] = 0, \tag{1}$$

$$\mathbf{u}_t + (\mathbf{u}\cdot\boldsymbol{\nabla})\,\mathbf{u} + g\boldsymbol{\nabla}\eta = (1+\beta)\,\frac{h}{2}\,\boldsymbol{\nabla}\left[\boldsymbol{\nabla}\cdot(h\mathbf{u}_t)\right] - \beta\,\frac{g\,h}{2}\,\boldsymbol{\nabla}\left[\boldsymbol{\nabla}\cdot(h\,\boldsymbol{\nabla}\eta)\right] - (1+\beta)\,\frac{h^2}{6}\,\boldsymbol{\nabla}\left(\boldsymbol{\nabla}\cdot\mathbf{u}_t\right) + \frac{g\,h^2}{6}\,\boldsymbol{\nabla}\left(\nabla^2\eta\right);\ t>0, \tag{2}$$

where $\eta = \eta(x,y,t)$ is the free surface displacement as it is measured from still water level and $\mathbf{u} = \mathbf{u}(x,y,t) = [u_1,u_2]^T$ is the depth-averaged horizontal velocity vector, $\boldsymbol{\nabla} = [\partial/\partial x, \partial/\partial y]^T$ the two-dimensional gradient operator, $h = h(x,y)$ is the still water depth, g the gravitational acceleration, β an appropriate constant and ∇^2 is the two-dimensional Laplace's operator.

For the one-dimensional propagation when $h_{xx} = 0$, $h = h(x)$, $u_1 \equiv u$ and $\tilde{\beta} = 1+\beta$ the system (1)-(2) gives

$$\eta_t + [(h+\eta)u]_x = 0, \tag{3}$$

$$u_t + uu_x + g\eta_x = \tilde{\beta}\,h\,h_x\,u_{xt} + \tilde{\beta}\,\frac{h^2}{3}u_{xxt} + \beta g\,h\,h_x\eta_{xx} + \beta\frac{gh^2}{3}\eta_{xxx};\ x\in\Omega,\ t>0. \tag{4}$$

The initial conditions are assumed to be of the form $u(x,0) = \eta(x,0) = 0$.

The numerical scheme

To obtain a numerical solution the region $R = \Omega\times[t>0]$ with its boundary ∂R is covered with a rectangular mesh, G, of points with coordinates $(x,t) = (x_m,t_n) = (L_0 + m\Delta x, n\Delta t)$ with $m = 0,1,...,N+1$ and $n = 0,1,...,$ in which Δx represents the space step, while Δt the time one.

Let the solution vectors be

$$\boldsymbol{\eta}^n = \boldsymbol{\eta}(t_n) = \left[\eta_1^n, \eta_2^n, ..., \eta_N^n, \eta_{N+1}^n\right]^T, \tag{5}$$

$$\mathbf{u}^n = \mathbf{u}(t_n) = \left[u_1^n, u_2^n, ..., u_N^n, u_{N+1}^n\right]^T. \tag{6}$$

The proposed method arises by considering that in Eq. (4) only the space partial derivatives are satisfied at the point $(m\Delta x,\ (n+\vartheta)\,\Delta t\,);\ \vartheta\in[0,1]$ of the grid G (see Bratsos et *al* [3]). This assumption for u_x gives

$$(\eta_x)_m^{n+\vartheta} = \vartheta\ (\eta_x)_m^{n+1} + (1-\vartheta)\ (\eta_x)_m^n \tag{7}$$

and analogous approximations for η_{xx} and η_{xxx}.

At the left-boundary point $x = L_0$ (*input*) the surface elevation is evaluated as $\eta(L_0,t) = f(t)$; $t>0$, where $f(t)$ is an appropriate function producing harmonic waves of period T and height H, while at the same point the depth-averaged velocity using the continuity equation for a progressive wave as $u(L_0,t) = \frac{\tilde{c}_0\,\eta(L_0,t)}{h_0+\eta(L_0,t)};\ t>0$, where $\tilde{c}_0$ and h_0 are the

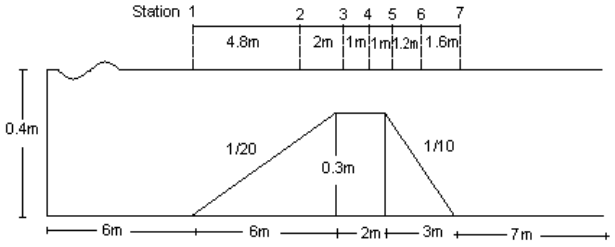

Figure 1: Bathymetry I

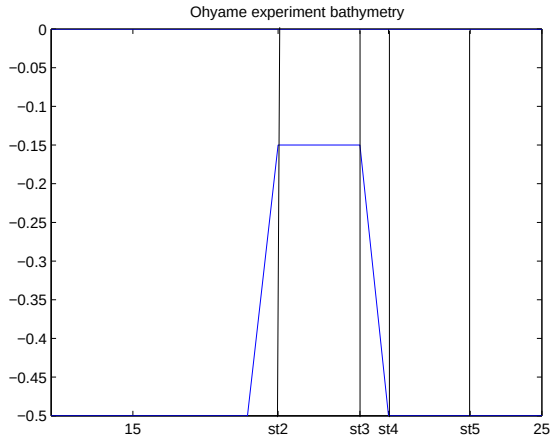

Figure 2: Bathymetry II

phase celerity and the water depth at $x = L_0$ respectively. At the outgoing boundary (*output*) $x = L_1$ the values $\eta(L_1, t)$ and $u(L_1, t)$ are evaluated from the radiation condition for both the surface displacement using the continuity equation and for the velocity from the momentum one.

Eq. (3) leads to a two-time level explicit finite-difference scheme for the unknown vector $\boldsymbol{\eta}^{n+1}$, while Eq. (4) to a linear system of the form $A\mathbf{u}^{n+1} = \mathbf{F}\left(\mathbf{u}^n, \boldsymbol{\eta}^{n+1}, \boldsymbol{\eta}^n\right)$ in which A is a tridiagonal matrix of order $N+1$ with appropriate entries. Then using a predictor-corrector scheme the values $\boldsymbol{\eta}^{n+1}$ are corrected using the values of $\mathbf{u}^{n+1}$ (see [3]).

Numerical experiments

The method developed in the previous Section was tested on the bathymetry I [1] (Fig. 1) and bathymetry II [5] (Fig. 2) using $\Delta x = 1/20\,\mathrm{m}$, $\Delta t = 1/150\,\mathrm{sec}$, while at each time step one prediction-correction was performed.

To investigate the effect of the parameter ϑ at the numerical solution of the system (3)-(4) the interval $[0, 1]$ was discretized into 20 subintervals each of width $\tilde{\vartheta} = 0.05$ and the method was applied for $t \in [0, 30]$ for each value $\tilde{\vartheta}$ using both the bathymetries [1], [5]. In order to evaluate the results, the solution for various values of ϑ was compared to the solution obtained by MIKE 21 BW [4]. Let ϑ^* to denote the value of ϑ which gives the solution, which fits best to [4]. From the experiments the following were deduced

A. Bathymetry I Data: $L_0 = 0\,\mathrm{m}$, $L_1 = 24\,\mathrm{m}$, $T = 2\,\mathrm{sec}$, $h_0 = 0.4\,\mathrm{m}$ (D1)

i. $H = 0.02\,\mathrm{m}$

- Peregrine's model (see [3] p. 131) when $\vartheta \in [0.4, 0.6]$ with $\vartheta^* = 0.525$,

- improved [2] using system (3)-(4) when $\vartheta \in [0.4, 0.65]$ with $\vartheta^* = 0.575$ due to the minimum error appeared in station 7 (Fig. 3).

ii. $H = 0.025\,\mathrm{m}$

- Peregrine's model when $\vartheta \in [0.4, 0.575]$ with $\vartheta^* = 0.55$ (Fig. 4),

- improved [2] using system (3)-(4) when $\vartheta \in [0.5, 0.7]$ with $\vartheta^* = 0.6$ (Fig. 5).

B. Bathymetry II Data: $L_0 = 0\,\mathrm{m}$, $L_1 = 30\,\mathrm{m}$, $T = 2\,\mathrm{sec}$, $H = 0.025\,\mathrm{m}$, $h_0 = 0.5\,\mathrm{m}$ (D2)

- Peregrine's model when $\vartheta \in [0.4, 0.55]$ with $\vartheta^* = 0.55$ (Fig. 6),

- improved [2] using system (3)-(4) when $\vartheta \in [0.45, 0.7]$ with $\vartheta^* = 0.6$ (Fig. 7).

This conclusion verifies that the introduced set of equations describes better the physical phenomenon and, also, prove that the introduced parameter ϑ influences the errors of the numerical method and the choice of $\vartheta = 0.5$ is not the ideal one (see analogous observation in [3]).

References

[1] S. Beji and J. A. Battjes, "Numerical simulation of nonlinear wave propagation over a bar", Coastal Eng. 23, pp. 1-16, 1994.

[2] S. Beji, and K. Nadaoka, "Formal derivation and numerical modelling of the improved Boussinesq equations for varying depth", Ocean Eng. 23, pp. 691-704, 1996.

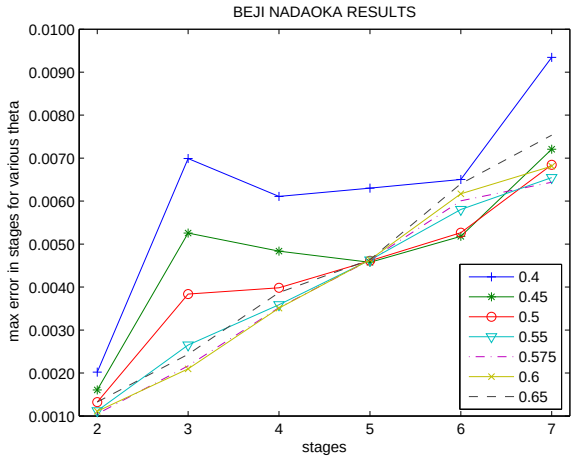

Figure 3: Bathymetry I using data (D1i) using model [2] and $\vartheta^* = 0.575$.

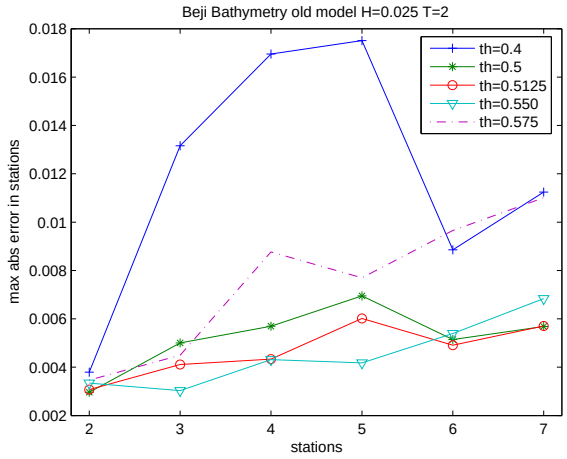

Figure 4: Bathymetry I with data (D1ii) using model [6] and $\vartheta^* = 0.55$.

[3] A. G. Bratsos, I. Th. Famelis, and A. M. Prospathopoulos, "A parametric finite-difference method for shallow sea waves", Int. J. Numer. Meth. Fluids 53, pp. 129 -147, 2007.

[4] DHI Software, MIKE 21 BW, User Guide, in: MIKE 21, Wave Modelling, User Guide, pp. 271-392, 2002.

[5] M. F. Gobbi and J. T. Kirby," Wave evolution over submerged sills: tests of a high-order Boussinesq model", Coastal Eng. 37, pp. 57-96, 1999.

[6] D. M. Peregrine, "Long waves on a beach", J. Fluid Mech. 27 (4), pp. 815-827, 1967.

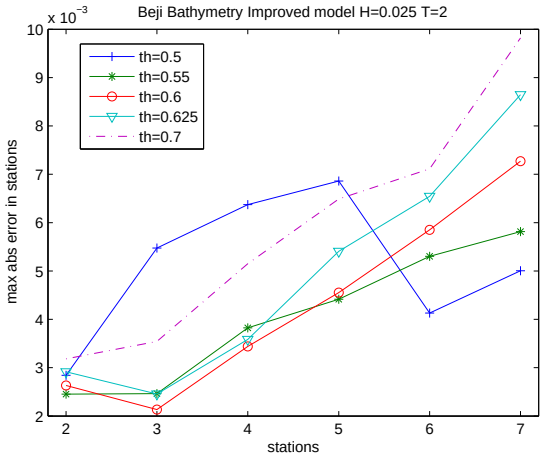

Figure 5: Bathymetry I with data (D1ii) using model [2] and $\vartheta^* = 0.6$.

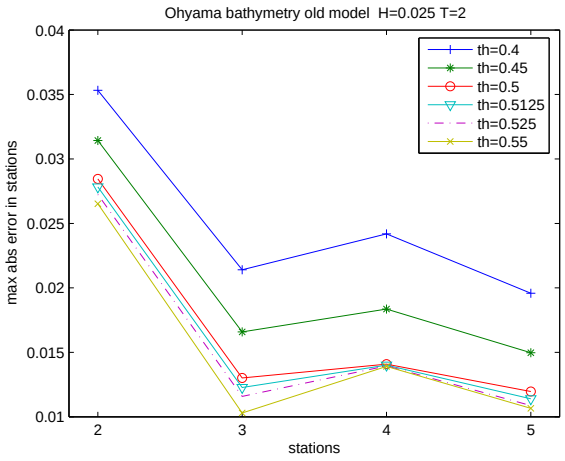

(a)

Figure 6: Bathymetry II with data (D2) using model [6] and $\vartheta^* = 0.55$.

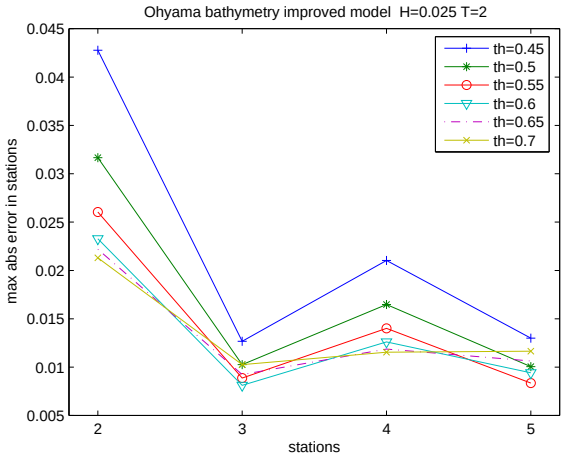

(b)

Figure 7: Bathymetry II with data (D2) using model [2] and $\vartheta^* = 0.6$.

NUMERICAL MODELING OF 1-D TRANSIENT POROELASTIC WAVES

G. Chiavassa[†], **B. Lombard**[‡,*], **J. Piraux**[‡]
[†] Ecole Centrale de Marseille and MSNM-GP, Marseille, FRANCE
[‡] Laboratoire de Mécanique et d'Acoustique, Marseille, FRANCE
[*] Email: lombard@lma.cnrs-mrs.fr

Abstract

Numerical modeling of transient poroelastic waves is studied in a one-dimensional geometry. The framework is the Biot's model in the low-frequency range. For realistic values of the physical parameters, waves with different properties coexist, leading to computational difficulties. A method is proposed to ensure efficient simulations.

Introduction

Porous media are made up of a solid matrix saturated by one or more fluids. Such media occur frequently in applications, for instance in geophysics [3]. The propagation of poroelastic waves has been analysed in [5], for linear models in the low-frequency range. Various time-domain numerical models have been proposed [4], [5], with null or low values of the viscosity of the interstitial fluid, simplifying greatly the modelisation. For realistic values, propagative and diffusive regimes coexist involving different scales of evolution and leading to important numerical difficulties. Moreover, the waves may propagate throught successive porous media, requiring an accurate treatment of the interfaces.

The aim of this study is to propose efficient numerical tools for such unfavourable situations. The 1D evolution equations are written as a first-order hyperbolic system with a source term. The proposed method is based on three different steps: a splitting to treat efficiently the source term, a mesh refinement to represent accurately the diffusive solution, and an interface method to account for discontinuies of parameters. Relevant numerical experiments are given.

Problem statement

We consider an elastic and isotropic solid saturated by a continuous and compressible liquid submitted to small perturbations whose wavelengths are much greater than the size of the pores. The relative motion of the fluid in the pores is assumed to be of the Poiseuille type. The framework is the theory of linear poroelasticity in the low-frequency range [2]. In 1D, the unknowns are the elastic velocity v_s, the filtration velocity $w = \Phi(v_f - v_s)$ (v_f is the acoustic velocity), the elastic stress σ and the acoustic pressure p. The solution $\boldsymbol{U} = {}^T(v_s,\, w,\, \sigma,\, p)$ satisfies the first-order system

$$\frac{\partial}{\partial t}\boldsymbol{U} + \frac{\partial}{\partial x}\boldsymbol{A}\boldsymbol{U} = -\boldsymbol{S}\boldsymbol{U}, \tag{1}$$

with

$$\boldsymbol{A} = \begin{pmatrix} 0 & 0 & -\rho_w/\chi & -\rho_f/\chi \\ 0 & 0 & \rho_f/\chi & \rho/\chi \\ -(\lambda_m + 2\,\mu) & -\beta\, m & 0 & 0 \\ \beta\, m & m & 0 & 0 \end{pmatrix},$$

$$\text{and } \boldsymbol{S} = \frac{\eta}{\kappa}\frac{\rho}{\chi}\begin{pmatrix} 0 & -\rho_f/\rho & 0 & 0 \\ 0 & 1 & 0 & 0 \\ 0 & 0 & 0 & 0 \\ 0 & 0 & 0 & 0 \end{pmatrix}.$$

The parameters are the density ρ_f and the dynamical viscosity η of the fluid, the density ρ_s and the shear modulus μ of the solid, the porosity $0 < \Phi < 1$, the tortuosity $a > 1$, the absolute permeability κ and the compressibility coefficients β, m, λ_m of the saturated material [3]. We set: $\rho_w = \dfrac{a}{\Phi}\,\rho_f$, $\rho = \Phi\,\rho_f + (1-\Phi)\,\rho_s$, $\chi = \rho\,\rho_w - \rho_f^2 > 0$. The eigenvalues of $\boldsymbol{A}$ are real: $\pm c_1$, $\pm c_2$, with $c_1 > c_2 > 0$. The spectral radius of $\boldsymbol{S}$ is $R(\boldsymbol{S}) = \frac{\eta}{\kappa}\frac{\rho}{\chi}$. For $\eta = 0$, the solution of (1) consists in two advection-like waves. For $\eta \neq 0$, the mechanical energy of the solution decreases [5]. The fast wave propagating at speed c_1 is slightly affected by the viscosity whereas the slow wave propagating at speed c_2 is highly damped, characterising a diffusive regime [3].

For non-homogeneous media, the physical parameters are piecewise constants. At an interface on $x = \alpha$, the simple model of open-pore jump conditions [6] is used

$$[\boldsymbol{U}]_\alpha = \boldsymbol{U}(\alpha^+,\, t) - \boldsymbol{U}(\alpha^-,\, t) = \boldsymbol{0}. \tag{2}$$

Numerical methods

Numerical scheme

We first consider an uniform grid with a mesh size $\Delta\, x$ and a time step $\Delta\, t$, in homogeneous medium. A classical approach is to discretize (1) directly [4], [5]. For standard schemes a Von-Neumann analysis of stability gives

$$\Delta\, t \leq \min\left(\frac{\Delta\, x}{c_1},\, \frac{2}{R(\boldsymbol{S})}\right). \tag{3}$$

With realistic values of the physical parameters η and κ, (3) may be very restrictive: in a sandstone saturated by bitumen, the CFL number is typically $c_1 \, \Delta t / \Delta x \approx 10^{-12}$.

We prefer a strategy of splitting, solving successively

$$\left\{ \begin{array}{l} \dfrac{\partial}{\partial t} \boldsymbol{U} + \dfrac{\partial}{\partial x} \boldsymbol{A} \boldsymbol{U} = \boldsymbol{0}, \\ \dfrac{\partial}{\partial t} \boldsymbol{U} = -\boldsymbol{S} \boldsymbol{U}. \end{array} \right. \tag{4}$$

The first equation may be solved by any flux-conservative scheme for hyperbolic systems, and we use the Lax-Wendroff method in the numerical experiments. For this step, one recovers the usual stability condition $c_1 \, \Delta t / \Delta x \leq 1$. Since $\exp(-\boldsymbol{S} t)$ is easy to compute, the second equation of (4) is solved exactly and no constraint about Δt is required. Then, a global solution is obtained by a classical second order Strang-splitting.

Mesh refinement

The phase velocity of the slow wave may be 1 or 2 orders of magnitude smaller than that of the fast wave. Consequently, a very fine grid is required to capture its evolution. Using uniform grid on the whole computational domain is out of reach in view of 2-D simulations. An alternative strategy is to use space-time mesh refinement techniques [7] near the points where these slow waves are generated, i.e. at sources and interfaces. Here, we adapt to (4) a flux-conservative method developped by [1]. Using adequate extrapolation formulas between different refinement levels ensures no spurious diffractions at grid interfaces. No complete theory exists but the numerical experiments indicate the stability of the method.

Interface method

For non-homogeneous media, it is necessary to modify the numerical scheme to account for the jump conditions at interfaces. We adapt to (1) the immersed interface method previously developped in the case of acoustics [8]. For the grid points where the stencil of the numerical scheme crosses the interface $x = \alpha$, modified values of the solution on the other side of α are used. These values are deduced from the numerical values of $\boldsymbol{U}$ on both sides of α but also from the jump conditions (2) satisfied by $\boldsymbol{U}$ and its successive spatial derivatives. The latter follow from time derivatives of (2) and from (1). Since $\boldsymbol{A}$ is piecewise constant, one gets for all $k \geq 0$

$$\left[\left(\boldsymbol{A} \frac{\partial}{\partial x} + \boldsymbol{S} \right)^k \boldsymbol{U} \right]_\alpha = \boldsymbol{0}. \tag{5}$$

In the limit-case of identical parameters on both sides of α, one recovers exactly the scheme for homogeneous medium. The subcell position of α is correctly described. The major part of the work is done during a preprocessing step, implying a negligible computational extra-cost during time-marching. Additional details may be found in [8].

Numerical experiments

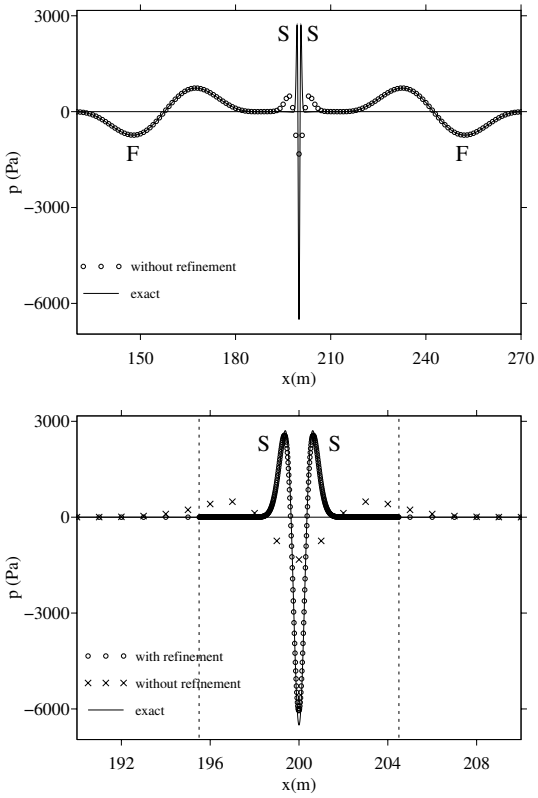

Figure 1: No mesh refinement (top); zoom around the source, with and without mesh refinement (bottom). F: fast wave, S: slow wave.

As a first test, we simulate the waves emitted by a ponctual source of stress in homogeneous sandstone saturated by water ($\eta \neq 0$) [4]. The source function is a time-bounded sinusoid with a central frequency 40 Hz [8]. The CFL number is 0.9, to be compared to 0.03 for a direct discretization (3). An exact solution is obtained by Fourier methods (idem for test 2). A snapshot of p is shown on the top of figure 1, after the extinction of the source. Fast waves are advected rightwards and leftwards while the slow waves remain localized around the source, varying strongly on small spatial scales. Their numerical estimations are highly smeared. In figure 1-(bottom), the crude solution is compared with a solution computed on a mesh refined 64 times around the source, between the two

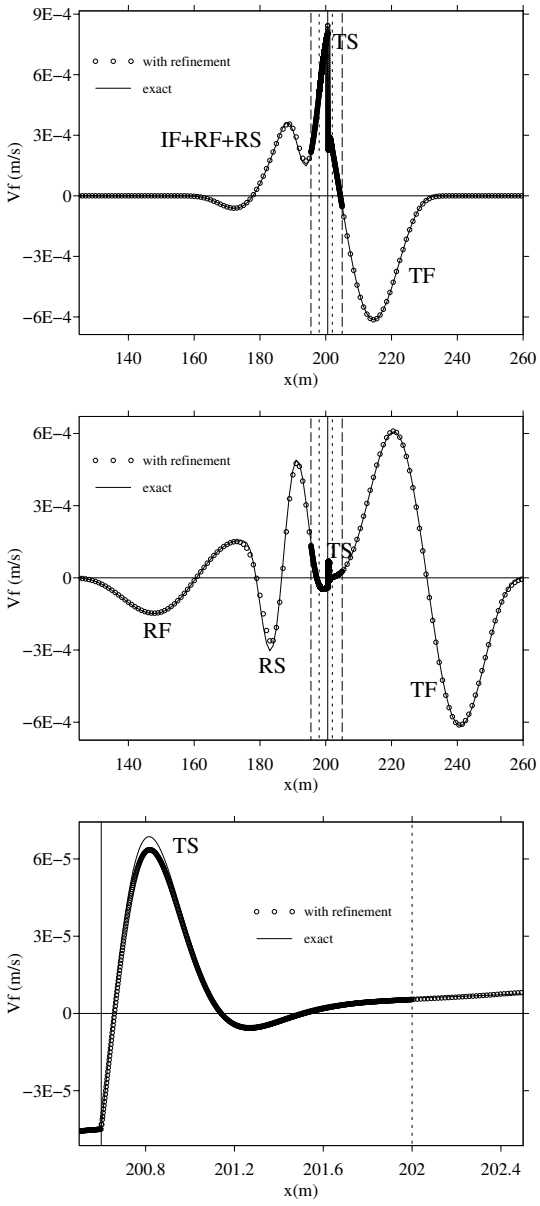

Figure 2: t_1 (top), $t_2 > t_1$ (middle), zoom around the interface at t_2 (bottom). I: incident, R: reflected, T: transmitted, F: fast wave, S: slow wave.

vertical dotted lines. A very good agreement between exact and numerical values is obtained.

As a second test, we consider the interface between sandstone saturated by a fluid with water properties (except $\eta = 0$) and sandstone saturated by a gas ($\eta \neq 0$) [4]. Two successive mesh refinements with factors 64 and 512 are used around the interface. The computation is initalized on the left of the interface by a right-going fast wave (F on the right of figure 1, top). Figure 2 shows snapshots of v_f at t_1 and $t_2 > t_1$. During the interaction of the incident wave with the interface (t_1, top), the slow waves have the larger magnitude. A poor estimation of these waves would invalidate the other ones. At t_2 (middle), the transmitted slow wave is greatly attenuated, and remains localized at α^+. Last figure (bottom) represents a zoom of the solution where the maximal refinement factor is used.

Conclusion

The slow waves generated across interfaces may vary sharply even if they are highly attenuated. They remain localized near interfaces, hence their role is crucial in the balance of mass and momentum. Consequently, they need to be computed very accurately. The proposed approach (splitting, mesh refinement and interface method) gives very promising results. An extension to 2D is in progress.

References

[1] M.J. Berger, R.J. LeVeque, "Adaptative Mesh Refinement Using Wave-Propagation Algorithms for Hyperbolic Systems", SIAM J. Numer. Anal., vol. 35-6, pp. 2298-2316, 1998.

[2] M.A. Biot, "Theory of Propagation of Elastic Waves in a Fluid-Saturated Porous Solid. I: Low-Frequency Range", J. Acoust. Soc. Am., vol. 28-2, pp. 168-178, 1956.

[3] T. Bourbié, O. Coussy, B. Zinszner, Acoustics of Porous Media, Gulf Publishing Company, 1987.

[4] N. Dai, A. Vafidis, E.R. Kanasewich, "Wave Propagation in Heterogeneous Porous Media: a Velocity-Stress, Finite-Difference Method", Geophysics, vol. 60-2, pp. 327-340, 1995.

[5] A. Ezziani, Modélisation de la propagation d'ondes dans les milieux viscoélastiques et poroélastiques, PhD thesis, University Paris-Dauphine, 2005.

[6] B. Gurevich, M. Schoenberg, "Interface Conditions for Biot's Equations of Poroelasticity", J. Acoust. Soc. Am. vol. 105-5, pp. 2585-2589, 1999.

[7] P. Joly, J. Rodriguez, "An Error Analysis of Conservative Space-Time Mesh Refinement Methods for the One-Dimensional Wave Equation", SIAM J. Numer. Anal., vol. 43-2, pp. 825-859, 2005.

[8] J. Piraux, B. Lombard, "A New Interface Method for Hyperbolic Problems with Discontinuous Coefficients: One-Dimensional Acoustic Example", J. Comput. Phys., vol. 168, pp. 227-248, 2001.

A COUPLED NEWMARK-DIFFUSIVE SCHEME FOR FRACTIONALLY DAMPED OSCILLATORS

J.-F. Deü[†,*], **D. Matignon**[‡,*]

[†]Laboratoire de Mécanique des Structures et des Systèmes Couplés, Cnam, 2 rue Conté, 75003 Paris, France
[‡]GET Télécom Paris, TSI dept. & CNRS UMR 5141, 37-39 rue Dareau, 75014 Paris, France.
[‡] Work supported by the CONSONNES project, ANR-05-BLAN-0097-01.
[*]Email: deu@cnam.fr, denis.matignon@enst.fr

Abstract

Mechanical systems with fractional damping have been studied in the literature since [1]. Resolution methods are either based on time discretization of the fractional dynamics (see e.g. [3], [2]), or on diffusive representation (cf. [5], [10], [4]). For large scale systems, the first method proves memory consuming whereas the second has no hereditary behavior and seems more appropriate. In this paper, a coupled Newmark-diffusive scheme is proposed and analyzed through a single degree-of-freedom example. Various strategies for choosing the diffusive parameters are presented and the numerical results are compared to those obtained with an original closed-form solution developed by the authors.

1 Model under study

The aim is to study fractionnaly damped oscillators using diffusive representations combined with Newmark integration scheme for mechanical systems of the form:

$$\mathbf{M}\,\ddot{\mathbf{u}}(t) + \mathbf{C}\,\dot{\mathbf{u}}(t) + \mathbf{C}_\alpha\,(d^\alpha \mathbf{u})(t) + \mathbf{K}\,\mathbf{u}(t) = \mathbf{f}(t)$$

where $d^\alpha \mathbf{u} = I^{1-\alpha}\dot{\mathbf{u}}$ is the Caputo derivative of order $\alpha \in (0,1)$, and $I^{1-\alpha}$ is the Riemann-Liouville fractional integral of order $1-\alpha$. Classically $\mathbf{M}, \mathbf{C}, \mathbf{C}_\alpha, \mathbf{K}$ are symmetric and positive matrices, $\mathbf{M}$ being positive *definite*.

2 A closed-form solution in fractional power series

Let us introduce an original closed-form solution for the following fractionally damped SDOF equation:

$$m\,\ddot{u}(t) + c\,\dot{u}(t) + c_\alpha\,(d^\alpha u)(t) + \kappa\,u(t) = f(t)$$

with $u(0) = u^0$, $\dot{u}(0) = v^0$, $\alpha = \dfrac{p}{q} \in (-1,1)$, $p \wedge q = 1$.

Here, three cases are investigated: the free vibrations (no external force $f \equiv 0$) due to **(a)** an initial displacement ($u^0 \neq 0$, $v^0 = 0$) or **(b)** an initial velocity ($v^0 \neq 0$, $u^0 = 0$), and **(c)** the dynamic response under a constant load ($f(t) = f^0 H(t)$, $u^0 = v^0 = 0$). We recall that (b) and (c) correspond to impulse and indicial responses.

The key point is to write this exact solution in terms of fractional power series as $u(t) = \sum_{j=0}^{\infty} U_j\, t^{j/q}$, where the corresponding U_j coefficients are defined by:

- for $j \leq 2q$, the U_j are zero except the following,
  case **(a)**: $U_0 = u^0$, $U_{2q} = -\kappa/(2m)\,u^0$;
  case **(b)**: $U_q = v^0$, $U_{2q} = -c/(2m)\,v^0$;
  case **(c)**: $U_{2q} = 1/(2m)\,f^0$;
- for $j > 2q$, the U_j are evaluated recursively by:

$$U_j = -\frac{1}{m}\frac{q^2}{j(j-q)}\left[c\,(\frac{j-q}{q})S_{j-q} + c_\alpha\,\frac{\Gamma\left(\frac{j+p-q}{q}\right)}{\Gamma\left(\frac{j-q}{q}\right)}S_{j+p-2q} + \kappa\,S_{j-2q}\right],$$

These coefficients have been obtained after some analytical calculations. Since u can be linearly decomposed into $2q$ Mittag-Leffler functions, see e.g. [8], and since the latter are entire functions, we know that the radius of convergence of the above series solution is infinite. In the sequel, it will be used to evaluate the accuracy of the Newmark-diffusive scheme for fractionally damped systems.

3 A coupled Newmark-diffusive numerical scheme

3.1 Diffusive schemes for fractional models

Following e.g. [5], [8]-[10], $d^\alpha \mathbf{u} = I^{1-\alpha}\mathbf{v}$ can be represented by the superposition of first-order systems :

$$\begin{aligned} \partial_t \boldsymbol{\varphi}(\xi,t) &= -\xi\,\boldsymbol{\varphi}(\xi,t) + \mathbf{v}(t),\ \xi > 0,\ \boldsymbol{\varphi}(0) = 0, \\ (I^{1-\alpha}\mathbf{v})(t) &= \int_0^\infty \boldsymbol{\varphi}(\xi,t)\,\mu_{1-\alpha}(\xi)\,d\xi\,. \end{aligned}$$

where $\mu_{1-\alpha}(\xi) = \frac{\sin\alpha\pi}{\pi}\,\xi^{-(1-\alpha)}$ for $\xi > 0$. Thus, stable numerical schemes can be derived, e.g. by standard *interpolation* $\int_0^\infty \boldsymbol{\varphi}(\xi)\,\mu_{1-\alpha}(\xi)\,d\xi \approx \sum_{k=1}^K \boldsymbol{\varphi}(\xi_k)\,\mu_k$, where ξ_k and μ_k must be chosen appropriately (see § 4.1).

3.2 Time-integration coupled scheme

Now, a predictor-corrector algorithm based on the Newmark integration scheme (see [7, chap 9.]) for the dynamic response of a fractionally damped system is proposed:

---

1. Initialization
   $\mathbf{S} = \mathbf{M} + \gamma\,\Delta t\,\mathbf{C} + \beta\,\Delta t^2\,\mathbf{K}$
   $\mathbf{u}(0) = \mathbf{u}^0$, $\mathbf{v}(0) = \mathbf{v}^0$, $\boldsymbol{\varphi}_k(0) = \mathbf{0}$ for $1 \leq k \leq K$
   $\mathbf{a}^0 = \mathbf{M}^{-1}(\mathbf{f}^0 - \mathbf{K}\,\mathbf{u}^0 - \mathbf{C}\,\mathbf{v}^0)$

2. Enter time step loop
   a) Prediction
   $\mathbf{u}_{\text{pr}}^{n+1} = \mathbf{u}^n + \Delta t\,\mathbf{v}^n + (0.5-\beta)\,\Delta t^2\,\mathbf{a}^n$
   $\mathbf{v}_{\text{pr}}^{n+1} = \mathbf{v}^n + (1-\gamma)\,\Delta t\,\mathbf{a}^n$
   b) Evaluation of $\boldsymbol{\varphi}_k^{n+1}$ for $1 \le k \le K$ and $\mathbf{a}^{n+1}$
   $\boldsymbol{\varphi}_k^{n+1} = \exp(-\xi_k\,\Delta t)\,\boldsymbol{\varphi}_k^n + \dfrac{1-\exp(-\xi_k\,\Delta t)}{\xi_k}\,\mathbf{v}_{\text{pr}}^{n+1}$
   $\mathbf{a}^{n+1} = \mathbf{S}^{-1}\Big(\mathbf{f}^{n+1} - \mathbf{C}\,\mathbf{v}_{\text{pr}}^{n+1} - \mathbf{C}_\alpha \sum_{k=1}^{K} \mu_k\,\boldsymbol{\varphi}_k^{n+1} - \mathbf{K}\,\mathbf{u}_{\text{pr}}^{n+1}\Big)$
   c) Correction
   $\mathbf{u}^{n+1} = \mathbf{u}_{\text{pr}}^{n+1} + \beta\,\Delta t^2\,\mathbf{a}^{n+1}$
   $\mathbf{v}^{n+1} = \mathbf{v}_{\text{pr}}^{n+1} + \gamma\,\Delta t\,\mathbf{a}^{n+1}$
3. Update time step and return to 2

Note that the prediction vectors $\mathbf{u}_{\text{pr}}$, $\mathbf{v}_{\text{pr}}$, and the diffusive components $\boldsymbol{\varphi}_k$ for $1 \le k \le K$ need not be stored.
Moreover, we use $\beta = 1/4$ and $\gamma = 1/2$ known as *average acceleration method* (i.e. the trapezoidal rule applied to the vector $(\mathbf{u}, \mathbf{v})$).

4 Numerical results

4.1 Various strategies for choosing diffusive parameters

Based on Bode diagrams, a heuristic choice of the $\{\xi_k\}_{1\le k\le K}$ is given by a geometric sequence on a frequency range of interest. Then, different choices are available for the $\{\mu_k\}_{1\le k\le K}$, see e.g. [5].

We first focus on the *analytical* evaluation of μ_k, using the hat functions $\Lambda_k(\xi)$ of P_1 interpolation, namely $\mu_k = \int_0^\infty \mu_{1-\alpha}(\xi)\Lambda_k(\xi)d\xi$, which gives, with $\lambda = \frac{\sin\alpha\pi}{(1+\alpha)\alpha\pi}$:

$$\mu_k = \lambda\left[\xi_{k+1}\left(\frac{\xi_{k+1}^\alpha - \xi_k^\alpha}{\xi_{k+1}-\xi_k}\right) - \xi_{k-1}\left(\frac{\xi_k^\alpha - \xi_{k-1}^\alpha}{\xi_k - \xi_{k-1}}\right)\right].$$

A second choice consists in *optimizing* the μ_k with respect to a weighted (W_l) least-squares criterion, see [6]:

$$\mathcal{C}(\boldsymbol{\mu}) = \sum_{l=1}^{L} W_l \left| \sum_{k=1}^{K} \frac{\mu_k}{i\,\omega_l + \xi_k} - \frac{1}{(i\omega_l)^{(1-\alpha)}} \right|^2,$$

where $\{\omega_l\}_{1\le l\le L}$ are angular frequencies, and $L \gg K$. Fig. 1 shows the analytical and optimal ($L = 10\,K$) values of μ_k, for geometrically spaced ξ_k in $[10^{-4},\ 10^4]$ and for $K = 10,\ 15$ and 20. We observe oscillations of the optimal μ_k around the analytical values, especially at the endpoints of the interval; even negative values can be found, which could be a problem for a further stability analysis.

The corresponding approximated Bode plots are shown in Fig. 2 below.

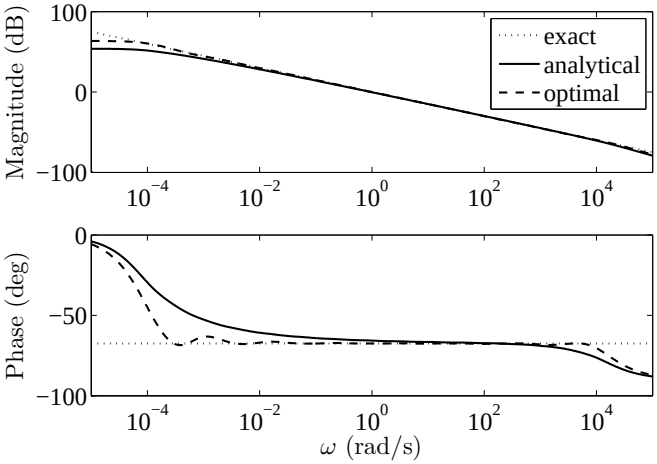

Figure 2: Exact and approximated Bode plots: analytical and optimal with $K = 15$ and $\xi_k \in [10^{-4}\ 10^4]$.

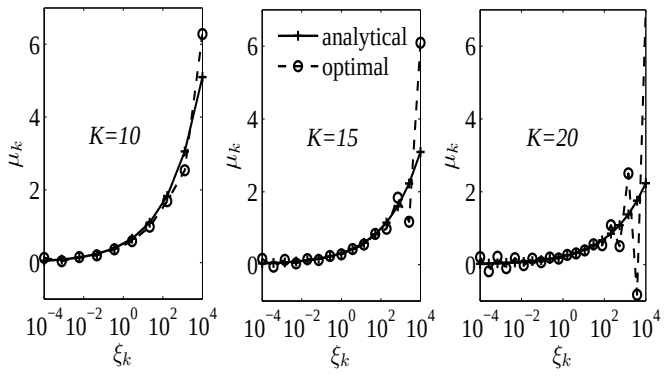

Figure 1: Evolution of μ_k versus ξ_k ($1 \le k \le K$)

4.2 Analysis of the SDOF case

Fig. 3 presents the time displacement and the phase diagram for $\alpha \in (0\,,1)$: one can see the continuity of the behaviour from the undamped to the viscous case.
The closed-form solution is used to evaluate the displacement error for the sdof in Fig. 4:

- for a given frequency range, the slope of the error clearly changes for $K = K^*$; oscillations occur in the second regime (due to the optimal choice of μ_k).
- as a consequence, for a given number K, the best choice of frequency range is first the smallest range for $K \le K_-^* \approx 10$, and finally the biggest range for $K \ge K_+^* \approx 20$.
- a smaller time step gives a smaller asymptotic displacement error, as K increases, whatever the frequency range (not shown).

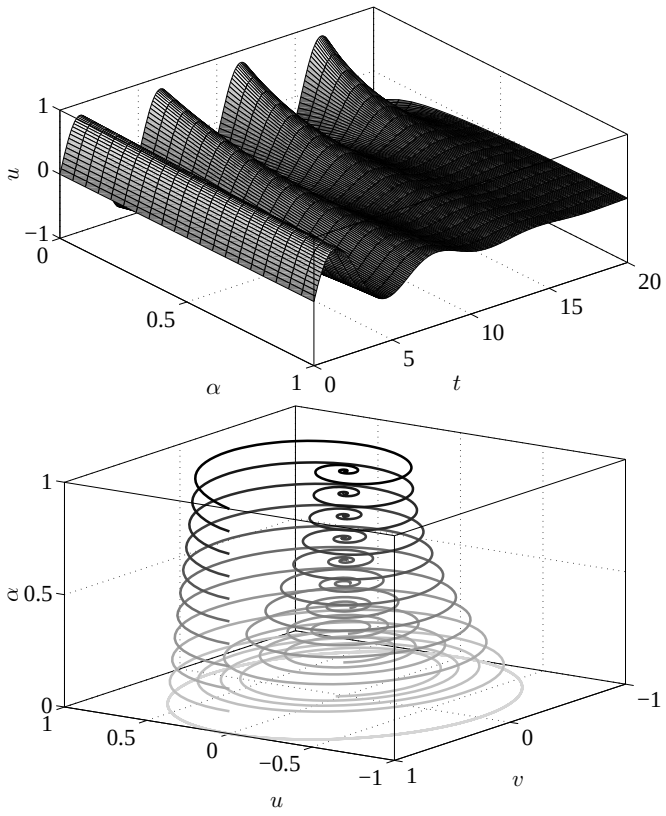

Figure 3: Displacement versus time (top) and phase diagrams (bottom) for various fractional orders α. Case **(b)**: $v^0 = 1$, $m = 1$, $c = 0$, $c_\alpha = 0.5$, $\kappa = 1$.

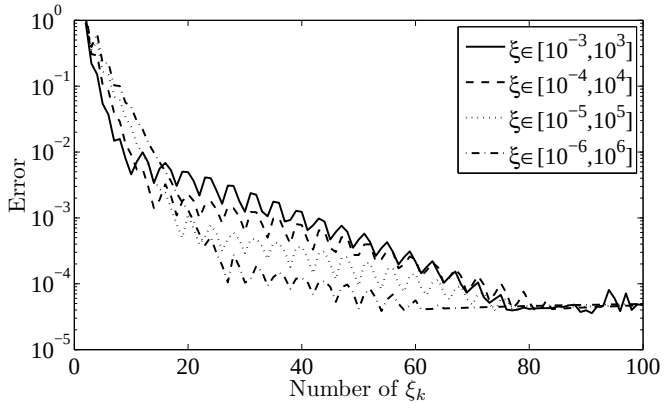

Figure 4: Displacement error versus K (number of ξ_k) for 4 different ranges of frequencies. Case **(b)**: $v^0 = 1$, $m = 1$, $c = 0$, $c_\alpha = 0.5$, $\kappa = 1$.

Conclusion and Perspectives

With this approach, complex mechanical systems with fractional damping can be efficiently simulated (in comparison to [3]), thanks to an appropriate finite element space discretization. Evaluation of the μ_k, which is a keypoint of the method, must be further investigated following the optimal approach.

Only $0 < \alpha < 1$ has been considered so far, but $1 < \alpha < 2$ can also be tackled through *extended* diffusive representations, the closed-form solution being still valid. Finally, a stability analysis of our coupled scheme has to be carried out, using energy balances, as in [4, chap. 3].

References

[1] R. L. Bagley and P. J. Torvik. Fractional calculus – a different approach to the analysis of viscoelastically damped structures. *AIAA J.*, 21(5):741–748, 1983.

[2] A.C. Galucio, J.-F. Deü, S. Mengué, and F. Dubois. An adaptation of the Gear scheme for fractional derivatives. *Comput. Methods Appl. Mech. Engrg.*, 1995(44-47):6073–6085, 2006.

[3] A.C. Galucio, J.-F. Deü, and R. Ohayon. Finite element formulation of viscoelastic sandwich beams using fractional derivative operators. *Computational Mechanics*, 33(4):282–291, 2004.

[4] H. Haddar and D. Matignon. Theoretical and numerical analysis of the Webster-Lokshin model. Technical Report, INRIA, 2007.

[5] D. Heleschewitz. *Analyse et simulation de systèmes différentiels fractionnaires et pseudo-différentiels linéaires sous représentation diffusive*. PhD thesis, ENST, December 2000.

[6] Th. Helie and D. Matignon. Representations with poles and cuts for the time-domain simulation of fractional systems and irrational transfer functions. *Signal Processing*, 86(10):2516–2528, 2006.

[7] T.J.R. Hughes. *The Finite Element Method: Linear Static and Dynamic Finite Element Analysis*. Prentice Hall, Englewood Cliffs, 1987.

[8] D. Matignon. Stability properties for generalized fractional differential systems. *ESAIM: Proceedings*, 5:145–158, 1998.

[9] D. Matignon. *An introduction to fractional calculus*, volume 1 of Scaling, Fractals and Wavelets of *Digital Signal and Image Processing Series*, chapter 4. Hermès–Lavoisier, 2007.

[10] D. Matignon and Ch. Prieur. Asymptotic stability of linear conservative systems when coupled with diffusive systems. *ESAIM: Control, Optimisation and Calculus of Variations*, 11(3):487–507, 2005.

EFFICIENT SOLUTION OF A WAVE EQUATION WITH FRACTIONAL ORDER DISSIPATIVE TERMS

H. Haddar[*], **J.-R. Li**[*], **D. Matignon**[†,‡]
[*]POems, INRIA-Rocquencourt, UMR 2706, B.P. 105, F-78153 Le Chesnay, France
[†]GET Télécom Paris, TSI dept. & CNRS UMR 5141. 37-39 rue Dareau, 75014 Paris, France
[‡] Work supported by the CONSONNES project, ANR-05-BLAN-0097-01.

Abstract

The dissipative model which describes acoustic waves traveling in a duct with viscothermal losses at the lateral walls is a wave equation with spatially-varying coefficients, which involves fractional-order integrals and derivatives. We first rewrite this model in a coupled form. Then the fractional integral is written in its diffusive representation; essentially, the fractional-order time kernel in the integral is represented by its Laplace transform. This allows for efficient time domain simulation because the value of integral at each time step can be updated from the value at the previous time step by operations which are local in time, contrary to a naive discretization of the fractional integral. An accurate and efficient quadrature for the inverse Laplace transform with an *a priori* error estimate is used and it is crucial in keeping the work at each time step reasonable; essentially, the number of quadrature points in the Laplace domain is $O(-\log(\Delta t))$. Thus, if M is the number of time steps, the numerical scheme we propose requires $O(M\log(M))$ work and $O(\log(M))$ memory, compared to $O(M^2)$ work and $O(M)$ memory of a naive discretization. The gain in efficiency makes long time simulations feasible.

1 Model under study

To simplify the presentation, we focus here on the one-dimensional Webster-Lokshin model of the form

$$\partial_t^2 w + a(z)\partial_t^{2-\beta} w + b(z)\partial_t w - \frac{1}{r^2(z)}\partial_z(r^2(z)\partial_z w) = 0,$$

for $t > 0$ and $z \in [0,1]$, where $\beta \in (0,1)$, $r, a, b \in L^\infty([0,1];\mathbb{R}^+)$; the radius of the duct satisfies $r \geq r_0 > 0$. The Riemann-Liouville fractional integral operator $\partial_t^{-\beta}$ is defined by

$$(\partial_t^{-\beta} f)(t) := \frac{1}{\Gamma(\beta)} \int_0^t \frac{f(\tau)}{(t-\tau)^{1-\beta}}\, d\tau. \qquad (1)$$

Working with $(p,\, v) := (\partial_t w,\, -r^2(z)\,\partial_z w)$ leads to the first order system:

$$\partial_t p = -r^{-2}\,\partial_z v - b\,p - a\,\partial_t^{-\beta}(\partial_t p)\ , \qquad (2)$$

$$\partial_t v = -r^2\,\partial_z p\ , \qquad (3)$$

which we supplement with the boundary conditions:

$$p_0(t) := p(z=0,\, t) = u(t)\ , \qquad (4)$$

$$v_1(t) := v(z=1,\, t) = 0. \qquad (5)$$

We assume that we have zero initial values.

2 Diffusive representation

We recall *diffusive* realizations for fractional integrals; we refer to [6, § 5] for the treatment of *completely monotone kernels*, and [4] for links between diffusive representations and fractional integral and differential operators.

The dynamical system with input $f \in L^2([0,T])$ and output $\theta^{[\beta]}(f) \in L^2([0,T])$:

$$\partial_t \varphi(\xi,t) = -\xi\varphi(\xi,t) + f(t),\ \forall \xi \in \mathbb{R}^+, \qquad (6)$$

$$\theta^{[\beta]}(f)(t) = \frac{1}{\Gamma(\beta)\Gamma(1-\beta)} \int_0^\infty \varphi(\xi,t)\,\xi^{-\beta}\ d\xi, \qquad (7)$$

given $\varphi(\xi,0) = 0$, provides a diffusive realization of the fractional integral $\partial_t^{-\beta}$: in the other words, it realizes the input-output relation $\theta^{[\beta]}(f) = \partial_t^{-\beta} f$. This can be seen from the relation:

$$\frac{1}{(t-\tau)^{1-\beta}} = \int_0^\infty e^{-\xi\,(t-\tau)} \frac{\xi^{-\beta}}{\Gamma(1-\beta)}\, d\xi, \qquad (8)$$

which in essence states that the convolution kernel in (1) is the inverse Laplace transform of $\frac{\xi^{-\beta}}{\Gamma(\beta)\Gamma(1-\beta)}$.

Using (6-7), the global system (2-5) can be put in the abstract form $\partial_t X + \mathcal{A}\,X = \mathcal{B}\,u$, with $X = \big(p,\, v,\, \varphi\big)^T$. We know from [2], [3] that operator $\mathcal{A}$ is maximal monotone on an appropriate functional space; thus, due to the Hille-Yosida theorem, the original problem is well-posed.

The efficient and accurate computation of (7) depends on finding a good quadrature for the integral in (8).

3 Optimized weights for diffusive representations

We follow, with slight modifications, the approach of [1] where the special case $\beta = \frac{1}{2}$ was considered. Due to the fact that as τ approaches t, the support of $e^{-\xi\,(t-\tau)}$ becomes infinite, we write $\theta^{[\beta]}(f)(t)$ as the sum of a local (in time) part

$$\theta^{[\beta,\,\mathrm{loc}]}(f)(t) = \frac{1}{\Gamma(\beta)} \int_{t-\Delta t}^t \frac{1}{(t-\tau)^{1-\beta}}\ f(\tau)\ d\tau,$$

and a historical part

$$\theta^{[\beta,\text{hist}]}(f)(t) = G\int_0^\infty \int_0^{t-\Delta t} e^{-\xi(t-\tau)}\xi^{-\beta}\, f(\tau)\, d\tau\, d\xi,$$

where $G = \frac{1}{\Gamma(\beta)\Gamma(1-\beta)}$. We use for $\theta^{[\beta,\,\text{loc}]}(f)(t)$ the approximation :

$$\theta^{[\beta,\,\text{loc}]}(f)(t) \approx \frac{1}{\Gamma(\beta)} f\left(t-\frac{\Delta t}{2}\right)\frac{\Delta t^\beta}{\beta},$$

and build a quadrature in ξ for

$$\int_0^\infty e^{-\xi\,(t-\tau)}\xi^{-\beta}\, d\xi \approx \sum_{j=1}^{M} e^{-\xi_j\,(t-\tau)}\xi_j^{-\beta}\, w_j,$$

which will be accurate for all $\tau \in [0,\, t-\Delta t]$. Removing the integrable singularity $\xi^{-\beta}$ at the origin will make the computation of the quadrature points simpler, so we make the change of variables, $\gamma = \frac{1}{1-\beta}$, $\eta = \xi^{\frac{1}{\gamma}}$, to obtain

$$\int_0^\infty e^{-\xi\,(t-\tau)}\xi^{-\beta}\, d\xi = \int_0^\infty \gamma\, e^{-(\eta^\gamma\,(t-\tau))} d\eta.$$

In essence, we will construct a quadrature with an error tolerance of ϵ:

$$\left|\int_0^\infty e^{-(\eta^\gamma\,\tau)} d\eta - \sum_{j=1}^{L^{\Delta t,\epsilon}} e^{-[(\eta_j^{\Delta t,\epsilon})^\gamma\,\tau]}\, \omega_j^{\Delta t,\epsilon},\right| \le \epsilon,$$

valid for all $\tau \in [\Delta t,\, t_f]$, where we have used the superscripts Δt and ϵ to indicate that the position, weight, and the number of quadrature nodes are dependent on those quantities.

First, we reduce the domain of integration to a finite interval. ¿From the relation

$$\int_{\eta_f}^\infty e^{-\eta^\gamma\,\tau} d\eta \le \frac{e^{-(\eta_f{}^\gamma\,\Delta t)}\Gamma(\frac{1}{\gamma})}{\gamma\,\Delta t^{(\frac{1}{\gamma})}},$$

we find that choosing $\eta_f = \left(\frac{-\log\frac{\gamma\,\epsilon/3\,\Delta t^l}{\Gamma(l)}}{\Delta t}\right)^l$, $l = \frac{1}{\gamma}$, ensures that

$$\left|\int_0^\infty e^{-\eta^\gamma\,\tau} d\eta - \int_0^{\eta_f} e^{-\eta^\gamma\,\tau} d\eta\right| \le \frac{\epsilon}{3}.$$

The parameter τ varies from Δt to t_f and we need to construct a single quadrature which accurately approximates the integral for this one-parameter family of integrands. Over any fixed subinterval in $[a,b]$, the integrand $e^{-\eta^\gamma\,\tau}$ varies from identically 1 to identically 0. A quadrature must approximate accurately this range of behavior. It is not difficult to see that the region of the most rapid range in the integrand $e^{-\eta^\gamma\,\tau}$ occurs at the inflection point, $\eta_{\text{i}} = \left(\frac{\gamma-1}{\gamma\,\tau}\right)^{\frac{1}{\gamma}}$.

To capture the clustering of support of the integrands toward $\eta = 0$ as τ becomes larger, we follow the development in [1] and use Gauss-Legendre quadrature points on dyadic intervals.

On a dyadic interval $[a,b]$, we choose the smallest order Gauss-Legendre quadrature which accurately computes to a tolerance $\frac{\epsilon}{3(b-a)}$:

$$\left|\int_a^b e^{-\eta^\gamma\,\tau} d\eta - \sum_{j=1}^{L^a} e^{-(\eta_j^a)^\gamma\,\tau}\, \omega_j^a,\right| \le \frac{\epsilon}{3(b-a)}, \quad (9)$$

for $\tau \in [\tau_{min}, \tau_{max}]$, where τ_{min} and τ_{max} are chosen by solving the following equations

$$e^{-a^\gamma\,\tau_{max}} = q,$$
$$e^{-b^\gamma\,\tau_{min}} = 1-q.$$

The number q is a small factor to indicate that the support of $\tau > \tau_{max}$ is mostly outside of $[a,b]$ and that for $\tau < \tau_{min}$ the integrand is almost identically 1. Hence, the only relevant τ for which the tolerance in (9) needs to be tested is between τ_{min} and τ_{max}. The number of quadrature points needed on $[a,b]$ are determined numerically by testing (9) for a range of values of τ in $[\tau_{min}, \tau_{max}]$.

If a t_f is chosen, then we solve for the largest a_{min} of the form $a_{min} = 2^{j_{min}}$ satisfying

$$e^{-a_{min}^\gamma\, t_f} \le q,$$

i.e., $e^{-\eta^\gamma\, t_f}$ is negligible outside of $[0, a_{min}]$ and we treat the interval $[0, a_{min}]$ like explained for the interval $[a,b]$, by numerically sastifying (9). But the number τ_{max} is now simply t_f. Clearly, if $a_{min} \le \frac{\epsilon}{3}$ this interval can be neglected. Thus, if $t_f = \infty$ is chosen, the smallest dyadic interval to be treated is $[2^{j_{min}}, 2^{j_{min}+1}]$ where j_{min} is the largest integer satisfying $2^{j_{min}} < \frac{\epsilon}{3}$.

	$\epsilon = 10^{-1}$	$\epsilon = 10^{-2}$	$\epsilon = 10^{-3}$
$\Delta t = 10^{-1}$	9 (13)	12 (22)	22 (54)
$\Delta t = 10^{-2}$	16 (18)	28 (48)	28 (60)

Table 1: Number of quadrature nodes $L^{\Delta t,\epsilon}$ for $\beta = \frac{1}{2}$, $t_f = 10$ ($t_f = \infty$).

The number of required quadrature nodes $L^{\Delta t,\epsilon}$ for a given Δt and ϵ is $O(-\log\Delta t, -\log\epsilon)$. In Table 1 above, $L^{\Delta t,\epsilon}$ for $\beta = \frac{1}{2}$, $t_f = 10$ and $t_f = \infty$ are given.

4 Numerical scheme and validation

Let Δt and $h = 1/N$ be, respectively, the time and spatial step sizes, N is the number of discretization points of $[0, 1]$. We set $z_i = ih$, $z_{i+\frac{1}{2}} = (i + \frac{1}{2})h$ and denote

$$p_i^n \approx p(ih, n\Delta t);\ v_{i+\frac{1}{2}}^{n+\frac{1}{2}} \approx v((i + \tfrac{1}{2})h, (n + \tfrac{1}{2})\Delta t).$$

Then a second order centered explicit scheme associated with (2-3) can be written as

$$\begin{aligned}\frac{p_i^{n+1} - p_i^n}{\Delta t} = &-\frac{1}{r^2(z_i)} \frac{v_{i+\frac{1}{2}}^{n+\frac{1}{2}} - v_{i-\frac{1}{2}}^{n+\frac{1}{2}}}{h} \\ &- b(z_i) \frac{p_i^{n+1} + p_i^n}{2} - a(z_i)\, \tilde\theta_i^{n+1/2}\,,\end{aligned} \tag{10}$$

for $n > 0$ and $0 < i \leq N$ and

$$\frac{v_{i+\frac{1}{2}}^{n+\frac{1}{2}} - v_{i+\frac{1}{2}}^{n-\frac{1}{2}}}{\Delta t} = -r^2(z_{i+\frac{1}{2}}) \frac{p_{i+1}^n - p_i^n}{h}\,, \tag{11}$$

where $\tilde\theta_i^{n+1/2}$ in (10) denotes an approximation of $\theta^{[\beta]}(\partial_t p)((n + \frac{1}{2})\Delta t))$. Based on the splitting of $\theta^{[\beta]}(f)$ in local and historical parts, we compute $\tilde\theta_i^{n+1/2}$ as

$$\tilde\theta_i^{n+1/2} = \frac{\Delta t^\beta}{\Gamma(\beta)\beta\ 2\Delta t}(p_i^{n+1} - p_i^{n-1}) + \sum_{j=1}^{L^{\Delta t,\epsilon}} \omega_j(\varphi_{i,j}^n + \varphi_{i,j}^{n-1})/2$$

where $(\xi_j, \omega_j)_{j=1,\cdots,L^{\Delta t,\epsilon}}$ is the quadrature associated with β and a given tolerance ϵ as derived in the previous section, and

$$\varphi_{i,j}^n = e^{-\xi_j \Delta t}\varphi_{i,j}^{n-1} + e^{-\xi_j \Delta t/2}(p_i^n - p_i^{n-1}), \tag{12}$$

is the centered approximation associated with

$$\partial_t(e^{\xi t}\varphi) = e^{\xi t}\partial_t p.$$

Unfortunately, the stability analysis derived in [3, chap. 3] does not apply any more to this scheme due to the shift introduced in the evaluation of $\tilde\theta_i^{n+1/2}$. Numerical experiments suggest, however, that the CFL is the same as for the scheme without dissipative terms. The proof of this result using Fourier analysis is under investigation.

We conclude this short presentation with a numerical validation in the case of the *Lokshin* model, i.e., when $r(z) = r_0$ and $b = (a/2)^2$. In this case, a closed-form solution is available in both time and frequency domains, see [5]: the output $p(z = 1, t) = h \star u$ can be decomposed into *wavetrains*, due to the fact that

$$h(t) = \sum_{k=0}^{\infty} (-1)^k\, \psi^{(2k+1)a}(t - (2k + 1))\,,$$

where $\psi^a(t) = \frac{a}{2\sqrt{\pi}\, t^{3/2}}\ \exp(-\frac{a^2}{4t})$ for $t > 0$. The following numerical example corresponds to $a = 0.4$, $\beta = 1/2$ and $r = 1$. The incident field is a Gaussian pulse.

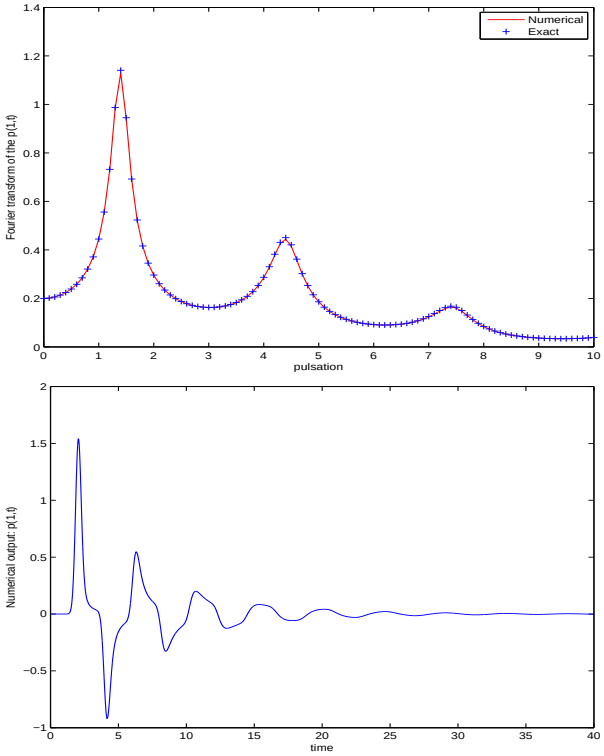

References

[1] L. Greengard and P. Lin. Spectral approximation of the free-space heat kernel. *Appl. Comput. Harmonic Anal.*, 9(1), p. 83–97, 2000.

[2] H. Haddar, Th. Hélie, and D. Matignon. A Webster-Lokshin model for waves with viscothermal losses and impedance boundary conditions. In *6th Waves conf.*, p. 66–71, Finland, July 2003. INRIA.

[3] H. Haddar and D. Matignon. Theoretical and numerical analysis of the Webster-Lokshin model. Technical Report, INRIA, 2007.

[4] D. Matignon. Stability properties for generalized fractional differential systems. *ESAIM: Proceedings*, 5:145–158, December 1998.

[5] D. Matignon and B. d'Andréa-Novel. Spectral and time-domain consequences of an integro-differential perturbation of the wave PDE. In *3rd Waves conf.*, p. 769–771, France, April 1995. INRIA, SIAM.

[6] O. J. Staffans. Well-posedness and stabilizability of a viscoelastic equation in energy space. *Trans. Amer. Math. Soc.*, 345(2):527–575, October 1994.

A finite volume method for the approximation of the two dimensional Maxwell equations on arbitrary meshes

S. Layouni[†,*], **P. Omnes**[‡], **F. Hermeline**[II]

[†]CEA/DEN/DANS/SFME/LMPE Saclay and UPS Toulouse, France
[‡] CEA/DEN/DANS/SFME/LMPE Saclay, France.
[II]CEA/DIF Bruyères-le-Chatel, France.
[*]Email: siham.layouni@cea.fr

Abstract

We present a new finite volume scheme for solving the two dimensional Maxwell equations. It is a generalization of the so-called covolume method ([4],[6]) to non-orthogonal, non-conforming meshes. It is also an extention of recent ideas developed in [1], [2], [3].
For an arbitrary mesh, the scheme preserves Gauss' law and a discrete energy and is stable under a CFL-like condition. In the case of regular cartesian grids, it degenerates into two Yee schemes [5]. Numerical tests show a second order convergence even on non conforming meshes and that the non conformity does not add parasitic reflections.

Discretization of Maxwell's system

For an arbitrary mesh that we call **primal mesh**, we associate with each primal cell P_p a primal point ξ_p (the centroid is a qualified candidate). By joining these points we obtain a second mesh called **dual mesh**. With each vertex x_d of a primal cell is associated a dual cell Π_d . A third mesh called **diamond mesh** is constructed by joining the points associated to two neighbor primal cells to the vertices of the side that they share.
For a side F_f of a primal cell P_p, we note $\mathbf{n}_{fp}$ the unit outward normal vector and $\mathbf{t}_{fp}$ the unit counterclockwise tangent vector. For a side Φ_f of a dual cell Π_d, we note ν_{fd} the unit outward normal vector and τ_{fd} the unit counterclockwise tangent vector.

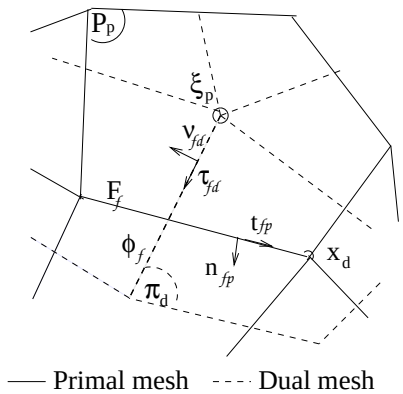

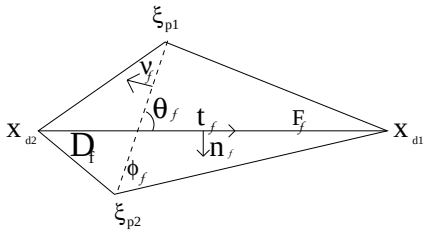

Figure 1: A diamond cell

Maxwell's equations are discretized such that magnetic field unknowns are located on the primal and dual cells; electric field unknowns are located on the diamond cells. And with a Leap-frog scheme for the time discretization, we get the following discrete Maxwell system:

$$
\begin{aligned}
B_p^{n+1} &= B_p^n - \frac{\Delta t}{|P_p|} \sum_{F_f \in P_p} |F_f| \mathbf{E}_f^{n+1/2} \cdot \mathbf{t}_{fp} \\
B_d^{n+1} &= B_d^n - \frac{\Delta t}{|\Pi_d|} \sum_{\Phi_f \in \Pi_d} |\Phi_f| \mathbf{E}_f^{n+1/2} \cdot \boldsymbol{\tau}_{fd} \\
\mathbf{E}_f^{n+1/2} &= \mathbf{E}_f^{n-1/2} - \frac{\Delta t}{\epsilon_0} \mathbf{J}_f^n \\
&+ \frac{c^2 \Delta t}{2|D_f|} \begin{pmatrix} [B^n(\mathbf{x}_{d_2}) - B^n(\mathbf{x}_{d_1})] \ |\Phi_f| \boldsymbol{\tau}_f \\ +[B^n(\boldsymbol{\xi}_{p_2}) - B^n(\boldsymbol{\xi}_{p_1})] \ |F_f| \mathbf{t}_f \end{pmatrix}
\end{aligned}
$$

In the case of regular cartesian grids, this system degenerates into two independent subsystems corresponding to two Yee schemes, one on the primal mesh, the other on the dual.

Properties of the scheme

Divergence preservation

The Discrete Gauss law, given below, is preserved for an adequate discretization of ρ and $\mathbf{J}$ and if it is satisfied by initial conditions .

$$
\begin{aligned}
\frac{1}{|P_p|} \quad & \textstyle\sum_{F_f \in P_p} |F_f| \, \mathbf{E}_f \cdot \mathbf{n}_{fp} && = \frac{\rho_p^{n+1/2}}{\epsilon_0} \\
\frac{1}{|\Pi_d|} \quad & \begin{pmatrix} \sum_{\Phi_f \in \Pi_d} |\Phi_f| \, \mathbf{E}_f \cdot \boldsymbol{\nu}_{fd} + \\ \frac{1}{2} \sum_{F_f \in \Pi_d \cap \partial\Omega} |F_f| \, \mathbf{E}_f \cdot \mathbf{n}_f \end{pmatrix} && = \frac{\rho_d^{n+1/2}}{\epsilon_0}
\end{aligned}
$$

Remark: $\Pi_d \cap \partial\Omega$ is not empty only for boundary dual cells.

Discrete electromagnetic energy conservation

The following discrete energy is conserved :

$$\begin{aligned}\mathbf{En}(t^n) &= \frac{\epsilon c^2}{4}\left(\sum_p |P_p| B_p^n B_p^{n+1} + \sum_d |\Pi_d| B_d^n B_d^{n+1}\right) \\ &+ \frac{\epsilon}{2}\sum_f |D_f| \left|\mathbf{E}_f^{n+1/2}\right|^2 .\end{aligned}$$

Stability

The scheme is stable under this CFL-like condition:

$$c\Delta t < min \left[\begin{array}{l} \min_p \max \left[\begin{array}{l} \min_{F_f \in P_p \backslash \partial\Omega} \sqrt{\frac{2|\Phi_f||P_p|\sin\theta_f}{N_p|F_f|(1+|\cos\theta_f|)}} \\ \min_{F_f \in P_p \backslash \partial\Omega} \sqrt{\frac{2|\Phi_f||P_p|\sin\theta_f}{(1+|\cos\theta_f|)|\partial P_p|}} \end{array} \right. \\ \min_d \max \left[\begin{array}{l} \min_{\Phi_f \in \Pi_d} \sqrt{\frac{2|F_f||\Pi_d|\sin\theta_f}{N_d'|\Phi_f|(1+|\cos\theta_f|)}} \\ \min_{\Phi_f \in \Pi_d} \sqrt{\frac{2|F_f||\Pi_d|\sin\theta_f}{(1+|\cos\theta_f|)|\partial\Pi_d|}} \end{array} \right. \end{array} \right.$$

where θ_f is the angle between a primal and a dual side, $N_p(N_d')$ the number of inner sides of a primal (dual) cell and $|\partial P_p|(|\partial\Pi_d|)$ represents the sum of lengths of inner sides of the primal (dual) cell.

In the case of regular cartesian grids, we get the same CFL condition as that of Yee's method ($\frac{c\Delta t}{h} \leq \frac{1}{\sqrt{2}}$).

Numerical results

Radiation from a dipole

We solve Maxwell's system on the domain $\Omega = [-1,1]^2$ with metallic boundary conditions, $\rho = 0$,

$$\mathbf{J} = \left(\omega + 4\, c^2 \frac{2r_0^6 + 2\, r^6 + 4 r_0^2\, r^4 - 7\, r_0^4 r^2)}{\omega(r_0^2 - r^2)^4} \right) \frac{2\, c\, \epsilon_0\, r_0^2\, \cos(\omega t)}{(r_0^2 - r^2)^2}\, \Xi(r)\, \exp\left(\frac{-r^2}{r_0^2 - r^2}\right) \begin{pmatrix} y \\ -x \end{pmatrix}$$

such that,
$r = \sqrt{x^2+y^2}$, $r_0 = \frac{1}{4}$,
$\Xi(r) = 1\, if\, r < r_0\, and\, \Xi(r) = 0\, if\, r \geq r_0$;

and the following initial conditions(with m=1):

$$\begin{aligned} B(0) &= \cos(\pi m x)\, \cos(\pi m y) \\ &+ \frac{4\, c\, r_0^2\, (\, r_0^4 - r^2\, r_0^2 - r^4\,)}{\omega\, (r_0^2 - r^2)^4}\, \Xi(r)\, \exp[\frac{-r^2}{r_0^2 - r^2}] \\ \mathbf{E}(0) &= 0\, . \end{aligned}$$

These functions have strong peaks in the neighborhood of the origin. The tests were performed on non conforming meshes having a refinement ratio of 4. An example of such meshes is given by figure 2. The choice of the ratio is due to a previous numerical study which showed that it is the best for this example.

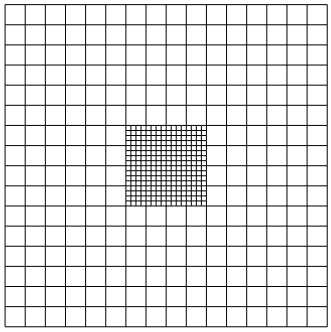

Figure 2: A locally refined mesh (refinement ratio=4)

Figure 3 displays the relative L^2 norm of the electric field error given by

$$e(\mathbf{E}) = \sqrt{\frac{\int_{9T}^{10T} |\mathbf{E} - \Pi\mathbf{E}|_{L^2}^2}{\int_{9T}^{10T} |\Pi\mathbf{E}|_{L^2}^2}},$$

where $\Pi\mathbf{E}$ is a suitable projection of the exact electric field on the diamond mesh. The figure shows a second order convergence. We get also similar results for the magnetic field error.

Incoming wave

Let $\Omega = [\,-1,1\,]^2$, $\rho = 0$, $\mathbf{J} = 0$. We consider a vanishing initial conditions and the following boundary conditions:

$$\begin{aligned} \mathbf{E}\cdot\boldsymbol{\tau} - cB &= 2\sin(\omega t + \frac{\omega}{c})\, ,\ on\ the\ left\ side \\ \mathbf{E}\cdot\boldsymbol{\tau} - cB &= 0\, ,\ on\ the\ right\ side \\ \mathbf{E}\cdot\boldsymbol{\tau} &= 0\, ,\ on\ the\ other\ sides \end{aligned}$$

We let the wave enter during only one period and we observe the magnetic field intensity on a vertex of a cartesian mesh with respect to time. Then we refine locally

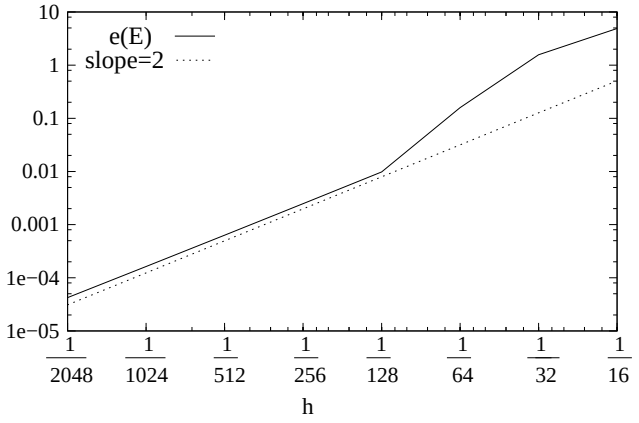

Figure 3: Relative L^2 norm of the electric field error

the mesh like in figure 2 and repeat the test with the same point. Figure 4 shows that, practically, local refinement

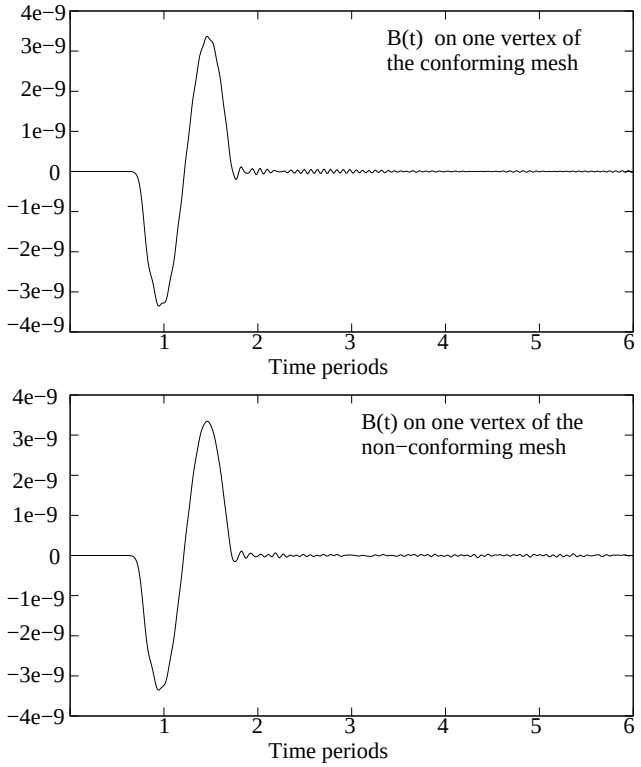

Figure 4: comparison of parasitic reflexions

does not amplify parasitic reflexions.
We repeated the test on different points and meshes, and we get similar results.

Remark

In this paper we considered Maxwell's equations in the vacuum. For benchmarks dealing with inhomogeneous media see [3].

References

[1] K. Domelevo and P. Omnes. "A Finite Volume method for the Laplace equation on almost arbitrary two-dimensional grids". ESAIM:M2AN. Vol. 39, N 6, pp. 1203-1249, 2005.

[2] S. Delcourte, K. Domelevo and P. Omnes. "A discrete duality finite volume approach to Hodge decomposition and div-curl problems on almost arbitrary two-dimensional meshes". Accepted in SIAM J. Numer. Anal. 2007.

[3] F. Hermeline. "A finite volume method for solving Maxwell equations in inhomogeneous media on arbitrary meshes". C. R. Acad. Sci. Paris, Ser. I 339, pp. 893-898. 2004.

[4] F. Hermeline. "Two coupled Particle finite volume methods using Delaunay-Voronoi meshes for the approximation of Vlasov-Poisson and Vlasov-Maxwell equations". J. Comput. Phys., 106, pp.1-18, 1993.

[5] K. S. Yee. "Numerical solution of initial boundary value problems involving Maxwell equations in isotropic media" IEEE Trans. Antennas and propag. 14. pp. 302-307. 1966

[6] R. A. Nicolaides and D.-Q. Wang. "Convergence analysis of a covolume scheme for Maxwell equations in three dimensions". Math. comput. 65. pp. 947-963. 1998.

Finite Element Study of Time-Dependent Maxwell's Equations in Dispersive Media

Jichun Li[†,*], **Yitung Chen**[‡,*]
[†]Dept. of Mathematical Sciences, University of Nevada Las Vegas, Las Vegas, NV 89154-4020, USA
[‡] Dept. of Mechanical Engineering, University of Nevada Las Vegas, Las Vegas 89154-4027, USA
[*]Email: jichun@unlv.nevada.edu

Abstract

In this paper, we consider the time-dependent Maxwell's equations in a bounded domain when dispersive media are involved. Crank-Nicolson scheme is developed to approximate the electric field equation by Nedelec edge elements and is proved to be optimal convergent in energy norm. The analysis is carried out for Debye medium, but the same results hold true for other dispersive media such as plasma and Lorentz medium. Furthermore, our analysis extends straightforward to cases when a dispersive medium and the standard simple medium are coupled.

Introduction

Dispersive electromagnetic media are ubiquitous, examples are human tissue, water, soil, snow, ice, plasma, optical fibers and radar-absorbing materials. Hence the study of electromagnetic wave interacting with dispersive media is a very important topic. Starting early 1990's, there is a growing interest in modeling of Maxwell's equations when dispersive media are involved (see [1, Ch.8] and [2, Ch.9] and references therein). However, most publications are exclusively restricted to the finite-difference time-domain (FDTD) methods due to its much simpler implementation compared to the finite element methods (FEM). In 2001, Jiao and Jin [3] initiated the application of time-domain finite element methods (TDFEM) for dispersive media. To our knowledge, there exists little theoretical analysis of TDFEM for Maxwell's equations in dispersive media except our initial effort in this direction [4], [5], where only first-order in time scheme was discussed. In this paper, we shall continue our initial effort and extend our analysis to the 2nd-order in time scheme (i.e., the Crank-Nicolson scheme). Optimal error estimates are proved for pure dispersive media and cases when dispersive media and the standard simple medium are coupled.

The governing equations

From [5], we can write out the governing equations for the single pole Debye model as follows:

$$\epsilon_0\epsilon_\infty \boldsymbol{E}_{tt} + \nabla \times (\mu_0^{-1}\nabla \times \boldsymbol{E}) + \frac{(\epsilon_s-\epsilon_\infty)\epsilon_0}{t_0}\boldsymbol{E}_t - \frac{(\epsilon_s-\epsilon_\infty)\epsilon_0}{t_0^2}\boldsymbol{E} - \boldsymbol{J}(\boldsymbol{E}) = 0, \quad (1)$$

where we denote ϵ_∞ the permittivity at infinite frequency, ϵ_s the permittivity at DC, t_0 the relaxation time, $\boldsymbol{E}$ the electrical field, and the polarization current

$$\boldsymbol{J}(\boldsymbol{E}) = \frac{(\epsilon_s-\epsilon_\infty)\epsilon_0}{t_0^3}\int_0^t e^{-\frac{t-s}{t_0}}\boldsymbol{E}(\boldsymbol{x},s)ds. \quad (2)$$

We assume the modeling domain is $\Omega \times (0,T)$, where Ω is a bounded Lipschitz polyhedral domain in $\mathcal{R}^3$ with connected boundary $\partial\Omega$. For simplicity, we assume that our model (1) satisfies a perfect conducting boundary condition

$$\mathbf{n} \times \boldsymbol{E} = 0 \quad \text{on} \quad \partial\Omega \times (0,T), \quad (3)$$

and the initial conditions

$$\boldsymbol{E}(\boldsymbol{x},0) = \boldsymbol{E}_0(\boldsymbol{x}), \quad \boldsymbol{E}_t(\boldsymbol{x},0) = \boldsymbol{E}_1(\boldsymbol{x}) \quad \boldsymbol{x} \in \Omega, \quad (4)$$

where $\boldsymbol{E}_0$ and $\boldsymbol{E}_1$ are given functions.

A fully discrete finite element scheme

To design our finite element methods (FEM), we partition Ω by a family of regular tetrahedra meshes T^h with maximum mesh size h. We like to remark that the results can extend to cubic elements without any difficult. Considering the usual low regularity of Maxwell's equations [6], we only employ the lowest order Nédélec edge element [7]: for any $K \in T^h$,

$$\mathbf{V}_h = \{\boldsymbol{v}_h \in H(\text{curl};\Omega) \mid \boldsymbol{v}_h|_K = \boldsymbol{a}_K + \boldsymbol{b}_K \times \mathbf{x}\},$$
$$\boldsymbol{V}_h^0 = \{\boldsymbol{v}_h \in H(\text{curl};\Omega), \boldsymbol{n} \times \boldsymbol{v}_h = 0 \text{ on } \partial\Omega\}. \quad (5)$$

where $\boldsymbol{a}_K, \boldsymbol{b}_K$ are constant vectors in R^3.

For any $\boldsymbol{u} \in H^\alpha(curl;\Omega)$, $\frac{1}{2} < \alpha \le 1$, it is well known [8] that its interpolant $\Pi_h\boldsymbol{u} \in \mathbf{V}_h$ can be defined on each

tetrahedron $K \in T^h$ by the degrees of freedom $\int_e \boldsymbol{u}\cdot\hat{\tau}$ on each edge e of K, where $\hat{\tau}$ is the unit vector along the edge e. Furthermore, for any $\frac{1}{2} < \alpha \le 1$, we have [8, (5.42)]:

$$||\boldsymbol{u}-\Pi_h\boldsymbol{u}||_0+||\nabla\times(\boldsymbol{u}-\Pi_h\boldsymbol{u})||_0 \le Ch^\alpha||\boldsymbol{u}||_{\alpha,\mathrm{curl}}. \quad (6)$$

Denoting by $P_h\boldsymbol{u} \in \boldsymbol{V}_h$ the standard $(L^2(\Omega))^3$-projection, we have

$$||\boldsymbol{u}-P_h\boldsymbol{u}||_0 \le Ch^\alpha||\boldsymbol{u}||_\alpha \quad \forall\boldsymbol{u}\in H^\alpha(\Omega). \quad (7)$$

To define our fully discrete scheme, we divide the time interval $(0,T)$ into M uniform subintervals by points $0 = t_0 < t_1 < \cdots < t_M = T$, where $t_k = k\tau$, and denote the k-th subinterval by $I_k = (t_{k-1}, t_{k+1}]$. Moreover, we define $\boldsymbol{u}^k = \boldsymbol{u}(\cdot, k\tau)$ for $0 \le k \le M$, and denote finite difference operators:

$$\partial_\tau\boldsymbol{u}^k = \frac{\boldsymbol{u}^k-\boldsymbol{u}^{k-1}}{\tau}, \quad \partial_\tau^2\boldsymbol{u}^k = \frac{\partial_\tau\boldsymbol{u}^k-\partial_\tau\boldsymbol{u}^{k-1}}{\tau},$$
$$\delta_{2\tau}\boldsymbol{u}^k = \frac{\boldsymbol{u}^{k+1}-\boldsymbol{u}^{k-1}}{2\tau}, \quad \overline{\boldsymbol{u}^k} = \frac{1}{2}(\boldsymbol{u}^{k+1}+\boldsymbol{u}^{k-1}).$$

Now we can formulate our fully discrete finite element scheme for the electric field equation (1) as follows:

$$\boldsymbol{E}_h^0 = P_h\boldsymbol{E}_0, \quad \boldsymbol{E}_h^1 = \boldsymbol{E}_h^0 + \tau P_h\boldsymbol{E}_t(0) + \frac{\tau^2}{2}P_h\boldsymbol{E}_{tt}(0), \quad (8)$$

and for $k = 1, 2, \cdots, M-1$, find $\boldsymbol{E}_h^k \in \boldsymbol{V}_h^0$ such that

$$\epsilon_0\epsilon_\infty(\partial_\tau^2\boldsymbol{E}_h^k, \boldsymbol{v}) + \mu_0^{-1}(\nabla\times\overline{\boldsymbol{E}_h^k}, \nabla\times\boldsymbol{v})$$
$$+\frac{(\epsilon_s-\epsilon_\infty)\epsilon_0}{t_0}(\delta_{2\tau}\boldsymbol{E}_h^k, \boldsymbol{v}) - \frac{(\epsilon_s-\epsilon_\infty)\epsilon_0}{t_0^2}(\overline{\boldsymbol{E}_h^k}, \boldsymbol{v})$$
$$-(\overline{\boldsymbol{J}}_h^k, \boldsymbol{v}) = 0 \quad \forall\boldsymbol{v}\in\boldsymbol{V}_h^0, \quad (9)$$

where for any $1 \le k \le M$,

$$\overline{\boldsymbol{J}}_h^0 = 0, \ \ \overline{\boldsymbol{J}}_h^k = \frac{1}{2}(1+e^{-\tau/t_0})\boldsymbol{J}_h^{k-1}$$
$$+\frac{(\epsilon_s-\epsilon_\infty)\epsilon_0}{t_0^3}\cdot\frac{\tau}{2}\cdot\frac{1}{2}(e^{-\tau/t_0}\boldsymbol{E}_h^{k-1}+\boldsymbol{E}_h^k), \quad (10)$$

and

$$\boldsymbol{J}_h^0 = 0, \ \ \boldsymbol{J}_h^k = e^{-\tau/t_0}\boldsymbol{J}_h^{k-1}$$
$$+\frac{(\epsilon_s-\epsilon_\infty)\epsilon_0}{t_0^3}\cdot\frac{\tau}{2}(e^{-\tau/t_0}\boldsymbol{E}_h^{k-1}+\boldsymbol{E}_h^k). \quad (11)$$

Here we denote $\boldsymbol{E}_h^k$ the finite element solution of $\boldsymbol{E}$ at time $t = t^k$.

The main results

It is easy to see that (9) has a unique solution for any $\tau \le t_0$ by Lax-Milgram lemma.

To prove our main results, we need the following lemmas, whose proofs will be provided in our full paper.

Lemma 0.1

$$(i)\ \|\partial_\tau\boldsymbol{u}^k\|_0^2 \le \frac{1}{\tau}\int_{t_{k-1}}^{t_k}\|\boldsymbol{u}_t(t)\|_0^2dt,$$
$$(ii)\ \|\overline{\boldsymbol{u}^k} - \frac{1}{2\tau}\int_{t_{k-1}}^{t_{k+1}}\boldsymbol{u}(t)dt\|_0^2 \le 2\tau^3\int_{t_{k-1}}^{t_{k+1}}\|\boldsymbol{u}_{tt}(t)\|_0^2dt,$$
$$(iii)\ \|\delta_{2\tau}\boldsymbol{u}_t^k - \partial_\tau^2\boldsymbol{u}^k\|_0^2 \le 2\tau^3\int_{t_{k-1}}^{t_{k+1}}\|\boldsymbol{u}_{t^4}(t)\|_0^2dt.$$

Lemma 0.2 *Let $\boldsymbol{J}^k \equiv \boldsymbol{J}(\boldsymbol{E}(\cdot,t_k))$ and $\overline{\boldsymbol{J}}_h^k$ be defined by (2) and (10), respectively. Then for any $1 \le k \le M$, we have*

$$|\overline{\boldsymbol{J}}_h^k - \overline{\boldsymbol{J}^k}|^2 \le C[\tau\sum_{l=0}^{k}|\boldsymbol{E}_h^l-\boldsymbol{E}^l|^2 +$$
$$\tau^4\int_0^{t_k}(|\boldsymbol{E}(t)|^2 + |\frac{\partial\boldsymbol{E}}{\partial t}(t)|^2 + |\frac{\partial^2\boldsymbol{E}}{\partial t^2}(t)|^2)dt].$$

Our main result is the following optimal error estimate in the energy norm:

Theorem 0.1 *Let $\boldsymbol{E}$ and $\boldsymbol{E}_h^n$ be the solutions of the electric field equation (1) and the finite element scheme (9) at time t and t^n respectively. Furthermore, we assume that*

$$\boldsymbol{E}, \boldsymbol{E}_t \in L^\infty(0,T;H^\alpha(curl;\Omega)), \boldsymbol{E}_{t^2} \in L^\infty(0,T;L^2(\Omega))$$
$$\boldsymbol{E}_{t^4}, \nabla\times\nabla\times\boldsymbol{E}_{tt} \in L^2(0,T;L^2(\Omega)),$$

Then for any $\tau < t_0/4$, there exists a constant $C = C(T,\epsilon_0,\epsilon_\infty,\mu_0,t_0,\boldsymbol{E})$, independent of both the time step τ and mesh size h, such that

$$max_{1\le n\le M}(\|\partial_\tau\boldsymbol{E}_h^n-\boldsymbol{E}_t^n\|_0+\|\boldsymbol{E}_h^n-\boldsymbol{E}^n\|_{0,curl}) \le C(\tau^2+h^\alpha),$$

Conclusions

In this paper, we develop the Crank-Nicolson scheme for solving the vector wave equation for a single pole Debye model. Optimal error estimates are proved. Similar results hold true for other dispersive media such as plasma and Lorentz model, and cases with coupled dispersive medium and a standard simple medium (such as air). Details will be provided in our forthcoming paper in this conference proceeding.

References

[1] K. Kunz and R.J. Luebbers, The Finite-Difference Time-Domain Method for Electromagnetics, CRC Press, Boca Raton, FL, 1993.

[2] A. Taflove and C. Hagness, Computational Electrodynamics: the Finite-Difference Time-Domain Method, 2nd ed., Artech House, Norwood, MA, 2000.

[3] D. Jiao and J.-M. Jin, Time-domain finite-element modeling of dispersive media, IEEE Microwave and Wireless Components Letters, vol. 11, pp. 220-223, 2001.

[4] J. Li and Y. Chen, Analysis of a time-domain finite element method for 3-D Maxwell's equations in dispersive media, Comput. Methods Appl. Mech. Engrg., vol. 195, pp. 4220-4229, 2006.

[5] J. Li, Error analysis of fully discrete mixed finite element schemes for 3-D Maxwell's equations in dispersive media, Comput. Methods Appl. Mech. Engrg. (in press).

[6] C. Amrouche, C. Bernardi, M. Dauge and V. Girault, Vector potentials in three-dimensional non-smooth domains, Math. Methods Appl. Sci. 21 (1998), 823-864.

[7] J.-C. Nédélec, Mixed finite elements in R^3, Numer. Math. 35 (1980), 315-341.

[8] P. Monk, Finite Element Methods for Maxwell's Equations, Oxford University Press, 2003.

Developing time-domain finite element methods for wave propagation in negative-index materials

Jichun Li[†,*], **Yitung Chen**[‡,*]
[†]Dept. of Mathematical Sciences, University of Nevada Las Vegas, Las Vegas, NV 89154-4020, USA
[‡] Dept. of Mechanical Engineering, University of Nevada Las Vegas, Las Vegas, NV 89154-4027, USA
[*]Email: jichun@unlv.nevada.edu

Abstract

In this paper, we develop a fully-discrete mixed finite element methods for modeling wave propagation in three-dimensional negative-index materials (NIMs). The NIMs model is formed as a time-dependent system involving four dependent vector variables: the electric and magnetic fields, and the induced electric and magnetic currents. Optimal error estimates for all four variables are proved for Nédélec tetrahedral elements.

Introduction

In 1968, Veselago postulated the existence of electromagnetic material in which both permittivity and permeability were negative real values, which result the negative refractive index. Until 2000, such materials were realized in practice by arranging periodic arrays of small metallic wires and split-ring resonators [1], [2]. These artificially structured periodic media have some exotic electromagnetic properties, which open potential applications in diverse areas such as interconnects for wireless telecommunications, radar and defense, nanolithography and medical imaging at subwavelength resolution et al. For more details, readers can consult the special issues [3], [4], [5] and references therein.

In the past several years, some numerical simulations have been performed for negative-index materials (NIMs, which have both negative permittivity and negative permeability) by finite element methods [6], [7]. Such simulation requires the 'ab-initio' numerical solution of Maxwell's equations in the time domain. In this paper we will continue our initial investigation on NIMs [8], where we developed time-domain finite element (TDFE) methods for solving Maxwell's equations involving NIMs. Here we will develop a fully-discrete scheme for solving all four physical variables: the electric and magnetic fields, and the induced electric and magnetic currents. Optimal error estimates are proved for Nédélec tetrahedral elements.

The governing equations

NIMs can be simulated using lossy Drude polarization and magnetization models [9]. The governing equations for modeling wave propagation in NIMs are [8]:

$$\epsilon_0 \frac{\partial \boldsymbol{E}}{\partial t} = \nabla \times \boldsymbol{H} - \boldsymbol{J}, \tag{1}$$

$$\mu_0 \frac{\partial \boldsymbol{H}}{\partial t} = -\nabla \times \boldsymbol{E} - \boldsymbol{K}, \tag{2}$$

$$\frac{1}{\epsilon_0 \omega_{pe}^2} \frac{\partial \boldsymbol{J}}{\partial t} + \frac{\Gamma_e}{\epsilon_0 \omega_{pe}^2} \boldsymbol{J} = \boldsymbol{E}, \tag{3}$$

$$\frac{1}{\mu_0 \omega_{pm}^2} \frac{\partial \boldsymbol{K}}{\partial t} + \frac{\Gamma_m}{\mu_0 \omega_{pm}^2} \boldsymbol{K} = \boldsymbol{H}, \tag{4}$$

where ϵ_0 is the vacuum permittivity, μ_0 is the vacuum permeability, ω_{pe} and ω_{pm} are the electric and magnetic plasma frequencies respectively, Γ_e and Γ_m are the electric and magnetic damping frequencies respectively, $\boldsymbol{E}(\boldsymbol{x}, t)$ and $\boldsymbol{H}(\boldsymbol{x}, t)$ are the electric and magnetic fields respectively, and $\boldsymbol{J}(\boldsymbol{x}, t)$ and $\boldsymbol{K}(\boldsymbol{x}, t)$ are the induced electric and magnetic currents respectively. The complex materials make solving the NIMs model more challenging, since the governing equations can not be reduced to a simple vector wave equation as in vacuum.

For simplicity, we assume that the modeling domain be $\Omega \times (0, T)$, where Ω is a bounded Lipschitz polyhedral domain in $\mathcal{R}^3$ with connected boundary $\partial\Omega$. Furthermore, we assume that the boundary of Ω is perfect conducting so that

$$\mathbf{n} \times \boldsymbol{E} = 0 \quad \text{on } \partial\Omega, \tag{5}$$

where $\mathbf{n}$ is the unit outward normal to $\partial\Omega$. Also we assume that the initial conditions are

$$\boldsymbol{E}(\mathbf{x}, 0) = \boldsymbol{E}_0(\mathbf{x}), \quad \boldsymbol{H}(\mathbf{x}, 0) = \boldsymbol{H}_0(\mathbf{x}),$$
$$\boldsymbol{J}(\mathbf{x}, 0) = \boldsymbol{J}_0(\mathbf{x}), \quad \boldsymbol{K}(\mathbf{x}, 0) = \boldsymbol{K}_0(\mathbf{x}).$$

A time-domain finite element scheme

To design our mixed finite element method, we partition Ω by a family of regular tetrahedral meshes T^h with maxmium mesh size h. Considering the usual low regularity of Maxwell's equations [10], [11], we only employ the lowest order Raviart-Thomas-Nédélec's mixed spaces [12]: for any $K \in T^h$,

$$\boldsymbol{U}_h = \{\boldsymbol{u}_h \in H(\text{div}; \Omega) \mid \boldsymbol{u}_h|_K = \boldsymbol{c}_K + d_K \mathbf{x}\},$$
$$\boldsymbol{V}_h = \{\boldsymbol{v}_h \in H(\text{curl}; \Omega) \mid \boldsymbol{v}_h|_K = \boldsymbol{a}_K + \boldsymbol{b}_K \times \mathbf{x}\},$$

where $\boldsymbol{a}_K, \boldsymbol{b}_K, \boldsymbol{c}_K$ are constant vectors in R^3, and d_K is a real constant.

For any $\boldsymbol{u} \in H^\alpha(curl;\Omega), \frac{1}{2} < \alpha \leq 1$, it is well known [12] that its interpolant $\Pi_h \boldsymbol{u} \in \mathbf{V}_h$ can be defined on each tetrahedron $K \in T^h$ by the degrees of freedom $\int_e \boldsymbol{u} \cdot \tau$ on each edge e of K, where τ is the unit vector along the edge e. Furthermore, we have (see [11] and [13, (5.42)]): for any $\boldsymbol{u} \in H^\alpha(curl;\Omega), \frac{1}{2} < \alpha \leq 1$,

$$||\boldsymbol{u}-\Pi_h\boldsymbol{u}||_0+||\nabla\times(\boldsymbol{u}-\Pi_h\boldsymbol{u})||_0 \leq Ch^\alpha||\boldsymbol{u}||_{\alpha,\text{curl}}. \quad (6)$$

Denoting by $P_h\boldsymbol{u} \in \mathbf{U}_h$ the standard $(L^2(\Omega))^3$-projection, we have

$$||\boldsymbol{u} - P_h\boldsymbol{u}||_0 \leq Ch^\alpha||\boldsymbol{u}||_\alpha \quad \forall \boldsymbol{u} \in H^\alpha(\Omega). \quad (7)$$

To define our fully discrete scheme, we divide the time interval $(0,T)$ into M uniform subintervals by points $0 = t_0 < t_1 < \cdots < t_M = T$, where $t_k = k\tau$, and denote the k-th subinterval by $I_k = (t_{k-1}, t_{k+1}]$. Moreover, we define $\boldsymbol{u}^k = \boldsymbol{u}(\cdot, k\tau)$ for $0 \leq k \leq M$, and denote finite difference operators:

$$\delta_{2\tau}\boldsymbol{u}^k = \frac{\boldsymbol{u}^{k+1} - \boldsymbol{u}^{k-1}}{2\tau}, \quad \overline{\boldsymbol{u}^k} = \frac{1}{2}(\boldsymbol{u}^{k+1} + \boldsymbol{u}^{k-1}).$$

Now we can formulate our fully discrete finite element scheme: for $k = 1, 2, \cdots, M$, find $\boldsymbol{E}_h^k, \boldsymbol{J}_h^k \in \mathbf{U}_h, \boldsymbol{H}_h^k, \boldsymbol{K}_h^k \in \mathbf{V}_h$ such that

$$\begin{aligned}
&\epsilon_0(\delta_{2\tau}\boldsymbol{E}_h^k, \boldsymbol{\phi}_h) - (\nabla \times \overline{\boldsymbol{H}_h^k}, \boldsymbol{\phi}_h) + (\overline{\boldsymbol{J}_h^k}, \boldsymbol{\phi}_h) = 0,\\
&\mu_0(\delta_{2\tau}\boldsymbol{H}_h^k, \boldsymbol{\psi}_h) + (\overline{\boldsymbol{E}_h^k}, \nabla \times \boldsymbol{\psi}_h) + (\overline{\boldsymbol{K}_h^k}, \boldsymbol{\psi}_h) = 0,\\
&\frac{1}{\epsilon_0\omega_{pe}^2}(\delta_{2\tau}\boldsymbol{J}_h^k, \tilde{\boldsymbol{\phi}}_h) + \frac{\Gamma_e}{\epsilon_0\omega_{pe}^2}(\overline{\boldsymbol{J}_h^k}, \tilde{\boldsymbol{\phi}}_h) = (\overline{\boldsymbol{E}_h^k}, \tilde{\boldsymbol{\phi}}_h),\\
&\frac{1}{\mu_0\omega_{pm}^2}(\delta_{2\tau}\boldsymbol{K}_h^k, \tilde{\boldsymbol{\psi}}_h) + \frac{\Gamma_m}{\mu_0\omega_{pm}^2}(\overline{\boldsymbol{K}_h^k}, \tilde{\boldsymbol{\psi}}_h) = (\overline{\boldsymbol{H}_h^k}, \tilde{\boldsymbol{\psi}}_h),
\end{aligned}$$

for any $\boldsymbol{\phi}_h \in \mathbf{U}_h$, $\boldsymbol{\psi}_h \in \mathbf{V}_h$, $\tilde{\boldsymbol{\phi}}_h \in \mathbf{U}_h$, $\tilde{\boldsymbol{\psi}}_h \in \mathbf{V}_h$, subject to the initial conditions

$$\begin{aligned}
&\boldsymbol{E}^h(0) = P_h\boldsymbol{E}_0, \quad \boldsymbol{H}^h(0) = \Pi_h\boldsymbol{H}_0,\\
&\boldsymbol{J}^h(0) = P_h\boldsymbol{J}_0, \quad \boldsymbol{K}^h(0) = \Pi_h\boldsymbol{K}_0.
\end{aligned}$$

Letting $\tilde{\boldsymbol{\phi}}_h = \boldsymbol{\phi}_h$ and $\tilde{\boldsymbol{\psi}}_h = \boldsymbol{\psi}_h$ in the 3rd and 4th equations respectively, then solving for $\boldsymbol{J}_h^{k+1}$ and $\boldsymbol{K}_h^{k+1}$ and substituting the resultants into the 1st and 2nd equations, we obtain

$$\begin{aligned}
&(\frac{\epsilon_0}{\tau} + \frac{\epsilon_0\omega_{pe}^2}{\tau^{-1}+\Gamma_e})(\boldsymbol{E}_h^{k+1}, \boldsymbol{\phi}_h) - (\nabla \times \boldsymbol{H}_h^{k+1}, \boldsymbol{\phi}_h)\\
&\quad = (f(\boldsymbol{E}_h^{k-1}, \boldsymbol{H}_h^{k-1}, \boldsymbol{J}_h^{k-1}), \boldsymbol{\phi}_h)\\
&(\frac{\mu_0}{\tau} + \frac{\mu_0\omega_{pm}^2}{\tau^{-1}+\Gamma_m})(\boldsymbol{H}_h^{k+1}, \boldsymbol{\psi}_h) + (\boldsymbol{E}_h^{k+1}, \nabla \times \boldsymbol{\psi}_h)\\
&\quad = (g(\boldsymbol{E}_h^{k-1}, \boldsymbol{H}_h^{k-1}, \boldsymbol{K}_h^{k-1}), \boldsymbol{\psi}_h).
\end{aligned}$$

Hence the coefficient matrix for the above system with the vector solution $(\boldsymbol{E}_h^{k+1}, \boldsymbol{H}_h^{k+1})'$ can be written as

$$Q \equiv \begin{pmatrix} A & -B \\ B' & C \end{pmatrix},$$

which is non-singular by noticing that the stiffness matrices $A = (\frac{\epsilon_0}{\tau} + \frac{\epsilon_0\omega_{pe}^2}{\tau^{-1}+\Gamma_e})(\mathbf{U}_h, \mathbf{U}_h)$ and $C = (\frac{\mu_0}{\tau} + \frac{\mu_0\omega_{pm}^2}{\tau^{-1}+\Gamma_m})(\mathbf{V}_h, \mathbf{V}_h)$ are symmetric positive definite, the matrix $B = (\nabla \times \mathbf{V}_h, \mathbf{U}_h)$, and the determinant of Q is $\det(Q) = \det(A)\det(C + B'A^{-1}B)$, which is non-zero.

The main results

Our main result is the following optimal error estimate:

Theorem 0.1 *Let $(\boldsymbol{E}^n, \boldsymbol{H}^n)$ and $(\boldsymbol{E}_h^n, \boldsymbol{H}_h^n)$ be the analytic and finite element solutions at time $t = t^n$, respectively. Under the regularity assumption*

$$\begin{aligned}
&\boldsymbol{E}, \boldsymbol{J} \in L^\infty(0,T;(H^\alpha(\Omega))^3),\\
&\boldsymbol{H}, \boldsymbol{K}, \boldsymbol{H}_t, \boldsymbol{K}_t \in L^\infty(0,T;H^\alpha(curl;\Omega)),\\
&\boldsymbol{E}_{tt}, \boldsymbol{H}_{tt}, \boldsymbol{J}_{tt}, \boldsymbol{K}_{tt} \in L^2(0,T;(L^2(\Omega))^3),\\
&\nabla \times \boldsymbol{E}_{tt}, \nabla \times \boldsymbol{H}_{tt} \in L^2(0,T;(L^2(\Omega))^3),
\end{aligned}$$

where $\frac{1}{2} < \alpha \leq 1$, there exists a constant $C = C(T, \epsilon_0, \mu_0, \omega_{pe}, \omega_{pm}, \Gamma_e, \Gamma_m, \boldsymbol{E}, \boldsymbol{H})$, independent of both the time step τ and the mesh size h, such that

$$\begin{aligned}
&\max_{1\leq n\leq M}(||\boldsymbol{E}^n - \boldsymbol{E}_h^n||_0 + ||\boldsymbol{H}^n - \boldsymbol{H}_h^n||_0\\
&+||\boldsymbol{J}^n - \boldsymbol{J}_h^n||_0 + ||\boldsymbol{K}^n - \boldsymbol{K}_h^n||_0) \leq C(\tau^2 + h^\alpha).
\end{aligned}$$

Conclusions

In this paper, we develop a fully-discrete TDFE scheme for solving Maxwell's equations when negative-index materials are involved. Optimal error estimates are proved. Details will be provided in our forthcoming paper in this conference proceeding.

References

[1] A. Shelby, D.R. Smith and S. Schultz, Experimental verification of a negative index of refraction, Science, vol. 292, pp. 489-491, 2001.

[2] D.R. Smith, W.J. Padilla, D.C. Vier, S.C. Nemat-Nasser and S. Schultz, Composite medium with simultaneously negative permeability and permittivity, Phys. Rev. Lett., vol. 84, pp. 4184-4187, 2000.

[3] N. Engheta and R.W. Ziolkowski (eds.), IEEE Trans. Antennas Propag. (Special Issue), Vol. 51, No. 10, Oct. 2003.

[4] T. Itoh and A.A. Oliner (eds.), IEEE Trans. Microw. Theory Tech. (Special Issue), Vol. 53, No.4, April 2005.

[5] J. Pendry (ed.), Optics Express (Focus Issue), Vol. 11, No.7, p. 639-760, April 2003.

[6] P. Kolinko and D.R. Smith, Numerical study of electromagnetic waves interacting with negative index materials, Optics Express, vol. 11, pp. 640-648, 2003.

[7] N. Engheta and R.W. Ziolkowski, A positive future for double-negative metamaterials, IEEE Trans. Microwave Theory and Techniques, vol. 53, pp. 1535-1556, 2005.

[8] J. Li, Error analysis of mixed finite element methods for wave propagation in double negative metamaterials, J. Comp. Appl. Math. (2006), doi:10.1016/j.cam.2006.10.031.

[9] R.W. Ziolkowski, Pulsed and CW Gaussian beam interactions with double negative metamaterial slabs, Optical Express, vol. 11, pp. 662-681, 2003.

[10] C. Amrouche, C. Bernardi, M. Dauge and V. Girault, Vector potentials in three-dimensional non-smooth domains, Math. Methods Appl. Sci., vol. 21, pp. 823-864, 1998.

[11] P. Ciarlet, Jr. and J. Zou, Fully discrete finite element approaches for time-dependent Maxwell's equations, Numer. Math., vol. 82, pp. 193-219, 1999.

[12] J.-C. Nédélec, Mixed finite elements in R^3, Numer. Math. 35 (1980), 315-341.

[13] P. Monk, Finite Element Methods for Maxwell's Equations, Oxford University Press, 2003.

REFLECTION AND TRANSMISSION OF TRANSIENT ACOUSTIC WAVES IN VISCOUS FLUIDS

A. Morro[†,*], **G. Caviglia**[‡,*]
[†]DIBE, University of Genoa, Genova, ITALY
[‡]Department of Mathematics, Genova, ITALY
[*]Email: morro@dibe.unige.it

Abstract

The paper investigates the reflection-transmission process, generated at the interface between two homogeneous half spaces, within the time domain. The governing equations are those for viscous fluids in the acoustic approximation. The incident and reflected waves are homogeneous and propagate in an inviscid fluid, the transmitted waves are inhomogeneous with frequency-dependent amplitudes. By means of Fourier analysis, reflected and transmitted waves are determined, in the time domain, in two cases: normal incidence on a viscous half-space and oblique incidence, beyond the critical angle, on an inviscid half-space.

Introduction

The aim of this paper is to determine the waves produced, at the interface between two homogeneous half spaces, by an oblique incident wave, within the time domain. The governing equations are those for viscous fluids in the acoustic approximation.

The subject is of interest in many respects. First, quite often reflection-transmission (RT) problems are investigated within the frequency domain. For linear problems, the inverse Fourier transform allows us to obtain the results in the time domain. While conceptually such is the case, in practice the inverse Fourier transformation may be quite involved and this gives reason for the relatively few results. Secondly, RT problems associated with a viscous half space cannot be solved directly within the time domain. The analysis within the frequency domain shows that the reflection and transmission coefficients are in fact functions of the frequency. While in general the inverse Fourier transform does not provide a closed-form solution in the time domain, it is of interest to find closed-form solutions in particular conditions or approximations. Thirdly, there is a renewed attention to direct and inverse problems for wave propagation in dissipative media [1].

Upon a general form of the RT problem, we determine the reflected and the transmitted waves, in the time domain, for normal incidence on a viscous half-space and oblique incidence, beyond the critical angle, on an inviscid half-space.

Model and method

Let $\Omega \subseteq \mathbb{R}^3$ be the region occupied by the fluid. Let $\mathbf{x} \in \Omega$ denote the position vector, $\mathbf{u}$ the displacement, $\mathbf{v}$ the velocity, ∇ the gradient operator, μ, λ the viscosity coefficients, $\mathbf{D} = \operatorname{sym} \nabla \mathbf{v}$ the symmetric part of the velocity gradient. Let ρ be the mass density at equilibrium and ϱ the perturbation mass density, $\wp$ the perturbation pressure, $\mathbf{1}$ the unit tensor. In the acoustic approximation, the governing equations are

$$\partial_t \varrho + \rho \nabla \cdot \mathbf{v} = 0,$$

$$\rho \partial_t \mathbf{v} = -\nabla \wp + \mu \nabla \cdot \mathbf{D} + \lambda \nabla (\nabla \cdot \mathbf{v}).$$

Let c^2 be the derivative of the pressure with respect to the mass density. The equation of motion becomes

$$\rho \partial_t^2 \mathbf{u} = \rho c^2 \nabla (\nabla \cdot \mathbf{u}) + \partial_t [(\mu + \lambda) \nabla (\nabla \cdot \mathbf{u}) + \mu \Delta \mathbf{u}].$$

Upon Fourier transformation,

$$\tilde{\mathbf{u}}(\mathbf{x}, \omega) = \int_{-\infty}^{\infty} \mathbf{u}(\mathbf{x}, t) \exp(-i\omega t) dt,$$

we have

$$-\rho \omega^2 \tilde{\mathbf{u}} = [\rho c^2 + i\omega(\mu + \lambda)] \nabla (\nabla \cdot \tilde{\mathbf{u}}) + i\omega \mu \Delta \tilde{\mathbf{u}}.$$

Wave solutions

Two wave solutions are found, say the transverse and the longitudinal waves (see [2], [3]). The transverse wave is characterized by

$$\tilde{\mathbf{u}} = \boldsymbol{\tau} \exp(-i\omega(\xi x + \sigma_\tau z)),$$

$$\boldsymbol{\tau} \cdot \nabla \tilde{u} = 0, \quad \sigma_\tau^2 = -i \frac{\rho}{\omega \mu} - \xi^2.$$

The longitudinal wave is characterized by

$$\tilde{\mathbf{u}} = \mathbf{l} \exp(-i\omega(\xi x + \sigma_l z)),$$

$$\mathbf{l} \times \nabla \tilde{u} = 0, \quad \sigma_l^2 = \frac{1}{c^2} \frac{1}{1 + i\omega(2\mu + \lambda)/\rho c^2} - \xi^2.$$

Both $\boldsymbol{\tau}$ and $\mathbf{l}$ are constant vectors parameterized by ω. The complex wave numbers σ_τ, σ_l are fixed by

$$\Re \sigma_\tau, \Re \sigma_l > 0, \quad \operatorname{sgn} \Im \sigma_\tau, \operatorname{sgn} \Im \sigma_l = -\operatorname{sgn} \omega$$

for forward-propagating waves (and by the opposite sign for backward propagating waves) in the z-direction.

Reflection-transmission problem

The interface $z = 0$ separates an inviscid fluid ($z < 0$) from a viscous fluid ($z > 0$). An incident, homogeneous wave is coming from $z < 0$ and produces a reflected wave, at $z < 0$, and a transverse and a longitudinal wave, at $z > 0$. Denote by the subscripts, or superscripts, I, R, T quantities pertaining to the incident, reflected, and transmitted waves. The solution $\tilde{\mathbf{u}}(\mathbf{x}, \omega)$ takes the form

$$\mathbf{l}_I \exp(-i\omega(\xi_I x + \sigma_I z)) + \mathbf{l}_R \exp(-i\omega(\xi_R x - \sigma_R z)),$$

if $z < 0$, and

$$\boldsymbol{\tau} \exp(-i\omega(\xi_\tau x + \sigma_\tau z)) + \mathbf{l}_T \exp(-i\omega(\xi_l x + \sigma_l z)),$$

if $z > 0$. The continuity of traction and velocity at the interface $z = 0$ implies that the values $\xi_I, \xi_R, \xi_\tau, \xi_l$ coincide; let ξ be the common value. Hence $\sigma_R = \sigma_I$ and

$$\tau_x \xi + \tau_z \sigma_\tau = 0, \quad l_x^T \sigma_l - l_z^T \xi = 0,$$

which follow from the vanishing of $\boldsymbol{\tau} \cdot \nabla \tilde{u}$, $\mathbf{l} \times \nabla \tilde{u}$. Also

$$l_x^I \sigma_I - l_z^I \xi = 0, \quad l_x^R \sigma_I + l_z^R \xi = 0.$$

In addition we have

$$l_z^I + l_z^R = \tau_z + l_z^T,$$
$$\tau_z \sigma_\tau + l_x^T \sigma_l + \xi(\tau_z + l_z^T) = 0,$$

$$\rho_- c_-^2 (l_x^I \xi + l_z^I \sigma_I + l_x^R \xi - l_z^R \sigma_I)$$
$$= (\rho_+ c_+^2 + i\lambda\omega)(l_x^T \xi + l_z^T \sigma_l) + i2\mu\omega(\sigma_\tau \tau_z + \sigma_l l_z^T),$$

the subscripts $\pm$ denoting the limit values as $z \to 0_\pm$. The RT problem amounts to the determination of the five unknowns $\tau_x, \tau_z, l_x^T, l_z^T, l_z^R$, parameterized by l_z^I, ξ, ω. We find that

$$l_z^T = \frac{2\rho_- \sigma_l \omega \mu (\sigma_\tau^2 - \xi^2)}{-i\rho_+\rho_-\sigma_l + i\omega^2\mu^2\sigma_I[(\sigma_\tau^2 - \xi^2)^2 + 4\sigma_l\sigma_\tau\xi^2]} l_z^I,$$

$$l_z^R = \frac{i\rho_+\rho_-\sigma_l + i\omega^2\mu^2\sigma_I[(\sigma_\tau^2 - \xi^2)^2 + 4\sigma_l\sigma_\tau\xi^2]}{i\rho_+\rho_-\sigma_l - i\omega^2\mu^2\sigma_I[(\sigma_\tau^2 - \xi^2)^2 + 4\sigma_l\sigma_\tau\xi^2]} l_z^I$$

$$\tau_z = \frac{4\rho_- \sigma_l \omega \mu \xi^2}{-i\rho_+\rho_-\sigma_l + i\omega^2\mu^2\sigma_I[(\sigma_\tau^2 - \xi^2)^2 + 4\sigma_l\sigma_\tau\xi^2]} l_z^I,$$

and $l_x^T = \xi l_z^T/\sigma_l$, $\tau_x = -\sigma_\tau \tau_z/\xi$.

Since $\tilde{\mathbf{u}}_R(\mathbf{x}, \omega) = \mathbf{l}_R(\omega) \exp[-i\omega(\xi x - \sigma_I z)]$ then $\mathbf{l}_R(\omega) = \tilde{\mathbf{u}}_R(0, \omega)$. Hence, by the inverse Fourier transform we have

$$u_z^R(\mathbf{x}, t) = \int_{-\infty}^{\infty} f(t, x, z; \omega) R(\omega) \tilde{u}_z^I(0, \omega) d\omega,$$

where $f(t, x, z; \omega) = \exp[i\omega(t - \xi x + \sigma_I z)]$. Replacing R with T and σ_I with $-\sigma_T$ gives u_z^T. Two simple cases are now examined which allow us to obtain definite results in the time domain.

Normal incidence on a viscous half-space

The relations for normal incidence follow by letting $\xi = 0$. First we find that $\boldsymbol{\tau} = 0$ and hence only longitudinal waves occur. Moreover, $l_x^T = 0$. The relations for l_z^T, l_z^R reduce to

$$l_z^T = \frac{2\rho_- \sigma_l \omega \mu \sigma_\tau^2}{-i\rho_+\rho_-\sigma_l + i\omega^2\mu^2\sigma_I\sigma_\tau^4} l_z^I,$$

$$l_z^R = \frac{i\rho_+\rho_-\sigma_l + i\omega^2\mu^2\sigma_I\sigma_\tau^4}{i\rho_+\rho_-\sigma_l - i\omega^2\mu^2\sigma_I\sigma_\tau^4} l_z^I.$$

We now investigate the form of the reflection and transmission coefficients

$$R(\omega) = \frac{l_z^R}{l_z^I}(\omega), \qquad T(\omega) = \frac{l_z^T}{l_z^I}(\omega).$$

By replacing l_z^R we have

$$R(\omega) = \frac{1 + \omega^2\mu^2\sigma_I\sigma_\tau^4/\rho_-\rho_+\sigma_l}{1 - \omega^2\mu^2\sigma_I\sigma_\tau^4/\rho_-\rho_+\sigma_l}.$$

Substitution for σ_τ^4/σ_l and some rearrangements yield

$$R(\omega) = \frac{1 - \nu^2|w|^2}{1 + 2\nu w_r + \nu^2|w|^2} - 2i\nu \frac{|w_i| \operatorname{sgn}\omega}{1 + 2\nu w_r + \nu^2|w|^2},$$

where

$$w = \frac{1}{\sqrt{2}}(\sqrt{\sqrt{1+\alpha^2}+1} + i\sqrt{\sqrt{1+\alpha^2}-1}\,\operatorname{sgn}\omega),$$

$$\alpha = \kappa\omega, \quad \kappa = \frac{2\mu + \lambda}{\rho_+ c_+^2}, \quad \nu = \frac{\rho_+ c_+}{\rho_- c_-},$$

and $w_r = \Re w$, $w_i = \Im w$. The dependence of R on $\operatorname{sgn}\omega$ is commented upon in [4], p. 153.

Likewise, by

$$T(\omega) = \frac{2\rho_- c_-}{\rho_- c_- + \rho_+ c_+ w}$$

we obtain

$$T(\omega) = \frac{2(1 + \nu w_r)}{(1 + \nu w_r)^2 + \nu^2 w_i^2} + 2i\nu \frac{|w_i| \operatorname{sgn}\omega}{(1 + \nu w_r)^2 + \nu^2 w_i^2}.$$

The dependence of R and T on ω does not allow a closed-form solution for the reflected and transmitted wave in the time domain. Yet, an interesting result follows if the incident wave allows us to work with band-limited data. In such a case

$$R(\omega) = \frac{1 - \nu}{1 + \nu} + i\frac{\nu\kappa}{(1 + \nu)^2}\omega,$$

$$T(\omega) = \frac{2}{1+\nu} + i\frac{2\nu\kappa}{(1+\nu)^2}\omega.$$

For normal incidence ($\xi = 0$), at $x = 0, z = 0_-$ we have

$$u_z^R(0,t) = \frac{1}{2\pi}\int_{-\infty}^{\infty} \exp(i\omega t) R(\omega)\tilde{u}_z^I(0,\omega)d\omega.$$

Since $i\omega\tilde{u}_z^I(\omega)$ is the Fourier transform of $\dot{u}_z^I$ we obtain

$$u_z^R(0,t) = \frac{1-\nu}{1+\nu}u_z^I(0,t) + \frac{\nu\kappa}{(1+\nu)^2}\dot{u}_z^I(0,t).$$

Likewise we find that, at $z = 0_+$,

$$u_z^T(0,t) = \frac{2}{1+\nu}u_z^I(0,t) + \frac{2\nu\kappa}{(1+\nu)^2}\dot{u}_z^I(0,t).$$

The reflected wave u_z^R and the transmitted wave u_z^T are linear combinations of the incident wave u_z^I and of the time derivative $\dot{u}_z^I$.

Oblique incidence on an inviscid half space

In inviscid fluids only longitudinal waves occur and hence $\boldsymbol{\tau} = 0$. The vector $\mathbf{l}^T$ is subject to $l_x^T\sigma_T - \xi l_z^T = 0$, $\sigma_T = \sigma_l$. Upon substitution for l_x^I, l_x^R, l_z^T and letting $\mu, \lambda = 0, \boldsymbol{\tau} = 0$ we find that

$$l_z^I + l_z^R = l_z^T, \qquad l_z^I - l_z^R = \frac{\rho_+\sigma_I}{\rho_-\sigma_T}l_z^T.$$

Hence we find that the reflection and the transmission coefficients, R and T, are given by

$$R = \frac{\rho_-\sigma_T - \rho_+\sigma_I}{\rho_-\sigma_T + \rho_+\sigma_I}, \quad T = \frac{2\rho_-\sigma_T}{\rho_-\sigma_T + \rho_+\sigma_I}.$$

If σ_T is real, and positive, then R and T are constants, independent of ω, and the passage to the time domain by the inverse Fourier transform is obvious.

Restrict now attention to the incidence beyond the critical angle. Letting $c_+ > c_-$ we assume that $\xi^2 c_+^2 > 1$, which means that the incidence angle is greater than the critical value. The transmitted wave is evanescent and

$$\sigma_T = -i\sqrt{\xi^2 - 1/c_+^2}\,\operatorname{sgn}\omega.$$

As a consequence, R and T depend on ω through the sign. Letting

$$\epsilon = \frac{\rho_+\sigma_I}{\rho_-|\sigma_T|} = \frac{\rho_+ c_+}{\rho_- c_-}\sqrt{\frac{1-\xi^2 c_-^2}{\xi^2 c_+^2 - 1}}$$

we find that

$$R(\omega) = \frac{1 - i\epsilon\operatorname{sgn}\omega}{1 + i\epsilon\operatorname{sgn}\omega}, \qquad T(\omega) = \frac{2}{1+\epsilon^2}(1 - i\epsilon\operatorname{sgn}\omega).$$

Both R and T are parameterized by ξ through ϵ. By applying the inverse Fourier transform to $\tilde{u}_z^R$ and $\tilde{u}_z^T$ we obtain the reflected wave and the transmitted wave in the time domain. Substitution of R, the convolution theorem and some rearrangements yield

$$u_z^R(\mathbf{x},t) = \frac{1-\epsilon^2}{1+\epsilon^2}u_z^I(0, t - \xi x + \sigma_I z) - \frac{1}{\pi}\frac{2\epsilon}{1+\epsilon^2}\int_{-\infty}^{\infty}\frac{1}{\zeta - (t - \xi x + \sigma_I z)}u_z^I(0,\zeta)d\zeta.$$

Hence the reflected wave is plane and homogeneous. The first term is merely proportional to u_z^I, evaluated at the retarded time $t - \xi x + \sigma_I z$. The second term is the Hilbert transform of u_z^I at time $(t - \xi x + \sigma_I z)$.

The transmitted wave is more involved. We find that

$$u_z^T(\mathbf{x},t) = u_z'(\mathbf{x},t) + u_z''(\mathbf{x},t)$$

where

$$u_z'(\mathbf{x},t) = \frac{1}{\pi}\frac{2}{\epsilon^2+1}\int_{-\infty}^{\infty} G(\mathbf{x},t,\zeta)u_z^I(0,\zeta)d\zeta,$$

$$u_z''(\mathbf{x},t) = \frac{1}{\pi}\frac{2\epsilon}{\epsilon^2+1}\int_{-\infty}^{\infty}\frac{1}{t-\zeta}u_z'(\mathbf{x},\zeta)d\zeta$$

where

$$G(\mathbf{x},t,\zeta) = \frac{|\sigma_T|z}{|\sigma_T|^2 z^2 + (t - \zeta - \xi x)^2}.$$

The dependence of G on z shows the spatial decay of the transmitted wave.

References

[1] F.D. Zaman, K. Masood, Z. Muhiameed, "Inverse scattering in multilayer inverse problem in the presence of damping", Appl. Math. Comp., vol. 176, pp. 455-461, 2006.

[2] N.H. Scott, "Inhomogeneous plane waves in compressible viscous fluids", Wave Motion, vol. 22, pp. 335-347, 1995.

[3] Ph. Boulanger, "Energy flux for damped inhomogeneous plane waves in viscoelastic fluids", Wave Motion, vol. 28, pp. 215-225, 1998.

[4] K. Aki, P.G. Richards, Quantitative Seismology, Freeman, San Francisco, 1980.

A UNIFORMLY EXPONENTIALLY STABLE SEMI-DISCRETIZATION FOR AN ABSTRACT WAVE-TYPE SYSTEM

K. Ramdani[†,‡,*], **T. Takahashi**[†,‡,*], **M. Tucsnak**[†,‡,*]
[†]Institut Elie Cartan, University of Nancy 1, Vandoeuvre-les-Nancy, France
[‡]INRIA Lorraine (Research Project CORIDA), Vandoeuvre-les-Nancy, France.
[*]Email: ramdani@loria.fr

Abstract

We propose in this contribution an approximation of a class of exponentially stable infinite dimensional linear systems modelling the damped oscillations of vibrating systems. The systems considered are essentially one-dimensional, since a spectral gap condition is assumed. Our abstract main result shows that, by adding a suitable artificial numerical viscosity term in the scheme, the approximations obtained are uniformly (with respect to the mesh size) exponentially stable. This result is applied to obtain uniformly stable approximations of a non homogeneous string equation.

Introduction

Given two Hilbert spaces H and U, we consider the closed-loop system described by

$$\begin{cases} \ddot{w}(t) + A_0 w(t) + B_0 B_0^* \dot{w}(t) = 0 \\ w(0) = w_0 \\ \dot{w}(0) = w_1 \end{cases} \tag{1}$$

where $A_0 : \mathcal{D}(A_0) \to H$ is a self-adjoint definite-positive operator with compact inverse and where the control operator $B_0 \in \mathcal{L}(U, H)$. The inner product in H is denoted by $\langle \cdot, \cdot \rangle$ and $\| \cdot \|$ stands for the corresponding norm. Assume that the damped system described by (1) is exponentially stable, i.e., there exist $M,\ \alpha > 0$ such that

$$E(t) := \left\{ ||\dot{w}(t)||^2 + ||A_0^{\frac{1}{2}} w(t)||^2 \right\} \leq M e^{-\alpha t} \quad \forall t \geq 0.$$

In order to simulate numerically the infinite dimensional system (A_0, B_0) described by (1), we need to derive finite dimensional approximations (A_{0h}, B_{0h}) of it (obtained for instance by finite element approximations). A natural question that arises in this context is the following: are the obtained semi-discretized (in space) systems uniformly exponentially stable, or, in other words, does their energy decrease exponentially when $t \to \infty$, **uniformly with respect to the discretization parameter** h? Due to the appearance during the discretization process of high frequency spurious modes that are only weakly damped by the feedback law, the answer to the above question can be negative (see [1] for more details).

Several remedies have been proposed in the literature to overcome this difficulty in the context of the control and stabilization of PDE's: Tychonoff regularization [2], mixed finite elements [3], filtering of high frequencies [4] and numerical viscosity method [5], [6].

In this contribution, we propose a uniformly exponentially stable semi-discretized Galerkin approximation of (1) in the particular case where the operator $A_0^{1/2}$ has simple eigenvalues satisfying a gap condition (see equation (2) in Theorem 1 below). The high frequency spurious modes are damped using an artificial numerical viscosity term. Let us emphasize that the construction of uniformly exponentially stable approximations of infinite dimensional systems is particularly crucial when dealing with LQR analysis of vibrating systems (cf. [6]). Indeed, it is one of the main assumptions to ensure the convergence of the discrete Riccatti operators towards the continuous one.

Remark 1 *Because of the gap condition the result of Theorem 1 essentially concerns one-dimensional problems. For higher dimensions, only results concerning specific vibrating systems exist. In particular, we proposed in [7] a uniformly exponentially stable finite difference semi-discretization for the internal stabilization of the Bernoulli-Euler plate equation in a square.*

Statement of the main result

Assume that $(V_h)_{h>0}$ is a sequence of finite dimensional subspaces of $\mathcal{D}\left(A_0^{1/2}\right)$, with $\dim(V_h) = N(h)$. The inner product in V_h is the restriction of the inner product $\langle \cdot, \cdot \rangle$ on H. We define the linear selfadjoint and positive-definite operator $A_{0h} \in \mathcal{L}(V_h)$ by

$$\langle A_{0h}\varphi_h, \psi_h \rangle = \langle A_0^{1/2}\varphi_h, A_0^{1/2}\psi_h \rangle \quad \forall \varphi_h,\ \psi_h \in V_h.$$

We also consider a sequence of subspaces (U_h) of U and we define the approximate operators $B_{0h} \in \mathcal{L}(U_h, V_h)$ by

$$B_{0h} u_h = \widetilde{\pi}_h B_0 u_h \qquad \forall u_h \in U_h,$$

where $\widetilde{\pi}_h$ is the orthogonal projection of H onto V_h.

We also suppose that the family of spaces (V_h) (respectively (U_h)) approximates the space $\mathcal{D}\left(A_0^{1/2}\right)$ (respectively U). More precisely, if π_h denotes the orthogonal projection of $\mathcal{D}\left(A_0^{1/2}\right)$ onto V_h, we suppose that there exist $\theta > 0$, $h^* > 0$ and $C_0 > 0$ such that, for all $h \in (0, h^*)$, we have:

$$\|A_0^{1/2}(\pi_h\varphi - \varphi)\| \leq C_0\, h^\theta \|A_0\varphi\|, \quad \forall \varphi \in \mathcal{D}(A_0),$$

$$\|\pi_h\varphi - \varphi\| \leq C_0\, h^{2\theta} \|A_0\varphi\|, \quad \forall \varphi \in \mathcal{D}(A_0),$$

Moroever, if ρ_h denotes the orthogonal projection of U onto U_h, we assume that

$$\lim_{h\to 0} \rho_h u = u \quad \text{in } U \quad \forall u \in U,$$

$$\|\rho_h B_0^*\varphi - B_0^*\varphi\|_U \leq C_0\, h^{2\theta} \|A_0\varphi\| \quad \forall \varphi \in \mathcal{D}(A_0).$$

The above assumptions are in particular satisfied when using classical finite elements for the approximation of PDE's.

Theorem 1 *Suppose that the above assumptions are satisfied. Moreover, assume that*

1. *$A_0^{1/2}$ has simple eigenvalues*

$$0 < \lambda_1 < \ldots < \lambda_m < \ldots$$

and there exists a constant $\gamma_0 > 0$ such that

$$\lambda_{m+1} - \lambda_m \geq \gamma_0 \quad \forall m \in \mathbb{N}^*. \tag{2}$$

2. *There exists a constant $\beta_0 > 0$ such that*

$$\|B_0^*\varphi\|_U \geq \beta_0 \tag{3}$$

for all normalized (in H) eigenvector φ of $A_0^{1/2}$.

Then the family of systems

$$\begin{cases} \ddot{w}_h + A_{0h} w_h + B_{0h} B_{0h}^* \dot{w}_h + h^\theta A_{0h} \dot{w}_h = 0 \\ w_h(0) = w_{0h} \in V_h \\ \dot{w}_h(0) = w_{1h} \in V_h \end{cases}$$

is uniformly exponentially stable, in the sense that there exist constants $M^*,\ \alpha^*,\ h^* > 0$ (independent of $h,\ w_{0h}$ and w_{1h}) such that for all $h \in (0, h^*)$ and all $t \geq 0$:

$$E_h(t) := \|\dot{w}_h(t)\|^2 + \left\|A_{0h}^{1/2} w_h(t)\right\|^2 \leq M^* e^{-\alpha^* t} E_h(0).$$

Sketch of proof

The first step is to rewrite the semi-discretized system (1) as a first order system on the space $X_h = V_h \times V_h$:

$$\begin{cases} \dot{z}_h(t) = A_h z_h(t) \\ z_h(0) = \begin{bmatrix} w_{0h} \\ w_{1h} \end{bmatrix}. \end{cases} \tag{4}$$

Next, we use the following characterization of uniform stability result given in [8, p. 162].

Theorem 2 *Let $(\mathbb{T}_h)$ be a family of contraction semigroups on a Hilbert space X_h and let (A_h) be the corresponding infinitesimal generators. The family $(\mathbb{T}_h)$ is uniformly exponentially stable if and only if the two following conditions are satisfied:*
i) For all $h \in (0, h^*)$, we have $i\mathbb{R} \subset \rho(A_h)$, where $\rho(A_h)$ denotes the resolvent set of A_h.
ii) $\sup_{h\in(0,h^*),\omega\in\mathbb{R}} \|(i\omega - A_h)^{-1}\|_{\mathcal{L}(X_h)} < +\infty.$

Condition $i)$ in the above Theorem can be easily checked for system (4). To prove condition $ii)$, we use a contradiction argument. Let then (h_n), (ω_n), and (z_n) be three sequences satisfying

$$\|z_n\| = 1 \qquad \forall n \in \mathbb{N}, \tag{5}$$

and

$$\|i\omega_n z_n - A_{h_n} z_n\| \to 0. \tag{6}$$

The main idea is then to decompose z_n into a low frequency wavepacket and a high frequency one. Given two fixed constants $\varepsilon > 0$ and $h^* > 0$, the sets of low and high frequencies respectively denoted $\mathcal{F}_L(h)$ and $\mathcal{F}_H(h)$ are defined for all $0 < h < h^*$as follows:

$$\mathcal{F}_L(h) = \{1 \leq m \leq N(h) \mid h^\theta \lambda_m^2 \leq \varepsilon\},$$

$$\mathcal{F}_H(h) = \{1 \leq m \leq N(h) \mid h^\theta \lambda_m^2 > \varepsilon\}.$$

With this definition, we show that the low frequency eigenelements of the discretized system are "close" to those of the continuous one. In particular, we prove that the gap condition (2) and the observability condition (3) which are the main assumptions in Theorem 1 still hold for the approximate problem **uniformly** for all $0 < h < h^*$ (provided ε is chosen small enough). Therefore, the low frequency part of (z_n) is damped to zero by the feedback control law. On the other hand, we prove using (6) that the artificial numerical viscosity term added in the scheme damps the high frequency part of (z_n). Thus, (z_n) converges to zero, and this contradicts (5).

Application : stabilization of a non homogeneous string

The vibrations of an elastic string of length 1 under a feedback damping supported in a subinterval $[a,b]$ of $[0,1]$ is described by the following system:

$$\begin{cases} \dfrac{\partial^2 w}{\partial t^2} - \dfrac{\partial}{\partial x}\left[p(x)\dfrac{\partial w}{\partial x}\right] + \chi_{[a,b]}\dfrac{\partial w}{\partial t} = 0 \\ w(0,t) = w(1,t) = 0 \quad \forall t \geq 0 \\ w(x,0) = w_0(x) \quad \forall x \in (0,1) \\ \dfrac{\partial w}{\partial t}(x,0) = w_1(x) \quad \forall x \in (0,1), \end{cases}$$

where $\chi_{[a,b]}$ is the characteristic function of $[a,b]$ and where the function describing the heterogeneity of the string $p \in C^1([0,1])$ is supposed to satisfy $p(x) > 0$ for all $x \in [0,1]$. One can check that the above system can be written in the abstract form (1), and that the corresponding operators A_0 and B_0 satisfy the assumptions (2) and (3) of our main result. Consequently, Theorem 1 implies (when using a $\mathbb{P}^1$ finite element approximation) that the solutions w_h of

$$\begin{cases} \langle \ddot{w}_h, \varphi_h \rangle + \left\langle p(x)\dfrac{\partial w_h}{\partial x}, \dfrac{d\varphi_h}{dx} \right\rangle + \displaystyle\int_a^b \dot{w}_h \varphi_h dx \\ \qquad\qquad + h\left\langle p(x)\dfrac{\partial \dot{w}_h}{\partial x}, \dfrac{d\varphi_h}{dx} \right\rangle = 0, \quad \forall \varphi_h \in V_h, \\ w_h(x,0) = w_{0h}(x) \qquad \forall x \in (0,1) \\ \dfrac{\partial w_h}{\partial t}(x,0) = w_{1h}(x) \qquad \forall x \in (0,1) \end{cases}$$

are uniformly exponentially stable.

References

[1] E. Zuazua, "Propagation, observation, and control of waves approximated by finite difference methods", SIAM Review, vol. 47, n 2, pp. 197-243, 2005.

[2] R. Glowinski, C.H. Li, J.-L. Lions, "A numerical approach to the exact boundary controllability of the wave equation. I. Dirichlet controls: description of the numerical methods", Japan J. Appl. Math., vol. 7, n 1, pp. 1-76, 1990.

[3] H.T. Banks, K. Ito, C. Wang, "Exponentially stable approximations of weakly damped wave equations", in Estimation and control of distributed parameter systems, Internat. Ser. Numer. Math., vol. 100, pp. 1-33, Birkhäuser, Basel ,1991.

[4] J.A. Infante, E. Zuazua, "Boundary observability for the space semi-discretizations of the 1-D wave equation", M2AN Math. Model. Numer. Anal., vol. 33, n 2, pp. 407-438, 1999.

[5] L.R. Tcheougoué Tebou, E. Zuazua, "Uniform exponential long time decay for the space semi-discretization of a localy damped wave equation via an artificial numerical viscosity", Numerische Math., vol. 95, n 3, pp. 563-598, 2003.

[6] K. Ramdani, T. Takahashi, M.Tucsnak, "Uniform exponential long time decay for the space semi-discretization of a localy damped wave equation via an artificial numerical viscosity", ESAIM COCV, to appear.

[7] K. Ramdani, T. Takahashi, M.Tucsnak, "Internal stabilization of the plate equation in a square : the continuous and the semi-discretized problems", J. Math. Pures Appl., vol 85, 17-37, 2006.

[8] Z. Liu, S. Zheng, Semigroups associated with dissipative systems, Chapman & Hall/CRC, Boca Raton, 1999.

TIME-DOMAIN SIMULATION OF FUNCTIONS AND DYNAMICAL SYSTEMS OF BESSEL TYPE

K. Trabelsi[†,*], **T. Hélie**[‡,*], **D. Matignon**[†,*]
[†]GET Télécom Paris, TSI dept. & CNRS UMR 5141. 37-39 rue Dareau, 75014 Paris, France
[‡]Ircam, Centre Pompidou, Analysis/Synthesis team & CNRS UMR 9912. 1 place Stravinsky, 75004 Paris, France.
[*]Email: karim.trabelsi@enst.fr, thomas.helie@ircam.fr, denis.matignon@enst.fr
[*] Work supported by the CONSONNES project, ANR-05-BLAN-0097-01.

Abstract

Two methods are investigated for the time-domain simulation of functions and dynamical systems of Bessel type, involved in wave propagation (see *e.g.* [1], [8], [2]). Both are based on complex analysis and lead to finite-dimensional approximations. The first method relies on optimized parametric contours and provides asymptotic convergence rates. The second is based on cuts and integral representations, whose approximations prove efficient, even at low orders, using ad hoc frequency criteria.

1 Model under study

For $\Re\mathrm{e}(s) > -\varepsilon$, let $\widehat{J^\varepsilon}(s) = [(s+\varepsilon)^2+1]^{-1/2}$ be the Laplace transform of $J^\varepsilon(t) = \mathrm{e}^{-\varepsilon t}\, J_0(t)$ for $t \geq 0$ (cf. [3]). The general formula can be derived:

$$J^\varepsilon(t) = \frac{1}{2i\pi}\int_{\mathbb{R}} \mathrm{e}^{\gamma(u)\,t}\widehat{J^\varepsilon}(\gamma(u))\,\gamma'(u)\,\mathrm{d}u, \qquad (1)$$

where the $\mathcal{C}^1$ parametrization $u \mapsto \gamma(u)$ defines a curve $\mathcal{C}$ which encloses all the singularities of $\widehat{J^\varepsilon}$: poles, branching points and cuts. In the case $\gamma(u) = \sigma + 2i\pi u$ for $\sigma > 0$, we recover the standard Bromwich formula.

2 Optimized parametrized Bromwich contours

In this section, we approximate $J^\varepsilon(t)$ on an interval $[t_0, t_1]$ following Talbot's approach, [11]. More precisely, we use two parametrized Bromwich contours proposed in [12], either the parabola $\gamma(u) = \mu(iu+1)^2 + \beta$, or the hyperbola $\gamma(u) = \mu(1+\sin(iu-\alpha)) + \beta$ where $u \in]-\infty, \infty[$, $\mu > 0$ regulates the width of the contours, β determines their foci, and α defines the hyperbola's asymptotic angle. The motivation for these choices is their simplicity and suitability for a trapezoidal approximation of (1) by:

$$J^\varepsilon_{h,N}(t) = \frac{h}{2i\pi}\sum_{n=-N}^{N} \mathrm{e}^{\gamma(nh)t}\widehat{J^\varepsilon}(\gamma(nh))\,\gamma'(nh). \qquad (2)$$

Indeed, one can assess the discretization errors by classical techniques (see [7], [10, § 3.2]) to obtain, for all $t \geq 0$,

$$|J^\varepsilon(t) - J^\varepsilon_{h,\infty}(t)| \leq E_d^-(t) + E_d^+(t) \text{ with } E_d^\pm = \frac{M^\pm(t)}{\mathrm{e}^{2\pi c^\pm/h} - 1},$$

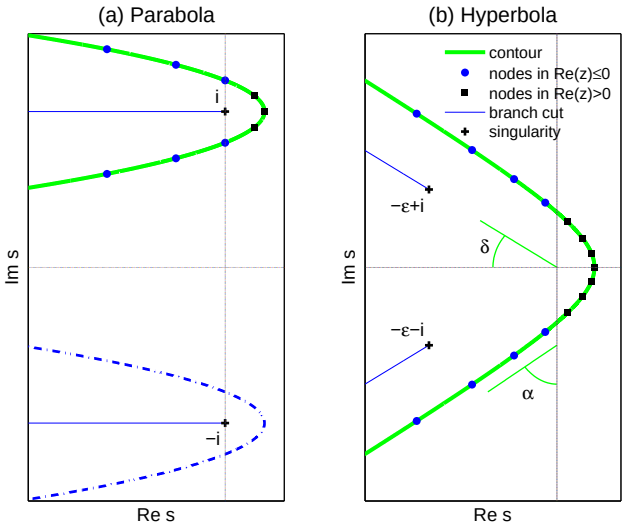

Figure 1: Parametrized Bromwich contours. (a) left: parabolas; (b) right: hyperbola.

owing to the holomorphic extension of the integrand in (1) to $\mathcal{U} = \{u \in \mathbb{C} : -c^- < \Im(u) < c^+\}$ (see [12, Th. 2.1]). For a given (t_0, t_1, N), the parameters μ, h and a range $]\alpha^-, \alpha^+[$ for α are derived in [12, § 3, 4] by asymptotically balancing the discretization errors $E_d^\pm$, and the truncation error E_t which is assumed to behave like the magnitude of the last term in (2), that is, $\mathcal{O}(|h\mathrm{e}^{\gamma(Nh)t}\widehat{J^\varepsilon}(\gamma(Nh))\gamma'(Nh)|)$. Parameter β is assumed to have a small real part.

2.1 *An optimized parabolic contour*

One way to simulate the Bessel function J^ε is to consider it as the *convolution* of the two functions $j^\varepsilon_\pm(t) = \mathcal{L}^{-1}[1/\sqrt{s+\varepsilon \mp i}] = (\pi t)^{-1/2}\mathrm{e}^{(\pm i-\varepsilon)t}$. The function j^ε_+ can be represented using a parabolic contour adapted to the cut $i - \varepsilon + \mathbb{R}^-$ (j^ε_- is straightforwardly inferred by hermitian symmetry, see Fig. 1a). However, two problems arise: first, the theoretical L^∞-error (see [12, §4])

$$E_N \triangleq \sup_{t\in[t_0,t_1]} |j^\varepsilon_\pm(t) - j^\varepsilon_{\pm,h,N}| = \mathcal{O}(\mathrm{e}^{-2\pi N/\sqrt{8\Lambda+1}}), \qquad (3)$$

where $\Lambda = t_1/t_0$, is not matched numerically. Nevertheless, this relation is recovered by taking $t_0' = 4\,t_0$, as observed in Fig. 2 (a possible reason could be the singularity

of $j_{\pm}^{\varepsilon}$ at $t = 0^+$). Second, numerical convolution fails for

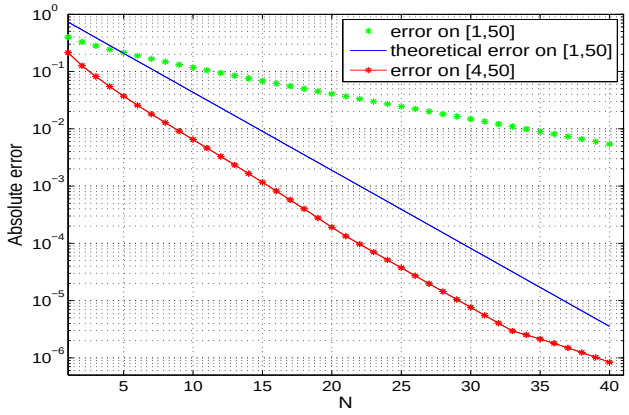

Figure 2: Approximation of $j_{\pm}^{0}$ for $(t_0, t_1) = (1, 50)$. Theoretical (-) and numerical (.,*) errors.

lack of information on the interval $[0, t_0[$ and badly approximated values on $[t_0, t_0']$. Using hyperbolic contours for J^{ε} will help cope with both these problems, due to the decomposition into *singular* functions $j_{\pm}^{\varepsilon}$.

2.2 An optimized hyperbolic contour

Here, we adopt the hyperbolic contour Fig. 1b, which is appropriate for our model problem, since the singularities lie in a *sectorial* region. In this case, the optimal convergence rate is:

$$E_N = \mathcal{O}(\mathrm{e}^{-B(\alpha,\Lambda)N}), \quad \alpha \in]\pi/4 - \delta/2, \pi/2 - \delta[, \quad (4)$$

where δ defines the sector the singularities lie in (see Fig. 1b) and B behaves like $(1/\ln\Lambda)$ for large Λ (see [12, § 4]). Further numerical simulations show that optimizing B w.r.t. α divides the rate by 10 at most, compared to the choice: $\alpha = \pi/4 - \delta/2 + 0$.

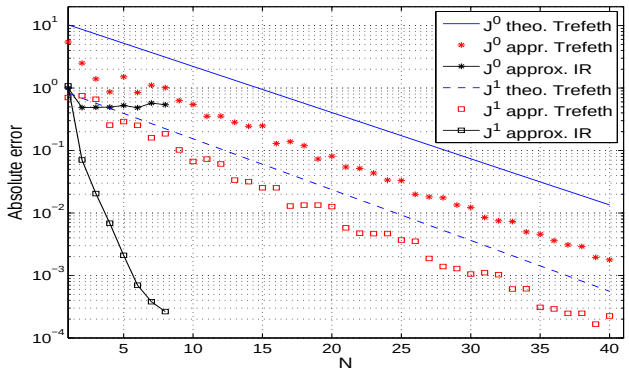

Figure 3: Approximation of $J_0(t)$ for $t \in [1, 5]$, and of $J^1(t)$ for $t \in [0.1, 50]$. Theoretical and numerical errors.

Figure 3 shows that the greater ε, the better the approximation: as ε gets smaller, the asymptotic sector widens; therefore, to yield comparable convergence rates in (4), one needs to take $\Lambda^{\varepsilon=1} = 100\,\Lambda^{\varepsilon=0}$. For $\varepsilon = 1$, β is zero, while for $\varepsilon = 0$, β has to be tuned heuristically, with a small real part (here, $\beta = 0.25$).

Improvements brought by hyperbolic over parabolic contours are yet unsufficient: a lingering problem is due to the nodes with a *positive* real part, which prevent simulation for $t \geq t_1$ (exponential divergence). This is tackled by the exact and approximated integral representations.

3 Optimal integral representations

The transfer function $\widehat{J^{\varepsilon}}(s)$ is analytic in the Laplace domain $\Re\mathrm{e}(s) > -\varepsilon$. In this section, we consider analytic continuations $\widehat{J_{\theta}^{\varepsilon}}$ of $\widehat{J^{\varepsilon}}$ over $\mathbb{C} \setminus (\mathcal{C}_{\theta} \cup \overline{\mathcal{C}_{\theta}})$, with the cuts $\mathcal{C}_{\theta} = \left(i - \varepsilon + \mathrm{e}^{i\theta}\mathbb{R}^{+}\right)$ and $\overline{\mathcal{C}_{\theta}}$, and $\widehat{J_{\theta}^{\varepsilon}}$ defined by:

$$\begin{aligned} \widehat{J_{\theta}^{\varepsilon}}(s) &= \frac{1}{\sqrt[(\theta)]{s+\varepsilon-i}\ \sqrt[(2\pi-\theta)]{s+\varepsilon+i}}, \quad (5) \\ \sqrt[(\theta)]{\rho\,\mathrm{e}^{i\phi}} &= \sqrt{\rho}\,\mathrm{e}^{i\phi/2}, \text{ if } \rho \geq 0,\ \phi \in]\theta - 2\pi, \theta[. \end{aligned}$$

3.1 Principle

For $u \geq 0$, let $\gamma_u = i - \varepsilon + \mathrm{e}^{i\theta}u$ be a parametrization of $\mathcal{C}_{\theta}$. Function $\widehat{J_{\theta}^{\varepsilon}}(s)$ has hermitian symmetric decomposition $\left(\widehat{J_{\theta}^{\varepsilon^+}}(s) + \overline{\widehat{J_{\theta}^{\varepsilon^+}}(\overline{s})}\right)/2$, with integral representation:

$$\begin{aligned} \widehat{J_{\theta}^{\varepsilon^+}}(s) &= \int_{\mathcal{C}_{\theta}} \frac{\mu_{\theta}(\gamma)}{s-\gamma}\,\mathrm{d}\gamma = \int_{\mathbb{R}^+} \frac{\mu_{\theta}(\gamma(u))}{s-\gamma(u)}\gamma'(u)\,\mathrm{d}u, \\ \mu_{\theta}(\gamma_u) &= \lim_{\eta\to 0^+} \frac{H_{\theta}(\gamma_u + i\gamma_u'\eta) - H_{\theta}(\gamma_u - i\gamma_u'\eta)}{2i\pi} \\ &= \left[\pi\sqrt{u}\ \sqrt[(\theta)]{2i + \mathrm{e}^{i\theta}u}\right]^{-1} \mathrm{e}^{i\frac{\pi-\theta}{2}} \quad (6) \end{aligned}$$

which fulfills the well-posedness criterion (see e.g. [6]):

$$\int_{\mathcal{C}_{\theta}} \left|\frac{\mu(\gamma)\,\mathrm{d}\gamma}{1-\gamma}\right| \triangleq \int_{\mathbb{R}^+} \left|\frac{\mu(\gamma_u)}{1-\gamma_u}\gamma_u'\right| \mathrm{d}u < \infty.$$

These systems are approximated by the finite-dimensional models:

$$\widetilde{H}_{\mu}(s) = \frac{1}{2}\sum_{k=0}^{K}\left[\frac{\mu_k}{s-\gamma_k} + \frac{\overline{\mu_k}}{s-\overline{\gamma_k}}\right], \quad (7)$$

where γ_k are a finite set of poles located on the cut $\mathcal{C}_{\theta}$. For a given location (so far, only a *heuristic* approach based on Bode diagrams is being used), the weights μ_k are optimized for the weighted least-squares criterion:

$$\mathcal{C}(\mu) \triangleq \int_{\mathbb{R}^+} \left|\widetilde{H}_{\mu}(2i\pi f) - \widehat{J^{\varepsilon}}(2i\pi f)\right|^2 w(f)\,\mathrm{d}f, \quad (8)$$

with the weight $w(f) = 1_{[f^-,f^+]}(f)/(f\,|\widehat{J^\varepsilon}(2i\pi f)|^2)$. The latter takes into account a bounded frequency range, a logarithmic frequency scale, and a relative error measurement (see [6] for details). Note that the Laplace transform of (2) is of the form (7) with $\gamma_k = \gamma(kh)$ and $\mu_k = 2h\,\gamma'(kh)\,\widehat{J^\varepsilon}\big(\gamma(kh)\big)$ for $0 \le k \le K = N$.

3.2 Numerical results

We consider four cases: **(C1)** J^0 with $\theta = \pi$, **(C2)** J^1 with $\theta = \pi$, **(C3)** J^0 with $\theta = \frac{\pi}{2}$, **(C4)** J^1 with $\theta = \alpha + \frac{\pi}{2}$. Results are presented on Fig. 4 for poles ($1 \le K \le 8$) on $\mathcal{C}_\theta$ with log-spaced u from $u_{min} = 5.10^{-4}$ to $u_{max} = 5.10^{3}$.

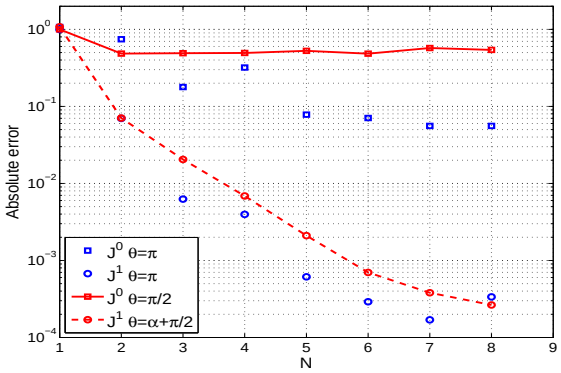

Figure 4: Approximations of J^0 and J^1 for various cuts ($\theta \approx \frac{\pi}{2}$ and $\theta = \pi$). Numerical errors.

Comparisons are also displayed in Fig. 3 for **(C3)** and **(C4)**. Note that horizontal cuts (i.e. $\theta = \pi$) improve the approximations significantly.

Conclusion and Perspectives

The first method seems appealing because of the a priori convergence rate, but this is only asymptotic. Other drawbacks are: sensitivity of the parameters of the contours, and existence of unstable nodes preventing long-range time simulation. On the contrary, the second method gives stable approximate systems, and the criterion used to build them is very flexible, user-designed; still, no theoretical convergence rate seems to be available, but low-order results can be very good.

Both these methods need to be tested on a wider family of transfer functions (see [3, chap. 4]). The role of the parameters in the first method has to be investigated more thoroughly and systematically. Another direction of research to be pursued in the near future is to compare our results with other techniques, based on Gauss-Legendre quadature points in the evaluation of the integral representation, which also have some very useful a priori error estimates, see e.g. [4].

References

[1] J. Audounet, D. Matignon, and G. Montseny. Perfectly absorbing boundary feedback control for wave equations: a diffusive formulation. In 5th *Waves conf.*, p. 1025–1029, Santiago de Compostela, Spain, July 2000. INRIA, SIAM.

[2] M. Duran, I. Muga, and J.-C. Nédélec. The Helmholtz equation in a locally perturbed half-plane with passive boundary. *IMA J. Appl. Math.*, 71 (2006), no. 6, 853–876.

[3] D. G. Duffy. *Transform methods for solving partial differential equations*. CRC Press, 1994.

[4] L. Greengard and P. Lin. Spectral approximation of the free-space heat kernel. *Appl. Comput. Harmonic Anal.*, 9(83), 2000.

[5] Th. Hélie and D. Matignon. Numerical simulation of acoustic waveguides for Webster-Lokshin model using diffusive representations. In 6th *Waves conf.*, p. 72–77, Jyväskylä, Finland, July 2003. INRIA.

[6] Th. Helie and D. Matignon. Representations with poles and cuts for the time-domain simulation of fractional systems and irrational transfer functions. *Signal Processing*, 86:2516–2528, jul 2006.

[7] P. Henrici. *Applied and computational complex analysis*, vol. 2. Wiley Interscience, 1977.

[8] D. Levadoux and G. Montseny. Diffusive realization of the impedance operator on circular boundary for 2D wave equation. In 6th *Waves conf.*, p. 136–141, Jyväskylä, Finland, July 2003. INRIA.

[9] D. Matignon. Stability properties for generalized fractional differential systems. *ESAIM: Proceedings*, 5:145–158, December 1998.

[10] F. Stenger. Numerical methods based on Whittaker cardinal, or sinc functions. *SIAM Rev.*, 23(2):165–224, 1981.

[11] A. Talbot. The accurate numerical inversion of Laplace transforms. *J. Inst. Math. Appl.*, 23(1):97–120, 1979.

[12] J. A. C Weideman and L. N. Trefethen. Parabolic and hyperbolic contours for computing the Bromwich integral. *Math. Comput.*, 2007. to appear.

Water Waves

Wave scattering by a circular ice floe of variable thickness and non-zero draught

L. G. Bennetts*, **N. R. T. Biggs**, **D. Porter**
Department of Mathematics, University of Reading, Reading, UK.
*Email: l.g.bennetts@rdg.ac.uk

Abstract

The problem of water wave scattering by a circular ice floe is considered under the assumptions of linear and time harmonic motions. Combining a Rayleigh-Ritz approximation of the vertical motion with a variational principle generates an approximation that may be made arbitrarily close to the full linear solution. This method allows for the introduction of axisymmetric variations in the thickness of the ice and bed shape, as well as the addition of submergence. A Fourier cosine expansion of the azimuthal coordinate simplifies the governing equations of the approximation to a finite set of ODEs. Numerical results are given to show the effect of the axisymmetric variations and submergence.

Introduction

Wave scattering by a circular ice floe has been considered previously (see, for example, [1]) but with the restrictions that the floe rests fictitiously on the fluid surface and has a constant thickness. Following [2], the problem in which axisymmetric variations and a physically correct draught are admitted is reformulated as a variational principle, and a Rayleigh-Ritz style approximation is generated through restriction of the vertical motion to a finite dimensional space. This creates a process of vertical averaging, which eliminates the vertical coordinate from the governing equations of the approximation. By selecting a suitably large dimension to represent the vertical motion, approximations may be obtained to an arbitrary degree of accuracy. Furthermore, a Fourier cosine expansion of the azimuthal coordinate leaves only a finite set of ODEs in the radial coordinate to be solved.

Formulation and solution method

All horizontal dependence is defined in terms of the polar coordinates (r,θ) that originate from the centre of the floe and we denote the radius of the ice floe to be R. To define the vertical structure of the geometry we use the cartesian coordinate z, which is directed upwards with its origin set to coincide with the equilibrium position of the unloaded fluid surface. For $r<R$, the undisturbed lower surface of the ice is given by the function $z=-d(r)$ and the thickness of the ice by $D=D(r)$. For $r>R$ the fluid is unloaded ($d=D=0$) and extends to infinity in all horizontal directions. The fluid is bounded below by a fixed, impermeable bed $z=-h(r)$, which is permitted to undulate only beneath the ice cover.

Under the usual assumptions of linear wave theory and the imposition of harmonic time dependence $\mathrm{e}^{-\mathrm{i}\omega t}$, the reduced velocity potential $\phi=\phi(r,\theta,z)$ must satisfy Laplace's equation in the fluid domain, the bed condition on $z=-h$ and the free-surface condition on $z=0$ for $r>R$. The fluid motion induces the periodic transverse oscillations $\eta(r,\theta)\mathrm{e}^{-\mathrm{i}\omega t}$ in the ice floe from its equilibrium position. Assuming these oscillations to be sufficiently small that linear theory applies and modelling the ice as a thin, elastic plate, we obtain the conditions

$$\nabla^2(\beta\nabla^2\eta)+F\eta-\phi=0,\ \nabla d.\nabla\phi+\phi_z=\kappa\eta\ \ (z=-d), \tag{1}$$

where ∇ denotes the horizontal Laplacian and $F\eta\equiv\{1-\kappa\alpha-\frac{1}{r^2}(1-\nu)(r\beta_r\partial_{rr}+r\beta_{rr}\partial_r+\beta_{rr}\partial_{\theta\theta})\}\eta$. These equations respectively represent the equation of motion of the plate and the kinematic condition at the water-ice interface. The various quantities appearing in these equations are defined as $\kappa=\omega^2/g$, $\alpha(r)=\kappa\rho_i D(r)/\rho_w$ and $\beta(r)=ED^3(r)/12\rho_w g(1-\nu^2)$, where ν is Poisson's ratio for ice, $\rho_w g\beta$ is its flexural rigidity and E is Young's modulus; ρ_i and ρ_w are respectively the densities of the ice and the fluid.

Forcing is induced by a plane wave, ϕ_I, and the scattered wave, ϕ_S, is subject to the Sommerfeld radiation condition. The full solution in the free surface region is therefore $\phi=\phi_I+\phi_S$, and it can be shown that $\phi_I=\phi_{I,0}w_0^{(0)}(z)$, where

$$\phi_{I,0}(r,\theta)=\mathrm{J}_0(k_0^{(0)}r)+2\sum_{m=1}^{\infty}\mathrm{i}^m\mathrm{J}_m(k_0^{(0)}r)\cos(m\theta),$$

and $\phi_S(r,\theta,z)=\sum_{n=0}^{\infty}\phi_{S,n}(r,\theta)w_n^{(0)}(z)$, where

$$\begin{aligned}\phi_{S,n}(r,\theta) &= B_{n,0}\mathrm{H}_0(k_n^{(0)}r)\\ &\quad+2\sum_{m=1}^{\infty}\mathrm{i}^m B_{n,m}H_m(k_n^{(0)}r)\cos(m\theta).\end{aligned}$$

Here $w_n^{(0)}=\cosh\{k_n^{(0)}(z+h)\}$, and J_m and H_m are respectively Bessel functions and Hankel functions of the

first kind. The quantities $k_n^{(0)}$ are the roots of the free surface dispersion relation $k^{(0)} \tanh k^{(0)} h = \kappa$, arranged such that $k_0^{(0)}$ is real and positive, which provides propagating waves. The roots $k_n^{(0)}$ $(n = 1, \dots)$ lie on the imaginary axis and are ordered in increasing magnitude, representing increasingly rapidly decaying evanescent waves. The amplitudes $B_{n,m}$ $(m, n = 0, \dots)$ are constants to be found as part of the solution process.

To ease the numerical calculations, we assume that there is a positive value $\epsilon < R$ for which, within the disc $r < \epsilon$, the ice is of constant thickness and the bed is flat. The solution within this region may be expressed as $\phi(r, \theta, z) = \sum_{n=0}^{\infty} \phi_n(r, \theta) w_n(z)$, where

$$\phi_n = A_{n,0} \mathcal{J}_{n,0}(r) + 2 \sum_{m=1}^{\infty} \mathrm{i}^m A_{n,m} \mathcal{J}_{n,m}(r) \cos(m\theta)$$

and $w_n = \cosh\{k_n(z + h)\}$. Here, the function

$$\mathcal{J}_{n,m}(r) \equiv \mathrm{J}_m(k_n r) + \varrho_{n,1} \mathrm{J}_m(\mu_1 r) + \varrho_{n,2} \mathrm{J}_m(\mu_2 r),$$

and the quantities k_n $(n = 0, \dots)$ are the roots of the dispersion relation

$$(1 - \alpha + \beta k^4) k \tanh k(h - d) = \kappa, \qquad (2)$$

ordered in the same manner as the free-surface case. The quantities μ_j $(j = 1, 2)$ are also roots of the dispersion relation but are (typically) complex and $\varrho_{n,j}$ $(j = 1, 2)$ are known weights. These values define waves that (typically) oscillate as well as attenuate. The amplitudes $A_{n,m}$ $(m, n = 0, \dots)$, like $B_{n,m}$, are unspecified constants. The corresponding displacement function η may be easily obtained from the interfacial conditions (1).

The governing equations are the natural conditions of Hamiltonian formulation of the problem as the variational principle, using functionals given in [2]. The continuity of fluid pressure and velocity beneath the ice edge is ensured by an interfacial functional. Additionally, through the variational principle we derive ice edge conditions that dictate no flow through the submerged portion of the ice edge and vanishing of the bending moment and shearing stress. At the internal interface $(r = \epsilon)$ the stationary value must satisfy a set of essential and natural conditions related to the continuity of the variables ψ and χ at that point, where the natural conditions are provided by the variational principle.

An approximation to the stationary point (ϕ, η) may be obtained by confining the dependence of the vertical coordinate, z, in the variational principle to a finite dimensional space and seeking the stationary point over this restricted space. An approximation to the displacement function, $\chi \approx \eta$, is then produced indirectly. Motivated by the forms of the full linear solutions in $r > R$ and $r < \epsilon$, we employ the approximation $\phi \approx \psi_N$, where

$$\psi_N(r, \theta, z) \equiv \sum_{n=0}^{N} \varphi_n(r, \theta) w_n(r, z) \quad (r < R),$$

and similarly $\psi_N(r, \theta, z) \equiv \sum_{n=0}^{N} \varphi_n^{(0)}(r, \theta) w_n^{(0)}(z)$ for $r > R$. The vertical modes $w_n(r, z) = \cosh\{k_n(r)(z + h(r))\}$ generalise those that appeared previously in $r < \epsilon$ to variable geometry so that, in the annulus of varying geometry $(\epsilon < r < R)$, the functions $k_n(r)$ $(n = 0, \dots)$ satisfy the dispersion relation (2) generated by the particular vertical structure at each radial value. It is therefore expected that φ_0 will represent modulated propagating waves and φ_n $(n = 1, \dots)$ the evanescent waves that are activated at the sources of scattering.

By restricting the vertical motion in the variational principle we generate a $(2N + 6)$-dimensional set of governing equations, independent of z, to be satisfied by the unknown functions φ_n and χ and a $(2N + 2)$-dimensional set of equations to be satisfied by $\varphi_n^{(0)}$, with corresponding matching conditions. The dimension of the approximation, N, may be increased to achieve an arbitrary degree of accuracy.

In the ice-free region it can be shown that the form of $\varphi_n^{(0)}$ is identical to $\phi_{I,0} + \phi_{S,n}$. Similarly, in the disc of uniform ice-cover $(r < \epsilon)$ we find that the form of φ_n is identical to ϕ_n but with the dimension-dependent quantities $\tilde{\mu}_j$ and $\tilde{\varrho}_{n,j}$ replacing $\varrho_{n,j}$ and μ_j respectively. A corresponding expression for χ in the disc $r < \epsilon$ may be deduced straightforwardly.

We therefore have analytic forms for the approximations in regions of uniform geometry, defined up to a set of unknown amplitudes. Consistent with these forms, we expand the azimuthal dependence of the unknown functions in the annulus of varying geometry in a Fourier cosine series, with

$$\varphi_n(r, \theta) = \varphi_{n,0}(r) + 2 \sum_{m=1}^{\infty} \mathrm{i}^m \varphi_{n,m}(r) \cos(m\theta),$$

and $\chi(r, \theta) = \chi_0(r) + 2 \sum_{m=1}^{\infty} \mathrm{i}^m \chi_m(r) \cos(m\theta)$. Our objective is now to find functions $\varphi_{n,m}$ $(n = 1, \dots, N)$ and χ_m $(m = 0, \dots)$, as well as the unknown amplitudes.

Due to the axisymmetry of the geometry the governing equations of the approximation decouple to leave a $(2N + 6)$-dimensional system of ODEs in the radial coordinate for each Fourier cosine mode. We then truncate

the expansions in the azimuthal coordinate to the finite dimension M that gives a desired accuracy. Each of the remaining $(M+1)$ ODE systems must be solved numerically over the interval $\epsilon < r < R$, with the interfacial conditions generated by the variational principle combined with the analytic expressions in $r < \epsilon$ and $r > R$ providing the boundary conditions at the points $r = \epsilon, R$.

Numerical results

In fig. 1 the effect of a quadratic increase in the thickness of the ice from 10cm at its edge $(r = R)$ to 1m at $r = \epsilon = R/2$ is considered. The uniform bed is $h = 20$m and the incident wavelength is chosen as $\lambda \equiv 2\pi/k_0^{(0)} = R/4$. Two problems of this form are shown. In one the thickness variation occurs on the lower surface of the ice $(\cdots)$ and in the other is on the upper surface of the ice $(\times)$. This is compared to a uniform floe of thickness 85cm $(-)$, which is chosen to give it an identical mass to the non-uniform floes. Results for a quadratic protrusion in the bed from 20m at $r = 50$m to 10m at $r = 25$m, beneath the uniform floe, are also shown $(\circ)$. We note that the two floes of varying thickness provide almost identical profiles. Despite a significant increase in the bed profile the displacements of the uniform floes are extremely similar. The relative differences between the sets of results indicates that variations to the thickness of the ice dominate over bed variations.

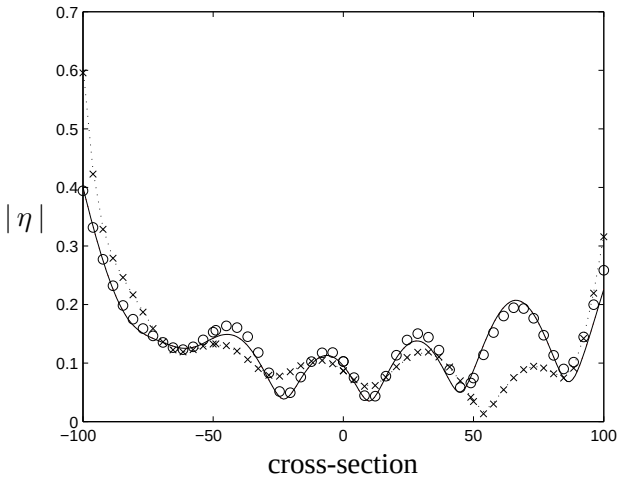

Figure 1: Introduction of geometrical variations

Fig. 2 displays the effect of introducing a physically correct Archimedean draught to floes of 50m radius and uniform thicknesses $D_0 = 1$m, 2m and 4m over a flat bed, $h = 20$m. The maximum value of the displacement of the floes, $\mathfrak{M}\eta \equiv \max|\eta|$, are given as functions of incident wavelength, $\lambda \in (5, 50)$m, for floes of a zero draught, $d = 0$, (solid line) and an Archimedean draught, $d = \rho_i D/\rho_w$, (dot-dash). As the floes become thicker, the displacement they experience decreases which is interpreted as a greater resistance to the incident wave. We note that the curves are monotonically increasing functions of wavelength for the longer incident waves. For shorter incident waves, this monotonicity is broken by the occurrence of local maxima. These maxima are more prevalent for the floes that incorporate a non-zero draught and thinner floes. At shorter wavelengths, there is a tendency for the floes of a non-zero draught to be displaced with a smaller magnitude than the corresponding floes of a zero draught, a tendency that is disrupted only by the occurrence of the maxima at short incident wavelengths. The point at which the floes of a non-zero draught begin to experience a smaller displacement is relative to the thickness of the floe, so that, the thicker the floe, the longer the incident wavelength that produces this behaviour.

Further results will be presented at the conference.

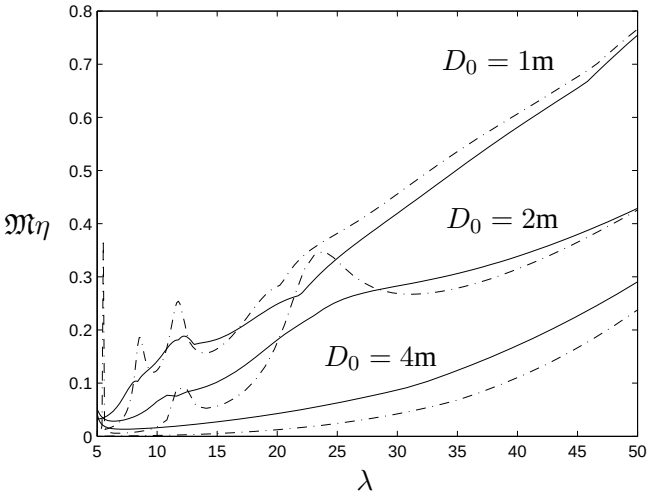

Figure 2: Introduction of Archimedean draught

References

[1] Peter, M. A., Meylan, M. H. & Chung, H., "Wave scattering by a circular elastic plate in water of finite depth: a closed form solution", IJOPE, vol. 14(2), pp. 81–85, 2004.

[2] Bennetts, L. G., Biggs, N. R. T. & Porter, D., "A multi-mode approximation to wave scattering by ice sheets of varying thickness", J. Fluid Mech., vol. 579, pp. 413–443, 2007.

An Idealised Model of Seiche Modes in the Northern Adriatic

N. R. T. Biggs[†,*], **A. J. Willmott**[‡]

[†]Department of Mathematics, University of Reading, P. O. Box 220, Whiteknights, Reading RG6 7AX, U.K.
[‡]Proudman Oceanographic Laboratory, Joseph Proudman Building, 6 Brownlow Street, Liverpool L3 5DA, U. K.
[*]Email: n.r.t.biggs@rdg.ac.uk

Abstract

Oscillations in a homogeneous uniformly rotating fluid with a free surface, contained in a semi-enclosed channel with mildly-sloping topography, are considered.

Introduction

In [1], it is demonstrated that in a 2D semi-enclosed basin the external (surface) seiche is sensitive to the water stratification. Here, we present a first step towards an analogous study of oscillations in a 3D model of the northern Adriatic, by considering a homogeneous uniformly rotating fluid with a free surface, contained in a semi-enclosed channel with mildly-sloping topography.

Governing equations

We adopt Cartesian coordinates (x, y, z), with z measured upwards from the undisturbed free-surface. The semi-infinite channel (see schematic in figure 1) is aligned so that its side-walls coincide with $y = \pm L$ for $x > -a$, and its end-wall is at $x = -a$ for $|y| \leq L$.

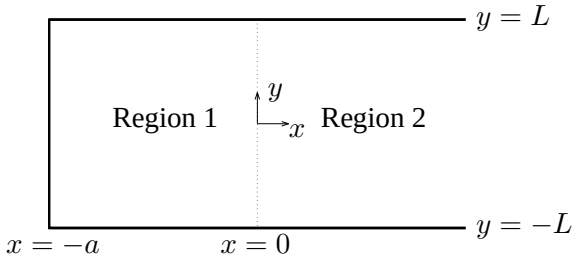

Figure 1: Schematic of channel geometry. In region 1, the fluid depth is allowed to increase linearly with x.

The flow is assumed to satisfy linearised shallow water theory. The momentum equations for regions 1 and 2 are

$$u_t - fv = -g\eta_x, \quad (1)$$
$$v_t + fu = -g\eta_y, \quad (2)$$

where u and v are the depth-averaged fluid velocities in the x and y directions respectively, and $\eta = h - H$ is the surface elevation, with h the total fluid depth and H the mean fluid depth. Lastly, f is the constant Coriolis parameter and g is the gravitational acceleration. In region 2, the channel is of constant depth $H_0^{(2)}$, but in region 1 the bed shoals gently as the end-wall is approached. The mean fluid depth is

$$H = H_0^{(1)} + \alpha x, \quad (3)$$

(see [2]), where $\alpha a / H_0^{(1)} \ll 1$. Thus, due to the similarity between the governing equations for the two regions, we consider the system

$$u_t - fv = -g\eta_x \quad (4)$$
$$v_t + fu = -g\eta_y \quad (5)$$
$$\eta_t + H_0(u_x + v_y) + \alpha u = 0 \quad (6)$$

from which the solutions for both regions can be deduced through appropriate choice of α and $H_0 = H_0^{(1)}$.

Harmonic time dependence of the form $e^{-i\omega t}$ is assumed and henceforth suppressed, where ω is a prescribed angular frequency. We are interested here in wave frequencies that are subinertial, that is $\omega < f$, and accordingly introduce the parameter

$$\sigma = \omega / f < 1. \quad (7)$$

The velocities u and v can be expressed as

$$u = \frac{g(i\sigma\eta_x - \eta_y)}{f(1-\sigma^2)}, \qquad v = \frac{g(\eta_x + i\sigma\eta_y)}{f(1-\sigma^2)}, \quad (8)$$

and can be eliminated from (6) to show that the free-surface elevation η satisfies

$$\eta_{xx} + \eta_{yy} + \frac{\alpha}{H_0}\eta_x + \frac{i\alpha}{\sigma H_0}\eta_y - \frac{1-\sigma^2}{R^2}\eta = 0, \quad (9)$$

where the radius of deformation is

$$R = \frac{\sqrt{gH_0}}{f}. \quad (10)$$

It is consistent with the shallow bottom-slope assumption for the frequency of oscillations to be very subinertial, i.e. $\omega << f$ (see [2]), and if this is the case then the third term in (9) is $O(\alpha^2)$, and can be discarded compared with the remaining $O(\alpha)$ terms. However, we here wish to stretch to the limit both the shallow slope assumption and the associated condition on the frequency, so we retain this term.

Infinite channel

In an infinite channel $|y| < L$, solutions of (9) are

$$\eta = e^{i\gamma x}(A^+ e^{\xi^+ y} + A^- e^{\xi^- y}), \tag{11}$$

for constants $A^\pm$, where $\xi^\pm$ are the two roots of

$$\xi^2 + \frac{i\alpha}{\sigma H_0}\xi - \lambda^2 = 0, \tag{12}$$

and

$$\lambda^2 = \gamma^2 + (1-\sigma^2)/R^2 - i\alpha\gamma/H_0. \tag{13}$$

A non-trivial solution which also obeys the no-normal flow conditions

$$\eta_x + i\sigma\eta_y = 0 \qquad (y = \pm L) \tag{14}$$

requires that the dispersion relation

$$\left[(\gamma + \sigma\xi^+)(\gamma + \sigma\xi^-)\right]\sinh[(\xi^+ - \xi^-)L] = 0 \tag{15}$$

be satisfied. Two distinct types of mode arise from this equation: modified Kelvin and Poincaré modes.

Modified Kelvin modes

If the first factor in (15) is zero, then we can write $\gamma^\pm = -\sigma\xi^\pm$, where $\xi^\pm$ is given from (12) and (13) as

$$\xi^\pm = \frac{-i\alpha}{2\sigma H_0} \mp \sqrt{\frac{1}{R^2} - \left(\frac{\alpha}{2\sigma H_0}\right)^2} \equiv \xi_0^\pm, \tag{16}$$

and so

$$\gamma^\pm = -\sigma\xi^\pm = \frac{i\alpha}{2H_0} \pm \sqrt{\left(\frac{\sigma}{R}\right)^2 - \left(\frac{\alpha}{2H_0}\right)^2} \equiv \gamma_0^\pm. \tag{17}$$

The square root is chosen here so that $\sqrt{c} = i\sqrt{-c}$ for $c < 0$, which ensures that γ_0^+ (γ_0^-) corresponds to modes propagating or decaying in the positive (negative) x-direction. Finally, returning to (11) and (15) we see that $A^\mp = 0$ for $\gamma = \gamma_0^\pm$ so that allowable solutions are

$$\eta_0^\pm(x,y) \propto e^{i\gamma_0^\pm x} e^{\xi_0^\pm y}. \tag{18}$$

For flat bottom topography ($\alpha = 0$), we have $\gamma_0^\pm = \pm\sigma/R$ and $\xi_0^\pm = \mp 1/R$, and we recover the classical right-trapped (in the Northern hemisphere) Kelvin modes

$$\eta_0^\pm(x,y) \propto e^{\pm i\sigma x/R} e^{\mp y/R}.$$

For $\alpha > 0$, modes decay in the positive x-direction (i.e. down-slope).

Modified Poincaré modes

If the second factor in (15) is zero, then $L(\xi^+ - \xi^-) = in\pi$ for integer n, from which $\gamma \equiv -i\gamma_n^\pm$ where

$$\gamma_n^\pm = \frac{\alpha}{2H_0} \pm \sqrt{\frac{1-\sigma^2}{R^2} + \left(\frac{n\pi}{2L}\right)^2 - (1-\sigma^2)\left(\frac{\alpha}{2\sigma H_0}\right)^2}. \tag{19}$$

Here the square root is chosen so that $\sqrt{c} = -i\sqrt{-c}$ for negative c, which ensures that γ_n^+ (γ_n^-) corresponds to modes which propagate or decay in the positive (negative) x-direction. The corresponding cross-channel wavenumbers are then found from (12) to be

$$\xi^\pm = -\frac{i\alpha}{2\sigma H_0} \pm \frac{in\pi}{2L} \equiv \xi_n^\pm. \tag{20}$$

Returning to (11) and (15), we have $A^-/A^+ \equiv \alpha_n^\pm$ where

$$\alpha_n^\pm = (-1)^{n+1}\frac{(-i\gamma_n^\pm + \sigma\xi_n^+)}{(-i\gamma_n^\pm + \sigma\xi_n^-)}, \tag{21}$$

giving the modified Poincaré modes

$$\eta_n^\pm(x,y) \propto e^{\gamma_n^\pm x}\left(e^{\xi_n^+ y} + \alpha_n^\pm e^{\xi_n^- y}\right) \qquad n = 1, 2, \ldots \tag{22}$$

If $\alpha = 0$ then $\gamma_n^\pm \in \mathbb{R}$ in the subinertial regime and give Poincaré modes which decay along the channel; if $\alpha > 0$ then some modified Poincaré modes may propagate.

To summarise, the solution η to equation (9) in conjunction with boundary conditions (14) is of the form

$$\eta(x,y) = \sum_{n=0}^{\infty} C_n^+ \eta_n^+(x,y) + C_n^- \eta_n^-(x,y), \tag{23}$$

where $\eta_0^\pm$ are modified Kelvin modes (18), $\eta_n^\pm$ ($n \geq 1$) are modified Poincaré modes (22), and the $C_n^\pm$ are constants.

Semi-infinite channel

In region 1, all modes from the expansion (23) are present, so we write the solution as

$$\eta_1 = \sum_{n=0}^{\infty} C_{n,1}^+ \phi_{n,1}^+ \psi_{n,1}^+ + C_{n,1}^- \phi_{n,1}^- \psi_{n,1}^-,$$

where $\phi_{0,1}^\pm(x) = e^{i\gamma_0^\pm x}$, $\psi_{0,1}^\pm(y) = e^{\xi_0^\pm y}$, and

$$\begin{cases} \phi_{n,1}^+(x) = e^{\gamma_n^+(x+a)}, \;\; \phi_{n,1}^-(x) = e^{\gamma_n^- x}, \\ \psi_{n,1}^\pm(y) = e^{\xi_n^+ y} + \alpha_n^\pm e^{\xi_n^- y}, \end{cases}$$

for $n = 1, 2, \ldots$ The subscript 1 denotes the region of validity of the expansion. In region 2, we allow an incoming Kelvin mode (i.e. one propagating from right to left)

of unit amplitude, an outgoing Kelvin mode, and those Poincaré modes which decay with x. Thus

$$\eta_2 = \phi^-_{0,2}\psi^-_{0,2} + \sum_{n=0}^{\infty} C^+_{n,2}\phi^+_{n,2}\psi^+_{n,2},$$

where $\phi^\pm_{0,2}(x) = e^{\pm i\sigma x/R}$, $\psi^\pm_{0,2}(y) = e^{\mp y/R}$, and

$$\left.\begin{array}{l}\phi^+_{n,2}(x) = e^{-x\sqrt{(1-\sigma^2)/R^2+(n\pi/2L)^2}} \\ \psi^+_{n,2}(y) = e^{in\pi y/2L} + \alpha^+_n e^{-in\pi y/2L}\end{array}\right\} \quad n = 0, 1, 2, \ldots$$

The unknown constants $C^+_{n,1}$, $C^-_{n,1}$ and $C^+_{n,2}$ are found from the no-normal flow condition at the channel-head,

$$u_1(-a, y) = 0 \qquad (|y| < L), \tag{24}$$

together with matching conditions at the shelf edge,

$$H^{(1)}_0 u_1(0, y) - H^{(2)}_0 u_2(0, y) = 0, \tag{25}$$

$$\eta_1(0, y) - \eta_2(0, y) = 0, \tag{26}$$

also for $|y| < L$, and where u_j is found via (8) from η_j.

The solution to this set of equations is determined approximately by truncating all summations at $n = 2M$, and then applying a Galerkin method. Thus we introduce the complete orthonormal sequence

$$\chi_m(y) = \frac{e^{im\pi y/L}}{\sqrt{2L}}, \qquad m = 0, \pm1, \pm2, \ldots, \tag{27}$$

and require that the residual of equations (24)-(26) is orthogonal to χ_m for $m = 0, \pm1, \ldots, \pm M$.

Results

Model parameter values which approximate the physical characteristics of the northern Adriatic are given in Table 1. Note that $\alpha a/H^{(1)}_0 = 0.96$ is not significantly smaller than unity, and that, whilst a sub-inertial regime, $\sigma = 0.70777$ does not conform to the regime $\omega \ll f$. In region 1, no modified Poincaré modes propagate, and the modified Kelvin waves oscillate but decay down-slope with an e-folding length-scale of ~ 1667km.

Table 1: Model parameter values, taken from [2].

L	100km	α	0.00054
a	800km	f	$1.03 \times 10^{-4}\mathrm{s}^{-1}$
$H^{(1)}_0$	450m	ω	$7.29 \times 10^{-5}\mathrm{s}^{-1}$
$H^{(2)}_0$	3500m	σ	0.70777

The solution for the model parameters, shown in Figure 2, displays an anticylonic gyre in the shelf region, and

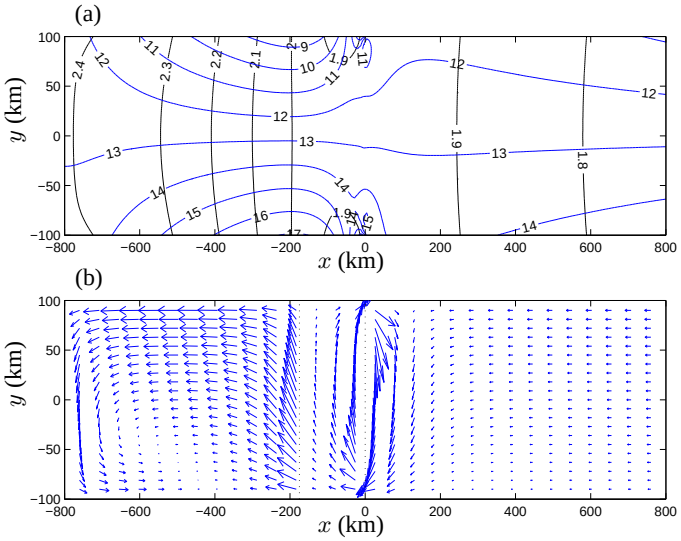

Figure 2: Simulation of the northern Adriatic, using the parameter values given in Table 1. Plotted are (a) $|\eta|$ in m (marked 1.8–2.4) and $\arg(\eta)$ in degrees (marked 9–17); (b) $|\mathrm{Re}(u, v)|$ (arrows). In (b), the top-left velocity vector has a magnitude of $0.027\mathrm{ms}^{-1}$; note also that velocity vectors between the vertical dotted lines ($x = 0, -175$km) have been shortened by a factor of 10.

the characteristics of a double Kelvin wave (DKW) propagating along the shelf edge. An exact superposition of DKWs which also obey the no-normal flow conditions on the channel wall is not possible at this frequency. Thus the modified Kelvin and Poincaré modes are reproducing the behaviour of a single DKW near the centre of the channel, but this combines with the effect of the channel walls at $y = \pm L$ to form a further anticylonic gyre centred on the shelf-edge itself.

Further results will be given in the presentation, including an investigation of near-resonances at certain critical values of the frequency parameter σ.

References

[1] B. Cushman-Roisin, A. J. Willmott, & N. R. T. Biggs, "Influence of stratification on decaying surface seiche modes", Continental Shelf Research, vol. 25, 227-242.

[2] B. Cushman-Roisin, Introduction to Geophysical Fluid Dynamics, Prentice Hall, 1994.

[3] V. Malačič, D. Viezzoli, & B. Cushman-Roisin, "Tidal dynamics in the northern Adriatic Sea", Journal of Geophysical Research, vol. 105, pp. 26265-26280, 2000.

INFLUENCE OF BOTTOM TOPOGRAPHY ON LONG WATER WAVES

F. Chazel
Institut de Mathématiques de Bordeaux, Université Bordeaux I, Talence, FRANCE
Email: florent.chazel@math.u-bordeaux1.fr

Abstract

This work deals with the water-waves problem for uneven bottoms in the long-wave framework on an unbounded two or three-dimensional domain. We aim here at constructing, justifying and comparing new asymptotic models taking into account the bottom topography. First, two new classes of symmetric Boussinesq-like models are derived by introducing two different regimes of bottom topography : one for small variations in amplitude, and one for strong variations. Then, starting from the two-dimensionnal version of the class corresponding to small topography variations, we recover a class of usual uncoupled Korteweg-de-Vries-like models. At this step, a discussion is performed and theses models are rigorously improved by adding correction terms linked to the bottom topography. Finally, all these models are integrated numerically : results are presented and commented.

Introduction

The water waves problem for uneven bottoms consists in describing the motion of the free surface and the evolution of the velocity field of a layer of ideal, incompressible and irrotationnal fluid. Our goal here is to rigorously derive new asymptotic models taking the bottom topography into account.

Starting from the classical water waves equations, we use the Bernoulli formulation and non-dimensionnalize the equations, which makes two parameters appear : ε which measures the ration between the typical amplitude of the waves and the mean depth and corresponds to a small parameter in our long-waves framework, and β which measures the ration between the typical amplitude of the variations of bottom topography and the mean depth. Finally we use the Zakharov formulation to get the following system, ψ being the velocity potential expressed at the free surface, η the free surface and b the bottom topography.

$$\left\{\begin{array}{l} \partial_t\psi - \varepsilon\partial_t\eta Z_\varepsilon(\varepsilon\eta,\beta b)\psi + \frac{1}{2}\left[\,|Z_\varepsilon(\varepsilon\eta,\beta b)\psi|^2\right. \\ \qquad\left. +\varepsilon\,|\nabla\psi - \varepsilon\,\nabla\eta Z_\varepsilon(\varepsilon\eta,\beta b)\psi|^2\,\right] + \eta = 0\ , \\ \partial_t\eta + \varepsilon\nabla\eta\cdot\left[\,\nabla\phi - \varepsilon\nabla\eta Z_\varepsilon(\varepsilon\eta,\beta b)\psi\,\right] \\ \qquad\qquad -\frac{1}{\varepsilon}\,Z_\varepsilon(\varepsilon\eta,\beta b)\psi = 0\ . \end{array}\right.$$

where $Z_\varepsilon(\varepsilon\eta,\beta b)$ is a Dirichlet-Neumann operator defined as $Z_\varepsilon(\varepsilon\eta,\beta b)f = \partial_z u_{|_{z=\varepsilon\eta}}$ with u solution of :

$$\left\{\begin{array}{l} \varepsilon\,\Delta u + \partial_z^2 u = 0, \quad -1+\beta\,b \le z \le \varepsilon\eta\ , \\ \partial_z u - \varepsilon\beta\,\nabla b\cdot\nabla u = 0, \quad z = -1+\beta b\ , \\ u(X,\varepsilon\eta) = f, \quad X\in\mathbb{R}^d\ . \end{array}\right.$$

Two classes of symmetric Boussinesq-like models

At this point, we use our long-waves framework to look for an asymptotic expansion of $Z_\varepsilon(\varepsilon\eta,\beta b)f$ in powers of ϵ. To this end, we distinguish two different regimes concerning the parameter β : $\beta = O(\varepsilon)$ for small bottom topography variations and $\beta = O(1)$ for large variations. Thanks to a general theorem, we are then able to rigorously compute two asymptotic expansions of $Z_\varepsilon(\varepsilon\eta,\beta b)f$ in the two previous regimes.

Small variations in amplitude of the bottom topography

If we plug the previous result for $\beta = O(\varepsilon)$ in the Zakharov formulation, we are able to derive a first Boussinesq-like model for slightly variating bottoms. Unfortunately, this model is ill posed. Thus we follow the global strategy put forward by Bona, Colin and Lannes in ([2]). This strategy consists in two successive changes of variable on the velocity field $V = \nabla\phi$, a pseudo-differential one and a non-linear one in which topography terms appear. The first change of variable helps to symmetrize the dispersive terms of the equations by introducing three arbitrary parameters, while the second one symmetrizes the non-linear terms. In the end, we get the following new class of symmetric models :

$$\left\{\begin{array}{l} (1-\varepsilon a_2\Delta)\,\partial_t V + \nabla\eta + \varepsilon\left[\frac{1}{4}\nabla|\eta|^2 + \frac{1}{4}\nabla|V|^2\right. \\ \left. +\frac{1}{2}(V\cdot\nabla)V + \frac{1}{2}\,V\,\nabla\cdot V - \frac{1}{2}\,b\,\nabla\eta + a_1\Delta\nabla\eta\right] = 0\,, \\ (1-\varepsilon a_4\Delta)\,\partial_t\eta + \nabla\cdot V + \varepsilon\left[\frac{1}{2}\nabla\cdot\Big((\eta-b)\,V\Big)\right. \\ \qquad\left. +a_3\Delta\nabla\cdot V\right] = 0\,. \end{array}\right.$$

where $a_1 = a_3, a_2 \ge 0, a_4 \ge 0$, these coefficients depending on the three previously introduced parameters.

All the symmetric systems of this class are proved to be well-posed on a long time interval $[0;\frac{T}{\varepsilon}]$, and we demonstrate that their solutions, up to the inversion of the two

previous change of variables, all furnish approximations of the water waves solutions at the order $O(\varepsilon^2 t)$ on $[0; \frac{T}{\varepsilon}]$.

Strong variations in amplitude of the bottom topography

This time, we plug the asymptotic expansion of $Z_\varepsilon(\varepsilon\eta, \beta b)f$ in the case $\beta = O(1)$ into the Zakharov formulation of the water waves problem, and get a first ill-posed Boussinesq-like model, more complex than the previous one. This time, we have to adapt our strategy because of the huge influence of the bottom topography in the equations. We propose two different changes of variable, first a non-linear one and then a pseudo-differential one. The first one symmetrizes both the order one derivative terms and the non-linear terms, while the second symmetrizes the dispersive terms thanks again to the introduction of three arbitrary parameters. We consequently derive a whole class of symmetric Boussinesq-like models for this regime, these models being written as :

$$\begin{cases} \left(1 - \frac{\varepsilon}{2}\mathcal{P}_h^1\right)\partial_t V + \sqrt{h}\,\nabla\eta + \frac{\varepsilon}{2}\left[F_h\begin{pmatrix} V \\ \eta \end{pmatrix}\right. \\ \left. +b_1\sqrt{h}\nabla\nabla\cdot(h^2\nabla\eta) + b_2\sqrt{h}\nabla(h\nabla h\cdot\nabla\eta)\right. \\ \left. +b_3\nabla h\nabla\cdot(h\sqrt{h}\nabla\eta) + b_4\sqrt{h}\nabla h(\nabla h\cdot\nabla\eta)\right] = 0 \ , \\ \left(1 - \frac{\varepsilon}{2}\mathcal{P}_h^2\right)\partial_t\eta + \nabla(\sqrt{h}\cdot V) + \frac{\varepsilon}{2}\left[f_h\begin{pmatrix} V \\ \eta \end{pmatrix}\right. \\ \left. +\nabla\cdot\Big(c_1 h^2\nabla\nabla\cdot(\sqrt{h}V) + c_2 h\nabla h\nabla\cdot(\sqrt{h}V)\right. \\ \left. +c_3 h\sqrt{h}\nabla(\nabla h\cdot V) + c_4\sqrt{h}\nabla h(\nabla h\cdot V)\Big)\right] = 0 \ . \end{cases}$$

with $h = 1 - b$ and where the coefficients (b_i) and (c_i) depending on the three parameters can be taken such that the whole system is symmetric. $\mathcal{P}_h^1$ and $\mathcal{P}_h^1$ are elliptic operators, and F_h and f_h correspond to the non-linear terms.

Here again, we are able to prove that all these symmetric systems are well-posed at least locally in time, and possibly on a long time interval when $\nabla b = O(\varepsilon)$. Up to the inversion of the two previous changes of variable, their solutions furnish approximations of the water waves problem solutions at the order $O(\varepsilon^2 t)$ on $[0; \frac{T}{\varepsilon}]$ when $\nabla b = O(\varepsilon)$. This result may hold without the last condition.

An improved class of uncoupled Korteweg-de-Vries-like models

We focus now on the case $\beta = O(\varepsilon)$ of slightly variating bottoms, and we start with any of the corresponding two-dimensionnal Boussinesq-like models previously derived. At this step, we aim at recover the classical uncoupled Korteweg-de-Vries approximation.

The usual uncoupled Korteweg-de-Vries approximation

Diagonalizing the system by introducing $U = V + \eta$ and $N = V - \eta$ leads to a new (class of) system. We look for approximate solutions of this system in the classical form $U_a = U_0(T, x - t) + \varepsilon U_1(T, t, x - t); N_a = N_0(T, x + t) + \varepsilon N_1(T, t, x + t)$ with $T = \varepsilon t$. Pluging this ansatz in the previous system leads to the following Korteweg-de-Vries uncoupled equations on U_0 and N_0 :

$$\begin{cases} \partial_T U_0 + \frac{3}{4}U_0\partial_x U_0 + (a_1 + \frac{a_2+a_4}{2})\partial_x^3 U_0 \\ \partial_T N_0 + \frac{3}{4}N_0\partial_x N_0 - (a_1 + \frac{a_2+a_4}{2})\partial_x^3 N_0 \end{cases}$$

and to an explicitly solvable equation on the correctors U_1 and N_1. The previous uncoupled Korteweg-de-Vries system of equations is similar to the one derived by Iguchi in his work ([5]) where he considered - like us - slightly variating bottoms.

Discussion and proposition of an improved model

The resulting Korteweg-de-Vries approximation consists in writing $v_{kdv} = \frac{U_0+N_0}{2}$ and $\eta_{kdv} = \frac{U_0-N_0}{2}$. Like Iguchi, we can prove that (v_{kdv}, η_{kdv}) approximates the solutions of the water waves problem at the order $O(\varepsilon)$ on a long time interval, but under the following conditions : both initial conditions (v_0, η_0) and bottom topography b must be very regular, f.e. belong to some weighted Sobolev space. Even if such an assumption is quite usual and acceptable on initial conditions, it is not the case as far as the bottom topography is concerned.

Indeed the validity of the approximation is governed by the estimates on the correctors U_1 and N_1 which must have at worse a sub-linear growth in time. Unfortunately, U_1 and N_1 contains topography terms that can have a linear growth in time in some cases where the bottom variation b is not L^2, f.e. a step. In such a case, these topography terms become so large on a long time intervall that U_1 and N_1 are not correctors anymore. Hence we have to adapt the ansatz to add these topography terms to the order one terms U_0 and N_0.

Consequently, we propose a new Korteweg-de-Vries approximation defined as the following :

$$\begin{cases} v_{kdv} = \frac{U_0+N_0}{2} + \varepsilon\frac{BT_1+BT_2}{2} \\ \eta_{kdv} = \frac{U_0-N_0}{2} + \varepsilon\frac{BT_1-BT_2}{2} \end{cases}$$

where BT_1 and BT_2 are topography terms coming respectively from U_1 and N_1. This new approximation is proved to be of order $O(\varepsilon)$ on a long time intervall as

long as initial conditions are regular enough and the bottom variation b is in $W_k^\infty(\mathbb{R})$ for k large enough.

Numerical comparison of the models

In this last part, we propose to compute and compare both previous Boussinesq-like and Korteweg-de-Vries-like models (classical and improved) in the case of slightly variating bottoms on a two-dimensionnal domain. We consider here the previously introduced case of a step on the bottom topography, and we study the propagation of a solitary wave over this step.

Presentation of the numerical schemes

The idea here is to consider quite simple and fast finite differences schemes that are able to reproduce faithfully the global behaviour of the solitary wave. To this end, we use a Crank-Nicholson scheme on both KdV-like uncoupled system and Boussinesq-like one. Non-linear terms are treated with a predictor term $U^{n+1/2}$ defined as $U^n = \frac{U^{n+1/2}+U^{n-1/2}}{2}$, in a way that preserves not only the symmetric structure of the Boussinesq-like system but also the discrete L^2 norm of (U, N) for the KdV-like one and a specific energy for the Boussinesq-like one.

Our aim here is to compare three models : our Boussinesq-like one, the classical uncoupled KdV-like model and our improved KdV-like one with topography terms. We propose to consider here a solitary wave which is propagated to the right by the first KdV equation : we take the known expression of such a wave at $t = 0$ as initial condition $U_0(t = 0)$ for the KdV-like model - and $N_0(t = 0) = 0$ - and we take $V(t = 0) = \eta(t = 0) = \frac{1}{2}U_0(t = 0)$ as initial conditions for the Boussinesq-like one.

Numerical results and comments

The following results have been obtained with $\varepsilon = 0.2$ and $a_1 = 0; a_2 = \frac{1}{6}; a_4 = \frac{1}{6}$. The figure shows the superposition of the free surface obtained numerically with each of the three models, in the case of a step at the bottom, for t=12 in non-dimensionnal variables.

We immediately observe that our Boussinesq-like and KdV-like models succeed in reproducing the phenomenon of reflexion on the bottom : a smaller wave appears and is propagated to the left at the same speed as the main wave. It is obviously not possible to reproduce this phenomenon with the classical uncoupled KdV-like model which propagates the wave indepently of the bottom topography. Moreover, our two new models successfully describe the following physical phenomenons : the shoaling which corresponds to the growth in amplitude of the wave after the step; the deceleration of the wave after the step : the waves obtained with our two new models are behind the one obtained with the usual KdV-like model; and finally the loss of symmetry of the wave, which can be remarked by comparing the resulting wave with the still symmetric one obtained with the usual KdV-like model.

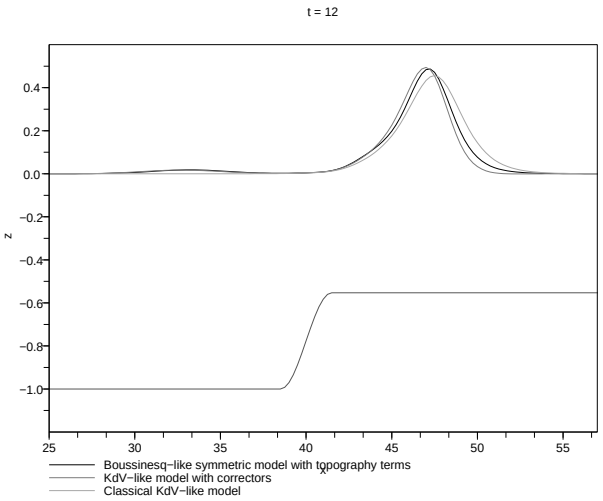

Figure 1: The case of a step

An interesting remark on our new KdV-like model is that we are able to identify precisely the role of each topography terms in the phenomena described below : BT_1 is responsible for the loss of symmetry and the deceleration of the wave after the step, while BT_2 generates the reflected wave and the shoaling effect. This a main advantage since these terms are calculated explicitly from the solution (U, N) of the uncoupled KdV-like system : we can thus easily isolate each phenomenon. Unfortunately, this model has the drawback of diverging quickly when time goes over $\frac{1}{\varepsilon}$. The Boussinesq-like model seems to diverge less quickly when time grows, but identifying the role of each term in the equations is significantly more difficult.

References

[1] J. L. BONA, M. CHEN, J.-C. SAUT, *Boussinesq Equations and Other Systems for Small-Amplitude Long Waves in Nonlinear Dispersive Media. II: Nonlinear Theory*, J. Nonlinear Sci. **12** (2002), 283-318.

[2] J. L. BONA, T. COLIN, D. LANNES, *Long Waves Approximations for Water Waves*, Arch. Rational Mech. Anal. **178** (2005) 373-410.

[3] M. CHEN, *Equations for bi-directional waves over an uneven bottom*, Mathematical and Computers in Simulation **62** (2003), 3–9.

[4] W. CRAIG, *An existence theory for water waves and the Boussinesq and Korteweg-de Vries scaling limits*, Comm. Partial Differential Equations **10** (1985), no. 8, 787–1003.

[5] T. IGUCHI, *A long wave approximation for capillary-gravity waves and an effect of the bottom*, Comm. Partial Differential Equations, 32 (2007), 37–85.

[6] D. H. PEREGRINE, *Long waves on a beach*, J. Fluid Mech., **27** (2005) No. 4, 815-827.

[7] G. SCHNEIDER, C. E. WAYNE, *The long-wave limit for the water-wave problem. I. The case of zero surface tension.*, COMM. Pure Appl. Math., **162** (2002), no. 3, 247–285.

THE INDUCED STOKES SURFACE WAVE BY STOKES INTERNAL WAVE

Y. L. Cheng
Dept. of Power Engineering, North China Electric Power University, Baoding, Hebei, PR China
Email: ylcheng001@163.com

Abstract

The induced Stokes surface waves by Stokes internal waves in the stratified ocean are investigated using the power series-Fourier series expansion and symbolic operation. The expressions of the waveforms and the frequency-dispersion relation of Stokes 5th-order surface waves and Stokes 5th-order internal waves are yielded by theoretical analysis for general cases. Then, the time evolutions of the waveforms, the frequency-dispersion curves of the induced Stokes surface waves are generated by numerical calculation for specific sea conditions. Moreover, the effects of relative density difference, depth ratio, wave length on the above frequency-dispersion curves under the different wave steepness are analyzed and compared.

Introduction

Stokes surface wave of a fluid is an interesting phenomenon studied since the famous work of Stokes [1]. Wu [2] did an exhaustive review on such problem. As we know, the surface wave can be induced by the internal wave underneath it. In fact, the shading and white stripes on the surface in the ocean can be treated with a kind of surface wave, which is modulated by the convergence and divergence of the sea water caused by the near–surface internal wave, and which can be imaged by radar such as satellite-borne Synthetic Aperture Radar (SAR) [3, 4]. The surface wave is a significant part of wave dynamics and has a practical application in many aspects, such as ocean engineering [5].

The main interest in this work is aimed at the Stokes surface waves, which propagate at the free surface and are induced by Stokes internal waves in the stratified ocean. The Stokes internal waves propagate at the interface between a heavy fluid and an upper light one. The two-layer fluid is bounded by the Stokes free surface wave and a rigid wall. In our investigation's scope, the literature concerning the induced Stokes surface waves by Stokes internal waves in the stratified ocean is sparse. Considering the known literature, it is found that the Stokes surface wave in non-stratified fluid, the nonlinear interfacial waves under some special cases and the Stokes internal waves without free surface are investigated. These are not enough for the in-deep study on the surface waves, such as that induced by internal waves. So, we try to present the general theory of the induced Stokes surface waves by Stokes internal waves in the stratified ocean.

The main strategy we used is solving the nonlinear boundary value problem of the stream function using the power series-Fourier series expansion and symbolic operation. After the series expansion of the fifth-order Stokes surface wave and internal waves are obtained, the waveforms up to the fifth order at different times and the frequency dispersion curves up to the fifth order are all plotted and compared with each other for the special sea condition. The effects of relative density difference, wavelength and depth ratio on the fifth-order non-dimension wave speed under the different wave steepness are analyzed and compared with each other.

Problem Formulation

Suppose that the two-layer fluid considered is immiscible incompressible inviscid one bounded by a free surface and a rigid wall with lighter layer of density ρ_1 and thickness h_1 above and the heavier one of density ρ_2 and thickness h_2 below, respectively, which are initially statically stable, i.e., $\sigma=\rho_1/\rho_2<1$, and at rest at infinity (see Figure 1).

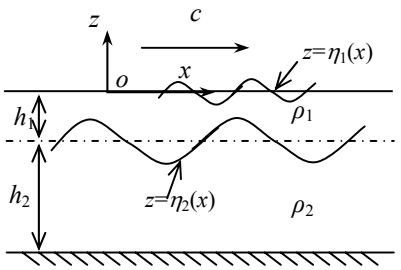

Figure 1: Sketch of the Stokes surface wave and interfacial wave in a two-dimensional Cartesian x, z coordinate system

Establishing the above two-dimensional Cartesian x, z coordinate system, the corresponding stream function $\psi_i(x, y, t)$ (i=1, 2) satisfy the following equations and boundary conditions:

$$\frac{\partial^2\psi_1}{\partial x^2}+\frac{\partial^2\psi_1}{\partial z^2}=0 \tag{1}$$

$$\frac{\partial^2\psi_2}{\partial x^2}+\frac{\partial^2\psi_2}{\partial z^2}=0 \tag{2}$$

$$\psi_2(x,-h)=0 \tag{3}$$

$$\psi_1\left[x,\eta_1(x)\right]=-Q_1 \tag{4}$$

$$\psi_2\left[x,-h_1+\eta_2(x)\right]=-Q_2 \tag{5}$$

$$\frac{1}{2}\left[\left(\frac{\partial\psi_1}{\partial x}\right)^2+\left(\frac{\partial\psi_1}{\partial z}\right)^2\right]+g[\eta_1(x)]=R_1 \tag{6}$$

$$\left.\frac{\partial\psi_2}{\partial x}\right|_{z=-h_1+\eta_2(x)}=\left.\frac{\partial\psi_1}{\partial x}\right|_{z=-h_1+\eta_2(x)} \tag{7}$$

$$\frac{1}{2}\left[\left(\frac{\partial\psi_2}{\partial x}\right)^2+\left(\frac{\partial\psi_2}{\partial z}\right)^2\right]+g[-h_1+\eta_2(x)]-R_2-(1-\sigma)$$
$$\times\left\{\frac{1}{2}\left[\left(\frac{\partial\psi_1}{\partial x}\right)^2+\left(\frac{\partial\psi_1}{\partial z}\right)^2\right]+g[-h_1+\eta_2(x)]-R_2\right\}=0 \tag{8}$$

in which $h=h_1+h_2$ is the total water depth, $\sigma=(\rho_2-\rho_1)/\rho_2$ is the relative density difference, Q_1 and Q_2 are both positive constants related to the total volume rate of flow underneath the Stokes surface wave and the Stokes internal wave per unit length normal to the (x, y) plane, R_1 and R_2 are also positive constants related to the Bernoulli's constant of the surface and the interface respectively.

Expressions of Stokes Surface Waves and Stokes Internal Waves

In order to obtain the expressions of Stokes surface waves and Stokes internal waves, a non-dimensional wave-amplitude $\varepsilon=kH/2$ is introduced being similar to Fenton [6]and Cheng [7], in which H is the wave height of the Stokes internal waves, and k is the wave number. The stream function, the surface elevation and the interfacial elevation are all expanded as the following power series-Fourier series expansion of ε and x. The quantities $\bar{u}$, Q_1, Q_2, R_1 and R_2 mentioned in the above expressions are all expanded as the power series of ε.

Substituting the above power series-Fourier series expansions into Eqs.1~8, then, expanding them into the series of ε and letting the coefficients of the same order of ε be identical with each other, the equations of all the undetermined and dimensionless coefficients with trigonometric functions are derived. Letting the coefficients of the same trigonometric functions of the same angle be identical with each other, the equations of all the undetermined and dimensionless coefficients without any trigonometric function are obtained. Solving these equations, thus, all the unknown coefficients will be determined, and then, the expressions of Stokes surface wave and internal wave are both produced.

The process of reducing and solving is heavy and complicated, but there are many analogous steps in it, which is adapted to program using computer algebra. Just by computer algebra software, the expressions of the fifth-order Stokes surface and internal waves are derived formally.

For the limited space, the solutions and all the derivations are also omitted.

Substituting the above solutions into the power series-Fourier series expansions of the stream function, the surface elevation and the interfacial elevation, the expressions the fifth-order frequency dispersion relation, the fifth-order waveform and the fifth-order stream functions of the Stokes surface waves and Stokes internal waves are all obtained

From the expressions, it can be seen that the Stoke surface waves are affected by the Stoke interfacial waves and the sea conditions of the stratified ocean and that there are two kinds of wave mode: internal wave mode and surface wave mode. It can be verified that the wave height of the induced Stoke surface waves is H times b_{111}, in which b_{111} is the coefficient of the first term in the power series-Fourier series of the $k\eta_1(x)$.

Case Study of Stokes Surface Waves Induced by Stokes Internal Waves

The four oceanic conditions are selected. They have been applied to the study of the second-order to the fifth-order theory of Stokes internal waves without free surface in [7]. In the following, they are used to discuss the characteristic of the induced Stokes surface waves.

According the simulations, the results of Stokes internal wave for internal wave mode and general case are similar to that without free surface [7]. In fact, the wave heights of the induced Stokes surface wave in the internal wave mode are all not very high that the effects of the induced Stokes surface wave on Stokes internal wave are less.

However, the wave heights of the induced Stokes surface wave in the surface wave mode are all higher. So, for this wave mode, the results of the induced Stokes surface wave, such as the frequency dispersion curves and the temporal evolution of the waveforms up to the fifth order, are investigated in the following. For brevity, only the results of case four are given below.

Case Four

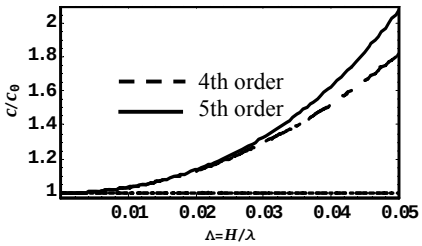

Figure 2: the fifth-order frequency dispersion curve and its comparison with the fourth-order curve for case four

The fifth-order frequency dispersion curve and its comparison with the fourth-order curve are plotted in Figure 2 above.

It can be seen from Figure 2 that the fifth-order frequency dispersion curve is obviously more than that of the fourth-order, which means that the wave speed will increase with the order and the fixed wave steepness as the fixed wave steepness is more than some value. In the figure c_0=0.999972, c/c_0=1+326.311Λ^2 for the 4th order curve and c/c_0=1+326.311Λ^2+ 41305.8Λ^4 for the 5th order curve.

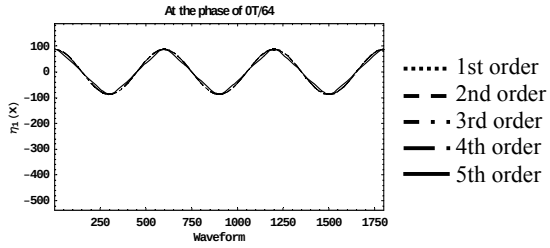

Figure 3 the waveforms up to the fifth and their comparison at a moment for case four

The time evolution of the waveforms up to the fifth of the induced Stokes surface wave for the surface wave mode are generated and compared with each other in Figure3.

It can be seen from Figure3 that the fifth-order waveform can be more acuminate and higher at the crest and more flat, wider and higher at the trough than the fourth-order waveform, which is similar to the characteristic of the Stokes internal wave for this case.

Factor Analysis on Fifth-order Wave Speed for Surface Wave Mode

In order to discuss the variation of wave speed for the surface wave mode with different sea condition and Stokes internal wave, the effects of relative density difference, wavelength and depth ratio on the fifth-order non-dimension wave speed under the different wave steepness are analyzed by numerical simulation in the figures. For the limited space, these figures are all omitted.

From these figures, it can be seen that for the surface wave mode the effects of relative density difference, wavelength and depth ratio on the fifth-order non-dimension wave speed under the different wave steepness are different from that for the internal wave mode [7].

Conclusions

Summarizing the above investigation, the following conclusions can be obtained.

The wave heights of the induced Stokes surface wave in the internal wave mode are all not very high that the effects of the induced Stokes surface wave on Stokes internal wave are less.

The wave heights of the induced Stokes surface wave in the surface wave mode are all higher. For this wave mode, the higher-order frequency dispersion curve is obviously more than that of the lower-order, which means that the wave speed will increase with the order and the fixed wave steepness as the fixed wave steepness is more than some value. Moreover, the higher-order waveform can be more acuminate and higher at the crest and more flat, wider and higher at the trough than the lower-order waveform, which is similar to the characteristic of the Stokes internal wave in the same case.

The effects of relative density difference, wavelength and depth ratio on the fifth-order non-dimension wave speed under the different wave steepness are different from that for the internal wave mode.

Acknowledgement

The work is supported by the National Natural Science Foundation of China (Grant 10672056) and the China Postdoctoral Science Foundation (Grant 2003034208).

References

[1] G.G. Stokes, “On the Theory of Oscillating Waves”, Trans Cambridge Philos Soc, Vol 8, pp.441-455, 1847.

[2] T.Y. Wu. “Advances in Water Wave Mechanics”, Advances in Mechanics, Vol 31, No 3, pp.327-343, 2001 (in Chinese).

[3] W. Alpers, “Theory of radar imaging of internal waves”, Nature, 314, pp.245-247, 1985.

[4] A.E. Gargett and B.A. Hughes, “On the interaction of surface and internal waves”, Journal of Fluid Mechanics, Vol 52, No 1, pp.179-191, 1972.

[5] T. Sarpkaya and M. Isaacson, “Mechanics of Wave Forces on Offshore Structures”, Van Nostrand Reinhold, New York, 1981.

[6] J.D. Fenton, “A Fifth-Order Stokes Theory for Steady Waves”, Journal of Waterway Port Coastal and Ocean Engineering-ASCE, Vol 119, No 5, pp.496-504, 1985.

[7] Y.L. Cheng, J.C. Li and L.S. An, “Stokes 5th-Order Internal Wave and Its Action on Cylindrical Piles”, in Proceedings of the Sixteenth International Offshore and Polar Engineering Conference, San Francisco, pp. 116-121, 2006.

FAST WAVES IN FLOW THROUGH A PERIODIC CHANNEL

Dick Kachuma[†,*], **Ian J. Sobey**[†]
[†]Oxford University Computing Laboratory, Oxford, UK
[*]Email: dick.kachuma@comlab.ox.ac.uk

Abstract

We compute numerical solutions to the 2D Navier-Stokes equations in a very long channel with a sudden expansion. The results show that, in the parameter regime of interest, the development of a vortex wave is followed by a faster and shorter wave. We carry out stability analysis which indicates that this faster wave is the result of a linear instability mechanism.

Introduction

Use of a stepped channel combined with unsteady laminar flow provides a powerful mixing mechanism that is particularly applicable to processes where the fluid contains delicate elements, for example, applications involving mass transfer in blood or in cell cultures. In such channel flows there are parameter regimes where the flow is described by the two-dimensional unsteady Navier-Stokes equations. Sobey [1] showed both experimentally and numerically that a standing wave of separated regions developed behind a channel step during oscillatory flow and called the resulting flow a vortex wave. Included in his experimental observations were vortex waves of extreme longitudinal extent and he conjectured that the wave formed was, under the correct parameter conditions, virtually undamped in the streamwise direction.

Ghaddar et. al. [2] considered flow through periodically grooved channels at moderate Reynolds numbers via spectral element solution of the two-dimensional Navier-Stokes equations. They developed a theory for the frequency selection in oscillations observed in flow based on linear stability analysis. They indicated that the observed oscillations resembled Tollmein-Schlichting waves forced by a Kelvin-Helmholtz shear layer instability. They noticed that the instability became self sustaining for Reynolds numbers above a critical value $\mathrm{R}e_c$ for channels of appropriate length.

In this work, we consider gradually accelerated flow through periodically grooved channels and we have have undertaken calculations in a different parameter region and this has been found to result in characteristically different bahaviour.

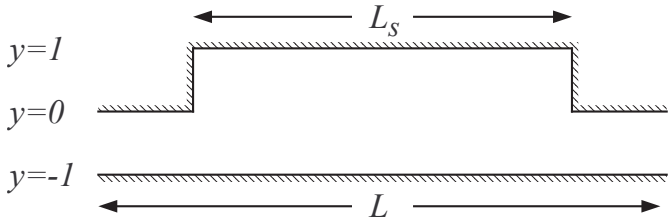

Figure 1: Geometry for a 2D plane flow through a periodic channel. The channel has a nondimensional minimum width 1, a maximum width 2, periodic length L and the length of the expansion is L_s.

Numerical method

We consider flow through a channel with a sudden expansion as shown in Figure 1. Our channels have a length that is characteristically much longer than the channels used by Ghaddar et. al. in [2]. Whereas they computed flows in channels in which L in Figure 1 was no larger than 10, we have undertaken computations is channels where L is around 100.

We solve the Navier-Stokes equations in dimensionless form with distances scaled with the minimum channel width h, velocities with the average velocity U, at peak volumetric flux, and time with the frequency of oscillation Ω. This gives two nondimensional paramaters: the Reynolds number $\mathrm{R}e = Uh/\nu$, ν being the kinematic viscosity and is the Strouhal number $\mathrm{S}t = \Omega h/U$. Solution is schieved by using in the streamfunction-vorticity formulation with the vorticity ω and streamfunction ψ defined in the usual way;

$$\omega = -\frac{\partial u}{\partial y} + \frac{\partial v}{\partial x}, \quad u = \frac{\partial \psi}{\partial y}, \quad v = -\frac{\partial \psi}{\partial x},$$

where u and v are the nondimensional velocities in x and y respectively. These definitions lead to the Poisson relationship;

$$\omega = -\left(\frac{\partial^2 \psi}{\partial x^2} + \frac{\partial^2 \psi}{\partial y^2}\right).$$

The 2D Navier-Stokes equations then lead to the vorticity transport equation

$$\mathrm{S}t\frac{\partial \omega}{\partial t} + \frac{\partial (u\omega)}{\partial x} + \frac{\partial (v\omega)}{\partial y} = \frac{1}{\mathrm{R}e}\left(\frac{\partial^2 \omega}{\partial x^2} + \frac{\partial^2 \omega}{\partial y^2}\right).$$

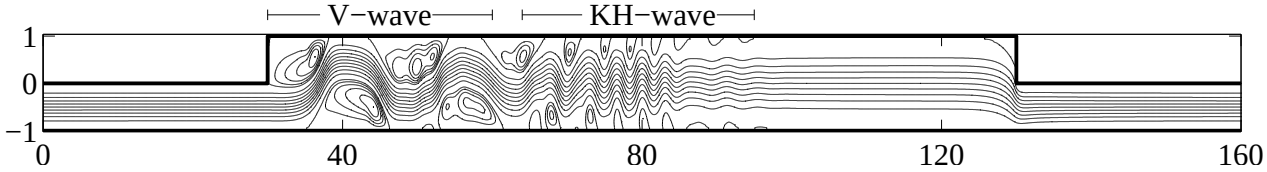

Figure 2: Instantaneous streamlines for flow through a periodic grooved channel showing the extent of the vortex wave and KH-wave. Geometry parameters $L = 160$, $L_s = 100$ and flow parameters $\mathrm{R}e = 400$, $\mathrm{S}t = 0.005$.

From the geometry in Figure 1 the boundary conditions are $u = v = 0$ on all solid surfaces. The total nondimensional volumetric flowrate is prescribed at $2q(t) = 2\sin(2\pi t)$ and this gives the boundary conditions

$$\begin{aligned} \psi &= q(t), \quad \text{at the top wall and;} \\ \psi &= -q(t), \quad \text{at the bottom wall.} \end{aligned}$$

Periodic boundary conditions are used in the streamwise coordinate giving

$$\psi(0, y, t) = \psi(L, y, t), \text{ and } \omega(0, y, t) = \omega(L, y, t).$$

Finite difference versions of these equations form the base of the numerical solution in a manner similar to [3]. The vorticity transport equation is used to step forward in time, the Poisson equation is then used to compute the streamfunction which gives the velocities at the next time step. Centred differences are used for second order accuracy and Lax-Wendroff discretisation is used for the vorticity transport equation. Several numerical tests have been carried out to confirm the validity of these computations and it is our conclusion that observed structures are actually physical and are not due to numerical artefacts.

Results

We find that a sequence of two events occurs: one is the formation of a vortex wave of finite extent (typically 2-4 vortices alternating on the two walls behind the step), in agreement to the experimental and numerical observations of [1]; the second is a subsequent rapidly propagating wave of regular but slightly smaller vortices. This second wave propagates at speeds that are much faster than those observed in [2]. We believe that this is as a result of the short channel lengths that they carried out their computations in: the lengths involved did not provide adequate room for the waves to develop. The propagation of this second wave is also such that its resolution would have been beyond that of the apparatus used in [1]. In this respect, we refer to the initial vortex wave as a "V-wave" and the fast wave as a "KH-wave" as shown in Figure 2. We observe that with periodic boundary conditions there is a critical length L_c below which the KH-wave is self-sustaining. With lengths less than L_c disturbances travel through to the downstream boundary of the channel and trigger further effects in the V-wave upstream and thus the resulting disturbance persists. For longer channels, the KH-waves are damped before reaching the downstream end of the channel.

Stability Analysis

In [4], Tutty and Pedley have developed a model for the evolution of an inviscid rotational core flow that is described by an evolutionary linearised Korteweg-de Vries (KdV) equation. This has been shown to be consistent with the genesis and evolution of the V-wave. Our computations on an extension of this model show that the V-wave can be accounted for by a similar KdV equation. This predicts correctly the phase and group velocity of the V-wave and also amplitude fluctuations in unsteady flow. However the model fails to account for the fast moving KH-waves as it assumes a long wavelength. As we believe that these are among the first calculations of these fast moving waves, we believe that there is no unifying theory to account for the existence of the KH-waves.

In order to understand the genesis of KH-waves we have undertaken a study of starting flows in which the fluid is accelerated from rest to either steady channel flux or a flux with a small oscillatory component. We have tested the hypothesis that the KH-wave results from an Orr-Sommerfeld type instability of nearly parallel but non-Poiseuille like flow. This has led us to study stability of a base flow

$$u_0(y) = \frac{3}{2}(1 - \sigma y)(1 - y^2), \quad -1 \le y \le 1,$$

where $\sigma = 0$ is Poiseuille flow and $\sigma > 1$ indicates reverse flow near one wall. That this might be a pluasible base flow comes from observations that the flow is nearly parallel over long sections of the channel and has a non-Pouseuille profile.

The development of KH-waves has been considered in channels with smoothly varying and sharp corners and us-

ing different numerical methods, as well as with different numerical resolution. We consider solutions of an Orr-Sommerfeld equation as the extent of a reverse flow region is varied and investigate the consequences of instability in the base flow on subsequent flow development. We present wavenumber and frequency predictions from this linear instability analysis. We also make approximations for the damping rates of these waves and investigate how these relate to the critical length of the channel.

The results we have indicate that the KH-wave is the result of a linear instability mechanism described by an Orr-Sommerfeld equation but with growth rates that are orders of magnitude greater than those for disturbances to symmetric Poiseuille flow and with instability occuring at relatively low Reynolds number.

The complexity of unsteady flows calculated from the full Navier–Stokes equations is remarkable and it is likely that flows in other parameter regimes are dominated by entirely different mechanisms.

References

[1] Sobey, I. J. (1985). Observation of waves during oscillatory flow. *Journal of Fluid Mechanics*, 151:395–426.

[2] Ghaddar, N. K., Korczak, K. Z., Mikic, B. B., and Patera, A. T. (1986). Numerical investigation of incompressible flow in grooved channels. Part 1. Stability and self-sustained oscillations. *Journal of Fluid Mechanics*, 163:99–127.

[3] Sousa, E. and Sobey, I. J. (1985). Numerical stability of unsteady stream-function vorticity calculations. *Communications in Numerical Methods in Engineering*, 19:407–419.

[4] Tutty, O. R. and Pedley, T. J. (1994). Unsteady flow in a nonuniform channel: A model for wave generation. *Physics of Fluids*, 6(6):199–208.

Waveguides

Transparent boundary conditions for the harmonic diffraction problem in an elastic waveguide

V. Baronian[†,*], **A. S. Bonnet-Ben Dhia**[†], **E. Lunéville**[†]
[†]POEMS, UMR 2706 CNRS-INRIA-ENSTA, Paris, France
[*]Email: vahan.baronian@ensta.fr

Abstract

This work concerns the numerical finite element computation, in the frequency domain, of the diffracted wave produced by a defect (crack, inclusion, perturbation of the boundaries etc..) located in an infinite elastic waveguide. The objective is to use modal representations to build transparent conditions on the artificial boundaries of the computational domain. This cannot be achieved in a classical way, due to non standard properties of elastic modes. In particular, the derivation of a "Dirichlet-to-Neumann" operator (relating the normal stress to the displacement) is not tractable. However, a biorthogonality relation allows to build an operator, relating hybrids displacement/stress vectors. An original mixed formulation is then derived and implemented, whose unknowns are the displacement field in the bounded domain and the normal component of the normal stresses on the artificial boundaries. Numerical validations are presented in the two-dimensional case.

1 The elastic waveguide

We consider a homogeneous isotropic elastic waveguide of section S (S is a bounded domain of $\mathbb{R}^2$), density ρ and Lamé's coefficients λ and μ, with a stress-free boundary. The domain is denoted by Ω ($\Omega = S \times \mathbb{R}$) and the propagation is modelized by the following classical equations ($\omega > 0$ denotes the pulsation and $\mathbf{u}$ the total displacement field) :

$$\begin{cases} -\operatorname{div}\sigma(\mathbf{u}) - \omega^2\rho\mathbf{u} = 0 & \text{in } \Omega, \\ \sigma(\mathbf{u}).\mathbf{n} = 0 & \text{on } \partial\Omega, \end{cases} \tag{1}$$

where $\sigma(\mathbf{u})$, the stress tensor, is related to the strain tensor $\varepsilon(\mathbf{u}) = 1/2(\nabla\mathbf{u} + \nabla^t\mathbf{u})$ by Hooke's law:

$$\sigma(\mathbf{u}) = \lambda \operatorname{div}(\mathbf{u}) Id + 2\mu\varepsilon(\mathbf{u}).$$

1.1 Elastic modes

Taking advantage of the cylindrical nature of the waveguide, the propagation properties are deduced from a modal analysis: the modes are the solutions of (1) of the form

$$\mathbf{u}(x_1, x_2, x_3) = \mathbf{v}(x_1, x_2)e^{i\beta x_3}, \quad \beta \in \mathbb{C}.$$

The dispersion relation can be calculated analytically in the particular case of a 2D plate (Lamb modes) and of a circular 3D rod (Pochammer modes). The corresponding spectra (symmetric with respect to $\Re e\,\beta = 0$ and $\Im m\,\beta = 0$) have been intensively studied [1]. At a given frequency, there exist infinitely many modes, that we can range in two categories: a finite number of propagative modes ($\beta \in \mathbb{R}$) and an infinity of evanescent modes ($\beta \notin \mathbb{R}$), which are generally also oscillating ($\Re e\,\beta \neq 0$). Dispersion curves of the propagative modes present some strange particularities, like a possible sign-shift of the group velocity. From the mathematical point of view, the related spectral problem is not self-adjoint and useful properties as completeness and orthogonality are not straightforward. We will assume completeness in the following (see [2] and [3] for a proof in 2D) and explain how to solve the question of orthogonality in the next section. Let us finally introduce the following definitions:

- An evanescent mode is said to be rightgoing (resp. leftgoing) if $\Im m\,\beta > 0$ (resp. $\Im m\,\beta < 0$).
- A propagative mode is said to be rightgoing (resp. leftgoing) if its group velocity $\partial\omega/\partial\beta$ is positive (resp. negative).

We will denote by $\mathbf{u}_n^+(x_1, x_2, x_3) = e^{i\beta_n x_3}\mathbf{v}_n^+(x_1, x_2)$ (resp. $\mathbf{u}_n^-(x_1, x_2, x_3) = e^{-i\beta_n x_3}\mathbf{v}_n^-(x_1, x_2)$) the rightgoing (resp. leftgoing) modes.

1.2 The diffraction problem

Let us consider now a perturbed waveguide, with a localized defect, a crack $\Gamma \subset \Omega$ for instance. Our purpose is the computation of the wave diffracted by the crack, when the incident wave is supposed to be a propagative mode:

$$\mathbf{u}_{inc}(x_1, x_2, x_3) = \mathbf{v}_{n_0}^+(x_1, x_2)e^{i\beta_{n_0}x_3}, \quad \beta_{n_0} \in \mathbb{R}.$$

The total displacement field $\mathbf{u}_{tot}$ then satisfies :

$$\begin{cases} -\operatorname{div}\sigma(\mathbf{u}_{tot}) - \omega^2\rho\mathbf{u}_{tot} = 0 & \text{in } \Omega\backslash\Gamma, \\ \sigma(\mathbf{u}_{tot}).\mathbf{n} = 0 & \text{on } \partial\Omega \cup \partial\Gamma, \end{cases} \tag{2}$$

where the diffracted wave defined as $\mathbf{u}_{dif} = \mathbf{u}_{tot} - \mathbf{u}_{inc}$ has to satisfy an outgoing radiation condition. More precisely, on each side of the perturbation, $\mathbf{u}_{dif}$ must be a superposition of outgoing modes. If $\Gamma \subset \{|x_3| < R\}$:

$$\begin{aligned} &\mathbf{u}_{dif}(x_1, x_2, x_3) = \sum_{n\in\mathbb{N}} a_n^{\pm}\mathbf{v}_n^{\pm}(x_1, x_2)e^{\pm i\beta_n x_3} \\ &\text{for } \pm|x_3| > \pm R \end{aligned} \tag{3}$$

In order to solve the problem with finite elements, one has to bound the computational domain. We will explain now how to build transparent boundary conditions which can be set on vertical artificial boundaries $\Sigma_{\pm R} = \{x_3 = \pm R\}$.

2 The semi-infinite waveguide

In this section, we consider the semi-infinite waveguide occupying the domain $\Omega_R^+ = S \times \{x_3 > R\}$. Usually (for the scalar problem for instance), to derive a Dirichlet-to-Neumann map on Σ_R, we solve the Dirichlet problem in Ω_R^+, with a Dirichlet condition on Σ_R and an outgoing condition at infinity; this is achieved through a modal decomposition. Here, this approach does not work because no orthogonality relations of the $\mathbf{v}_n^+$ are available. Besides, well-posedness of the Dirichlet problem is not guaranteed. The way to proceed relies on a generalized orthogonality relation, known as the biorthogonality relation of Fraser [4], which is detailed now.

2.1 Biorthogonality

Consider two rightgoing modes $\mathbf{v}_n^+$ and $\mathbf{v}_m^+$. From the ealstodynamic equations, one can derive the following relation:

$$(\beta_n^2 - \beta_m^2) \int_S (v_1^{m+}\sigma_{31}^{n+} + v_2^{m+}\sigma_{32}^{n+}) - v_3^{n+}\sigma_{33}^{m+} = 0. \quad (4)$$

Introducing the two vectors $X = (v_1, v_2, \sigma_{33})$ and $Y = (\sigma_{31}, \sigma_{32}, v_3)$, this relation becomes

$$(X_m^+, Y_n^+)_{Fr} \stackrel{def}{=} J_n^+ \delta_{nm} \quad (5)$$

where we have set

$$(X_m^+, Y_n^+)_{Fr} \stackrel{def}{=} \int_S (v_1^{m+}\sigma_{31}^{n+} + v_2^{m+}\sigma_{32}^{n+}) - v_3^{n+}\sigma_{33}^{m+}.$$

In general J_n^+ does not vanish except at particular frequencies where the group velocity of the n^{th} mode vanishes. We assume we are not in this case.

2.2 Modal representation

Thanks to Fraser relation (5), any vector X given on Σ_R can be expanded on rightgoing modes as follows:

$$X = \sum_{n\in\mathbb{N}} \frac{(X, Y_n^+)_{Fr}}{J_n^+} X_n^+$$

(a similar relation holds for Y). This leads naturally to consider the following exterior problem, where the usual Dirichlet condition has been replaced by a mixed condition $X = X_R = (g_1, g_2, h_3)$ on Σ_R, for given data $g_1, g_2 \in H^{1/2}(\Sigma_R)$ and $h_3 \in H^{-1/2}(\Sigma_R)$:

$$\begin{cases} -\operatorname{div}\sigma(\mathbf{u}) - \omega^2\rho\mathbf{u} = 0 & \text{in } \Omega_R^+, \\ \sigma(\mathbf{u}).\mathbf{n} = 0 \text{ on} & \partial S \times \{x_3 > R\}, \\ u_1 = g_1, u_2 = g_2, \sigma_{33} = h_3 & \text{on } \Sigma_R \end{cases} \quad (6)$$

The solution of this problem has the following expression:

$$\mathbf{u} = \sum_{n\in\mathbb{N}} \frac{(X_R, Y_n^+)_{Fr}}{J_n^+} \mathbf{v}_n^+ e^{i\beta_n(x_3 - R)}.$$

The complementary Cauchy data $Y_R = (\sigma_{31}, \sigma_{32}, u_3)$ on Σ_R can be recovered thanks to the following expansion:

$$Y_R = \sum_{n\in\mathbb{N}} \frac{(X_R, Y_n^+)_{Fr}}{J_n^+} Y_n^+.$$

Summing up, we have built a generalized Dirichlet-to-Neumann map T_R^+ such that

$$T_R^+ X_R = Y_R$$

where X_R and Y_R are the Cauchy data associated to the outgoing solution of (6).

3 The mixed formulation

Using the previous boundary maps, the original diffraction problem has the following equivalent formulation on the bounded domain $\Omega_R = S \times \{|x_3| < R\}$ (the free surface is denoted by $\Gamma_S = \partial S \times \{|x_3| < R\}$):

$$\begin{cases} -\operatorname{div}\sigma(\mathbf{u}_{tot}) - \omega^2\rho\mathbf{u}_{tot} = 0 & \text{in} \quad \Omega_R\backslash\Gamma, \\ \sigma(\mathbf{u}_{tot})\cdot\mathbf{n} = \mathbf{0} & \text{on} \quad \Gamma_S, \\ Y_{tot} - T_R^+(X_{tot}) = 0 & \text{on} \quad \Sigma_R. \\ Y_{tot} - T_R^-(X_{tot}) = Y_{inc} - T_R^-(X_{inc}) & \text{on} \quad \Sigma_{-R} \end{cases} \quad (7)$$

where X_{inc} and Y_{inc} are related to the incident field.

To take into account the transparent boundary conditions on $\Sigma_{\pm R}$ in a variational formulation, we introduce an additional unknown, say $\xi = \sigma_{33}$, defined only on $\Sigma_{\pm R}$ and we get the following mixed formulation:

find $\mathbf{u} \in V$ and $\xi \in W$ such that $\forall \mathbf{v} \in V, \forall \theta \in W$

$$\begin{cases} a(\mathbf{u}, \mathbf{v}) + b(\xi, \mathbf{v}) = & l_1(\mathbf{v}) \\ -b(\theta, \mathbf{u}) + c(\xi, \theta) = & l_2(\theta) \end{cases} \quad (8)$$

where $V = H^1(\Omega_R\backslash\Gamma)$ and $W = H^{-1/2}(\Sigma_R) \times H^{-1/2}(\Sigma_{-R})$. The first equation is derived from the elastodynamic equation by a Green formula; the stresses appearing in the boundary terms are replaced by either the

new unknown or their expression resulting from the transparent conditions. The second equation is the weak form of the relation between u_3 and X, also coming from the transparent conditions.

A similar approach in the scalar case leads to a coercive + compact formulation. We observe here that some useful properties of the bilinear forms are still valid (symmetry, positivity...) and we conjecture that problem (8) is also of Fredholm type. However, a rigorous analysis requires new results concerning completeness of modes and Sobolev trace spaces caracterization in terms of modes.

This variational framework is well-suited for a finite element approximation. As it is (probably) of Fredholm type, no inf-sup condition is required and any conformal discretizations of V and W are allowed. Notice that the bilinear forms involve infinite modal series expansions which have to be truncated in practice.

4 Numerical results

The method has been implemented in the 2D case using the code MELINA [5]. More precisely, we deal with a steel plate of thickness 2 mm. The velocities of longitudinal and transversal waves are given by $c_L = 6020ms^{-1}$ and $c_T = 3220ms^{-1}$. The computations are made for a frequency $f = \omega/2\pi$ =2MHz. At this frequency, it can be shown that exactly 5 Lamb modes can propagate in the plate : the two symmetric modes S0 and S1, and the three antisymmetric ones A0, A1 and A2.

We use P2 Lagrange finite elements for both unknowns $\mathbf{u}$ and ξ, and we keep 35 terms in the modal expansions. The method has been first validated in the case of a safe plate (no crack) to check the transparency of the boundary conditions. Then, as an example, we deal with a planar crack of length 1.4 mm. Below are the isovalues of the real part of u_3 for the total and the diffracted fields.

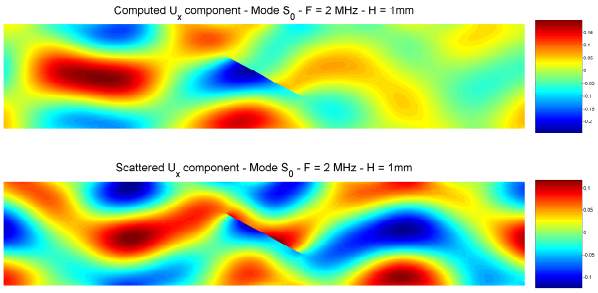

The extension to the 3D case is in progress : in the case of a general section S, it requires a preliminary numerical determination of the modes, contrary to the 2D case where Lamb modes are known analytically.

References

[1] D. ROYER AND E. DIEULESAINT, *Ondes élastiques dans les solides*, Tome 1, Masson (1996).

[2] P. KIRRMANN, *On the completeness of Lamb modes*, J. of Elastic., 37 (1995), pp. 39–69.

[3] H. BESSERER AND P. G. MALISCHEWSKY, *Mode series expansions at vertical boundaries in elastic waveguides*, Wave Motion, 39 (2004), pp. 41–59.

[4] V. PAGNEUX AND A. MAUREL, *Lamb wave propagation in inhomogeneous elastic waveguides*, Proc. R. Soc. Lond. A, 458 (2002), pp. 1913–1930.

[5] D. MARTIN, *On line documentation of* MÉLINA, http://perso.univ-rennes1.fr/daniel.martin/melina.

NUMERICAL STUDY OF TIME REVERSAL IN A 2-D WAVEGUIDE

C. Ben Amar [†,‡,*], **N. Gmati**[†], **C. Hazard**[‡], **K. Ramdani** [**]
[†]LAMSIN, ENIT Campus universitaire B. P. 37 1002 Tunis Belvedére TUNISIE
[‡]POEMS, ENSTA 32, Boulevard Victor 75739 Paris Cedex 15 FRANCE.
[**] INRIA (Projet CORIDA) et Institut Elie Cartan Université de Nancy Vandoeuvre-les-Nancy, 54506 FRANCE
[*] Email: chokri.benamar@lamsin.rnu.tn

Abstract

We study the time reversal phenomenon in a waveguide. We show the effectiveness of the DORT (french acronym for Decomposition of the Time Reversal Operator) method for selective focusing on small scatterers and we prove the advantage of the waveguide boundaries and multipath propagation by comparing the results to the case of free space.

Introduction

Time reversal techniques have been studied in ultrasonics and underwater acoustics environments. In this paper, we are concerned with the DORT method resulting from the analysis of the iterative time reversal process which can be described as follows. A Time Reversal Mirror (TRM), composed of an array of transducers, £rst emits an acoustic wave in a non dissipative medium containing some unknown obstacles, then measures the diffracted £eld. The measured £eld is then time reversed and reemitted. The time reversal operator T is obtained by iterating this procedure twice.

The D.O.R.T method consists in calculating the eigenelements of T for a £xed frequency. In this case, reversing the time amounts to a conjugation. It was shown [5] that for small and distant enough scatterers in the free space, the number of signi£cant eigenvalues of T is exactly the number of obstacles and each eigenvector corresponding to a nonzero eigenvalue of T provides the signals to be sent to the transducers in order to focus on one scatterer.

We are interested in this paper in studying the focusing properties of the eigenvectors of T when the medium of propagation is a two-dimensional waveguide. The main object is to study the effect of the multiple diffusion due to the interfaces of the waveguide on the focusing. We are then interested uniquely to the interactions between the obstacles and the interfaces, and between the obstacles themselves, the ones between the TRM and the obstacles studied in [1] are neglected here. Therefore, we consider a non intrusive TRM (whose presence do not perturb the acoustic wave) constitued of pointlike transducers as in Prada et al. [5].

Note the waveguide $= \{x = (x_1, x_2) \in I\!R^2, 0 \quad x_2 \quad H\}$ and consider N_t pointlike transducers placed at $x_1 = a_1$ and some bounded scatterers. We denote by $\mathcal{O}$ the union of these obstacles and by $\Gamma = \partial\mathcal{O}$ the union of their boundaries (see £gure 1).

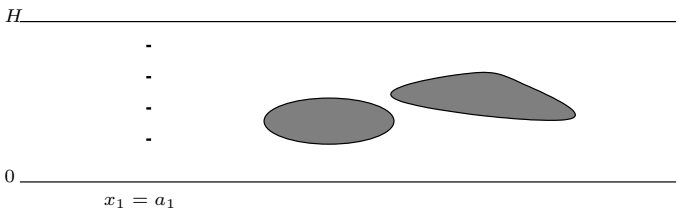

Figure 1: The waveguide, the scatterers and the transducers.

Time reversal process

The time reversal process is described as follows : let $A_i,\ i = 1$ to N_t, be the points of $\setminus\ \overline{\mathcal{O}}$ where are placed the transducers. As the transducers are supposed to be pointlike, each one emits an incident £eld proportional to the Green's function $G(A_i, .)$ de£ned in (3). The incident £eld φ_I is then :

$$\varphi_I(x) = \sum_{i=1}^{N_t} G(A_i, x) g_i \tag{1}$$

where g_i represents the emission intensity of the transducer A_i, $1 \quad i \quad N_t$.

The diffracted £eld by the obstacles φ_D is then the *outgoing* solution of the problem :

$$\begin{cases} \varphi_D + k^2\varphi_D &= 0 & \setminus\ \overline{\mathcal{O}} \\ \dfrac{\partial\varphi_D}{\partial n} &= -\dfrac{\partial\varphi_I}{\partial n} & \Gamma \\ \varphi_D &= 0 & \partial \end{cases} \tag{2}$$

The condition *outgoing* means that we consider only the evanescent and the guided modes that propagate towards in£nity (*outgoing* modes).

At the reception, each transducer measures the value of the diffracted £eld without perturbing it. The measured signal g_R is then de£ned by

$$g_R = \{\varphi_D(A_i)\}_{1 \le i \le N_t}$$

g_R is then conjugated and used to generate the incident £eld in the next iteration.

Let g denote the vector composed of the complex amplitudes g_i of transducers at the emission step and by D, the transfer matrix describing the three successive steps : Emission-Diffraction-Measure. Then, we have $Dg = g_R$. The time reversal matrix T is obtained by iterating the time reversal process (Emission-Diffraction-Measure-Conjugation) twice. T is de£ned by

$$Tg = \overline{D\overline{Dg}}, \text{ or } T = \overline{D}D.$$

For $x \in$, we de£ne the Green's function in the waveguide $G(x,.)$ as the *outgoing* solution of the following problem :

$$\begin{array}{rcl} G(x,.) + k^2 G(x,.) & = & x \\ G(x,.) & = & 0 \quad \partial \end{array} \tag{3}$$

Different methods can be used to £nd an explicit representation of the Green's function. For numerical reasons, we have chosen to decompose G on the modes of the waveguide. By considering a source $A(a = (a_1, a_2))$ and by projecting the function $x_2 \to G(a = (a_1, a_2), x = (x_1, x_2))$ on a basis composed of eigenvectors of the operator $-\partial^2/\partial x_2^2$ in $H_0^1(0, H)$, we obtain the series decomposition of G [2]:

$$G(a,x) = \frac{1}{H} \sum_{n=1}^{+\infty} \frac{1}{ik_n} \sin \frac{n \ x_2}{H} \sin \frac{n \ a_2}{H} \ e^{ik_n |x_1 - a_1|} \tag{4}$$

where $k_n = \sqrt{k^2 - (\frac{n}{H})^2}$ and Imag(k_n) 0.

It is obvious from its expression that G is symmetric on $\times$.

We de£ne the Green's function G_D like φ_D but associated to the incident £eld G instead of φ_I, we have then

$$T_{ij} = \sum_{n=1}^{N_t} \overline{G_D(A_n, A_i)} G_D(A_j, A_n)$$

By proving the symmetry of G_D (see [1]), we deduce the following proposition :

Proposition T is a hermitian and positive matrix. Its eigenvalues $(\ _i)_{1 \le i \le N_t}$ are then positive numbers.

Numerical results

The numerical simulation of the time reversal process is realized using the Finite Elements (FE) code MELINA [4]. The method of resolution is a coupling technique between the FE method and the integral representation [3].

We consider two disks of centers $(0, 0.5)$ and $(0.6, 0.5)$ and of radius $r_1 = 0.02$ and $r_2 = 0.01$ respectively, N_t uniformly distributed transducers are placed at $a_1 = -2.8$ (we set $N_t = 9$).

We present in the £gures 2 and 3 the eigenvalues of T according to k respectively in the case of a non intrusive TRM in the free space (when considering the Green's function in the free space) and the model considered here for a waveguide of height $H = 1$.

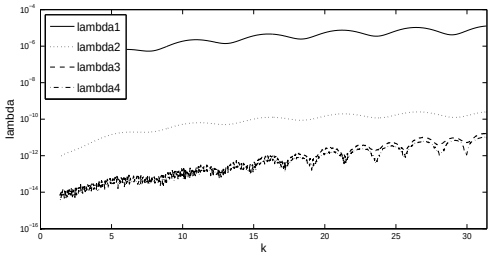

Figure 2: 4 £rst eigenvalues of T according to k (free space).

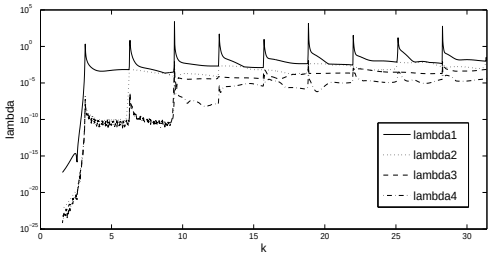

Figure 3: 4 £rst eigenvalues of T according to k (waveguide).

We remark that in the free space case (£gure 2), there is only one signi£cant eigenvalue (the ratio between the £rst eigenvalue and the second is of order 10^4) which means that the greatest obstacle masks the smallest one and we can not focus selectively on them.

We are interested now in the case of the waveguide (£gure 3). Note £rst that the picks represent the cutoff frequencies ($k_n = n \ /H = n \ $) for which the problem (3) is ill-posed.

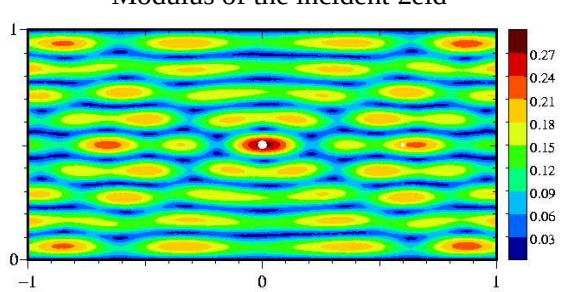

Figure 4: Emission of the £rst eigenvector $k = 30$.

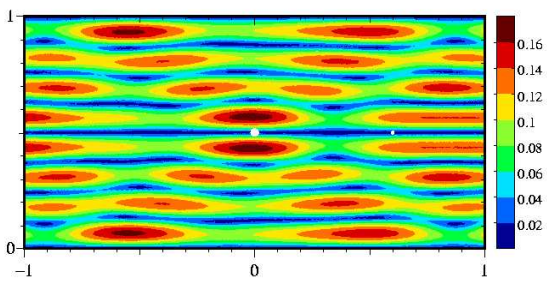

Figure 5: Emission of the second eigenvector $k = 30$.

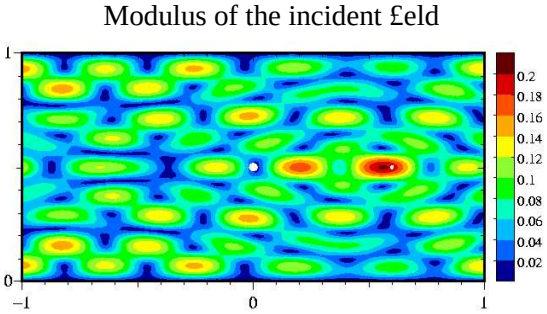

Figure 6: Emission of the third eigenvector $k = 30$.

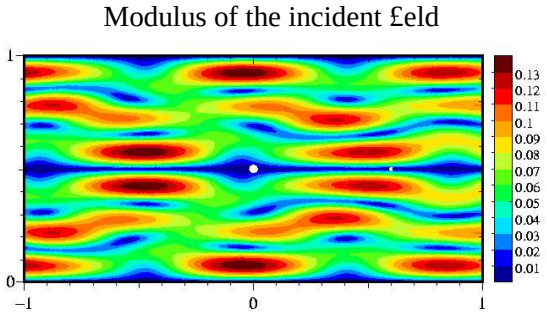

Figure 7: Emission of the fourth eigenvector $k = 30$.

At low frequencies, most precisely, when $k <$, we remark that the eigenvalues are very small (even the £rst); this is can be explained by the fact that there are only evanescent modes and then the incident £eld decreases rapidly and the scattered £eld received by the TRM is of low intensity.

When $< k < 2$, there is only one signi£cant eigenvalue due to the presence of one propagative mode but, as the precedent case, we can not focus selectively on the obstacles.

When k increases ($k > 2$), the second eigenvalue becomes signi£cant but the relation : "number of signi£cant eigenvalues = number of obstacles" is not in general satis£ed : there is not a clear separation between the two £rst eigenvalues and the following ones.

For $k = 30$, the £rst eigenvalues are $_1 = 1.54\ 10^{-2}$, $_2 = 1.5\ 10^{-3}$ and $_3 = 5\ 10^{-4}$. The £gure 4 (resp. 6) shows that the emission of the £rst (resp. the third) eigenvector allows to focus selectively on the greatest obstacle (resp. the smallest). Note that in this case, the obstacles are small and distant. In addition, the selective focusing has taken place for only a few number of transducers contrarily to the case of free space where the transducers must be well-distributed and their number suf£ciently large.

To explain the presence of more than two signi£cant eigenvalues, we have studied the case where there is only one obstacle in the waveguide. In particular, we have found that $_1$(only the smallest obstacle is present) $= 1.05\ 10^{-3} \simeq\ _2$(only the greatest one is present) $= 8.6\ 10^{-4}$ which explains that the second and the third eigenvalues of T in presence of the two obstacles are comparable and that in this case it's the third eigenvector which focuses on the smallest disk.

The numerical results presented in this paper seem in contradiction with the ones obtained in [6], where a far-£eld model for time-reversal in a waveguide containing sound-soft scatterers (Dirichlet condition) is investigated. In particular, a mathematical justi£cation of selective focusing for small obstacles is provided in [6] when the number of propagating modes of the waveguide is large enough. In our case, the number of propagative modes does not exceed nine and probably this is the reason why the number of signi£cant eigenvalues is not equal to the number of obstacles.

References

[1] C. Ben Amar, N. Gmati, C. Hazard and K. Ramdani, "Mathematical and numerical study of a time reversal mirror", Waves, Brown USA, June 2006.

[2] R.E. Collin, Field theory of guided waves, IEEE Press, 1991.

[3] A. Jami and M. Lenoir, "A variational formulation for exterior problems in linear hydrodynamics", Comput. Methods Appl. Mech. Engrg., vol. 16, pp. 341-359, 1978.

[4] D. Martin, http://www.maths.univ-rennes1.fr/ dmartin/melina/www/homepage.html.

[5] C Prada, S. Maneville, D. Spoliansky and M. Fink, "Decomposition of the time reversal operator : Detection and selective focusing on two scatterers," The Journal of The Acoustical Society of America, vol. 99, no. 4, pp. 2067-2076, 1996.

[6] B. Pinçon and K. Ramdani, "Selective focusing on small scatterers in acoustic waveguides using time reversal mirrors", Inv. Pb., vol. 23, pp. 1-25, 2007.

AN IMPROVED MULTIMODAL METHOD IN WAVEGUIDES WITH NONUNIFORM IMPEDANCE BOUNDARY CONDITIONS

W. P. Bi*, **V. Pagneux, D. Lafarge, Y. Aurégan**
Laboratoire d'Acoustique de l'Universit du Maine, AV. O. Messiaen, Le Mans, 72000, France
*Email: wenping.bi@univ-lemans.fr

Abstract

An improved multimodal method is proposed for modeling time harmonic acoustic propagation in a waveguide with nonuniform impedance boundary condition without or with uniform flow. The impedance is axially segmented uniform, but varies circumferentially. The sound pressure is expanded in term of rigid waveguide modes and an additional function that carries the information about the impedance boundary. The rigid waveguide modes and the additional function are known *a priori* so that calculations of the modes, which are difficult, are avoided. By matching the pressure and axial velocity at the interface between different uniform segments, scattering matrices are obtained for each individual segment; these are then combined to construct a global scattering matrix for multiple segments. The radial rate of convergence is shown to be $O(n^{-4})$, where n is the radial mode indices.

Introduction

Numerous methods have been proposed to study sound propagation in waveguides with locally reactive liners which are mathematically represented by an impedance boundary condition. In the presence of circumferential variations of the lining impedance (e.g., hard walled splices in the lined intakes of an aeroengine), the problem to solve is fully three dimensional. When dimensionless frequency K is high, where $K = kR$, $k = 2\pi f/c$, f is frequency, c is sound velocity in air, and R is the radius of waveguide, it turns to be challenging to model it efficiently.

In Ref. [1], we proposed a multimodal propagation method (MPM) to study sound propagation in a nonuniform lined waveguide without flow. The sound pressure is expressed as a double series of the rigid waveguide modes which are known *a priori*. The boundary condition is satisfied in the integral sense. Calculations of the eigenmodes of nonuniform lined waveguides, which are very difficult, are avoided. Because the individual rigid waveguide mode does not satisfy the impedance boundary condition, the radial convergence rate is only $O(n^{-2})$, where n is the radial mode indices.

In this paper, we improve the MPM[1] by accelerating the radial convergence rate. The sound pressure is expressed as a double series of the rigid waveguide modes and an additional function which carries the information of the impedance boundary. This is motivated by Ref. [2] which studies water waves over variable bathymetry regions, and Ref. [3] and [4] which study sound propagation in rigid waveguides with varying cross section. It is shown that the radial convergence rate of the double infinite series is improved from $O(n^{-2})$ to $O(n^{-4})$.

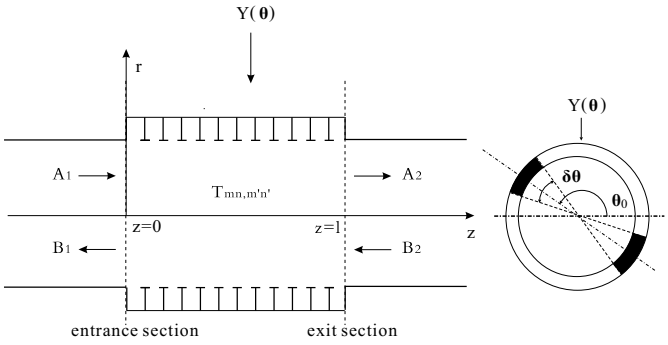

Figure 1: Configuration of one axial segment nonuniform lined waveguide.

Derivation of the multimodal equations

We consider an infinite rigid waveguide with circular cross section lined with a region of nonuniform liner. The liner properties are assumed to be given by a distribution of locally reacting impedance. Without significant loss of generality, the distribution may be assumed axially segmented, i.e., the impedance is set piecewise constant along the waveguide, while being arbitrarily variable along the circumference of each segment. In Fig. 1 the configuration of one axial segment of lining impedance is depicted, the circumferential variation of impedance is presented as two acoustically rigid splices, which is a typical configuration in the intake of an aeroengine. Linear and lossless sound propagation in air is assumed. With time dependence $\exp(j\omega t)$ omitted, the three dimensional wave equation with uniform flow is

$$\frac{1}{r}\frac{\partial}{\partial r}(r\frac{\partial p}{\partial r}) + \frac{1}{r^2}\frac{\partial^2 p}{\partial \theta^2} + \frac{\partial^2 p}{\partial z^2} - D_t^2 p = 0, \qquad (1)$$

where $D_t = jK + M_0\partial_z$, M_0 is the mach number of uniform flow. The radial boundary condition is

$$\frac{\partial p}{\partial r} = -\frac{Y(\theta)}{K^2} D_t^2 p, \quad \text{at} \quad r = 1, \tag{2}$$

where $Y(\theta) = -jK\beta(\theta)$, and $\beta(\theta)$ is the liner admittance.

Circumferentially uniform impedance boundary condition without flow

When there is no flow, and the impedance boundary condition is circumferentially uniform, the boundary condition is $\partial p/\partial r = Y_0 p$, where $Y_0 = -jK\beta_0$, and β_0 is the liner admittance and it is a complex constant.

The solution of Eq. (1) is expressed as an infinite series and an additional function in order to satisfy the boundary condition

$$p_m(r,\theta,z) = \sum_{n=0}^{\infty} P_{mn}(z)\Psi_{mn}(r,\theta) + A_m(z)\chi_m(r)e^{-jm\theta}, \tag{3}$$

where P_{mn} are the expansion coefficients, m and n refer to azimuthal and radial mode indices respectively. The basis functions

$$\Psi_{mn} = \frac{1}{\sqrt{\pi\Lambda_{mn}}} \frac{J_m(\alpha_{mn}r)}{J_m(\alpha_{mn})} e^{-jm\theta}, \tag{4}$$

are the eigenfunctions of the hard walled cylindrical circular waveguide, where J_m is the m order first kind Bessel function, Λ_{mn} refers to the normalized constant.

In order to choose $A_m\chi_m$, two conditions can be imposed on $\chi_m(r)$

$$\chi_m(r)|_{r=1} = 0, \tag{5a}$$

$$\frac{d\chi_m(r)}{dr}|_{r=1} = 1. \tag{5b}$$

Substitution of the conditions (5) into the boundary condition yields

$$A_m(z) = Y_0 \sum_{n=0}^{\infty} \frac{P_{mn}(z)}{\sqrt{\pi\Lambda_{mn}}}. \tag{6}$$

Functions which satisfy the conditions (5) may be not unique. One choice may be

$$\chi_m(r) = \frac{-1}{\beta_{m,0} J_{m+1}(\beta_{m,0})} J_m(\beta_{m,0} r), \tag{7}$$

where $\beta_{m,0}$ refers to the roots of the m order first kind Bessel function.

For calculating $P_{mn}(z)$, we project $p(r,\theta,z)$ on the basis Ψ_{mn}. Following the matricial terminology, Eq. (3) is written

$$p(r,\theta,z) = \mathbf{\Psi}^T \mathsf{M} \mathbf{P}, \tag{8}$$

where $\mathbf{P}$ and $\mathbf{\Psi}$ are column vectors, the superscript "^{T}" indicates the transpose. M is a matrix, it is equal to

$$\mathsf{M} = \mathsf{I} + 2\pi Y_0 \mathsf{N} \mathbf{\Phi}^* \mathbf{\Phi}^T, \tag{9}$$

where I refers to the identity matrix, N is a diagonal matrix, its elements in the main diagonal are $1/(\alpha_{mn}^2 - \beta_{m,0}^2)$. They come from the projection of χ_m over the rigid mode eigenfunctions. $\mathbf{\Phi}$ is a column vector, its elements are $1/\sqrt{\pi\Lambda_{mn}}$.

Using Eqs. (8) and (9), we project Eq. (1) to yield

$$\mathsf{M}\mathbf{P}'' + \mathsf{A}\mathbf{P} = 0, \tag{10}$$

where matrix A is

$$\mathsf{A} = (K^2\mathsf{I} - \mathsf{L})\mathsf{M} + 2\pi Y_0 \mathbf{\Psi}^*(1,\theta)\mathbf{\Psi}^T(1,\theta), \tag{11}$$

L is a diagonal matrix, its elements in the main diagonal are α_{mn}^2, the double prime refers to the second derivative with respect to axial coordinate z.

Circumferentially nonuniform impedance boundary condition without flow

When the boundary condition is circumferentially nonuniform, we have to solve a full 3D problem. The sound pressure cannot be separated in the $r-\theta$ plane. Similarly to Eq. (3), the sound pressure is expressed as

$$\begin{aligned} p(r,\theta,z) &= \sum_{m=-\infty}^{\infty} \sum_{n=0}^{\infty} P_{mn}(z)\Psi_{mn} \\ &+ \sum_{m=-\infty}^{\infty} A_m(z)\chi_m(r)e^{-jm\theta}. \end{aligned} \tag{12}$$

As in the above section, substitution of Eq. (12) into the boundary condition, yields

$$\begin{aligned} A_m(z) = & \sum_{m'=-\infty}^{\infty} \frac{1}{2\pi} \int_0^{2\pi} Y(\theta) e^{-j(m'-m)\theta} d\theta \\ & \times \sum_{n'=0}^{\infty} \frac{P_{m'n'}(z)}{\sqrt{\pi\Lambda_{m'n'}}}, \end{aligned} \tag{13}$$

where we have used Eq. (4) and imposed the conditions (5). Function χ_m, satisfying conditions (5), is the same as in Eq. (7). After we yield A_m, the rest is similar to the above section to yield an equation as Eq. (10).

Matching between segments

Equation (10) is a constant coefficient matrix differential equation when the axial lining impedance is uniform in one segment. Its solution can be directly written as

$$\mathbf{P} = \mathsf{X}\mathsf{D}(z)\mathbf{C_1} + \mathsf{X}\mathsf{D}(l-z)\mathbf{C_2}, \qquad (14)$$

where $\mathbf{C_1}$ and $\mathbf{C_2}$ are amplitude vectors of dimension N_t ($M \times N$, where M and N refer to the truncated dimensions of mode indices m and n), X is the $N_t \times N_t$ matrix whose columns are the generalized eigenvectors $\mathbf{X}_n$ of matrix $\mathsf{M}^{-1}\mathsf{A}$, and $\mathsf{D}(z)$ and $\mathsf{D}(l-z)$ are diagonal matrices with $\exp(-j\nu_n z)$ and $\exp(-j\nu_n(l-z))$ respectively on the main diagonal, with $\nu_n = \sqrt{d_n}$, d_n being the generalized eigenvalues of matrix $\mathsf{M}^{-1}\mathsf{A}$. In the form of Eq. (14), numerical stability is ensured because the propagation matrices $\mathsf{D}(z)$ and $\mathsf{D}(l-z)$ have only positive arguments and contain no exponentially diverging terms due to the evanescent modes. By matching the pressure and axial velocity at the interfaces of the segment, the coefficients of transmission and reflection are yielded. Scattering matrices are then obtained for each individual segment; these are combined to construct a global scattering matrix for multiple segments.

Circumferentially uniform impedance boundary condition with uniform flow

Consider the waveguide to include uniform flow. p in Eq. (1) and boundary condition (2) refers to displacement potential. The coefficient A_m in Eq. (3) is difficult to be decided explicitly as in Eq. (6). A_m is then decided numerically by an additional equation which is obtained by projecting Eq. (1) over $\chi_m \exp(jm\theta)$.

Convergence analysis

The radial convergence properties are numerically shown in Fig. 2 for fixed m.

The parameters are noted in Fig. 2. In this example, incident modes $(m = 2, n = 0)$ and $(m = 98, n = 0)$ are only scattered in corresponding radial modes of $m = 2$ and $m = 98$ respectively. The truncated dimension is $N = 1000$. It is clearly shown that for incident mode $(2, 0)$, the convergence rate is $O(n^{-4})$, when $n > 10$. However, the rate $O(n^{-4})$ takes place after $n > 200$ for incident mode $(98, 0)$. In the transient region $n < 200$, the convergence rate is slower, about $O(n^{-3})$ in the region $20 < n < 200$, and $O(n^{-2})$ in the region $n < 20$.

It is important to point out that in Fig. 2, although the transient region is longer for the modes with $m = 98$ than for the modes with $m = 2$, and in the transient region

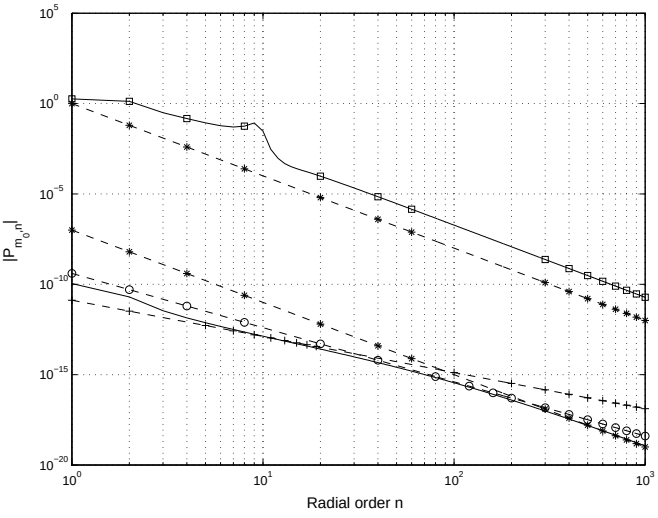

Figure 2: Convergence rates of radial order n for different incident modes $(m_0, 0)$. Solid line refers to $m_0 = 98$, solid line with squares refers to $m_0 = 2$, dashed line with stars refers to n^{-4}, dashed line with circles refers to n^{-3}, and dashed line with plus refers to n^{-2}. $K = 31.26$, $Z/\rho c = 2 - j$, no splice, no flow.

the convergence rate is slower, the amplitudes $|P_{98,n}|$ are already much smaller than $|P_{2,n}|$.

References

[1] W. P. Bi, V. Pagneux, D. Lafarge, and Y. Aurégan, "Modelling of sound propagation in a non-uniform lined duct using a multi-modal propagation method," J. Sound Vib. **289**, 1091–1111 (2006).

[2] G. A. Athanassoulis and K. A. Belibassakis, "A consistent coupled-mode theory for the propagation of small-amplitude water waves over variable bathymetry regions," J. Fluid Mech. **389**, 275–301 (1999).

[3] C. Hazard and V. Pagneux, "Improved multimodal approach in waveguides with varying cross-section," *Proceedings of the International Congress on Acoustics*, Rome, 2001, Vol. 25, No. 1–3, pp. 3–4.

[4] C. Hazard and E. Lunéville, "Multimodal approach and optimum design in non uniform waveguides," Workshop on the Method of Numerical and Electromagnetism, Toulouse, 2002.

MULTIMODAL ADMITTANCE METHOD IN WAVEGUIDE AND BEHAVIOR AT HIGH FREQUENCY

V. Pagneux
Laboratoire d'Acoustique de l'Université du Maine, Faculté des sciences, 72085 LE MANS, France
Email: vpagneux@univ-lemans.fr

Abstract

This work presents a multimodal method for the propagation in waveguide. The coupled mode equations is obtained by projecting the Helmholtz equation on the local transverse modes. To solve this problem we integrate the Riccati equation governing the admittance matrix (DtN operator). For many propagating modes, ie at high frequencies, the numerical integration of the Riccati equation shows that this operator has quasi-singularities associated to quasi-trapped modes.

Introduction

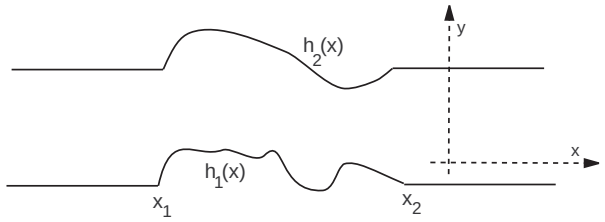

Figure 1: geometry of the 2D waveguide

The aim is to solve the helmholtz equation

$$\triangle\phi + k^2\phi = 0 \tag{1}$$

in the waveguide shown in figure 1 with Dirichlet boundary conditions at the wall ($\phi = 0$ for $y = h_1(x)$ and for $y = h_2(x)$). The same method could be also applied for Neumann or mixed boundary conditions but we take here the Dirichlet condition for the sake of clarity.

We first write the Helmholtz as a firt order evolution equation along the direction x of the waveguide

$$\partial_x \begin{pmatrix} \phi \\ \psi \end{pmatrix} = \begin{pmatrix} 0 & 1 \\ -\partial_{y^2} - k^2 & 0 \end{pmatrix} \begin{pmatrix} \phi \\ \psi \end{pmatrix}. \tag{2}$$

Then, the transverse modes of the waveguide are used to discretize the problem along the transverse direction y so that ϕ and ψ are projected on the modes as

$$\begin{array}{rcl} \phi & = & \sum_{n=1}^{+\infty} a_n(x) g_n(x;h) \\ \psi & = & \sum_{n=1}^{+\infty} b_n(x) g_n(x;h) \end{array}, \tag{3}$$

where

$$g_n(x;h) = \sqrt{\frac{2}{h}} sin(\frac{n\pi y}{h}) \tag{4}$$

and $h = h_2 - h_1$.

The projection of the evolution equation 2 yields the coupled mode equation for the component on the modes $a_n(x)$ and $b_n(x)$:

$$\begin{array}{rcl} a' & = & -Fa + b \\ b' & = & -K^2 a + F^T b \end{array} \tag{5}$$

where primes denote differentiation with respect to x, a (resp. b) is the vector of components a_n (resp. b_n) with $n \geq 1$, F is a matrix with non-diagonal elements ($n \neq m$) given by

$$F_{nm} = -\frac{nm}{m^2 - n^2} \frac{2}{h} \left((-1)^{n+m} h_2' - h_1' \right)) \tag{6}$$

and $F_{nn} = 0$, and K is the diagonal matrix of the mode wavenumbers given by $K_{nm} = k_n \delta_{nm}$ with $k_n = \sqrt{k^2 - n^2\pi^2/h^2}$. Since the implicit harmonic time dependance here is $e^{-i\omega t}$ the square root for k_n is chosen such that $Re(k_n) \geq 0$ and $Im(k_n) \geq 0$.

The coupled mode equations (5) cannot be integrated directly as an initial value problem for two reasons: firstly, the problem is posed as a boundary value problem with a radiation condition given, say, at the right, and a source given, say, at the left. Secondly, as an initial value problem the system (5) is unstable because of the evanescent modes that cause exponential divergence of the errors [1]. The method chosen here to solve this problem is to define the admittance matrix as

$$b = Ya. \tag{7}$$

This admittance matrix is the representation of the DtN operator on the mode basis. By inserting equation (7) into the system (5), a Riccati equation is obtained for the admittance matrix Y:

$$Y' = -K^2 - Y^2 + YF + F^T Y. \tag{8}$$

The Riccati equation (8) is a first order differential equation that enables us to obtain the admittance matrix (DtN operator) for all x from the initial value of Y

given by the radiation condition at, say, the right of the waveguide ($x = x_2$ see figure 1). This initial condition is $Y(x_2) = Y_c$ for the radiation condition corresponding to only right-going waves in the region $x > x_2$, where the matrix Y_c is $Y_c = iK$; this initial condition is the same as the DtN condition imposed in finite elements method. Note that the same kind of method had been presented in [1] and in [2].

Calculation of the wave field

If one is interested in the calculation of the whole field in the waveguide, once the Riccati equation (8) has been solved and the matrix Y has been stocked along x, it is sufficient to solve the first equation of the coupled mode equations (5) where $b = Ya$. It gives the first order equation for a:

$$a' = (Y - F)a. \tag{9}$$

Reflection and transmission matrix

The admittance matrix is directly related to the reflection matrix by

$$R = (Y_c + Y)^{-1}(Y_c - Y), \tag{10}$$

where the waves has been decomposed into right and left going parts as $a = a^+ + a^-$ and $b = Y_c(a^+ - a^-)$, and the reflection matrix has been defined by $a^- = Ra^+$.

It is also possible to get the transmission matrix of the waveguide at the same time as the Y matrix by defining the propagator matrix G such that

$$a(x_2) = G(x_2, x)a(x), \tag{11}$$

where $x_2 \geq x$ and $G(x_2, x_2) = Id$. The equation governing G is then found to be

$$G' = -G(-F + Y), \tag{12}$$

with the initial value $G(x_2, x = x_2) = Id.$ and the transmission matrix is given by

$$T = G(x_2, x = x_1)(I + R) \tag{13}$$

(the definition of the transmission matrix is the classical one: $a^+(x_2) = Ta^+(x_1)$).

To summarize, starting from $x = x_2$ equations (8) and (12) are integrated for $x \leq x_2$ with the initial conditions $Y(x_2) = Y_c$ and $G(x_2, x = x_2) = I$, and they yield the reflection and transmission matrix by equations (10) and (13). The great advantage of the method in this case is that the matrices (Y and G) do not have to be stocked during the integration of the differential equations (8) and (12) along x.

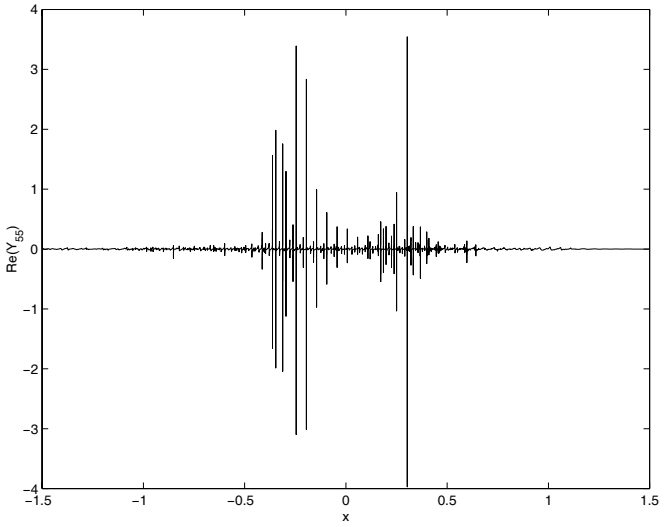

Figure 2: Real part of Y_{55} as a function of x for a case with 20 propagating modes and showing the quasi-singularites

Numerical integration

The Riccati equation (8) can be numerically integrated owing to a classical scheme as the Runge-Kutta method for instance. Nevertheless, as the frequency is increased the admittance matrix Y show more and more quasi-singularities that makes this kind of method very time consuming or even useless. Figure (2) displays the behavior of the real part of the diagonal element Y_{55} for a frequency corresponding to 20 propagating modes. The quasi-singularities are apparent and necessitate very small step size with a Runge-Kutta method. An alternative has been proposed to avoid this problem by Schiff and Shnider [3]: it consists in using the numerical integration by a Magnus method of the linear system from which the Riccati equation comes from (here the system (5)). Besides, for the high frequencies, the Magnus method (see [4]) is a very efficient method that necessitate very few points to describe wildly oscillating solutions. So this method is applied and enables us to get rather easily solutions at high frequencies

Quasi-singularities of Y and quasi-trapped modes

The quasi-singularities of the matrix Y correspond to an eigenvector of Y with a very high eigenvalue. For this eigenvector $Ya_s = \lambda_s a_s$ with $\lambda_s \to \infty$ so that $a_s = 1/\lambda_s b_s \to 0$ ($b_s = Ya_s$). That means that the eigenvector associated to a quasi-singularity can be also associated to a quasi-trapped mode of the geometry. Practically, if there is a quasi-singularity at $x = x_s$ for Y, we take the associated eigenvector a_s as an initial condition of the

evolution equation (9) and we calculate the values of $a(x)$ for $x_s \leq x \leq x_2$. The resulting quasi-trapped modes are shown in the figures (3) and (4) for two different values of the quasi-singularity locations $x_s = 1.1157$ and $x_s = -0.294$, in the case of a waveguide with semicircle indentation. The frequency is such that $kh_0 = 22.3\pi$ where h_0 is the height of the waveguide in the leads. That means that at this frequency there are 22 propagating modes in the leads.

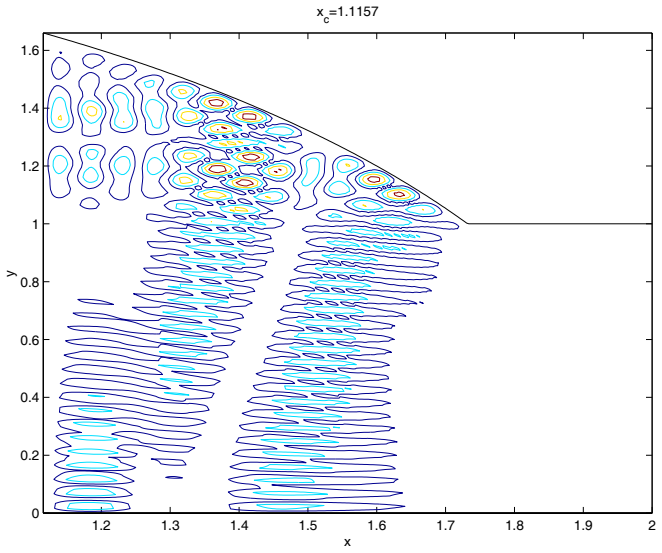

Figure 3: Quasi-trapped mode for a quasi-singularity at $x_s = 1.1157$ for the semi-circle geometry at $kh_0 = 22.3\pi$

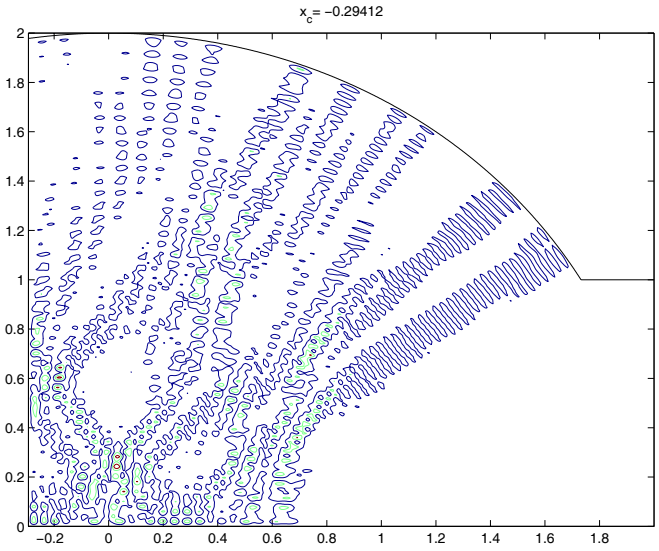

Figure 4: Quasi-trapped mode for a quasi-singularity at $x_s = -0.294$ for the semi-circle geometry at $kh_0 = 22.3\pi$

References

[1] V. Pagneux, N. Amir & J. Kergomard, "A study of wave propagation in varying cross-section waveguides by modal decomposition - Part I: theory and validation." *J. Acoust. Soc. Am.* **100**, 2034–2048, 1996.

[2] Y.Y. Lu & J.R. McLaughlin, "The Riccati method for the Helmholtz equation." *J. Acoust. Soc. Am.* **100**, 1432–1446, 1996.

[3] J. Schiff & S. Shnider "A natural approach to the numerical integration of Riccati differential equations." *SIAM J. Numer. Anal.* **36**, 1392–1413, 1999.

[4] A. Iserles, A. Mathisen & S.P. Norsett "On the implementation of the method of Magnus series for linear differential equations." *BIT* **39**, 281–304, 1999.

Asymptotic analysis of partial reflection of modes in slowly inhomogeneous elastic waveguides

Maria V. Perel
Department of Mathematical Physics, Physics Faculty, St.Peterburg University, Russia
Email: perel@mph.phys.spbu.ru

Abstract

An asymptotic study of reflection of modes in a slowly varying plane elastic waveguide is presented. The reflection occurs in the vicinity of a cross section where the wave frequency coincides with the cut-off frequency. Elastic constants and the volume density are assumed to be even functions of the distance from this section. Partial reflection and transmission of modes take place near this section. Results are obtained by the method of matched asymptotic expansions and are formulated in the general form so that they can be applied to the waves of another nature.

Introduction

The propagation of elastic waves in an inhomogeneous plane elastic waveguide has been considered in the literature (see [1] - [4] and references therein). We assume that the properties of the waveguide vary smoothly and slowly in the lateral direction, along the axis of the waveguide, being constant in transverse directions. The width of the waveguide is constant. The problem contains a small parameter that is the ratio of the wavelength and the scale of the lateral inhomogeneity. The wave field in such a waveguide is the superposition of modes which propagate independently of one another. Their amplitudes vary in such a way that the flux of energy in each mode is conserved. We say that they propagate adiabatically. The adiabatic approach fails to work near the cross section where the phase speeds of two modes coincide. We call the coordinate of a cross section where the coincidence occurs a degeneracy point. The transformation of energy between the degenerate modes takes place near the degeneracy point. Our aim here is to develop an asymptotic theory for describing this transformation.

The problem of describing the transformation of modes in slowly inhomogeneous waveguides has a long history (see, for example, [5]-[10]). Asymptotic formulae, which arises, are similar to waves of a different nature: acoustic, electromagnetic, elastic waves and so on. We formulate the problem in general terms. All lines of argument and results can be applied to problems of the propagation of waves of another nature.

The asymptotic theory of modes transformation in a slowly varying elastic waveguide has been developed in paper [10]. We treat here the same problem but we do it under another assumptions of lateral inhomogeneity near a degeneracy point. It has been shown in [10] that the points of the degeneracy are points where the frequency of waves coincides with the cut-off frequency. It has been obtained that a mode which runs in the direction of the cut-off section reflects totally near this section and the asymptotic description of this phenomenon has been done. The consideration in [10] has been carried out in the assumption that the properties of the waveguide vary in the monotone way near the cut-off section. Here we assume that the cut-off section is a specific section for the inhomogeneity. It is a section of symmetry of the waveguide and all the parameters of the waveguide, i.e., the elastic constants and the density, are even functions of the distance from this section.

In our considerations we use the method developed in [8], [9], [10]. We rewrite the elastic equations in the form of a Schrödinger type equation. We construct the asymptotic formulae for modes in the adiabatic approach. Next we consider reference homogeneous waveguides which possess the same properties as the inhomogeneous waveguide in the cut-off cross section and near it. We obtain expansions of the phase speed of degenerating mode and of its vertical structure in the reference waveguide in terms of the distance from the cut-off cross section by using the perturbation method. These expansions helps to estimate the width of the resonance zone in the inhomogeneous waveguide near the cut-off section where the adiabatic approach fails to hold. To do this, we examine the singularities that occur near cut-off section in all terms of the adiabatic expansion. Then we introduce a scaled distance variable and construct an inner asymptotic solution dependent on this variable, which works in the resonance zone. We call it the resonance expansion. It describes the common field of both degenerating modes. Finally we match the inner and outer expansions in the common zones of their validity.

The results are as follows. The transformation of energy between two modes occurs near a cut-off section where the phase speeds of these modes coincides. A degenerating mode incident on the cut-off section partially reflects and partially penetrates to the other side of it. The reflection and the transmission coefficients are calcu-

lated. An asymptotic expansion near the cut-off section is found.

Elastic equations and their reduction to a Schrödinger type equation

The time-harmonic displacements in a linear isotropic elastic plate $-\infty < x_1, x_2 < \infty, -H \le x_3 \le H$ are described by the Lamé equations which are accompanied by the traction-free boundary conditions on the faces:

$$-i\rho\omega^2 u_q = \frac{\partial \sigma_{qj}}{\partial x_j}, \quad \sigma_{qj} = \delta_{qj}\lambda\frac{\partial u_k}{\partial x_k} + \mu(\frac{\partial u_q}{\partial x_j} + \frac{\partial u_j}{\partial x_q}),$$

where u_q is the qth component ($q = 1, 2, 3$) of the vector of displacements, σ_{qj} is the stress tensor, ρ is the density, ω is frequency, λ, μ are the Lamé coefficients, and summation on repeated indices is assumed. Lamé equations are to be considered in conjunction with the traction-free boundary conditions $\sigma_{q3}|_{x_3=-H} = \sigma_{q3}|_{x_3=H} = 0$, $q = 1, 2, 3$. We assume that all the components u_q, σ_{qj} do not depend on x_2, i.e., the wave propagates along the axis x_1. All the variables here are dimensionless. We assume that the waveguide is slowly irregular along the axis x_1 and $\mu = \mu(\varepsilon x_1)$, $\lambda = \lambda(\varepsilon x_1)$, $\rho = \rho(\varepsilon x_1)$, where $\varepsilon \ll 1$. In what follows, we use two new variables $x = \varepsilon x_1$ and $z = x_3/H$ that are of order of unity. We reduce the Lamé equations to a Schrödinger type equation in the same way as was done in [10]:

$$\mathbf{K}\mathbf{\Psi} = -i\varepsilon\mathbf{\Gamma}\frac{\partial \mathbf{\Psi}}{\partial x}, \quad \mathbf{B}\mathbf{\Psi}_{|\,z=1} = \mathbf{B}\mathbf{\Psi}_{|\,z=-1} = \mathbf{0}. \quad (1)$$

Here $\mathbf{\Psi}$ is the four component vector

$$(\mathbf{\Psi})_1 = -i\omega u_1, \quad (\mathbf{\Psi})_2 = -i\omega u_3,$$
$$(\mathbf{\Psi})_3 = \sigma_{11}, \quad (\mathbf{\Psi})_4 = \sigma_{13} = \sigma_{31},$$

the matrix operators $\mathbf{K}$, $\mathbf{\Gamma}$ and $\mathbf{B}$ are defined in such a way:

$$\mathbf{K} = \begin{pmatrix} -\omega\rho & 0 & 0 & i\frac{\partial}{\partial z} \\ 0 & -\omega\rho - \frac{1}{\omega}\frac{\partial}{\partial z}\frac{4\mu(\lambda+\mu)}{2\mu+\lambda}\frac{\partial}{\partial z} & i\frac{\partial}{\partial z}\frac{\lambda}{2\mu+\lambda} & 0 \\ 0 & i\frac{\lambda}{2\mu+\lambda}\frac{\partial}{\partial z} & \frac{-\omega}{2\mu+\lambda} & 0 \\ i\frac{\partial}{\partial z} & 0 & 0 & \frac{-\omega}{\mu} \end{pmatrix},$$

$$(\mathbf{\Gamma})_{1j} = \delta_{3j}, (\mathbf{\Gamma})_{2j} = \delta_{4j}, (\mathbf{\Gamma})_{3j} = \delta_{1j}, (\mathbf{\Gamma})_{4j} = \delta_{2j},$$

$$\mathbf{B} = \begin{pmatrix} 0 & 0 & 0 & i \\ 0 & -\frac{4\mu(\lambda+\mu)}{\omega(2\mu+\lambda)}\frac{\partial}{\partial z} & i\frac{\lambda}{(2\mu+\lambda)} & 0 \\ 0 & 0 & 0 & 0 \\ 0 & 0 & 0 & 0 \end{pmatrix},$$

where δ_{ij} is the Kronecker δ.

We introduce the inner product of two four-component vector-functions $\mathbf{f}(z)$ and $\mathbf{g}(z)$ as $(\mathbf{f}, \mathbf{g}) = \int_{-1}^{1} \overline{f}_j(z) g_j(z)\, dz$, where summation is taken over the repeated subscripts and $\overline{f}_j(z)$ denotes the complex conjugate of $f_j(z)$. The matrix $\mathbf{G}$ is symmetric, and the operator $\mathbf{K}$ is Hermitian $(\mathbf{f}, \mathbf{K}\mathbf{g}) = (\mathbf{K}\mathbf{f}, \mathbf{g})$ on the functions $\mathbf{f}(z)$ and $\mathbf{g}(z)$ satisfying the boundary conditions.

Every solution of problem (1) satisfies the conservation law $(\mathbf{\Psi}, \mathbf{\Gamma}\mathbf{\Psi}) = \mathrm{Const}$, which follows from (1) and the fact that $\mathbf{K}$ is Hermitian. It can be interpreted as the conservation of the average x - component of the flux of energy (see [3]). Let $\mathbf{\Psi}_1$ and $\mathbf{\Psi}_2$ be any two different solutions of Eq. (1). The conservation law can then be generalized in the following way $(\mathbf{\Psi}_1, \mathbf{\Gamma}\mathbf{\Psi}_2) = \mathrm{Const}$.

Modes in the adiabatic approximation

The standard asymptotic series for a mode reads [10]

$$\mathbf{\Psi}_n = \mathbf{\Phi}_n \exp\left(\tfrac{i}{\varepsilon}\int_{x_*}^{x} \beta_n(x')dx'\right), \quad (2)$$

$$\mathbf{\Phi}_n = \tfrac{\boldsymbol{\varphi}_n}{\sqrt{N_n}} + \varepsilon\mathbf{\Phi}_n^{(1)} + \varepsilon^2\mathbf{\Phi}_n^{(2)} + \ldots, \quad (3)$$

where β_n and $\boldsymbol{\varphi}_n$ are consequently the eigenvalue and the corresponding eigenelement, respectively, of the spectral problem

$$\mathbf{K}\boldsymbol{\varphi}_n = \beta_n\mathbf{\Gamma}\boldsymbol{\varphi}_n, \qquad \mathbf{B}\boldsymbol{\varphi}_{n|z=1} = \mathbf{B}\boldsymbol{\varphi}_{n|z=-1} = \mathbf{0}.$$

We deal here with modes corresponding to real eigenvalues. Then the notation N_n in (3) means that $N_n = (\boldsymbol{\varphi}_n, \mathbf{\Gamma}\boldsymbol{\varphi}_n)$. It ensures that the average x - component of the flux of energy of a mode is preserved and is equal to unity in modulus. The sign of it determines the direction in which the mode carries energy. For the sake of definiteness, $0 \le arg(\sqrt{N_n}) < \pi$. The approximations $\mathbf{\Phi}_n^{(m)}$ are determined from the recurrent system $\mathbf{K}\mathbf{\Phi}_n^{(m)} = \beta_n\mathbf{\Gamma}\mathbf{\Phi}_n^{(m)} - i\frac{\partial \mathbf{\Phi}_n^{(m-1)}}{\partial x}$ and boundary conditions (1).

Our aim is to investigate the case where the adiabatic approximation does not work. It happens at such distance x_* that $N_n = 0$ and $\mathbf{\Phi}_n$ has a singularity. At this distance, the frequency of the wave coincides with the cut-off frequency and eigenvalues of two modes, say β_1 and β_2, coincides. We choose the amplitudes of eigenelements $\boldsymbol{\varphi}_1$ and $\boldsymbol{\varphi}_2$ in such a way that $\boldsymbol{\varphi}_1(x_*, z) = \boldsymbol{\varphi}_2(x_*, z)$ and $N_1 = (\beta_2 - \beta_1)\zeta$, $N_2 = (\beta_1 - \beta_2)\zeta$ near x_*. The parameter ζ is equal to ± 1, it depends on the behaviour of the dispersion curves near cut-off frequency [10]. The functions $\boldsymbol{\varphi}_1, \boldsymbol{\varphi}_2$ are of order of unity.

The crucial point in what follows is an investigation of the dependence of eigenvalues on the distance from the cut-off section. It is shown here that, under some conditions,

$$\beta_1 - \beta_2 = B(x - x_*) + o(x - x_*), \quad B = \text{const}.$$

For example, this is the case when the elastic constants and the volume density are even smooth functions of $x - x_*$. We show that the singularities in higher-order terms $\varepsilon^m \mathbf{\Phi}_n^{(m)}, m = 1, 2, \ldots$ increase as $\varepsilon^m/(x - x_*)^{2m}$. This implies that the width of the resonance zone is of order $\sqrt{\varepsilon}$.

Transmission and reflection of modes near a cut-off section

The main result of the paper is an asymptotic description of the process of reflection and transmission of modes near a cut-off section in the case where this section is a section of symmetry of the waveguide.

To the mode carrying energy in the positive direction of x-axis we assign the number one; therefore $N_1 > 0$. The mode carrying energy in the negative direction has number two, we obtain $N_2 < 0$. The first mode is incident on the cut-off section. In the resonance zone, the interaction of the first and second modes occurs, which produces the reflected mode of number 2 for $x < x_*$ and the transmitted mode behind the cut-off section for $x > x_*$. Outside the resonance zone, we have

$$\begin{aligned} \mathbf{\Psi}(x,z) &= \mathbf{\Psi}_1(x,z) + R\mathbf{\Psi}_2(x,z), \quad x_* - x \gg \sqrt{\varepsilon}, \\ \mathbf{\Psi}(x,z) &= T\mathbf{\Psi}_1(x,z), \qquad\qquad\quad x - x_* \gg \sqrt{\varepsilon}, \end{aligned}$$

where R and T are the reflection and the transmission coefficients, respectively. The process of modes interaction is described by an inner asymptotic expansion, which is valid in the resonance zone. This expansion incorporates the contributions of both modes interacting in the resonance zone. This expansion is constructed, and the main term of it is as follows:

$$\begin{aligned} &\mathbf{\Psi}(x,z) = AD_\mu(t)\boldsymbol{\varphi}(x_*,z)e^{i\theta(x)} + \ldots, \\ &\theta(x) = \int_{x_*}^{x} \frac{\beta_1(x') + \beta_2(x')}{2} dx', \\ &\boldsymbol{\varphi}(x_*,z) = \boldsymbol{\varphi}_1(x_*,z) = \boldsymbol{\varphi}_2(x_*,z), \\ &t = e^{-i\pi/4}\sqrt{2B}(x - x_*)/\sqrt{\varepsilon}, \end{aligned}$$

where the positive square root is understood, $D_\mu(t)$ stands for the parabolic cylinder function, which is the solution of the differential equation

$$\frac{d^2 D_\mu(t)}{dt^2} + (\mu + \frac{1}{2} - \frac{t^2}{4})D_\mu(t) = 0$$

(see [11]). Here ζ is chosen equal to -1.

The constants A, R and T are determined from the matching of the inner expansion and the adiabatic expansion in the common zone of their validity. The matching gives the following values:

$$R = T = \frac{1}{\sqrt{2}}, \qquad A = \frac{e^{-i\pi/8}}{2^{3/4}B^{1/4}}.$$

References

[1] J. D. Achenbach, Wave Propagation in Elastic Solids, North-Holland, Amsterdam, 1973.

[2] V. T. Grinchenko, V. V. Meleshko, Garmonic vibrations and waves in the elastic bodies, Naukova Dumka, Kiev, 1981 (In Russian).

[3] I. P. Getman, J. A. Ustinov, The mathematical theory of the irregular solid waveguides, Rostov-na-Donu Univ. Press, Rostov-na-Don, 1993 (In Russian).

[4] J. G. Harris, Linear Elasic Waves, Cambridge, New York, 2001.

[5] K. G. Budden, "The theory of coupling of characteristic radio waves in the ionosphere", J. Atmos. Terr. Phys. vol.34, pp. 1909–1921, 1972.

[6] K. G. Budden, "The critical coupling of modes in a tapered Earth-ionosphere waveguide", Math. Proc. Cambridge Phil. Soc., vol. 77, pp. 567–580, 1975.

[7] I. A. Molotkov, "The behavior of waveguide modes in the vicinity of the cut-off cross-section", Journal of Soviet Mathematics, vol. 9, 1978.

[8] M. V. Perel, "Overexcitation of modes in an anisotropic Earth - ionosphere waveguide on transequatorial paths in presence of two degeneracy points", Radiophysics and Quantum Electronics, vol. 33, pp. 882–889, 1990.

[9] M. V. Perel, I. V. Fialkovksy, and A. P. Kiselev, " Resonance interaction of bending and shear modes in nonuniform Timoshenko beam", Journal of Mathematical Sciences, No 6, pp.198-218, 2002.

[10] M.V. Perel, Yu.D. Kaplunov, G.A. Rogerson, "An Asymptotic Theory for Internal Reflection in Weakly Inhomogeneous Elastic Waveguides", Wave Motion, vol. 41(2), pp. 95-108, 2005.

[11] E. T. Whittaker, G. N.Watson, A course of modern analysis, Cambridge, Cambridge Univ. Press, 1952.

COMPUTING SECOND HARMONIC GENERATION IN PIECEWISE UNIFORM WAVEGUIDES

Lijun Yuan[†], **Ya Yan Lu**[†,*]
[†]Department of Mathematics, City University of Hong Kong, Kowloon, Hong Kong
[*]Email: mayylu@cityu.edu.hk

Abstract

An efficient numerical method is developed for second harmonic generation in two-dimensional wave-guiding structures composed of segments that are invariant in the main propagation direction. The method marches two operators and two functions along the waveguide axis. A Chebyshev collocation method is used to discretize the longitudinal direction in each segment for computing the Dirichlet-to-Neumann map and the locally generated second harmonic wave.

Introduction

The nonlinear optical phenomenon of second harmonic generation (SHG) has found applications in many fields. In a number of applications, it is desirable to have SHG in optical waveguides. SHG can be enhanced by a periodic structure along the waveguide axis [1], [2], [3]. Efficient numerical methods are needed to analyze SHG in such piecewise uniform and periodic wave-guiding structures. To analyze linear waves in piecewise uniform waveguides, the eigenmode expansion method (EEM) and the bidirectional beam propagation method (BiBPM) are particularly efficient. In [2] and [3], the BiBPM and the EEM are extended to handle SHG, respectively. However, both methods become very complicated due to the inhomogeneous term in the governing equation of the second harmonic wave. In a recent work [4], we developed an efficient method for linear waves in piecewise uniform waveguides based on the Dirichlet-to-Neumann (DtN) maps. For a uniform segment from z_{j-1} to z_j, the DtN map M is an operator that maps the wave field at z_{j-1} and z_j to the z-derivative of the wave field there. A highly accurate Chebyshev collocation method is used for discretizing z in each uniform segment. In this paper, we extend the DtN map method to SHG.

Operator marching scheme

We consider a two-dimensional (2D) wave-guiding structure in the xz plane and assume that both the fundamental frequency and second harmonic waves are given in the transverse electric (TE) polarization. Therefore, the y-component of the electric field is the real part of $ue^{-i\omega t} + ve^{-2i\omega t}$, where ω is the angular frequency of the fundamental frequency wave. Although higher harmonics can also be generated by the second order nonlinear effect, they are typically very weak and can thus be ignored. The governing equations for SHG are

$$\partial_z^2 u + \partial_x^2 u + [k_0 n^{(1)}]^2 u = -k_0^2 \chi^{(2)}\, \bar{u} v, \quad (1)$$

$$\partial_z^2 v + \partial_x^2 v + [2k_0 n^{(2)}]^2 v = -2k_0^2 \chi^{(2)}\, u^2, \quad (2)$$

where $k_0 = \omega/c$ is the free space wavenumber, c is the speed of light in vacuum, $n^{(1)}$ and $n^{(2)}$ are the linear refractive index functions at ω and 2ω, respectively, $\chi^{(2)}$ is an element in the second order nonlinear susceptibility tensor. We assume that the structure is linear for $z < 0$ and $z > a$ and piecewise uniform (i.e., z-invariant) with longitudinal discontinuities at $z_0,\ z_1,\ \ldots,\ z_m$ satisfying $0 = z_0 < z_1 < \ldots < z_m = a$. For the segment (z_{j-1}, z_j), we have $\chi^{(2)} = \chi_j^{(2)}(x)$, $n^{(l)} = n_j^{(l)}(x)$ for $l = 1, 2$. This is valid even for $j = 0$ and $j = m+1$ if we define $z_{-1} = -\infty$ and $z_{m+1} = +\infty$. Notice that $\chi_0^{(2)} = \chi_{m+1}^{(2)} = 0$. For a given incident wave u^+ (at the fundamental frequency) in $z < 0$, we have transmitted waves in $z > a$ and reflected waves in $z < 0$ for both frequencies. With a proper definition of the square root operators $L_j^{(l)} = \sqrt{\partial_x^2 + [k_0 n_j^{(l)}]^2}$, we can write down the boundary conditions as:

$$\partial_z u + iL_0^{(1)} u = 2iL_0^{(1)} u^+(x, 0-), \quad z = 0, \quad (3)$$

$$\partial_z u - iL_{m+1}^{(1)} u = 0 \quad \text{at} \quad z = a, \quad (4)$$

$$\partial_z v + iL_0^{(2)} v = 0 \quad \text{at} \quad z = 0, \quad (5)$$

$$\partial_z v - iL_{m+1}^{(2)} v = 0 \quad \text{at} \quad z = a. \quad (6)$$

Under the undepleted-pump approximation, the effect of the second harmonic wave on the fundamental frequency field is ignored. Eq. (1) is then replaced by the linear homogeneous Helmholtz equation:

$$\partial_z^2 u + \partial_x^2 u + [k_0 n^{(1)}]^2 u = 0. \quad (7)$$

This approximation is appropriate for the examples considered in this paper. Since $\chi^{(2)}$ is small, the magnitude of v is still much smaller than that of u.

In principle, the method developed here can be used in an iterative procedure to solve the fully nonlinear SHG problem without the undepleted-pump approximation.

The DtN marching method for u satisfying (7,3,4) was developed in [4]. Here, we concentrate on the second harmonic v and extend the method to the inhomogeneous Helmholtz equation (2). For all solutions of (2) and (6), we define the operators Q_j, Y_j and functions $g_j(x)$, $f_j(x)$ to satisfy

$$\partial_z v_j = Q_j\, v_j + g_j, \tag{8}$$
$$Y_j\, v_j = v_m + f_j, \tag{9}$$

where $v_j = v(x, z_j)$, $v_m = v(x, a)$, $\partial_z v_j = \partial_z v(x, z_j)$. Condition (5) is excluded in the definition, therefore, the above equations are valid for infinitely many solutions of v. When the transverse variable x is truncated and discretized by N points, Q_j and Y_j are $N \times N$ matrices, f_j and g_j are column vectors of length N. From the boundary conditions at $z = a$ and the definitions, we have

$$Q_m = iL_{m+1}^{(2)}, \quad g_m = 0, \quad Y_m = I, \quad f_m = 0, \tag{10}$$

where I is the identity operator. In the definition, the functions f_j and g_j are the contributions of the right hand side of (2). If Eq. (2) becomes homogeneous, then $g_j = f_j = 0$ for all j. This implies that the operators Q_j and Y_j are defined independent of the inhomogeneous term. Therefore, they can be marched exactly the same way as in [4]. For the segment (z_{j-1}, z_j), we define the local DtN map M by

$$M \begin{bmatrix} s(x, z_{j-1}) \\ s(x, z_j) \end{bmatrix} = \begin{bmatrix} \partial_z s(x, z_{j-1}) \\ \partial_z s(x, z_j) \end{bmatrix}, \tag{11}$$

where $s = s(x, z)$ is an arbitrary solution of the homogeneous Helmholtz equation at 2ω:

$$\partial_z^2 s + \partial_x^2 s + [2k_0 n_j^{(2)}]^2 s = 0, \quad z_{j-1} < z < z_j. \tag{12}$$

If we write down the DtN map in 2×2 blocks

$$M = \begin{bmatrix} M_{11} & M_{12} \\ M_{21} & M_{22} \end{bmatrix},$$

then the two operators Q_j and Y_j can be marched from z_j to z_{j-1} by the following formulas [4]:

$$Z = (Q_j - M_{22})^{-1} M_{21}, \tag{13}$$
$$Q_{j-1} = M_{11} + M_{12} Z, \tag{14}$$
$$Y_{j-1} = Y_j Z. \tag{15}$$

To find the marching formulas for the functions g_j and f_j, we consider an arbitrary solution v of (2) and (6) and split it as $v = w + s$ in the segment (z_{j-1}, z_j), where w satisfies the inhomogeneous Helmholtz equation

$$\partial_z^2 w + \partial_x^2 w + [2k_0 n_j^{(2)}]^2 w = -2k_0^2 \chi_j^{(2)}\, u^2, \tag{16}$$

for $z_{j-1} < z < z_j$ and zero Dirichlet boundary conditions $w = 0$ at $z = z_{j-1}$ and z_j. Notice that w corresponds to the locally generated second harmonic wave in the segment. Meanwhile, s satisfies the homogeneous equation (12). We can evaluate $\partial_z v$ at z_{j-1} and z_j through (8), as well as through $v = w + s$ and the DtN map M for s. This gives rise to

$$g_{j-1} - \partial_z w|_{z_{j-1}} = (M_{11} - Q_{j-1}) v_{j-1} + M_{12} v_j$$
$$g_j - \partial_z w|_{z_j} = M_{21} v_{j-1} + (M_{22} - Q_j) v_j.$$

Together with (13) and (9), the above leads to

$$h = (Q_j - M_{22})^{-1} \left(g_j - \partial_z w|_{z_j} \right), \tag{17}$$
$$g_{j-1} = \partial_z w|_{z_{j-1}} - M_{12} h, \tag{18}$$
$$f_{j-1} = f_j + Y_j h. \tag{19}$$

Starting from the initial values given in (10) and following the marching formulas (13-19), we can calculate Q_0, Y_0, g_0 and f_0, then the second harmonic field at $z_0 = 0$ and $z_m = a$ can be solved from

$$\left[Q_0 + iL_0^{(2)} \right] v_0 = -g_0, \quad v_m = Y_0\, v_0 - f_0. \tag{20}$$

In each step, we need to find the local DtN map M (if it is not already available), to find the locally generated second harmonic field w, to solve linear systems with coefficient matrix $Q_j - M_{22}$ for Z and h, and to find the matrix products $M_{12}Z$ and $Y_j Z$, etc. When x is discretized by N points, the operators Q_j, Y_j, Z, M_{11}, M_{21}, etc, are approximated by $N \times N$ matrices. Therefore, $O(N^3)$ operations are required for computing Z and h, $M_{12}Z$ and $Y_j Z$. It turns out that M and w can be obtained in less operations. Therefore, the total required number of operations in each step is still $O(N^3)$. For a structure with m uniform segments, the method requires $O(mN^3)$ operations. To take advantage of the property that the structure is piecewise z-invariant, we discretize z by a Chebyshev collocation method. If the segment (z_{j-1}, z_j) is discretized by q points, then q is typically much smaller than N. The DtN map M can be found in $O(qN^2)$ operations. To find w, we need to solve the inhomogeneous equation (16) with zero Dirichlet boundary conditions. This can be done in $O(q^2 N)$ operations.

A numerical example

We consider an example originally studied Locatelli *et al.* in [2]. It is a 2D model (top view) of a deeply etched waveguide with a semiconductor core. Starting from a symmetric slab waveguide with air claddings and a core of width 2.5 μm, we introduce eight equally spaced air gaps in the waveguide core. The length of these air gaps is 0.2 μm. There are seven guiding segments between the air gaps. The length of each guiding segment is 0.837 μm. More precisely, we have $z_{2k} = 1.037\,k\,(\mu m)$, $z_{2k+1} = 1.037\,k + 0.2\,(\mu m)$ for $k = 0, 1, ..., 7$. The total length of the z-varying part of the structure is $a = z_{15} = 7.459$ μm. In the waveguide core, we have a refractive index $n^{(1)} = 3.15$ at the fundamental frequency and $n^{(2)} = 3.3$ for the second harmonic. In our notation, these two values correspond to $n^{(l)}_{2k}(x)$ for $|x| < 1.25$ μm, $l = 1, 2$ and $0 \le k \le 8$. The second order nonlinear coefficient is assumed to be $\chi^{(2)}_{2k}(x) = 300$ pm/V in the waveguide core ($|x| < 1.25$ μm) for the seven guiding segments ($1 \le k \le 7$). Notice that $\chi^{(2)}$ is assumed to be zero for $z < 0$ and $z > a$. The incident wave is the fundamental mode of the original symmetric slab waveguide with a maximum electric field amplitude of 10^6 V/m.

We first calculate the linear transmission and reflection properties of this structure. It is found that a transmission resonance around 1.55 μm matches well with another transmission peak around 0.775 μm. Using the method described earlier, we calculate the second harmonic field for a number of wavelengths. The maximum absolute value of the generated second harmonic wave at $z = a$ is shown versus the free space wavelength λ at the fundamental frequency in Fig. 1. At $\lambda = 1.55$ μm, the maximum we obtained is 5.37×10^3 V/m. This is slightly larger than the value 5.1×10^3 V/m reported in [2]. Our numerical results are obtained with $q = 35$ for the guiding segments and $q = 10$ for the air gaps. The x variable is discretized form -2.5 μm to 2.5 μm with 201 points. Perfectly matched layers are used at the two ends of the interval.

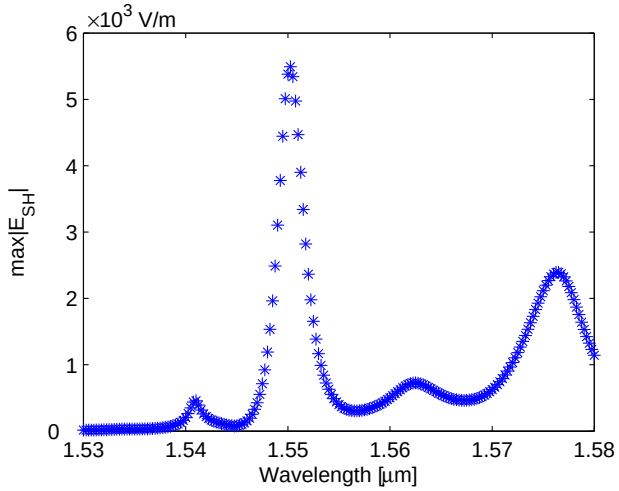

Figure 1: Maximum amplitude of the generated second harmonic wave at $z = a$.

Conclusions

We have developed a marching scheme for second harmonic generation (SHG) in piecewise uniform waveguides based on Dirichlet-to-Neumann (DtN) maps. It is an extension of our earlier work [4] for linear waves. Due to an inhomogeneous term in the governing Helmholtz equation of the second harmonic wave, existing methods for SHG require additional analytic approximations. Our method solves the inhomogeneous Helmholtz equation rigorously. Compared with the linear DtN map method, the additional effort required for computing SHG is insignificant. The total required number of operations for computing the second harmonic wave in a structure with m segments is $O(mN^3)$, where N is the number of points for discretizing the transverse variable. To take advantage of the piecewise uniform nature of the structure, a highly accurate Chebyshev collocation method is used to discretize z in each segment for computing the DtN map and the locally generated second harmonic field.

References

[1] Y. Dumeige, F. Raineri, A. Levenson and X. Letartre, "Second-harmonic generation in one-dimensional photonic edge waveguides", Phys. Rev. E , Vol. 68, 066617, 2003.

[2] A. Locatelli, D. Modotto, C. De Angelis, F. M. Pigozzo and A. D. Capobianco, "Nonlinear bidirectional beam propagation method based on scattering operators for periodic microstructured waveguides", J. Opt. Soc. Am. B , vol. 20, pp. 1724-1731, 2003.

[3] B. Maes, P. Bienstman and R. Baets, "Modeling second-harmonic generation by use of mode expansion", J. Opt. Soc. Am. B, vol. 22, pp. 1378-1383, 2005.

[4] L. Yuan and Y. Y. Lu, "An efficient bidirectional propagation method based on Dirichlet-to-Neumann maps", IEEE Photon. Technol. Lett., vol. 18, pp. 1967-1969, Sept. 2006.

AUTHOR INDEX

The 8th International Conference on Mathematical and Numerical Aspects of Waves (Waves 2007) was held at the University of Reading, organised jointly with INRIA, 23-27 July 2007. This conference series is one of the main venues where signifi cant advances in the analysis and computational modelling of wave phenomena and exciting new applications are presented.

Major themes of the conference included periodic media and photonic crystals, metamaterials and propagation in complex and random media, nonlinear wave phenomena in optics and fluid dynamics, inverse problems and optimization, numerical methods for time domain problems, resonances and trapped modes, fi nite element methods for the Helmholtz equation and Maxwell system, absorbing boundary conditions, elastic waves, gravity waves, and brain waves and cognitive neurodynamics.

The conference included an embedded Workshop on High Frequency Propagation and Scattering, as a satellite meeting of the Isaac Newton Institute Programme on Highly Oscillatory Problems: Computation, Theory and Application.

Published by:
Department of Mathematics
School of Mathematics, Meteorology and Physics
University of Reading
Whiteknights
P.O. Box 220
Reading
RG6 6AX, U.K.
https://www.waves2007.org/

ISBN: 0 704998 80 7

The 8th International Conference on Mathematical and Numerical Aspects of Waves (Waves 2007) was held at the University of Reading, organised jointly with INRIA, 23-27 July 2007. This conference series is one of the main venues where signifi cant advances in the analysis and computational modelling of wave phenomena and exciting new applications are presented.

Major themes of the conference included periodic media and photonic crystals, metamaterials and propagation in complex and random media, nonlinear wave phenomena in optics and fluid dynamics, inverse problems and optimization, numerical methods for time domain problems, resonances and trapped modes, fi nite element methods for the Helmholtz equation and Maxwell system, absorbing boundary conditions, elastic waves, gravity waves, and brain waves and cognitive neurodynamics.

The conference included an embedded Workshop on High Frequency Propagation and Scattering, as a satellite meeting of the Isaac Newton Institute Programme on Highly Oscillatory Problems: Computation, Theory and Application.

Published by:
Department of Mathematics
School of Mathematics, Meteorology and Physics
University of Reading
Whiteknights
P.O. Box 220
Reading
RG6 6AX, U.K.
https://www.waves2007.org/

ISBN: 0 7049 9880 7